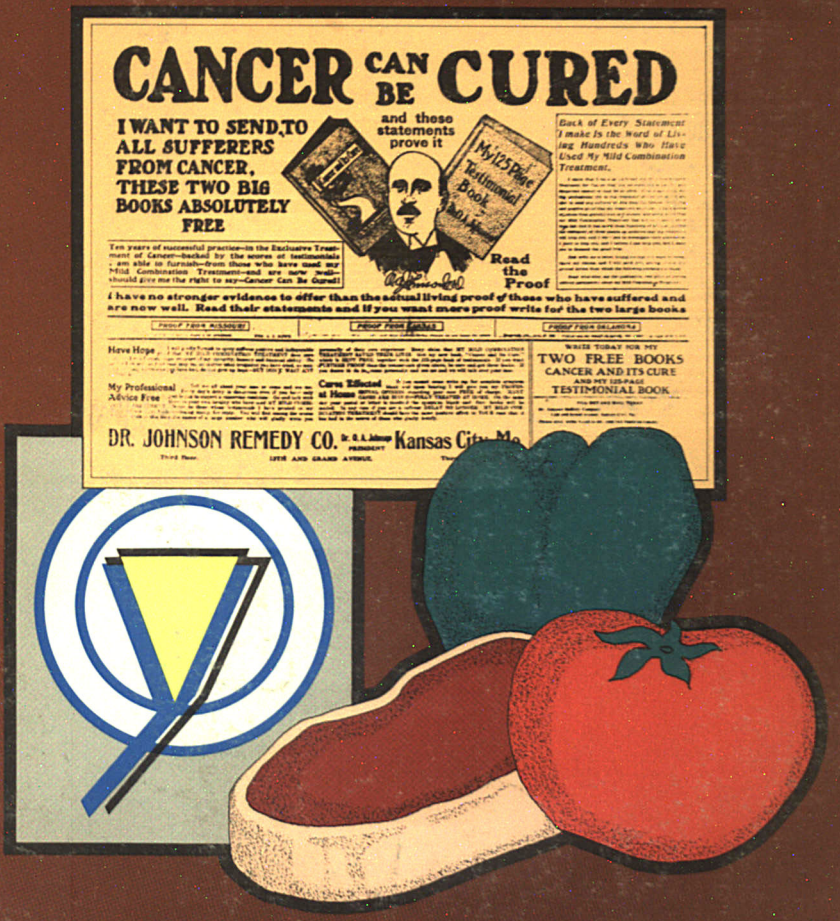
FEBRUARY 1978

analytical chemistry



Cancer Treatments: Science vs. Quackery 197A
Nutrient Trace Elements in Foods 190A
1978 Pittsburgh Conference 119A

NEW X-Y RECORDER

MORE RELIABLE
LESS EXPENSIVE
BECAUSE...

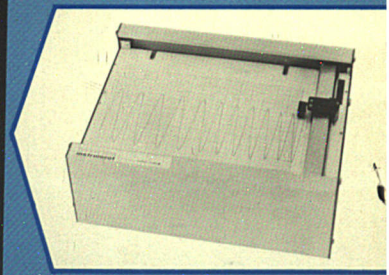
"THE POT IS NOT"

A capacitance feedback transducer replaces the potentiometer and slidewire -

neatly eliminating the most troublesome components in X-Y servo systems

* No more slidewire cleanser
* No more slidewire lubricant
* No more slidewire





Prices start at $895.*

Send today for complete information on the Series 100 – a new concept in low cost X-Y recorders.

houston instrument

THE RECORDER COMPANY

A DIVISION OF BAUSCH & LOMB

ONE HOUSTON SQUARE (at 8500 Cameron Road) AUSTIN, TEXAS 78753
(512) 837-2820 TWX 910-874-2022 cable HOINCO
TELECOPIER

EUROPEAN OFFICE Rochesterlaan 6 8240 Gistel Belgium
Phone 059/277445 Telex Bausch 81399

* U S Domestic Price only

Visit us at Booth #223 at the Pittsburgh Conference in Cleveland Feb. 27–Mar. 25

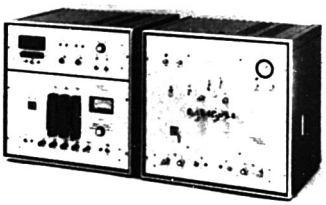
CIRCLE 88 ON READER SERVICE CARD

Even Better Ways of Doing What Dohrmann Does Best

Detecting halides for GC

The Dohrmann® DE-20, a new *low cost* halide specific detector for gas chromatography, offers *sensitivity, linearity* and *simplicity*. When combined with the Dohrmann CP-1 continuous purge module, it measures total purgeable organic halides in drinking water to *±1 ppb*. For details circle No. 58 or call our specialist, Doug Jones, collect at (408) 249-6007.





Analyzing water for ppb organic carbon

Dohrmann has added the DC-54 ultra-low-level organic carbon analyzer to its well established line of versatile TOC instruments. The DC-54 brings *speed, convenience* and *precision* to low-level TOC analysis: purgeables to *±1 ppb*, non-purgeables to *±10 ppb*.

For details on Dohrmann TOC analyzers, circle No. 59 or call our TOC specialist, Leon Hiam collect at (408) 249-6002.

Measuring traces of nitrogen, sulfur, and halides

Dohrmann microcoulometric systems are leaders in the field for *fast, accurate* and *sensitive* determinations of traces of N, S and Cl in solids, liquids and gases.

New from Dohrmann, the DN-10 total nitrogen analyzer, using oxidative pyrolysis and chemiluminescence detection, offers even greater *convenience* when measuring traces of nitrogen in organics.

For details, circle No. 60 or call our specialist, Doug Jones, collect at (408) 249-6007.

For literature on all Dohrmann products described above, write or circle the reader service number below.



ENVIROTECH

DOHRMANN

3240 Scott Boulevard
Santa Clara, California 95050

CALL TOLL FREE
(800) 538-7708

In Alaska, California, Hawaii, Puerto Rico, call collect (408) 249-6000

See these new instruments in Cleveland at the Pittsburgh Conference, Booth 808
CIRCLE 42 ON READER SERVICE CARD

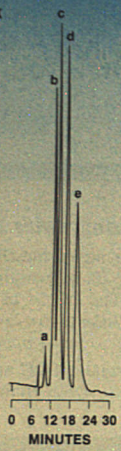
หอสมุด กรมวิทยาศาสตร

Two great microparticle columns

for high performance ion exchange LC:

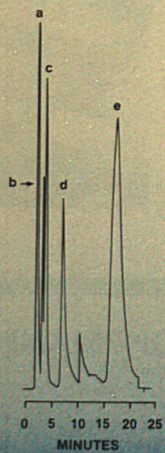
CEPHALOSPORINS ON PARTISIL-10 SAX

Operating Conditions—
Column:
PXS-1025 SAX; 4.6 mm x 25 cm
Mobile Phase:
0.25M Na Acetate, pH 5.0
Flow Rate:
0.5 ml/min
Pressure:
150 psi
Detection:
UV @ 254 nm
Peaks—
a. 6-Aminopenicillanic Acid*
b. Cephaloglycin (Kafocin - Lilly)
c. Cephalexin (Keflex - Lilly)
d. 7-Aminocephalosporanic Acid*
e. 7-Aminodeoxycephalosporanic Acid*
*Intermediates courtesy of Eli Lilly & Co.



WATER SOLUBLE VITAMINS ON PARTISIL-10 SCX

Operating Conditions—
Column:
PXS-1025 SCX; 4.6 mm x 25 cm
Mobile Phase:
0.1M $(NH_4)_2HPO_4$, pH 2.2
Flow Rate:
1 ml/min
Pressure:
(Unknown)
Detection:
UV @ 280 nm. Atten.:
0.02 x 10 mV for peaks a, b, c, d;
0.02 x 1 mV for peak e
Peaks—
a. Sodium ascorbate
b. Pyridoxine hydrochloride
c. Niacinamide
d. Riboflavin
e. Thiamine mononitrate



Partisil™-10 SAX
Partisil™-10 SCX

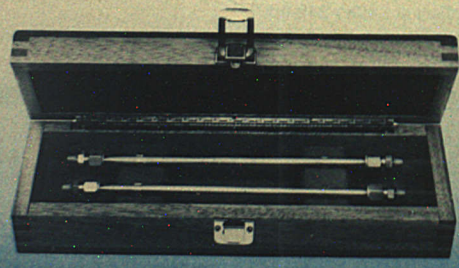
Analytical or Semi-preparative.

If your compounds have ionizable functional groups they can very probably be separated better on our HPLC ion exchanger columns than any other way. Better resolution (at ambient column temperatures), better reproducibility, higher speeds. Siloxane bond stability. Very high efficiencies. On your liquid chromatograph, whatever make or model.

Partisil-10 SAX columns are strong anion exchangers with $-NR_3^+$ functional groups; Partisil-10 SCX columns are strong cation exchangers with $-SO_3^-$ functional groups. Selectivities are similar to conventional exchange resins, but there the similarities stop. In performance they aren't comparable to anything but each other.

The same packings are available in our 9.4 mm ID Magnum 9 semi-preparative columns; eight times as much packing. Remarkable performance. Really remarkable.

Whatman Inc. • 9 Bridewell Place, Clifton, New Jersey 07014 • (201) 777-4825 • Telex 133426.



Whatman

CIRCLE 235 ON READER SERVICE CARD

Volume 50, No. 2, February 1978
ANCHAM
50(2) 99A-306A/193-384 (1978)
ISSN 0003-2700

analytical chemistry

© Copyright 1978
by the American Chemical Society

Permission of the American Chemical Society is granted for libraries and other users to make reprographic copies for use beyond that permitted by Sections 107 or 108 of the U.S. Copyright Law, provided that, for all articles bearing an article code, the copying organization pay the stated per-copy fee through the Copyright Clearance Center, Inc. For further information, write to Office of the Director, Books and Journals Division, ACS, 1155 16th St., N.W., Washington, D.C. 20036.

Published monthly with review issue added in April and Laboratory Guide in August by the American Chemical Society, from 20th and Northampton Sts., Easton, Pa. 18042. Executive and Editorial headquarters, American Chemical Society 1155 16th St. N.W., Washington, D.C. 20036 (202) 872-4600. Second class postage paid at Washington, D.C., and at additional mailing offices.

1978 Subscription prices—including surface postage

	1 yr	2 yr	3 yr
MEMBERS:			
Domestic	$10.00	$18.00	$25.00
Foreign	19.00	36.00	52.00
NONMEMBERS—PERSONAL:			
Domestic	14.00	26.00	38.00
Foreign	23.00	44.00	65.00
INSTITUTIONAL:			
Domestic	14.00	26.00	38.00
Canada	23.00	44.00	65.00
Other foreign	29.00	54.00	77.00

Airmail and air freight rates are available from Membership & Subscription Services, ACS, P.O. 3337, Columbus, Ohio 43210 (614) 421-7230.

New and renewal subscriptions should be sent with payment to the Office of the Controller at the ACS Washington address.

Subscription service inquiries and changes of address (include both old and new addresses with ZIP code and *recent mailing label*) should be directed to the ACS Columbus address noted above. Please allow six weeks for change of address to become effective.

Claims for missing numbers will not be allowed if loss was due to failure of notice of change of address to be received in the time specified; if claim is dated (a) North America: more than 90 days beyond issue date, (b) all other foreign: more than one year beyond issue date; or if the reason given is "missing from files".

Microfiche subscriptions are available at the same prices but are mailed first class domestic and airmail foreign. Inquiries and payments to Microform Program, ACS Washington address.

Single issues, current year, $3.00 except review issue and Labguide, $4.00; **back issues and volumes; microfilm editions** from volume 1 to present: *write or call* Special Issues Sales, ACS Washington address (202) 872-4365.

Advertising Management: Centcom, Ltd., 25 Sylvan Road South, Westport, Conn. 06880 (203) 226-7131

CONTENTS

REPORT

Wayne R. Wolf discusses the current challenges in generating data for the nutrient trace element composition of foods **190 A**

REPORT

The Food and Drug Administration's efforts to fight cancer quackery are reviewed by Wallace F. Janssen **197 A**

INSTRUMENTATION

A simple hardware control approach for sequencing chemical instruments is presented by S. R. Crouch, D. N. Baxter, E. H. Pals, and E. R. Johnson **291 A**

PITTSBURGH CONFERENCE

The 29th Pittsburgh Conference on Analytical Chemistry and Applied Spectroscopy will be held February 27–March 3, 1978, in Cleveland, Ohio. The complete technical program is presented **119 A**

NEW PRODUCTS

Products to be featured at the 1978 Pittsburgh Conference Exposition are introduced **173 A**

NEWS

Technical programs of interest to analytical chemists at the 175th ACS National Meeting in Anaheim, Calif., March 12–17, 1978, are given. ANALYTICAL CHEMISTRY appoints Catherine C. Fenselau, Gary M. Hieftje, and C. David Miller to its Instrumentation Advisory Panel **211 A**

BOOKS

Books on lasers, fine particles, and liquid chromatography are reviewed by Fred E. Lytle, B. J. Rubin and G. L. Beyer, and Joseph Sherma **267 A**

EDITORS' COLUMN

Analytical chemistry is needed to determine the composition of cancer "cure" compounds, the latest of which is Laetrile **283 A**

EDITORIAL

Selection of appropriate analytical methods and definition of sensitivity limits are important in the regulation of carcinogens in the environment **193**

Technical Contents/Briefs **102 A**

Author Index **IBC**

Future Articles **IBC**

Meetings **240 A**

Short Courses **240 A**

Manufacturers' Literature **261 A**



Our cover highlights three of this month's features

ห้องสมุด กรมวิทยาศาสตร

Briefs

Purification of Analytical Reagents and Other Liquids by Low Temperature Vacuum Sublimation 194

Low temperature sublimation is shown to be applicable for processing a broad range of liquids which includes analytical reagents, inorganic halides, organic solvents, and other compounds.

J. W. Mitchell, Bell Laboratories, Murray Hill, N.J. 07974 *Anal. Chem., 50 (1978)*

Fluorescence Photometric Quantitation of Procainamide and *N*-Acetylprocainamide in Plasma after Separation by Thin-Layer Chromatography 197

A precision of better than 4% is obtained for the simultaneous estimation of these compounds in plasma at therapeutic levels.

Ram N. Gupta,* Francis Eng, and Diane Lewis, Department of Laboratory Medicine, St. Joseph's Hospital, McMaster University, Hamilton, Ontario, Canada *Anal. Chem., 50 (1978)*

Competitive Intrinsic Factor Binding Assay Technique for Cobalamins in Natural Waters 200

Benzyl alcohol extractable cobalamins at concentration levels of 10^{-12} g/mL are quantitatively assayed on the basis of competitive intrinsic factor binding with radioactive ^{57}Co-cyanocobalamin with a 10.98% relative standard deviation.

Robert A. Beck, Department of Chemistry, Framingham State College, Framingham, Mass. 01701 *Anal. Chem., 50 (1978)*

Determination of Chlorine Dioxide in Sewage Effluents 202

A colorimetric method for the direct determination of chlorine dioxide in sewage effluent samples is presented. The results are verified by electron spin resonance spectrometry.

J. Ross Knechtel,* Wastewater Technology Centre, Burlington, Ontario, and **Edward G. Janzen and Edward R. Davis,** University of Guelph, Ontario *Anal. Chem., 50 (1978)*

Kinetic Microdetermination of Manganese in Nonferrous Alloys, and of Nitrilotriacetic Acid, Ethylenediaminetetraacetic Acid, and Diethylenetriaminepentaacetic Acid 205

Manganese in the 10^{-8}–10^{-6} M level, and NTA, EDTA, and DTPA in the 10^{-7}–10^{-6} M level are determined with an average error of about 2%. and measurement times of 10–100 s.

D. P. Nikolelis and T. P. Hadjiioannou,* Laboratory of Analytical Chemistry, University of Athens, Athens, Greece *Anal. Chem., 50 (1978)*

Directly Digital Flow Controller with Rapid Response Time and High Precision 209

The new transducer is rapid, reproducible, predictable, and compatible with most digital electronic devices, making it suitable as a computer-controlled valve for either gases or liquids.

T. W. Hunter and G. M. Hieftje,* Department of Chemistry, Indiana University, Bloomington, Ind. 47401 *Anal. Chem., 50 (1978)*

Comparisons between Hydrogen Bond Donor–Acceptor Parameters and Solvatochromic Red Shifts 212

Perturbation influences associated with hydrogen bonding solvents are identified in correlations between empirical solvent polarity factors and the transition energies for red shift solvatochromic dyes.

Orland W. Kolling, Chemistry Department, Southwestern College, Winfield, Kan. 67156 *Anal. Chem., 50 (1978)*

Fundamental and Second Harmonic Alternating Current Cyclic Voltammetric Theory and Experimental Results for Simple Electrode Reactions Involving Amalgam Formation 216

AC cyclic voltammetry is extended to the simple amalgam case, $O + ne \rightleftharpoons R(Hg)$. Experimental data for several Nernstian and non-Nernstian processes are in excellent agreement with theoretical predictions.

Alan M. Bond* and Roger J. O'Halloran, Department of Inorganic Chemistry, University of Melbourne, Parkville, Victoria, 3052, Australia, and **Ivica Ruzic and Donald E. Smith,*** Department of Chemistry, Northwestern University, Evanston, Ill. 60201 *Anal. Chem., 50 (1978)*

Electrochemistry of the Ruthenium(3+,2+) Couple Attached to Graphite Electrodes 223

Cyclic voltammetry and differential pulse voltammetry are used to compare the electrochemical behavior of the attached complexes and to measure surface concentrations.

Carl A. Koval and Fred C. Anson,* Arthur A. Noyes Laboratory, California Institute of Technology, Pasadena, Calif. 91125 *Anal. Chem., 50 (1978)*

Electrochemical Behavior of the Selenocyanate/Triselenocyanate Redox Couple in Acetonitrile on Platinum Electrodes 229

A reversible $(SeCN)_3^-/SeCN^-$ redox couple is formed on clean Pt when KSeCN solutions in ACN, containing $[(Et)_4N]ClO_4$ as supporting electrolyte are electrolyzed.

M. E. Martins, C. E. Castellano, A. J. Calandra, and A. J. Arvía,* Instituto de Investigaciones Fisicoquímicas Teóricas y Aplicadas, División Electroquímica, Universidad Nacional de La Plata, 1900 La Plata, Argentina *Anal. Chem., 50 (1978)*

Direct Potentiometric and Titrimetric Determination of Methadone in Urine with Plastic Electrodes Selective for Hydrophobic Cations 232

A hydrophobic ion selective electrode is used to determine methadone levels in urine at concentrations down to 5×10^{-5} M without prior separation, both by a single potential measurement (±15% accuracy) and by titrating with sodium tetraphenylboron (±2% accuracy).

Songsak Srianujata, Wesley R. White, Takeru Higuchi, and Larry A. Sternson,* Department of Pharmaceutical Chemistry, University of Kansas, Lawrence, Kan. 66044 *Anal. Chem., 50 (1978)*

* Corresponding author.

LOOKS LIKE *A* pH METER.



WORKS LIKE *A* COMPUTER.

a digital specific ion meter

ORION has developed the Model 901 to further simplify all analyses made using pH, specific ion, and gas-sensing electrodes. A series of operating modes covers the full range of analytical methods used for performing electrode analyses:

direct reading concentration	
incremental methods:	**known (standard) addition**
	known subtraction
	analate (sample) addition
	analate subtraction
absolute and relative millivolts:	**Gran's plots and titrations**
pH	

Results are calculated in real time with an accuracy that will satisfy the most demanding research applications – yet the 901 is simple enough to be used in all routine quality control applications.

Analytical parameters are entered on the digital switches on the control panel, with standardization and blank correction accomplished at the push of a button. Results are read directly from the LED display in the unit system of your choice. The 901 completely eliminates the use of calibration curves, tables, or calculations.

how the 901 works

The Model 901 has a high input impedance analog amplifier and analog-to-digital converter similar to that used in digital pH/mv meters. The output of the converter is fed to a microprocessor which is pre-programmed with equations for calculating pH's and concentrations. Parameters needed to solve the electrode equations are supplied to the microprocessor from the switches and pushbuttons on the front panel.

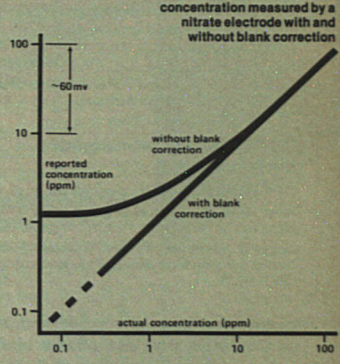
Twice each second the electrode's potential is digitalized and fed to the microprocessor, and the analytical result is calculated using the pre-programmed equations. A concentration result ranging between .000 and 999. is shown on the LED display in a three-digit floating decimal point format. Calculated pH results between 0.000 and 13.999 are displayed.

pushbutton blank correction

The 901 has a blank correction feature that is especially useful in overcoming two problems frequently encountered in making low-level measurements: slow time response of the electrode and deviation of the electrode response from theoretical.

In the first case a background level of the species measured is added to all samples and standards to bring the concentration up to the region of fast time response. The blank correction feature is used to automatically subtract this background level from the result.

In the second case the electrode potential in the blank solution is entered into the microprocessor's memory by pushbutton so that the results are automatically corrected over the region of nontheoretical response.



volume correction

When analyses are carried out by one of the incremental methods, the volume change that takes place when the standard is added to the sample (or vice versa) should be taken into consideration if a correct result is to be calculated. The various incremental modes include a volume correction factor that the microprocessor uses in calculating the result.

call us

Can we discuss applications for the 901 – or arrange a demonstration in your laboratory? Call us toll-free at 800-225-1480 (except Mass.) and ask for one of our Technical Service Representatives. In Canada call 800-363-9270.

ORION RESEARCH

380 Putnam Ave., Cambridge, MA 02139

CIRCLE 157 ON READER SERVICE CARD

Briefs

Controlled-Potential Coulometric Determination of Plutonium 236

An application of the Nernst equation is used to accurately determine the fraction of the sample electrolyzed without exhaustive electrolysis. A 40% decrease in determination time is achieved without loss in precision or accuracy.

Michael K. Holland,* Jon R. Weiss, and Charles E. Pietri, New Brunswick Laboratory, United States Department of Energy, 9800 South Cass Avenue, Building 350, Argonne, Ill. 60439

Anal. Chem., 50 (1978)

Chromatographic Determination of Chromium(VI) with Coulometric Detection Based on the Electrocatalysis by Adsorbed Iodine of the Reduction at Platinum Electrodes in Acidic Solutions 240

Determination of Cr(VI) in a coulometric flow-through electrode is possible in the range 0.4 ng to 80 μg.

J. H. Larochelle and D. C. Johnson,* Department of Chemistry, Iowa State University, Ames, Iowa 50011 *Anal. Chem., 50 (1978)*

Determination of Polycyclic Aromatic Hydrocarbons in the Environment by Glass Capillary Gas Chromatography 243

Polycyclic aromatic hydrocarbons are isolated by a sequence of solvent extraction, gel filtration, and adsorption chromatography and individual concentrations determined by capillary gas chromatography.

Walter Giger* and Christian Schaffner, Swiss Federal Institute for Water Resources and Water Pollution Control (EAWAG), CH-8600 Dübendorf, Switzerland *Anal. Chem., 50 (1978)*

Gel Permeation Chromatography of Fluoroether Polymers 249

GPC with porous silica-packed columns is used to determine molecular weight distributions of fluorinated polymers in the molecular weight range of 1400 to 30 000.

Roger A. Korus and Robert W. Rosser,* Ames Research Center, National Aeronautics and Space Administration, Moffett Field, Calif. 94035 *Anal. Chem., 50 (1978)*

Collection of Chlorpyrifos and Other Pesticides in Air on Chemically Bonded Sorbents 251

A procedure is described for the collection and determination of chlorpyrifos in air at the low parts-per-trillion level for sampling periods of 10 min up to 16 h.

Richard G. Melcher,* Warren L. Garner, Loren W. Severs, and James R. Vaccaro, Analytical and Industrial Hygiene Laboratories, Dow Chemical U.S.A., Midland, Mich. 48640

Anal. Chem., 50 (1978)

Selective Separation of Metal Ions by a Chelating Agent-Loaded Anion Exchanger 255

Fe(III), Cr(III), Cu(II), and Pb(II) are selectively separated from slightly acidic aqueous solutions by anion exchangers loaded with sulfonated chelating agents.

Kil Sang Lee, Won Lee, and Dal Woon Lee,* Department of Chemistry, Yonsei University, Seoul, Korea

Anal. Chem., 50 (1978)

Kinetics of Ion Exchange in Polydisperse Systems 258

Theoretical and experimental investigations reveal that monitoring in such systems only the solution concentration will simulate an equilibrium, which is not yet attained by the ion exchanger particles.

Kurt Bunzl, Gesellschaft für Strahlen- und Umweltforschung mbH München, Institut für Strahlenschutz, 8042 Neuherberg, West Germany *Anal. Chem., 50 (1978)*

Determination of Sulfur Compounds in High-Boiling Petroleum Distillates by Ligand-Exchange Thin-Layer Chromatography 268

Mercaptans, sulfides, and disulfides are separated from aromatic hydrocarbons by ligand-exchange TLC on mercury-loaded silica gel.

Takashi Kalmai* and Atsushi Matsunaga, Nippon Mining Co., Ltd., Technical Research Center, 3 Niizo-Minami, Toda, Saltama 335, Japan *Anal. Chem., 50 (1978)*

Packed Microcapillary Columns in High Performance Liquid Chromatography 271

Basic parameters of column performance are investigated for the newly developed packed microcapillary columns.

Takao Tsuda and Milos Novotny,* Department of Chemistry, Indiana University, Bloomington, Ind. 47401

Anal. Chem., 50 (1978)

Determination of Penicillamine in Blood and Urine by High Performance Liquid Chromatography 276

Procedures using HPLC coupled with a Hg-based electrochemical detector are described for determining reduced and oxidized penicillamine in the nonprotein fraction of plasma, erythrocytes, whole blood, and urine.

Rolf Saetre and Dallas L. Rabenstein,* Department of Chemistry, University of Alberta, Edmonton, Alberta, Canada

Anal. Chem., 50 (1978)

Liquid Chromatographic Analysis of Analgesic on Amberlite XAD-7 280

Analgesics are determined in tablets using organic mobile phases selected on the basis of plots of log adjusted retention volume vs. composition.

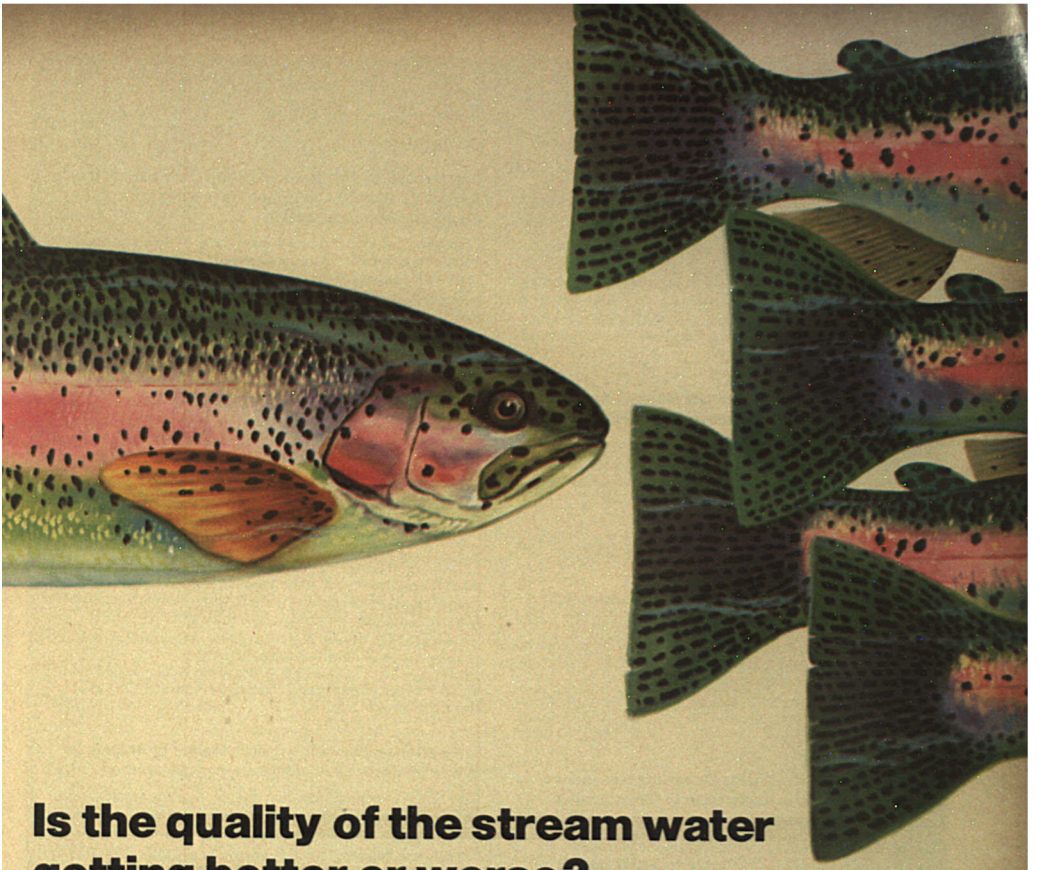
Robert G. Baum and Frederick F. Cantwell,* Department of Chemistry, University of Alberta, Edmonton, Alberta, Canada, T6G 2G2 *Anal. Chem., 50 (1978)*

Quantitative Ion Probe Measurement Using Matrix Ion Species Ratios 285

Accurate results are obtained for multielement analysis of steels, aluminum alloys, and copper alloys using matrix ion species ratios to calibrate empirically derived elemental sensitivity factors.

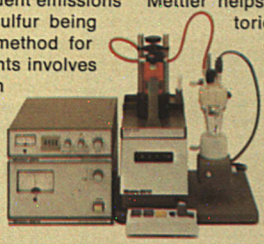
J. D. Ganjei, D. P. Leta, and G. H. Morrison,* Department of Chemistry, Cornell University, Ithaca, N.Y. 14853

Anal. Chem., 50 (1978)



Is the quality of the stream water getting better or worse?

Many environmental standards for effluent emissions are concerned with the amount of sulfur being discharged into streams. A reliable method for determining total sulfur in plant effluents involves the use of a Mettler automatic titration system. Stream samples are collected, oxidized and chemical interferences removed. Then the samples are titrated with a lead specific-ion electrode. This method can detect sulfur levels as low as 10 to 0.1 ppm.



Mettler helps solve problems in analytical laboratories and on the production floors of industry. We market a great variety of weighing and measuring instruments. All of them made with the world-renowned Mettler craftsmanship. All of them backed by a worldwide team of service specialists who can be there whenever you need them.

Mettler – instruments and people you can depend on.

Depend on Mettler for the answer.

Mettler

Electronic balances and weighing systems · Thermoanalytical instruments · Automatic titration systems · Laboratory automation

6272.72

Mettler Instrumente AG, CH-8606 Greifensee-Zürich, Switzerland · Mettler-Waagen GmbH, D-63 Giessen 2, Postfach 2840, BRD
Mettler Instrumenten B.V., Postbus 68, Arnhem, Holland · Mettler Instrument Corporation, Box 100, Princeton, N.J. 08540, USA

CIRCLE 145 ON READER SERVICE CARD

Briefs

Measurement of Electron Capture Rates for Chlorobenzene with Negative Ion Plasma Chromatography 290

Theory and experimental procedures are developed to allow measurement of ion–molecule reaction rates with plasma chromatography. Diagnostics are performed with the dissociative electron capture process for chlorobenzene.

Glenn E. Spangler,* MERADCOM, Attn: DRDME-O, Fort Belvoir, Va. 22060, and **Phil A. Lawless,** Research Triangle Institute, Research Triangle Park, N.C. 27709 *Anal. Chem., 50 (1978)*

Determination of Molybdenum by Neutron Activation and Srafion NMRR Ion Exchange Resin Separation 294

Srafion NMRR resin is used to separate Mo during neutron activation analysis of standard samples of steel, rock, coal, and plant and animal material with an accuracy of 1–8% and precision of 5–9%.

R. A. Nadkarni and G. H. Morrison,* Department of Chemistry, Cornell University, Ithaca, N.Y. 14853 *Anal. Chem., 50 (1978)*

Determination of Silica in Bulk Iron Ore Samples by Neutron Activation Analysis 296

Silica is determined in dried 30-kg iron ore samples with an accuracy of better than ±0.34% SiO_2 at the 95% confidence level for silica concentrations of up to 10%.

Mihai Borsaru* and Ralph J. Holmes, CSIRO Division of Mineral Physics, P.O. Box 124, Port Melbourne, Victoria 3207, Australia *Anal. Chem., 50 (1978)*

Feedback Excitation Nuclear Magnetic Resonance Spectrometry and Its Application to Simultaneous Temperature Measurement 298

Calibrations given permit temperature measurement ±1° between −50 and +60 °C. ^{19}F chemical shifts relative to ^{1}H TMS for several compounds are measured at different temperatures.

Drouet Warren Vidrine and Paul E. Peterson,* Chemistry Department, University of South Carolina, Columbia, S.C. 29208 *Anal. Chem., 50 (1978)*

Electron Spin Resonance Spectrometric Study of Free Radicals in Coals 303

The presence, concentration, and nature of free radicals in several coals, coal fractions, and pyrolyzed coals are ascertained by electron spin resonance spectrometry.

Leon Petrakis* and D. W. Grandy, Gulf Research & Development Company, P.O. Drawer 2038, Pittsburgh, Pa. 15230 *Anal. Chem., 50 (1978)*

Interference of Salt Matrices in the Determination of Copper by Atomic Absorption Spectrometry with Electrothermal Atomization 309

Concentration dependent interferences of alkali halides and oxyhalides and their elimination by Na_2O_2 are explained by an occlusion mechanism.

D. J. Churella and T. R. Copeland,* Department of Chemistry, Northeastern University, Boston, Mass. 02115 *Anal. Chem., 50 (1978)*

Determination of Industrial Dyes in Water by Laser Excited Resonance Raman Spectrometry 315

Industrial fabric dyes are detected in distilled water at concentrations below 100 ppb and identified at concentrations below 200 ppb by resonance Raman spectrometry.

Laurent Van Haverbeke, Patricia F. Lynch, and Chris W. Brown,* Department of Chemistry, University of Rhode Island, Kingston, R.I. 02881 *Anal. Chem., 50 (1978)*

Analytical Chemistry of Amygdalin 317

Analytical protocols for the specific identification and quantitation of amygdalin and its epimers are described by the use of HPLC, ^{13}C-NMR, GC/FID, and GC-MS.

Thomas Cairns,* Jerry E. Froberg, Steve Gonzales, William S. Langham, and John J. Stamp, U.S. Food and Drug Administration, Los Angeles, Calif. 90015, and **John K. Howie and Donald T. Sawyer,** Department of Chemistry, University of California, Riverside, Calif. 92521 *Anal. Chem., 50 (1978)*

Ionic Interference in the Determination of Arsenic in Water by Silver Diethyldithiocarbamate Method 322

The SDDC method provides reliable data for arsenic, even in fairly polluted water and its recovery up to 0.5 μg (0.01 mg L^{-1}) from such waters is quantitative.

Shingara S. Sandhu,* Claflin College, Orangeburg, S.C. 29115, and **Peter Nelson,** South Carolina State College, Orangeburg, S.C. 29117 *Anal. Chem., 50 (1978)*

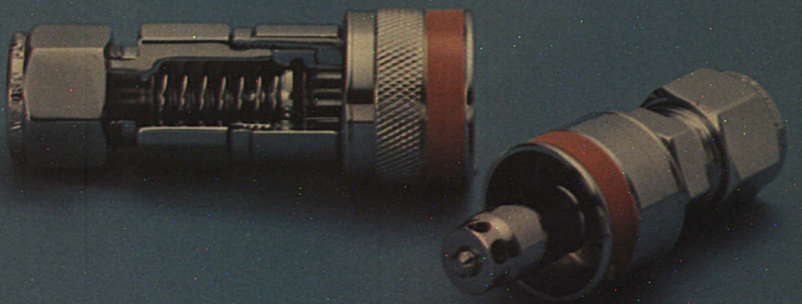
Determination of Sulfides and Application to Shale Oil Analysis 326

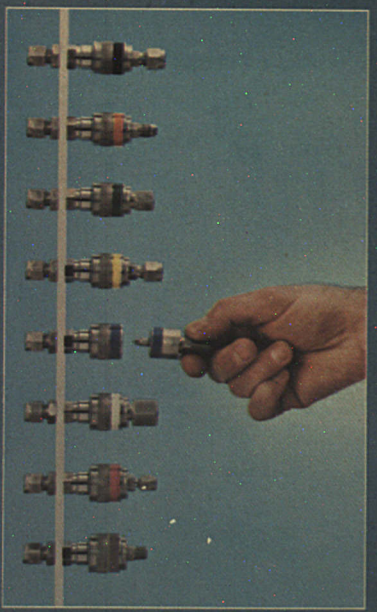
Organic sulfides are oxidized by sodium metaperiodate and the iodate formed is determined by atomic absorption after precipitation with silver. Precision is ±2.0–4.0% over a range of 1.0–5.0 μmol/mL of sulfide.

Raphael P. D'Alonzo, Alan P. Carpenter, Jr., Sidney Siggia,* and Peter C. Uden, Department of Chemistry, GRC Tower I, University of Massachusetts, Amherst, Mass. 01003 *Anal. Chem., 50 (1978)*

© 1977 MARKAD SERVICE CO /all rights reserved ©SC

You can't mis-connect this QUICK-CONNECT!





Swagelok® "Keyed" Quick-Connects prevent accidental intermixing of fluids in multiple line systems. Bodies and stems are "keyed," numbered and color coded to guarantee proper connections.

Eight different "keys" are available. Each "key" has a positive mechanical lockout system to prevent stems and bodies of unmatched "keys" from coupling with each other, or interchanging with any other type of quick-connect.

Automatic shut-off minimizes pressure loss or fluid spillage during uncoupling. An attempt to couple unlike "keys" will not open the shut-off valve and allow accidental flow.

Available in brass or 316 stainless steel, with tube connections or NPT pipe ends in 1/8", 1/4", 3/8" and 1/2" sizes. Immediate availability from local distributor stocks.

Patented

Swagelok®

CRAWFORD FITTING COMPANY
29500 Solon Road, Solon, Ohio 44139
Crawford Fittings (Canada), Ltd., Ontario

CIRCLE 32 ON READER SERVICE CARD

Briefs

Micro-Size Potentiometric Probes for Gas and Substrate Sensing 330

A micro air-gap sensor suitable for measuring dissolved gases and for fabricating a micro biosensor is reported.

C. P. Pui, G. A. Rechnitz,* and R. F. Miller, Departments of Chemistry and Physiology, State University of New York, Buffalo, N.Y. 14214 *Anal. Chem., 50 (1978)*

Identification of Fuel Oils by Low Temperature Luminescence Spectrometry 334

Low temperature luminescence spectra show more structure than room temperature fluorescence spectra, thereby enhancing oil identification capabilities.

Scott H. Fortier and DeLyle Eastwood,* U.S. Coast Guard Research and Development Center, Avery Point, Groton, Conn. 06340 *Anal. Chem., 50 (1978)*

Dual-Flame Photometric Detector for Sulfur and Phosphorus Compounds in Gas Chromatograph Effluents 339

A new flame photometric detector achieves uniform response to different sample compounds by first decomposing samples in one flame and generating optical emission in a second flame.

Paul L. Patterson,* Robert L. Howe, and Ahmad Abu-Shumays, Varian Instrument Division, 2700 Mitchell Drive, Walnut Creek, Calif. 94598 *Anal. Chem., 50 (1978)*

Comparison of Quenching Effects in Single- and Dual-Flame Photometric Detectors 345

Light emission is severely quenched by the presence of a hydrocarbon background in single-flame photometric detectors. A dual-flame detector minimizes this quenching effect.

Paul L. Patterson, Varian Instrument Division, 2700 Mitchell Drive, Walnut Creek, Calif. 94598 *Anal. Chem., 50 (1978)*

Simultaneous Determination of Vancomycin, Anisomycin, and Trimethoprim Lactate by High Pressure Liquid Chromatography 349

Precision of the high pressure liquid chromatographic assay is ±1.8%, ±1.1%, and ±2.2% for vancomycin, anisomycin, and trimethoprim lactate respectively (two standard deviations relative to the average).

R. L. Kirchmeier* and R. P. Upton, Pfizer Inc., Quality Control, Special Testing and Analytical Development Laboratories, Groton, Conn. 06340 *Anal. Chem., 50 (1978)*

Thin-Mercury-Film Voltammetry of Inorganic Lead(II) Complexes in Seawater 351

Cyclic and anodic stripping voltammetry of model solutions and seawater reveals poor correlations between peak current values and Pb(II) concentrations at high pH due to PbOH electrochemical inactivity.

Lloyd M. Petrie* and Rodger W. Baier, Graduate School of Oceanography, University of Rhode Island, Kingston, R.I. 02881 *Anal. Chem., 50 (1978)*

Solvent Extraction Method for Determination of Plutonium in Soft Tissue 357

Recovery of plutonium in human soft tissues ranges from 49–85% with a mean of 61%.

Narayani P. Singh,* Shawki Amin Ibrahim, Norman Cohen, and McDonald E. Wrenn, Institute of Environmental Medicine, New York University Medical Center, 550 First Avenue, New York, N.Y. 10016 *Anal. Chem., 50 (1978)*

Improvement of Detection Limits in Laser-Excited Atomic Fluorescence Flame Spectrometry 360

Laser-excited atomic fluorescence flame spectrometry is investigated in terms of optimization of the analytical experimental system. The analytical figures of merit are discussed and detection limits reported for 23 elements.

S. J. Weeks, H. Haraguchi, and J. D. Winefordner,* Department of Chemistry, University of Florida, Gainesville, Fla. 32611 *Anal. Chem., 50 (1978)*

Trimethylsilyl Ether Formation to Quantitate Hydroxyls by Nuclear Magnetic Resonance Spectrometry 368

Model compounds are used to demonstrate the enhancement in proton NMR sensitivity from their TMS derivatives. Hydroxyl content is found with an average error of 5%. The method is applied to coal liquefaction products.

F. K. Schweighardt,* H. L. Retcofsky, S. Friedman, and M. Hough, U.S. Department of Energy, Pittsburgh Energy Research Center, 4800 Forbes Avenue, Pittsburgh, Pa. 15213 *Anal. Chem., 50 (1978)*

Correspondence

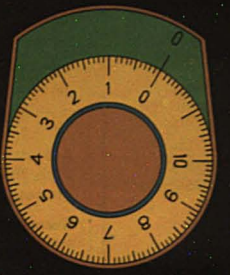
Chemical Ionization Mass Spectrometry as a Tool for the Elimination of Surface Related Phenomena in the Spectra of Unstable Compounds 371

Richard D. Smith* and Philip W. Ryan, Chemical Methods and Kinetics Section, Physical Sciences Department, Battelle, Pacific Northwest Laboratories, Richland, Wash. 99352 *Anal. Chem., 50 (1978)*

Simplified Solids Mass Spectrometer Combining a Glow Discharge Source with a Quadrupole Mass Filter 373

C. G. Bruhn, B. L. Bentz, and W. W. Harrison,* Department of Chemistry, University of Virginia, Charlottesville, Va. 22901 *Anal. Chem., 50 (1978)*

The fast get faster.



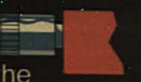
Now the Ohaus Dial-O-Gram 1600 Series has a 10-gram dial; you can read to 0.1 gram directly, so every measurement is easier, faster.

We've also increased capacity to 2610 g with three weights that are easily attached, and store conveniently in the contoured base.



We've kept the over 20 special advantages that make the Dial-O-Gram 1600's all best-sellers.

For example, a lever system to make these Ohaus balances insensitive to out-of-level conditions. Or the patented Ohaus tare poise: it's internally threaded and contains a flat spring which allows you to slide it along the beam for rough taring and rotate for fine adjustment.

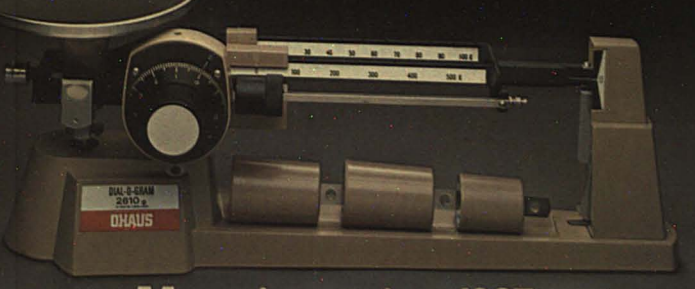




If you'd like to find out how beautifully engineered a balance can be, write: Ohaus Scale Corporation, 29 Hanover Rd., Florham Pk., N.J. 07932.

CIRCLE 158 ON READER SERVICE CARD

OHAUS



Measuring up since 1907

Marine Chemistry in the Coastal Environment



ACS Symposium Series No. 18

Thomas M. Church, *Editor*

A special symposium sponsored by the Middle Atlantic Region of the American Chemical Society.

Now available—a comprehensive volume containing the most recent advances in this new and increasingly important field.

The collection represents an indispensable source of information for every marine scientist. Emphasis is not merely on describing coastal problems but on showing the potential in applying the tools of modern oceanography and chemistry to solve these problems.

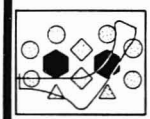
Forty-one chapters cover six major areas:

physical, organic, and tracer marine chemistry; estuarine geochemistry; hydrocarbons and metals in the estuarine environment; ocean disposal forum; applications and resources in marine chemistry; and organic and biological marine chemistry.

710 pages (1975) Clothbound $35.75
(ISBN 0-8412-0300-8) LC 75-28151

Order from:
Special Issues Sales
American Chemical Society
1155 Sixteenth St., N.W.
Washington, D.C. 20036

Electrochemical Studies of Biological Systems



ACS Symposium Series No. 38

Donald T. Sawyer, *Editor*
University of California

A symposium sponsored by the Division of Analytical Chemistry of the American Chemical Society.

The twelve papers in this significant new collection provide a representative cross section of the kinds of electrochemical methods used to characterize biological systems, as well as the kinds of biological problems that are being studied by such methods.

CONTENTS

vitamin B_{12} and related cobalamins • bioelectrochemical modelling of cytochrome c • potentials of metal ion couples in complexes • metalloporphyrins in aprotic solvents • N-bridged dimer in nonaqueous media • reduction of nitrogenase substrates • manganese (II) and -(III) 8-quinolinol complexes • interfacial behavior of purines • coulometric titration of biocomponents • rotating ring disk enzyme electrode • left ventricle/aorta simulator • EDTA and NTA in phytoplankton media

216 pages (1977) clothbound $15.50
LC 76-30831 ISBN 0-8412-0361-X

Order from:
SIS/American Chemical Society
1155 16th St., N.W./Wash., D.C. 20036

Briefs

Data Treatment in Cyclic Voltammetry 375

Gregory Ginzburg, Department of Chemistry, Ben Gurion University of the Negev, Beer Sheva, Israel *Anal. Chem., 50 (1978)*

Comment on Determination of Fluoride by Neutron Activation Analysis 376

Ernest S. Gladney,* and David B. Curtis, Los Alamos Scientific Laboratory, P.O. Box 1663 MS 490, Los Alamos, N.M. 87545 *Anal. Chem., 50 (1978)*

Aids for Analytical Chemists

Automated Analysis for Trace Organic Components in 32% Hydrochloric and 28% Hydrobromic Acid Process Streams 377

Kenneth W. Grubaugh* and Gerald E. Stobby, Analytical Laboratories, 258 Building, Dow Chemical U.S.A., Midland, Mich. 48640 *Anal. Chem., 50 (1978)*

Gas Chromatography of High Molecular Weight Hydrocarbons with an Inorganic Salt Eutectic Column 379

Lloyd R. Snowdon,* Institute of Sedimentary and Petroleum Geology, 3303-33rd Street N.W., Calgary, Alberta, Canada, and **Eric Peake,** Environmental Sciences Centre (Kananaskis), University of Calgary, Calgary, Alberta, Canada *Anal. Chem., 50 (1978)*

Drying Small Amounts of Solvent for Use in Nuclear Magnetic Resonance Spectrometry 381

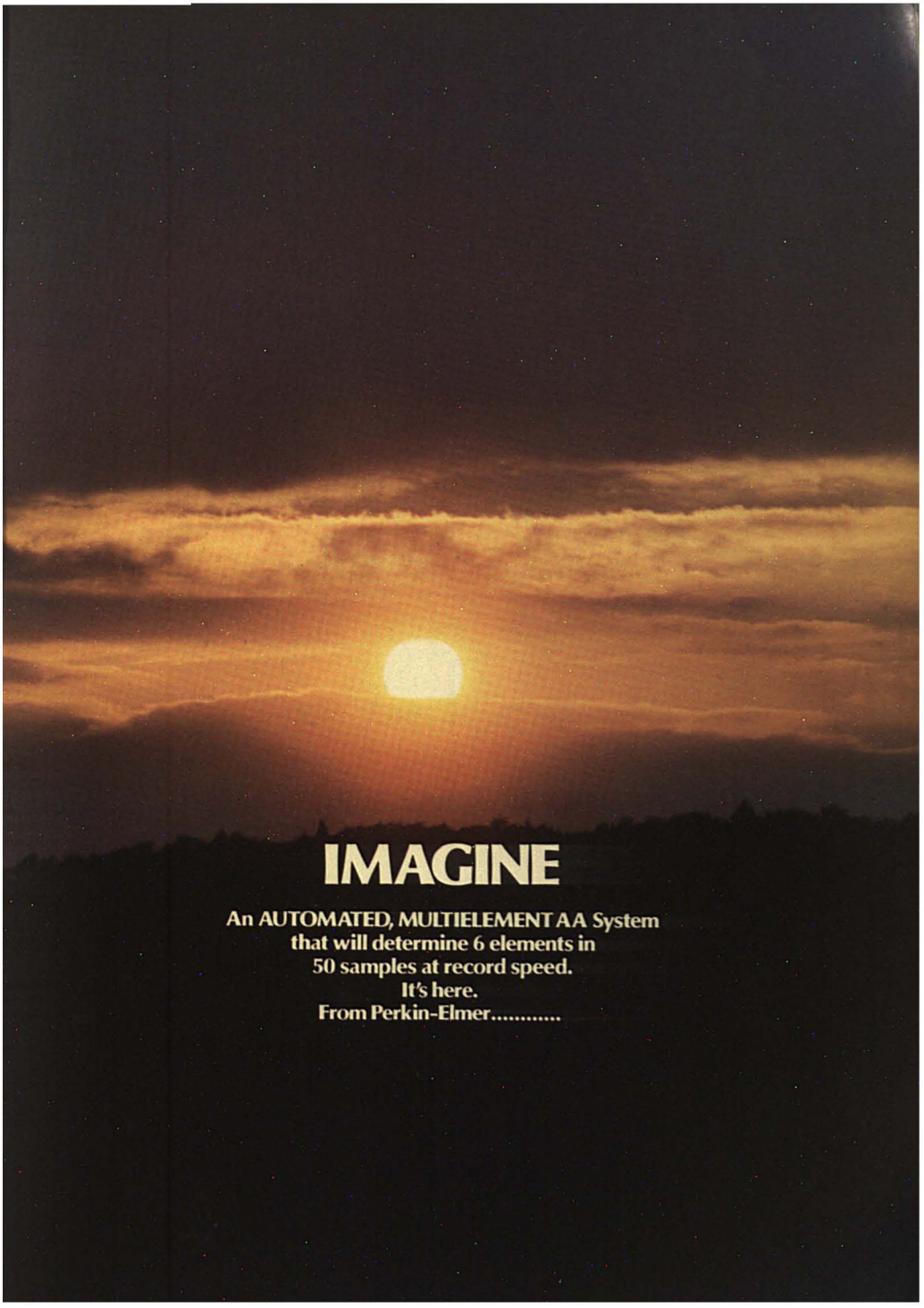
Joseph B. Alper, Department of Biochemistry, College of Agricultural and Life Sciences, University of Wisconsin–Madison, Madison, Wis. 53706 *Anal. Chem., 50 (1978)*

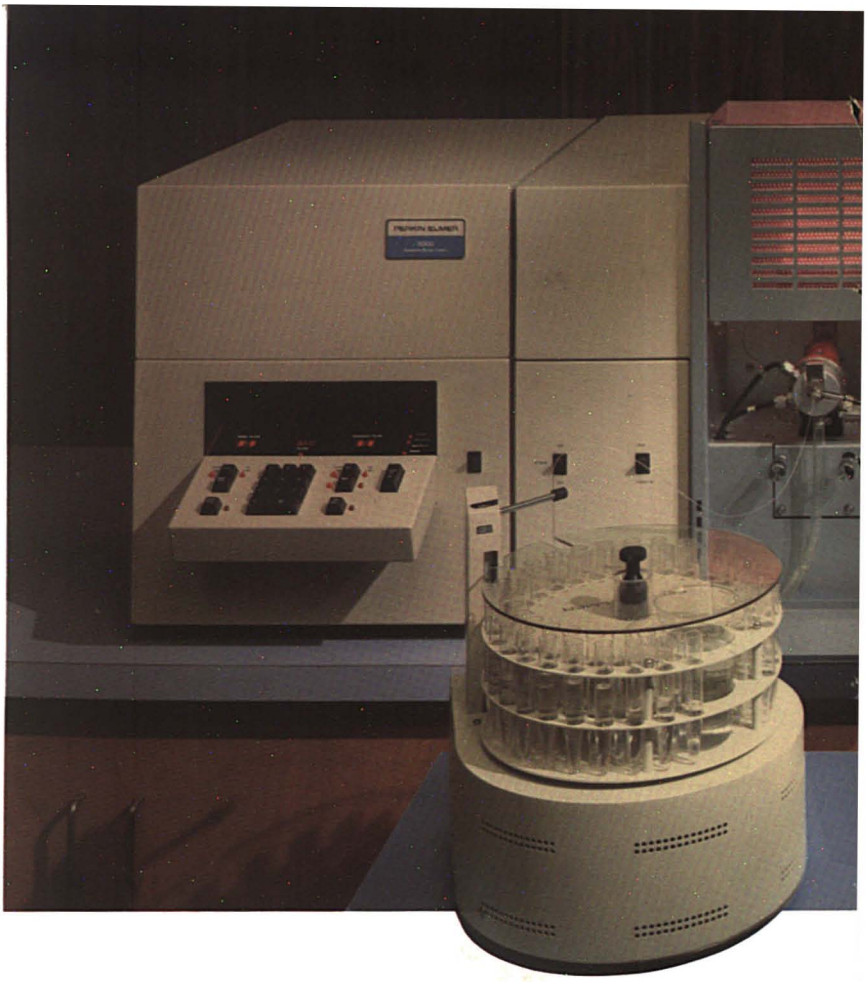
Vacuum Envelope for High Pressure Mass Spectrometry Applications 382

Eric Grimsrud, Department of Chemistry, Montana State University, Bozeman, Mont. 59717 *Anal. Chem., 50 (1978)*

Correction. Chemically-Bonded Aminosilane Stationary Phase for the High-Performance Liquid Chromatographic Separation of Polynuclear Aromatic Compounds 384

S. A. Wise, S. N. Chesler, H. S. Hertz, L. R. Hilpert, and W. E. May


IMAGINE
An AUTOMATED, MULTIELEMENT AA System
that will determine 6 elements in
50 samples at record speed.
It's here.
From Perkin-Elmer.....



THE MODEL 5000 AA. REVOLUTIONARY.

Never before has an atomic absorption spectrophotometer with its accessories combined so much convenience with so much performance.

The Perkin-Elmer Model 5000 is a totally new instrument. The most completely automated of its kind. It's designed to minimize human error and effort, while maximizing performance and analytical throughput. It has every function under microcomputer control. Its built-in memory stores all analytical conditions for up to six elements.

Automatically, the Model 5000 analyzes up to 50 samples for six elements in about an hour – without operator attention.

Automatically, the Model 5000 selects all instrument parameters, including calibration values, with the simple insertion of a preprogrammed magnetic card.



FROM PERKIN-ELMER.

Automatically, the Model 5000 interchanges monochromator gratings, selects wavelengths, varies slit widths and heights, changes lamps, varies flames and flame conditions, and performs numerous other operations and adjustments.

Along with all these advances in convenience, the Model 5000 represents a breakthrough in performance. It sets a new standard for top-of-the-line atomic absorption spectrophotometers.

Even the cost is a major advantage. The Model 5000 carries a price tag lower – surprisingly lower – than you'd expect.

Some of the Model 5000's exciting new accessories are described on the next page.

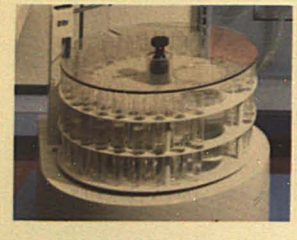


IMAGINE

FAST, AUTOMATIC, HIGH-VOLUME ANALYSIS AT A PRICE LOWER THAN YOU'D EXPECT.

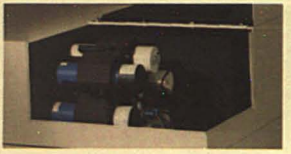
Besides making your AA analyses fast, precise and virtually effortless, the Model 5000 helps you watch your budget. You select specific options for the type of work you do. Here are a few of the more important accessories.

The AS-50 Auto Sampler speeds through 50 samples automatically, then either reindexes to the original position and analyzes the samples for the next element, or signals the completion of the series. It triggers calibration functions automatically. It lets you recalibrate automatically during a run for utmost accuracy. And it enables you to select aspiration times best suited to the element you're measuring.

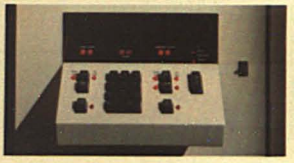


Background Correction is double-beam, both UV and visible, completely contained within the instrument. Source selection is automatic, depending on the wavelength range.

The Six-Lamp Turret is motor-driven, changing lamps in accordance with the instrument's programming directions. Designed for hollow cathode lamps (HCLs) powered from the basic instrument supply, the turret is also usable with electrodeless discharge lamps (EDLs)* powered by the single or dual-element power supplies available only from Perkin-Elmer.



The Automatic Burner Control is keyboard-controlled. Of course, there are pressure sensors, flame sensors, burner head sensors, a drain sensor and LEDs which show their status. It's so safe, you can let it run automatically. And digital flow control means that you can select the precise gas flows which are optimum for *each* element you are going to measure.



The HGA-500 Graphite Furnace is also microcomputer-controlled. It can store six programs with nine different program steps. You can select ramp and hold times and temperatures, normal heating or rapid heating, alternate inert gas flows, recorder or printer, and even auto zero just before the read cycle – whatever will provide the most accurate results. And there are alarms to signal low cooling water flow, lack of inert gas, or the approaching end of the tube's useful life.



The Card Reader makes it possible to store permanently all analytical conditions for as many as 12 elements on one magnetic card. It will read preprogrammed cards and store within the instrument all parameters and calibration values for up to 6 elements at a time that otherwise are handled manually via the keyboard. The card stores such instructions as wavelengths, slit widths and heights, lamp position and current, flame type, gas flows, and standard concentrations.



Our new motion picture clearly demonstrates all the features and improvements you'll find in the Model 5000. To arrange a showing or to obtain detailed literature, contact your local Perkin-Elmer representative, or write Perkin-Elmer Corp., MS-12, Main Avenue, Norwalk, CT 06856. For immediate action, call (203) 762-6681.

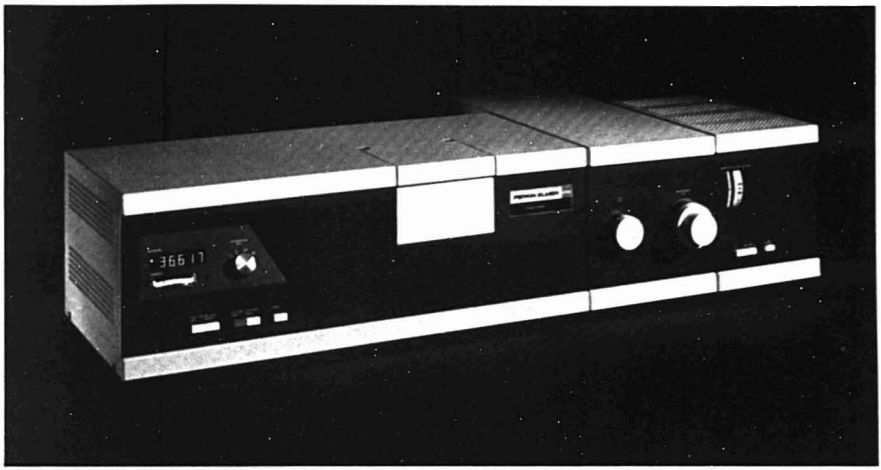
*U.S. Patent No. 3,873,884

Circle Reader Service Card No. 172

PERKIN-ELMER

Expanding the world of analytical chemistry.

THE ALL-PURPOSE POLARIMETER



This is the Perkin-Elmer 241 MC polarimeter. The top of our line.

We call it all-purpose because it has the flexibility for handling the widest variety of applications, whether research or routine.

That's not all. The Model 241 MC performs with more precision, reliability, and convenience for the money than any polarimeter you've ever used. Consider now some of the practical features of the 241 MC that lead us to make such a statement.

SIMPLICITY OF OPERATION

Standard items include automatic lamp ignition as well as rapid-change source mounts. Fully automatic gain and balance along with cell holder construction ensure reproducible results.

FLEXIBILITY

The Model 241 MC has four light sources. A mercury lamp is built in. Sodium, deuterium, and quartz-iodine lamps are supported on prealigned rapid-change mounts. A grating monochromator gives you the choice of 21 major spectral lines or continuous measurements from 250 nm to 650 nm for the generation of ORD curves. An illuminated + or — sign shows dextro or levo rotary values. Standard and micro cells are available in a wide range of path lengths to complete your analytical package.

HIGH ACCURACY

The measurement principle allows an accuracy of ± 0.002° for rotations $\leq 1°$. Selectable integration times and beam apertures, together with automatic gain and continuously selectable slit width, guarantee high accuracy even with strongly absorbing samples.

These are among the advances in high performance that make the Model 241 MC so convenient for measuring optically active substances. It aids in the determination of concentrations, characterization of pure compounds, kinetic studies and polarimetric titrations. It's being used now for analysis of sugars, proteins, drugs, amino acids, and other biological, pharmaceutical, and industrial compounds.

GET MORE DETAILS

Find out firsthand if polarimetry is a better tool for your work. Contact Dr. Greg McClure at (203) 762-1642 or your local Perkin-Elmer representative for more information. Write for literature to Perkin-Elmer Corp., MS-12, Main Avenue, Norwalk, CT 06856.

PERKIN-ELMER

Expanding the world of analytical chemistry.

CIRCLE 214 ON READER SERVICE CARD

LABORATORY DATA HANDLING AND AUTOMATION SYSTEMS



SIGMA 10... THE CHROMATOGRAPHY MASTERMIND FROM PERKIN-ELMER

No other data handling device in its price range is so capable and practical as Perkin-Elmer's new Model SIGMA 10 Chromatography Data Station.

Costing little more than an integrator, it makes integrators look primitive. Especially since SIGMA 10 offers the dual benefits of both storage and programmability. Other systems with comparable features are far more costly, far more complex.

MULTIPLE FUNCTIONS WITH MULTIPLE CHROMATOGRAPHS

With the SIGMA 10 Chromatography Data Station, you have a fast, versatile resource center for chromatography data. You can plug in four chromatographs at once – gas or liquid, whether Perkin-Elmer's or not. It works with them all.

It collects, integrates, and performs calculations on the information they develop. It can also control their operation. With six time-controlled relays on every channel and the ability to sense "ready" signals, it synchronizes automatic analyses from several chromatographs and autosamplers. It delivers annotated chromatograms and stores multiple data files and methods.

EVERYTHING MADE EASY

You can have your SIGMA 10 equipped with firmware for chromatography, or add an optional programmable accessory for writing your own programs in BASIC. And you don't have to be a computer expert. The SIGMA 10 guides you through every step, with a lighted display and printed message on its thermal printer/plotter. It even signals your mistakes. With all the sophistication of a computer system, it still works as simply as an integrator.

EXPANSION POTENTIAL

The entire SIGMA 10 system is housed in a single compact unit containing a keyboard, lighted display panel, CPU, memory, printer/plotter, and I/O for chromatographic instruments. Along with BASIC programmability, other optional features include a magnetic tape cassette for additional data storage and an RS-232C interface for external devices.

And for advanced laboratory data control, you can use several SIGMA 10 stations. Eventually, you can incorporate them into a central data management system, along with other instrumentation. Let us give you full details on the potential of this remarkable device. Contact your local Perkin-Elmer representative now. To request literature, call us at (203) 762-6853. Or write Perkin-Elmer Corp., MS-12, Main Ave., Norwalk, CT 06856.

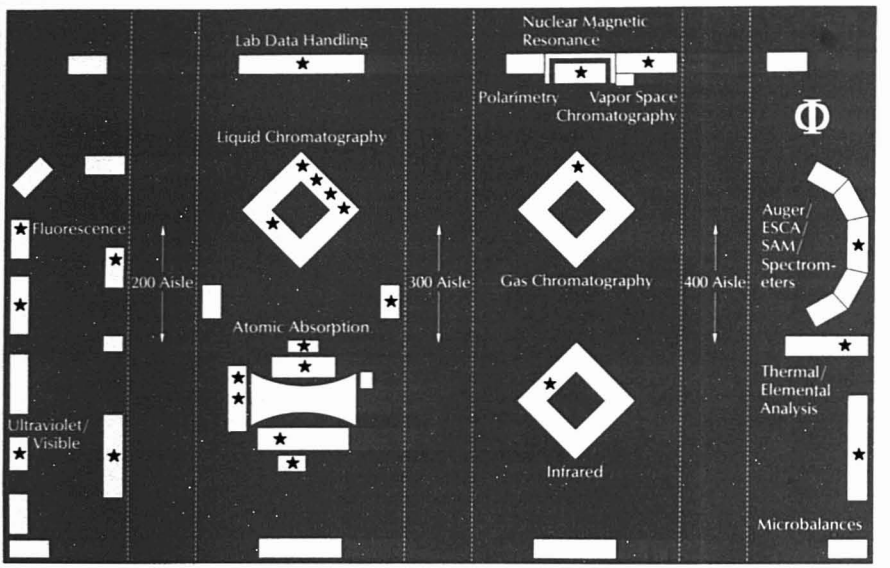
PERKIN-ELMER

Expanding the world of analytical chemistry.

CIRCLE 185 ON READER SERVICE CARD

A GUIDE TO OUR BIGGEST-EVER EXHIBIT AT THE PITTSBURGH CONFERENCE

★ Indicates a Perkin-Elmer system, instrument or accessory never before shown at a Pittsburgh Conference.



Perkin-Elmer is taking the biggest booth in our history – plus three extra demonstration rooms – to show you the broadest product line in our history. Included in our booth this year will be our new subsidiary, Physical Electronics Industries, Inc. Visit us February 27 – March 2 in Cleveland and see all the latest systems, instruments and accessories.

And be sure to get your mug on one of our mugs. Once again, this year we'll give you a mug with your photo on it.

Perkin-Elmer Corporation, MS-12, Main Avenue, Norwalk, CT 06856.

PERKIN-ELMER

Expanding the world of analytical chemistry.

CIRCLE 163 ON READER SERVICE CARD



PITTSBURGH CONFERENCE

Cleveland Convention Center
Cleveland, Ohio
February 27-March 3, 1978

The 29th Pittsburgh Conference on Analytical Chemistry and Applied Spectroscopy will feature a technical program appealing to the wide range of interests of chemists and spectroscopists. The 80 technical sessions scheduled include 15 planned symposia and a total of 668 papers. In addition, the Exposition of Modern Laboratory Equipment, held in conjunction with the meeting will feature the largest exhibition in conference history with 350 exhibitors showing the latest analytical instrumentation and related chemicals and supplies.

Preregistration is urged. Registration forms mailed before February 8, 1978, can be processed so that a badge, program, and souvenir will be ready for attendees on their arrival at the Convention Center. Registration fees are $10 for preregistration, $15 for regular registration, and $3.00 for students and are payable when badges are picked up. A pocket admission tab for the exposition only will be provided free of charge. Registration and housing forms may be obtained by contacting Mrs. Margaret Davison, Cleveland Convention Bureau, 511 Terminal Tower, Cleveland, Ohio 44113 (212-621-4110).

During the Conference several awards will be presented to honor scientists who have made outstanding contributions to analytical chemistry and spectroscopy. The Pittsburgh Spectroscopy Award, the Pittsburgh Applied Analytical Chemistry Award, and the Stephen Dal Nogare Award will be presented at an Awards Symposium Wednesday afternoon.

The 1978 Pittsburgh Spectroscopy Award will be presented by the Spectroscopy Society of Pittsburgh to E. Bright Wilson, Harvard University. Professor Wilson will be honored for his contributions to vibrational and microwave spectroscopy. His award address is entitled "Some Impacts of Microwave Spectroscopy on Chemistry".

The Society for Analytical Chemists of Pittsburgh will present the 1978 Pittsburgh Applied Analytical Chemistry Award to George M. Janini, University of Kuwait, and Kevin Johnston and Walter L. Zielinski, Jr., NCI Frederick Cancer Research Center. The award is given for their paper entitled "Use of a Nematic Liquid Crystal for Gas-Liquid Chromatographic Separation of Polyaromatic Hydrocarbons" [ANAL. CHEM., 47, 670–4 (1975)]. Dr. Janini will present the award address.

Csaba Horvath, Yale University, will receive the Stephen Dal Nogare Award sponsored by the Chromatography Forum of Delaware Valley for his significant contributions to chromatographic theory.

On Thursday afternoon the 1978 Coblentz Award will be presented to Lester Andrews, University of Virginia, for his contributions to the understanding and interpretations of vibrational spectra. Dr. Andrews will speak on the spectroscopy of transient species and molecular ions in matrices.

The Society for Analytical Chemists of Pittsburgh will present an Outstanding Analytical Chemist Award to Howard V. Malmstadt, University of Illinois. This award will honor Professor Malmstadt for his many achievements in the field of analytical instrumentation and his impact on the education of analytical chemists. The award will be presented at the Keeping Up with Microcomputers Symposium on Monday morning.

The social program will begin Sunday evening with a 2-hour performance of the Duquesne University Tamburitzans in a pageant of folk music, songs, and dances portraying the Slavic cultures of the world. The performance will be held in the Music Hall at the Convention Center, and admission will be by registration badge. Other planned activities include a Hawaiian luau, conference mixer, dinner-theater party, and wine-tasting party. In addition, a special nontechnical program has been planned for spouses attending the meeting.

Technical tours have been planned during the week to Republic Steel Corp., Cuyahoga County Coroner's Laboratory, Goodyear World of Rubber, Lubrizol Corp., NASA Lewis Research Center, B. F. Goodrich Research and Development Center, and Standard Oil Research Center.

The American Chemical Society will present five short courses just preceding and following the conference. For titles, fees, and other details, see page 240 A, this issue. During the meeting Kontes will present a seminar on quantitative thin-layer chromatography and SAVANT (Sloane Audio-Visuals for Analysis and Training) will offer two audiovisual courses on liquid chromatography and atomic absorption. Further information on these can be found in the January issue, page 54 A.

During the course of the week, various committees and subcommittees of the American Society for Testing

1978 CONDENSED PROGRAM

All Sessions Are in the Cleveland Convention Center

February 27

MONDAY MORNING	
Emission Spectroscopy—Chemical	Room 205
Biochemical Analysis	Room 239
Fluorescence and Phosphorescence—Instrumental	Room 3A
New Instrumentation	Club Room B
Symposium: Biomedical Applications of Ion Selective Electrodes I	Room 235A
Symposium: Coal Liquefaction Products—New Separations Challenge for Liquid Chromatography	Room 235B
Gas Chromatography—General	Little Theater
Atomic Absorption Spectroscopy I	Ball Room
Symposium: Keeping Up with Microcomputers I	Music Hall

MONDAY AFTERNOON	
Magnetic Resonance and Mössbauer Spectrometry: Particle Size Analysis	Room 205
Biochemical Analysis and Food Analysis	Room 239
Fluorescence and Phosphorescence—Applications	Room 3A
New Instrument Concepts	Club Room B
Symposium: Biomedical Applications of Ion Selective Electrodes II	Room 235A
Liquid Chromatography—General I	Room 235B
Symposium: Glass Capillary Gas Chromatography for Routine Analysis	Little Theater
Atomic Absorption Spectroscopy II—Flameless	Ball Room
Instrument Automation	Music Hall

February 28

TUESDAY MORNING	
Emission Spectroscopy	Room 205
Forensic, Drug, and Pharmaceutical Analysis	Room 239
Symposium: Quantitative Infrared Spectroscopy by FT–IR	Room 3A
Electroanalytical Chemistry I	Club Room B
Symposium: Advances in Applied Surface Analysis I (ASTM E-42)	Room 235A
Liquid Chromatography—General II	Room 235B
Gas Chromatography—Applications	Little Theater
Atomic Absorption Spectroscopy III	Ball Room
Symposium: Keeping Up with Microcomputers II	Music Hall

TUESDAY AFTERNOON	
Surface Analysis I	Room 205
Clinical Chemistry and Biochemical Analysis	Room 239
Symposium: Chemical Analysis as Applied to Steel Industry	Room 3A
Electroanalytical Chemistry II	Club Room B
Symposium: Laboratory Automation I—Computerization: Some Case Studies	Room 235A
Liquid Chromatography—Detectors	Room 235B
Gas Chromatography—Inlet Systems & General	Little Theater
Atomic Absorption Spectroscopy IV	Ball Room
Symposium: Spectroscopy in England	Music Hall

March 1

WEDNESDAY MORNING	
Raman Spectroscopy	Room 205
Atomic Fluorescence Spectroscopy	Room 239
Fourier Transform Infrared Spectroscopy	Room 3A
Laboratory Management and Automation	Club Room B
Symposium: Advances in Applied Surface Analysis II	Room 235A
Symposium: Toxicology in Industry	Room 235B
Gas Chromatography—Novel Detectors	Little Theater
Ion Exchange and Ion Chromatography	Ball Room
Environmental Analysis—General I	Music Hall

WEDNESDAY AFTERNOON	
Surface Analysis II	Room 205
ICP–Atomic Emission	Room 239
Oil and Other Organic Pollutants Analysis I	Room 3A
Raman Instrumentation and General Spectroscopy	Club Room B
Symposium: Laboratory Automation II—Computer Information Handling in Clinical Laboratory (ASTM E-31)	Room 235A
Symposium: OSHA—Industrial Hygiene and the Analytical Chemist	Room 235B
1978 Awards Symposium	Little Theater
Liquid Chromatography—Columns	Ball Room
Environmental Analysis—Organic	Music Hall

March 2

THURSDAY MORNING	
UV–VIS Spectrophotometry	Room 205
Symposium: Speedy Spectroscopy (How Fast Is Fast?)	Room 239
X-ray Fluorescence	Room 3A
Infrared Spectroscopy	Club Room B
Symposium: Airborne Contaminants	Room 235A
Liquid Chromatography—Applications	Room 235B
Automated Analysis	Little Theater
Computerized Mass Spectrometry and GC/MS	Ball Room
Polymer Analysis	Music Hall

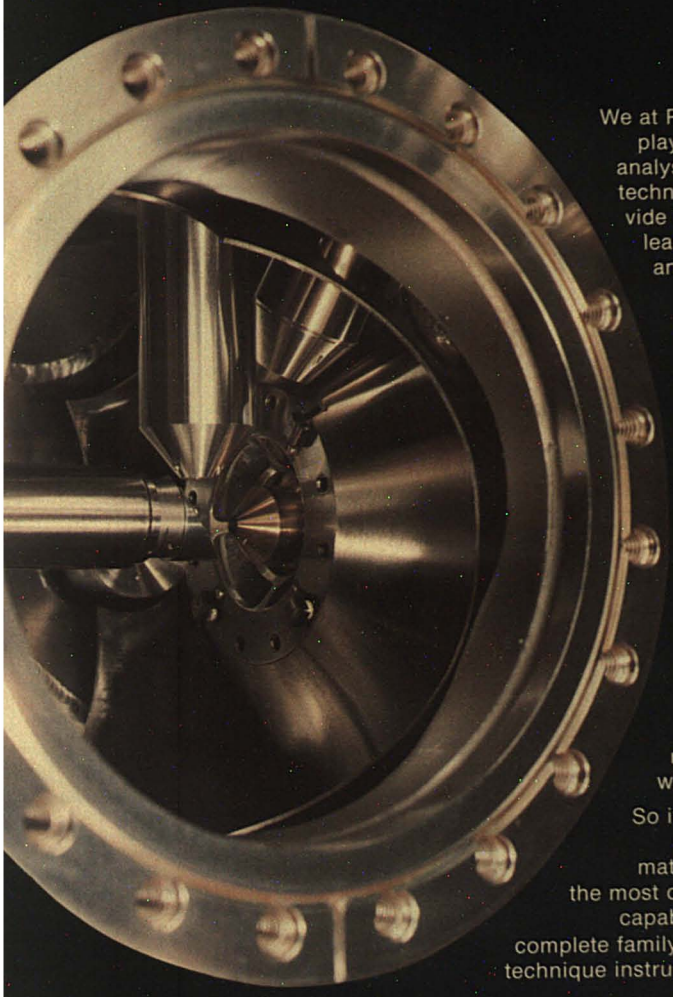
THURSDAY AFTERNOON	
General Analysis I	Room 205
Flame Atomic Emission	Room 239
Oil and Other Organic Pollutants Analysis II	Room 3A
Thermal Analysis	Club Room B
Environmental Analysis—General II	Room 235A
Liquid Chromatography—Instrumentation	Room 235B
Coblentz Society Award and Symposium: Applications of Fourier Transform Infrared Spectroscopy	Little Theater
Mass Spectrometry (EI, CI, FI, API)	Ball Room
Symposium: Automation Comes of Age	Music Hall

March 3

FRIDAY MORNING	
General Analysis II	Room 205
Trace Analysis	Room 239
Acoustic Spectroscopy/Fuels	Room 3A
Environmental Analysis—Air Pollution	Room 235A
Thin Layer/Gel Permeation Chromatography	Room 235B
Statistics, Mathematics, & Models	Little Theater

SYNERGISM...

when one plus one is greater than two.



We at PHI have found that synergism plays an important role in surface analysis. When two or more surface techniques are combined, they provide complementary information — leading to a more comprehensive analysis and a greater likelihood of finding solutions to many materials problems. For this reason, PHI has pioneered the development of multiple-technique surface analysis instrumentation.

And one look inside our test chamber will convince you — PHI offers the most versatile multiple-technique surface analysis systems available ... ESCA, AES, SAM, SESD, SIMS, UPS, all performed on the same specimen area ... without changing specimen position ...with optimized performance for all techniques ... with rapid sample turnaround ... and with complete computer control.

So if you need solutions to surface problems in almost any area of materials technology... if you need the most comprehensive surface analysis capability available ... investigate the complete family of high performance multiple-technique instruments from PHI... **Call PHI.**

View of analysis station in a typical PHI multiple-technique instrument, the Model 550 ESCA/SAM.

See the latest PHI equipment at the Pittsburgh Conference, Booth 432.

PHYSICAL ELECTRONICS INDUSTRIES, INC.

6509 Flying Cloud Drive Eden Prairie, Minnesota 55343
(612) 941-5540 Telex 29-0407

CIRCLE 211 ON READER SERVICE CARD

and Materials will meet. Executive and governing board meetings of other societies are also scheduled, and ANALYTICAL CHEMISTRY's Instrumentation Advisory Panel will meet.

An employment bureau will be in operation in Room 216 at the Convention Center. This service is available to all registrants without charge. Advance registration is urged. Job candidate or employer forms are available from Hector Silva, Westinghouse Research Laboratories, Beulah Road, Pittsburgh, Pa. 15235 (412-256-7617).

Further information on the meeting is available from Edwin S. Hodge, Carnegie-Mellon University, Mellon Institute, 4400 Fifth Ave., Pittsburgh, Pa. 15213 (412-578-3260).

The following pages of ANALYTICAL CHEMISTRY contain the complete technical program and coverage of new products to be shown at the Exposition.



J. H. Judd



H. L. Retcofsky



R. W. Baudoux



R. M. Raybeck



D. P. Manka

Conference Officials

1978 Board of Directors

President: Jane H. Judd, *Westinghouse Electric Corp.*

Vice President: Herbert L. Retcofsky, *PERC/DOE*

Chairman (Society for Analytical Chemists of Pittsburgh): Bruce M. LaRue, *National Steel Corp.*

Chairman-Elect (Society for Analytical Chemists of Pittsburgh): Robert W. Baudoux, *U.S. Steel Corp.*

Chairman (Spectroscopy Society of Pittsburgh): Allen J. Sharkins, *alcoa Technical Center*

Chairman-Elect (Spectroscopy Society of Pittsburgh): Richard Obrycki, *Koppers Research Laboratories*

Past Conference Chairman: John F. Jackovitz, *Westinghouse Research Laboratories*

Treasurer: Ralph M. Raybeck, *Jones and Laughlin Steel Corp.*

Assistant Treasurer: John E. Graham, *Koppers Research Laboratories*

Executive Secretary: Rita Bastiani, *Pittsburgh, Pa.*

Conference Committees

Administrative Activities:

Eleanor L. Saier, *Allegheny General Hospital;* Edwin S. Hodge, *Mellon Institute*

Activities:

Chairlady: Marilyn V. Senneway, *ARCO/Polymers, Inc.*

Chairman-Elect: J. Kevin Scanlon, *PPG Industries, Inc.*

Assistant: Norma Bottone, *Union Carbide Corp.*

Audiovisuals:

Chairman: George Vassilaros, *Colt Industries, Inc.*

Chairman-Elect: Charles D. Gaitanis, *Alcoa Technical Center*

Employment:

Chairman: Hector Silva, *Westinghouse Research Laboratories*

Chairman-Elect: Peter M. Castle, *Westinghouse Research Laboratories*

Exposition:

Chairman: Dan P. Manka, *Consultant*

Chairman-Elect: Allen J. Sharkins, *Alcoa Technical Center*

Assistant: Nancy Kotsko, *University of Pittsburgh*

Assistant: Ralph Host (*Retired*)

Housing:

Chairman: Paul Bauer, *Westinghouse Electric Corp.*

Chairman-Elect: Charles R. Hines, *National Forge Co.*

Nontechnical Program:

Chairlady: Louise Manka, *Pittsburgh, Pa.*

Chairlady-Elect: Irene McCafferty, *Pittsburgh, Pa.*

Program:

Chairman: Robert W. Baudoux, *United States Steel Corp.*

Chairman-Elect: S. David Cifrulak, *Calgon Corp.*

Printing:

Chairman: John Snodgrass, *Shenango, Inc.*

Chairman-Elect: John A. Queiser, *PERC/DOE*

Publicity:

Chairman: Florence A. Eggers, *Pittsburgh, Pa.*

Chairman-Elect: Charles J. Belle, *Ferro Corp. Tech. Center*

Cleveland Liaison: Allen T. Pollock, *Harshaw Chemical Co.*

Assistant: Joseph Drost, *Alcoa Technical Center*

Registration:

Chairman: Richard S. Danchik, *Alcoa Technical Center*

Chairman-Elect: Richard Obrycki, *Koppers Research Laboratories*

Assistant: Jay Auses, *Alcoa Technical Center*

Assistant: Rita Bastiani, *Pittsburgh, Pa.*

Assistant: Marlene Bauer, *Pittsburgh, Pa.*

Assistant: Jack Petty, *Calgon Corp.*

GCA
CORPORATION



FREE TEST KIT AND 30 DAYS

Let us send you a factory-fresh McPherson 700 spectrophotometer to use in your lab on your work for 30 days.

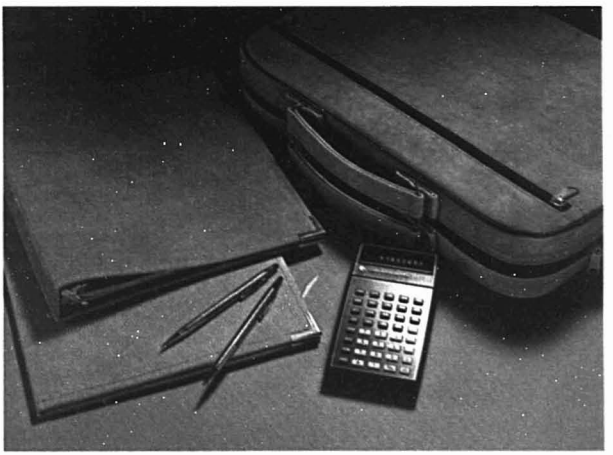
We want you to have the time for a really objective appraisal, the kind just not possible from a quick look at a salesman's demonstrator.

With your 700, you will also receive a kit. Complete instructions, plus a TI SR-40 calculator, a notepad and diary, as well as a Cross pen and pencil to document your findings.

After 30 days, you either buy the 700 or tell us to come and get it. In any event, you keep the test kit.

Call Jay Iannini toll free at 800-621-8820. He'll configure your 700 with the functions you need. Wavelength scanning, gel scanning, kinetics, automatic sampling, whatever your work requires. Offer expires September 1, 1978.

Or for more information on McPherson instruments, write **GCA/Precision Scientific Group,** 3737 West Cortland Street, Chicago, Illinois 60647.



McPHERSON™

DOES IT WITH PRECISION

See us at the Pittsburgh Conference, booths 520 & 522

CIRCLE 82 ON READER SERVICE CARD

Society Meeting Coordination:

Chairman: Frank W. Plankey, *University of Pittsburgh*

Special Projects:

Chairman: Harold A. Sweeney, *Koppers Research Laboratories*

Chairman-Elect: William M. Hickam, *Westinghouse Research Laboratories*

Special Assistant to the President:

Joseph R. Ryan, *Harbison-Walker Refractories (Deceased)*

Advisory to the President:

Gerald L. Carlson, *Westinghouse Research Laboratories;* Robert Mainier, *Koppers Research Laboratories*

Long-Range Planning Committee:

Chairman: John F. Jackovitz. Joseph A. Feldman, Alex J. Kavoulakis, Robert E. Witkowski, Charles J. McCafferty, Jr., Harry Fracek

Award Winners



G. M. Janini



W. L. Zielinski, Jr.



K. Johnston

Pittsburgh Applied Analytical Chemistry Award



L. Andrews
Coblentz Award



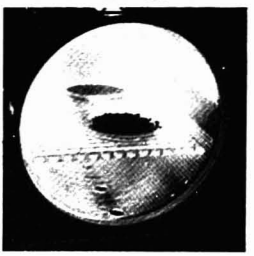
C. Horvath
Dal Nogare Award



E. B. Wilson
Pittsburgh Spectroscopy Award

Three new reasons why your department should

TAKE ANOTHER LOOK AT PLASMA ASHING



1. New End-of-Ashing Detector. We've incorporated an optical feedback mechanism that uses spectral analysis to determine if any ashing is going on. If the sample is entirely ashed, or needs stirring, your IPC system will let you know.

2. New Temperature Control. Transferring technology we developed in maintaining a critical temperature envelope for semiconductor manufacturing, we have built a sophisticated temperature probe into our ashing chamber for real-time control over temperature *at the sample.*

3. New Heat Lamps. Until now, the only benefit you derived from plasma ashing was its speed at low temperatures. Now you can enjoy plasma's cleanliness, safety and inexpensive unattended operation and get rid of your expensive and hazardous perchloric acid. These are important advantages when you need speed and are ashing a lot of samples. Now you can do high temperature ashing simply with our efficient new built-in heat lamps.

So. Three good new reasons. And there are many more that won't fit this space. Please let us tell you our complete story and show what other chemists and spectroscopists are doing in the **QC Laboratory** with our ashers. Analyzing plastics, paints, foods, drugs and more. Call or write Dick Bersin; ask for IPC Bulletin 4802.

IPC

International Plasma Corporation, 31159 San Benito Street, Box 4136, Hayward, CA 94544. (415) 489-3030.

CIRCLE 111 ON READER SERVICE CARD
See us at the Pittsburgh Conference, Booth #710

With all the spectrophotometers on the market, how do you choose your next one? **Ask yourself questions like these and draw your own conclusions.**

If you want to change from enzyme kinetics to thermal melts, from scanning wavelength to scanning gels, from sucrose gradient studies to column chromatography, etc, do you have to change spectrophotometers too? Maybe use your neighbor's instrument and (especially if it's a Gilford) stand in line? **Our Model 250 accommodates a variety of sample handling systems, and its unrestricted sample space even lets you design your own special-purpose devices. That tells you something about versatility.**

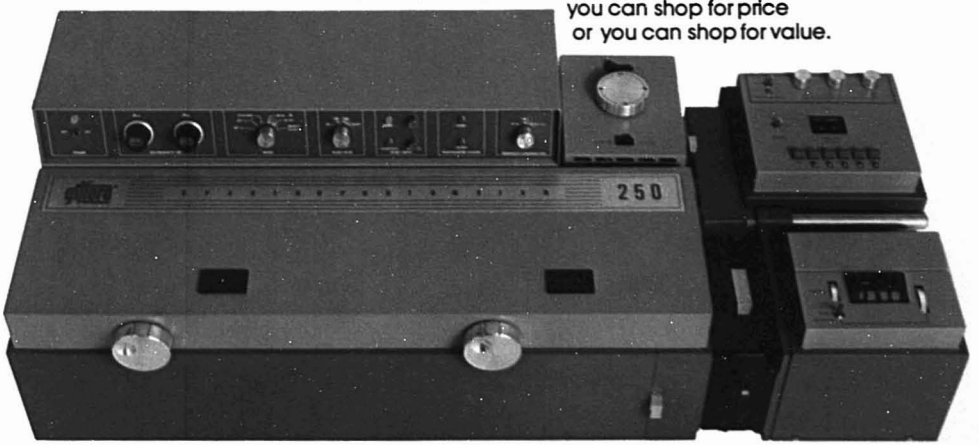
How important are the critical areas of measurement? The low UV, the dense sample, operation with flow-through or microcuvettes? **Model 250's throughput is exceptional; the proof lies in an absorbance range 50% greater than most (3A instead of 2A) and in sensitivity to 0.0001A. That also tells you something about routine performance.**

Which spectrophotometer is used to check questionable results from other instruments? **With Model 250's wavelength and absorbance standards directly traceable to NBS, verification of results is easy. That tells you something about accuracy.**

What's the oldest UV-VIS spectrophotometer still in use in your building? **There's every chance that it's a Gilford; and if so, there's also a good chance that it's using an accessory or two not listed on the original order. That tells you something about durability.**

Versatility, performance, accuracy, and durability: *that tells you something about Gilford.* As we see it, you have but two choices when it comes time to select your spectrophotometer:

you can shop for price
or you can shop for value.



The Gilford Model 250: All the spectrophotometer you will ever need.

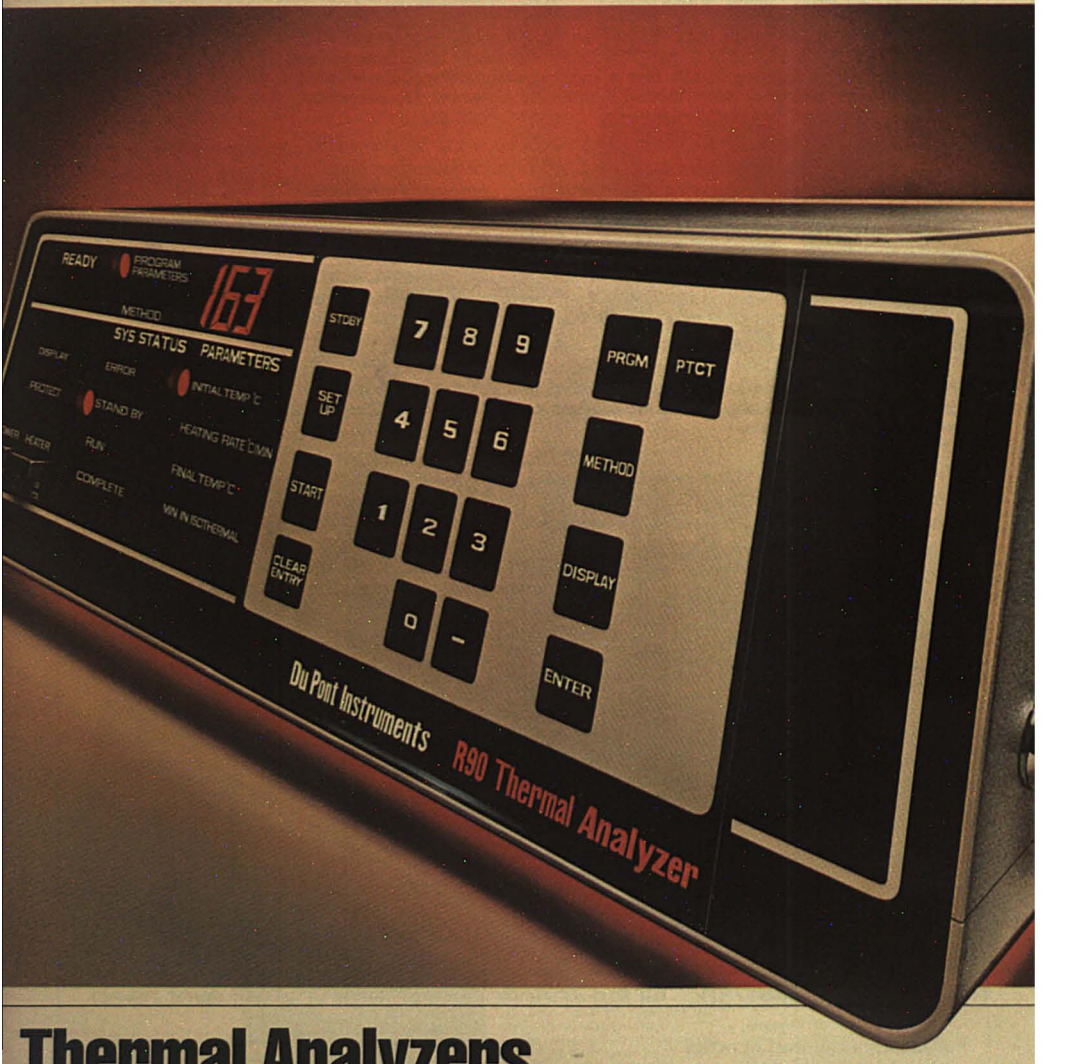
For information call or write
Gilford Instrument Laboratories Inc, Dept.7-9-16
Oberlin OH 44074 (216) 774-1041.

CIRCLE 80 ON READER SERVICE CARD

gilford® INSTRUMENT

Oberlin, Ohio 44074
Paris (Malakoff), France
Düsseldorf, W. Germany
Teddington, Middx., England
(216) 774-1041 Telex: 98-0456

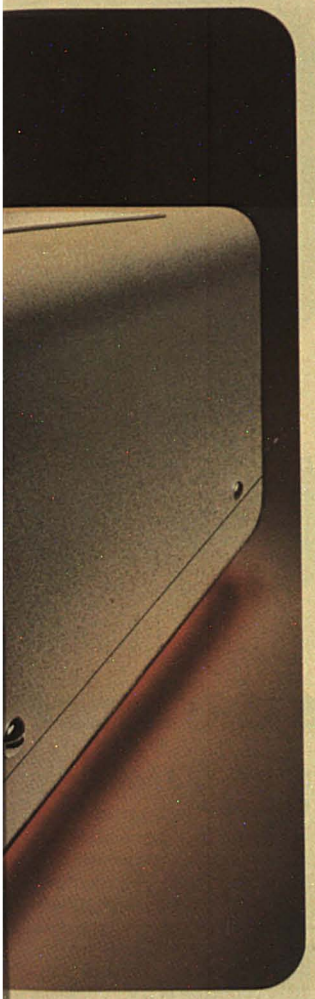
Du Pont's new R90 the cost of routine



Thermal Analyzers

Scientific & Process Instruments Division

programmer lowers thermal analysis.



The ideal answer to a wide range of quality and process control problems in polymer, chemical, automotive and electronic fields.

This new microprocessor-controlled programmer can be used with the DuPont Differential Scanning Calorimeter, Thermogravimetric Analyzer and Thermomechanical Analyzer to provide an economical system with practical features:

Pushbutton-actuated microprocessor control for reliability, simplicity of operation, minimal operator involvement. "Set up" and "Start" are the only operating buttons in routine use.

9-method memory for testing that's repeatable as well as accurate and simple.

Lockout key avoids accidental program change. Only the supervisor can change programs.

Automatic set up. Instrument establishes initial conditions; ready light alerts operator that test can be started.

Complete visual display. Operator knows test status and program conditions at a glance. Easy-to-read digital LED display confirms programmer command.

Plug-in circuit boards and subassemblies for easy servicing.

Get detailed information on the new R 90 programmer by writing to DuPont or using the reader service card. For assistance in exploring the use of thermal analysis, drop us a note outlining your needs. For immediate action, call our TA hotline (302) 772-5134. DuPont Instruments, Room 36250, Wilmington, DE 19898.

See the DuPont R 90 and other thermal analysis instruments at the Pittsburgh Conference, Booth 125.

DUPONT

REG. U.S. PAT. & TM. OFF.

CIRCLE 35 ON READER SERVICE CARD



DuPont announces the most

If you want the GC/MS/DS with the best combination of sensitivity, speed, resolution, reproducibility, stability, data handling capability, versatility and ease of operation, you want the new DuPont DP-1 Mass Spectrometer. Here's why:

Unmatched control and data processing

Fully integrated system controls the GC/MS and acquires data faster than any analytical GC/MS. Dynamic range is unequalled. Special software assures proper abundance and true mass spectra that are comparable with reference data.

Total data display on a single screen with foreground/background processing gives automatic real-time display of routines simultaneously with data acquisition. Selective ion monitoring is standard and quantitative. Routines are written in FORTRAN IV to facilitate user programming. Storage capability is the highest available today—up to 15 megabytes of disc storage, plus provision for archival storage.

Simple and fast operation

Human engineering for mass spectrometers is at a dramatic new level. Operation and control are greatly simplified, with tuning prompted by the data system. Diagnostic software pinpoints malfunctions and suggests corrective action.

Instant EI to CI switching

The DP-1 uniquely integrates instant EI to CI switching with



advanced GC/MS/DS ever built.

data acquisition and programming. Unique ability to program ionization mode and reagent gas during a run helps you use CI to best advantage.

Automatic source revitalization

Innovative gold sputtering process renews critical ion source surfaces, restores source performance without shutting down, reduces frequency of cleaning.

Outstanding capillary column interface

Available capillary column inlet provides optimum resolution for high performance GC columns.

To get full details on the DP-1, and explore the potential of mass spectrometry in your work, write to DuPont Instruments, Room 36262, Wilmington, DE 19898. For immediate assistance call our hotline, (302) 772-5429.

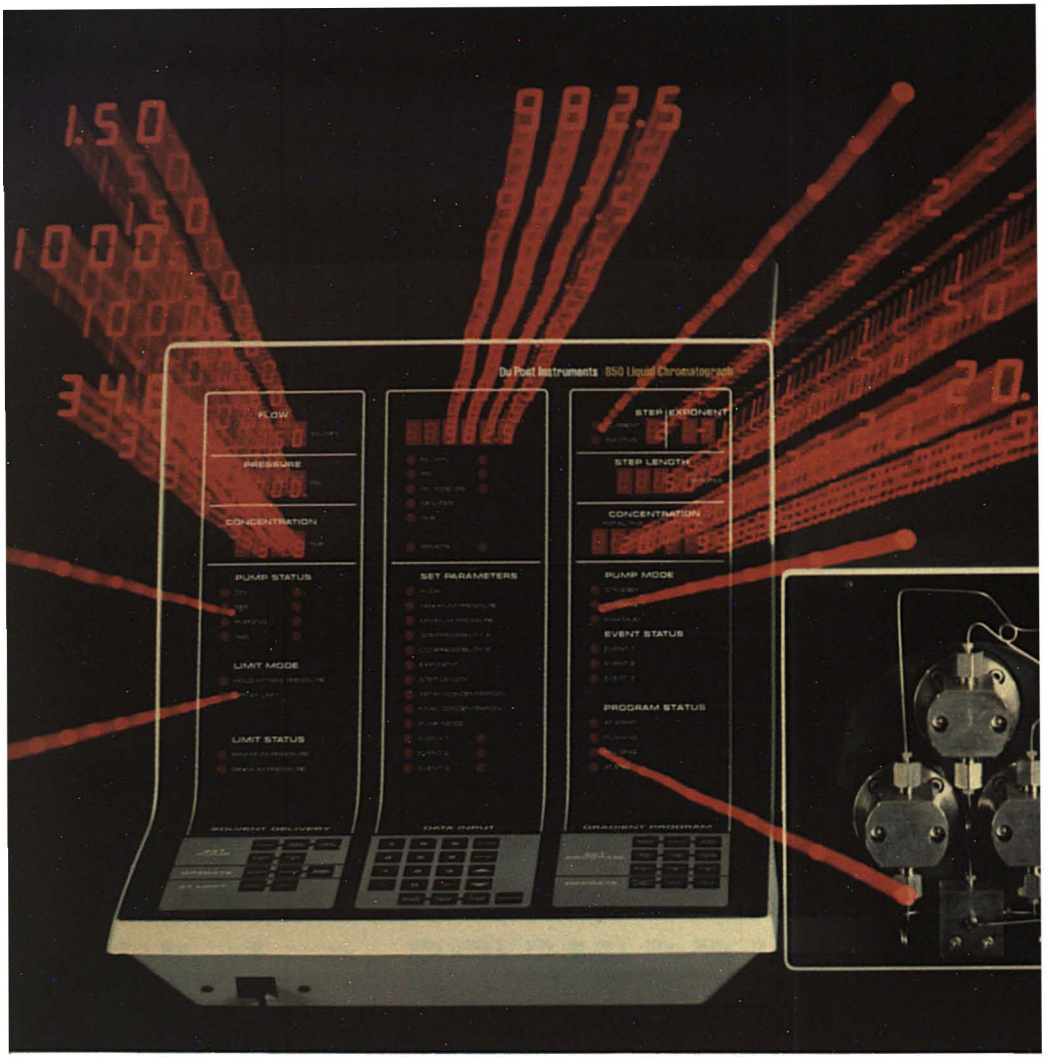
See the new DuPont DP-1 GC/MS/DS at the Pittsburgh Conference, Booth 125.

Mass Spectrometers

Scientific & Process Instruments Division

DUPONT

CIRCLE 36 ON READER SERVICE CARD



An outstanding combination of features

- **Visual display of operating parameters**
- **Constant-volume three-piston pump**
- **Microprocessor control of components**
- **Immediate operator access while system is running**

This new DuPont LC system offers the chromatographer more than outstanding reproducibility and reliability. It solves the man-machine interface problem by giving the operator immediate call-out knowledge of all key operating parameters and the ability to effect a change in those parameters while the system is running.

Design features of the innovative system include

- automatic gradient programming
- a precision constant-volume three-piston pump
- a versatile microprocessor to control components, insure reliability and simplify parameter selection
- precise control of thermal environment

Not just an instrument... a totally new Du Pont LC system.



- built-in computerized diagnostics
- universal port for data processing
- guaranteed column performance.

The new system—designated the Model 850—is designed to meet the most demanding requirements of the research scientist as well as the dedicated needs of the quality control analyst. In any situation, the chromatographer is in total charge—with complete authority to change vital parameters without interrupting data reporting.

Get full details by writing DuPont Instruments, Room 36300, Wilmington, DE 19898. Or, if you have immediate need, please telephone 302-772-5139.

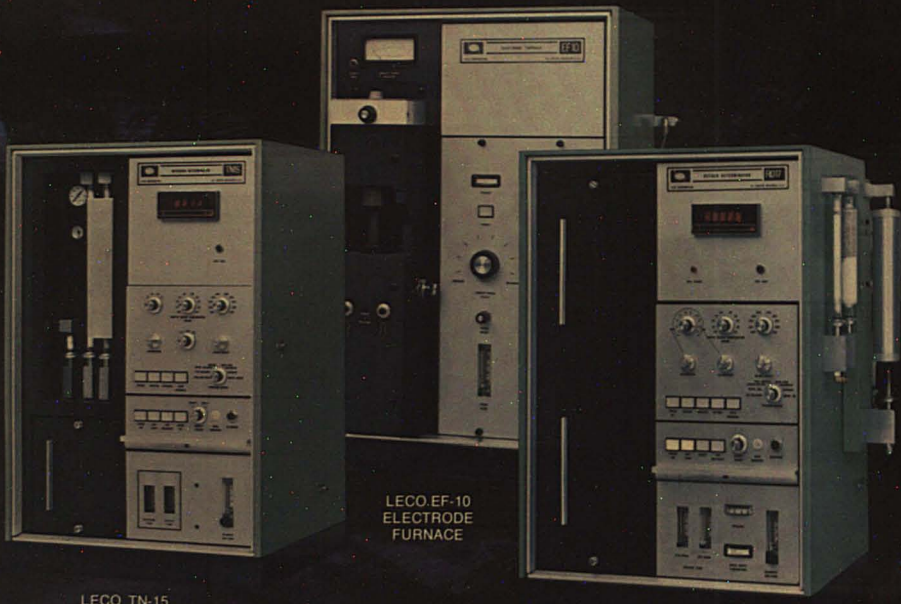
Liquid Chromatographs

Scientific & Process Instruments Division

DUPONT

CIRCLE 40 ON READER SERVICE CARD

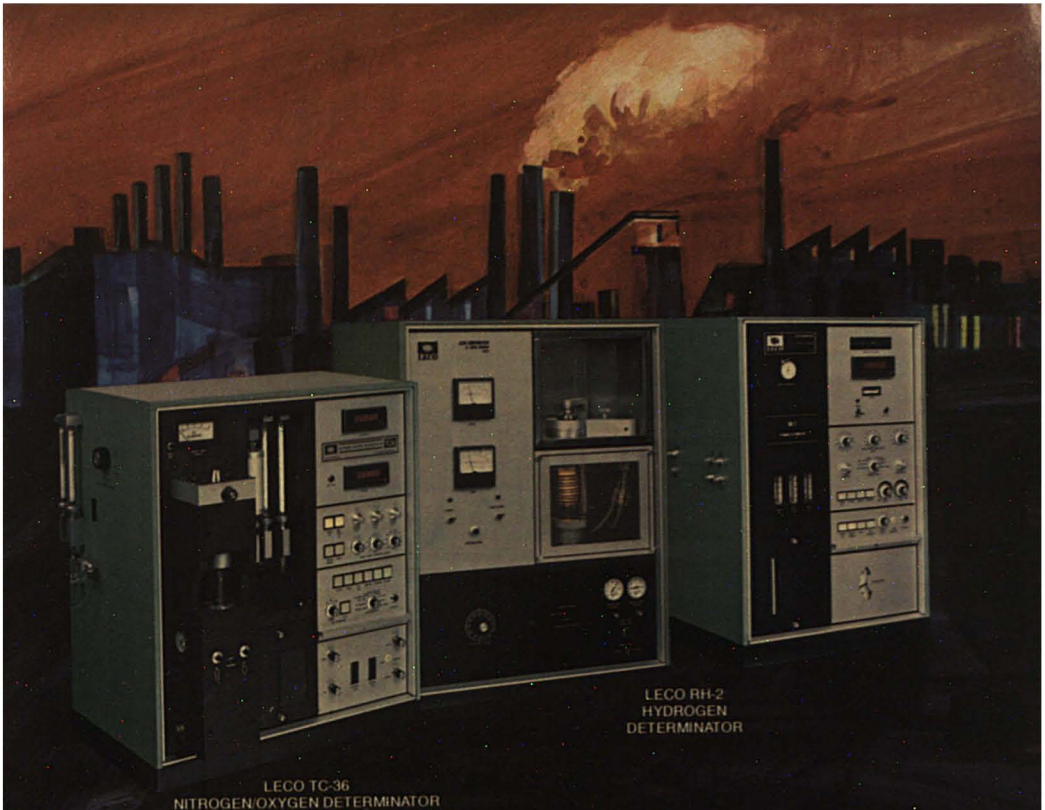
LECO® is No.1 in analyses of gases in metals



LECO TN-15
NITROGEN DETERMINATOR

LECO EF-10
ELECTRODE
FURNACE

LECO RO-17
OXYGEN DETERMINATOR



LECO RH-2
HYDROGEN
DETERMINATOR

LECO TC-36
NITROGEN/OXYGEN DETERMINATOR

LECO® Gas Determinators for the Rapid and Accurate Determination of Nitrogen, Oxygen, and Hydrogen in Metals.

LECO® offers a complete line of instruments for determining oxygen, nitrogen and hydrogen in ferrous and non-ferrous metals, and other inorganic materials. These instruments are ideal for both laboratory and production control applications and are available with data output interfaces for remote printout and computer compatibility.

Contact LECO Today!

LECO CORPORATION 3000 Lakeview Ave. St. Joseph, MI 49085, U.S.A. Phone: (616) 983-5531

CIRCLE 175 ON READER SERVICE CARD

LECO

PROGRAM

Monday, February 27

Emission Spectroscopy—Chemical

Monday Morning, Room 205
J. E. Paterson, *Presiding*

8:30 Evaluation of Sequential Multielement Argon Radio Frequency Induction Coupled Plasma Optical Emission Analysis (Smear FICPA). M. D. Silvester, F. N. Abercrombie, D. J. Koop, R. B. Cruz, Barringer Research Ltd.

8:50 Nebulous Aspects of Simple Introduction into Argon Induction Coupled Plasma. F. N. Abercrombie, M. D. Silvester, R. B. Cruz, D. J. Koop, Barringer Research Ltd.

9:10 Advanced Curve-Fitting Technique for Direct Reading Spectrometer. R. L. Crawford, Fisher Scientific Co.

9:30 New Inductively Coupled Plasma Sequential Spectrometer: JY38P. J. M. Lerner, ISA, J. P. Ellerbach

9:50 Spectrochemical Analysis of Resulfurized Steels, Pb in Steels, and Bi in Malleable Cast Irons. R. F. Jarrell, V. A. Cannavo, Fisher Scientific Co.

10:20 Changes in Background Radiation Due to Variation in Major Alloying Elements with Traditional Spark Excitation and Computer Correction for Such Effects. R. F. Jarrell, H. LeFebvre, J. Gardner, Fisher Scientific Co.

10:40 Spectral Characteristics of ICP Discharge. G. Horlick, U of Alberta

11:00 Multielement Instrumental Neutron Activation Determination of Al, Cu, Mn, and V in Raw and Drinking Water. V. Lavrakas, P. Bouvier, Jr., U of Lowell

11:20 Polymer-Bound Cupric Ion Selective Chelating Agents. G. L. Carlson, J. T. McCall, Mayo Clinic and Mayo Foundation

11:40 Investigation of Metal Chelation by Metallothionein Using Differential Pulse Polarography—New Method for Investigation of Metalloproteins. W. B. Tucker, Colorado State U, D.F.S. Natusch, P. G. Schmidt

Biochemical Analysis

Monday Morning, Room 239
E. L. Saier, *Presiding*

8:30 Use of On-Line Instruments and Computers for Study of Enzyme-Catalyzed Reactions. J. W. Frazer, Lawrence Livermore Lab, L. P. Rigdon, C. L. Pomernacki, H. R. Brand, J. A. Brubaker

8:50 Mathematical Modeling for Multidimensional Enzyme Reaction System. H. R. Brand, Lawrence Livermore Lab, C. L. Pomernacki, J. W. Frazer, T. A. Brubaker

9:10 Method for Numerically Characterizing Enzyme Reaction System Flow Dynamics. C. L. Pomernacki, H. R. Brand, J. W. Frazer, Lawrence Livermore Lab

9:30 Rapid Characterization and Assay of Enzymes by Kinetic Measurements. L. P. Rigdon, J. W. Frazer, Lawrence Livermore Lab

9:50 Adenosine Deaminase Assay Using HPLC. R. Hartwick, A. Krstulovic, P. R. Brown, U of Rhode Island

10:20 Evaluation of Conditions for Storage of Blood Fluids Prior to HPLC Analysis for Nucleosides and Bases. M. McKeag, P. R. Brown, U of Rhode Island

10:40 HPLC Analysis of Indomethacin and Asperin in Plasma Using UV and Fluorescence Detectors. T. M. MacNeil, P. R. Brown, U of Rhode Island

11:00 Rapid Method for Preparation of Serum Samples for HPLC Analyses for Nucleosides and Bases. R. A. Hartwick, P. R. Brown, U of Rhode Island

11:20 Serum Profiles of Patients with Breast Cancer and Benign Fibrocystic Changes; High-Pressure Liquid Chromatographic Study of Nucleosides and Bases. A. M. Krstulovic, P. R. Brown, D. M. Rosie, U of Rhode Island

11:40 Analysis of Naproxen in Serum Using High-Pressure Liquid Chromatography. R. F. Burgoyne, P. R. Brown, U of Rhode Island

Fluorescence and Phosphorescence—Instrumental

Monday Morning, Room 3A
G. L. Carlson, *Presiding*

8:30 J-Y 4, A Videospectrofluorometer. M. M. Young, B. Rosovsky, Instruments SA

8:50 Recent Advances in Video Fluorometry. G. D. Christian, D. W. Johnson, L. W. Hershberger, J. B. Callis, U of Washington

9:10 New Multiple-Sample Capacity Fluorophotometer for Routine Analysis. J. P. Salsgiver, R. L. MacLure, United Technical Corp.

9:30 Characterization of Trace Impurities in Minerals Using Cathodoluminescence Microscope Attachment—the Luminoscope. D. J. Marshall, Nuclide AGV Div., A. N. Mariano

9:50 Digital Research Phosphorimeter. D. Kolb, S. DiGregorio, Spex Industries

10:20 New Reference Spectroradiometer for Luminescence Spectrometry. K. D. Mielenz, NBS

10:40 Luminescence/Absorption Spectrophotometer. H. Madlin, S. Cravitt, M. Dachs, E. A. Kallet, Farrand Optical Co.

11:00 Pulsed Laser Excited Phosphorimetry. G. D. Boutilier, J. D. Winefordner, U of Florida

11:20 Utilization of Microprocessor to Obtain Fluorescence Derivative, Polarization, and Anisotropy Spectra. J. L. Dicesare, N. A. Sebestyen, Perkin-Elmer

11:40 Use of Differential and Derivative Techniques for Obtaining Corrected Fluorescence Spectra. D. A. Terhaar, T. J. Porro, Perkin-Elmer

New Instrumentation

Monday Morning, Club Room B
J. R. Ryan, *Presiding*

8:30 New Ultrasonic Methods in Analytical Chemistry. H. Alliger, Heat Systems-Ultrasonics

8:50 Versatile Look-in Amplifier Using Tapped Analog Delay Line. E. G. Codding, M. M. Schoenmann, U of Calgary

9:10 Bipolar Pulse, Differential Electrolytic Conductivity Detector. R. C. Hall, P. W. Thiede, B. J. Ehrlich, Tracor

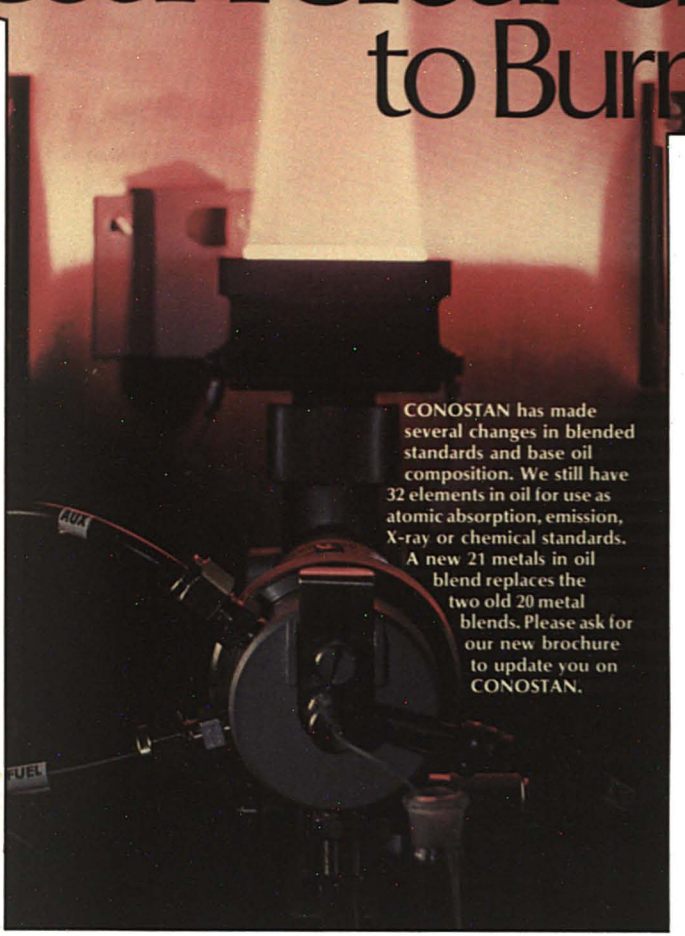
9:30 TG-DTA: Design and Performance of New Instrument in Thermal Analysis. K. Meier, Mettler Instrumente AG

9:50 Sequential Exponential Diluter. T. Hirschfield, Block Engineering

10:20 Videospectrofluorometer "JY-4". B. Rosovsky, ISA, M. Young, M. Saguem, A. Samoun

10:40 Infrared "Answer Machine". R. J. Obremski, A. Way, T. Reid, J. W. Mohar, Beckman Instruments

New Standards to Burn



CONOSTAN has made several changes in blended standards and base oil composition. We still have 32 elements in oil for use as atomic absorption, emission, X-ray or chemical standards. A new 21 metals in oil blend replaces the two old 20 metal blends. Please ask for our new brochure to update you on CONOSTAN.

CONOSTAN

CONOSTAN DIVISION
Continental Oil Company • P.O. Box 1267 • Ponca City, Oklahoma 74601 • (405) 762-3456

The doubly convenient Double Beam.

Introducing
the Zeiss DM 4 Spectrophotometer.

It's the most convenient double-beam instrument on the market in the spectral range of 195–850mm—for two reasons:

1. The controls are few and logically placed (see the control panel in the upper illustration). Automatic lamp switch-over adds more convenience, especially when the DM 4 is used for wavelength scanning.

2. The extra-large, 6-position sample compartment is located right up front for ready accessibility. It can accommodate 6 sample and up to 6 reference cells.

CIRCLE 235 ON READER SERVICE CARD

Versatile. Accurate. Reliable. Compact.

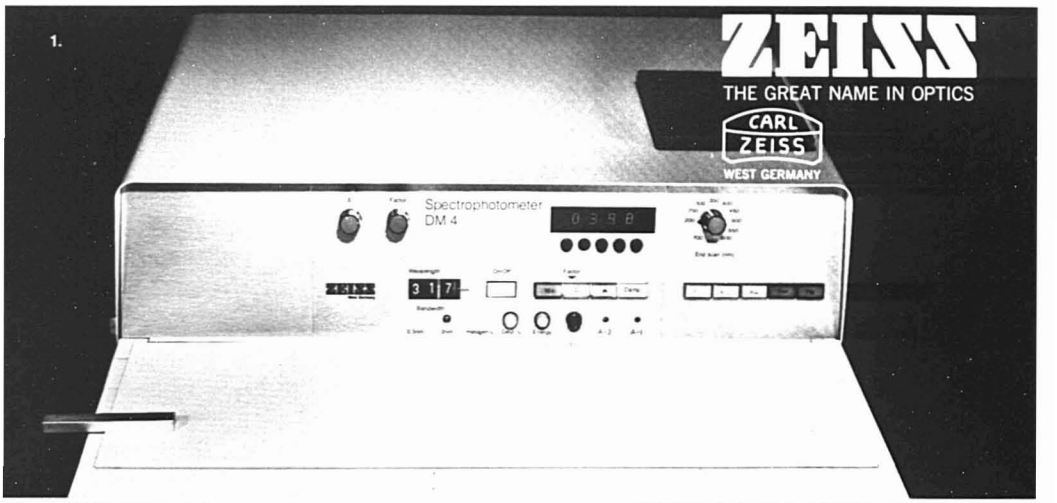
Whether you use the DM 4 for routine quantitative absorption determinations, for sensitive reaction studies, such as enzyme kinetics, or for demanding qualitative wavelength scanning, you'll find it has all the accuracy and reliability associated with the Zeiss name. For instance, the baseline flatness is ± 0.002A, and photometric accuracy can be easily determined by internal standards.

The DM 4 is equipped with digital and analog outputs with suppression of up to 2.0A. The programmable sample changer features selectable dwell and cycle times.—Most existing recorders are compatible.

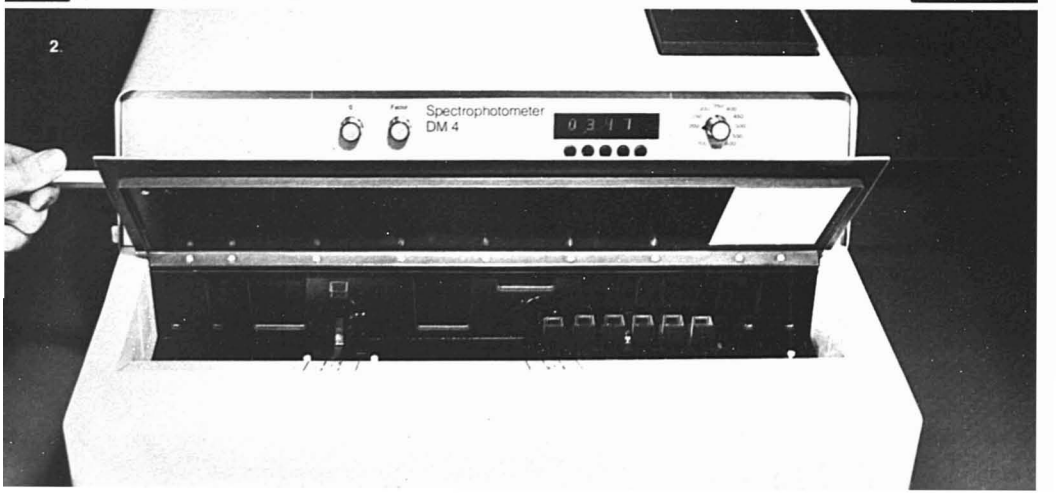
Nationwide sales and service only from Zeiss.

Carl Zeiss, Inc., 444 5th Avenue, New York, N.Y. 10018 (212)730-4400. Branches in: Atlanta, Boston, Chicago, Columbus, Houston, Los Angeles, San Francisco, Washington, D.C. In Canada: 45 Valleybrook Drive, Don Mills, Ont., M3B 2S6. Or call (416)449-4660.

1.



2.



11:00 New Microprocessor-Based Double-Beam UV/Visible Spectrophotometer. D. Irish, R. J. Francis, Pye Unicam Ltd.

11:20 In Situ Rejuvenation of Mass Spectrometer Ion Sources via Gold Sputtering. C. W. Hull, C. G. Blanchard, R. F. Howard, Du Pont

11:40 New Color-Measuring System. D. Irish, A.R.L. Moss, Pye Unicam Ltd.

Symposium: Biomedical Applications of Ion Selective Electrodes I

Monday Morning, Room 235A

H. Freiser, *Presiding*

8:30 Diagnostic Polarographic Enzyme Electrodes. L. C. Clark, Jr., Children's Hospital Medical Center

9:30 Liquid Membrane Electrodes of Biomedical Applicability. W. Simon, Eidgenossiche Technische Hochschule

10:45 Bio-Selective Membrane Electrodes. G. A. Rechnitz, U of Delaware

Symposium: Coal Liquefaction Products—New Separations Challenge for Liquid Chromatography

Monday Morning, Room 235B

P. C. Talarico, *Presiding*

8:30 Keynote Address—Coal Liquefaction Products—New Challenge for the Analyst: An Overview. A. G. Sharkey, PERC/DOE

9:05 Chromatographic Analysis of Benzene Carboxylic Acids. J. Litton, J. R. Graham, Occidental Petroleum

9:35 Rapid Liquid Chromatographic Determination of *n*-Paraffins in Coal Liquids. D. Jewell, R. Ruberto, Gulf Research and Development

10:25 Role of HPLC in Analysis of H-Coal Liquids. A. W. Fort, IMMR, N. L. Holy

10:55 Role of LC and LC/MS in Separation and Characterization of Coal Liquefaction Products. W. A. Dark, Waters Associates, W. A. McFadden

11:25 Separation and Isolation of Coal Liquefaction Products. T. F. Yen, I. Schwager, J. T. Kevan, W. C. Lee, P. A. Farmanian, V. Weinberg, J. G. Miller, U of Southern California

Gas Chromatography—General

Monday Morning, Little Theater

A. J. Kavoulakis, *Presiding*

8:30 Designing New Chromatograph for Tomorrow's Applications. M. J. Murphy, E. Zerenner, Hewlett-Packard

8:50 Capillary System for $400 and One Week's Labor. H. M. McNair, S. K. Gangwal, VPI & SU

9:10 Rapid GC Separations Using Short Glass Capillary Columns. T. A. Rooney, L. H. Altmayer, Hewlett-Packard

9:30 Use of Polar Phase (Silar 10C) Coated Glass Capillary Columns in GC. S. Ramachandran, B. L. Reinbold, R. S. Henly, Applied Science Labs

9:50 Fresh Design for Thermal Conductivity Detectors. J. Craven, D. Clouser, Hewlett-Packard

10:20 Column Switching and Backflush Techniques with Open Tubular and Packed Columns in Gas Chromatography. B. Welton, J. E. Purcell, E. W. March, Perkin-Elmer

10:40 Determination of Pesticides with Photoionization Detector. J. Ford, J. N. Driscoll, HNU Systems

11:00 Selective Nitrogen and Phosphorus Detection with Electrically Heated Alkali Beads. P. L. Patterson, R. Howe, V. Hornung, C. H. Hartmann, Varian

11:20 Extended Capability for Detection of Nitrogen and Phosphorus Compounds. R. C. Hall, P. W. Thiede, Tracor

11:40 Low-Pressure Ashing Plasma as Halogen Selective Detector for Gas Chromatography. B. D. Quimby, R. J. Winslow, J. L. Fan, R. M. Barnes, P. C. Uden, U of Massachusetts

Atomic Absorption Spectroscopy I

Monday Morning, Ball Room

J. F. Bukowski, *Presiding*

8:30 Roadside Heavy Metal Profiles in Southern New Hampshire. E. F. Barry, J. N. LePage, U of Lowell

8:50 Analysis of Sand by Atomic Absorption Spectroscopy. D. R. Hilligoss, r. C. Burton, Ball Corp.

9:10 Determination of Microgram Amounts of Tellurium in All Types of Steels by Atomic Absorption Spectroscopy. M. der Bedrossian, Armco Steel Corp.

9:30 Lithium Isotope Ratio Technique for Tracer or Tagging Applications in Natural Water Samples. H. E. Taylor, L. J. Schroder, U.S. Geological Survey

9:50 Use of Sodium Borohydride as Reductant in Mercury Determinations. S. M. Gamache, Perkin-Elmer, E. Wiedeking

10:20 Determination of Trace Elements in Brine by Atomic Absorption Spectroscopy. D. E. Harrington, B. A. Leone, W. R. Bramstedt, Diamond Shamrock Corp.

10:40 Further Studies on Effect of Helium on Quantitative Analysis for Certain Metals in Air–Acetylene Flames. N. C. Clampitt, F. Guaqueta, M. Siracusano, U of Nebraska

11:00 Surface Adsorption of Trace Metals: Retardation by Competitive Complexation. W. C. Hoyle, A. Atkinson, Miami U

11:20 Enhanced Nebulization Efficiency with Nonsegmented Continuous Flow Sampling. W. R. Wolf, F. E. Greene, K. K. Stewart, USDA

11:40 New Nebulizer for Atomic Spectroscopy. J. J. Sotera, S. B. Smith, Jr., J. C. Tzavaras, Instrumentation Lab

Symposium: Keeping Up with Microcomputers I

Monday Morning, Music Hall

F. W. Plankey, *Presiding*

8:30 Introduction and Overview. F. W. Plankey, U of Pittsburgh

8:40 Electronics and Chemical Instrumentation—Perspective and Preview. H. V. Malmstadt, U of Illinois

9:25 Basic Architecture of Microprocessor Devices. G. Horlick, U of Alberta

10:20 Interfacing Domain Converters to Microcomputer. C. G. Enke, Michigan State U

11:05 Microcomputer Peripherals. S. R. Crouch, Michigan State U

11:50 Outstanding Analytical Chemist Award. Presented to **H. V. Malmstadt** by **B. M. Larue,** Chairman, Society for Analytical Chemists of Pittsburgh

Magnetic Resonance and Mössbauer Spectrometry: Particle Size Analysis

Monday Afternoon, Room 205

H. L. Retcofsky, *Presiding*

1:30 Quantitative Evaluation of *y*-Acetoxytiglic Aldehyde by NMR Spectroscopy. V. S. Venturella, C. T. Williams, Hoffman-La Roche

1:50 Determination of Fuel Content of Devonian Shale by Pulsed NMR. A. Attalla, B. D. Craft, Mound Lab

2:10 Pulse and Multiple-Pulse NMR Studies of ^{1}H, ^{13}C, and ^{19}F in Coals and Fluorinated Coals. B. C.

Gerstein, R. G. Pembleton, P. D. Murphy, L. M. Ryan, U.S. Department of Energy

2:30 Electron Spin Resonance Studies of Coals and Coal Liquefaction. H. L. Retcofsky, M. R. Hough, U.S. Department of Energy

2:50 Te_{011} Coaxial Microwave Cavity for Improved Electron Spin Resonance Sensitivity with Lossy Solvents. R. D. Allendoerfer, J. Carroll, Jr., SUNY

3:20 Ferric/Ferrous-Iron Ratios in USGS Rock-Standards GSP-1, AGV-1, BCR-1, PCC-1, and DTS-1 by Mössbauer Spectroscopy. C. Riddle, Ministry of Natural Resources, G. M. Bancroft, L. Aldridge, T. E. Smith, A. Turek

3:40 Determination of Particle Size Distribution of Salt Crystals in Aqueous Slurries. A. G. Miller, Rockwell Hanford Operations

4:00 Design Concepts and Performance of New Disc Centrifuge Photosedimentometer for Routine Quality Control of Latex Particle Size Distribution. R. A. Zander, Glidden Coatings & Resins, T. Provder, R. M. Holsworth, G. A. Levcun, J. A. Frijouf

4:20 Particle-Size Distribution from Low-Angle Laser Light Scattering. R. W. Wallace, W. J. Wiley, Chromatix

4:40 Applications of Particle Size Analysis by Low-Angle Laser Light Scattering. M. L. McConnell, R. W. Wallace, W. J. Wiley, Chromatix

Biochemical Analysis and Food Analysis

Monday Afternoon, Room 239

R. E. Hein, *Presiding*

1:30 Efficiency of TCA-Amine-Freon Sample Preparation Procedure for Use Prior to HPLC Analysis for Nucleotides and Nucleosides in Blood Samples. D. Van Haverbeke, P. R. Brown, U of Rhode Island

1:50 Rapid Method for Urinary 1-Methylnicotinamide and Methylated Purines by Ion-Pair HPLC. W. L. Zielinski, Jr., B. Shaikh, N. J. Pontzer, Frederick Cancer Research Center

2:10 Biochemical Applications of Spectrofluorometric Detection in HPLC. Example: Simultaneous Determination of Tryptophan Metabolites. J. Montastier, J. Yvon, C. Sterboul, J. Levine, J. P. Garnier, C. Dreux, B. Bousquet

2:30 Analysis of Selected Drugs by Liquid Chromatography/Mass Spectrometry. R. F. Skinner, Finnigan Instruments Div., D. C. Bradford, W. H. McFadden, S. Matin, T. Jennison

2:50 Biological Digestion of Fruit Juices for Pb Analysis Using Graphite Furnace AAS. R. Rouseff, Florida Department of Citrus

3:20 Polarographic and Voltammetric Determination of Vitamins. L. R. Taylor, Princeton Applied Research Corp.

3:40 Quality Control in Food Industry with HPLC. R. Schuster, Hewlett-Packard

4:00 Determination of Organophosphate and Carbamate Pesticides in Toxicological Samples. H. M. Stahr, W. Hyde, M. Gaul, R. Moore, Iowa State U

4:20 On-Line Application of Magnesium Trisilicate and Dowex 50W-X4 in Automated Fluorometric Analysis of Calcium Pantothenate from Multivitamin Preparations. R. B. Roy, A. Buccafuri, Technicon Industrial Systems

4:40 High-Performance, Liquid Chromatographic Analysis of Nonesterified Fatty Acids Extracted from Margarine. J. D. Stuart, A. G. Bailie, Jr., R. G. Jensen, U of Connecticut

Fluorescence and Phosphorescence—Applications

Monday Afternoon, Room 3A

F. E. Lytle, *Presiding*

1:30 Structure of Reactively Produced Chloropropene Cations by Laser Photodissociation. R. C. Dunbar, R. G. Orth, Case Western Reserve U

1:50 Mixture Analysis via Two-Photon Excited Fluorescence. M. J. Wirth, F. E. Lytle, Purdue U

2:10 Multicomponent Luminescence Analysis of Aromatic Mixtures. L. P. Giering, A. W. Hornig, Baird-Atomic

2:30 Techniques in Using Time Correlated Single Photon Counting for Measurement of Nanosecond Fluorescent Lifetimes. L. J. Cline Love, L. Upton, A. Ritter, Seton Hall U

2:50 Microenvironmental Effects on Excited State Electronic Properties of Selected Drug Series. L. J. Cline Love, L. Upton, A. Ritter, Seton Hall U

3:20 Chemiluminescence Determination of Reductants in Biological Fluids. R. L. Veazey, T. A. Nieman, U of Illinois

3:40 Time-Resolved Matrix Isolation Fluorometry. R. B. Dickinson, Jr., R. R. Gore, E. L. Wehry, U of Tennessee

4:00 Effect of Ortho Substitution on Benzoic Acid Fluorescence. G. H. Schenk, L. Beaubien, I. Khasawneh, Wayne State U

4:20 Quinine Sulfate Dihydrate: Fluorescence Standard Reference Material. R. A. Velapoldi, K. D. Mielenz, NBS

4:40 Trace Cobalt Determination via Lucigenin Chemiluminescence. J. D. Ingle, Jr., L. A. Montano, Oregon State U

New Instrument Concepts

Monday Afternoon, Club Room B

N. E. Gordon, *Presiding*

1:30 Hydrogen Sulfide Analysis Method and Its Calibration Using Standard Sample Generator. C. L. Kimbell, Houston Atlas

1:50 Mass Spectral Search System Based on Novel Data Compression Scheme. G. T. Rasmussen, U of North Carolina, J. C. Marshall, T. L. Isenhour

2:10 Application of Signal Processing Techniques in Electrochemistry. P. Kaerk, Princeton Applied Research

2:30 TN-1710 DARSS System: Hardware and Software Capabilities for Optical Spectral Measurement. D. E. Osten, Tracor Northern

2:50 Evaporative Rate Analysis: Technique for Chemical Characterization of Surfaces. J. L. Anderson, ERA Systems

3:20 Angle Resolved Mass Spectrometry. J. J. Carmody, J. A. Laramee, R. G. Cooks, Purdue U

3:40 Microcomputer-Based Pulsed Ion Cyclotron Resonance Spectrometer. J. D. Breshears, U of California

4:00 Minicomputer System for Automation of Multiple Laboratory Instruments in Industrial Research Center. T. F. Niemann, Glidden Coatings & Resins, T. Provder, V. Metzger, R. J. Kearney

4:20 Laboratory Application of Microprocessor-Controlled 7-Channel Programmable Timer. A. J. Martin, Marlabs, M. Martin, E. J. Levy

4:40 Results of Computerization and Automation of Perkin-Elmer 240 Carbon, Hydrogen, and Nitrogen Analyzer. W. R. Bramstedt, L. D. Vargyas, D. E. Harrington, Diamond Shamrock Corp.

Symposium: Biomedical Applications of Ion Selective Electrodes II

Monday Afternoon, Room 235A

H. Freiser, *Presiding*

1:30 Automated Ion Selective Electrode Measurements Based on Flow Injection System with Lim-

1978 "PITTSBURGH" SPECIAL
Valid thru April 30, 1978

To Owners and Operators of the

Perkin-Elmer Model 240 Elemental Analyzer

and those who wish they had one.

C-H-N-S-O

To those of you who have a 240, we offer:—

1. Full automation of sample injection and all calculations of an existing 240 to handle 64 samples without operator attendance, including freight, field installation, and operator training — $10,400.
2. Single sample data handling system (all calculations) with solid state timing control of the 240 to increase production by 25% (5 samples per hour instead of 4), including freight, field installation, and operator training — $ 7,850.
   Single sample automatic injector for the above — 480.
3. Reconditioning of one existing 240 if ordered with item 1, or 2; parts at list price, no labor charge if done at our facility ((freight extra)
4. Any model Cahn automatic electro balance, less 10% if ordered with item 1, 2, or 5.

To those who wish you had a 240, we offer:—

5. Fully reconditioned, used 240's (subject to prior sale)
   - Automated as per item 1 — $14,400.
   - As per item 2, with single sample automatic injector — $12,330.

We accept surplus 240's as trade-in, and are also interested in purchasing used 240's outright.

Last, but not least, we sell tubes, supplies, and service parts for the 240 analyzers at savings up to 50% over P-E prices - and we like to serve you.

TERMS: 1% 10 - Net 30 Days. Prices valid in continental U.S.A. only.

WARRANTY: One year on parts and labor, F.O.B. our factory, except input/output printers, and Cahn balances, where manufacturers warranty applies.



CONTROL EQUIPMENT CORPORATION

220 TANNER STREET, LOWELL, MASS. 01851 • (617) 459-0573

CIRCLE 67 ON READER SERVICE CARD

An Award Winning Analytical Technique

ION CHROMATOGRAPHY

1977
I-R 100 AWARD
PITTSBURGH
APPLIED ANALYTICAL
CHEMISTRY AWARD
AND
VAALER AWARD
WINNER



Ion Chromatography (IC) analyzes ions in solution. IC is generally applicable to the separation and ppm-ppb detection of: **INORGANIC ANIONS, ORGANIC ACIDS, ORGANIC PHOSPHATES, AMMONIA, AMINES, QUATERNARY AMMONIUM SALTS, ALKALI METALS, ALKALI EARTH METALS.**

Due to the fact that IC analyzers separate the ions in a sample and detect them from 1% to trace level makes IC most appropriate in the following areas: (1) analysis in complicated matrices; (2) analysis of more than one ion simultaneously in a sample; (3) analysis of ions at low concentration in a large concentration of other ions; (4) analysis of trace (ppb) levels of ions; (5) the analysis of several samples of a given type, then several of a different type, etc.; and (6) automated analysis.

APPLICATION AREAS

AIR POLLUTION
Analysis of ambient aerosol filter extracts for nitrate and sulfate, sulfuric acid (SO_3) in stack gas, sulfite and sulfate in FGD scrubber liquors and trace ions in rain water.

WATER POLLUTION
Ion characterization of waste effluents, routine ion analysis of ground waters, nitrate-N and phosphate-P in hatchery and bio-pond water, chloride, sulfate and oxalate in paper mill effluent.

ELEMENTAL ANALYSIS
Trace level and interference free analysis of organic fluorine, chlorine, bromine, iodine, sulfur and phosphorus after Schoniger oxidation.

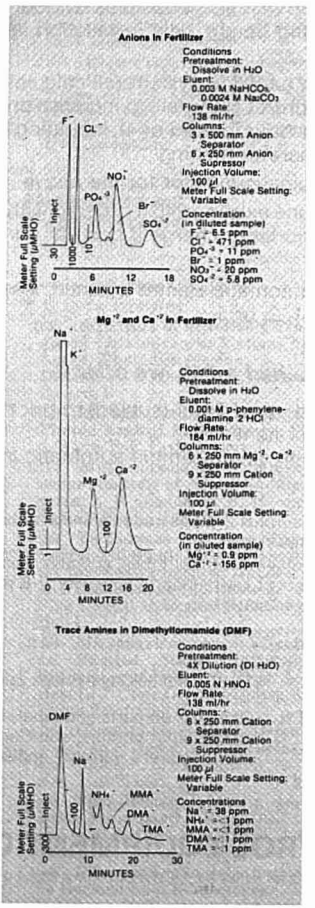
SOIL ANALYSIS
Direct anion analysis of KCl, ammonium acetate and ammonium fluoride, sulfuric acid or bicarbonate soil extracts.

BRINE ANALYSIS
Direct analysis of chlorate, sulfate, calcium and magnesium in 25% brine and 50% caustic solutions; phosphate, bromide, nitrate, sulfate, calcium and magnesium in 2% brine.

POWER PRODUCTION
Trace ion analysis in boiler, boiler feed and cooling tower waters.

QUALITY CONTROL
Fluoride, chloride, sulfate and chromate in plating bath process water, trace ions in electronic device process water, glycolate in surfactants, monomethyl amine in ethylenedichloride, thioacetic, thiolactic and thioglycolic acid in water, tetra-ethylammonium and tetra-N-butyl-ammonium bromide in water, mono-methylamine, dimethylamine and tri-methylamine in water, mono and dibutyl phosphate in water and halides and sulfate in foods and food additives.

NEW APPLICATIONS



UPCOMING EVENTS

SEMINAR SERIES PLANNED
Dionex will be conducting a one day seminar series in the following cities. There will be a formal slide presentation on the technique and applications of Ion Chromatography and an instrument will be available for demonstration and sample running. Please call us directly at 408-737-0700 (X224) to register or to request further information.

In the United States . . .

DATE/CITY	LOCATION
Monday, February 13 Atlanta	Peachtree Center Plaza 2110 Peachtree St. Atlanta, GA
Wednesday, February 15 Chattanooga	Red House & Motor Inn 9th & Broad Street Chattanooga, TN
Friday, February 17 Oakridge-Knoxville	Hyatt House 500 Hill Avenue Knoxville, TN

In Canada . . .

Monday, March 27, Toronto

Wednesday, March 29, Ottawa

Friday, March 31, Montreal

Shows

Pittsburgh Conference
February 27-March 3

Dionex will exhibit both a Model 10 & a Model 14 Ion Chromatograph in Booth 712. Representatives will be available to discuss the technique and applications. On Tuesday, 2/28, and Thursday, 3/2, from 4:30-7:00 at the Holiday Inn Lakeside there will be a cocktail session featuring a slide presentation on IC.

For information regarding applications of IC, circle the appropriate number on the information card or call the Dionex applications laboratory to discuss your particular application.

AIR POLLUTION
WATER POLLUTION
ELEMENTAL ANALYSIS
SOIL ANALYSIS
BRINE ANALYSIS
POWER PRODUCTION
QUALITY CONTROL
NEW APPLICATIONS

DIONEX™
A LICENSEE OF THE DOW CHEMICAL CO

Dionex Corporation
In the US contact: 1228 Titan Way, Sunnyvale, CA 94086, 408-737-0700
In Europe contact: 77 Tudor Drive, Yateley, NR. Camberley, Surrey GU17 7DB England, 01-464-7632

CIRCLE 41 ON READER SERVICE CARD

ited Dispersion. J. Ruzicka, Technical U of Denmark

2:15 New Developments in Chemically Sensitive Field Effect Transistors. J. Janata, U of Utah

3:10 Application of Field Effect Transistors to Chemical Sensing. P. Cheung, Case Western Reserve U

4:00 Panel Discussion on Current Status and Future of ISE's in Biomedical Applications. All Symposium Speakers

Liquid Chromatography—General I

Monday Afternoon, Room 235B

A. E. Kostyo, *Presiding*

1:30 Amberlite XAS Copolymers in HPLC: Separation of Sulfas. R. Sydor, D. Pietrzyk, U of Iowa

1:50 Use of Flat Bottom pH Electrodes and Flow-Through Assemblies in Liquid Chromatography. R. C. Barabino, P. J. Breno, M. H. Keyes, Owens-Illinois

2:10 Applications of High-Performance Paired Ion Liquid Chromatography in Pharmaceutical Analysis. L. G. Meehan, C. D. Muller, Smith Klein & French

2:30 Identification of Trace Metal Species in Water by Liquid Chromatography with Atomic Spectrometric Detection. G. N. Coleman, J. A. Koropchak, U of Georgia

2:50 Separation and Spectroscopy—Rapid Isolation and Identification via HPLC. R. W. Yost, J. M. Attebery, A. F. Poile, R. D. Conlon, Perkin-Elmer

3:20 Liquid Chromatography of Low Polarity Samples Using Infrared Detection. N. A. Parris, Du Pont

3:40 Precolumn Derivatization for Liquid Chromatography. F. L. Vandemark, G. J. Schmidt, W. Slavin, Perkin-Elmer

4:00 Protocol for Sample Analysis by HPLC. R. W. Stout, G. Dallas, S. D. Abbott, N. A. Parris, Du Pont

4:20 New Results and Developments in Preparative Liquid Chromatography. J. Levine, Instruments SA, J. Montastier, J. Huau, M. Porthault, Z. El Rassi

4:40 Design and Applications of New High-Temperature GPC/LC. R. J. Limpert, J. R. Nelson, W. A. Dark, Waters Associates

Symposium: Glass Capillary Gas Chromatography for Routine Analysis

Monday Afternoon, Little Theater

W. H. Suits, *Presiding*

1:30 New Developments in Glass Capillary GC (Plenary Lecture). G. Schomburg, Max-Plank Institute für Kohlenforshung

2:30 Importance of Sample Preparation for Reproducible Environmental Analysis. S. N. Chesler, H. Hertz, W. Mays, NBS

3:15 Method for Isolation, Identification, and Comparison of Tobacco Essential Oil Components. R. A. Lloyd, R. J. Reynolds Tobacco Co.

3:40 Role of Retention Indices and Wide Bore Glass Capillaries for Isolation and Identification of Essential Oil Components. J. Walradt, International Flavor and Fragrances

4:05 Columns vs. Glass Capillaries. D. Ottenstein, Supelco

4:30 Column Selection and Operating Parameters to Consider for High-Speed Analysis with Glass Capillaries. M. J. Hartigan, W. Averill, Perkin-Elmer

Atomic Absorption Spectroscopy II—Flameless

Monday Afternoon, Ball Room

J. D. Sember, *Presiding*

1:30 Determination of Gold and Copper Levels in Serum, Tissue, and Separated Serum Protein Fractions by Atomic Absorption Spectrometry Using Carbon Furnace Atomization. W. E. Smith, U of Strathclyde, D. H. Brown, H. Kamel, J. M. Ottaway

1:50 Phosphorus Determination Using Graphite Furnace Vaporization Coupled to Flame Photometry. W. R. Seitz, A. Driedger, U of New Hampshire

2:10 Rapid Determination of Low Concentrations of Lead in Paint by Flameless Atomic Absorption Spectroscopy. C. E. Cowan, C. H. Ke, PPG Industries

2:30 Flameless Atomic Absorption Determination of Gold in Potassium Cyanide Solution. J. D. Sember, M. B. Linkenheimer, S. D. Cifrulak, Calgon Corp.

2:50 Direct Determination of Copper and Iron in Solutions of Acrylamide by the Heated Graphite Atomizer. M. S. Vigler, A. Strecker, A. Varnes, Sohio Research

3:20 Investigation of Influence of Furnace Conditions on Matrix Effects in Graphite Furnace Atomic Absorption. R. D. Beaty, F. J. Fernandez, A. R. Knott, Perkin-Elmer

3:40 Further Developments and Applications of Profiled Tube Graphite Atomizer. R. A. Newstead, P. J. Whiteside, M. P. Wassall, Pye Unicam Ltd.

4:00 Determination of Volatile Metals in Biological Samples by Flameless Atomic Absorption Spectrometry. H. J. Issaq, NCI Frederick Cancer Research Center

4:20 Increased Accuracy and Precision in Furnace Atomic Absorption. M. W. Routh, Varian, K. G. Brodie, P. A. Bennett

4:40 Interferences in Determination of Lead with Graphite Furnace. D. C. Manning, W. Slavin, Perkin-Elmer

Instrument Automation

Monday Afternoon, Music Hall

H. Schultz, *Presiding*

1:30 Interfacing Dichrograph to Signal Averager or Minicomputer. D. O. Landon, ISA, A. Darier, W. Ungerer

1:50 Automated Data Reduction for Gel Permeation Chromatography. H. L. Silverman, D. Baker, R. Howard, Hewlett-Packard

2:10 Computer Automation of Cary CD Spectropolarimeter. V. C. Zadnik, R. Megargle, K. H. Pearson, Cleveland State U

2:30 Microcomputer - Assisted Photoacoustic Spectroscopy of Amorphous Solids. H. E. Eaton, J. D. Stuart, U of Connecticut

2:50 Spectral Fractionation of Mixtures Using Computerized Dispersive IR Spectrometer. R. W. Hannah, Perkin-Elmer

3:20 Microcomputer-Based Detector System for Coherent Raman Spectroscopy. D. J. Wallan, G. P. Ritz, M. D. Morris, U of Michigan

3:40 Simple Automated Infrared Analysis of Trace Contaminants in (Gasified) Liquid Oxygen. R. S. Sheinson, A. Kravitz, O. Ahmed, F. W. Williams, Naval Research Lab

4:00 Computerized Quality Control. P. O. Shapiro, H. C. Brunner, E. Godwin, R. Y. Shatz, Whatman

4:20 Foreground / Background Microprocessor Program for Real Time Data Manipulation and Large Computer Interface. A. F. Witt, S. L. Cooke, U of Louisville

4:40 Real Time Data Acquisition and Control Microcomputer System that Executes EPROM Resident Basic Application Programs. M. D. Maples, M & E Associates

Tuesday, February 28

Emission Spectroscopy

Tuesday Morning, Room 205

C. B. Clark, *Presiding*

8:30 Microwave-Induced Doped Helium Electrical Discharges. C.

K. Kohlmiller, T. H. Risby, Pennsylvania State U

8:50 Building of Low-Cost ICP–OES for Radionuclide Analysis. T. J. Golembeski, W. J. Lynch, New England Nuclear Corp.

9:10 Use of ICP–OES for Analysis of Highly Radioactive Samples. T. J. Golembeski, W. J. Lynch, New England Nuclear Corp.

9:30 Interelement Effects Observed When Ultrasonically Generated Aerosols Are Analyzed by Inductively Coupled Plasma–Atomic Emission Spectroscopy. R. E. Adams, K. W. Olson, V. A. Fassel, Iowa State U

9:50 Studies of Metal Excitation in Argon Intensity/Time Studies by Various Chamber Pressures. J. A. Norris, NBS

10:20 Approaches for Improvement of Accuracy in Simultaneous Multielement Determinations by Plasma Emission Spectroscopy. W. J. Haas, Jr., R. K. Winge, V. A. Fassel, R. N. Kniseley, Iowa State U

10:40 Optical Emission Analysis of Aluminum with Low-Voltage Discharge in Argon. P. D. Dalager, R. L. Conrad, A. L. Davison, Applied Research Labs

11:00 Advanced Readout Design for Optical Emission Spectrometers. J. K. Finster, R. M. Ajhar, R. J. Baker, A. L. Davison, Applied Research Labs

11:20 Plasma-Impedance of Inductively Coupled Plasma Torch and Its Variations. C. D. Allemand, Fisher Scientific, R. M. Barnes

11:40 New Direct Reading Spectroanalyzer: JY48. G. S. Hayat, ISA, I. M. Gani

Forensic, Drug, and Pharmaceutical Analysis

Tuesday Morning, Room 239

N. L. Alpert, *Presiding*

8:30 Computer Dispersive Spectroscopy Used in Forensic Applications. S. C. Pattacini, R. W. Hannah, Perkin-Elmer

8:50 Criteria for Determining Chemical and Radiochemical Purity of Drugs Derived from Synthesis. E. G. E. Jahngen, J. L. Percival, New England Nuclear Corp.

9:10 Characterizing Trace Evidence Samples by Gel Permeation Chromatography. K. E. Coraine, Waters Associates, W. W. McGee, J. R. Strimaitis

9:30 Quick, Quantitative, Picomole Esterification Procedure for Drug Analysis by Electron-Capture Gas Chromatography. J. Rudy, Pennsylvania State Harness Racing Commission

9:50 Separation of Heimia Alkaloids by Adsorption and Reverse-Phase High-Performance Liquid Chromatography. J. E. Zarembo, B. Douglas, J. Weisbach, E. R. White, L. B. Killmer, Smith Kline Corp.

10:20 Pharmaceutical Applications of Quantitative Florine-19 NMR Spectroscopy. D. B. Staiger, R. J. Warren, J. E. Zarembo, Smith Kline Corp.

10:40 Ion-Pair and Hydrophobic Chromatography of Pharmaceutical Compounds on Ultrahigh-Efficiency Reverse-Phase Columns. E. R. White, J. E. Zarembo, Smith Kline Corp.

11:00 Fluorometric Determination of Chlorzoxazone in Dosage Forms and Biological Fluids. J. T. Stewart, C. W. Chan, U of Georgia

11:20 Comparison of Drug Analysis by PID and FID. L. Jamarillo, J. N. Driscoll, J. Ford, HNU Systems

11:40 Improving Antiepileptic Drug Analyses by Using Multiple Internal Standards and Data Systems. H. B. Bente, Hewlett-Packard

Symposium: Quantitative Infrared Spectroscopy by FT–IR

Tuesday Morning, Room 3A

J. R. Durig, *Presiding*

Twelfth Meeting of Fourier Transform Spectroscopy Group

8:30 FT–IR Current and Future Utilization in Industry. S. T. Dunn, J. I. Steele, Dunn Technology

9:05 Adaptation of Quantitative FT–IR to Process Control. D. R. Mattson, R. L. Julian, Nicolet Instrument Corp.

9:40 Quantitative Measurements by Diffuse Reflectance Infrared Fourier Transform (DRIFT) Spectroscopy. P. R. Griffiths, M. P. Fuller, Ohio U

10:30 Quantitative Determinations in Absorbance Subtraction. K. Krishnan, Digilab

11:00 Quantitative FT–IR Spectroscopy of Polymer Surfaces Using Variable Angle ATR. D. F. Smith, Union Carbide

11:30 Molecular Interactions in Hemoglobin and Other Biological Materials. J. O. Alben, Ohio State U

Electroanalytical Chemistry I

Tuesday Morning, Club Room B

R. T. Oliver, *Presiding*

8:30 Simplified Computing Polarographic Analyzer. E. P. Kujawa, Brinkmann Instruments, J. D. McLean, J. F. Holland, K. Hertach

8:50 Speciation of Trace Level Arsenic(III) and Arsenic(V) by Differential Pulse Polarography. T. M. Thorpe, F. T. Henry, T. O. Kirch, Miami U

9:10 Intermodulation Polarograph. W. J. Mergens, Hoffman-La Roche, G. W. Ewing

9:30 Spinning Dropping Mercury Electrode and Electrochemical Theory. H. J. Mortko, R. E. Cover, St. John's U

9:50 Voltammetric Determination of Ferrous and Ferric Iron. W. M. Moore, Standard Oil Co. (Ohio)

10:20 Recent Advances in Voltammetric Electrode Systems. J. L. Smith, B. N. Whitlock, R. A. Nadolny, Princeton Applied Research

10:40 Evaluation of Accuracy and Reproducibility of Anodic Stripping Voltammetry by Automatic Instrumentation. E. Kral, Princeton Applied Research

11:00 Minicomputer - Controlled, Background-Corrected, Rapid-Scan Stripping Voltammetry. S. D. Brown, B. R. Kowalski, U of Washington

11:20 Computer-Optimized Potential-Step Voltammetry. P. A. Boudreau, L.H.L. Miaw, S. P. Perone, Purdue U

11:40 Characterization of Voltammetric Electrode Processes by Pattern Recognition Techniques. R. A. DePalma, Q. V. Thomas, S. P. Perone, Purdue U

Symposium: Advances in Applied Surface Analysis I (ASTM E-42)

Tuesday Morning, Room 235A

N. S. McIntyre, *Presiding*

8:30 Introduction to Symposium. D. M. Hercules, U of Pittsburgh

8:40 Auger Electron Spectroscopic Studies of Semiconductor Surfaces. P. H. Holloway, Sandia Labs

9:15 Energy Calibration of Electron Spectrometers. C. D. Wagner

10:10 Electron Spectroscopy in Catalysis Research. J. S. Brinen, American Cyanamid

10:45 Corrosion Studies Using Electron Spectroscopy. J. E. Castle, U of Surrey

11:20 Ion Bombardment for Depth Profiling. R. E. Honig, RCA Labs

Liquid Chromatography—General II

Tuesday Morning, Room 235B

C. G. Creed, *Presiding*

Our gases are rare. Our hardware is not.



Every rare and specialty gas you'll ever need—from Argon and CO to SO_2 and Xenon. Plus every piece of hardware and equipment you'll ever need to use them. Like these valves, for example. Plus flowmeters, regulators and aluminum sample cylinders—the works. For your *free* copy of our new 1977 catalog listing them all, and including complete physical properties and equipment recommendations, call Hank Grieco at (201) 464-8100. Or send this coupon to Airco Industrial Gases.

Name_____ Title _____

Company_____

Address_____

City_____ State_____ Zip_____

Airco Industrial Gases, Rare & Specialty Gases Dept., 575 Mountain Ave., Murray Hill, NJ 07974.

CIRCLE 48 ON READER SERVICE CARD

PROGRAM

8:30 Increased Efficiency and Reproducibility in HPLC by Use of Coaxial Frit Injector. V. S. Venturella, B. Buglio, Hoffman-La Roche

8:50 Rapid Scan of Technical Literature for LC Problem Solving. J. M. Attebery, R. W. Yost, Perkin-Elmer

9:10 Reversed-Phase HPLC Solvent Selectivity. S. R. Bakalyar, Spectra-Physics

9:30 Effect of Change in Solvent on Chromatographic Peak Shapes. P.K.C. Tseng, L. B. Rogers, U of Georgia

9:50 Effect of Guard Column on HPLC Column Life and Performance. D. K. Igou, R. C. Williams, Du Pont

10:20 Column Selection for Totally Automated HPLC. J. R. Gant, Technicon Industrial Systems

10:40 Development of Separation Method in High-Performance Liquid Chromatography (HPLC). M. Riedmann, Hewlett-Packard

11:00 Versatile New Microprocessor Controller Gradient Elution System for Liquid Chromatography. S. J. Moulton, M. Hewins, Pye Unicam Ltd.

11:20 Column Temperature Effects in Reversed-Phase High-Performance Liquid Chromatography. D. R. Baker, D. R. Gere, Hewlett-Packard

11:40 Column Temperature Effects in HPLC. D. Colby, H. McNair, VPI & SU

Gas Chromatography—Applications

Tuesday Morning, Little Theater

M. V. Senneway, *Presiding*

8:30 Applications of Glass Capillary Gas Chromatography in Field of Nuclear Fuels Reprocessing and Waste Management. S. J. Johnson, Rockwell Hanford Operations

8:50 Pyrolysis Gas Chromatography of Coal Tar and Petroleum Pitches. J. L. Glajch, J. A. Lubkowitz, L. B. Rogers, U of Georgia

9:10 Identification of 1,8, 1,2, and 2,3 Dibasic Acids of Naphthalene as Oxidation Products of Solvent Refined Lignite. R. C. Duty, R. Hayatsu, R. Scott, L. Moore, M. Studier, R. Winans, Illinois State U

9:30 Determination of Equol in Commercial Conjugated Estrogen Formulations. K. M. McErlane, G. Carignan, N. M. Curran, B. A. Lodge, Drug Research Labs

9:50 Novel and Rapid Method for Preparation of Methyl Esters for Gas Chromatography: Application to Determination of Fatty Acids of Edible Fats and Oils. W. C. Kossa, D. K. McCreary, R. R. Kurtz, S. Ramachandran, R. S. Henly, Applied Science Labs

10:20 Synthesis and Gas-Liquid Chromatographic Application of New Nematic Liquid Crystals. W. L. Zielinski, Jr., G. M. Janini, G. M. Muschik, R. I. Sato, NCI Frederick Cancer Research Center

10:40 Substantially Improved Method for Separation and Analysis of Metabolic Phenol Isomers of Benzo(a)Pyrene by Gas-Liquid Chromatography on Liquid Crystals. W. L. Zielinski, Jr., NCI Frederick Cancer Research Center, G. M. Janini, G. M. Muschik, R. I. Sato, R. M. Young, D. M. Jerina, D. Thacker, H. Yagi, W. Levin

11:00 Adsorption Study of Solute-Brush Interactions on Chemically Bonded Phase. H. L. Liao, Lederle Labs, N. M. Trieff

11:20 Response Surface Methodology in Gas Chromatography. S. L. Morgan, C. A. Jacques, U of South Carolina

11:40 Rapid Determination of Vapor Concentration in Atmosphere Using New Preconcentration Gas Chromatography Technique. A. Linenberg, Xonics, R. Siegel, R. N. Matherne

Atomic Absorption Spectroscopy III

Tuesday Morning, Ball Room

J. J. McGovern, *Presiding*

8:30 Extending Dynamic Range of Atomic Absorption Spectrometry. T. C. O'Haver, J. M. Harnley, U of Maryland

8:50 Determination of Detection Limits for Complex Samples Analyzed by Graphite Furnace Atomic Absorption. J. M. Harnely, T. C. O'Haver, U of Maryland

9:10 Loss of Lead from Digested Whole Blood in Flameless AA Analysis. R. Heaton, U of Rhode Island, J. Maney, J. Fasching

9:30 Application Areas of High-Performance Background Correction System for Atomic Absorption Spectrophotometers. R. A. Newstead, P. J. Whiteside, Pye Unicam Ltd.

9:50 Novel Autosampler for AA Furnace Atomization. R. G. Schleicher, D. A. Leighty, Instrumentation Lab

10:20 New Multielement Atomic Absorption and Fluorescence Instrument. E. D. Salin, J. E. Ingle, Jr., Oregon State U

10:40 Methods Development for Sequential Multielement Atomic Absorption Analysis. R. D. Ediger, W. B. Barnett, S. M. Gamache, D. L. Wilson, Perkin-Elmer

11:00 Two-Channel Analysis by Atomic Absorption Spectroscopy. R. H. Emmel, H. L. Kahn, Instrumentation Lab

11:20 Automated AA Spectrophotometer. T. W. Barnard, W. B. Barnett, C. G. Fisher III, D. L. Smith, A. J. Russo, Perkin-Elmer

11:40 Study of Sample Handling and Calibration for Electrothermal Atomic Absorption Spectrophotometry Using Solid Samples. R. A. Newstead, W. J. Price, P. J. Whiteside, T. C. Dymott, I. Bowater, Pye Unicam Ltd.

Symposium: Keeping Up with Microcomputers II

Tuesday Morning, Music Hall

J. M. Rombough, *Presiding*

8:30 Introduction and Overview. F. W. Plankey, U of Pittsburgh

8:40 Software at Machine and Assembly Language Levels. C. Titus, Tychon

9:25 Convers—A Modular Software Package. M. B. Denton, U of Arizona

10:20 In-Depth Study of Signal Processing Application of Microcomputer. T. C. O'Haver, U of Maryland

11:05 Roundtable Discussion. F. W. Plankey, Chairman. Panelists: H. V. Malmstadt, G. Horlick, C. E. Enke, S. R. Crouch, C. Titus, M. B. Denton, T. C. O'Haver

Surface Analysis I

Tuesday Afternoon, Room 205

G. C. Mateescu, *Presiding*

1:30 Auger Electron Spectroscopic Study of Impurity Segregation in Various Forms of Titanium. C. P. Lofton, General Electric, W. E. Swartz, Jr.

1:50 Auger/X-ray Photoelectron Spectroscopic Depth Profiling Techniques Applied to Ultrathin Titanium Films. W. E. Swartz, Jr., U of South Florida, C. P. Lofton

2:10 Trace Arsenic Analysis with ESCA. M. B. Carvalho, D. M. Hercules, U of Pittsburgh

2:30 ESCA and Auger Study of Iron Borides. D. J. Joyner, O. Johnson, D. M. Hercules, U of Pittsburgh

2:50 Quantitative Analysis of Chemical Composition of Silicon Nitride Films by Means of X-ray Photoelectron Spectroscopy. K. Usami, K. Mukai, E. Kitazume, A. Hiraiwa, Hitachi, Ltd.

3:20 ESCA Studies of Lead Sulfide Oxidation. D. S. Zingg, D. M. Hercules, U of Pittsburgh

How Carle's Patented* "HTS" makes GC analysis of samples with hydrogen easy and practical

It's no secret to chromatographers that hydrogen spells trouble—which is why Carle scientists invented the HTS. Determining hydrogen is devilish because of a TCD's non-linear, low sensitivity response to hydrogen when helium is the carrier.

"HTS" stands for Hydrogen Transfer System—a unique device just granted a patent in January, 1978*. Taking advantage of the remarkable properties of a palladium alloy, the HTS beats the devil by selectively transferring the *entire* hydrogen peak from the column effluent into a nitrogen carrier—while leaving all other components in the helium carrier.

Carle "puts a price on the answer" with eight different factory-dedicated gas chromatographs incorporating an HTS. Priced from $3690 to $7435, each one analyzes a different type of hydrogen containing sample. These "answers for a price" all depend on the Hydrogen Transfer System for their unique ability to detect hydrogen in complex mixtures.

The HTS chromatographs, a Carle exclusive, offer five significant benefits to anyone who needs to analyze a mixture containing hydrogen:

1) Excellent, near-equal sensitivity for both hydrogen and all the other components—regardless of whether major or minor H_2 concentrations are involved.

2) Practical for analyzing virtually all sample types that have hydrogen present—from refinery gases to chlorine streams.

3) Predictable response to hydrogen from 150 ppm up to 100%. In many cases detection limit extends down to 20 ppm.

4) All positive peaks without any type of polarity switching during the analysis.

5) Eliminates the errors inherent in other approaches using multiple instruments on the same sample.



To learn more about the Hydrogen Transfer System, send for your free copy of The HTS Story—16 pages explaining how it works, detailing operational parameters and showing performance data and sample chromatograms. Circle the number below or call Carle direct at our new Anaheim facility (714) 761-9000.



*T. Johns and E. A. Berry, U.S. Patent No. 4,067,227. Mr. Johns is Director of Research at Carle Instruments and Mr. Berry is Senior Electronic Engineer.

CARLE
INSTRUMENTS, INC.
A Hach Company

1200 Knollwood Circle, Anaheim, CA 92801, (714) 761-9000

Circle No. 53

See HTS gas chromatographs at Cleveland: Booths 709/711

3:40 In-Situ AES and ESCA Analysis of Electrochemically Formed Iron Oxides. D. A. Stout, Ohio State U, J. B. Lumsden, R. W. Staehle, G. Gavelli

4:00 XPS Quantitative Studies of Mixed Oxide-Metal Surfaces. N. S. McIntyre, Atomic Energy of Canada, Ltd.

4:20 Characterization of Adhesive-Adherend Interphase by Auger Electron Spectroscopy. J. S. Solomon, U of Dayton, N. T. McDevitt

4:40 Surface Analysis and Adhesive Bonding. III. Titanium 6-4. D. W. Dwight, W. Chen, J. P. Wightman, VPI & SU

Clinical Chemistry and Biochemical Analysis

Tuesday Afternoon, Room 239

R. M. Windisch, *Presiding*

1:30 HPLC Analysis of Acetaminophen and Its Metabolites in Serum. B. Haeckler, Duquesne U, J. Feldman, C. Corder

1:50 Rapid Determination of Quinidine in Plasma by High-Performance Liquid Chromatography. R. G. Achari, J. L. Baldridge, L. Yu, Cooper Labs

2:10 Determination of Theophylline by HPLC. D. J. Popovich, E. T. Butts, C. J. Lancaster, Whatman

2:30 Determination of Steroids by LC Using Fluorescence Labeling. G. J. Schmidt, F. L. Vandemark, W. Slavin, Perkin-Elmer

2:50 New Approach to Enzyme Assay Accessories for UV/Visible Spectrophotometers. D. Irish, J. E. Steward, A.R.L. Moss, Pye Unicam Ltd.

3:20 Calcium Ion-Selective Electrodes for Biomedical Applications. J. D. R. Thomas, G. J. Moody, N. S. Nassory, UWIST

3:40 Determination of Thyroxine by Fluorodensitometry of Thin-Layer Chromatograms. J. C. Touchstone, U of Pennsylvania, M. F. Dobbins, L. M. Cummins

4:00 Study of Hydrophobically Immobilized Lipase for Analysis of Serum Triglycerides. R. S. Schifreen, U of Minnesota, P. W. Carr, M. M. Miller

4:20 Pyrolysis Gas-Liquid Chromatography of Enzymes. N. D. Danielson, J. L. Glajch, L. B. Rogers, U of Georgia

4:40 Metabolic Profiles of Low-Molecular-Weight Constituents of Human Cerebrospinal Fluids. S. L. Smith, Indiana U, M. Novotny, E. L. Weber

Symposium: Chemical Analysis as Applied to Steel Industry

Tuesday Afternoon, Room 3A

B. M. LaRue, *Presiding*

1:30 Separation and Selective Determination of Nitride Phases in Steel. D. Svedung, Jernkontoret, Sweden

2:20 Universal Technique for Rapid Dissolution of Materials Encountered in Steel Industry. O. P. Bhargava, Steel Co. of Canada, Ltd.

3:30 Sampling and Sample Preparation of Molten Steel in Steel Industry. R. L. Zickefoose, National Steel Corp.

4:15 Reference Material for Iron and Steel Industry. R. E. Michaelis, NBS

Electroanalytical Chemistry II

Tuesday Afternoon, Club Room B

J. P. McKaveney, *Presiding*

1:30 Dual-Test Electrode for Programmed Potential Analysis. P. H. Davis, W. R. Matson, W. W. Mogayzel, R. Vitukevich, E. W. Zink, Environmental Sciences Associates

1:50 Charge Transfer Analysis of Anions and Cations at Trace Levels. P. H. Davis, W. R. Matson, W. W. Mogayzel, R. Vitukevich, E. W. Zink, Environmental Sciences Associates

2:10 Power-of-Time Chronopotentiometry. L. H. Chow, Warner-Lambert Co., G. W. Ewing

2:30 Ion-Selective Electrode Control of H_2S in Industrial Effluents. R. T. Oliver, Foxboro Co.

2:50 Conductimetric Gas Sensor—New Approach to Gas Sensing Electrodes. M. J. Brand, H. A. Himpler, Texas A & M U

3:20 Estimation of Ion-Selective Instrument Parameters. T. A. Brubaker, Colorado State U, R. W. Tracy, J. W. Frazer

3:40 Self-Modifying Potentiometric Titrations for Use with Ion-Selective Electrodes. J. W. Frazer, Lawrence Livermore Lab, L. P. Rigdon, R. W. Tracy

4:00 Determination of Halides and Titanium by Controlled Potential Coulometry. W. M. Peterson, Princeton Applied Research

4:20 Controlled Current Coulometric Titration of Acids and Bases. J. A. Dougherty, Petrolite Instruments

4:40 New Coulometric Water Titrator. K. A. Lindblom, L. B. Eppstein, J. K. Kroeger, M. Weiser, G. B. Levy, Photovolt Corp.

Symposium: Laboratory Automation I—Computerization: Some Case Studies

Tuesday Afternoon, Room 235A

G. A. Gibbon, *Presiding*

1:30 Computerization—A Laboratory Manager's Overview. H. Schultz, PERC/DOE

1:45 Developing Specification for Computerization of Analytical Laboratory. G. Gould, V. Mazzone, Warner Labs

2:25 Implementation of Specification for Analytical Laboratory. M. P. Lepanto, Purvis Systems

3:30 From Chemistry to Fortran—An In-House Approach. J. M. Rombough, USS Chemicals

4:10 Instrument Vendor's View of Laboratory Automation, Now and the Future. D. L. Harris, L. Mikkelsen, Hewlett-Packard

4:50 Discussion

Liquid Chromatography—Detectors

Tuesday Afternoon, Room 235B

C. E. Gonter, *Presiding*

1:30 Evolution of Spectroscopic Detectors in LC. R. D. Conlon, C. C. Helms, E. B. Delany, Perkin-Elmer

1:50 Low-Cost, High-Performance Multiwavelength Detector for HPLC. D. F. Schaack, A. L. Cordry, R. W. Allington, Instrumentation Specialties Co.

2:10 HPLC Applications with High Sensitivity Discrete Wavelength UV Detector. D. W. Janzen, B. E. Leaver, P. J. Mondron, Laboratory Data Control

2:30 Fundamental and Practical Aspects of 214-nm Discrete Wavelength Detection for HPLC. M. N. Munk, D. W. Janzen, B. E. Leaver, Laboratory Data Control

2:50 New Low-Cost Filter Fluorescence Detector for Liquid Chromatography. B. E. Leaver, D. W. Janzen, P. J. Mondron, Laboratory Data Control

3:20 Fast Scanning UV Detector for High-Pressure Liquid Chromatography. L. J. Anthony, K. Biemann, MIT

3:40 Voltammetric/Amperometric Detector for Nano and Subnanogram Levels in HPLC. E. P. Kujawa, Brinkmann Instruments, P. Rach, S. L. Migdal

4:00 Advantage of Multiple Detectors in High-Performance Liquid Chromatography. R. E. Majors, S. R. Abbott, E. L. Johnson, Varian

MOLECULAR WEIGHT DISTRIBUTION IN MINUTES:

The End to GPC Column Calibration and Manual Calculations.

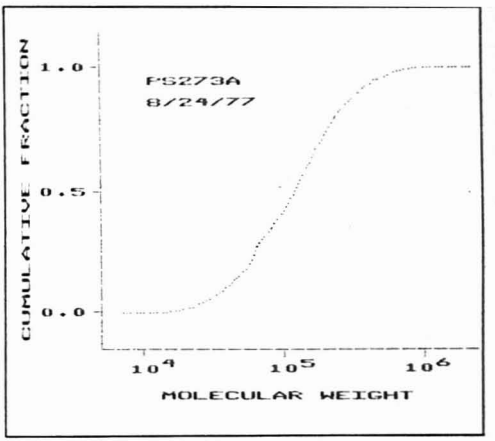
Now, molecular weight distributions can be calculated in real-time and plotted automatically with the new Chromatix KMX-6/DP Molecular Weight Data Processor. No GPC column calibration or manual calculations are required.

This unique new device operates in conjunction with the KMX-6 Low Angle Light Scattering Photometer and a gel permeation chromatograph. While your sample elutes from the GPC, the KMX-6/DP acquires data from the KMX-6 and the GPC. Simultaneously, the KMX-6/DP calculates the absolute solute molecular weight (not molecular size, as with conventional GPC techniques).

Within minutes after sample elution, you have a complete plot of the molecular weight distribution, plus the number-average, weight-average, and z-average molecular weights as well.

Whether you have one sample or a hundred, the KMX-6/DP can be preprogrammed for sequential analysis of samples with an auto-sampler equipped GPC.

If you'd like to learn more about how to reduce your polymer characterization workload, circle the numbers below or contact Chromatix for complete information. **Circle No. 37** for brochure. **Circle No. 38** for application information. **Circle No. 39** to have a technical representative call.

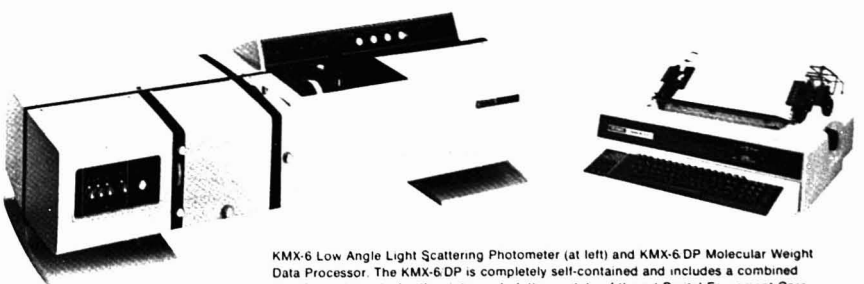


Portion of KMX-6/DP printout showing plot of molecular weight distribution.

chromatix

560 Oakmead Parkway
Sunnyvale, CA 94086
Phone: (408) 736-0300

D6903 Neckargemünd 2
Unterestrasse 45a
West Germany
Phone: (06223) 7061/62
Telex: 461691



KMX-6 Low Angle Light Scattering Photometer (at left) and KMX-6/DP Molecular Weight Data Processor. The KMX-6/DP is completely self-contained and includes a combined input/output terminal with printer and plotter, a state-of-the-art Digital Equipment Corp. LSI-11 microcomputer, instrument interfaces, and complete software for both on-line GPC analyses and static weight-average molecular weight calculations.

4:20 Nitrogen-Selective Detector for Liquid Chromatography. K. R. Hill, Agricultural Research Service, H. Crist

4:40 Electron Capture Detector for Liquid Chromatography. S. J. Moulton, P. J. Ridgeon, Pye Unicam Ltd.

Gas Chromatography—Inlet Systems & General

Tuesday Afternoon, Little Theater
J. Q. Walker, *Presiding*

1:30 Ghost-Cut-Type Sample Injection Port for Gas Chromatograph. K. Shiomi, Y. Hayashi, T. Haruki, Shimadzu Seisakusho Ltd.

1:50 Modern Third-Generation Sampling Systems for Laboratory Gas Chromatographic Instruments. E. W. March, Perkin-Elmer, B. Kolb, B. Welton

2:10 Semiautomatic Accessory for Gas Chromatographic Head-Space Analysis. B. Kolb, P. Pospisil, M. Jaklin, D. Boege, Bodenseewerk Perkin-Elmer

2:30 Headspace Gas Chromatography. I. Design of Automatic Sampler for High-Temperature Headspace Analysis. R. E. Arner, D. E. White, J. B. Pausch, G. F. Pfeiffer, BF Goodrich

2:50 Headspace Gas Chromatography. II. Performance of Automatic Sampler for High-Temperature Headspace Analysis. R. P. Lattimer, J. J. Cangemi, J. B. Pausch, BF Goodrich

3:20 Automated Capillary GC Splitless Sampling. A. C. Brown III, F. J. Yang, S. P. Cram, Varian

3:40 High-Performance Radial Chromatography (HPRC). R. K. Vitek, D. M. Kent, Camag

4:00 Applications of New GC Precolumn Venting System. R. H. Waltz, D. Newhouse, L. D. Johnson, F. Kaiser, Analytical Biochemistry Labs

4:20 Evaluation of Nonmetallic Ferrules Used in Sealing Gas Chromatographic Glass Columns (Graphite, Teflon, and Vespel). N. W. Armstrong, E. N. Armstrong, M. J. Dreksler, J. Scully, L. C. Co.

4:40 Comparison of High-Temperature Septa for Gas Chromatography. V. M. Olsavicky, Mobay Chemical Corp.

Atomic Absorption Spectroscopy IV

Tuesday, Afternoon, Ball Room
E. S. Hodge, *Presiding*

1:30 New Atomic Absorption Spectrophotometer with Novel Data Readout System. S. B. Smith, Jr., P. Moran, R. G. Schleicher, Instrumentation Lab

1:50 Comprehensive Low-Cost Data Processing System for Atomic Absorption Spectrophotometry. R. A. Newstead, T. J. Stockdale, P. J. Whiteside, Pye Unicam Ltd.

2:10 Fundamental Aspects of Sputtering Atomization Cell. D. A. McCamey, T. M. Niemczyk, U of New Mexico

2:30 Experience with Demountable, High-Intensity Lamp. S. A. Myers, Perkin-Elmer

2:50 Comparison of Intensity of Hollow Cathode Lamps to 300-W Eimac Xenon Arc Lamp for Continuum-Source Atomic Absorption Spectrometry. T. C. O'Haver, U of Maryland, J. M. Harnley, A. T. Zander

3:20 Wider Working Range in Flame Atomic Absorption. M. W. Routh, Varian, K. G. Brodie, P. A. Bennett

3:40 Nonspecific Resonance Monochromator for Atomic Absorption. J. N. Bower, J. D. Winefordner, U of Florida

4:00 Some Observations on Nebulizer-Spray Chamber Design, Construction and Operation as Sample Introduction Systems for Use in Atomic Flame Emission, Absorption, and Fluorescence Spectrophotometry. J. Bradshaw, S. Bayer, S. Weeks, H. Haraguchi, J. D. Winefordner, U of Florida

4:20 Measurement of Relative Atomic Transition Probabilities Using Flame Atomic Absorption Spectroscopy. R. J. Brown, M. L. Parsons, Arizona State U

4:40 Spatial Distribution of OH Radicals in Air Acetylene Flame. G. J. Keefe, G. J. Bastiaans, Georgetown U

Symposium: Spectroscopy in England

Tuesday Afternoon, Music Hall
N. Sheppard, *Presiding*

1:30 Structural Investigations. E.A.V. Ebsworth, U of Edinburgh

2:15 Resonance Raman Spectra of Inorganic Molecules and Ions. R. J. Clark, University College

3:20 Spectroscopy in British Industry. H. A. Willis, ICI Ltd.

4:10 Infrared and Raman Spectroscopic Studies of Molecules Chemisorbed on Catalysts. N. Sheppard, U of East Anglia

Wednesday, March 1

Raman Spectroscopy

Wednesday Morning, Room 205
F. R. Brown, *Presiding*

8:30 MOLE: Some Applications of Molecular Microprobe to Microanalytical Problems. M. Leclercq, Lirinord Instruments, D. O. Landon

8:50 Resolution Enhancement in Raman Spectra. B. J. Bulkin, K. Krishnan, Polytechnic Institute of New York

9:10 Temperature Regulated 180°-Excitation Raman Cell for Biological Samples. J. S. Ard, USDA

9:30 Computer-Controlled Coherent Anti-Stokes Raman Spectroscopy. G. W. Martin, L. B. Rogers, L. A. Carreira, U of Georgia

9:50 Development of CARS as Tool for Combustion Diagnostics. S. Lemont, Naval Research Lab, W. M. Shaub, R. W. Gammon, A. B. Harvey

10:20 Catecholamine Assay by Coherent Raman Spectroscopy. J. Haushalter, M. D. Morris, U of Michigan

10:40 Surface Reactions on Silver-Zeolite Molecular Sieves Monitored by Laser-Raman Spectroscopy. P. J. Trotter, Eastman Kodak

11:00 Detection and Identification of Phenolic Pollutants in Water by Resonance Raman Spectroscopy. L. Van Haverbeke, Rijksuniversitair Centrum Antwerpen, M. A. Herman, C. W. Brown

11:20 Infrared and Raman Spectra of Corrosion Films on Iron. R. J. Thibeau, C. W. Brown, A. Z. Goldfarb, R. H. Heidersbach, U of Rhode Island

11:40 Raman and Infrared Spectra of CF_3OOX Compounds. A. S. Manocha, Kansas State U, D. D. Des Marteau, R. M. Hammaker, C. J. Marsden

Atomic Fluorescence Spectroscopy

Wednesday Morning, Room 239
M. L. Parsons, *Presiding*

8:30 Some Considerations of Design and Use of Flame Atomic Fluorescence Spectrometer for Analysis of Clinical Materials. R. G. Michel, U of Strathclyde, M. L. Hall, J. M. Ottaway, G. S. Fell

8:50 CW Laser-Excited Atomic Fluorescence in Flames. M. Blackburn, J. Mermet, J. D. Winefordner, U of Florida

Cahn now makes it easier



with the
NEW
CAHN Series-20
Balances

The new Series-20 digital Balances automatically weigh up to 3.5g and offer sensitivity to 0.1μg. The new push-button tare system is unique and the only full-range tare system available. High sensitivity weighing is exceptionally fast and precise with these new Series-20 Balances. There is no doubt about it – Cahn Now Makes It Easier! There's a new Series-20 model for every requirement and price range.

CAHN 25 The full capability balance with portability; a unique push-button tare; full plus/minus ranges of 2, 20, 200 and 1000mg; widest range electrical zero; higher capacity of 3.5g; ultimate sensitivity and precision of 0.1μg.

CAHN 27 The full capability balance with a free-standing weighing chamber for remote and weigh-below applications.

CAHN 23 Users requiring only the more popular 20mg range, 1.5g capacity and 1.0μg sensitivity will benefit from this more economically priced model.

CAHN 21 For applications not requiring push-button tare even greater economy is found in this model. All other Series-20 features included.

For complete details ask your Cahn representative for the new Cahn Series-20 brochure or contact:

precision balances for 100 grams and less.



Ventron

CAHN

Cahn Instruments/A Division of Ventron Corporation
16207 South Carmenita Road/Cerritos, CA 90701 U.S.A.
Telephone 213-926-3378 • TWX 910-583-4806

CIRCLE 46 ON READER SERVICE CARD

The New...

See us at booth 1522
"Pittsburgh 78"

NEC

EXAC™ Energy Dispersive X-Ray Spectrometers



Solve today's problems with the *most flexible* computer-based system available...and be ready for tomorrow's challenges!

EXAC™ Features...

- Comprehensive library of programs written in the Spectroscopy Language of Today—NEC BASIC II
- Unique operating simplicity via conventional push button control panel—and easy-to-write programs in user-interactive NEC BASIC II
- Unexcelled expandability in hardware and software

Find out more about NEC's bulk and micro-analysis x-ray spectrometer systems. Phone or write:

Nuclear Equipment Corporation
963 Industrial Road
San Carlos, California 94070
Phone: (415) 591-8203

78/02

CIRCLE 143 ON READER SERVICE CARD

9:10 Fluorescence Spectrometry in Inductively Coupled Plasma Using Continuous Wave Dye Laser. B. D. Pollard, M. B. Blackburn, S. Nikdel, J. D. Winefordner, U of Florida

9:10 Application of Synchronously Pumped Dye Laser to Atomic Fluorescence Spectroscopy. W. T. Barnes, F. E. Lytle, Purdue U

9:50 Pulsed Laser-Excited Atomic Fluorescence. S. Weeks, H. Haraguchi, J. D. Winefordner, U of Florida

10:20 Tilting Filter Atomic Fluorescence Spectrometry. F. Lipari, F. W. Plankey, U of Pittsburgh

10:40 Trace Metal Analyses of Petroleum, Petroleum Products, and Substitutes by Atomic Fluorescence Spectrometry. D. W. Brinkman, M. L. Whisman, ERDA

11:00 Evaluation of Eimac Xenon Source for Excitation in Atomic and Molecular Luminescence Spectrometry. K. M. Aldous, J. S. Garden II, New York State Department of Health

11:20 Optimization and Signal-to-Noise Ratio Studies of Flame Atomic Absorption, Emission, and Fluorescence Measurements. J. D. Ingle, Jr., N. W. Bower, Oregon State U

11:40 Trace Metal Determinations in Real Samples Using Computer-Controlled Slew-Scan Atomic Emission/Fluorescence Spectrometer. A. H. Ullman, B. D. Pollard, G. D. Boutilier, J. D. Winefordner, U of Florida

Fourier Transform Infrared Spectroscopy

Wednesday Morning, Room 3A

J. G. Grasselli, *Presiding*

8:30 Far-IR Studies of Molecular Sieve. D. D. Saperstein, A. J. Rein, Merck Sharp and Dohme Research Laboratories

8:50 Fourier Transform Infrared Studies of Metal-18-Crown-6 Complexes. A. J. Rein, Merck Sharp & Dohme, D. D. Saperstein, R. H. Herber

9:10 Vibrational Spectroscopic Study of Bromination of Diethyl Fumarate on Silica Surface. J. M. Casper, J. E. Rice, Polytechnic Institute of New York

9:30 Instant Sample Preparation for FT-IR. T. Hirschfeld, Block Engineering

9:50 High-Resolution FT-IR Experiments. C. A. Anderson, D. R. Mattson, R. L. Julian, Nicolet Instrument Corp.

10:20 FT in FT-IR. D. R. Mattson, Nicolet Instrument Corp.

10:40 Quantitative FT-IR—Test Spectra Selection Criteria and Interpretation. D. R. Mattson, Nicolet Instrument Corp.

11:00 Confidence Spectra. T. Hirschfeld, Block Engineering

11:20 Scatter Elimination in FT-IR Spectra. T. Hirschfeld, Block Engineering

11:40 Fourier Transform Ion Cyclotron Resonance. C. L. Wilkins, M. L. Gross, R. B. Spencer, S. Ghaderi, U of Nebraska

Laboratory Management and Automation

Wednesday Morning, Club Room B

S. Pollack, *Presiding*

8:30 Microprocessor Automation Using BASIC. E. R. Fisher, U of California

8:50 Laboratory Sample Management. H. S. Ames, U of California

9:10 Scheduling Laboratory Automation Projects. H. S. Ames, U of California

9:30 Minicomputer-Based Laboratory Management and Control System. G. G. Idnani, Computer Sciences Corp.

9:50 Syncrude's Lab Data Handling System. J. A. Bloxham, W. A. Foster, D. D. Ritz, G. M. Burns, A. P. Reuvers, Syncrude Canada, Ltd.

10:20 Impact of Instrumentation Automation Parameters on Microcomputer Design. W. S. Woodward, U of North Carolina

10:40 Microcomputer Control of ESCA Spectrometer. J. Hinderlitersmith, W. S. Woodward, C. N. Reilley, U of North Carolina

11:00 Interactive Microcomputer Program for Curve-Fitting of ESCA Data. D. F. Smith, R. W. Murray, U of North Carolina

11:20 Modular Microcomputer-Controlled Multinuclear FT-NMR. B. W. Good, Philip Morris, U.S.A., J. P. Koontz, W. S. Woodward, C. N. Reilley

11:40 Microcomputer-Based Data Acquisition and Instrument Control System for FT-NMR. J. P. Koontz, Burroughs Wellcome Co., W. S. Woodward, C. N. Reilley

Symposium: Advances in Applied Surface Analysis II

Wednesday Morning, Room 235A

D. M. Hercules, *Presiding*

8:30 Opening Remarks. D. M. Hercules

8:35 Data Treatment in Electron and Ion Spectroscopy. W. L. Baun, Air Force Materials Lab

9:15 Ion Scattering Spectroscopy. E. Tanglauer, Max Planck Institut für Plasmaphysik

10:15 Surface Ionization Mass Spectrometry in Multitechnique Approach to Surface Analysis. H. W. Werner, Philips Research Center

10:55 Electron Spectroscopic Studies in Metallurgy. A. Joshi, Physical Electronics

11:30 Applications of X-ray Photoelectron Spectroscopy to Atmospheric Studies. T. Novakov, Lawrence Berkeley Lab

Symposium: Toxicology in Industry

Wednesday Morning, Room 235B

J. A. Feldman, *Presiding*

8:30 Overview of Industrial Toxicology. H. N. MacFarland, Gulf Oil Corp.

9:30 Impact of Regulatory Developments on Industrial Toxicology. M. Eisler, Diamond Shamrock Corp.

10:45 Practical Applications of Industrial Toxicology. L. W. Keller, PPG Industries

Gas Chromatography—Novel Detectors

Wednesday Morning, Little Theater

P. C. Uden, *Presiding*

8:30 Glass Capillary GC/MS for Biomedical Analyses. R. Jenkins, R. F. Skinner, Finnigan Instrument Div.

8:50 Detection Capability of Multiple-Ion Detection in GC/MS. E. M. Chait, Du Pont

9:10 Advantages of Rapid Switching CI/EI Source for GC/MS. E. M. Chait, Du Pont

9:30 Use of Capillary for GC/MS Columns. E. M. Chait, Du Pont

9:50 Automated Selected Ion Monitoring for GC/MS. J. Michnowicz, A. Anderson, Hewlett-Packard

10:20 FT-IR and Chromatography. D. W. Virdrine, D. R. Mattson, Nicolet Instrument Corp.

10:40 Spectroscopic Detectors for Gas Chromatography. M. J. Hartigan, J. E. Baudean, J. E. Purcell, Perkin-Elmer

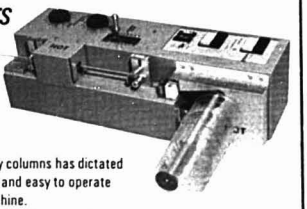
11:00 New Instrument for Effective Low-Cost GC/IR. V. Rossiter, Accuspec, Ltd.

11:20 Combined GC/AA Systems. B. R. Bartschmid, H. M. McNair, VPI & SU

11:40 Development of Practical Microwave Emission Spectro-

The New RFR Capillary Drawing Machine

Now — An Instrument Designed To Control ALL Capillary Drawing Parameters



The growing interest in analytical work utilizing glass capillary columns has dictated the need for a reliable and easy to operate capillary drawing machine.

RFR Corp. has designed the Capiliform™ II from the "USER'S-POINT-OF-VIEW" incorporating such features as: *QUICK CHANGE GEAR SHIFT* for changing draw ratios from 75 to 125; *POSITIVE DRIVE PUSH AND PULL ROLLERS AND COILING TUBE TEMPERATURE CONTROL* to ensure reproducible capillary columns.

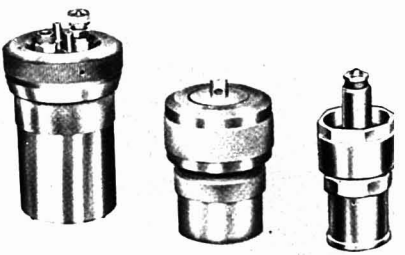
Immediate delivery available from stock. Write for more information.

See a Demonstration at the Pittsburgh Conference in Booth No. 1417.

RFR Corp. 1 Main Street Hope, R. I. 02831

CIRCLE 181 ON READER SERVICE CARD

PARR® BOMBS

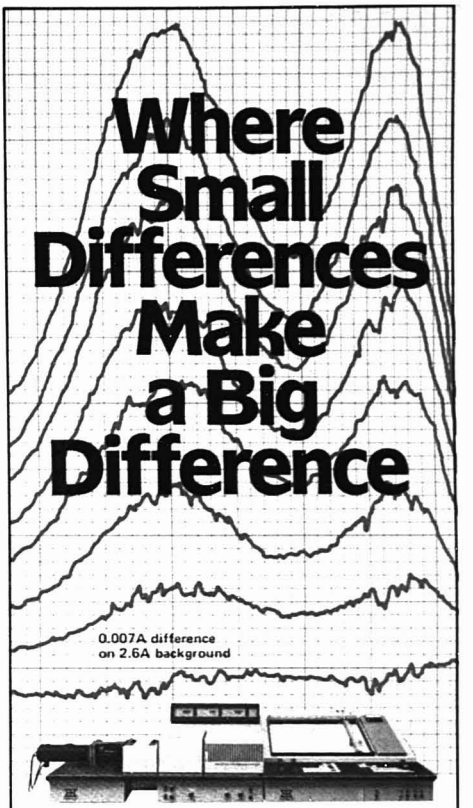


For Oxygen Combustion
For Acid Digestion
For Alkaline Fusion

Standard procedures for sulfur and halogens depend upon Parr oxygen or peroxide combustion bombs for oxidizing solid or liquid samples rapidly with complete recovery of all combustion products; while Parr digestion and fusion bombs give the analyst several effective systems for dissolving silicates, ores and other difficult materials in strong acids or alkalis without losing trace constituents. For details, write or phone: Parr Instrument Company, Moline, Illinois 61265. 309/762-7716

CIRCLE 169 ON READER SERVICE CARD

Where Small Differences Make a Big Difference



The Aminco DW-2a™ UV-VIS Spectrophotometer Extends the Range of Sample Investigations!

With our DW-2a spectrophotometer, small differences can lead to new research territories in UV-VIS spectrophotometry. The reason? Our painstaking improvements in such parameters as photometric accuracy, stability, and system versatility lead to substantial increases in overall system performance. Now, you can reliably record and reproduce absorbance differences as small as 0.0005A, even with extremely concentrated samples. This means that trace components can be easily detected in near-opaque samples.

See us at the Pittsburgh Conference of Applied Spectroscopy and Analytical Chemistry, AMINCO Booth 902.

AMINCO®

DIVISION OF TRAVENOL LABORATORIES, INC. Silver Spring, Md. 20910 Phone: 301-589-1727
European Headquarters: Rue Dautzenberg 36-38, 1050 Brussels Belgium. Phone: (02) 648-30-02

Circle No. 7 For more information
Circle No. 8 To have Sales Representative call

©1977 Travenol Laboratories, Inc.

metric Detector for Gas Chromatography. J. E. Gebhart, U of Iowa, C. W. Frank, D. Gay

Ion Exchange and Ion Chromatography

Wednesday Morning, Ball Room

T. S. Stevens, *Presiding*

8:30 Anionic Behavior of Uranium(VI) in Sulfate–Sulfuric Acid System. J. Rego, R. Carver, U of California

8:50 Effect of Calcium Solutions on Conversion of Strongly Acid Cation Exchange Resins. L. J. Cummings, Bio-Rad Labs

9:10 Concentration Gradient Elution of Metal Chloride Complexes on Dowex 1×8. H. G. Hicks, P. C. Stevenson, J. S. Schweiger, U of California

9:30 Ion Chromatographic Determination of Microgram Quantities of Anions Collected on Cellulose Fiber Filters. D. A. Otterson, NASA

9:50 Baseline Precipitation Chemistry Measurements by Ion Chromatography. D. C. Bogen, S. J. Nagourney, G. A. Welford, ERDA

10:20 Rapid Analysis of Boiler Water to Parts per Billion Level by Ion Chromatography. M. A. Fulmer, Westinghouse Electric Corp., R. J. Nadalin, J. Penkrot, C. Anderson

10:40 Determination of Ionic Impurities in Power Plant Steam/Water Using Ion-Exchange Concentrator Columns and Ion Chromatography. G. L. Carlson, M. A. Fulmer, Westinghouse R&D

11:00 Application of Ion Chromatography to Analysis of Solid Geological Samples for Anions. D. J. Koop, M. D. Silvester, F. N. Abercrombie, I. Thomson, Barringer Research Ltd.

11:20 Ion Chromatographic Analysis of Trace Anions in Brines. R. C. Chang, L. A. Woodruff, Dionex Corp.

11:40 Applications of Ion Chromatography for Oxyanion Analyses in Field of Nuclear Fuels Reprocessing and Waste Management. S. J. Johnson, Rockwell Hanford Operations

Environmental Analysis—General I

Wednesday Morning, Music Hall

J. O. Frohliger, *Presiding*

8:30 Carbon Partitioning of Aquatic Ecosystem by Using Organic Carbon Analyzer. J. C. Perkins, P. E. Edmunds, Duke Power Co.

8:50 Diffusion Tubes as Primary Standard for OSHA-Type Calibration. F. J. Debbrecht, D. T. Daugherty, E. M. Neel, Analytical Instrument Development

9:10 Differential Thermal Analysis (DTA) with Minicomputer Programming and Data Handling. O. Menis, NBS, J. A. Mackey, P. C. Ruegg, J. F. Barkley, P. D. Garn

9:30 Automatic Analyzer for Traces of Dispersed Oils in Wastewater by Solvent Extraction–Infrared Spectrophotometry. N. Yamaguchi, R. Suzuki, R. Matsumoto, Nippon Steel Corp.

9:50 Automated Determinations of Sulfur in Fossil Fuels. D. Gibboney, Fisher Scientific Co.

10:20 Improved Design for Analysis of Microliter Samples by Fluorescence and Room Temperature Phosphorescence. G. Walden, J. Bradshaw, J. D. Winefordner, U of Florida

10:40 Analytical Performance of Room Temperature Phosphorimetry. E. L. Yen, J. D. Winefordner, U of Florida

11:00 Application of Microwave Plasma Detector to Problems in Environmental Pollution. J. S. Hobbs, Applied Chromatography Systems, Ltd.

11:20 Investigation of Error in Low-Range Chemical Oxygen Demand Determination. L. L. Stookey, B. A. Klein, Manchester Labs

11:40 Total Carbon, Total Organic Carbon, and Carbonate Carbon Determinations in Water and Various Solid Materials Using Coulometrics Carbon Analyzer. E. W. D. Huffman, Jr., Huffman Labs

Surface Analysis II

Wednesday Afternoon, Room 205

W. E. Swartz, Jr., *Presiding*

1:30 Computer-Based System for Quantitation of ESCA Data. W. M. Riggs, L. E. Davis, P. W. Palmberg, Physical Electronics Industries

1:50 Flexible ESCA Spectrometer Data Acquisition and Control System. K. R. Thompson, Nuclear Data

2:10 Combined AES and SIMS System with Differentially Pumped Ion Gun. R. C. Hedtke, R. L. Gerlach, Physical Electronics Industries

2:30 Concerted ESCA–ISS–SIMS: New Approach to Molecular Structure and Surface Investigation. G. D. Mateescu, Case Western Reserve U, G. R. Sparrow

2:50 New Means for Extended Analysis of Metals, Alloys, and Composites: Combination of ESCA, ISS, and SIMS. G. R. Sparrow, 3M Co., G. C. Mateescu

3:20 Oscillations in Compositional Depth Profile of Cu/Ni Alloys: Study of UPS. I. Lindau, D. T. Ling, J. N. Miller, W. E. Spicer, P. M. Stefan, P. Pianetta, Stanford Electronics Labs and Stanford Synchrotron

3:40 Organic SIMS. H. Grade, R. J. Day, R. G. Cooks, Purdue U

4:00 Ion Scattering Spectrometry (ISS) for Analysis of Copper in Thin Vapor Deposited Al–Cu Films. D. L. Malm, Bell Labs, H. H. Strehblow

4:20 Comparative AES, ESCA, and SIMS Investigation of Oxide Films on FE–NI–CR Alloys. G. R. Conner, Inficon Leybold-Heraeus

4:40 Applications of SIMS Technology. C. E. Badgett, A. Jaclenques, A. Diebold, Instruments SA

ICP–Atomic Emission

Wednesday Afternoon, Room 239

H. F. Beeghly, *Presiding*

1:30 Multielement Ore Analysis Using ICP–AES Method. S. E. Church, Applied Research Labs

1:50 Use of Inductively Coupled Argon Plasma Spectroscopy for Analysis of Undigested Organic Materials and Oils. C. D. Carr, J. Borst, Applied Research Labs

2:10 Some Aspects of Standard Reference Material (SRM) Certification Process Using Inductively Coupled Plasma (ICP) Technique. R. L. Watters, Jr., J. A. Norris, NBS

2:30 Simultaneous Multielemental Major, Minor, and Trace Analysis in Metals and Alloys Using ICAP. A. F. Ward, Fisher Scientific Co.

2:50 Analytical Aspects of ICAP in Elemental Determination of Energy Sources. A. F. Ward, L. F. Marciello, Fisher Scientific Co.

3:20 Comparison of Inductively Coupled Plasma Emission Spectroscopy with Atomic Absorption and X-ray Fluorescence for Determination of Wear Metals in Lubricating Oil. A. W. Varnes, T. E. Andrews, Sohio Research

3:40 Evaluation of Cobalt as Internal Standard for Wear Metal Determination in Lubricating Oil via Induced Coupled Plasma Optical Emission Spectroscopy. A. W. Varnes, T. E. Andrews, Sohio Research

4:00 Effects of Operational Parameters of ICAP on Line to Background Ratios in Aqueous Solutions. R. L. Crawford, Fisher Scientific Co.

4:20 New Nebulizer for Analysis of High Salt Content Solutions with ICP. R. F. Suddendorf, K. W. Boyer, FDA

We supply
complete LC Systems . . .
from injectors to
Data Systems



or . . .

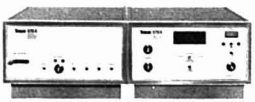


we can upgrade
your present LC
(even other makes)
with our components . . .

The 980A
Solvent Programmer
can be added to the
intake side of any low
internal volume, recipro-
cating pump to provide
up to 11 different solvent gradients.



The 970A
Variable Wavelength
UV Detector
is now available
with manual or
Auto Scanning
capability.



The 970A employs true double beam
optics for maximum stability. Reference
cells are available which make it
unnecessary to pre-scan your mobile
phase.

Tracor Liquid Chromatography

The Leaders in LC and GC Detector Technology

Tracor Instruments

Tracor, Inc 6500 Tracor Lane Austin, Texas 78721 Telephone 512 926 2800

CIRCLE 201 ON READER SERVICE CARD

your pipeline to high performance results



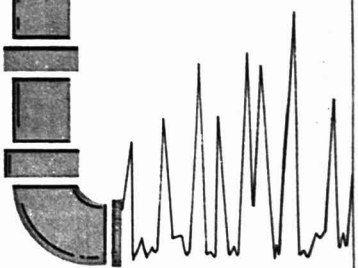
the Aminco HPLC System

It starts where others stop

Increased detectability and selectivity due to:
- a superior fluorescence detector - 1000 fold more sensitive than absorbance
- a unique resin
- the ability to perform chemical derivatizations

A detector to fit your needs:
- fluorescence detector
- electro-chemical
- UV
- ninhydrin
- colorimetric

Unattended, 24 hours/day operation with automatic sample injection and temperature programming



Circle No. 16 for more information.
Circle No. 17 to have sales representative call.

AMERICAN INSTRUMENT COMPANY
DIVISION OF TRAVENOL LABORATORIES, INC.
Silver Spring, Maryland 20910-Phone: 301-589-1727

AMINCO®

See us at the Pittsburg Conference of Applied Spectroscopy and Analytical Chemistry, **AMINCO Booth 902.**

*1977 Travenol Laboratories, Inc.

4:40 Some Applications of Plasma Emission Spectrometry with ICP Source and Discrete Sample Introduction. G. F. Kirkbright, A. Gunn, D. Millard, Imperial College

Oil and Other Organic Pollutants Analysis I

Wednesday Afternoon, Room 3A
A. P. Bentz, *Presiding*

1:30 Introductory Remarks. A. P. Bentz

1:35 Weighting Factors for Infrared Data Points in Pattern Recognition for Oil Identification. C. P. Anderson, U of Connecticut, T. J. Killeen, A. P. Bentz

2:00 Oil Matching Using Single Vector Method. T. J. Killeen, U of Connecticut, D. Eastwood, M. S. Hendrick

2:25 New Method of Petroleum Analysis—Computerized Infrared Spectra of Solutions. C. W. Brown, M. Ahmadjian, S. L. Pavignano, U of Rhode Island

2:50 Improved Techniques for Isolation and Quantitative Estimation of Hydrocarbon Content of Tissues and Sediments. D. W. Mayo, D. S. Page, Bowdoin College

3:30 Correlation of Petroleum Hydrocarbons in Clams and Sediments by GC, IR, and UV. F. E. Franklin, J. Kostyla, C. W. Brown, U of Rhode Island

3:55 Initial Classification of Oily Wastewater Components from U.S. Navy Vessels. D. H. Freeman, J. J. Zyren, U of Maryland

4:20 Use of GC/Mass Spectrometry in Settling High Volume-High Cost Oil Spills by Nonjudicial Means. J. W. Barron, EPA, B. M. Wright

4:40 Trace Metal Analysis (V/Ni) by Argon Plasma Optical Emission Spectrometry for Weathered Oil Identification. M. S. Hendrick, D. Eastwood, U.S. Coast Guard

Raman Instrumentation and General Spectroscopy

Wednesday Afternoon, Club Room B
D. H. Finseth, *Presiding*

1:30 Rapid Scanning Raman Spectroscopy with Ramanor HG2S. D. O. Landon, ISA, M. Delhaye, E. DaSilva

1:50 Signal-to-Noise Improvements in Time-Resolved Raman Spectroscopy. T. L. Gustafson, F. E. Lytle, Purdue U

2:10 Problems in Raman Spectroscopy. S. DiGregorio, Spex Industries

2:30 Low-Frequency Raman Spectra with Spatial Filter. W. Walker, S. DiGregorio, Spex Industries

2:50 Through Stray Light Barrier—Raman Spectroscopy Below 20 cm^{-1}. C. J. Vear, Anaspec Ltd.

3:20 Infrared Study on $Ru_3(CO)_{12}$-Impregnated χ-Al_2O_3 Fischer-Tropsch Hydrocarbon Synthesis Catalyst. R. Bouwman, I.L.C. Freriks, C. van der Woude, M. J. Doyle, Koninklijke/Shell-Laboratorium

3:40 New Device for Reflectance Spectroscopy of Powders. R. McKenzie, J. A. Miller, Beckman Instruments

4:00 Reflectance Measurements for Small or Odd-Shaped Samples—New Sphere and Accessory. J. A. Miller, R. McKenzie, Beckman Instruments

4:20 Application of Derivative Spectroscopy to Reflectance Measurements. J. A. Miller, Beckman Instruments

4:40 Determination of Cesium Vapor Densities over Pure Metal and Various Amalgams by Tunable Dye Laser Spectroscopy. P. M. Castle, J. F. Lowry, Westinghouse R&D Center

Symposium: Laboratory Automation II—Computer Information Handling in Clinical Laboratory (ASTM E-31)

Wednesday Afternoon, Room 235A
R. Megargle, *Presiding*

1:30 Data Acquisition and Sample Identification in Clinical Chemistry. M. Rubin, Georgetown U

2:05 Comparison of Data Entry Methods in Clinical Laboratory Systems. G. Braley, Honeywell

2:40 Handling of Medical Data with Micro and Mini Computers. A. O. Wist, Virginia Commonwealth U

3:35 Report Formatting by Clinical Laboratory. R. E. Horowitz, Saint Joseph Medical Center

4:10 Laboratory Communication with the Physician. S. Raymond, Hospital of U of Pennsylvania

4:45 Discussion

Symposium: OSHA—Industrial Hygiene and the Analytical Chemist

Wednesday Afternoon, Room 235B
O. E. Wilkinson, *Presiding*

1:30 Occupational Safety and Health Act—An Overview. D. Dowdell, U.S. Department of Labor

2:10 Industrial Hygiene: Viewpoint from Management. R. A. White, Mobay Chemical Corp.

2:50 Chemist Beware: Cautions in Industrial Hygiene Measurements. K. Cohen, U.S. Navy

3:40 Development and Applications of Standard Methods of Analysis in Industrial Hygiene. F. Madson, OSHA

4:20 NBS Standard Reference Materials for Industrial Health Measurements. R. Alvarez, NBS

1978 Awards Symposium

Wednesday Afternoon, Little Theater
Jane H. Judd, 1978 Conference President, *Presiding*

1:30—Presentation of 1978 Pittsburgh Spectroscopy Award
By
Allen J. Sharkins
Chairman, Spectroscopy Society of Pittsburgh
To
Professor E. Bright Wilson
Harvard University
Cambridge, Mass.
Award Address
Some Impacts of Microwave Spectroscopy on Chemistry

2:30—Presentation of the 1978 Pittsburgh Applied Analytical Chemistry Award
By
Bruce M. LaRue
Chairman, Society for Analytical Chemists of Pittsburgh
To
George M. Janini
University of Kuwait
Kuwait, Kuwait
And
Keven Johnston and Walter L. Zielinski, Jr.
NCI Frederick Cancer Research Center
Frederick, Md.
Award Address
Novel High-Temperature Gas Chromatographic Separations Using Liquid Crystal Stationary Phases
George M. Janini

3:15—Presentation of Dal Nogare Award
By
The Chromatography Forum of Delaware Valley
To
Csaba Horvath
Yale University
Award Address

Absorption Spectroscopy—IR & General

4:00 Infrared CO Analysis. B. Krakow, ARO, M. G. Davis, H. Grassman

Improved! Solvent Delivery Pumps for Liquid Chromatography



REDUCES ANALYSIS TIME 15-TO 20 FOLD OVER HYDROSTATIC PRESSURE METHODS!

- FULL FLOW RANGE FROM 0 TO 1164 ML/HOUR.
- ACCURATE AT PRESSURES TO 100 P.S.I.G.
- REPEAT YOUR FLOW SETTINGS TO WITHIN 0.1%.
- DRIFT-FREE ACCURACY FOR LONG RUNS.
- REVERSIBLE WHILE RUNNING FOR QUICK COLUMN BACK FLUSH AND REGENERATION.
- SOLVENTS ONLY CONTACT HARD ALUMINA CERAMIC AND T.F.E.
- ABRASION RESISTANT CERAMIC PISTON AND CYLINDER LINER.
- QUIET SYNCHRONOUS STEPPER MOTOR DRIVE.
- SMALL: ONLY 10.7" X 5" X 3.2" WIDE AND 8 POUNDS LIGHT.
- INEXPENSIVE: *RP1SYCSC F.M.I. LAB PUMP $450.00
  *R428 MICROMETER KIT $ 40.00
  *R479 ¼-28 T.F.E. PORT ADAPTERS NO CHARGE
  COMPLETE F.O.B. PRICE $490.00
  NOTE: FOR EXPLOSION-PROOF DRIVE, SPECIFY RP1SYXCSC, R428, AND R479 ONLY $630.00

FMI FLUID METERING, INC.
P.O. BOX 507, OYSTER BAY, N.Y. 11771 • (516) 922-6050

CIRCLE 71 ON READER SERVICE CARD

UNBREAKABLE



Graphic Controls

COMBINATION ELECTRODE

With Spin-Off Protected Tip

You can stir solutions with this new combination electrode... it's virtually unbreakable! Of sealed polymer body design, it also has a unique spin-off cap to protect the bulb. Makes cleaning easier, too. For more information, use the coupon.

- Sealed reference...no filling required.
- Low impedance for fast response.
- Virtually unbreakable.
- Ultra stable Ag/AgCl internal electrode design.
- Measures full pH range (0-14 at 0°C to 100°C.)

RECORDING CHART DIVISION
GRAPHIC CONTROLS CORPORATION
Box 1271, Buffalo, NY 14240 AC-117
Attn: Mr. Robert P. Vail or call 716/853-7500

I'd like more information on your new Spin-Off Protected Tip Combination Electrode.

Name _____ Title _____

Company _____ Phone _____

Address _____

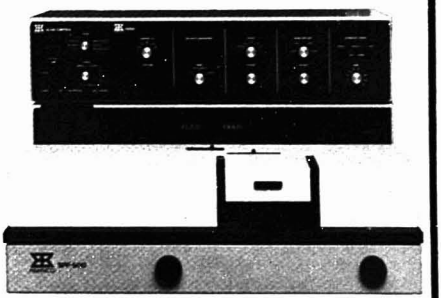
City _____ State _____ Zip _____

Visit booths 510–512 at the Pittsburgh Conference

CIRCLE 78 ON READER SERVICE CARD

KISS

Keep It Simple Spectrofluorometer



The AMINCO SPF–500™ Spectrofluorometer simplifies the measurement process by using the unique AUTORANGING SYSTEM that automatically performs all scaling functions and range selection without operator intervention. The SPF–500™ Spectrofluorometer measurements simplify to:

1. inserting sample
2. closing sample compartment cover
3. reading digitally displayed value

Other outstanding features of the SPF–500 Ratio and Corrected Spectra Spectrofluorometers include:

- superior resolution and sensitivity
- high-intensity excitation source
- digital readouts
- 4-cell sample compartment
- flexibility
- ease-of-operation

From Aminco, the leader in the fluorescence field.

See us at the Pittsburgh Conference of Applied Spectroscopy and Analytical Chemistry, Aminco Booth 902.

For further details, contact your local representative or

AMINCO®
AMERICAN INSTRUMENT COMPANY
DIVISION OF TRAVENOL LABORATORIES, INC.
Silver Spring, Maryland 20910 • Phone: 301-589-1727

Circle 14 for more information
Circle 15 for sales representative to call

©1977 Travenol Laboratories, Inc.

4:20 Quantitative Applications of Laser Stark Spectroscopy: Measurement of Carbon Isotope Ratios. D. M. Sweger, NBS, R. B. Murphy

4:40 Separation and Spectral Characterization of Coal-Derived Asphaltenes. D. H. Finseth, C. E. Schmidt, H. L. Retcofsky, PERC/DOE

Liquid Chromatography—Columns

Wednesday Afternoon, Ball Room

J. Lengyel, *Presiding*

1:30 Microcolumns in Liquid Chromatography: Their Potential and Limitations. M. Novotny, T. Tsuda, Indiana U

1:50 Disposable Low-Pressure Silica Columns and Their Correlation to TLC. T. Beesley, M. Mazzei, Whatman

2:10 Preparative Reverse-Phase Liquid Chromatography Using Radially Compressed Columns. H. M. Quinn, Waters Associates

2:30 New Comprehensive Family of Bonded Phases—Column Packings for HPLC. M. Telepchak, ES Industries

2:50 Preparative Reversed-Phase HPLC with Lobar Prepacked Columns. F. Eisenbeiss, E. Merck, A. Henke

3:20 High-Performance Organic Resins for Liquid Chromatography. R. A. Henry, Altex Scientific, J. R. Benson, V. A. McKay

3:40 Advances in Quantity Production of High-Efficiency HPLC Columns. P. J. Mondron, P. G. Bonnett, Laboratory Data Control

4:00 New Techniques for Prolonging LC Column Life. F. M. Rabel, A. G. Caputo, E. T. Butts, Whatman

4:20 New 5-μm Bonded Reversed-Phase LC Packing. F. M. Rabel, D. J. Popovich, C. J. Lancaster, Whatman

4:40 Use of Reversed-Phase Packing for Both Reversed-Phase and Adsorption Separations. E. T. Butts, D. J. Popovich, C. J. Lancaster, Whatman

Environmental Analysis—Organic

Wednesday Afternoon, Music Hall

R. M. Raybeck, *Presiding*

1:30 Concentration and Analysis of Organic Compounds from Air and Water. W. Averill, J. E. Purcell, Perkin-Elmer

1:50 Determination of Trace Organic Impurities in Water Using Thermal Desorption from XAD Resin. J. S. Fritz, J. Ryan, Iowa State U

2:10 Analysis of Carcinogenic Gases in Ambient Urban Air. B. Kibbekus, J. Bozzelli, New Jersey Institute of Technology

2:30 Trace Organic Compounds in Water by Liquid Chromatography. H. F. Walton, G. A. Eiceman, U of Colorado

2:50 Concentration and/or Separation of Organics in Ecosystems by Functional Group Specific Polymer Resins. T. J. Mourey, R. Kostyla, S. Siggia, U of Massachusetts

3:20 Comparison of Two Techniques for Collection and Analysis of Polynuclear Aromatics in Ambient Air. J. L. Lindgren, Texas Air Control Board, H. J. Krauss, M. A. Fox

3:40 Collection and Quantitative Analysis of Some C_1–C_{12} Hydrocarbons in Texas Urban Air. J. L. Lindgren, Texas Air Control Board

4:00 Determination of Volatile *N*-Dialkylnitrosamines in Ambient Air. J. A. Cucco, P. R. Brown, U of Rhode Island

4:20 New Column Technology in Analysis of Organics in Water by Gas Chromatography. R. Mindrup, Supelco

4:40 Monitoring of Freshwater Organics. J. A. Pattison, Digicolor, G. Amey

Thursday, March 2

UV–VIS Spectrophotometry

Thursday Morning, Room 205

J. A. Queiser, *Presiding*

8:30 Computerized Derivative UV–VIS Spectroscopy Qualitative and Quantitative Roles. J. W. Mohar, J. A. Miller, Beckman Instruments

8:50 Microcomputer Automation of High-Accuracy Spectrophotometer. J. F. Barkley, F. E. Ruegg, R. Mavrodineau, NBS

9:10 Conversion of Single to Double-Beam Recording Spectrophotometer for Biochromatic Analyzer. K. M. Walczak, H. V. Malmstadt, U of Illinois

9:30 Advances in Microspectrophotometry: I. Reflectance, Absorbance, and Corrected Fluorescence Measurements in Visible and Deep Red Regions Using Computerized Microspectrophotometer. V. J. Coates, Nanometrics

9:50 Isolating Sample from Difficult Matrix Using Laboratory Computer and UV–Visible Spectrophotometer. J. W. Mohar, J. A. Miller, Beckman Instruments

10:20 Advances in Microspectrophotometry: II. Near Infrared Absorption Studies of Particles and Fibers Using Conventional Optical Microscope. V. J. Coates, Nanometrics

10:40 UV–VIS–NIR Recording Spectrophotometer with Newly Designed Double Monochromator. Y. Tsunazawa, O. Akiyama, M. Nishida, M. Takada, S. Tezuka, Shimadzu Seisakusho Ltd.

11:00 Photometric Capabilities of Varian Cary 219 Spectrophotometer. M. J. Kelly, D. Priesner, Varian

11:20 Standard Reference Materials to Verify Transmittance Accuracy in Molecular Absorption Spectrometry. R. Mavrodineau, NBS

11:40 Performance Details of Original and Replicated Holographic Diffraction Gratings. D. Irish, R. J. Francis, Pye Unicam Ltd.

Symposium: Speedy Spectroscopy (How Fast Is Fast?)

Thursday Morning, Room 239

W. G. Fateley, *Presiding*

8:30 Historical Development and Directions in Infrared Time Resolved Spectroscopy. W. G. Fateley, Kansas State U

8:55 Infrared Double-Resonance Investigations of Excited Molecules and Coherent Transient Spectroscopy. J. I. Steinfeld, MIT

9:30 Time Resolved Infrared Spectroscopy Utilizing Fourier Transform Techniques. A. W. Mantz, Digilab

10:15 Picosecond Time Resolved Spectroscopy in Chemical and Biological Systems. P. M. Rentzepis, Bell Labs

10:50 Time Resolved Laser Induced Fluorescence Spectroscopy. F. E. Lytle, Purdue U

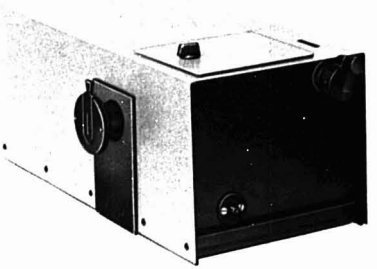
11:25 Use of Laser Mode Noise as Probe for Fast Spectroscopic Events. G. M. Hieftje, Indiana U

X-ray Fluorescence

Thursday Morning, Room 3A

C. J. McCafferty, Jr., *Presiding*

8:30 Application of Energy-Dispersive X-ray Fluorescence Spectroscopy to Analysis of Contaminants in Fuels and Lubricants. M.



Who put all those wonderful specifications in one little monochromator?

Who but **Jarrell-Ash,** for over half-a-century a leader in monochromator engineering. J-A's newest ¼-meter, the Mark X, brings you more great features than ever:

- Dramatically improved focal-plane accessibility. Lets you use the latest **multi-element arrays** (Vidicon, Pyrocon, charge-coupled devices, etc.) as well as photomultipliers. Incomparably versatile!
- New optical design that **intrinsically** eliminates re-entry spectra at all wavelengths.
- Superb infrared as well as visible and UV capability.
- Choice of **10** quick-change pre-aligned gratings — a 175nm-40μ range. With remarkable dispersion (e.g., 3.0nm/mm with our 1200g/mm grating).
- Finest resolution in its field. Better than 0.6nm with 1200 g/mm grating). On our parabolic-mirror model Mark X, it's **0.3nm!**
- Minimal scattered light. At 500nm, it's less than **0.05%!**
- A beautiful selection of accessories to make your lab life easier. Like digital Omni-Drive (1-200nm/minute) . . . quantum photometer . . . filter wheels to expedite fluorescence, phosphorescence, luminescence, polarization and photometry studies . . . **and much more.**

Use Mark X as a heavy-duty monochromator or as a spectrograph. In instruction **or** research. It's all in a handsome little package with a handsome little price. Not $2500, not $2000, but — thanks to volume production — a little over $1000.

Incidentally, we **call** it a quarter-meter. Actually we've made it 275mm for greater dispersion, improved focal plane. The extra 25mm are on the house.

The monochromator people

Jarrell-Ash

590 Lincoln St
Waltham MA 02154
(617) 890-4300

A Division of Fisher Scientific Company

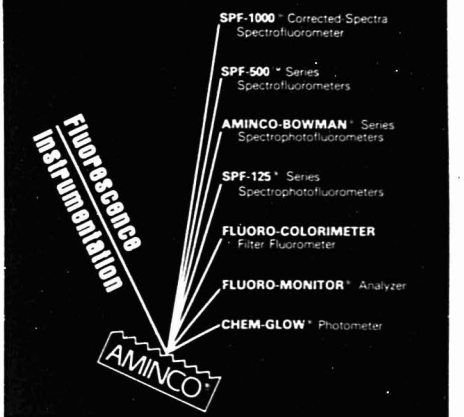
Look for Mark X at the Pittsburgh Conference

CIRCLE 75 ON READER SERVICE CARD

ANNOUNCING

the newest entry to the Full Spectrum —see it at the Pittsburgh Conference

THE FULL SPECTRUM



SPF-1000® Corrected-Spectra Spectrofluorometer — top-of-the-line instrument for the most sophisticated research applications.

SPF-500™ Series Spectrofluorometers — quality grating instruments for today's research needs with a sensitivity and resolution comparable to the SPF-1000 instrument.

AMINCO-BOWMAN® Series Spectrofluorometers — provide wavelength scanning with high-quality grating separation of wavelength. Over 5,000 units are currently in use.

SPF-125® Series Spectrofluorometers — for non-scanning or scanning applications using grating separation of wavelength.

FLUORO-COLORIMETER for filter fluorometry, colorimetric, tubidimetric, and nephelometric applications.

FLUORO-MONITOR® Analyzer — for high-performance liquid chromatography fluorescence applications.

CHEM-GLOW® Photometer — for bioluminescent and chemiluminescent applications.

© 1977/1978 Travenol Laboratories, Inc.

AMINCO®
AMERICAN INSTRUMENT COMPANY
DIVISION OF TRAVENOL LABORATORIES, INC., Silver Spring, Md. 20910 Phone: 301-589-1727
European Headquarters: Rue Dautzenberg 36-38, 1050 Brussels, Belgium Phone (02) 648-50-02

Circle No. 5 for more information
Circle No. 6 to have Sales Representative call

K. Greenberg, F. M. Newman, Southwest Research Institute

8:50 Self-Optimization of X-ray Fluorescence System. J. C. Russ, R. B. Shen, Edax Labs

9:10 Chemical Analysis of Stainless Steel by Energy-Dispersive X-ray Fluorescence. B. Wheeler, N. Jacobus, Ortec

9:30 Multiple-Element Geochemical Analysis by Energy-Dispersive X-ray Spectrometry. W. H. Lemons, Wyoming Mineral Corp.

9:50 Energy-Dispersive X-ray Analysis of Coatings Systems. R. M. Holsworth, T. Provder, Glidden Coatings and Resins

10:20 Accurate X-ray Spectrochemical Determination of Tungsten in Ore Concentrates. J. S. Mras, J. R. Barton, R. Dyck, GTE Sylvania

10:40 Use of Dedicated X-ray Analyzer for Quality Control of Lead in Paint. G. P. Cunningham, C. E. Cowan, PPG Industries

11:00 Flux Fusion Methods and Their Roles in X-ray Fluorescence Spectrometry—A Review. P. M. Welch, Johnson, Matthey Chemicals Ltd.

11:20 Filter Deposition X-ray Fluorescence Spectrometry for Analysis of Elements in Parts-per-Billion Range. K. J. Garska, Union Carbide

11:40 Determination of Trace Elements in Fuel Oil by Energy-Dispersive X-ray Fluorescence Analysis. J. S. Mgebroff, J. S. Payne, Texas Air Control Board

Infrared Spectroscopy

Thursday Morning, Club Room B

J. F. Jackovitz, *Presiding*

8:30 Multisample-Controlled Environment Infrared Cell. J. L. White, C. F. Schanke, Purdue U

8:50 Vapor-Phase Infrared Library Search (and Seizure) System. M. F. Delaney, D. E. Henderson, P. C. Uden, U of Massachusetts

9:10 Computerized Infrared Spectroscopy as Separation Technique—Analysis of Complex Organic Mixtures Extracted from Water. P. F. Lynch, M. M. Brady, U of Rhode Island

9:30 Infrared Spectroscopic Techniques Applied to Analysis of Asbestos. J. P. Coates, M. J. Lewis, Perkin-Elmer

9:50 Computerized Infrared Analysis of Flame Retardant Fabric Additives. M. V. Zeller, R. W. Hannah, Perkin-Elmer

10:20 Infrared Analysis of Lubricant Blends by Computerized Dispersive Spectroscopy. J. P. Coates, Perkin-Elmer

10:40 Computerized Difference Spectroscopy—Factors That Effect the Final Spectrum. J. P. Coates, M. J. Lewis, Perkin-Elmer

11:00 Dispersive Infrared-Computer System: Its Usefulness in Quantitative Analysis. J. W. Mohar, R. J. Obremski, Beckman Instruments

11:20 On-Line Quantitative Analysis of Multicomponent Mixtures Using Infrared Techniques. R. J. Obremski, J. W. Mohar, Beckman Instruments

11:40 Spectral Subtraction: Its Usefulness and Limits in Qualitative Analysis Using Dispersive Infrared Instrumentation. J. W. Mohar, R. J. Obremski, Beckman Instruments

Symposium: Airborne Contaminants

Thursday Morning, Room 235A

R. W. Freedman, *Presiding*

8:30 Continuing Problems in Sampling and Chemical Speciation of Sulfate in Airborne Particles. R. L. Tanner, Brookhaven National Labs

9:10 Critique of Procedures for Nitrogen Oxides. B. Saltzman, U of Cincinnati

10:00 Analysis of Human Carcinogens in Polluted Atmospheres. E. Sawicki, National Environmental Research Center

10:40 Various Difficulties Associated with Field Sampling of Airborne Particulates. M. Corn, N. A. Esmen, U of Pittsburgh

11:20 Polynuclear Aromatic Hydrocarbons in Environmental Samples—Their Characterization by X-ray Excited Optical Luminescence Technique. V. A. Fassel, C. S. Woo, A. P. D'Silva, Iowa State U

Liquid Chromatography—Applications

Thursday Morning, Room 235B

N. Kotsko, *Presiding*

8:30 Rapid Analysis of Xanthene Group Dyes by High-Speed Liquid Chromatography. Y. Ohtsu, I. Matsumoto, Shiseido Labs

8:50 Determination of Parathions and Atrazine in Runoff Water with HPLC. D. C. Paschal, Illinois State U

9:10 Improved HPLC–Fluorometric Labeling Parameters for Determination of Carbamate Insecticide Residues. R. T. Krause, FDA

9:30 Analysis for Oxygenated Metabolites of Polycyclic Aromatic Hydrocarbons in Marine Organisms by High-Pressure Liquid Chromatography. L. C. Thomas, W. D. MacLeod, Jr., D. C. Malins, National Oceanic and Atmospheric Administration

9:50 Molecular Weight Distribution of Mineral Oils and Waxes as Studied by HPLC and Mass Spectrometry. H. H. Lo, Chesebrough Pond's

10:20 Reverse-Phase Chromatography of Urinary Catecholamines with Fluorescent Detection. L. D. Mell, Jr., Naval Medical Research Institute, C. W. Gehrke, Jr.

10:40 Total HPLC Automation of Cephalosporin Analysis. J. H. Kaufman, R. W. Lamoureux, Bristol Labs

11:00 Reverse-Phase High-Pressure Liquid Chromatography of Short-Chain Peptides. E. P. Kroeff, D. J. Pietrzyk, U of Iowa

11:20 HPLC Analyses of Aminoglycoside Antibiotics. T. McCorkle, S. Gruber, Schering Corp.

11:40 Preparation of Drugs and Lipids by HPLC. P. T. Pei, S. Ramachandran, R. S. Henly, Applied Science Labs

Automated Analysis

Thursday Morning, Little Theater

Michael J. F. DuCros, *Presiding*

8:30 Automated Procedure for Simultaneously Determining Specific Conductance and pH in Natural Waters. D. E. Erdmann, H. E. Taylor, U.S. Geological Survey

8:50 Simplified Automated System for Titrimetric Procedures. W. D. Barnes, E. P. Kujawa, C. F. Chiarelly, Brinkmann Instruments

9:10 Application of New Automatic Titrator for Individual Analysis. O. Siroky, Ciba-Geigy AG, P. Fruh

9:30 Design of ISE Analysis System Using Tektronix GS 4051 for Data Acquisition and Control. K. A. Gertz, U of California

9:50 Using Tektronix 4051 for Data Acquisition and Control in Ion Selective Electrode Analyzer. A. M. Kray, U of California

10:20 Application of Automated Thermometric Analysis—Fertilizer and Aluminum Industries. N. B. Sherry, J. DiLiddo, Technicon Industrial Systems

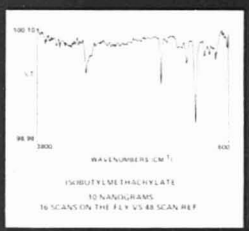
10:40 Evaporation to Dryness—New Module for Automated Chemical Analysis. A. Pietrantonio, Technicon Industrial Systems

11:00 Acid Scrubber for Rapid Digestion Equipment. A. F. Buccafuri, R. Delgrosso, Technicon Industrial Systems

Digilab GC/IR

Digilab Means Sensitivity

In GC/IR, the most critical parameter is SENSITIVITY. GC fractions are measured in nanograms, so you need maximum sensitivity to obtain positive IR spectra. Digilab Fourier transform spectrometers with GC/IR provide better than 100 nanogram sensitivity on-the-fly; and better than 10ng in trap mode. These numbers are your assurance of receiving clear functional group identification of fractions virtually as fast as the GC separates them. The on-the-fly IR spectrum, below, of a 10ng fraction demonstrates Digilab's GC/IR sensitivity.



SYSTEM UTILITY and FLEXIBILITY are vitally important to GC/IR analysis. Digilab GC/IR uses your chromatograph and takes full advantage of its detector output. Digilab flexibility is evident in the switch-selectable external GC/IR on dual-beam FTS® instruments. Digilab's IMX-RDOS® software provides proven utility in GC/IR processing . . . from rapid data acquisition to spectral differentiation of the components in unresolved GC peaks. Digilab is the ultimate refinement in high sensitivity GC/IR.

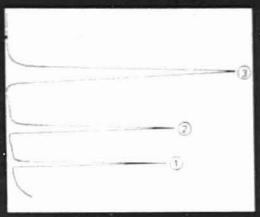


External GC/IR sampling accessory on Digilab model FTS-15C spectrometer.

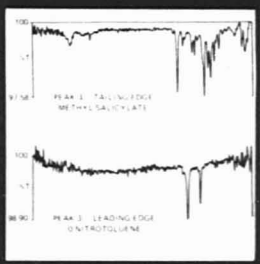
To learn more, see "High Sensitivity Infrared Spectroscopy of Gas Chromatographic Peaks," Wall and Mantz, APPL. SPEC *31*,6,1977,P.552.

3 GC = 4 GC/IR

Take a look at the chromatogram. It's a read-out of a four component mixture – with equal concentration of each component. Yet there are just three peaks. Without the help of Digilab's infrared Fourier Transform Spectrometer with GC accessory,



you'd never know that Peak 3 is a blend of two components – o-nitrotoluene and methyl-salicylate (separated in the spectra below).



What you don't know can hurt you – and your research findings. But with Digilab you'll be sure.

But don't just take our word for it. Call or write us today for a free brochure and ask about our demonstration program.

DIGILAB INC

Subsidiary of Block Engineering, Inc.
237 Putnam Avenue, Cambridge, MA 02139 Telephone (617) 868-4330

Put us to the test.

See us at the Pittsburgh Conference, Booths 846, 848, 945 and 947. Application seminars daily, Room TM-11.

11:20 Automated Extraction Based on Flow Injection Principle. B. I. Karlberg, S. Thelander, Astra Pharmaceuticals AB

11:40 Band Spreading in Unsegmented Continuous Flow Analysis. K. K. Stewart, C. W. Hendrix, USDA

Computerized Mass Spectrometry and GC/MS

Thursday Morning, Ball Room

D. K. Bakale, *Presiding*

8:30 Leadoff Lecture: **Data Interpretation for Computerized Mass Spectrometry.** F. W. McLafferty, Cornell U

9:10 Updating and Computerizing 21-103 and Similar Mass Spectrometers. T. J. Eskew, G. L. Brezler, L. F. Herzog, Nuclide Corp.

9:30 Improving Dynamic Mass Spectrometer Detection Limits by Rejection of Background. L. F. Herzog, T. J. Eskew, T. L. Strand, Nuclide Corp.

9:50 Integration of Central Processor into Control System of Digital GC/MS. C. W. Hull, Du Pont, W. N. Huse, R. L. Mack, W. H. Holt

10:20 Applications-Oriented Software for Solution of GC/MS Problems. E. M. Chait, W. N. Huse, C. W. Hull, Du Pont

10:40 Applications of Spark Source Mass Spectrometry to Analysis of Coal Conversion Process Streams. R. G. Lett, PERC/DOE, R. R. DeSantis, D. W. Koppenaal

11:00 Mass Spectrometric Analysis of Gases Dissolved in Transformer Oil. K. C. Linn, G. B. Bunyard, B. A. Raby, UTI

11:20 GC/MS System for Alternately Scanning Positive and Negative Ions. J. R. Reeher, G. C. Stafford, G. C. Cox, Finnigan Instruments Div.

11:40 Simultaneous EI/CI Computer Mass Spectrometry System. P. S. Berger, Teknivent Corp., T. A. Patterson

Polymer Analysis

Thursday Morning, Music Hall

R. F. Kratz, *Presiding*

8:30 Quantitative Determination of Oil Content in Oil-Modified Ortho-Phthalic Polyester Resins Using Infrared Spectroscopy. J. A. Vance, Lilly Industrial Coatings, N. B. Brakke, P. R. Quinney

8:50 Inelastic Electron Tunneling Spectroscopy as Probe of Polymer Structure. J. P. Luongo, R. F. Roberts, Bell Labs

9:10 Infrared Analysis of Carbon Containing Black Rubbers and Polymers. R. W. Hannah, Perkin-Elmer, A. Toivo, L. Kalervo

9:30 Quality Control of Thermosets by Dynamic Mechanical Analysis. L. Woo, R. L. Hassel, Du Pont

9:50 Polymer Evaluation Using Dynamic Mechanical Analysis Quantitative Damping. R. L. Hassel, R. L. Blaine, Du Pont

10:20 Polymer Analysis by Dynamic Measurement of Evolved Gases. R. M. Lum, Bell Labs

10:40 New, Automated, Simultaneous, Thermal Analysis Techniques for Polymer Characterization. B. Cassel, W. P. Brennan, Perkin-Elmer

11:00 Comparative Evaluation of Degree of Cure of Phenolic Systems by DMA, DSC, and TMA. K. F. Baker, Du Pont

11:20 Total Thermal Analysis of Moldable Thermosetting Resins—A Case History. R. L. Blaine, K. F. Baker, Du Pont

11:40 Automated Dynamic Mechanical Spectra. C. W. Macosko, U of Minnesota, J. M. Starita

General Analysis I

Thursday Afternoon, Room 205

J. E. Willis, *Presiding*

1:30 New Liquid Sample Handling Accessory for CHN Analyzer. R. F. Culmo, Perkin-Elmer

1:50 Critical Study of Brilliant Green as Spectrophotometric Reagent for Determination of Antimony and Its Application in Zinc Industry. H.K.L. Gupta, Texasgulf Canada, Ltd.

2:10 Determination of Total Phosphorus on Activated Carbon. J. D. Sember, M. B. Linkenheimer, S. D. Cifrulak, Calgon Corp.

2:30 New Analytical Procedure for Arsenic in Water. R. J. Matthews, S. R. Goode, U of South Carolina

2:50 Stability of Low-Level Sulfur Gases in Volatile Hydrocarbon Matrixes Contained in High-Pressure Aluminum Cylinders. F. Kramer, Jr., S. G. Wechter, Airco Industrial Gases

3:20 Thermal Method of Analysis—High-Speed Dilatometry for Study of Metallic Alloys. J. Giglio, G. R. Cizeron, ISA

3:40 Analysis of Ash Deposits Using Heated Stage and Scanning Electron Microscopy. D. K. Rindt, W. Beckering, Grand Forks Energy Research Center

4:00 SEM Examination of Quinoline Insoluble Particulates in Pitch. J. W. Bluhm, Koppers Co.

4:20 New Approach to Organic Microanalysis: Microwave Plasma Analyzer with Multielement Capabilities. J. S. Hobbs, Applied Chromatography Systems, Ltd.

4:40 Spectrophotometric Determination of Tantalum(V) with Gallic Acid and 1,2-Diaminocyclohexanetetraacetic Acid. K. Srinivasulu, M. S. Rao, Vikram U

Flame Atomic Emission

Thursday Afternoon, Room 239

S. D. Cifrulak, *Presiding*

1:30 Advances in Laser Microspectrochemical Analysis. R. McGillivray, ICI Fibres

1:50 Atomic Flame Spectroscopy Using Laser-Enhanced Ionization. G. C. Turk, NBS, J. C. Travis, J. R. DeVoe, T. C. O'Haver

2:10 Development of Air Plasma Torch and Its Applications. S. Hanamura, NBS

2:30 Matrix Interference Effects in Determination of La in Barium Titanate by Flame Molecular Emission Spectrometry. T. Y. Kometani, Bell Labs

2:50 Atom Vapor Transport in Analytical Flames. K. P. Li, U of Florida

3:20 Spatially Resolved Flame Temperature Measurements by Slope Method. M. A. Fernandez, G. J. Bastiaans, Georgetown U

3:40 Use of CH Sensitized Silver Emission for Flame Photometric Determination of Total Organic Content in Aqueous Solutions. R. S. Fike, C. W. Frank, U of Iowa

4:00 Mechanism and Use of In-Flame, Gas-Solid Interactions for Direct Determination of Copper in Sheet Metals. R. S. Fike, C. W. Frank, U of Iowa

4:20 Experimental Studies of Direct Current Plasma Jet. G. N. Coleman, W. P. Braun, A. M. Allen, U of Georgia

4:40 Plasma Characteristics of Hollow Cathode Discharge. D. M. Mehs, T. M. Niemczyk, U of New Mexico

Oil and Other Organic Pollutants Analysis II

Thursday Afternoon, Room 3A

D. Eastwood, *Presiding*

1:30 Further Investigations in Fluorescence and Low-Temperature Luminescence for Oil Identification. D. Eastwood, M. S. Hendrick, U.S. Coast Guard

1:50 Total Luminescence Study of Effects of Artificial Weathering on

PGT
PRINCETON GAMMA-TECH

X-ray Fluorescence
Analyzers

Computer-based PGT-500 Spectrochemical X-ray Analyzer
New PGT-260 Multichannel Materials Analyzer
Versatile bench-top PGT-100 Chemical Analyzer

Microanalysis
Systems

New PGT-1000 XCEL
the computer that analyzes–the analyzer that computes

are going to
Pittsburgh

(in Cleveland)
if you've got the time, we've got the place
Booths 516-518

Box 641 • Princeton, N.J. 08540 • Tel: 609 924-7310 • Telex: 843486

CIRCLE 153 ON READER SERVICE CARD

Oils. A. W. Hornig, L. P. Giering, Baird-Atomic

2:10 **Identification and Quantitation of Isomeric Polycyclic Aromatic Hydrocarbons in Mixtures by Matrix-Isolation Fluorescence Spectroscopy.** E. L. Wehry, G. Mamantov, P. Tokousbalides, R. C. Stroupe, R. B. Dickinson, Jr., U of Tennessee

2:30 **Fluorescence Excitation-Emission Contour Mapping of HPLC Eluates.** J. R. Jadamec, U.S. Coast Guard, W. A. Saner, E. Kallet, S. Cravitt, Y. Talmi

2:50 **Characterization of HPLC Eluates Using OMA for UV Absorption and Fluorescence Mapping.** W. A. Saner, U.S. Coast Guard, J. R. Jadamec, Y. Talmi

3:20 **Laboratory Weathering of Petroleum.** G. A. Flanigan, U.S. Coast Guard

3:40 **Automatic Analysis of Organic Pollutants in Water via GC/MS.** D. Beggs, Hewlett-Packard, B. Holtz

4:00 **Pollutant Analysis via Negative Ion Chemical Ionization Mass Spectrometry.** D. Beggs, A. Melera, G. Mathers, Hewlett-Packard

4:20 **Field Ionization Mass Spectra of Nitramines and Related Compounds.** D. O. Helton, G. Radolovich, Midwest Research Institute

4:40 **Automated Analysis of Volatile Organic Compounds in Water.** W. D. Snyder, Hewlett-Packard

Thermal Analysis

Thursday Afternoon, Club Room B

R. E. Witkowski, *Presiding*

1:30 **Characterization of Oil Shales by Thermal Analysis.** P. S. Gill, R. L. Blaine, Du Pont

1:50 **Thermal Analysis in Rubber Industry.** R. L. Hassel, R. L. Blaine, Du Pont

2:10 **Thermal Stability of Potentially Hazardous Materials.** K. F. Baker, Du Pont

2:30 **Thermal Methods of Analysis as Applied to Study of Alkali Metal–Concrete Interactions.** G. C. Burrow, R. E. Witkowski, R. G. Charles, Westinghouse R&D Center

2:50 **Detection of Phase Transitions in Nickel and Titanium Alloys by Derivative Differential Thermal Analysis.** J. S. Fipphen, C. A. Seymour, Wyman Gordon Co.

3:20 **Metrication of Thermal Analysis—Conversion to SI Units.** R. L. Blaine, Du Pont

3:40 **New High-Temperature DTA Module—Performance and Applications.** W. P. Brennan, B. Cassel, H. I. Hill, S. D. Norem, M. J. O'Neill, Perkin-Elmer

4:00 **Unique Thermogravimetric Analysis Study of Curie Point and Crystallization Temperatures of Amorphous Metals.** R. L. Fyans, Perkin-Elmer

4:20 **Recent Applications of Thermal Analysis for Quality Control in Electronics Industry.** W. P. Brennan, B. Cassel, Perkin-Elmer

4:40 **Energy Conservation: Contributions of Thermal Analysis Instrumentation.** B. Cassel, W. P. Brennan, R. L. Fyans, Perkin-Elmer

Environmental Analysis—General II

Thursday Afternoon, Room 235A

J. P. Auses, *Presiding*

1:30 **Computation of Error Estimates in Total Elemental Content Passive Dosimeters.** J. G. Montalvo, Jr., Gulf South Research Institute

1:50 **Improved Data Processing Software for Glass Capillary Separations of Complex Environmental Samples.** E. B. Overton, C. F. Steele, J. L. Laseter, U of New Orleans

2:10 **Field Measurements of Atmospheric Methane with Two-Wavelength Laser System.** C. F. Dewey, Jr., MIT

2:30 **Application of Glass Open Tubular Gas Chromatography to Environmental Samples.** S. C. Madden, W. L. Winterlin, J. N. Seiber, T. J. Mast, U of California

2:50 **Collection and Determination of Trace Amounts of Organo-Thiophosphates in Air Using XAD-2 Resin.** F. Kaminski, R. G. Melcher, Dow Chemical U.S.A.

3:20 **Determination of Nickel Carbonyl.** J. E. Campana, T. H. Risby, Pennsylvania State U

3:40 **Collection, Separation, and Analysis of Organic Vapors by Computerized GC/IR.** D. Goldfarb, C. W. Brown, U of Rhode Island

4:00 **In Situ Determination of Total Particulate and Dissolved Organic Matter.** G. V. Winters, D. E. Buckley, Geological Survey of Canada

4:20 **Simplified Techniques for Perchlorination of Polychlorinated Biphenyls in Environmental Samples.** O. W. Berg, G.A.V. Rees, M. S. Ali, Ministry of the Environment

4:40 **Stabilization of I pph Hg (II) Solutions Stored in Polyolefin Containers.** R. W. Heiden, D. A. Aikens, Rensselaer Polytechnic Institute

Liquid Chromatography—Instrumentation

Thursday Afternoon, Room 235B

E. W. Albaugh, *Presiding*

1:30 **Influence of Flow-Cell Characteristics on Liquid Chromatographic Resolution and Fluorescence Sensitivity.** T. J. Porro, R. D. Conlon, J. L. DiCesare, N. A. Sebestyen, Perkin-Elmer

1:50 **High-Efficiency Preparative Liquid Chromatography by Automatic Repetitive Injection and Fraction Collection.** D. Kohler, M. Telepchak, ES Industries

2:10 **Programmable, Software-Controlled Variable-Wavelength Detector for Liquid Chromatography.** A. Maute, Hewlett-Packard

2:30 **New Design Concepts in Liquid Chromatography Instrumentation.** D. H. Rodgers, Tracor Instruments

2:50 **High-Performance Liquid Chromatography Analyzer.** J. I. Fernandez, Technicon Industrial Systems

3:20 **Practical Applications of Programmed Runs: Use of New Automatic Liquid Chromatograph.** L. B. Sybrandt, Spectra-Physics

3:40 **New Approach to Automated HPLC, a Modular Microprocessor System Controller.** R. Stevenson, J. Loram, H. Magnussen, M. Go, Altex Scientific

4:00 **Unique Processor for Liquid Chromatography.** B. A. Bidlingmeyer, D. Friswell, R. McNeil, Waters Associates

4:20 **New LC/MS System.** J. W. Serum, A. Melera, Hewlett-Packard

4:40 **Automation and Liquid Chromatography.** R. Majors, E. L. Johnson, R. Pecsar, Varian

Coblentz Society Award and Symposium

Thursday Afternoon, Little Theater

P. R. Griffiths, *Presiding*

1:30—Presentation of 1978 Coblentz Award

By

Peter R. Griffiths

President of the Coblentz Society

To

Professor Lester Andrews

University of Virginia

Charlottesville, Va.

Award Address

Spectroscopy of Transient Species and Molecular Ions in Matrices

TRACOR SPECTROSCOPY

New instrumentation spanning the spectrum from X-rays to the near-IR.

TN-2000 X-ray Elemental Analysis System brings the full power of x-ray energy spectroscopy to your laboratory in an affordable, convenient, easy-to-operate system. System TN-2000 is easily expandable from qualitative to quantitative capability, with proven software capabilities to meet your analytical needs, *now and in the future.*

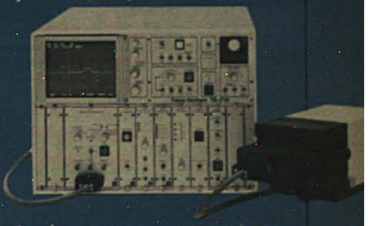
TN-1710 Signal Averager, a new microcomputer-based signal



analysis system. Modular software and hardware allow you to precisely tailor the system to your analytical needs. Powerful data acquisition and processing are under convenient pushbutton *"firmware"* control, with features that include bipolar memory, versatile I/O interfaces, comprehensive alpha-numeric display information, a full repertoire of data processing operations, higher-level interactive programming, and support modules for fast pulse counting, four-input averaging, and parametric sweep averaging.

Visit us at the Pittsburgh Conference, booths 1138, 1140, 1142.

Diode Array Rapid Scan Spectrometer performs rapid



simultaneous measurement from 2000 to 1100 nm with the widest dynamic range and highest sensitivity available, enabling the spectroscopist to perform analyses that are difficult or impossible with conventional instrumentation.

Applications include:

Detector lag-free UV-VIS absorption measurements for chemical kinetics studies.

Measurement of flame and DC arc emission spectra for simultaneous multielement analyses.

Fluorescence, chemiluminescence, and Raman spectral measurements.

UV-VIS absorption/fluorescence measurements for LC peak characterization.



Tracor Northern

Tracor Europa B.V.
Schiphol Airport Amsterdam
Building 706, The Netherlands
Telephone (020) 41 1865
Telex 13695

2551 West Beltline Highway
Middleton, Wisconsin 53562
(608) 831-6511
TWX 910 280-2521

CIRCLE 102

CIRCLE 103

CIRCLE 104

PROGRAM

Applications of Fourier Transform Infrared Spectroscopy

J. L. Koenig, *Presiding*

2:50 Polarized Infrared Emission Spectra from Operating Bearings. J. L. Lauer, Rensselaer Polytechnic Institute

3:25 Fourier Transform Infrared Studies of Coal and Its Derived Products. P. Painter, M. M. Coleman, Pennsylvania State U

4:00 General Meeting—Coblentz Society

Mass Spectrometry (EI, CI, FI, API)

Thursday Afternoon, Ball Room

B. S. Freiser, *Presiding*

1:30 Leadoff Lecture: **Direct Analysis of Complex Mixtures by Mass Spectrometry.** R. G. Cooks, Purdue U

2:10 ICR–The Mass Spectrometer That's Something Else. B. S. Freiser, Purdue U

2:30 Design and Operation Principles of Instrument Providing Simultaneous Separate EI and CI Mass Spectra. M. W. Siegel, Extranuclear Labs

2:50 Analytical Advantages of Simultaneous but Separate CI/EI in GC/MS Analysis. D. K. Bakale, M. W. Siegel, Extranuclear Labs

3:20 Modified Chemical Ionization Source for Elemental Analysis of Electrically Conducting Solids. B. N. Colby, TRW Systems Group, C. W. Hull

3:40 Comparative Chemical Ionization and Electron Impact Mass Spectrometric Studies of Mucohalic Acids and Related Molecules. R. D. Moore, Miami U, J. E. Katon, T. Y. Yu

4:00 Identification of Isomers by Pulsed Positive Negative Ion Chemical Ionization Mass Spectrometry (PPNICI). J. A. Poppiti, G. C. Stafford, Finnigan Instrument Div.

4:20 New Developments in API–MS Applications. M. W. Siegel, Z. C. Curry, Extranuclear Labs

4:40 Identification of Clusters Produced by Atmospheric Pressure Ionization (API) by Collisional Dissociation Method. H. Kambara, Y. Mitsui, I. Kanomata, Hitatchi, Ltd.

Symposium: Automation Comes of Age

Thursday Afternoon, Music Hall

P. B. Stockwell, *Presiding*

1:30 Developments in Philosophy of Automatic Analysis. P. B. Stockwell, Laboratory of the Government Chemist, England

2:10 Specification for Laboratory Automation. S. P. Perone, Purdue U

2:40 Principles Involved in Automation of Manual Procedures for Assay of Water Soluble Vitamins in Food. R. B. Roy, Technicon Industrial Systems

3:30 Automated Reaction Rate Methods of Analysis. H. V. Malmstadt, U of Illinois

4:00 New Concept in Automation of Industrial Analytical Chemistry. R. W. Ardnt, Mettler Instrument Corp., Switzerland

4:30 Teaching Graduate-Level Course in Automatic Analysis or How to Avoid Pedagogical Peristalsis. R. F. Browner, Georgia Institute of Technology

Friday, March 3

General Analysis II

Friday Morning, Room 205

H. Fracek, *Presiding*

8:30 New Instrument for Molecular Emission Cavity Analysis (MECA). S. L. Bogdanski, A. C. Calokerinos, A. Townshend, U of Birmingham

8:50 Combination of Chromatographic and Spectroscopic Techniques with Respect to Photoproduct Analysis. A. Ehrl, Gesellschaft für Strahlen-und Umweltforschung

9:10 Use of Chromatography Data System for Complex Chromatography Calculations. L. S. Ettre, H. D. Hoberecht, J. E. Baudean, Perkin-Elmer

9:30 Application of Nonlinear Pressure Programs and Modification of Mobile Phase Composition in Supercritical Fluid Chromatography. J. A. Graham, J. E. Conaway, L. B. Rogers, U of Georgia

9:50 Vapor Pressure of Tetrachloro-*m*-Dicyanobenzene in Range 90–145 °C by Effusion Method. R. S. Depablo, Diamond Shamrock Corp.

10:20 Reticulated Vitreous Carbon Flow-Through Electrodes. D. J. Curran, A. N. Strohl, U of Massachusetts

10:40 Analysis of Gravimetric Precision over Extended Period. J. W. Mills, Lif-O-Gen, J. Graver

11:00 Extending Wavelength Range of Angstrom V-70 Optical Emission Spectrometer. E. Dubois, J. M. Carrol, P. W. Flynn, Angstrom

11:20 Design Considerations and Performance of UV–VIS Spectrophotometer System. J. Duffield, V. Chupp, K. George, Varian

11:40 Digital Data Acquisition and Processing in Auger Electron Spectrometer. Y. E. Strausser, N. J. Taylor, T. A. Pandolfi, Varian

Trace Analysis

Friday Morning, Room 239

F. P. Byrne, *Presiding*

8:30 Glass: Preconcentrator for Trace Metals. T. S. Wasco, J. L. Fasching, U of Rhode Island

8:50 Survey of Instrumentation Used for Monitoring Metals in Water. M. S. Quinby-Hunt, U of California

9:10 Cylinder Gas Standards: How Much Accuracy Do You Need? C. W. Keith, H. A. Grieco, Airco Industrial Gases

9:30 Matrix Effects in Trace Metal Analysis of Goods by Emission Spectrometry. A. J. Pyzik, W. R. Wolf, USDA

9:50 Trace Element Analysis of Pharmaceuticals by PIXE. R. Litman, A. Mittler, U of Lowell

10:20 Mixing of Solid Standard Reference Materials. R. M. Lindstrom, B. S. Carpenter, NBS

10:40 Determination of Trace Amounts of Polycyclic Aromatic Hydrocarbons in Aqueous Samples. K. Ogan, W. Slavin, Perkin-Elmer

11:00 Instrument and Method for Quantitative Analysis of Trace Hydrazine Vapors in Air. J. R. Stetter, K. Tellefsen, Energetics Science

11:20 Real-Time Analysis of Trace Toxic Contaminants in Ambient and Occupational Environment at Sub-ppb Level. N. M. Reid, J. B. French, J. A. Buckley, D. A. Lane, A. M. Lovett, Sciex

11:40 Detection of Trace Amounts of Organometallics and Other Gaseous Encapsulated Elements. G. A. Capelle, K. R. Westberg, D. G. Sutton, Aerospace Corp.

Acoustic Spectroscopy/Fuels

Friday Morning, Room 3A

J. K. Scanlon, *Presiding*

8:30 Scanning Laser Acoustic Microscope (SLAM). L. W. Kessler, D. E. Yuhas, Sonoscan

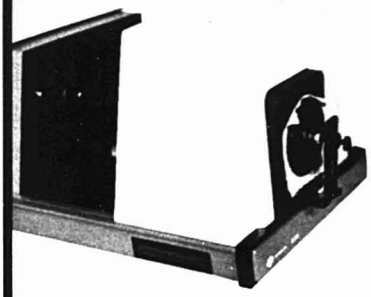
Accurate spectral data come fast and easy with the new **Hunterlab D54P-5 Spectrophotometer,** with the versatility to handle batch adjustment or color formulation.

The **Optical Sensor** features a range of 400 to 710 nanometers in a 3 second scan.

The separate **Signal Processor** contains a microcomputer that prints out the corrected data in 10 or 20 nanometer intervals, and computes color coordinates, color difference and metamerism index.

Tell us your requirements and we'll send more details.

Is the color the same from batch to batch?





HunterLab

Hunter Associates Lab., Inc.

9529 Lee Highway, Fairfax, Virginia 22030 • Telephone: (703) 591-5310

CIRCLE 105 ON READER SERVICE CARD

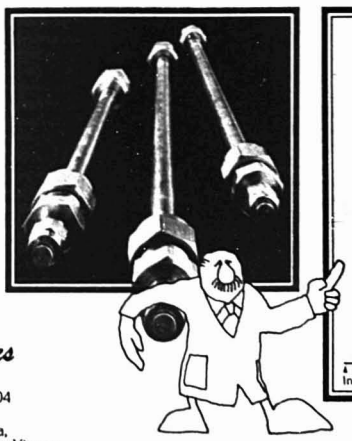
Since the column is the least expensive part of your liquid chromatograph, why not use the best?

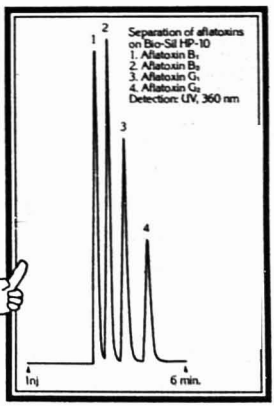
Bio-Rad's new HPLC columns

Bio-Rad's HPLC columns are the best available. That's because Bio-Rad brings more than 20 years of liquid chromatography experience to HPLC technology. Bio-Rad provides columns with guaranteed efficiency (up to 25,000 plates/meter), guaranteed peak symmetry, and superior performance with your instrumentation (or we'll take it back!)

Bio-Rad has the best columns available for adsorption (Bio-Sil HP-10), reverse phase (Bio-Sil ODS-10), and ion-exchange (Aminex resins) chromatography.

Bio-Rad has prepared an eye-opening guide to HPLC column evaluation. For your copy, contact:





BIO-RAD *Laboratories*

2200 Wright Avenue • Richmond, CA 94804
Phone (415) 234-4130
Also in: Rockville Centre, N.Y.; Mississauga, Ontario; London; Milan; Munich; Sao Paulo; Vienna.

CIRCLE 26 ON READER SERVICE CARD

8:50 Resonant Optoacoustic Spectroscopy Sample Cell. S. Rosenstark, R. Lee, J. W. Bozzelli, New Jersey Institute of Technology

9:10 Luminescence Quantum Efficiency Measurements by Optoacoustic Spectroscopy. G. F. Kirkbright, M. J. Adams, J. G. Highfield, Imperial College

9:30 Versatile Double-Beam UV–VIS Instrument for Photoacoustic Spectroscopy (PAS). R. E. Blank, T. Wakefield, Gilford Instrument Labs

9:50 Industrial Applications of Photoacoustic Spectroscopy. H. Pawlowski, Gilford Instrument Labs

10:20 Toxic Gas Monitor with ppb Sensitivity Using Automated Laser Optoacoustic Spectrometer. T. Wakefield, R. E. Blank, Gilford Instrument Labs

10:40 Photoacoustic Spectroscopy Studies of Laser Window and Thin Film Materials. N. Fernelius, U of Dayton

11:00 Optical Activity of Shale Oil. D. L. Lawlor, U.S. Department of Energy, D. R. Latham, R. O. Asplund

11:20 Optical Activity Parameters of Chiral Alkanes from Oil Shale. R. O. Asplund, U of Wyoming, D. L. Lawlor

11:40 Determination of Aromaticity of Fuels and Lubricant Basestocks by Ultraviolet Spectroscopy. F. M. Newman, M. K. Greenberg, Southwest Research Institute

Environmental Analysis—Air Pollution

Friday Morning, Room 235A

J. E. Snodgrass, *Presiding*

8:30 Analytical Chemistry and Best Available Technology for Air Pollution Control. R. T. Oliver, Foxboro Co.

8:50 Atmospheric Sulfur Analyzer. M. J. Trzeciak, IBM

9:10 Analytical Methodology for Measurement of Biogenic Sulfur Emissions. S. O. Farwell, U of Idaho, D. F. Adams, W. L. Bamesberger

9:30 Applicatior of Instrumental Neutron Activation Analysis to Determination of in Vitro Solubility of Fly Ash Particles. S. H. Weissman, K. F. McCarty, Lovelace Biomedical and Environmental Research Institute

9:50 Laser Optoacoustic Detection of Ozone, Ammonia, and Particulates. J. W. Bozzelli, D. R. Castellano, S. Rosenstark, R. Lee, New Jersey Institute of Technology

10:20 ESCA Study of Air Filters. J. M. Blaisdell, G. R. Grieger, Walter C. McCrone Associates

10:40 Technique for Determining Minimum Level of a Variable Consistent with a Set of Environmental Data. J. L. Fasching, U of Rhode Island

11:00 Sampling and Determination of Diesel Particulate. S. R. Prescott, T. H. Risby, Pennsylvania State U

11:20 Determination of Benzo(a)-pyrene and Other Polynuclear Aromatic Hydrocarbons in Airborne Particulate Material by Ultrasonic Extraction and Reverse-Phase HPLC with Fluorescence Techniques. C. Golden, E. Sawicki, EPA

11:40 Simultaneous Multielement Preparation of Air Particulate Standard Reference Materials and Their Application in Intercalibration of Analytical Instrumentation. K. W. Olson, V. A. Fassel, Iowa State U

Thin Layer/Gel Permeation Chromatography

Friday Morning, Room 235B

M. A. Phillips, *Presiding*

8:30 On the Stability of Benzo(a)-pyrene in Solution and or Thin-Layer Chromatographic Plates. H. J. Issaq, G. M. Janini, E. W. Barr, NCI Frederick Cancer Research Center

8:50 Determination of Boron by Spectrodensitometry of Thin-Layer Chromatograms. J. C. Touchstone, M. F. Dobbins, G. J. Hansen, D. R. Rossien, U of Pennsylvania

9:10 Reversed-Phase (C_{18}) TLC and Its Correlation to Partisil 10 (C_{18}). T. Beesley, M. Mazzei, E. Heilwiel, Whatman

9:30 Correlation of TLC, HPTLC, and PMD Results and Their Transfer to HPLC Systems. H. J. Issaq, B. Shaikh, N. J. Pontzer, E. W. Barr, NCI Frederick Cancer Research Center

9:50 Electrophoretic Study of Ions on Filter Paper. H. G. Mukherjee, S. K. Dutt, Calcutta U

10:20 GPC of Aqueous Soluble Polymers. F. E. Regnier, K. M. Gooding, K. C. Lu, Purdue U

10:40 Cleanup of Vegetable, Straw, and Forage Plant Samples for Organophosphate Residue Analysis Utilizing Methylene Chloride/Cyclohexane Solvent System with Automated Gel Permeation Chromatography. C. M. Schofield, L. D. Johnson, R. W. Leicht, R. H. Waltz, Analytical Biochemistry Labs

11:00 Design and Applications of New Microcomputer Data System for GPC-Coupled Low-Angle Laser Light Scattering. M. L. McConnell, F. C. Siu, P. J. Christ, Chromatix

11:20 Copolymer Analysis with Gel Permeation Chromatography and Computerized IR Spectroscopy. E. G. Bartick, R. W. Hannah, Perkin-Elmer

11:40 Data Treatment in High-Performance Size Exclusion Chromatography. S. D. Abbott, Du Pont

Statistics, Mathematics, & Models

Friday Morning, Little Theater

P. M. Castle, *Presiding*

8:30 Pattern Recognition: Informational Content of Training Vectors Applied to Serum Chemistries. J. C. MacDonald, T. J. Mercolino, Fairfield U

8:50 On-Line Pattern Recognition System for Structural Interpretation of Mass Spectra. S. L. Kaberline, C. L. Wilkins, U of Nebraska

9:10 Adaptable Algorithm for Computer Comparison of Mass Spectra. S. Sokolow, Finnigan Instruments Div.

9:30 Practical Considerations for IR Spectra Identification by Band Searching of Large Computer Data Base. C. D. Craver, N. N. Tompkins, D. J. Derges, IRGO-Chemir Labs

9:50 New Method for Nonlinear Mapping That Includes Analytical Uncertainties. J. C. Rossell, J. L. Fasching, U of Rhode Island

10:20 Calibration and Quality Cortrol in Routine Chemical Analysis. D. G. Mitchell, J. S. Garden, New York State Department of Health

10:40 Variable-Variance Regression Techniques for Calibration Curve-Based Analysis. J. S. Garden, D. G. Mitchell, W. N. Mills, New York State Department of Health

11:00 Theory of Tolerable Error in Factor Analysis. E. R. Malinowski, H. Rozyn, Stevens Institute of Technology

11:20 Fundamental Parameters vs. Regression Analysis Accuracy. D. M. Bartell, D. A. Gedcke, B. D. Wheeler, Ortec

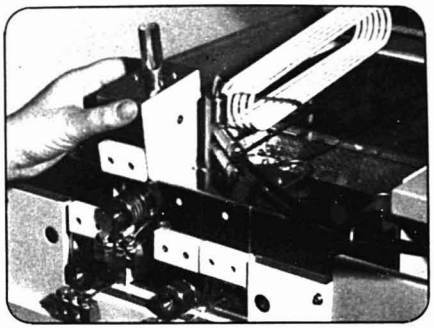
11:40 Curve Smoothing Attachment to Stripchart Recorder. J. Ketseas, J. Rendina, Spex Industries

GAS CHROMATOGRAPH SPECTROPHOTOMETER

Only From Shimadzu

★

A Unique Analytical Cartridge System For Gas Chromatographs.



GC-6AM Gas Chromatograph

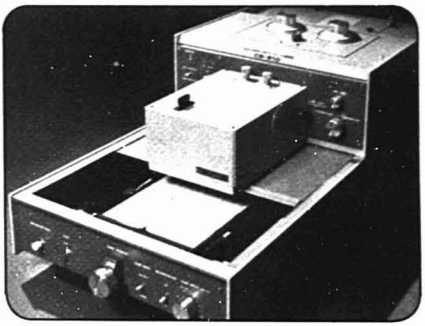
Only Shimadzu offers the Analytical Cartridge System combining detector, column and injection port in a single unit.

1. Quick, easy interchangeability of analytical system using cartridge units.
2. Large selection of cartridge combinations to meet your analytical demands.
3. On column, on detector, all glass system to minimize sample/component degradation.
4. Minimizes down time when cleaning injection port, detector, or changing columns.
5. Four cartridge capacity.
6. Twelve different cartridge selections to chose from.

★ **U.S. PATENT 4,044,593**

★★

A New Generation of TLC and Gel Scanner.



CS-910 TLC Scanner

Only Shimadzu offers a TLC Scanner combining the quantitative accuracy of TLC densitometry with the high resolutions of gel scanning.

1. DUAL-WAVELENGTH METHOD eliminates baseline fluctuations caused by local irregularities in thin-layers or gels.
2. ZIG-ZAG SCANNING TECHNIQUE eliminates errors caused by the irregular shape of the developed spots.
3. Unique WORKING CURVE LINEARIZER provides excellent linearity over a wide density range—eliminates errors resulting from different size spots.
4. Built-in BACKGROUND CORRECTOR minimizes the effects of contamination on TLC plates.
5. Extremely sensitive FLUOROMETRY MODE permits precise quantitation of ultra-micro content samples.
6. TRANSMISSION ON REFLECTION METHOD can be easily selected.

★★ **U.S. PATENT 4,013,364 and 3,994,587**

See SHIMADZU at the Pittsburgh Conference, Booths 1509–1519

SHIMADZU SCIENTIFIC INSTRUMENTS, INC.
OAKLAND RIDGE INDUSTRIAL CENTER, 9147-H RED BRANCH ROAD COLUMBIA MARYLAND 21045
PHONE (301) 596-6978, (301) 997-1227 TELEX 87-959

SHIMADZU SEISAKUSHO LTD.
KYOTO JAPAN

CIRCLE 193 ON READER SERVICE CARD

See us at booth 1201-1206

Waters Has Everything for the Liquid Chromatographer

NEW! Waters' Controlled-Temperature Liquid Chromatograph/Gel Permeation Chromatograph Model 150C.

For facts, see page opposite. For new brochure ...
CIRCLE 236 ON READER SERVICE CARD

NEW! Waters' Liquid Chromatographic Solvents

Manufactured and tested for quality and reproducibility for your applications success. To ensure high quality, each solvent batch is serial numbered and quality controlled to rigidly-set end-use LC standards. Solvents available include: Acetonitrile, tetrahydrofuran, methylene chloride, methanol, hexane, and chloroform.
CIRCLE 237 ON READER SERVICE CARD

NEW! Waters' SEP-PAK Cartridges for Rapid Sample Preparation.

Whatever the analytical method used for final analysis, small, self-contained SEP-PAK™ cartridges will drastically reduce sample preparation to no more than a few steps which can be performed in a matter of minutes.
CIRCLE 238 ON READER SERVICE CARD

AND . . . WISP™, Waters' Intelligent Sample Processor.

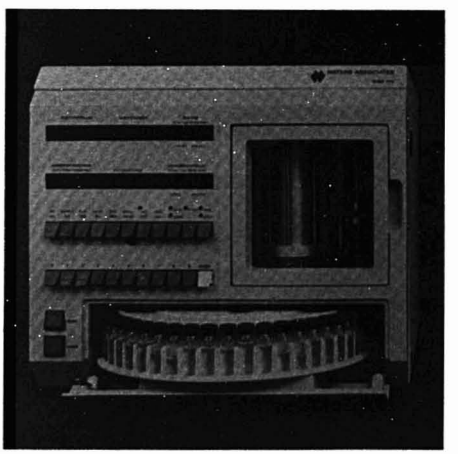
One in a family of "intelligent modules" designed to operate independently or interactively with other Waters' modules. WISP automatically injects 48 different samples. YOU program the number of injections per vial and the sample volume per vial. YOU set the time for each analysis. WISP allows you to load the carriage, set the operating parameters, and walk away — run samples overnight if you wish.
CIRCLE 239 ON READER SERVICE CARD

NEW! Waters' PrepPAK/C_{18} Cartridges.

For the PrepLC™/System 500 Preparative Liquid Chromatograph. Multigram purification in minutes in a reverse-phase mode is now possible with PrepPAK™-500/C_{18} cartridges for use with Waters' PrepLC/System 500 preparative liquid chromatograph. PrepPAK-500/C_{18} cartridges are second in the family of prepacked cartridges for PrepLC.
CIRCLE 240 ON READER SERVICE CARD

NEW! Waters' Fluorescence Detector

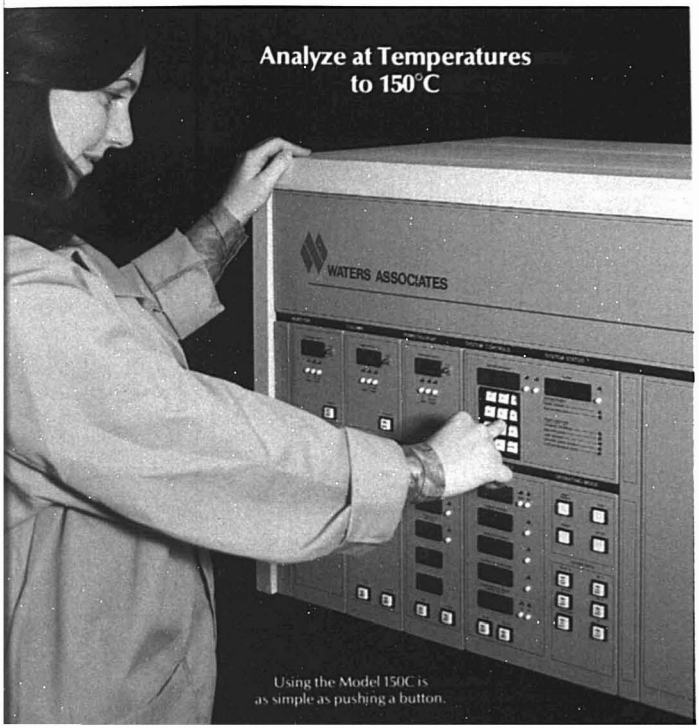
The Model 420 detector is a highly sensitive instrument for the detection of fluorescent compounds. Uniquely designed, flow-through sample chamber, of less than 10 microliters volume, minimizes band-spreading. Modular design incorporates LED readouts with reliable solid state integrated electronics. Excitation and emission filters, lamp and flowcell assembly are all readily accessible to the user, and easily changeable.
CIRCLE 241 ON READER SERVICE CARD



Waters
137 Maple Street, Milford, MA 01757
Telephone (617) 478-2000
The Liquid Chromatography People

From Waters — Originator of the Gel Permeation Chromatograph

Controlled-Temperature Liquid Chromatograph/ Gel Permeation Chromatograph



Now, you can analyze materials that dissolve only at elevated temperatures or require elevated temperatures to reduce viscosity. With Waters "Hot One", the Model 150C, you can analyze these materials in minutes!

The Model 150C provides:

- **Rapid Results**
  Sample Preparation
  7-15 Minute Separations
  Data Reduction
- **Ease of Operation**
  Simple
  Reliable
  Microprocessor Controlled
- **Flexibility**
  Factory Preprogrammed
  Operator Programmed
- **Safety**
  Totally Self-Contained Environment
  Zero Voltage Switching
  Multiple Internal Sensors and Alarms
  Coupled with Microprocessor Controls for Corrective Action
  No External Hot Solvents

First-generation controlled-temperature liquid chromatograph/ gel permeation chromatograph, The GPC 200.

Second-generation controlled-temperature liquid chromatograph/ gel permeation chromatograph, the Model 150C.

With the new Model 150C you benefit from all the experience and knowledge gained since Waters introduced the first commercial GPC instrument in 1963.



For more information on the Model 150C, send now for this brochure.



Waters

137 Maple Street, Milford, MA 01757
Telephone (617) 478-2000
The Liquid Chromatography People

CIRCLE 242 ON READER SERVICE CARD



Plasma AtomComp III

The instrument you asked Jarrell-Ash to make.

The newest Plasma AtomComp — **Mark III** — is the instrument hundreds of laboratories we surveyed asked us to produce.

It is a fully digital, easy-to-use system with an integral computer. A **PDP-11** computer.

This direct-reading plasma spectrometer actually matches AA in sensitivity. But to this sensitivity it adds a remarkable **capacity.** It can determine up to 48 elements simultaneously, in any combination, in any concentration, in a little over a minute.



The Mark III's computer: a PDP-11. It serves as spectrochemical controller and as manager of data acquisition-&-handling.

Just what the doctor ordered, when the problem is trace metals in solution, no matter what the field. Water, wastewater, air, soils, food, alloys, wear metals in petroleum, metabolites in biologicals — the Mark III will **expedite** your workloads.

Not an add-on.

Unlike other systems on the market, the new third-generation Plasma AtomComp from Jarrell-Ash was designed **from the start** as a computer-controlled, computer data-managing instrument. This gives the Mark III a number of advantages over analog systems with a computer add-on.

For example, it has a significantly smaller number of parts — hence there's less possibility of downtime. It has self-diagnostic capability — hence there's no tedious check-out of electronics.It achieves a new level of speed — its 48 detectors can be read computer-fast, not one-at-a-time over a period of time. And it brings a new level of precision to the field — because its detectors are read with a sensitivity that is ultimately a **digital number,** not an analog approximation.

Easy does it.

The system is as easy to operate as a typewriter. No computerese spoken here. You can tell your Mark III to erase all previous analytical results . . . run new samples in replicate . . . average the data . . . print out in % concentration, ppm, ppb, or any other units you need. You can even have different elements in the **same** sample print out in different units. You're boss.

You get automatic analysis over a dynamic concentration range of **100,000** — in a single sample — without changing a single parameter. And sequential analysis of widely differing concentrations from one calibration.

Mark III's integral PDP-11 gives it greater capabilities than ever — faster. Printout and subsequent runs can overlap, if you wish. You get outstanding storage **flexibility.** And you can expand into higher-level languages for data-handling when your needs change.

Plasma AtomComp III from Jarrell-Ash. In this age of crucial trace-metal and effluent analyses, can you settle for less?

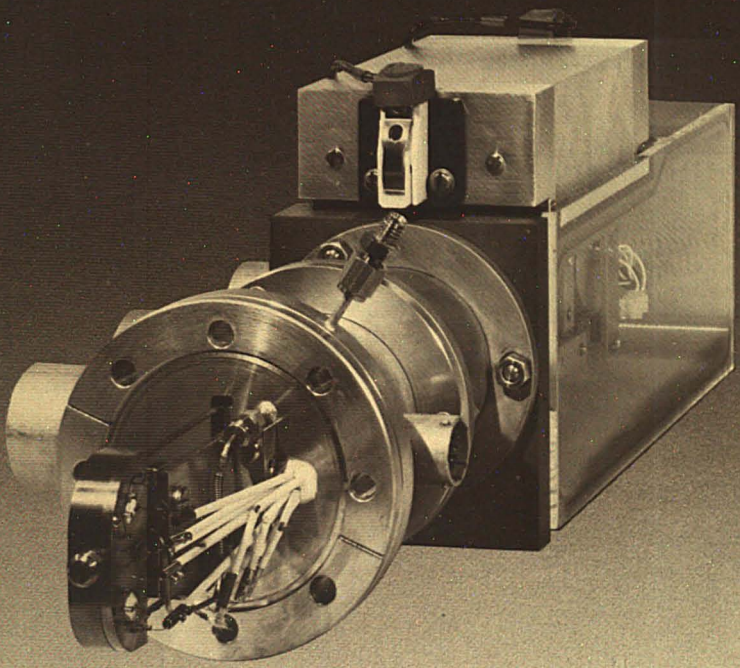
To talk plasma spectrometry with an expert, call Dr. Arthur Ward at Jarrell-Ash headquarters. He knows the Mark III. The phone is **617-890-4300.** For product literature, use the reader-service number below.

Jarrell-Ash
A Division of Fisher Scientific Company
590 Lincoln Street Waltham, MA 02154

Be sure to see Jarrell-Ash at the 1978 Pittsburgh Conference. Exhibits, workshops, demonstrations.

CIRCLE 73 ON READER SERVICE CARD

LC/MS NOW



HIGH CHROMATOGRAPHIC INTEGRITY
HIGH SENSITIVITY LC DETECTION
HIGH SAMPLE YIELD
FREE CHOICE EI/CI IONIZATION
NO INTERFERENCE WITH GC/MS OR PROBE OPERATION

ASK THE SPECIALISTS — ASK FINNIGAN

finnigan INSTRUMENTS
845 W. MAUDE
SUNNYVALE, CALIFORNIA 94086
Visit us at the Pittsburgh conference, booth 315–320
CIRCLE 77 ON READER SERVICE CARD

New Products-A Preview

Exposition of Modern Laboratory Equipment
Cleveland Convention Center
February 27-March 2, 1978

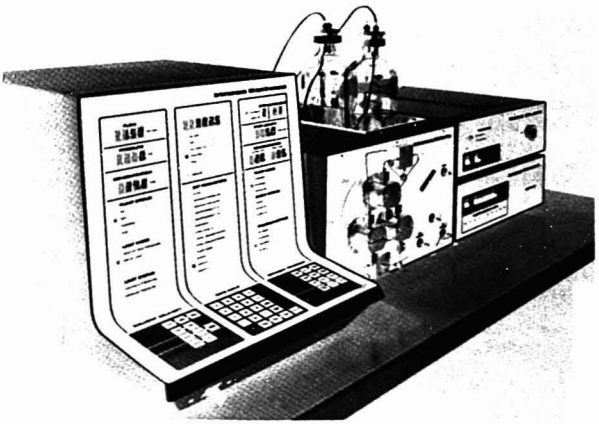
Voltametric/Amperometric Detector for HPLC

The Metrohm V/A Detector E 611 incorporates a flow-through "wall-jet" cell with a glassy carbon or carbon paste electrode coupled to a voltametric/amperometric detector. It features a large dynamic range and good reproducibility. With the instrument the investigator can choose from four different detection modes: DC polarography, DC Tast polarography, and two differential pulse polarography modes. Initial potential, pulse heights, and integration times can be chosen in accordance with the exact application. Brinkmann Instruments Inc. **433**

Polarographic Liquid Chromatography Detector

Model 310 uses the Model 303 static mercury drop electrode module to achieve ppb level sensitivities for pharmaceuticals, pesticides, vitamins, additives, pollutants, and many other compounds. It incorporates a specially designed, minimal dead volume glass cell, within which the LC eluate is led up and around the mercury droplet. All substances that exhibit polarographic responses can be detected. Model 310 can be connected to any LC without hardware modification. Princeton Applied Research Corp. **431**

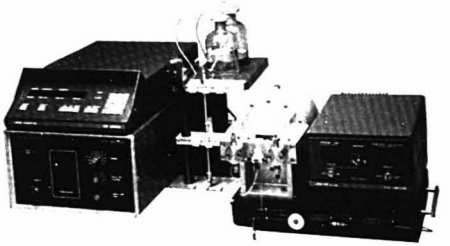
For more information on listed items, circle the appropriate numbers on one of our Readers' Service Cards



Model 850 high-performance liquid chromatography system, designed for either isocratic or gradient operation, features a central digital controller with a visual display. It provides convenient random operator access to all key system parameters. Several vital parameters can be changed at any time without interrupting an analysis. The controller can also be used diagnostically to isolate the causes of component malfunction. The pumping system controls flow rate by combining the digital controller with a low internal volume (50 μL/stroke), trihead, reciprocating piston pump. This provides more uniform delivery of mobile phase throughout the flow and pressure range. The oven in the column compartment keeps solvent, columns, and samples at the same temperature (range is 35–140 °C). Digital control is also extended to the UV/VIS absorbance detector (sensitivity 0.002 AUFS ± 1% noise). Other features for gradient elution include mixing of solvents on the low side of the pressure pump; a low-volume, high-efficiency mixing chamber; and a degassing system to eliminate bubble formation. The system can be interfaced with data handling and reduction systems. Du Pont Instruments **401**

Liquid Chromatography Supports

Chromosorb LC-6 is a fully porous microparticulate silica highly selective in separating close polarity compounds with an isocratic solvent system, or in separating wider polarity range mixtures with gradient elution. Chromosorb LC-7 is prepared by chemically bonding an octadecyl group to a silica support through a silicon–oxygen–silicon–oxygen type bond. A closely controlled reaction provides a C_{18} nonpolar stationary phase of excellent performance in either partition or ion pair chromatography modes. Chromosorb LC-8 is prepared by chemically bonding a cyano-type group to a Chromosorb LC-6 silica surface. It is highly polar and very efficient in separating polar compounds. Johns-Manville **420**



The XP-liquid chromatography system features microprocessor control, a gradient programmer, a solvent delivery system, and a wide range of detectors. Resolution of % B in A is controlled to ±0.5% to give the highest repeatability of retention times. The gradient programmer requires only one pump. It provides nine segments, each up to 99 min, and each capable of being programmed with a choice of 99 curve shapes plus a step function. High-pressure capability is made possible through the digital solvent delivery system, which gives smooth, pulse-free operation up to 10 000 psi with flow rates up to 10 mL. Detectors available include: a fixed wavelength UV detector that operates at 254 nm; a variable wavelength UV detector that operates at 190 nm; an electron capture detector; and a universal flame ionization detector. Philips Electronic Instruments, Inc. **402**

HPLC Detection System

The MM 700 memory module for automatic baseline correction eliminates the problems associated with solvent slopes and other absorption phenomena not related to the sample being examined. The MM 700 can be added along with the SFA 339 wavelength scan drive to the SF 770 UV–VIS monitor for greatly enhanced utility and flexibility. Scannable wavelength is 190–700 nm (in two steps), and resolution is 0.1% of the full scale value selected. Output is compatible with any 10-mV recorder. Information regarding retrofitting of SF 770 units currently in use with the new modules is available. The MM 700 memory module is $1980, and the SFA 339 wavelength scan drive is $585. Schoeffel Instrument Corp. **423**

High-Performance Radial Chromatography

The system includes the Nanomat automatic spotter, a U-chamber for radial development, and a radial scanner to quantitate separations. Both the automatic spotter and scanner can be used also for classical, linear TLC. The system produces high-resolution separations in less than 5 min on 5 × 5 cm HPTLC plates. Retention data are reproducible to ±0.01 Rf units. Experimental parameters are fully controllable. The HPRC system can be used as a pilot technique for high-performance columns. Camag Inc. **427**

For more information on listed items, circle the appropriate numbers on one of our Readers' Service Cards

Microsample Chromatograph

The Familic-100 features the ability to handle and separate samples as small as 0.1–1.0 μL. Material is processed in any of four discrete flow rates: 2, 4, 8, and 16 μL/min. Using a very small precolumn followed by a small final column, the Familic-100 requires only about 1% of the amount of packing of conventional columns, requires less of a sample, and feeds directly into UV absorbance detector equipment. The column is Teflon to resist corrosion and contamination of the sample. Jasco Inc. **426**

Automatic Samplers

A new line of automatic samplers can accommodate from 40 to 120 samples per batch. One model can also operate as a fraction collector using the timed flow method. The units are offered for OEM as end-user applications. Remote switching capacity is standard and facilitates operator intervention or interfacing with other equipment. Lachat Instruments **436**

Liquid Chromatographs

The Analyst Series 7800 are integrated high-performance isocratic and gradient systems designed for economy and ease of operation. The isocratic system includes a 5000 psi pump and controller, with a choice of fixed or variable wavelength UV detectors (and others), plus a section for mounting columns, injection valve, and housing solvents and effluent containers. The gradient system includes two 5000 psi pumps with a complete nine-function gradient forming controller, and variable or fixed wavelength detectors. Facilities are also included for column mounting, sample injection, and solvent storage. Laboratory Data Control **405**

HPLC System Controller

The Model 420 microprocessor system controller is compatible with all recent Altex hardware. It is designed to control and program the functions of sample injection, solvent selection, automatic recycle and column switching, total flow rate, solvent composition, and chart speed. Programs are easy to write, and up to 10 separate methods can be written and stored in the controller. These can be recalled at any time or can be looped together sequentially for unattended methods development. Altex Scientific Inc. **432**

HPLC Columns

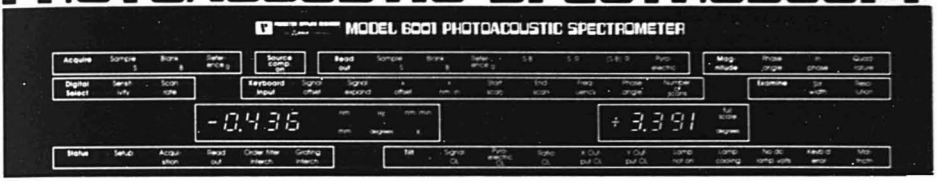
Six new packed columns, all 4.6 mm i.d. × 25 cm long and using LiChrosorb packings, are available. The two ion-exchange columns include 10-μ high-efficiency, high-capacity AN and KAT units. For the adsorption phase, a 10-μ Alox T column is offered. The three reverse-phase columns include two 10-μ units, the RP-2 and RP-18, and a 5-μ RP-18 with 24 000 plates/m. All three feature a symmetry of 1.8. Each column is shipped with its own test chromatogram and is guaranteed with respect to minimum plates per meter and peak symmetry. Rheodyne, Inc. **428**



Model 860 high-performance liquid chromatograph is designed as a rugged and reliable instrument for repetitive analysis such as quality control. The manually controlled 860 consists of three main modules: solvent delivery, heated column compartment, and detector. The solvent delivery system is a constant-volume, dual-piston reciprocating pump with flow rate precision of ±1% at 0.1–9.9 cm^3/min. The heated column compartment provides temperature control to ±1 °C over the entire useful chromatographic range. Rapid solvent changeover is facilitated by a solvent flushing valve in the oven compartment with an exterior drain. Other features include preheated mobile phase and injector, and UV/VIS detector with autozero and high sensitivity. Du Pont Instruments **403**

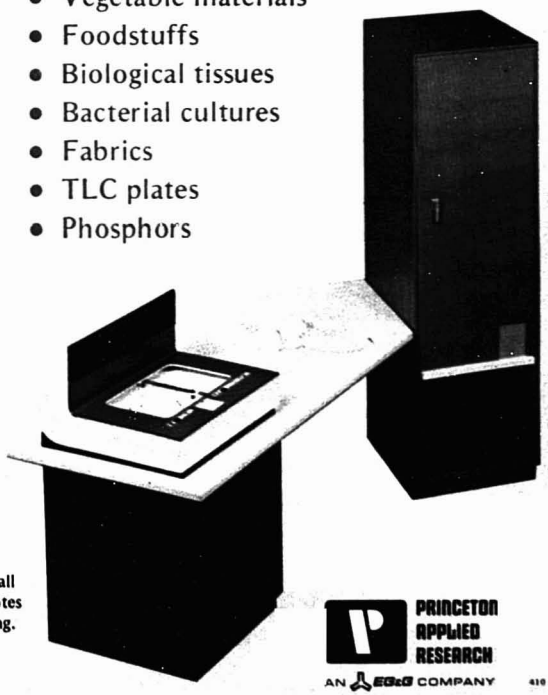
Analyze from another point of view...

PHOTOACOUSTIC SPECTROSCOPY



... such varied samples as:

- Pharmaceuticals
- Gels
- Rare earths
- Suspensions
- Semiconductors
- Cosmetics
- Catalysts
- Plastics
- Organometallic compounds
- Polymers
- Clays
- Paint chips
- Vegetable materials
- Foodstuffs
- Biological tissues
- Bacterial cultures
- Fabrics
- TLC plates
- Phosphors



THE PARC MODEL 6001 FEATURES:

- Microprocessor control
- 200 nm–1600 nm spectral range
- 2 nm spectral bandwidth
- Realtime source compensation
- Self-contained memory & X-Y recorder
- Differential and ratiometric capability
- Multiple scan averaging

Get the full story on the Model 6001 from PARC. Call or drop us a note. We have brochures, application notes and a bibliography which are yours free for the asking. Princeton Applied Research Corporation, P. O. Box 2565, Princeton, New Jersey 08540; phone: 609/452-2111.

PRINCETON APPLIED RESEARCH
AN EG&G COMPANY

410

Circle #165 for Salesman to Call. Circle #204 for Additional Information Only.
See these instruments at the Pittsburgh Conference, booth #117–124.



in a beautiful new package

Versatility.

LDC announces two new HPLC systems with some exceptional advantages over ordinary systems. In the new Analyst 7800 series individual modular components can be taken out as easily as removing a bureau drawer, for use in another part of the laboratory. Yet the Analyst is delivered as a completely interconnected system, in a compact, functional housing.

If you already have LDC modular components, they can be used in the new Analyst 7800 series.



ANALYST 7800
ISOCHRATIC

Economy.

The Analyst 7800 dual pump gradient system with variable wavelength UV detection is available for under $13,000. The isochratic system with variable wavelength UV detection is available for under $9,000.

Mail the coupon for the complete story of the Analyst 7800.

Liquid chromatography by LDC

CIRCLE 248 ON READER SERVICE CARD

LABORATORY DATA CONTROL
Division of Milton Roy Co.
P.O. Box 10235, Riviera Beach, Fl. 33404
305/844-5241. Telex 513479 (148)

Please send me the Analyst 7800 brochure

Name _____

Institution _____

Address _____

City _____

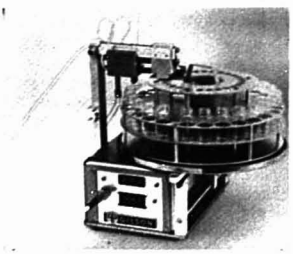
State _____ Zip _____



The Nanomat automated TLC spotter uses an electromagnetic field control system to deliver quantitative and qualitative samples to high-performance and classical TLC plates. It can also use specially designed Pt–IR tipped pipets to apply samples as small as 5 nL. Each spot is precisely positioned and is identical in volume and diameter to previously applied samples. Spot size and volume are determined by the length of time the pipet is in contact with the layer, which is controlled by the Nanomat. Camag Inc. **407**

Monolayer-Bonded Phases

Zorbax particles are composed of tiny, extremely uniform silical sol beads agglutinated in a patented polymerization process to produce a spherical particle with exceptional control of pore structure and particle size. Packing uniformity is excellent due to its uniform spherical shape and narrow particle distribution. All Zorbax-bonded phases (ODS, CN, and C-8) are produced from monofunctional silanes. The use of these silanes and associated reaction technology results in monolayer-bonded phases with maximum surface coverage. The use of monofunctional silanes is the best way to achieve reproducible chromatographic packings. Zorbax ODS is a reversed-phase packing for compounds of moderate to low polarity. Zorbax C-8 is a reversed-phase packing for compounds with moderate to high polarity. Zorbax CN is a polar-bonded phase for use in both normal and reversed phase. Du Pont Instruments **435**



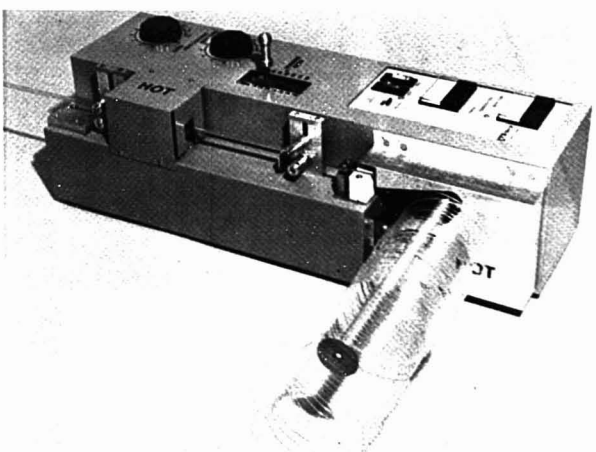
The Mini-Escargot fraction collector for liquid chromatography features a wide selection of rack combinations including a scintillation vial rack holding twenty-seven 28 × 57 mm vials, and racks holding 9-mL glass and 6- and 15-mL polypropylene tubes. It collects by drop counting or time mode operation and contains a 3-digit light emitting diode display. Volume collection can be achieved by combination with the constant flow Minipuls pump. Gilson Medical Electronics, Inc. **404**

Nitrogen Detector for GC

Model 705 gas chromatograph/chemiluminescent nitrogen detector provides specific detection of chromatographic peaks containing chemically bound nitrogen (ppb level). It uses the chemiluminescent detection method to sense the presence of nitric oxide. Compounds eluted from the column are pyrolyzed in a furnace and contacted with ozone. The light resulting from the flameless reaction between nitric oxide and ozone is monitored by a photomultiplier tube. The 705 GC/CND can be used with virtually any gas chromatograph. Other features include a diagnostic display with lights indicating operational discrepancies, digital display of signal integration, and analog output for a 0–1-mV recorder. Antek Instruments, Inc. **421**

Reversed-Phase Thin-Layer Chromatography Plates

The 5 × 20 cm EM brand TLC plates are coated with an organosilane derivatized silica gel sorbent with two carbons (RP-2), available with and without fluorescent (F-254) indicator. The plates facilitate the separation of lipophilic samples soluble in moderately polar solvents. The RP surface can be used in a wide pH range of 1–8 without swelling. MC/B Manufacturing Chemists **424**



The Capilliform II capillary drawing machine features oven and bent tube temperature controls and readouts, quick change "gear shift" that permits the selection of eight drawing ratios without the use of special tools, and optional coil length indicator for direct readout of capillary length. Columns of various ID can be drawn. The drawing speed is 50 m/h; drawing ratios available are 75, 82, 90, 100, 105, 112, and 125. RFR Corp. **406**

FID Flow Meter

The FID flow meter is a three-tube unit that serves as a control center to monitor and permit regulation of the fuel gas, air, and the carrier gas in FID gas chromatography. The three tubes are properly sized for air, hydrogen, and nitrogen or helium flows. Control valves are located at the flow meter outlets to allow precise flow controls. The unit is rated at 200 psi to fit the specific needs of an FID system. Available in either aluminum or stainless steel. Matheson **430**

HPLC Sorbents

LiChroprep, an EM brand sorbent, is available as derivatized silica gel for preparative reversed-phase chromatography (RP-2, 8, and 18) and underivatized silica gel for adsorption-normal phase chromatography (silica gel Si-60). Particle size ranges are 15–25 or 25–40 μ. These particle sizes enable the chromatographer to easily pack his own columns, either dry packed or slurry packed, under hydrostatic pressure. MC/B Manufacturing Chemists **425**

GC Precolumn Venting System

Model 250 is suitable for use with all detector types and adapts easily to most chromatographs. Control of the precolumn separation is achieved by a split jacket cold spot chamber that distributes liquid CO_2 coolant around a discrete section of the precolumn. Column head pressure is accurately controlled during venting, permitting its use with flow sensitive detectors. The unit eliminates the need to reduce samples to small volumes or dryness where components of interest may be partially lost; it permits the injection of halogenated solvents when electron capture detectors are used. It can also be used as a splitless injector for capillary column applications. Venting of solvent, excess derivatizing agents, and unwanted reaction by-products, as well as flushing of unwanted late eluting compounds, can all be accomplished. Analytical Biochemistry Laboratories, Inc. **422**

Hydrogen Transfer System

The HTS, incorporated into the Series-S gas chromatographs, ends the trouble hydrogen causes because of unpredictable, nonlinear response when measured in a helium carrier. The device uses the properties of a palladium alloy in a double-wall tube design that selectively transfers hydrogen into a nitrogen carrier while leaving all other components in the helium carrier. The result is excellent sensitivity and predictable, linear response to hydrogen. Carle Instruments, Inc. **434**

Computerized IR Spectrophotometer

Integrated with the research grade 4260 IR spectrophotometer is a basic computer, a complete signal interface box, and applications software on floppy disc storage. The turnkey IR system can digitize and store spectra on floppy disc, process the data fully through 12 operational programs, and transmit to a printer or plotter for final answers. Computer operations typically include spectral subtraction, addition, signal averaging, along with a peak pick/search/match routine for compound identification. Each user can build a high-speed personalized data file for exact identification since spectra comparison operations are completely flexible. An operator can place a sample in the 4260 for final answers to complex identifications. Beckman Instruments, Inc. **438**

Digital Phosphorimeter

Based on a pulsed source and gated photomultiplier, the phosphorimeter is designed as an accessory to the Fluorolog spectrofluorometer. Features include variable delay time, data acquisition time, flash repetition frequency, and data integration. Initiated by pulses from the excitation lamp, the timing sequences consist of a delay time variable from 1 μs to 10 ms and a data acquisition window from 10 μs to 1 s. Spex Industries **439**

Curve Smoothing

A simple device that solves the equations for 7-point smoothing of data is offered as an adjunct to Spex spectrometer systems. The device continuously smooths incoming data before they are plotted. Spex Industries **440**

Spectrofluorometer

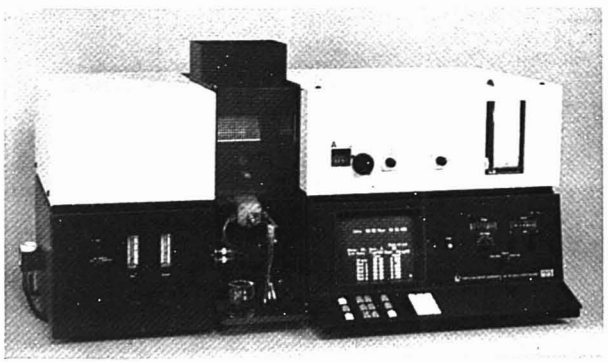
Model MK-2 features improved performance, simplified push-button operation, automatic selection of sensitivity scale corresponding to sample signal intensity, digital display of luminescence with serial BCD output, and a sealed lamp housing that eliminates ozone. The modular design concept permits use of the full range of available accessory equipment including corrected spectra, double-beam differential fluorescence and absorption, TLC scanners, and phosphorescence capability. Farrand Optical Co., Inc. **442**

Thermoelectric Temperature Control

This temperature control system is offered as an accessory to all PM 6 spectrophotometers. The unit comes with a 4-position cell carrier that can be cooled or heated over a range from 0 to 100 °C. Any selected temperature can be maintained with an accuracy of better than 0.1 °C. With an optional temperature sweeper, temperature changes can be programmed linearly with time over a range of 50 °C. Temperatures within a sample can be monitored with an auxiliary probe and can also be displayed on the control unit. Carl Zeiss, Inc. **441**

Automated Spectrofluorometers

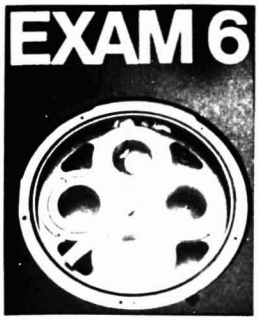
The Autoprocessor-1 is a microprocessor system for automating the MK-1 and MK-2 scanning spectrofluorometers. In conjunction with the corrected excitation module that provides real time data, all functions performed by the Autoprocessor-1 are continuously and automatically updated. Functions include corrected spectra, instantaneous recalibration of corrected emission, differential fluorescence, ratio fluorescence, and absorption and transmission. The system permits repetitive scanning of either monochromator or both monochromators synchronously between preselected wavelengths. Four-digit display of excitation and emission wavelength with parallel BCD output is included. Farrand Optical Co., Inc. **443**



Model IL551 Video I atomic absorption spectrophotometer, a microcomputer-equipped instrument, presents all required analytical information on a 23 × 17 cm CRT display. The data handling system is operated with 12 pushbuttons. It is designed to satisfy two different functions: to be set up optimally and precisely for any type of AA research or analysis and for use by personnel with a minimum of training. Features of the Video I include a "cookbook" option for displaying the required analytical conditions for the element of interest, and a "curve storage" option for retaining corrected working curves for 10 elements. The instrument can routinely analyze a series of samples and present complete statistical information, including relative standard deviation and a running mean value. A graphics option is also available for display of absorption and emission readings and a running display of the working curve. Instrumentation Laboratory, Inc. **408**

Does your present elemental analysis pass the test?

Take an EXAM:



What's the *high precision* energy dispersive X-ray spectrometer?

ANSWER

EXAM 6

Interactive computer control, coupled with *precise* techniques for sample handling, positioning and spinning, set the standard for analytical precision. Optional 12 or 60 position sample loaders. **Circle Reader No. 177**



What's the *only* XRF macroanalyzer you can get?

ANSWER

EXAM/MAX

Table top unit for elemental macroanalysis of bulk samples. Binocular viewing with X-Y-Z specimen stage for area selection. Samples to 3 inches in diameter.
Circle Reader No. 178



What's the fast, simple, versatile **EXAM** workhorse?

ANSWER

EXAM 2

Flexible, simple qualitative system upgradable to full quantitative analysis. **Circle Reader No. 179**



What's the *new authoritative* book by Russ, Jenkins & Shen?

ANSWER

EXAM: Principles and Experiments

A definitive text with an extended series of practical experiments for *any* eds user. **Circle Reader No. 180**

See us at the Pittsburgh Conference—Booths 601-608 and TM-10

PHILIPS

N.V. Philips' Gloeilampenfabrieken
M.I.G Science & Industry
Lelyweg 1
Almelo, Nederland

Philips Electronic Instruments, Inc.
85 McKee Drive
Mahwah, New Jersey 07420
A North American Philips Company

Atomic Absorption Data Center

The AA data system incorporates the SP2900 spectrophotometer and a programmable printing microcomputer. The system provides accurate and complete automatic concentration readout with the curvature correction method most appropriate to the application. Programs are stored on magnetic cards and are available for three methods of curve correction, automatic sampling, and statistical analysis. Standard addition calibrations and calibrations with standard reference materials are also available. Philips Electronic Instruments, Inc. **444**

Inductively Coupled Argon Plasma Emission Spectrometer

Plasma Scan Model 700 has been designed to offer an economical alternative to atomic absorption spectrometry for the analysis of solutions. Detection is from the nanogram level with improved sensitivity for a number of elements. The Plasma Scan uses digitally controlled optical scanning and is under the command of a microprocessor computer readout. The system is easy to automate and is capable of expanding for use in simultaneous analysis using the polychromator. Labtest Equipment Co. **437**

Ultraviolet/Visible Scanning Spectrophotometer

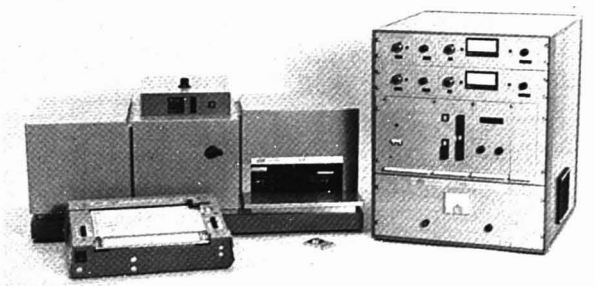
The SP8-200 system provides full instrument parameter control as well as data handling with a microprocessor system. Parameter programs can be set up via the keyboard or from an externally stored program on punched tape or magnetic tape. A set of instrument parameters constituting a complete program can be stored for future recall and use. The setting of every major control can be accessed remotely if necessary from a computer or minicomputer. In addition, five significant digits of photometric data are available 20 times/s for external computer processing. Other features include a master, blazed, holographic grating; automatic baseline correction; a unique Synchrosean recording system; and a wide range of accessories. Philips Electronic Instruments, Inc. **445**

Photomultiplier Tube

The subnanosecond photomultiplier tube features a risetime of about 300 ps and a gain of 10^5. The detector can be furnished with many cathode and window types and will be useful in fast kinetics work. Hamamatsu Corp. **448**

UV Filters

Stable, efficient filters for vacuum UV and middle UV applications are available in the 120–300-nm spectral region. They have 30–40% minimum peak transmission bandwidths of 300–500 Å and have visible and IR transmission ranging from 0.1% to less than 0.01%. The filters are made with nonfluorescent materials and have high radiation resistance. Standard 1-in. filters are stocked; large aperture and custom filters are available on request. Acton Research Corp. **446**



Model R-1500 photoacoustic spectrometer is a dual-beam instrument for obtaining UV–VIS–NIR absorption spectra or thermal diffusivity data from solids, semisolids, or liquids. It uses the technique of acoustic detection of the thermal deexcitation produced by the periodic monochromatic irradiation of samples. Gilford Instrument Laboratories, Inc. **409**



Model 21000 variable temperature cell is designed so that liquid and solid samples can be examined spectroscopically over the temperature range −190 to +250 °C with stability better than 0.1 °C. The cell fits most IR spectrophotometers. Temperature is controlled by either manual or automatic control. A vacuum-tight liquid cell is fitted with AgCl windows, and windows in any of the IR or UV transmitting materials can be supplied on request. Path lengths of 0.025, 0.05, 0.1, 0.2, 0.5, and 1.0 mm are available. Precision Cells Inc. **410**

Monochromator

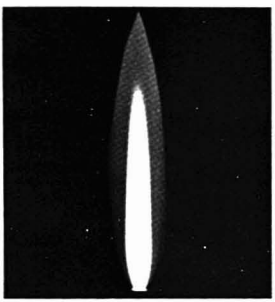
The Mark X is a versatile quarter-meter monochromator. Its optical design intrinsically eliminates reentry spectra for all wavelengths, from ultraviolet through infrared, and for all grating choices. It offers a choice of 10 gratings, with a range of 200 nm to 40 μ. Resolution is better than 0.6 nm at 435.8 nm first order, with 2400 g/mm grating and spherical mirrors. Scattered light is less than 0.05% at 500 nm, using a broad-band lamp and high-pass filter, and less than 0.001% at 10 nm from the 632.8-nm laser line. A 4-digit Veeder-Root wavelength counter gives actual wavelengths in nanometers, accurate to 1 nm. Jarrell-Ash Div., Fisher Scientific Co. **449**

Digital Scan Controller

The McPherson Model 786 is computer compatible and offers a wide degree of control flexibility since it may be operated remotely or from its own control panel. It operates within a speed range of 0.05–500 nm/min with 13 speed selections. The internal clock input allows the operator to pick speeds other than those preselected. The computer input/output feature provides remote stop-start and directional control. The digital scan controller is compatible with the McPherson Model 218 and 2051 monochromators. GCA/Precision Scientific Group **447**

Let our Answer Machines be YOUR Solution







Environmental Analyses

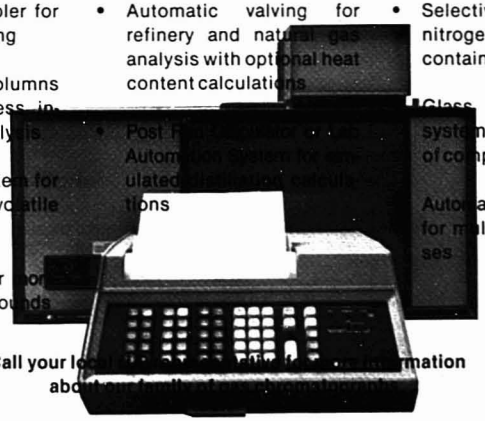
- Automatic air sampler for in-plant air monitoring
- Glass capillary columns with purged splitless injection for trace analysis
- Purge and Trap system for concentration of volatile organics in water
- Specific detectors for monitoring specific compounds

Energy Analyses

- Automatic valving for refinery and natural gas analysis with optional heat content calculations
- Post run calculation of GC/MS Automation system for simulated distillation calculations

Bioscience Analyses

- Selective detection of nitrogen and phosphorus-containing compounds
- Glass capillary column system for high resolution of complex mixtures
- Automatic sample injection for multiple sample analyses

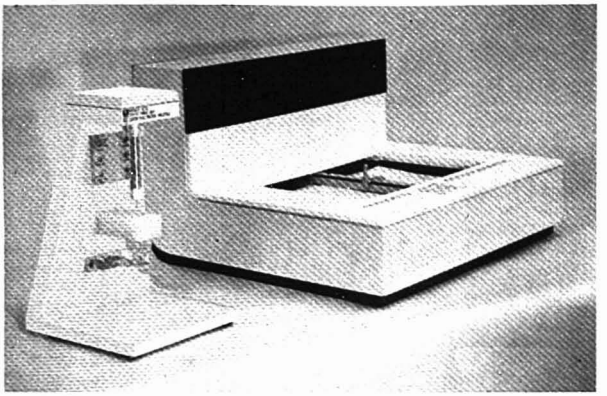


Call your local ... for more information about our family of gas chromatographs

HEWLETT hp PACKARD

Rt. 41, Avondale, Pennsylvania 19311
CIRCLE 101 ON READER SERVICE CARD

43711



Model 303 static mercury drop electrode module improves detection levels by at least an order of magnitude compared with conventional dropping mercury electrode assemblies. The stable, static drop permits use of substantially larger drop areas. In addition, baseline distortions from background current changes produced by drop size changes are eliminated. Each mercury droplet remains stationary over the course of each current measurement. Drops can be formed within 50 ms, permitting rapid polarographic scans. The Model 303 can be used for either polarography or stripping voltammetry. The module includes the mercury electrode, a reference electrode, a counter electrode, a purge tube, an electronics package, and a stand with built-in tray. It is easily interfaced with the Model 174A, 374, and 364 polarographic analyzers. Princeton Applied Research Corp. **411**

Polarographic Analyzer

Model 374-3 combines the Model 303 static mercury drop electrode module with a microprocessor-based analyzer. The baseline storage feature of the analyzer, coupled with the reduced background current and increased drop area of the 303 module, creates a very favorable signal-to-noise ratio. All set-up, scan, data reduction, calculation, and chart-labeling operations are monitored and controlled by the built-in 16-bit microprocessor. Blank and sample scans are stored in separate memories, permitting automatic blank subtraction during the data reduction and calculation stage. Twenty-two override switches permit a high degree of operator flexibility during methods development. Princeton Applied Research Corp. **456**

Automatic Control and Data Handling

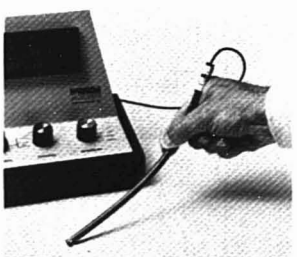
The Auto Chem Package is a collection of programs to control and analyze data from complex laboratory equipment (spectrometers, analyzers, gas chromatographs). It is written in Basic or Fortran and is fully conversational. The programs can be tailored to the user's operating needs. Features available include programs for calibration, sample identification, automatic standardization, instrument control, data output, data transmission, diagnostics, and documentation. Process Corp. **457**

Printer/Plotters

The Versatec 3000 series offers 12 line printers, plotters, and printer/plotters with a choice of resolution (100 or 200 dots/in.), printing speed (500 or 1000 132-column LPM), plot speed (1 or 2 in./s), and packaging (desktop or rack-mountable). All models use 500-ft-long, 11-in.-wide roll paper. These units are well suited for OEM systems and mobile operations. Price range from $8550 to $11 400. Versatec **451**

Field Conductivity Meter

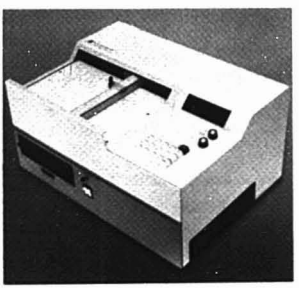
The Model 10 is capable of directly measuring solutions from pure water to twice the salinity of seawater without calculations or balancing. Special field features include a rugged corrosion-resistant housing, analog readout for visibility in direct sunlight, battery operation, and a compact carrying case. Five conductivity ranges permit measurements from 0.1 to 100 000 μmho on a single cell, with a relative accuracy on any range to $\pm 1\%$. Repeatability is to $\pm 0.5\%$ of reading. $275. Markson Science Inc. **450**



The 28XX Series pHlexiMark pH electrodes are constructed of polymer inner and outer tubes and thus are virtually unbreakable. The only glass is in the bulb. The electrodes are prefilled with a special gel and sealed during manufacture. No significant loss of gel will occur for at least two years, eliminating refilling. The 28XX Series is available in four sizes; all have a full 0–14 pH range and 0–70 °C sample temperature range. Priced from $78 to $158. Markson Science Inc. **412**

Oxygen Analyzer

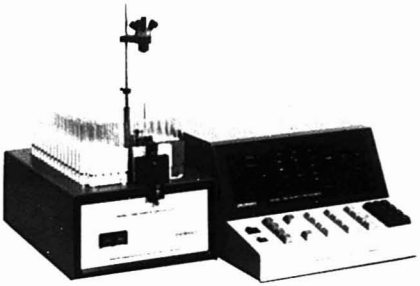
The Model 0260 combines digital display and simplified operation for laboratory analysis of gaseous oxygen (0–100%) and dissolved oxygen (0–199 ppm). It also doubles as a digital laboratory thermometer, measuring 0–100 °C. Features include: "Auto read", which automatically determines when the measurement is stable; a signal for connection to a recorder; and a BCD output to interface with a printer or computer. The meter provides expanded readout to 0.01 at values below 20 ppm or 20% O_2. Manual or automatic temperature compensation is provided, as well as a test function to check for proper operation. Beckman Instruments **453**



Series 8000 electronic recorders are microprocessor-based, multichannel recorders with data processing and flexible disk storage. Data are acquired at high speed from any of eight channels, stored on flexible disks with capacity equivalent to 100 yards of chart paper, retrieved selectively, processed, and displayed graphically. The data can also be manipulated via mathematical functions prior to display. Five models range from $3700 to $4900. Bascom-Turner Instruments **413**

A new name from an old company:

Instrumentation Specialties Co. introduces ChemResearch instruments



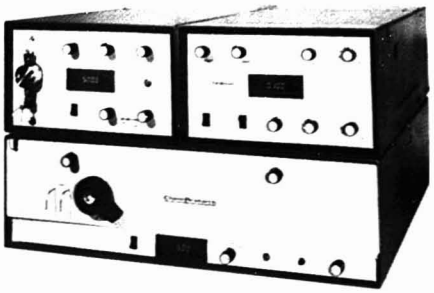
...for automatic sample processing

You can completely automate even your most complex lab procedures with the ChemResearch sample processor – it will do virtually everything you can do manually, but with better precision and repeatability. In addition to simple chemical analyses, it is suitable for such diverse purposes as tissue culture growth; automatic control of complex process reactors such as peptide synthesizers; biochemical processing; and the fundamental characterization of reactions by varying experimental parameters through practically infinite permutations.

Up to 210 samples can each be processed through 960 steps, involving reagent addition from up to 40 sources, agitation, incubation, and many other events. It can measure pH, optical absorbance, or other characteristics at any time, and will vary the program in response to these measurements.

Utilizing an integral microprocessor-based computer, the sample processor is quickly programmed by simple keystrokes. You don't have to know a computer language, and an annunicator display even tells you what to enter next.

Put a ChemResearch sample processor to work for you – save your technician for the easy jobs.



...for high performance liquid chromatography

The ChemResearch liquid chromatograph is a modular unit suitable for a wide range of analytical and semi-preparative applications. This compact HPLC system offers many conveniences: LED readouts monitor 15 operating parameters; all valve and column plumbing projects from the oven when the door is opened; a precisely reproducible injection mark is automatically made every time the valve is operated; and pressure and temperature are controlled by cutoffs with alarms.

Detector choices include a multi-wavelength UV/visible photometer and variable wavelength spectrophotometer. The isocratic pumping system has a sophisticated feedback control which compensates for valve action and other irregularities to produce extremely smooth solvent flow. An optional two-pump gradient system can be quickly set for a wide variety of gradients.

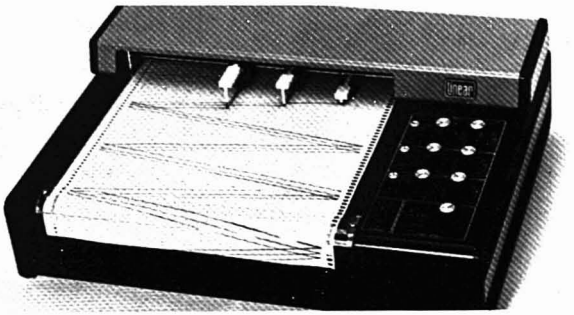
The internally mounted injection valve matches column temperature to provide better reproducibility and to prevent precipitation of samples which require heat to remain in solution. The oven accomodates four 25cm columns or two 50cm columns, with ±1°C temperature control.

ChemResearch

For more information on ChemResearch instruments, dial direct, toll free (800) 228-4250 (continental U.S.A. except Nebraska). Or write Instrumentation Specialites Company , P.O. Box 5347, Lincoln, Nebraska 68505.

See us at the Pittsburgh Conference – Booths 1017 and 1019

CIRCLE 109 ON READER SERVICE CARD



Model 395 strip chart recorder is a three-pen unit with a 250-mm chart width, 12 input spans ranging from 1 mV to 50 V, and 22 chart speeds from 1 cm/h to 30 cm/min. Special features include automatic electronic power shutdown, remote chart control and programming, paper release clutch, push-button zero, 100% suppression, and long life disposable fiber-tipped pens. $1475. Linear Instruments Corp. **414**

Display Monitor

Model 624 offers a brightness of 40 f L for easy viewing in room light. A 12 mil spot size assures crisp, detailed displays and is held over a wide range of brightness levels. The 10 × 12 cm viewing area represents about the maximum size that the viewer can take in as a whole rather than concentrating on a subsection of the display. Other features include choice of ac or dc power supply, UL recognition and UL listing, and 70 ns risetime for x, y, and z axes. A number of options allow the user to fit the 624 to his specific application. Priced at approximately $1000. Tektronix, Inc. **459**

Join the Barnes Special-of-the-Month Club and save on analytical accessories.

Each month in 1978 Barnes is featuring a special on IR analytical accessories. Offers include 10 and 20% discounts on transmission windows and cells, free gifts and useful application notes.

Each offer will be effective for one month only. To know about them in advance, join the Barnes Special-of-the-Month Club. Simply send us your name, title, organization. Clip out this ad and return it to us. We'll send you Barnes latest Infrared Analytical Accessories Catalog as well. You can't get the specials until Barnes gets your name, so act now! Write Barnes Engineering Co., 30 Commerce Rd., Stamford, Ct. 06904; or call us toll-free at (800) 243-3498.

BARNES

Name_____

Title_____

Address_____

City/State/Zip_____

AC-2

CIRCLE 52 ON READER SERVICE CARD

Calibrator

Model GRC 101 for calibrating voltage indicating instruments is a compact, miniaturized, solid state instrument, powered by internal batteries. Features include output setting from 1 mV to 1 V in 4 decades, 1-V functional output, linearity within 0.1%, and stable auxiliary 10-V output. Time base is crystal controlled to better than 0.02% accuracy, with settings of 1 s to infinity. The voltage output may be set to DC, staircase, square, or pulse waveforms. $145. Linear Instruments Corp. **455**

pH Meter

Model 3560 incorporates the "Auto Read" electronic circuit that automatically determines when a pH reading has stabilized, then signals when to take a measurement. In addition to pH, the 3560 also doubles as a digital laboratory thermometer with readings from 0 to 100 °C. It spans the full 0–14 pH and ±1999 mV ranges with accuracy of ±0.01 pH. Other features include an electronic test switch, wide range zero control, slope control, and BCD output. Beckman Instruments, Inc. **452**

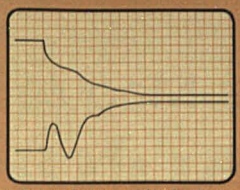
CRT Camera

Model C-28 features an electric shutter for remote operation of the camera for operator convenience or system control. Magnification can be changed from 0.67 to 0.85 to permit full-frame photographs or both 8 × 10 and 10 × 12 cm displays. The f 2.8 lens provides the performance needed in general CRT photography. Two film backs are included, a Graflok 4 × 5 in. roll film back and a Polaroid Type 405 back. $1085. Tektronix, Inc. **458**

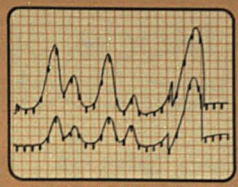
Precision Laboratory Calibrator

The Model 450 is a convenient, accurate laboratory calibration source for recorders, integrators, computers, oscilloscopes, and other laboratory instruments. It simulates chromatographic peaks or a constant voltage output for calibrating data measurement systems. Seven DC outputs from 1 mV to 10 V are available with the additional ability to select 0, 25, 50, 75, and 100% of these values for a total of 21 voltage calibration values. The Model 450's triangular wave output permits checking and calibrating slope detection of integrators and computers as well as area counts, linearity, span, reproducibility, zero, and response time. Analytical Bio Chemistry Laboratories, Inc. **454**

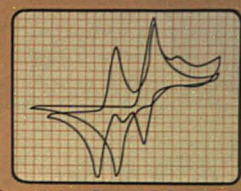
(*Continued on page 252 A*)



100 ms Voltage Transient and Its First Derivative



UV - Absorbance of Density Gradient Fractions



Current-Voltage Curves in Cyclic Voltammetry

Introducing the Series 8000 Electronic Recorders with Data Processing and Storage

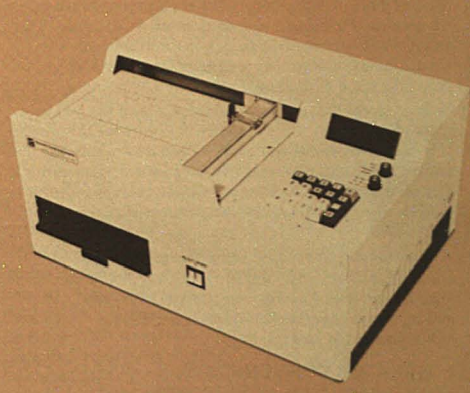
A major advance in recorders, the Bascom-Turner Series 8000 are new, electronic, multi-channel recorders with data processing and storage.

With the Series 8000 you can digitize, record, and process up to eight channels of analog data. Raw or processed data are graphed in real time on strip or X-Y chart paper and stored on flexible disk.

The Series 8000 lets you specify a wide variety of modes for data acquisition. You can record on preset triggering or on event triggering at speeds up to 10,000 points per second for a single channel. Alternatively, you can record at regular intervals as few as two points per day. In all cases, you have the advantages of superior accuracy offered by digital electronics and an input impedance of 100 megohms on all channels and all ranges.

A simple key sequence allows you to process data before plotting. For example, data from any channel can be integrated, differentiated, smoothed, normalized, converted to logarithms or reciprocals. Or, you can compare data from any two channels, or sequences of data from a single channel, and plot their difference, average, or quotient.

Storage is convenient, economical, and efficient. Each flexible disk is equivalent to 100 yards of chart paper. Yet, any sequence of data can be retrieved in graphical form in a few seconds.



For all their versatility, Series 8000 recorders are priced from $3,700 to $4,900.

For more information, call Bob Sanford at (800) 225-3298

Bascom-Turner Instruments
A Division of EIC Corporation
111 Chapel Street Newton, Massachusetts 02158 U.S.A.

CIRCLE 23 ON READER SERVICE CARD

See us at the Pittsburgh Conference, Booth #1545

Introducing The Model 303 Static Mercury Drop Electrode Module...

See what you've been missing!

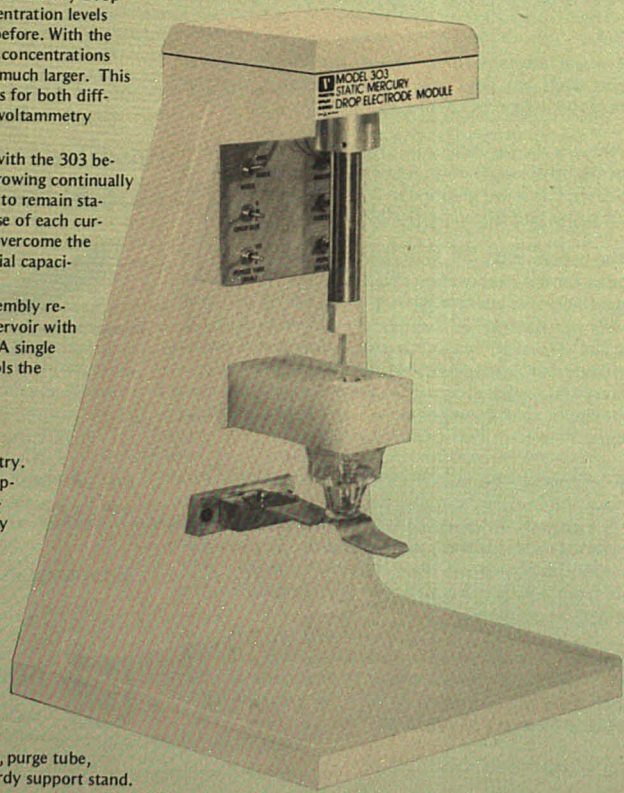
- Higher Sensitivity
- Greater Convenience
- Lower Cost

• HIGHER SENSITIVITY

The name of the game! The new 303 Static Mercury Drop Electrode Module gets you down to concentration levels that you were probably only guessing at before. With the 303 electrode, baseline distortions at ppb concentrations are drastically lowered and drop sizes are much larger. This means you'll get improved detection limits for both differential pulse polarography and stripping voltammetry (using the same static drop).

Hang in there! You get higher sensitivity with the 303 because each mercury droplet, rather than growing continually as in the conventional approach, is caused to remain stationary at the optimum size over the course of each current measurement. This is a great way to overcome the baseline distortion caused by the differential capacitance curve.

And talk about simplicity! There's no assembly required of the operator. Simply fill the reservoir with mercury and start running your analyses. A single moving part within the 303 Module controls the extrusion of each mercury drop.



• GREATER CONVENIENCE

Simple switchover! Use the Model 303 for either polarography or stripping voltammetry. Convert from one mode to the other by flipping a single panel switch. No other adjustments are necessary since the same capillary serves both techniques. And you'll appreciate the additional controls for purge, purge times, drop size, drop extrusion and drop dislodge.

• LOWER COST

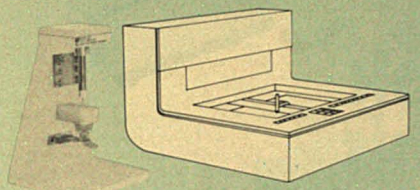
Now that's progress! The Model 303 costs less than the two previous electrode assemblies you needed for doing polarography and stripping voltammetry. The 303 Module includes the mercury electrode, reference and counter electrodes, purge tube, cell bottoms, electronics package and a sturdy support stand.

See how it's used...

A GREAT INSTRUMENT MADE BETTER . . .

THE MODEL 374-3 MICROPROCESSOR-BASED ANALYZER SYSTEM

When your samples demand the utmost in voltammetric sensitivity and capability we've got it. The 374-3 combines the new Model 303 Static Mercury Drop Electrode Module with the popular Model 374 microprocessor-based polarographic analyzer to yield a truly unique approach to ultra-high sensitive voltammetry. The increased drop area of the 303 Module, the greatly reduced background current and the baseline storage feature of the microprocessor-based analyzer all combine to create the most favorable signal-to-noise ratio available in any commerical polarographic instrument.

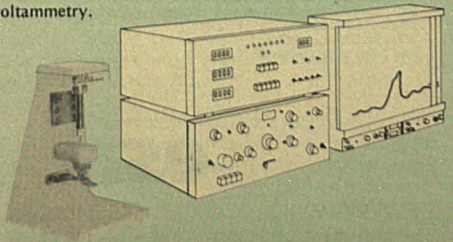


A simple but elegant approach is used to create reproducible stationary mercury drops within the 374-3 System. A single vertically moving part controls the extrusion of each drop. Drops formed in this manner are stable for as long as you want. All set-up, scan, data reduction, calculation and symbolization steps are monitored and controlled for you by the built-in 16-bit microprocessor. Blank and sample scans are stored in separate 750 point memories within the 374-3 to give you automatic blank subtraction during the data reduction and calculation stages. And for your methods development work you'll appreciate the 22 override switches which provide a high degree of analytical flexibility.

AN ECONOMICAL, HIGHLY SENSITIVE PACKAGE . . .

THE MODEL 174 POLAROGRAPHIC ANALYZER SYSTEM

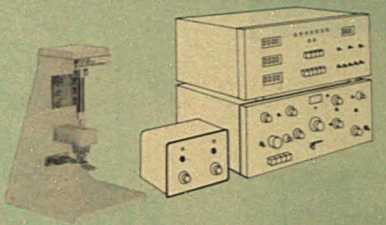
This system combines the new 303 Module with the versatile Model 174A Polarographic Analyzer, the 315A Automated Electroanalyis Controller and the 9002A X-Y recorder—a complete package for polarography and stripping voltammetry.



ANALYZE IT CONTINUOUSLY WITH . . .

THE MODEL 318 AUTOMATED BATCH SAMPLER INTERFACE

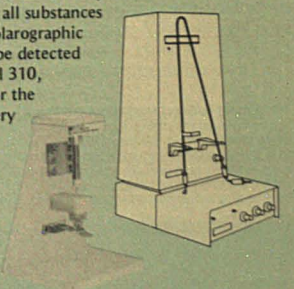
Now you can apply automated voltammetry to the analysis of process streams, reservoirs, holding tanks, plating baths and the like with our new Model 318 Automated Batch Sampler Interface. The 318 incorporates an electronic control package and a cell that is automatically refilled at regularly timed intervals with aliquots of the solution to be analyzed. The 318, shown here with the new Model 303 Static Mercury Drop Electrode Module, can be used with the 174A Polarographic Analyzer/315A Automated Electroanalysis Controller combination or with the 374-1 and 374-3 Polarographic Analyzers.



A UNION OF TWO POWERFUL TECHNIQUES . . .

THE MODEL 310 POLAROGRAPHIC LIQUID CHROMATOGRAPHY DETECTOR

The Model 310 Detector employs the new PARC Model 303 Static Mercury Drop Electrode Module to achieve ppb-level sensitivities for pharmaceuticals, pesticides, vitamins, metals, additives, pollutants and many other compounds. Typically 10 ng. ascorbic acid can be measured with little difficulty. The 310 Detector incorporates a specially-designed cell in which the LC eluate is led up and around the static mercury droplet. Since all substances that exhibit polarographic responses can be detected with the Model 310, applications for the detector are very broad.



For more information on these new products, contact: Princeton Applied Research Corporation, P.O. Box 2565, Princeton, NJ 08540; or phone 609/452-2111.

PRINCETON APPLIED RESEARCH

AN EG&G COMPANY

See these instruments at the Pittsburgh Conference, booth #117–124



Model 3010A
Trace Metals Analyzer.
Measures up to 200 micro or macro samples daily at 90 seconds or less per sample using a rapid exchange reagent. Cost per sample: about one-third that of conventional methods. Excellent accuracy and precision at the nanogram level. **Circle No. 18**



Model 4000
ZnP Hematofluorometer.
Determines the amount of zinc protoporphrin in whole blood without sample preparation. Principle approved by the Center for Disease Control of HEW for lead intoxication and/or iron deficiency anemia.
Circle No. 29



Model 3040
Charge Transfer Analyzer.
For electro-chemical analyses, measuring chemical levels or changes in solutions, selection and detection of complex compounds, process control, and similar applications. Pushbutton programmable. Available with flow cells, trap cells, and other sensors. **Circle No. 45**



Model 2014 Multiple Anodic Stripping Analyzer.
A laboratory instrument that will perform quantitative or qualitative analyses on trace metals in numerous matrices without destroying the sample. Available with extender units to handle up to 12 discrete samples simultaneously, and with a variety of equipment options for routine analysis or basic research. **Circle No. 136**



ANALYTICAL INSTRUMENTS

ANALYTICAL INSTRUMENTS

Look at this trace metals complex



Model 2011 Single Cell Anodic Stripping Voltammeter.
A portable, single cell version of the Model 2014 that will operate on line power or from a 12-volt storage battery and inverter.
Circle No. 33

ANALYTICAL INSTRUMENTS

RESEARCH AND DEVELOPMENT

The R&D Laboratory consists of both in-house and consulting groups for development of hardware, and for analytical projects ranging from emission surveys from power plants and smelters to the effectiveness of existing techniques for controlling the environment. **Telephone or letterhead request only, please.**

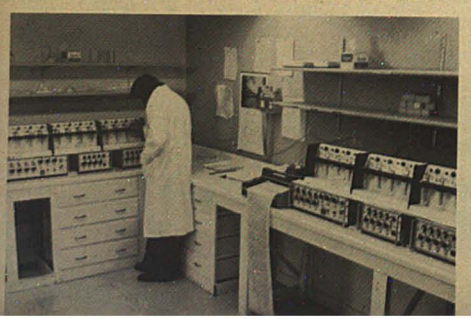
...and for halides, chemicals, and other substances and solutions, too.

ESA is a multi-faceted company with capabilities in such diverse areas as industrial hygiene, clinical laboratories and health care centers, industrial processes, environmental technology, and quality control. We operate one of the largest private blood lead screening laboratories in the world, provide the food industry with instruments for measuring and monitoring trace metals in food products and containers, test air filters, and analyze water and soil for lead, tin, cadmium, copper, arsenic, mercury, bismuth, thallium and other heavy, precious, or toxic metals in a variety of matrices. Look us over—then tell us your requirements.

SERVICE LABORATORIES

SYSTEM ACCESSORIES

Screening Laboratories for screening of children and industrial personnel for blood and urine lead, erythrocyte protoporphrin, and hematology testing.... determining the presence and amount of lead, cadmium, copper, mercury, arsenic, tin, bismuth, and thallium in various matrices.... or for intermediate or massive repetitive analyses of other trace elements in solids and aqueous solutions. **Circle No. 34**



Sampling Kits for obtaining, handling, shipping, and storing blood or other biologicals. **Circle No.155**

Fast Exchange Reagents that obsolete preparative chemistry for lead in food, water, blood, urine.... and other trace substances in different matrices. **Circle No. 167**

Flow Cells and Sensors for continuous or batch measurement and monitoring of chemical and industrial processes, capturing and eliminating undesirable ingredients, and other uses. **Circle No.194**

esa

ENVIRONMENTAL SCIENCES ASSOCIATES, INC.

45 Wiggins Avenue, Bedford, MA. 01730–Telephone: 617-275-0100

SEE US AT THE PITTSBURGH CONFERENCE BOOTHS 702 AND 704

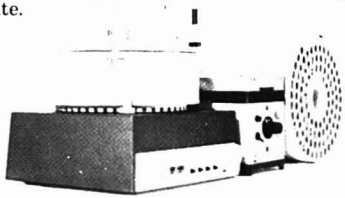
The New LKB Fraction Collector



There is no mistake! The NEW LKB 2120 Vario Perpex II Pump really is a fraction collector.

A new fraction collecting method

Each movement of the pump's stepping motor produces a signal which can be collected in the new LKB RediRac fraction collector. Each signal means a certain volume of liquid displaced by the pump head. By simply dialling in on the preset counter of RediRac you can select precisely the fraction volume you want; you collect *precise-volume* fractions, irrespective of changes in surface tension or applied flow rate.

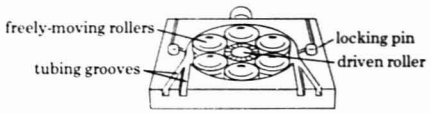


VarioPerpex II Pump is now better than ever

In addition to the new fraction collecting feature, we have added to the popular VarioPerpex Pump a button for immediately obtaining the maximum flow rate. With its wide range of variable flow rates this makes VarioPerpex II Pump more than ever the best you can buy.

The unique roller system

All LKB Perpex Pumps use the same unique system, in which 6 freely-rotating rollers move around an inner driven one. This design gives you minimum pulsation flow, since the increase in pressure on the tubing occurs gradually.



The drag on the tubing is so low that you do not need clips or special tubing. You can use a variety of tubing types and sizes – silicon rubber, Tygon, Viton – just pick the most suitable for you.

LKB family of Perpex Pumps

LKB 10200 Perpex Pump is a single-channel pump, with up to 10 optional gearboxes available to give flow rates of 0.013–800 ml/h.

LKB 2115 MultiPerpex Pump is a variable-speed pump; its four channels and 3 different gearboxes give flow rates of 5–5,000 ml/h per channel.

LKB 2120 VarioPerpex II Pump provides variable flow rates over the range 0.6–400 ml/h, with an optional gearbox giving 0.2–104 ml/h.

LKB

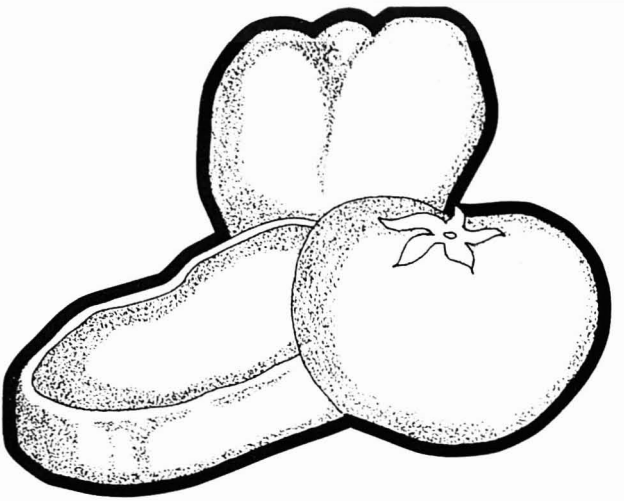
LKB Instruments Inc.
12221 Parklawn Drive, Rockville, Maryland 20852
Tel: (301) 881-2510

230

See us at the Pittsburgh Conference, Booths 1227–29–31

CIRCLE 127 ON READER SERVICE CARD

Wayne R. Wolf
U.S. Department of Agriculture
Agricultural Research Service
Nutrition Institute
Nutrient Composition Laboratory
Beltsville, Md., 20705



The rapid, fairly recent developments of trace element research in the area of nutrition have led to a need to accurately and precisely know the content of these micronutrients in the diet. In the past several decades the analytical chemistry community has made great advances in improvements in sensitivity, selectivity, and accuracy of analytical methodology. In general, however, these advances have not been routinely applied to the determination of trace element content of foods. The problems involved in food analysis at the parts-per-million or parts-per-billion levels required for many of the newer essential trace elements have not been well defined. The present state of analytical and nutritional knowledge varies with each of the elements. Since neither resources nor scientific knowledge indicates the feasibility of a full attack on each element, priorities must be established on the basis of immediate scientific need and the possibility of success. I will limit the present discussion to those trace elements and problems of a nutritional nature and defer discussion of those trace elements that act, as far as is presently known, only in toxic or detrimental modes and that were discussed in a recent issue of this JOURNAL (*1*).

For definition of the problems involved in food analysis, it is necessary to consider the data required for foods and to then ask if these requirements can be met for each element. Analytical data in nutrition are used to: establish the essentiality of a nutrient; establish requirements; identify adequate, subadequate, or marginal intakes in selected populations; and prevent nonoptimal intakes (*2*).

The present state of knowledge of the essentiality of trace elements in nutrition is shown in Table I. The knowledge that small amounts of metals are needed in the diet goes back several hundred years to the discovery of a requirement for iron and over a hundred years to the discovery of an iodine requirement. Requirements for the trace elements copper, manganese, zinc, and cobalt were discovered in the 1920's and 1930's in conjunction with the discovery and identification of another class of micronutrients, the vitamins. Not until the 1950's were three more trace elements—molybdenum, selenium, and chromium—added to the list. Very recently, the six "newer trace elements", tin, vanadium, fluorine, silicon, nickel, and arsenic, were discovered to have a nutritional requirement. These discoveries parallel advances in analytical determination of small amounts of metals. Emission spectroscopic methods were developed in the 1920's and 1930's, atomic absorption spectroscopy in the 1950's, and several very sensitive techniques, such as activation analysis and new advances in spectroscopic techniques, by the 1970's. These new, highly sensitive analytical techniques, in conjunction with the development of isolator techniques for carrying out growth studies in controlled atmospheres, allowed the discovery and identification of the "newer trace elements" (*3*).

The second need for analytical data in foods is to define requirements or amounts needed in the diet. Normally, requirements are defined by assessing balance studies on controlled populations and gaining some knowledge of the biological role of the trace element. Total dietary intake of the trace element is monitored under experimental conditions to determine the

Table I. Trace Elements in Human Nutrition

Element	Discovery of requirement[a]	RDA established[b]	Subadequate intakes identified	Fortification recommendations
Iron	17th Century	Yes	Yes	Yes
Iodine	1850	Yes	Yes	Yes
Copper	1928	Pending	?	More data needed
Manganese	1931	No	No	No
Zinc	1934	Yes	Yes	Yes
Cobalt	1935	No (B_{12})	No (B_{12} yes)	No
Molybdenum	1953	Pending	No	No
Selenium	1957	Pending	Yes	More data needed
Chromium	1959	Pending	Yes	More data needed
Tin	1970	No	Experimental	Unknown
Vanadium	1971	No	Experimental	Unknown
Fluorine	1972	Pending	Experimental	Unknown
Silicon	1972	No	Experimental	Unknown
Nickel	1973	No	Experimental	Unknown
Arsenic	1975	No	Experimental	Unknown

[a] Ref. 3. [b] Ref. 5.

This article not subject to U.S. Copyright
Published 1978 American Chemical Society

Nutrient Trace Element Composition of Foods: Analytical Needs and Problems

amount required to balance the amount excreted. Alternatively, diets with different levels of trace elements are fed, and an identified biological parameter affected by the trace element is monitored to find dietary levels for optimum function. An example of such a parameter is blood hemoglobin levels which are used to monitor the effect of dietary iron. Recommended Dietary Allowances (RDA) have been set for iron, iodine, and zinc where knowledge is sufficient and a need for a requirement was shown for each (Table I). For copper the issuance of an RDA is pending. Selenium, chromium, and fluorine are under discussion; further study is needed before an RDA can be established. Only tentative recommendations for the "newer" trace elements in the form of a range of values can be presently proposed. To more firmly establish these recommendations, knowledge of the content of each of these trace elements in the diet is necessary.

Knowledge of the trace element content of foods is also necessary to identify adequate, subadequate, and marginal intakes in selected populations or trace element deficiency-related diseases. Several large-scale surveys and epidemiological studies indicated that trace element levels in water might be potentially correlated with major diseases such as cancer and heart disease (*4*). Further exploration of these correlations and expansion of epidemiological studies depend upon accurate, extensive knowledge of trace element distribution in the food supply.

The final application of data on trace element content of food is to provide optimal intakes of these nutrients for the population. That application could take the form of public health programs, dietary recommendations such as the RDA's, dietetic services, possible fortification recommendations and actions, and educational programs and food labeling. For example, the last column in Table I shows the trace elements for which specific subadequate intakes have been identified and fortification programs recommended. The occurrence of iron deficiency and the iron fortification program of bread plus the occurrence of iodine deficiency in the United States "goiter belt" and the iodization of salt are well documented. More recently, the recognition of possible marginal zinc deficiency in the U.S. has led to some recommendations for zinc fortification by the Food and Nutrition Board Subcommittee (*5*). These recommendations have been implemented by most manufacturers of infant foods (*6*). Recent analytical methods have produced data indicating that the average daily copper intake is probably 1 mg or about half the estimated human requirement (*7, 8*). More data generated by modern methods are needed to correctly assess the requirements and intakes of copper. For selenium, soil and plant deficiencies are known, and supplementation of animal feeds is practiced widely. Marginal human intakes have been identified in New Zealand (*9*). Selenium content should be determined for additional foods so that the nutritional status, as regards selenium, of the U.S. population can be evaluated. Chromium deficiency occurs during protein-caloric malnutrition (*10*) and is suspected to occur marginally in elderly people in the U.S. The human requirement for chromium cannot be defined at present because of problems of analysis and incomplete knowledge of availability. Additional data are needed to assess chromium status. For the "newer" trace elements, deficiencies in animals have been produced experimentally. Human requirements and distribution in foods are unknown and must be determined before human nutritional status can be evaluated.

Available data on food composition are presented in Agriculture Handbook No. 8, "Composition of Foods, Raw, Processed, Prepared" (*11*). This handbook gives some food composition data on iron. A recently updated section of Handbook 8 (*12*) gives some data on zinc, but the data are, in general, of a provisional nature because they are based upon a limited number of analyses on a limited number of foods. Data are not presented for the other trace elements listed in Table I. Thus, additional food composition data are needed for all the trace elements known to have dietary requirements, particularly for those elements of greatest current interest in the nutrition community: iron, zinc, copper, selenium, and chromium. Such data can only be generated by the use of critically evaluated, well-defined analytical methodology.

Evaluation of Methodology

Criteria must be developed for the evaluation of analytical methodology. Basic criteria are specificity, precision, sensitivity, accuracy, and suitability for quality control and automation. The methodology must be capable of a specific analysis of the nutrient of interest and be relatively free of interferences. This criterion can be attained by either separation of the nutrient from the bulk food or a specific detection system or both. The precision of the method must be sufficient to study and define food variations associated with processing, geographical, seasonal, and genetic factors plus oth-

Sample	Percentage recovered COPPER $\bar{x}$	COPPER SD[a]	ZINC $\bar{x}$	ZINC SD[a]
09-265	96.8	5.6	103.2	0.5
09-281	98.3	0.6	104.5	2.0
09-281	97.2	5.5	96.8	1.6
09-271	98.6	2.7	100.4	0.3
09-266	100.3	3.9	99.3	1.5
09-265	96.8	3.2	98.4	1.8
07-119	101.4	2.2	104.3	3.5
08-175	96.4	0.8	98.6	1.5
07-143	96.1	1.4	99.2	3.0
07-141	98.6	4.3	100.6	4.6
	$\bar{x}$ = 98.05 ± 1.7 SD		100.5 ± 2.6 SD	

[a] Each analysis done in triplicate.

Sample digest	ZINC (μg/mL) Standard addition	Curve calibration	% Deviation	COPPER (μg/mL) Standard addition	Curve calibration	% Deviation
08-175	1.13	1.18	+4.4	0.204	0.239	+17.2
07-119	0.66	0.67	+1.5	0.211	0.241	+14.2
07-141	0.89	0.91	+2.2	0.158	0.189	+19.6
07-143	0.97	1.02	+5.2	0.339	0.375	+10.6
09-281	0.73	0.73	0	0.282	0.300	+6.4
09-271	1.05	1.10	+4.8	0.200	0.217	+8.5
09-266	0.57	0.61	+7.0	0.351	0.371	+5.7
09-265	1.43	1.32	−8.3	0.199	0.217	+9.0
09-281	0.75	0.74	−1.4	0.174	0.172	−1.2
NBS SRM 1571	0.89	0.85	−4.7	0.421	0.458	+8.8
NBS SRM 1577	0.87	0.84	−3.6	1.182	1.269	+7.4
Wheat sample AACC-1	1.60	1.77	+10.6	0.304	0.350	+15.1

Sample	Date	COPPER (μg/g) $\bar{x}$	COPPER (μg/g) SD[a]	ZINC (μg/g) $\bar{x}$	ZINC (μg/g) SD
AACC-1	7/14	4.22	0.20	23.26	0.24
Whole wheat—	8/10	3.94	0.04	24.92	0.67
ground	8/17	4.01	0.51	22.35	0.20
	8/20	4.66	0.34	25.37	0.31
	9/14	3.77	0.05	25.10	0.65
	9/22	4.06	0.05	25.35	1.34
Mean		4.11 ± 0.31		24.39 ± 1.27	
AACC value[b]		4.65 ± 0.85 (n = 15)		25.3 ± 3.1 (n = 18)	
AACC-2	7/1	1.73	0.06	6.08	0.07
Refined wheat—	7/20	1.53	0.10	7.62	0.64
ground	7/21	1.75	0.26	6.47	0.58
	8/17	1.94	0.20	6.69	0.28
	8/25	1.41	0.05	6.55	0.18
	8/25	1.45	0.10	7.37	0.41
	8/25	1.63	0.08	5.87	0.49
Mean		1.63 ± 0.19		6.66 ± 0.64	
AACC value[b]		1.65 ± 0.15 (n = 15)		6.55 ± 1.6 (n = 18)	

[a] Each analysis done in triplicate on a separate day. [b] Values of a round robin analysis: American Association of Cereal Chemists, Doris Baker, private communication.

ers. These variations may be meaningful in the range 5–10%. The precision of the methodology must be well enough defined so that data can be evaluated and compared among different groups of workers.

The method must be sufficiently sensitive for analysis, at naturally occurring levels, of the total content of the trace element and the content of the individual fractions or different chemical forms of the element. For the degree of precision required, the analyses must be carried out at least 10–20 times above the detection limits of the methods. For some trace elements such as chromium, this requires detection limits in the low nanogram or picogram range.

For each type of food, the methodology must be critically evaluated for accuracy and possible matrix effects. Recovery of added metal, analysis of certified reference materials, and agreement of data between the test method and independent analysis of the same sample are all areas that must be evaluated in the development of a methodology. Not only the detection system, but the sample preparation must be checked for accuracy. For routine use the method, once developed, must have sufficient quality control to ensure accuracy on a day-to-day basis. One method of quality control is the routine analysis of a primary Standard Reference Material.

It is generally necessary to have a method as highly automated as possible to eliminate human error, allow savings in time and labor, and to allow the analysis of enough control samples to maintain the proper level of quality control. The need for highly automated, rapid analysis techniques is especially important because of the enormous number of food products and the number of elements of interest. The advantages of multielement analysis are apparent. However, each trace element has unique chemical and analytical properties. Adequate methods must be perfected for each element separately before multielement methods can be developed.

For some of the trace elements, such as iron, zinc, and copper, basic analytical methodology is under control. For these metals, present emphasis should be placed on the development of rigidly defined, rapid, accurate methods for analyzing a significant number of foods in large-scale studies to determine the effects of distribution and processing of food on their trace element content. For example, in our laboratory we have developed a procedure for rapid analysis of zinc and copper in foods. We have used this procedure to analyze a series of composites of daily diets at the rate of 25–30 per week in triplicate, with re-

producibility and accuracy within 5–10%. In this method we use a sulfuric acid–hydrogen peroxide digestion procedure capable of simultaneous digestion of 30–40 samples. Solutions of digested samples are analyzed by flame atomic absorption spectrometry with automatic sample introduction. The system has been automated with a stream sampling system to introduce discrete amounts of liquid samples into the spectrometer at the rate of 120/h; the readout is equipped with digital integration and automatic data reduction (*13*).

Some of the data generated with this system are shown in Tables II–IV. Table II shows the quantitative recovery of added metal from a series of daily diet composite samples (*7*). Table III shows that severe matrix effects were absent in the comparison of data from standard additions and calibration curves for analysis of the composites and reference material samples. Table IV shows the day-to-day reproducibility of data for several wheat samples that served as controls in the analysis. The data illustrate the quality control methodology that would be required routinely for generation of valid trace element data.

Problems and Needs

For other trace elements, such as selenium, chromium, and the more recently defined essential trace elements, the basic analytical methodology is not presently under control. Analytical problems must be defined and solved before a large amount of reliable data can be generated. A recent round robin comparison of the trace element content of a Standard Reference Material (NBS SRM 1577–Bovine Liver) demonstrated the extent of the analytical problem for chromium in biological materials (*14*). The investigators reported fairly good agreement of data on copper content for which the analytical methodology is under control. For the chromium content, however, the range of reported values was three orders of magnitude. With such variable analytical results, consensus of agreement as to the content of chromium in foods is impossible. Over the past several years, work in our laboratory and in others has identified some of the problems associated with the analysis of chromium. Errors are mainly due to the very low levels in biological materials (low parts per billion), the problems of external contamination at these low levels, and the extreme sensitivity of different chemical forms of chromium to losses in various sample digestion and preparation procedures. Losses of significant amounts of chromium by volatilization during sample preparations have been demonstrated (*15*). Recently, the National Bureau of Standards released a biological Standard Reference Material (SRM 1569–Brewers Yeast) certified for chromium content by several independent methods in light of recent understanding of the various analytical problems. This standard material should be a great help in further development of methodology and comparisons between laboratories.

The difficulty of the analysis of chromium in foods illustrates another very real problem in defining nutrient composition of foods— namely, chemical speciation of the trace elements. Different chemical species containing a trace element may be present in the food, and each species may have a widely different biological activity or role. The availability of the metal to the organism depends greatly upon the chemical species. Interest is increasing in this aspect of trace element nutrition. It is necessary to know not only the total content of trace element, but also the content of the different fractions containing the element in the specific chemical form. For example, inorganic chromium is poorly utilized nutritionally, whereas an organic complex of chromium known as the "glucose tolerance factor" is highly utilized (*16*). Present evidence suggests that the nutritionally important form of chromium is contained in a difficult-to-analyze organic fraction much more susceptible than inorganic chromium to matrix effects and loss during sample preparation (*17*). Therefore, data on the biologically active fraction of chromium content in foods may be more important than data on total chromium content. The Brewers Yeast SRM contains a fraction of chromium that has biological activity. It is therefore a better choice for a reference material for food chromium than SRM 1571 Orchard Leaves that contains no biologically active chromium (*17*), even though the total chromium levels of the two are similar. The SRM 1569 Brewers Yeast is a good example of the type of reference material required for development and validation of methods to give meaningful food composition data. Appropriate biological standard reference materials are needed for all types or classes of foods.

Iron also illustrates the need for speciation data. Recent work has indicated that iron availability and utilization might be defined by two types of iron in foods, the heme and nonheme fractions. It is thought that knowledge of the contents of those two fractions and of several other factors, such as the amount of meat protein and vitamin C, would allow calculation of the total available iron in a meal (*18*). Consequently, a method to specifically determine heme iron is needed to generate food composition data for heme and nonheme iron.

Several general problems affect the analyses of trace elements in foods. These problems involve sampling, sample storage, sample preparation, and sample throughput. It is imperative that representative samples be taken of selected items from the food supply. Some 60 000 different food items are available in the U.S. food supply, and often there are numerous processing plants for each food item. Generation of a complete data base of trace element content of every available item would be impossible. Therefore, some consideration must be given as to which items are to be analyzed, how many of each item, and the source of each sample. In reporting analytical data, it would be necessary to give a full description of each item, complete with brand names, lot numbers, and source.

Generally, it is practical to collect more samples than can be analyzed immediately; therefore, the samples must be stored until analysis. For dry or canned samples, storage problems generally are not serious for total trace element content. For samples with considerable moisture content, such as meat, fresh fruits, and vegetables, significant changes in weight and subsequently in composition can be caused by loss or gain of moisture during storage. Changes during storage have not been reported for the specific chemical forms of the trace elements, but so few data are available that no conclusions are possible.

Once the sample is taken into the laboratory, some sample preparation is necessary before analysis. In the most specific and interference-free systems of analysis, the element or species of interest is separated and then detected by a sensitive, precise instrumental system. In these samples, levels of trace elements are very low, and great care must be taken to prevent contamination or losses during preparation. Airborne particulate matter can contain large amounts of trace elements and must be removed from the laboratory atmosphere. A central air system with some filtering and laminar flow clean air work areas are required. Proper care to avoid contamination from reagents and containers must become routine to the analyst. Proper checks and control of blank levels and contamination control must be a part of the quality control procedures. One of the first indications of uncontrolled contamination is the lack of day-to-day reproducibility. In addition to contamination, the possibility of loss of the analyte of interest must be considered. As mentioned above for chromium, the defi-

nition and solution of problems may require extensive research efforts. Lastly, all analytical methodology used to determine trace element composition of foods must be verified by an alternate technique to ensure against systematic bias.

The present challenges in generating data for the trace element composition of foods can be summarized by the statement: The great advances by the analytical community in sensitivity, selectivity, and accuracy need to be applied in critically evaluated, well-defined analytical methodology to generate the large amount of data required to evaluate foods as sources of the trace elements.

References

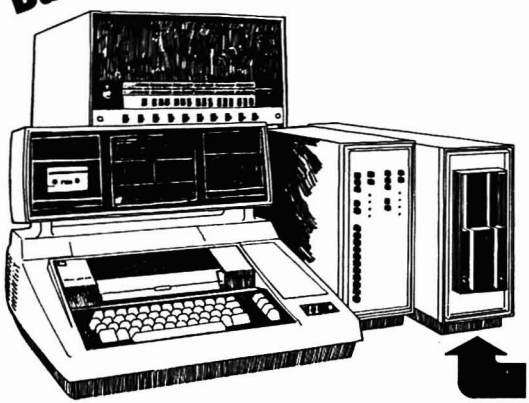
(1) G. B. Morgan and E. W. Bretthauer, *Anal. Chem.*, **49**, 1210A (1977).
(2) W. Mertz, in "Proceedings of Western Hemisphere Nutrition Congress", IV, p 141, 1974.
(3) K. Schwarz, in "Trace Element Metabolism in Animals", W. G. Hoekstra et al., Eds., Vol 2, p 355, University Park Press, Baltimore, Md., 1974.
(4) R. Masironi, *Bull. WHO*, **42**, 103 (1970).
(5) Food and Nutrition Board, "Recommended Dietary Allowances", National Research Council, Washington, D.C., 1974.
(6) W. Mertz, *Ann. N.Y. Acad. Sci.*, in press (1977).
(7) W. R. Wolf, J. M. Holden, and F. E. Greene, *Fed. Proc.*, **36**, 1175 (1977).
(8) L. M. Klevay, *Nutr. Rep. Int.*, **11**, 237 (1975).
(9) M. F. Robinson, in "The Moonstone, More About Selenium", pp 13–30, Nutrition Society of New Zealand, Palmerston North, New Zealand, 1975.
(10) C. T. Gurson and G. Saner, *Am. J. Clin. Nutr.*, **26**, 988 (1973).
(11) B. K. Watt and A. L. Merrill, in "Composition of Foods, Raw, Processed, Prepared", Agriculture Handbook No. 8, U.S. Department of Agriculture, Washington, D.C., 1963.
(12) L. P. Posati and M. L. Orr, in "Composition of Foods: Dairy and Egg Products", Agriculture Handbook 8-1, U.S. Department of Agriculture, Washington, D.C., 1976.
(13) W. R. Wolf and K. K. Stewart, Pittsburgh Conference on Analytical Chemistry and Applied Spectroscopy, Paper #108, Cleveland, Ohio, 1977.
(14) R. W. Parr, Joint Research Program on Trace Elements in Cardiovascular Disease, Research Coordination, Meeting WHO/IAEA, Vienna, Austria, 1973.
(15) W. R. Wolf, W. Mertz, and R. Masironi, *J. Agric. Food Chem.*, **22**, 1037 (1974).
(16) W. Mertz, E. W. Toepfer, E. E. Roginski, and M. M. Polansky, *Fed. Proc.*, **33**, 2275 (1974).
(17) W. R. Wolf, *ibid.*, **34**, 972 (1975).
(18) U.S. Department of Agriculture—Workshop on the Calculation of Available Dietary Iron, Seattle, Wash., Sept. 1976.

Presented at the Division of Agricultural and Food Chemistry, 173rd Meeting, ACS, New Orleans, La., March 1977.



Wayne R. Wolf is a research chemist at the Nutrient Composition Laboratory, USDA. His research interests include the development of sensitive accurate methods for analysis of the trace element content of foods and other biological materials utilizing spectroscopic and combined chromatographic-spectroscopic techniques for chemical speciation of the trace elements. Of particular interest have been chromium analysis in biological materials, automated procedures for flame atomic absorption, development of appropriate reference materials for nutrient content of food, and multielement analytical techniques.

GC-LC Data Processing



Tracor 812
Analytical Processor

Highest Precision
Peak detection software uses both first and second derivative of chromatographic signal to interpret the chromatogram precisely.

Easiest to operate
User communicates with system by responding to system-initiated dialogue in *chromatographic terms*, not obscure codes.

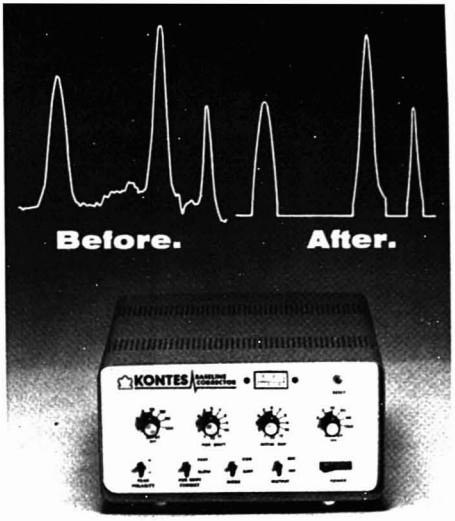
Clear, Concise Reporting

New
Expanded Capability
Dual Disc Accessory

Contact us for a demonstration.

Tracor Instruments Tracor, Inc. 6500 Tracor Lane Austin, Texas 78721 Telephone 512:926 2800

CIRCLE 202 ON READER SERVICE CARD



Dial out baseline drift and noise.

Our new and unique Kontes Baseline Corrector can modify the output signal from an analytical instrument and compensate for electronic drift, background noise, or other stray electronic signals.

The resultant clean, corrected baseline can then be reduced to significant data by means of a standard chart recorder, digital integrator, or other EDP hardware.

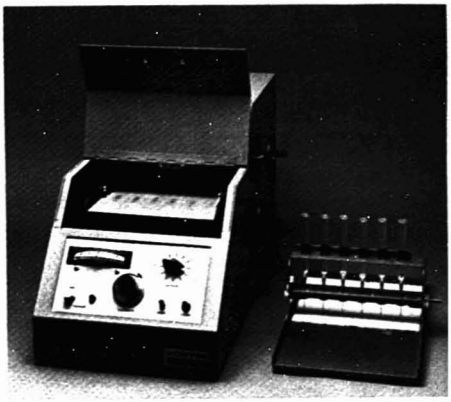
Specially designed solid-state circuitry in our Baseline Corrector permits a broad range of sensitivity adjustment and a high degree of baseline determination accuracy.

Dial out drift and noise and dial in accuracy and reproducibility. Baseline Corrector complete, ready for hook-up $925.

For more details or a demonstration, contact your Kontes representative or send for Bulletin K-21.

KONTES
Vineland, N.J. 08360

Exclusive Distributors: **KONTES OF ILLINOIS**, Evanston, Illinois
KONTES OF CALIFORNIA, San Leandro, California
KONTES (U.K.) LTD., Carnforth, England
CIRCLE 118 ON READER SERVICE CARD



Patented and proven.
The Kontes low-cost, quantitative TLC system.

Here is the proven Kontes system that offers high resolution, quantitative TLC analysis at low cost.

The brain of the system is the unique and patented Kontes Densitometer*[1]. It utilizes a rugged and highly reliable fiber optic scanner to create outputs compatible with all conventional data processing. It features single or double beam scanning in four modes—diffused reflectance, visible transmission, flourescence, and flourescence quenching. The densitometer sells for $2875 in U.S.

Our air-manifold Chromaflex® Spotter**[2] is the heart of the system. It consistently makes uniformly-sized spots on all standard TLC plates. Up to 2 ml of solvent extract can be spotted to a controlled diameter of 6mm or less with a reproducibility of ±2%. The Chromaflex Spotter sells for $150 in U.S.

In combination, our densitometer and spotter afford reproducible, quantitative analysis at a cost unmatched by other methods. The practicality of the Kontes system is documented by a bibliography of applications and a comprehensive manual.

For further information contact your Kontes representative or send for our detailed literature.

1. *U.S. Patents 3,562,539 and 3,924,948. "Determination of Reflectance of Pesticide Spots on Thin-Layer Chromatograms, Using Fiber Optics", Morton Beroza, K. R. Hill, Karl H. Norris, ANALYTICAL CHEMISTRY, September 1968.
2. "An automatic spotter for quantitative thin layer and paper chromatographic analysis by optical scanning", Melvin E. Getz, Journal of the AOAC, Volume 54, No. 4, 1971. **U.S. Patent 3,843,053

KONTES
Vineland, N.J. 08360

Exclusive Distributors: KONTES OF ILLINOIS, Evanston, Ill. • KONTES OF CALIFORNIA, San Leandro, Calif.
KONTES (U.K.) LTD., Carnforth, England
CIRCLE 119 ON READER SERVICE CARD

Matheson has...

Gases And Equipment For Gas Chromatography

We are proud of our expertise in the laboratory — we were manufacturing quality gases and mixtures for more than a decade before GC was introduced. We have maintained our position as leaders ever since.

Calibration Standards



Matheson Primary and Certified Standards are the workhorses of the analytical laboratory. Primary Standards are mixed gravimetrically to the highest accuracy and precision on a high load, high sensitivity analytical balance. Primary Standard accuracies often exceed the capability of your instrumentation. Certified Standards are recommended where the critical accuracy of Primary Standard is not required. Most standards are traceable to the NBS.

CIRCLE 128 ON READER SERVICE CARD

Regulators



The Matheson 3104 regulator is a high purity, two-stage regulator with a stainless steel diaphragm. Two-stage design provides even regulation regardless of cylinder pressure changes. Stainless steel diaphragm minimizes inboard leakage of air or water from the atmosphere, and does not outgas impurities into carrier or fuel gas systems. Five minute helium leak rate is $<2 \times 10^{-9}$ ccs. Excellent for applications involving trace components.

CIRCLE 132 ON READER SERVICE CARD

Zero Gases

For the carrier gas, fuel gas, and oxidizer gas—all required for flame ionization and flame photometric gas chromatography —Matheson offers Ar, He, H_2, N_2, 40% H_2/60% N_2, and 40% H_2/60% He Zero Gases each having a total hydrocarbon content of less than 0.5 ppm (as CH_4). Air, Zero Gas is available with hydrocarbon content <2.0 ppm.

CIRCLE 129 ON READER SERVICE CARD

High Purity Carrier Gases

Matheson makes carrier gases available in a variety of purity classifications — choose the specifications that most nearly meet your requirements. Routine analyses can be performed using Helium, High Purity, 99.995%. For more critical applications, you may choose Ultra High Purity 99.999% and Matheson Purity 99.9999%. For other applications, Argon, Hydrogen, and Nitrogen are all available in a variety of purities.

CIRCLE 133 ON READER SERVICE CARD

Purifiers





Matheson recommends the use of purifiers in all flow systems for the purpose of keeping false peaks and background interferences to a minimum. Two types are available: The Hydrox Purifier is a gettering furnace capable of reducing impurity levels of 100 ppm water and oxygen to 0.1 ppm each.

Models 450 and 460 Line Purifiers use interchangeable cartridges containing molecular sieves, charcoal, and special filters. They will remove oil, water, foreign particles, etc. The 460 will also remove most heavy hydrocarbons.

CIRCLE 130 ON READER SERVICE CARD

Filters



Matheson recommends No. 6164T High Purity Line Filters in all carrier and stream gas lines. It is stainless steel, heliarc welded — capable of removing particles 0.3 microns or larger, with a filtration efficiency of 99.999%. Using these filters minimizes background noise, and virtually eliminates the possibility of permanent damage by larger particles to sensitive valves, meters, and other parts of your system.

CIRCLE 134 ON READER SERVICE CARD

Chart

Matheson offers, free of charge, a six-page brochure: "How to Succeed at Gas Chromatography." Inside, a 3-page chart details exactly what you require for a high performance GC set-up. Included are specifications for carrier gases, regulators, filters, tubing, etc., as they apply for the different methods of gas chromatography. Suggestions are also made for gas sampling techniques to minimize error and contamination.

CIRCLE 131 ON READER SERVICE CARD

2132

Matheson®

Lyndhurst, N.J. 07071

East Rutherford, N.J. 07073
Morrow, Georgia 30260
Gloucester, Massachusetts 01930
Joliet, Illinois 60430
La Porte, Texas 77571

Cucamonga, California 91730
Newark, California 94560
Whitby, Ontario, Canada L1N 5R9
Edmonton, Alberta, Canada T5B 4K6
B 2431 Oevel, Belgium

Wallace F. Janssen
Food and Drug Administration
5600 Fishers Lane
Rockville, Md. 20857

Report

The Cancer "Cures": A Challenge to Rational Therapeutics

"Quackery kills a larger number annually of the citizens of the United States than all the diseases it pretends to cure."

So wrote an American physician in 1861, in an unsigned article published in the *National Quarterly Review*.

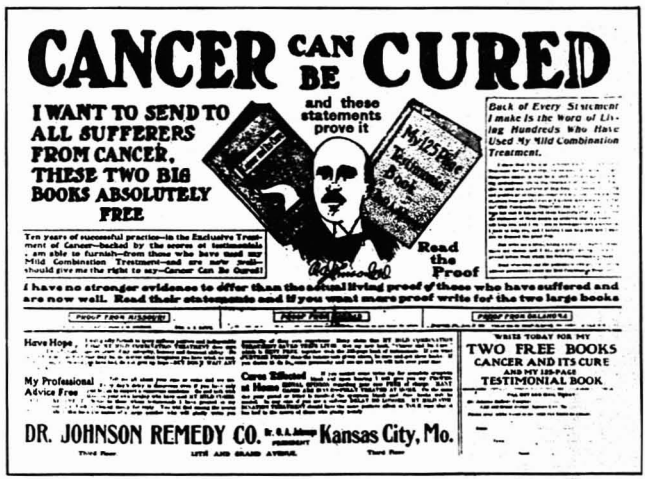
In the context of the times, the golden age of quackery, this was not an extreme statement.

One Samuel Thompson had explained the situation in his "New Guide to Health", first published in 1822. "The people," he said, "regard it among their vested interests to buy and swallow such physick as they in their sovereign will and pleasure shall determine, and in this free country denounce all restrictions upon quackery as wicked monopolies for the benefit of physicians."

Thompson's highly popular guide promoted his patented system for treating all diseases by means of heat, herbal laxatives, and emetics. Thompsonianism spread like wildfire, dominating medical practice for decades, especially in the Southern and Western States, and undoubtedly killing many thousands, but finally becoming discredited and replaced by other theories of healing.

Today we are in the midst of another nationwide health fad, the Laetrile panacea for all forms of cancer. When it has run its course, as it inevitably will, people will look back with amazement that so many were so gullible at a time when reliable health information was readily available.

Why is it that the American public seems to learn so little from experience in the area of health? Something must be lacking in health education.



We can vaccinate successfully against infectious diseases but not against the lure of a painless, easy, but worthless treatment for cancer. One reason, no doubt, is that today's generation has no memory of the conditions that resulted in enactment of the nation's laws to ensure drug safety and effectiveness.

Significant but forgotten is the fact that it was a fake cancer treatment which led Congress to pass the first Federal law against false claims for drugs.

In 1910 the Bureau of Chemistry (now FDA) attempted to prosecute the promoter of Dr. Johnson's Mild Combination Treatment for Cancer. At the time everyone thought the new Food and Drugs Act of 1906 would do away with the thousands of worthless and dangerous "patent medicines" then on the market, a major public health problem. But the Supreme Court ruled in the Johnson case that the law did not prohibit false "therapeutic" claims on drug labels but only false statements about the identity or composition of drugs.

Justice Oliver Wendell Holmes, Jr., son of the famous American poet and physician, who wrote the majority

This article not subject to U.S. Copyright
Published 1978 American Chemical Society

"The people . . . denounce all restrictions upon quackery as wicked monopolies for the benefit of physicians."—1822

opinion, could not believe Congress intended to legislate in the complex area of therapeutics. He concluded that Johnson could not be prosecuted for "mistaken praise" of his treatment, even though the indictment charged that he knew his claims were false.

Justice Charles Evans Hughes, one of three dissenters, thought just the opposite. The law prohibited labeling that was "false or misleading in any particular", and Hughes believed Congress meant what it said. In his view the courts had been made responsible for determining from the evidence whether or not a drug was misbranded. He saw the Holmes decision as opening the door to every kind of quackery, which indeed it did.

President Taft at once called on Congress to close this dangerous gap in the law. What he said applies as much today as in 1912:

> "There are none so credulous as sufferers from disease. The need is urgent for legislation which will prevent the raising of false hopes of speedy cures of serious ailments by misstatement of facts as to worthless mixtures on which the sick will rely while their disease progresses unchecked."

Congress responded with the Sherley Amendment, which made it a crime to label drugs with false and fraudulent claims of therapeutic effectiveness. Unfortunately, the words "and fraudulent" made it difficult for the Government to prosecute, in many cases, because it was necessary to prove the defendent *intended* to swindle the purchaser. Twenty-six years later, in 1938, Congress passed a new food and drug law which eliminated the so-called "fraud joker" and required scientific proof of safety before a new drug could be sold. And in 1962 the Congress voted unanimously for even stronger drug controls which required effectiveness as well as safety to be established before a drug goes on the market, a milestone advance in medical history. Opposition to the legislation continued in the courts, but in 1973 the Supreme Court unanimously upheld the law and the FDA's enforcement program.

A tremendous improvement in the quality and reliability of drugs has resulted from the drug effectiveness law. In the area of prescription drugs, for example, more than 6800 products have been removed from the market since 1962 because of the lack of evidence that they were effective, and the labeling of some 2000 others has been changed to reflect today's medical knowledge. Even more important, the law made the drug manufacturers responsible for proving the merits of their products, rather than requiring the Government to go into court in each case to show that a drug was misrepresented or unsafe.

But it was the unproven cancer treatments that demonstrated most strikingly the need to establish effectiveness of drugs *before* allowing them on the market.

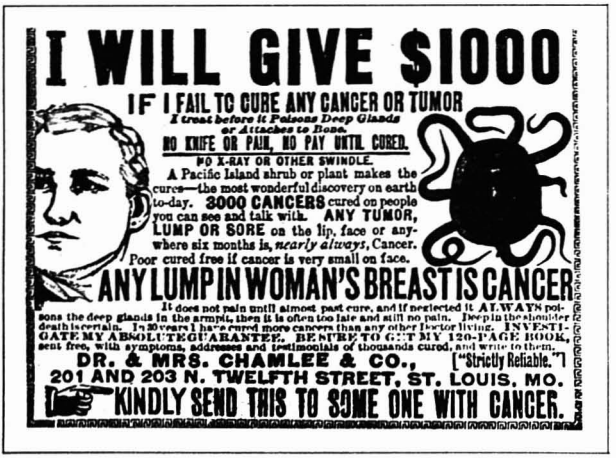
The Koch Treatment—Distilled Water

The great cancer swindle of the 1940's and early 1950's, and one of the greatest medical hoaxes of all times, was promoted by William F. Koch, M.D., of Detroit, who did business as the "Christian Medical Research League". Dr. Koch's treatment was a bonanza. Analysis showed it to be distilled water of extraordinary purity, but Dr. Koch claimed it contained 1 part of its alleged active ingredient, the chemical glyoxylide, in 1 trillion parts of water! A Federal prosecutor said this dilution was like dumping a cocktail into the Detroit River and expecting to get a kick from the water flowing over Niagara Falls. There was no evidence that glyoxylide had any therapeutic effect. But a great many people believed in it—over 3000 health practitioners across the nation paid $25 per ampul for it, and charged patients as much as $300 for a single injection! In 1942 the Federal Trade Commission, seeking evidence to ban Dr. Koch's advertising as false and misleading, held hearings in 21 cities. Local practitioners who testified ranged from reputable doctors who were misled by the advertising to fakers with no medical training whatever.

In 1943 the FDA prosecuted Dr. Koch. The trial lasted 18 weeks. Forty-three expert witnesses testified that the Koch products were misbranded and not effective in the treatment of cancer or any other disease. The defense had 104 witnesses who said the products were efficacious in the treatment of 69 different diseases, from acute appendicitis to *herpes zoster*, with special emphasis on cancer, tuberculosis, and coronary thrombosis. After 9000 pages of testimony (2 250 000 words) the case went to the jury, which deliberated 8 days without reaching a verdict, and was dismissed.

A poll of the jurors showed three who had insisted on acquittal from the outset. Human credulity had again been shown to be a major factor in the success of quackery.

Dr. Koch was tried again in 1946, but after five months a juror became ill and a mistrial was declared. In 1948, after an FDA inspection of



Chemical analysis of "Chamlee's Cancer Specific" from a "Pacific island shrub" showed only alcohol, water, and small amounts of iron, strychnine, and saccharin. Ads such as this appeared until the 1930's when stronger laws and rigorous enforcement put an end to them

Koch's laboratories, he announced he was retiring and went to live in Brazil. For a time the business was continued by Koch's associates under the name of the Christian Medical Research League. A product known as the "Koch Treatment" continued to be sold in Mexico long after it disappeared in the United States.

Harry Hoxsey's Herbal Tonic

The biggest health hoax of the 1950's was the Hoxsey Treatment for internal cancer. There were two products: the "pink medicine" composed chiefly of lactated pepsin and potassium iodide, and the "black medicine" composed of a common laxative (cascara) in an extract of prickly ash bark, buckthorn bark, red clover blossoms, barberry root, burdock root, licorice root, pokeweed, and alfalfa.

Harry Hoxsey, in his ghost-written book, "You Don't Have to Die", attributed this 1840 formula to his great grandfather whose horse was said to have recovered from a leg cancer after grazing in a pasture where such plants were growing. Apart from the laxative and potassium iodide, which have no value for cancer, all of the ingredients had long been discarded for any medical use.

Hoxsey was a medicine man all his life. After being prosecuted for violating the medical practice laws of several states, he finally set up a "clinic" at Dallas, Tex., where the judge of the Federal Court was a believer in "the treatment" even though his wife had died of cancer after using it.

The Hoxsey Clinic offered a package deal consisting of a perfunctory examination by a salaried osteopath and some routine blood and urine tests, after which the patients were told they had cancer and then the treatment was prescribed. This cost $400 for a lifetime supply of the two medicines. At the peak of the business over 10 000 people were getting the medicines.

Hoxsey had a large income from oil leases as well as the clinic, and he fought the Government both in the courts and with publicity. Writers and editors were paid to publish pro-Hoxsey articles. A "crusade of prayer" launched a write-to-Congress campaign against the FDA. Nevertheless, the medicines were found worthless by two Federal Courts after lengthy trials, one before a jury. In preparing for the litigation, FDA inspectors investigated some 400 cases of persons who were claimed by Hoxsey to have been cured of cancer by the treatment. The results formed a typical and significant pattern:

One group of these victims had diagnosed themselves or had never had a biopsy showing they had cancer.

> *"There are none so credulous as sufferers from disease."—1912*

A second group had cancer and had been treated for it by accepted and effective methods, but had later gone to the Hoxsey Clinic fearing they had not been cured.

The remaining cases were people who had received the Hoxsey treatment and had died of cancer (the majority) or still had it. No case of a bona fide cure was found. Public warnings issued by the FDA saved thousands from being victimized; in 1960, after 10 years of litigation, a Federal Court injunction finally stopped the sales of the Hoxsey treatment in the United States. Announcing the conclusion of the case, FDA estimated that cancer patients had paid over $50 million for the drugs. How many had paid with their lives was unknown. But like the Koch treatment, Hoxsey's medicines continued to be offered by practitioners in Mexico.

Krebiozen—Mineral Oil Injections

While the FDA was battling the Hoxsey treatment, another very different cancer drug was also making headlines and converts. This was *Krebiozen*, an alleged investigational drug said to be manufactured from the blood serum of horses inoculated with a mold that causes a disease known to veterinarians as "lumpy jaw".

Unlike Harry Hoxsey's backwoods herb remedy, Krebiozen had an aura of high scientific prestige. It was sponsored by the famous Dr. Andrew C. Ivy of the University of Chicago, who had joined forces with Stephan and Marko Durovic, Yugoslav immigrants, who said they made their discovery in Argentina. Ivy's announcement and endorsement of the drug at a lay press conference in 1951 was greeted with indignation by his university colleagues, the scientific community, and the American Medical Association, which regarded him as a defector from respectable science. But Dr. Ivy's prestige gained widespread confidence and credibility among cancer patients. To many he became a hero battling for humanity against the "Medical Trust".

A book would be needed to tell the entire story of Krebiozen. Thousands of cancer victims eagerly sought it, and thousands of doctors prescribed it as an investigational drug at $9 per ampul—billed as a "donation". But the cancer experts who suspected Krebiozen from the beginning were vindicated in 1963 when a team of FDA chemists, analyzing the only sample of the substance ever obtained from the sponsors, found it to be creatine monohydrate, an amino acid present in all animal tissue and without value in the treatment of cancer. At the same time, analysis of the drug as packaged for injection into patients showed that only mineral oil was present!

Krebiozen inspired an emotionally charged, organized following of people who were convinced that the scientific establishment was suppressing the use of a drug which could save lives. Nevertheless, when the FDA became convinced that the law had been violated, Dr. Ivy, the Durovics, and their Krebiozen Research Foundation were prosecuted. A Federal grand jury investigation resulted in an indictment on 49 counts of fraud and conspiracy to carry out a gigantic hoax. But on January 31, 1966, after a nine-month jury trial at Chicago, all defendants were found not guilty. Later, an investigation of jury tampering led to the conviction of one of the jurors, who served a six-month prison term.

The acquittal verdict meant that the Government had failed to prove deliberate action to defraud the public. It had no bearing on the lack of scientific evidence on the effectiveness or safety of Krebiozen, nor did it change the fact that the ampuls contained only mineral oil. Interstate distribution continued to be illegal.

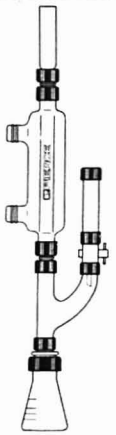
On March 28, 1966, the first of a series of demonstrations and "sit ins" by Krebiozen supporters blocked access to the FDA Commissioner's office. On succeeding days the group beseiged the HEW Secretary and their representatives in Congress to make the FDA back down and allow the continued shipment of Krebiozen. HEW officials held a public meeting with the group to hear their protest and explain the Government's position, but to no avail. Eleven U.S. Senators called for another start in determining whether the drug had any value for cancer. The pressure was intense. But the FDA did not back down. To have done so would have meant that for every cancer patient who thought he was helped, there would be many others who could lose their lives by stopping, or not getting, effective treatment.

FDA's Commissioner, Dr. James L. Goddard, put it this way:

> "I know there are several hundred people who believe in their hearts that Krebiozen will cure them. And

NEW!

REACTI-WARE© SYSTEM



THE ALL NEW MICRO-SCALE GLASSWARE SYSTEM

FEATURING:

- Grease Free Micro-connectors* for an all Glass and Teflon® System
- Screw-together Components for Fast, Positive Assembly

FOR:

- Derivatization
- Sample Isolation/Purification
- Micro-distillation
- Micro-column Chromatography
- Sample Concentration
- AND MORE!

Our new Vials & Closures Brochure gives full details on Reacti-Ware℠ and other unique laboratory aids. Ask for your FREE copy today!
Patent Pending

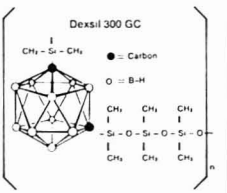
PIERCE
CHEMICAL COMPANY
Box 117, Rockford, Illinois 61105

CIRCLE 217 ON READER SERVICE CARD

DEXSIL®

High Temperature GC Phases

Extended column life at 400° and beyond



Separate amino acids, drugs, paraffins, hydrocarbons, natural waxes, pesticides, fatty acids, steroids, alcohols, etc. – at column temperatures of 400° C and more. Routinely. With outstanding selectivity.

Columns packed with Dexsil 300GC have shown negligible bleed from 20° to 450° C. Limited life applications can be performed at temperatures to 500° C. Two other Dexsil polymers – 400GC and 410GC – can be selected according to application, and used at temperatures to 400° C.

When used at lower temperatures up to 350° C, the Dexsils offer the advantages of using more sensitive GC settings and increasing column life because of the Dexsils' low bleed. Users report column life under routine conditions at 2, 3, 4 years and more.

Dexsil is available NOW, either directly or from your regular supplier. Write for details, and an exhaustive bibliography of over 200 Dexsil applications.

DEXSIL 295 Treadwell Street ● Hamden, CT 06514
(203) 288-3509

® Registered Trade Mark Dexsil Chemical Corporation Hamden CT.

CIRCLE 69 ON READER SERVICE CARD

GFS CHEMICALS

YOUR MOST
DIRECT SOURCE
FOR THE FINEST COMMERCIALLY AVAILABLE
ANALYTICAL CHEMICALS

IT'S WISE TO KNOW YOU CAN
BUY DIRECT in ANY QUANTITY
FROM THE MANUFACTURER

1928 50 YEARS 1978 GFS

ANALYTICAL CHEMICALS SINCE 1928

G. FREDERICK SMITH CHEMICAL COMPANY

867 McKinley Ave.
Columbus, Ohio 43223

FOR PROMPT SHIPMENT
614 224-5343



Contact us or circle Reader Service Card for YOUR 50th ANNIVERSARY GENERAL CATALOG
...it's FREE

GFS CHEMICALS

CIRCLE 247 ON READER SERVICE CARD

"The sponsors . . . have held out false hope to unknown numbers of cancer victims . . ."—1966

I have deep sympathy for these people. But there are 198 million people whose health and safety depend in some measure on the integrity of FDA . . .. The sponsors of krebiozen have not fulfilled the requirements of the laws passed by the Congress for the introduction of safe and effective drugs to the American public. They have held out false hope to unknown numbers of cancer victims . . .. The Commissioner of Food and Drugs has neither the moral nor the legal right to disregard the laws of Congress and the evidence of science. We cannot and will not permit the introduction of Krebiozen into interstate commerce."

Like believers in the Hoxsey Treatment, Krebiozen advocates demanded a "fair test" of the drug. But Dr. Ivy had never submitted evidence sufficient to demonstrate the existence of an active substance. Animal test data—essential to justify FDA clearance of an investigational drug—were totally inadequate to justify tests in humans. Yet, in 15 years of illegal distribution as an investigational drug, Krebiozen *was* tried on thousands of cancer patients—with no credible effects. A National Cancer Institute committee of 24 leading cancer experts reviewed 504 case histories provided by Dr. Ivy and found unanimously that Krebiozen was ineffective as an anticancer agent.

What happened afterward? The Krebiozen boom collapsed. Stephan Durovic abruptly left the United States, via Cuba, to Paris, and then to Switzerland where he had banked his profits. Marko Durovic, the lawyer brother, spent years in controversy with the Internal Revenue Service. He died in 1976. And Dr. Ivy continued to dispense Krebiozen from his office in Chicago, changing the name to "Carcalon", which he claimed to be an improved product, and which he continued to prescribe until retirement a year ago.

Miscellaneous, But Remarkable

The Koch, Hoxsey, and Krebiozen treatments overlapped in time, and there were numerous other cancer frauds during the 30-plus years that saw their rise and fall. Most remarkable was the fact that so many believed in them.

Mucchoricin, extracted from moldy, decayed wheat, was made and sold by Philip Drosnes, a former tire salesman, and Lillian Lazenby, an excafeteria worker, who opened a "clinic" at Detroit. Promoted as an "antibiotic", it had a bacteria population which made it a dangerous drug as well as an ineffective one.

The Sanders treatment, offered by an Oklahoma motel operator, kept his 70-unit facility running at capacity, day after day. It was made of ground warts from horses, in a sour milk suspension.

Millrue, an herbal extract with iron and vitamins, was prescribed and dispensed by Roy Paxton, an Illinois healer, who diagnosed all diseases by feeling the patients' feet. After serving a three-year sentence for violating the Federal Food, Drug and Cosmetic Act, he became a director of the National Health Federation, the leading advocate of quackery under the slogan "freedom of choice".

Orgone energy, the nonexistent universal force imagined by psychiatrist Wilhelm Reich, exploited hundreds of cancer victims who rented "orgone accumulators" for $250 per month. Patients sat inside the box-like devices to absorb the "orgone".

The Rand Vaccine, a sensation in 1966, was much more effective as a stock promotion than as a cancer treatment. The Rand Development Corp. supplied it free of charge, but the stock of the company leaped from $7 to $50 a share and then fluctuated widely. In January 1967 the Securities and Exchange Commission suspended trading, and James H. Rand was subsequently indicted for stock fraud.

The "vaccine" was crudely made from the blood of animals which had been injected with material from human cancers collected indiscriminately from hospital operating rooms.

Extensive publicity from stories planted in newspaper financial pages and a national magazine brought thousands of cancer patients to Ohio physicians and hospitals, where the "vaccine" was generally thought to be a legal investigational drug. The one obstacle to nationwide distribution was the Federal Food, Drug and Cosmetic Act. An application to FDA to show that the vaccine was reasonably safe for use in man failed in every respect. Investigation disclosed toxic effects, heavy bacterial contamination, and in one study (not disclosed by the sponsor) that the vaccine actually hastened the growth of cancer in test animals.

On February 7, 1967, on evidence provided by the FDA, a Federal Court order stopped further manufacture and distribution, and a few weeks later Rand consented to a permanent ban after a full hearing. The stock fraud indictment was dismissed.

The reaction to the ban was intense. Public sympathy was aroused by press headlines—"Court Ban Like Death Sentence", "Cancer Victims Fight For Hope"—but the facts did not permit a retreat. Organizations and individuals who had backed Krebiozen now backed the Rand treatment. In a week after the ban a petition with 25 000 signatures was being circulated in Washington urging that supplies of the vaccine be continued. The tragic stories of those who had been duped were ignored. But the Rand "cure" declined almost as quickly as it had arrived.

And Now—Laetrile

Today's cancer fad is Laetrile, also known as amygdalin and vitamin B-17. It is heavily promoted by well-organized groups who are using all the mass-communication techniques. The product is different, but the claims (to prevent cancer as well as treat it) are as extreme and dangerous as those used pre-1912.

FDA's Laetrile file begins with a memorandum of a visit by a Mrs. Moriarity to the Chicago district office on November 30, 1945. She had come to tell the Agency that a Dr. Ernest T. Krebs, M.D., of San Francisco, had a new drug which had cured her of cancer. The FDA was not impressed by this testimonial; cancer "cures" were a dime a dozen. But some 16 months later inspectors interviewed Dr. Krebs, his son E. T. Krebs, Jr., and a Dr. Gurchot. The drug they were shipping, for cancer, was not Laetrile but "Mutagen", a brand name for chymotripsen, an enzyme derived from the pancreas of cattle.

In 1952 the FDA learned that Dr. Krebs had a different cancer treatment, made from apricot kernels, which he first called "Lyotral", and which was not yet available even for investigational use. But soon it was learned that a patent had been granted and was being used to promote the drug in California. The first Federal action against Laetrile came in 1960 when an interstate shipment was seized from an osteopath who had taken over the operation of the Hoxsey Cancer Clinic at Dallas, Tex. There was no contest. The record shows that immediately after the clin-

". . . with a little luck, proper timing and a good promotion program, a bag of asafetida with a unique chemical side chain can be made to look like a wonder drug".—1977

ic was enjoined from using the Hoxsey treatment they had switched to Laetrile.

The second Laetrile case was a criminal prosecution of three Los Angeles practitioners for shipping the drug illegally to a lay person in Idaho. The Government charged that the new drug, labeled for investigational use, was not shipped to "an expert qualified by scientific training and experience to investigate the safety of said drug", as required by law. Two of the three defendants were M.D.'s past 80 years of age. They consented to a court order to stop distributing the drug. The third defendant was the notorious medical con-man, Roy De Welles, whose main business was promoting enemas for the treatment of all diseases. A warrant for his arrest was never served, the reason being that he was being prosecuted in the Federal Court at Indianapolis for mail fraud. Convicted, he served a 10-year prison sentence.

The Krebs, father and son, did business as the "John Beard Memorial Foundation". In the third FDA legal action involving Laetrile, the Krebs and their Foundation were charged with shipping another new drug which had not been cleared as safe under the law. This was an alleged "Vitamin B-15", also known as "pangamic acid". It was claimed to be effective as a heart stimulant and for improving the performance of race horses. In this case, E. T. Krebs, Jr., and the Foundation pleaded guilty to five counts of violating the new drug law, and a total fine of $3 755 was imposed. Krebs, Jr., was put on probation for three years, on condition that he would not ship any new drugs, including Laetrile, without approval from the FDA. A supply of Laetrile already manufactured was permitted by the court to be sent to the McNaughton Foundation of Montreal, Canada, for research purposes.

At this point two things happened: First, a promotional paperback book, "Laetrile—Control for Cancer", appeared in newstands, book stores, and thousands of health food stores across the country.

Second, Laetrile, which had never been legally available in the United States, became readily available in Canada and Mexico.

Neither of these developments could be dealt with by the Food and Drug Administration. Publicizing of the treatment in the press, dangerous as it is to desperate, frightened cancer victims, is protected by the first amendment to the Constitution. And the prescribing and dispensing of drugs in other countries is, of course, beyond the reach of U.S. law.

This leaves, as the only means available to protect U.S. consumers, the authority of the Government to bar the importation and interstate distribution of illegal drugs.

The Laetrile Challenge

The significant difference between the Laetrile craze and its predecessors is the power of the promotion behind it and the damage it threatens to the laws which insure drug safety and effectiveness. Laetrile has become a *cause célèbre*, promoted by both organized quackery and its misguided followers. The situation has been aptly described as an "unhealthy alliance of promoters, fighting for the right to cheat, and victims fighting for the right to be cheated". The slogan of the movement, "Freedom of Choice", is but one side of a counterfeit coin. The other side is freedom for swindlers to sell worthless drugs to desperate victims who will pay any price and clutch at any straw. For many the consequences are fatal—because the lure of easy, painless treatment for cancer is irresistible.

The "sit-in" demonstrations by Krebiozen followers in 1966 were a preview of the pressures applied to State legislatures by Laetrile lobbyists, beginning in 1976. To date, 13 States have enacted laws to "legalize" the drug by stopping enforcement of their drug and medical practice laws. More serious are bills in the Congress to repeal the effectiveness requirements of the 1962 Drug Amendments. Some 125 House members and four Senators have endorsed this legislation. It seems incredible in the light of the legislative history of the 1962 law, enacted unanimously by the Congress, that so many members have gone on record against its most important requirement.

The hearings held by Senator Kefauver disclosed that false claims for prescription drugs were hardly less prevalent and no less dangerous than those for the so-called "patent medicines" at the turn of the century. As one witness put it, "If an automobile does not have a motor, no amount of advertising can make it appear to have one. On the other hand, with a little luck, proper timing and a good promotion program, a bag of asafetida with a unique chemical side chain can be made to look like a wonder drug." To this we can add that placebo effects and mass hysteria make the promotion of cancer panaceas the easiest of all drug swindles. Consumers, law makers, and even many physicians can be blinded to the consequences.

As another witness pointed out at the hearings, the average practicing physician just does not have the time, facilities, skill, or training to be an expert on drug safety. Without an agency to assure safety and effectiveness, every physician would have to be his own Pasteur, and the American people a willing army of guinea pigs.

The Supreme Court of the United States in 1973 upheld specifically and in great detail the FDA's powers to administer the 1962 drug effectiveness law. Yet in 1977, a U.S. District Court Judge ordered this Agency to stop action against the distribution of Laetrile. Incredibly, this decision presumes the 296 judges of Federal District Courts qualified to make the final judgments on medical policy and products.

We have not seen the last of the Laetrile issue. It is a fundamental challenge to the credibility of science and the future of rational therapeutics.



Wallace F. Janssen is FDA historian and author of numerous articles on FDA activities. Previously as FDA's information chief, he was primarily involved with problems of health misinformation and quackery. Janssen was instigator of FDA's public warning which saved more than 6000 persons from being victimized by the Hoxsey cancer treatment.

X-ray analytical equipment is a big investment. Don't you deserve a look at the best investment?

Whether it be spectrometers or diffractometers, Siemens analytical x-ray units are the best investment.

Siemens SRS 200 is a sequential spectrometer that uses x-ray fluorescence methods to non-destructively analyze solid, powder, and liquid samples for all elements from fluorine to uranium. Sample changers are available to accommodate up to 80 specimens. That's flexibility.

For process control applications demanding speed and accuracy, the MRS 400 spectrometer provides up to 28 simultaneous analyses in less than one minute. That's speed.

Siemens D 500 diffractometer provides for material examination; including structure and layer determination, texture and stress measurement, and phase analysis.

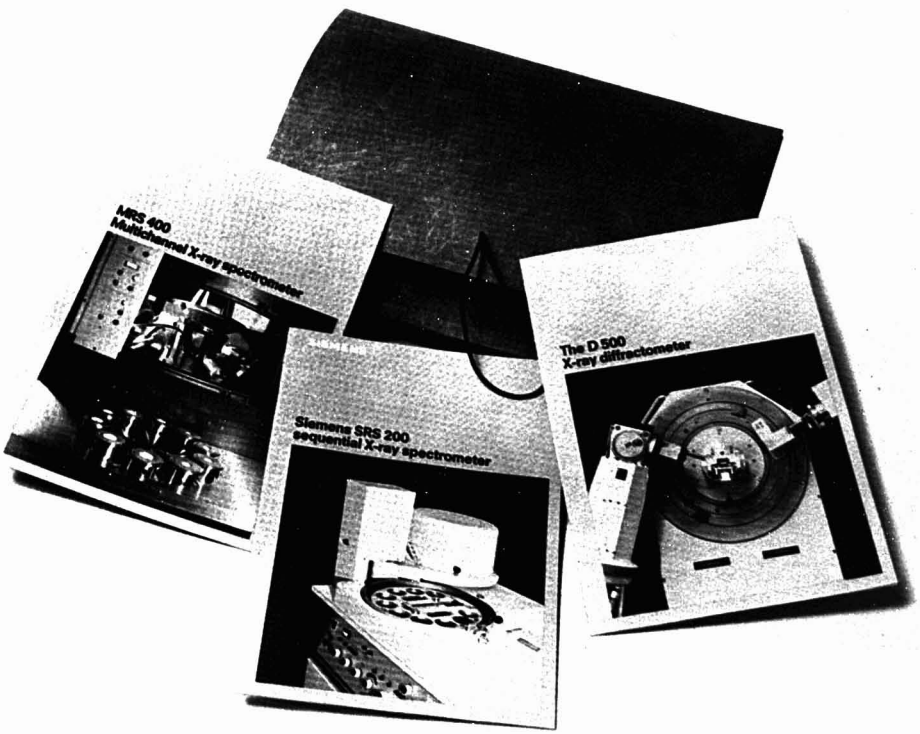
The D 500 is available with 1, 30, or 80 specimen magazines, with sample rotation capabilities... perfect for the routine analysis of a large number of samples.

All three units are designed and built to be either automatic or manual. So when you invest in an automatic unit, you get an automatic unit, not just a retrofitted manual instrument.

For more information on your best x-ray analytical investment and a free x-ray periodic table chart, write or call: Mr. Pedro Arredondo, Siemens Corporation, Analytical Systems Division, 1 Computer Drive, Cherry Hill, N.J. 08002, (609) 424-9212.

SIEMENS

CIRCLE 190 ON READER SERVICE CARD



Laboratory tools worth your careful attention.



Versatile automatic titrator

Newest Titralyzer® II has most versatile sampling you'll see anywhere. Microprocessor-controlled sampler handles 32x100 ml, 32x200 ml or 21x400 ml — or any partial loads you dial in. Printout of results to nearest 0.01 ml titrant; also important analytical information before-&-after titration via pH/mV printout. Continuous LED display. Single, dual endpoints with proportional anticipation. Expanded-range electrometer for exotic applications. Photometric as well as potentiometric automation. First derivatives too. In short: versatility at a surprisingly modest price. (Smartest way we know to handle large-scale wet-analysis workloads.)

For data, circle 84.



See these – and many more from the Fisher product "think tank" – at the Pittsburgh Conference.

Booths 301-310.

Ultra-filtered HPLC solvents

Fisher Certified HPLC solvents are ready-to-use reagents controlled for every parameter vital to high-pressure liquid chromatography. Consistent results, bottle to bottle, lot to lot. Now a stringent specification for these distilled-in-glass solvents becomes even more stringent. They're submicron filtered (0.5μ), to protect pumps and columns.

For data, circle 85.







Simplified phenol, Hg tests

Two new portable Fisher analyzers vastly simplify measurement of total phenol in water/wastewater, and free mercury in solids, liquids and gases. ONE: Dedicated UV phenol-analyzer virtually eliminates sample prep, dramatically reduces reagent consumption, lets one operator do work of 4 or 5. Range 5 ppb to 20 ppm. TWO: Equally dedicated UV mercury-analyzer permits even inexperienced operators to achieve accurate reproducible measurements fast, provides automatic background compensation. Range: 0.2 ng to 600 ng.

For data, circle 89.

Space-saving pH-meters

Full-performance pH-meters tend to be either squat-bulky . . . or high-rise skinny. Not the newest Accumet* models. Series 600 is more compact, more space-saving than ever. Yet low-silhouette, for stability. Total swivel, for optimum viewing. And ingenious 3-electrode arm that's almost as flexible as the human kind. Accumet 600. New high in convenience. New low in space needs.

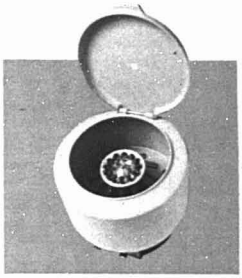
For data, circle 86.



Extra-rugged centrifuge

New Centrific™ is the strongest tabletop centrifuge you'll hope to find. A roomy bright-yellow portable, ideal for large-volume testing, student labs, etc. Where conventional aluminum guard bowls are pierced through by flying-shield tests, Fisher bowl will display only a dent. Reason: its crosslinked high-density polyethylene is ultra-high impact. Speeds from below — 1000 to 4750 rpm. Takes 2 ml to 100 ml tubes. Uses your present heads. Truly quiet. And economical.

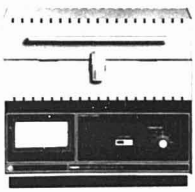
For data, circle 90.



Speedy furnace heats

Isotemp* furnaces are true portables. Tube models are a scant 10 kg; muffle models, 16 kg. And they're true speedsters. Reach maximum (1000°C for tube models, 1100°C for muffles) in as little as 12 minutes. Rapid cooldown and recovery time, too. Automatic compensation for voltage and ambient variations. Miserly power consumption. Five models to choose from.

For data, circle 87.







Fully reproducible sulfurs

Here, now, the industry's first affordable sulfur analyzer with full inter-lab reproducibility. Detects available sulfur to 0.005%. Displays results directly in % or ppm on LED readout in 2 minutes. Lowest test cost (5¢ expendables). Uses patented amperometric titration, hence unaffected by interferences plaguing other methodologies. Safe, clean, speedy, accurate, automated — and $6000 less than anything comparable to date.

For data, circle 91.

Battery-pack balance

A truly carefree electronic toploader for field tests. Our Model A-200BP, providing freedom from line power for 8 hours at a stretch. Only 5 kg; balance and battery-pack fit into briefcase! No leveling needed — use anywhere. 200g capacity, 0.01g sensitivity are ideal for broad range of field monitoring. Single touch-bar operation (including taring). Instant LED digital readout. Also a-c versions, from 20g to 2000g, in this line of rugged briefcase-slim balances.

For data, circle 88.



We Know Laboratories

Fisher Scientific Company

711 Forbes Avenue
Pittsburgh, PA 15219
(412) 562-8543

Three major technical advances have made Neslab's constant temperature circulating baths the most advanced laboratory cooling baths available. The temperature range of +250 down to −100°C only hints at the new lows we've reached.

Multi-point sensing probes housed in a stainless steel sheath read the temperature three times per second at three different points in the bath. Unavailable in laboratory baths at any price, Neslab's 3-point sensing virtually eliminates overshoot and lag, and keeps control deviations lower than ever before possible.

The proportional IC controller provides unmatched short-term control without long-term instability or drift. Four integrated circuits provide stability of a low ±0.02°C or less. Conservatively.

The new circulating pump is adjustable from 0 to 13 liters/minute. It combines a specially designed motor, industrial grade ball bearings, a multi-bladed rotor and a massive ½" diameter shaft, reducing vibration and noise to a new low. With no sacrifice in flow or pressure.

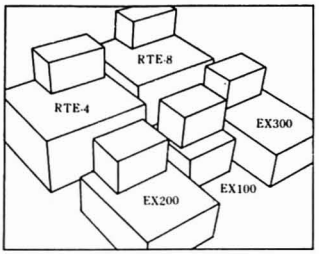
The efficient, progressive cavity pump design reduces mechanical heat input to a new low. It can operate with a wide range of temperatures, bath fluids and viscosity conditions, and is designed to run for years. Continuously.

Lowest of all is the price tag. Neslab's baths actually cost less than others not having their exclusive features. And we think that's the best low of all.

Phone right away. Or write away.

NESLAB INSTRUMENTS, INC., 871 Islington St., Portsmouth, N.H. 03801 U.S.A., (603) 436-9444.

NESLAB



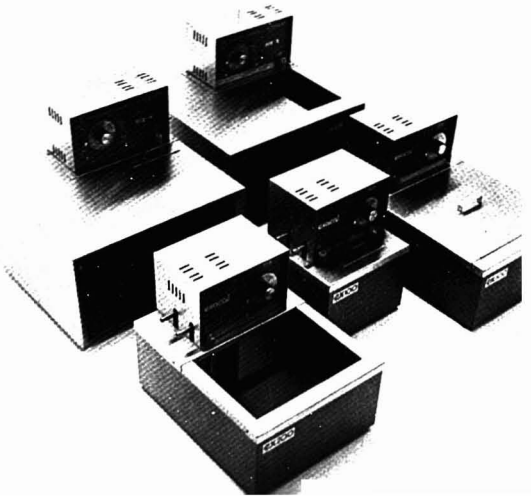
EXACAL BATH CIRCULATORS provide constant temperatures from −35 to + 150°C. Stability: ±0.02°C or less. Work areas: up to 10" x 12" x 5¼" deep. Accessories: refrigeration units; electronic temperature programmer.

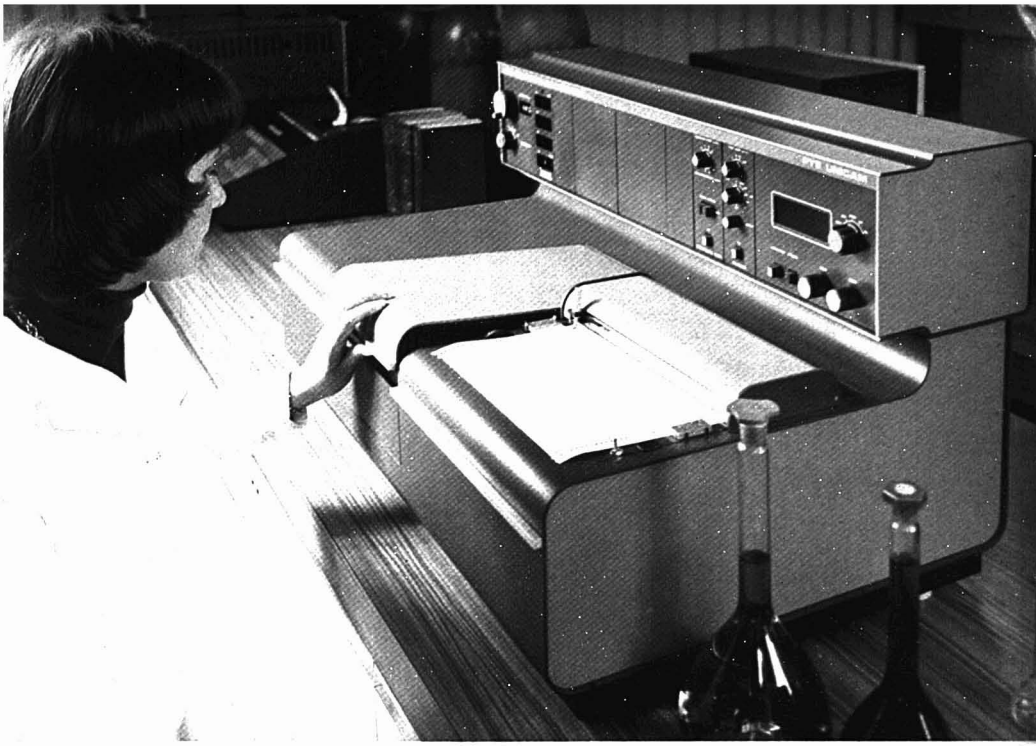
RTE-4 & 8 REFRIGERATED BATH CIRCULATORS have 20-30% greater cooling capacity than most baths. From −30 to + 100°C. Stability: ±0.02°C. Work areas: up to 8¼" x 4¼" x 9" deep. Accessory: electronic temperature programmer.

LT-9 LOW-TEMPERATURE BATH CIRCULATOR (not illustrated) can maintain a high 300 watt heat removal capacity at −70°C. From + 10°C to −70°C. Stability: ±0.05°C. Work area: 6¼" dia. x 8" deep. Accessory: electronic temperature programmer.

We've reached some new lows in temperature control.

CIRCLE 144 ON READER SERVICE CARD





Get more UV-VIS spectrophotometer than your budget allows!

Now from Philips, the Pye Unicam SP8-100 high performance spectrophotometer.

You'll be most pleasantly surprised when you see the features packed into the SP8-100 . . . and learn how affordable it is. Get our brochure and compare this system with any other.

The SP8-100 is built by Pye Unicam, a leader in UV-VIS spectrophotometry, and is backed by Philips, a world leader in high technology systems. Our applications specialists and accessories will help you get the most from your studies, including:

- reaction rate analysis
- kinetic analysis
- color measurements



- fluorescence
- densitometry
- column monitoring
- turbid samples
- automated measurements

Stretch your budget . . . and your capabilities . . . with the Pye Unicam SP8-100.

Philips Electronic Instruments, Inc.
A North American Philips Company.

85 McKee Drive, Mahwah, NJ 07430
Telephone (201) 529-3800 International, contact Pye Unicam Ltd., York Street, Cambridge, England CB1 2PX. Telephone Cambridge (0223) 58866. Telex 817331

PHILIPS **Electronic Instruments**

Call, write or use the reader reply service for your copy of the SP8-100 brochure.

PHILIPS

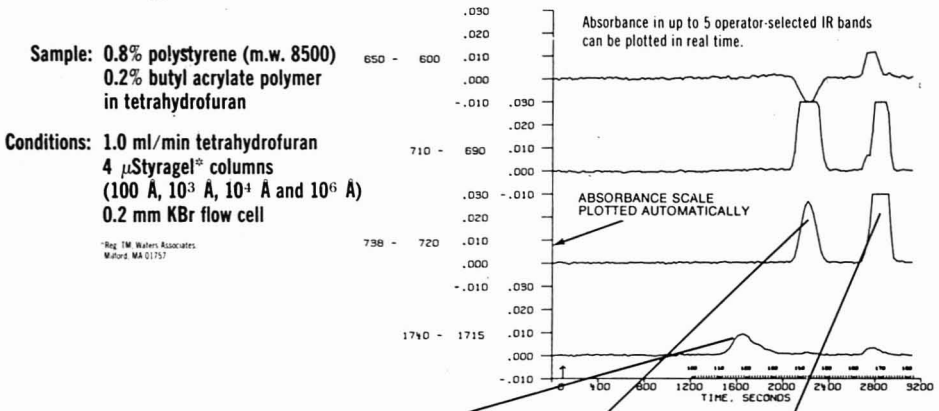
Be sure to visit our display at the Cleveland Conference, Booth #601–608.
CIRCLE 198 ON READER SERVICE CARD

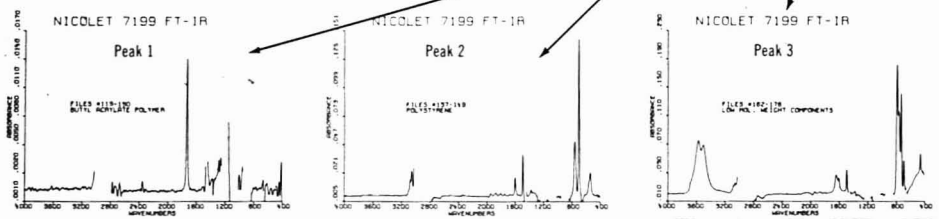
Revolutionize your LC measurements with the amazing new Nicolet LC-IR *CHEMIGRAM*™

Sample: 0.8% polystyrene (m.w. 8500)
0.2% butyl acrylate polymer
in tetrahydrofuran

Conditions: 1.0 ml/min tetrahydrofuran
4 μStyragel* columns
(100 Å, 10^3 Å, 10^4 Å and 10^6 Å)
0.2 mm KBr flow cell

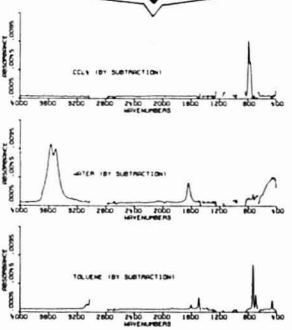
*Reg. TM. Waters Associates
Milford, MA 01757





- Routinely determine polymer chemical composition versus molecular weight.
- Use automatic flow programming.
- Use stopped flow for maximum sensitivity.
- Solvent programming is possible.

Unresolved components can be separated by absorbance subtraction.



See a demonstration of the Nicolet LC-IR CHEMIGRAM at the Pittsburgh Conference, Booths 517-523.

NICOLET INSTRUMENT CORPORATION
5225 Verona Road
Madison, Wisconsin 53711
Telephone: 608/271-3333

CIRCLE 146 ON READER SERVICE CARD



The big HPLC system breakthrough

The breakthrough in flexibility

Buy a packaged HPLC system and you're out of luck when any part of it becomes obsolete or when it no longer matches your needs. Your Altex system, however, is always at a state-of-the art level. It consists of smart modules coordinated by an even smarter controller. It is exactly right for the work you are doing today. And since you can expand its capabilities at any time, it will still be exactly right for the work you are doing five years from now. In fact, an Altex system is the only HPLC system whose flexibility and versatility you cannot outgrow.

The breakthrough in programming

At your fingertips you have command over your Altex HPLC System unequalled in systems costing much more. All changes in flow rate, composition, chartspeed . . . all commands to valves, injectors, fraction collectors can be programmed to occur automatically for maximum reproducibility, speed and convenience. A unique, programmable audible signal alerts you when an important event is occurring. Ten numbered programs with different values can be stored for repeated use. The system can be run while a new program is being written and additional steps can be manually inserted at any time without affecting the basic stored program. Finally, what other microprocessor system will greet you in the morning, and have your first cup of coffee waiting!

ALTEX

ALTEX SCIENTIFIC INC. 1780 Fourth St.
Berkeley, California 94710 (415) 527-5900
CIRCLE 12 ON READER SERVICE CARD

Reliable. Fast and Easy. MCI automatic analyzer.

Incorporates coulometry principle applied to Karl Fischer titration. Operation is full-automatic. Measuring time is shortened. Accuracy is within 5μg for 10μg—1mg H_2O and within 0.5% for 1—30mg H_2O. Wide-range applications include measurement of ultra-trace water content in liquids, solids and gases. Range: 10μg—30mg H_2O.
An optional water vaporizer for speedy and accurate measurement of water content in plastics, grain, etc.

Printer (optional)



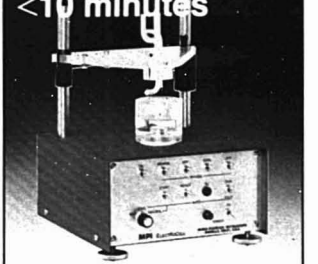
CA-02 Moisture Meter with Printer

MITSUBISHI CHEMICAL INDUSTRIES LIMITED
Instruments Dept., Mitsubishi Bldg., 5-2, Marunouchi 2-chome, Chiyoda-ku, Tokyo, 100 Japan Telex: J24901 Cable Address: KASEICO TOKYO

CIRCLE 139 ON READER SERVICE CARD

Rapid TRACE METAL ANALYSIS

0.1 ppb detection limit reached in <10 minutes



ElectRoCell
Electroanalytical Rotated Cell

Quantify small amounts of Pb, Cu, Ni, Cd, Zn, and other metals in solution by rapid anodic stripping analysis.

Extremely efficient and reproducible stirring action speeds analysis time. ElectRoCell's unique rotating action holds the 15 ml sample in a thin film on the cell's wall by centripetal force where O_2 is sparged in 75 seconds or less. The cell is then switched to its back-and-forth stirring mode during amalgam accumulation. Aliquoting and cleaning time included, it takes less than 10 minutes for a complete ppb range analysis. That's only about 2/3 of the time required for sparging alone with a conventional cell.

Optional 1502B Control Electronics also accept a variety of other cells for different electro-analytical techniques. TTL level signals are available for complete, programmed operation.

Pacific Photometric Instruments
formerly McKee-Pedersen Instruments
5675 Landregan St.
Emeryville, CA 94608
(415) 654-6585

Booth 421
Pittsburgh
Conference

CIRCLE 175 ON READER SERVICE CARD

LIFE CAN BE SIMPLER



HPRC develops reproducible picogram separations in four minutes like these carotinoids used in liquors. Screening is important because price varies considerably with the origin of these carotinoids. HPRC can help you with pharmaceuticals, pesticides, narcotics, oils, etc. And correlate to your HPLC columns with confidence.

Make life more pleasant for yourself by letting CAMAG High Performance Radial Chromatography serve you.

Pittsburgh Conference-Booth #708, Paper #269

HPRC: Carotinoids in liquors

CAMAG Inc.
16229 West Ryerson Road / P.O. Box 183
New Berlin, Wisconsin 53151

CIRCLE 49 ON READER SERVICE CARD

1978 ACS National Meeting

Anaheim
March 12–17, 1978

Anaheim, home of the magical kingdom of make-believe, Disneyland, will extend its hospitality to the attendees of the 175th National Meeting of the American Chemical Society, March 12–17, 1978. This spring the meeting is scheduled a few weeks earlier than usual and the city will be particularly delightful for those attendees descending from those parts of the country still suffering from freezing temperatures. The meeting will feature technical sessions and professional and social activities that will attract more than 8 000 attendees. In all, 24 of the Society's 29 divisions and a number of committees will participate in the five days of technical sessions. The technical program will include over 2 500 papers to be presented in almost 350 planned symposia sessions. Two additional activities to note are the ACS Award Dinner on Monday, March 13, and the meeting of the ACS Council on Wednesday, March 15.



The Analytical Chemistry Division will hold 18 half-day sessions at which close to 100 papers will be presented. These sessions are composed of five symposia of 14 sessions and four general sessions. Among the symposia topics are: the ACS award in analytical chemistry, new applications of lasers to chemistry, selective detectors for chromatography, Divisional instrumentation award, and analysis of high-purity materials. Of these the first two symposia with 17 and 18 presentations each at four respective sessions seem to dominate the technical program of the Division. The four general sessions will cover the areas of spectroscopy, electroanalytical chemistry, chromatography, and general analytical chemistry.

The Division program will be highlighted by the presentation of the two ACS awards and the Divisional instrumentation award. The ACS Analytical Chemistry Award, consisting of a $2000 honorarium and an etching and sponsored by Fisher Scientific, will be presented to Henry Freiser of the University of Arizona. His award address on the structure and behavior of organic analytical reagents will be delivered on Monday morning at the symposium dedicated to the award. The ACS Chromatography Award will be presented to the Nobel Laureate and the originator of gas chromatography, A.J.P. Martin. This award, which consists of a $2000 honorarium and a certificate, is sponsored by Supelco, Inc. Dr. Martin's award address will be presented on Wednesday morning at the symposium on selective detectors for chromatography. Finally, the Analytical Chemistry Division Instrumentation Award will be presented to James D. Winefordner of the University of Florida. The award, consisting of a $2000 honorarium and a wall plaque, is cosponsored by the Division and the Instrumentation Specialties Co. of Lincoln, Neb. At the opening of the symposium dedicated to the award on Thursday morning, Dr. Winefordner will speak on the trace analysis of atoms and molecules by new approaches.

In addition to these programs for which the Analytical Division is the primary sponsor, the Division will participate in a two-session symposium on nondestructive and analytical chemical techniques in nuclear safeguards. The primary sponsor of the symposium is the Division of Nuclear Chemistry and Technology.

Other topics that are not necessarily related to the analytical chemistry discipline itself, but rather relevant to the entire chemical profession can also be found. Just to name a few of these, the topics include: problems of toxic materials in the academic laboratory, by the Division of Chemical Health and Safety; biochemistry in introductory organic courses: how to teach it and how much to teach in the full-year course, by the Division of Chemical Education; How to prepare for retire-



DIANO XRD diffraction-emission systems and XEG on-line gauges have offered spectroscopists and diffractionists greater analytical speeds and capabilities through DIANO improvements. Like DIANO'S solid-state detector electronics for improved reliability. DIANO'S patented Dual-Target™ X-ray tube for extra precision and convenience. And DIANO'S fully programmed computer-controllers for added productivity.

DIANO still leads the way.

Last year, DIANO introduced fully automated, microprocessor-based data collection . . . and greatly expanded system control through remote devices.

For 1978, DIANO announces the most advanced system yet . . . the high-performance XRD-8500. This operator-oriented system features PDP-11 Fortran capability, dual floppy discs, and peripheral flexibility.

For design leadership and innovations in X-ray systems, one name *never* changes . . . DIANO. See our nearby DIANO representative, or write.

DIANO CORPORATION
8 COMMONWEALTH AVENUE
WOBURN, MASSACHUSETTS 01801 U.S.A.
TEL.(617)-935-4310 TELEX 94-9306
American designed, engineered and manufactured

CIRCLE 57 ON READER SERVICE CARD

ment: where to go and why? Is a chemist a professional?, both by the Division of Professional Relations. The Division of Environmental Chemistry will also hold symposia in topical areas of interest to analytical chemists in the environmental and toxic substances fields.

All sessions sponsored by the Analytical Division will be held in the Sheraton-Anaheim hotel, two blocks away from the Anaheim Convention Center. The symposium sponsored jointly with the Division of Nuclear Chemistry and Technology will be held in the Anaheim Convention Center.

The Analytical Chemistry Division social hour and dinner will be held Tuesday, March 14 at 6:30 and 7:30 p.m., respectively, at the Twin Dragon restaurant (Shanghai-Mandarin Chinese food), 1550 South Harbor Blvd., Anaheim, Calif. Tickets for the dinner can be purchased in advance (See *Chem. Eng. News*, December 19) or at the meeting for $10.

The chemical exposition will be jointly sponsored by ACS and the Orange County Section. More than 300 exhibit areas will be available for companies to show their equipment, services, and publications.

Several ACS courses given in conjunction with the meeting before and after the meeting will be of interest to analytical chemists. For more information, see page 240 A.

The detailed technical program given below includes all the Analytical Division sessions and those cosponsored by the Division.

Preregistration forms and housing information are contained in *Chem. Eng. News*, December 19, 1977. The complete technical program for the meeting will appear in *Chem. Eng. News*, February 6, 1978.

DIVISION OF ANALYTICAL CHEMISTRY

D. M. Hercules, *Chairman*
A. J. Cunningham, *Secretary*

MONDAY MORNING

SECTION A

Sheraton-Anaheim

Symposium on ACS Award in Analytical Chemistry

H. A. Mottola, *Presiding*

9:00—Introductory Remarks. **H. A. Mottola.**



BOD!

You can use it to run the 5-day BOD in just 3 days! Expect "significantly greater precision" than with other methods. For full details, circle readers' service card number 159.

COD!

Triple your output of Chemical Oxygen Demand test results, and cut reagent consumption to *one twentieth* of that required in the reflux method. Circle 160 for complete information.

TOC!

Top precision and high speed in a complete total carbon system. Run a sample a minute or better. Analyzes TOC in high chloride, particles, salt, acids, and in conventional effluents and aqueous samples. Circle 161.

OCEANOGRAPHY INTERNATIONAL CORPORATION

512 West Loop P.O. Box 2980, College Station, Texas 77840 (713) 693-1711

See us at the Pittsburgh Conference, booth #1704 & 1705.

add
state-of-the-art
quantitative
capability
to your
microscope



NanoSpec™/10
COMPUTERIZED
MICROSPECTROPHOTOMETER
SYSTEMS
for absorption,
reflectance, and
fluorescence measurements
in the ultraviolet
visible and near infrared.

NANOMETRICS

NANOMETRICS INCORPORATED
1030 West Maude Avenue, S-502
Sunnyvale, California 94086
(408) 735-1044
CIRCLE 142 ON READER SERVICE CARD

News

9:15—1. *Award Address* (ACS Award in Analytical Chemistry, sponsored by Fisher Scientific Co.) Structure and Behavior of Organic Analytical Reagents 1948–1978. **H. Freiser.**
10:15—Intermission.
10:30—2. Porphyrins as Analytical Reagents. **A. Corsini, H. Mehdi, O. Herrman.**
11:00—3. Ester Adducts of Lanthanide Shift Reagents. **A. Merali, J. T. Edward, J. Fresco.**
11:30—4. Relating Molecular Structure to Metal Chelate Stability and Reagent Selectivity: An Evaluation of Methodologies. **D. L. Duewer, A. M. Harper.**

SECTION B

Sheraton-Anaheim

Symposium on New Applications of Lasers to Chemistry

G. Hieftje, *Presiding*

9:00—Introductory Remarks. **G. Hieftje.**
9:10—5. High Resolution Spectroscopy with Lasers. **T. W. Hansch.**
9:50—6. Two-Photon Excited Molecular Fluorescence. **F. E. Lytle.**
10:25—Intermission.
10:40—7. Selective Excitation of Probe Ion Luminescence. **J. C. Wright.**
11:15—8. Application of Tunable Diode Lasers to Chemical Analysis. **J. F. Butler, K. W. Nill.**

MONDAY AFTERNOON

SECTION A

Sheraton-Anaheim

Symposium on ACS Award in Analytical Chemistry

A. Corsini, *Presiding*

2:00—9. Metal-Binding in Medicine. **J. L. Walter.**
2:30—10. Ion Microscopy in Biology and Medicine. **G. H. Morrison.**
3:15—Intermission.
3:30—11. Gas Phase Ion Chemistry and Photochemistry of Ions Generated from Trifluorotoluene. **R. B. Cody, B. S. Freiser.**
4:00—12. Rapid Consecutive Gas-Chromatographic Separation and Determination of Rare-Earth Elements. **T. Fujinaga.**

SECTION B

Sheraton-Anaheim

Symposium on New Applications of Lasers to Chemistry

G. Hieftje, *Presiding*

2:00—13. Laser Excited Atomic Fluo-

WESCAN'S
NEW
MOLECULAR
WEIGHT
APPARATUS..



COMBINES EASE
WITH PRECISION.

- Molecular weights 100 to 25,000
- Temperature range 25°C to 130°C
- Digital readout with analog recorder output
- Aqueous or organic solvents with no change in thermistors
- Priced under $5000

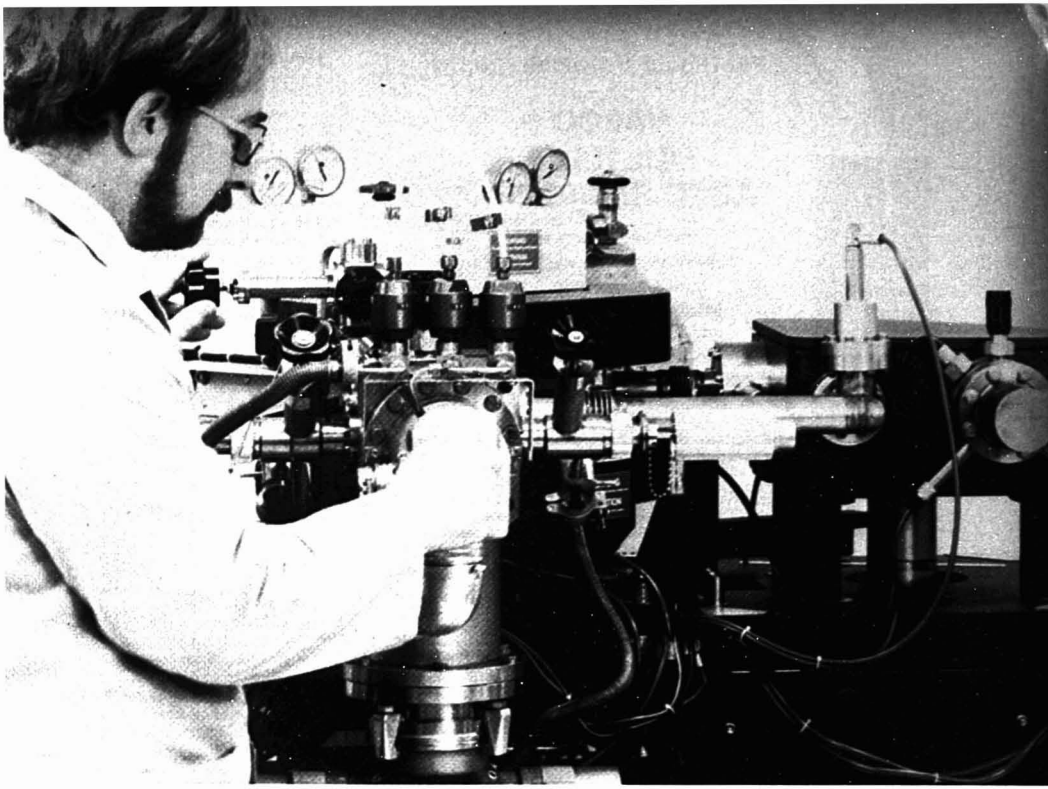
The WESCAN Model 233 Molecular Weight Apparatus is a convenient and easy means for routine determination of molecular weights up to 10,000, and with slightly greater care, up to at least 25,000. It works on the well established principle of differential vapor pressure measurement using two thermistors in a closed chamber.

Incorporation of the latest circuitry, and the same measurement chamber used in the Corona/Wescan Model 232A, provides an instrument which is more precise and stable than earlier designs. Yet the Model 233 includes a number of operating conveniences which make it easy to use.

For more information, contact

WESCAN
INSTRUMENTS, INC.

WESCAN INSTRUMENTS, INC.
3018 Scott Blvd. • Santa Clara, CA 95050
CIRCLE 231 ON READER SERVICE CARD



What's behind Varian M.A.T.'s leadership in high resolution mass spectrometry?

The secret of our sales leadership is simple: R&D. The largest — and most active — R&D program in the field.

Our continuing R&D commitment assures you of the instrumentation advances essential to your state-of-the-art research activities.

The Varian MAT 311A, a double-focusing mass spectrometer with high performance for both low and high resolution analyses, reflects this commitment. As do our other high resolution sector field instruments, models 731 and 112S.

Among their features are:

- Turbomolecular pumps for exceptionally clean background
- Proven FD/FI/EI ion source
- Temperature-programmable direct probe
- Proven CI/EI source for optimized ion source chamber geometry in both modes, with dual electronic controls
- "DADI" metastable analysis
- Field-regulated magnets

Throughout 1978 and the coming years, we will continue to provide the mass spectrometry community with quality without compromise which results in a significant technological edge.

Give yourself that edge. Send today for our informative catalog or contact us for a demonstration.

Varian MAT
Mass Spectrometry
25 Hanover Road
Florham Park, NJ 07932
Tel. (201) 822-3700

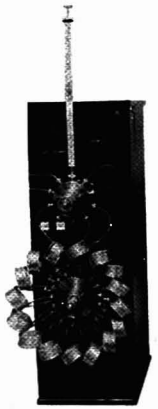
varian

Varian MAT GmbH, Postfach 14 4062, Barkhausenstr 2, 2800 Bremen 10, West Germany • Telephone (0421) 54 931
Varian Associates, Ltd., 18, Manor Road, Walton-on-Thames/Surrey, United Kingdom • Telephone 43741

Be sure to visit our display at the Cleveland Conference.

CIRCLE 227 ON READER SERVICE CARD

For Liquid Chromatography



VALCO'S MULTI LOOP AUTO SAMPLER . . .

the automatic sample injection system that lets you Minimize Sample Waste, Maximize System Efficiency



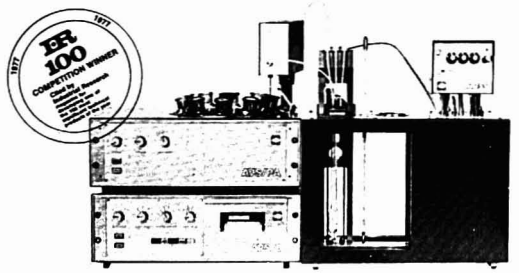
All for under $3,000.

- Ideal for low waste applications where very little sample is available
- Small uniform bore minimizes error due to sample carry-over
- Improves repeatability of recorded area and retention times
- Up to 150° continuous operation in high temperature GPC (optional)
- No pressurized gas required for sample loading into injection valve
- No bottles to fill, break, or lose
- All Hastalloy C and nickel flow path available for reactive samples (optional)
- BCD samples number identification for use with computers or integrators
- Pulse and continuous contact closures available
- Up to 4 injections per sample
- Simplicity of operation

VALCO instruments co

P.O. Box 18032 Houston, Tx 77024
713-688-8345
TX3 910-881-6500
Telex 79-0033

CIRCLE 218 ON READER SERVICE CARD



Save Lab Time

Automatic Viscosity Measuring Systems — AVS — Automates Capillary Viscosity Measurements.
System AVS/PA with 10 sample capacity employs one capillary viscometer and performs selected test programs of testing single or repeat measurements, discharge, rinsing and sample change automatically.
AVS/G base unit in conjunction with AVS/PA provides a seven digit tape print out with a 0.01 sec resolution.
Efflux time is measured opto-electronically resulting in accuracy of measurement of 0.1%. Covers measuring range of 0.3 to 30.000 cSt at temperatures up to +150°C.
AVS systems for single and serial measurement also available.

Send for descriptive color brochure now.

SCHOTT MAINZ

SCHOTT

JENAer GLAS JENAer GLASWERK SCHOTT & GEN., INC.
11 East 26th Street • New York, New York 10010 • (212) 679-8535

CIRCLE 205 ON READER SERVICE CARD
See us at the Pittsburgh Conference, Booth 1308

News

rescence Spectrometry. **J. D. Winefordner.**
2:40—14. Laser Fluorimetry. **R. N. Zare.**
3:15—15. New Fluorescence Spectroscopic Methods. **T. Hirschfeld.**
3:50—16. Recent Applications of Resonance Ionization Spectroscopy to the Study of Single Atoms. **J. P. Young, C. E. Bemis, S. D. Kramer, S. L. Allman, G. S. Hurst.**
4:25—17. Laser Enhanced Ionization Spectrometry in Flames. **J. C. Travis, G. C. Turk, R. B. Green.**

TUESDAY MORNING

SECTION A

Sheraton-Anaheim

Symposium on ACS Award in Analytical Chemistry

B. E. McClellan, *Presiding*

9:00—18. Solvent Extraction of Stearate Ion with Metal-Triethylenetetramine Complex Ions. **D. Jeffries, J. Fresco.**
9:30—19. Determination of Nickel and Cadmium in Air Samples by Extraction-Furnace Atomic Absorption Spectrometry. **B. E. McClellan, K. R. Jolly.**
10:00—Intermission.
10:15–20. Flow Effects in Gradient Elution Liquid Chromatography. **R. L. Stevenson.**
10:45—21. A Comparison of the Thorin and Modified Methylthymol Blue Method for the Determination of Micro-Amounts of Sulfate. **G. Colovos, E. P. Parry, A. M. Miles, R. Panesar, E. Rodes.**
11:15—22. Kinetic Parameters Relevant to Repetitive Determinations via Transient Signals. **H. A. Mottola.**

SECTION B

Sheraton-Anaheim

Symposium on New Applications of Lasers to Chemistry

G. Hieftje, *Presiding*

9:00—Introductory Remarks. **G. Hieftje.**
9:10—23. Proton and Electron Transfer by Picosecond Spectroscopy. **P. M. Rentzepis, K. Peters.**
9:50—24. The Study of Biological Surfaces by Electrophoretic Light Scattering. **B. R. Ware.**
10:25—Intermission.
10:40—25. Measurement of Nanosecond and Subnanosecond Chemical Events with a CW Laser. **G. M. Hieftje.**
11:15—26. Laser Applications in Photoelectrochemistry. **S. P. Perone, J.**



EM-360L

The leading family of permanent-magnet NMR spectrometers has a new addition!

Varian's line-up of low-cost, high-performance permanent-magnet NMRs now includes the EM-360L—a 60-MHz instrument of extraordinary experimental flexibility. Like the EM-360A and EM-390, the EM-360L offers you ease of operation, low utility costs (it requires no cooling water and uses very little electric power), a convenient desk-type console with built-in 11x17" flatbed recorder, pneumatic sample handling for reduced breakage, and optional variable-temperature capability utilizing Joule-Thomson cooling (no liquid nitrogen). And the EM-360L is, like its cousins, backed by the name of the world's largest manufacturer of high-resolution, permanent-magnet NMR systems.

Whether your lab is considering an analytical NMR for the first time or replacing an existing instrument, check out the leading family first:

EM-360A

Along with its predecessor model, the EM-360A is unquestionably the most popular low-cost 60-MHz NMR; almost 700 EM-360s and EM-360As are now



EM-360A

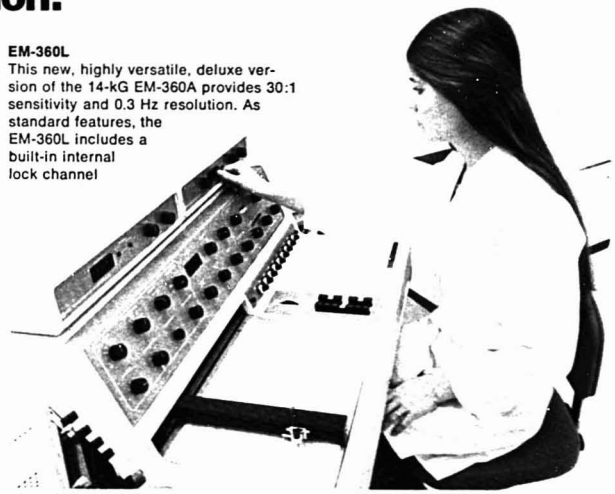
installed around the globe! Designed for routine proton analysis, the EM-360A delivers a guaranteed sensitivity of 25:1 (5-mm sample; 1% ethylbenzene) and 0.5 Hz (FWHM) resolution—but it can also tackle research problems with the addition of lock/decoupler, variable temperature, and signal averager accessories. In fact, the EM-360A is the only 60-MHz NMR in its class to offer VT operation (−100°C to +150°C).

Circle Reader Service Number 1.

EM-360L

This new, highly versatile, deluxe version of the 14-kG EM-360A provides 30:1 sensitivity and 0.3 Hz resolution. As standard features, the EM-360L includes a built-in internal lock channel with AutoShim™ (automatic Y-gradient homogeneity adjustment), wide sweeps (0.2 to 100 ppm) and digitally selectable offsets (−200 to +200 ppm), 25-kHz modulation frequency with single sideband detection, and fast normalization of spectrum and integral amplitudes. The EM-360L can also readily be extended to double-resonance experiments (decoupling, spin tickling, and INDOR), VT (−100°C to +175°C), ^{19}F, ^{31}P, and sensitivity enhancement (signal averager or rapid-scan correlation NMR).

Circle Reader Service Number 2.



EM-360L operating console—engineered for maximum functionality.



EM-390

EM-390

This spectrometer has all the functional features and options of the EM-360L, but affords the high sensitivity (50:1) and chemical shift dispersion of 21-kG (90-MHz) operation. The latter are particularly attractive to investigators dealing with limited amounts of sample, sparingly soluble substances, or large, complex molecules. The EM-390 is rapidly becoming the high-performance standard of analytical NMR spectroscopy.

Circle Reader Service Number 3.

If you wish to discuss the leading family of permanent-magnet NMR spectrometers with a Varian representative, circle Reader Service Number 4. Or write: Varian Instrument Division, 611 Hansen Way, Palo Alto, CA 94303.

varian

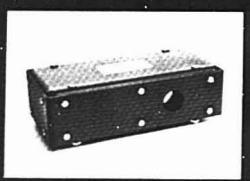
Varian ultra-fast response PMT's...

Detect 50 picosecond pulses.

For high-data-rate laser communication systems, Varian offers two types of photodetectors with ultra-fast response, high quantum yield over a broad spectrum and high gain.



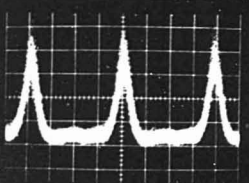
4-stage Static Crossed Field PMT's (VPM-148 Series): Provide 120 picosecond rise times for DC to 3 GHz detection with 10^3 gain. Your choice of cathode types determines spectral response.



6-stage Static Crossed Field PMT's (VPM-154 Series): Feature 150 picosecond rise times for DC to 2.5 GHz detection with 10^5 gain. A variety of cathode types are available.



All-Electrostatic PMT (VPM-152 Series): Less expensive and easy to use, these tubes can be fabricated to provide 10^1 to 5 x 10^6 gain with rise times from 320 to 500 picoseconds for detection from DC to 1 GHz. Spectral response is dependent upon cathode material specified.



VPM-154 response to a 50 picosecond rise time laser pulse.
Scale: Horiz.—200 ps/division
Vertical—1mV/division

Varian has the fast photodetectors you need. For details and application assistance, contact Varian, LSE Division, 601 California Avenue, Palo Alto, California 94304. Telephone (415) 493-4000, extension 3608 or 3094.

varian

CIRCLE 219 ON READER SERVICE CARD

News

Richardson, B. S. Shephard, J. Rosenthal, J. Harrar, S. George.

TUESDAY AFTERNOON

SECTION A

Sheraton-Anaheim

ACS Award in Analytical Chemistry Symposium

J. L. Moyers, *Presiding*

2:00—**27.** Analytical Chemistry Training as Background for Chemical Invention. **J. P. McKaveney.**
2:30—**28.** The University Analytical Center—Analytical Chemistry Applications at the University of Arizona. **J. L. Moyers.**
3:00—Intermission.
3:15—**29.** The Role of Solvent Extraction at the Hanford Operation. **C. B. Honaker.**
3:45—**30.** Novel Thermal Methods for Characterization of Uranium Ores. **R. G. Charles.**

SECTION B

Sheraton-Anaheim

Symposium on New Applications of Lasers to Chemistry

G. Hieftje, *Presiding*

2:00—**31.** Coherent Anti-Stokes Raman Scattering Spectroscopy. **B. S. Hudson.**
2:40—**32.** Inverse Raman Spectroscopy. **E. S. Yeung.**
3:15—**33.** Single Photon Absorption Reaction Chemistry in the Solid State. **E. Catalano, R. E. Barletta.**
3:50—**34.** Time-Resolved Resonance Raman Spectroscopy (TR^3): Vibrational Spectra in 10 Nanoseconds. **W. H. Woodruff.**
4:25—**35.** Analytical Applications of the NBS Laser-Raman Microprobe. **E. S. Etz, G. J. Rosasco.**

WEDNESDAY MORNING

SECTION A

Sheraton-Anaheim

Symposium on Selective Detectors for Chromatography

D. H. Freeman, *Presiding*

9:00—Introductory Remarks. **D. H. Freeman.**
9:05—**36.** *Award Address* (ACS Award in Chromatography, sponsored by SUPELCO, Inc.) The Development of an Idea. **A.J.P. Martin.**
10:00—**37.** Computer-Controlled Optical Multichannel Analyzers for Recording UV Fluorescence and Absorption Spectra of HPLC Eluants. **J. R. Jadamec, W. A. Saner.**

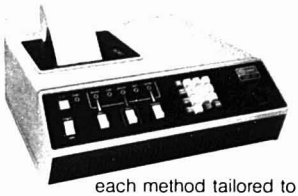
Planning GC automation?

If you are, check with Varian to make sure that you are getting the best automation system for your particular needs and budget.

We can help you because our automation systems are completely modular and offer you the opportunity to choose a system very closely tailored to your specific application at reasonable cost.

If you need the most powerful automatic gas chromatograph, Varian has it. Or if you want only automatic data handling or automatic sampling, that is available, too.

You can start with one modular component and add other automation capabilities later to match changing needs. You have great flexibility. You can start automating your GC analyses anywhere that is right for you. For example:



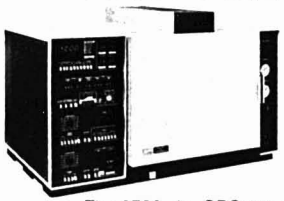
The CDS-111 chromatography data system

The CDS-111 will automatically quantitate the output from most any gas or liquid chromatograph. You can switch it from one instrument to another, even move it from lab to lab for most efficient use of capital equipment. And the CDS-111 is easy to use. It is preset to automatically quantitate most chromatograms entirely on its own. It holds up to nine analysis methods in memory, each method tailored to control a complex analysis from start to finish. It will even automatically calculate the results from a single injection up to nine different ways. For complete automation, the CDS-111 combines with the Model 3700 Gas Chromatograph and the Model 8000 AutoSampler.™



Model 8000 AutoSampler

The reliable, proven Model 8000 AutoSampler obtains injection reproducibility that sets the standard for automatic gas chromatography and far surpasses the precision of human operation. Sample cross contamination is virtually eliminated. It will handle up to 60 samples in a single unattended run. Model 8000 can be used with any gas chromatograph. Or it can be microproccesor controlled by the CDS-111 in a completely automatic closed-loop system with the Model 3700 Gas Chromatograph.



Model 3700 automatable gas chromatograph

3700 series dual-column gas chromatographs are modular and automatable. TCD, FID, ECD, FPD and multi-detector models are offered tailored to handle any GC application from simple routine to the most demanding research. Performance features include: highest sensitivity detectors, dual-flame FPD, the first easy to use capillary system, large column oven and separate pneumatics compartment for versatility and convenience.

The 3700, the CDS-111 and the 8000 AutoSampler are designed to combine to form many different automation configurations including the powerful Model 3711 series of Automatic Gas Chormatographs that automate the entire chromatography process from injection through separation, calculations and final report.

We've been helping chromatographers for over 20 years. Let us help you.

For immediate assistance, phone your nearest Varian field office:

Downey, CA	(213) 927-3415	Park Ridge, IL	(312) 825-7772	Florham Park, NJ	(201) 822-3700
Los Altos, CA	(415) 968-8141	Louisville, KY	(502) 897-0171	Syracuse, NY	(315) 437-6464
Wheatridge, CO	(303) 425-0413	Cheverly, MD	(301) 772-3683	Euclid, OH	(216) 261-2115
Atlanta, GA	(404) 955-1392	Waltham, MA	(617) 890-8430	Houston, TX	(713) 783-1800

For detailed information circle the indicated Reader Service Numbers:

222 CDS-111 Chromatography Data System
223 Model 8000 AutoSampler
224 Model 3700 Gas Chromatographs
225 Model 3711 Automatic Gas Chromatographs
226 Have a representative call

varian

10:30—Intermission.
10:40—**38.** The Use of Electrochemical Detection of HPLC for the Speciation of Organometals. **W. A. MacCrehan, R. A. Durst.**
11:10—**39.** The Determination of Phenols and Hydroxylated PAHs by HPLC with Electrochemical Detection. **S. A. Wise, W. J. Bonnett.**
11:35—**40.** Speciation of Selenium Compounds by Liquid Chromatography–Zeeman AA. **T. M. Vickrey, H. Howell.**

SECTION B

Sheraton-Anaheim

General Papers: Spectroscopy

H. V. Drushel, *Presiding*

9:00—**41.** Monitoring of PNA in Fugitive Emissions and By-Product Waters from Synfuel Operations. **T. Vo-Dinh, R. B. Gammage, A. R. Hawthorne, J. H. Thorngate.**
9:20—**42.** Determination of Ge, As, Se, Sn, and Sb in Biological Samples Utilizing Hydride Generation Chromatographically Coupled to a Microwave Induced Ar/He Plasma. **W. B. Robbins, J. A. Caruso, F. L. Fricke.**
9:40—**43.** Nitrogen Compounds in Fossil Fuels by Gas Chromatography with a Chemiluminescent Detector. **H. V. Drushel.**
10:00—**44.** Constant Temperature vs. Pulsed Furnace Atomizers. **R. Woodriff.**
10:20—Intermission.
10:40—**45.** Fourier Transform Mass Spectrometry for Analysis. **C. L. Wilkins, M. L. Gross, R. B. Spencer, S. Ghaderi.**
11:00—**46.** Coupling of a Quadrupole Mass Filter and a Hollow Cathode Ion Source for Trace Element Analysis by Mass Spectrometry. **B. L. Bentz, C. G. Bruhn, W. W. Harrison.**
11:20—**47.** A Proposed Circular Dichroism Standard: Preparation and Properties. **K. H. Pearson, J. L. Scott, V. C. Zadnik.**
11:40—**48.** Trace Analysis of Mercury by Photoacoustic Spectroscopy. **D. K. Roe, R. Cary.**

WEDNESDAY AFTERNOON

SECTION A

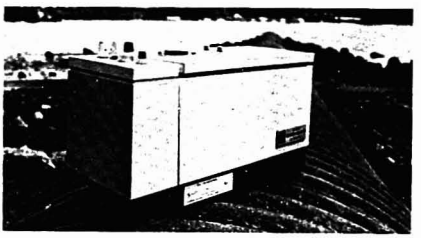
Sheraton-Anaheim

Symposium on Selective Detectors for Chromatography

C. Feldman, *Presiding*

2:00—**49.** Application of a Thermionic Detector to the Gas Chromatographic Determination of Nitrogen Compound Distribution in Petroleum. **D. K. Albert.**
2:35—**50.** Spectroscopic Element Detector for Gas Chromatography. **C. Feldman, D. A. Batistoni.**
3:00—**51.** Use of a Gas Chromatograph–Microwave Plasma Detector for the Determination of Tetraalkyl Lead and Alkyl Selenide Species in the Atmosphere. **D. C. Reamer, W. H. Zoller, T. C. O'Haver.**
3:25—Intermission.
3:40—**52.** Evaluation of a Microwave Plasma Detector at Atmospheric Pressure for Capillary Columns. **S. P. Wasik, F. P. Schwartz, W. Braun.**
4:05—**53.** A Submicroliter Flow Cuvette for Fluorescence Detection of Chromatographic Effluents. **G. D. Christian, L. W. Hershberger, J. B. Callis.**
4:25—**54.** Determination of Halogenated Anilines and Related Compounds by HPLC with an Electrochemical Detector. **E. M. Lores, D. W. Bristol, R. F. Moseman.**

The Auto Analyzer is the standard*



and ALPKEM rebuilds the standard.

* Rebuilt AutoAnalyzer instruments
* Full line of accessories & supplies
* Applications Engineering

ALPKEM Corporation
1234 S.E. Union Ave., Portland, OR 97214
503 - 233-3626 or **800 - 547-5535**
*Trademark Technicon Corp.

See us at Pittsburgh Conference booth #1524
CIRCLE 51 ON READER SERVICE CARD



Our specialty is saving you money.
We buy and sell surplus or used, gas and liquid, chromatographs.
We guarantee everything we sell.
Send for our catalog of budget stretchers.

L.C. COMPANY, INC.
619 Estes Avenue, Schaumburg, Ill. 60193
Telephone: (312) 529-1880

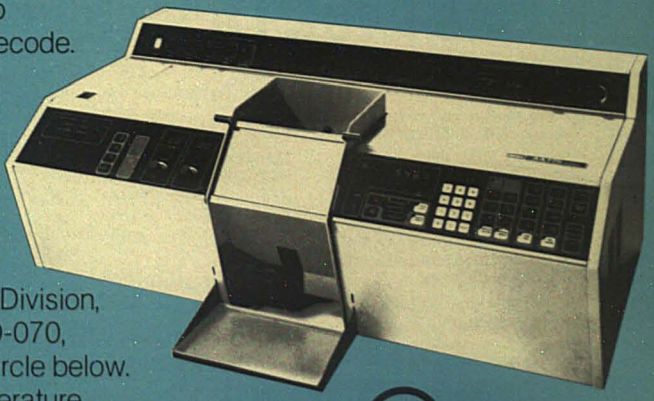
See us in Cleveland at Booth #1701
CIRCLE 148 ON READER SERVICE CARD

Heralding Varian's AA-775... Sophisticated, Accurate, Simple.

Sophisticated. Microprocessor calibration, integration, peaks, emission, statistics—even standard additions by regression. Then it divides by the sample weight. Four-lamp turret. Superbly automatic gas control. New high-performance monochromator. No compromises. Sophisticated.

Accurate. The best, most accurate curve corrector in the business (Pat App). Up to five standards. Calibration on the mean, not just on one reading. Peak height and area on the same peak, statistics on both. Elegant. Accurate.

Simple. Designed by users, not just microprocessor engineers. Touch-buttons with flashing lights that say 'push me'. Detects and corrects operator errors. Obvious operation, even for the beginner. No computer language to decode. No 'where was I' when you come back from that phone conversation. Obvious. Simple.



Maybe this really is the perfect AA instrument. Write Varian Instrument Division, 611 Hansen Way, Box D-070, Palo Alto, CA94303 or circle below.
Circle 196 for product literature
Circle 197 for a Varian representative to call.
See it at Cleveland.

varian

SECTION B

Sheraton-Anaheim

General Papers: Electroanalytical Chemistry

D. K. Roe, *Presiding*

2:00—55. Differential Pulse Polarographic Analysis of Cyanide in Combustion Products. **J. C. Spurgeon, R. E. Feher.**

2:20—56. Electrochemistry of Decyl Mercuric Halides. **B. C. Willett, D. G. Peters.**

2:40—57. Concentration- and Temperature-Dependent Polarographic Phenomena for Reduction of Alkyl Halides at Mercury. **W. F. Carroll, Jr., D. M. La Perriere, E. C. Torp, D. G. Peters.**

3:00—58. Electrochemical Reduction of 1-Bromo-5-Decyne and 1-Iodo-5-Decyne at a Mercury Cathode in Dimethylformamide. **D. M. La Perriere, D. G. Peters.**

3:20—Intermission.

3:40—59. Chronopotentiometric Determination of Catalytic Rate Constants of Electrogenerated Species. **S.-M. Park, D. A. Tryk.**

4:00—60. Electrochemistry of Nickel in Molten Sodium Tetrachloroaluminate. **R. A. Osteryoung, B. Gilbert.**

4:20—61. Determination of Oxygen in Organic Compounds Using a Controlled Pyrolysis System and Coulometric Finish. **E.W.D. Huffman, Jr., E.W.D. Huffman, Sr.**

4:40—62. Speciation of Aqueous Trace Metals: Comparison of Chelex Resin and Voltammetric Methods for Determining Labile and Nonlabile Fractions in the Presence of Model Ligands. **P. Figura, B. McDuffie.**

THURSDAY MORNING

SECTION A

Sheraton-Anaheim

Divisional Instrumentation Award Symposium

M. Parsons, *Presiding*

9:00—Introductory Remarks. **M. Parsons.**

9:05—63. *Award Address* (Divisional Award in Chemical Instrumentation) Trace Analysis of Atoms and Molecules—New Approaches. **J. D. Winefordner.**

10:00—Intermission.

10:15—64. Spectral Considerations in the Application of Flame Atomic Absorption and Emission Spectrometry to Nonaqueous Systems. **R. J. Sukasiewicz.**

10:45—65. Flameless Atomic Absorption Spectrometric Determination of Trace Metallic Elements in Uranium without Prior Chemical Separation. **B. M. Patel, P. M. Bhatt, B. D. Joshi.**

11:15—66. Pulsed RF EDL for Atomic Absorption and Atomic Fluorescence Spectroscopy. **J. W. Novak, Jr., R. F. Browner.**

SECTION B

Sheraton-Anaheim

General Papers: Chromatography

R. U. Robinson, *Presiding*

9:00—67. Pulse Dampening System for HPLC. **D. A. Ventura, J. G. Nikelly.**

9:20—68. Liquid Chromatography of Drugs on Macroporous Nonionic Adsorbents. **F. F. Cantwell, H. Y. Mohammed, R. G. Baum, S. Puon.**

9:40—69. High-Pressure Liquid-Chromatographic Separation and Identification of Epimeric 17-Ketone Impurities Found in a Commercial Sample of Dexamethasone Sodium



How To Know When You Need A Gas Leak Detector

- **When you have instrumentation, like GC, under pressure.**
- **When you have valves, regulators, piping, tubing fittings, connections or joints.**
- **When you have processes in plant or lab using refrigeration, incubation, etc.**

Inefficient operation of any of the above can and frequently does ruin the most careful work.

GOW-MAC's new Gas Leak Detector can prevent a lot of this grief. Sensitivity is 1×10^{-6} cc/sec. for helium, producing a 10% deflection full scale. For CO_2 1.1×10^{-5} cc/sec. These are leaks too small to bubble but they are possibly critical.

The new GLD is portable, easy to read, and economical. Line operated and battery operated options available. Also optionally available audio signal with built in speaker.

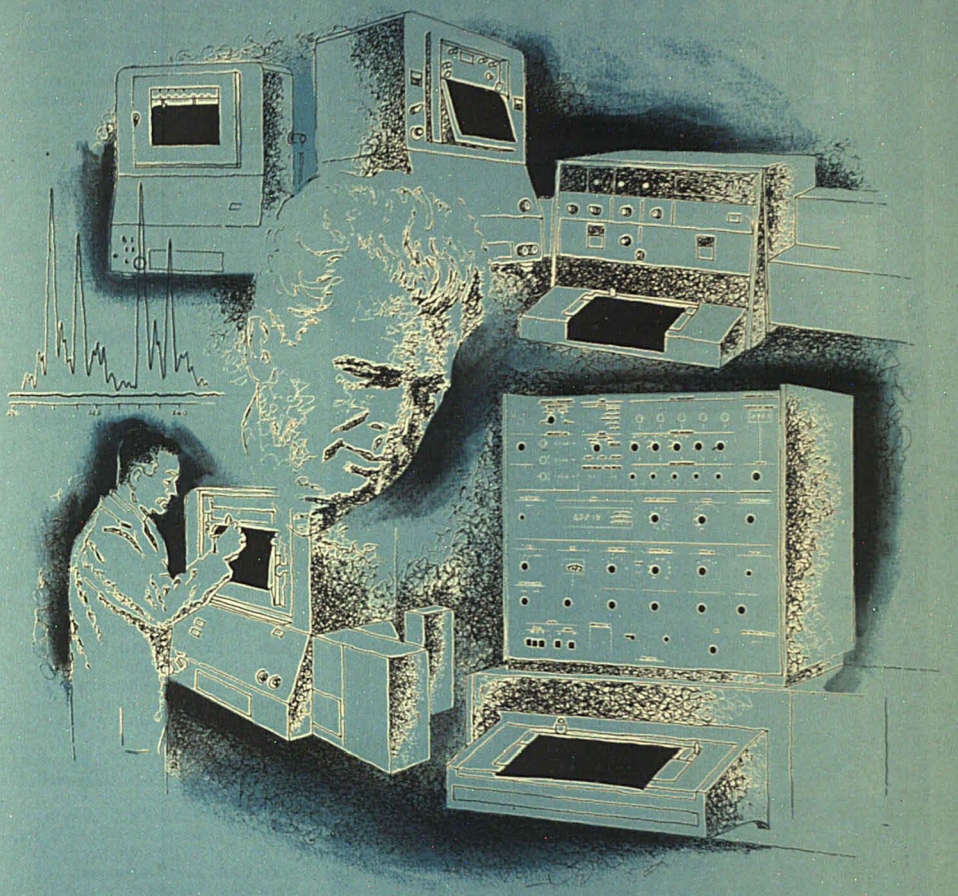
You should send for our bulletin SB-21 because it gives prices, operating particulars, and technical specifications. Use the reader service number or contact GOW-MAC.

GOW MAC

GOW-MAC INSTRUMENT CO.
P.O. Box 32, Bound Brook, NJ 08805
Telephone: (201) 560-0600
Shannon Free Airport, Co. Clare, Ireland
Telephone: 61632 Telex: 6254

CIRCLE 81 ON READER SERVICE CARD

This Varian Cary 219 UV-Vis spectrophotometer affirms a 30-year tradition for instrumental excellence...



in a class affordable to all users.

Our all new Cary spectrophotometer is a thoroughbred in every way. It traces its genealogy back to the world's first direct ratio recording UV-Vis spectrophotometer, the Cary model 11. It inherits the precision, versatility and "research grade" aura which made the models 14, 17/17D and the model 118 legend among the world's foremost spectroscopists.

But when it comes to purchase price, the model 219 breaks cleanly with the past. There's no need to anticipate budget submittals in the $25K range for this unequalled performance. With all of its precision, versatility and elegant operability, the Varian Cary 219 can be yours for approximately half that figure.

If you have plans to acquire any new UV-Vis spectrophotometer, there's no reason to accept less than a Cary. Be sure you are fully informed on the model 219's performance characteristics, accessories capabilities and operating ease—all typically Cary.

Request the Cary 219 information package today!

Varian Instrument Division, 611 Hansen Way, Box D-070, Palo Alto, CA 94303.

Circle 220 for brochure, performance proofs and price list. Circle 221 our tech rep will contact you.

varian

*Prices slightly higher outside USA

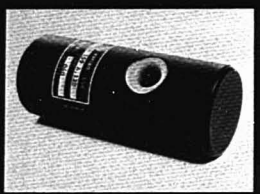
Varian low-noise, high-sensitivity PMT's . . .

More choice in III-V PMT's.

Varian offers a wide selection of high performance semiconductor cathode photomultiplier tubes for photon counting applications in the UV, visible and near IR.



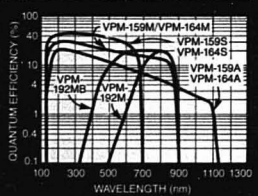
VPM-164: Varian's III-V photocathode end-window tube for photon counting applications where low dark counts and high sensitivity are of the greatest importance.



VPM-159: A less expensive relative of the VPM-164 with a ½" side window for extremely low-light-level applications.



VPM-192M/MB: Low dark count end-window PMT's with a choice of large GaAs narrow or broad spectrum cathodes for retrofitting older instruments for higher performance and for new designs.



Typical Quantum Efficiency of various cathode types.

Select the performance you need, then contact Varian, LSE Division, 601 California Avenue, Palo Alto, California 94304. Telephone (415) 493-4000, extension 3608 or 3094.

varian

CIRCLE 232 ON READER SERVICE CARD

Phosphate. **E. C. Juenge, J. F. Brower.**

10:00—Intermission.

10:20—**70.** Determination of Coumestrol in Soybean Extracts by High-Performance Liquid and Thin-Layer Chromatography. **G. L. Lookhart, B. L. Jones, K. F. Finney.**

10:40—**71.** Use of the *S*-Pyridylethyl Derivative for Determination of Cysteine During Protein Sequencing. **B. L. Jones, G. L. Lookhart, A. S. Mak.**

11:00—**72.** On Stream Computer-Controlled Gas Chromatograph for the Analysis of Interreactor Catalytic Reformer Products. **J. H. Stockinger, R. B. Callen, W. E. Kaufman.**

11:20—**73.** Total and Organic Carbon Analysis of Fluvial Sediments. **M. M. Reddy, E. Canelli, K. V. Krishnamurty.**

THURSDAY AFTERNOON

SECTION A

Sheraton-Anaheim

Divisional Instrumentation Award Symposium

M. Parsons, *Presiding*

2:00—**74.** The Development of a Scanning Echelle Monochromator. **M. L. Parsons, A. R. Forster, D. L. Anderson.**

2:30—**75.** Study of the Mechanism of Formation of Alkaline Earth Phosphate Compounds by Atomic Absorption Inhibition Release Titration. **D. Stojanovic, J. D. Winefordner, J. Bradshaw.**

3:00—**76.** Recent Applications of Coherent Anti-Stokes Raman Spectroscopy. **B. W. Smith, A. Eckbreth.**

3:30—**77.** The Future of Fluorescence Immunoassays. **C. M. O'Donnell, S. C. Suffin.**

4:00—**78.** Recent Developments in Multicomponent Analysis by Room Temperature Phosphorimetry. **T. Vo-Dinh, R. B. Gammage.**

4:30—**79.** C. Veillon.

SECTION B

Sheraton-Anaheim

Symposium on Analysis of High-Purity Materials

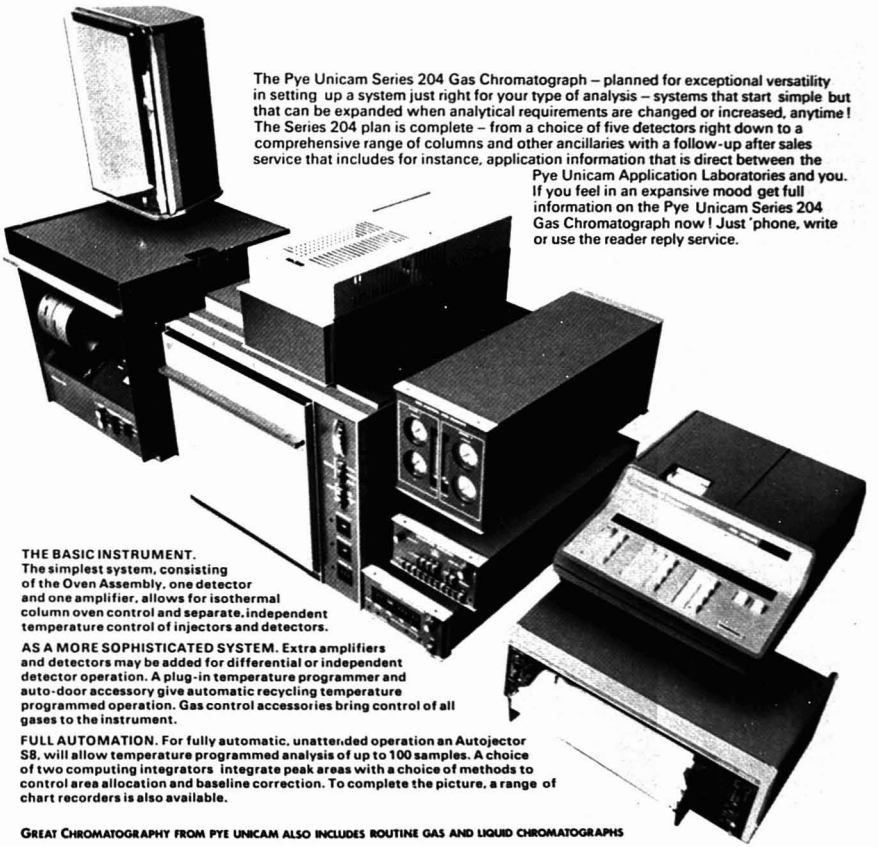
H. J. Keily, *Presiding*

2:00—Introductory Remarks. **H. J. Keily.**

2:05—**80.** X-ray Excited Optical Luminescence and Its Applications to High-Purity Material Analyses. **V. A. Fassel, E. L. DeKalb, A. P. D'Silva.**

2:50—**81.** Determination of Impurities

The 204 Chromatograph expansion plan



The Pye Unicam Series 204 Gas Chromatograph – planned for exceptional versatility in setting up a system just right for your type of analysis – systems that start simple but that can be expanded when analytical requirements are changed or increased, anytime! The Series 204 plan is complete – from a choice of five detectors right down to a comprehensive range of columns and other ancillaries with a follow-up after sales service that includes for instance, application information that is direct between the Pye Unicam Application Laboratories and you. If you feel in an expansive mood get full information on the Pye Unicam Series 204 Gas Chromatograph now! Just 'phone, write or use the reader reply service.

THE BASIC INSTRUMENT. The simplest system, consisting of the Oven Assembly, one detector and one amplifier, allows for isothermal column oven control and separate, independent temperature control of injectors and detectors.

AS A MORE SOPHISTICATED SYSTEM. Extra amplifiers and detectors may be added for differential or independent detector operation. A plug-in temperature programmer and auto-door accessory give automatic recycling temperature programmed operation. Gas control accessories bring control of all gases to the instrument.

FULL AUTOMATION. For fully automatic, unattended operation an Autoject S8, will allow temperature programmed analysis of up to 100 samples. A choice of two computing integrators integrate peak areas with a choice of methods to control area allocation and baseline correction. To complete the picture, a range of chart recorders is also available.

GREAT CHROMATOGRAPHY FROM PYE UNICAM ALSO INCLUDES ROUTINE GAS AND LIQUID CHROMATOGRAPHS

Pye Unicam Ltd
York Street, Cambridge, England CB1 2PX
Cambridge (0223) 58866. Telex: 817331

A member of the Pye of Cambridge Group

CIRCLE 164 ON READER SERVICE CARD

The Pye Unicam SP 8-100



UV/Visible Spectrophotometer

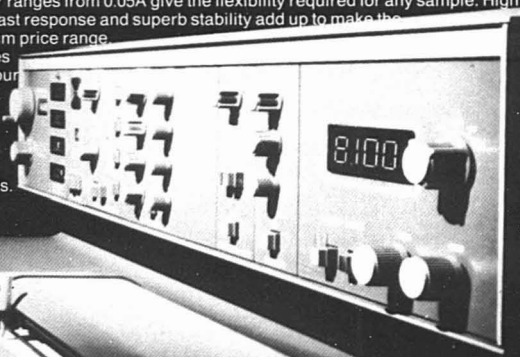
The Pye Unicam SP8-100 is a major development in the design of precision instrumentation for applications which include scanning and reaction kinetics. High performance is combined with extreme simplicity of operation in a neat and compact package. Bench space is preserved by the built-in recorder and accessories which plug into the control console or fit within the vast sample compartment.

The unique 'Synchroscan' recording principle provides calibrated spectra automatically. 5 bandwidths, 5 chart speeds, 5 scan speeds and 9 recorder ranges from 0.05A give the flexibility required for any sample. High photometric accuracy up to 3A, low noise, fast response and superb stability add up to make the SP8-100 the highest performer in the medium price range.

The very wide selection of accessories includes quick-change attachments for colour measurement, fluorescence, densitometry, column monitoring, turbid samples and automated measurements.

So whatever your application, we're certain that you will discover an SP8-100 system that's Simply the Best for your needs.

Write, phone or use the reader reply service now for full details.



Pye Unicam Ltd

York Street, Cambridge, England CB1 2PX.
Cambridge (0223) 58866. Telex: 817331.

CIRCLE 168 ON READER SERVICE CARD

PACKARD CHROMATOGRAPHY



See our instruments at Booth Nos. 335 337 339

NEW DIMENSIONS IN...

Multi-Application Capability

- The microprocessor-controlled 429 Series GC (shown above) can store and execute up to 18 user/application programs. All important parameters, including temperature, flow rates (optional), detector sensitivity and attenuation, polarity and auto-zero routines are programmable on a time basis.
- The unique Analytical Module further enhances flexibility of the 429 GC's. It is an integral assembly of two injection ports and detector block mounted on a removable column oven cover. For critical applications, including trace analysis, interference from other samples is avoided by employing a module exclusively for a particular analysis.

Analytical Flexibility

- Back-flushing (standard), heart cutting and solvent venting enhances performance of the chromatography system. These routines are provided as standard, and selection of any one of these three within their individual user application program is possible.
- Near ambient (within 20°C above room temperature) oven temperature operation permits accurate analysis of low-boiling compounds.
- All-glass chromatography is achieved through use of quartz jet FID's and glass-lined ECD's, permitting quantitative analysis of labile substances.

User Convenience

- Eye level 360° access to column connections is provided with the Analytical Module in the raised position. During automatic cool-down, the module remains in the lower position (a second fan circulates cold air through the oven). The front oven cover can also be rapidly removed to gain access to columns.

For additional information, request Bulletin 1245.

NEW DIMENSIONS IN...

Radiochromatography - 7200 Series

- A gas proportional counter, a complete counting system which can interface to gas chromatographs.
- Paper and thin-layer (TLC) strip scanner to detect radioactivity on chromatograms.
- A two-dimensional scanner to measure the distribution of radioactivity on chromatograms up to 20 cm x 20 cm; will also accommodate multiple chromatograms on the sample carrier.

For additional information, request Bulletin 1250.

Packard

PACKARD INSTRUMENT COMPANY, INC.
2200 WARRENVILLE RD • DOWNERS GROVE ILL 60515
PACKARD INSTRUMENT INTERNATIONAL S.A.
RENGGERSTRASSE 3 • CH-8038 ZURICH, SWITZERLAND
SUBSIDIARIES OF AMBAC INDUSTRIES, INC.

CIRCLE 212 ON READER SERVICE CARD

Packard



Microanalysis is our game...

so if you are investigating the choice and possible purchase of instrumentation—don't take a chance... with us you can be a winner. Our product line represents the finest analytical instrumentation available in the world—TODAY!
See us at the Pittsburgh Conference Booths 1708-1709, February 27 to March 3, 1978.

CAMECA
INSTRUMENT, INC.
37 Brownhouse Road
Stamford, Connecticut 06902
Tel: 203/348-5252
A Subsidiary of Thomson-CSF

CIRCLE 66 ON READER SERVICE CARD

HIGH RESOLUTION MASS SPECTRA FOR DOLLARS INSTEAD OF THOUSANDS

Are you typical of the chemist who needs high resolution mass spectral data, but cannot justify the expenditure of thousands of dollars for the equipment?



A high and low resolution MS-30 mass spectrometer with a combined gas chromatographic inlet is available to serve your needs.

Solids, liquids, or gases—low molecular weight or high (up to 2400)—are easily and quickly analyzed.

The gas chromatographic inlet facilitates the identification of minor impurities in foods, drugs, solvents, or other chemicals.

Pesticides, drugs, or other foreign chemicals are easily and unambiguously identified in water, body fluids, soil, or agricultural products.

Elemental compositions are determined from mass measurements with accuracies better than ten parts per million.

You can now obtain mass spectral data from the most sophisticated instrumentation available—and at reasonable prices.

Results are totally computerized, leading to speed, accuracy, and convenience of the final output.

Contact: Stephen R. Shrader, Ph. D.
SHRADER ANALYTICAL & Consulting Laboratory, Inc.
3450 Lovett Ave.
Detroit, Mich. 48210
(313) 825-5550

CIRCLE 244 ON READER SERVICE CARD

News

in Silicon by Low-Temperature Fourier Transform Infrared Spectroscopy. **S. C. Baber.**
3:30—Intermission.
3:45—**82.** Purity Analysis in Liquid Crystal Material. **E. M. Barrall III.**
4:15—**83.** Application of DSC to the Analysis of High-Purity Materials. **J. P. Elder.**

FRIDAY MORNING

SECTION A

Sheraton-Anaheim

General Papers

J. Osteryoung, *Presiding*

9:00—**84.** Determination of Acrylamide in a Potable Water Reservoir During a Clay/Polymer Soil-Sealing Treatment. **G. L. Jewett, D. R. Bell, F. J. Beafore.**
9:20—**85.** Determination of Lead in Plants. **F. Wahdat, M. Shamsipoor.**
9:40—**86.** Potentiometric Titration of Alkyl Aromatic Sulfonates Using a PVC Membrane Electrode. **S. H. Hoke.**
10:00—Intermission.
10:20—**87.** Factors Controlling in Situ Trace Precipitation on Reactive Ion-Exchange Resins. The Dowex 50W-Cu(II)-Hexacyanoferrate(II) System. **W. E. Bernier, G. E. Janauer.**
10:40—**88.** A Report on the Development of a Single Reagent Procedure for the Quantitative Determination of Phosphorus in Serum and Urine. **J. M. Hayes, M. E. Hutchinson.**
11:00—**89.** A New Analytical Tool for Characterizing Coal. **V. Weinberg, T. F. Yen.**
11:20—**90.** Quantitation of Transition Metals in Sera of Sickle-Cell Disease Patients Using X-ray Fluorescence Techniques. **G. W. Jackson, R.L.R. Towns.**
11:40—**91.** Determination of Some Azomethine-Containing Pesticides Using Differential Pulse Polarography. **M. R. Smyth, J. G. Osteryoung.**

SECTION B

Sheraton-Anaheim

Symposium on Analysis of High-Purity Materials

H. J. Keily, *Presiding*

9:00—**92.** Spark Source Mass Spectrometric Determination of Trace Elements Using Stable Isotope Dilution. **P. J. Paulsen, M. G. Diaz, L. P. Dunstan.**
9:45—**93.** The Analysis of High-Purity Standard Reference Materials for

Our Newest Lab Automation System

Hewlett-Packard's newest disc-based system maintains the easy operation previously available while adding many major improvements. These include:

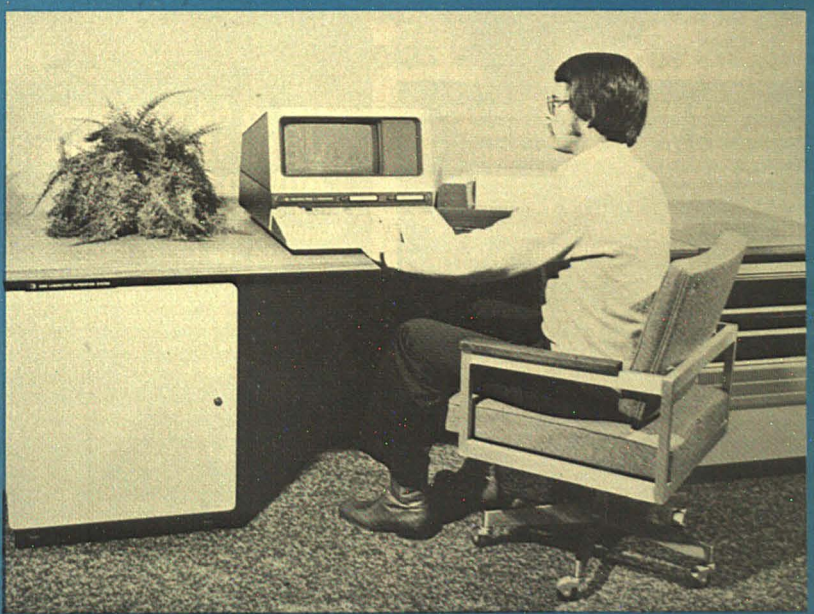
- Capable of 45 analog and digital interfaces
- Display of stored chromatograms on HP's 2648 Graphics CRT
- Additional data storage on magnetic tape
- Data transfer on magnetic tape to other computers

For complete information on all the new systems and the other members of our Laboratory Automation Family, contact your local HP representative.

See our new system displayed at the Pittsburgh Conference.

HEWLETT hp PACKARD

Rt. 41, Avondale, Pennsylvania 19311



CIRCLE 100 ON READER SERVICE CARD

Micromeritics: Puts Performance Into HPLC



Micromeritics' Model 7000B HPLC combines operational ease with exacting instrument standards to provide the performance your application demands.

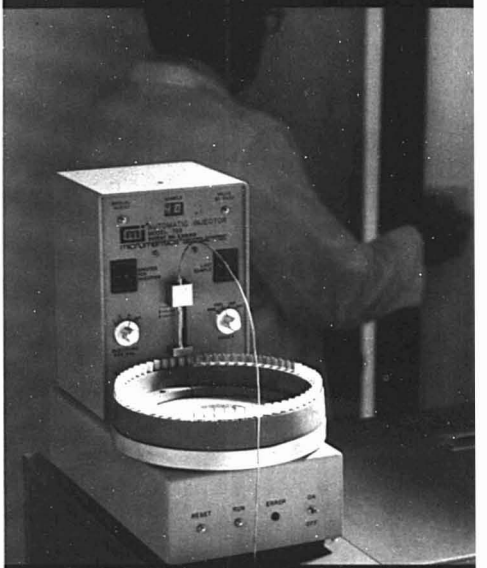
- Patented flow multiplexing compensates for differences in solvent compressibility to provide a constant pulseless flow solvent delivery system.
- Gradient and isocratic systems available with or without microprocessor control.
- Worldwide service, sales and applications support.
- Applications-oriented design allows operator to change columns, modes, solvents, and solvent conditions in minutes.

For more information, contact Micromeritics Instrument Corporation, Telephone (404) 448-8282 or write 5680 Goshen Springs Road, Norcross, Georgia 30093.

micromeritics® instrument corporation

CIRCLE 137 ON READER SERVICE CARD

Micromeritics: Automatic Injector For Unattended HPLC



Up to 64 samples Up to 192 injections Automatically

Micromeritic's Model 725 Automatic Injector for HPLC

- Microprocessor operation controls injections per sample, injection time, rinse between samples and automatic shutdown.
- Positive flow design requires only 0.75 ml of sample, allows precise, reproducible sample volumes.
- Adaptable to any HPLC solvent delivery system—can be externally controlled by computing integrator.

For more information, contact Micromeritics Instrument Corporation, Telephone (404) 448-8282 or write 5680 Goshen Springs Road, Norcross, Georgia 30093.

micromeritics® instrument corporation

CIRCLE 138 ON READER SERVICE CARD



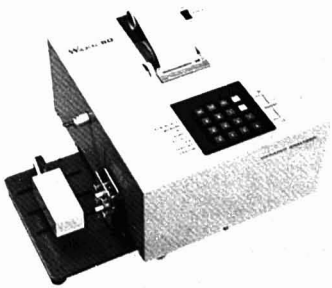
You can do accurate quantitative analyses of gas, liquid and solid samples with GC, LC or UV....

Even if you've never used an infrared analyzer, the Wilks MIRAN® 80 is so easy to operate . . . and so fast . . . you'll quickly be doing routine quantitative analyses in under two minutes per sample. That's up to 20-times faster than GC, LC or UV. And, best of all, the MIRAN 80 does quantitative analysis on all types of materials including solids, liquids, gases, films — even opaque solids and highly absorbing liquids.

The high performance of this compact single-beam analyzer results from:

- A built-in programmable microcomputer which does all the calculations and data reductions in seconds.
- Rapid sample preparation — no sample dilution or precise sample quantities required for analysis.
- Accuracy is high — 0.1% — 1% relative.
- Fast changeover from program-to-program.

but...you can do the same 5-times faster with the MIRAN 80



Increase your productivity, lower your cost per analysis and cut raw material usage. You'll do all this with the speed — and ease — of the Wilks MIRAN 80 Analyzer. Just fill a cell, press a button, and — in less than 2 minutes — the analysis is printed out in parts per million or per cent, etc., whether it is a single or multi-component analysis.

For a copy of our new MIRAN 80 brochure and complete details on this significant advance in routine quantitative analysis, call or write Foxboro/Wilks, Box 449, S. Norwalk, CT. 06856 (203) 853-1616.

*Registered trademark of Foxboro/Wilks, Inc.

WILKS
Foxboro/Wilks, Inc.

See us at the Pittsburgh Conference Booths 826–830

CIRCLE 234 ON READER SERVICE CARD

SUPERB NEW GLASS CAPILLARY COLUMNS FOR GAS CHROMATOGRAPHY

Get tomorrow's high technology columns—today—from

QUADREX

Several new stationary phases has been added to our expanded list. These include a C–87 hydrocarbon (Kovats) with an upper temperature limit of ~230°C and a new, very stable Carbowax HP of high purity, whose polarity does not significantly differ from that of Carbowax 20M—but has an extremely useful extended temperature range approaching 280°C. Although we have a limited supply at the moment, it looks like a real winner—destined to become very widely used in many different applications. With these additions, we are able to offer you the highest quality capillary columns—coated with any of the following materials:

SE-30	C-87 hydrocarbon (Kovats)	Carbowax HP	Dexsil 300	Polyphenyl ether (6 rings)
OV-101	Squalane	SP-2340	Dexsil 400	Polyphenyl ether (20 rings)
OV-17	Apiezon L	FFAP	Dexsil 410	Silar 5C
OV-225	Carbowax 20M	Ethylene glycol adipate	DC-550	Silar 10C

Other phases, custom coated upon request,

A wide variety of column diameters and lengths to fit every need:

0.25 mm (0.010″) i.d. X 25, 50, 75 and 100 meters (ultra high resolution)
0.35 mm (0.013″) i.d. X 25 and 50 meters (high resolution and moderate sample capacity)
0.50 mm (0.020″) i.d. X 25 and 50 meters (moderate resolution and high sample capacity)

Guaranteed high performance

0.25 mm i.d. columns yield 3000–4500$^+$ theoretical plates/meter at k > 3–4
0.35 mm i.d. columns yield 2000–3000$^+$ theoretical plates/meter at k > 3–4
0.50 mm i.d. columns yield 1500–2250$^+$ theoretical plates/meter at k > 3–4

The most unique and outstanding deactivation technology for the binding of the active sites of the glass. Almost all manufacturers, to remain competitive, claim that they thoroughly deactivate the surfaces of their non-polar columns. In our experience with comparison testing however, with the exception of a European group, this has proved to be wishful thinking indeed. Try our columns and note the difference!

Only one type of column available—*the highest quality—at very modest prices*

*All columns:	25 meters	$225
	50 meters	350
	75 meters	450
	100 meters	525

*An additional $35 charge for columns coated with Dexsils

A complete line of accessories for use with glass capillary columns. These include split and splitless sample introduction systems, low dead volume connectors, graphite ferrules, cages, glass lined tubing, nickel tubing, heat shrinkable teflon tubing, straight glass capillary tubing, and T pieces for make up gas.

Write for our brochure. If you have any problems with capillary columns why don't you call us.

We will be delighted to have our experts help you.

QUADREX CORPORATION
P.O. Box 3881
Amity Station
New Haven, Connecticut 06525
Tel: 203-389-6620

CIRCLE 249 ON READER SERVICE CARD

News

Trace Constituents. **H. L. Rook.**
10:30—94. Phase Solubility Analysis for Determining the Purity of Organic Compounds. **H. J. Keily, H. G. Higson, F. J. Reavis.**
11:15—95. Total and Organic Carbon Analysis of Fluvial Sediments. **M. M. Reddy.**

DIVISION OF NUCLEAR CHEMISTRY AND TECHNOLOGY

B. J. Dropesky, *Chairman*
R. L. Hahan, *Secretary*

MONDAY AFTERNOON

SECTION B

Anaheim Convention Center

Symposium on Nondestructive and Analytical Chemical Techniques in Nuclear Safeguards
Joint with Division of Analytical Chemistry

E. A. Hakkila, Organizer, *Presiding*

2:00—Introductory Remarks.
2:05—9. Safeguard Needs in the Measurement Area. **G. Hammond, C. Auerbach.**
2:35—10. Standards for Chemical or NDA Measurements for Nuclear Materials Safeguards—A Review. **C. D. Bingham.**
3:05—11. Nuclear Safeguards and the NBS Standard Reference Materials Program. **W. P. Reed, H. T. Yolken.**
3:25—Intermission.
3:40—12. Decision Analysis for Nuclear Safeguards. **J. P. Shipley.**
4:10—13. A Nonlinear Method for Including the Mass Uncertainty of Gravimetric Standards and the System Measurement Errors in the Fitting of Calibration Curves. **W. L. Pickles, J. W. McClure, R. H. Howell.**
4:40—14. U and Pu Analysis with Well-Type Germanium Detectors. **F. P. Brauer, W. A. Mitzlaff, J. E. Fager.**
5:15—*Divisional Business Meeting.* (See Section A for location).
5:45—*Divisional Social Hour.* (See Section A for location.)

TUESDAY MORNING

SECTION B

Anaheim Convention Center

Symposium on Nondestructive and Analytical Chemical Techniques in Nuclear Safeguards

Rigaku is there

For every application WORLDWIDE there is a Rigaku X-Ray System

From leading universities, corporate laboratories and national research institutes; from heavy machinery, metal processing, oil refining and the manufacture of cement to chemicals, paper, pulp, leather and food processing . . . Wherever the need exists for reliable, accurate X-Ray analysis . . . **RIGAKU IS THERE!**

From laboratory studies to process control in the field, in over 50 countries, . . . **RIGAKU IS THERE!** . . . With the world's widest range of industrial X-Ray analytical equipment.

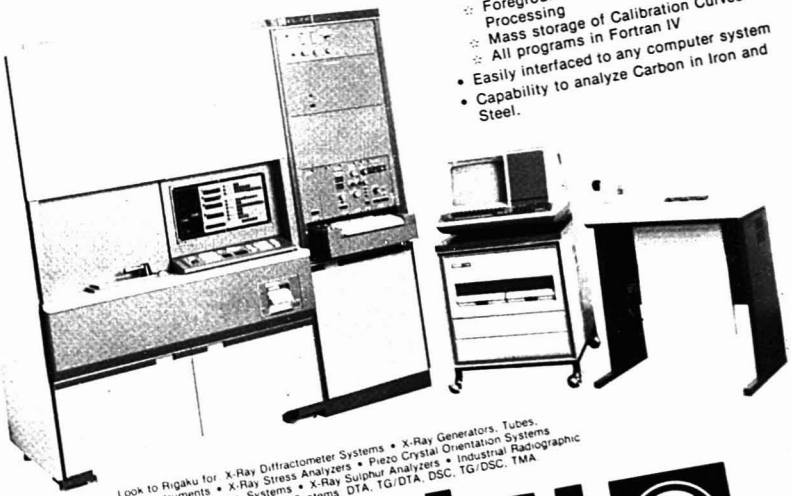
We back it up with a worldwide sales/service network with application laboratories on 3 continents. At our Danvers, Massachusetts Laboratory, our staff engineers can demonstrate a full line of operating equipment and apply their knowledge of all operating and analytical conditions to your specific application. **RIGAKU IS THERE!**

HOW RIGAKU GOT THERE is demonstrated very well by the 3064 X-Ray Spectrometer.

The Rigaku 3064 Geigerflex Sequential X-Ray Spectrometer System provides unsurpassed versatility and reliability in data collection and processing.

UNMATCHED ADVANTAGES:

- End Window Rhodium X-Ray Tube
- 8 Crystal Changer
- Core Memory Microprocessor
- Dataflex™ System for Data Processing includes:
  - Foreground/Background Data Processing
  - Mass storage of Calibration Curves
  - All programs in Fortran IV
- Easily interfaced to any computer system
- Capability to analyze Carbon in Iron and Steel.



Look to Rigaku for X-Ray Diffractometer Systems • X-Ray Generators, Tubes, Film Instruments • X-Ray Stress Analyzers • Piezo Crystal Orientation Systems • X-Ray Spectrometer Systems • X-Ray Sulphur Analyzers • Industrial Radiographic Equipment • Thermal Analysis Systems DTA, TG/DTA, DSC, TG/DSC, TMA

Rigaku

Rigaku/USA, Inc.

Sales and Service:
3 Electronics Avenue, Danvers, Massachusetts 01923, U.S.A.
Phone: (617) 777-2446

CIRCLE 182 ON READER SERVICE CARD

CSI Quality: built from experience

Over the years the name Columbia Scientific Industries has become synonymous with quality instrumentation. This quality is the result of years of valuable experience accrued by CSI's personnel in their given field. In most cases CSI's engineers have been involved in a particular discipline since its inception. CSI experience runs deep in such areas as integrators, mass spectrometer data analysis, x-ray analysis, and thermal analysis.

This wealth of experience has been parlayed into a line of high quality instruments that feature accuracy, advanced design, and serviceability. . . prime components for quality instruments.

CSI Supergrators

The Name in Computing Integrators

Versatile

- Handles up to 31 different programs
- 4 discrete inputs may be preselected for automatic operation
- Performs all needed calculations: external standard, internal standard, and normalization

Economic

- Directs up to 4 chromatographs to a single recorder
- Recorder does not require costly thermal paper
- 3 different programmable models are available for the most efficient utilization

Reliable

- 6th generation instrument combining years of experience derived from earlier models
- Minimum down time due to only 2 mechanical parts, self-diagnostics, and unmatched serviceability

Accurate

- Yields data on both peak height and area mode
- Sophisticated 2nd derivative signal analysis produces highly accurate results even in complex chromatography

Model 38 (Mini-Lab)
CSI also offers an inexpensive ($1995) digital integrator.

CSI-260

High Speed Data System for Mass Spectrometers

The only instrument that provides an economic alternative to a dedicated computer system, for a fraction of the price



- Measures peaks at a rate of 1000/sec.
- Obtains good heights on peaks as narrow as 100 microseconds
- Calculates mass numbers and normalizes peak heights of 256 peaks in a 6 second repetitive cycle
- Eliminates peaks below a selectable percentage of maximum peak height

Models 700 and 720

Portable X-Ray Analyzers

- Compact, truly portable
- Minimum sample preparation required
- In-depth application support from recognized industry expert



Model 700

- Non destructive measurement of elements in solids and liquids from atomic numbers 20-83

Model 720

- Measures sulfur in hydrocarbons and lead in gasoline

ARC

Thermal Kinetic Screening Device

Combining the company's experience in thermal analysis equipment with Dow Chemical's experience in reactive chemicals, CSI introduces the ARC, an advanced accelerating rate calorimeter. The ARC is used for hazard evaluation of reactive chemicals. By using a sophisticated microprocessor, the ARC performs fully automated tests and records data acquired from the reaction of chemicals under programmed conditions. It searches for and tracks exotherms created by the reaction within the experimental parameters of time, temperature, and heat rate. This data is useful to the operator in predicting possible thermal runaway of reactive chemicals.



Air Quality Monitoring Equipment
CSI also offers monitors for ozone and oxides of nitrogen

P.O. Box 9908, Austin, TX 78766 (512) 258-5191
Outside Texas Call Toll Free (800) 513-5003
TWX 910-874-1364

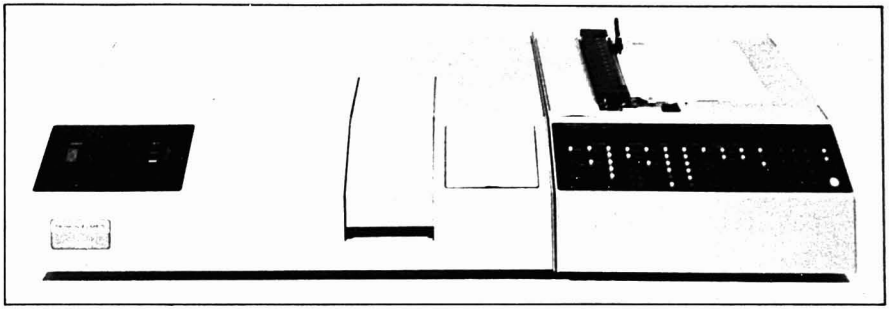
Booths 218, 220, 222, and 224 at the Pittsburgh Conference

CSI COLUMBIA SCIENTIFIC INDUSTRIES CORP.



CIRCLE 54 ON READER SERVICE CARD

THINKING UV? THE MODEL 554 DOES.



MICROCOMPUTER CONTROL

The microcomputer at the heart of Perkin-Elmer's new Model 554 medium-priced spectrophotometer does most of your thinking in recording UV spectra. Simply enter operating parameters on the keyboard, and the instrument's own Flowchart Recorder™ displays the spectra.

HIGH AUTOMATION

The Model 554 has been designed for routine scanning without sacrifice of photometric accuracy. High automation of both instrument and sample programmer, achieved through microcomputer control, is perfect for reaction rate analysis. The microcomputer calculates and controls the abscissa and ordinate values for the built-in Flowchart Recorder, checks the OA/100%T balance, and automatically calculates concentration factors at the push of a button. It also flattens the instrument's baseline and permits recording of the first or second derivative of the spectrum. Wavelength limits for repetitive scanning, or up to seven discrete wavelengths for wavelength programming, are entered into the microcomputer's memory, and subsequent spectra may be recorded either sequentially or overlayed. The microcomputer controls the digital display of ordinate, abscissa and selected parameter values and outputs these values to data handling systems via a low cost, dedicated interface.

ADVANCED TECHNOLOGY

The keyboard provides the operational simplicity inherent in microcomputer controlled instruments. A selected value is simply entered via the keyboard and the monochromator is positioned automatically to this preselected wavelength by pushing a button. Upper and lower ordinate limits for the recorder, range limits for repetitive scanning, and wavelength values for wavelength programming are all entered via the keyboard. All stored values can be recalled on the display even while a spectrum is being scanned, without interrupting scanning.

The built-in Flowchart Recorder uses the patented * Perkin-Elmer Flowchart-lock™ system for abscissa synchronization so that the recorder pen is always in coordination with the monochromator. Manual correlation of monochromator and chart, required with conventional instruments, is not necessary.

TECHNICAL INFORMATION

For immediate answers about our full range of Perkin-Elmer UV spectrophotometers, please call (312) 887-0770, Ext. 100, or write directly to Perkin-Elmer Corporation, M/S-12, Main Avenue, Norwalk, Connecticut 06856, or Bodenseewerk Perkin-Elmer & Co., GmbH, Postfach 1120, 7770 Uberlingen, Federal Republic of Germany.

For more information on the "Thinking UV", circle Reader Service Number:
208 for information about the Model 554
209 for an immediate demonstration
210 for a schedule of demonstrations in your area

*U.S. Patents Number 4,038,664, Foreign Patents Pending

PERKIN-ELMER

Expanding the world of analytical chemistry.

Joint with Division of Analytical Chemistry

C. Auerbach, *Presiding*

9:00—Introductory Remarks.
9:05—20. Progress in the Verification of the Reprocessing In-Put Analysis for Nuclear Materials Safeguards. **L. Koch, E. Mainka.**
9:30—21. Nuclear Safeguard Applications of Energy-Dispersive Absorption Edge Densitometry. **T. R. Canada.**
10:00—Intermission.
10:20—22. Isotopic Safeguards Techniques. **C. L. Timmerman, K. B. Stewart, B. A. Napier, J. C. Bower, D. E. Christensen.**
10:50—23. Measurement of Nuclear Fuel Burnup Using Inexpensive Chemical Techniques. **S. F. Marsh, M. R. Ortiz, J. E. Rein.**
11:10—24. Application of On-Line Alpha Monitors to Process Streams at the Barnwell Nuclear Fuel Plant. **K. J. Hofstetter, G. M. Tucker, J. H. Gray, G. A. Huff.**
11:30—25. Portable Calorimeter Systems for Nondestructive Assay of Mixed-Oxide Fuels. **C. T. Roche, R. B. Perry, R. N. Lewis, E. A. Jung.**

ANALYTICAL CHEMISTRY Appoints Three New Instrumentation Advisory Panel Members

ANALYTICAL CHEMISTRY has appointed three new members to its Instrumentation Advisory Panel. They are Catherine C. Fenselau, the Johns Hopkins University; Gary M. Hieftje, University of Indiana; and C. David Miller, American Instrument Co.

Members who are leaving the panel after serving three-year terms are Robert W. Hannah, Perkin-Elmer Corp.; R. K. Skogerboe, Colorado State University; and Donald E. Smith, Northwestern University.

The six members who will continue to serve on the panel are Gary D. Christian, University of Washington; Nathan Gochman, Veterans Administration Hospital and University of California at San Diego; Gary Horlick, University of Alberta, Canada; Peter T. Kissinger, Purdue University; James N. Little, Waters Associates; and Sidney L. Phillips, Lawrence Berkeley Laboratory, University of California.

The Advisory Panel members lend their expertise to the continued development of interesting and provocative editorial coverage of the interdisciplinary field of instrumentation. They aid both in the selection of subject matter and possible authors and in the development of the scope and aims of the feature itself. Panel members also review material for the feature and sometimes contribute directly as authors or coauthors of articles.

The goal of the instrumentation feature is to help broaden and deepen the reader's knowledge in related disciplines so that cross-fertilization of ideas might provoke original and useful thinking in the area of instrumentation for solving analytical problems. The articles are written by the specialist but directed toward the nonspecialist. They are not intended to be lengthy review articles but should serve to introduce and promote interest in the subject under discussion. Areas of interest include not only instrument design but also specific applications. Experts in disciplines other than chemistry are often invited as authors when the topic has great potential application to analysis. Although articles are normally invited, unsolicited articles are also considered if the topic is appropriate.



Catherine C. Fenselau



Gary M. Hieftje



C. David Miller

Brief biographical sketches of the new panel members follow.

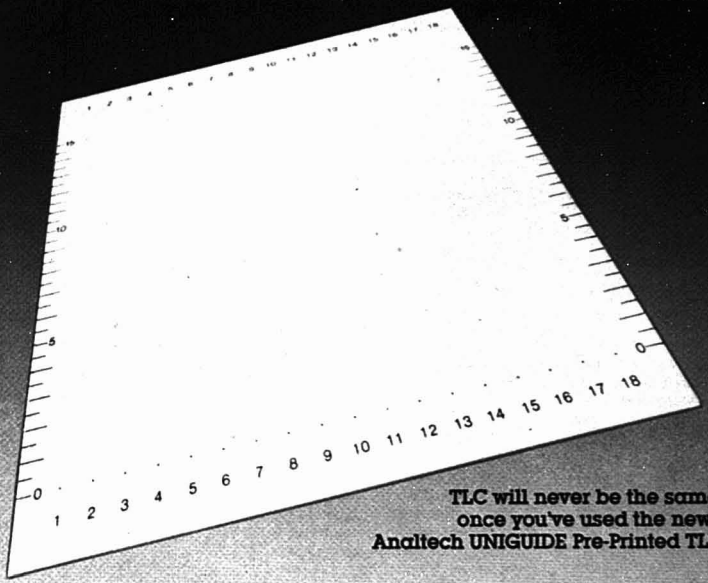
Catherine C. Fenselau is associate professor in the Department of Pharmacology and Experimental Therapeutics, the Johns Hopkins University School of Medicine. She received her AB degree from Bryn Mawr College and her PhD degree from Stanford University. She joined the faculty at Hopkins after two years of postdoctoral research with Melvin Calvin and A. L. Burlingame at the University of California at Berkeley. Her current research programs, in which mass spectrometry and combined gas chromatography–mass spectrometry are the principal techniques, include the synthesis and characterization of glucuronides, and studies of drug metabolism and pharmacokinetics. Her research group is also active in developing new reagent gases for chemical ionization mass spectrometry and in elucidating mechanisms of fragmentation. She is an active member of the Analytical Chemistry and Medicinal Chemistry Divisions of the American Chemical Society, and of the American Society for Mass Spectrometry. She is coeditor-in-chief of the international journal, *Biomedical Mass Spectrometry.*

Gary M. Hieftje is professor of chemistry at Indiana University. He received his AB degree from Hope College in 1964, after working several years at Miles Laboratories in Zeeland, Mich. From 1964 to 1965, he served as a research assistant in physical chemistry at the Illinois State Geological Survey. He earned his PhD degree in 1969 from the University of Illinois under the direction of H. V. Malmstadt. In the same year, he was

UNIGUIDE™

Template-Printed TLC Plates

MARKEDLY BETTER



TLC will never be the same once you've used the new Analtech UNIGUIDE Pre-Printed TLC plates.

UNIGUIDE is faster - place sample spots directly on the printed dots. No template necessary. Channels are numbered for maximum convenience.

UNIGUIDE is more accurate - read Rf values easily, precisely with printed metric scale on every plate. Printed points-of-origin provide positive spike for densitometry plus guide for accurate alignment.

UNIGUIDE is easier - abrasion-resistant surface permits stacking plates without damage and can be written on. Spots scrape cleanly without flaking for sample recovery.

Complimentary samples of the ultimate convenience in TLC with your call or letterhead request.

75 Blue Hen Drive • P.O. Box 7558 • Newark, Delaware 19711
TOLL FREE 1-800-441-7540
In Delaware (302) 737-6960

ANALTECH THE PREFERRED SOURCE FOR THIN LAYER CHROMATOGRAPHY

PRE-COATED / PRE-SCORED / PRE-PRINTED / PRE-CHANNELED / PRE-ADSORBENT

CIRCLE 9 ON READER SERVICE CARD

appointed assistant professor of chemistry at Indiana University and was promoted to associate professor in September 1973 and to full professor in July 1977. His research interests include the investigation of basic mechanisms in atomic emission, absorption, and fluorescence spectrometric analysis, and the development of atomic methods of analysis. He is also interested in the on-line computer control of chemical instrumentation and experiments, the use of time-resolved luminescence processes for analysis, the application of information theory to analytical chemistry, and the use of stochastic processes to extract basic and kinetic chemical information. He is a member of the American Chemical Society, the Society for Applied Spectroscopy, the Optical Society of America, Sigma Xi, and Phi Mu Alpha. He currently serves on the editorial boards of *Spectrochimica Acta, Part B,* and *Analytica Acta.*

C. David Miller is director of Research, Development and Engineering at the American Instrument Co. Division of Travenol Laboratories, Inc. He received his AB degree in chemistry from Columbia University in 1952. After working for Du Pont Co. and serving with the Army Chemical Corp., he earned his MS degree in organic chemistry from the University of Maryland in 1959. He interrupted his later employment at the American Instrument Co. to earn his PhD degree in analytical chemistry from the University of Florida in 1964. His research interests include instrumental aspects of microanalysis, atomic and molecular fluorescence/absorption/emission spectrometry, electrochemistry, gas chromatography, and thermal and clinical methodologies. He has numerous publications and patents in these areas. Dr. Miller is a member of the American Chemical Society and its Analytical Chemistry Division, the Society for Applied Spectroscopy, the Electron Microscopy Society of America, and the Optical Society of America.

Bell Labs Spectroscopist Receives Award

Darwin L. Wood of Bell Labs, Murray Hill, N.J., has received a medal of honor for his outstanding achievements in spectroscopy from the New York Section of the Society for applied Spectroscopy. The award, which has been sponsored by the Society annually since 1952, was presented at a symposium held in Dr. Wood's honor during the 1977 Eastern Analytical Symposium.

Dr. Wood, supervisor of the Optical Spectroscopy Group at Bell Labs, has contributed to the understanding of the structure and energy levels of such materials as laser crystals, magnetic materials, gems, and quartz through the use of spectroscopy. Many of these materials are important in solid-state electronic devices. Recently, Dr. Wood, together with two Bell Labs scientists, developed a new device called a Direct Reading TV Spectrometer. The device is an ingenious combination of television, a spectrograph, and a computer, designed for analysis of a wide variety of materials, particularly those materials widely used in telecommunications networks.



Darwin L. Wood (right) receives the medal from Bernard J. Bulkin, chairman of the New York Section of SAS

Rensselaer Professor Honored

Fred W. Billmeyer, Jr., professor of analytical chemistry at Rensselaer Polytechnic Institute, has received the Armin J. Brunning Award of the Federation of Societies for Coatings Technology at the Federation's annual meeting in Houston, October 28, 1977.



Fred W. Billmeyer

The award was established in 1962 in memory of Armin Brunning, a pioneer in the application of color science to paint technology.

The award cites Professor Billmeyer's outstanding contribution to the science of color in the field of coatings technology. At the Rensselaer Color Measurement Laboratory, Professor Billmeyer oversees graduate research and industrial liaison in the science and technology of color. He joined the faculty in 1964 after nearly 20 years in plastics research at Du Pont. He earned his PhD at Cornell University.

Radioiodine Monitor Developed by NRL Scientists

A radioiodine monitor capable of detecting trace quantities of radioactive $^{129}I_2$ in the atmosphere has been developed by two Naval Research Laboratory scientists, J. R. McDonald and Andrew Baronavski. The new device can detect less than 10^{-8} g of $^{129}I_2$ per liter of air at 1 atm. The principle of detection is based on a coincidence between $^{129}I_2$ absorption lines and a helium–neon laser (operating with a particular neon isotope, ^{22}Ne). This particular radioiodine must be monitored at nuclear reprocessing plants during the processing of material for storage and fuel recovery. However, the detection by radiocounting tech-

We made a good recorder better...

Introducing Model SRG-2 single pen and Model DSRG-2 dual pen potentiometric recorders. The latest in the Sargent-Welch family of recorders designed with the chemist in mind.

Both include linear and logarithmic operation. Log conversion is completely electronic —no gears to change. And the log range is expandable from ½ to 3 full cycles.

Ten spans from 1 mV to 1000 mV, calibrated or variable expansion in each span, and 9 chart speeds offer maximum flexibility.

Signals are traced by a disposable, fiber tip pen on metric chart paper with a 24 cm scale graduated −2 to 100.

Other features such as automatic gain control, zero adjust up and down scale and fast pen response combined with years of experience designing and building recorders result in unsurpassed versatility and dependability.

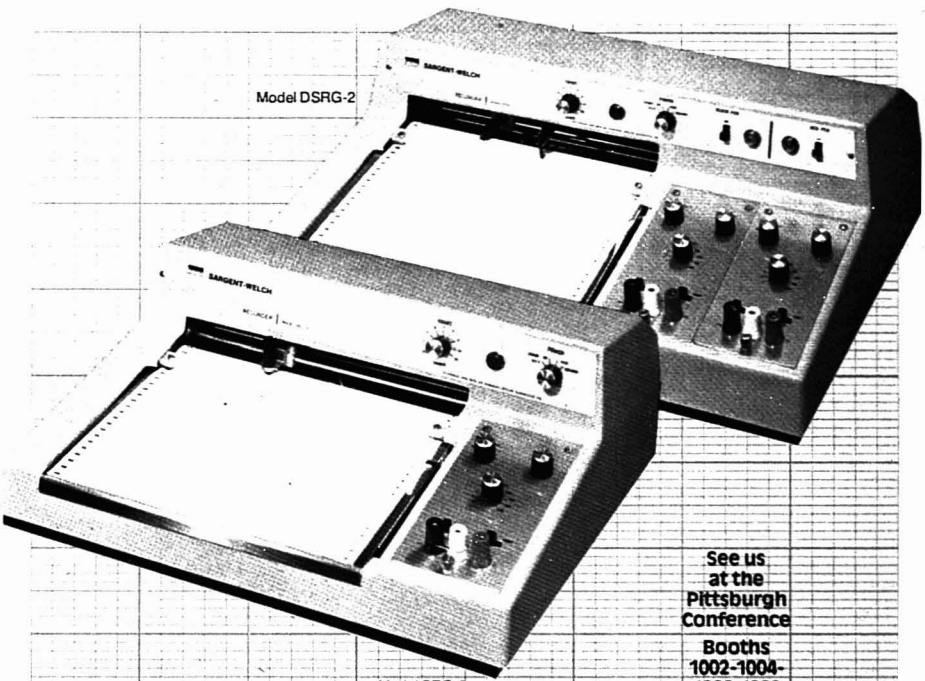
Optional accessories include an event marker and new electronic integrator.

To learn more about how we made a good recorder better, call or write today.

Sargent-Welch Scientific Company
7300 North Linder Avenue
Skokie, Illinois 60076
(312) 677-0600

SARGENT-WELCH

Single and dual pen, linear/log, strip chart recorders



See us at the Pittsburgh Conference

Booths 1002-1004-1006-1008

Anaheim/Birmingham/Chicago/Cincinnati/Cleveland/Dallas/Denver/Detroit/Springfield, N.J./Toronto/Montreal

CIRCLE 192 ON READER SERVICE CARD

THE LANGUAGE OF SCIENCE
Plenum
PUBLISHING CORPORATION

Introduction to X-Ray Spectrometric Analysis
by **Eugene P. Bertin,** RCA Laboratories

This new text, suitable for self-instruction or university courses and workshops, provides detailed descriptions and explanations of X-ray spectrometric principles, instrumentation, and techniques. approx. 475 pp., illus., 1978, $28.50

Applied Atomic Spectroscopy
edited by **E. L. Grove,** IIT Research Institute

Experts in the field provide chemists with a basic understanding of the fundamental principles and latest developments in atomic spectroscopy, including emission and atomic absorption. Two-volume set in *Modern Analytical Chemistry*.
Volume 1: approx. 330 pp., illus., 1978, $39.50
Volume 2: approx. 315 pp., illus., 1978, $39.50
Two-volume set: $75.00

Laser and Coherence Spectroscopy
edited by **Jeffrey I. Steinfeld,** Massachusetts Institute of Technology

Active researchers in the field of chemical physics examine coherent absorption and scattering phenomena in the spectroscopy of atoms and molecules. approx. 515 pp., illus., 1978, $45.00

Contemporary Topics in Analytical and Clinical Chemistry
edited by **David M. Hercules,** University of Pittsburgh; **Gary M. Hieftje,** Indiana University; **Lloyd R. Snyder,** Technicon Instruments Corporation; and **Merle A. Evenson,** University of Wisconsin

Volume 1

Presents chemists with the latest developments in the field, and delineates the relationship of analytical chemistry to other areas, such as air and water pollution, oceanography, earth sciences, and various aspects of biomedical science and technology. 342 pp., 1977, $25.00

Visit the Plenum Booth #1406 at the Pittsburgh Conference

PLENUM PUBLISHING CORPORATION, 227 West 17th Street, New York, N.Y. 10011
Prices subject to change without notice. Prices slightly higher outside the U.S.

CIRCLE 173 ON READER SERVICE CARD

niques is difficult because of the long half-life and low specific activity of $^{129}I_2$ and because this isotope occurs together with other isotopes of iodine with short half-lives. Since the new detector is insensitive to other isotopes of iodine, the NRL scientists conclude that the monitor can be used even in the presence of a large excess of other iodine radioisotopes.

Alcohol That Stimulates Plant Growth

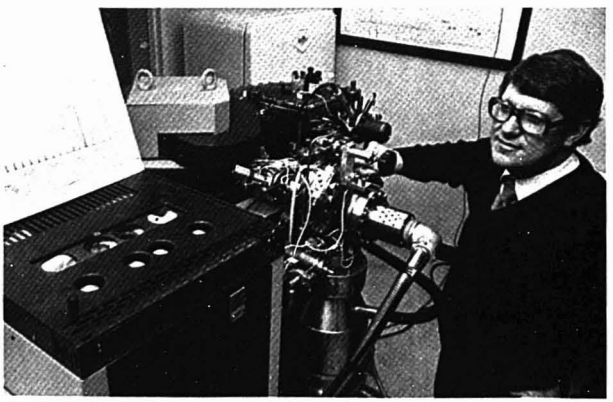
While to the casual observer the recent Arab oil embargo and the discovery of the growth stimulating natural alcohol might seem to have little connection, the two events are linked in a remarkable story. The embargo led to a general increase in the price of all forms of energy, especially of natural gas, the source of hydrogen used for the production of nitrogen fertilizers. As a result a team of scientists led by Stanley K. Ries of Michigan State University thought perhaps the nitrogen-rich forages like alfalfa leaves could be substituted for chemical fertilizers in an emergency.

In the first part of their investigation, chopped alfalfa hay was placed below and to the side of the crop seeds. The results of the experiment were better than expected, since the increase in growth of the plants was actually greater than that produced by equivalent amounts of nitrogen fertilizer. After a series of further experiments, they were able to purify a crystalline substance from the chloroform extract of alfalfa hay. When the substance was applied to the plants as a foliar spray, the growth of the plants proved indeed that this substance was responsible for the growth stimulating effect.

Dr. Ries then turned to analytical chemist, Charles C. Sweeley, also of Michigan State University, for the identification of the compound. The crystalline substance was identified by mass spectrometry as triacontanol, a straight-chain 30 carbon saturated alcohol, $CH_3(CH_2)_{28}CH_2OH$. When the crystals were dissolved in hexane, the mass spectrum was identical to that of a sample of triacontanol synthesized by Analabs, North Haven, Conn. In addition, the gas chromatographic retention times were similar to those of an authentic sample, and the melting points of the crystals, the authentic material, and a mixture of both were similar to that reported for triacontanol. Triacontanol, which was first isolated and identified in 1933 by the English scientist A. C. Chibnall, is the principal component of wax derived from alfalfa leaves.

Further experiments showed that application of synthetic triacontanol in concentrations as low as 10 μg/L of nutrient solution resulted in an increase of the yields of most crops including navy beans, asparagus, sweet corn, carrots, cucumbers, lettuce, radishes, and tomatoes. In addition, the compound does not appear to be a pollution hazard since it already occurs naturally in fairly high concentrations.

Despite this success, Dr. Ries remains cautious because he still does not know "much at all about how this alcohol biochemically causes the plants to grow and yield more". He



Charles C. Sweeley is shown at the controls of a mass spectrometer during a sample identification run

says that he cannot "predict how triacontanol will work outside of the particular climate. It is still possible that the chemical won't work in other important crop production areas such as the tropics or more arid locales. In fact, it may not work in Michigan next year."

Cancer Research Aided by GC/MS

The analytical systems that combine the superior separation capabilities of gas chromatography and the detection sensitivity and specificity of mass spectrometry (GC/MS) are playing an increasingly important role in biomedical research. An "Award of Appreciation" presented recently to the Du Pont Co. by a major cancer research institution highlights a case of such applications.

For its contributions in the development of two GC/MS systems now used for immunology research, Du Pont's Instrument Products Division was honored by the City of Hope. The development was a joint venture between Du Pont and the City of Hope, a nonprofit organization dedicated to the treatment of patients (without charge) with major diseases and the conduct of basic biomedical research. The systems, which were designed to meet the needs of the Division of Immunology at the City of Hope, are Du Pont's 321 digital GC/MS and 492 GC/MS. The 321 is equipped for high resolution measurements, and the 492 for multiple specific ion detection. The high sensitivity of the 321 makes it ideal for biomedical research where only trace amounts of samples are available. The research at the City of Hope is centered on identification and structural elucidation of cellular antigens, with particular emphasis on tumor immunology.

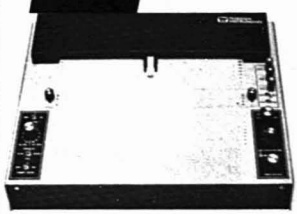


The award is presented to Du Pont's president, Edward R. Kane (right), by Charles W. Todd of the City of Hope



Glass Plumber—Repairing the device made out of glass is Gary Seaver, resident glassblower at the Akron Central Research Laboratory of the Firestone Tire & Rubber Co. The apparatus is a high vacuum oil diffusion pump used in reactor experiments conducted at the laboratory. Seaver blows air from the tube in his mouth through the pump to the spot being repaired. This keeps the glass from collapsing as it melts. Specially tinted glasses shield his eyes from the bright glare of the torch

WORKHORSES



Pedersen builds strip chart recorders so accurate, flexible, easy to operate, free of trouble and easy to buy, we call them "Workhorses." First, the single channel Model 27MR. Second, the 27MR with Integrator or Event Marker. Third, the 37MR Dual Channel Model. And fourth, exciting new recorders on the drawing boards. For particulars, write or call Svend Pedersen.

From $695.00

Pedersen

Pedersen Instruments of Walnut Creek
2772 Camino Diablo
Walnut Creek, CA 94596
(415) 937-3630

CIRCLE 195 ON READER SERVICE CARD

New Oxford® Adjustable SAMPLER® Micropipette

OXFORD

Set any volume
Continuously adjustable
Slim line design
Consistent accuracy
Exceptional precision
Quick and easy adjustment
Rugged construction
One-hand tip ejector
Soft plunger action
Unique balance
No carry-over
Insulated handle
Positive calibration stop
1-year guarantee
Hand-contoured handle
Tips available bulk, "rack pack," sterile
Two tips cover entire range.

Cat. No.	Range	Tip No.
3001	2-10 μL	910
3002	10-50 μL	910
3003	50-200 μL	910
3004	200-1000 μL	911

Order from your national laboratory distributor

OXFORD LABORATORIES

Subsidiary of G. D. Searle & Co.
Foster City, California 94404
Toll-free: 800/227-0276
From California and Canada call collect: 415/573-1343



CIRCLE 156 ON READER SERVICE CARD

News

Meetings

The following meetings are newly listed in ANALYTICAL CHEMISTRY. *The 1978 meetings listed earlier appear in the January issue*

- **Symposium on HPLC with Application to the Pharmaceutical and Food Industries.** Apr. 10–14. Sunderland, England. *Contact: R. Dennis, School of Pharmacy, Sunderland Polytechnic, Chester Rd., Sunderland, Tyne & Wear, SR1 3SD, England*
- **9th International Symposium on Chromatography and Electrophoresis.** May 15–16. Riva Del Garda, Lake of Garda, Italy. *Contact: Alberto Frigerio, Istituto de Ricerche Farmacologiche, Mario Negri, Via Eritrea 62, 20157 Milan, Italy. Page 44 A, Jan.*
- **5th International Symposium on Mass Spectrometry in Biochemistry and Medicine.** June 19–21. Rimini, Italy. *Contact: Alberto Frigerio, Istituto de Ricerche Farmacologiche, Mario Negri, Via Eritrea 62, 20157 Milan, Italy. Page 44 A, Jan.*
- **6th Discussion Conference on Macromolecules: Chromatography of Polymers and Polymers in Chromatography.** July 17–21. Prague. *Contact: P. M. M. Secretariat, c/o Institute of Macromolecular Chemistry, 162 06 Prague 616, Czechoslovakia*
- **Inter/Micro-78.** July 24–27. McCormick Inn, Chicago. Sponsored by McCrone Research Institute. Emphasis on new techniques in acoustic, infrared, interference microscopy; uses of laser Raman microprobe; techniques of modulation contrast, and combinations of microscopes and computers. *Contact: McCrone Research Institute, 2508 S. Michigan Ave., Chicago, Ill. 60616. 312-842-7105*
- **6th International Conference on Raman Spectroscopy.** Sept. 4–9. Bangalore, India. *Contact: J. R. Durig, College of Science & Mathematics, U. of South Carolina, Columbia, S.C. 29208. 803-777-2505*
- **176th ACS National Meeting.** Sept. 10–15. Miami Beach, Fla. *Contact: A. T. Winstead, American Chemical Society, 1155 16th St., N.W., Washington, D.C. 20036*
- **ISA/78.** Oct. 15–19. Philadelphia. *Contact: Instrument Society of America, 400 Stanwix St., Pittsburgh, Pa. 15222. Page 44 A, Jan.*
- **5th Annual Meeting of the Federation of Analytical Chemistry and Spectroscopy Societies.** Oct. 30–Nov. 3. Boston. *Contact; Paul Lublin, GTE Laboratories, 40 Sylvan Rd., Waltham, Mass. 02154. 617-890-8460. Page 44 A, Jan.*

Short Courses

ACS Courses. For more information, contact: Department of Educational Activities, American Chemical Society, 1155 Sixteenth St., N.W., Washington, D.C. 20036. 202-872-4508

Column Selection in Gas Chromatography
Cleveland. Feb. 25–26. Harold M. McNair and Walter R. Supina. $165, ACS members; $205, nonmembers

Capillary Gas Chromatography
Cleveland. Feb. 25–26. Stuart Cram and Milos Novotny. $245, ACS members; $295, nonmembers

Thermal Methods of Analysis
Cleveland. Feb. 25–26. Wesley W. Wendlandt and Ilya M. Sarasohn. $195, ACS members; $235, nonmembers

Statistics for Experimental Design
Cleveland. Feb. 25–26. John Hromi. $195, ACS members; $235, nonmembers

Thin-Layer Chromatography
Cleveland. Mar. 3–4. Victor W. Rodwell and Donald J. McNamara. $195, ACS members; $235, nonmembers

Solving Problems with Modern Liquid Chromatography
Cleveland. Mar. 3–5. J. J. Kirkland and Lloyd R. Snyder. $225, ACS members; $265, nonmembers

Electroanalytical Chemistry
Anaheim, Calif. Mar. 10–12. Dennis Evans and Paul Whitson. $225, ACS members; $305, nonmembers

Carbon-13 NMR Spectroscopy
Anaheim, Calif. Mar. 10–12. George Levy and Paul Ellis. $255, ACS members; $305, nonmembers

Modern Techniques in Gas Chromatography
Anaheim, Calif. Mar. 11–12. Harold McNair and Stuart Cram. $195, ACS members; $235, nonmembers

Statistics for Experimental Design
Anaheim, Calif. Mar. 11–12. John Hromi. $195, ACS members; $235, nonmembers

What's your precision weighing need? A Torbal balance will give you more years of trouble-free performance.



The TORBAL TB-160S best-value digital electronic analytical balance of its scope on the market. Full digital outputs, industry compatible. Completely automatic for most applications. Electronic null indicator speeds weighing, minimizes errors.
Capacity: 160 g
Readability: 0.1 mg
48 grams of tare without use of built-in internal weights.

CIRCLE 97



The TORBAL EA-1 analytical balance with electronic speed and the highest standards of accuracy, operating ease and retained sensitivity.
Capacity: 160 g
Precision: 0.03 mg
8-10 g dial-in-tare, extended, tare range to 208 grams.

The TORBAL SEA-1 student analytical balance; similar to EA-1, except taring to 159 g with built-in weights.

CIRCLE 98



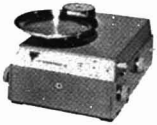
The TORBAL ET-1 is the only 160 g capacity top-loading balance that gives 1 mg accuracy, complete digital display without optics or verniers. Electronic null readout speeds up weighing and minimizes errors.
Capacity: 160 g
Accuracy: 0.001 g
48 grams of tare without the use of built-in internal weights.

CIRCLE 106



The TORBAL ST-1 is a low cost rugged, accurate laboratory balance.
Capacity: 310 grams without use of loose weights
Accuracy: 0.01 g
Heavy base and sturdy frame
Dial range from 0 to 10 grams by 0.01 grams (with vernier)
"C"-type bow for easy access
5" diameter stainless steel pan.

CIRCLE 107



The TORBAL PL-12D balance has
Capacity: 2000 g
Precision: ±0.07 g
Readability: 0.1 g (digital)
Tare: 1125 g
Quality optics provide sharp image and high illumination.

The TORBAL PL-3D similar to above with 3000 g capacity.

CIRCLE 120

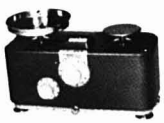


The TORBAL IL-11 high capacity, notched-beam balance for convenient, accurate, economical weighing to 4.5 Kg with 0.1 g sensitivity.

The TORBAL DH-4a similar to the IL-11, except 0.2 g sensitivity.

The TORBAL DH-2a 2 Kg capacity and 0.07 g sensitivity.

CIRCLE 124



The DWM3V is a TORBAL top-loader that makes weighing five times faster than graduated beam balances.
Capacity: 200 g
Weight control dial and fine weighing dial with vernier give direct readings from 100 grams to 0.01 grams.
Magnetic damping
Stainless steel pans

CIRCLE 151



The TORBAL DWM2 and the DWM2-1: rugged, fast, accurate top-loaders for "semi-analytical" weighing.
Capacity: 120 g
Readability: 2 mg
Dial reading: 10 g to 0.01 g
Magnetic damping

The TORBAL DWM5 similar to DWM2, except 500 g capacity ...dial reading 100 g to 0.1 g.

CIRCLE 152

TORBAL WEIGHTS: Torsion Balance manufactures and supplies a variety of individual weights and weight sets—in stainless steel and brass and in aluminum and tantalum for fractional weights—from 1 mg to 1 Kg. Weights available in Class S, S-1 and P, traceable to National Bureau of Standards.

CIRCLE 203

For complete information on *all* of the above products, circle number 252.

The Torsion Balance Company has one of the most versatile lines of precision balances. You can now select a TORBAL laboratory balance for virtually any purpose, and you can save a great deal of time and expense when you do it. With TORBAL's low maintenance you'll also save money with years of trouble free performance.

Newer models have full, industry-compatible digital outputs.

All TORBAL balances feature rugged torsion-band suspension making them far more reliable and durable than knife-edge balances. With torsion band fulcra there are no knife edges, no metal-to-metal wear, and no bearings to accumulate dust or dirt. And the weighing mechanism is not affected by corrosion or abrasive dusts in the atmosphere either.

Write today for literature detailing any of TORBAL's balances. There is a TORBAL laboratory balance to meet virtually any precision weighing need.

TORBAL®

THE TORSION BALANCE CO.

Main Office and Factory:
Clifton, N.J. 07012

Sales Offices:
Chicago, IL; Temple City, CA and Salem, OR

SPECTRASPAN III

versatility in element analysis from trace to major levels



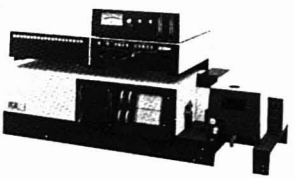
The unmatched versatility and performance of Spectraspan III plasma-emission spectrometers ensure high productivity in a wide variety of analytical applications.

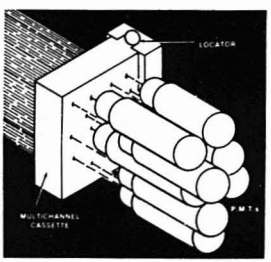


In the quantitative mode of operation, a built-in microprocessor and programmed cassettes permit either sequential analysis of single elements automatically, or **simultaneous analysis of up to 20 different elements.** No special techniques are required to set up the cassettes, and conversion from one type of analysis to the other can be achieved quickly. And for rapid, comprehensive qualitative analysis of unknown elements even at trace levels, or for troubleshooting, Spectraspan III converts to operation as a high-resolution spectrograph in less than one minute.

Other unique features of Spectraspan III total-measurement systems include:

- **The ability to handle solutions with dissolved-solids contents as high as 20 per cent.**
- **Reduced chemical and spectral interferences.**
- **Improved detection limits and wider linear dynamic range.**
- **Broad application.**
- **Modular construction to permit future expansion.**
- **Low initial cost.**





In addition, Spectraspan III systems are safe and economical to operate because the plasma is sustained in low-cost inert argon which eliminates the need for lamps and explosive gases.

So if you want to establish and maintain the high accuracy and productivity that characterize today's analytical requirements, and do it as economically as possible, look to versatile Spectraspan III. It's today's most innovative plasma spectrometer from the acknowledged leader . . .

SMI

SPECTRAMETRICS INCORPORATED
204 ANDOVER STREET, ANDOVER, MA 01810
(617) 475-7015

See our New Spectrajet III at Booth 1146 & 1148
CIRCLE 206 ON READER SERVICE CARD

News

Solving Problems with Modern Liquid Chromatography
Anaheim, Calif. Mar. 11–12. J. Kirkland and Lloyd Snyder. $225, ACS members; $265, nonmembers

Effective Writing for Scientists and Engineers
Anaheim, Calif. Mar. 15–17. Henrietta Tichy and Sylvia Fourdrinier. $225, ACS members; $275, nonmembers

Thin-Layer Chromatography
Anaheim, Calif. Mar. 16–17. Victor Rodwell and Donald McNamara. $195, ACS members; $235, nonmembers

Microprocessors and Minicomputers
Blacksburg, Va. Mar. 19–24, June 11–16. Raymond Dessy. $425, ACS members; $485, nonmembers

Capillary Gas Chromatography
Washington, D.C. May 19–20. Stuart Cram and Milos Novotny. $245, ACS members; $295, nonmembers

Laboratory Safety—Recognition and Management of Hazards
New York City. May 22–24. Norman Steere and Maurice Golden. $255, ACS members; $305, nonmembers

Gas Chromatography—Theory and Practice
Blacksburg, Va. June 6–9. Harold McNair. $425, ACS members; $485, nonmembers

High-Pressure Liquid Chromatography Workshop
Boston. June 24–25. David Freeman. $195, ACS members; $235, nonmembers

---

Laser Anemometry: Theory, Application, and Techniques for Researchers New to the Field
Houston, Tex., Feb. 13–15; Washington, D.C., Apr. 24–26; Dayton, Ohio, May 22–24. *Contact:* TSI, Inc., 500 Cardigan Rd., P.O. Box 3394, St. Paul, Minn. 55165. 612-483-0900

Applied X-ray Spectrometry and X-ray Powder Diffraction
U. of Denver. Mar. 13–17. C. S. Barrett, D. E. Leyden, J. B. Newkirk, C. O. Ruud, and P. K. Predecki. *Contact:* Mildred Cain, Denver Research Institute, U. of Denver, Denver, Colo. 80208. 303-753-2141

Chicago Gas Chromatography Discussion Group 16th Annual Introductory Course
Chicago. Mar. 21–24. *Contact:* J. B. Himes, Richardson Co., 2701 W. Lake St., Melrose Park, Ill. 60160

X-ray Spectrometry
State U. of New York at Albany. June 5–16. First week: Basic Principles and Techniques, $400. Second week: Fundamentals and Practical Applications, $400. $750 for both. *Contact:* Henry Chessin, State U. of New York at Albany, Dept. of Physics, 1400 Washington Ave., Albany, N.Y. 12222. 518-457-8339

Advanced Microcomputer Interfacing and Programming Workshop
On board the *TSS Carnivale* in the Carribean. June 17–24. $975. *Contact:* Norris Bell, Virginia Polytechnic Institute and State University, Continuing Education Center, Blacksburg, Va. 24061 (703-951-6208). Page 54 A, Jan.

X-ray Powder Diffraction
State U. of New York at Albany. June 19–30. First week: Basic Principles and Techniques, $400. Second week: Fundamentals and Practical Applications, $400. $750 for both. *Contact:* Henry Chessin, State U. of New York at Albany, Dept. of Physics, 1400 Washington Ave., Albany, N.Y. 12222. 518-457-8339

Concepts of Radiation Measurement
Philadelphia. July 24–28. Lectures and/or laboratory. *Contact:* Grafton D. Chase, Dept. of Chemistry, Philadelphia College of Pharmacy and Science, Philadelphia, Pa. 19104. 215-386-5800

Radioimmunoassay and Other Competitive Radioassays
Philadelphia. July 31–August 11. Lectures and/or laboratory. *Contact:* Grafton D. Chase, Dept. of Chemistry, Philadelphia College of Pharmacy and Science, Philadelphia, Pa. 19104. 215-386-5800

For Your Information

Micrometrics (5680 Goshen Springs Rd., Norcross, Ga. 30093) marks its 15th year in the analytical instrumentation business with the opening of two new district offices in the Chicago and Pennsylvania areas. In addition to manufacturing, selling, and servicing of analytical instruments for measuring pore size and volume, particle size, materials density, etc., Micrometrics produces a line of instruments for liquid chromatographs. Some of these include pulseless flow pumps, injectors, detectors, and complete accessories

SPECTRASPAN IV

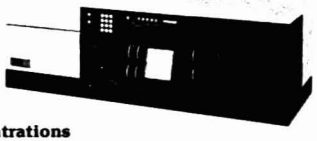
plasma spectrometry at atomic absorption prices



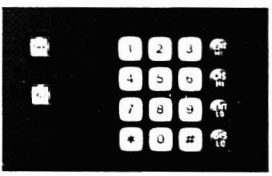
Spectraspan IV computer-aided plasma-emission spectrometers offer far more capabilities than atomic absorption units, yet are competitively **priced.**

Think about it. For about the cost of an atomic absorption unit, you can have a simple totally-integrated system that performs all common atomic absorption analyses **plus** analysis of:

- **Boron and phosphorus**
- **Elements which form refractory compounds**
- **Complex solutions having dissolved-solids contents as high as 20 per cent**
- **High acid concentrations**
- **Trace to major element concentrations**
- **Difficult elements including some non-metals**



All Spectraspan IV systems are compact bench-top units designed for sequential quantitative analysis of most elements automatically. Rapid comprehensive qualitative analysis is also available. Conversion from one mode of operation to the other can be accomplished in seconds.



These low-cost systems feature unique Echelle Grating Spectrometers that provide high dispersion of all wavelengths from 190 to 800nm, and powerful dedicated INTEL microprocessors that improve operating efficiency by providing overall control, calibration, monitoring, and reporting with minimum operator attention. In addition, Spectraspan IV systems consume little power, and operate on safe, inert argon which eliminates the need for lamps and explosive gases.

If you want to increase your capabilities to meet today's analytical requirements without increasing costs, invest in Spectraspan IV. Call SMI now for details. SMI is an acknowledged leader, and the company that has more plasma-emission spectrometers in use by satisfied customers throughout the world than any other manufacturer.



SMI

SPECTRAMETRICS INCORPORATED
204 ANDOVER STREET, ANDOVER, MA 01810
(617) 475-7015

See our new Spectrajet III at the Pittsburgh Conference, Booths 1146 & 1148
CIRCLE 207 ON READER SERVICE CARD

The best GC/MS Data System just keeps getting better

When you look at the Riber 150 GC/MS Data System you may say it looks like the System Industries System 150.

Right and wrong.

The Riber 150 is based on the hardware and software of SI's System 150 first developed for use with quadrupole GC/MS in '69. It's now in use in hundreds of laboratories around the world.

But, we've already made a number of key hardware and software improvements to the system to increase it's capabilities for you. And, there are more in process.

Whether you're considering automating magnetic sector or quadrupole GC/MS, you won't find a data system that gives you better price/performance ... now or in the future.

That's because we've concentrated on developing a truly versatile data system that can easily be adapted to any GC/MS instrument. The Riber 150's modular flexibility lets you economically tailor a data system to meet your most exacting requirements.

In addition, we are carrying out an aggressive upgrade program with Ribermag, the number one GC/MS company in Europe, to insure the data system will keep pace with your state-of-the-art.

If you're considering automating your GC/MS instrumentation, find out more about the Riber 150, its proven price/performance and our plans to continually improve its value in your lab.

RIBER DATA SYSTEMS

1020 Corporation Way • Palo Alto, CA 94303 • (415) 961-2012
Telex 910-379-6474



In Europe contact:
RIBERMAG, Rueill
Malmaison, France,
Tel. 977.92.05

See us at the Pittsburgh Conference, ISA Booths 1033–1047
CIRCLE 184 ON READER SERVICE CARD

News

for HPLC. The two new sales offices are located at **2020 Oakton St., Park Ridge, Ill. 60068** (312-696-3418); and **120 South Warner Rd., King of Prussia, Pa. 19406** (215-687-6920).

Syntex Corp. and Varian Associates have announced an agreement for **Syntex to acquire Varian's interest in Syva,** a joint venture of subsidiaries of Syntex and Varian. Under the terms of the agreement, Varian will receive the amount of its investment in Syva plus a cash payment of approximately $3.5 million and royalties on certain future sales. Syva developed and markets EMIT diagnostic assay systems for monitoring drug treatment for neurological and cardiovascular patients and for drug abuse monitoring. Syva assays for the principal antiepileptic drugs, for digoxin, and for drugs of abuse are widely used in clinical laboratories. Syva will continue to operate as a separate and distinct organization with the existing management from its Palo Alto, Calif., location.

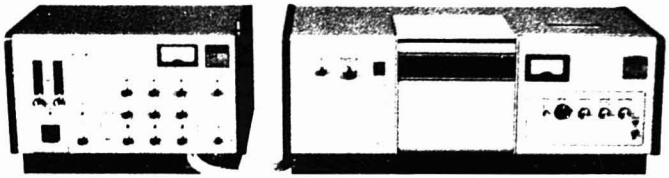
Kinney Vacuum Co. of Boston, Mass., the leading manufacturer of vacuum pumping equipment for science and industry, will relocate in the fall of 1978. The new plant and home office will be designed and built by the Carlson Corp. on a 14-acre site on Route 138, about 15 miles south of Boston.

Rhoads Scientific Co. is a new independent research, testing, and consulting laboratory specializing in general analytical chemistry, metabolism, method development, radiochemistry, radioimmunoassays, and residue determinations. For further information, contact: Rhoads Scientific Co., 4620 Edison Ave. (B), Colorado Springs, Colo. 80915 (303-574-6400).

Metrication for the Manager is a comprehensive manual published by the American National Metric Council (ANMC), a nonprofit organization whose purpose is to provide guidance and coordination for voluntary conversion. The 48-page, 8½ by 11-in. manual outlines the entire metrication process step-by-step, from investigation and planning through marketing and servicing a metric product. Copies are available from ANMC, 1625 Massachusetts Ave., N.W., Washington, D.C. 20036, at the following rates: single copies, $4.50; 2–9 copies, $4.00; 10 or more, $3.50.

Hitachi Polarized Zeeman

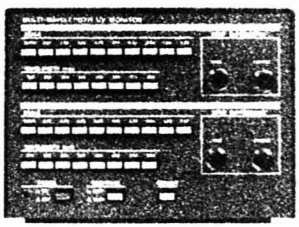
Atomic Absorption Spectrophotometer



- Direct analysis of most samples including blood, urine, organic material, sea water, acids, etc.
- Eliminates most, if not all, sample preparation
- 10 times better accuracy and precision
- Precise background correction to 1.7A—up to 5 times better than conventional deuterium lamp techniques.
- Simple, easy operation—few controls, no alignment
- Automatic Sampling Accessory

Hitachi LC Detector

NEW

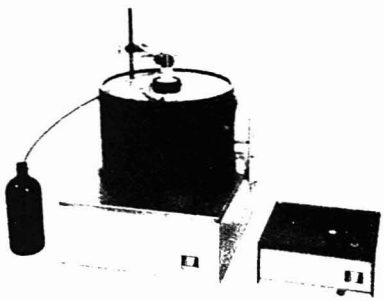


New Simultaneous Dual Beam, Dual-Channel, Multi-Wavelength UV Detector for Liquid Chromatography

- Dual beam simultaneously monitors and records two selected wavelengths from 210 to 280 nm
- Provides differential recording between two wavelengths
- Simple push-button operation
- Increases detectability and accuracy

Hitachi Preparative LC

NEW



New Centrifugal Liquid Chromatograph

- Large sample volume—up to 500 ml
- High speed—5 times faster
- Excellent separation—up to 550 theoretical plates

See these new Instruments, Accessories and other products at

Booth 1612-14-16 Pittsburgh Conference

February 27 thru March 3, 1978

NSI HITACHI
SCIENTIFIC INSTRUMENTS

392 Potrero Avenue, Sunnyvale, CA 94086 (408) 737-2522

CIRCLE 141 ON READER SERVICE CARD

OUR NEW 1978
CHROMATOGRAPHY
CATALOG
IS NOW AVAILABLE

FREE



MAY WE SEND YOU ONE?

WRITE:
ALLTECH ASSOCIATES
202 CAMPUS DRIVE • ARLINGTON HEIGHTS, ILLINOIS 60004 • 312-392-2670

CIRCLE 10 ON READER SERVICE CARD

Gilson Spectra/Glo Fluorometer

—for liquid chromatography
column monitoring of
Fluorescence-labeled compounds

- MUCH GREATER SENSITIVITY
- SPECIFICITY OF MEASUREMENT
- NEWEST L.C. TECHNIQUE

More sensitive measurement than UV or visible absorption monitoring



More specific method of measurement because fewer compounds exhibit fluorescing property • **Fluorophors** are stable for L.C. uses • **As little as** 10 to 40 nanograms of protein can be detected.

Call or write
Gilson Medical Electronics, Inc.
Box 27, Middleton, WI 53562
Phone 608/836-1551 • Telex: 26-5478

CIRCLE 83 ON READER SERVICE CARD

LABORATORY SERVICE CENTER

Acetylenedicarboxylic Acid Monopotassium Salt • p-Aminoacetophenone
Ammonium Reineckate • Anisoin • o,o'-Biphenol • 1-Chloropentane
Cinchophen • 2,5-Diethoxytetrahydrofuran • Diethyl Adipate • Digitonin
Dimethyl Acetone Dicarboxylate • 2,6-Dimethyl-g-Pyrone • Dulcitol
Furoic Acid • D(+)Galactosamine HCl • HABA • INT • α-Ketoglutaric Acid
Malonamide • Mandelic Acid • Phenolphthalein • o-Phthalaldehyde
Sodium Malonate • Sodium Pyruvate • Suberic Acid • Sulfosalicylic Acid
Taurine • Tetrahydrofurfuryl Acetate • Thionalide • Traumatic Acid

Write for our Products List of over 3000 chemicals

Tel: 516-273-0900 TWX: 510-227-6230

EASTERN CHEMICAL BOX 2500 K
Division of GUARDIAN CHEMICAL CORP. HAUPPAUGE, N. Y. 11787

LAB SAFETY
Send for 1978 Catalog
LAB SAFETY SUPPLY CO.
P.O.Box 1422, Janesville, WI 53545

Microparticle Standards

Large assortment of well-characterized microspheres and micropowders for analytical, research, and testing applications. Range of diameters from .05 to 500 microns (μm). Size and other physical properties are listed for each product. Materials include polystyrene, glass, pollens, minerals, many others. Write or telephone for Data File 45.

Duke Scientific Corporation
445 Sherman Avenue
Palo Alto, CA 94306
Phone (415) 328-2400

Carbon 13
15 years' experience in synthesising
LABELLED COMPOUNDS
Prochem
19 Ox Bow Lane
Summit, N.J. 07901
201-273-0440
NEW CATALOG AVAILABLE

NEW: LIQUID CHROMATOGRAPHY
PLUS, MASS SPECTROMETRY
GAS CHROMATOGRAPHY
AND MORE
GOLLOB ANALYTICAL SERVICE CORP.
Write For Brochure
47 Industrial Road, Berkeley Heights, N.J. 07922 (201) 464-3331

Laboratory Service Center (Equipment, Materials, Services, Instruments for Leasing), Maximum space — 4 inches per advertisement. Column width, 2-3/16"; two-column width, 4-9/16". Artwork accepted. No combination of directory rates with ROP advertising. Rates based on number of inches used within 12 months from date of first insertion. Per inch: **1" — $58; 12" — $57; 24" — $56; 36" — $55; 48" — $54.**

CALL OR WRITE BARBARA AUFDERHEIDE

ANALYTICAL CHEMISTRY
25 Sylvan Road, So.
Westport, Ct. 06880
203-226-7131

INDEX TO ADVERTISERS IN THIS ISSUE

CIRCLE INQUIRY NO.	ADVERTISERS	PAGE NO.
11	* Academic Press Flamm Advertising	269A
48	* Airco Industrial Gases Hammond Farrell Inc.	143A
10	* Alltech Associates Chromad	246A
51	Alpkem Corporation Alpkem Advertising Company	220A
12	* Altex Scientific Inc. Oliver Smith Advertising, Inc.	209A
5–6, 7–8, 14–15, 16–17	* American Instrument Company Industrial Advertising Associates	151A, 153A, 155A, 157A
9	* Analtech, Inc. Robert J. Allen	235A
62	Analytical Instrument Development, Inc. Mercer Associates	258A
13, 44	Antek Instruments, Inc. Cooley & Shillinglaw, Inc.	276A, 280A
21, 22	J. T. Baker Chemical Company Naimark & Barba, Inc.	259A, 285A
20	Balston, Inc. Levy Advertising Associates, Inc.	268A
52	Barnes Engineering Company Jarman, Spitzer & Felix, Inc.	184A
23	Bascom-Turner Instruments Tolland Associates	185A
19, 30, 43	* Beckman Instruments, Inc. N W Ayer ABH International	272A, 274A, 278A, 302A–303A
24	* Berghof Tubinger Satzatelier	261A
50	Biomation Regis McKenna, Inc.	273A
26	* Bio-Rad Fred Schott & Associates	165A
28	* Brinkmann Instruments, Inc. Blatt Advertising, Inc.	OBC
47	Broadley-James Corporation Wescon Advertising	297A
27	* Bruker Instruments Schwietzer Advertising	306A
56	Buchler Instruments Fletcher-Walker-Gesell, Inc.	284A
92, 93	Buck Scientific, Inc. Leif W. Hansen	293A, 297A
31	Burdick & Jackson Laboratories, Inc. Studio 5 Advertising, Inc.	264A
25	Burrell Corporation The Agency of Pittsburgh	260A
46	* Cahn Instruments Marketing Directions, Inc.	149A
49	Camag, Inc. Donald E. Heinz and Associates	210A
66	* Cameca Instruments SSS Art Service	226A
53	* Carle Instruments Knollwood Advertising Group	145A
37–39	* Chromatix, Inc. David R. McClurg	147A
54	Columbia Scientific Industries Columbia Advertising Assoc.	232A
xx	* Conostan Division, Continental Oil Co.	135A
67	Control Equipment Corp.	139A
61	Coulometrics Mike Rasmussen Advertising	293A
68	Crane Company Doremus Uptown	268A
32	* Crawford Fitting Company Falls Advertising Company	107A
69	Dexsil Chemical Corp. Kenyon Hoag Associates	200A
57	Diano Corporation Design Associates	212A
55	Digilab, Inc. Conrad, Inc.	159A
42, 58–60	* Dohrmann Fred Schott & Associates	99A
35, 36, 40	* E. I. DuPont de Nemours & Co., Inc. N W Ayer ABH International	126A–127A, 128A–129A, 130A–131A
41	* Durrum Instrument Corporation	140A
63	* Eastman Kodak Company Rumrill-Hoyt, Inc. Advertising	301A
65	* Eberbach Corporation Drury, Lacy, Inc.	262A
18, 29, 33, 34, 45, 136, 155, 167, 194	* Environmental Science Associates, Inc. Marketing Dimensions, Inc.	188A
64	Extranuclear Laboratories, Inc. Al Bierman and Associates	271A
70, 233	Farrand Optical Company, Inc.	290A
77	* Finnigan Instruments John Feack	172A
72, 73, 75, 84–91	* Fisher Scientific Company Tech Ad Associates	157A, 170A–171A, 204A–205A, 256A
71	Fluid Metering, Inc. Arnold H. Nachman Associates	155A
76	Fluidyne Instrumentation	297A
82	GCA/Precision Scientific Winterkorn, Hammond and Lillis, Inc.	123A
80	* Gilford Instrument Laboratories, Inc. Oberlin Industrial Advertising	125A
83	* Gilson Medical Electronics, Inc. Towell, Inc. Advertising	246A
79	* Glenco Scientific Boone Advertising, Inc.	278A
123	Gould, Inc. Carr Liggett Advertising, Inc.	253A
81	* Gow-Mac Instrument Company Kenyon Hoag Associates	222A
78	Graphic Controls Corporation Conklin, Labs & Bebee, Inc.	155A
96	* Hamilton Company Mealer & Emerson, Inc.	255A
94	* Hellma International, Inc. Miller Advertising Agency	260A
100, 101	Hewlett-Packard CK Associates Advertising	181A, 227A
95	* Hewlett-Packard Dancer Fitzgerald Sample, Inc.	281A
99	* Houston Instrument Cooley & Shillinglaw, Inc.	IFC
105	Hunter Associates Lab, Inc. Lin Lockhart Advertising, Inc.	165A
110	Inficon The Rath Organization	288A
74, 115–117	Instrumentation Laboratories, Inc. Aries Advertising, Inc.	275A
112, 113	* Instruments SA, Inc. J-Y Optical Systems Division Kathy Wyatt & Associates	263A
111	* International Plasma Corporation Paul Pease Advertising, Inc.	124A
108	International Scientific Instruments, Inc. Fred Schott & Associates	260A
109	ISCO Farneaux Associates Advertising	183A
114	JEOL Analytical Instruments, Inc. Weinrich Associates, Inc.	277A
118, 119	* Kontes Aitkin-Kynett Company, Inc.	195A
121–122	* Kratos, Inc. Mesa Copy	287A
126	* Labindustries Fred Schott & Associates	286A
248	Laboratory Data Control Kelleher, Bamberger, Levy	176A
148	L C. Company, Inc. M. J. Dreksler Associates	220A
125	Leco Corporation F Y I	132A–133A
127	LKB Instruments Inc. Jarman, Spitzer & Felix, Inc.	189A
147	3M New Business Ventures Div. Kerker & Assoc.	282A
128–134	* Matheson Kenyon Hoag Associates	196A
135	MC/B Manufacturig Chemists, Inc. Liebel & Company, Advertising	251A
145	* Mettler Instrument Corp. Harris D. McKinney, Inc.	105A
137–138	* Micromeritics Instrument Corporation Adgraphics	228A
150	Millipore Corporation Schneider Parker, Inc.	265A
139	* Mitsubishi Chemical Industries Ltd. Global Advertising Company, Ltd.	210A
149	Munich Fair Authority Kallman Associates	263A
142	Nanometrics, Inc. Design + Plus	214A
144	* Neslab Instruments, Inc. The Ramphastos Agency	206A
146	Nicolet Instrument Corporation Technical Communications	208A
141	* Nissei Sangyo Instruments Kaneko-Murakami, Inc. Advertising	245A

INDEX TO ADVERTISERS IN THIS ISSUE

CIRCLE INQUIRY NO.	ADVERTISERS	PAGE NO.
140	* Norton Plastics & Synthetics Division Northlich, Stolley of Akron, Inc.	295A
143	Nuclear Equipment Corporation KREatiVELY Designed	149A
159–161	* Oceanography International Corporation Gianturco & Michaels, Inc. Advertising	213A
158	* Ohaus Scale Corporation Michel-Cather, Inc.	109A
157, 162	* Orion Research, Inc. OBC Advertising	103A, 293A
156	Oxford Laboratories Inc. O/L Advertising	240A
175	Pacific Photometrics Elizabethan Advertising	210A
212	Packard Instruments Mandabach & Simms, Inc.	225A
169	Parr Instrument Company F. Willard Hills Advertising	151A
176	PCR Research Chemicals, Inc. Media Marketing Inc.	278A
195	* Pedersen Instruments Benjamin Paul Harold Advertising	239A
163, 172, 185, 186, 214, 215	* Perkin-Elmer Corporation Marquardt & Roche, Inc. Advertising	111A–114A, 115A, 116A–117A, 118A, 264A, 270A
208–210	Perkin-Elmer, Coleman Instrument Division	233A
213	Phase Separations, Limited Peter Kershaw Associates	259A
170–171, 177–180	* Philips Electronic Instruments, Inc.	136B, 136C, 179A
174, 198	* Philips Electronic Instruments, Inc. Shepherd, Tibball, Galog Associates	207A, 289A
211	* Physical Electronics Industries, Inc. Visual-Media, Inc.	121A
217	Pierce Chemical Company Pierce Ad-Graphics	200A
173	Plenum Publishing Company	238A
154	* Precision Sampling Corporation William U. Stracener	280A
165, 166, 204	* Princeton Applied Research Corporation The Message Center	175A 186A–187A
153	* Princeton Gamma-Tech. Raytector, Inc.	161A
164, 168	Pye Unicam, Ltd.	224B, 224C
249	QuadRex J. Wethersbee & Assoc.	230A
243	Regis Chemical Company Dick Loew & Associates Advertising	249A
245	Reliance Glass Co.	258A
181	RFR Corporation Alden Advertising Inc.	151A
183	* Rheodyne Bonfield Associates, Inc.	286A
184	Riber Data Systems Marken Communications Associates	244A
182	Rigaku Harry B. Hill Company	231A
187	Sadtler Research Laboratories, Inc. Stephen & Sons Enterprises	283A
192	* Sargent-Welch Scientific Company Polytech Advertising	237A
216	* Schoeffel Instrument Corporation Tek-Mark, Inc.	288A
205	Schott & Gen., Inc. Bloom-Zagoren, Inc.	216A
191	Scientific Glass Engineering Arden Advertising Agency	279A
246	The Separations Group	288A
193	Shimadzu Scientific Instruments, Inc.	167A
244	Shrader Analytical and Consulting Laboratories, Inc.	226A
190	* Siemens Hanson, Fassler, Kolody, Inc.	203A
247	* G. Fredrick Smith Chemical Co. Andrew Show Advertising	200A
206, 207	Spectramétrics S. Gunnar Myrbeck & Company, Inc.	242A, 243A
189	Spectra Physics Paul Pease Advertising, Inc.	304A–305A
188	SPEX Industries Seymour Nussenbaum	249A
199	* Techne Incorporated Brunswick Advertising	259A
200	Tektronix-IDP Young, White & Roehr, Inc.	299A
97, 98, 106, 107, 120, 124, 151, 152, 203, 252	* The Torsion Balance Company Douglas Turner, Inc.	241A
201, 202	* Tracor Analytical Instruments Aim Advertising Agency	153A, 194A
102–104	Tracor Northern Aitchnew Energetics	163A
218	* Valco Instruments Company Cooley & Shillinglaw, Inc.	216A
1–4, 196–197, 220–221, 222–226	* Varian Moran, Lanig & Duncan Advertising	217A, 219A, 221A, 223A
219, 232	* Varian, LSE Division Tycer-Fultz Ltd.	218A, 224A
227	Varian-MAT Shepherd, Tibball, Galog Associates	215A
236–242	* Waters Associates Edward W. Fischer & Assoc.	168A–169A
229	* Waters Associates Marketing Dimensions, Inc.	257A
231	Wescan Instruments, Inc. W. W. Love Advertising	214A
230	* Whatman, Inc. J. S. Lanza & Associates	100A
228	John Wiley & Sons, Inc. 605 Advertising Group	266A
234	* Wilks Scientific WILSCI Advertising	229A
235	Carl Zeiss Young & Rubicam, Inc.	136A

** See ad in ACS Laboratory Guide*

*** Company so marked has advertisement in the foreign regional edition only*

Advertising Management for the American Chemical Society Publications

CENTCOM, LTD.

Thomas N. J. Koerwer, President; James A. Byrne, Vice President; Clay S. Holden, Vice President; Benjamin W. Jones, Vice President; Robert L. Voepel, Vice President; C. Douglas Wallach, Vice President, 25 Sylvan Rd. South, Westport, Connecticut 08880 (Area Code 203) 226-7131

ADVERTISING SALES MANAGER
James A. Byrne

SALES REPRESENTATIVES

Atlanta, GA . . . Robert E. Kelchner, CENTCOM, Ltd. Telephone: 203-226-7131

Boston, MA . . . Don Davis, CENTCOM, LTD. Telephone 203-226-7131

Chicago . . . Thomas Hanley, CENTCOM, LTD., 540 Frontage Rd., Northfield, Ill. 60093. 312-441-6383.

Cleveland . . . James Pecoy, CENTCOM, LTD., Suite 205, 18615 Detroit Ave., Lakewood, Ohio 44107. 216 228-8050.

Houston . . . Robert LaPointe, CENTCOM, LTD., 415-692-0949.

Denver . . . Clay S. Holden, CENTCOM LTD., 213-776-0552.

Los Angeles 90045 . . . Clay S. Holden, CENTCOM, LTD., Newton Pacific Center, 3142 Pacific Coast Highway, Suite 200, Torrance, CA 90505, 213-325-1903

New York 10017 . . . Don Davis, Richard L. Going, CENTCOM LTD., 60 East 42nd St., 212-972-9660

Philadelphia . . . Richard L. Going, CENTCOM LTD., GSB Building, Suite 510 1 Belmont Avenue Bala Cynwyd, Pa. 19004. Telephone: 215-667-9666

San Francisco, CA . . . Robert LaPointe, CENTCOM, LTD., Room 235, 1499 Bayshore Highway, Burlingame, CA 94010. Telephone: (415) 692-0949

Westport 06880 . . . Don Davis, CENTCOM, LTD., 25 Sylvan Rd. So., 203-226-7131.

Manchester, England . . . Jill E. Loney, Technomedia Ltd., 216, Longhurst Lane, Mellor, Stockport, SK6 5PW, Telephone: 061-427-5660

Reading, England . . . Malcolm Thiele, Technomedia Ltd., Wood Cottage, Shurlock Row, Reading, RG10 OOE. Telephone 073-581-302

Paris, France . . . Patric B. Hale, Technomedia Ltd., 18 Rue Gounod, 92 Saint-Cloud, Paris. Telephone: 602-24-79

Tokyo, Japan . . . Haruo Moribayashi, International Media Representatives Ltd., 1, Shibe-Kotohiracho, Minato-ku Tokyo. Telephone: 502-0656

PRODUCTION DEPARTMENT

Production Director
Joseph P. Stenza

Advertising Production Assistant
Barbara Aufderheide

For Silylation in Gas Chromatography if

BSTFA

bis(trimethylsilyl)trifluoroacetamide

is your reagent of choice specify

REGISIL™

from REGIS

Here are some good reasons why:

■ With REGISIL from REGIS you obtain BSTFA from its prime source ... REGISIL is manufactured by REGIS under license, U.S. Patent 3,415,864 (1968).

■ REGISIL is the highest quality BSTFA available anywhere...99+% pure.

■ REGIS is known for its derivatization technology . . . its chromatography group is skilled in derivatization practices, procedures, and new product development to aid you in your GC, TLC and HPLC work.*

*Exclusive Regis products developed by the Regis chromatography group: Regisil, TAB Reference Standards, Tabsorb, Sterosorb, Col-Treet, Fluorotags, Chromotags, Tuned Solvents, PMD.

REGIS offers REGISIL:

	Code No.	Price
BSTFA (neat)	270124	$44/100 g
BSTFA - 1% TMCS	270134	$44/100 g
BSTFA - 10% TMCS	270132	$17/4x5 g

REGIS also offers deuterated —BSTFA for GC/MS work. The complete Regis chromatography line, with price and product description is presented in a new Regis Chromatography Catalog available upon request.

SPECIAL OFFER

A Regis exclusive . . . a 228 page book titled A USER'S GUIDE TO CHROMATOGRAPHY featuring helpful, practical information on GC, TLC, and HPLC. Over 30 pages in the GUIDE are devoted to derivatization, including extensive BSTFA references and application data. The GUIDE sells for $5.95 (including postage and handling). Send check or purchase order. With your GUIDE purchase you will receive a $5 REBATE COUPON applicable to your first REGISIL order or any other items in the GUIDE totaling $25 or more.

Here is how to get on the Regis mailing list to receive the new Regis Chromatography Catalog and other Regis mailings helpful to you . . .

Phone REGIS 312-967-6000
TWX REGIS 910-223-0808

Write REGIS, or if you find it easier, use the READER SERVICE POSTAGE PAID REPLY CARD herewith.

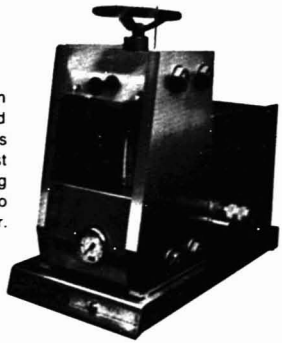
REGIS CHEMICAL COMPANY
8210 Austin Avenue, Morton Grove, IL 60053

Visit Regis booths No. 311 & 313 at the Pittsburgh Conference

CIRCLE 243 ON READER SERVICE CARD



30-ton motorized hydraulic press for safe, fast reproducible pressing of pellets 13-mm to 44-mm in diameter.



SPEX INDUSTRIES INC.
P.O. BOX 798, METUCHEN, N.J. 08840
(201) 549-7144

CIRCLE 188 ON READER SERVICE CARD

FIRST CLASS
Permit No. 25682
Philadelphia, Pa. 19101

BUSINESS REPLY CARD
No postage stamp necessary if mailed in the United States

POSTAGE WILL BE PAID BY

ANALYTICAL CHEMISTRY
P. O. Box #8660
Philadelphia, Pennsylvania 19101

NEW PRODUCTS, CHEMICALS, LITERATURE: 401 402 403 404 405 406 407 408 409 410 411 412 413 414 41
416 417 418 419 420 421 422 423 424 425 426 427 428 429 430 431 432 433 434 435 436 437 438 439 440 441 44
443 444 445 446 447 448 449 450 451 452 453 454 455 456 457 458 459 460 461 462 463 464 465 466 467 468 46
470 471 472 473 474 475 476 477 478 479 480 481 482 483 484 485 486 487 488 489 490 491 492 493 494 495 49

ADVERTISED PRODUCTS: 1 2 3 4 5 6 7 8 9 10 11 12 13 14 15 16 17 18
20 21 22 23 24 25 26 27 28 29 30 31 32 33 34 35 36 37 38 39 40 41 42 43 44 45
47 48 49 50 51 52 53 54 55 56 57 58 59 60 61 62 63 64 65 66 67 68 69 70 71 72
74 75 76 77 78 79 80 81 82 83 84 85 86 87 88 89 90 91 92 93 94 95 96 97 98 99
101 102 103 104 105 106 107 108 109 110 111 112 113 114 115 116 117 118 119 120 121 122 123 124 125 126
128 129 130 131 132 133 134 135 136 137 138 139 140 141 142 143 144 145 146 147 148 149 150 151 152 153
155 156 157 158 159 160 161 162 163 164 165 166 167 168 169 170 171 172 173 174 175 176 177 178 179 180
182 183 184 185 186 187 188 189 190 191 192 193 194 195 196 197 198 199 200 201 202 203 204 205 206 207
209 210 211 212 213 214 215 216 217 218 219 220 221 222 223 224 225 226 227 228 229 230 231 232 233 234
236 237 238 239 240 241 242 243 244 245 246 247 248 249 250 251 252 253 254 255 256 257 258 259 260 261

Name_____ Position_____

Company_____

Street_____ City_____

State_____ Zip_____ Telephone_____

USE . . .

these postage paid reply cards for free data

on all products advertised in this issue.

nalytical Chemistry FEBRUARY 1978 Valid through June 1978

EW PRODUCTS, CHEMICALS, LITERATURE:																									
5	417	418	419	420	421	422	423	424	425	426	427	428	429	430	431	432	433	434	435	436	437	438	439	440	441	442
3	444	445	446	447	448	449	450	451	452	453	454	455	456	457	458	459	460	461	462	463	464	465	466	467	468	469
0	471	472	473	474	475	476	477	478	479	480	481	482	483	484	485	486	487	488	489	490	491	492	493	494	495	496

DVERTISED PRODUCTS:								1	2	3	4	5	6	7	8	9	10	11	12	13	14	15	16	17	18	19
0	21	22	23	24	25	26	27	28	29	30	31	32	33	34	35	36	37	38	39	40	41	42	43	44	45	46
7	48	49	50	51	52	53	54	55	56	57	58	59	60	61	62	63	64	65	66	67	68	69	70	71	72	73
4	75	76	77	78	79	80	81	82	83	84	85	86	87	88	89	90	91	92	93	94	95	96	97	98	99	100
1	102	103	104	105	106	107	108	109	110	111	112	113	114	115	116	117	118	119	120	121	122	123	124	125	126	127
8	129	130	131	132	133	134	135	136	137	138	139	140	141	142	143	144	145	146	147	148	149	150	151	152	153	154
5	156	157	158	159	160	161	162	163	164	165	166	167	168	169	170	171	172	173	174	175	176	177	178	179	180	181
2	183	184	185	186	187	188	189	190	191	192	193	194	195	196	197	198	199	200	201	202	203	204	205	206	207	208
9	210	211	212	213	214	215	216	217	218	219	220	221	222	223	224	225	226	227	228	229	230	231	232	233	234	235
6	237	238	239	240	241	242	243	244	245	246	247	248	249	250	251	252	253	254	255	256	257	258	259	260	261	262

ame_____ Position_____

ompany_____

reet_____ City_____

ate_____ Telephone_____

FIRST CLASS
Permit No. 25682
Philadelphia, Pa.
19101

BUSINESS REPLY CARD
No postage stamp necessary if mailed in the United States

POSTAGE WILL BE PAID BY

ANALYTICAL CHEMISTRY
P. O. Box #8660
Philadelphia, Pennsylvania 19101

Students Instructors Researchers Problem-Solvers . . .

keep on top of recent advances in analytical chemistry.



MODERN CLASSICS IN ANALYTICAL CHEMISTRY

Volume II

Edited by Alvin L. Beilby

A selection from the best feature articles that appeared in issues of ANALYTICAL CHEMISTRY from 1970 through 1975.

Particularly suitable as supplementary reading for the advanced student of analytical chemistry and for those who must keep up with the latest developments in analytical chemistry and instrumentation, this convenient collection of source material contains valuable information presented only in outline form in many modern textbooks.

Volume II 314 pages (1976) $8.50 paperbound
Volume I 268 pages (1970) $5.75 paperbound

CONTENTS (Volume II)

- Development of Analytical Chemistry
- Spectroscopy (11 articles)
- Electrochemistry (2 articles)
- Chromatography (3 articles)
- Automation and Instrumentation(6 articles)
- Measurement Techniques (7 articles)
- The Analytical Approach (9 articles)
- Art Conservation (2 articles)

SIS/American Chemical Society
1155 16th St., N.W./Wash., D.C. 20036
Please send the following books:
Modern Classics in Analytical Chemistry
_____ (Vol. II $8.50 paperbound)
_____ (Vol. I $5.75 paperbound)
☐ My check for $_____ is enclosed. ☐ Bill me. Postpaid in U.S. and Canada, plus 40 cents elsewhere. (Prices subject to change without notice.)
Name
Address
City State Zip

Just the Right Combination.



A delicate cheese with a fine, light wine. Each brings out the best in the other. And the same holds true for any great combination.

MC/B and EM have created a strong, diversified resource for the full range of laboratory chemicals. The result is just the right combination of sales and marketing, manufacturing, research and service.

MC/B, as an associate of E. Merck, Darmstadt, Germany, serves the market with reagents and specialties for laboratory testing and research, and intermediates for chemical processing. An innovative, new resource capable of responding quickly to your particular needs.

MC/B and EM. Just the right combination for you.

MC/B® MANUFACTURING CHEMISTS, INC.

Associate of E. Merck, Darmstadt, Germany

2909 Highland Avenue, Cincinnati, Ohio 45212 Telephone: (513) 631-0445

REGIONAL SALES OFFICES

East
Suite #16
4 Cornwall Drive
East Brunswick, N.J. 08816
(201) 257-7900

Central
Suite #404
9575 West Higgins Rd.
Rosemont, Ill. 60018
(312) 823-1778

West
P.O. Box 7203
2121 S. Leo Avenue
Los Angeles, Ca. 90022
(213) 685-5280

CIRCLE 135 ON READER SERVICE CARD

. . . continued from page184 A

Differential Refractometer

The KMX-16 has a coherent laser source that provides greater beam collimation than the mercury or tungsten light sources of conventional instruments. A telescope increases the effective moment arm. Sensitivity is improved tenfold, to 2×10^{-7} refractive index units. Other features include front panel digital readout and closely regulated test cell temperatures (−10 to +165 °C). Reproducibility is specified as 1×10^{-6} refractive index units. Chromatix **460**

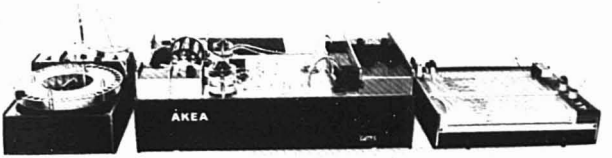
Reaction Calorimeter

Featuring a versatile, stirred reactor combined with an automatic adiabatic temperature control system, this calorimeter provides complete facilities for handling chemical reactions under heat and pressure to 350 °C and 200 psig, and for measuring, controlling, and recording temperature changes associated with such reactions. Precise thermal control is provided by supporting the pressure reactor within a temperature-controlled, spherical chamber in which the temperature can be maintained at any desired working level or matched continuously to the temperature within the reactor itself. All instrumentation is rack mounted for complete flexibility in adapting the calorimeter to meet individual research requirements. Parr Instrument Co. **461**

Ultrasonic Processing System

Model 190 is a 900-W system for processing dispersions, emulsions, or solutions. It is suitable for laboratory or pilot use and may be used for sample treatment in a beaker or in a processing cell at a rate of up to 3 gal/min. Features include modular construction, adjustable power output, a timer and output meter, solid state circuitry, automatic tuning, and a fanless converter. Branson Sonic Power Co. **468**

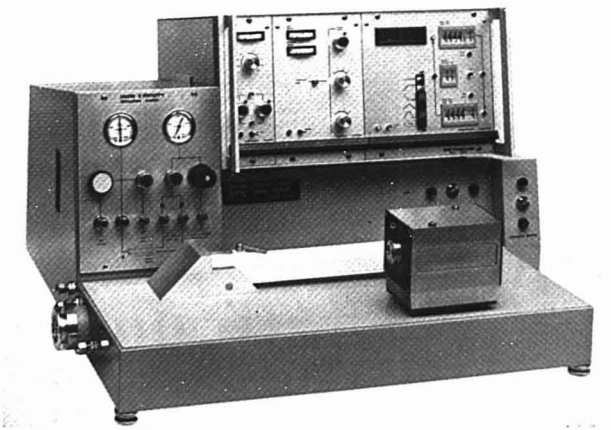
For more information on listed items, circle the appropriate numbers on one of our Readers' Service Cards



This continuous flow automatic chemical analyzer features compactness, portability, and economy. The system automates both industrial and clinical analyses, operating from one to four channels at a rate of up to 80 samples/h. Design flexibility facilitates operator innovation and assembly of analytical manifolds as well as complete factory-prepared units. The system is supported by complete technical services, glassware, and reagents. Lachat Instruments **415**

Accelerating Rate Calorimeter

The ARC is a new analyzer for hazard evaluation of reactive chemicals. Exothermic reactions starting at temperatures between 0 and 500 °C can be studied by permitting a contained sample to undergo thermal decomposition under adiabatic conditions. Data acquired by monitoring this thermal runaway are useful for determining kinetic parameters that describe the decomposition reaction and are helpful for hazard prediction. A built-in microprocessor performs fully automated temperature control and data acquisition. Columbia Scientific Industries **462**



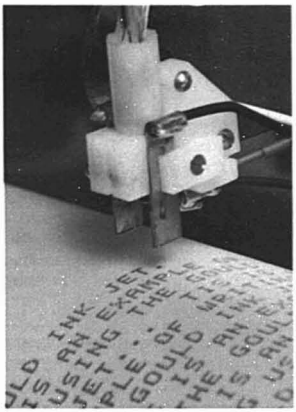
The Setaram differential scanning calorimeter is based on the Calvet detector principle. It features expanded sample volume to 0.4 mL, expanded temperature range of −123 to 827 °C, self-contained gas circulation and pressure control system, vertical or horizontal orientation of the detector, a completely digital, microprocessor-based push-button temperature programmer, and the ability to accept samples either with or without sample cells. Marche Instruments, Inc. **416**

INK JET WILL TELL YOU WHAT HAPPENED, WHEN IT HAPPENED.

Gould's new Ink Jet annotation device allows you to automatically print time, date and other data parameters alongside your Gould analog traces.

The Ink Jet writing system employs the most advanced technology consisting of ink reservoir and electrostatic charging and deflection plates to print highly legible characters in a 5 x 7 dot matrix at chart speeds of up to 50 mm/sec. Any desired annotation of up to 256 characters may be entered by means of our optional keyboard or from an external ASCII parallel data source.

Designed to complement the Gould 2000 Series pressure ink direct writing recorders, Ink Jet

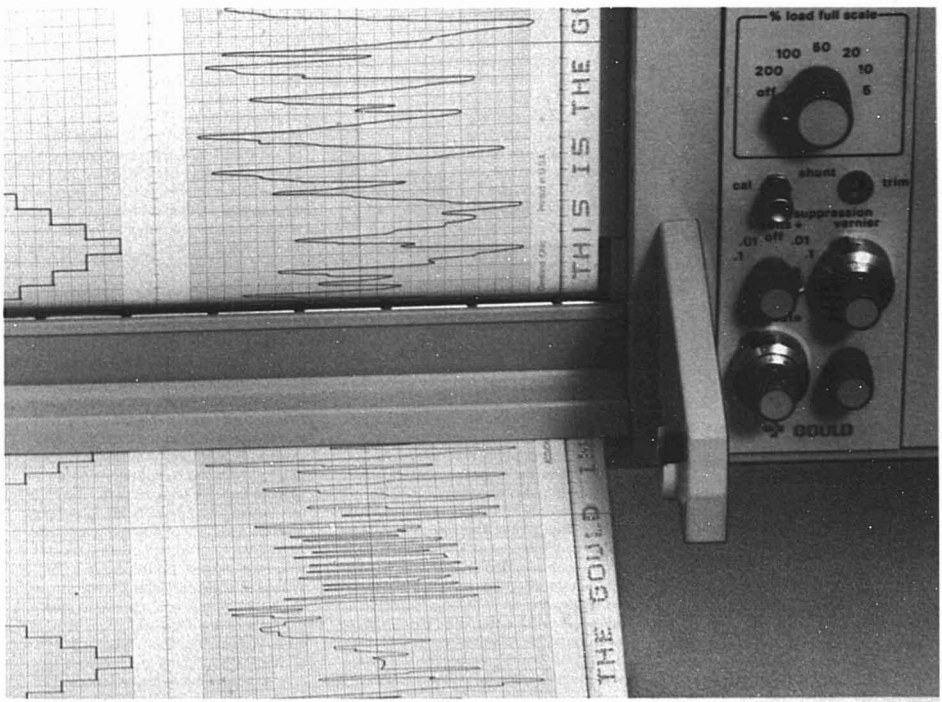


adds an entirely new dimension to analog data display. Medical, industrial, research and engineering users now have a means of immediately annotating all pertinent information while a study is taking place.

Consider the additional breadth of data display that only Ink Jet applications will bring to you. For more information contact, Gould Inc., Instruments Division, 3631 Perkins Ave., Cleveland, O. 44114. Or Gould Alco S.A., 57 rue St. Sauveur, 91160, Ballainviliers, France. **For brochure, call toll free (800) 325-6400, Ext. 77.**

In Missouri: (800) 342-6600.

GOULD



CIRCLE 123 ON READER SERVICE CARD

Alternative Cooling Methods

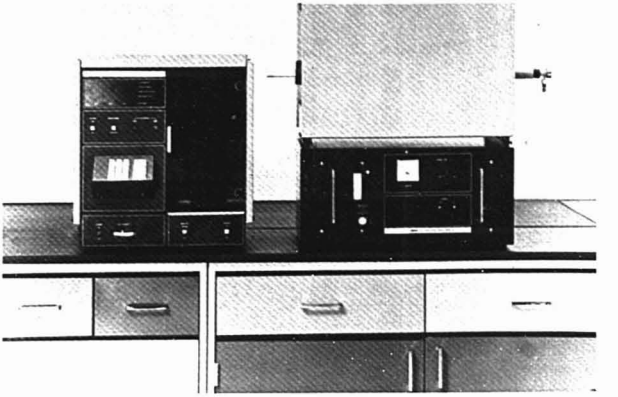
Three "Cooling Packages" are offered as alternatives to the normal additions of dry-ice or liquid N_2 for removing heat at a controlled rate from all types of exothermic reactions. The three basic configurations offered are: (1) a mechanically refrigerated self-contained, temperature-controlled bath that will accept reaction vessels of up to 7½ in. (190 mm) diameter and attain a temperature of −130 °C; (2) a remote-operated "cold-probe" in almost any shape that will fit into existing dewars of various sizes and configurations for maintaining temperature to −100 °C; (3) a circulation pump that can transfer refrigerated fluid from a low-temperature bath to a secondary vessel location. FTS Systems, Inc. **463**

Thermoprogrammer

Designed for applications such as DNA thermal denaturation-renaturation studies, enzyme rates, and microtubule studies, the thermoprogrammer with four individual quartz cuvettes uses a thermoelectric copper block for fast and precise temperature control. The cuvettes, stable over a wide temperature range, are open at the top, making them easier and quicker to fill and empty. Gilford Instrument Laboratories Inc. **469**



The NanoSpec/AFT automatic film thickness gauge is designed for precise and nondestructive measurement of the thickness of dielectric film layers in functional areas as small as 5 μ diameter on patterned wafers and microcircuits. It is computer programmed to measure silicon dioxide, silicon nitride, resist, polysilicon, and other dielectric films with high precision. The NanoSpec/AFT uses a conventional reflection-type optical microscope to measure thickness by the optical interference method. Measurements are automatically made in less than 60 s using the microprocessor-based computer that controls the measurement cycle, does the computation, and provides a printed record of all test data. $20 000. Nanometrics, Inc. **417**



The sulfur analyzer consists of two modules, a sulfur analyzer and a high-temperature resistance tube furnace. The analyzer uses a patented amperometric titration technique, developed specifically to measure sulfur content, and a microprocessor (operated by simple keyboard command) to handle computations. Features include complete automation, digital readout, high precision (±2%) and accuracy (±3%), and results reported in % and ppm sulfur. Preweighed samples can be analyzed at the rate of one every 2 min. Fisher Scientific Co. **418**

Process Gas Analyzer

The MA-3A precisely monitors and controls process gases in petrochemical, chemical, and gas production application. The instrument operates by a unique mass spectrometer concept. Continuous "real time" mass spectra are available on an oscilloscope, simultaneously with recorded outputs for complete analysis. The system can provide concentrations for an uniimited number of gases (0–600 amu mass range). Sensitivity is in the ppm range. A computer system is also available for data handling. CVC Products, Inc. **466**

Automated Batch Sampler

Model 318 incorporates an electronic control package and an automatically refilled cell, and is designed to sample process streams, reservoirs, holding tanks, plating baths, etc., at regularly timed intervals. It operates unattended on a 24-h basis, and delay times between samples can be varied between 0, 15, and 30 min. The Model 318 interfaces to the Model 303 static mercury drop electrode module or PARC's existing electroanalytical accessories. It can be used with the 174A polarographic analyzer–315A automated electroanalysis controller combination or with the 374-1 and 374-3 polarographic analyzers. Princeton Applied Research Corp. **467**

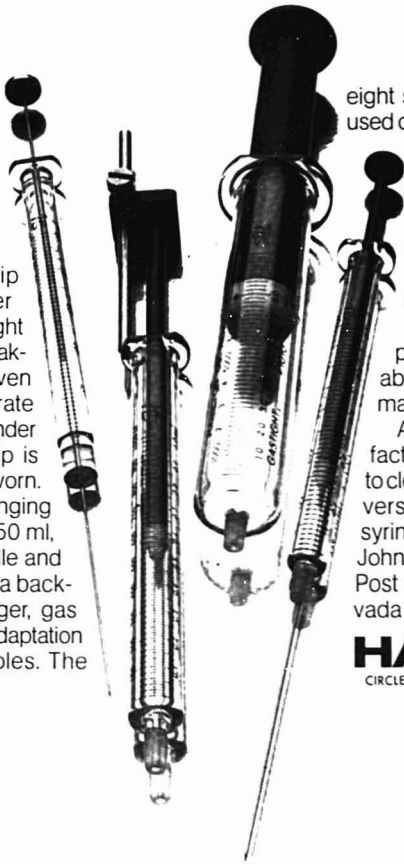
Liquid Circulator

Model C-400 has a built-in temperature control unit and is designed to pass thermostatically controlled liquid through jacketed equipment or through small open or closed vessels. Features include: design for any flow rate between 0 and 15 L/min, temperature stability better than ±0.1 °C over the whole range of −20 to 80 °C, overheat cut-out and liquid level fail safe system, and solid state proportional control with zero voltage switching. Techne Inc. **465**

Centrifugal Freeze Dryer

Spin-Freeze is a small, lightweight centrifuge that freezes and lyophilizes small samples without the use of refrigeration. By connecting the Spin-Freeze to a vacuum pump, the pressure over the samples is lowered causing rapid evaporation. It uses the rapid evaporation to lower the temperature of the sample until freezing occurs. The rotor has both ½- and ⅜-in. holes to accommodate a variety of sample tube sizes. A totally enclosed ball bearing motor spins the rotor at 1600 rpm. The Spin-Freeze is equipped with a timer for 0–60 min of spin and a brake to stop the rotor at any time during the process. A ¾-in. aluminum tube and 3 ft of gum rubber tubing are provided for connection to the vacuum source. Labconco Corp. **464**

THE SYRINGES WITH 99.9% VERSATILITY.



It may not solve all your sample handling problems, but a Hamilton 1000 Syringe may be the most useful syringe you could have around your lab. Just look at this versatility.

The exclusive Teflon tip at the end of the plunger makes the syringe gas tight and liquid tight. There's no leakage at pressures up to seven atmospheres and a leak rate of less than 3 μl per hour under partial vacuum. And the tip is replaceable if it becomes worn.

There are 11 models ranging in capacities from 50 μl to 50 ml, with a wide variety of needle and plunger options, as well as a backfill plunger, threaded plunger, gas tight valve needle, and an adaptation for flushing out gas samples. The eight syringes over 500 μl may be used over a wide temperature range.

The 1000 syringes are ideal for precision measurement of gases, and are equally suited for handling highly corrosive, viscous, or normal liquids.

Your sample contacts essentially inert glass and Teflon.

All barrels, plungers and plunger tips are interchangeable within a given capacity, and may be purchased separately.

Add to all those features the fact that a 1000 syringe is easy to clean and you have almost 100% versatility for an all-purpose lab syringe. For more details, write to John Nadolny, Hamilton Company, Post Office Box 10030, Reno, Nevada 89510.

HAMILTON

CIRCLE 96 ON READER SERVICE CARD



This flameless AA hardware gives you 238 data points a second — not 5.

Until now, flameless atomic absorption was often flameless atomic **assumption.** Conventional systems were simply too slow to provide all the facts you need in the course of an event that's over in less than a second.

Some remarkable Jarrell-Ash hardware has changed all that. Our Model 850 (world's first totally digital, integral-computer-controlled spectrophotometer). And our FLA-100 graphite tube atomizer. Together, their ultra-fast 100% digital electronics can produce **238** readings per second. That's 238 data points per second, one every 4 **milliseconds!** Not the miserly 4 or 5 per second of other systems.

That's why we use an **oscilloscope** (coupled to a data-translator accessory) to provide all the details for our flameless AA system. (Strip-chart recorders simply couldn't keep up.) Now for the first time you can see complete flameless AA results. Explore **every aspect** of this high-speed excitation chemistry.

The oscilloscope tracing presents the exact peak shape. (No need to guess what's happening between dots.) You can compare sample runs at various temperatures for **best results** — they're conveniently superimposed on the cathode-ray tube. See any signal distortion from matrix interferences. Determine rate of atom production. Learn exactly when the first atoms appear during an analysis. (Should there be any error in the curve, you can adjust furnace controls pronto.)

All this information was always "there," of course. It took Jarrell-Ash to make it **visible.**

Send today for product literature. And make a note to yourself to see our system **in action** at the Pittsburgh Conference.

CIRCLE 72 ON READER SERVICE CARD



Jarrell-Ash
A Division of Fisher Scientific Company

711 Forbes Avenue
Pittsburgh PA 15219
(412) 562-8543

The Intelligent Approach to LC.

Intelligence adds a critical new dimension to today's most dynamic analytical problem solver—Liquid Chromatography.

Waters, building on its proven base of leadership in LC instrumentation, has developed a new generation of "Intelligent" LC modules.

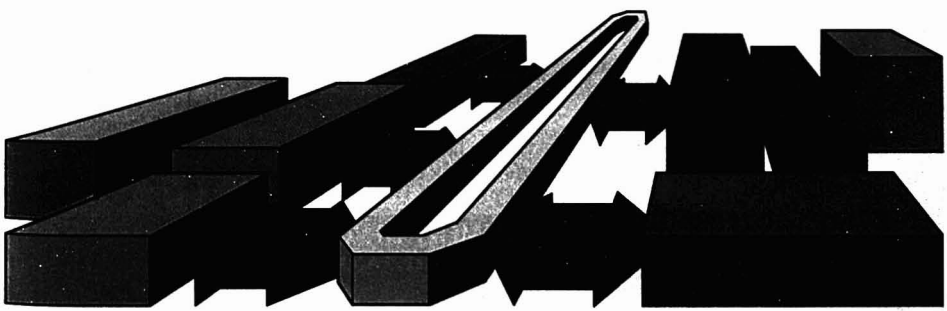
This Intelligent Approach incorporates microprocessor-based Intelligence in every module that does more than just automate specific fixed functions. These modules can stand alone, perform independently, and communicate with each other. The user can now tailor his LC instrumentation to meet specific problem-solving needs.

This is all possible because of a unique system architecture called Intelink™. Intelink permits Distributed Chromatographic Processing (DCP™)—total system coordination without inflexible central control. Intelligent LC instrumentation has the capacity to evolve—new modules can be added anytime.

Advanced equipment design is just one aspect of The Intelligent Approach to LC. Our application support, training programs, specialized technical representatives, and worldwide seminars ensure unrivaled levels of customer success. Our position as world leader in LC is the result of our total commitment to provide you with advanced products and successful solutions.

Find out what Waters' Intelligent Approach means to you. Write for complete information.

Waters Associates
Milford, Massachusetts 01757



CIRCLE 229 ON READER SERVICE CARD

NEW
*THREAD-TITE™ ⅝ MINI VIALS

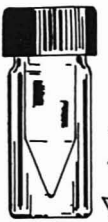
SAVE

BUY MINIVIALS DIRECT FROM MANUFACTURER

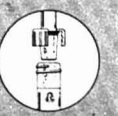
SAVE up to 25%

Quantity discounts available

Send for list of sizes, related accessories, and prices!



*THREAD–TITE™ MINI–VIALS



•Threaded ⅝ outer joint provides positive pressure and vacuum connections to glassware assemblies.
•Compatible with ⅝ 14/20 glassware.
•Syringe penetrable closures.

*Patent pending

*THREAD–TITE™ MICRO SYSTEMS



•Fractional distillation
•Reflux
•Freeze drying
•Derivatization
•Radiosyntheses
•Extraction
•Concentration

Available in organic kits for both Micro and Semi-Micro scale.

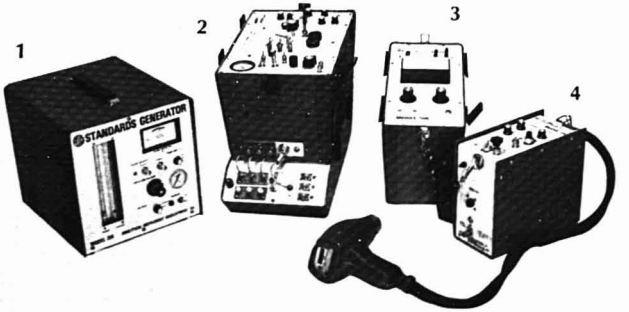
RELIANCE GLASS WORKS, INC.

17 Gateway Rd. Dept. AC-28 Bensenville, IL 60106 (312) 766-1816

CIRCLE 245 ON READER SERVICE CARD

THE AID FAMILY

SEE US AT BOOTH 1144 THE PITTSBURGH CONFERENCE



1. STANDARDS GENERATOR
2. PORTABLE GAS CHROMATOGRAPH
3. PORTABLE OZONE ANALYZER
4. PORTABLE TOTAL HYDROCARBON ANALYZER

AID MANUFACTURES A LINE OF INSTRUMENTS TO MEET THE SCIENTIST'S NEEDS IN THE FIELD OR IN THE LABORATORY. CHECK THE NUMBER BELOW OR WRITE AID FOR THE FULL FAMILY STORY.

ANALYTICAL INSTRUMENT DEVELOPMENT, INC.

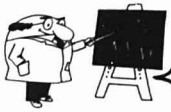
RT. 41 & NEWARK RD., AVONDALE, PA. 19311

215-268-3181 TELEX 835441

CIRCLE 62 ON READER SERVICE CARD

"Most chromatographers accept that whichever way you look at it, angular particles are not as good for HPLC use as spherical particles."





"The ideal shape for HPLC adsorbents is spherical - smooth and uniform in size and having constant capacity."

"This should result in the most unbelievable versatility giving value for money, the best separation (with exceptionally fast results because of its optimum packing) and producing the finest peaks."

"HOWEVER, THERE IS ONE PROBLEM !!!"

"It is very difficult to make good, spherical HPLC adsorbents."



But there is a Solution

"Phase Sep have large stocks of spherical materials and can supply many varieties off the shelf. This material has been in successful production for six years and is well known both in Europe and America."

*"Its name? - **SPHERISORB**. We don't make any claim for its performance or structure other than that which is already on the shelf."*



Summary of Spherisorb Range of Materials

Code	Basic Material	Mean Particle Diameter (micron)	Chemical Bonding	Phase Sep Column Typical Efficiency per metre.
S5W	silica	5	–	70000
S10W	silica	10	–	35000
A5Y	alumina	5	–	65000
A10Y	alumina	10	–	35000
A20Y	alumina	20	–	15000
S5ODS	silica	5	ODS	38000
S10ODS	silica	10	ODS	16000
S5CN	silica	5	Nitrile	60000 (in partition mode)

PLUS TWO NEW TYPES TO BE RELEASED ON STAND 629 AT THE PITTSBURGH CONFERENCE ON ANALYTICAL CHEMISTRY AND APPLIED SPECTROSCOPY.

PHASE SEPARATIONS LIMITED

255 Oser Ave, Hauppauge, NY 11787, USA
Telephone (516) 231-3380 and 3389

Deeside Industrial Estate, Queensferry, Clwyd, Great Britain
Telephone Chester (0244) 816444 Telex 61459

CIRCLE 213 ON READER SERVICE CARD

ULTRAPURE
chemicals

When you simply can't tolerate impurities or uncertainties in your reagents

Over 100 of the purest reagents and chemicals available anywhere in the world. Every product is accompanied by a detailed **Certificate of Analysis** of the actual lot supplied. In terms of spectrochemically detectable impurities, **ULTREX** products are typically **99.995%** to **99.99995%** pure. And the extremely low content of all impurities (often at the parts per billion level) satisfies the most rigid use requirements.

Whenever your requirements for purity and product definition are stringent, ULTREX ultrapures can indeed insure against loss of time, effort, and other expenses.

Consider ULTREX when you just can't afford to gamble with impurities or uncertainties.

ULTREX®

Write for new ULTREX ultrapure Reagent brochure.

J. T. Baker Chemical Co.
Phillipsburg, N.J. 08865
201 859-5411

J.T.Baker® CHEMICALS

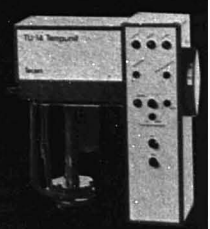
CIRCLE 21 ON READER SERVICE CARD

Immersion Circulators

See these brand new advanced temperature controllers

0.005°C

Controlling to within 0.005°C and working over a range −20°C to +180°C, the Tempunit is in a class by itself. Features include fail safe cut-outs, variable and preset temperature controls, adjustable proportional band-width and a highly efficient pump/stirrer.

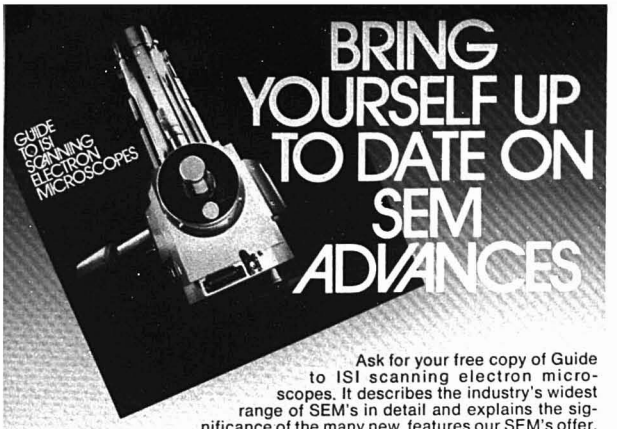


The Tempette is the controller for standard water bath applications. This unit offers with elegant simplicity 0.02°C control over a 0°C to 80°C range.

Techne

Techne Incorporated
3700 Brunswick Pike
Princeton, New Jersey 08540
(609) 452-9275 Telex 84 3319

CIRCLE 199 ON READER SERVICE CARD



BRING YOURSELF UP TO DATE ON SEM ADVANCES

Ask for your free copy of Guide to ISI scanning electron microscopes. It describes the industry's widest range of SEM's in detail and explains the significance of the many new features our SEM's offer. For example, why is dual magnification display useful? What's gamma control? How do you mate SEM's and X-ray spectrometers? That and much more in the *Guide*.

Request your copy now. From ISI, the most popular choice for SEM's the world over.

ISI **International Scientific Instruments, Inc.**
3255-6C Scott Boulevard • Santa Clara, CA 95050
Phone (408) 249-9840

Europe– International Scientific Instruments, Inc., GmbH, 8 Munchen 90, Rotbuchenstrasse 1/West Germany/phone 089/690 0696/7.
U.K.– ISI, Inc., Waterwitch House, Exeter Road, New Market, Suffolk, England. Phone: Newmarket (0638) 5031; TLX =817278.

CIRCLE 108 ON READER SERVICE CARD

CHEMICAL CARCINOGENS

A tape recorded in-depth look at the problem of hazardous substances in the environment.

5 Speakers
Length: 164 Minutes
14 Figures

The Speakers:

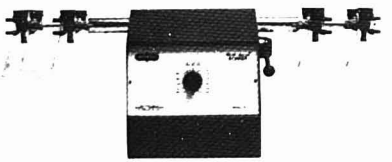
H.H. Fawcett—Purpose of Symposium
B. Carroll (N.I.O.S.H.)—Toxic Substances List—What, Why, How, For Whom
W.F. Malone (Nat'l. Cancer Inst.)—Occupational Cancer Control and Prevention
N. Meade (EPA)—Actual vs. Acceptable Risks from Asbestos
W.S. Wood (Wood Assoc.)—Engineering Approach to Control of Chemical Carcinogen Exposure

PRICE: $18.00 (Cassettes Only)
(Postpaid, includes printed copies of slides used)

Order From: American Chemical Society
1155 Sixteenth Street, N.W.
Washington, D.C. 20036
ATTN: Dept. AP

Name _____
Address _____
City _____
State _____ Zip _____
(allow 4 to 6 weeks for delivery)

Reliable Shakers

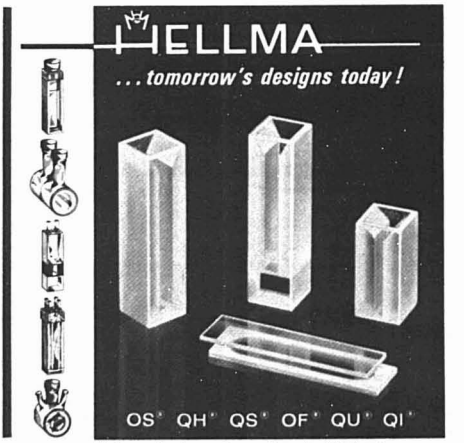


When it comes to reliable performance, you can count on Burrell Wrist-Action™ Shakers. They're ruggedly built for long life . . . some units have been in operation over forty years. Burrell Shakers duplicate a hand-mixing swirl with an even motion at all speeds for as long as necessary. And Burrell's unique Build-Up® System lets your Shaker grow as your lab grows . . . from a Shaker that holds 1 to 4 flasks to a Shaker that holds 24. Burrell parts and accessories are interchangeable. Burrell Wrist-Action Shakers with Build-Up design . . . the Reliable Shaker.

Write for our literature.

BURRELL **BURRELL** CORPORATION
2223 Fifth Avenue Pittsburgh, Pa. 15219
Telephone 412-471-2527

CIRCLE 25 ON READER SERVICE CARD



Hellma—the largest assortment of highest precision glass and quartz cells.
Standard · Flow-through · Constant-temperature
Anaerobic · Special Designs
Also available—ULTRAVIOLET LIGHT SOURCES
Deuterium Lamps · Mercury Vapor Lamps
Hollow Cathode Lamps · Power Supplies

HELLMA CELLS, INC.

Write for literature
Box 544
Borough Hall Station
Jamaica, New York 11424
Phone (212) 544-9534

CIRCLE 94 ON READER SERVICE CARD

Manufacturers' Literature

Pellicular Column Packings. Pellicular media and the newer microparticle media are compared and found to be complementary with a place for each type in HPLC. 12 pp. Whatman Inc. **470**

Fluorescence Spectrophotometers. Describes features, applications, and accessories for the MPF-44A and MPF-43A high-performance fluorescence spectrophotometers. 12 pp. Perkin-Elmer Corp. **471**

Carbon Bed Adsorption Monitoring System. Based on a Miran-II infrared analyzer, the system can be sensitized to measure either a specific organic solvent or to make a total hydrocarbon measurement and to monitor air at the inlet and outlet of the adsorption beds. 2 pp. Wilks Scientific Corp. **472**

Toxicity Testing of Chemical Products. Describes laboratory methods for determining toxicologic hazards posed by chemical products intended for industrial or consumer use. 6 pp. United States Testing Co., Inc. **473**

Chromatography. *Chromatogram,* Vol. 1, No. 1, features articles on analysis of theophylline in body fluids by LC, practical LC solvent considerations, and effect of column diameter on LC column performance. 4 pp. Altex Scientific Inc. **474**

Temperature Detectors. Describes the Type 100 R 30 Thermafilm platinum resistance temperature detectors. 4 pp. Matthey Bishop, Inc. **475**

Gas Chromatography. *Gas-Chrom Newsletter,* November 1977, features articles on packed GC columns, a new reagent for resolving enantiomeric amines and alcohols, high-temperature liquid crystal GC phases, and mycotoxin standards. 12 pp. Applied Science Laboratories **476**

Strip Chart Recorders. Describes six single pen and integrating recorders including Models 70-700, 70-750, 70-800, 70-300, 70-900, and 70-950. 3 pp. Gow-Mac Instrument Co. **477**

Balances. Features a balance selector chart that enables weighing requirements for scientific, educational, and many industrial applications to be matched with the capabilities of a wide range of balances. 16 pp. Ohaus **478**

Liquid Chromatography. Applications notes 33, 34, and 35 cover HPLC analysis of cyclopeptide toxins in *Amanita Phalloide* mushrooms, analysis of theophylline in plasma by reverse-phase LC, and trace determination of linear alkylbenzene-sulfonate surfactants in wastewater using reverse-phase ion pair partition chromatography. Varian Instrument Div. **479**

Benzene in Gasoline. The latest issue of *Current Peaks* describes the use of a Series-S gas chromatograph to measure benzene in gasoline by the latest ASTM method. 3 pp. Carle Instruments, Inc. **480**

Impurities in Ethylene. An application note describes the use of a Series-S gas chromatograph for the analysis of impurities in ethylene, including CO and CO_2. 4 pp. Carle Instruments, Inc. **481**

Lasers. Data sheet outlines the diverse line of lasers including helium neon, CO_2, and argon/krypton ion lasers. 1 p. Coherent **482**

Ozone Meter. Describes the Model 2000 portable chemiluminescent ozone meter. 8 pp. Columbia Scientific Industries Corp. **483**

Chromatography Supplies. The second issue of *The Chromatography Optimizer,* a newsletter of new accessories and supplies for both gas and liquid chromatography, includes information on three fraction collectors, a water bath, and air sampling devices. 4 pp. Varian Instrument Div. **484**

Organic Custom Chemicals. Outlines the capabilities and facilities for the custom manufacture of organic chemicals. 4 pp. J. T. Baker Chemical Co. **485**

Spectrum Analysis. Describes and explains theory, implementation, and applications of modern FFT instrumentation. 48 pp. Rockland Systems Corp., 230 W. Nyack Rd., West Nyack, N.Y. 10994

Chromatography and Mass Spectrometry Accessories. Features capillary columns and accessories as well as jet separators, high-temperature micro needle valves, and various other pieces of hardware for GC/MS operation. 16 pp. Scientific Glass Engineering, Inc. **486**

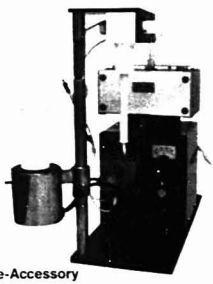
For more information on listed items, circle the appropriate numbers on one of our Readers' Service Cards



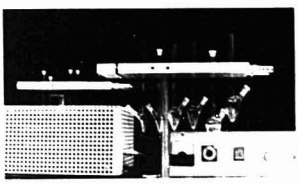
Autoclaves
50 ml to 750 ml
PTFE lined



Digestion Bombs
with PTFE-vessel 10 ml and 250 ml



Hg-, As-, Se-Accessory
for Atomics



Micro-Refluxer for GC + HPLC

Fractioner for UZ · UF-Membranes
PTFE-Labware · SiC-Fibers
Customer-Research · Electronic Business

BERGHOF
West Germany
P.O.Box 1523
D-7400 Tübingen 1

CIRCLE 24 ON READER SERVICE CARD

Multigas IR/UV Analyzer. Describes the Perco II, a nondispersive, single-cell, multiwavelength analyzer for the measurement of one, two, three, or four gas concentrations simultaneously and continuously from one sample. 4 pp. CEA Instruments, Inc. **487**

Tunable Lasers. Wall chart includes 71 common wavelengths for spectroscopic calibration, general physical constants, spectral conversion equivalents, conversion equations, and tuning ranges for the CMX-4 tunable laser. Chromatix **488**

Plastic Products. Features full line of plastic and plastic-lined products including pipe and fittings, valves, expansion joints, flexible couplings, vessels, and vessel accessories. 8 pp. Peabody Doré Corp. **489**

Monitoring Airborne Contaminants. Explains the procedures for collecting aerosol contaminants that occur in particulate form and the air sampling monitors and membrane filters available. 6 pp. Millipore Corp. **490**

Catalogs

Research Products. Features liquid scintillation counting chemicals and accessories, contamination and radiation monitoring instruments, carbon-14 and tritium-labeled compounds, antisera, enzyme substrates, and over 200 research biochemicals. 136 pp. Research Products International Corp. **491**

Instruments and Reagents for Water, Ecology, and Industrial Testing. Catalog 77A describes the expanded line of instruments, testing outfits, and labware and reagents for field or lab tests in public health, ecology, educational, and industrial or energy-related applications. 78 pp. Hellige, Inc. **492**

ACS Solvents. Lists 32 reagent ACS grade solvents and provides extensive information on storage and handling conditions, health and safety precautions, spill and disposal procedures, and DOT hazard regulations. 40 pp. Publication No. JJ-283 available from Eastman Kodak Co., Department 412-L, Rochester, N.Y. 14650

Petroleum Test Instruments. Features the complete line of Herzog instruments including aniline point, automatic breaking point, automatic cloud point, automatic cold filter plugging point, and automatic ring and ball testers. Also includes distillation apparatus and automatic viscometers. 16 pp. Utopia Instrument Co. **495**

Pesticides. Lists nearly 400 purified pesticides for use in pesticide research and analysis. Kits available cover the general categories of fungicides, insecticides, herbicides, and plant growth regulators. 78 pp. Chem Service, Inc. **496**

Glass Columns for Gas Chromatography. Features silane treated glass columns available either empty or packed with stock tested or custom packings as well as column filling accessories, ferrules, and reducers. 16 pp. Supelco, Inc. **493**

Specialty Gases. Details full line of ultrapure specialty gases and gas mixtures and an expanded line of gas handling equipment. 80 pp. MG Scientific Gases **494**







ELECTRO-ANALYTICAL APPARATUS

ELECTRO-ANALYZER, Cat. 1000. For simultaneous or individual determination of copper, lead, zinc, nickel, antimony, cadmium by electro-deposition. For 115/230v, 50/60 Hz. . . without electrodes $1400.00

ULTRA-SPEED ELECTRO-ANALYZER, Cat. 1250. For high speed determinations of copper and lead by electro-deposition. Deposits 1 gram of copper in 8 minutes. Single position instrument. For 115v, 50/60 Hz. . .without electrodes $1550.00

DYNA-CATH, Magnetic Mercury Cathode, Cat. 1510. For rapid separation of metals. For example, analysis of aluminum in zinc-base alloys. For 115v, 50/60 Hz. . .with platinum electrodes $2250.00

Eberbach CORPORATION
P.O. BOX 1024
ANN ARBOR, MICHIGAN
48106

Visit our Booth # 236 at Pittsburgh Conference CIRCLE 65 ON READER SERVICE CARD

Analytica 78

International Exhibition of Biochemical and Instrumental Analysis with European Conference „Biochemische Analytik"

Munich

18 - 22 April 1978

Coupon - Analytica 78

Please, submit further information

Name

Address

Gerald G. Kallman Associates,
30 Journal Square, Jersey City, N.J. 07306,
Tel.: (201) 653 3304, Telex: 710-730-5380 Goodword jcty.

CIRCLE 149 ON READER SERVICE CARD

The answer to your fluorescence problems...

ISA SPECTRO FLUOROMETER



Our JY-3 incorporates the latest developments in optical and analytical technology, offering the best results at the lowest cost. Standard features include:

- Holographic concave grating for the highest possible sensitivity.
- 150 Watt stabilized Xenon source with elliptical focussing mirror
- Ratio reference module
- Superb spectral resolution of 2 to 10 nm, with interchangeable slits
- 5 position multi-cell compartment

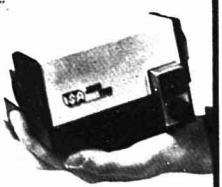
Instruments SA, Inc., J-Y Optical Systems Division, 173 Essex Avenue, Metuchen, N.J. 08840 (201) 494-8660, Telex 844 516. In Europe, Jobin Yvon, Division d'Instruments SA, 16-18 Rue du Canal, 91160 Longjumeau, France, Tel. 909.34.93, Telex JOBYVON 842-692882.

JOBIN YVON Instruments SA, Inc. J-Y Optical Systems Division

CIRCLE 112 ON READER SERVICE CARD

Our SMALL Monochromator

The reasonably priced H-10 measures only 4" x 5" x 3½". It is the perfect monochromator for the OEM manufacturer, or for any application requiring high purity monochromatic light in a compact package. Unique optical design features J-Y's revolutionary new Type III aberration-corrected holographic grating.



FEATURES

100 nm focal length, F/3 aperture, spectral domain 200 to 800 nm or 300 to 1200 nm, resolution 1 nm or better, very low stray light. Full line of accessories. Call or write today for more information on the H-10 and J-Y's comprehensive line of monochromators.

Instruments SA, Inc.
J-Y Optical Systems Division
173 Essex Avenue Metuchen, New Jersey 08840
201-494-8660 Telex 844 516

CIRCLE 113 ON READER SERVICE CARD



Don't inventory all those grades of a solvent when ONE from B&J will do the job... better

- Fewer bottles mean greater safety—fewer hazards.
- Fewer bottles mean less storage space—more lab space.
- Fewer bottles mean lower inventory costs.

You get the best when you order high purity solvents from Burdick & Jackson Laboratories, Inc. All solvents are available in either gallons or quarts.

Send for BJ-25.

BURDICK & JACKSON LABORATORIES, INC.
MUSKEGON, MICHIGAN 49442 (616) 726-3171

CIRCLE 31 ON READER SERVICE CARD

SEE ALL THIS AT CLEVELAND—AND MORE!



You'll miss plenty if you don't see our new thermal analysis equipment at the Pittsburgh Conference.

From the leader: DSC-2 Differential Scanning Calorimeter ■ TGS-2 Thermogravimetric Analyzer ■ TMS-2 Thermomechanical Analyzer ■ Model 240 Automatic Elemental Analyzer ■ and a new microprocessor-controlled temperature programmer. If you can't come—write! Perkin-Elmer Corp., M.S.12, Main Avenue, Norwalk, CT 06856. Or Telephone: (203)762-6915.

PERKIN-ELMER
Expanding the world of analytical chemistry.

CIRCLE 215 ON READER SERVICE CARD

THE ONLY SYSTEM THAT DELIVERS REAGENT GRADE WATER, WITHOUT WATERED-DOWN SERVICE.

Milli-Q.™ From Millipore.

When you buy one, you get more than reagent grade water that exceeds standard purity specifications, you get support and service that exceed what the competition can offer.

Because other systems are mainly sold through distributors; and distributors simply don't have the staff, the expertise, and often the motivation to help in your application.

In contrast, Milli-Q is sold to you direct. And the service you receive from the staff at our network of support centers is total. From the very beginning, you'll have on-site technical assistance, plus help in planning future costs for upkeep.

But more about the Milli-Q itself.

The system takes water that's been pretreated (deionization, distillation or reverse osmosis) and processes it through an activated carbon cartridge to remove dissolved organics; then through two strong acid/strong base mixed-bed ion-exchange cartridges to remove dissolved inorganics; and finally, through a Twin-90 membrane filter to remove all microorganisms and particles larger than 0.22 microns.

The result is the purest water available. And a resistivity meter that comes with the system makes it easier to see that it stays that way.

The cartridges and filter units are disposable. And can be replaced in a couple of minutes without the use of tools.

For more information, call toll-free, 800-225-1380. Or write to us directly. In Massachusetts, call 617-275-9200.

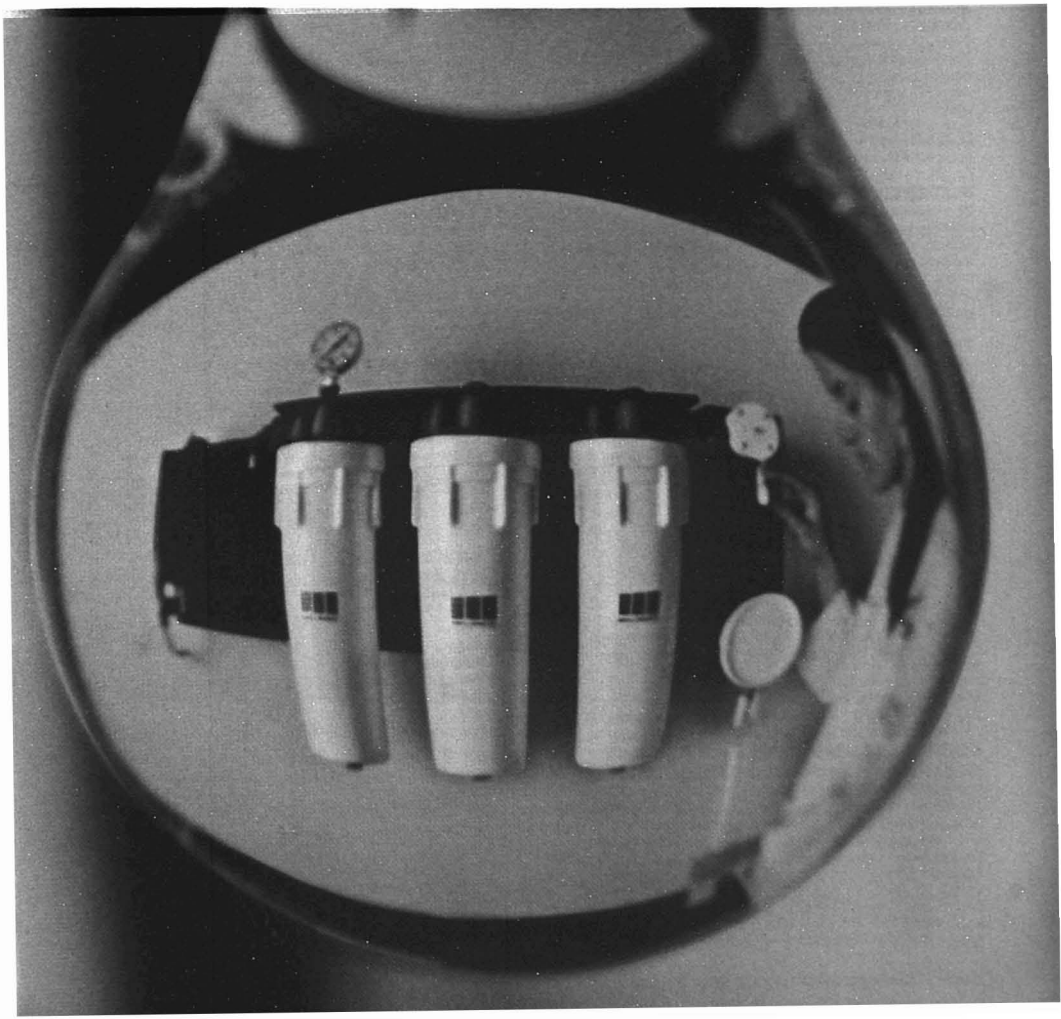
Milli-Q. From Millipore.

Reagent water. Without the watered-down service.

Millipore Corporation, Water Systems Division, Bedford, Mass. 01730.

MILLIPORE®

CIRCLE 150 ON READER SERVICE CARD



Analytical Highlights From Wiley-Interscience

PRACTICE OF THIN LAYER CHROMATOGRAPHY

Joseph C. Touchstone & Murrell F. Dobbins

Explains in easily understood language the hows and whys of performing thin layer chromatography. Each chapter is self-contained and presents all the basics needed to perform a particular separation and the tasks related to it. This is believed to be the first "how-to" book on the subject, offering a practical understanding of TLC.

approx. 416 pp. (1-88042-6) **Dec. 1977** $19.95

PHOTOMETRIC AND FLUOROMETRIC METHODS OF ANALYSIS Metals, Part I

Foster Dee Snell

Condenses all recently published photometric and fluorometric methods for the determination of 57 common and uncommon metals and the rare earths. Each chapter is a quasi-monograph on the determination of one element with references to the original literature. The book reflects the recent development of instruments permitting more rapid, accurate, and economical methods.

approx. 864 pp. (1-81014-2) **March 1978** $99.50 (tent.)

POTENTIOMETRIC WATER ANALYSIS

Derek Midgley & Kenneth Torrance

Describes in detail the theories and practice of potentiometric water analysis and methods for using ion-selective electrodes developed in the past ten years. Emphasizing practical aspects, it covers experimental limitations, statistical treatment of results, titration procedures, and operational features of apparatus.

approx. 384 pp. (1-99532-0) **Feb. 1978** $29.95 (tent.)

THE MINICOMPUTER IN THE LABORATORY With Examples Using the PDP-11

James W. Cooper

Covers in detail the use of the minicomputer for the acquisition and analysis of laboratory data and describes the programming of the DEC PDP-11 minicomputer in language understandable to the beginner. Examples and problems take the reader through each phase of the programming language.

365 pp. (1-01883-X) **1977** $19.50

PATTY'S INDUSTRIAL HYGIENE AND TOXICOLOGY, 3rd Ed. Volume 1: General Principles

Edited by George D. Clayton & Florence E. Clayton

Updated, revised, and expanded first volume of the classic reference work in industrial hygiene. The third edition incorporates recent developments in the field, including major advances since the passage of the Occupational Safety and Health Act of 1970. The scope of the book has been broadened to include agriculture, quality control, environmental pollution, and much more.

approx. 1,504 pp. (1-16046-6) **April 1978** $60.95 (tent.)

TECHNIQUES OF CHEMISTRY, Vol. 12 Separation and Purification, 3rd Ed.

Edited by Edmond S. Perry

The revised third edition of this collection of techniques for the isolation and purification of compounds. **Contents:** Purity: Concepts and Reality, *Morris Zief & A.J. Barnard, Jr.* Solvent Selection for Separation Processes, *Lloyd R. Snyder.* Liquid-Liquid Extraction, *Edward G. Scheibel.* Ion Exchange Chromatography, *Phyllis R. Brown & Anté M. Krstulovic.* Affinity Chromatography, *Sheldon W. May.* Centrifuging, *Charles M. Ambler & Frederick W. Keith, Jr.* Filtration as a Laboratory Tool, *C.S. Oulman & E.R. Baumann.*

approx. 400 pp. (1-02655-7) **April 1978** $27.50 (tent.)

COLORIMETRIC DETERMINATION OF NONMETALS, 2nd Ed.

Edited by the late David F. Boltz & James A. Howell

The second edition is devoted exclusively to the colorimetric determination of traces of nonmetals. New chapters on carbon and oxygen have been included. Chapters have been extensively revised or rewritten, reflecting the development of new and improved methods for the determination of nonmetals in the past twenty years.

approx. 560 pp. (1-08750-5) **Feb. 1978** $33.95

TREATISE ON ANALYTICAL CHEMISTRY PART 2: Analytical Chemistry of Inorganic and Organic Compounds, Vol. 10

Edited by I.M. Kolthoff, Philip J. Elving, & Robert S. Braman

A new volume in this respected series.

Contents: Borons, *Robert S. Braman.* Carbon, *W.E. Chambers, Paul D. Coulter, & Ronald A. Greinke.* Analytical Chemistry of Arsenic, *Richard F. Skonieczny & Richard B. Hahn.* Antimony, *Richard B. Hahn.* Molybdenum, *Gordon A. Parker.* Tungsten, *Gordon A. Parker.* Acknowledgement. References. Index.

approx. 624 pp. (1-49998-6) **March 1978** $34.50

ANALYTICAL APPLICATIONS OF NMR

D.E. Leyden & R.H. Cox

An introduction to the principles, practices, instrumentation, and applications of nuclear magnetic resonance in analytical chemistry. Discusses the theory of NMR, experimental and instrumental aspects, analysis of spectra and determination of structure, carbon-13 NMR, and methods of quantitative measurements, and gives examples of analytical applications.

456 pp. (1-53403-X) **1977** $27.50

THE ANALYTICAL CHEMISTRY OF SYNTHETIC DYES

Edited by K. Venkataraman

A comprehensive survey by numerous authorities. Begins with a classification of dyes for analytical purposes and describes all the important methods for making this analysis, giving examples of structure determination and the disclosure of structures of several commercial dyes. Offers special techniques for ecological and toxicological monitoring.

591 pp. (1-90575-5) **1977** $42.50

SURFACTANTS AND INTERFACIAL PHENOMENA

Milton J. Rosen

This book applies theoretical surface chemistry to understanding the action of surfactants in modifying interfacial phenomena. Surveys the structural types of commercially available surfactants, and discusses interfacial phenomena, the physicochemical principles underlying the action of surfactants in each phenomenon, and the effect of structural changes in the surfactants and environmental changes on their action.

approx. 288 pp. (1-73600-7) **April 1978** $20.00 (tent.)

Available at your bookstore or write to Nat Bodian, Dept. A8504



WILEY-INTERSCIENCE
a division of John Wiley & Sons, Inc.
605 Third Avenue, New York, N.Y. 10016
In Canada: 22 Worcester Road, Rexdale, Ontario

Prices subject to change without notice. 092 A 8504-51

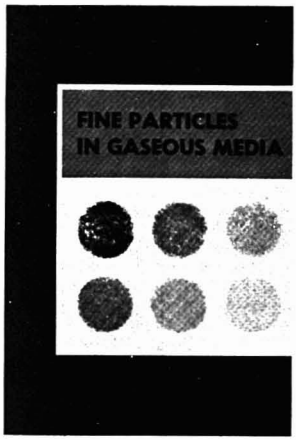
CIRCLE 228 ON READER SERVICE CARD

Particle Analysis

Fine Particles in Gaseous Media. Howard E. Hesketh. Ann Arbor Science Publishers, Inc., P.O. Box 1425, Ann Arbor, Mich. 48106. 1977. $24

Reviewed by B. J. Rubin and G. L. Beyer, Research Laboratories, Eastman Kodak Co., Rochester, N.Y. 14650

This book is recommended especially to professionals engaged in environmental engineering and air pollution studies, but it will also be valuable for anyone working with small particles. The first half provides an excellent summary of forces acting upon particles; this is presented in very readable style, but with enough math to allow particle force calculations by a specialist in the field. Because the principles are developed clearly and concisely, the book might be used by someone entering the field or as a text at the university level.



The chapter on particle collection applies principles already discussed to techniques for air pollution control and measurement of the efficiency of particle removal. A chapter on size measurement provides information on one cascade impactor, but little detail on other sizing techniques, and is the least satisfactory portion of the book.

A final chapter describes simple apparatus that can be constructed and used for flow measurement and particle collection. This is followed by a set of problems involving different sections of the book. These problems and the apparatus might have been more useful if they were appropriately located throughout the text.

The book definitely fills a need as a single source reference depicting the forces that affect small particles, and as such is a worthwhile addition to the library of any professional working with small particles.

Chemical and Biochemical Applications of Lasers, Vol. II. C. Bradley Moore, Ed. ix + 288 pages. Academic Press, Inc., 111 Fifth Ave., New York, N.Y. 10003. 1977. $15

Reviewed by Fred E. Lytle, Dept. of Chemistry, Purdue University, West Lafayette, Ind. 47907

The rapid maturation and commercialization of laser devices continue to have a tremendous impact in all areas of spectroscopy. Treatises discussing these new sources of radiation are quite often concerned with operational principles and basic quantum electronics, leaving the potential user to bridge the gap between theory and practice on his own. The original and continuing aim of this series has been the presentation of introductory expositions that convincingly document the value of the laser to the general audience. As in the initial effort, this second volume achieves that broad goal.

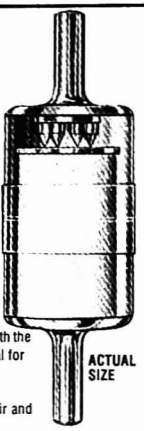
The text is a collection of six independently written chapters. As a result, Volume II has half the topical coverage of the first volume, although the reduction in length of the book and the switch to camera-ready copy kept each article to about the same number of words. The editor has again demonstrated his ability to carefully choose material descriptive of potential or existing broad areas of interest. In addition, all of the authors are recognized scientists who have contributed substantially to the field of laser spectroscopy.

D. H. Levy, L. Wharton, and R. E. Smalley have authored a well-written and organized chapter on laser spectroscopy in supersonic jets. This technique provides a source of molecules having virtually no vibrational or rotational excitation and having an extremely narrow velocity distribution. Consequently, excitation of such samples can yield spectra with a greatly reduced number of bands. As such, the work described should appeal to those analytical chemists interested in high resolution techniques. In this chapter the basic experiment is described in an understandable fashion, while both the capabilities and pitfalls of the equipment are discussed. The examples were well chosen, starting with simple diatomic systems that demonstrate key points, and progressing to complicated systems such as tetrazine and weakly bonded complexes. In addition to the structural studies, one dynamic process is considered, that of Van der Waals' photochemistry. The circle is completed by a final discussion relating how these results can be used to study the supersonic jet itself.

F. Legay is author of a chapter on the use of lasers in the study of solid state vibrational relaxation. In this experiment the sample and an inert gas matrix are codeposited on a surface cooled to a very low temperature. After preparation, some specific vibrational level of the ground electronic state is populated by one of several suitable optical techniques. The time-dependent distribution of this excess energy is then determined by monitoring either the decrease in population of the initially excited level or the increase in population of other levels. The described work should appeal to those analytical chemists interested in applications of matrix isolation spectroscopy. The author attempts to outline the theory, describe the experiment and survey some experimental results. On the whole, the material was hard to assimilate, and the examples did not progress in the smooth autotutorial style of the first chapter. Much of the difficulty presenting the material seemed to be centered about the scarcity of experimental data. The latter fact is constantly demonstrated by the large number of references to unpublished results.

A. Laubereau and W. Kaiser have authored a well-written chapter on the use of lasers in the study of vibrational relaxation in polyatomic molecules in liquids. In these investigations the sample, either neat or dissolved in an

**At last—
a disposable filter
so good, it can
sterilize air—
so economical, you
won't mind
replacing it!**



Balston's new Microfibre* Disposable Filter Unit gives you truly high efficiency filtration—to the sterile level in gases, and 98% retention of 0.3 micron particles in liquids—combined with the convenience of complete disposability. It's ideal for

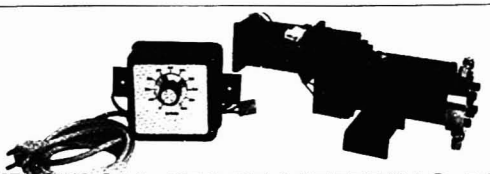
- sterilizing air and other gases—autoclavable
- filtration of samples to analyzers
- complete removal of oil, dirt and water from air and gases to 125 psig
- filtration of small quantities of liquids with minimum hold-up and no cross-contamination

All this at a price of only about $2.75 each.
For more detailed information, use the Reader Service Card. For a FREE SAMPLE, write on your letterhead, describing your application. Address Dept. AC-17.



BALSTON, INC.
P.O. Box C, 703 Massachusetts Ave
Lexington, Massachusetts 02173
(617) 861-7240 · (617) 862-7455
Telex 92-3481

CIRCLE 20 ON READER SERVICE CARD



OUR SMALL-SPACE METERING PUMP IS BIG ON ACCURACY.

Our Series 20 Chem/Meter hydraulic diaphragm metering pump will give you repetitive accuracy within ± 1% or better.

Measuring only 9¾" x 4⅛" x 3⅛", it's designed for steady, continuous feeding of clear fluids. How? The programmed cam drive produces a constant velocity discharge—when the full displacement of two plungers working 180° apart are combined in a common manifold, a steady flow is established. And it provides capacities to 4.9 and 16.0 ML/min—with pressures to 1000 psig.

The series 20 Chem/Meter's wetted parts are made of corrosive resistant stainless steel with sapphire ball-seats and teflon diaphragms. With its totally enclosed, no-seal leakproof design and remote capacity control, its features make it ideal for applications such as chromatography columns, laboratory apparatus and industrial wet process analytical equipment.

To get all the details on why our little Chem/Meter is a big performer, write Chempump Division, Crane Co., Warrington, Pa. 18976.

CRANE **CHEMPUMP**

CIRCLE 68 ON READER SERVICE CARD

appropriate solvent, is excited to some high vibrational level of the ground electronic state. Two different types of measurements are described. First, coherent probing is used to determine the length of time required for collisions, energy transfer, etc., to dephase the excited vibrations. Second, incoherent Raman scattering is used to monitor the decrease in population of the same state. The work described should appeal to those analytical chemists interested in time-resolved spectroscopy or the use of coherent scattering techniques such as CARS. An overall balance was attained between theory, experiment, and results. In particular, there are several very useful discussions about potential experimental pitfalls. The examples were well chosen to both represent the two methods of excitation and to discuss the dephasing and depopulating data. The chapter ends on a positive note by presenting the results, obtained for coumarin 6, which is composed of ~50 atoms.

R. D. Levine and A. Ben-Shaul have written a chapter on the thermodynamics of molecular disequilibrium, with emphasis on applications relevant to chemical lasers. The discussion is divided into three sections. First, information theory is used to develop state functions useful for systems in molecular disequilibrium. Second, these results are used to synthesize the energy state distribution of nascent, unrelaxed collision products. And finally, by use of a maximum entropy approach it is shown how the time-dependent energy distribution of the products can be predicted. The work described should appeal to those analytical chemists interested in bond-specific infrared photochemistry. The chapter is very heavy on theory and will probably prove difficult going for the average reader. Surprisingly, the reviewer found the first section on information theory the easiest to comprehend because it assumed a weaker prior knowledge than the last two parts.

B. R. Ware is author of a fascinating chapter on the applications of laser velocimetry in biology and medicine. In this experiment the Doppler shift in the frequency of light scattered from a moving object is used to compute its velocity. The work described should have a broad appeal while providing specific examples of interest to a bioanalytical chemist. In this chapter, the basic experiment and operational principles are very briefly described, while most of the coverage is reserved for length descriptions of selected experiments. The discussion of

Fourier Transform Infrared Spectroscopy

APPLICATIONS TO CHEMICAL SYSTEMS/VOLUME 1

Edited by JOHN R. FERRARO and LOUIS J. BASILE

FROM THE PREFACE:

Many of the problem areas being investigated by FT-IR are in the field of chemistry. It is to chemical applications that the first volume attempts to address itself. A second volume is in the planning stage at present to include applications not included in Volume 1, and to add the new applications surfacing daily.

Volume 1 contains 8 chapters. The chapters are written by scientists who are very active in FT-IR, and, in particular, the areas they discuss. The aim of the chapters and the book is to serve both research and analytical chemists in acquainting them with applications of FT-IR, and, hopefully, finding a pathway toward solution of their problems.

The applications discussed are in the areas of gas chromatography FT-IR, polymers and biological macromolecules, emission spectroscopy, matrix isolation, high-pressure interferometry, far infrared interferometry and surfaces. A final discussion is made concerning the use of FT-IR toward solving National Technical Problems (NTP). The NTP discussed are atmospheric pollution, space exploration, and energy related subjects, such as solar energy, magnetohydrodynamics, fusion and nuclear reactions, and coal liquefaction and gasification.

1978, 320 pp., $25.00/£16.25 ISBN: 0-12-254101-4

Polymer Sequence Determination: Carbon-13 NMR Method

By JAMES C. RANDALL

CONTENTS: Polymer Structure and Carbon-13 NMR. Number-Average Sequence Lengths in Vinyl Polymers. Number-Average Sequence Lengths in Copolymers and Terpolymers. Statistical Analyses of Monomer Distributions and Number-Average Sequence Lengths. Experimental Design for Quantitative FT-NMR Measurements. A Survey of Carbon-13 NMR Studies of Vinyl Homopolymers and Copolymers.

1977, 176 pp., $16.50/£11.70 ISBN: 0-12-578050-8

Analytical Methods for Pesticides and Plant Growth Regulators

Edited by GUNTER ZWEIG

VOLUME IX/SPECTROSCOPIC METHODS OF ANALYSIS

Edited by GUNTER ZWEIG and JOSEPH SHERMA

CONTENTS: *J. F. Ryan*, Residue Analysis Applications of Mass Spectrometry. *N. Cyr et al.*, Nuclear Magnetic Resonance Spectroscopy. *T. Cyr et al.*, Spectrophotometric Methods. *R. J. Argauer*, Fluorescence Methods for Pesticides. *T. Cyr et al.*, Infrared Spectrometry. *P. A. Giang*, Library of Infrared Spectra of Important Pesticides.

1977, 320 pp., $32.00/£22.70 ISBN: 0-12-784309-4
*Subscription price:$27.50**

Annual Reports on NMR Spectroscopy

Edited by E. F. MOONEY

VOLUME 6C Edited by E. F. MOONEY

Annual Reports On NMR Spectroscopy is well established as a medium for communicating recent progress in NMR and its applications to the specialist and non-specialist alike. The series is a vital source of information for workers in all branches of chemistry, including biochemistry and pharmaceutics, and will continue to be a valuable source of information for all analytical, structural and physical chemists.

CONTENTS: *P. W. Hickmott et al.*, NMR data on organic-metal carbonyl complexes (1965-1971).

1977, 672 pp., $65.50/£33.50 ISBN: 0-12-505347-9

VOLUME 7

Edited by G. A. WEBB

CONTENTS: *R. Fields*, Fluorine-19 NMR spectroscopy of fluoroalkyl and fluoroaryl derivatives of transition metals. *M. Witanowski et al.*, Nitrogen NMR spectroscopy. *R. E. Wasylishen*, Spin-spin coupling between carbon-13 and the first row nuclei.

1977, 310 pp., $31.25/£16.00 ISBN: 0-12-505307-X

Instrumental Organic Elemental Analysis

Edited by R. BELCHER

CONTENTS: *M. R. Cottrell and F. H. Cottrell*, The Perkin-Elmer Model 240 Elemental Analyzer: Carbon, Hydrogen and Nitrogen. The Perkin-Elmer Model 240 Elemental Analyzer: Sulphur or Oxygen. *C. J. Howarth*, The Carlo Erba Analyzer: Carbon, Hydrogen, Nitrogen and Oxygen. *R. Kubler*, Instrumental Methods for the Determination of Organic Carbon in Water. *P. I. Brewer*, The Determination of Nitrogen by the Merz Modification of the Dumas Method. *F. C. A. Killer*, Microcoulometric Methods for the Determination of Sulphur, Chlorine, Nitrogen and Individual Compounds.

1977, 300 pp., $27.35/£14.00 ISBN: 0-12-085950-5

* Subscription prices for individual volumes valid only on orders for the complete set received before publication of the last volume. Subscription prices are not valid in the United Kingdom, Australia, or New Zealand.

Send payment with order and save postage plus 50¢ handling charge.

Prices are subject to change without notice.

ACADEMIC PRESS, INC.

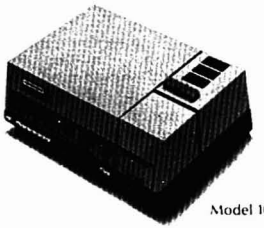
A Subsidiary of Harcourt Brace Jovanovich, Publishers

111 FIFTH AVENUE, NEW YORK, N.Y. 10003

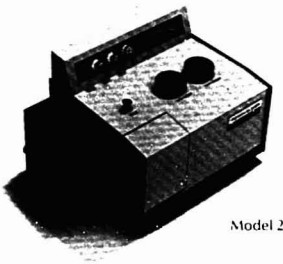
24-28 OVAL ROAD, LONDON NW1 7DX

CIRCLE 11 ON READER SERVICE CARD

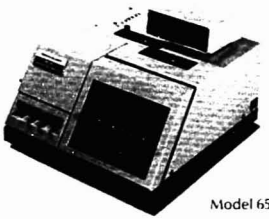
SUPERSENSITIVE LC DETECTION



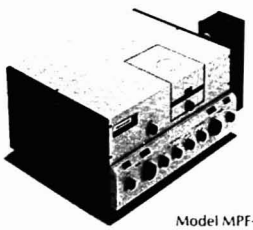
Model 1000/2000



Model 204A/S



Model 650-10M/S



Model MPF-43A/44A

You can make your LC detection vastly more sensitive and selective simply by using one of these versatile Perkin-Elmer fluorescence spectrophotometers as a fluorescence detector. Whatever LC separates in the picogram range, they'll detect by means of the stop-flow technique, scanning either excitation or emission spectra, and delivering the superior identification capability you want. The key is their novel low-scattering 20 µl flow cell that has excellent flow characteristics and can be pressurized up to 600 psi or better.

They'll work with a wide variety of compounds like amino acids, vitamins, porphyrins, steroids, peptides, polycyclic aromatics, drugs, dyes, or non-fluorescing compounds derivatized with a fluorophor. And the choice of four models fits your requirements and your budget. Get the details on these instruments and their use in this remarkable detection technique. Contact your local Perkin-Elmer representative now. Or write Perkin-Elmer Corp., Main Ave., M.S.12, Norwalk, CT 06856. Telephone: 203-762-4639.

PERKIN-ELMER

Expanding the world of analytical chemistry.

CIRCLE 186 ON READER SERVICE CARD

Books

applications in electrophoretic light scattering includes such diverse samples as protein solutions, cells, bacteria, colloids, and polystyrene spheres. In addition, the swimming speed distributions of organisms such as spermatozoa and bacteria are included. Finally, several studies of blood flow and protoplasmic streaming are covered to demonstrate the wide range of subjects successfully investigated by the technique.

J. J. Ewing has written a needed chapter on new laser sources. While the presentation is essentially an update of material appearing in Volume I, the scope is restricted to a discussion of efficient, high-powered ultraviolet and infrared lasers. As such, the work described should appeal to analytical spectroscopists interested in photochemical applications. The author covers the details of a large variety of systems and where possible includes a discussion of basic molecular spectroscopy and reaction kinetics. Specific examples of ultraviolet devices encompass both electron beam and electric discharge-driven rare gas lasers, rare gas excimer lasers, and molecular halogen lasers. The coverage of infrared devices is comprised mostly of electrically, optically, or chemically driven high-pressure gas lasers and to a lesser extent those based on nonlinear techniques.

The book is well documented with 522 references and possesses a very complete index. The camera-ready copy proves to be quite readable, and the text contains very few typographical errors. The only stylistic change that this reviewer would suggest is a return to the format of Volume I in which the table of contents is broken up and appears at the start of each chapter. The book is reasonably priced, and individual ownership should be considered by the laser aficionado or by those specialists interested in any particular topic covered.

Journal of Chromatography Library, Vol. 5: Instrumental Liquid Chromatography. N. A. Parris. x + 329 pages. Elsevier Scientific Publishing Co., P.O. Box 211, Amsterdam, The Netherlands; 52 Vanderbilt Ave., New York, N.Y. 10017. 1976. $38.50. Dfl 100

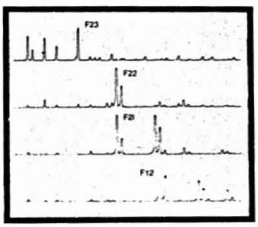
Reviewed by Joseph Sherma, Dept. of Chemistry, Lafayette College, Easton, Pa. 18042

The subtitle of this volume is "A Practical Manual on High-Performance Liquid Chromatographic Methods", and the emphasis should certainly be on the word *practical.* The book was written by an author

How in the world can four metal rods lend a hand to nature's balancing act?

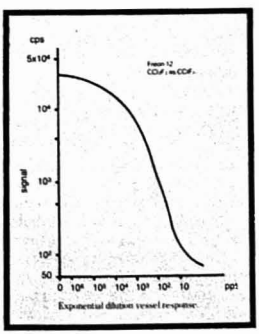
Some 35 kilometers above us is a subject of global significance. There, shielding the earth from excessive UV radiation, is a naturally balanced concentration of gas . . . ozone. The potential destruction of the ozone layer by trace quantities of fluorochlorocarbons is alarming because of the relationship between UV radiation and the incidence of skin cancer.

In an effort to determine the ozone depletion, if any, researchers are asking: what were the ozone concentrations and normal fluctuations before the introduction of fluorochlorocarbons into the atmosphere? What are the concentration levels, travel patterns and collection altitudes of the fluorochlorocarbons? What are the reaction mechanisms, the fundamental rate constants and competing mechanisms of all the interacting species? That the new, anomalous ozone destruction mechanism involves the recycling of chlorine atoms, derived from fluorochlorocarbons, is now understood. This only reaffirms the basic problem of low level fluorochlorocarbon detection.



Extranuclear Laboratories, Inc. has answered this challenge by pursuing the development of Atmospheric Pressure Ionization, a promising ionization technique in mass spectrometry for the ultra-trace analysis of reactive compounds. Detection of fluorochlorocarbons at the ppt level is possible.

For the research scientist, this provides the analytical tool with which to address the fluorochlorocarbon questions. For the rest of us, it could mean a secure life under earth's protective ozone umbrella.



Atmospheric Pressure Ionization for mass spectrometry uses thermal energy ion-molecule reactions at high gas pressure to produce positive and/or negative ions characteristic of the trace contaminants in the gas. Polar or heteroatom organic compounds (e.g., drugs and pesticides) and many inorganic molecules (e.g., pollutants and hazardous chemicals) respond to this ionization method with detection limits approaching 1×10^{-15} gm.



We're using atmosphere to save this atmosphere.

And the four metal rods? They're the heart of our quadrupole mass spectrometer systems.

Extranuclear Laboratories, Inc.
P.O. Box 11512 / Pittsburgh, Pennsylvania 15238 (412) 782-3884
Telex: 812-316 Extralab Pgh

CIRCLE 64 ON READER SERVICE CARD
See us at the Pittsburgh Conference, Booth #941–944.

FREE $100 IR ACCESSORY.

If you're planning to purchase any dispersive IR scanning spectrophotometer in the next few months, be sure to talk to your Beckman representative before making your final decision.

Just for giving him the chance to discuss in person the Beckman IR capability in your lab, he'll give you a precision accessory worth $100—as soon as you have actually purchased the IR spectrophotometer of your choice. Be it a Beckman or even a competitive unit.

If you are interested, just clip the coupon below and mail it to the attention of the IR Product Line Manager, Scientific Instruments Division, Beckman Instruments, Inc., P.O. Box C-19600, Irvine, CA 92713. Or for immediate action, call the IR Product Manager collect at (714) 833-0751.

BECKMAN®

Free $100 IR Accessory Offer
Have a Beckman Representative contact me. I realize I am not obligated to purchase a Beckman product to receive my free accessory.
Act now. Offer expires July 1, 1978.

NAME

ORGANIZATION

PHONE

STREET

CITY

STATE ZIP

with a background as an LC user in industrial analytical laboratories and currently an applications chemist with an instruments company producing LC equipment, rather than by the more typical academic, theoretically oriented specialist. This appears to have been an ideal perspective from which to produce a practical, comprehensive, authoritative laboratory manual based on personal experience, containing the minimum amount of theory to allow an understanding of the basic principles of LC without an excess of experimental detail.

The book is divided into four major sections. The first section titled "Fundamentals and Instrumentation" contains five chapters covering history, principles and terminology, column technology, instrumentation, and detectors.

Containing probably the best material in the entire book, the second section on factors influencing selectivity has five chapters on separation mechanisms and properties of column packings and mobile phases for adsorption, partition, ion exchange (including ion-pair partition), and steric exclusion chromatography. Sections on the range of sample applicability for each technique and a general discussion of methods development provide a rational basis for deciding the best mode to apply for a particular desired separation.

Section three on uses of LC procedures contains chapters on optimization of qualitative, quantitative, trace, and preparative LC. Especially useful is an outline of sources of errors in the various steps of a quantitative analysis.

The final section is a listing of over 200 literature references on applications of LC arranged according to compound type. Although a few references are as current as 1975, most literature cited in all chapters of the volume was published between 1970 and 1974.

The book concludes with four appendices, including a listing of hardware suppliers and directions for preparing and using simple liquid stationary phases, and a subject (but no author) index.

This attractively produced, reasonably sized, and generally well-written, error-free volume is highly recommended to any scientist using HPLC. It must be realized, however, that the book was published in 1976; because of the normal lag between writing and publication and the intense activity in the field in recent years, coverage of some topics is already badly out of date at this time.

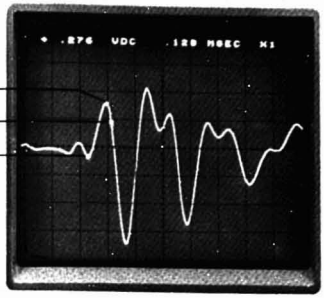
New Books

Methods of Air Sampling and Analysis, 2nd Ed. Morris Katz, Ed. xxii + 984 pages. American Public Health Association, 1015 18th St., N.W., Washington, D.C. 20036. 1977. $45

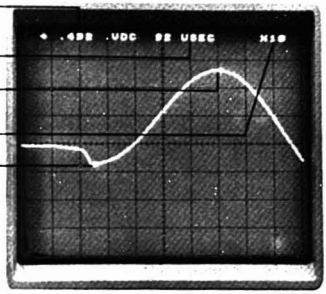
Most of the methods in this manual originally appeared in the American Public Health Association publication, *Health Laboratory Science* (starting with Volume 6, No. 2, April 1969). The first edition, published in 1972, contained 57 methods. In this edition there are 136 methods for the sampling and analysis of ambient and workplace air. Most of these are, however, designated as "tentative". The elevation of "tentative" methods to "recommended" procedure takes place only after satisfactory completion of a cooperative test program conducted by the Intersociety Committee. The Intersociety Committee is composed of one representative each from 13 relevant professional societies (including the American Chemical Society) for the purpose of developing standardized methods for sampling and analysis of ambient and workplace air. Major topics discussed include general precautions and techniques, state-of-the-art reviews, recommended factors and conversion units for analysis of air pollutants, and methods for analysis of chemicals in workplace air and biological samples. Also included are ambient air sampling and analytical procedures for carbon compounds, halogen and halogen compounds, metals, inorganic compounds and oxidants, particulate matter, radioactivity, and sulfur compounds.

Mass Spectrometry in Drug Metabolism. Alberto Frigerio and Emilio L. Ghisalberti, Eds. xii + 532 pages. Plenum Publishing Corp., 227 West 17th St., New York, N.Y. 10011. 1977. $42.50

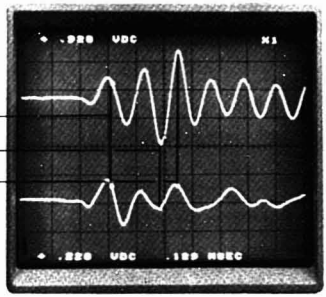
Thirty-two original research papers and review articles are collected in this volume on the application of mass spectrometry to the study of drug metabolism. Originally presented at the International Symposium on Mass Spectrometry in Drug Metabolism held in Milan, Italy, June 1976, the papers are divided into three major areas: drug metabolism, developments in methodology, and drug abuse. Drug metabolism is further arranged into identification (nine papers), quantitation (eight) and reactivity of intermediates (two). Methodology development is concerned with isotope labeling, chemical ionization mass spectrometry, field desorption mass spec-



Biomation's new 820 Digital Storage Oscilloscope captures one-shot analog events, converts them to digital form, then holds them in memory. Exclusive pre-trigger recording lets you keep as much of the signal prior to the trigger point as you want. You can set the trigger level high enough to avoid false triggers. The delayed trigger stops the recording process trapping information before and after the event.

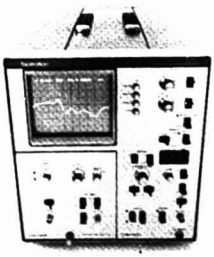


Biomation's new 820 Digital Storage Oscilloscope offers you 4 MHz input bandwidth and 20 MHz A/D conversion rate to capture a broad spectrum of analog signals. Move the cursors to measure time and voltage and read them out on the CRT along with a display expansion factor. You have up to a X50 digital expansion of the display for close examination of your analog data.



Biomation's new 820 Digital Storage Oscilloscope has a 2048 word memory which can be split in half to record separate analog events. Record one test signal, change a test parameter, and test again. Then you can compare the before and after signals and their voltage and time measurements right on the display.

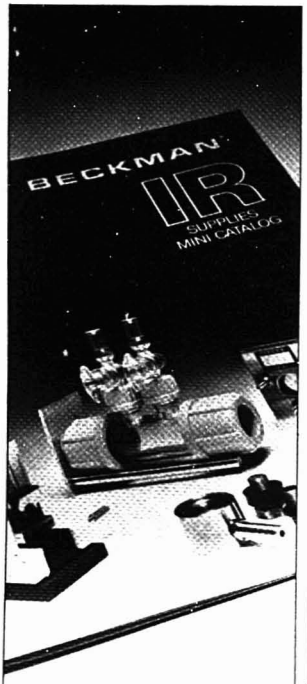
We've just changed the way you look at things.



Our new 820 Digital Storage Oscilloscope offers you high performance analog capture capabilities that let you trap events you've never seen before and built-in display features that let you see that information in a whole new way. To start to put our 820 to work on your problem, call now and arrange for a demonstration. Ask for Roy Tottingham, Product Manager, (408) 255-9500. Or write Biomation, 10411 Bubb Road, Cupertino, CA 95014.

biomation

CIRCLE 50 ON READER SERVICE CARD



New IR catalog is free from Beckman.

Prices, specifications, and full ordering information for your most needed IR supplies and accessories are all included in our new "Mini Catalog."

Get yours free now and solve the supplies search. Just circle the reader service number or contact Scientific Instruments Division, Beckman Instruments, Inc., P.O. Box C-19600, Irvine, CA 92713.

BECKMAN®

See us at the Pittsburgh Conference
CIRCLE 43 ON READER SERVICE CARD

Books

trometry, and the use of computers in GC/MS systems. The last section on drug abuse deals with the determination of cannabinoids and other illicit street drugs in urine and blood plasma by MS and GC/MS systems.

Anionic Surfactants—Chemical Analysis. John Cross, Ed. xvi + 251 pages. Marcel Dekker, Inc., 270 Madison Ave., New York, N.Y. 10016. 1977. $29.75

This text is designed for those with a basic understanding of classical and modern instrumental methods of analysis. Consequently, the introduction to analytical techniques has been kept to a minimum. For instance, the chapter on gas chromatographic analysis presents no discussion on principles of separation, detector choice, etc. However, no extensive familiarity with surfactants or surface activities is assumed. Nine authors contribute six self-contained chapters on detection, separation, and isolation of anionic surfactants; identification by absorption spectroscopy techniques; gas chromatography for the analysis of anionic surfactants; nuclear magnetic resonance spectrometry of anionic surfactants; the colorimetric estimation of anionic surfactants; and the volumetric estimation of anionic surfactants. The list of references given at the end of each chapter contains the titles of the articles in addition to the usual bibliographic information. The book is a good quality photo-offset copy of typewritten text.

Biomedical Applications of Immobilized Enzymes and Proteins, Vol. 2. Thomas Ming Swi Chang, Ed. xx + 359 pages. Plenum Publishing Corp., 227 West 17th St., New York, N.Y. 10011. 1977. $39.50

A total of 22 chapters contributed by 42 international experts review the wide-ranging analytical and diagnostic methods based on immobilized enzymes and proteins. These methods are used to diagnose bacterial infections, parasitic diseases, hepatitis, etc., to cite only a few. In addition to these chapters devoted principally to a review of biomedical applications, there are others dealing solely with the development of methodology itself.

Electrodeposition of Chromium from Chromic Acid Solutions. George Dubpernell. 93 pages. Pergamon Press, Inc., Maxwell House, Fairview Park, Elmsford, N.Y. 10523. 1977. $12.50

This short monograph reviews in great detail the chemistry of chromium plating from the initial introduction of the process by Colin G. Fink and Charles H. Eldridge in 1924–1926 to the present commercial scale electroplating process. In six chapters it discusses the historical development, economic importance of chromium deposition, two common forms of deposited chromium, the catalyst balance, empirical tests for catalyst concentration and bath balance, and fluoride and complex fluoride-catalyzed baths.

Continuing Series

Infrared and Raman Spectroscopy, Part C. Edward G. Brame, Jr., and Jeanette G. Grasselli, Eds. ix + 323 pages. Marcel Dekker, Inc., 270 Madison Ave., New York, N.Y. 10016. 1977. $36.50

Part C completes Volume 1 (in three parts) of the new "Practical Spectroscopy Series" initiated in 1976 for the review of all possible applications of the varied aspects of spectroscopy. All three parts are devoted entirely to infrared and Raman spectroscopy. Part C contains three chapters: 11–13 of the volume. Coauthored by George J. Thomas, Jr., and Yoshimasa Kyogoku, Chapter 11 deals with the applications of infrared and Raman spectroscopic methods in the biological sciences. Principles and experimental procedures, as well as recent applications, are reviewed. Chapter 12, written by Sandra C. Brown and Albert B. Harvey, deals with the applications of the method to polymer analysis. Since a full coverage of this subject in limited space is not possible, only the prime utility of the techniques in both qualitative and quantitative analyses is presented. Chapter 13, which is the final chapter in the book and also in Volume 1, gives a comprehensive review, by Clara D. Craver, of the use of the Raman and infrared techniques in analyzing various kinds of surfaces.

Advances in Infrared and Raman Spectroscopy, Vol. 3. R.J.H. Clark and R. E. Hester, Eds. xiv + 285 pages. Heyden & Son Inc., Kor-Center East, Bellmawr, N.J. 08030. 1977. $35

This series presents review articles in both the fundamentals and applications of infrared and Raman spectrometry. In this volume Chapter 1 by W. Kiefer surveys the advances in the field during the past few years. However, the review is not intended to be comprehensive; only some novel techniques of practical utility are reviewed. The second chapter by N.W.B. Stone and G. W. Chantry reviews advances in Fourier transform interferometric spectrometry. Topics discussed are high-precision intensity

New IL Atomic Absorption Equipment Includes a Video Readout and a Unique Autosampler.

AT THE PITTSBURGH CONFERENCE, COME SEE THIS ALL-NEW LINEUP:

The IL551 Video I™ AA Spectrophotometer is the first to read out on a 23 x 17-cm video display. Built-in cookbook, storage of 10 analytical curves, graphics option, statistics, much more. Versatile yet easy to use; microcomputer needs only 12 function keys.

CIRCLE 115 ON READER SERVICE CARD

The FASTAC™ system (Flame/Furnace Autosampler with Automatic Calibration) presents up to 95 samples to flame or furnace in an innovative manner. Advantages include controllable furnace sensitivity (either higher or lower than conventional), faster sampling speed, and great cost effectiveness.

CIRCLE 116 ON READER SERVICE CARD

The IL157/257 AA Spectrophotometers are low-to-medium in cost. Microcomputer has novel feature called "running mean," which tells operator when the analytical result is as good as it can be. Must be seen to be appreciated. Come appreciate it.

CIRCLE 117 ON READER SERVICE CARD

And the well-established two-channel IL751, still the only modern AA instrument that can determine two different elements simultaneously. The microcomputer has even more power this year.

CIRCLE 74 ON READER SERVICE CARD

"Live" demos all day every day in Room M-134 on the exhibit floor in Cleveland. Seminars at 10:30 Tuesday, Wednesday, Thursday, 2:30 Monday, Tuesday, Wednesday. IL users-only meeting Wednesday 4:30.

THERE REALLY IS A DIFFERENCE BETWEEN AA INSTRUMENTS AND IT'S GROWING WIDER ALL THE TIME.



Instrumentation Laboratory
Analytical Instrument Division

and wavenumber measurements on gases and the monitoring of trace gases in the high atmosphere, measurements of the dielectric properties of strongly absorbing solids and liquids, and time-resolved spectrometry of transient plasmas. Chapter 3 by P. Gans is concerned with the long-established subject of force-constant calculations. In Chapter 4, I. W. Shepherd surveys the contributions made by the polarized Raman technique in the elucidation of polymer structures. Chapter 5, dealing with vibrational spectra of nonaqueous solutions, is contributed by D. J. Gardiner. This review concentrates on solutions either totally or partially inorganic, and only a few examples of totally organic systems are discussed. In Chapter 6 M. Lapp and C. M. Penney review applications of the Raman scattering technique as a probe of combustion systems used to determine temperatures and densities of the main constituents.

Vibrational Spectra and Structure, Vol. 6. James R. Durig, Ed. viii + 397 pages. Elsevier Scientific Publishing Co., P.O. Box 211, Amsterdam, The Netherlands; 52 Vanderbilt Ave., New York, N.Y. 10017. 1977. $59.60

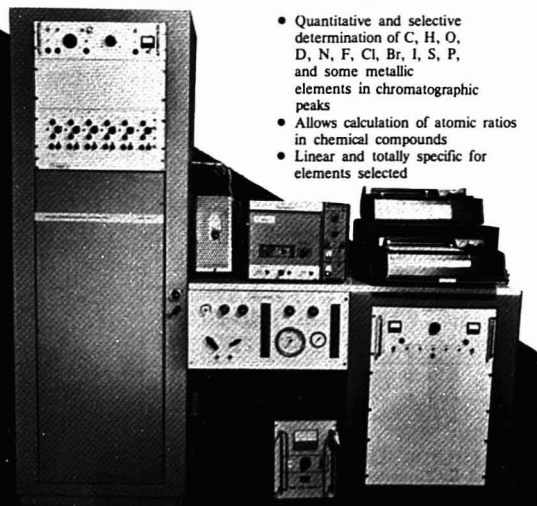
The purpose of this series is to provide critical summaries of recent developments in the field of vibrational spectrometry. Volume 6 contains five chapters written by nine experts. Chapter 1 by James K. G. Watson is a coherent development of some aspects of quartic and and sextic centrifugal effects on rotational energy levels. In Chapter 2, H. F. Shurvell and J. T. Bulmer discuss the application of factor analysis and band contour resolution to infrared and Raman studies of equilibria in solution. The third chapter by J. W. Nibler, W. M. Shaub, J. R. McDonald, and A. B. Harvey treats the rapidly expanding field of coherent anti-Stokes Raman spectrometry (CARS). A brief introduction to the CARS method and some recent results are included. To assess future expectations for the method, some of its shortcomings are discussed. In Chapter 4 D. C. Moule reviews developments in the evaluation of the structural parameters of molecules in their excited electronic states, with emphasis on the polydimensional Frank-Condon method. In chapter 5 James E. Griffiths discusses molecular reorientation of symmetric top molecules in the liquid state. The literature citations include some as recent as 1977. The book is reproduced from typewritten text.

Annual Reports on Analytical Atomic Spectroscopy, Vol. 6. C. W. Fuller, Ed. vii + 282 pages. The Chemical Society, Burlington House, London W1V 0BN, England. 1977. $36

This annual review volume on analytical atomic spectroscopy surveys the original research papers and review articles published mostly in 1976, with some from 1975. It includes a total of 1682 literature citations. The text is divided into two parts. Part I is further divided into light sources, excitation sources and atomizing systems, optics, detector systems, data processing, complete instruments, and fundamental studies. Part II is devoted to discussion of applications. It also includes lists of new books and meetings of 1976 which are relevant to analytical atomic spectroscopy.

Antek's MPD 850

M/S Capabilities at a Fraction of the Cost.



- Quantitative and selective determination of C, H, O, D, N, F, Cl, Br, I, S, P, and some metallic elements in chromatographic peaks
- Allows calculation of atomic ratios in chemical compounds
- Linear and totally specific for elements selected
- Capable of monitoring up to 12 elements simultaneously
- Basic unit (with single amplifier and detectors for 4 elements) starts at under $30,000

The Antek MPD-850 microwave plasma detector interfaces to virtually any commercially available gas chromatograph to provide quantitative, selective, and sensitive determination of individual elements normally found in organic peaks.

Relying on the principle that a plasma emission source can be used as the basis for an elemental analyzer, the MPD-850 allows accurate interpretation of complex gas chromatograms and determination of the structure of unknown compounds.

See us at the Pittsburgh Conference booths 413, 415, and 416.

ANTEK® INSTRUMENTS, INC.

6005 North Freeway
Houston, Texas 77076
Tel: (713) 691-2265 TWX: 910-881-1792

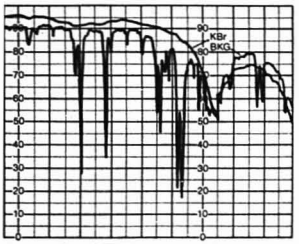
CIRCLE 13 ON READER SERVICE CARD

"OMNI" is coming to FT NMR

JEOL
Analytical Instruments, Inc.

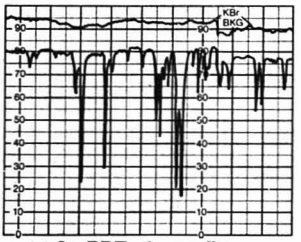
SEE "OMNI" at the Pittsburgh Conference
(BOOTHS 615-621)

CIRCLE 114 ON READER SERVICE CARD



5μg DDT—1 mm pellet

WITHOUT



5μg DDT—1 mm pellet

WITH

Only the Beckman 4200 IR Spectrophotometers have spatial imaging.

And spatial imaging is the easiest way to minimize the aperture effects encountered in microsampling.

For proof, just check the 5-microgram scans of DDT shown above.

Note the flat base line with spatial imaging. Then make a note to get full technical information on the one IR system that combines center-beam focusing and spatial imaging for the ultimate in high-performance microsampling capability.

Contact Scientific Instruments Division, Beckman Instruments, Inc., P.O. Box C-19600, Irvine, CA 92713.

Innovation in IR since 1940

See us at the Pittsburgh Conference

BECKMAN®

CIRCLE 30 ON READER SERVICE CARD

Attention Gas Chromatographers
Derivatizing Agents

The following are some of the derivatizing agents available from PCR stock.

27090-0	Chloromethyldimethylchlorosilane	50g–$20.00; 250g–$90.00
34040-6	N,N-Diethylaminotrimethylsilane (Trimethyl-N,N-diethylaminosilane)	10g–$20.00; 50g–$80.00
13090-6	Heptafluorobutyric acid	50g–$18.00; 250g–$73.00
13100-3	Heptafluorobutyric anhydride	25g–$30.00; 100g–$90.00
13120-1	Heptafluorobutyryl chloride	25g–$22.50; 100g–$75.00
34020-8	Hexamethyldisilazane (HMDS)	100g–$12.00; 500g–$25.00
34090-1	1,1,3,3-Tetramethyldisilazane	25g–$21.00; 100g–$65.00
11023-9	Trifluoroacetic acid, highest purity	250g–$22.50; 1 kg–$75.00
13200-1	Trifluoroacetic anhydride	100g–$12.00; 500g–$54.00
27490-2	Trimethylchlorosilane (TMCS)	1 pt–$11.00; 1 qt–$15.00
27650-1	Trimethylbromosilane	25g–$15.00; 100g–$55.00

Attention NMR Spectroscopists

Standards for both ^1H and ^{19}F NMR

11850-5	Hexafluorobenzene (min. 99.7%)	25g–$30.00; 100g–$90.00
15771-9	Hexafluoroacetone sesquideuterate D/D+H>99.8%	10g ampoule–$22.50; 50g–$85.00
10103-0	Fluorotribromomethane	10g–$20.00; 50g–$72.00
16060-6	2,2,2-Trifluoroethanol	250g–$28.00; 1kg–$90.00
29200-3	Tetramethylsilane, NMR Grade	25g–$12.00; 100g–$30.00
11857-0	Hexamethyldisiloxane, NMR Grade	25g–$12.00; 100g–$21.50

NOTE: Minimum order $25.00.

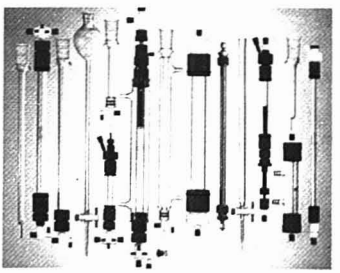
Ask for our FREE General Catalog if you don't have yours yet.

PCR RESEARCH CHEMICALS, INC.
P.O. BOX 1778 GAINESVILLE, FLORIDA 32602
(904) 376-7522

CIRCLE 176 ON READER SERVICE CARD



The proof is in the chromatogram.





When the quality is in the product, you can read it in the chromatogram. Glenco supplies a *complete* line of high-quality liquid chromatography products:

- HPLC System I
- A complete line of prepacked HPLC columns
- An exclusive line of classical LC columns
- High-quality packings, syringes and dispensers

Write for our new catalog.

GLENCO

Glenco Scientific Inc.

The total LC supplier since 1959
2802 White Oak Drive
Houston, Texas 77007
713/861-9123

See us at booth 1005, 1007, Pittsburgh Conference.

CIRCLE 79 ON READER SERVICE CARD

Pittsburgh Conference Booths 1546–1548

Super SCOTS

For faster, better results

At S.G.E., we make both SCOT and WCOT columns in glass. Without a doubt, WCOT columns are the ultimate when it comes to separation. But.... they present many problems for the normal chromatographer who does not have the time or staff to overcome instrumental problems associated with WCOT's. Not to mention the worries of non linear splitting.

Which is why we believe that the SCOT column provides the ideal compromise for most chromatographers.

SCOT columns are easier to use than WCOT 's, they take larger samples without the need of a splitter, and are very tolerant with beginners.

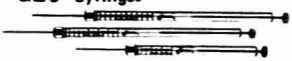
We offer several phases and each phase is available with varying numbers of effective plates so you only pay for what you want to use.

In the end though, what is important is that they normally give better, faster results than packed columns

Data Sheets are available. **Why not write for information now ?**

S.G.E.

GLC Syringes



Top quality with emphasis on long life and reliability. Strengthened plungers, removable needles, low cost repair kits, variable needle lengths, capacities from 0.5µl - 1ml.

GLC, HPLC, GC-MS
Glass Lined Tubing



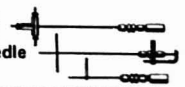
Another S.G.E. invention. Stainless steel tubing with fused glass insert combining strength of steel with chemical inertness of glass. Overcomes such problems as catalytic adsorption. Suitable for columns, flow lines "T's" Enables virtually all glass systems to be built. Available in 1/16", 1/8" and 1/4" O.D.s with many I.D.s

GLC GC-MS
Graphlok™ Ferrules



Another breakthrough from S.G.E. High purity graphite ferrules, can be used at up to 500°C. Suitable for GLT, glass, and steel tubing. Accept tube sizes from 1/4" down to 0.8mm. Ideal for capillary columns.

GC-MS Microneedle Valves



Available options include two or three arms, with or without GLT terminals. Micrometer type control gives infinite flexibility over ratios. Can be used as outlet splitters.

S.G.E.

Scientific Glass Engineering Pty. Ltd.

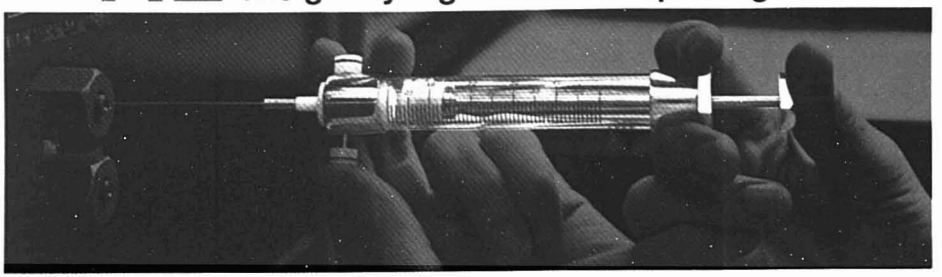
Head Office:
111 Arden Street,
North Melbourne,
Victoria 3051, Australia.

European Office:
657 North Circular Road,
London NW2 7AY,
Great Britain.

USA Office:
2800 Longhorn Blvd,
Suite 104, Austin,
Texas 78759, USA.

CIRCLE 191 ON READER SERVICE CARD

Pressure-Lok®
A-2 The gas syringe with the stop and go valve.



Pressure Lok® A-2. The rapid-action, push-button valve member of the Pressure Lok® line of gas chromatography syringes. Green button in, valve's open. Red button in, it's closed. Fast.

This precision instrument is a modified version of the Series A gas syringe which uses a valve activated by turning. With both, samples can be trapped and transported leak-tight, vacuum to 250 psi.

Pressure Lok® A-2 is particularly suitable for pre-injection pressurizing techniques. Injection under pressure sharpens peaks and improves reproducibility. Error from carrier gas back-flushing and sample diffusion is eliminated. †

A-2 embodies all of the advances made by the Pressure Lok® models. Long-life, durable seals are achieved by Teflon* plungers and internal O-rings, defeating cold flow and eliminating dead volume. Positive rear stops prevent blow-back.

Gas sampling needles for the A-2 are luer tapered, easily removable, and easily replaced. They are leak-tight, Teflon*-bonded and crafted with low dead volume fittings.

Pressure Lok® A-2. Another remarkable member of a long line of workhorse syringes for precise gas chromatography.

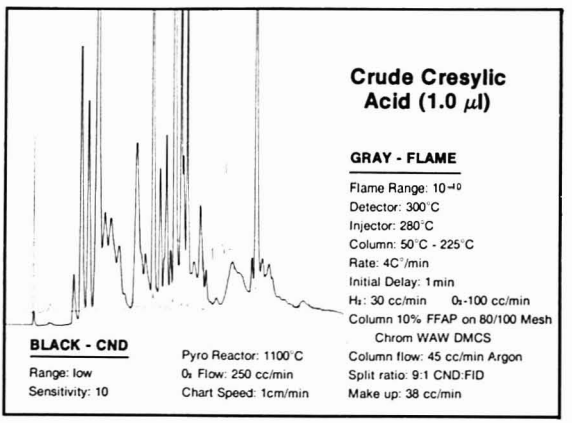
* Reg. DuPont Trademark † Literature discussing these advanced techniques will be forwarded upon request.

PRECISION SAMPLING CORPORATION
Post Office Box 15119
Baton Rouge, Louisiana 70815
Telephone 504-927-1128

CIRCLE 154 ON READER SERVICE CARD

Antek's New Model 705 GC/CND*

Specific detection of chromatographic peaks containing bound nitrogen



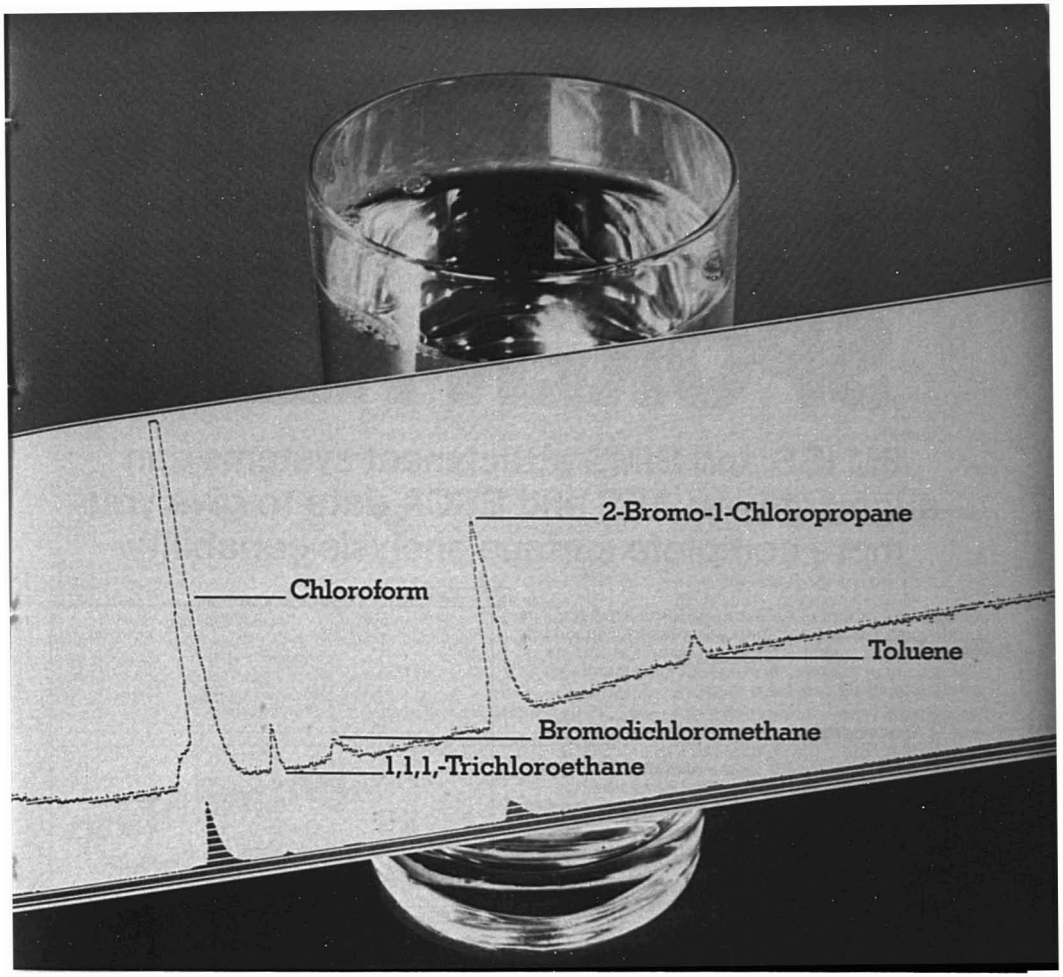
- Totally specific measurement of nitrogen in the ppb level
- Can be used with virtually any existing chromatograph
- Proven chemiluminescent detection method

*** Gas Chromatograph/Chemiluminescent Nitrogen Detector**

ANTEK INSTRUMENTS, INC.
6005 North Freeway
Houston, Texas 77076
TELEPHONE (713) 691-2265 TWX: 910-881-1792

See us at the Pittsburgh Conference booths 413, 415 and 416.

CIRCLE 44 ON READER SERVICE CARD



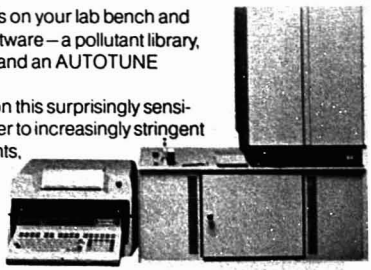
Low-cost GC/MS identifies sub-ppb pollutants in drinking water.

Talk about price/performance! Our HP 5992A GC/MS positively identifies and quantitates exceedingly low levels of chloroform, 1,1,1-trichloroethane, bromodichloromethane, 2-bromo-1-chloropropane (internal standard) and toluene in ordinary drinking water.

Moral: if you're struggling to meet TSCA or other Federal standards (air, water or solid), an HP 5992A can make your job a lot easier. And it can do it for about half the cost of any other GC/MS with data system.

The HP 5992A is easy to use (desktop computer-controlled), fits on your lab bench and comes with powerful software – a pollutant library, selected ion monitoring and an AUTOTUNE program, for example.

For detailed specs on this surprisingly sensitive and affordable answer to increasingly stringent government requirements, call your local HP office or write to the address below.



HEWLETT hp PACKARD

For assistance call: Washington (301) 948-6370; Chicago (312) 255-9800; Atlanta (404) 955-1500; Los Angeles (213) 877-1282.

1507 Page Mill Road, Palo Alto, California 94304

CIRCLE 95 ON READER SERVICE CARD

23705

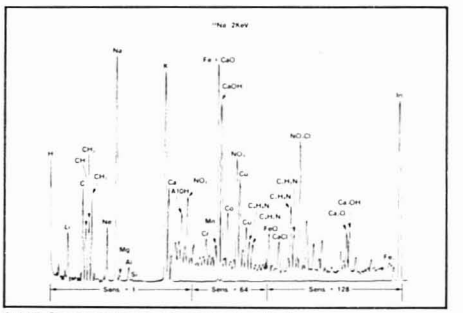
SURFACE ANALYSIS SPOKEN HERE

3M ISS and SIMS attachment systems can augment your AES and ESCA data to give you more complete surface analysis capability.

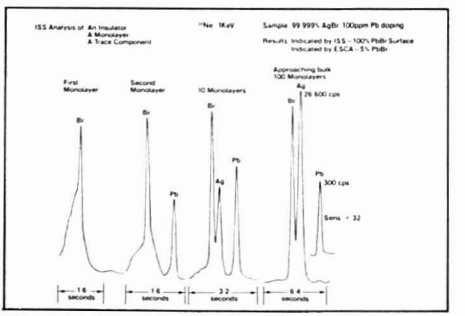
Growing numbers of AES and ESCA users have come to the realization that their present capabilities can't solve all their everyday, real-world problems. Their companies need and expect more complete surface analysis data from them.

As a result, more and more of these users are turning to 3M Analytical Systems. That's because only 3M offers complete, fully compatible ISS and SIMS Attachment Systems for their existing AES or ESCA equipment. Complete, operational systems—not just bits and pieces. Systems for which 3M assumes "turnkey" responsibility.

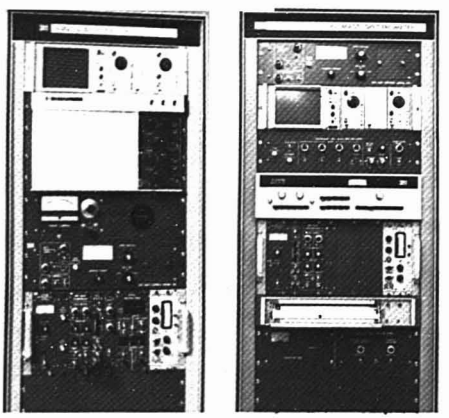
If your present surface analysis equipment isn't telling you the whole surface story, talk to us. We can help translate your problems into solutions. Call 612/733-3909, or write: Analytical Systems, 3M Company, 3M Center, Building 209, St. Paul, MN 55101. In Europe: Cambridge Instruments, GmbH, Dortmund, Germany.



SIMS Spectra: Contaminated Indium Foil



ISS spectra showing: Analysis of insulators; Monolayer sensitivity; Trace detection



We speak your language

3M COMPANY

CIRCLE 147 ON READER SERVICE CARD

"Laetrile Warning"

"Laetrile is worthless. Laetrile is dangerous." So read the posters signed by Food and Drug Administration head, Donald Kennedy, and posted in Federal and state buildings, post offices, and in other public places. Kennedy believes strongly in public education as an effective weapon in FDA's arsenal.

What is new about Laetrile and FDA's efforts to combat its use in the U.S. for cancer treatment? Not much. For perspective on this subject, read Janssen's article, page 197 A. The article describes FDA efforts in past years to fight cancer quackery, from Dr. Johnson's Mild Combination Treatment for cancer in 1910 to the more recent Krebiozen cancer "cure" in the 1960's. Laetrile proponents have come upon the scene just as the public has become particularly alarmed at the strong regulatory arm of the Federal government. Laetrile promoters have latched onto this and secured some support from those concerned with freedom of choice and the right of privacy.

Further, Laetrile promoters have used the media to advantage in their battle to overcome FDA restrictions on its importation, transport, and prescription. A striking example of this was given at Senator Edward Kennedy's Subcommittee hearings on the controversial cancer drug last July. Mike Wallace's TV show, "60 Minutes", and the book, "World Without Cancer", were mentioned by the widow of a cancer patient as sources of information leading her to seek advice from Dr. Krebs. Both media mentioned Dr. Krebs. Dr. Krebs persuaded her to use Laetrile rather than surgery for her husband's diagnosed lung cancer. Although the lung cancer was reported by physicians to be about 90–95% curable at the time of discovery, the patient was influenced by his wife to use Laetrile treatment. The patient died.

Both the chemical identity and the suggested mode of action of Laetrile are moving targets by proponents of the drug in its forays with the medical establishment. In testimony before Senator Kennedy's Subcommittee, Laetrile was carefully defined as "vitamin B-17, the extracted form of the chemical amygdalin, usually made from apricot kernels" by its proponents. It was purported to be a cancer "control, part of a total metabolic program for cancer in which Laetrile may be seen as the crown jewel in a total treatment diadem".

Proponents originally had claimed that Laetrile would be broken down by an enzyme (beta-glucosidase) in

announcing...

The Sadtler Handbooks of Reference Spectra

- INFRARED
- PROTON NMR
- ULTRAVIOLET

available individually or as a set

Special Pre-Publication Offer!

THREE THOUSAND OF THE MOST COMMONLY REFERRED TO COMPOUNDS HAVE BEEN SELECTED FOR INCLUSION, FROM OVER 200,000 SADTLER REFERENCE SPECTRA. THE SPECTRA OF EACH OF THE 3,000 COMPOUNDS HAVE BEEN PUBLISHED USING IR, PROTON NMR; AND, WHERE APPROPRIATE, UV.

- A CONVENIENT DESK SET FOR CHEMISTS AND SPECTROSCOPISTS
- A PRACTICAL AND CONVENIENT TEACHING TOOL
- ALL SPECTRA ARE ARRANGED BY CHEMICAL CLASS AND ARE THOROUGHLY INDEXED

For more information, circle No. 159 on Readers' Inquiry Card or contact:

Sadtler Research Laboratories, Inc.
Subsidiary of Block Engineering, Inc.
3316 Spring Garden Street
Philadelphia, Pennsylvania 19104
(215) 382-7800

CIRCLE 187 ON READER SERVICE CARD

From Buchler...keeping pace with the age of discovery:

An ALL NEW digital power supply.

Buchler introduces the first laboratory power supply with large, bright L.E.D. digital readout and instant pushbutton selection of constant-*power*, constant-*voltage*, or constant-*current* modes.

The bright L.E.D. display means easy reading, even from across the room, without the distraction of dual or multifunction scales.

Overvoltage and overcurrent protection are built in; control circuits operate at low voltage for long life and reliability.

This is the only truly contemporary power supply. It's new from Buchler. Available through your leading laboratory supply house.

SEARLE

Buchler Instruments
Division of Searle Diagnostics Inc.
1327 Sixteenth Street
Fort Lee, New Jersey 07024 U.S.A.
201-224-3333



Buchler Instruments: made in the United States, sales and service worldwide.

CIRCLE 56 ON READER SERVICE CARD

Editors' Column

cancerous tissues to liberate cyanide, which would kill the cancer. When scientific evidence was used to refute this claim, the theory was advanced that the material is a vitamin which prevents cancer and that cancer is a manifestation of a vitamin deficiency. However, no properties of a vitamin have been associated with this compound as presented to FDA, nor has a deficiency disease been associated with its lack.

Identity and analysis form cornerstones of any Federal action on drugs. In the past, accurate and careful analysis has helped squelch some so-called cancer "cures". Examples are Dr. Koch's treatment in the 1940's and 1950's. Analysis showed the material to be distilled water of unusual purity. Dr. Koch claimed it contained 1 part of the chemical glyoxylide in 1 trillion parts of water! We wonder how Dr. Koch determined this amount in those days!

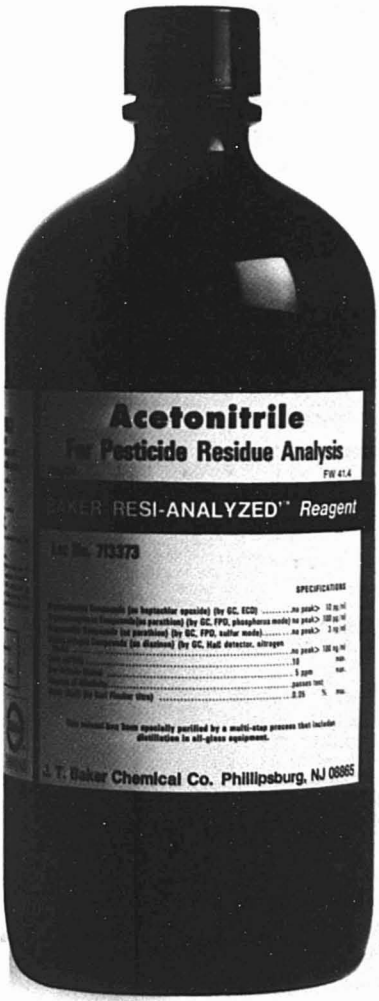
Two decades later, another cancer "cure", Krebiozen, was found to contain only creatine monohydrate, an amino acid present in all animal tissues and without value as a cancer treatment. Ampuls for injection contained only mineral oil.

Commissioner Kennedy has run into severe roadblocks in his efforts to protect the public from Laetrile promoters. The most recent court decision by District Court Judge Luther Bohanon in Oklahoma City directs the Federal government, in an unusual Nationwide ruling, to cease interfering with the importation, introduction, delivery, or use of the controversial cancer drug Laetrile. The Food and Drug Administration has no choice other than appeal to support the necessity for scientific validation of drugs rather than "witchcraft".

Surprisingly, the court also ruled that Laetrile is not a "new" drug, although the FDA maintains that the material cannot be "grandfathered". "There is no evidence that experts in 1962 recognized Laetrile to be safe and effective in the treatment and management of cancer; none of the experts who submitted testimony to FDA knows of scientific reports on which such recognition could have been predicated." Further, and most important, FDA's Kennedy reports that "numerous variations of the identity of Laetrile make it certain that before 1938, and probably even in 1962, the material now understood to be Laetrile was a different compound or compounds entirely". See "The Analytical Chemistry of Amygdalin", page 317, this issue.

Josephine M. Petruzzi

'Baker Resi-Analyzed'™ Solvents for pesticide residue analysis



Application	Instrumental Method
Recommended for evaluation of pesticide and other organic residues.	Gas chromatography (ECD, FPD, etc.)

Quality/Characterization

The 'Baker Resi-Analyzed' brand has the highest assurance of performance for any solvents designed for pesticide residue analysis. They exhibit no extraneous peaks, have excellent baseline stability, show a narrow solvent front, and return rapidly to the baseline.

'Baker Resi-Analyzed' solvents are controlled by 8 or more quality tests, including 4 GC determinations (ECD, FPD for P and S, Hall conductivity detection for N).

The testing also includes water, APHA color, non-volatile matter and substances darkened by H_2SO_4.

Solvents Available

Acetone
Acetonitrile
Benzene
Chloroform
Cyclohexane
Ether, Anhydrous
Ethyl Acetate
Heptane
Hexanes
Methanol
Methylene Chloride
Pentane
Petroleum Ether, 30-60°C
2-Propanol
Toluene
1, 1, 2-Trichloro-1, 2, 2-Trifluoroethane
2, 2, 4-Trimethylpentane

'Baker Resi-Analyzed' solvents are stocked right where you need them. Contact one of the more than 120 Baker distributor locations in the U.S. and Canada to implement a stocking program to suit your needs.

For emergency shipments your distributor can provide special Baker Super Service by calling a Baker Super Service Center for immediate shipment to you.

For instrumental analysis . . . the professional chooses J.T. Baker

For more information use coupon or write to J.T. Baker Chemical Co., Phillipsburg, New Jersey 08865 or call 201-859-2151

J.T.Baker® CHEMICALS

See us at the Pittsburgh Conference, Booths 405–411

J.T. Baker Chemical Co.
Phillipsburg, New Jersey 08865

Yes, Please send me more information for the following:

- ☐ ULTREX® Solvents
- ☐ 'Baker Instra-Analyzed'® Solvents
- ☐ PHOTREX® Solvents
- ☐ LSC Solvents
- ☐ HPLC Solvents
- ☐ 'Baker Resi-Analyzed'® Solvents

Name _____
Title _____
Dept. _____
Organization _____
Address _____
_____ zip

CIRCLE 22 ON READER SERVICE CARD

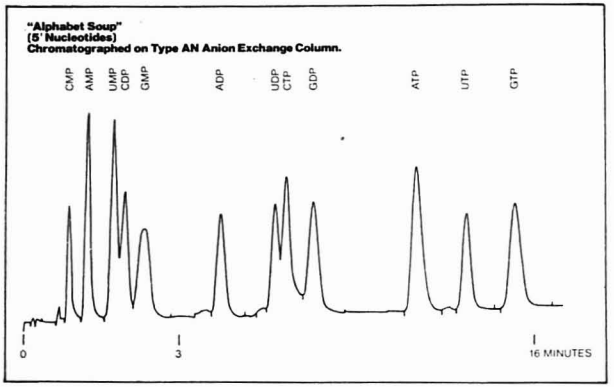
Six New HPLC Columns

Two ion exchange columns
Now you can purchase high efficiency, high capacity, 10 micron ion exchange columns. They're Brownlee Labs packed columns and they're available now from Rheodyne. Look at the chromatogram below!

Are you in Reverse Phase?
Choose RP-2, RP-8, or RP-18 (new). To help you decide which one to use, we have a little note for you.

It is Technical Note #910 and it compares the three reverse phase packings and gives a useful insight into their application.

Fully specified and doubly guaranteed
Brownlee Labs guarantees each column with respect to plates per meter and peak symmetry. Each column is shipped with its own test chromatogram which shows completely specified test conditions and results.



Brownlee HPLC columns* available through Rheodyne

Guaranteed Minimum Specifications		Plates per meter	Symmetry
Reverse Phases			
RP-2 (new)	10 micron	12,000	1.8
RP-8	10 micron	18,000	1.6
RP-8	5 micron	36,000	1.6
RP-18 (new)	10 micron	12,000	1.8
RP-18 (new)	5 micron	24,000	1.8
Adsorption Phases			
Si 100	10 micron	20,000	1.6
Si 100	5 micron	36,000	1.6
Alox T (new)	10 micron	14,000	1.6
Polar Bonded Phases			
NH2	10 micron	18,000	1.6
DIOL	10 micron	16,000	1.6
Ion Exchangers			
AN (new)	10 micron	10,000	2.0
KAT (new)	10 micron	16,000	2.0

*Column packings are LiChrosorb (a trademark of E. Merck, Darmstadt, Germany).
All columns are 4.6 mm I.D. x 25 cm long.

Write for price list and Technical Note #910.
Please address Rheodyne, Inc., 2809 Tenth Street, Berkeley, Calif. 94710. For even faster service, phone (415) 548-5374.

RHEODYNE
THE LC CONNECTION COMPANY
CIRCLE 183 ON READER SERVICE CARD

Another innovation from L/I:
The REPIPET® II dispenser
Virtually unbreakable!

Better than any $85 plastic dispenser! But only $52.50!*

Here it is, the best value ever offered in reagent dispensers. The tough REPIPET II reflects more than 14 years of L/I's experience in liquid dispensing—your best assurance of quality and performance. All REPIPET II dispensers feature the use of fluorocarbon and extra-thick borosilicate glass for strength and durability. They're tough lab workhorses, virtually impossible to break.

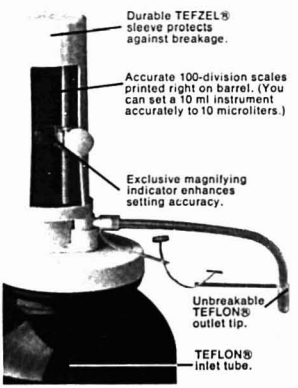
Note the 100-division scales, printed where they should be—on the glass barrel, not on an elastic plastic! L/I's exclusive sturdy magnifying indicator is a further aid to precise volume settings.

L/I guarantees accuracy of 1.5% full scale and 0.2% reproducibility for all REPIPET II dispensers. They are suitable for use with all laboratory reagents (except HF).

(Although TEFZEL® plastic and TEFLON® plastic are chemically inert to all laboratory reagents, slight distortions may occur at autoclaving temperatures and with some strong solvents.)

REPIPET II dispensers are offered in three popular sizes, 5, 10, and 20 ml. Price of 5 and 10 ml units is $52.50; 20 ml, $58.50.

To order, contact your distributor. For literature, write, call or circle the reader service number below.



LABINDUSTRIES
620 Hearst Avenue, Berkeley, CA 94710
Phone (415) 843-0220
CIRCLE 126 ON READER SERVICE CARD

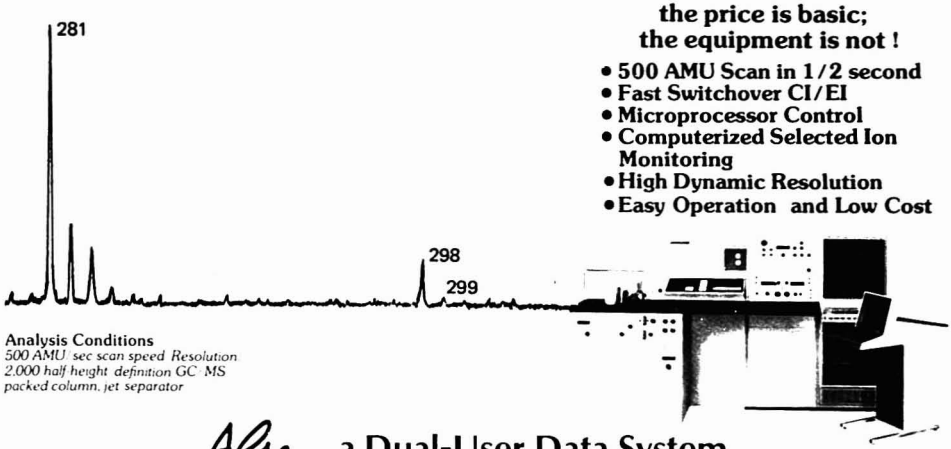
New at the Pittsburgh Conference... Booths 639-645

GC/MS

300 femtomole full spectrum

**The KRATOS MS-25—
the price is basic;
the equipment is not !**

- **500 AMU Scan in 1/2 second**
- **Fast Switchover CI/EI**
- **Microprocessor Control**
- **Computerized Selected Ion Monitoring**
- **High Dynamic Resolution**
- **Easy Operation and Low Cost**



Analysis Conditions
500 AMU/sec scan speed Resolution 2,000 half height definition GC/MS packed column, jet separator

Also... a Dual-User Data System

Add any of the KRATOS DS50S Data Systems (right, in photo above) and the MS-25 becomes an integrated GC/MS/DS system—a high-performance package offering the absolute latest in all three technologies.

DS50S-Series Data Systems are available for operation with a single GC/MS unit . . . with two units . . . or in stereo versions for up to four instrument operation.

Talk to us in Cleveland

While at the Conference, also talk to us about the other products that have made KRATOS *the* source for fine analytical instruments:

•ESCA/Auger •X-Ray Diffraction
•High-Resolution Mass Spectrometry

KRATOS, INC.
AEI Scientific Instruments
8322 Clairemont Mesa Blvd.
San Diego, CA 92111
Telephone (714) 292-0925

KRATOS, LTD.
AEI Scientific Instruments
Barton Dock Road, Urmston, Manchester
England M31 2LD
Telephone 061-865-4466

Circle 121 For Literature
Circle 122 For Salesman to call

The VYDAC™ Family for your HPLC Separation needs

I	Vydac SC 37u, 10m²/ gm
II	Vydac TP 10u, 100m²/ gm
III	Vydac IR 10u, 350m²/ gm
IV	Phases: RP-2, RP-8, RP-18, oxynitrile, Adsorbent, SAX, SCX, WAX
V	Pre-packed columns 3.2mm, 4.6mm, 10mm
VI	Bulk material
VII	Simple Slurry Packing set-up for packing your own columns
VIII	Empty columns, zero dead volume end fittings and etc.
IX	All Vydac materials are made and manufactured in the U.S.A.

by

THE SEP/A/RA/TIONS GROUP

P.O. BOX 867
HESPERIA CALIFORNIA 92345

Booth 1246, 1248, at the Pittsburgh Conference

CIRCLE 246 ON READER SERVICE CARD

The only thing variable about the SF 770 Spectroflow Monitor for liquid chromatography ...is the wavelength!

- It consistently offers highest sensitivity with low noise and baseline drift.
- It classically follows Beer's law in its measurements.
- It routinely includes an automatic gain control and zero suppression.
- It equally interfaces with all Liquid Chromatography systems.
- It inconspicuously takes up very little room.
- It uniquely incorporates a double-beam design.
- It invariably is an honest instrument, not relying on gimmicks to achieve unrealistic specs.
- It indubitably is preferred by more liquid chromatographers than all other models combined.



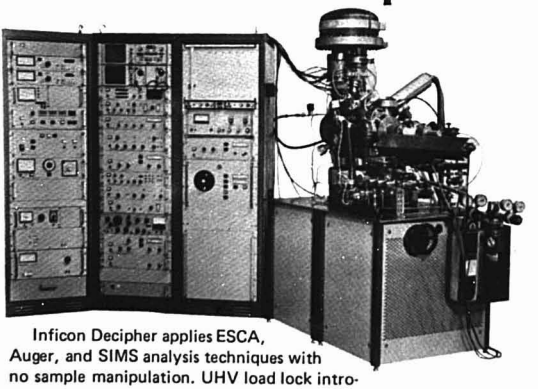
Call or write now!

24 BOOKER STREET, WESTWOOD, NEW JERSEY 07675
(201) 664-7263

SCHOEFFEL INSTRUMENT CORPORATION

See us at the Pittsburgh Conference, booths 845–847
CIRCLE 216 ON READER SERVICE CARD

One Surface Analysis Instrument Now Deciphers All



Inficon Decipher applies ESCA, Auger, and SIMS analysis techniques with no sample manipulation. UHV load lock introduces samples in seconds; unique energy analyzer secures constant sample area. It's the most advanced complete instrument of its type.

Write for 16-page color booklet.

Infinitely better,

INFICON LEYBOLD-HERAEUS

5 Adler Drive, East Syracuse, NY 13057
Phone 315/437-0377 TWX 710 541-0594

Inquiries outside North America to: Leybold-Heraeus GMBH & Co. KG
Gaedestrasse, D-5000 Cologne 51, West Germany

CIRCLE 110 ON READER SERVICE CARD



New from Philips: Atomic Absorption programmed for your applications.

Introducing the Pye Unicam SP2900 double-beam AA spectrophotometer with powerful Data Center.

This versatile Atomic Absorption system features a microprocessor-based Data Center offering the user unprecedented flexibility. With the program cards provided, you can easily tailor system performance to meet your own individual operating requirements.

Data Center's program cards offer a wide variety of different curve corrections and calibrations. The SP2900 provides simultaneous high accuracy background correction over a wider absorbance range. Data Center does the calculations, thus allowing you to do the chemistry!

You'll find that the SP2900 system offers a new level of precision, sensitivity and detection limits, all of which are backed up with fully-published specifications.

Beyond its pace-setting performance, there are many more reasons to see the SP2900 in action: Every Pye Unicam Atomic Absorption system is backed by comprehensive applications, sales and service assistance throughout North America and overseas.

Invest a few minutes of your time to request our Atomic Absorption information package, or see a demonstration of this powerful system. We think you'll find it programmed for *your* applications.



Philips Electronic Instruments, Inc.
A North American Philips Company

85 McKee Drive, Mahwah, N.J. 07430
Telephone (201) 529-3800

International — Contact Pye Unicam Ltd.
York Street, Cambridge, England CB1 2PX
Telephone, Cambridge (0223) 58866
Telex 817331

PHILIPS **Electronic Instruments**

PHILIPS

Be sure to visit our display at the Cleveland Conference, Booth #601–608
CIRCLE 174 ON READER SERVICE CARD

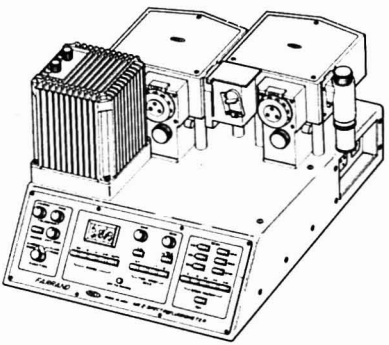
Reach New Levels
in fluorescence and absorption spectroscopy

ECONOMY . . . PERFORMANCE . . . DEPENDABILITY

MK-2 SPECTROFLUOROMETER

Operational simplicity and automated features bring a bright new dimension to our world-renowned Spectrofluorometers.

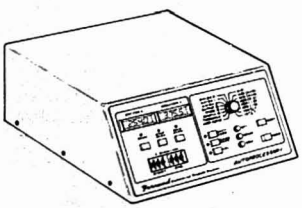
- *auto-ranging continuously selects sensitivity scale corresponding to sample signal intensity*
- *improved electro-optical design resulting in 1 part per trillion quinine sulfate sensitivity*
- *simplified pushbutton operation*
- *digital display of luminescence with serial BCD output*
- *synchronous scanning*
- *sealed lamp housing eliminates ozone*
- *xenon arc stabilizer eliminates arc fluctation, increases source stability, and extends lamp life*



Circle Reader Service Card No. 70

Modular design concept permits use of Corrected Spectra, Double-Beam Differential Fluorescence and Absorption, TLC scanners, and Phosphorescence accessories.

AUTOPROCESSOR-1



Circle Reader Service Card No. 233

FARRAND
THE FINEST IN
FLUORESCENCE
FOR OVER 30 YEARS

Advanced automation for our MK-1 and MK-2 Spectrofluorometers. This new Microprocessor system simplifies the most complex analytical research. In conjunction with the Corrected Excitation module which provides real time data, all functions performed by the Autoprocessor-1 are continuously and automatically updated. Can also be used with FARRAND's Auto Sampler for research and routine batch analyses.

Your Autoprocessor-1 performs the following functions:

- *corrected spectra*
- *instantaneous recalibration of corrected emission*
- *differential fluorescence*
- *ratio fluorescence*
- *absorption and transmission*
- *repetitive scanning between preselected wavelengths*
- *4-digit display of excitation and emission wavelength with parallel BCD output*

FARRAND OPTICAL CO., INC./Commercial Products Division/117 Wall St., Valhalla, N.Y. 10595/(914) 428-6800

COME SEE US AT PITTSBURGH CONFERENCE — Booths 336 and 338

FOCI

S. R. Crouch,[1] D. N. Baxter,[2]
E. H. Pals, and E. R. Johnson[3]
Department of Chemistry
Michigan State University
East Lansing, Mich. 48824

Simple Hardware Control Approach for Sequencing Chemical Instruments

In modern analytical instrumentation, digital controllers have become more and more complex and flexible as instruments have become more highly automated. The controller directs the sequencing of various instrument functions. For example, in an automated gas chromatography system, the controller might be required to send signals to an automatic sampler for introduction of the sample into the column, to control the oven temperature and its temperature program, to control the sensitivity of the detection system, and to control the detection and integration of the various chromatographic bands as they elute from the column. Such controllers may be simple fixed order sequencers or may require branching to skip certain functions if certain instrument conditions are set by the user (i.e., unless the temperature program button and rate have been set, the GC controller would skip this part of its sequence).

In modern instruments, controllers take the form of hardwired logic systems, minicomputers or microprocessors. The microprocessor is certain to become the controller of choice in the future for many operations, because the program (sequence) can be altered without changes in hardware. Also, even the most complex control operations, with multiple and nested branches, can be readily carried out under the supervision of a microprocessor. However, the microprocessor requires the instrument designer to be re-educated in terms of software and processor capabilities. This education process may require months to years in order to get working systems into the laboratory with "intelligent" instrument controllers.

A few years ago our research group became heavily involved in controllers when we decided to undertake a project that involved the spatial profiling of atomic concentration above a filament-type electrothermal atomizer using atomic absorption spectrometry. We desired to automate fully the operations of sample introduction to the filament, movement of the filament in both x and y directions away from the AA optical axis to predetermined destinations, temperature programming of the filament, data acquisition of background-corrected peak area, and automatic return to position "zero" for pickup of a new sample. The filament position controller was intended to move the atomization cell freely over a total displacement of 1 in. in either of two dimensions, through the use of stepper motor-driven micrometer translation stages. The controller was required to function in either a "local" mode, in which the desired filament position could be set by the user via front panel BCD switches, or in an "on line" mode in which the controller received binary information from a minicomputer and functioned as a hardware slave to the processor. In addition, we required the controller to convert BCD position code to binary code in the local mode, to use position instead of displacement as the input (i.e., to remember where it is and to determine the direction to move and how far to go), and to be capable of a hardware reset to an optically defined reference position. Finally, we required the controller to correct for backlash in the leadscrews of the translation stages in that if a requested movement was in the positive direction (away from the optical reference), the controller would intentionally move the cell to a known distance beyond the desired destination and then return to the true destination, in contrast to movement in the negative direction, which would proceed directly to the destination without such overshoot. In this manner, no matter whether the net movement was positive or negative, the cell would be moved last in the negative direction, thus leaving the leadscrews tightly meshed in that direction of movement.

Because of the complexity of our application, we did not look forward to relearning combinatorial and sequential logic methods, component minimization techniques, and other forgotten digital design methods. Microprocessor approaches were considered but later abandoned because the interleaving of real-time tasks each with their own timing requirements put the problem on a level of complexity where our then meager microprocessor experience could not hope to reach in a reasonable time. Fortunately, the sinking feeling we had originally experienced was short-lived when we discovered the simple approach to the design of complicated controllers described in this paper. Even for our complex application, this systems-level approach to controller design enabled us to design in about 3 h a unit requiring over 50 IC's per motor controller. Construction and debugging of the position controller required additional time, of course. The speed of our design was made possible by the use of a method, originally described by Richards (*1*), that allows all the complex sequential operations to be treated by using only a simple flow chart description at the beginning and by implementing the flow chart with 3-4 MSI IC's.

To understand the approach, we present in the first section of this paper the general concepts and principles of the "state" of a controller (*2*) and the simple implementation that results from the Richards (*1*) approach. We then present a chemical example of a "fall-through" sequencer

[1] To whom correspondence should be addressed.
[2] Present address, Eastman Kodak Co., Kodak Park, Building 82, Rochester, N.Y. 14650.
[3] Present address, Department of Chemistry, Wayne State University, Detroit, Mich. 48202.

0003-2700/78/0350-291A$01.00/0
© 1978 American Chemical Society

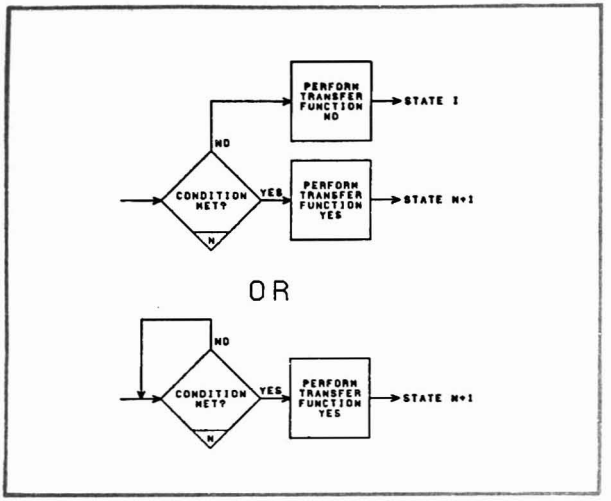


Figure 1. Basic flow chart units for transfer conditions and transfer functions. N: state number

that controls an automatic fraction collector used in elution chromatography. In the last section we describe a branching sequencer and illustrate its use as an electrothermal atomizer position controller.

Concept of the State

Automatic sequencing of measurement and control operations is highly desirable for modern chemical instruments. We assume here that the operations to be sequenced are ON-OFF operations that can be controlled by logic level signals. The sequencer must then produce logic level outputs for each controlled operation and must be responsible for the timing relationships of the appropriate logic level signals. There are a variety of approaches to the design of sequencers (*3*). However, the systematic approach presented here allows even the most complex sequencing applications to be handled with ease.

To help understand this approach, several terms must be defined. This can be done most conveniently with the aid of an example. Consider the controller for the thermostat on a temperature bath. The method described by Richards (*1*) considers it to have three states: State 0 = thermostat off–heater off; State 1 = heater on; and State 2 = heater off. In State 0 the thermostat controller waits for the condition of the thermostat power switch to be on. The on condition of the switch then is referred to as a *transfer condition*. When the transfer condition for State 0 is true, i.e., the switch is on, the controller advances to State 1. The process of this advance causes a *transfer function* to occur. The heater is turned on. The second state (State 1) tests to see if the bath temperature exceeds the limit set on the thermostat. When the bath temperature does exceed the limit, the controller steps to State 2, which causes another transfer function to occur. The heater is turned off. The transfer condition for State 2 is a bath temperature below the thermostat limit. When this condition is met, no transfer function is required except to return to State 0 and repeat the cycle.

Viewing such a trivial example in terms of states, transfer conditions, and transfer functions may seem overly complicated, but it is useful for two reasons. First, the method is also applicable to much more complex control applications. Second, with this approach the circuit design is greatly simplified by use of a standard circuit for the heart of the controller.

The application of this approach involves first converting the states, transfer conditions, and transfer functions into a standard flow chart format. The two basic flow chart units for each state are shown in Figure 1. The unit used depends on what is to occur at that particular state. Either unit contains a diamond-shaped box that represents the state and contains the transfer condition. Depending on the application, the basic unit will also contain one or two rectangles that represent the transfer functions which are to occur when the transfer conditions are met or not met. In this method the transfer function on the "no" leg (if one exists) is available only if the transfer condition not being met causes a move to a State 1 other than the present one. This transfer function, if it is used, is called a *secondary transfer function*, as opposed to the *primary transfer function* on the "yes" leg. Figure 2 shows the flow chart for the bath thermostat example. No secondary transfer functions are required for this application; therefore, the controller is an example

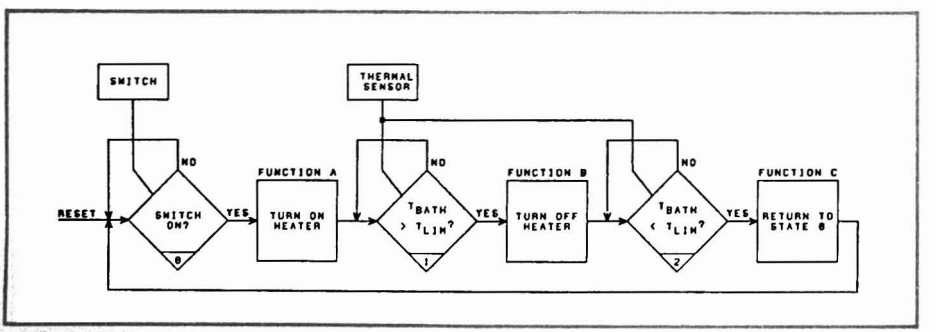


Figure 2. Sequencer flow chart for bath thermostat example

Coulometrics means Carbon Analyzers

- TOTAL CARBON
- ORGANIC CARBON
- MINERAL CARBON





COULOMETRICS MEANS VERSATILITY

COULOMETRICS carbon analyzers use a new coulometric carbon dioxide titrator to provide a new standard of accuracy, reliability and versatility in carbon determinations. They provide rapid analysis with minimal operator attention. Digital readout in micrograms of carbon. No standards or calibration required.

Look for us in Booth No. 1105 at the Pittsburgh Conference or call or write us for detailed information.

Coulometrics Incorporated

3830 High Ct., Box 544
Wheat Ridge, Colorado 80033
(303) 425-0799

CIRCLE 61 ON READER SERVICE CARD

WE TOO... Have New Accessories



For
- Atomic Absorption
- Infrared and
- Ultraviolet—Visible SPECTROPHOTOMETRY

Send for your own FREE 32 page 1978 Gold Book Catalog from

BUCK Scientific, Inc.

58 Fort Point Street, East Norwalk, Conn. 06855
(203) 853-9444

See us at the Pittsburgh Conference Booths 321-323

CIRCLE 93 ON READER SERVICE CARD

move fluids accurately with Sage syringe pumps



- set the flow rates you want at the turn of a dial
- models that hold up to three syringes
- models that will both infuse and withdraw
- nonpulsatile flow - insensitive to back pressure
- flow rates from 10's of milliliters per minute to microliters per day - depending on syringe used

SAGE INSTRUMENTS
380 Putnam Avenue
Cambridge, MA 02139 U.S.A.

CIRCLE 162 ON READER SERVICE CARD

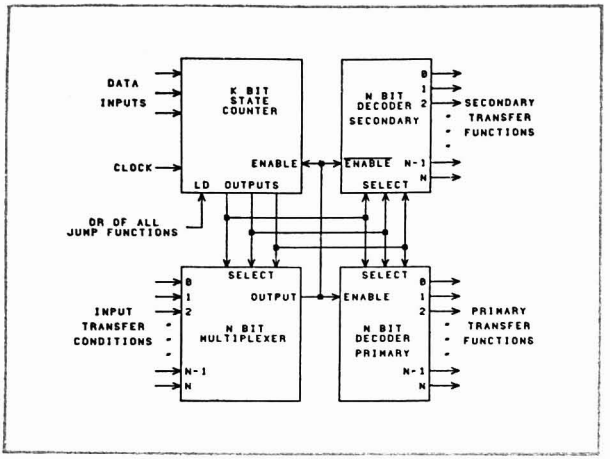


Figure 3. General schematic diagram of controller

of a *fall-through sequencer* (no conditional branches).

The "heart" of a sequencer based on this approach can be implemented with the standard integrated circuits shown in Figure 3. From the flow chart, the number of states in the sequence and the various transfer conditions and functions are known. If no secondary transfer functions are necessary, the secondary n-bit decoder can be eliminated. Thus, the heart of a sequencer consists of a k-bit counter, an n-bit multiplexer, and one or two n-bit decoders, where n is the number of states in the sequence and $n \leq 2^k$.

The k-bit counter keeps track of the state of the controller. Logic level signals representing the various transfer conditions are connected to the n-bit multiplexer. The outputs of the state counter determine which transfer condition is supplied by the multiplexer to one or two n-bit decoders. The multiplexer output also allows the state counter to increment to the next state on the next clock pulse after a "true" transfer condition. The presence of a "true" transfer condition at the multiplexer output causes the appropriate primary transfer function (as selected by the state counter) at the output of the decoder to go true. However, only a pulse occurs on the selected decoder output line, because the next clock pulse increments the state counter to the next state. If the transfer condition is false, either a secondary transfer function can be generated (at the secondary decoder output), or the sequencer merely waits in the same state until the transfer condition becomes true. To provide the capability for the sequencer to skip certain states under the appropriate conditions, a state counter capable of parallel loading is used. When a jump or branch in the sequence is necessary, the load (LD) line of the state counter is activated, and the new state is loaded into the counter through the data inputs.

An eight-state sequencer can be readily implemented with a 74163 counter, a 74151 multiplexer, and one or two 7442 decoders. At current single unit prices, they can be obtained for just over $3.00.

Fall-Through Sequencer

The fall-through sequencer is the simplest type. In this sequencer the only decision to be made is whether to remain in the present state or proceed to the next state. In a closed-loop operation this decision is based on receiving an "all done" signal (flag) from a previously actuated circuit. In an open-loop operation the change of state may be immediate or may occur upon receiving a signal that a time delay has elapsed.

A chemical example of a fall-through sequencer is a controller for an automatic fraction collector used in elution chromatography. Typically, the fraction collector has a rotatable tray that contains vials sequentially rotated beneath the column outlet valve. When a vial is directly beneath the outlet valve, the valve is opened for a preset time, then closed, and the next vial rotated into the receiving position. These motions are repeated until the desired number of fractions has been collected.

In Figure 4 the decisions and actions involved in controlling this apparatus are represented in flow diagram form, along with the external inputs used to make the decisions. Assume that the operator has initialized the apparatus, by rotating the first vial into position beneath the valve, and loaded the number of fractions desired into a counting register. Also, assume that the controller is initially in State 0. Condition A is satisfied since the counter is nonzero; therefore, the controller generates Function A, which is to open the delivery valve and to start the delay timer. Now the controller moves to State 1 and repeatedly queries the delay timer until it signals that enough solution has been de-

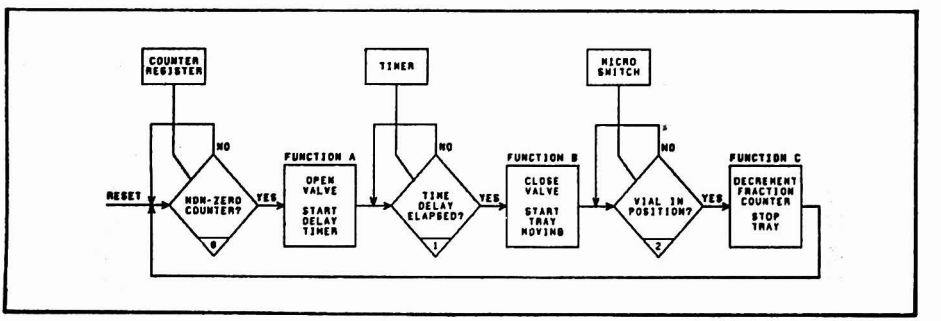


Figure 4. Sequencer flow chart for automatic fraction collector


Tygon® tubing
The one tubing that's right throughout the lab
Tygon laboratory tubing is specifically formulated to meet the high standards of quality and reliability required by laboratories everywhere.
Tygon is versatile enough to excel in almost any application. It has a broad range of chemical compatibility and safely handles most chemicals found in the lab.
But that's just part of the Tygon story. Tygon tubing is built tough to last. It resists aging and oxidation for a superior service life . . . which makes Tygon economical for even routine uses like with water and air. And because Tygon is glass-clear, you can check flow at any point.
But most important, Tygon will not affect the solutions or gases it carries. That's because it's non-contaminating, and has a smooth inner bore that resists residue build-up. You're assured of reproducible results, even when tests are made over a period of time. Tygon is available in popular vacuum tubing sizes as well.
Tygon Tubing Hot-Line: 800-321-9634
Specify the one tubing that's right throughout the lab — Tygon tubing. Call us toll-free for complete chemical resistance information, and the location of your nearest Tygon lab supply house. In Ohio, call collect 216-633-3224.
NORTON PLASTICS AND SYNTHETICS DIVISION
P.O. BOX 350 AKRON, OHIO 44309 TEL: (216) 633-3224
See us at booths 817, 819 Pittsburgh Conference
CIRCLE 140 ON READER SERVICE CARD

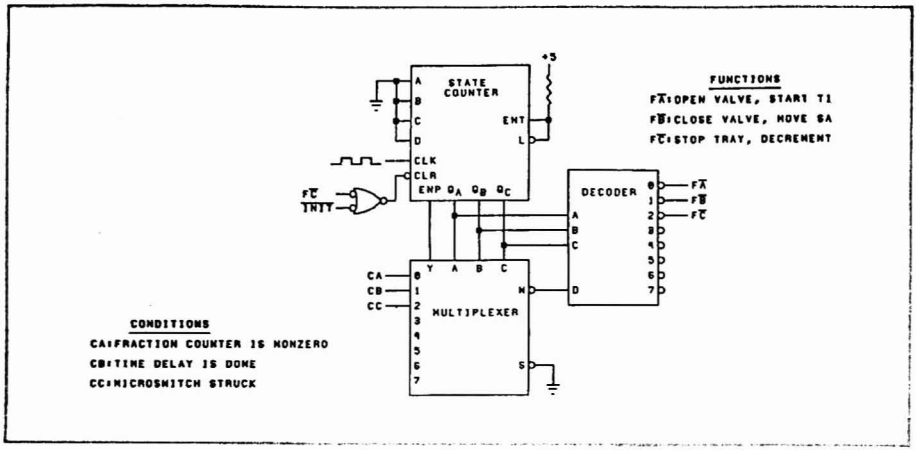


Figure 5. Schematic diagram of fraction collector controller

livered (Condition B). When Condition B has been satisfied, the controller closes the valve and starts the vial tray moving (Function B). Now the controller moves to State 2 and waits for a position indicator microswitch beneath the outlet valve to be tripped (Condition C). When Condition C is met, the controller must decrement the fraction counter register, stop the tray, and effect a jump back to controller State 0 (Function C). This sequence is then repeated until the fraction counter register is decremented to zero. When this happens, Condition A can never be met. The apparatus halts since it becomes hung up in State 0.

This controller can be quite easily implemented with three IC's: a 74163 counter, a 74151 multiplexer, and a 7442 decoder. Of course, additional packages may be necessary for such things as delay timing, but these three IC's handle the generation of all the signals necessary to initiate the actions at the appropriate times. Figure 5 shows how these IC's are interconnected and also the input and output signals required in this particular application. When power is turned on, an initialize pulse ($\overline{\text{INIT}}$) is required to clear the fraction counter register and to assert the CLEAR (CLR) input of the state counter. This forces the state counter to State 0. The Q_A, Q_B, and Q_C outputs of the state counter are all LO (zero), which sets the multiplexer's Y output LO. This LO signal is fed to the state counter's ENABLE P (EN P) input, which inhibits the counter from counting clock pulses at its CLOCK (CLK) input. Thus, it remains in State 0. The multiplexer's W output (the complement of the Y output) is directed to the decoder's D input. Output W is HI, and examination of the truth table for the decoder indicates that the 0–7 decoder outputs must be HI when D is HI (LO true logic is used at these outputs so that a function is generated only when the output goes LO). This means that initially none of the functions is being asserted. When the operator gives the "GO" command, the number of fractions desired is loaded into the fraction counter register, and Condition A is satisfied. Now the multiplexer's W output goes LO, and the decoder points to a decimal 0, which asserts the Function A signal ($F\overline{A}$).

Function A triggers external circuitry to open the delivery valve and start a time delay circuit. In addition, the multiplexer Y output is HI, so that the state counter's ENABLE P input is asserted, and on the first clock pulse the counter is incremented once (State 1). Now the multiplexer shifts from selecting data channel 0 (Condition A) to data channel 1 (Condition B). If the required time delay has not yet elapsed, Condition B is not yet satisfied so that the multiplexer Y output falls, locking the state counter in State 1, and the W output goes HI, concluding function A and inhibiting the decoder from generating any functions.

When the required time delay has elapsed, Condition B is satisfied, and a similar sequence occurs in the state counter, multiplexer, and decoder. The multiplexer's W output enables the decoder, and its A, B, C, and D inputs point to decimal 1. Thus, output 1 (Function B) is asserted. This triggers the valve to close and starts the tray moving. The multiplexer Y output goes HI, allowing the counter to count one pulse and move to State 2. Now the state counter requests the multiplexer to address the status of Condition C.

When the new sample vial reaches the position beneath the outlet valve, a microswitch is tripped and Condition C is satisfied. Again this activates the decoder, and Function C is asserted. Function C stops the tray and decrements the fraction counter register. Also, since this is the last function in the sequence, it is used to assert the CLEAR input of the state counter and return the controller to State 0.

Unless this was the last fraction to be collected, the fraction counter register will be nonzero when the state counter enters State 0 so that Condition A is immediately satisfied. Thus, as soon as the Function C pulse has cleared the state counter to State 0, Function A will be generated, and on the next clock pulse State 1 will be achieved. This entire delivery sequence will continue until the fraction counter register reaches zero, which prevents Condition A from being satisfied. Then the apparatus will halt because the controller becomes hung up in State 0 until the operator intervenes to start a new collection sequence.

Branching Sequencer

In many cases, it is desirable to have a sequencer capable of branching; that is, one in which sections of the basic state sequence may be skipped, repeated, or otherwise altered as requested by the instrumentation under control. An example of such a sequencer is the electrothermal atomizer position controller mentioned previously.

Flat surface Combination pH Electrode



Special Introductory Offer

$55 SALE PRICE

regularly 85.00

Flat surface pH and reference constructed into a single probe.

0 - 14pH

0 to 80° C

12mm x 145mm long

High impact epoxy body

Used for flat surface pH measurements such as: Skin Cultures Soil, etc.

Sealed, gel-filled calomel reference.

MODEL 9113

Specify type or pH meter or plug when ordering.

BROADLEY-JAMES-CORPORATION

1714 South Lyon Street, Santa Ana, CA 92705

(714) 547-8061

– Limited time offer –

CIRCLE 47 ON READER SERVICE CARD

RECYCLED Instruments Save Money!

- YOU CAN HAVE INSTRUMENTS pre-owned but completely refurbished and fully warranted . . . Save 50% of the new replacement cost from the nation's leader in REBUILT Atomic Absorption, Infrared and Ultraviolet-Visible Spectrophotometers.
- WE CURRENTLY STOCK reconditioned instruments from: Beckman, Coleman, Hitachi, Leads & Northrup, Perkin-Elmer, Varian and Others.
- WE PROVIDE SERVICE repair and preventative maintenance at rates lower than the original equipment manufacturers.

Call or write for our latest FREE brochure of REMANUFACTURED ANALYTICAL INSTRUMENTS.

See us at the Pittsburgh Conference Booths 321-323

BUCK Scientific, Inc.

58 Fort Point Street, East Norwalk, Conn. 06855

(203) 853-9444

CIRCLE 92 ON READER SERVICE CARD

In data acquisition a computer/calculator can win half the battle.

Winning the other half is our job.

Putting computer/calculators to work in process control and data acquisition is our business. We're helping to assemble custom, cost effective interface systems from coast to coast, from cement plants to research laboratories. Put your computer/calculator to work.

Call 415-444-2376 and ask John Peddie how Fluidyne can help win your interface battle. Or write Fluidyne Instrumentation, 1631 San Pablo Ave., Oakland, CA 94612.



Fluidyne

The Interface People

CIRCLE 76 ON READER SERVICE CARD

The flow diagram of its sequence is shown in Figure 6. The system waits in State 0 until data representing a new location are received, and a command to move is given. Upon receipt of this command, the overflow flag is cleared, and the system determines if it is being operated under local or computer control. If control is local, the desired destination has been entered in BCD format from front panel thumb-wheel switches, which requires a BCD to binary conversion. A check is made to see if the system is free of overflow; if so, another check is made to see if BCD to binary conversion is complete. If conversion is not complete, the registers are clocked, and the checks for overflow and complete conversion are repeated. If an overflow should occur, the sequence will abort to State 0 with the overflow flag set. (Overflow results from entering a destination outside the defined limits of the system.) If no overflow occurs, then upon completion of the conversion, the stepper motor direction is determined, and the stage begins to move. If control is from the computer, the BCD to binary conversion is unnecessary. Thus, this section of the sequence is omitted.

The stage moves until the destination is reached. At this point the system checks to see if the direction of movement was positive. If so, the stage continues to move 10 additional increments positive, and when finished, reverses direction and comes back 10 increments negative. If movement was originally negative, the sequence is concluded immediately. In this manner, gear play is removed from the mechanism by assuring that movement always occurs last in the negative direction.

To implement a branching sequencer such as this, it is necessary to add only one additional decoder IC to the basic controller circuit. The actual wiring is shown in Figure 7. The actions of this controller are identical to the simpler three-chip system previously discussed as long as the basic, nonbranching sequence is followed. If a branch is called for, however (if the selected data channel of the multiplexer is LO when a potentially branchable state is reached), the following events occur. The LO state of output Y from the multiplexer causes the function pulse to be generated by the second decoder instead of the first decoder. This function pulse is used by the instrument to perform tasks in the same manner as any function pulse from the first decoder. In addition, this pulse is also fed back to the state counter where it serves simultaneously to provide binary data representing the state to which to branch as well as to load those data into the state counter. For example, in the positioner sequence, if the system is under computer control when State 1 is entered, the LO level at the data Channel 1 of the multiplexer disables the first decoder, but causes the second decoder to generate Function B2. Function B2 is used in the circuitry to update the direction of movement and start the motor, just as Function D1 of the first decoder does under local control. But it is also present at the C and Load (L) inputs of the state counter so that as it occurs, the state counter is forced to skip directly to State 4 through parallel loading. All additional functions that are part of other such branches are similarly directed back to the Load and appropriate data inputs of the state counter, by use of simple gates as shown to OR them together as required.

By adding additional multiplexer and decoder chips to the controller, it is possible to produce sequencers of even greater complexity in which the branches consist not only of single

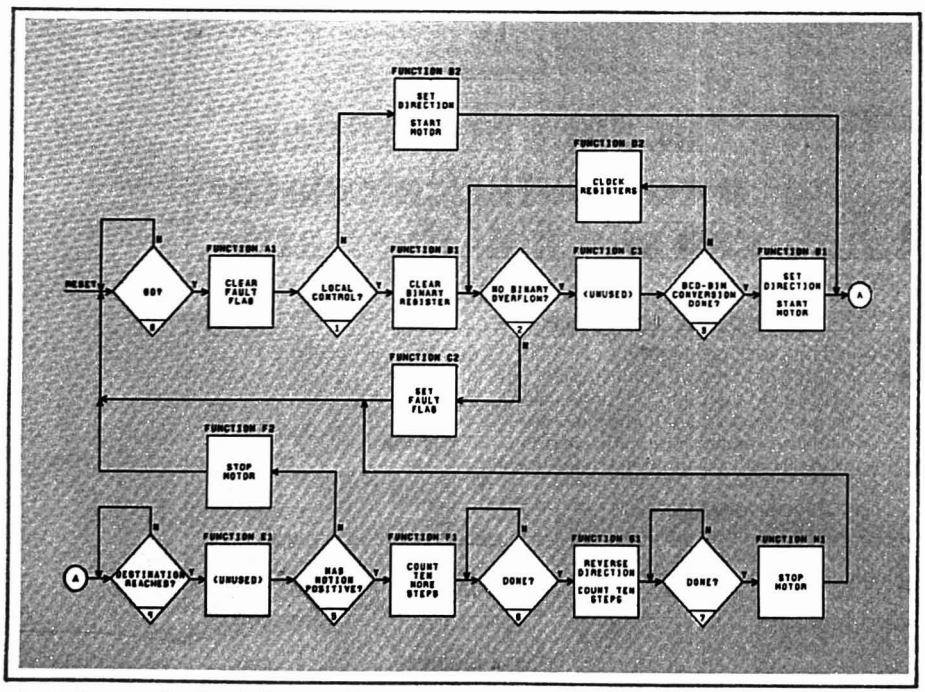


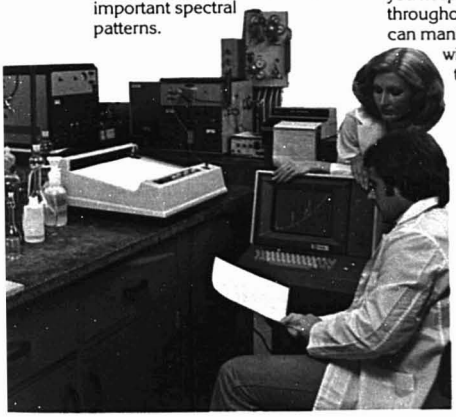
Figure 6. Sequencer flow chart for filament positioner

"With Graphics I can see at a glance what used to take hours to uncover."



You can get clean, sharp, hard copies from the 4631 Hard Copy unit; local storage with the 4923 Digital Cartridge Tape Recorder; and multicolor plots from the 4662 Interactive Digital Plotter, shown left.

Problem: Data reduction can be the weakest link in your analytical chain.
Every time you have to analyze spectral data from lists of numbers, you not only lose a world of time, you risk not recognizing important spectral patterns.



Solution: Tektronix Interactive Graphics can replace manual operations with precise, instant visual displays.
Tektronix Graphics Terminals let you keep to waveform display throughout your processing. You can manipulate data at will—without tedious and time-consuming manual translation. **You can see Graphic results immediately.** You can integrate and scale, correct baselines, perform mathematical transforms, and command camera-ready hard copy all with unequalled interactivity and simplicity.

Keeping your eyes on the display keeps your mind on the solution. Tektronix Graphics is priced right to begin with, and more than pays for itself in performance. And because it's from Tektronix, you know it's got the reliability that's been respected by research for years.

To get the whole Graphics story, talk to your Tektronix Sales Engineer, or write Tektronix.



Tektronix, Inc.
Information Display Group
P.O. Box 500
Beaverton, OR 97077
Tektronix Datatek N.V.
P.O. Box 159, Badhoevedorp,
The Netherlands

Copyright © 1977, Tektronix, Inc.
All rights reserved
OEM Information Available

CIRCLE 200 ON READER SERVICE CARD

Tektronix
COMMITTED TO EXCELLENCE

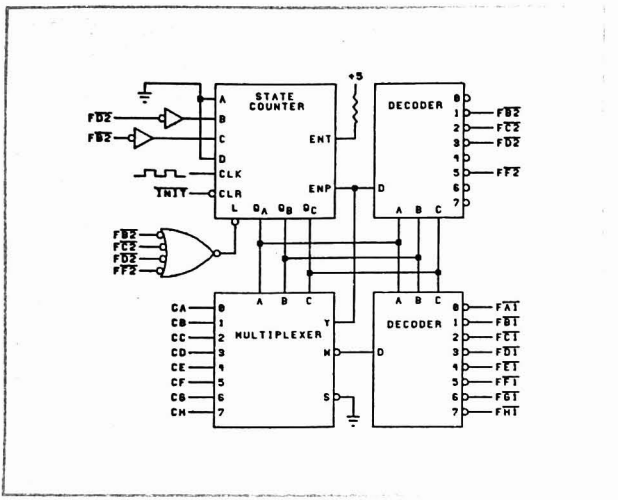


Figure 7. Schematic diagram of filament positioning controller

function pulses, but also of additional states or even complete subsequences reminiscent of nested computer subroutines (*1*). Similarly, it is also possible to substitute basic chips different from those employed here to produce sequences of more than eight basic states. However, such systems can quickly become unwieldy in their complexity and might very well be better performed using microprocessor-managed controllers even if the user has no previous experience with such devices (*4–6*).

Conclusions

We have described in this paper a hardware approach for designing instrument sequencers. We feel that this approach greatly reduces design time, yet allows complex sequences to be readily implemented. The increasing education of chemists as to the potential, the software, and the interfacing of microprocessors will certainly lead to a level of controller complexity at which a microprocessor is the sequencer of choice. Even so, the concepts presented here should enable simple controllers to be designed and implemented readily by chemists unfamiliar with microprocessors or for applications in which it is undesirable to "tie up" the processor in simple, unchanging control tasks.

In addition, the hardware approach is advantageous for high-speed control functions and for applications that involve the interleaving of tasks with quite dissimilar timing requirements. In fact, we have found in our own laboratories that hardware sequencers are important adjuncts to instrumentation systems supervised by minicomputers or microcomputers. Besides the electrothermal atomizer positioning systems, we have used this approach to design a minicomputer data acquisition system and a communications network between several microprocessors and a minicomputer. The simplicity and power of the approach should prove valuable to other chemists involved in the automation of chemical instrumentation.

Acknowledgment

We are grateful to T. V. Atkinson for his assistance in the use of a computerized graphics facility for the production of our figures.

References

(1) C. L. Richards, *Electronics*, 46 (3), 107 (1973).
(2) T. R. Blakeslee, "Digital Design with Standard MSI and LSI", pp 117–20, Wiley-Interscience, New York, N.Y., 1975.
(3) H. V. Malmstadt, C. G. Enke, and S. R. Crouch, "Electronic Measurements for Scientists", pp 662–7, Benjamin, New York, N.Y., 1973.
(4) D. R. McGlynn, "Microprocessors", Wiley-Interscience, New York, N.Y., 1976.
(5) B. Soucek, "Microprocessors and Microcomputers", Wiley-Interscience, New York, N.Y., 1976.
(6) T. R. Blakeslee, "Digital Design with Standard MSI and LSI", pp 150–232, Wiley-Interscience, New York, N.Y., 1975.

D.N.B. was recipient of both a summer and full-year ACS Analytical Fellowship under the sponsorship of Procter & Gamble Co., Cincinnati, Ohio.



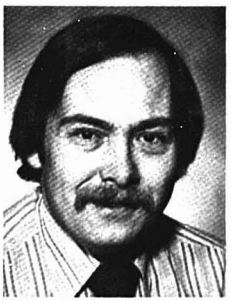
S. R. Crouch



D. N. Baxter



E. H. Pals



E. R. Johnson



FOR THE CREATIVE CHEMIST:

EASTMAN REAGENTS FOR GEL ELECTROPHORESIS.

Colorful currents soaring from the universe? No. It's actually a photomicrograph of EASTMAN Organic Chemical 8154, Phthalaldehyde, by John Delly, McCrone Research Institute. It demonstrates what can happen when you use your imagination and our chemicals.

For everyday applications, you'll appreciate the quality of our more than 120 Eastman gel-forming reagents, catalysts/initiators; buffers, dyes, stains, and other reagents for creative chemists working in acrylamide gel electrophoresis.

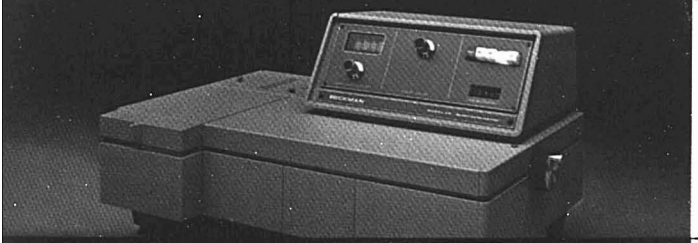
Dealers offering EASTMAN Organic Chemicals can also offer you thousands of other organics for electrophoresis: liquid scintillation counting; protein chemistry; dyes, stains, and indicators. See them for fast, reliable delivery and service; and a free reminder that chemistry is creative.

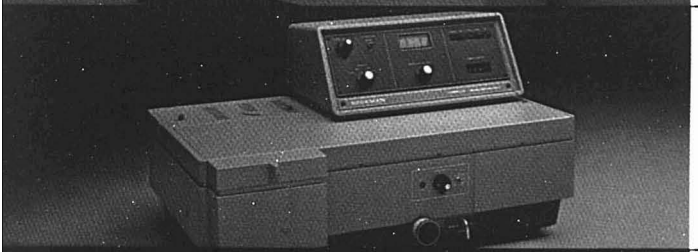
For a detailed description of Eastman reagents for gel electrophoresis, send for free technical literature, JJ-11. Write Eastman Organic Chemicals, Eastman Kodak Company, Dept. 412L, Rochester, N.Y. 14650.

Take a close look at EASTMAN Organic Chemicals. Dealers handling EASTMAN Organic Chemicals: American Scientific & Chemical, Bio Clinical Laboratories, Brand-Nu Laboratories, Inc., Bryant Laboratory, Inc., Custom Chemical Laboratories, Inc., Fisher Scientific, GAC Laboratories, Inc., Labproducts, Inc., Midland Scientific, Inc., North-Strong, Inc., Preiser Scientific, Sargent-Welch Scientific Products, Scientific & Industrial Sales & Service, Inc., VWR Scientific Inc., Ward's Natural Science Establishment, Inc.

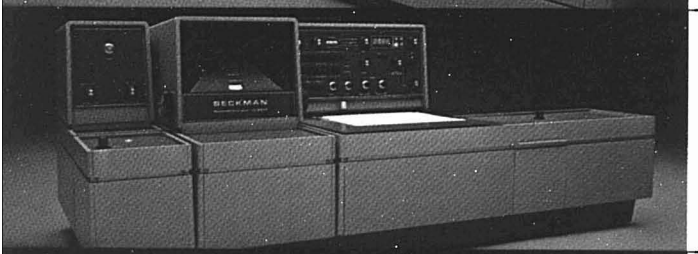
CIRCLE 63 ON READER SERVICE CARD

Only Beckman backs up a full UV line with a full 37 years of UV experience.











And that's why all our instruments from the workhorse 25 to the state-of-the-art 5270 offer exceptional reliability and performance.

They feature, too, genuine human engineering factors, the kind that simplify the acquisition of superior quality answers, and are only learned from years of hands-

Model 24/25 Considered by many to be the standard for a high performance workhorse, the 24/25 series offers a unique *common optics* system and double beam capability at a single beam price. Minimal controls, formatted chart paper, digital

Model 34/35 The new series 34/35 instruments offers a broad range of convenience, performance, and precision design features previously unavailable on medium-priced units. A *common optics* system with a common beam aperture, a program-

Model 3600 The new 3600 features a high performance holographic grating monochromator teamed with common optics, programmable or fixed slits, automatic source change, and an advanced recorder. Pushbutton selection of 11 chart speeds,

Model 5230 The 5230 is a complete research grade instrument designed with a classical superstructure for long-term optical stability and overall ruggedness and reliability. Exceptional quality supporting hardware includes an innovative holo-

Model 5270 No short form list of performance characteristics can sum up the 5270. It is, for many researchers in biomedicine and chemistry, simply the best UV instrument that has ever been made. And you might say that excellence was 37 years

on field experience. As for breadth of applications, that's where experience can be critical. Since 1941 and the first DU,® we've developed over 40 major accessory systems to specialize an instrument (at a minimum cost) for a specific application.

Today, the Beckman tradition of UV innovation continues with special capabilities for such applications as: Gel Scanning. Scatter Transmission. Kinetic Monitoring. Wavelength Programming. Column Monitoring. Reflectance Measurement—Specular and Diffuse. And Dissolution Monitoring to meet the most stringent government standards.

In short, whatever your budget or whatever your application, the Beckman UV team can help. Check out the instruments below to find the one that meets your needs exactly. Then for more information contact Scientific Instruments Division, Beckman Instruments, Inc., P.O. Box C-19600, Irvine, CA 92713.

Innovation in UV since 1941.

---

readout, and a long record for stable performance all work to make the 24/25's simple to operate, fast and precise.

---

mable slit system, automatic absorbance overrange detection, 0-3 absorbance range, *k Factor,* fast scanning speeds, expanded scales, and time constant selection are just some of the 34/35's attributes.

---

5 scan speeds, and 7 ordinate spans directly calibrated in absorbance provide a variety of convenient formats. Other capabilities include: Readout in absorbance, concentration, or percent transmission with first and second derivative recording, multi-

wave length programming, 0-3 absorbance range, and 4 Time Constant Selection.

---

graphic grating, true ratio recording capability, servo-operated slits, stepper motor drive, and computer compatible digital output to provide truly excellent performance for the instrument dollar.

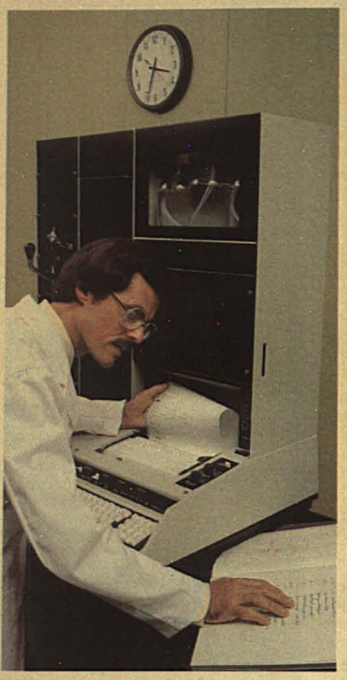
---

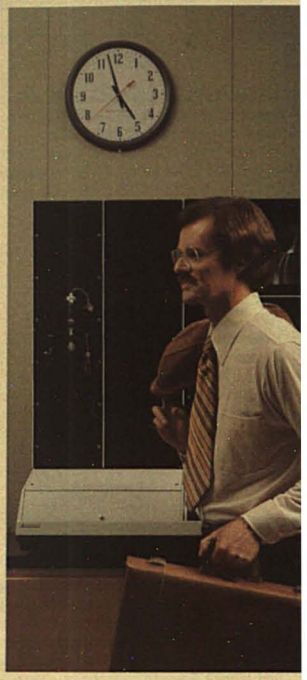
in the making. Of course, if you can't put one in your lab on tomorrow's budget, we'd like you to remember that all Beckman Instruments share in the DU heritage and our 37 year commitment to UV analysis.

See our complete line of products at the Pittsburgh Conference

BECKMAN®

'Round-the-Clock HPLC: Development and





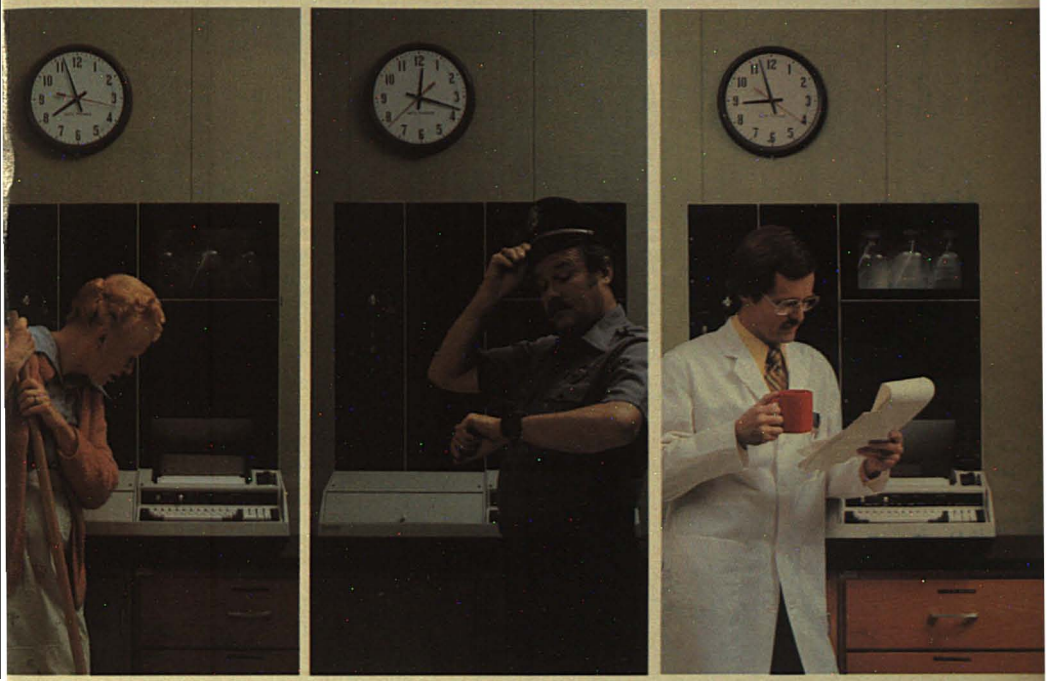
Ternary gradient capability, automatic sample injection, programmable chromatographic parameter changes, a dual-channel data system, and printer/plotter output make SP 8000 the first *truly automatic* HPLC.

Cut methods development time by up to 75%.
LC methods development calls for the systematic changing of chromatographic conditions: temperature, flow rate, mobile phase composition and other variables. SP 8000, by means of its microprocessor and keyboard programming, is the first HPLC to control all these things automatically.

Faster, more complete separations.
HPLC has always been viewed as potentially more powerful than GC because its mobile phase is an active partner in the separation process. Now recent work has shown that different solvent ratios in ternary mobile phases produce markedly different separations. For example: the selectivity of a reversed-phase column can be changed by varying the ratio of water, methanol, and acetonitrile. SP 8000, with its microprocessor-controlled, three-solvent, single-pump gradient system, puts this added separation power at your command.

Improved quantitative results and finished reports.
SP 8000's powerful *dual-channel* data system provides extensive report formatting and post-run calculation capabilities. Its functions include internal/external standardization and normalization; multi-level calibration; bracketing; statistical analyses; molecular weight distribution; and simultaneous dual-detector analysis, all recorded on a built-in printer/plotter. It's the kind of advanced system you'd expect to get

Unattended Methods Repetitive Analysis.



from the company that invented the computing integrator.

There's a configuration *for your laboratory.*

Within its basic 33-inch-wide cabinet, SP 8000 can be configured in a variety of ways to fill a specific need and a specific budget. Options include an oven, a gradient programmer, a data system, an autosampler, detectors, and columns. It's the most advanced modular design of any HPLC.

Drop us a line for details. We'll be happy to show you how you can do 'round-the-clock HPLC.

See SP 8000 in Booths 841-844 at the Pittsburgh Analytical Conference February 27th thru March 3rd.

Spectra-Physics, 2905 Stender Way, Santa Clara, California 95051 U.S.A.

In Europe: Spectra-Physics GmbH, Alsfelder Strasse 12, 6100 Darmstadt, West Germany.



SP 8000 HPLC

OK. OK. I'm interested in SP 8000.

☐ Have someone give me a call.

My need is ☐ Immediate ☐ 5-6 months out ☐ Long-term ☐ Send literature.

( ) -

Phone

Name

Title

Organization

Department

Address

City State

Country Zip (In U.S.A.)

Mail to: Spectra-Physics, 2905 Stender Way, Santa Clara, California 95051 U.S.A.

In Europe: Spectra-Physics GmbH, Alsfelder Strasse 12, 6100 Darmstadt, West Germany.

AC 2/78

Spectra-Physics

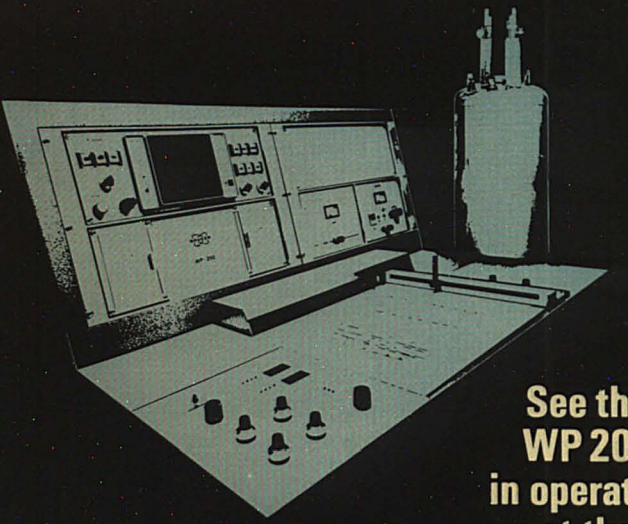
Innovators in Chromatography

CIRCLE 189 ON READER SERVICE CARD

BRUKER

WP 200

LOW-COST SUPERCON



A New Generation in NMR Spectroscopy

- HIGH FIELD PERFORMANCE ... 200 MHz for Proton
- LOW COST ... $160,000 for Proton and Carbon FT
- LOW OPERATING COST ... Approx. 25 l Helium per month

See the WP 200 in operation at the Pittsburgh Conference

Cleveland — Feb. 27 to March 3

For more information on this exciting new spectrometer, call or write:

BRUKER INSTRUMENTS, INC.
Manning Park
Billerica, Mass. 01821
Tel: 617 667-9580

BRUKER INSTRUMENTS, INC.
539 Beall Avenue
Rockville, Maryland 20850
Tel: 301 762-4440

BRUKER INSTRUMENTS, INC.
1801 Page Mill Road, Suite 212
Palo Alto, California 94304
Tel: 415 493-3173

BRUKER SPECTROSPIN LTD.
2410 Dunwin Drive, Unit 4
Mississauga, Ontario, Canada
L5L 1J9 Tel: 416 625-2374

BRUKER - WORLD LEADER IN MAGNETIC RESONANCE

Use this card to receive 1978
your own monthly copy of
ANALYTICAL CHEMISTRY

Start my subscription as follows:

	U.S.	Can.**	Foreign**
ACS Members*	☐ $10.00	☐ $19.00	☐ $19.00
Nonmembers (Personal)	☐ $14.00	☐ $23.00	☐ $23.00
Institutional	☐ $14.00	☐ $23.00	☐ $29.00

☐ Bill me ☐ Bill Company ☐ Payment enclosed
(Make payable: American Chemical Society)

Name _____

Position _____

Your Employer _____
☐ Home
Address ☐ Business _____

City _____ State _____ ZIP _____

Employer's business ☐ Manufacturing ☐ Academic
☐ Government ☐ Other

If manufacturer, type of products produced _____

*Subscriptions at ACS member rates are for personal use only.
**Payment must be made in U.S. Currency, by international money order, UNESCO coupons, U.S. bank draft, or through your book dealer.
Allow 60 days for your first copy to be put in the mail. 9998-G

Mail this postage-free card today

Use this card to receive 1978
your own monthly copy of
ANALYTICAL CHEMISTRY

Start my subscription as follows:

	U.S.	Can.**	Foreign**
ACS Members*	☐ $10.00	☐ $19.00	☐ $19.00
Nonmembers (Personal)	☐ $14.00	☐ $23.00	☐ $23.00
Institutional	☐ $14.00	☐ $23.00	☐ $29.00

☐ Bill me ☐ Bill Company ☐ Payment enclosed
(Make payable: American Chemical Society)

Name _____

Position _____

Your Employer _____
☐ Home
Address ☐ Business _____

City _____ State _____ ZIP _____

Employer's business ☐ Manufacturing ☐ Academic
☐ Government ☐ Other

If manufacturer, type of products produced _____

*Subscriptions at ACS member rates are for personal use only.
**Payment must be made in U.S. Currency, by international money order, UNESCO coupons, U.S. bank draft, or through your book dealer.
Allow 60 days for your first copy to be put in the mail. 9998-G

Mail this postage-free card today

FIRST CLASS
Permit No. 1411-R
Washington, D.C.

BUSINESS REPLY MAIL
No postage stamp necessary if mailed in the United States

Postage will be paid by

AMERICAN CHEMICAL SOCIETY
1155 Sixteenth Street, N. W.
Washington, D.C. 20036

ATTN: G. HEBRON

FIRST CLASS
Permit No. 1411-R
Washington, D.C

BUSINESS REPLY MAIL
No postage stamp necessary if mailed in the United States

Postage will be paid by

AMERICAN CHEMICAL SOCIETY
1155 Sixteenth Street, N. W.
Washington, D.C. 20036

ATTN: G. HEBRON

analytical
chemistry

Editor: **Herbert A. Laitinen**

EDITORIAL HEADQUARTERS
1155 Sixteenth St., N.W.
Washington, D.C. 20036
Phone: 202-872-4570 Teletype: 710-8220151

Managing Editor: Josephine M. Petruzzi
Associate Editor: Andrew A. Husovsky
Associate Editor, Easton: Elizabeth R. Rufe
Assistant Editors: Barbara Cassatt, Nancy J. Oddenino, Deborah C. Stewart
Production Manager: Leroy L. Corcoran
Art Director: John V. Sinnett
Designer: Alan Kahan
Artist: Diane Reich

Advisory Board: Donald H. Anderson, Peter Carr, Velmer Fassel, David Firestone, Kurt F. J. Heinrich, Philip F. Kane, Barry L. Karger, J. Jack Kirkland, Lynn L. Lewis, Marvin Margoshes, Harry B. Mark, Jr., J. W. Mitchell, Harry L. Pardue, Garry A. Rechnitz, W. D. Shults

Instrumentation Advisory Panel: Gary D. Christian, Catherine Fenselau, Nathan Gochman, Gary M. Hieftje, Gary Horlick, Peter J. Kissinger, James N. Little, C. David Miller, Sidney L. Phillips.

Contributing Editor: Claude A. Lucchesi
Department of Chemistry, Northwestern University, Evanston, Ill. 60201

Published by the
AMERICAN CHEMICAL SOCIETY
1155 16th Street, N.W.
Washington, D.C. 20036

Books and Journals Division
Director: D. H. Michael Bowen
Editorial: Charles R. Bertsch
Magazine and Production: Bacil Guiley
Research and Development: Seldon W. Terrant
Circulation Development: Marion Gurfein

Manuscript requirements are published in the January 1978 issue, page 189. Manuscripts for publication (4 copies) should be submitted to ANALYTICAL CHEMISTRY at the ACS Washington address.

The American Chemical Society and its editors assume no responsibility for the statements and opinions advanced by contributors. Views expressed in the editorials are those of the editors and do not necessarily represent the official position of the American Chemical Society.

Regulation of Carcinogens in the Environment

At the Chicago ACS meeting, a paper was presented to describe proposed new regulations to be invoked by NIOSH (National Institute of Occupational Safety and Health) to regulate carcinogens in the environment. Two sets of regulations are involved, one for the immediate environment of the industrial worker and the other for continuous exposure of the general population in the general environment. In each case, the regulations are expressed in terms of a reliable, sensitive analytical method appropriate to each application, and the regulation requires that each carcinogen be present in concentrations below the detection limit of the test. This type of regulation raises several questions from the analytical viewpoint.

First, there is the matter of choice of test. It is expected that a personal monitor of some sort would sample the actual immediate surroundings of each worker during a working day, and the analysis itself would be a simple one, perhaps a color change in the monitor itself. More elaborate and sensitive methods would be appropriate to testing the overall environment. It can be anticipated that a great deal of argument can arise about the choice of tests.

Then there is the question of proper sampling. A gaseous pollutant presents a relatively simple problem compared with airborne particulates, which have health effects related to particle size distribution.

Assuming that sampling is properly done, what about the anaiysis itself? Some of the proposed regulations are written in terms of elements, and thus ignore chemical species completely, even though carcinogenic activity is known to be sensitive to chemical differences in a given element and sometimes even physical differences in a given compound. A great deal of work is indicated to pinpoint the actual carcinogens and their detection.

A definition of detection limit is needed for each method. A straightforward definition is possible for repetitive instrumental response in terms of signal-to-noise ratio, but for simple color tests the definition becomes less rigorous.

Finally, and most seriously, the question of ultimate limits needs to be faced. Given a need, the science of analytical chemistry can push sensitivity essentially without foreseeable limit, as witnessed for example by announcements of single atom detection. It is easy to foresee that, especially in the open environment, the detection limit would be below the natural background level, defined as that existing in nature without the intervention of human activities. There is also the distinct possibility that an element may be essential to human health at one concentration, carcinogenic at another, and chemically toxic at still another.

Admittedly, it is not an easy task to set finite limits on safe exposure to carcinogens. The proposed regulations avoid the problem of "absolute zero" but introduce the almost equally knotty problem of selection of appropriate analytical methods and defining their sensitivity limits.



Purification of Analytical Reagents and Other Liquids by Low Temperature Vacuum Sublimation

J. W. Mitchell

Bell Laboratories, Murray Hill, New Jersey 07974

Small batch quantities (≤50 mL) of 15% hydrogen peroxide, doped originally with 1 μg/mL of Fe, Co, Cr, Mn, Cu, Zn, Ni, and V, have been sublimed cryogenically under vacuum. Quantitative analysis of 10 mL of the purified product by Coprex x-ray fluorescence showed amounts of the doped traces to be ≤0.1 μg. Monitoring the process by a more sensitive radiotracer method indicated less than 2 ng/g of Fe, Cr, Co, and Mn in the processed reagent. After a single sublimation treatment, decontamination factors determined by neutron activation analysis were 1107, 2680, and 323, respectively, for Mn, Co, and As. Low temperature sublimation is shown to be applicable for processing a broad range of liquids which includes analytical reagents, inorganic halides, organic solvents, and other compounds.

Sublimation has been documented well as a highly efficient technique for purifying appropriate solid compounds (*1*), but has not been used generally to decontaminate compounds that are liquids at ambient conditions. For the latter the liquid–vapor transition, distillation, has been conventionally exploited for obvious reasons. Distillation, because of advances such as controlling environmental factors, preventing violent boiling, improving still designs to eliminate entrainment (*2*), and constructing stills from Teflon and quartz (*3*, *4*), will continue to be an irreplaceable tool for ultrapurifying some analytical reagents. Sublimation, however, has the principal advantage over distillation of always occurring at a lower temperature. Water, for example, can be sublimed as ice, which has a vapor pressure of 3 mm at −5 °C, while distillation takes place at 100 °C at 760 mm. The former process, lyophilization, has been established as a convenient method for drying heat-sensitive biological fluids (*5*).

As shown by any familiar phase diagram of water, ice is in equilibrium only with water vapor at temperatures and pressures below the triple point. Except for the slope of the solid–liquid equilibrium arising from the expansion of water on freezing, similar phase diagrams should exist for other aqueous-like and certain organic compounds. For those with vapor pressures greater than ice, cryogenic sublimation should be possible below the triple point temperature and pressure.

In this paper, the results of an investigation to survey the types of compounds amenable to cryogenic sublimation are reported. The application of the method for purification of reagents that are in the liquid state at ambient conditions has also been demonstrated by the example, hydrogen peroxide.

EXPERIMENTAL

Apparatus. The apparatus used for preliminary tests of various compounds to determine their sublimability is shown in Figure 1. For these preliminary tests, the components of the apparatus were constructed from borosilicate glass. A polyfluorocarbon grease was used on joints and vacuum stopcocks. However, in subsequent purification runs, quartz vessels with Teflon stopcocks and Teflon sleeves for joints were used to minimize contamination. The reagent was sublimed from vessel A and the sublimate collected in chamber C. The collector (C) was placed in a Dewar flask, which was filled with either liquid nitrogen, a dry ice–acetone mixture, or some other liquid that was capable of maintaining sub-zero temperatures. A vacuum pump with a suitable cold-trap to prevent cross contamination of the product with hydrocarbon vapors or the pump with the reagent, was connected to B at position 3.

Sublimation was accomplished as follows: The assembled apparatus (parts B and C of Figure 1) was evacuated to a few mm of Hg pressure by positioning the three-way stopcocks (2, 4, 5) appropriately and by attaching a vacuum pump at position 3. A small volume of the test solution (up to 100 mL) was frozen in a thin shell on the walls of vessel A by rotating the container and its contents continuously in a dry ice–acetone bath. The round-bottom flask (A) was then connected to B at position 1 via a standard taper joint and held in place until stopcock 2 was positioned to allow the pressure in the entire apparatus to be reduced to a steady-state value that was governed by the sample being vaporized.

During sublimation, a source for the latent heat of sublimation was provided by keeping vessel A in contact with room air at 22 °C. Occasionally additional heat to prevent ice formation on the outside of the flask was provided with a heat lamp. Mass flow of vapors from the sublimer (A) to the collector (C) was induced by continuous evacuation of the apparatus. The reagent was collected by reverse sublimation onto the walls of collector C. Under these conditions a compound was labeled as cryogenically sublimable if 90% of the frozen material in the sublimer was transferred to and collected in the condenser. When the bulk of the reagent had sublimed from A, the stopcock (2) was positioned to seal the collector compartment under vacuum. Stopcock 2 was then adjusted to release the vacuum in vessel A.

Procedures. After a 15% solution of H_2O_2 was doped with 1 μg/mL of each of the elements, Fe, Co, Cr, V, Ni, Mn, and Cu, 50 mL of the solution was subjected to a one-stage sublimation. The sublimate was tested for H_2O_2 by titrating a small aliquot with ceric sulfate solution using ferroine as indicator. A second test on a portion of the trapped sublimate was made by adding 5 mL of 0.05 M sodium sulfide, acidifying the resulting solution with HNO_3 and by adding 1 mL of 0.1 M barium nitrate solution. The immediate precipitation of barium sulfate showed the presence of H_2O_2.

After subliming the reagent, a 10-mL sample of the purified reagent (sublimate of originally doped H_2O_2) was analyzed by an x-ray fluorescence technique using a Coprex procedure (*6*). Another portion of H_2O_2 was doped with 1 μg/mL of the trace elements and also spiked with ^{59}Fe, ^{51}Cr, ^{54}Mn, and ^{60}Co. In this case the amount of added tracer was negligible and produced no change in the total concentration of any element. Ten milliliters of this solution contained $\sim 1.60 \times 10^4$ counts of γ-ray activity per minute per milliliter for each isotope. The total γ-ray activity of the original reagent and activities of the individual isotopes at characteristic energies were measured before and after sublimation with a TMC Model 1001 multichannel analyzer equipped with a 3 inch × 3 inch well-type sodium iodide detector. A second sample (a 50-mL volume of 15% reagent) was doped with 1 μg/mL of As^{3+}, Co^{2+}, and Mn^{2+}. After sublimation, samples were packaged, transported to the reactor in the frozen state, and irradiated simultaneously with standards in a flux of $\sim 10^{13}$ n/cm^2 s^{-1} for 20 min. Decontamination factors (*DF* = concentration of element per mL in original reagent/concentration per mL in sublimed reagent) were then calculated after analysis of the purified product by neutron activation.

RESULTS AND DISCUSSION

Effect of Temperature on Purification Efficiency. Several practical advantages are derived from conducting a

0003-2700/78/0350-0194$01.00/0 © 1978 American Chemical Society

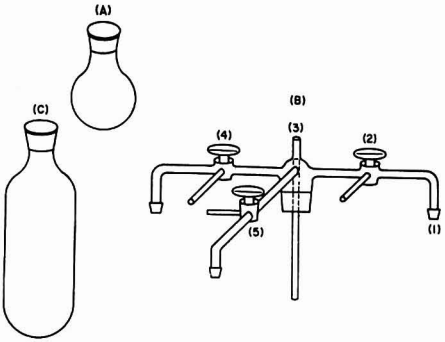


Figure 1. Vacuum sublimation apparatus

process for purification at low temperature. A primary limiting factor in ultrapurification of liquids, contamination by storage vessels (*7*), is reduced considerably by storage of pure chemicals in the frozen state (*8*). The chemical reactivity of hydroscopic or fuming liquids is reduced at low temperature and extremely toxic reagents can be processed more safely in the solid state. In addition to these practical advantages of performing purification processes at low temperature, considerations of thermodynamic concepts also suggest that greater efficiency of purification is achieved as the temperature at which the process is executed is lowered. In the case of the fractional distillation of liquids, the Clausius–Clapeyron Equation,

$$\frac{d(\ln P_1^\circ)}{dT} = \frac{\Delta H_1^v}{RT^2} \tag{1}$$

gives the relationship between temperature and the vapor pressure (P_1°) of a pure liquid that has a constant heat of vaporization (ΔH_1^v) over a short temperature range. A similar equation,

$$\frac{d(\ln P_2^\circ)}{dT} = \frac{\Delta H_2^v}{RT^2} \tag{2}$$

can be written for a second liquid. In a mixture of these two compounds the less volatile specie is designated by subscript 1, and the more volatile by 2.

Let the mole fraction of 1 in the liquid be X_1 and X_1' be the mole fraction of the component in the vapor phase above the liquid. The larger the ratio X_1/X_1' the better is the separation of the liquids by distillation. The mole fraction of liquid 1 in the vapor is given by Dalton's law,

$$X_1' = P_1/(P_1 + P_2) \tag{3}$$

where P_1 and P_2 are the partial pressures of the vapors in equilibrium with the liquid. The values of P_1 and P_2 are given by Raoult's law,

$$P_1 = P_1^\circ X_1 \text{ and } P_2 = P_2^\circ X_2 \tag{4}$$

The expression for the ratio, X_1/X_1', can then be written as

$$X_1/X_1' = (P_1 + P_2)/P_1^\circ \tag{5}$$

which reduces upon substitution of the relationships given in Equation 4 to

$$X_1/X_1' = X_1 + X_2\,(P_2^\circ/P_1^\circ) \tag{6}$$

From this it is seen that the ratio X_1/X_1' is increased, corresponding to better fractionation, by any factor that increases the term $(P_2^\circ/P_1^\circ)X_2$. The ratio, P_2°/P_1°, is altered for a two component mixture of liquids by the temperature as shown in the following sequence of equations.

Equations 1 and 2 can be combined to give

$$\frac{d(\ln (P_2^\circ/P_1^\circ))}{dT} = \frac{\Delta H_2^v - \Delta H_1^v}{RT^2} \tag{7}$$

which can be rearranged to

$$\frac{d(\ln(P_2^\circ/P_1^\circ))}{d(1/T)} = \frac{\Delta H_2^v - \Delta H_1^v}{R} \tag{8}$$

Assuming the heats of vaporization to be constant over a small temperature interval, integration of Equation 8 gives

$$\ln(P_2^\circ/P_1^\circ) = -\frac{\Delta H_2^v - \Delta H_1^v}{RT} + C \tag{9}$$

where C is the constant of integration. Since the liquid having the higher boiling point (lower vapor pressure) will usually have the higher heat of vaporization, ΔH_1^v will be greater than ΔH_2^v and the ratio, P_2°/P_1°, will decrease with increasing temperature. It can, therefore, be stated as a general rule that the fractional distillation of a given nearly ideal solution is more efficient, the lower the temperature at which it is carried out (*9*).

An equation corresponding to Equation 8 can be written for the sublimation of a two component mixture. In this case the Clausius–Clapeyron equation takes the form,

$$\frac{d(\ln(P_2^\circ/P_1^\circ))}{d(1/T)} = -\frac{\Delta H_2^{sub} - \Delta H_1^{sub}}{RT} + C \tag{10}$$

Here the heats of sublimation, ΔH_2^{sub} and ΔH_1^{sub} are assumed to remain constant over a short temperature interval. In a mixture of two chemically similar solids, i.e., amorphous compounds and others with similar crystal structures, lattice energies, phase transitions, and molecular interactions in the solid state, the more volatile component 2, will usually have the smaller heat of fusion. These seemingly restrictive requirements of similarity in the solid state are not limited to ideal or hypothetical systems. This behavior commonly occurs during the formation of solid solutions which result during quick freezing of mixtures of chemically similar liquids. Furthermore, the trace impurities most difficult to remove from a liquid are usually quite similar in structure, physical properties, and in chemical behavior to the major component. Also the ultrapurification of a reagent closely approximates the treatment of an infinitely dilute solution.

Since the general conclusion stated previously for fractional distillation applies equally as well for decontamination of solids by sublimation, it follows that the vapor phase produced by cryogenic sublimation of a mixture of two solids (frozen liquids) should contain a smaller quantity of the less volatile component than would be found in the vapor phase created by distillation at higher temperatures. Thus, collection of the gaseous phase produced by low temperature sublimation should permit the preparation of extremely pure compounds. Results of experimental tests of this principle are reported in this paper.

Compounds amenable to cryogenic sublimation are listed in Table I. Without detailed measurements of vapor pressure–temperature relationships or phase diagrams, no general prediction of compounds capable of being sublimed in this way is possible. However, it was observed that compounds with freezing points between −25 to 20 °C and boiling points less than 150 °C sublimed readily from vessel A, exposed to surrounding air at 20 °C. Optimization of sublimation rates by adjustment of vacuum conditions, by controlling temperature of the collector and sublimation chamber, and by selecting appropriate surface to sublimate ratios in the condenser should allow liquids with physical

Table I. Liquids Sublimable at Low Temperature

Analytical reagents and solvents	mp, °C	bp, °C
Water	0	100
Hydrogen peroxide (15%)	0.5	150
Acetic acid (99.5%)	16.6	118.5
Formic acid	8.4	100.7
Ammonium hydroxide (15%)	...	...
Hydrazine (95%)	1.4	113.5
Benzene	5.5	80
p-Dioxane	11.8	101
Carbon tetrachloride	−23	76.8
Cyclohexane	6.5	80.7
Bromoform	8.3	149.5
CVD reagents and other inorganic halides		
Arsenic trichloride	−8.5	130.2
Silicon tetrabromide	5.4	154
Arsenic trifluoride	−8.5	
Bromine trifluoride	−2(8.8)	135
Tungsten hexafluoride	2.5	17.5
Phosphorus oxychloride	2.0	105.3
Antimony pentachloride	2.8	79

properties lying beyond these ranges to be treated. These engineering considerations are being optimized in continuing investigations.

Purification of Hydrogen Peroxide. Ultrapure H_2O_2 (≤100 ng/g total cationic impurities) is required frequently as a strong oxidant during determinations of trace constituents. The adjustment of the oxidation state of elements to be determined by substoichiometric isotope dilution is a typical example (*10*). This reagent is also used for separating trace elements, for purifying ion-exchange resins, and a product containing ultralow levels of As, Sb, and Bi was sought recently for processing semiconductor devices (*11*).

Hydrogen peroxide of moderate purity can be obtained from several commercial suppliers. Apache Chemicals markets a 30% electronic grade reagent for which a purity quotation of 6 N (1 μg/mL of impurities) is given (*12*). J. T. Baker Chemical Co. supplies 30% H_2O_2 for electronic purposes. Their lot analysis indicates 0.5 μg/mL of Fe and 1 μg/mL of heavy metals (as Pb) (*13*). Fisher's 30% reagent is stated to contain 0.5 μg/mL Fe, 0.1 μg/mL Cu and Ni and 1 μg/mL heavy metals (*14*). These products contain concentrations of trace elements several orders of magnitude higher than other analytical reagents now supplied commercially (*13*).

Because of the sensitivity of H_2O_2 to decomposition, precautions are usually taken to use mild temperature conditions during purification. Procedures based on preliminary purifications by vacuum distillation (*15*, *16*) and further refinement by subsequent ion-exchange purifications at 0–3 °C have been reported (*17*). In the new procedure described in this paper, highly pure H_2O_2 (9%) is prepared from reagent grade stock (15%) at sub-zero temperatures by sublimation and can be stored in the solid state. The low temperature employed in this procedure minimizes decomposition of the reagent and also reduces reactivity of H_2O_2, a particularly reactive agent that is catalytically decomposed by some trace cations and acts as an avid scavenger of others (*18*).

The recovery of H_2O_2 after sublimation was determined by titration with ceric sulfate. Following sublimation of 50 mL of a 15% solution 45 mL were recovered by melting the sublimate. The product was shown by titration to contain 9% H_2O_2. During routine purifications ~20% (by volume) of the reagent in the sublimer is allowed to remain as a crude product in which the nonvolatile impurities are concentrated. Retention of impurities has also been provided by adding a mixture of cationic and anionic exchange resins to the reagent in vessel A prior to purification by sublimation. In this manner purification by ion exchange is supplemented by cryogenic sublimation. Ionic organic degradation products from the ion-exchange resin and minute quantities of other nonvolatile impurities that would not be retained completely by the resin are prevented from contaminating the purified reagent. Alternatively, it should be possible to increase the retention of cationic impurities during sublimation by adding nonvolatile complexing agents such as EDTA to the solution prior to freezing it in vessel A.

X-Ray fluorescence analysis of 10 mL of the purified solution indicated that all of the cations (originally doped at 1 μg/mL) were below the detection limit of 0.1 μg. These results suggested that a single purification caused at least a 100-fold decrease in the concentration of each impurity in the reagent. The effectiveness of the sublimation process for the decontamination of H_2O_2 was also monitored by a sensitive radioisotope technique. The methodology was selected to obtain an unequivocal assessment of the efficiency of the sublimation method for removing trace elements initially present in the reagent. Ten mL of 15% solution, doped with 1 μg/mL of Fe, Co, Cu, Ni, V, Mn, and Cr and also spiked with ^{60}Co, ^{51}Cr, ^{59}Fe, and ^{54}Mn, was prepared to generate a total γ-ray count rate of 8.18×10^5 counts/min from all photopeaks of these isotopes. After sublimation, 8.7 mL of the purified fraction was recovered. The γ-ray activity of this product, 7 counts/min, indicated that less than 2×10^{-3}% of the original total quantity of Fe, Co, Cr, and Mn remained in the purified fraction (i.e., ≤2 ng/mL. Thus, entrainment is negligible during the low temperature sublimation process. Further investigations were made by neutron activation. Since data obtained by neutron activation are reasonably free of blank problems, the total amount of several impurities remaining in the purified reagent could be measured directly, and reliably reflect the purity of the reagent. Decontamination factors for Mn, Co, and As during a single sublimation at initial levels of 1 μg/mL were 1107, 2680, and 323, respectively.

These data obtained on small test samples indicate that low temperature sublimation is well-suited for the preparation of high purity chemicals. The general utility of the process for purification of certain liquids is apparent from the variety of sublimable reagents reported in Table I. Additional details of the process are reported elsewhere (*19*) and applications and equipment designs are continuing.

LITERATURE CITED

(1) J. W. Mullin, *Ind. Chem.*, 540, Nov. (1955).
(2) D. Balerew and N. Kolarow, *Fresenius Z. Anal. Chem.*, **107**, 30 (1936).
(3) E. C. Kuehner, R. Alvarez, P. J. Paulsen, and T. J. Murphy, *Anal. Chem.*, **44**, 2050 (1972).
(4) P. P. Coppola and R. C. Hughes, *Anal. Chem.*, **24**, 768 (1952).
(5) M. Nord, *Chem. Eng.*, 157, Sept. (1951).
(6) C. L. Luke, *Anal. Chim. Acta*, **41**, 237 (1968).
(7) J. W. Mitchell, *Anal. Chem.*, **45**, 492A (1973).
(8) M. Zief and J. W. Mitchell, "Contamination Control in Truce Element Analysis", Wiley Interscience, New York, N.Y., 1976, pp 27, 71. (NBS report on storage.)
(9) J. H. Hildabrand and R. L. Scott, "The Solubility of Nonelectrolytes", Dover Publications, New York, N.Y., 1964, pp 24–25.
(10) J. Ruzicka and J. Stary, "Substoichiometry in Radiochemical Analysis", Pergamon Press, New York, N.Y., 1968.
(11) John Pudvin, personal communications.
(12) "Ultra Pure Metals and Salts", Apache Chemicals, Rockford, Ill., 1970.
(13) J. T. Baker Laboratory Chemicals and Products, J. T. Baker Chemical Company, Phillipsburg, N.J.
(14) Fisher Chemical Index 71C, Fisher Scientific Company, Pittsburgh, Pa.
(15) A. K. Dunlop, D. R. Douglin, and G. J. Pierotti, U.S. Patent 2,695,217, Nov. 23, 1954.
(16) D. Gold and S. S. vorm Roessler, Br. Patent 710,169, June 9, 1954.
(17) M. Stanislaw, C. Jadwiga, K. Janusz, and J. Platek, *Chem. Abstr.*, **69**, 53300d (1968). (Pol. Patent 55,378) Jan. 25, 1968.
(18) F. A. Cotton and G. Wilkinson, "Inorganic Chemistry", Interscience Publishers, New York, N.Y. 1966.
(19) J. W. Mitchell, U.S. Patent 3,992,159, Nov. 16, 1976.

RECEIVED for review September 16, 1977. Accepted November 16, 1977.

Fluorescence Photometric Quantitation of Procainamide and *N*-Acetylprocainamide in Plasma after Separation by Thin-Layer Chromatography

Ram N. Gupta,* Francis Eng, and Diane Lewis

Department of Laboratory Medicine, St. Joseph's Hospital, McMaster University, Hamilton, Ontario, Canada

A thin-layer chromatographic method for the estimation of procainamide and its major metabolite, *N*-acetyl-procainamide, in plasma is described. The method involves a plasma extraction at alkaline pH with dichloromethane to isolate the drug and its metabolite. *p*-Amino-*N*-(2-dipropylaminoethyl)-benzamide and its *N*-acetyl derivative are added to the plasma prior to extraction as internal standards. A solvent system is selected which allows excellent separation of the four compounds from each other; from plasma constituents and other drugs commonly prescribed with procainamide. It is demonstrated that densitometric scanning in the fluorescent mode is a precise and specific technique to quantitate procainamide and *N*-acetylprocainamide separated by thin-layer chromatography.

In the past, plasma procainamide (PA) levels have been determined in clinical laboratories as a guide to effective therapy (*1*). *N*-Acetylprocainamide (NAPA), the major metabolite of PA, also has an antiarrythmic effect, with potency similar to that of PA (*2–4*). The estimation of PA and NAPA is a more effective guide to therapy than the determination of PA concentration alone.

Several methods for the simultaneous determination of PA and NAPA have been described.

The simplest procedure that can be carried out in any clinical laboratory is the colorimetric procedure (*5, 6*). In this technique, hydrolysis is used to convert NAPA to PA. The concentration of PA in the extract is measured with and without hydrolysis using Bratton-Marshall reagent. The NAPA concentration is determined by the difference between the two measurements. This procedure lacks specificity. Benzodiazepines and their metabolites produce amines on hydrolysis which react with Bratton-Marshall reagent, producing the same purple color as PA.

In the fluorometric procedure (*7*), the concentration of NAPA is measured at pH $\simeq$ 1 at λ_{ex} = 288 nm, λ_{em} = 341 nm and the concentration of PA is measured at alkaline pH at λ_{ex} = 298 and λ_{em} = 354 nm. This procedure also lacks specificity because other compounds that may fluoresce under the same conditions are not removed and it has a limited linear range.

A number of gas chromatographic (GC) procedures have been described (*2, 8–11*). All are more specific but are slow. The retention time for NAPA is more than 20 min. In these procedures, a single compound, similar in properties to those of PA, has been used as an internal standard. As a result, the quantitation of NAPA has not been ideal. A number of high performance liquid-chromatographic (HPLC) procedures have been described for the simultaneous estimation of PA and NAPA (*12–14*). The elution time for PA and NAPA in HPLC is much shorter than the elution time of these compounds in GC. However, it is also a relatively slow technique since only one sample can be chromatographed at a time.

To meet the increasing demands for drug analysis, we have opted to use thin-layer chromatographic (TLC) techniques wherever possible. The instrument used for quantitation, a TLC spectrophotometric scanning system, is capable of estimating quantitatively a number of preseparated samples relatively rapidly. Spectrophotometric and fluorometric modes are available to quantitate the separated compounds by reflectance, by transmittance, or by simultaneous reflectance and transmittance. In addition, the separated compounds on TLC plates can be chemically converted to colored or fluorescent products, an ability that is not generally available in the commercial HPLC instruments.

A TLC procedure for the estimation of PA and NAPA has been described (*3*). The quantitation has been carried out by measuring the quenching of a fluorescent indicator incorporated into the TLC plate by the separated compounds. This technique has been shown to be erroneous (*15*). More recently, a TLC procedure has been published where PA and NAPA have been estimated by UV reflectance (*16*).

We describe a TLC procedure where PA and NAPA and their corresponding internal standards are separated and then estimated by fluorometric densitometry.

EXPERIMENTAL

Instrumentation. A TLC scanning spectrophotometer model KM3 (Carl Zeiss Canada Ltd., Don Mills, Ontario) was used in the fluorescent mode with a mercury vapor lamp as the light source for excitation and a Zeiss No. M365 filter for isolation of the emitted light. Both a strip-chart recorder (Linear Instruments Corp., Irvine, Calif.) model 355, and an Autolab System IV computing integrator (Spectra-Physics, Santa Clara, Calif.) were used for calculation.

Silica gel 60 glass plates, 20 × 20 cm, without fluorescent indicator (E. M. Merck, No. 5763) were developed in TLC tanks with twin chambers (Terochem Laboratories, Edmonton, Alberta).

Reagents. All reagents were of analytical grade and were used without further purification unless otherwise specified.

Procainamide Stock Standard. Procainamide hydrochloride was purchased from Pfaltz and Bauer, Inc., Flushing, N.Y. A stock solution of PA (1 mg/mL) was prepared by dissolving 57.7 mg of PA·HCl in 50 mL of methanol.

N-Acetylprocainamide Stock Standard. N-Acetylprocainamide was prepared by treating 57.7 mg of PA·HCl with 100 μL of acetic anhydride and 200 μL of redistilled pyridine. The mixture was placed in a boiling water bath for 2 h, dried in a current of dry nitrogen, and dissolved in 50 mL of methanol to give a concentration of NAPA 1 mg/mL.

No trace of unreacted PA was detected when 10 μg of the acetylated product was chromatographed and sprayed with Bratton-Marshall reagent: sequential spraying of TLC plate with: 20% (v/v) sulfuric acid; 1% (w/v) sodium nitrite; 5% (w/v) ammonium sulfamate and 1% methanolic solution of *N*-1-naphthylethylenediamine dihydrochloride. Under similar conditions, 10 ng of PA produced an intense purple spot.

p-Amino-N-(2-dipropylaminoethyl)benzamide (BA) Stock Standard. BA·HCl was kindly supplied by E. R. Squibb & Sons, Inc., Princeton, N.J. A stock solution of BA (1 mg/mL) was

Table I. R_f Values of PA, NAPA, BA, and NABA

Solvent systems	R_f values PA	NAPA	BA	NABA
1. Benzene:ethyl acetate:ethanol:ammonia (15:15:5:1)	0.38	0.29	0.64	0.51
2. Benzene:ethyl acetate:methanol:ammonia (160:80:160:1)	0.26	0.26	0.64	0.70
3. Benzene:ammonia:1,4-dioxane (10:5:80)	0.54	0.42	0.80	0.71
4. Isopropanol:chloroform:ammonia (45:45:2)	0.45	0.52	0.87	0.88
5. Benzene:ammonia:acetone:dioxane (10:4:60:20)	0.70	0.67	0.92	0.87
6. Benzene:ethyl acetate:methanol:ammonia (20:10:20:1)	0.70	0.71	0.88	0.87
7. Ethyl acetate:methanol:ammonia (42:5:2)	0.52	0.42	0.80	0.66
8. Isopropanol:chloroform:ammonia (45:45:5)	0.67	0.73	0.92	0.94
9. Ethyl acetate:methanol:ammonia (88:8:4)	0.32	0.23	0.74	0.62

prepared by dissolving 29 mg of BA·HCl in 25 mL of methanol.

N-Acetyl-p-amino-N-(2-dipropylaminoethyl)benzamide (NABA) Stock Standard. NABA (1 mg/mL) was prepared and checked as for NAPA stock standard. The stock solutions were stored at 4 °C and were stable for at least three months.

Plasma Standards. Combined plasma standards containing 5, 10, 15, and 20 mg/L of both PA and NAPA were prepared by adding appropriate volumes of the stock (1 mg/mL) solutions of PA and NAPA to drug free pooled plasma. The plasma standards were divided into 2-mL aliquots and frozen until assay.

Internal Standard. A combined internal standard solution containing 10 mg/L BA and 10 mg/L NABA was prepared on the day of analysis by diluting appropriate volumes of the stock solutions of these compounds with dichloromethane.

Patient Samples. Venous blood from patients receiving procainamide therapy was drawn 1 h after the last dose into evacuated heparinized blood collection tubes. Plasma was separated within 2 h of collection and stored at 4 °C until analyzed. The samples were frozen when they were to be stored for more than 24 h.

Procedure. *Extraction.* To 0.5 mL of spiked plasma (standards) or patient plasma in 16 × 125 mm glass culture tubes with Teflon-lined screw caps, 0.5 mL of internal standard solution, 0.1 mL of 1 M sodium hydroxide and 5 mL of dichloromethane were added. The tubes were shaken on a mechanical shaker for 2 min. Approximately 5 g of anhydrous sodium sulfate was added to each tube and the tubes were again shaken for 2 min and centrifuged. The dichloromethane layer from each tube was decanted into correspondingly labeled 16 × 100 mm glass test tubes and evaporated in a water bath at 45–50 °C. The residue was dissolved in 100 μL of methanol.

Chromatography. Methanol residue, 1 μL from each tube was spotted 15 mm apart on a TLC plate. The plate was developed in solvent No. 9 (Table I) to a height of about 15 cm and air dried for 10 min. The residues of the standard plasmas were spotted on each plate if more than one was chromatographed.

Detection. A. The plate was then scanned along the direction of the solvent flow using the Zeiss Chromatogram scanner. The scanner was used in the fluorescence (M-PR) mode (λ_{ex} = 313 nm and M365 filter for emission; slit length = 10 mm and slit width = 0.3 mm).

The emission peaks were recorded on the strip chart recorder and also simultaneously integrated by the electronic integrator. Under these conditions, peaks due only to PA and BA and the solvent front were observed.

B. The same TLC plate was then placed into the equilibrated dry chamber of the twin chamber developing tank. The other chamber contained 10 mL of concentrated hydrochloric acid. The plate was exposed to the acid for 15 min and then exposed to air for 5 min and then rescanned (λ_{ex} = 297 nm and M365 emission filter; slit length = 10 mm and slit width = 1.5 mm). The only emission peaks observed were due to NAPA, NABA, and the solvent front.

The plasma PA or NAPA concentrations were determined from standard curves established by plotting peak area ratios of standard/internal standard (PA/BA or NAPA/NABA) against PA and NAPA concentrations of the standards.

RESULTS AND DISCUSSION

Recovery from plasma spiked with PA, NAPA, BA, and NABA at a concentration of 10 mg/L was determined by comparing each extracted compound with the area of corresponding amounts of methanolic standards spotted directly. The recoveries varied from 88–98%. During extraction there is no change in the ratio of PA and its internal standard, BA, or NAPA and its internal standard, NABA, when mixed in ratios of 0.5 to 5. The addition of internal standards (BA and NABA) prior to extraction to all plasmas (standards and patient sera) obviates the need of a quantitative procedure for extraction and for precise spotting of the residue on TLC plates. The use of internal standards compensates for extraction irregularities or unforeseen losses.

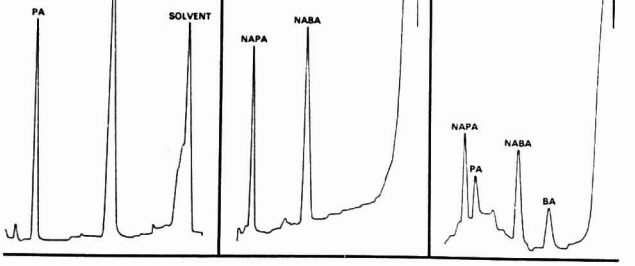


Figure 1. Chromatograms of PA, BA, NAPA, and NABA. (A) Fluorescent mode; alkaline pH, λ_{ex} = 313 nm, λ_{em} = 365 nm, slit width 0.3 mm. (B) Fluorescent mode; acidic pH, λ_{ex} = 297, λ_{em} = 365 nm, slit width 1.5 mm. (C) UV reflectance mode; alkaline pH, λ = 265 nm, slit width 0.5 mm.

Table II. Estimation of Precision

A. Within-batch variation

	PA			NAPA		
Mean	2.0[a]	6.4[a]	10.5[a]	2.0[a]	6.4[a]	9.9[a]
ISD	0.08	0.10	0.14	0.09	0.21	0.24
N	9	10	10	8	10	9
RSD	3.7%	1.5%	1.3%	4.5%	3.2%	2.5%

B. Between-batch variation

	PA	NAPA
Mean	5.4[a]	5.4[a]
ISD	0.085	0.182
N	10	10
RSD	1.6%	3.4%

[a] mg/L.

Table III. R_f Values by Fluorescent Detection before or after Exposure to HCl

	R_f value
PA	0.32
NAPA	0.23
BA	0.74
NABA	0.62
1. Caffeine	-
2. Carbamazepine	-
3. Chloropromazine	-
4. Codeine	-
5. Diazepam	-
6. Diphenhydramine	-
7. Flurazepam	-
8. Isoniazid	-
9. Librium	-
10. Lidocaine	-
11. Meprobamate	-
12. Methaqualone	-
13. Methylprylon	-
14. Phenozuximide	-
15. Primidone	-
16. Propanalol	0.51
17. Quinidine Sulfate	0.42
18. Theophylline	-

Plasma standards containing known amounts of PA and NAPA are processed with each plate to obtain a standard curve. The spotting of methanolic standards has been found to be unnecessary.

A number of solvent systems were tried for the separation of PA, NAPA, BA, and NABA. The results are summarized in Table I. The solvent system selected: ethyl acetate: methanol:ammonia (88:8:4), allows optimal separation of these compounds and shows minimal edge effect.

It has been shown that procainamide has good native fluorescence (λ_{ex} = 298 nm, λ_{em} = 354 nm) at pH 11.0 and *N*-acetyl procainamide has fair native fluorescence (λ_{ex} = 288 nm, λ_{em} = 341 nm) at pH 1.0 (7). The internal standards, BA and NABA, behave similarly to PA and NAPA in their fluorescence characteristics. Since the developing solvent contains ammonia, the pH of the TLC plate, even after drying, is optimal for fluorescence photometry of PA and BA. The baseline is steady and essentially noise free (Figure 1), and PA and BA show excellent response.

After exposure to acid, NAPA and NABA become fluorescent; however, the fluorescence exhibited is less than that for the same concentration of PA or BA, therefore the slit width is increased from 0.3 to 1.5 mm to achieve greater response. The baseline is still quite stable (Figure 1).

The procedure is linear from 1 mg/L to 30 mg/L of PA and NAPA (RSD of PA = ±2.7%, N = 6, and RSD of NAPA = ±1.2%, N = 6).

The precision of this procedure for both PA and NAPA is excellent. Within-batch precision was tested with plasma samples between 2 and 10 mg/L. Between-batch variation was tested using a plasma at a level of 5 mg/L for both PA and NAPA in ten consecutive runs (Table II). Throughout this investigation, only one lot of pre-coated silica gel plates was used. The incorporation of a standard curve on each plate chromatographed in this technique should eliminate problems encountered with minor deviations in plates.

The plasma samples in the procedure are subjected to a simple dichloromethane extraction at an alkaline pH. A number of neutral and basic compounds other than PA, BA, NAPA, and NABA could also be extracted if present in the plasma. As shown in Table III, some of the drugs which may be administered along with procainamide do not interfere. Fluorescence adds to the specificity of the thin-layer chromatographic procedure.

The need to scan the TLC plate twice for the quantitation of PA and NAPA in this procedure is time consuming; however, we have not been able to find conditions where both the compounds could be quantitated simultaneously by fluorodensitometry.

The separated compounds can be quantitated simultaneously by UV reflectance either before or after exposure to acid vapors. One internal standard is adequate for the quantitation of PA and NAPA by this method. However, in the UV reflectance mode, the baseline is not as stable as in the fluorometric mode (Figure 1).

The procedure is very sensitive. There is no problem distinguishing plasma containing 0.5 mg/L of PA or NAPA from a blank plasma. If required, as little as 50 μL of plasma can be assayed. The amounts of internal standards are correspondingly decreased and the residue of the extracts are reconstituted in smaller volumes of methanol. We conclude that the quantitative TLC procedure described here for PA and NAPA is an acceptable routine method.

LITERATURE CITED

(1) J. Koch-Weser and S. W. Klein, *J. Am. Med. Assoc.*, **215**, 1454 (1971).
(2) J. Elson, J. M. Strong, W.-K. Lee, and A. J. Atkinson Jr., *Clin. Pharmacol. Ther.*, **17**, 134 (1975).
(3) M. M. Reidenberg, D. E. Drayer, M. Levy, and H. Warner, *Clin. Pharmacol. Ther.*, **17**, 722 (1975).
(4) W.-K. Lee, J. M. Strong, R. F. Kehoe, J. S. Dutcher, and A. J. Atkinson, Jr., *Clin. Pharmacol. Ther.*, **19**, 508 (1976).
(5) E. V. Giardina, J. Dreyfuss, J. T. Bigger Jr., J. M. Shaw, and E. C. Schreiber, *Clin. Pharmacol. Ther.*, **19**, 339 (1976).
(6) N. A. Klitgaard, *Arch. Pharm. Chemi, Sci. Ed.*, **4**, 61 (1976).
(7) E. Matusik and T. P. Gibson, *Clin. Chem. (Winston-Salem, N.C.)*, **21**, 1899 (1975).
(8) E. Karlsson, L. Molin, B. Norlander, and F. Sjoqvist, *Br. J. Clin. Pharmacol.*, **1**, 467 (1974).
(9) K. Frisild, J. E. Bredesen, and P. K. M. Lunde, *Clin. Chem. (Winston-Salem, N.C.)*, **21**, 1180 (1975).
(10) R. L. Gallazzi, L. B. Sheiner, T. Lockwood, and L. Z. Benet, *Clin. Pharmacol. Ther.*, **19**, 55 (1976).
(11) E. V. Giardina, R. M. Stein, and J. T. Bigger, *Circulation*, **55**, 388 (1977).
(12) K. Carr, R. L. Woosley, and J. A. Oates, *J. Chromatogr.*, **129**, 363 (1976).
(13) L. R. Shukur, J. L. Powers, R. A. Marques, M. E. Winter, and W. Sadee, *Clin. Chem. (Winston-Salem, N.C.)*, **23**, 636 (1977).
(14) R. M. Rocco, D. C. Abbott, R. W. Giese, and B. L. Karger, *Clin. Chem. (Winston-Salem, N.C.)*, **23**, 705 (1977).
(15) V. Pollak, *J. Chromatogr.*, **133**, 49 (1977).
(16) B. Wesley-Hadzija and A. M. Mattocks, *J. Chromatogr.*, **143**, 307 (1977).

RECEIVED for review August 9, 1977. Accepted November 21, 1977.

Competitive Intrinsic Factor Binding Assay Technique for Cobalamins in Natural Waters

Robert A. Beck

Department of Chemistry, Framingham State College, Framingham, Massachusetts 01701

A competitive intrinsic factor binding (CIFB) method for the determination of 10^{-12} g/mL concentration levels of benzyl alcohol extractable cobalamins in natural waters has been developed. Purified cobalamin extracts assayed by the CIFB protocol were 76.9% of those concentrations determined for the same samples using high pressure liquid chromatographic analysis, and demonstrated a 10.98% relative standard deviation for a series of 32 CIFB assays. Application of the CIFB technique to natural waters indicated a sensitivity ranging from 9.98–187.98 pg/mL.

The environmental occurrence of cobalamins in natural waters may be significantly implicated with the productivity of phytoplankton and dinoflagellates (*1*, *2*).

Traditional methods for the routine assessment of cobalamins in environmental systems have relied on bioassays (*1–7*) which are tedious and may be potentially inaccurate in the milieu of biochemically complex samples (*8*, *9*).

A more direct analysis of environmental cobalamins using high pressure liquid chromatography (HPLC) has been developed for the quantitation of 1.0–10.0 μg of benzyl alcohol extractable cobalamins (*10*). Although the HPLC method has an analytical capability for the assay of cobalamin-rich environmental samples, this method clearly lacks the required sensitivity for determining pg/mL concentrations which normally occur in natural waters.

Because of the limitations of both bioassay methods and the HPLC technique, a more sensitive assay method for benzyl alcohol extractable cobalamins in natural waters has been developed which utilizes the basic principles involved in the measurement of an endogenous substrate by competitive protein binding. For this analytical method, the thermolabile glycoprotein, intrinsic factor (IF), serves as a nondiscriminative binding reagent for both radioactive ^{57}Co-cyanocabalamin (vitamin B_{12}) and nonradioactive cyanocobalamin as well as its derivatives. Consequently, in the case of a fixed concentration of radioactive cyanocobalamin, an inverse relationship is observed between the amount of radioactivity bound to IF and increasing concentration levels of nonradioactive cyanocobalamins. This principle permits the determination of cyanocobalamin concentrations in samples ranging from 50–1600 pg/mL.

Clinical applications of this competitive intrinsic factor binding (CIFB) technique have been widely reported (*11–13*) but the reliability of the method for quantitating environmental cobalamins has not been described.

EXPERIMENTAL

Reagents. All reagents for the CIFB assay of cobalamins including ^{57}Co-cyanocobalamin, IF, and hemoglobin coated charcoal were obtained from RIA Products, Inc., Waltham, Mass. Standard concentration levels of cyanocobalamin used for HPLC quantitation of cobalamin extracts were prepared from cyanocobalamin obtained from Sigma Chemical Co., St. Louis, Mo. All other reagents, including benzyl alcohol, chloroform, sodium cyanide, sodium chloride, and sodium sulfate, were analytical reagent grade.

Instrumentation. Radioassay of ^{57}Co-cyanocobalamin, bound to IF during the CIFB protocol, was determined by using a Beckman LS-100C Liquid Scintillation Counting System under conditions detailed previously by Gutcho et al. (*14*). Low potassium glass scintillation vials were used in conjunction with a cocktail of Ready-Solve GP obtained from Beckman Instruments, Irvine, Calif.

Procedure. *Evaluation of CIFB Assay Technique.* Evaluation of the CIFB assay technique for quantitation of environmental cobalamins was based on the preparation of cobalamin-rich extracts derived from activated sewage sludge (*10*). The cobalamin extracts were purified by triplicate acetone precipitations (*15*) prior to quantitative HPLC analysis (*10*). These extracts were subsequently diluted with 0.9% saline solution, through a multiplicity of serial dilution schemes, to a speculated concentration of less than 1600 pg/mL. The CIFB assay for cobalamins was performed according to the protocol outlined by RIA Products, Inc. (*16*), which is essentially the method reported by Lau et al. (*11*) and others (*12*, *17*).

All quantitative assays of cobalamin extracts were based on duplicate assays of eight replicative cyanocobalamin standards representing seven different concentrations ranging from 0 to 1600 pg/mL. On the basis of these data, a standard regression line plot of logit B/B_0 values (ordinate) vs. the log of standard cyanocobalamin concentrations (abscissa) was determined. The logit B/B_0 values were calculated for standard and unknown cobalamin concentration levels using the standard radioassay formula of $\ln [(B/B_0)/(1- B/B_0)]$, where B is the counts per minute (cpm) observed for ^{57}Co-cyanocobalamin bound to IF during the radioassay and B_0 represents the cpm for ^{57}Co-cyanocobalamin bound at the "zero" cyanocobalamin concentration level.

Assay of Total Cobalamins in Natural Waters. Vitamin B_{12} related cobalamins in natural waters were prepared for CIFB assays by mixing a water sample with sodium nitrite and sodium cyanide in a ratio of 0.5:0.2 g/100 mL and the pH was adjusted to 4.0 using concentrated hydrochloric acid. The sample was then boiled for 15 min under a well ventilated hood, sodium sulfate (20% w/v) was dissolved in the sample, and it was subsequently extracted three times with one-tenth volume of benzyl alcohol. The combined benzyl alcohol extracts were mixed with one-half volume of chloroform and the resulting solvent phase was extracted three times with one-tenth volume of water (*10*). As previously reported, radioactive ^{57}Co-cyanocobalamin tracer studies have indicated cobalamin extraction efficiencies of 92.3 to 80.2% for natural water samples having respective volumes of 100 and 500 mL (*10*).

Emulsions generated during the course of the previous extraction steps were easily eliminated by centrifugation for 10 min at 2500 × *g*.

After concentrating cobalamins in a combined aqueous phase, this sample was further concentrated by lyophilization, only when necessary, to achieve a preferred analytical cobalamin concentration of 200–800 pg/mL.

The salinity of the aqueous cobalamin extract was adjusted to 0.9% by adding sodium chloride and a 200-μL aliquot of this solution was assayed by the CIFB technique as previously described.

Because of the analytical sensitivity of this procedure, all portions of the assay must be carried out in scrupulously clean, acid washed glassware.

RESULTS AND DISCUSSION

Quadruplicate HPLC analyses of three independently prepared cobalamin extract preparations from activated

0003-2700/78/0350-0200$01.00/0 © 1978 American Chemical Society

Table I. Quantitative Comparison of Cobalamin Extract Concentrations Based on HPLC Analyses and CIFB Assays

Calculated concentrations for a series of cobalamin rich extracts based on HPLC analysis	Competitive intrinsic factor binding assay data for samples			
	Cobalamin concentration (mean pg/mL ± 2 s)	No. of assays (n)	Rel std dev (percent ± 2 s)	Percent of calculated concentration based on HPLC analyses
549.1	415.69 ± 24.85	8	8.63 ± 4.23	75.7
436.6	336.67 ± 21.66	16	13.25 ± 4.59	77.1
314.0	244.41 ± 18.76	8	11.08 ± 5.43	77.8

Table II. Quantitative Comparison of Cobalamin Concentration Levels in Filtered and Unfiltered Natural Water Samples Based on CIFB Assays

Sample origin	Unfiltered natural water samples			Filtered natural water samples[a]		
	Mean cobalamin concentration (pg/mL ± 2 s)	No. of assays (n)	Rel std dev, % (mean ± 2 s)[b]	Mean cobalamin concentration (pg/mL ± 2 s)	No. of assays (n)	Rel std dev, % (mean ±2 s)[b]
University of Massachusetts Marine Field Station, Rockport, Mass.	37.91 ± 1.84	7	6.54 ± 3.42	19.40 ± 2.21	7	15.39 ± 8.06
Boston Edison Nuclear Power Plant Breakwater, Plymouth, Mass.	30.55 ± 3.18	8	15.02 ± 7.36	9.98 ± 0.91	8	9.35 ± 4.58
Harbor Breakwater Plymouth, Mass.	187.98 ± 52.54	12	34.93 ± 19.76	33.40 ± 2.49	8	10.75 ± 5.27
Sudbury Dam, Fayville, Mass. (oligotrophic reservoir)	34.47 ± 2.95	8	12.37 ± 6.06	10.33 ± 1.24	8	12.26 ± 6.01
Hager Pond, Marlborough, Mass. (eutrophic pond)	61.26 ± 5.05	8	11.90 ± 5.83	18.81 ± 0.80	8	4.35 ± 2.13
Treated sewage effluent, Easterly Water Pollution Control Facility, Marlborough, Mass.	67.92 ± 5.03	8	10.69 ± 5.24	16.42 ± 1.58	8	13.86 ± 6.79

[a] Samples were filtered through 0.22 μm Millipore G.S. filters. [b] Between assays reported for each set of samples.

sewage sludge were determined to have concentrations of 10.98 ± 0.24, 8.73 ± 0.19, and 6.27 ± 0.11 μg/10 μL. A series of variable dilution schemes for each extract, effecting a dilution of 1:20 000, resulted in respective anticipated cobalamin concentrations of 549.10, 436.60 and 314.00 pg/mL.

The CIFB assays for these samples accordingly resulted in concentrations of 415.69 ± 24.85, 336.67 ± 21.66, and 244.41 ± 18.76 pg/mL (Table I). These concentrations represented 76.9% of the respective cobalamin concentrations calculated for the same samples based on HPLC analyses and demonstrated a 10.98% mean relative standard deviation for 32 samples assayed. Moreover, studies of the same cobalamin extracts conducted by a reference laboratory (RIA Products, Inc., Waltham, Mass.) resulted in concentration levels 90.3 ± 9.6% of the values reported in Table I.

In addition to the results outlined above, a high degree of comparability was noted for regression line plots of logit B/B_0 values (ordinate) vs. the log of concentrations (abscissa) for both cyanocobalamin standards (slope: −2.15; y-intercept: 6.13) and benzyl alcohol extractable cobalamins (slope: −2.55; y-intercept: 7.17) over a concentration range of 50–1600 pg/mL. The correlation coefficient for both regression lines was 0.99.

Although benzyl alcohol extractable cobalamins exhibited a statistical logit plot which was almost identical to that calculated for a series of standard cyanocobalamin concentrations, the fact remains that CIFB assays for the cobalamin extracts averaged 76.9% of those levels calculated for the same samples using HPLC analysis. A conclusive rationale for this disparity has not been formulated, but it has been widely recognized that analogues of the basic cyanocobalamin structure are distributed widely in nature. Furthermore, many of these analogues are devoid of biological and clinical activities associated with cyanocobalamin. On this basis it is tempting to speculate that a portion of the purified cobalamin extracts studied here may consist of a minor cobalamin fraction which exhibits less quantitative interaction with IF than other cobalamins more closely reminiscent of the cyanocobalamin structure.

The total cobalamin concentrations determined for unfiltered freshwater and ocean water specimens varied from 30.55–187.98 pg/mL depending on the origin of the sample (Table II). Water samples found to have the highest concentrations were obtained from a eutrophic freshwater pond (Hager Pond, Marlborough, Mass.) and ocean water sampled 800 m from a treated sewage effluent discharge point (Plymouth Harbor Breakwater, Plymouth, Mass.). The mean relative standard deviation for cobalamin concentrations in all unfiltered water samples was 15.24%. The 34.93% relative standard deviation displayed by Plymouth Harbor Breakwater samples was attributable to high population numbers of zooplankton and phytoplankton suspended in the water column at the time of sampling.

As a result of cobalamins bound to microorganisms and other organic material, all water samples filtered through a 0.22-μm Millipore GS filter (Millipore Corp., Inc., Bedford, Mass.) consistently displayed smaller cobalamin concentration levels than unfiltered water samples (Table II). Bioassays have previously suggested (*18*) that up to 25.0 pg of free cobalamins contained in a water sample may be bound to this type of mixed cellulose acetate and nitrate filter. However, radioactive ^{57}Co-cyanocobalamin tracer studies conducted in this investigation demonstrated a maximum binding of only 16.0 pg. Therefore, all cobalamin concentrations reported for filtered water samples in Table II have been tabulated in view of this consideration.

It should also be recognized that all concentrations detailed in Table II were based on the analysis of aqueous cobalamin extracts in the concentration range of 200–800 pg/mL. This analytical range was preferred since logit plot regression lines

may be statistically dubious at higher or lower concentrations. For those instances where natural water samples failed to provide an aqueous cobalamin extract with a minimum 200 pg/mL concentration, the extract was lyophilized to dryness and reconstituted to a smaller volume with 0.9% saline solution prior to CIFB analysis.

Aside from the fact that the CIFB assay method is less time consuming and tedious than bioassays, it permits the analysis of cobalamins in a more representative size water sample and substantially eliminates interference of noncobalamin compounds in quantitative assays through implementation of selective benzyl alcohol extraction and concentration procedures. Moreover, the CIFB assay method described in this paper provides a means for evaluating cobalamin concentrations in natural waters on a routine basis using a sensitive analytical approach other than traditional bioassays.

ACKNOWLEDGMENT

Thanks are expressed to Charles Zapsalis and Richard F. Milaszewski for helpful discussions.

LITERATURE CITED

(1) L. Provasoli, "Algal Nutrition and Eutrophication" in "Eutrophication: Causes, Consequences, Correctives", Proceedings of a Symposium, National Academy Science, Washington, D.C., 1969, pp 574–593.
(2) J. Cairns, G. R. Lanza, and B. C. Parker, "Pollution Related Structural and Functional Changes in Aquatic Communities with Emphasis on Freshwater Algae and Protozoa", *Proc. Acad. Nat. Sci. Philadelphia*, **124** (5), 79 (1972).
(3) A. F. Carlucci and S. B. Silbernagel, *Limnol. Oceanogr.*, **11**, 642 (1966).
(4) S. R. Hoover, L. Jasewicz, J. B. Pepinsky, and N. Porges, *Sewage Ind. Wastes*, **24**, 38 (1952).
(5) H. Y. Neujahr, *Acta, Chem. Scand.*, **9**, 622 (1955).
(6) R. Strohecker and H. M. Henning, "Vitamin Assay—Tested Methods", Chemical Rubber Co. Press, Cleveland, Ohio, 1965.
(7) W. H. Sebrell and R. S. Harris, "The Vitamins", Vol. II, Academic Press, New York, N.Y., 1968, pp 120–258.
(8) E. L. Smith, "Vitamin B_{12}", John Wiley and Sons, New York, N.Y., 1960.
(9) W. Shive, J. M. Ravel, and W. M. Harding, *J. Biol. Chem.*, **176**, 991 (1948).
(10) R. A. Beck and J. J. Brink, *Environ. Sci. Technol.*, **10**, 173 (1976).
(11) K-S. Lau, C. Gottlieb, L. R. Wasserman, and V. Herbert, *Blood*, **26**, 202 (1965).
(12) L. Wide and A. Killander, *Scand. J. Clin. Lab. Invest.*, **27**, 151 (1971).
(13) C. Rosenblum, *Talanta*, **11**, 255 (1964).
(14) S. Gutcho, J. Johnson, and H. McCarter, *Clin. Chem.* (*Winston-Salem, N.C.*), **19**, 998 (1973).
(15) H. H. Fricke, U.S. Patent 2,582,589 (1952).
(16) RIA Products, Inc., "In Vitro Quantitative Measurement of Serum Vitamin B_{12} by Radioassay", Waltham, Mass., 1977.
(17) Y. K. Liu and L. W. Sullivan, *Blood*, **39**, 426 (1972).
(18) B. C. Parker, *J. Phycol.*, **5**, 124 (1969).

RECEIVED for review September 14, 1977. Accepted November 21, 1977.

Determination of Chlorine Dioxide in Sewage Effluents

J. Ross Knechtel*

Wastewater Technology Centre, Burlington, Ontario L4R 4A6

Edward G. Janzen and Edward R. Davis

University of Guelph, Guelph, Ontario N1G 2W1

A spectrophotometric method is developed for the determination of chlorine dioxide in sewage treatment plant effluents. The decrease in absorbance at 550 nm of acid chrome violet K (ACVK) enables the direct spectrophotometric determination of ClO_2 in sewage effluent samples. Centrifugation is employed to remove suspended solids. In a NH_4Cl–NH_3 buffer of pH 8.1 to 8.4, no interference from active chlorine, hypochlorites, chlorites, chloramines, and nitrites was observed. The results obtained using the ACVK technique were verified against electron spin resonance spectrometry.

The subject of this paper is the use and measurement of chlorine dioxide in sewage treatment plant effluents. There were three good reasons for the consideration of chlorine dioxide as an alternative to chlorine (*1*). In the first place, chlorine dioxide is a much stronger oxidizing agent than chlorine. Because of this, a smaller dosage of chlorine dioxide than chlorine should be possible for disinfection purposes. Because a smaller dosage is possible, a lower residual could result. The second reason for the choice of chlorine dioxide over chlorine was that chlorine dioxide does not react with ammonia to form chloramines as does chlorine (*2*). The reaction of chlorine with ammonia does two things. It reduces the oxidizing power of the oxidant and produces a toxic by-product. The third reason for the choice of chlorine dioxide was that it oxidizes the phenolic ring in phenols (*3*), whereas, chlorine forms phenolic chlorides when it combines with phenols. This could produce taste and odor problems in potable water supplies.

Several published methods (*4–9*) exist for ClO_2 determination in water but not for sewage effluents. These techniques are not entirely specific for ClO_2 because the measurement includes other chlorine species (*7*). Modifications in some of these procedures are suggested to mask or remove these effects.

In the effluent disinfection project itself, the chlorine dioxide residues were measured amperometrically (*9, 10*) using phenylarsineoxide (PAO) as titrant. The chlorine dioxide values reported were not verified by a referee method.

Because of the uncertainties of this technique and the results, work was undertaken to examine an alternative method. The method selected (*8*) to measure chlorine dioxide depends on the selective decolorization of a dye (acid chrome violet K). The relationships between the level of chlorine dioxide initially present and the amount of decolorizing which occurs obeys Beer's law up to 200 μg ClO_2. The maximum absorbance of the complex formed occurs at 550 nm.

A study was undertaken to investigate the feasibility of using the acid chrome violet K technique for the measurement of ClO_2 in sewage effluent samples. The results obtained on sewage effluent samples using this technique were verified using an electron spin resonance method. The chlorine dioxide molecule is the only stable chlorine species which contains an unpaired electron and which is capable of existing in

0003-2700/78/0350-0202$01.00/0 © 1978 American Chemical Society

solution. Thus, electron spin resonance should provide an accurate means of verifying any method for the determination of chlorine dioxide in solution.

EXPERIMENTAL

Apparatus. The colorimetric measurements were made on a Bausch and Lomb Spectronic 100 equipped with a 1-cm micro flow-through cell. This particular spectrophotometer has an expanded readout feature which permits the measurement of concentrations much lower than conventional spectrophotometers.

The electron spin resonance (ESR) measurements were made on a Varian E-104 instrument using a Varian aqueous solution flat cell (fused quartz construction).

Reagents. *Sodium Chlorite.* Technical grade sodium chlorite (80% $NaClO_2$, 20% NaCl) was obtained from Kingsley & Keith Ltd., (Toronto, Ontario, Canada).

Chlorine Dioxide was prepared by reacting sodium chlorite with hydrochloric acid (*11*). Equal volumes of sodium chlorite solution (55.1 g/L $NaClO_2$) and 2 N hydrochloric acid were mixed. The gas produced was scrubbed to remove any chlorine present by passing through a saturated solution of sodium chlorite (39 g/100 cm^3 of $NaClO_2$ at 17 °C). The purified chlorine dioxide was dissolved in distilled water. This reaction was allowed to proceed to completion (about 30 min). The solution was standardized using an iodometric titration with sodium thiosulfate (*12*).

Acid Chrome Violet K. A stock solution was prepared by suspending 175 mg of acid chrome violet K (ESBE Laboratory Supplies, Toronto, Ontario) in distilled water. To the suspension were added 20 mg of purified sodium metaphosphate, 48.5 g of analytical grade ammonium chloride, and 5.3 mL of concentrated ammonium hydroxide solution (29% NH_3). The suspension was finally diluted to 1 L with distilled water, thoroughly mixed, and set aside for 24 to 48 h to stabilize. The suspension was then filtered through a 0.45-μm membrane filter under vacuum. Our experience has shown that this solution is stable for at least 1 month. To prevent interference from active chlorine, hypochlorites, chlorites, and chlorates, the pH of the solution must be between 8.1 and 8.4. This is achieved after a 10-fold dilution of the ACVK solution with the sample to be analyzed. The absorbance of a 10% dilution of this ACVK stock with distilled water at 550 nm (the absorbance maximum) should be between 0.15 and 0.19 using the Bausch and Lomb Spectronic 100 (the spectrophotometer used in this study).

Recommended Procedure. *Standardization.* Twenty milliliters of the acid chrome violet K solution are introduced into a 200-mL flask. A known amount of chlorine dioxide up to 200 μg is added, taking care that the solution drops directly into the reagent without running along the walls of the vessel. The solution is diluted to 200 mL with distilled water and the absorbance at 550 nm is read using distilled water as a blank. The absorbance of a 10% dilution of the ACVK reagent is measured also. The values of ∇A (absorbance of the 10% dilution of the reagent minus the absorbance of the decolorized sample) vary linearly with the amount of chlorine dioxide added up to 200 μg ClO_2.

Analysis of Residual ClO_2 in Samples. For the analysis of chlorine dioxide in samples, 20 mL of the ACVK reagent is diluted to 200 mL with sample. The sample is centrifuged and the absorbance at 550 nm of the clear supernatant liquid is measured (Reading 1). At the same time, 20 mL of the ACVK reagent is diluted to 200 mL with the same sample material containing no chlorine dioxide. This is accomplished by either taking a sample at a point in the sewage treatment process just prior to the addition of chlorine dioxide or by eliminating the ClO_2 in the sample by the introduction of 5 mg of phenol per liter. The solids are centrifuged as outlined above. The optical density of 550 nm of this second sample containing no ClO_2 is measured (Reading 2). The difference between these two readings (∇A) is then translated to micrograms of ClO_2 from the relationship derived in the previous (standardization) section. The concentration of chlorine dioxide in the sample, in mg/L, is obtained by dividing the micrograms of chlorine dioxide found by the aliquot of sample taken (mL).

RESULTS AND DISCUSSION

Interferences. By a procedure identical to that for standardization, the acid chrome violet K reagent was allowed to react with chlorine, hypochlorite, chlorite, chloramine T, and nitrite. These potential interferences were allowed to react together and in various combinations with acid chrome violet K both in the presence and absence of chlorine dioxide. The concentrations of various species which did not interfere are shown in Table I.

Table I. Species Found Not to Interfere with Chlorine Dioxide Determination

ClO_2, mg/L	Species and concentration level (mg/L) Tested
0.2	Chlorine (Cl_2) up to 20 mg/L
0.2	Hypochlorite (ClO^-) up to 20 mg/L
0.2	Chlorite (ClO_2^-) up to 50 mg/L
0.2	Chloramine up to 1000 mg/L
0.2	Nitrite (NO_2^-) up to 20 mg/L

Table II. General ESR Instrument Parameters (for 52 mg ClO_2/L)

Microwave frequency	9.495 GHz	Scanning time	30 min
Field	3370 Gauss	Receiver gain	2×10^4
Scanning range	1000 Gauss	Modulation amplitude	1 Gauss
Modulation frequency	100 KHz	Time constant	2 s



Figure 1. ESR spectrum of 52 mg ClO_2/L in distilled water at room temperature

Reproducibility. A volume of a nonchlorinated final effluent from a sewage treatment plant was treated with 4.0 mg/L chlorine dioxide. The suspension was mixed using a magnetic stirrer for 5 min. A sufficient quantity of acid chrome violet K reagent was added to bring its concentration to 10% by volume and the suspension was thoroughly mixed. Ten samples of 50 mL each were withdrawn, centrifuged, and readings taken on the Bausch and Lomb Spectronic 100 in the expanded concentration mode. The range of results calculated from these 10 readings was 0.38 to 0.40 mg ClO_2/L.

Verification of Colorimetric Procedure. The chlorine dioxide molecule contains an unpaired electron. This property makes the molecule paramagnetic. No other stable chlorine species capable of existing in solution contains an unpaired electron. Chlorine dioxide shows no tendency to dimerize (*2*). Any dimer found (Cl_2O_4) would not have an unpaired electron and thus would not exhibit electron spin resonance. The electron spin resonance technique should thus be able to provide an accurate measurement of the chlorine dioxide concentration in samples and a means of verifying the colorimetric procedure. As well, the ESR technique has been advocated as a primary standard method for the analysis of ClO_2 (*13*).

A characteristic ESR trace of chlorine dioxide is shown in Figure 1. This particular curve is a trace resulting from the ESR analysis of a solution containing 52 mg ClO_2/L. The spectrum shape is in agreement with that found by another author (*13*). The ESR instrumental parameters used are listed in Table II.

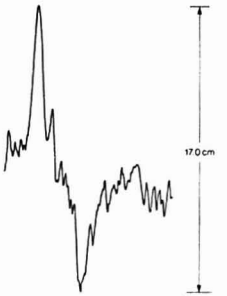


Figure 2. ESR spectrum of 1.3 mg ClO_2/L in distilled water at room temperature

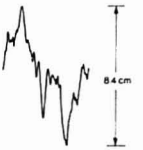


Figure 3. ESR spectrum of 0.65 mg ClO_2/L in distilled water at room temperature

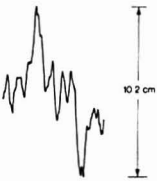


Figure 4. ESR spectrum of sewage effluent sample No. 1 at room temperature

Before a comparison of results obtained using the acid chrome violet K test and the electron spin resonance method can be made, one important difference between the two tests must be discussed. The acid chrome violet K test gives the chlorine dioxide concentration in the sample at the time the dye (ACVK) is added to and reacts with the chlorine dioxide. The ESR method gives a dynamic measurement—the chlorine dioxide concentration could likely be decreasing during the period of the measurement. The two tests must thus be made on the same sample as close as possible to each other in time.

Figure 2 represents the spectrum of a 1.3 mg ClO_2/L; Figure 3 represents the spectrum of a 0.65 mg ClO_2/L. The instrumental parameters for these spectra are listed in Table II, with the exceptions of receiver gain (5×10^5), modulation amplitude (0.5×10^2), and the time constant (4 s).

A sample of nonchlorinated effluent from a sewage treatment plant was treated with 6.5 mg/L chlorine dioxide. The reaction was allowed to proceed for a pre-determined time period after which the sample was divided into two parts—one for electron spin resonance, and one for ACVK colorimetric analysis. The ESR scan was then started. After the first peak in the scan was obtained (see Figure 4), the ACVK colorimetric test was carried out on the other part of the sample. The time elapsed between the start of the ESR scan and the beginning ACVK test was about 5 min. The length of time required for the complete ESR scan was $2^1/_4$ min. Based on known decay curves of chlorine dioxide, a time of $2^1/_4$ minutes should not

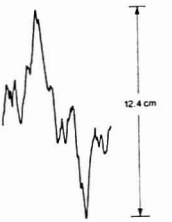


Figure 5. ESR spectrum of sewage effluent sample No. 2 at room temperature

Table III. Chlorine Dioxide Measurement in Sewage ESR vs. ACVK Measurements

Sample/ standard	ESR amplitude, cm	ClO_2 content		% Difference
		ESR	ACVK	
Standard 1	8.4	0.65	...	...
Standard 2	17.0	1.30	...	...
Sample 1	10.2	0.78	0.85	9
Sample 2	12.4	0.95	0.89	6

amount to more than a 5% decay. Thus, the procedure used for comparing the methods as outlined in the previous paragraph should be valid. The ESR scans of two such samples are shown in Figure 4 and 5. The ESR instrumental parameters were the same as those for Figures 2 and 3.

For this application of ESR, the maximum to minimum amplitude in an ESR spectrum is proportional to the concentration of the material present which exhibits the paramagnetism (*14*). When this measurement is made on two standards run earlier, 1.3 and 0.65 mg/L, a calibration for the analysis of samples with unknown ClO_2 content can be set up. A similar measurement of the two samples referred to earlier can be made, and the chlorine dioxide content of these samples calculated. The maximum to minimum amplitudes along with the corresponding chlorine dioxide concentrations for standards and samples, as well as the differences between chlorine dioxide measurements obtained on the sewage samples using the two different techniques are shown in Table III.

From this last Table III, it is clear that the measurements obtained using both techniques (ACVK–colorimetric and ESR) are comparable. The ACVK technique should be reliable for the direct colorimetric measurement of chlorine dioxide in sewage effluent.

ACKNOWLEDGMENT

The authors earnestly thank Fritz Engler of the Ontario Ministry of the Environment (Pollution Control Branch) for his kind technical assistance and the use of his Bausch and Lomb Spectronic 100 during the study.

LITERATURE CITED

(1) F. A. Tonelli, Ontario Ministry of the Environment, Toronto, Ontario personal communication, 1977.
(2) D. H. Rosenblatt, "Chlorine Dioxide—Chemical and Physical on Ozone/Chlorine Dioxide Oxidation of Organic Materials", Cincinnati, Ohio, November 1976.
(3) Olin Chemicals Report (Stamford, Conn.), "Treatment of Water Supplies with Chlorine Dioxide (ClO_2)" (1975).
(4) M. A. Post, and W. A. Moore, *Anal. Chem.*, **31**, 1872 (1959).
(5) R. N. Ashton, *J. Am. Water Works Assoc.*, **42**, 151 (1950).
(6) J. E. Haller, and S. S. Listek, *Anal. Chem.*, **20**, 639 (1948).
(7) G. C. White, "Handbook of Chlorination", Van Nostrand-Reinhold, Toronto, 1972, pp 612–13.
(8) W. Masschelein, *Anal. Chem.*, **38**, 1839 (1966)
(9) Standard Methods for the Examination of Water and Wastewater, 14th Ed., 1975, APHA–AWWA–WPCF, p 357.
(10) R. W. Andrew, and G. E. Glass, "Amperometric Titration Methods for Total Residual Chlorine, Ozone, and Sulphite", U.S. EPA report unpublished, 1974.

(11) L. Beuermann, *Gas Wasserfach.*, **106**, 78 (1965) (in German).
(12) Ref. 9, p 342.
(13) C. B. Murphy, and E. C. Tifft, Jr., "A Novel Application of Electron Spin Resonance, The Analysis of Chlorine Dioxide in Wastewater", (unpublished) Northeast Regional Meeting, American Chemical Society, Rochester, N.Y., October 1975.
(14) J. E. Wertz, and J. R. Bolton, "Electron Spin Resonance–Elemental Theory and Practical Applications", McGraw-Hill, New York, N.Y., 1972, pp 462–463.

RECEIVED for review September 5, 1977. Accepted November 14, 1977.

Kinetic Microdetermination of Manganese in Nonferrous Alloys, and of Nitrilotriacetic Acid, Ethylenediaminetetraacetic Acid, and Diethylenetriaminepentaacetic Acid

D. P. Nikolelis and T. P. Hadjiioannou*

Laboratory of Analytical Chemistry, University of Athens, Athens, Greece

An automatic spectrophotometric kinetic method is described for the ultramicrodetermination of manganese, based on its catalytic effect on the periodate–antimony(III) reaction. The method is also used for the determination of nitrilotriacetic acid (NTA) and of ethylenediaminetetraacetic acid (EDTA) and diethylenetriaminepentaacetic acid (DTPA), on the basis of their activating and inhibitory effect, respectively, on the manganese-catalyzed periodate–antimony(III) reaction. The time required for the reaction to consume a fixed amount of periodate is measured automatically and related directly to the catalyst or activator or inhibitor concentration. Manganese in the 10^{-8}–10^{-6} M level, and NTA, EDTA, and DTPA in the 10^{-7}–10^{-6}M level were determined with an average error of about 2%. The method has been applied to the determination of manganese in nonferrous alloys.

The phenomenon of catalysis has been widely used for the kinetic determination of trace amounts of various elements (*1*). In the case of metal ion catalysis, complexing agents forming highly stable metal complexes with such catalysts act as inhibitors and they can be determined on the basis of their inhibitory effect on the metal ion-catalyzed reactions (*2–4*). In other cases, the rate-increasing effect of complexing agents on the metal ion-catalyzed reactions has been used for their determination (*4–7*).

In a study of periodate reactions, it was found that the reactions of periodate with mercury(I) and antimony(III) which proceed at a measurable rate at room temperature are highly accelerated by trace amounts of manganese, in the ppb range. The periodate–antimony(III) reaction was found to be more sensitive. In this paper, a kinetic spectrophotometric method for the ultramicrodetermination of manganese(II) is described, based on its catalytic effect on the periodate–antimony(III) reaction

$$IO_4^- + Sb(III) + 2H^+ \xrightarrow[\text{catalyst}]{\text{manganese}} IO_3^- + Sb(V) + H_2O$$

The method has also been used for the determination of trace amounts of nitrilotriacetic acid (NTA) on the basis of its activating effect on the manganese-catalyzed periodate–antimony(III) reaction, and of ethylenediaminetetraacetic acid (EDTA) and diethylenetriaminepentaacetic acid (DTPA) on the basis of their inhibitory effect on the aforementioned reaction. In all cases, the time required for the periodate–antimony(III) reaction to consume a fixed amount of periodate, and thus for the absorbance to decrease by a preselected amount, is measured automatically with a solid state "double-switching" network (*3, 8*) and related directly to the catalyst (Mn) or activator (NTA) or inhibitor (EDTA or DTPA) concentration.

Rapid operation, good accuracy, and high sensitivity are the main features of the automatic method. Ultramicroamounts of manganese in the range 0.1–2 μg (4.6×10^{-7}–9.1×10^{-6} M) in the absence of NTA, and 4–40 ng (1.8×10^{-8}–1.8×10^{-7} M) in the presence of NTA, were determined with an average error and relative standard deviation of about 2%. Measurement times varied from a few seconds to about 2 min. The method has been applied successfully to the determination of manganese in nonferrous alloys. Also, nanogram amounts of NTA and microgram amounts of EDTA and DTPA were determined with the same degree of accuracy and precision.

EXPERIMENTAL

Apparatus. As previously described (*3, 8*). The "double-switching" network was adjusted to measure the time required for the recorder pen to cross preselected positions in the chart, corresponding to 0.84 and 0.79 absorbance unit.

Reagents. Water was purified by doubly distilling de-ionized water through an all borosilicate-glass still. This water passed the dithizone test (*9*) and was used throughout this work.

Antimony Trichloride Stock Solution, 0.0041 M. $SbCl_3$, 0.9352 g, is dissolved in 1 L of 3 M HCl. More dilute solutions are prepared daily by dilution.

Buffer, sodium periodate, manganese(II), and ligands solutions are prepared as previously described (*3, 10*).

The very dilute NTA, EDTA, and DTPA solutions ($<10^{-6}$ M) are prepared just before the measurements. All working standards, reagent solutions, and samples are kept in a water bath at 20 ± 0.1 °C. The stock NTA, EDTA, and DTPA solutions are stored in polyethylene bottles.

Procedure. The equipment and the nonferrous alloys samples were prepared as previously reported (*3, 10*).

Measurement Step. Determination of Manganese. Into the thermostated reaction cell kept at 20 °C, pipet 1.00 mL of phosphate buffer 0.5 M, pH 6.70, and 4.00 mL of sample or standard manganese solution, and inject 0.100 mL of 0.015 M sodium periodate solution into the cell using a 0.1-mL Hamilton microliter syringe. Start the reaction by injecting 0.250 mL of 4.1×10^{-4} M antimony trichloride, with a 0.25-mL hypodermic syringe with a Teflon needle. Close the compartment and press *at once* the start button on the universal digital instrument (UDI). The measurement is completed automatically and the number

0003-2700/78/0350-0205$01.00/0 © 1978 American Chemical Society

Table I. Effect of Various Ions on Manganese Determination at a Concentration of 9.1×10^{-8} M (5 ppb)

Ion[a]	Source	Ratio of added ion concn to Mn concn	Ion[b]	Source	Ratio of added ion concn to Mn concn
Mo(VI)	$(NH_4)_6Mo_7O_{24}\cdot 4H_2O$	3	Cr(III)	$Cr(NO_3)_3$	6
V(IV)	$VOSO_4$	5	Fe(II)	$FeSO_4\cdot 7H_2O$	10
Al(III)	$Al(NO_3)_3\cdot 9H_2O$	50	Cu(II)	$CuSO_4\cdot 5H_2O$	20
Zn(II)	$ZnSO_4\cdot H_2O$	50	Ni(II)	$Ni(NO_3)_2\cdot 6H_2O$	140
Fe(III)	$Fe(NO_3)_3\cdot 9H_2O$	55	Pb(II)	$Pb(NO_3)_2$	250
			Co(II)	$Co(NO_3)_2\cdot 6H_2O$	270
			Cd(II)	$3CdSO_4\cdot 8H_2O$	500

[a] These ions in the stated ratio caused a positive relative error of less than 5%. [b] These ions in the stated ratio caused a negative relative error of less than 5%.

on the UDI is recorded. Press the Reset button and empty the cell with suction. Repeat the procedure for each analysis.

Determination of Manganese in the Presence of NTA Activator. As in the determination of manganese, but after the addition of the buffer, inject 0.050 mL of 0.0100 M NTA solution, using a 0.05-mL Hamilton microliter syringe.

Determination of NTA. Into the thermostated reaction cell, pipet 1.00 mL of phosphate buffer 0.5 M, pH 6.70, and 4.00 mL of sample or standard NTA solution and inject 0.100 mL of 5 ppm manganese solution. Continue as in the determination of manganese from the point of sodium periodate addition.

Determination of EDTA and DTPA. Into the thermostated reaction cell, pipet 1.00 mL of phosphate buffer 0.5 M, pH 6.70, and 4.00 mL of sample or standard EDTA or DTPA solution and inject 0.100 mL of 10 ppm manganese solution. Continue as in the determination of manganese from the point of sodium periodate addition.

RESULTS AND DISCUSSION

Basic considerations concerning reducing and oxidizing agents, contamination, control of experimental conditions, and preparation of calibration curves are similar to those previously reported (*11*).

The reaction is critically pH-dependent and therefore the pH should be kept constant to better than ±0.1 pH unit. The optimum pH is in the range 6.6–6.7.

Variation in sodium periodate concentration showed that the reaction rate, the sensitivity, and the blank increased with increasing concentration of this reagent. Variation in antimony trichloride concentration showed that the blank and the reaction rate decreased, whereas the sensitivity increased with decreasing concentration of this reagent. The concentrations chosen for the determination of manganese are a compromise to ensure small blanks and measurement times in the range 10–100 s.

The reaction can be started by either antimony(III) or periodate. The antimony (III) approach was chosen because of better precision.

The rate of the catalyzed reaction and the accuracy of the method decrease with an increase in ionic strength of the solution. Manganese can be determined even in solutions of high ionic strength, provided that the composition of the standard manganese solutions is similar to that of the samples. Otherwise, the standard addition method should be used (*11*).

Linear calibration curves are obtained in the temperature range 20–29 °C. Within this range, the blank increases with increasing temperature, while the sensitivity remains practically constant. A temperature of 20 °C was chosen to secure a small blank.

It was found that citrates, tartaric acid, 2,2′-bipyridine, NTA, 1,10-phenanthroline, and ethyleneglycol-bis(2-aminoethylether)-*N,N,N′,N′*-tetraacetic acid (EGTA) enhance the catalytic effect of manganese(II) on the periodate–antimony(III) reaction. These findings parallel reported data on the activating effect of NTA, EGTA, and 1,10-phenanthroline on the manganese-catalyzed reactions of periodate with malachite green (*5–7*), triethanolamine (*10*), and hypophosphite (*4*). These facts point to the independence of ligand modification from the indicator reaction, and suggest that this modification operates via a true metal complex catalysis by complexation of, probably, manganese(III) (*6, 12, 13*). NTA was chosen as activator for the determination of manganese, because it increased the sensitivity and the detectability of the method to a larger extent than the other tested compounds and because of its lower cost. Thus, the limit of detection was decreased from 100 ng in the absence of NTA to 4 ng in its presence. Intermediate values were obtained with the other activators. The activating effect of NTA increased with increasing NTA concentration in the range 10^{-5}–10^{-4} M and remained practically constant at higher NTA concentrations.

Table II. Results for the Determination of Mn(II) in Aqueous Solutions

Reciprocal time, $s^{-1} \times 10^3$	Manganese, μg/4 mL		Relative error, %
	Taken	Found[a]	
12.4	0.100	0.100	0.0
16.0	0.200	0.190	−5.0
25.8	0.400	0.404	+1.0
39.9	0.750	0.700	−6.7
53.4	1.00	0.98	−2.0
77.6	1.50	1.50	0.0
101.8	2.00	2.01	+0.5
			Av 2.2

[a] From straight-line calibration curve, average of two values.

From Arrhenius plots of log (initial rate, $(dA/dt)_0$) vs. reciprocal of absolute temperature, the activation energy of the uncatalyzed reaction was calculated to be 19.9 kcal/mol.

To investigate the effect of various ions that might interfere with the determination of manganese (in the presence of NTA), the measurement step was modified as follows. After the addition of a manganese standard (5 ppb) and NTA, 0.250 mL of water or of the solution of the ion being examined was injected into the reaction cell. Strongly alkaline solutions were neutralized with sulfuric acid and acidic solutions with sodium hydroxide, before their effect on the reaction rate was studied. The following ions did not affect the rate of the manganese-catalyzed reaction even when their concentrations were several thousand times that of the manganese:potassium, sodium, calcium, and magnesium. Table I shows the effect of interfering ions on the manganese determination.

Determination of Manganese. Analysis of aqueous manganese solutions of known concentrations, in the absence and in the presence of NTA, gave the results shown in Tables II and III, respectively. The data indicate that ultramicroamounts of manganese in the range 0.1–2 μg in the absence of NTA and 4–40 ng in the presence of NTA can be determined with an average error of about 2%. The reaction is

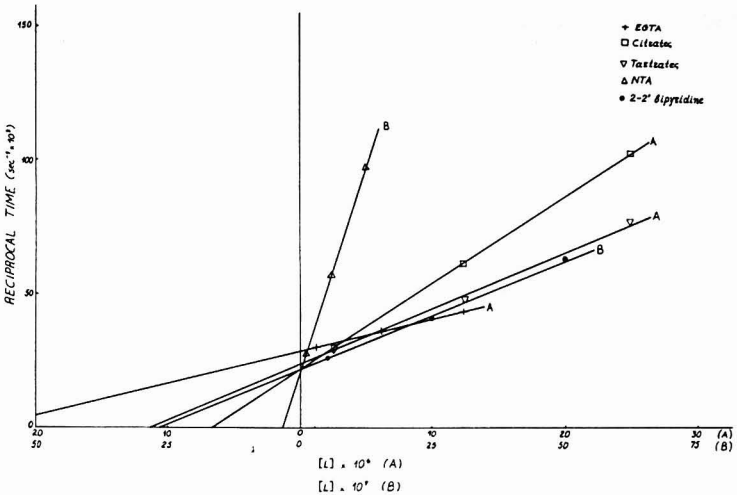


Figure 1. Activating effect of complexing agents, L, on the manganese-catalyzed periodate-antimony(III) reaction. Conditions as under Procedure

Table III. Results for the Determination of Mn(II) in Aqueous Solutions with NTA as an Activator

Reciprocal time, $s^{-1} \times 10^3$	Manganese, ng/4 mL		Relative error, %
	Taken	Found[a]	
28.2	4.00	4.20	+5.0
46.0	10.0	10.0	0.0
76.2	20.0	20.0	0.0
105.0	30.0	29.2	−2.7
138.5	40.0	40.2	+0.5
			Av 1.6

[a] From straight-line calibration curve, average of two values.

pseudo-first-order with respect to manganese in the aforementioned range. The reaction becomes too fast to be followed at higher manganese concentrations and therefore the manganese concentration of such samples should be brought in the aforesaid ranges by dilution. The relative standard deviation was 2.1% for a 250-ppb manganese sample in the absence of NTA and 2.7% for a 5-ppb sample in the presence of NTA (n = 6).

Addition of a complexing agent to a metal ion-catalyzed reaction may result in true metal–complex catalysis, ligand promotion or inhibition (*14*). Figures 1 and 2 show the effect of various complexing agents on the rate of the periodate–antimony(III) reaction. There is a linear relationship between reaction rate and ligand concentration, thereby making possible the determination of several ligands. NTA was determined on the basis of its activating effect, and EDTA and DTPA were determined on the basis of their inhibitory effect, to show the possibilities of the method. For the determination of NTA, variation in manganese concentration showed that the sensitivity increased and the blank decreased with increasing concentration of this reagent. The concentration chosen for the determination of NTA is a compromise to ensure small blanks and measurement times in the range 10–40 s. As is shown in Figure 2, the linear relationship between reaction rate and EDTA or DTPA concentration extends over a wide concentration range (at least a decade), thereby making possible the determination of EDTA and

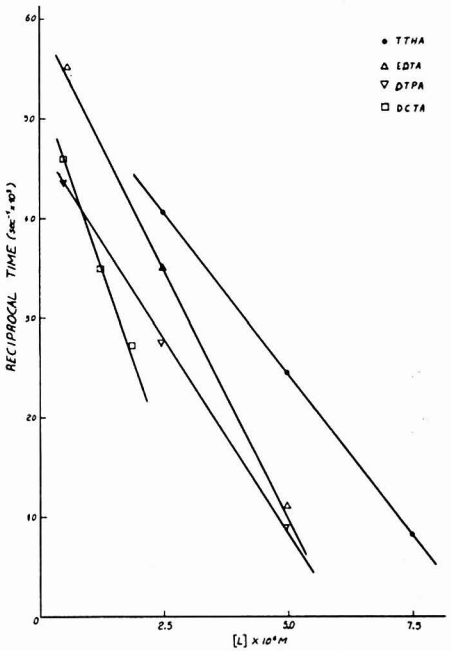


Figure 2. Inhibitory effect of complexing agents, L, on the manganese-catalyzed periodate–antimony(III) reaction. Conditions as under Procedure

DTPA in very dilute solutions (10^{-7}–10^{-6} M). Manganese concentrations smaller than 3.3×10^{-7} M were tested, but the catalysis was insufficient to give a measurable change in reaction rate under the chosen experimental conditions. On

Table IV. Results for the Determination of NTA, EDTA, and DTPA in Aqueous Solutions

NTA, ng/4 mL		Relative	EDTA, μg/4 mL		Relative	DTPA, μg/4 mL		Relative
Taken	Found[a]	error, %	Taken	Found[a]	error, %	Taken	Found[a]	error, %
95.6	95.6	0.0	0.744	0.744	0.0	0.787	0.779	−1.0
239	239	0.0	1.86	1.92	+3.2	1.97	2.08	+5.6
478	459	−4.0	3.72	3.72	0.0	3.93	3.93	0.0
717	727	+1.4	5.58	5.96	+6.8	5.90	6.29	+6.6
956	995	+4.1	7.44	7.37	−0.9	7.87	7.95	+1.0
		Av 1.9			Av 2.2			Av 2.8

[a] From straight-line calibration curve, average of two values.

Table V. Effect of Foreign Species on the NTA, EDTA, and DTPA Determination Using the Mn(II)-Catalyzed Periodate-Sb(III) Reaction

	Concn level, M, that gives 5% positive error in the determination of			Concn level, M, that gives 5% negative error in the determination of		
Foreign species	NTA[a]	EDTA[b]	DTPA[c]	NTA[a]	EDTA[b]	DTPA[c]
Nitrilotriacetic acid (NTA)					1.2×10^{-8}	1.2×10^{-8}
Ethylenediaminetetraacetic acid (EDTA)			1.2×10^{-7}	1.2×10^{-7}		
Diethylenetriaminepenta-acetic acid (DTPA)		1.2×10^{-7}		1.2×10^{-7}		
1,2-Diaminocyclohexanetetra-acetic acid (DCTA)		1.2×10^{-7}	1.2×10^{-7}	1.2×10^{-7}		
Sodium oxalate		2.5×10^{-6}	1.2×10^{-6}	5.0×10^{-7}		
Triethylenetetraaminehexa-acetic acid (TTHA)		1.2×10^{-6}	1.2×10^{-6}	1.2×10^{-6}		
Potassium biphthalate		1.0×10^{-5}	1.0×10^{-5}	1.0×10^{-5}		
Sodium citrate	1.2×10^{-5}				1.2×10^{-5}	1.2×10^{-5}
Tartaric acid	1.2×10^{-5}				1.2×10^{-5}	1.2×10^{-5}
Ethyleneglycol- bis(2-amino-ethylether)-*N,N,N',N'*-tetraacetic acid (EGTA)	8.0×10^{-5}				1.2×10^{-5}	1.2×10^{-5}

[a] NTA: 6.25×10^{-7} M. [b] EDTA: 2.50×10^{-6} M. [c] DTPA: 2.50×10^{-6} M.

the other hand, for manganese concentrations higher than 3.3 $\times 10^{-6}$ M the sensitivity increases and the range at which EDTA can be determined is extended. However, the purpose of the present study was to determine EDTA at lower concentration levels.

Determination of NTA, EDTA, and DTPA. Analysis of aqueous NTA, EDTA, and DTPA solutions of known concentrations gave the results shown in Table IV. The data indicate that microamounts of NTA (0.1–1 μg, 1.25×10^{-7}–1.25×10^{-6} M), and EDTA and DTPA (0.8–8 μg, 5.0×10^{-7}–5.0×10^{-6} M) can be determined with an average error of about 2%. The relative standard deviation for 6.25×10^{-7}M NTA, 2.50×10^{-6} M EDTA and 2.50×10^{-6} M DTPA solutions were 3.2%, 2.9% and 2.1%, respectively ($n = 6$).

NTA, EDTA, and DTPA analogues which can be expected to interfere in their determination on the basis of their stability constants include: EGTA, 1,2-diaminocyclohexanetetraacetic acid (DCTA), and triethylenetetraaminehexaacetic acid (TTHA). Potential interfering substances including the above compounds, sodium oxalate, and citrate, tartaric acid, and potassium biphthalate were tested and the results are summarized in Table V.

The kinetic method was tested for the determination of manganese in nonferrous alloys. Satisfactory results were obtained in the analysis of National Bureau of Standards Bronze 62 (Mn%: found 1.60, 1.57, 1.58, 1.61; reported 1.59) and Thorn Smith Dow metal 4 (Mn%: found 0.53, 0.54, 0.51, 0.51; reported 0.52).

CONCLUSION

A method for the determination of trace amounts of NTA and of EDTA and DTPA, on the basis of their activating and inhibitory effect, respectively, on the manganese-catalyzed periodate–antimony(III) reaction has been developed. Although the application reported here deals with the catalytic determination of manganese in nonferrous alloys, the scope of the method is intended to be more general. A basic procedure and general considerations for the determination of manganese are given so that the method can be adapted to many specific cases—e.g., natural waters, urine, tissues, bones, blood, etc.

LITERATURE CITED

(1) K. B. Yatsimirskii, "Kinetic Methods of Analysis", Pergamon, Oxford, 1966.
(2) H. A. Mottola and H. Freiser, *Anal. Chem.*, **39**, 1294 (1967).
(3) D. P. Nikolelis and T. P. Hadjiioannou, *Mikrochim. Acta*, **9**, 125 (1977).
(4) D. P. Nikolelis and T. P. Hadjiioannou, *Analyst, (London)*, **102**, 591 (1977).
(5) H. A. Mottola and C. R. Harrison, *Talanta*, **18**, 683 (1971).
(6) H. A. Mottola and G. L. Heath, *Anal. Chem.*, **44**, 2322 (1972).
(7) E. W. Chlapowski and H. A. Mottola, *Anal. Chim. Acta*, **76**, 319 (1975).
(8) C. E. Efstathiou and T. P. Hadjiioannou, *Anal. Chim. Acta*, **89**, 55 (1977).
(9) E. B. Sandell, "Colorimetric Determination of Traces of Metals", 3rd ed., Interscience, New York, N.Y., 1965, pp 17–18.
(10) C. E. Efstathiou and T. P. Hadjiioannou, *Anal. Chem.*, **49**, 414 (1977).
(11) T. P. Hadjiioannou and T. A. Kefalas, *Mikrochim. Acta*, **1**, 1215 (1969).
(12) H. A. Mottola, *Anal. Chim. Acta*, **71**, 443 (1974).
(13) H. A. Mottola, *Crit. Rev. Anal. Chem.* **4**, 229 (1975).
(14) A. E. Martell, *Pure Appl. Chem.*, **17**, 129 (1968).

RECEIVED for review September 6, 1977. Accepted November 14, 1977.

Directly Digital Flow Controller with Rapid Response Time and High Precision

T. W. Hunter and G. M. Hieftje*

Department of Chemistry, Indiana University, Bloomington, Indiana 47401

A new, directly digital device for automated gas flow control at a fixed pressure level is described. Being a pneumatic analog to a weighted-resistor, digital-to-analog converter, the transducer controls gas flow by summing the flow from selected parallel paths. The new transducer exhibits rapid response time, excellent reproducibility and linearity over its entire operating range. Although the present device is intended for gas flow control and operates over an 8-bit (256-fold) flow range, simple modifications would enable its use for liquid flow control or for different flow ranges.

Advances in computer technology have led to increasingly sophisticated control of scientific experimentation and industrial process streams. In many of these applications, on-line computers not only log data but also control many of the experimental or process parameters. With this increased degree of control, improvements in transducer design are imperative for optimal transfer of computer commands to the subservient unit. To achieve optimal transfer of control information, the transducer should ideally be directly digital and respond as rapidly as the computer itself.

One parameter which often must be controlled in an automated system is gas flow. When the flow is to be controlled by a computer or other digital network, it is common to employ a transducer consisting of a needle valve connected to the shaft of a stepper motor. With such a device, the magnitude of flow is a function of the position of the valve stem which in turn is governed by the number of increments the stepper motor has moved in relation to an indexed location. Unfortunately, mechanical backlash and changes in valve stem position can lead to irreproducible or unpredictable flows when the stepper motor is returned to a previous location or sent to a new position. Stepper-motor-driven needle valves also suffer from rather slow response times, because of the need to drive the finely pitched screw of the valve over a substantial distance and because of the limited angular rotation rate of most stepper motors. Other disadvantages of this type of flow transducer are the nonlinear relationship of flow as a function of valve stem location and the need to initialize the transducer upon start up (i.e., to relate stem location to an index).

This paper presents an improved approach to automated control of gas flow which eliminates the shortcomings of the previously described device. The new approach employs a flow network which is analogous to a parallel, weighted resistor ladder used for digital-to-analog conversions; a schematic diagram is shown in Figure 1.

As shown in Figure 1, the new controller consists of a number of selectable, parallel flow paths, each of which can be opened or closed, depending on the state of a solenoid valve (S) located in each path. The output gas flow from the transducer is then the sum of the flows through all of the open, individual paths. For convenience and binary compatability, each successive path is adjusted for a flow twice that of the preceding path, so that the total flow is directly proportional to the binary word corresponding to the state of the series of solenoid valves.

This new method of fluid control requires a minimum of mechanical movement and therefore displays greatly improved response time and reproducibility. When used to control the flow of air, the transducer exhibited a reproducibility of about 2% over two months and showed no significant difference between calculated and observed flows from combined flow paths. However, the present experimental configuration does nothing to eliminate irreproducibility arising from thermally produced expansion and contraction of the needle valve stem. This problem, which is common to all flow-regulating systems which incorporate a needle valve, can be overcome with modifications to be suggested later.

DESIGN CONSIDERATIONS

The application for which the new flow controller was designed, atomic absorption flame spectrometry, requires the metering of two gases (air and acetylene). A block diagram for the final system used in this dual-flow application is shown in Figure 2. Just as its electronic analog must have a constant voltage across the resistor ladder network, so must the pneumatic transducer have a pressure applied over its alternative, parallel flow paths which is constant regardless of the flow rate. It was found that a 12-L shunt ballast tank, placed after a dual-stage regulator, made it possible to maintain a sufficiently constant pressure across the transducer (~20 psig) regardless of the gas flow rate within the range 0–16 L/min.

Both transducers were constructed with input and output tubes 40.6 cm long and 2.54 cm in diameter and fabricated from either brass for transducer 1 (air) or stainless steel for transducer 2 (acetylene). Because of the formation of potentially explosive copper acetylides, it is unwise to employ copper components in any flow system intended for use with acetylene. One should also keep the use of brass to a minimum. The input and output tubes are connected by eight parallel flow paths of $^1/_8$-in. tubing (brass and stainless steel, respectively), each of which contains a subminiature solenoid valve (Angar, Roseland, N.J., Model 10, normally closed) and a needle valve (Nupro, Cleveland, Ohio, either models SA or MA) in series. The individual needle valves were adjusted so that the gas flow rates through successive parallel paths increased by a factor of two.

The state (open or closed) of each solenoid valve, S_i, is determined by the transducer controller. An eight-bit control word and the occurrence of load pulses are employed by the controller circuitry to determine which solenoid valves of each flow transducer are to be open. Auxiliary emergency sensors are also provided, so that all solenoid valves can be closed independently of the eight-bit control word if some defined shutdown condition occurs. In the present application, a photoelectric sensor provides such a shutdown indication if the flame being supported is somehow extinguished. Also contained in the controller is circuitry which amplifies the control word logic information to the voltage and current levels necessary to drive the solenoids.

In the present configuration, the load pulses and the eight-bit control word can originate in either of two places: from the digital output of the computer or from a local hardwired selector. The hardwired selector consists simply

0003-2700/78/0350-0209$01.00/0 © 1978 American Chemical Society

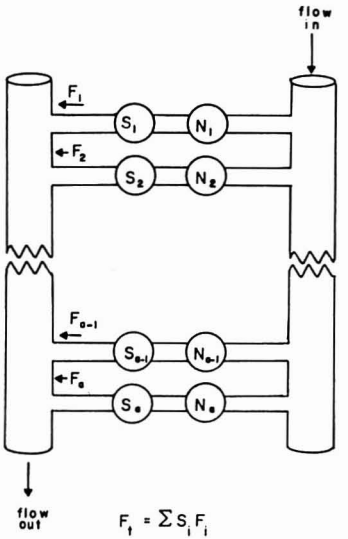


Figure 1. Schematic diagram of flow transducer. S_i and N_i are the solenoid valve and needle valve, respectively, in the ith flow path. F_i is the gas flow through the ith flow path. F_t is the total flow from the transducer

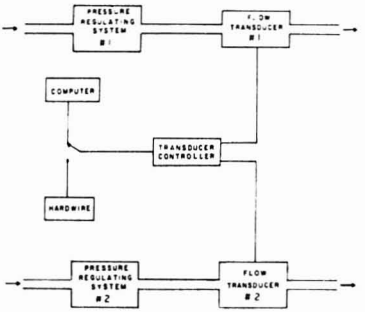


Figure 2. Functional organization of the automated gas flow controller designed to control two gases

of a bank of eight toggle switches which generates an eight-bit word, and two push-button switches which provide the load-command pulses. These push-button switches select the transducer to which the control word is to be directed. The ten switches are located on the front of the controller. Also on the front of the controller are a switch, termed *mode control*, which determines the source, either local or remote, of the eight-bit control word, two light-emitting-diode displays which indicate which solenoid valves are to be open, and shutdown controls. The designated control word can be loaded from either the computer or the hardwired device.

Control and Driving Circuitry. Figure 3 shows a detailed schematic diagram of the circuitry involved in controlling a single solenoid valve. One bit each of the control words from the computer and the local circuitry are fed into a digital multiplexer, M. Which of these two inputs is to appear at the M output is governed by the position of mode switch, S1. The output of the multiplexer is fed in parallel to the inputs of two data latches, one for each flow transducer to be controlled. This design enables the same control word input (hardwired or computer interfaced) to be used for all flow transducers, thereby minimizing the number of required control lines. Which of the flow controllers is to be addressed is governed by the load command system (described below).

In Figure 3, only the data latch and subsequent circuitry for one controller are shown. When the data latch receives a pulse through gate G1 from either the local command circuitry or the computer, the control logic level at input D appears at output Q. Output $\bar{Q}$ (whose logic level is the complement of Q) is used to drive a light-emitting-diode display lamp on the front panel. The output at Q is then fed to a driving transistor T1 through AND gate G2. The passage of the control signal through gate G2 is determined by the "shutdown" input, whose level indicates the existence of safe operating conditions. In the present system, a high or "1" logic level at the shutdown input indicates that the flame is on. Obviously, this input must be temporarily overridden by switch S2 when the flame is first ignited.

If the logic level from gate G2 is high, transistor T1 is biased "on", activating the solenoid valve; if T1 is biased off by the G2 AND gate output being low, the solenoid is turned off. Therefore, if a control bit is loaded high and no shutdown conditions are activated, the solenoid is opened, whereas if the loaded control bit is low or if shutdown is indicated, the solenoid is closed. In Figure 3, signal diode D1 protects the TTL control logic from any switching transients fed back through T1; resistor R1 limits the base current to transistor T1.

The solenoid valves used in the present circuitry require a larger current to drive them open (250 mA) than is required to maintain an open condition, once it has been established. This high initial driving current is supplied by capacitor C1, which stores energy until T1 first turns on. When T1 is saturated, capacitor C1 dumps its stored charge through the solenoid, pulling it in. Resistor R2 limits the final collector current to the 50 mA needed to hold the solenoid valve open. Rectifier diode D2 keeps the transistor base-collector junction forward-biased as the magnetic field in the solenoid collapses when the transistor shuts off. The 24-V and 5-V power supplies can deliver 24 W and 5 W, respectively.

Not shown in Figure 3 are two status flags which are available to the computer. One flag when high indicates that a shutdown condition has occurred. The other flag is high for about 10 ms after a load pulse has been received by the control circuitry. This latter flag can be used by the computer as a hardwired delay so that the computer with its cycle time of 1.6 μs does not overrun the flow transducer (the solenoid valves have an opening (pull-in) time of 5 ms).

EXPERIMENTAL

Gas flows were measured with three different devices to cover the wide range of flow rates selectable with the transducer. Two different wet test meters (Precision Scientific Co., Chicago, Ill.) with full scale capacities of 3 L (model 63114) and 0.25 ft^3 (model 63118) and accuracies of $\pm^1/_2$% were used to measure flows from 16 to 0.5 L/min. A 22-mL capacity bubble meter was used to measure flows of less than 0.5 L/min. Flow rates were determined by dividing the capacity of the measuring device by the time required for that volume of calibrating gas to flow from the transducer. In this study, the calibration gas used was dry air (Matheson Gas Co., East Rutherford, N.J.). After this initial calibration, other gases could be used with the flow controllers merely by correcting for the differences in gas densities and viscosities.

CHARACTERIZATION

To assess the performance of this new approach to automated flow control, flow rates for each parallel flow path and

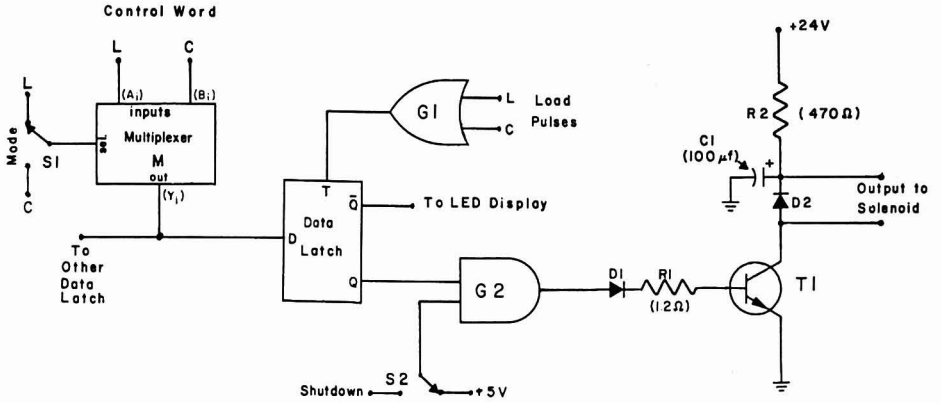


Figure 3. Schematic diagram of digital and analog circuitry used to control the state of a single solenoid valve. Multiplexer, M, and data latch are integrated circuits SN74157 (parenthetical pin designation same as used in manufacturer specifications) and SN7475 (Texas Instrument, Inc., Houston, Texas), respectively; T1 is a NPN, h_{fe} = 60 transistor. Designations C and L refer to computer or local control, respectively

Table I. Statistical Summary of Observed Flow Rates (L/min) from Individual Flow Paths

	Binary weight of flow								
	2^0	2^1	2^2	2^3	2^4	2^5	2^6	2^7	Av
Average of 5 data sets	0.0641	0.129	0.257	0.540	0.998	2.04	4.11	8.07	
Std dev among sets	0.0024	0.004	0.009	0.003	0.003	0.03	0.003	0.06	
Std dev within a set	0.008	0.001	0.002	0.009	0.02	0.01	0.02	0.04	
% Rel std dev among sets	3.7	3.1	3.5	0.6	0.3	1.5	0.7	0.7	1.8
% Rel std dev within a set	1.2	0.8	0.8	1.6	2.0	0.5	0.5	0.5	0.88

for combinations of paths were determined periodically over a two-month period. In order to characterize the reproducibility of flow rates and the uncertainty of a single flow measurement, the flow rates from the individual paths were measured a minimum of three times and then averaged. On five different occasions, the average flow rates for all eight flow paths were determined. The averages of the five average flow rates for each flow path are listed in Table I along with the standard deviations among the five sets of data. Also listed in Table I are the standard deviations within a set of observations (obtained by pooling all observed standard deviations for that flow path). For purposes of comparison, relative standard deviations are also included in Table I. Even though deviations between days of observations are small, analysis of variance reveals that, at the 95% confidence level, these differences are significant and are probably due to temperature and slight delivery pressure changes from day to day. On the average, day-to-day irreproducibility for all flow paths was about 2% while the uncertainty in a single flow measurement was found to be less than 1%.

If the flow transducer were to perform as expected, the observed flow rates for a combination of opened flow paths should equal the sum of the flows through the individual paths. When each of 49 observed flow rates was compared to its calculated flow rate, eight theoretical flow rates were not encompassed by the two-standard-deviation error range of the average observed flow rate. Because the calculated sum of flows is based on measured flows which have an associated error themselves, the calculated flows therefore have an associated uncertainty which has not been taken into account. When propagation of error is used to estimate uncertainties in the calculated flows and the difference between observed and expected flows is statistically tested at the 95% level, only three comparisons showed a statistically significant difference. One would expect that of 49 samples from a normal distribution, 2.45 samples would lie outside the 95% confidence range. Therefore, the three noted differences of the 49 comparisons are probably not significant and the transducer performs as theorized.

The same accuracy and precision as stated above were obtained from the new transducer over a wide range of applied pressures. This fact makes it possible to employ the same transducer for a wide range of flows, merely by adjusting the applied gas pressure. Moreover, re-tuning of the parallel flow paths (adjustment of the needle valves) is unnecessary, once their relative flows have been established.

CONCLUSIONS

The approach of adding flows from parallel flow paths has been shown to be a feasible method of automated flow control. This type of flow transducer has the advantages of minimal mechanical motion, fast response time, good long-term reproducibility, and directly digital operation. The experience gained with this first prototype has shown that performance can probably be improved by further regulation of the gas pressure system and possibly by thermostating the transducer. In addition, the susceptibility of the present device to temperature fluctuations could be greatly minimized if the needle valves were replaced by a set of preset, fixed orifices such as watch jewels. The diameters of fixed orifices would be selected so that a relationship between their transmitted flows exhibited the binary relationship required of the parallel flow paths. In such a device, the desired flow range used could be finally set by adjusting the pressure across the transducer.

ACKNOWLEDGMENT

The authors acknowledge Maurice Williams and John Dorsett for their help in the construction of the flow transducers used in this study. Thanks are also due to Robert

Ensman, Nick Loy, and Steve Williams for their advice in the design and construction of the electronic circuitry.

RECEIVED for review September 16, 1977. Accepted October 31, 1977. Presented in part at the Centennial Meeting of the American Chemical Society, New York, N.Y., April 1976; taken in part from the Ph.D. thesis of T. W. Hunter, Indiana University, Bloomington, Ind., 1976. Support of this work by Grant PHS GM 17904-04A1 from the National Institutes of Health is gratefully acknowledged.

Comparisons between Hydrogen Bond Donor–Acceptor Parameters and Solvatochromic Red Shifts

Orland W. Kolling

Chemistry Department, Southwestern College, Winfield, Kansas 67156

Transition energies were tabulated for three bathochromic indicators in representative nonpolar, polar aprotic, and amphiprotic solvents. Nonlinear statistical correlation functions previously used for comparing the dye transition energy with a second solvent polarity parameter were resolved into linear equations for polar aprotic solvents and a deviation variable for hydrogen bond donor solvents. In these comparisons, the Gutmann acceptor number was useful as a second empirical parameter responsive to solvent polarity. For the lower alcohols, acetic acid, chloroform, and acetonitrile, the qualitative trend in the deviation variable parallels the order obtained with the Kamlet–Taft α-scale for hydrogen bond donor solvents. Similar correlations between transition energies for the bathochromic dyes and enthalpy-based measures of donor–acceptor interactions generally failed.

Solvatochromic indicators having chromophoric groups absorbing in the UV-visible region have been used to define empirical scales of solvent polarity. The most commonly used scales deduced from blue-shift chromophores are the Kosower *Z* values and the Dimroth–Reichardt numbers. These have been found to be most adequate for representing hydrogen bonding and dielectric characteristics of polar nonaqueous solvents, but are less satisfactory as measures of solvent basicity for nonpolar and aprotic solvents (*1*). A series of red-shift (bathochromic) dyes have been developed which are more capable of representing distinctions among polar aprotic and nonpolar solvents (*2–4*) and their transition energies can be used to quantify medium effects in some instances where the Kosower and Dimroth values fail. Recently, Taft and Kamlet have devised a double scale for hydrogen bond donor and acceptor solvents which is derived from the solvatochromic shifts of nitroanilines and nitrophenols (*5*, *6*).

In previous investigations on the solvatochromism of three bathochromic dyes (Phenol Blue, Nile Blue A oxazone, and Brooker's dye VII) a general nonlinear correlation was found between the transition energy (E_T) of the indicator and the ^{19}F NMR shift and the ^{14}N ESR hyperfine splitting constant for selected model basic probes of solvent polarity (*7*). A purely statistical treatment of all of the data for both hydrogen bonding and nonhydrogen bonding solvents produced the rational correlation function given in Equation 1

$$P_r = \frac{cE_T - a}{E_T - b} \qquad (1)$$

where P_r is the probe variable, E_T the transition energy (kcal/mol) for the solvatochromic indicator, and a, b, and c are constants.

The present paper is concerned with the results of a more detailed examination of bathochromic shifts by the three model dyes in pure hydrogen bond donor solvents with the objective of resolving the influence of hydrogen bonding from the correlated parameters of solvent polarity incorporated into Equation 1. For the latter, the Gutmann donor (*DN*) and acceptor (*AN*) numbers were selected for the P_r variables. The Figueras concept of an additive perturbation energy contribution was extended to the response to the probe in hydrogen bond donor solvents (*4*).

EXPERIMENTAL

Solvents. Seven solvents were included in this study for which bathochromic shifts of the dyes had not been determined in previous work. These are: benzonitrile, carbon tetrachloride, absolute ethanol, *n*-hexane, methylene chloride (re-determination), nitrobenzene, and 2-propanol. In all cases, the liquid was initially dried for 1 week over anhydrous calcium sulfate. Subsequent steps in purification are those specified below.

Anhydrous ethanol was prepared by the usual refluxing over fresh CaO, followed by fractional distillation. Isopropyl alcohol was treated with clean magnesium ribbon prior to fractional distillation.

Carbon tetrachloride, dichloromethane, and *n*-hexane were further dried by passing through a chromatographic column of alumina and then re-distilled. Benzonitrile was passed through two alumina columns, but not re-distilled. Purified nitrobenzene was obtained by reduced pressure (7 Torr) fractional distillation.

Solvatochromic Dyes. Purified samples of Phenol blue and Nile Blue A oxazone were prepared by the procedures for recrystallization and column chromatography reported earlier (*8*, *9*). Literature melting points and thin layer chromatography were again used as criteria for purity of the products.

Spectra. Measurements of the absorption maxima for specific dye solutions in the visible region were made with a Perkin-Elmer-Coleman 111 spectrophotometer, following the methods previously described (*8*).

RESULTS AND DISCUSSION

Additional experimental values for the transition energies of Phenol blue and Nile Blue A oxazone in nonaqueous solvents are given in Table I, along with published data for Brooker's dye VII. Representative parameters measuring solvent basicity which were used in previous work on red shift vs. basicity correlations were re-examined with special attention being given to the bathochromic shifts in hydrogen bond donor solvents. Possible relationships to enthalpy-based

0003-2700/78/0350-0212$01.00/0 © 1978 American Chemical Society

Table I. Spectral Data for Solvent Polarity Probes (at 25 °C)

Solvent	Electronic E_T (kcal/mol)			^{14}N ESR A_N radical 1[d]	Gutmann AN[e]
	X_R[a]	PB[b]	NBAO[c]		
1. Acetic acid	···	47.14	51.24	16.420	52.9
2. Acetone	45.7	49.14	53.64	15.527	12.5
3. Acetonitrile	45.7	48.97	53.74	15.666	19.3
4. Benzene	46.9	49.73	55.87	15.404	8.2
5. Benzonitrile	43.3	47.90	52.77	···	15.5
6. Carbon disulfide	···	50.87	55.46	15.289	···
7. Carbon tetrachloride	48.7	50.61	55.09	15.331	8.6
8. Chloroform	44.2	48.13	53.24	15.863	23.1
9. Diethyl ether	48.3	51.58	56.39	15.334	3.9
10. *N,N*-Dimethyl formamide	43.7	48.06	52.85	15.635	16.0
11. Dimethyl sulfoxide	42.0	47.26	52.17	15.692	19.3
12. 1,4-Dioxane	48.4	50.07	55.19	15.452	10.8
13. Ethanol	43.9	47.20	52.10	16.030	37.1
14. *n*-Hexane	50.9	51.96	56.50	15.134	0.0
15. Methanol	43.1	47.03	51.98	16.210	41.3
16. Methylene chloride	44.9	48.46	53.52	15.752	20.4
17. Nitrobenzene	42.6	47.26	52.36	···	14.8
18. Nitromethane	44.0	48.39	52.85	15.759	20.5
19. 2-Propanol	44.5	47.96	52.94	15.973	33.5
20. Pyridine	43.9	47.98	52.55	15.608	14.2
21. Tetrahydrofuran	46.6	48.72	53.31	15.373	8.0
22. Water	68.9	···	···	17.175	54.8

[a] Values from Brooker's mercyanine dye (VII), L. G. S. Brooker et al. (*2*). [b] Re-evaluated and new data for Phenol blue as well as earlier values: J. Figueras (*4*); O. Kolling and J. Goodnight (*8*); O. Kolling (*9*). [c] Literature values and new experimental results for Nile Blue A oxazone: M. M. Davis and H. Hetzer (*3*); O. Kolling (*9*). [d] Hyperfine splitting constants for di-*tert*-butyl nitroxide radical: B. Knauer and J. Napier, *J. Am. Chem. Soc.*, 98, 4395 (1976). [e] Solvent acceptor numbers: V. Gutmann (*10*).

scales for hydrogen bond donor–acceptor interactions were included as well.

Gutmann Donor and Acceptor Numbers. The donor number (*DN*) of Gutmann is defined as $-\Delta H$ (in kcal/mol) for the reaction between a given Lewis base and $SbCl_5$ as the reference acid, and the numbers are evaluated in very dilute solutions of the reactants in 1,2-dichloroethane as the solvent (*10*). The broad scale of donor numbers ranges from 0.1 for benzene to 61.0 for triethylamine; and extensive empirical correlations between *DN* values and the effects of donor solvents upon redox and ligand substitution reactions have been developed by Gutmann.

In an important critical review of the data for enthalpies of formation for hydrogen bonded adducts between different donors and common acceptors, Arnett, Mitchell, and Murty noted that the uncertainty in enthalpy changes predicted from DN values is ±0.4 kcal/mol and that the *DN* scale provides a fairly adequate measure of the hydrogen bond acceptor capacities of a variety of Lewis bases (*11*). Among the various Lewis acids which have been used as reference acceptors, antimony(V) chloride appears to be among the stronger if one compares the electrostatic contributions to adduct formation from the acidic reactants. For example, on the Drago–Wayland E-C scale the E_A value of 7.38 for $SbCl_5$ is comparable to that of BF_3 and is well above the values for phenol and *p*-fluorophenol (*12*). Thus, positive correlations between donor numbers and solvent parameters would be expected for interactions characterized by significant electrostatic (or Coulombic) contributions.

The Kosower *Z* scale derived from pyridinium iodides as blue shift chromophores has been successfully used as a measure of solvent polarity in polar and hydroxylic solvents (*13*). Gutmann has noted a seemingly linear correlation for *Z* vs. *DN* (*10*); however, there is extensive scattering of points along the linear plot with no visible pattern to deviations when comparing hydrogen bonding to nonhydrogen bonding solvents. When similar plots are made for *DN* vs. E_T for the data of the three model red shift dyes in Table I, no clear trend is observed among either the hydrogen bond donor or acceptor solvents. (The figures are not included herein.) Pairwise comparisons between bathochromic shifts and other enthalpy parameters for hydrogen bond donor–acceptor interactions (*11*) do not exhibit any significant correlations.

By contrast to the donor scale, the Gutmann acceptor number (*AN*) values are spectral parameters derived from the ^{31}P NMR shift for triethylphosphine oxide as the reference base dissolved in single solvents or in mixed solvents (*10*). However, *AN*-scale values are normalized shift numbers based upon an assigned value of 100 for the 1:1 adduct, $SbCl_5$:Et_3PO, in 1,2-dichloroethane and for *n*-hexane as zero for the reference solvent. A connective function between *DN* and *AN* has been developed (*14*).

Because of the structural similarity of the basic functional group in triethylphosphine oxide to the dialkyl nitroxide radical, the interaction of a given solvent with the oxygen atom of the probe species would be expected to be comparable, as well. As noted in the earlier review (*7*), hyperfine splitting constants (A_N) for di-*tert*-butyl nitroxide exhibit a regular though nonlinear trend when related to the red shift of solvatochromic indicators. Therefore, the initial new correlation examined was that between *AN* (triethylphosphine oxide) and the A_N of dibutyl nitroxide, using the data from Table I. The resulting graph in Figure 1 conforms to the linear regression function of Equation 2.

$$AN = 44.36\,(A_N - 15.23) \qquad (2)$$

Here, the regression coefficient is 0.986 based upon 17 solvents, including hydrogen bond donors as well as aprotic solvents. If the ^{14}N ESR measurements are used with Equation 2 as a predictive function for *AN* values, the uncertainty in the computed results is ±0.9 (std dev). A similar regression function can be established for *AN* vs. ^{19}F chemical shift for 3-fluoropyridine in the same set of solvents; however, the regression coefficient is lower (0.956) because of the greater experimental uncertainties in NMR shifts for the fluoropyridines (*7*). Gutmann has noted a correlation (with negative slope) between *AN* and ^{13}C NMR shifts for the carbonyl group of acetone in polar and hydrogen bond donor solvents (*10*).

Table II. Derived Parameters for Hydrogen Bonding Solvents (at 25 °C)

Solvent	Δ(AN) from: X_R	PB	NBAO	α_{KT}[a]	E_A[b]	S_B[c]
Acetic acid	···	33.7	31.8	0.79	···	0.005
Acetonitrile	7.7	7.0	6.3	0.29	···	−0.104
Chloroform	8.3	7.6	8.3	0.0	3.02	−0.200
Ethanol	21.8	18.1	18.3	0.850	3.41	0.000
Methanol	24.0	21.7	22.4	0.990	3.91	0.050
Methylene chloride	7.4	6.1	6.7	···	1.66	···
Nitromethane	5.3	5.9	4.5	···	···	···
2-Propanol	19.4	16.8	17.8	0.687	2.59	−0.041

[a] Alpha scale values from R. W. Taft and M. Kamlet (*6*). [b] Data from R. Drago and B. Wayland, *J. Am. Chem. Soc.*, 87, 3571 (1965); R. Drago, G. Vogel, and T. Needham, *ibid.*, 93, 6014 (1971); D. Martire, et al., *ibid.*, 98, 3101 (1976). [c] S. Brownstein, *Can. J. Chem.*, 38, 1590 (1960).

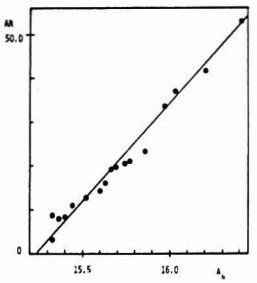


Figure 1. Correlation diagram for Gutmann acceptor numbers (*AN*) with ^{14}N ESR hyperfine splitting constants (A_N) di-*tert*-butylnitroxide for the solvents listed in Table I

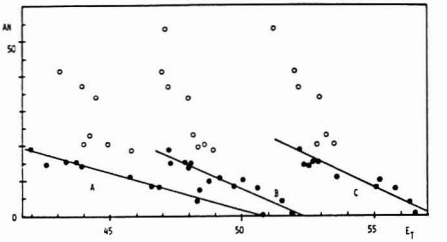


Figure 2. Comparison of Gutmann *AN* values with the transition energies (E_T) for three bathochromic indicators: (A) Brooker's dye (VII); (B) Phenol blue; (C) Nile Blue A oxazone. (●) Aprotic solvents, (O) hydrogen bonding solvents

Hydrogen Bond Donor–Acceptor Parameters. From the preceding investigations on red shift indicators, linear free energy functions were found between E_T and ΔG_f for the phenol–DMSO complex in polar aprotic solvents (*15*); and detailed treatment of the specific case of Phenol blue has demonstrated that E_T is linearly related to the McRae two-variable equation when restricted to pure aprotic solvents (*4*). Therefore, one may infer that the transition energies of each of the three solvatochromic dyes included in this study will, in general, be linearly correlated to a second idealized solvent polarity parameter for those nonaqueous media in which hydrogen bonding and other specific solvent–solute interactions are absent.

If the above deduction is correct, then one approach to the resolution of hydrogen bonding effects from the intrinsic solvent polarity included within empirical but nonlinear correlations is to employ the assumption of Figueras, i.e., that the deviation in the measured parameter is proportional to the perturbation energy caused by hydrogen bonding (*4*). The usefulness of this assumption has been demonstrated by Taft and Kamlet in their "solvatochromic comparison method" (*5, 6*). The Gutmann *AN* data appear to conform to the Figueras concept and the graphs of *AN* vs. E_T for the three model bathochromic indicators in Figure 2 were prepared from the data summarized in Table I. Regression functions for the best-fit lines within the data points for the nonhydrogen bonding and basic solvents are given by Equations 3–5.

$$\text{Curve A: } AN = -2.12\,(E_T - 51.1) \quad (3)$$

$$\text{Curve B: } AN = -3.61\,(E_T - 52.46) \quad (4)$$

$$\text{Curve C: } AN = -3.43\,(E_T - 57.31) \quad (5)$$

The enhanced response or perturbation in the acceptor number for each hydrogen bond donor solvent is represented as the displacement (ΔAN) from the linear function. Numerical ΔAN values for the eight donor solvents are listed in Table II for the curves of the three bathochromic dyes.

A sequence of decreasing ΔAN for the nonaqueous hydrogen bond donors is visible from the data in Table II: HOAc > CH_3OH > C_2H_5OH > i-C_3H_7OH > $CHCl_3$ > CH_2Cl_2 ~ CH_3CN > CH_3NO_2. The deviation in *AN* yields a linear function of positive slope when correlated with the Kamlet–Taft α values for the alcohols and chloroform (with acetonitrile and acetic acid as outlying points); and the same sequence is observed with the Brownstein *S* parameter as well. It should be emphasized in this regard that ΔAN does not relate directly with ν_{max} values for the nitroanilines used by Kamlet and Taft as the solvatochromic indicators but qualitatively relates only to the derived α values. However, there is seemingly no correspondence between ΔAN and the Drago E_A-C_A parameters or their ratio. Infrared frequency shifts for the free –OH bond in reference solute–donor solvent systems follow the order noted above with the exception of nitromethane: HOAc > CH_3OH > C_2H_5OH > i-C_3H_7OH > CH_3NO_2 > $CHCl_3$ (*16*).

The enhanced response shown by the Gutmann acceptor number for hydrogen bond donors appears to parallel other measures of donor capacity (*6*) and can be identified within parameter correlations to solvent polarity data derived from the solvatochromic dyes. The same conclusion applies also to other correlations between the bathochromic E_T and the ^{19}F NMR shifts of the fluoropyridines or ^{14}N ESR splitting constants of the alkyl nitroxide radicals; however, the exact placement of nitromethane in the lower portion of the resulting qualitative sequence remains uncertain.

When the McRae equation is used to calculate an intrinsic solvent polarity contribution to E_T of the bathochromic dye as was done by Figueras (*4*), the difference between that calculated E_T and the experimental value (as a ΔE_T) can be viewed as one measure responsive to hydrogen bonding. The

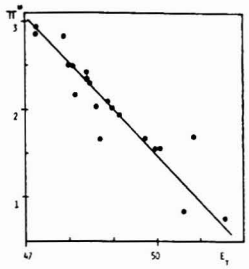


Figure 3. Correlation of π^* scale (Kamlet–Taft) with E_T of Phenol blue in polar and nonpolar aprotic solvents. Both coordinates in units of kcal/mol. Data from literature sources (*4*, *7*, *9*, *17*)

limited data reported on Phenol blue derivatives seem to parallel the above order for ΔE_T in several donor solvents (*4*); however, when the more complete data on Phenol blue are examined (including those solvents in Table I), only the gross form of the sequence among the stronger donors is the same: HOAc > CH_3OH > C_2H_5OH > i-C_3H_7OH ≫ CH_3CN. The ambiguity in the order among the weaker hydrogen bond donors in this case appears to reflect the statistical limits of reliability within the McRae equation itself as well as small nonadditive contributions ΔE_T from specific solvent effects (*8*).

A further test for the resolution of the data points as shown in Figure 2 was obtained from the recent proposal of Kamlet, Abboud, and Taft (*17*) for representing solvatochromic effects by the summation in Equation 6.

$$P_r = P_{ro} + a\alpha + b\beta + s\pi^* \quad (6)$$

Here, a, b, and s are empirical slope coefficients, α and β the previously defined hydrogen bond acidities and basicities, respectively (*5*, *6*), and π^* the parameter depicting the intrinsic solvent polarity-polarizability. For aprotic solvents in which the contributions of α and β are essentially zero, the probe response would be expected to be a simple linear function of π^* with intercept P_{ro}. The plot of E_T data for Phenol blue in polar aprotic solvents vs. π^* (converted to kcal/mol) shown in Figure 3 confirms this expectation. The correlation coefficient is 0.97 for 19 solvents (excluding CS_2 as an outlying point) and a value of −0.52 is obtained for s in Equation 6.

In the absence of any single general parameter which can be used as a quantitative measure of solvent polarity, it is important to examine correlations between the empirical responses of a variety of probes for medium effects upon reactions. Comparisons among various spectroscopic shifts, including those of a number of solvatochromic indicators and NMR and ESR probe species, seem to give evidence for common and consistent responses in polar aprotic media. The extensive investigations of Taft and Kamlet and of Figueras, as well as findings reported here, indicate that abnormal spectral shifts observed in the stronger hydrogen bonding solvents can be treated as additive perturbation energy contributions induced by the donor solvents.

LITERATURE CITED

(1) F. Fowler, A. Katritzky, and R. Rutherford, *J. Chem. Soc. B*, **1971**, 460.
(2) L. G. S. Brooker et al., *J. Am. Chem. Soc.*, **87**, 2443 (1965).
(3) M. M. Davis and H. Hetzer, *Anal. Chem.*, **38**, 451 (1966).
(4) J. Figueras, *J. Am. Chem. Soc.*, **93**, 3255 (1971).
(5) M. Kamlet and R. Taft, *J. Am. Chem. Soc.*, **98**, 377 (1976).
(6) R. Taft and M. Kamlet, *J. Am. Chem. Soc.*, **98**, 2886 (1976).
(7) O. Kolling, *Anal. Chem.*, **49**, 591 (1977).
(8) O. Kolling and J. Goodnight, *Anal. Chem.*, **45**, 160 (1973).
(9) O. Kolling, *Anal. Chem.*, **48**, 884 (1976).
(10) V. Gutmann, *Chem. Tech.*, **7**, 255 (1977).
(11) E. Arnett, E. Mitchell, and T. Murty, *J. Am. Chem. Soc.*, **96**, 3875 (1974).
(12) R. Drago, G. Vogel, and T. Needham, *J. Am. Chem. Soc.*, **93**, 6014 (1971).
(13) E. M. Kosower, *J. Am. Chem. Soc.*, **80**, 3253 (1958).
(14) U. Mayer, V. Gutmann, and W. Gerger, *Monatsh. Chem.*, **106**, 1275 (1975).
(15) O. Kolling, *Anal. Chem.*, **48**, 1814 (1976).
(16) A. Lemley, in "The Chemistry of Nonaqueous Solvents", Vol. IV, J. Lagowski, Ed., Academic Press, New York, N.Y., 1976, 19–43.
(17) M. Kamlet, J. Abboud, and R. Taft, *J. Am. Chem. Soc.*, **99**, 6027 (1977).

RECEIVED for review September 12, 1977. Accepted November 7, 1977.

Fundamental and Second Harmonic Alternating Current Cyclic Voltammetric Theory and Experimental Results for Simple Electrode Reactions Involving Amalgam Formation

Alan M. Bond* and Roger J. O'Halloran

Department of Inorganic Chemistry, University of Melbourne, Parkville, Victoria, 3052, Australia

Ivica Ruzic[1] and Donald E. Smith*

Department of Chemistry, Northwestern University, Evanston, Illinois 60201

The technique of ac cyclic voltammetry is extended to treat the case involving the simple electrode reaction, $O + ne \rightleftarrows R$, in which the electrode product forms an amalgam. Rate laws are presented for the ac cyclic response at a stationary sphere mercury electrode. Experimental data for several redox systems give excellent agreement with theoretical predictions for both Nernstian and non-Nernstian conditions. The fundamental and second harmonic ac cyclic responses both prove to give sensitive measures of the amalgam and sphericity effects, and complement conventional dc cyclic measurements.

In a previous communication (*1*), the ac cyclic voltammetric method was studied for simple solution-soluble redox couples. Excellent correlation of theory and experiment was obtained using the versatile digital simulation approach to solve for the dc component of the boundary value problem. The ac component was treated by standard analytical procedures (*1*). With rate laws derived in this manner, it was found that ac cyclic voltammetry presents a powerful method for elucidating electrochemical kinetic parameters. The investigation will now be extended to cover the analogous case in which the electrode product forms an amalgam:

$$O + ne \underset{k_b}{\overset{k_f}{\rightleftharpoons}} R(Hg) \qquad (1)$$

Several investigations of ac polarography and ac anodic stripping voltammetry involving amalgam formation have been undertaken elsewhere. It was clearly evident that modifications to existing electrochemical theories were required to account for the amalgam behavior (*2–6*). For dc cyclic voltammetry of amalgam systems, it is observed that there is a current enhancement on the reverse (anodic or stripping) peak (*7*). Preliminary studies by Blutstein and Bond (*6*) also have shown that, on the reverse scan of the ac cyclic voltammogram, amalgam formation at a spherical electrode is associated with a marked increase in current relative to the forward (cathodic) sweep. This phenomenon of enhanced anodic scan current is illustrated in Figure 1 for the techniques of dc and fundamental and second harmonic ac cyclic voltammetry.

For the ac observables with Nernstian dc processes, the enhanced anodic scan, with its attendant scan rate and switching potential dependence (see below), provides a major and obvious distinction between amalgam-forming systems and those where the reduced form is solution-soluble (*1*). In the latter case, one predicts and observes negligible differences in forward and reverse scan peaks and no scan rate or switching potential dependence (*1*). Our ability to quantitatively interpret these special amalgam effects is a question of considerable interest and the prime topic of this report.

For the case of dc cyclic voltammetry, Beyerlein and Nicholson (*7*) have shown that electrode sphericity has a substantial influence on amalgam systems. The nature of the ac polarographic amalgam response also has been reported to show a marked dependence on spherical diffusion (*8–13*). From these precedents, it would be anticipated that a significant effect of electrode sphericity should be observed in the ac cyclic voltammetry of amalgam systems.

THEORY

The amalgam case defined by Equation 1 can be regarded as a special case of the simple solution-soluble redox couple investigated previously (*1*). The same set of expressions as defined there (assuming the slow scan limit) will give the ac amalgam response, since all influences of electrode geometry and spherical diffusion (which will be different for the amalgam case) are included only in the dc surface concentration terms. No attempt is made to analytically solve for these dc terms, but digital simulation, as described by Feldberg (*14*), can successfully account for the electrode geometry and amalgam formation to give accurate estimates for the surface concentrations. The essence of spherical electrode simulation may be found in the work of Ruzic and Feldberg (*15*).

Simulation parameters were chosen so that further optimization produced negligible improvement. Typical values of simulation parameters used were: (a) a radius increment of 1/900 the drop radius; (b) at least the first 150 of these elements nearest the electrode surface had to be considered, although 350 were employed in most calculations; (c) a dc potential increment of 1.0 mV; (d) a maximum dimensionless simulation diffusion coefficient, DDMAX (*14*), of 0.32.

Notation definitions employed here are conventional and are given elsewhere (*1*).

EXPERIMENTAL

Cyclic voltammograms were recorded on a Princeton Applied Research Corp. (PAR) Model 170 Electrochemistry System, modified as detailed previously (*1*).

The working electrode was a Metrohm Hanging Mercury Drop Electrode (HMDE) BM-503. Ag/AgCl (1 M NaCl) was used as the reference electrode and platinum wire as the auxiliary electrode. All solutions were deoxygenated with argon and thermostated at 25.0 ± 0.1 °C. Positive feedback circuitry was used to minimize iR drop. The following solutions were prepared using supplied AR grade materials: (i) 1.0×10^{-3} M Cd(II) in 1.0 M NaCl. (ii) 1.0×10^{-3} M Cd(II) in 1.0 M Na_2SO_4. (iii) 2.0×10^{-3} M Zn(II) in 1.0 M KCl/1.0×10^{-3} M HCl. These systems were chosen to give a range of k_s and α values that have been extensively investigated by other workers (*16–23*).

[1] On leave from the Center for Marine Research, Ruder Boskovic Institute, Zagreb, Yugoslavia, 1972–1975.

0003-2700/78/0350-0216$01.00/0 © 1978 American Chemical Society

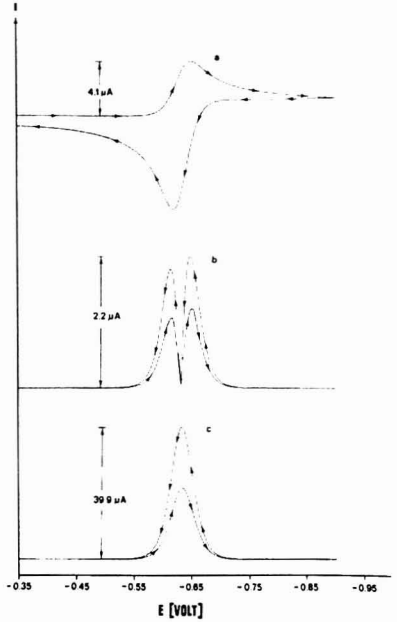


Figure 1. Comparison of dc and fundamental and second harmonic ac cyclic voltammograms for 1.0×10^{-3} M Cd(II) in 1.0 M NaCl at a HMDE. $A = 0.0086$ cm^2, $T = 25$ °C, $v = 50$ mV s^{-1}, $E_i = -0.35$ V, $E^0 = -0.635$ V, $E_s = -0.90$ V [all potentials relative to Ag/AgCl (1.0 M NaCl)], $\omega = 2\pi \times 400$ s^{-1}, $\Delta E = 5$ mV. (a) = dc; (b) = second harmonic; (c) = fundamental harmonic

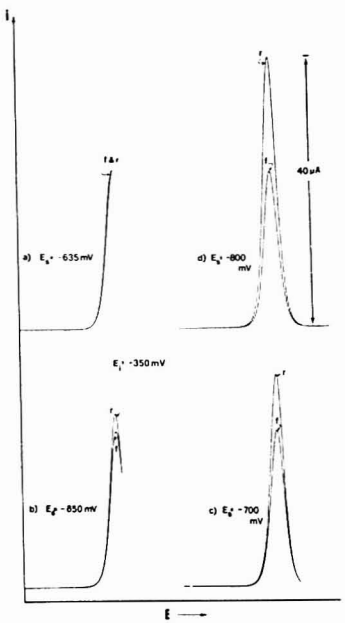


Figure 2. Influence of switching potential (E_s) on observed fundamental harmonic ac cyclic response for Cd(II) system as described in Figure 1. $E_i = -350$ mV for all voltammograms, f = forward scan, r = reverse (anodic) scan

Reversible $E_{1/2}{}^r$ values used in theoretical calculations were obtained from dc polarograms, and E^0 values were determined using published diffusion coefficients (*16–23*).

The surface area of the HMDE was calculated by weighing 20 mercury drops, and any shielding due to the point of attachment to the capillary was neglected.

RESULTS AND DISCUSSION

Because of the large number of independently variable parameters which significantly influence the ac cyclic experiment when amalgam formation occurs, the most expedient way to investigate the theoretical predictions is to discuss several real electrode processes. General predictions (e.g., construction of working curves of ΔE_p vs. log k_s) are not simple because of the marked dependence on the switching potential and scan rate. Thus, kinetic parameters for three electrochemical systems were obtained from the literature, and the predicted ac cyclic response was computed. Actual experiments were then performed under conditions matching those used in the calculation, and theory–experiment correlation was made.

Reversible Case (dc and ac Senses). The first example considered is the reduction of 1.0×10^{-3} M Cd(II) in 1.0 M NaCl

$$Cd(II) + 2e \rightleftharpoons Cd(Hg) \qquad (2)$$

The k_s and α values for this system have been reported as 1.2 cm s^{-1} and 0.46, respectively (*16*). This satisfies the requirements for a reversible dc process (*24*, *25*) and the k_s is sufficiently large for effectively reversible ac behavior to prevail under the conditions employed here (*26*). This system should thus enable the effects of amalgam formation to be observed, uncomplicated by heterogeneous charge transfer kinetic factors.

Fundamental Harmonic Case. It is observed that the most important factor in determining the nature of reversible fundamental harmonic ac cyclic voltammograms is the extent to which amalgam formation occurs. This is determined predominantly by the time during which the applied dc potential is more negative than the $E_{1/2}{}^r$ value. Two factors determine this time: the rate of voltage scan (v) and the switching potential (E_s). In Figure 2, a series of experimental fundamental harmonic ac cyclic voltammograms with variable E_s values are shown. Figure 2(a) illustrates that, if the scan is reversed at the peak potential of the forward sweep, $(E_p)_f$, then the forward and reverse scans overlap within limits of experimental error. As the switching potential is made more negative, the reverse peak becomes progressively larger because of the greater anodic stripping effect. The influence of scan rate on the reverse sweep is shown in Figure 3. As expected, the slower the scan rate, the larger the reverse peak becomes relative to the forward peak, since there is a longer time available for amalgam formation.

Another factor which will determine the extent of current enhancement on the reverse scan is the sphericity of the mercury drop. Data in Table I show that the ratio of forward to reverse peak currents, $(I_p)_f/(I_p)_r$, increases with drop size. This is qualitatively in agreement with expectation: as the size of the mercury drop increases, the concentration buildup near its surface due to the convergent nature of spherical diffusion decreases, since the inner volume into which the amalgam species diffuses is relatively larger.

Several important observations become apparent on studying experimental data for the cadmium system in 1 M

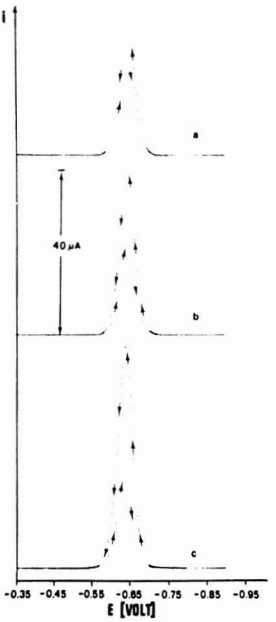


Figure 3. Influence of scan rate on observed fundamental harmonic ac cyclic response for Cd(II)/1 M NaCl as detailed in Figure 1. (a) v = 100 mV s^{-1}; (b) v = 50 mV s^{-1}; (c) v = 20 mV s^{-1}

Table I. Dependence of Fundamental Harmonic ac Cyclic Peak Currents for 1.0 × 10^{-3} M Cd(II)/1.0 M NaCl on Area of Mercury Drop

	$(i_p)_f$ (μA)		$(i_p)_r$ (μA)	
A, cm^2	Exptl	Theory	Exptl	Theory
0.0086	21.4	21.4	39.9	43.4
0.0138	35.0	33.8	56.8	61.6
0.0180	42.9	43.8	66.7	73.7

[a] E_i = −0.350 V, E_s = −0.900 V, v = 50 mV s^{-1}, ΔE = 5 mV, $\omega = 2\pi \times 400$ s^{-1}, E^0 = −0.635 V, T = 298 K. Theoretical figures calculated using data from Reference 16. All potentials measured relative to Ag/AgCl (1 M NaCl).

NaCl. The position and height of the peak on the forward scan is independent of scan rate within limits of experimental error and, in fact, predictions for the forward scan closely resemble the non-amalgam case, except that the current magnitude is larger for the amalgam system: e.g., 19.6 μA (theoretical, non-amalgam) vs. 21.4 μA (theoretical, amalgam) for v = 50 mV s^{-1} and A = 0.0086 cm^2. The half-width is 45.5 ± 0.5 mV for forward and reverse scans, so the waveshape on the reverse scan is similar to the forward scan despite the difference in current magnitude. Furthermore, within limits of experimental error, the peak potentials of both scans coincided under all conditions studied. Experimentally, a linear dependence of both the forward scan peak current, $(I_p)_f$, and the reverse peak current, $(I_p)_r$, on ΔE was found for $\Delta E \leq 5$ mV (at 400 Hz). Over the frequency range 100 to 600 Hz, a direct relationship of $(I_p)_f$ and $(I_p)_r$ with $\omega^{1/2}$ was found for ΔE = 5 mV. For both these instances, the scan rate was 50 mV s^{-1} and the drop area 0.0086 cm^2. The phase angle at the

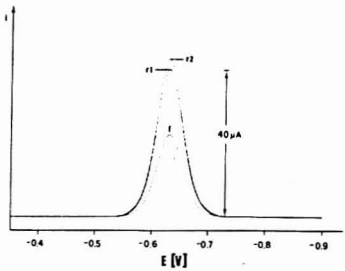


Figure 4. Theory–experiment comparison for fundamental harmonic ac cyclic response for Cd(II)/1 M NaCl as detailed in Figure 1. D_O = 0.68 × 10^{-5} cm^2 s^{-1}, D_R = 1.6 × 10^{-5} cm^2 s^{-1}, f = forward scan. r1 = reverse (anodic) scan, experimental; r2 = theoretical reverse scan, data from Reference 16. f = forward scan for theory and experiment (Experimental results normalized to forward theoretical scan.)

Table II. Theoretical Results Showing Effect of D_O and D_R on the Fundamental Harmonic ac Cyclic Response of 1.0 × 10^{-3} M Cd(II)/1 M NaCl System

		E_f	i_f	E_r	i_r	i_f/i_r
$D_R \times 10^5$	0.68	−0.6350	21.51	−0.6350	38.05	0.5653
(cm^2 s^{-1})	1.0	−0.6336	21.48	−0.6334	40.12	0.5354
	1.2	−0.6325	21.46	−0.6322	41.43	0.5180
	2.0	−0.6294	21.37	−0.6292	45.34	0.4713
$D_O \times 10^5$	0.4	−0.6272	16.22	−0.6269	31.92	0.5081
(cm^2 s^{-1})	0.6	−0.6299	20.07	−0.6297	40.32	0.4978
	0.9	−0.6326	24.76	−0.6323	51.56	0.4802
	1.2	−0.6345	28.72	−0.6343	61.87	0.4642

[a] Unless otherwise stated, D_O = 0.68 × 10^{-5} cm^2 s^{-1}, D_R = 1.6 × 10^{-5} cm^2 s^{-1}, E_i = −0.350 V, E_s = −0.900 V, E^0 = −0.635 V, v = 50 mV s^{-1}, $\omega = 2\pi \times 400$ s^{-1}, ΔE = 5 mV, A = 0.0086 cm^2, α = 0.5, k_s = 1.2 cm s^{-1}, T = 298 K. All potentials are in V (relative to Ag/AgCl (1 M NaCl)) and currents in μA and refer to peak values.

peak potential of the forward scan was 44 ± 2°; and for the reverse peak, 42 ± 1°, at 400 Hz. Within experimental error, all these latter data closely match expectations for the reversible response.

Theoretical ac cyclic predictions for the Cd/NaCl system were obtained via digital simulation using the following data (k_s, D_O, D_R, and α from Reference 16): k_s = 1.2 cm s^{-1}, α = 0.5, D_O = 0.68 × 10^{-5} cm^2 s^{-1}, D_R = 1.6 × 10^{-5} cm^2 s^{-1}, $\omega = 2\pi \times 400$ s^{-1}, ΔE = 5 mV, E_i = −0.350 V, E_f = −0.900 V, E^0 = −0.635 V, A = 0.0086 cm^2, v = 50 mV s^{-1}. All potentials are relative to Ag/AgCl (1 M NaCl). Theory–experiment fit is very good (see Figure 4). A small discrepancy can be observed in the current magnitude of the reverse sweep. Experimentally, it is found that the reverse peak current (being larger) is more sensitive to iR compensation than the forward peak current. Any degree of uncompensated resistance will thus cause a relative decrease in the magnitude of the observed reverse peak. The discrepancy between observed and calculated $(I_p)_r$ values is within acceptable limits. Uncertainties in D_O and D_R used in the simulation, together with experimental inaccuracies associated with uncompensated resistance and errors in switching potential and scan rate are sufficient to account for the small difference.

For this reversible Cd(II) system, changes in k_s and α had an insignificant effect on the predicted ac cyclic response, such that any $k_s > 1$ cm s^{-1} gives acceptable experiment–theory fit. The effect of changes in D_O and D_R on the computed response is shown in Table II. The diffusion coefficient of the amalgam species, D_R, has negligible effect on the magnitude of the forward peak current, but the reverse peak increases sub-

Table III. Influence of the Size of the Mercury Drop on Simulated Second Harmonic ac Cyclic Voltammograms. $I_f = (i_{p^+} + i_{p^-})^a$ for Forward Scan, $I_r = (i_{p^+} + i_{p^-})$ for Reverse Scan[b]

A, cm²	Forward scan i_{p^+}	Forward scan $(E_{in} - E^\circ)$	Forward scan i_{p^-}	Reverse scan i_{p^+}	Reverse scan $(E_{in} - E^\circ)$	Reverse scan i_{p^-}
0.0086	1.039	5.5	1.163	2.057	5.6	2.295
I_f/I_r = 0.55 (exptl)	[23.3]		[−13.2]	[22.9]		[−12.4]
= 0.506 (theor)						
0.0138	1.659	5.5	1.813	2.918	5.5	3.173
I_f/I_r = 0.62 (exptl)	[23.3]		[−13.0]	[23.0]		[−12.3]
= 0.570 (theor)						
0.0180	2.159	5.5	2.333	3.571	5.5	3.842
I_f/I_r = 0.68 (exptl)	[23.4]		[−12.9]	[23.1]		[−12.3]
= 0.608 (theor)						

[a] i_{p^+} = peak current of anodic peak (absolute value). i_{p^-} = peak current of cathodic peak (absolute value). [b] All potentials in mV, currents in μA. Figures in brackets are peak potentials relative to E° (i.e., $E_p - E^\circ$). E_{in} = inflection (current minimum) potential. Other parameters are the same as those in Table II.

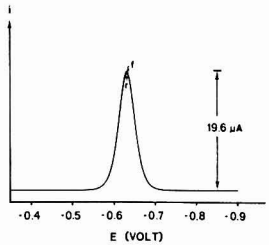


Figure 5. Simulated fundamental harmonic ac voltammogram for the same system as in Figure 4, but considering the reduced species to be solution-soluble (i.e., neglecting amalgam formation); f = forward scan, r = reverse scan

stantially as D_R is made larger. The influence of D_O is more complicated, affecting both forward and reverse scans to a marked degree. Of course, the position of $E_{1/2}^r$ and the ac peak potentials, relative to E^0, are also affected by D_O/D_R. The Cd(II)/NaCl system thus gives reversible behavior, and the ac cyclic results allow no conclusions regarding the precise magnitudes of k_s and α.

To show the differences between amalgam and nonamalgam systems, a calculation was performed using the same set of parameters as those for Cd(II)/NaCl, but considering the reduced species to be solution soluble. The differences are quite evident, especially on the reverse scan, as shown in Figure 5. The very slight inequality in forward and reverse scan peak magnitudes shown in Figure 5 arises from the spherical diffusion effect combined with the more than factor-of-two difference in diffusion coefficients (see Figure 4 legend) (9). While such a diffusion coefficient difference is perfectly realistic for amalgam-forming systems, it is highly unlikely when species O and R are solution phase-soluble. The more nearly equal diffusion coefficients characterizing solution-soluble redox couples lead to disappearance of this forward and reverse scan difference (9). The same observations apply to the second harmonic polarogram shown below in Figure 6b.

Second Harmonic Case. Figure 6a shows theoretical and experimental second harmonic ac cyclic voltammograms for the reduction of Cd(II) in 1.0 M NaCl. For comparison, a corresponding voltammogram, calculated using the same parameters, but considering both species to be solution-soluble, also is included (Figure 6b). The influence of amalgam formation can be seen in the current enhancement of the reverse sweep, and in the enlargement of the lobes at more negative potentials. Again, the observed reverse peaks are marginally lower than predicted, and similar discussions as

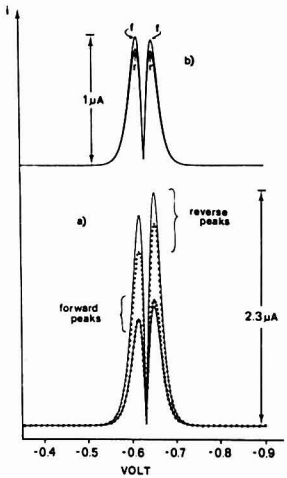


Figure 6. Second harmonic ac cyclic voltammograms for Cd(II)/1.0 M NaCl system as detailed in Figure 4. (a) (——) = theoretical prediction (···) = experimental observation (normalized to i_{p^+} on forward scan); (b) theoretical results as for (a) but neglecting influence of amalgam formation; f = forward scan, r = reverse scan

applied to the fundamental harmonic case are still relevant. Experimental and simulation results showed a linear dependence of the peak currents on both $\omega^{1/2}$ (for ΔE = 5 mV) and ΔE^2 (at 400 Hz), as expected. A drop area of 0.0086 cm² and scan rate of 50 mV s⁻¹ were used in these measurements. The influence of drop size (sphericity) is shown by some data in Table III. As the drop increases in size, effects due to amalgam formation diminish since, as discussed previously, the concentration buildup of the amalgam near the surface decreases. The predominance of the current lobe at more negative potential over that at more positive potential decreases, and the enhancement of current on the reverse scan falls off.

The effect of scan rate on the second harmonic response was similar to that for the fundamental harmonic. In Table IV, theoretical and experimental data are presented for several scan rates. As the scan rate decreases, the extent of amalgam formation becomes greater, and so its consequences become more marked: cathodic peaks increase their predominance over anodic peaks, and the reverse scan increases in current magnitude.

Table IV. Dependence of Second Harmonic ac Cyclic Voltammograms on Scan Rate. Experimental System 1.0 × 10^{-3} M Cd(II)/1.0 M NaCl[a]

	Forward scan			Reverse scan		
v, mV s^{-1}	i_{p^+}	$(E_{in} - E^0)$	i_{p^-}	i_{p^+}	$(E_{in} - E^0)$	i_{p^-}
20	1.503	5.6	1.257	2.518	5.6	3.008
(theoretical)	[23.2]		[−13.5]	[22.3]		[−12.7]
I_f/I_r = 0.418						
20	1.1	5	1.3	2.4	5	2.9
(experimental)	[24]		[−13]	[23]		[−13]
I_f/I_r = 0.45						
50	1.039	5.5	1.163	2.057	5.6	2.295
(theoretical)	[23.3]		[−13.2]	[22.9]		[−12.4]
I_f/I_r = 0.506						
50	1.1	5	1.2	2.0	5	2.2
(experimental)	[24]		[−13]	[23]		[−13]
I_f/I_r = 0.55						
100	1.035	5.6	1.119	1.729	5.6	1.864
(theoretical)	[23.5]		[−12.8]	[23.2]		[−12.2]
I_f/I_r = 0.599						
100	1.1		1.2	1.8		1.9
(experimental)	[24]		[−13]	[23]		[−13]
I_f/I_r = 0.62						

[a] All potentials in mV, currents in μA. Figures in brackets are peak potentials relative to E^0 (i.e., $E_p - E^0$). Other parameters as in Table II.

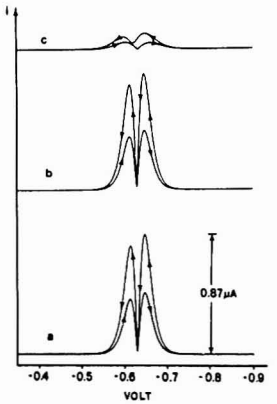


Figure 7. Predicted second harmonic ac cyclic voltammograms for Cd(II)/1.0 M NaCl system as detailed in Figure 4: influence of changing k_s ($\omega = 2\pi \times 49$ s^{-1}). (a) k_s = 12.0 cm s^{-1}; (b) k_s = 0.12 cm s^{-1}; (c) k_s = 0.012 cm s^{-1}

Data in Table V show that the value of D_R mainly influences the reverse scan, similar to the analogous fundamental harmonic predictions. Figure 7 shows voltammograms computed for order of magnitude changes of k_s around the accepted value. As would be anticipated for a reversible system, increasing k_s has negligible effect, but decreasing k_s significantly lowers the current magnitude and increases the peak-to-peak separation, as ac quasi-reversible behavior is reached.

Quasi-reversible ac but Nernstian dc Case. *Fundamental Harmonic Case.* The ac cyclic voltammetric response of 1.0 × 10^{-3} M Cd(II)/1.0 M Na_2SO_4 was studied to provide an example of a system reversible in the dc sense, but with a quasi-reversible ac response. The kinetic parameters for this system (unacidified Na_2SO_4) have been reported as α = 0.30 and k_s = 0.20 cm s^{-1} (*21*). Other values of α = 0.30, k_s = 0.15 cm s^{-1} (*18*); α = 0.35, k_s = 0.20 cm s^{-1} (*19*); α = 0.35, k_s = 0.19 cm s^{-1} (*20*); α = 0.47, k_s = 0.27 cm s^{-1} (*23*) and α = 0.22, k_s = 0.063 cm s^{-1} (*16*) are also presented in the literature.

Table V. Influence of D_R on the Predicted Second Harmonic ac Cyclic Response for 1.0 × 10^{-3} M Cd(II)/1.0 M NaCl[a]

$D_R \times 10^5$, cm^2 s^{-1}	Forward scan			Reverse scan		
	i_{p^+}	$(E_{in} - E^0)$	i_{p^-}	i_{p^+}	$(E_{in} - E^0)$	i_{p^-}
0.68	1.059	0.7	1.162	1.848	0.7	2.000
	[18.0]		[−18.0]	[17.8]		[−17.8]
1.0	1.053	2.8	1.164	1.931	2.8	2.105
	[20.2]		[−15.8]	[19.9]		[−15.5]
1.2	1.046	3.6	1.161	1.976	3.7	2.178
	[21.4]		[−14.9]	[21.1]		[−14.2]
2.0	1.031	7.1	1.166	2.125	7.2	2.372
	[24.8]		[−11.8]	[24.2]		[−11.1]

[a] Notation as in Table III. D_O = 0.68 × 10^{-5} cm^2 s^{-1}. Other parameters as in Table II.

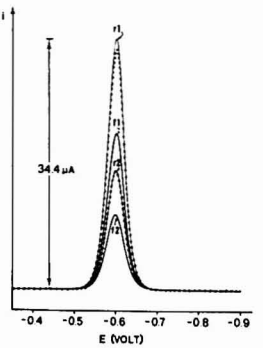


Figure 8. Comparison of theoretical and experimental fundamental harmonic ac cyclic voltammograms for 1.0 × 10^{-3} M Cd(II)/1.0 M Na_2SO_4. Experimental parameters: E_i = −0.35 V, E_s = −0.90 V, E^0 = −0.605 V, ν = 50 mV s^{-1}, $\omega = 2\pi \times 400$ s^{-1}, ΔE = 5 mV, T = 298 K, A = 0.0086 cm^2. (——) = theoretical predictions, (•••) = experimental. f1 and r1 are respectively forward (cathodic) and reverse (anodic) scans calculated using k_s = 0.20 cm s^{-1}, α = 0.3, D_O = 0.60 × 10^{-5} cm^2 s^{-1}, D_R = 1.6 × 10^{-5} cm^2 s^{-1}. f2 and r2 are corresponding results calculated using data from Reference 16

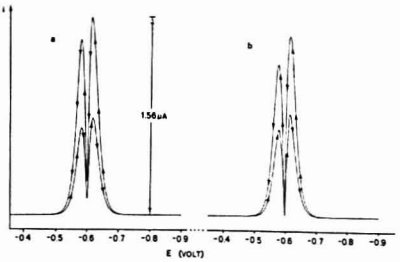


Figure 9. Comparison of theoretical and experimental second harmonic ac cyclic voltammograms for Cd/Na_2SO_4 system as detailed in Figure 8. (a) theoretical (from Reference 21); (b) experimental

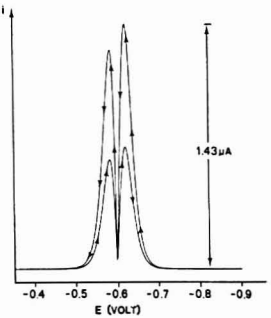


Figure 10. Simulated second harmonic ac cyclic voltammogram as for Figure 9, but $\alpha = 0.5$

As is evident from Figure 8, very good theory–experiment correlation is found using the kinetic data from References 19, 20, and 21. The fundamental harmonic current response is practically independent of α with this k_s value, and so no worthwhile conclusions as to its precise magnitude can be drawn. Cot ϕ measurements were insufficiently accurate to compute α by the recommended procedure (*26*). There is negligible peak potential separation of the forward and reverse scans, but current magnitudes are significantly lower than for the reversible Cd(II)/NaCl case. At a frequency of 400 Hz, $\Delta E = 5$ mV and $v = 50$ mV s^{-1}, the half-widths of both forward and reverse waves were measured experimentally as 48 ± 1 mV, which agrees with a value of 48 mV computed using data from References 19, 20, or 21. The calculated phase angle at the peak potential of both forward and reverse scans was 33°; experimentally it was found to be 35 ± 2°. Again, the only noteworthy discrepancy was a small deviation on the reverse scan. Similar discussions as those applied to the reversible case are still pertinent regarding this small disparity.

Computations based on data from References 16 and 27 (k_s = 0.063 cm s^{-1}) gave unsatisfactory results in regard to current magnitude (see Figure 8) and phase angle (22°). Studies in Reference 27 were performed in acidified (pH 4) Na_2SO_4 media. It thus seems that, for this Cd(II)/Cd(Hg) system, the apparent k_s value is pH dependent, a fact which may have significant implications (*23*).

Second Harmonic. Figure 9 shows experimental and theoretical second harmonic ac cyclic voltammograms for the Cd/Na_2SO_4 electrode process. The consequences of spherical diffusion and amalgam formation are evidenced by the enhanced reverse sweep current, and in the enlargement of the lobe at more negative potentials. Comparison of Figures 9a and b indicates good theory–experiment agreement, except

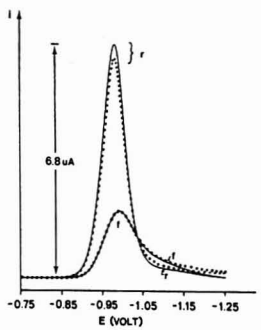


Figure 11. Comparison of theoretical and experimental fundamental harmonic ac cyclic voltammograms for 2.0×10^{-3} M Zn((II)/1.0 M KCl–10^{-3} M HCl. $D_O = 0.7 \times 10^{-5}$ cm^2 s^{-1}, $D_R = 2.0 \times 10^{-5}$ cm^2 s^{-1} using parameters from Reference 12 (see text). (——) = theoretical; (···) = experimental. Experimental parameters: E_i = −0.75 V, E_s = −1.25 V, E^0 = −1.005 V, v = 50 mV s^{-1}, f = 400 Hz, ΔE = 5 mV, T = 298 K, A = 0.0086 cm^2. $k_s = 4 \times 10^{-3}$ cm s^{-1}, $\alpha = 0.3$. f = forward (cathodic) scan, r = reverse (anodic) scan

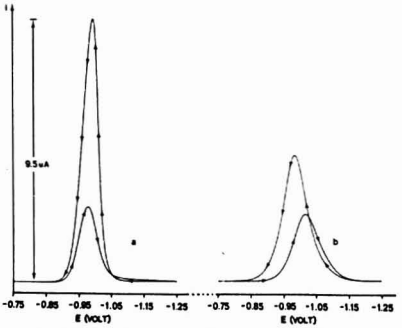


Figure 12. Calculated fundamental harmonic ac cyclic response for Zn(II) system as detailed in Figure 11 showing effect of α. (a) α = 0.1; (b) $\alpha = 0.5$

for the minimum current (especially on the reverse scan) which does not reach zero in the theoretical curve, but nearly does so in the ac cyclic experimental data. Figure 10 depicts a theoretical second harmonic ac cyclic voltammogram for α = 0.5 (same k_s). It shows better agreement with experiment regarding both the current minimum and the peak current magnitudes. One concludes from the ac cyclic data that α = 0.5 for this system. AC polarographic data in both fundamental (*16*, *19*, *20*, *23*) and second harmonic (*18–21*) modes clearly disagree on this point ($\alpha \cong 0.3$). That this experimental disparity is real has recently been shown by running successive fundamental harmonic ac polarographic and ac cyclic experiments on the same solution (same day). The digital FFT approach (*23*) was employed, which provides sufficiently accurate data to permit evaluation of α from the cot ϕ observable. A 0.35 ± 0.03 value was indicated for α by the ac polarographic mode and ac cyclic voltammetry suggested $\alpha = 0.47 \pm 0.05$, both in complete agreement with the corresponding analog measurements. A plausible qualitative explanation for the disparity has been advanced (*23*), but it remains to be confirmed by experimental investigations. For present purposes, it is sufficient to recognize that excellent theory–experiment agreement is obtained for the ac cyclic experiment using a k_s value which is consistent with literature

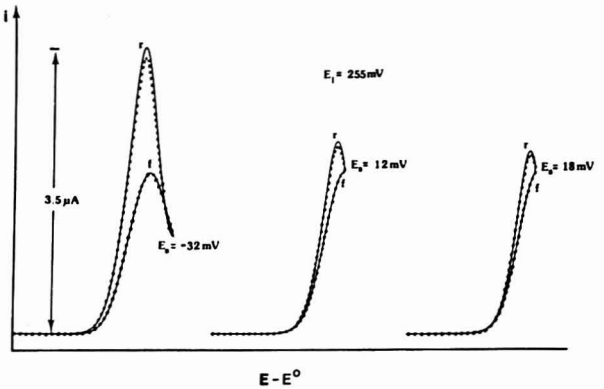


Figure 13. Fundamental harmonic ac cyclic response for Zn(II) system as detailed in Figure 11 showing effect of switching potential, E_s. E_i constant at +255 mV (relative to E^0). (——) = theoretical; (···) = experimental

reports and an α value which agrees better with the fundamental theory of heterogeneous electron transfer (*28*) than the ≃0.3 value previously advanced.

Quasi-reversible in Both dc and ac Senses. *Fundamental Harmonic.* As an example of a dc quasi-reversible amalgam system, the electrode reaction of 2.0×10^{-3} M Zn(II) in 1.0 M KCl/10^{-3} M HCl was chosen. Literature values of its kinetic parameters have been reported as $k_s = 3.8 \times 10^{-3}$ cm s^{-1}, $\alpha = 0.30$ (*17*), $k_s = 4.0 \times 10^{-3}$ cm s^{-1}, $\alpha = 0.30$ (*12*); and $k_s = 3.3 \times 10^{-3}$ cm s^{-1}, $\alpha = 0.27$ (*22*). A comparison of theoretical and experimental curves is shown in Figure 11. The best agreement was obtained using the results quoted in Reference 12.

The effect of α upon the quasi-reversible system is quite marked, as is evident from Figure 12. Computations using $\alpha = 0.1$ and $\alpha = 0.5$ result in significantly different curve shapes, and only α values close to 0.3 give results in agreement with experiment. At a frequency of 400 Hz, $\Delta E = 5$ mV and $v = 50$ mV s^{-1}, the peak separation between forward and reverse scans was experimentally 10 mV, a figure which was obtained with $\alpha = 0.28$ and $k_s = 4.0 \times 10^{-3}$ cm s^{-1}.

As in the previous systems, the current magnitude of the reverse peak was slightly lower than calculated. For the dc quasi-reversible case, the simulated voltammograms are very sensitive to small changes in the system parameters and this, together with uncompensated resistance effects, could explain the discrepancy.

Theoretical calculations predicted that the fundamental harmonic response would be practically independent of frequency in the range 49 to 400 Hz, and this was confirmed experimentally. The phase angle of both forward and reverse peaks was observed to be close to 0°, in good agreement with the computed value of 2° for the forward peak and 4° for the reverse peak.

A selection of voltammograms with different switching potentials is shown in Figure 13. Differences to analogous observations with the reversible case are apparent, especially as the forward and reverse scans do not overlap when the potential scan is switched at potentials more positive than the forward peak, reflecting the dc quasi-reversibility of this process. As can be seen from the figure, theoretical calculations gave similar results.

Second Harmonic. Figure 14 shows a comparison of theoretical and experimental second harmonic ac cyclic voltammograms for the zinc system. Good agreement between theory and experiment is observed.

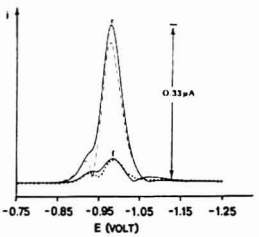


Figure 14. Comparison of theoretical and experimental second harmonic ac cyclic voltammograms for Zn(II) system described in Figure 11. (——) = theoretical, f = forward scan, r = reverse scan; (···) = experimental, forward (cathodic) scan; (- - -) = experimental, reverse scan

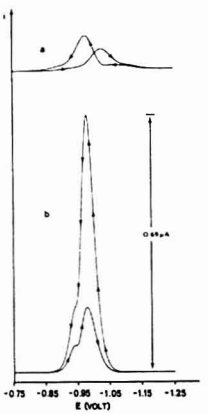


Figure 15. Simulated second harmonic ac cyclic voltammograms for Zn(II) system as detailed in Figure 11: influence of α. (a) $\alpha = 0.5$; (b) $\alpha = 0.1$

In Figure 15, simulated second harmonic ac cyclic voltammograms showing the influence of α at this low k_s, are plotted. A marked α-dependence is evident. As for the fundamental harmonic, observed voltammograms are only

consistent with an α value close to 0.3.

CONCLUSION

The combined digital simulation–analytical solution approach to the ac cyclic rate law with amalgam-forming redox systems has proved successful. Kinetic parameters calculated from this theory using fundamental and second harmonic observables agree well with accepted results in most instances. In this case the reverse (anodic) sweep ac response is not so useful as for the non-amalgam case because of its marked sensitivity to many parameters (e.g., scan rate, switching potential, diffusion coefficients), even for the pure reversible (Nernstian) response. For dc quasi-reversible conditions, no parallel with the α-dependent crossover potential (*1*) is found. However, predictions for the reverse scan are very close to the experimental results presented here, indicating the satisfactory nature of the theoretical model used.

To obtain previously unevaluated heterogeneous charge transfer kinetic parameters, k_s and α, from experimental ac cyclic data on amalgam-forming systems, the recommended approach is use of the phase angle cotangent in the standard manner (*26*). This observable remains independent of the troublesome operating parameters like scan rate, switching potential, electrode radius, and scan direction (*1*), which are invariably of significance with amalgam-forming systems, as shown above. Although phase angle data provided by the instrument used in this work were of insufficient accuracy and precision for this purpose, the desired data quality has been achieved with computerized FFT instrumentation (*23*). Should it be necessary to employ current amplitude data, the use of the frequency spectra of the ac cyclic peaks is recommended to obtain reasonable estimates of k_s and α. These observable's shape characteristics, and their dc potential dependence, also are negligibly influenced by the "troublesome parameters" mentioned above. Of course, if scan rate, switching potential, and electrode radius are held fixed, and diffusion coefficients are known (usually the case), theoretical working curves of any potentially useful ac cyclic observable (e.g., peak width, peak location, forward and reverse scan peak separation, etc.) can be generated for the specified operating conditions. In short, the message is that insurmountable data analysis problems do not exist with ac cyclic data on amalgam-forming systems following Reaction 1, despite the more complicated parametric dependences. In most cases, the usual cot ϕ data analysis strategy (*26*) will suffice, as has been demonstrated (*23*).

LITERATURE CITED

(1) A. M. Bond, R. J. O'Halloran, I. Ruzic, and D. E. Smith, *Anal. Chem.*, **48**, 872 (1976).
(2) W. L. Underkofler and I. Shain, *Anal. Chem.*, **37**, 218 (1965).
(3) N. Velghe and A. Claeys, *J. Electroanal. Chem.*, **35**, 229 (1972).
(4) D. I. Levitt, *Anal. Chem.*, **45**, 1291 (1973).
(5) E. D. Moorhead and P. H. Davis, *Anal. Chem.*, **45**, 2178 (1973).
(6) H. Blutstein and A. M. Bond, *Anal. Chem.*, **46**, 1934 (1974).
(7) F. H. Beyerlein and R. S. Nicholson, *Anal. Chem.*, **44**, 1647 (1972).
(8) T. Biegler and H. A. Laitinen, *Anal. Chem.*, **37**, 572 (1965).
(9) J. R. Delmastro and D. E. Smith, *Anal. Chem.*, **38**, 169 (1966).
(10) J. R. Delmastro and D. E. Smith, *Anal. Chem.*, **39**, 1050 (1967).
(11) T. G. McCord and D. E. Smith, *Anal. Chem.*, **41**, 131 (1969).
(12) T. G. McCord and D. E. Smith, *Anal. Chem.*, **42**, 126 (1970).
(13) I. Ruzic and D. E. Smith, *Anal. Chem.*, **47**, 530 (1975).
(14) S. W. Feldberg in "Electroanalytical Chemistry", Vol. 3, A. J. Bard, Ed., Marcel Dekker, New York, N.Y., 1969, pp 199–296.
(15) I. Ruzic and S. W. Feldberg, *J. Electroanal. Chem.*, **63**, 1 (1975).
(16) J. K. Frischmann and A. Timnick, *Anal. Chem.*, **39**, 507 (1967).
(17) B. Timmer, M. Sluyters-Rehbach, and J. H. Sluyters, *J. Electroanal. Chem.*, **14**, 181 (1967).
(18) T. G. McCord and D. E. Smith, *Anal. Chem.*, **41**, 131 (1969).
(19) D. E. Glover and D. E. Smith, *Anal. Chem.*, **44**, 1140 (1972).
(20) D. E. Glover and D. E. Smith, *Anal. Chem.*, **45**, 1869 (1973).
(21) M. Hirota, Y. Umezawa, H. Kojima, and S. Fujiwara, *Bull. Chem. Soc. Jpn.*, **47**, 2486 (1974).
(22) M. Hirota, Y. Umezawa, and S. Fujiwara, *Bull. Chem. Soc. Jpn.*, **48**, 1053 (1975).
(23) A. M. Bond, R. J. Schwall, and D. E. Smith, *J. Electroanal. Chem.*, **85**, 231 (1977).
(24) R. S. Nicholson and I. Shain, *Anal. Chem.*, **36**, 706 (1964).
(25) R. S. Nicholson, *Anal. Chem.*, **37**, 1351 (1965).
(26) D. E. Smith in "Electroanalytical Chemistry", Vol. 1, A. J. Bard, Ed., Marcel Dekker, New York, N.Y., 1966, pp 1–155.
(27) D. J. Kooijman and J. H. Sluyters, *Electrochim. Acta*, **12**, 693 (1967).
(28) R. A. Marcus, *J. Chem. Phys.*, **43**, 679 (1965).

RECEIVED for review August 15, 1977. Accepted October 28, 1977.

Electrochemistry of the Ruthenium(3+,2+) Couple Attached to Graphite Electrodes

Carl A. Koval and Fred C. Anson*

Arthur A. Noyes Laboratory, California Institute of Technology, Pasadena, California 91125

Procedures are presented for attaching pyridine–pentaammineruthenium(II) complexes to graphite electrodes by covalent bonding and irreversible adsorption. Cyclic voltammetry and differential pulse voltammetry are used to compare the electrochemical behavior of the attached complexes and to measure surface concentrations. Different orientations of the anisotropic graphite affect the quantity of reactant that can be attached as well as the voltammetric responses. Attachment by irreversible adsorption yields larger quantities of complex on the electrode surface but the covalently attached complex persists on the surface for a longer time.

A number of schemes for the attachment of a variety of molecules to electrode surfaces have been proposed and tested recently (*1–12*). In only a few instances have the attached molecules exhibited the long-lived, reversible electrochemical behavior that would be essential for effective catalysis of charge transfer reactions involving less reactive substrates to be realized. In preliminary experiments (*4*) directed at such an objective, we reported some examples of reactants containing multiple aromatic rings (e.g., 9,10-phenanthrenequinone, iron protoporphyrin IX, and iron tetraphenylporphyrin) which attach themselves to graphite electrodes by spontaneous, irreversible adsorption. In media free of attached reactant, these surface species remain adsorbed for hours and can be cycled repeatedly between oxidation states electrochemically. The tendency of sufficiently large, aromatic molecules to adsorb on graphite has also been exploited to attach a simple transition metal complex, $Ru(NH_3)_5L^{2+}$ (L is the large, aromatic ligand), to a graphite electrode and to examine its electrochemical behavior in the attached state (*12*).

In the present paper, methods similar to those described by Miller and co-workers (*2*) were used to attach the same

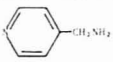
0003-2700/78/0350-0223$01.00/0 © 1978 American Chemical Society

ruthenium redox couple to graphite electrodes by coordinating the metal to a pyridine ligand which was, in turn, covalently linked to the graphite surface. The objective was to compare the two methods of attachment with respect to the electrochemical behavior of the redox center and to the longevity of the attachment.

EXPERIMENTAL

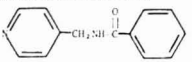
Materials. *Graphite.* The pyrolytic graphite was commercially available material (Union Carbide Corp., Parma, Ohio). It was obtained in the form of cylindrical rods in which the layered (basal) planes of graphite were either parallel or perpendicular to the axis of the rod. In the former case surfaces cut perpendicular to the rod axis presumably contain a large number of "edge" carbon atoms and will be termed edge pyrolytic graphite (EPG). In the latter case, cut surfaces contain mostly basal planes and are termed basal pyrolytic graphite (BPG).

Complexes. $[Ru(NH_3)_5Cl]Cl_2$ was prepared from $Ru(NH_3)_6Cl_3$ by standard procedures (*13*). $[Ru(NH_3)_5L](PF_6)_2$ where L = pyridine, 4-aminomethylpyridine, (AMP),



AMP

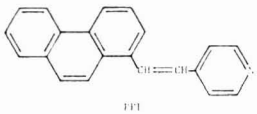
and *N*-(4-picolinic)-benzamide, (PBA),



PBA

were synthesized by adaptation of a procedure described in reference (*14*): To a solution of $Ru(NH_3)_5(OH_2)^{2+}$, generated by reduction of $Ru(NH_3)_5Cl^{2+}$ with zinc amalgam, a fivefold excess of L was added and the reaction allowed to proceed for ca. 1 h. The resulting solution was filtered and the desired complex precipitated by addition of solid NH_4PF_6.

The ligand, PBA, was synthesized by the reaction of benzoyl chloride and 4-aminomethylpyridine in benzene. The crude product was recrystalized from benzene yielding white needles which gave the following elemental analysis (%): C, 73.69, H, 5.79, and N, 13.13. Calculated for $C_{13}H_{12}N_2O$: C, 73.56, H, 5.70 and N, 13.20. The preparation of the ligand, 1-(9-phenanthrene)-2-(4-pyridine)ethene, (PPE),



PPE

and its ruthenium complex have been described (*12*).

Other chemicals, solvents and supporting electrolytes were reagent grade and were used as received.

Apparatus. Cyclic voltammograms and differential pulse voltammograms were obtained by means of a Princeton Applied Research Model 174 Polarographic Analyzer. Conventional two-compartment cells were employed with a platinum wire auxiliary electrode and a saturated calomel reference electrode. Both BPG and EPG electrodes were in the form of disks. Disks were obtained from rods of basal plane pyrolytic graphite by slicing with a razor blade. Those from edge pyrolytic graphite rods were cut on a lathe. Both types of electrode were mounted in the Teflon holder shown in Figure 1. The O-ring seal defines a reasonably reproducible surface area of ca. 0.12 cm^2 and there was no evidence of the solution leaking under the O-ring even after several hours of use. The holder allows electrodes to be mounted in less than 1 min which is highly desirable when a large number of electrodes are being screened. The electrode surface is recessed ca. 2 mm below the outer orifice of the removable Teflon cap but it did not prove difficult to stir the solution well enough to ensure that the solution layer at the electrode surface was representative of the bulk solution composition.

Procedures. The graphite disks were subjected to various treatments designed to clean and oxidize the surface, to attach

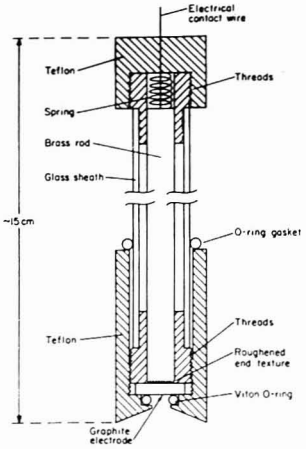


Figure 1. Teflon holder for pyrolytic graphite disk electrodes

ligands to the surface and to form ruthenium complexes with the attached ligands.

Treatment I. EPG disks were abraded in air with clean, AG2-400 silicon carbide paper (Minnesota Mining & Manufacturing Co., Minneapolis, Minn.) to expose fresh graphite. The surface of these disks was flat but visibly rough. They were not polished further for fear of decreasing the number of exposed "edge" carbon sites. Loose graphite particles were removed by vigorous washing with water and the disks were dried under vacuum. Treatments of BPG electrodes began with cleavage of a thin layer from the surface to expose fresh graphite instead of abrading the surface with silicon carbide paper. Both types of disks were then heated in air at 400 °C for 4 h, cooled, treated in a Soxhlet extractor with distilled water for 12 h and dried under vacuum.

Treatment II. Disks from Treatment I were subjected to Soxhlet extraction with benzene for 12 h and dried under vacuum.

Treatment III. Disks from Treatment I were stirred over-night in a refluxing solution of benzene (10 mL) containing 2 mL of 4-aminomethylpyridine. The disks were rinsed with several portions of benzene and then subjected to 12 h of Soxhlet extraction with benzene, removed, and dried under vacuum.

Treatment IV. Disks from Treatment I were stirred in a refluxing mixture of benzene (5 mL) and thionyl chloride (5 mL) for 8 h, rinsed with pure benzene and then subjected to Treatment III.

Treatment V. A 0.01 M solution of $Ru(NH_3)_5OH_2^{2+}$ was prepared by dissolving $[Ru(NH_3)_5Cl]Cl_2$ in a 0.1 M solution of sodium trifluoracetate (pH 6–7) and reducing the Ru(III) to Ru(II) at a stirred mercury pool electrode at −700 mV vs. SCE under argon. The resulting solution was transferred under argon to a second vessel containing the disk electrodes which were soaked in the solution for 30 min, rinsed thoroughly with water, and air dried.

Electrochemical measurements were conducted at room temperature (22 ± 2 °C) in solutions freed of oxygen by bubbling with argon that had been passed through a vanadium(II) solution. All potentials are quoted vs. the saturated calomel electrode (SCE).

RESULTS

Relevant Formal Potentials of Unattached Ruthenium Complexes. Formal potentials for the couple $Ru(III)(NH_3)_5X + e^- = Ru(II)(NH_3)_5X$ have been measured in a variety of supporting electrolytes for a considerable number of heteroligands, X (*15*, *16*). Those most relevant to the present study are collected in Table I and include values, measured as part of the present study, for complexes for which no previous potentials were available in the desired acidic electrolyte.

Table I. Formal Redox Potentials of Some Selected Complexes of Ru(III)-Ru(II)

Complex[a]	E^f, mV vs. SCE	Supporting electrolyte[b]	Ref.
$Ru(NH_3)_6^{3+,2+}$	−194	0.1 F $NaBF_4$	(15)
	−191	1 M HTFA	This work
	−210	1 M HCl	This work
$Ru(NH_3)_5py^{3+,2+}$	60	0.1 F NaTFA-0.1 F HTFA	(15)
	48	1 F HTFA	This work
	26	1 F HCl	This work
$Ru(NH_3)_5L^{3+,2+}$			
L = AMP	95	1 F HTFA	This work
	76	1 F HCl	This work
L = PBA	44	1 F HTFA	This work
	23	1 F HCl	This work
$Ru(NH_3)_5OH_2^{3+,2+}$	−179	0.1 F NaTFA-0.1 F HTFA	(15)
$Ru(NH_3)_5Cl^{2+,3+}$	−287	0.2 F NaTFA	(15)

[a] py = pyridine. [b] HTFA = trifluoroacetic acid. NaTFA = sodium trifluoroacetate.

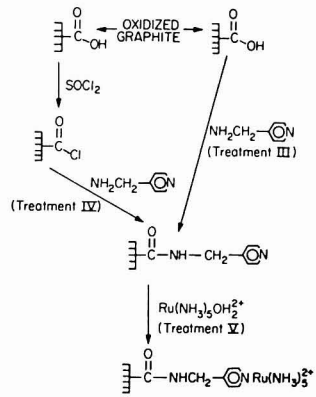


Figure 2. The likely surface chemistry involved in the attachment of $Ru(II)(NH_3)_5^{2+}$ to graphite electrode surfaces

Supporting electrolytes consisting of 1 M acids were employed in the present case in order to shift the inevitably present, pH-dependent waves associated with oxidation and reduction of the graphite electrode surface out of the potential region characteristic of the ruthenium complexes investigated. Differential pulse voltammetry was used to measure the formal potentials in Table I using EPG electrodes which had been subjected to Treatment I (see Experimental section). The width at half-peak height of the differential pulse voltammograms was typically 90 to 95 mV compared with the expected 90.4 mV for a one-electron Nernstian reaction, indicating that high electron transfer rates prevail between the dissolved complexes and the EPG graphite electrodes. The small differences in the formal potentials in Table I for hydrochloric acid and trifluoroacetic acid supporting electrolytes are most likely reflections of differences in the extent of ion pairing between the cationic reactants and the supporting electrolyte anions in the two cases.

Attachment of $Ru(II)(NH_3)_5^{2+}$ to Graphite Electrode Surfaces by Means of a Covalently Bound, Pendant Pyridine Ligand. Graphite disks were subjected to Treatments III and IV (see Experimental section) in order to produce a surface containing 4-aminomethylpyridine groups and to Treatment V to attach the $Ru(NH_3)_5^{2+}$ moiety to the pendant pyridine ligand. The likely surface chemistry is indicated in Figure 2.

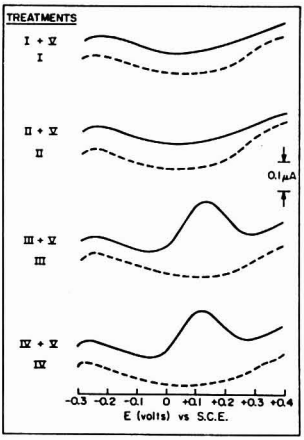


Figure 3. Differential pulse voltammograms recorded at EPG disks. The disks have undergone the treatments indicated (see Experimental section). Supporting electrolyte: 1 M trifluoroacetic acid. Scan rate: 2 mV s^{-1}. Modulation amplitude: 5 mV

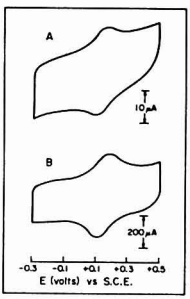


Figure 4. Cyclic voltammograms of covalently attached $Ru(NH_3)_5$-(CAAMP). Supporting electrolyte: 1 M trifluoroacetic acid. Scan rates: (A) 0.1 V s^{-1}, (B) 5.0 V s^{-1}

The unabraded graphite disks with chiefly basal planes exposed (BPG) showed no detectable attachment under any of the reaction conditions investigated. By contrast, attachment to EPG disks was successful. Figure 3 shows typical differential pulse voltammograms recorded at EPG disks following the treatments used to achieve attachment of the Ru(II) complex. The surfaces of the disks show no apparent changes to the eye at any stage of the treatments and the differential pulse voltammograms recorded at any point prior to Treatment V are virtually identical (Figure 3). However, disks subjected to Treatments III and IV and then soaked in a solution of $Ru(NH_3)_5OH_2^{2+}$, i.e., Treatment V, yield a prominent differential pulse voltammetric peak centered at ca. +135 mV.

Cyclic voltammograms recorded at EPG disks that have undergone Treatments III and V or IV and V are displayed in Figure 4. The waves have the symmetric shape characteristic of a surface redox couple (11); however, the peak potentials are not identical. They differ by 40 mV (Figure 4A). Furthermore, the width at half-peak height is 145 mV (Figure 4A or 4B) compared to the theoretical value of 90 mV

(17). The area under the waves in Figure 4 corresponds to a surface concentration of 4.6×10^{-10} mol cm^{-2} (geometric area).

Repeated scanning of these waves between the potential limits shown causes no change in their size or shape. However, if the electrode potential is maintained in the range between +0.5 and 1.0 V for several minutes, the peak current of subsequently recorded voltammograms is decreased markedly. Disks that have undergone Treatments III and V or IV and V can be stored in air for up to a day without significant changes in the wave at +135 mV. As expected, the wave can be entirely eliminated by abrading the electrode with silicon carbide paper.

Control Experiments. The possibilities that during Treatment V the $Ru(NH_3)_5OH_2^{2+}$ might seep into microcrevices in the disks or react with groups present on the surface of the oxidized graphite to (somehow) produce an attached or adsorbed ruthenium complex were examined by exposing disks that had been subjected only to Treatments I or II to the solution of $Ru(NH_3)_5OH_2^{2+}$. The lack of any detectable differential pulse peak using such disks (Figure 3) is strong evidence against these possibilities.

Additional control experiments that produced no sign of attachment included the exposure of disks subjected to the Treatments I, II and III or IV to 0.01 M solutions of $Ru(NH_3)_6^{3+}$, $Ru(NH_3)_6^{2+}$, or $Ru(NH_3)_5Cl^{2+}$. These results confirmed the absence of significant porosity in the pyrolytic graphite employed as well as demonstrating that a labile coordination position in the ruthenium complex is required for the attachment reaction to be successful.

The (remote) possibility that the attachment process, instead of proceeding as suggested in Figure 2, involved a very strong ion-pair interaction between anionic groups on the oxidized graphite surface and the cationic aminomethylpyridine pentaammineruthenium complex was eliminated by soaking graphite disks in 0.01 M solutions of $[Ru(NH_3)_5(AMP)](PF_6)_2$ at pH 1 or 7. (Samples of solid $[Ru(NH_3)_5(AMP)](PF_6)_2$ invariably contained $Ru(NH_3)_5(OH_2)(PF_6)_2$ as an impurity. It was therefore necessary to add a slight excess of 4-aminomethylpyridine during these experiments.) Disks subjected to these treatments showed no electrochemical response in the range of potentials where the peaks were obtained in Figure 3.

Peak Potentials. The peak potential (135 mV in 1F HTFA; 115 mV in 1F HCl) of the waves shown in Figure 3 falls in the expected range for a pentaammineruthenium complex in which a π-acid such as pyridine occupies one of the coordination sites. If the sixth coordination site were occupied by a ligand such as an ammine, a halide anion, or water, the peak potential would appear at potentials 200 to 300 mV more negative (Table I).

In order to compare the peak potentials of the attached ruthenium couple with those of unattached complexes containing a sixth ligand more closely resembling the one which is believed to bind the ruthenium to the graphite surface, the differential pulse voltammetry of the complexes $Ru(NH_3)_5L^{2+}$ (L = AMP, PBA) was examined. The peak potentials of these complexes, given in Table I, fall very close to that of the corresponding pyridine complex. From this it may be inferred that the 40 to 90 mV difference between the peak potentials of the attached ruthenium complex and unattached model complexes does not result from the presence of the aminomethyl group in the 4 position of the pyridine ligand or from the amidization of this group.

Attachment of $Ru(NH_3)_5L^{2+}$ to Graphite Electrode Surfaces by Means of the Irreversible Adsorption of the Pendant Ligand, L. The preparation of the ligand PPE and its complex with pentaammineruthenium(II) was recently

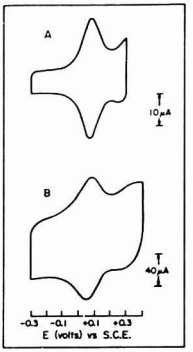


Figure 5. Cyclic voltammograms of adsorbed $Ru(NH_3)_5(PPE)^{2+}$ on a BPG electrode (A) and an EPG electrode (B). Supporting electrolyte: 1 M trifluoroacetic acid. Scan rate: 2.0 V s^{-1}

reported along with a preliminary description of its electrochemical behavior (12). The phenanthrene group of the ligand serves as an "aromatic anchor" by spontaneously adsorbing on the surface of graphite electrodes and carrying with it the ruthenium complex attached to the pyridine group in the ligand. In contrast to the covalent attachment scheme which depends upon the presence of an adequate number of appropriate functional groups on the electrode surface, attachment by means of pendant aromatic anchors proceeds readily on BPG as well as on EPG electrodes. Figure 5A shows a cyclic voltammogram obtained with a BPG disk that had been soaked in a dilute solution (less than 1 mM) of $Ru(NH_3)_5(PPE)^{2+}$ in 1:1 acetone–water for 15 min, removed, washed thoroughly with water, and dried in air before being mounted in the electrode holder (Figure 1). The well-formed waves have the symmetrical shape, identical peak potentials, and nearly the 90 mV width at half-peak height characteristic of reactants which undergo rapid electron transfer and are confined to the surface of an electrode (17). The area encompassed by either the anodic or cathodic wave corresponds to a surface concentration of 5.2×10^{-11} mol cm^{-2} (geometric area).

Figure 5B is a cyclic voltammogram obtained with a EPG disk which was subjected to the same treatment as the BPG disk in Figure 5A. The waves are not as well separated from the background currents, their shape is less symmetrical, the peak potential separation appears to be greater than was true with the BPG electrode, and the width at half-peak height is 115 mV. Nevertheless, the apparent surface concentration evaluated by integration of the cyclic voltammogram, 2.8×10^{-10} mol cm^{-2}, is significantly greater than that at the BPG electrode. The differences in the behavior exhibited by the two types of electrode are believed to be the results of the significantly larger microscopic area of the EPG electrode which produces greater background currents associated with double layer charging and surface oxide formation and reduction. These background currents are asymmetric within the potential region where the cyclic voltammetric waves of the adsorbed reactant fall and the resulting asymmetric summing of the background and faradaic currents causes the two peak currents to appear at different potentials. Comparison of the two voltammograms in Figure 5 makes it clear that BPG electrodes are preferable for inspecting the electrochemical response of reactants which are attached to the electrode surface by means of aromatic anchors.

Sweep Rate Dependence of Faradaic Currents for Attached Complexes and Background Currents at

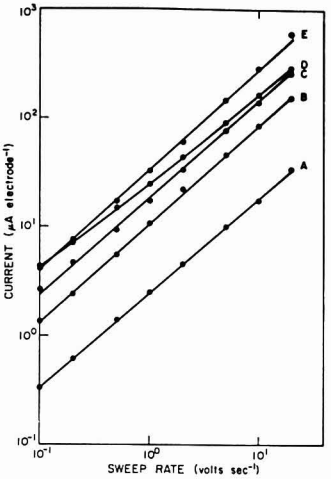


Figure 6. Log current vs. log scan rate for voltammetric peak and background currents. (A) Background current at −200 mV for BPG electrode. (B) Peak current for $Ru(NH_3)_5(PPE)^{2+}$ adsorbed on BPG electrode. (C) Peak current for covalently attached $Ru(NH_3)_5$(CAAMP) on EPG electrode. (D) Background current at −200 mV for EPG electrode. (E) Peak current for $Ru(NH_3)_5(PPE)^{2+}$ adsorbed on EPG electrode

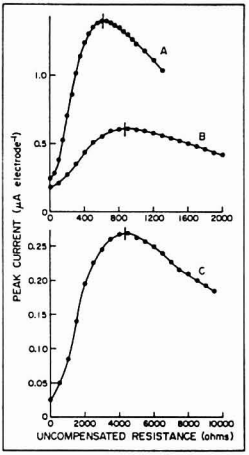


Figure 7. Differential pulse voltammetric peak current vs. uncompensated resistance added to the circuit. (A) $Ru(NH_3)_5(PPE)^{2+}$ adsorbed on EPG electrode. (B) Covalently bound $Ru(NH_3)_5$(CAAMP) on EPG electrode. (C) $Ru(NH_3)_5(PPE)^{2+}$ adsorbed on BPG electrode

Graphite Electrodes. In cyclic voltammetry, the relatively small faradaic currents that result with reactants attached to the electrode surface are often obscured by the background currents which are also present. The component of the background current arising from double layer charging, i_{dl}, is given by Equation 1

$$i_{dl} = C_{dl}A\nu \tag{1}$$

where C_{dl} is the double layer capacitance, A is the electrode area, and ν is the rate of potential scan. The faradaic current arising from the presence of Γ mol cm^{-2} of an attached reactant that obeys the Nernst equation is (*4*)

$$i_f = \frac{n^2F^2\Gamma A\nu}{4RT} \tag{2}$$

Since both currents depend linearly on the rate of potential scan, one would not expect to be able to improve the ratio of faradaic to double-layer charging current by increasing the scan rate. However, comparison of the two cyclic voltammograms in Figure 4 shows that the faradaic peak becomes somewhat more prominent at the higher scan rate. This type of behavior was observed with EPG electrodes independent of the mode of attachment of the reactants.

Figure 6 summarizes the observed sweep rate dependence of background and faradaic currents for both EPG and BPG electrodes. (Double layer charging current, i_{dl}, was measured as one half the distance between anodic and cathodic traces on the cyclic voltammograms.) With the exception of Curve D, all of the data lie close to the straight lines of unit slope expected on the basis of Equations 1 and 2. The smaller slope of Curve D, which represents the background current at an EPG electrode, means that the faradaic current increases more rapidly than the background with EPG electrodes so that the prominence of faradaic peaks is enhanced at higher scan rates. The origin of this effect is most likely associated with the kinetics of the formation (and removal) of graphite oxides on the EPG electrode surface which constitutes a major component of the background current. Curve A in Figure 6 shows that BPG electrodes yield smaller background currents which exhibit the expected linear dependence on scan rate.

Cyclic voltammetry at appropriate scan rates is a useful procedure with high surface concentrations of attached reactants but at lower concentrations its sensitivity is inadequate at any scan rate and the differential pulse technique becomes preferable (*4*, *11*).

Evaluation of Surface Concentrations with Differential Pulse Voltammetry. The general properties of differential pulse voltammograms recorded with reactants attached to electrodes have been discussed recently (*11*). By restricting measurements to sufficiently slow scan rates (1 mV s^{-1} or less) peak potentials are obtained that fall close to the formal potentials of the attached reactants and are independent of the direction of the scan. Introducing (uncompensated) resistance in series with the indicator electrode produces an enhancement in the peak current and provides a method for estimating the amount of reactant attached to the electrode (*11*). Figure 7 shows plots of differential pulse voltammetric peak currents for both forms of attached reactant vs. the amount of uncompensated resistance present in the circuit controlled by the pulse polarograph. The maximum peak current occurs at the value of the uncompensated resistance, R_u, given in Equation 3 (*11*):

$$(R_u)_{max} = t(C_{dl} + C_f)\Gamma^{-1} \tag{3}$$

where t is the time at which differential pulse current is sampled and C_f is the faradaic pseudocapacitance which is given by Equation 4 for Nernstian reactants (*11*)

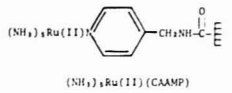
$$C_f = \frac{n^2F^2A\Gamma}{4RT} \tag{4}$$

The surface concentration can then be determined by measuring $(R_u)_{max}$ and C_{dl} and applying Equation 5:

$$\Gamma = \frac{4RT}{n^2F^2A}\left(\frac{t}{(R_u)_{max}} C_{dl}\right) \tag{5}$$

As is clear from Figure 5, the effective value of C_{dl} obtained from cyclic voltammetry and Equation 1 depends somewhat

upon the scan rate employed, especially with EPG electrodes. The appropriate value of C_{dl} to use in Equation 5 seems likely to be that resulting from a voltammogram recorded at a scan rate corresponding to the ratio of the pulse magnitude to the current sampling time employed in the differential pulse voltammetry. For the PAR 174 instrument, the current sampling time is 48 ms and 5-mV pulse amplitudes were used so the value of C_{dl} was evaluated from cyclic voltammetric currents measured at a scan rate of $5/48 = 0.105$ V s^{-1}. The resulting values of Γ estimated from Equation 5 are 2.9×10^{-10} and 1.0×10^{-9} mol cm^{-2} for $Ru(NH_3)_5(PPE)^{2+}$ adsorbed on BPG and EPG graphite, respectively, and 1.8×10^{-10} mol cm^{-2} for covalently linked Ru(II)$(NH_3)_5$(CAAMP)



$(NH_3)_5Ru(II)$(CAAMP)

on EPG graphite. The corresponding values estimated from the areas of the cyclic voltammograms recorded at the same time as the data in Figure 7 are 4.0×10^{-10}, 2.3×10^{-9}, and 1.2×10^{-10} mol cm^{-2}. The agreement between the two sets of values of Γ is well within the estimated uncertainties that are known to be associated with the use of Equation 5 (*11*).

The considerably greater surface concentration obtained with adsorptive attachment on EPG disks probably reflects the larger microscopic area of this form of graphite. The adsorption of more than a monolayer of the reactant may also be occurring since the aromatic anchors might be expected to attach to themselves about as readily as to the graphite surface.

Rates of Loss of Attached Reactants from the Electrode Surface. The slow decrease in the magnitude of differential pulse voltammetric peak currents was used to monitor the loss of reactants from the electrode surface. (Between scans the electrodes were potentiostated at −0.15 V. Detached reactants were removed by periodically flushing the cell with fresh electrolyte solution.) The data, plotted semilogarithmically in Figure 8, indicate that the rates of detachment of both adsorbed and covalently linked reactants follow first-order kinetics only after a significant fraction of the initially attached species has been removed. The half-lives evaluated from the linear portions of the plots for the loss of adsorbed $[Ru(NH_3)_5(PPE)]^{2+}$ and covalently linked Ru$(NH_3)_5$(CAAMP) were 313 and 1080 min, respectively. The adsorbing reactant, $[Ru(NH_3)_5(PPE)]^{2+}$, can readily be reattached to electrodes from which it has desorbed. However, the diminishing pulse voltammetric waves for the covalently linked complex cannot be restored by exposing the spent electrodes to fresh solutions of $Ru(NH_3)_5OH_2^{2+}$. This might be taken as an indication that it is the rupture of the amide bond holding the ligand to the electrode surface which determines the rate of loss of the covalently linked complex.

DISCUSSION

The experimental results summarized here make it clear that attachment of electrochemically active reactants to the surface of graphite electrodes can be readily achieved both by spontaneous adsorption via "aromatic anchors" as well as by the controlled synthesis of suitable functionalities on the electrode surface (cf. Figure 2). The two routes to attachment differ markedly in the longevity of the attached reactants (Figure 8) but, at least for the Ru(III)/Ru(II) couples studied here, the electrochemical behavior of the two types of attached reactant is virtually identical. It may be that the very high intrinsic electron transfer rates of ruthenium–pentaammine complexes effectively mask real differences in electrochemical reactivities of the two forms of attached reactants so that the attachment of a less reactive redox couple would provide a more sensitive test of this question.

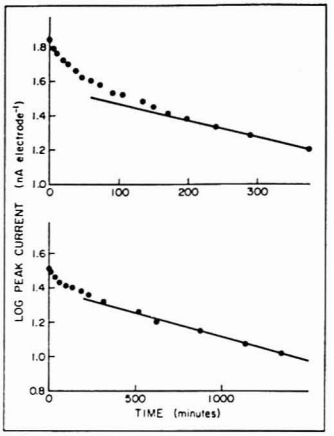
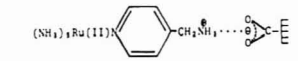


Figure 8. Semilogarithmic plot of differential pulse voltammetric peak current vs. the time the electrode was exposed to the supporting electrolyte solution. (A) $Ru(NH_3)_5(PPE)^{2+}$ adsorbed on EPG electrode. (B) Covalently attached $Ru(NH_3)_5$(CAAMP) on EPG electrode. Supporting electrolyte: 1 M trifluoroacetic acid

The surface chemistry indicated in Figure 2 is based, in part, on the established presence of carboxylic acid functionality on high area, oxidized graphites (*18*). The fact that 4-aminomethylpyridine could be successfully attached to EPG but not (detectably) to BPG electrodes supports the proposition that the attachment requires an abundance of oxidized functionalities on the surface. However, it is somewhat surprising that the attachment of 4-aminomethylpyridine, if accomplished by means of a simple amide bond, was just as great at oxidized electrodes which were not treated with thionyl chloride as at those which were. Nevertheless, we are convinced that the attachment described does involve a covalent bond because the control experiments clearly rule out spontaneous adsorption of $[Ru(NH_3)_5(AMP)]$ as well as the possibility of ionic bonding such as



Furthermore, the durability of the attached ruthenium complex, $t_{1/2} \sim 18$ h, is inconsistent with anything but a strong covalent attachment bond.

Finally, it may be worth pointing out that Ru(III)/Ru(II) complexes were selected for this study because their chemistry features several extremely desirable virtues: (i) Both halves of the redox couple are sufficiently substitutionally inert that the complex is not chemically destroyed within a few cycles of oxidation and reduction; (ii) the standard electron transfer rate constant for the Ru(III)/Ru(II) pentaammine complex is quite high (~ 1 cm s^{-1}) assuring Nernstian behavior with correspondingly sharp differential pulse and cyclic voltammetric responses; (iii) the formal potentials of the attached redox couples can be adjusted over a considerable range by selection of the sixth ligand in the metal's coordination sphere. To match these chemical properties with other, particularly first-row, transition metal complexes will probably require the use of multidentate ligands.

ACKNOWLEDGMENT

We are grateful to Alan Brown for helpful discussions and the synthesis of the ligand PPE.

LITERATURE CITED

(1) R. F. Lane and A. T. Hubbard, *J. Phys. Chem.*, **77**, 1401, 1411 (1973).
(2) B. F. Watkins, J. R. Behling, E. Kariv, and L. L. Miller, *J. Am. Chem. Soc.*, **97**, 3549 (1975).
(3) B. E. Firth, L. L. Miller, M. Mitani, T. Rogers, J. C. Lennox, and R. W. Murray, *J. Am. Chem. Soc.*, **98**, 8271, (1976).
(4) A. P. Brown, C. Koval, and F. C. Anson, *J. Electroanal. Chem.*, **72**, 379 (1976).
(5) R. J. Burt, G. J. Leigh, C. J. Pickett, *J. Chem. Soc., Chem. Commun.*, 1940 (1976).
(6) M. Fujihira, T. Matsue and T. Osa, *Chem. Lett.*, 875 (1976).
(7) P. R. Moses and R. W. Murray, *J. Am. Chem. Soc.*, **98**, 7435 (1976); *J. Electroanal. Chem.*, **77**, 393 (1977).
(8) J. R. Lenhard and R. W. Murray, *J. Electroanal. Chem.*, **78**, 195 (1977).
(9) S. Mazur, T. Matusinovic, and K. Cammann, *J. Am. Chem. Soc.*, **99**, 3888 (1977).
(10) J. F. Evans, T. Kuwana, M. T. Henne, and G. P. Royer, *J. Electroanal. Chem.*, **80**, 409 (1977).
(11) A. P. Brown and F. C. Anson, *Anal. Chem.*, **49**, 1589 (1977).
(12) A. P. Brown and F. C. Anson, *J. Electroanal. Chem.*, **83**, 203 (1977).
(13) P. Ford, D. Rudd, R. Gaunder, and H. Taube, *J. Am. Chem. Soc.*, **90**, 1187 (1968).
(14) C. G. Kuehn and H. Taube, *J. Am. Chem. Soc.*, **98**, 689 (1976).
(15) H. S. Lim, D. J. Barclay, and F. C. Anson, *Inorg. Chem.*, **11**, 1460 (1972).
(16) T. Matsubara and P. C. Ford, *Inorg. Chem.*, **15**, 1107 (1976).
(17) E. Laviron, *J. Electroanal. Chem.*, **39**, 1 (1972) and references therein.
(18) H. P. Boehm, *Adv. Catal.*, **16**, 179 (1964).

RECEIVED for review September 12, 1977. Accepted November 14, 1977. This work, Contribution No. 5659, was supported by a grant from NSF-RANN.

Electrochemical Behavior of the Selenocyanate/Triselenocyanate Redox Couple in Acetonitrile on Platinum Electrodes

M. E. Martins, C. E. Castellano, A. J. Calandra, and A. J. Arvía*

Instituto de Investigaciones Fisicoquímicas Teóricas y Aplicadas, División Electroquímica, Universidad Nacional de La Plata, 1900 La Plata, Argentina

A reversible $(SeCN)_3^-/SeCN^-$ redox couple is formed on clean Pt when KSeCN solutions in ACN, containing $[(Et)_4N]ClO_4$ as supporting electrolyte are electrolyzed. The reaction is studied by triangular potential sweep voltammetry and the RDE technique. The main overall process corresponds to that of the $(SeCN)_3^-/SeCN^-$ redox couple. The kinetic relationships obtained at 30 mV/s $\leq v \leq$ 300 mV/s can be interpreted with the formal reaction pathway already known.

The anodic oxidation of potassium selenocyanate dissolved in methanol was attempted about 50 years ago as a method for the preparation of selenocyanogen (*1*). Later, the same electrochemical process was used to obtain organic chemicals with the SeCN group (*2*). The electrochemical selenocyanation of organic molecules on platinum proceeds with a relatively high yield when acetonitrile is used as solvent (*3*). Under these conditions the $SeCN^-$ ion is electrooxidized to $(SeCN)_2$, via the SeCN radical. The dimer, however, decomposes to $Se(SeCN)_2$ and $Se(CN)_2$ and its electroreduction yields $SeCN^-$ ions and $(CN)_2$ (*4*). During the anodic oxidation of the $SeCN^-$ ion, the existence of the $(SeCN)_3^-$ complex ion was evidenced by electrochemical as well as spectrophotometric methods and its dissociation equilibrium constant was evaluated (*5*).

The most probable species participating in these electrochemical reactions, namely $SeCN^-$ and $(SeCN)_3^-$ ions and $(SeCN)_2$ are isoelectronic with the halogen-containing equivalent species whose electrochemical behavior in acetonitrile on platinum has been already investigated (*6, 7*). The present work refers to the kinetic behavior of the redox couples involved in the electrolysis of KSeCN solutions in ACN through the analysis of voltammetric data, following the experimental approach previously reported in the study of the KSCN in the same solvent (*8*). The mechanism of the $(SeCN)_3^-/SeCN^-$ redox couple fits the simple dimerization reaction pathway already suggested by other authors (*5*) but including the chemical equilibrium related to the $(SeCN)_3^-$ ion formation.

EXPERIMENTAL

The conventional three-compartment electrolysis cell as described earlier (*8*) consisted of a Pt working disk electrode (0.071 cm^2) placed into a Teflon holder, a Pt counter electrode and a saturated calomel electrode as reference. The electrolytic solution was prepared from KSeCN (Schuchardt-München) dissolved in ACN (U.C.B.) and 0.5 M $[(Et)_4N]ClO_4$ as supporting electrolyte. The solvent was purified as indicated elsewhere (*8*). The KSeCN concentration was varied from 5×10^{-3} to 10^{-2} M. The solution was kept continuously under a purified N_2 atmosphere during the measurements.

Experiments were performed at 0 °C and 25 °C under cyclic triangular voltammetry with ohmic drop compensation either with a single triangular potential scan or under repetitive conditions, the working electrode being either at rest or under rotation. The linear potential sweeps covered the range from 1 to 900 mV/s while the rotation speed of the working electrode was varied between 300 and 1500 rpm. The circuitry employed was the same as already mentioned in previous publications (*6, 8*).

The reproducibility of the experimental results depended on the electrode treatment. Thus, the best reproducibility and reversible behavior of the electrochemical system was achieved when the Pt electrode surface was mechanically polished to a mirror surface with a suspension of fine alumina powder in ethanol. Previous electrochemical treatments, either anodic or cathodic, gave only poorly reproducible results, the electrochemical system approaching a relatively more irreversible behavior than that obtained with the mechanical polishing.

RESULTS

Voltammetric Data. Voltammograms run from −0.30 V up to ca. 0.50 V using single symmetric triangular potential scans (Figure 1) exhibit two anodic current peaks, in the 0.20 to 0.35 V range. The returning potential scans involve a net cathodic current peak at ca. 0.15–0.20 V and also a shoulder at about 0.35 V which is associated with the second anodic peak. Repetitive triangular potential scans run between −0.25

0003-2700/78/0350-0229$01.00/0 © 1978 American Chemical Society

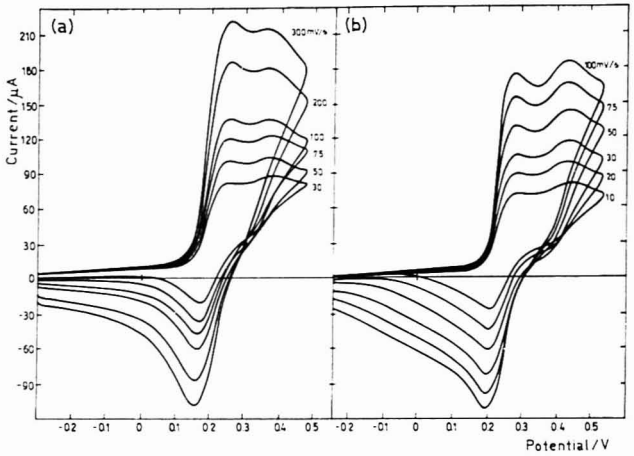


Figure 1. Single triangular potential sweep voltammograms run at different potential sweep rates. (a) 7.5×10^{-3} M KSeCN + 0.5 M $[(Et)_4N]ClO_4$; 25 °C. (b) 10^{-2} M KSeCN + 0.5 M $[(Et)_4N]ClO_4$; 0 °C

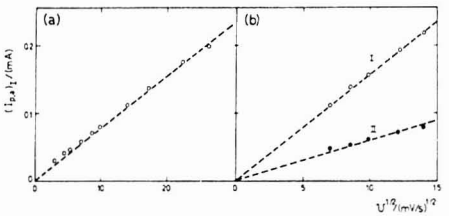


Figure 2. Dependence of the anodic current peak heights on $v^{1/2}$. (a) 5×10^{-3} M KSeCN + 0.5 M $[(Et)_4N]ClO_4$; 25 °C. (b) 10^{-2} M KSeCN + 0.5 M $[(Et)_4N]ClO_4$; 25 °C. (○) First anodic current peak; (●) second anodic current peak

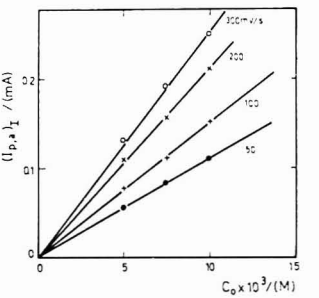


Figure 3. Dependence of the first anodic current peak height on KSeCN concentration at 25 °C, for different potential sweep rates

V and 0.55 V at $30 \leq v \leq 700$ mV/s are coincident without any hysteresis.

The heights of the two anodic and the cathodic current peaks increase linearly with the square root of the potential sweep rate (Figure 2) and the corresponding current peak potentials obtained from the E/I voltammograms run with mechanically polished electrodes are independent of the potential sweep rate.

The ratio of the first anodic current peak height to the cathodic current peak height, $(I_{ap})_I/I_{cp}$, read from the voltammograms recorded within the region of the first anodic current peak, is very close to unity. In addition, the height of the first anodic current peak depends linearly on the $SeCN^-$ ion concentration (Figure 3).

The difference between the potential of the first anodic current peak, and its value at $(I_{ap})_I/2$, namely $[(E_{ap}) - E_{ap})/2]_I$ lies between 57 and 65 mV at 25 °C. The plot, $(I_{ap})_I/v^{1/2}$ vs. $v^{1/2}$, (Figure 4) deviates from a horizontal line when $v < 30$ mV/s.

To compare the heights of both anodic current peaks, the baseline for the second one was obtained by extrapolation of the first E/I profile towards higher potentials on the assumption that the former corresponds to a simple reversible electrochemical reaction and that the current decay fits a $t^{-1/2}$ law taking as $t = 0$ the current peak potential value plus 30 mV. The height ratio, $(I_{ap})_I/(I_{ap})_{II}$, thus obtained is close to 2. The difference of the corresponding current peak potentials

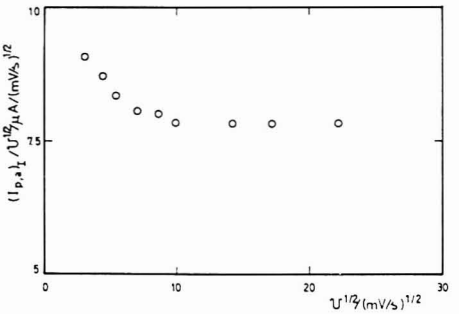


Figure 4. Dependence on the $(I_{ap})_I/v^{1/2}$ ratio on $v^{1/2}$. 5×10^{-3} M KSeCN + 0.5 M $[(Et)_4N]ClO_4$, 25 °C

lies between 0.105 and 0.135 V, at 25 °C, apparently depending on the concentration of the $SeCN^-$ ion.

Rotating Disk Electrode Data. Under the most favorable and reproducible conditions, the E/I characteristics obtained with the Pt RDE, run at 1 mV/s exhibit two successive anodic waves. The ratio between the first to the second limiting

currents, $(I_{a,lim})_I/I_{a,lim})_{II}$, particularly for the experiments run at the highest concentration and the lowest temperature, is close to 2.

The same result is obtained from any E/I curve although the first anodic wave is sometimes rather poorly defined. The latter can be estimated on the assumption that it corresponds to a reversible electron transfer reaction using the diffusion coefficient of the $SeCN^-$ ion derived from voltammetry.

The height of the total limiting current, I_L, increases linearly with the concentration of the $SeCN^-$ ion and both anodic limiting currents increase linearly with the square root of the rotating speed of the working electrode.

DISCUSSION

The anodic oxidation of the $SeCN^-$ ion dissolved in ACN on Pt electrodes under potentiodynamic conditions, at $v > 30$ mV/s, exhibits a behavior which resembles that of the iodide ion dissolved in aprotic solvents on the same metal electrodes, where two anodic waves are recorded associated with either one or two cathodic waves, depending on the solution composition (*5, 6, 9, 10*).

The redox couples related to the halogen or pseudohalogen electrodes, involve an equilibrium such as

$$X_2 + X^- = X_3^- \quad (1)$$

where X^- is the halide or pseudohalide ion, X_2 is the molecular species in solution, and X_3^- the corresponding complex ion. If equilibrium 1 is fast and the stability constant of X_3^- formation is large, then a solution containing an excess of X^- will mainly contain X^- and X_3^- as the reacting species at the metal solution interface, while with an excess of X_2, the reacting species will be X_2 and X_3^-. The former situation applies to the present electrochemical system since here the existence of the $(SeCN)_3^-$ ion and the $(SeCN)_2$ dimer has been demonstrated (*5*).

The analysis of the first current peak exhibited by the potentiodynamic E/I profiles at $v > 30$ mV/s is made in terms of the following diffusion controlled overall reaction:

$$3\,SeCN^- = (SeCN)_3^- + 2e^- \quad (2)$$

This reaction can be interpreted as an electrochemical dimerization process as already discussed by Cauquis and Pierre (*3–5*) followed by a homogeneous fast chemical equilibrium according to the following consecutive reaction pathway:

$$(SeCN^-)_e = (SeCN^-)_e + e^- \quad (2a)$$

$$2(SeCN^-)_e = (SeCN)_2 \quad (2b)$$

$$[(SeCN)_2 + SeCN^- = (SeCN)_3^-] \quad (2c)$$

where the subscript e means the species at the electrode surface. The E/I profile can be reproduced reasonably well with the theoretical equation derived for such reaction scheme, taking the number of electrons per mole of reacting species equal to 2/3 and the diffusion coefficient of the $SeCN^-$ ion in these solutions as 1.5×10^{-5} cm^2/s. The latter has been calculated from the slope of the $(I_{ap})_I$ vs. $v^{1/2}$ relationship and concides with that calculated from the total limiting current obtained with the rotating disk electrode.

The experimental first anodic E/I profile can also be reproduced with the current functions calculated for reaction 2 according to Shuman (*11*), but a larger value of the diffusion coefficient is then required.

The cathodic current peak also exhibits the characteristics of a reversible process. The difference between the first anodic current peak potential and the cathodic current peak potential is a constant for any value of v and lies at 0.070 ± 0.010 V, namely within the potential range corresponding to a reversible electrode process. The difference $[E_{1/2} - (E_{ap/2})_I]$ and the ratio $I_{cp}/(I_{ap})_I$, agree with the establishment of the reversible redox couple $(SeCN)_3^-/SeCN^-$ at the Pt electrode.

Unfortunately the interpretation of the second anodic process which implies the electrochemical oxidation of the $(SeCN)_3^-$ species is more speculative. The potential corresponding to the initiation of this process corresponds to an interface whose electrolyte composition is different from the bulk solution. According to the anodic limiting current ratio, the overall reaction at the interface should be

$$2(SeCN)_3^- = 3(SeCN)_2 + 2e^- \quad (3a)$$

followed again by the homogeneous fast chemical equilibrium:

$$(SeCN)_2 + SeCN^- = (SeCN)_3^- \quad (3b)$$

Under the present circumstances the cathodic current associated with the dimer appears only as a shoulder at around 0.35 V and it makes any quantitative evaluation from it quite unreliable. The sequence of the overall processes associated with each anodic current peak explains why the ratio of current heights is equal to 2.

The characteristics of the E/I profiles at potential sweep rates lower than 30 mV/s are not clear. Probably they involve the contribution of other processes coupled to the electrochemical reaction, such as a chemical reaction between the pseudohalogen molecule and the solvent probably similar to that earlier described for the electrochemistry of hydrogen halides in aprotic solvents (*12*).

LITERATURE CITED

(1) L. Birchenbach and K. Kellermann, *Chem. Ber.*, **58**, 786 (1925).
(2) N. N. Melnikov and E. M. Cherkasova, *J. Gen. Chem. USSR*, **16**, 1025 (1946).
(3) G. Cauquis and G. Pierre, *C. R. Hebd. Seances Acad. Sci., Ser. C*, **272**, 609 (1971).
(4) G. Cauquis and G. Pierre, *C. R. Hebd. Seances Acad. Sci., Ser. C*, **269**, 740 (1969).
(5) G. Cauquis and G. Pierre, *Bull. Soc. Chim. Fr.*, 1225 (1972).
(6) V. A. Macagno, M. C. Giordano, and A. J. Arvía, *Electrochim. Acta*, **14**, 335 (1969).
(7) T. Iwasita and M. C. Giordano, *Electrochim. Acta*, **14**, 1045 (1969).
(8) R. Pereiro, A. J. Calandra, and A. J. Arvía, *Electrochim. Acta*, **17**, 1723 (1972).
(9) M. C. Giordano, J. C. Bazán, and A. J. Arvía, *Electrochim. Acta*, **11**, 741 (1966); **11**, 1553 (1966); **12**, 723 (1967).
(10) A. J. Arvía, M. C. Giordano, and J. J. Podestá, *Electrochim. Acta*, **14**, 389 (1969).
(11) M. S. Shuman, *Anal. Chem.*, **42**, 521 (1970).
(12) M. Michlmayr and D. T. Sawyer, *J. Electroanal. Chem.*, **23**, 387 (1969).

RECEIVED for review April 25, 1977. Accepted October 25, 1977. A. J. Calandra acknowledges Aluar Saic Argentina for permission to participate in the present work. This work is part of the research program of the Electrochemistry Division of INIFTA, sponsored by the Universidad Nacional de La Plata, the Consejo Nacional de Investigaciones Científicas y Técnicas of Argentina and the Comisión de Investigaciones Científicas (Provincia de Buenos Aires).

Direct Potentiometric and Titrimetric Determination of Methadone in Urine with Plastic Electrodes Selective for Hydrophobic Cations

Songsak Srianujata, Wesley R. White, Takeru Higuchi, and Larry A. Sternson*

Department of Pharmaceutical Chemistry, University of Kansas, Lawrence, Kansas 66044

Methadone was determined in acidified (pH 2 to 3) urine samples by using a miniaturized hydrophobic-cation-selective plastic membrane electrode. The selectivity of this electrode permitted the determination to be made at 5×10^{-6} M in urine samples without prior separation. Determinations of about ±15% accuracy were possible with a single potential measurement; better than ±2% accuracy could be obtained by titrating the sample with a solution of sodium tetraphenylboron and monitoring the decrease in methadone activity potentiometrically.

The use of methadone in opiate-addiction treatment programs has created a need for rapid, simple, yet accurate analytical methods for monitoring drug levels in biological fluids, in order to evaluate patient compliance. Some of the earlier reported (*1–5*) clinical methods for the drug lacked the specificity required to obtain meaningful results. Beckett (*6*) has described a gas–liquid chromatographic technique for analysis of methadone and its metabolites in microsomal homogenates, and Valentine (*7*) reports an alternative GLC procedure for quantitation of the analyte in human urine samples. These methods, while highly specific, are time consuming and require substantial sample manipulation. They are not ideally suited for routine monitoring of methadone levels in an outpatient setting. What is needed is a direct method, requiring a minimal number of steps and time to specifically detect and quantitate the drug in urine. Urine was chosen as the test biological fluid because of its ready accessibility and because a significant fraction of the drug is eliminated intact by the kidney.

Structurally, methadone is a γ-keto-tertiary amine. In this report we describe a clinically applicable method for methadone, based on its hydrophobicity and ability to form cationic species at low pH.

Higuchi (*8*) has described an ion-selective membrane electrode, which responds preferentially to hydrophobic cations. The membrane is composed of a poly(vinylchloride) (PVC)–dioctylphthalate (DOC) mixture. The selective response of the electrode for cations is made possible by specific anionic sites in the membrane (*9*), while the preference for hydrophobic species is derived from the hydrophobicity of the membrane itself, i.e., response is related to the difference in chemical potential of the analyte in the aqueous vs. membrane phase. The potential of this electrode is directly related to the activity of hydrophobic cations in aqueous solution (*8*) and response is Nernstian. Although these characteristics seem to make the electrode a useful probe for drug analysis, the cumbersome nature of the original assembly prevented application of the electrode to clinical analysis. Coated-wire ion-selective electrodes have been further discussed by Freiser et al. (*10, 11*).

This report describes the design of a modified version of this electrode which is smaller, less fragile, more stable, and provides a faster response time. This electrode was then used to monitor urinary levels of methadone, a hydrophobic drug which is made cationic at low pH because of protonation of the amine. Measurement could be made either by direct potentiometric monitoring of acidified urine samples or by potentiometric titration of the analyte in urine with tetraphenylboron (TPB).

EXPERIMENTAL

Apparatus. Potential measurements were made with an Orion Model 801 Ionalyzer.

Materials. Tetraphenylboron (sodium salt) was purchased from Matheson, Coleman and Bell Chemical Company and methadone hydrochloride was obtained as 10-mg tablets (Dolophine) from Eli Lilly Inc. Dolophine tablets (10 mg) were crushed, a portion of the resulting powder was weighed, and the weight of methadone calculated assuming that the average weight of methadone hydrochloride per tablet in the sample taken is exactly 10 mg. The electrode membrane was prepared with poly(vinylchloride) (PVC) resin [(Bakelite QYKV Blend 1) Union Carbide Corp.], PVC (molding resin) purchased from Diamond Shamrock Corp., dioctylphthalate (DOC) (Analabs Chemical Co.), and 1,2-dichloroethane (obtained from Fisher Scientific Co.).

Electrode Construction. Silver wire ($^1/_2$-inch, No. 0 gauge) was soldered to a shielded wire connected to a standard glass electrode plug. A glass tube ($^1/_4$-inch diameter) was used as the electrode body and the wire was sealed into the tapered end of the tubing with epoxy resin so that the silver wire protruded about 3 mm from the tube. The protruding silver wire was then melted into a ball point (Figure 1). The entire electrode was then coated with a nonsensitive hard plastic (prepared by dipping the electrode in a solution prepared by dispersing 20 g of PVC in 200 mL of 1,2-dichloroethane, heating at 60° for 6 h, then adding a few drops of DOC and heating for an additional hour) to obtain a coating of ca. 0.5-mm thickness. One and one-half millimeters of plastic were removed from the tip of the wire (Figure 1). The exposed tip was then chloridized electrolytically for 30 min in 0.1 N HCl solution (*12*), after which the electrode tip was immersed in 0.1 M KCl solution. The sensitive polymer membrane solution was prepared as a 1:1 mixture of PVC (Diamond Shamrock) and DOC in 1,2-dichloroethane maintained at 60 °C. The Ag/AgCl electrode tip was then dipped into this polymer solution a total of 4 to 6 times, and allowed to dry after each treatment. The electrode was finally equilibrated with 0.1 M KCl solution for 12 h before use.

Analysis for Methadone in Urine. Urine samples containing methadone were diluted with one volume of water and acidified to pH 2–3 with 5 M H_2SO_4. The electrode assembly was then introduced into the solution and the mixture titrated with a 4.98×10^{-4} M solution of tetraphenylboron (sodium salt). Alternatively, the urine samples were assayed by a single direct potentiometric measurement.

RESULTS AND DISCUSSION

Electrode Design. A simplified version of a hydrophobic cation specific electrode was constructed by affixing a PVC–DOC membrane onto a silver wire coated with AgCl. Effective construction depends on developing electrical contact between the metal and polymer membrane surfaces, which in turn establishes a constant potential which is responsive

0003-2700/78/0350-0232$01.00/0 © 1978 American Chemical Society

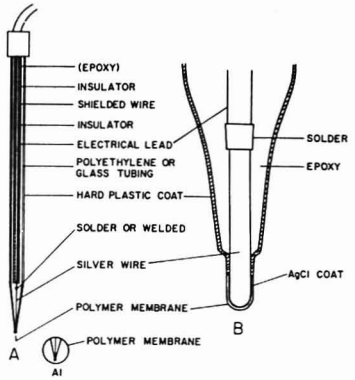


Figure 1. (A) Miniaturized electrode bodies for coated wire electrodes. (B) Magnified view of the tip of a coated wire electrode

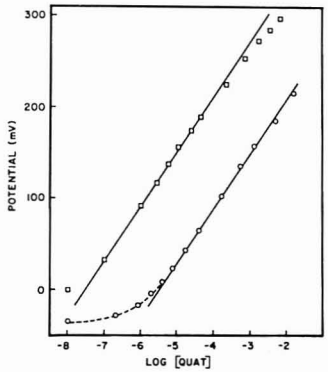


Figure 2. Response of a coated wire plastic electrode towards tetrabutylammonium bromide (O) and tetrapentylammonium bromide (□) in distilled water. The lines drawn are theoretical lines with slope of 59 mV

to the external solution. It is unlikely that such contact takes place directly, because of large differences in the physical properties of the metal surface and hydrophobic membrane. It is assumed that electrical contact between these surfaces is made through a thin layer of aqueous salt solution, which originates from transfer of water through the thin membrane by diffusion and from the established osmotic gradient. The potential develops through the aqueous phase between the wire-membrane interface. The most reproducible and stable electrode configuration was acquired by immersing the Ag/AgCl wire in a 0.1 M KCl solution *after* coating it with the polymeric membrane. A reproducible aqueous interphase was thus generated. The resulting electrode, shown in Figure 1, has an internal reference solution and is in a less fragile, more stable configuration than the electrode previously described (*8*). A typical cell used for measuring the potentials developed was:

$$\mathrm{Ag/AgCl}\left|\ 0.1\ \mathrm{M\ KCl}\ \right|\begin{matrix}\text{plastic}\\ \text{membrane}\end{matrix}\Bigg|\ \Bigg|\begin{matrix}R_4N^+\\ \text{test soln.}\end{matrix}\Bigg|\ \mathrm{SCE}$$

The observed response of coated wire plastic electrodes toward varying concentrations of tetrabutylammonium

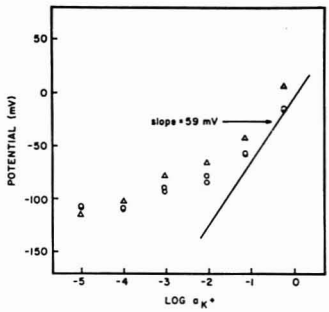


Figure 3. Response of two coated wire plastic electrodes in p chloride aqueous solutions. The line drawn is a theoretical slope of 59 mV

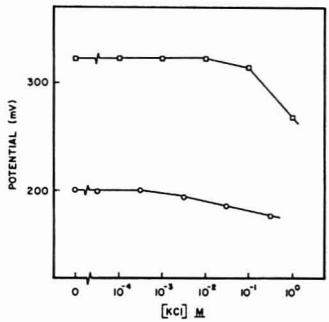


Figure 4. Response of a coated wire plastic electrode towards tetrapentylammonium bromide 1×10^{-4} M (O) and benzalkonium chloride 1.38×10^{-4} M (□) in distilled water, in the presence of varying concentration of potassium chloride

bromide (TBA) and tetrapentylammonium bromide (TPA) in water is illustrated in Figure 2. The electrode gave a good, apparently Nernstian response over a wide range of concentrations. The sensitivity limit appears to be approximately 1×10^{-6} M for TBA and 1×10^{-8} M for TPA. These results are similar to those obtained with the original design of the electrode (*8*).

Interference of common inorganic cations with electrode response was studied both in solutions containing the primary hydrophobic cation and in its absence. The electrode response to sodium ion and hydronium ion was essentially insignificant in the concentration range from 1×10^{-5} M to 1 M. However, the response toward potassium ion in KCl solution was appreciable (Figure 3), particularly at concentrations greater than 1×10^{-2} M, where a slope of about 48 mV per decade change in concentration was observed. However, in the presence of a hydrophobic cation, the interference from potassium ion was not appreciable (Figure 4). The slight change in potential for TBA ion at higher KCl levels may be due to changes in the ionic strength of the solution. In the case of benzalkonium chloride, at the 1 M KCl level, the observed drop in potential may be accounted for by micellular aggregation of the ions. The electrode failed to respond to calcium ion at concentrations less than 0.5 M. Shatkay (*13*) previously found that a PVC membrane in which tributylphosphate and theonyltrifluoroacetone were incorporated could serve as a calcium ion selective electrode.

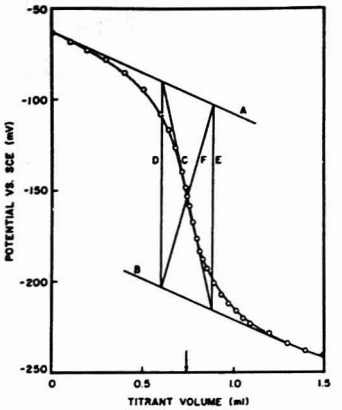


Figure 5. Typical potentiometric titration curve of methadone in distilled water, with graphical lines drawn for locating of the equivalence point, titrated with sodium tetraphenylboron

The response time of the coated wire electrode towards 1×10^{-6} M TBA in aqueous solution (taken as >98% of peak) was less than 50 s; after removal of the electrode from the test solution and immersion in "clean" buffer, the equilibrium potential was reestablished within 20 s. Response time was concentration-dependent, taking up to 3 min to obtain equilibrium potentials in very dilute solution, e.g., 1×10^{-7} M TBA. Response time was also dependent on the composition and thickness of the membrane and the time allowed for equilibration of the membrane with salt solution before use.

Direct Potentiometric Analysis for Methadone. The response of the coated wire plastic electrode towards varying concentrations of methadone hydrochloride in water was identical to that seen with TBA (Figure 2). A linear, Nernstian response was observed in the range from 1×10^{-6} M to 1×10^{-2} M with a slope of 59 mV/decade change in concentration of methadone. Measurements for methadone were made in acidic solution to ensure protonation of the tertiary amine group. Standard curves, similar to those generated in aqueous solution, were obtained with known concentrations of methadone present in unprocessed, acidified urine. The electrode did not respond to any of the many cationic constituents of normal urine, presumably because they are too hydrophilic to influence the sensor, even when methadone was present at levels as low as 1×10^{-5} M.

The usefulness of the coated wire plastic electrode is still somewhat unsatisfactory for direct potentiometric measurement because of the need for frequent standardization of the electrode. However, for some applications, where the highest accuracy is not required, it might be possible to estimate the methadone concentration from a single potentiometric measurement.

Titrimetric Analysis for Methadone. Tertiary ammonium salts can be titrated with sodium tetraphenylboron (*14*), the resulting complex forming a stable precipitate. The specificity and sensitivity of the method is then dependent, in part, on the dissociation constant for the complex and the constants for potential interferents. This reagent was used to titrate the protonated form of methadone, the decrease in analyte activity being followed using the plastic electrode.

A typical titration curve for the drug in aqueous solution, which results from plotting electrode potential vs. titrant volume, is shown in Figure 5. Potentiometric titration curves

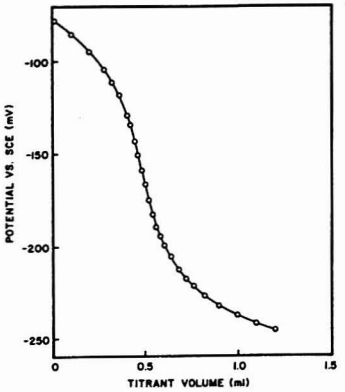


Figure 6. Potentiometric titration curve of methadone in patient's urine. Two mL of the urine sample, titrated with sodium tetraphenylboron solution, 4.98×10^{-4} M

for methadone in acidified urine are shown in Figure 6. The curve shows a sharp equivalence point even though the sample was diluted with one volume of water before titration. The apparent equivalence point for these titrations was determined graphically as follows: Line A was drawn with minimum slope, tangent to the initial part of the titration curve; line B was then drawn parallel to A, tangent to the final portion of the titration curve; line C was then drawn with maximum slope tangent to the region of the equivalence point; lines D and E were drawn vertically so as to pass through the intersections of line C with A and B; line F was drawn from the intersection of lines A and E to the intersection of lines B and D. The intersection of lines F and C was then taken to be the equivalence point.

The equivalence point of the titrations was alternatively determined by a computerized curve-fitting technique. The curve-fitting was performed on the HP 2100 computer by a modified version of the GCSL055-Omega nonlinear regression program developed at Goddard Computer Science Institute and distributed by Hewlett-Packard as Program No. 22188A. This program uses the Gauss–Newton (*15*) method to minimize the sum of the squares of the differences between the data points and the function being fitted. If it is assumed that the product of TPB and MH ion concentrations is a constant, an equation can be derived relating the electrode potential to the volume of TPB solution added [(Equation 1) Appendix].

$$E = E^0 + x\frac{RT}{F} \times \ln\left\{\frac{-t(V - V_{eq}) + \sqrt{t^2(V_{eq} - V)^2 + 4K(V + W)^2}}{2C^0(V + W)}\right. \quad (1)$$

where E is the electrode potential, C^0 is the standard state concentration of MH, E^0 is E at C^0, x is the electrode response factor, t is the titrant concentration, V is the titrant volume, V_{eq} is V at the equivalence point, K is the product of MH and TPB ion concentrations, W is the initial volume in the titration vessel, and R, T, and F have their usual meanings. This equation was fitted to each of the titration curves by allowing E^0, V_{eq}, and K to vary, taking C^0 to be 1 M. In Table I the results of a typical fitting are shown in comparison with actual titration data.

In all cases, the computerized fitting was quite successful; the standard deviation of the fitted equation from the actual

Table I. Results of Curve-Fitting the Data from a Typical Titration of Methadone in Aqueous Solution Using Nonlinear Regression Analysis[a,b,c]

Titrant volume, mL[d]	Potential, mV	Predicted potential, mV	Error, mV
0.00	−105.0	−105.18	0.18
0.10	−112.6	−111.79	−0.81
0.14	−115.8	−114.86	−0.94
0.18	−118.6	−118.24	−0.36
0.22	−121.8	−122.03	0.23
0.26	−126.1	−126.32	0.21
0.30	−130.5	−131.26	0.76
0.34	−136.5	−137.07	0.57
0.38	−142.8	−144.04	0.12
0.42	−152.5	−152.55	0.48
0.44	−157.8	−157.45	−0.35
0.48	−163.2	−162.76	−0.44
0.49	−168.1	−168.34	0.24
0.50	−174.8	−174.00	−0.80
0.52	−180.1	−179.50	−0.60
0.54	−185.1	−184.65	−0.45
0.56	−189.7	−189.36	−0.34
0.58	−193.4	−193.61	0.21
0.60	−196.5	−197.43	0.93

[a] Titration of 5 mL of 4.8×10^{-5} M solution of methadone hydrochloride with 4.98×10^{-4} M solution of sodium tetraphenylboron. [b] K (1:1 complex) = 1.89×10^{-11}; E° = 164.3 mV; x = 1.053. [c] From Equation 2: σ = 0.558 mV. [d] 4.98×10^{-4} M solution of sodium tetraphenylboron.

Table II. Summary of Titration Results[a]

Sample type	Standard added, mL	Volume taken, mL[b]	V_{eq}[c] Graphical	V_{eq}[c] Curve-Fitting
Aqueous soln.	0.5[d]	5.0	0.485	0.4897
Aqueous soln.	1.0[d]	2.0	0.384	0.3849
Aqueous soln.	2.0[d]	2.0	0.750	0.7595
Aqueous soln.	4.0[d]	2.0	1.520	1.5526
Urine	0.5[e]	5.0	···	0.5066
Urine	1.0[e]	2.0	0.430	0.4445
Urine	2.0[e]	2.0	0.815	0.8502
Urine	4.0[e]	2.0	1.600	1.6346

[a] All titrations were carried out at 25 °C. The potential of the plastic electrode (vs. the reference solution) was monitored using an Orion Ionanalyzer Model 801-Digital pH meter. Titrant was a standardized solution (4.98×10^{-4} M) of sodium tetraphenylboron. [b] Volume of sample used for titration. [c] Volume of titrant necessary to reach equivalence point; equivalence point determined as described in the text. [d] Volume of 9.67×10^{-4} M stock solution of methadone hydrochloride used; diluted to 10 mL with water. [e] Volume of 9.67×10^{-4} M stock solution of methadone hydrochloride used; diluted to 10 mL with urine acidified to pH 2–3 with 5 M sulfuric acid.

data was less than a millivolt. The standard deviation was calculated as follows (Equation 2)

$$\sigma = \sqrt{\frac{\sum_{i=1}^{N} d_i^2}{N-1}} \qquad (2)$$

where σ is the standard deviation, d_i is the difference between the data point and the function at corresponding values of the independent variable (volume), and N is the number of data points.

Since the uncertainty in the potential measurement is approximately $^1/_2$ mV, almost all of the standard deviation can be ascribed to this phenomenon. The fitted equation would have described the data even better if the uncertainties in the volume measurements had been taken into account in the fitting procedure. However, the procedure was more than adequate for identifying the equivalence point, so no more refined mathematical analysis was attempted. The results of the graphical analysis and curve-fitting are presented in Table II. Any small (about 1%) difference between the two techniques appears to be well within expected experimental error.

Table III. Accuracy of the Titration of Methadone Solution with Tetraphenylboron

Sample type	Volume taken, mL	Standard added, mg/mL[a]	Concentration found, mg/mL	Recovery, %
Aqueous	5.0	0.0443	0.0435	98.2
Aqueous	2.0	0.0443	0.0420	94.8
Aqueous	2.0	0.0443	0.0420	94.8
Urine	2.0	0.0211	0.0219	103.8
Urine	2.0	0.0211	0.0217	102.8
Urine	2.0	0.0211	0.0217	102.8

[a] Calculated on the basis that one methadone tablet contained exactly 10 mg of methadone hydrochloride.

Table IV. Comparison of Single Potentiometric and Titrimetric Determinations of Methadone in Aqueous and Urine Samples

Sample type	$E_{initial}$, mV	V_{eq}, mL[a]	V_{eq}, mL[b]	Ratio[c]
Aqueous	−105	0.497	0.490	0.985
Aqueous	−88	0.319	0.385	1.207
Aqueous	−63.8	0.718	0.760	1.057
Aqueous	−46.8	1.566	1.553	0.991
Patient's urine	−77.7	0.474	0.488	1.029
Patient's urine	−67.4	0.658	0.694	1.056
Patient's urine	−59.1	0.854	0.892	1.045
Patient's urine	−47.2	1.207	1.252	1.037
Patient's urine	−32.5	1.616	2.135	1.321

[a] Obtained from initial potential measurement and solving Equation 3. [b] Calculated by curve fitting of data from potentiometric titration with tetraphenylboron. [c] $V_{eq}{}^b$ (curve fit)/$V_{eq}{}^a$ (single potential measurement).

Methadone can be determined titrimetrically to levels of 5×10^{-5} M in urine samples without prior separation, with an accuracy of ±5% (Table III) and precision of ca. 1%.

Standard addition curves for aqueous and urine solutions of methadone were constructed by plotting concentration of analyte found vs. amount added. The curves were linear with slopes very nearly equal to one, indicating the absence of any important interference in any of the samples. Identical lines resulted when either graphically or computer-generated equivalence points were used in constructing these plots. Potassium ion did not interfere in the titration, since the solubility product of potassium tetraphenylborate exceeds that of methadone tetraphenylborate by a factor of 10^5. Thus all the methadone present in the sample is titrated well before potassium tetraphenylborate concentration approaches the solubility product.

For some applications, where highest accuracy is not acquired, it is possible to estimate methadone concentration from a single potentiometric measurement. In Table IV are presented the initial potential measurements for all the ti-

trations in this study, and the equivalence point volumes calculated from these potentials, using the values of E^0 and n found in the curve-fitting for that titration in the following equation:

$$V_{eq} = \frac{W}{t} \times e^{\frac{(E - E^\circ)F}{nRT}} \quad (3)$$

In all cases the agreement between V_{eq} (calculated) and V_{eq} (curve-fit) agree within 15%, and for some applications, this is adequate. Presumably, if care were taken to maintain uniform pH and ionic strength from one sample to the next, and if the electrode were standardized periodically, E^0 and n could be maintained sufficiently constant so that by making a single potentiometric measurement, the methadone content of a sample could be calculated, or read off a calibration curve.

Thus, in conclusion a miniaturized plastic electrode is described which selectively responds to hydrophobic cations. This probe was used to monitor methadone levels directly in urine either by direct potentiometric measurement or by potentiometric titration with sodium tetraphenylboron.

APPENDIX

Derivation of the Equation Representing the Titration Curve for the Computer Curve Fitting Model. For the titration of B^+ with A^-, if it is assumed that the product of the concentrations of B^+ and A^- is constant, the amount of the anion A^- in the titrating solution can be expressed as:

$$A^- = \frac{K_{sp}(W + V)^2}{B^+} \quad (1A)$$

where K_{sp} = the ionic product of B^+ and A^-, W = initial volume of the titer solution, and V = volume of the titrant added.

The amount of the cation B^+ present in the titrating solution at any time can be expressed as:

$$B^+ = V_{eq} \cdot t - V \cdot t + A^- \quad (2A)$$

where t is the concentration of the titrant. Substituting A^- from Equation 1A in Expression 2A and rearranging yields Equation 3A.

$$B^+ = (V_{eq} - V) \cdot t + \frac{K_{sp}(W - V)^2}{B^+}$$

$$B^{+2} - (V_{eq} - V) \cdot t \cdot B^+ - K_{sp}(W + V)^2 = 0 \quad (3A)$$

This cubic equation can be solved to give a function of B^+; the concentration of B^+ is obtained by dividing the positive root of Equation 3A by the total volume in the titration cell as in Equation 4A.

$$[B^+] = \frac{(V_{eq} - V)t + \sqrt{(V_{eq} - V)^2 t^2 + 4K_{sp}(W + V)^2}}{2(W + V)} \quad (4A)$$

Assuming that the electrode responds only to the cation B^+, an equation can be written relating the electrode potential to the volume of the titrant added (Equation 5A).

$$E = E_0' + x \frac{RT}{F} \times \ln \left[\frac{(V_{eq} - V)t + \sqrt{(V_{eq} - V)^2 t^2 + K_{sp}(W + V)^2}}{2(W + V)} \right] \quad (5A)$$

where E is the electrode potential, E_0' is the standard potential of the electrode at 1 M concentration of B^+, x is the electrode response factor, and R, T, and F have their usual meanings.

LITERATURE CITED

(1) E. J. McGonigle, *Anal. Chem.*, **43**, 966 (1971).
(2) J. E. Wallace, H. E. Hamilton, J. T. Payte, and K. Plum, *J. Pharm. Sci.*, **61**, 1397 (1972).
(3) R. C. Baselt and L. J. Casarett, *Clin. Pharmacol. Ther.*, **13**, 64 (1972).
(4) J. C. Rickards, G. E. Boxer, and C. G. Smith, *J. Pharmacol. Exp. Ther.*, **98**, 380 (1950).
(5) E. L. Way, B. T. Signorotti, C. H. March, and C. Peng, *J. Pharmacol. Exp. Ther.*, **101**, 249 (1951).
(6) A. H. Beckett, M. Mitcharo, and A. A. Shihab, *J. Pharm. Pharmacol.*, **23**, 347 (1970).
(7) J. L. Valentine, P. E. Wiegart, and R. L. Charles, *J. Pharm. Sci.*, **61**, 796 (1972).
(8) T. Higuchi, C. R. Illian, and J. L. Tossounian, *Anal. Chem.*, **42**, 1674 (1970).
(9) J. R. Luch, Ph.D. Thesis, University of Kansas, Lawrence, Kansas, (1976); manuscript in preparation.
(10) R. W. Cattrall and H. Freiser, *Anal. Chem.*, **43**, 1905 (1971).
(11) R. W. Cattrall, S. Tribuzio, and H. Freiser, *Anal. Chem.*, **46**, 2223 (1974).
(12) D. J. G. Ives and G. J. Janz, "Reference Electrode, Theory and Practice", Academic Press, New York, N.Y., 1961, pp 203–207.
(13) A. Shatkay, *Anal. Chem.*, **39**, 1056 (1967).
(14) C. E. Moore, *Crit. Rev. Anal. Chem.*, **2**, 1ff (1971).
(15) H. O. Hartley, *Technometrics*, **3**, May 1961.

RECEIVED for review September 7, 1977. Accepted November 7, 1977.

Controlled-Potential Coulometric Determination of Plutonium

Michael K. Holland,* Jon R. Weiss, and Charles E. Pietri

New Brunswick Laboratory, United States Department of Energy, 9800 South Cass Avenue, Building 350, Argonne, Illinois 60439

A non-empirical method for the controlled-potential coulometric determination of plutonium has been proposed. The method utilizes an application of the Nernst equation to reduce the determination time by 40% without loss in precision or accuracy. A fraction greater than 99% of the total plutonium content was accurately determined and corrected for background current and for the fraction not electrolyzed. One hundred thirty-five standards from eleven preparations were assayed yielding a mean recovery of 100.01% with a standard deviation of 0.06% using an electrical calibration factor.

Following the proposal of analysis using controlled-potential coulometry by Hickling in 1942, early investigations required electrolysis times in excess of one hour (*1–7*). These long electrolysis times initiated the development of various time-saving improvements such as predictive and empirical end-point determinations as well as cell and stirrer modifications.

Predictive end-point methods based on the exponential current decay equation eliminate the need for electrolysis to completion (*4–8*). However, the time required in calculating

0003-2700/78/0350-0236$01.00/0 © 1978 American Chemical Society

the integrated current value often cancels the savings in electrolysis time. Application of computer techniques for predicting the integrated current value has eliminated these computational time losses (*8*). Electrolysis times for many applications have been reduced through the use of empirical end-point techniques in which the analysis is terminated at a point where the integrated current is not significantly changed by further electrolysis (*2*).

Cell modifications which increase the electrode surface to electrolyte volume ratio and improved stirring techniques which minimize the diffusion layer thickness have decreased the long electrolysis times to the several-minute range (*9–14*).

Alternatively, automated coulometric systems have substantially reduced operator time which diminishes concern about less than optimum electrolysis times (*15–17*).

A controlled-potential coulometric system with an improved cell and stirrer assembly was developed at this laboratory (*18, 19*). A further study of this method showed that the procedure could be modified to reduce the electrolysis times substantially. The modified method differs from the previously described methods in that the electrolysis of 99.6%–99.8% of the sample is to constant background current, and the end point and calculations are non-empirical.

THEORY

The controlled-potential coulometric determination of plutonium normally involves a preliminary reduction to the Pu^{3+} oxidation state. The reduction is followed by oxidation of Pu^{3+} to Pu^{4+} at a control potential approximately 0.18 V above the formal potential, $E^{o\prime}$, of plutonium in the electrolyte used (*20*). The oxidation is considered complete when the current reaches a constant value, i.e., the constant background current (*21, 22*). At this time, the control potential is equal to the potential of the Pu^{4+}/Pu^{3+} redox couple at the species concentration (that is, the potential that would be measured at an inert electrode immersed in the solution) hereafter called the solution redox potential. The solution redox potentials may be used with Equation 5 (derived below) to determine the fraction of the plutonium electrolyzed (*22, 23*).

The Nernst equation (Equation 1) may be solved for the ratio of ox/red:

$$E - E^{o\prime} = \frac{RT}{nF} \ln \frac{\text{ox}}{\text{red}} \tag{1}$$

$$\frac{\text{ox}}{\text{red}} = \exp\left[(E - E^{o\prime})/k\right] \tag{2}$$

where E is the solution redox potential, $E^{o\prime}$ is the formal potential, k is the logarithm coefficient (RT/nF which, for a one-electron reaction at 25 °C, equals 0.025692 V), ox is the fraction in the oxidized state, and red is the fraction in the reduced state. Substituting red = 1 – ox in Equation 2 and solving for ox and red:

$$\text{ox} = \frac{\exp\left[(E - E^{o\prime})/k\right]}{1 + \exp\left[(E - E^{o\prime})/k\right]} \tag{3}$$

and

$$\text{red} = 1 - \frac{\exp\left[(E - E^{o\prime})/k\right]}{1 + \exp\left[(E - E^{o\prime})/k\right]} \tag{4}$$

By substituting the solution redox potential after reduction, S_{red}, for E in Equation 3 and the solution redox potential after oxidation, S_{ox}, for E in Equation 4, the sum of ox and red is equal to the fraction of the total plutonium which was not electrolyzed for the given S_{red} and S_{ox} pair. Subtraction of the fraction not electrolyzed from unity yields the correction factor, f, i.e., the fraction of the plutonium electrolyzed, which simplifies to:

$$f = \frac{\exp\left[(S_{ox} - E^{o\prime})/k\right]}{1 + \exp\left[(S_{ox} - E^{o\prime})/k\right]} - \frac{\exp\left[(S_{red} - E^{o\prime})/k\right]}{1 + \exp\left[(S_{red} - E^{o\prime})/k\right]} \tag{5}$$

Equation 5 permits the calculation of the plutonium content of a sample for any set of reduction and oxidation potentials.

Within a range of potentials that do not cause competing reactions, the control potential may be varied during the electrolysis of a reversible couple without affecting the final correction for the fraction electrolyzed. The ability to adjust the control potential to equal the solution redox potential takes advantage of the fast initial electrolysis rate.

The modified sample reduction and oxidation cycles can be started at control potentials further away from the redox couple formal potential than the control potentials used to terminate the electrolysis. Adjusting the control potential until the current decreases to background sets the control potential equal to the solution redox potential. When the solution redox potentials are far enough from the redox couple formal potential to eliminate errors due to the uncertainty in the formal potential and in the solution redox potential measurements, accurate correction factors for quantities of material not electrolyzed can then be calculated.

For example, in the oxidation step, the accurately-known starting solution redox potential is between 0.50 and 0.52 V vs. the saturated calomel electrode, SCE. Initiating the oxidation with the control potential at +0.92 V vs. SCE, causes a rapid initial change in the solution redox potential. As the current exponentially decays, so does the rate of change of the solution redox potential. When the solution redox potential increases to an arbitrary point between 0.83 and 0.85 V vs. SCE, the control potential is adjusted to this potential, thereby ending the electrolysis at the background current. Reduction to a solution redox potential more negative than 0.52 V vs. SCE and oxidation to a solution redox potential more positive than 0.83 V vs. SCE, yields an accurate value for the fraction of the plutonium electrolyzed. Monitoring of the solution redox potential is not necessary. The time required to reach the desired reduction and oxidation solution redox potentials is very reproducible. The desired range is reached when the current is approximately 0.4% of the initial current.

EXPERIMENTAL

Apparatus and Instrumentation. The cell, composed of a gold working electrode, platinum counter electrode, and saturated calomel reference electrode, and its performance have been described in detail (*24–27*). The routine treatment and cleaning of the electrodes have also been described in detail (*25*). The controlled-potential coulometer system has been previously discussed (*28, 29*). A Hewlett-Packard 3455A digital-voltmeter was used for all voltage measurements. An electronic calibrator with a Julie Research 100-Ω precision resistor and an Electronics Research quartz crystal clock, accurate to ±0.01 s, with digital readout, was used to determine the integrator electrical calibration factor, C (*25*).

$$C = \frac{(V)(T)\ (\text{g Pu/equiv})(1000\ \text{mg/g})}{(E)(R)(F)} \tag{6}$$

where V is the voltage drop across the precision resistor of value R, T is the calibration time in seconds, E is the voltage readout of the integrated current, and F is the Faraday (96484.56 C/equiv).

Operating Conditions. Results obtained in this study were achieved using solutions prepared sufficiently in advance to ensure equilibration to room temperature. Variations in room temperature caused a shift in the electrical calibration factor. Instrument recalibration was performed whenever the room temperature shifted more than 1 °C.

Sample Material. Sample solutions containing 6–12 mg of plutonium were prepared from National Bureau of Standards SRM 949e plutonium metal and SRM 944 plutonium sulfate tetrahydrate, and subsequently fumed to dryness in sulfuric acid.

Blank Determination. A solution of three drops of saturated sulfamic acid in 20 mL of 1 N nitric acid was used as the electrolyte. Reduction was accomplished by maintaining the control potential at 0.40 V vs. SCE until the cell current dropped to 30 μA, (approximately 15 s elapsed time). The control potential was adjusted to approximately 0.20 V vs. SCE. After the current 0.50 V vs. SCE became constant (approximately 30 s), the control potential was measured using the HP 3455A DVM and the value recorded. All control potential measurements were made to 0.0001 V.

Oxidation was accomplished by maintaining the control potential at 0.92 V vs. SCE until the cell current dropped to 30 μA, (approximately 15 s elapsed time). The control potential was then adjusted to approximately 0.85 V vs. SCE. After the current became constant (approximately 30 s), the voltage readout of the integrated current and the exact time since the oxidation was initiated were recorded. A second voltage readout of the integrated current and the exact time was taken after approximately one additional minute. The control potential was then measured and the value recorded. The readout of the blank, V_0, corrected for constant background current was calculated:

$$V_0 = E_2 - (E_2 - E_1)t_2/(t_2 - t_1) \quad (7)$$

where t_1 and t_2 are the first and second elapsed times, respectively. E_1 and E_2 are the voltage readouts of the integrated current at t_1 and t_2, respectively. Meites and Moros have discussed extensively the use of Equation 7 to correct for constant background current and the use of the result, V_0, to correct for faradaic and charging background current (*30*).

Sample Determination. The fumed, dried sample was dissolved by transferring the solution on which the blank was determined to the dry sample in the cell beaker. Reduction was accomplished by maintaining the control potential at 0.40 V vs. SCE until the current level dropped below 200 μA, (approximately 4.5 min elapsed time). The current was monitored on the ammeter of the potentiostat as the control potential adjustments were made. The control potential was adjusted to the solution redox potential by increasing the control potential until constant background current was obtained. The control potential was measured using the HP 3455A DVM and the value recorded. Oxidation was accomplished by maintaining the control potential at 0.92 V vs. SCE until the current level dropped below 200 μA, (approximately 4.5 min elapsed time). The control potential was adjusted to the solution redox potential by decreasing the control potential until constant background current was obtained. The exact time since oxidation initiation and the voltage readout of the integrated current were recorded. A second voltage readout and the exact time were taken after approximately two more minutes. The control potential was measured and the value recorded. The blank, V_0, corrected for constant background current was adjusted for the solution redox potentials determined from the sample analysis. The adjusted blank, V_0', was calculated as follows:

$$V_0' = V_0\left[\frac{S_{ox} - S_{red}}{B_{ox} - B_{red}}\right] \quad (8)$$

where B_{ox} and B_{red} were the solution redox potentials at the termination of the blank oxidation and reduction, respectively. S_{ox} and S_{red} were the solution redox potentials at the termination of the sample oxidation and reduction, respectively. The readout of sample, V_1, was corrected for constant background current using Equation 7 with V_1 substituted for V_0. The sample was calculated by first determining f using Equation 5, then using Equation 9 to determine the total quantity of plutonium present:

$$\text{Pu(mg)} = (V_1 - V_0')C/f \quad (9)$$

RESULTS AND DISCUSSION

Routine plutonium coulometry shows a precision of about 0.1% to 0.2% relative standard deviation, RSD, with no significant bias, although relative standard deviations of about 0.05% have also been reported (*31*, *32*). An examination of the data in Table I shows that the improved method provides results at least comparable to the state of the art.

Table I. Determination of Plutonium Using the Present Method

Preparation	Std type	No. of aliquots[a]	Mean recovery, %	RSD, %	Standard error, %
A	949e	5	99.96	0.07	0.03
B	949e	11	100.03	0.06	0.02
C	949e	11	99.99	0.06	0.02
D	949e	9	99.99	0.03	0.01
E	944	5	100.02	0.05	0.02
F	944	17	100.01	0.07	0.02
G	944	39	100.01	0.06	0.01
H	944	11	99.98	0.05	0.02
I	944	7	100.03	0.04	0.02
J	944	18	100.02	0.05	0.01
K	944	2	100.00	0.01	0.01
Total		135	100.01	0.06	0.01

[a] 6-12 mg Pu aliquots.

Table II. Data from a Typical Determination of Plutonium

Calibration	Blank	Sample
V = 0.92004 V	B_{red} = 0.5017 V	S_{red} = 0.6093 V
T = 250.19 s	B_{ox} = 0.8494 V	S_{ox} = 0.8501 V
E = 6.0984 V	t_1 = 1.00 min	t_1 = 5.00 min
R = 100.00 Ω	t_2 = 2.00 min	t_2 = 7.00 min
	E_1 = 0.0127 V	E_1 = 10.7758 V
	E_2 = 0.0129 V	E_2 = 10.7760 V

All calculations are based on National Bureau of Standards certified values corrected for ^{239}Pu and ^{241}Pu decay. The data were collected over a one-year period to assure the long term reliability of the method. There was no difference in results based on sample size in the 6- to 12-mg plutonium range studied. These results were achieved with a 40% reduction in total analysis time. If individual blank determinations were replaced with an average blank value, an additional 10% time savings would be realized.

Typical data are given in Table II and are used in the following example. Application of Equation 6 yields C = 0.935273 mg Pu/V, Equation 7 (for the blank determination) yields V_0 = 0.0125 V, Equation 8 yields V_0' = 0.0123 V, Equation 7 (for the sample determination) yields V_1 = 10.7753 V, Equation 5 with $E^{o\prime}$ equal to 0.6742 V vs. SCE yields f = 0.997309, and finally Equation 9 yields Pu (mg) = 10.0935. It is important to note that these calculations can be readily performed using a pocket calculator while subsequent determinations are in process.

This procedure is intended for use with high-purity plutonium materials where Pu^{6+} does not exist. For plutonium-bearing samples subject to commonly encountered interferences from impurities, organic materials, salts, and where Pu^{6+} is present, plutonium oxidation state adjustment and prior separation of plutonium by the New Brunswick Laboratory anion exchange procedure is recommended (*33*).

The solution redox potential span of greater than ±0.15 V from the formal potential was mathematically selected by assigning a conservative measurement uncertainty of ±0.005 V to the formal potential and determining the span necessary to ensure an uncertainty of less than 0.01% in the correction factor, f. It should be possible, in some applications, to use a span of less than ±0.15 V to provide shorter electrolysis time without sacrificing accuracy in the determination of f, the

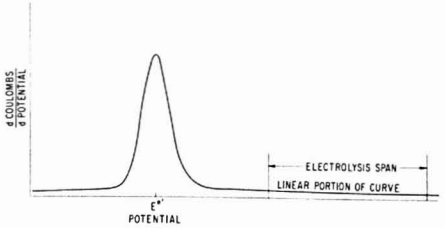


Figure 1. Differential coulogram of a faradaic constituent of the supporting electrolyte

fraction of the sample electrolyzed. However, efforts at this laboratory are being directed toward improving the accuracy of the determination of the solution redox potential and the formal potential before attempting to further decrease analysis time with a smaller potential span.

In utilizing the control potential adjustment technique, it was necessary that the dependence of the blank magnitude on the control potential span be well known. The correction of the blank for the solution redox potentials used in the sample electrolysis, Equation 8, is an experimentally verified equation based on the theory of background current (*30*). Constant background current has been corrected using Equation 7. This leaves only the faradaic and charging constituents of the blank. If it is assumed that faradaic constituents of the supporting electrolyte have formal potentials outside of the electrolysis span employed, then it can be seen from Figure 1 that the faradaic background current is proportional to the electrolysis span. From the definition that capacitance equals charge divided by voltage, it is clear that the charging (condensor) background current is proportional to the electrolysis span. Thus, the ratio of the sample potential span to the blank potential span provides a factor for correcting the blank, V_0, for the difference between the background current measured in the blank determination and the background current obtained during sample electrolysis. Since the entire blank represented less than 0.2% of the sample, the magnitude of the potential correction and its uncertainty have a negligible impact on the sample determination. Table III shows the behavior of a representative blank which has been repetitively electrolyzed. The ratio of V_0 to $B_{ox} - B_{red}$ was experimentally found to be constant which verifies the applicability of Equation 8.

The most important feature of this control potential adjustment concept is that it should be applicable to many other coulometric procedures for the determination of plutonium with only minor modification. Methods such as the ASTM controlled-potential coulometric method for plutonium which uses features such as a chemical calibration and an empirical end point, and avoids background current and individual blank corrections (*34*), should still be compatible with the control potential adjustment technique.

For the methods which use chemical calibration and are adapted to use the control potential adjustment technique, the correction for the fraction of the sample electrolyzed (Equation 5) may be eliminated, providing that the fraction of both the sample and the standard electrolyzed is the same. However, ensuring that the fraction electrolyzed for all standards and samples is the same, may prove more difficult than actually performing the correction.

There are several advantages in using this coulometric method in preference to the other coulometric methods routinely employed for the determination of plutonium. First, a non-empirical time-saving technique which is independent of the exponential decay equation is used. Second, an

Table III. Experimental Verification of Equation 8

B_{red}, V	B_{ox}, V	Blank potential span, V ($B_{ox} - B_{red}$)	Blank[a] (V_0)	$V_0/(B_{ox} - B_{red})$
0.470	0.851	0.381	0.0130	0.0341
0.470	0.841	0.371	0.0127	0.0342
0.470	0.830	0.360	0.0122	0.0339
0.470	0.820	0.350	0.0120	0.0343
0.470	0.810	0.340	0.0116	0.0341
0.470	0.800	0.330	0.0113	0.0342
0.470	0.791	0.321	0.0105	0.0340
0.470	0.780	0.310	0.0150	0.0339
0.480	0.841	0.361	0.0123	0.0341
0.490	0.841	0.351	0.0119	0.0339
0.501	0.841	0.351	0.0115	0.0338
0.511	0.841	0.330	0.0114	0.0345
0.521	0.841	0.320	0.0109	0.0341
			Average =	0.0341

[a] Corrected for constant background current (Equation 7).

electrical calibration, precise to about 0.003% RSD, eliminates the need for expensive, high quality plutonium standard materials for instrument calibration. Furthermore, since this method is based directly on the Faraday and the Nernst equation, it is capable of independent characterization of chemical standards.

Although only the Pu^{4+}/Pu^{3+} couple has been discussed, this method is applicable to other couples provided they are reversible.

LITERATURE CITED

(1) A. Hickling, *Trans. Faraday Society*, **38**, 27 (1942).
(2) J. J. Lingane, "Electroanalytical Chemistry", 2nd ed., Interscience Publishers, New York, N.Y., 1958, pp 452, 462–463.
(3) P. Delahay, "New Instrumental Methods in Electrochemistry", Interscience, New York, N.Y., 1954, pp 287–289.
(4) W. M. MacNevin and B. B. Baker, *Anal. Chem.*, **24**, 986 (1952).
(5) S. Hanamura, *Talanta*, **9**, 901 (1962).
(6) L. Meites, *Anal. Chem.*, **31**, 1285 (1959).
(7) S. Hanamura, *Talanta*, **2**, 278 (1959).
(8) F. B. Stephens, F. Jakob, L. P. Rigdon, and J. E. Harrar, *Anal. Chem.*, **42**, 764 (1970).
(9) A. J. Bard, *Anal. Chem.*, **35**, 1125 (1963).
(10) W. D. Shults, "Standard Methods of Chemical Analysis", 6th ed., Vol. 3, Part A, F. J. Welcher, Ed., D. Van Nostrand, Princeton, N.J., 1966, Chapter 23.
(11) G. L. Booman, *Anal. Chem.*, **29**, 213 (1957).
(12) G. C. Goode and J. Herrington, *Anal. Chim. Acta*, **33**, 413 (1965).
(13) R. G. Clem, F. Jakob, D. H. Anderberg, and L. D. Ornelas, *Anal. Chem.*, **43**, 1398 (1971).
(14) R. G. Clem, *Anal. Chem.*, **43**, 1853 (1971).
(15) G. E. Peoples, S. A. Malone, J. R. Weiss, A. W. Wenzel, and C. E. Pietri, *U.S. Energy Res. Dev. Administration Rep.*, **NBL-277**, 80 (1976).
(16) J. P. Phillips, "Automatic Titrators", Academic Press, New York, N.Y., 1959, Chapter VI.
(17) G. Phillips, D. A. Newton, and J. D. Wilson, *J. Electroanal. Chem.*, **75**, 77–96 (1977).
(18) E. F. Groh, D. A. Cassidy, and J. R. Weiss, Application for Patent, Attorney's Docket Number S-48147 (1977).
(19) G. E. Peoples, S. A. Malone, M. K. Holland, J. R. Weiss, and C. E. Pietri, *U.S. Dept Energy Rep.*, **NBL-288**, in preparation.
(20) O. J. Wick, Ed., "Plutonium Handbook — A Guide to the Technology", Vol. 2, Gordon and Breach Science Publishers, New York, N.Y., 1967, p 712.
(21) R. A. Day, Jr., and A. L. Underwood, "Quantitative Analysis", 2nd ed., Prentice-Hall, Englewood Cliffs, N.J., 1967, p 243.
(22) F. A. Scott and R. M. Peekema, *U.S. At. Energy Comm. Rep.*, **HW-58491** (1958).
(23) W. D. Shults, *Talanta*, **10**, 833 (1963).
(24) K. Lewis, *U.S. At. Energy Comm. Rep.*, **NBL-265**, 58 (1972).
(25) R. J. Greer, G. E. Peoples, S. A. Malone, J. R. Weiss, A. W. Wenzel, and C. E. Pietri, *U.S. Energy Res. Dev. Administration Rep.*, **NBL-277**, 71 (1976).
(26) S. A. Malone, R. J. Greer, and G. E. Peoples, *U.S. Energy Res. Dev. Administration Rep.*, **NBL-277**, 86 (1976).
(27) R. J. Greer, C. E. Pietri, J. R. Weiss, and A. W. Wenzel, *U.S. Energy Res. Dev. Administration Rep.*, **NBL-277**, 89 (1976).
(28) J. E. Harrar and E. Behrin, *Anal. Chem.*, **39**, 1230 (1967).
(29) Controlled-Potential Coulometry System Model 3 Operating and Service Manual, M-T Electronics Co.

(30) L. Meites and S. A. Moros, *Anal. Chem.*, **31**, 23 (1959).
(31) Safeguards Analytical Laboratory Evaluation, *U.S. Energy Res. Dev. Administration Rep.*, **NBL-282** (1976).
(32) Safeguards Analytical Laboratory Evaluation, *U.S. Energy Res. Dev. Administration Rep.*, **NBL-283** (1977).
(33) J. R. Weiss, C. E. Pietri, A. W. Wenzel, and L. C. Nelson, Jr., *U.S. At. Energy Comm. Rep.*, **NBL-265** (1972).
(34) "1976 Annual Book of ASTM Standards", American Society for Testing and Materials, Easton, Md., (1976), Part 45, Nuclear Standards, pp 211–214.

RECEIVED for review August 10, 1977. Accepted November 3, 1977.

Chromatographic Determination of Chromium(VI) with Coulometric Detection Based on the Electrocatalysis by Adsorbed Iodine of the Reduction at Platinum Electrodes in Acidic Solutions

J. H. Larochelle[1] and D. C. Johnson*

Department of Chemistry, Iowa State University, Ames, Iowa 50011

Adsorbed iodine at a Pt electrode is demonstrated to be an electrocatalyst for the irreversible electrochemical reduction of Cr(VI) in HCl and H_2SO_4 solutions. Determination of Cr(VI) in a coulometric flow-through electrode is possible in the range 0.4 ng to 80 μg. No interference by dissolved O_2 is observed. Application of the coulometric detector for chromatographic determinations of Cr(VI) is presented.

The maximum concentration of Cr(VI) presently permitted in drinking water by the Safe Drinking Water Act (*1*) is 0.05 μg/mL (50 ppb). Cr(III) is of less concern and, consequently, analytical techniques must be specific for Cr(VI).

We have been interested in the development of a general methodology for determining ionic species at trace levels in complex aqueous samples based on liquid chromatographic separation with in-stream amperometric and coulometric detection (*2–5*). Results of this work have convinced us that determinations of many species by this technique can be made with detection limits at the part-per-billion level or lower (*3, 5*). We report here the determination of Cr(VI) without interference from a large number of inorganic species including oxygen by liquid chromatography with coulometric detection.

Iodine is rapidly adsorbed at Pt electrodes in acidic solutions of iodide salts (*6–8*). A maximum of approximately 1.5×10^{-9} mol/cm^2 is adsorbed from solutions containing as little as 2 μM NaI. The adsorption is irreversible and desorption does not readily occur even if the electrode surface is bathed with pure water. Lane and Hubbard (*9*) determined that the I^- from solution is adsorbed as a neutral species, whereas F^-, Cl^-, and Br^- are adsorbed as anions. Adsorbed I is removed at large positive potential ($E > 1.2$ V vs. SCE in 1.0 M H_2SO_4) with concurrent oxidation to IO_3^- (*7*). The surface of the Pt electrode is oxidized simultaneously. No adsorption of I occurs at a Pt surface covered with oxide (*6–8*).

Electrocatalysis of several irreversible reactions by halogens adsorbed at Pt electrodes has been reported. Anson (*10*) determined that adsorbed Br^- catalyzed the oxidation of the EDTA-Co(II) anion. Hubbard and co-workers (*11–14*) reported the accelerating influence of free halide ions on the interconversion of Pt(II) and Pt(IV) complexes at Pt electrodes. Davenport and Johnson (*15*) reported the electrocatalysis of the irreversible oxidation of Sb(III) by adsorbed I and Taylor and Johnson (*3*) applied the electrocatalyzed reaction for determination of Sb(III) by liquid chromatography with coulometric detection. Lane and Hubbard (*16*) reported the electrocatalysis of the oxidation of ascorbic acid by adsorbed I at a Pt electrode. Recently, Johnson and Resnick (*17*) reported that the reduction of Fe(III) in $HClO_4$ solutions is irreversible in the absence of traces of dissolved halides but is dramatically catalyzed by addition of halide salts, including I^-, at micromolar levels.

The $Cr_2O_7^{2-}$–Cr^{3+} system is well known to be irreversible at Pt electrodes in acidic solutions (*18*). The cathodic reduction of $Cr_2O_7^{2-}$ was reported by Kabasakaloglu and Uneri (*19*) to occur at the same potential as for reduction of Pt oxide. These factors are undoubtedly responsible for the observed deviations of the potentiometric titration curve from theory for the titration of Fe^{2+} by $Cr_2O_7^{2-}$. The deviation occurs when the $Cr_2O_7^{2-}$–Cr^{3+} couple is predominately responsible for establishing the electrode potential, i.e., beyond the equivalence point (*20*). Liteanu and Haiduc (*21*) studied the effects of various electrode pretreatment and observed that the titration curve was closer to theory when the Pt electrode was pretreated by oxidation with *aqua regia* followed by reduction of the surface oxide with an iodide solution. They noted that iodide is adsorbed at Pt electrodes.

EXPERIMENTAL

Reagents. All chemicals were Baker Reagent Grade except as specified. Water was triply distilled with deionization in a mixed-bed ion-exchange column after the first distillation and the second distillation was from alkaline permanganate solution. The separation column was prepared from Fisher A-540 Adsorption Alumina which was ground wet with a porcelain mortar and pestle. The ground alumina was then sieved while being flooded with deionized water to facilitate the sieving process. A retainer of sintered glass was constructed in one end of the glass tube to be used for the chromatographic column by partial fusion of a plug of finely ground glass. The column was filled by transfer of a water slurry of the 180–250 mesh fraction of the ground alumina. Water was drawn out of the tube during packing by gentle suction applied to the tube end with the sintered plug. The column was installed in the chromatograph so that the sintered glass retainer was at the low pressure end of the packed column, thereby preventing loss of alumina due to eluent flow.

Instrumentation. Preliminary voltammetric data were obtained with a rotating Pt-disk electrode (RPtDE) with an area of 0.47 cm^2. The electrode was constructed by Pine Instrument

[1] Present address, Department of Chemistry, St. John's University, Collegeville, Minn. 56321.

0003-2700/78/0350-0240$01.00/0 © 1978 American Chemical Society

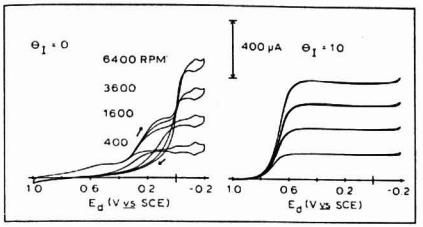


Figure 1. I_d–E_d curves for Cr(VI) at RPtDE in 1.0 M H_2SO_4. 2×10^{-4} M $Cr_2O_7^{2-}$; 2.0 V/min scan; θ_I = fractional surface coverage of electrode by adsorbed I

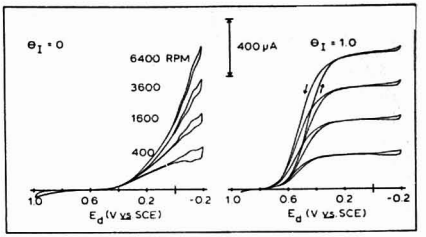


Figure 2. I_d–E_d curves for Cr(VI) at RPtDE in 1.0 M HCl. 2×10^{-4} M $Cr_2O_7^{2-}$; 2.0 V/min scan; θ_I = fractional surface coverage of electrode by adsorbed I

Co. of Grove City, Pa., and was rotated in a PIR rotator also from Pine Instrument Co.

The liquid chromatograph was essentially that described in Reference 2. The volume of the sample loop was 0.504 mL and the glass chromatographic column had internal dimensions of 2 × 80 mm. The flow-through detector was the packed Pt tubular electrode designated Detector C in Reference 2. Instrumentation for potentiostatic control of the detector potential, current measurement, and peak integration was constructed in our laboratory from operational amplifiers according to conventional designs. Some recorded chromatographic peaks were integrated by a Kueffel and Esser compensating planimeter.

Procedures. Activation of the RPtDE was achieved by immersion into a solution of approximately 0.1 M NaI followed by rinsing with distilled water. Activation of the chromatographic detector was achieved by injecting several 0.5-mL samples of 0.1 M KI into the chromatographic system.

Preliminary investigations with the flow-through electrode were performed without the presence of the alumina column in the liquid chromatograph. Aqueous solutions of 0.01668 M (0.1001 N) $K_2Cr_2O_7$ were injected into a water stream which was subsequently mixed with a reagent stream of 4.0 M HCl. The resultant stream passed through the detector. Study of the effects of fluid flow rate in the detector was made by controlling the sample stream at 0.1–0.2 mL/min and varying the reagent stream from 0.1–5 mL/min.

The separation procedure ultimately determined to provide the most satisfactory analytical results was as follows: The aqueous sample of Cr(VI) was injected into a stream of 0.18 M HCl flowing through the alumina column at 0.5 mL/min. Seven minutes after sample injection, the eluent was changed to 1.8 M HCl to bring about elution of Cr(VI) from the column. The effluent was continuously mixed with the stream of 4.0 M HCl flowing at 3.0 mL/min prior to passage through the detector. Complete elution occurred within 5 min at which time the eluent was changed to 4.0 M HCl to wash the column and ensure complete desorption of all sample components. After a 4-min washing, the eluent was changed back to 0.18 M HCl. Injection of a subsequent sample was delayed until 4 min after the final eluent change to ensure the complete removal of 4.0 M HCl from the chromatograph.

Water Sample. A water sample (No. 10334) was obtained from the Veterinary Diagnostic Laboratory at Iowa State University. The sample was obtained from the effluent stream of a tannery and had been acidified with 10% by volume of concentrated HCl. Dilution of the sample was necessary prior to analysis to decrease the HCl concentration. A 1.00-mL aliquot of the sample as received was pipetted into each of six 50-mL volummetric flasks. To the flasks were added sequentially 0.00, 0.25, 0.50, 1.00, 1.50, and 2.00-mL aliquots of a standard aqueous solution containing 1.73 ppm Cr(VI) was $K_2Cr_2O_7$. The contents of each flask were diluted to volume, mixed, and analyzed.

RESULTS AND DISCUSSION

Electrocatalysis at RPtDE. Current–potential (I–E) curves obtained at the RPtDE for reduction of Cr(VI) are shown in Figure 1 for a supporting electrolyte of 1.0 M H_2SO_4 and in Figure 2 for 1.0 M HCl. The I–E curves shown were obtained at four values of rotational velocity for the presence

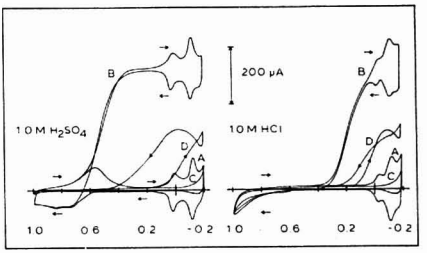


Figure 3. I_d–E_d curves for O_2 at RPtDE in 1.0 M H_2SO_4 and 1.0 M HCl. 2×10^{-4} M $Cr_2O_7^{2-}$; 6.0 V/min scan; (A) residual, 0 μM I^-; (B) air saturated, 0 μM I^-; (C) residual, 4 μM I^-; (D) air saturated 4 μM I^-

and absence of adsorbed I on the electrode surface. With the absence of adsorbed I, the cathodic waves are markedly irreversible. The current appears to approach a limiting value in the region of $E < 0.1$ V and it may be possible that hydrogen adsorbed on the Pt electrode for $E < 0.0$ V electrocatalyzes the reduction process. The apparent reversibility of the reduction of Cr(VI) is dramatically improved by the presence of adsorbed I at the electrode surface. In both solutions extensive potential ranges exist, as a result of the adsorbed I, for which the cathodic current is potential independent and appears limited by the rate of mass transport. A linear plot with zero intercept was obtained for the limiting current measured in the plateau region of the I–E curves for each electrolyte as a function of the square root of rotational velocity for velocities <1600 rev/min (<168 rad/s).

Cathodic applications of Pt electrodes in acidic solutions at potentials more negative than 0.5 V are usually subject to interference by dissolved O_2 which is reduced in this potential region. I–E curves for air-saturated solutions of 1.0 M H_2SO_4 and 1.0 M HCl are shown in Figure 3. Curves are also shown which were obtained following addition of 4 μM NaI to the solutions. Residual I–E curves obtained following deaeration with N_2 are shown for reference. This concentration of I^- is sufficient for the formation of a complete monolayer of adsorbed I at the Pt electrode surface but the anodic wave for oxidation of bulk I^- is insignificant at the current sensitivity used for recording these curves. Virtually identical results are obtained if the electrode is dipped in a solution of NaI and rinsed with distilled water prior to placement in the test solution. The presence of adsorbed I significantly inhibits reduction of O_2 under these conditions. Judging from the I–E curves in Figures 1 and 2, a potential in the range 0.2–0.5 V for 1.0 M H_2SO_4 and 0.2–0.3 V for 1.0 M HCl is suitable for amperometric detection of Cr(VI) without interference from dissolved O_2. The analytical results reported here for the flow-through detector were obtained with HCl as the sup-

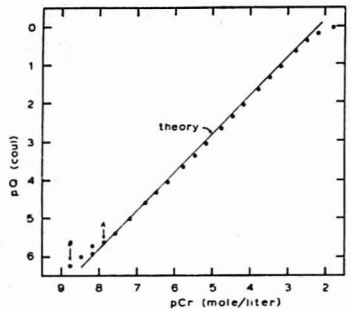


Figure 4. Calibration curve for Cr(VI) in flow-through detector. (A, B) see Figure 5

porting electrolyte. The choice was made because of the lower level of electrical noise observed for the HCl in comparison with the H_2SO_4 solutions. The source of noise related to the identity of the electrolyte is not yet clearly understood.

Voltammetry in the Tubular Detector. The voltammetric behavior of an electroactive species can be obtained for a flow-through detector by plotting peak currents observed for sequential injections of the analyte into the electrolyte stream as a function of electrode potential. The detector potential is maintained constant during the period of a single current peak and changed by a small increment prior to the succeeding injection. Just as useful are plots of Q vs. E where Q is the time integral of the current peak obtained for a single injection. Based on our experience, values of $E_{1/2}$ calculated from data obtained by either method are virtually identical. This technique is particularly useful for qualitative study of an electroactive component of an unknown mixture separated by the chromatographic system. Q-E data were obtained for Cr(VI) injected into the chromatographic system without the presence of the alumina column. The value of $E_{1/2}$ was approximately 0.6 V in fair agreement with Figure 2.

Detector Efficiency. The electrolytic efficiency of the detector was determined at 0.25 V as a function of the flow rate of the combined sample and reagent streams. The efficiency was calculated for a reduction of Cr(VI) to Cr(III). The average efficiency was ≥98% for $V_f \leq 1.0$ mL/min.

A coulometric detector (100% efficiency) has the advantage of being an absolute detector. The number of moles (N) of the electroactive analyte corresponding to a chromatographic peak is calculated from Q using Faraday's law.

$$N = Q/nF$$

Departure from coulometric efficiency does not detract from analytical applicability so long as a means of calibration is available and the electrolytic efficiency does not vary significantly with time.

Calibration. Values of pQ (coul) are plotted in Figure 4 as a function of pCr (mol/L Cr). The calibration is linear for the approximate range pCr = 7.8–2.5 which corresponds to 0.4 ng–80 μg Cr. The volume of the sample loop was 0.504 mL and 0.4 ng Cr(VI) corresponds to approximately 0.8 part per billion. The detector response for injections of 1.33×10^{-8} M and 1.67×10^{-9} M Cr(VI) (points A and B in Figure 4) is shown in Figure 5 together with the response to blank injections. All data in Figure 4 were corrected for the blank.

Negative deviation from linearity at high concentrations undoubtedly occurs because large cell currents passing through the region of uncompensated resistance can produce significant departure of the potential drop across the electrode–solution interface from the value of 0.25 V applied by the potentiostat

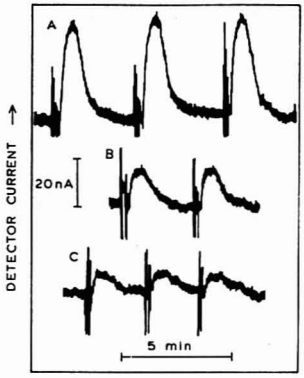


Figure 5. Detector response at low Cr(VI) concentrations. (A) 1.33×10^{-8} M (0.349 ng); (B) 1.67×10^{-9} M (43.8 pg); (C) blank

to a value at which the reaction is not mass-transport limited. The analyst is advised to consider dilution of highly concentrated samples prior to analysis.

The fact that a linear calibration curve is applicable over nearly six decades in the concentration range makes the electrochemical detector somewhat unique among detectors for liquid chromatography. Furthermore, the detection limit is very impressive. By way of comparison, we estimate that equivalent spectrophotometric detection at 0.001 absorbance unit for 0.8 ppb Cr(VI) in a 1-cm cell would require production of a metallochromic compound having a molar absorptivity of approximately 7×10^4 L/mol-cm. There was no evidence in later chromatographic experiments for movement of the Cr(VI) band on the alumina column during extensive elution with 0.18 M HCl and the authors are certain that sample loops much larger than 0.5 mL could be used to achieve detection of Cr(VI) at concentrations much less than 0.8 ppb.

Chromatographic Separations. The requirements set for the chromatographic separation were as follows: quantitative retention of $Cr_2O_7^{2-}$ from aqueous samples by the column packing; rapid elution of cationic and neutral components of the sample; separation of $Cr_2O_7^{2-}$ from common electroactive anionic species; and elution of $Cr_2O_7^{2-}$ in a narrow band by a dilute acid compatible with the detection system. Several popular packing materials capable of anion exchange were tested using both dilute H_2SO_4 and HCl as eluents. The most satisfactory results were obtained with alumina as the packing material and dilute HCl as the eluent. The exact conditions for separation were described in a previous section.

Cations present in samples of $Cr_2O_7^{2-}$ are not retained by the alumina column and, therefore, cannot interfere with the separation. Metal cations which may possibly be deposited on the detector at potentials used for detecting Cr(VI) were not tested for their interferences because they can be easily shunted around the detector by slight modification of the chromatographic design.

The common monovalent anions NO_3^-, Br^-, I^-, F^-, ClO_4^-, and CH_3COO^- are not electroactive at 0.25 V and are not adsorbed by the alumina. Hence, they produce no interference either chromatographically or electrochemically. High concentrations (>0.1 M) of SO_4^{2-}, HPO_4^{2-} and PO_4^{3-} were observed to affect the separation by displacement of adsorbed $Cr_2O_7^{2-}$. Of the electroactive anions NO_2^-, MnO_4^-, BrO_3^-, and IO_3^-, only IO_3^- was found to be adsorbed significantly by the alumina. However, Cr(VI) was resolved from IO_3^- by the

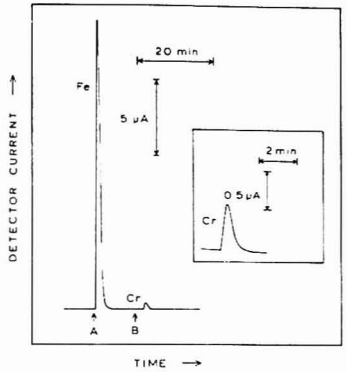


Figure 6. Chromatogram of water sample. (A) sample injection; (B) eluent switched from 0.18 M HCl to 1.8 M HCl; inset shows only Cr(VI) peak recorded at higher sensitivity

prescribed chromatographic procedure.

Precision. Replicate analysis of samples containing Cr(VI) throughout the range 90 ppb–3.5 ppm produced results with average deviations less than 2%. The areas of I–t recordings for this concentration range were measured on the recorder chart with a planimeter. Accurate electronic integration was possible for concentrations above 3.5 ppm and the average deviation for replicate analyses was approximately 0.3%.

Water Sample. A water sample containing Cr(VI) was supplied by the Veterinary Diagnostic Laboratory of Iowa State University. The sample had been acidified with HCl prior to receiving and was consequently diluted as described in a previous section. Chromatograms for the sample obtained at two recorder sensitivities are shown in Figure 6. The large peak obtained shortly after sample injection resulted predominately from reduction of Fe(III) in the sample. The concentration of Cr(VI) was determined by the technique of standard additions to be 1.04 ppm.

ACKNOWLEDGMENT

The authors are grateful to Ronda Snider and H. Mike Stahr of the Veterinary Diagnostic Laboratory for providing the water sample.

LITERATURE CITED

(1) *Fed. Registr.*, **40**, No. 248 (1975).
(2) D. C. Johnson and J. H. Larochelle, *Talanta*, **20**, 959 (1973).
(3) L. R. Taylor and D. C. Johnson, *Anal. Chem.*, **45**, 262 (1974).
(4) R. J. Davenport and D. C. Johnson, *Anal. Chem.*, **45**, 1971 (1974).
(5) R. W. Andrews and D. C. Johnson, *Anal. Chem.*, **48**, 1056 (1975).
(6) V. E. Kazarinov and N. A. Balashova, *Dokl. Akad. Nauk SSSR*, **134**, 864 (1960).
(7) A. T. Hubbard, R. A. Osteryoung and F. C. Anson, *Anal. Chem.*, **38**, 692 (1966).
(8) D. C. Johnson, *J.. Electrochem. Soc.*, **119**, 331 (1972).
(9) R. F. Lane and A. T. Hubbard, *J. Phys. Chem.*, **79**, 808 (1975).
(10) F. C. Anson, *J. Electrochem. Soc.*, **110**, 436 (1963).
(11) J. P. Cushing and A. T. Hubbard, *J. Electroanal. Chem.*, **23**, 183 (1969).
(12) A. L. Y. Lan and A. T. Hubbard, *J. Electroanal. Chem.*, **24**, 237 (1970); *ibid.*, **33**, 77 (1971).
(13) C. N. Lai and A. T. Hubbard, *Inorg. Chem.*, **11**, 2081 (1972).
(14) R. F. Lane and A. T. Hubbard, *J. Phys. Chem.*, **77**, 1401, 1411 (1973).
(15) R. J. Davenport and D. C. Johnson, *Anal. Chem.*, **45**, 1755 (1973).
(16) R. F. Lane and A. T. Hubbard, *Anal. Chem.*, **48**, 1287 (1976).
(17) D. C. Johnson and E. W. Resnick, *Anal. Chem.*, **49**, 1918 (1977).
(18) I. M. Kolthoff, *Chem. Weekblad.*, **16**, 450 (1919).
(19) M. Kabasakologlu and S. Uneri, *Commun. Fac. Sci. Univ. Ankara, Ser. B*, **14**, 59 (1967); *Chem. Abstr.*, **70**, 173524d (1967).
(20) H. A. Laitinen and W. E. Harris, "Chemical Analysis", 2nd ed., McGraw-Hill Book Co., New York, N.Y., 1975, pp 286–290.
(21) C. Liteanu and I. Halduc, *Rev. Roum. Chim.*, **14**, 1039 (1969).

RECEIVED for review August 29, 1977. Accepted November 14, 1977. Work supported by the National Science Foundation through grant GP-40646X.

Determination of Polycyclic Aromatic Hydrocarbons in the Environment by Glass Capillary Gas Chromatography

Walter Giger* and Christian Schaffner

Swiss Federal Institute for Water Resources and Water Pollution Control (EAWAG), CH-8600 Dübendorf, Switzerland

Polycyclic aromatic hydrocarbons (PAH) are isolated by a sequence of solvent extraction, gel filtration, and adsorption chromatography. The separation of the PAH concentrates into quantifiable individual constituents is then achieved by glass capillary gas chromatography using 20-m long capillaries coated with SE-52. Precision and accuracy of the determination of five individual PAH are presented. Representative analyses are reported for samples of recent lake and river sediments, river particulates, street dust, and airborne particulates. Benzo[*a*]pyrene levels in surface sediments range from 0.2 to 0.6 μg/g dry material and in river particulates and street dust from 2 to 4 μg/g. A sample of airborne particulates contained 40 μg benzo[*a*]pyrene per g.

Polycyclic aromatic hydrocarbons (PAH) have long been recognized as hazardous environmental chemicals. Several members of this class of compounds show considerable carcinogenic activity (*1*, *2*).

Analytical methods for PAH are basically three-step procedures: (1) Extraction and isolation of the PAH from the sample matrix, (2) Separation of the PAH mixture into subgroups or individual constituents, (3) Characterization of these subgroups or compounds (identification and quantitative determination). Two facts call for a quantitative determination of individual PAH in environmental samples. First, the biological activity of a particular chemical is very much dependent on its structure. It is well established, for example, that of the two isomeric benzopyrenes, only the asymmetric benzo[*a*]pyrene shows a carcinogenic activity (*1*, *2*). Second, if extensive characterization of PAH mixtures is based on analyses of individual constituents rather than unresolved mixtures, we can improve our ability to describe the sources and the fates of these chemicals in the environment.

We are involved in studies of the origin and fate of a number of different organic compounds in the aquatic environment. Within this area of interest, we have been investigating PAH in recent lake sediments (*3*). In this paper we present our methods which are used to achieve quantitative determi-

0003-2700/78/0350-0243$01.00/0 © 1978 American Chemical Society

nations of individual PAH in various environmental samples. PAH are isolated by a two-step column chromatography procedure and are subsequently analyzed by glass capillary gas chromatography. A limited number of representative analyses will demonstrate the feasibility of our procedures.

EXPERIMENTAL

Materials. All solvents were of "Nanograde" quality (Mallinckrodt Inc., St. Louis, Mo.) and were used without further purification. Glass-fiber extraction thimbles (Keller, Basel, Switzerland) were cleaned in potassium dichromate–sulfuric acid solution, washed with tap and distilled water, and dried at elevated temperature (approx. 120 °C). Granulated copper was activated by stirring in 2 N hydrochloric acid, washing with water and methanol, and vacuum drying.

Sephadex LH-20 (Pharmacia Fine Chemicals, Uppsala) was conditioned in benzene–methanol (1:1) and washed with the same solvent after wet packing into the column. Silica gel (Kieselgel 40, 70–230 mesh, Merck) was activated for 17 h at 260 °C.

PAH and alkane reference compounds (Fluka, Buchs, Switzerland, and K&K Laboratories, Plainview, N.Y.) and the internal GC-standard 1-chlorotetradecane (Fluka, Buchs) were used as received from the suppliers.

Samples and Sample Preparation. The lake sediment samples were taken with a gravity coring device; river sediments were collected with a grab sampler. All sediment samples were frozen immediately after recovery. The cores were then sectioned into layers of 3–5 cm. Samples of 30 to 70 g wet sediment were frozen in a cooled isopropanol bath under continuous rotation. Subsequently the samples were evaporated and freeze-dried. Lyophilization times varied between 4 and 14 h at a pressure of approximately 0.05 Torr. Freeze drying of the samples was chosen because it allows a much cleaner sample storage and handling. No significant losses of the compounds of interest were observed. Air drying at slightly elevated temperatures (40 °C, over-night) has been checked and can also be used with no detrimental effects. River particulates were obtained by filtering river water through pre-extracted paper filters (2-μm pore size), followed by air drying. Airborne particulate matter was sampled on glass fiber filters in the urban area of Zurich by the Institute of Hygiene of the Swiss Federal Institute of Technology. Street dust was swept from a street with heavy motor traffic in Dübendorf.

Extraction and Isolation of PAH (Figure 1). The dry samples (corresponding to approximately 20 g wet sediment) were Soxhlet-extracted in glass-fiber thimbles with methylene chloride (70 mL) for 6 h. Longer extraction times (an additional 20 h) did not provide significantly higher yields (less than 5%). Extraction was performed with methylene chloride because this solvent is low boiling, easily purified, and provides a sufficient extraction yield for the relatively nonpolar substances of interest. In our opinion, methylene chloride can adequately replace the toxicologically suspicious benzene. The extracts were concentrated to 3 mL in a rotary evaporator at room temperature.

After adjusting the volume of the extract to a known value (1, 2, or 5 mL), the weight of the extractable matter was measured using a Cahn 4100 electrobalance. Small aliquots (10–40 μL) were transferred with a microliter syringe to the aluminum pan of the balance, and weighed after cautious air-drying on a hot plate.

Elemental sulfur was then removed from the extracts by percolating through a column of activated copper (12 g). The methylene chloride eluates were carefully evaporated to dryness, taken up in 2 mL of benzene–methanol (1:1), and subjected to gel permeation/adsorption chromatography. For this purpose Sephadex LH-20 (20 g) in benzene–methanol (1:1) was packed in a glass column (50 × 1.6 cm). The same solvent mixture was used to elute two fractions of 50 mL each. Another 50 mL was then used to flush the column before applying the next sample. The column chromatography on Sephadex LH-20 is influenced simultaneously by exclusion and adsorption processes. In the way it is used in our procedure (i.e., as a simple, coarse prefractionation technique), it is favorably characterized by its speed, the high column capacity, and the possibility of reusing the column for many samples. Both fractions were cautiously evaporated to dryness (rotary evaporator, reduced pressure, approximately 30 °C), taken up in 1 mL of *n*-pentane, and applied to silica gel columns (1-cm i.d., 10-mL bed volume). Twenty-five mL of

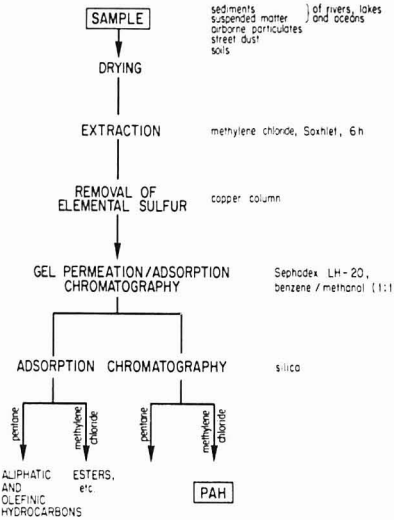


Figure 1. Procedure for the isolation of polycyclic aromatic hydrocarbons from environmental samples

pentane and 25 mL of methylene chloride yielded two eluates of low and medium polarity, respectively. Column chromatography was performed under a slight pressure of nitrogen, giving flow rates of approximately 2 mL/min. The cutpoints of these separation steps were established based on the elution volumes of naphthalene and coronene.

This separation procedure provided two sufficiently pure concentrates: aliphatic and olefinic hydrocarbons in the pentane eluate of the first Sephadex fraction, and polycyclic aromatic hydrocarbons in the methylene chloride fraction of the material which had been more retained on the Sephadex column (i.e., second Sephadex fraction). The PAH concentrates could also be characterized by low voltage mass spectroscopy after probe distillation (*4*). We have not encountered any cases where it would be recommendable to perform the complex formation step with trinitrofluorenone which was included in the method of Giger and Blumer (*4*). The fraction weights were determined by the same procedure used for weighing the total extracts.

Gas Chromatography. For subsequent GC analyses, the samples were concentrated at room temperature in a stream of nitrogen to volumes of 0.1–0.2 mL. The internal standard (1-chlorotetradecane) was added as a hexane solution yielding a concentration of 1–10 μg of internal standard per sample.

Gas chromatography was performed on a Carlo Erba apparatus (Model 2101 AC) with a flame ionization detector. Two types of inlet ports with built-in septum flushing were used. One type is manufactured by Carlo Erba, Milan, according to Grob and Grob (*5*). The second type (called Model 76) is a modified version (*6*) and was purchased from Brechbühler AG, Urdorf, Switzerland. The glass capillary columns (20 m × 0.3 mm) were kindly supplied by K. and G. Grob. SE-52 was the stationary phase chosen for quantitative determinations, whereas many qualitative analyses have been performed with OV-101 columns. Columns prepared by the barium carbonate procedure (*7*) were best suited for quantitative work. The lifetime of the capillary columns was four to six months of daily use, corresponding to about 240 GC runs.

Aliquot samples of 1–2 μL were injected without stream splitting onto the column at ambient temperature. The injector temperature was held at 270 °C. After 30 s, the split valve was opened, allowing the septum and injection port to be purged at a flow rate of 50 mL/min. Subsequent to the elution of the solvent, the oven temperature was raised rapidly to 60 °C and then at 2.5 °C/min up to 250 °C. Hydrogen was used for carrier

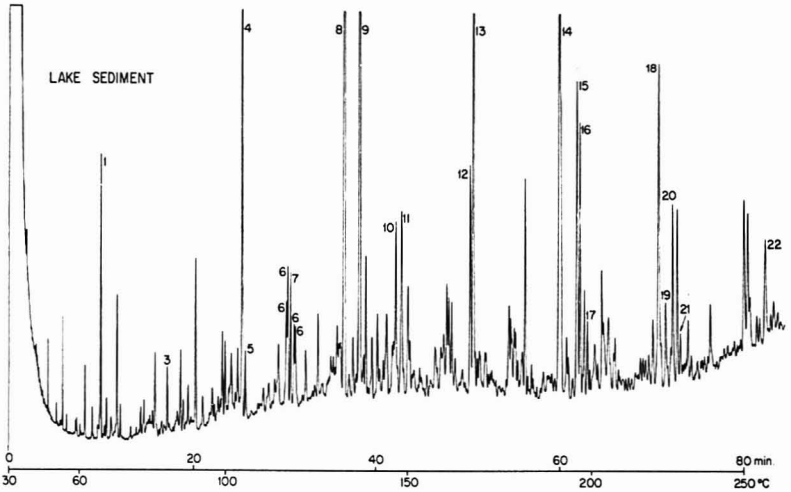


Figure 2. Gas chromatogram of polycyclic aromatic hydrocarbons isolated from the surface layer (0–3 cm) of recent lake sediments (Greifensee, Switzerland). Numbers refer to identified components listed in Table I. S: internal standard. GC conditions: 20 m × 0.3 mm i.d. glass capillary column with barium carbonate interlayer and coated with SE-52, 0.8 atm hydrogen as carrier gas, flame ionization detector, column at ambient temperature during injection and elution of the solvent, then programmed from 60 °C to 250 °C at a rate of 2.5°/min

gas with the flow adjusted so that coronene eluted at about 250 °C from columns with 0.1-μm thick films. Back pressures of approximately 0.5–1.0 atm were needed depending on the particular column dimensions. Our GC procedure basically follows the description given by Grob and Grob (*5*).

Electronic integration of the gas chromatographic peak areas was performed by a digital integrator (Minigrator, Spectra-Physics).

Procedure Blank and Recoveries. An empty thimble was extracted in the Soxhlet apparatus with 70 mL of methylene chloride for 6 h. The extract was then carried through the entire procedure as described above. The resulting gas chromatograms of several such blank analyses did not display any peaks interfering with the compounds of interest.

The recovery studies were performed using a standard mixture containing approximately 5 μg of each constituent. This solution was analyzed omitting the extraction step.

Gas Chromatography/Mass Spectrometry. For mass spectrometric identification and mass specific detection, a Finnigan GC/MS system (Model 1015 D) combined with an on-line computer (Model 6000) was used. The glass capillary column was directly coupled to the mass spectrometer by means of a platinum capillary. Helium was used for carrier gas. The MS operating conditions were: electron energy, 70 eV; emission current, 350 μA; preamplifier sensitivity, 10^{-6} A/V.

RESULTS AND DISCUSSION

Qualitative Analysis. Figure 2 shows a typical gas chromatogram of a PAH mixture isolated from recently deposited lake sediment. The major peaks were found to be unsubstituted PAH ranging from two-ring (biphenyl) to seven-ring compounds (coronene). Constituents positively identified by GC/MS and co-injection of authentic reference compounds are listed in Table I.

Two and more isomers with the same number of condensed aromatic rings occur in this PAH mixture. Phenanthrene and anthracene can readily be separated by the glass capillary column used in Figure 2. Some other isomeric unsubstituted PAH, however, are not as well resolved, such as triphenylene and chrysene (peak 13) or the several benzofluoranthenes (peak 14). No significantly better separation of these isomeric PAH was achieved by using longer columns (50 m). These isomeric PAH can be resolved on more polar columns with higher selectivities (coated e.g. with polyphenyl ether, carbowax, or silar phases). However, we did not routinely use such columns because of their reduced practical temperature range and because of their lower intrinsic separation efficiency (due to coating on a more intensely roughened support surface). Thus, our choice of 20-m long SE-52 columns is a compromise between resolution efficiency and practicality (analysis time and column temperature).

The gas chromatogram is also characterized by a large number of poorly resolved minor peaks which are due to substituted PAH. A detailed qualitative analysis by mass chromatographic methods (*3*) has shown that these PAH mixtures contain, in addition, great numbers of homologous and isomeric alkylated PAH. Methylphenanthrenes (peaks

Table I. Polycyclic Aromatic Hydrocarbons Identified in Environmental Samples. Numbers Refer to Figures 2–4

No.	Compound
1	Biphenyl
2	Acenaphthene
3	Fluorene
4	Phenanthrene
5	Anthracene
6	Methylphenanthrenes
7	4,5-Methylenephenanthrene
8	Fluoranthene
9	Pyrene
10	Benzo[*a*]fluorene
11	Benzo[*b*]fluorene
12	Benz[*a*]anthracene
13	Chrysene/triphenylene
14	Benzofluoranthenes
15	Benzo[*e*]pyrene
16	Benzo[*a*]pyrene
17	Perylene
18	Dibenzanthracenes
19	Indeno[1,2,3-*cd*]pyrene
20	Benzo[*ghi*]perylene
21	Anthanthrene
22	Coronene

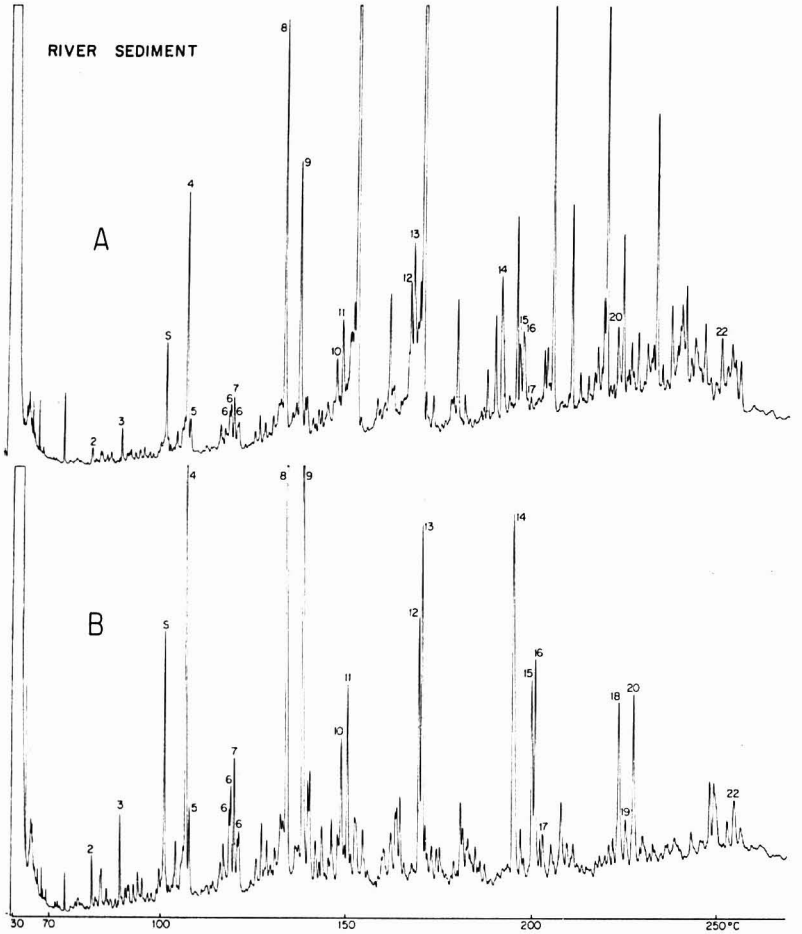


Figure 3. Gas chromatograms of fractions isolated from a river sediment (Mönchaltorfer Aa, Switzerland). (A) Aromatic fraction after column chromatography on silica. (B) PAH fraction after column chromatography on Sephadex and silica. Numbers refer to identified components listed in Table I. S: internal standard. GC conditions as for Figure 2

No. 6) and 4,5-methylenephenanthrene (peak No. 7) are readily detected even with nonspecific flame ionization detection.

As shown in Figure 2, the compositional complexity of the PAH in this environmental sample cannot be completely resolved by the capillary columns which we applied. Similar results were reported by authors who performed PAH analyses by capillary GC in tobacco smoke (*8*) and airborne particulates (*9, 10*). Therefore, we strongly feel that the objective to quantitate individual PAH in environmental samples needs the most efficient separation technique available, namely capillary GC. Packed column GC or HPLC clearly does not have sufficient separation power.

The complexity of sedimentary PAH as uncovered here by capillary GC is in agreement with observations by other authors who have applied mass spectrometric (*4, 11–13*) or gas chromatographic (*13–15*) techniques to study samples of soils and recent sediments of rivers and the ocean.

Rationale for PAH Isolation Scheme. Our scheme for the isolation of PAH from other extracted materials is a modification of the method of Giger and Blumer (*4*) which has been successfully used for investigations of PAH in sediments and soils (*11, 12*). The intent during the development of the isolation procedure presented in this paper was to simplify the cleanup scheme as much as possible. It was thought that a highly efficient characterization technique like capillary GC should need less preseparation steps than low voltage mass spectrometry or absorption spectrometry with their intrinsic lower specifity.

We began by separating the extract only by adsorption chromatography on silica into two fractions containing aliphatic and aromatic hydrocarbons, respectively. Figure 3a depicts the resulting gas chromatogram of such an aromatic fraction isolated from a river sediment. PAH can still be

Table II. Relative Standard Deviations, Recoveries, and Gas Chromatographic Response Factors

	Rel std dev,[a] ± %	Recovery,[b] %	Response factor[c] I	II	III
Phenanthrene	17	99 ± 5	0.74	0.77	0.84
Fluoranthene	16	107 ± 4	0.78	0.83	1.00
Pyrene	12	109 ± 3	0.79	0.86	1.02
Benzo[*a*]pyrene	22	113 ± 5	1.03	1.35	2.95
Perylene	10	115 ± 5	1.02	1.35	2.97
n-Heptadecane	3	87 ± 5	0.82	0.82	0.81
n-Pentacosane	15	101 ± 1	1.10	0.99	1.25

[a] Triplicate analyses of a lake sediment sample containing 0.1–1 μg of individual component per g dry sediment. [b] Three determinations of a standard mixture containing 5–7 μg of each component. [c] With respect to the internal standard 1-chlorotetradecane. For explanation of I, II, and III, see text.

recognized in the chromatogram, but they are superimposed by a series of more abundant constituents. For many PAH, a quantitative determination would be very questionable because of overlapping peaks. The structures of the major interfering compounds have been tentatively elucidated: Long chain wax esters.

The insertion of a column chromatography step using Sephadex LH-20 prior to silica gel chromatography, leads to a fraction which contains predominantly PAH and provides a gas chromatogram much more suitable for quantitative analyses of individual PAH (see Figure 3b).

The described PAH isolation procedure is quite rapid and easy to perform. Minimum solvent volumes are required in comparison to previous methods. Consequently, evaporation steps, of which only one needs to go completely to dryness, are minimized. The simple column chromatographic steps (only two fractions) are also very clean operations compared to liquid–liquid partitioning or preparative thin layer chromatography. This latter aspect is of particular importance considering the health hazard inherent to PAH.

Quantitation. Table II lists relative standard deviations for replicate analyses and analytical recoveries for five individual PAH and two *n*-alkanes. The reproducibility has been determined by triplicate analyses of a well homogenized lake sediment sample containing 0.1–1 μg of individual PAH per gram dry sediment. The precision of the method is most acceptable considering the fact that the concentration levels are in the range of tenths of μg/g in a complex sample matrix which requires sophisticated separation techniques. The precision attained is certainly adequate for applications in environmental and geochemical investigations.

The PAH recoveries (Table II) show unusual values which are higher than 100% with a tendency to increase towards larger PAH. The *n*-alkanes in comparison have "normal" recoveries. This phenomenon is not understood at present. Formation during the isolation procedure or in the GC can be excluded based on blank experiments. Preliminary evidence hints that processes occurring in the injection system may be responsible. This can be suggested based on experiments with a GC system in which the sample is injected directly onto the column, omitting an evaporation in the inlet system (*16*).

Two parts of the gas chromatographic system are crucial for the quality of the quantitative determinations of individual PAH: primarily the capillary column but also the geometry of the inlet system. Precision and accuracy as given in Table II were achieved with glass capillary columns which were coated with SE-52 by K. and G. Grob according to their barium carbonate procedure (*7*). Furthermore the newest version of a Grob-type inlet system (Model 76, see Experimental) was used.

Table II also gives gas chromatographic response factors with respect to the internal standard (1-chlorotetradecane) for three different chromatographic systems. The values of column I were measured with the setup eventually used for the precision and accuracy reported in Table II (Model 76 inlet system, barium carbonate SE-52 capillary). The response factors of column II were obtained with the same capillary column but with the older version of an inlet system with built-in septum flushing (*5*), while the figures in column III were taken from measurements with the older injection port and with capillaries coated on bare silica surface (*6*). In system I, the response factors vary only from 0.74 for phenanthrene to 1.0 for perylene. The response factors of the larger PAH are increased in system II and much more drastically in system III. This means that losses of the larger, less volatile PAH occur in the last two chromatographic systems. This increase of the response factors was strictly parallel to a deterioration of precision and accuracy. Hence, the reliable quantitative performance of the GC system can be already checked based on the changes of the response factors.

Applications. The analytical method presented in this paper is currently being used for investigations of the origin and fate of PAH in lake sediments. Here we report resulting data of five representative environmental samples to illustrate the feasibility of our procedure. Table III lists the concentrations of seven individual PAH and two *n*-alkanes in samples of lake and river sediments, river particulates, street dust, and airborne particulates. In addition, Figure 4 shows the gas

Table III. Hydrocarbon Concentrations in Selected Environmental Samples[d]

	Recent sediments				
	Lake[b]	River[c]	River particulates[c]	Street dust	Airborne particulates
Total extract[a]	8.02 × 10³	0.65 × 10³	8.78 × 10³	7.2 × 10³	155 × 10³
Aliphatic/olefinic[a] hydrocarbons	499	93	2 320	1 090	34 850
Aromatic hydrocarbons[a]	110	53	673	500	5 390
Phenanthrene	0.34	0.21	1.6	3.5	3.4
Anthracene	0.03	0.02	0.33	0.45	0.22
Fluoranthene	0.42	0.39	5.7	10.0	12.9
Pyrene	0.38	0.33	6.0	7.2	18.0
Benzo[*e*]pyrene	0.21	0.15	3.5	3.9	48.0
Benzo[*a*]pyrene	0.16	0.19	3.9	2.7	40.5
Perylene	0.04	0.03	0.66	0.66	9.3
n-Heptadecane	24.0	0.08	2.8	0.25	17.7
n-Pentacosane	0.87	0.38	4.0	0.68	222

[a] Fraction weights. [b] Greifensee, Switzerland surface layer sediment (0-3 cm). [c] Mönchaltorfer Aa, Switzerland. [d] Values are μg/g dry material.

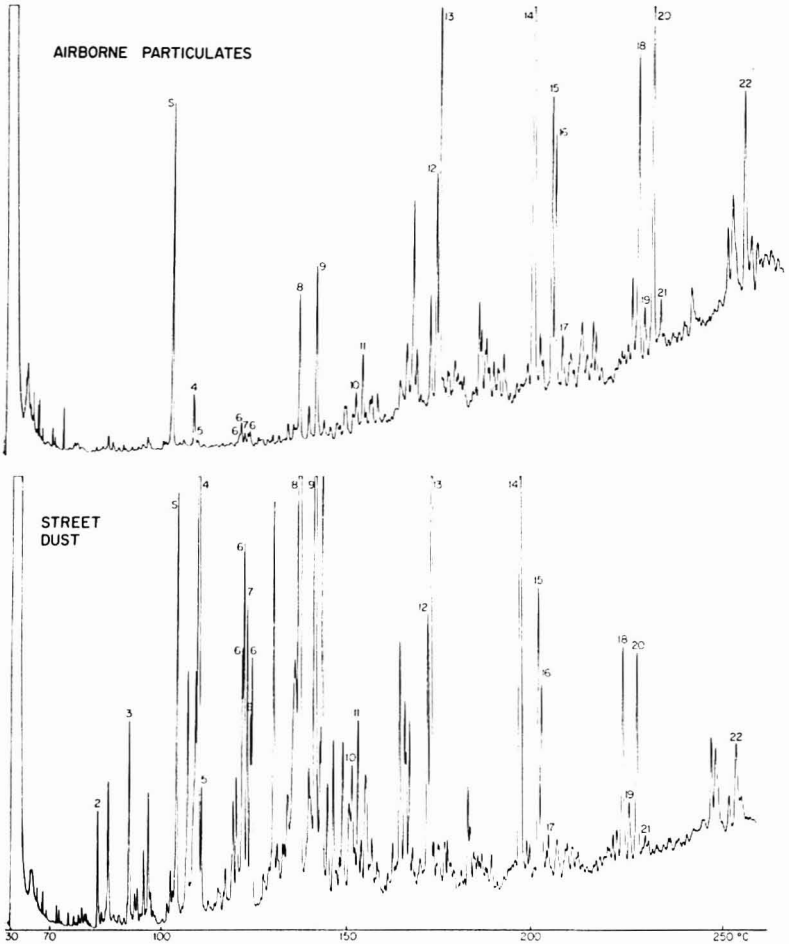


Figure 4. Gas chromatograms of polycyclic aromatic hydrocarbons isolated from street dust and airborne particulates. Numbers refer to identified components listed in Table I. S: internal standard. GC conditions as for Figure 2

chromatograms of PAH mixtures extracted from street dust and airborne particulate matter. A corresponding analysis of the suspended matter in a river is not shown because it is very similar to the chromatograms of the sediment samples (Figures 2 and 3b).

In a qualitative sense, the samples presented in this paper contain very similar PAH assemblages. The unsubstituted PAH detected in recent lake and river sediments (Figures 2 and 3b) are also predominant in the possible source materials (Figure 4). The PAH mixture contained in airborne particulates is shifted towards a higher boiling range. We suspect, however, that this is due to a sampling artifact caused by losses of smaller, more volatile PAH in the high volume air sampler. Otherwise the relative distributions of the unsubstituted PAH in the different samples do not vary drastically. Phenanthrene, for instance, is always much more abundant than the isomeric anthracene.

The concentrations of individual PAH in both recent sediments are in the range of tenths of $\mu g/g$ on a dry weight basis (Table III). Fluoranthene and pyrene are the two most abundant components in all samples except the airborne particulate matter which is again likely caused by a sampling artifact. The two isomeric benzopyrenes are almost equally abundant. One could choose benzo[a]pyrene (BaP, the active isomer) as a guide component as is done in many studies of environmental PAH. BaP concentrations in surface lake sediments ranged from 0.2 to 0.6 $\mu g/g$. With increasing depth in sediment cores, a rapid decrease was detected in most cases.

Our analyses of river particulates, street dust, and airborne particulates (Table III) characterize possible source materials of PAH which are eventually deposited in lake or ocean sediments. In the case of the Greifensee, a small lake in a densely populated area, we believe that the major origin of the sedimentary PAH is run-off material from streets which

is then transported through rivers. Much lower values were found in soils (0.03–0.09 μg BaP/g dry soil), and BaP was not measurable in a more remote mountain lake (<0.01 μg/g dry sediment).

Besides the discussed environmental samples, we have successfully applied our analytical scheme for PAH contained in ancient sediments such as oil shales and bituminous limestones and dolomites.

The described GC method can be complemented by PAH analyses based on mass spectral characterization after probe distillation (*4*, *11–13*). The GC method aims at the determination of individual PAH with maximum separation efficiency. The probe distillation method, on the other hand, describes the molecular weight distribution in series of alkyl homologues with maximum sensitivity but without distinguishing between different isomers. The PAH homologue patterns contain a large amount of information with regard to formation and alteration of PAH assemblages. For the assessment of biological effects, however, only the gas chromatographic approach can provide reliable data, because accurate quantitation of individual compounds is needed for this purpose.

ACKNOWLEDGMENT

The authors thank K. and G. Grob for supplying glass capillary columns and for very valuable advice throughout the project. We are grateful to S. G. Wakeham and J. C. Westall for their suggestions on the manuscript. The Institute for Hygiene of the Swiss Federal Institute of Technology Zurich is acknowledged for collecting the sample of air particulates.

LITERATURE CITED

(1) National Academy of Sciences (USA), Particulate Polycyclic Organic Matter, Washington, D.C., 1972.
(2) R. Freudenthal and P. W. Jones, Ed., "Polynuclear Aromatic Hydrocarbons: Chemistry, Metabolism, and Carcinogenesis", Raven Press, New York, N.Y., 1976.
(3) W. Giger and C. Schaffner, *Adv. Org. Geochem.*, **1975**, 375; R. Campos and J. Goni, Ed., ENADIMSA, Madrid, 1977.
(4) W. Giger and M. Blumer, *Anal. Chem.*, **46**, 1663 (1974).
(5) K. Grob and G. Grob, *Chromatographia*, **5**, 3 (1972).
(6) K. Grob, private communications, 1977.
(7) K. Grob, G. Grob, and K. Grob, Jr., *Chromatographia*, **10**, 181 (1977).
(8) M. L. Lee, M. Novotny, and K. D. Bartle, *Anal. Chem.*, **48**, 405 (1976).
(9) M. L. Lee, M. Novotny, and K. D. Bartle, *Anal. Chem.*, **48**, 1566 (1976).
(10) R. C. Lao, R. S. Thomas, and J. L. Monkman, *J. Chromatogr.*, **112**, 681 (1975).
(11) M. Blumer and W. W. Youngblood, *Science*, **188**, 53 (1975).
(12) W. W. Youngblood and M. Blumer, *Geochim. Cosmochim. Acta*, **39**, 1303 (1975).
(13) R. A. Hites and W. G. Bleman, *Adv. Chem.*, **147**, 188 (1975).
(14) G. Müller, G. Grimmer, and H. Böhnke, *Naturwissenschaften*, **464**, 427 (1977).
(15) G. Grimmer and H. Böhnke, *Cancer Lett.*, **1**, 75 (1975).
(16) K. Grob and K. Grob, Jr., *J. Chromatogr.*, **1977**, in press.

RECEIVED for review August 15, 1977. Accepted November 4, 1977. This work was supported in part by the Swiss Department of Commerce (Commission of the European Communities Project COST 64b).

Gel Permeation Chromatography of Fluoroether Polymers

Roger A. Korus[1] and Robert W. Rosser*

Ames Research Center, National Aeronautics and Space Administration, Moffett Field, California 94035

A method is described for determining the molecular weight distribution of fluorinated polymers by gel permeation chromatography. Porous silica-packed columns are used with Freon 113 as the chromatographic solvent. Fluoroether oligomers are used for column calibration in the molecular weight range of 1400 to 12 000.

Molecular weight measurements have been a major problem in the characterization of fluorinated polymers. Such measurements are severely limited by the low solubility of fluorinated polymers in most organic solvents. Sufficiently high solubility is usually obtained only in fluorinated solvents such as 1,1,2-trichloro-1,2,2-trifluoroethane (Freon 113). Molecular weight measurements of fluorinated polymers by light-scattering have low sensitivity because of the small refractive index difference between fluorinated polymers and fluorinated solvents (*1*). Gel permeation chromatography (GPC) has not been successfully applied to fluorinated polymers because the microporous polystyrene gels normally used as column packing shrink in the presence of fluorinated solvents. We now wish to report a rapid and convenient technique for measuring molecular weight distributions of fluoropolymers which overcomes many of the inherent limitations of other analytical methods.

Table I. Nominal Molecular Weight Separation Ranges of Silica GPC Columns

Designation	Supplier	Nominal separation range
SE 60	DuPont	100–5 000
SE 100	DuPont	2 000–50 000
SE 500	DuPont	10 000–500 000
E 300	Waters	3 000–100 000

Recently we have been examining perfluoroalkylene ether polymers for use as high-temperature elastomers (*2*). These polymers have high thermal stability, high chemical resistance, and low glass-transition temperatures. Until recently, perfluoroether synthesis has been limited to low molecular weight polymers. However, we have been able to obtain linear polymers with weight average molecular weights of approximately 20 000. To determine molecular weight distributions of these fluorinated polymers, we have used GPC with small particle silica column packing. This rigid packing is compatible with fluorinated solvents and should be applicable to other fluorinated polymers. Since chromatograms can be obtained in 10 to 20 min, this method provides a rapid means of molecular weight determination for fluorinated polymers.

EXPERIMENTAL

Apparatus and Materials. All GPC measurements were made with the Waters ALC-GPC 202/401 liquid chromatograph,

[1] Research Associate, San Jose State University, San Jose, Calif. 95192.

0003-2700/78/0350-0249$01.00/0 © 1978 American Chemical Society

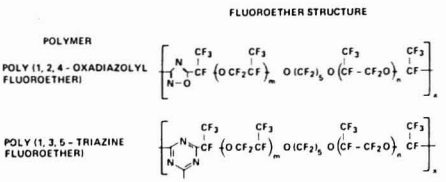


Figure 1. Heterocyclic perfluoroether polymers (*2*)

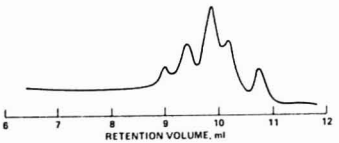


Figure 2. Chromatogram of 1,2,4-oxadiazole fluoroether polymer with $m + n = 6$. SE 60 and SE 100 columns, refractive index detector, 1 mL/min flow rate, 2 mg sample injected in 50 μL Freon 113. Refractive index decreases during polymer elution, and the maximum change was 7×10^{-6} RI

Waters Associates, Milford, Mass. This instrument is equipped with dual refractive index and ultraviolet (UV) detectors. Detection by UV absorption was at 254 nm. UV absorption spectra were recorded with a Cary 14 Spectrophotometer. All measurements were made at ambient temperatures.

Two types of porous silica packings were examined: μBONDAGEL columns, obtained from Waters Associates, and DuPont size exclusion (SE) columns, purchased from DuPont Instruments, Wilmington, Del. All columns were prepacked by the suppliers. The nominal molecular weight separation ranges of the columns are shown in Table I. The DuPont SE columns are 6.2 mm i.d. by 25 cm in length. The μBONDAGEL columns are 4 mm by 30 cm in length.

1,1,2-Trichloro-1,2,2-trifluoroethane (Freon 113) was purchased from E. I. du Pont de Nemours & Co., Wilmington, Del.

RESULTS AND DISCUSSION

Chromatograms of Fluoroether Oligomers. The molecular weight distributions of two classes of fluoroether polymers were determined by GPC. The chemical structures of these two polymers are shown in Figure 1. The values of $m + n$ range from 2 to 6. For an $m + n$ value of 6, the molecular weight of the repeating unit for the 1,2,4-oxadiazole fluoroether polymer is 1546. A representative chromatogram of a sample of this polymer with a low degree of polymerization is shown in Figure 2. This chromatogram shows five distinct peaks, which can be attributed to monomer, dimer, trimer, tetramer, and pentamer. The 1,2,4-oxadiazole fluoroether polymer has a UV absorption maximum at 230 nm. The refractive index detector shows a higher sensitivity than the UV detector, which operates at 254 nm. The assignment of elution volumes was verified for monomer and dimer from chromatograms of the monomer and the dimer obtained under the same conditions as in Figure 2. The structures of monomer and dimer were verified by infrared spectrometry, gas chromatography, and end-group analysis (*2*).

A representative chromatogram of a triazine fluoroether polymer with a low degree of polymerization is shown in Figure 3. This oligomer has an $m + n$ value of 3. The UV absorption maximum of the triazine polymer is 260 nm; in this case, the UV detector is more sensitive than the differential refractomer. The chromatogram of Figure 3 shows seven distinct peaks, corresponding to dimer through octamer. As a result of the method of polymerization, the monomer does not have a triazine moiety. Therefore, the monomer of the triazine fluoroether does not appear in the UV chromatogram.

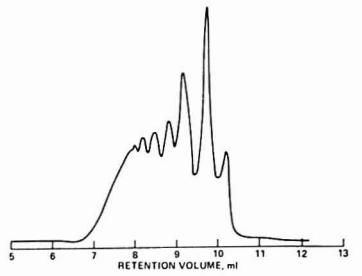


Figure 3. Chromatogram of triazine fluoroether polymer with $m + n = 3$. SE 60 and SE 100 columns, UV detector at 254 nm, 1 mL/min flow rate, 0.54 mg sample injected in 20 μL Freon 113. Maximum absorbance corresponds to 0.04 absorbance unit

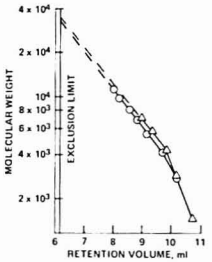


Figure 4. Calibration curve of SE 60/SE 100 columns. △ indicates retention volume of oligomer peaks from Figure 2 and ⊙ indicates retention volume of oligomer peaks from Figure 3

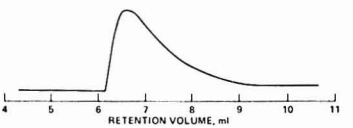


Figure 5. Chromatogram of high molecular weight 1,2,4-oxadiazole fluoroether polymer with $m + n = 6$. SE 60 and SE 100 columns, refractive index detector, 1 mL/min flow rate, 0.58 mg sample injected in 20 μL Freon 113. Maximum decrease in refractive index was 3×10^{-6} RI

Calibration of GPC Columns. A major problem in applying gel permeation chromatography to molecular weight determinations of a newly synthesized polymer is the calibration of the GPC columns used. Whenever possible, it is desirable to use molecular weight standards of the polymer of interest. Fortunately, our fluoroether oligomers provide a means of column calibration up to a molecular weight of approximately 12000. The retention volumes of the oligomer peaks of monomer through octamer can be determined from Figures 2 and 3. This provides a calibration curve as shown in Figure 4. This calibration curve is linear over a molecular weight range of 4000 to 12000. The calibration curve can be extrapolated to higher molecular weights to estimate molecular weights at higher retention volumes.

Chromatograms of Higher Molecular Weight Polymers. Several configurations of the silica columns shown in Table I were used for gel permeation chromatography of fluoroether polymers. For polymers not containing fractions with molecular weight greater than approximately 30000, the best column arrangement was the DuPont SE 60 column in

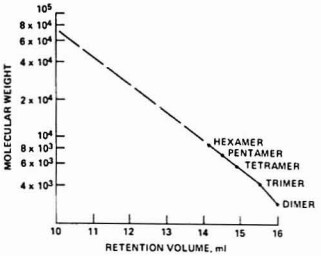


Figure 6. Calibration curve obtained with triazine fluoroether polymer for SE 60/SE 100/SE 500 columns

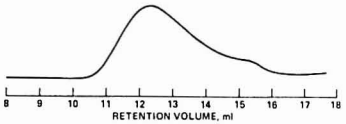


Figure 7. Chromatogram of high molecular weight 1,2,4-oxadiazole fluoroether polymer with $m + n = 6$. SE 60, SE 100, and SE 500 columns, refractive index detector, 1 mL/min flow rate 2.3 mg sample injected in 50 μL Freon 113. Maximum decrease in refractive index was 6×10^{-6} RI

series with either the DuPont SE 100 column or the Waters E 300 column. The chromatogram of a higher molecular weight oxadiazole polymer is shown in Figure 5. Similar chromatograms were obtained for several high molecular weight oxadiazole and triazine polymers. All of these chromatograms showed a rapid increase in UV absorbance and a rapid change in refractive index, indicating elution of polymer beginning at 6.17 mL. The position of this exclusion limit is shown in Figure 4 and corresponds to a molecular weight of approximately 32 000.

To extend molecular weight measurements to higher molecular weights, the DuPont SE 500 column was placed in series with other columns with lower molecular weight ranges. Using three DuPont columns, SE 60, SE 100, and SE 500, resolution of the fluoroether oligomers was reduced, and only distinct peaks up to the hexamer could be observed in chromatograms of low molecular weight triazine fluoroethers. The calibration curve obtained for these three columns is shown in Figure 6. The oxadiazole polymer used to obtain the chromatogram of Figure 5 was injected into this three-column set, and the resulting chromatogram is shown in Figure 7. The calibration curve of Figure 6 can be applied to the chromatogram in Figure 7 to compute the weight and number average molecular weights of the oxadiazole polymer (*3*). Thus $\bar{M}_w$ equals 19 500 and $\bar{M}_n$ equals 13 200. In this way, it is possible to calculate the various molecular weight averages of fluoroether polymers.

LITERATURE CITED

(1) G. A. Morneau, P. I. Roth, and A. R. Shultz, *J. Polym. Sci.*, **55**, 609 (1961).
(2) R. W. Rosser, J. A. Parker, R. J. DePasquale, and E. C. Stump, Jr., *ACS Symposium Series*, *No. 6*, *Polyethers*, 185 (1975).
(3) F. L. McCrackin, *J. Appl. Polym. Sci.*, **21** 191 (1977).

RECEIVED for review August 25, 1977. accepted November 7, 1977.

Collection of Chlorpyrifos and Other Pesticides in Air on Chemically Bonded Sorbents

Richard G. Melcher,* Warren L. Garner, Loren W. Severs, and James R. Vaccaro

Analytical and Industrial Hygiene Laboratories, Dow Chemical U.S.A., Midland, Michigan 48640

A procedure is described for the collection and determination of chlorpyrifos [*O,O*-diethyl *O*-(3,5,6-trichloro-2-pyridyl)-phosphorothioate] in air at the low parts per trillion level for sampling periods of 10 min up to 16 h. Worker breathing zone or area samples are collected by pumping air through a small tube containing a chemically bonded sorbent, GC Durapak–Carbowax 400/Porasil F. Samples are analyzed by desorption in diethyl ether and injection into a gas chromatograph equipped with a Poly I-110 column and an electron capture detector. Preliminary results for ronnel, lindane, carbaryl and diazinon indicate applicability of this technique to a wide range of pesticides.

A wide variety of sampling techniques have been applied to the determination of pesticides in air, and are described in a recent review (*1*). Most of the earlier methods for sampling pesticide vapors utilized solvent absorbent impingers; however, recently the general emphasis is toward the use of solid sorbents. Solid sorbents are now being used successfully for the collection of a variety of solvent vapors in work atmospheres. A small tube containing a solid sorbent is convenient to use, provides concentration of the trace pollutants, and can be attached to the worker for determination of actual breathing zone exposures for periods up to eight hours.

Some work has been reported in the literature (*2*, *3*) using solid adsorbents such as silica gel and activated charcoal for the sampling of some pesticides in air. However, when these adsorbents were tried for the collection of chlorpyrifos [*O,O*-diethyl *O*-(3,5,6-trichloro-2-pyridyl)phosphorothioate] at the trace amounts which may be found in work atmospheres, very low recoveries were obtained.

A highly sensitive method has been developed by Russell (*4*) for chlorpyrifos and ronnel [*O,O*-dimethyl *O*-(2,4,5-trichlorophenyl)phosphorothioate] using a sampling tube filled with 20% DC 200 chromatographic packing, and analyzed by thermal desorption directly into a gas chromatograph. This

0003-2700/78/0350-0251$01.00/0 © 1978 American Chemical Society

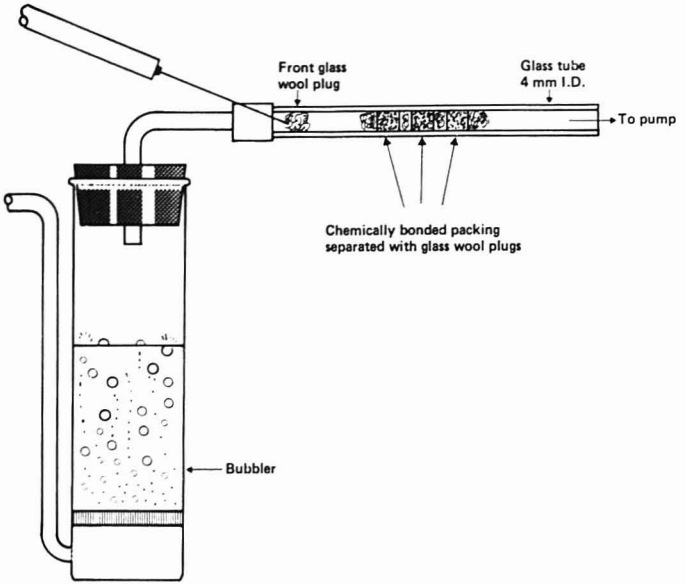


Figure 1. Experimental apparatus for determining breakthrough and recovery

technique can be adapted to personnel sampling but the analysis requires a somewhat specialized technique and the information obtainable is limited due to the "one shot" nature of the analysis.

The use of liquid-coated cloth screens and supports has been suggested (*5*, *6*); however, this suffers the disadvantage of coextraction of the liquid phase, which may lead to analytical problems. This problem can be avoided by the use of porous polymers or chemically bonded packings. Thomas and Seiber (*7*) have reported the use of Chromosorb 102 for a series of pesticides including chlorpyrifos. The procedure involved the collection on 4–5 g of Chromosorb 102 at the sampling rate of 12 to 13 L/min. The compounds were analyzed by gas chromatography following a 1-h Soxhlet extraction and a vacuum evaporation concentration step. Similar methods using XAD-2 resin (*8*) and polyurethane foam (*9*) for the collection of various pesticides have been reported. Aue and Teli (*10*) reported a brief experiment showing the collection of several chlorinated hydrocarbon insecticides on a support-bonded silicone, $(C_{18}H_{32}SiO_{3/2})_n$, prepared by them. Collection was on a large cartridge with a flowrate of 10 to 20 L/min. The cartridge was extracted by the circulation of 200 mL of pentane which was subsequently concentrated by evaporation and analyzed by gas chromatography. Although all these techniques are highly sensitive for pesticides in ambient air, they are not applicable to personnel breathing zone sampling, and the analytical procedures are lengthy.

This paper describes the development of a procedure for the collection and determination of chlorpyrifos in air at the low parts per trillion level for sampling periods of 10 min up to 16 h. Preliminary testing on a number of other pesticides has also been successful. Samples are collected on a small tube containing a commercially available chemically bonded sorbent and are subsequently analyzed by desorption in a small amount of solvent and direct injection into a gas chromatograph. The technique has been tested in a number of plant and field applications. The solvent desorption system described in this paper permits duplicate analyses by different techniques, treatment to eliminate, separate, and identify interferences, and also permits automatic injection by available liquid handling systems.

EXPERIMENTAL

Apparatus. The laboratory experimental setup is shown in Figure 1. The 8-cm glass tube (4-mm i.d.) contained three 5-mm sections of the sorbent separated by small glass wool plugs. The humidity was controlled by attaching a bubbler containing a saturated solution of either potassium carbonate (45% relative humidity) or ammonium sulfate (80% relative humidity).

A Hewlett-Packard Model 5710A gas chromatograph equipped with a hydrogen flame ionization detector or an electron capture ^{63}Ni detector was used to perform analyses. Chromatographic separations were accomplished on one of two phases, either a 1.8-m glass column packed with 3% SE-30/3% QF-1 or a 0.9-m glass column packed with 3% Poly I-110, at a column temperature of 200 °C, injection port 200 °C, detector 250 °C, and a carrier flow of 35 mL/min. The collection sorbents used in this study were: GC Durapak-Carbowax 400/Porasil F, 100–120 mesh; GC Durapak-*N*-Octane/Porasil C, 100–120 mesh; GC Durapak-Phenylisocyanate/Porasil C, 80–100 mesh; and GC Durapak OPN/Porasil C, 80–100 mesh, all obtained from Supelco Inc., Bellefonte, Pa. These sorbents were used with no prior treatment and showed no interferences for the pesticides tested. New batches of the packings should be tested before use and rinsed with diethyl ether if the background level is too high. The glass wool and glass tubes (8 cm × 4 mm i.d.) were rinsed with diethyl ether. The portable pump used for personnel sampling was either a Sipin Model SP-1 or an SKC personnel pump.

Collection and Recovery Studies. Solutions of the various pesticides were prepared in a volatile solvent, diethyl ether or methanol, at concentrations of 0.1 to 1.0 mg/mL. Two to 20 μL of the solution was injected into a separate glass wool plug in the front end of the collection tube, while air was being pumped through the system. For the humidity studies, the bubbler was immediately attached to the inlet of the collection tube after

Table I. Laboratory Collection and Recovery Experiments for Selected Pesticides on Bonded Packings

Pesticide	Sorbent[a]	Amount Added (μg)	Amount Found (μg) Front Section	Back Section	% Recovery
Ronnel [O,O-dimethyl O-(2,4,5-trichlorophenyl) phosphorothioate]	1	54.5	47.3	0.5	88
	2	51.3	41.1	2.6	85
	3	50.5	35.7	5.3	81
	4	39.0	25.4	1.9	70
Lindane (1,2,3,4,5,6-hexachlorocyclohexane)	1	5.93	5.68	0.002	96
	2	5.21	4.56	0.05	88
	3	5.97	5.74	0.004	96
	4	5.90	5.53	0.02	94
Carbaryl (naphthyl N-methyl carbamic acid)	1	6.4	6.0	Not detected	94
	2	11.8	3.6	" "	31
	3	7.5	4.8	" "	72
	4	9.6	2.4	" "	25
Diazinon (diethyl 6-isopropyl-2-methyl-4 pyrimidinyl phosphorothionate)	1	1.2	1.0	" "	83

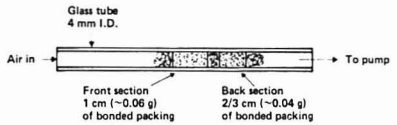


Figure 2. Sampling tube

injection, as shown in Figure 1.

A collection tube for plant, field, and personnel samples was designed and is shown in Figure 2. A collection and storage study was conducted using this size collection tube with a front glass wool plug added for injection of the concentrated solution. Samples for the storage study were collected for 8 h at the concentration of $^1/_{10}$ the TLV (threshold limit value) and stored on the bench top for periods of 1 to 7 days.

Recovery experiments for ronnel, lindane, carbaryl, and diazinon were carried out using the two section tubes. All pesticide loadings were at or below $^1/_2$ the TLV level. In each experiment, air of 45% relative himidity was drawn through the tube at 0.1 L/min for 4 h, and the front glass wool plug and sorbent sections were analyzed separately.

Sample Analysis. After the sampling period, the separate front glass wool plug and each section was analyzed for chlorpyrifos separately by shaking with 2 mL of diethyl ether for 15 min. In the storage study, the front glass wool plug was analyzed the day of collection. Three microliters of the extract was injected into a gas chromatograph equipped with an electron capture detector and either the Poly I-110 or the SE-30/QF-1 column. Some of the field samples were analyzed using a flame photometric detector to obtain additional specificity. The extracts of ronnel and lindane were chromatographed using the Poly I-110 column with an electron capture detector and extracts of carbaryl and diazinon were chromatographed using the Poly I-110 column and a hydrogen flame ionization detector.

Concentrations of compounds in air were calculated from the equation:

$$\text{ppb (vol/vol in air)} = \frac{\mu\text{g found} \times 24.45 \times 10^3}{\text{liters of air collected} \times \text{molecular weight}}$$

The factor 24.45 is the volume occupied by 1 g molecular weight of gas at 25 °C and 760 mm of mercury pressure.

Personnel Monitoring. Personnel working in the plant and applying pesticide formulations were monitored for chlorpyrifos exposures by attaching a collection tube to the worker. The collection tube was connected with flexible tubing to a small battery operated pump calibrated to pump 100 mL of air per minute. The pump was placed in the workers breast or back pocket.

Table II. Laboratory Collection and Recovery Experiment for Chlorpyrifos on Durapak-Carbowax 400/Porasil F

Amount Added (ng)	Flow Rate Liters/Min.	Time, Hrs	% Rel. Hum.	% Recovery[a]	Concentration (ppb v/v)
8.3	1.0	0.2	45	88.6	0.04
986	1.0	0.5	45	92.6	2.1
1060	0.5	1	45	94.5	2.4
758	0.5	1	80	98.9	1.7
160	0.5	1	45	97.3	0.43
195	0.5	2	45	100	0.21
188	0.1	16	45	91.4	0.14

DISCUSSION AND RESULTS

The low recoveries of polar compounds of low volatility, particularly the organophosphate pesticides, from the commonly used solid adsorbents promoted the search for a suitable solid adsorbent for air sampling. The chemically bonded packings, developed for gas chromatography, were shown to have excellent collection and recovery properties. These packings, commonly called "brush" packings (*11*) because of the orientation of the organic moiety on the surface of the support, have been reported (*12*) to retain the organic compounds through the dominant mechanism of adsorption on the brush. The high liquid desorption recoveries of the pesticides can be attributed to the deactivated solid support and to the thin layer and low amount of bonded liquid phase.

Initial experiments were performed using a specialized chemically bonded packing which had been prepared using a procedure developed by Nestrick and Stehl (*13*). Additional experiments used the commercially available bonded packing, Durapak–Carbowax 400/Porasil F, and similar collection and recovery properties were observed. Three other available bonded packings were tested on several types of pesticides, Table I. The Durapak–Carbowax 400/Porasil F gave the best recoveries of the commercial sorbents and was used for the in-depth study of chlorpyrifos in air. An additional bonded packing, Durapak–Carbowax 400/Porasil C is available, which contains 7.86% bonded phase compared to 1.41% on the Porasil F (*12*). This packing was not tested because the extraction blank was high and the material would require prior treatment before use.

The experimental data for chlorpyrifos are summarized in Tables II and III. Even under extreme conditions of high humidity, high concentrations, high solvent vapor concentrations and storage periods of 7 days, the recovery was 95

Table III. Collection of Chlorpyrifos on Bonded Durapak-Carbowax 400/Porasil F Storage Study

Storage Time (days)	% Relative Humidity	Amount[a] Collected (ng)	% Recovery	Concentration (ppb v/v)
1	30	888	99.4	2.0
1	30	892	98.5	2.0
3	30	911	95.0	2.1
3	30	872	96.3	2.0
7	30	851	96.1	2.0
7	30	908	98.8	2.1
7	80	784	91.9	1.8

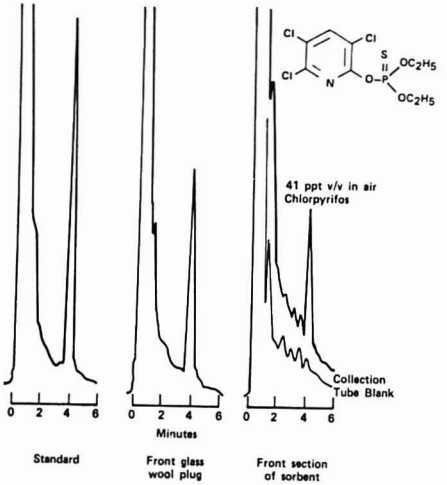


Figure 3. Laboratory experimental run. Collection: 10 min at 1.0 L/min. Gas chromatographic conditions: 0.9 m × 3 mm, glass column, 3% Poly I-110, 200 °C, Carrier gas 35 mL/min argon + 5% methane, electron capture detector attenuation, ×8

± 7% at the 95% confidence level, with only a small amount (less than 5%) found in the back-up section. Recoveries were calculated with the assumption that the amount of pesticide not found on the front glass wool plug had been carried as the vapor into the adsorbent sections. The amount found on the front glass wool plug was usually less than 10% of the total amount injected except for short term samples as shown in Figure 3. Desorption of the bonded packing was rapid and simple. Complete desorption took place in 15 min with gentle shaking.

In a plant study, two areas were surveyed using isooctane impingers and chemically bonded sorbent collection tubes. Two impingers were required to cover the total sampling time in each area while one bonded sorbent tube was used. The two impingers for each area were combined and analyzed. The time weighted average concentration of chlorpyrifos was 2.9 and 9.4 ppb v/v in air compared to the bonded sorbent values of 3.0 and 9.3 ppb, respectively. A few examples of field and plant applications are summarized in Table IV.

The chromatogram in Figure 4 shows the typical sensitivity obtained for field samples using an electron capture detector. This sample was collected for 4 h at 75 mL/min during the spraying of formulations containing chlorpyrifos. The peak represents 10.9 ng in 2 mL of diethyl ether and 40 ppt v/v as the time weighted average concentration in air. The limit of detection was 2 to 4 ng per sample at a signal-to-noise ratio

Table IV. Determination of Chlorpyrifos in Field Samples Collected on Durapak-Carbowax 400/Porasil F

Sample	Vol. (Liters)	Amount Found (μg) Front Section	Back Section	% In Back	Concentration (ppb v/v)
Moved around following a sprayer in a confined area 2.5 hr	30	5.83	0.15	2.5	6.4
Breathing zone personnel monitor spraying four lawns 55 minutes	11	0.272	0.004	1.5	1.7
Breathing zone personnel monitor spraying five buildings	15.2	0.123	0.002	1.6	0.57
Near Plant equipment (under cover)	4.8	8.11	0.14	1.7	122
Control panel	2.7	0.293	0.004	1.4	7.7
100 meters downwind	9.5	– None detected at sensitivity of 0.02 ppb –			

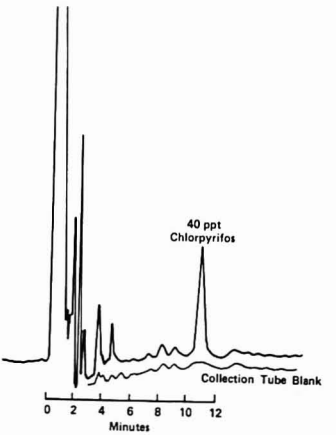


Figure 4. Four-hour breathing zone sample. Gas chromatographic conditions: 1.8 m × 3 mm glass column. 3% SE-30/3% QF-1, carrier gas 35 mL/min argon + 5% methane, electron capture detector attenuation, ×8

of 3:1. No interferences were observed in the field samples even in the presence of high concentrations of solvents present in the formulations.

The technique allowed breathing zone personnel samples for long periods. No other technique for this type of sample has previously been successful for chlorpyrifos. By using collection rates of 1 L/min, short sampling periods may be used to monitor peak exposures during operations which take place for only a few minutes. Another advantage of the bonded packing collection system is its low retention of water and solvent vapors. Solvent vapors, from the formulations, readily pass through the bonded sorbent without increasing breakthrough of the chlorpyrifos. This reduces interferences and will allow solvent vapors to be collected on activated charcoal in a section following the bonded sorbent.

The results for the collection of several other types of pesticides indicate that this technique may be applied to a wide range of compounds. Further development of various bonded packings for the collection of compounds which are difficult to determine in air is under way.

LITERATURE CITED

(1) L. P. van Dyk and K. Visweswariah, *Residue Rev.*, **55**, 91 (1975).
(2) W. N. Yule, A. F. W. Cole, and I. Hoffman, *Bull. Environ. Contam. Toxicol.*, **6**, 289 (1971).
(3) L. A. Jonas and J. A. Rehrmann, *Carbon*, **10**, 657 (1972).

(4) J. W. Russell, *Environ. Sci. Technol.*, **9**, 1175 (1975).
(5) J. D. Tessari and D. L. Spencer, *J. Assoc. Offic. Anal. Chem.*, **54**, 1376 (1971).
(6) R. W. Risebrough, R. J. Huggett, J. J. Griffin, and E. D. Goldberg, *Science*, **159**, 1233 (1968).
(7) T. C. Thomas and J. N. Seiber, *Bull. Environ. Contam. Toxicol.*, **12**, 17 (1974).
(8) S. O. Farwell, F. W. Bowes, and D. F. Adams, *J. Environ. Sci. Health*, **B12**, 71 (1977).
(9) B. C. Turner and D. E. Glotfelty, *Anal. Chem.*, **49**, 7 (1977).
(10) W. A. Aue and P. M. Teli, *J. Chromatogr.*, **62**, 15 (1971).
(11) I. Halasz and I. Sebestian, *Angew. Chem., Int. Ed. Engl.*, **8**, 453 (1969).
(12) J. J. Pesek and J. E. Daniels, *J. Chromatogr. Sci.*, **14**, 288 (1976).
(13) T. J. Nestrick and R. H. Stehl, The Dow Chemical Company, unpublished work.

RECEIVED for review July 20, 1977. Accepted November 10, 1977.

Selective Separation of Metal Ions by a Chelating Agent-Loaded Anion Exchanger

Kil Sang Lee, Won Lee, and Dai Woon Lee*

Department of Chemistry, Yonsei University, Seoul, Korea

A conventional anion exchanger loaded with sulfonated chelating agents, such as 5-sulfosalicylic (SSA), chromotropic (CTA), and 7-iodo-8-hydroxyquinoline-5-sulfonic (IHQS) acid has been applied to the selective and quantitative separation of Fe(III), Cu(II), Cr(VI), and Pb(II) from aqueous solutions. The optimum conditions were determined with respect to the pH, shaking time, and the effect of anion concentration in the medium. The total absorption capacities of the loaded resins were; 1.28 mmol Fe and 1.07 mmol Cu per gram of SSA-loaded resin, 0.65 mmol Fe and 1.14 mmol Cr per gram of CTA-loaded resin, and 0.73 mmol Cu and 0.70 mmol Pb per gram of IHQS-loaded resin. A few examples of the separation from the synthetic mixtures of the metal ions were examined by the elution method.

The selective and quantitative separation of metal ions from aqueous solutions, which is closely related to water pollution problems, has been extensively investigated with a number of materials. The materials studied are conventional (*1–4*) and chelating ion-exchange resins including inorganic ion exchangers (*5–11*), solvent-impregnated resins (*12, 13*), controlled pore glass (*14*), foamed plastics (*15–17*), and so on. It is well known that the chelating resins were recognized as being potentially useful for the selective separation of the specific metal ions. On the other hand, the use of chelating resins is limited by difficulties in their synthesis and high cost.

The purpose of the present work is to examine the application of the sulfonated chelating agent-loaded anion exchangers for the selective and quantitative separation of some metal ions from the aqueous solutions. The chelating agents studied here are 5-sulfosalicylic (SSA), chromotropic (CTA), and 7-iodo-8-hydroxyquinoline-5-sulfonic (IHQS) acid which are held strongly by the anion exchanger. The chelating agents loaded into the exchanger react to form colored stable chelates in the resin with the metal ions existing in the solutions.

It might be applicable to separate the specific metal ions and to remove them from the aqueous solutions for industrial use as well as for laboratory works. In this paper, all experiments were carried out with only the synthetic solutions of metal ions. There are two main advantages: The first is that the preparation of the chelating agent-loaded resins is quite simple, and the second is that the absorption of metal ions on the loaded resins is visible.

EXPERIMENTAL

Apparatus and Materials. A Cary 14 Recording Spectrophotometer, Beckman Infrared Spectrophotometer Model IR-12, and Perkin-Elmer Atomic Absorption Spectrophotometer Model 303 with hollow cathode lamps were used in this work.

The chloride form of a strongly basic anion exchanger, Dowex 1-X8 (50–100 mesh) was used for the preparation of the chelating agent-loaded resins. The chelating agents, 5-sulfosalicylic, chromotropic, and 7-iodo-8-hydroxyquinoline-5-sulfonic acid, and all other chemicals used were of analytical reagent grade.

For the elution method, the chelating agent-loaded resins were placed in a borosilicate glass column of 1.0 × 50 cm furnished with Teflon (Du Pont) fittings and porous Teflon bottom. The column was washed thoroughly with deionized water using a Serva Elutionpumpe, and then the resin bed was adjusted to the required height.

Preparation of Chelating Agent-Loaded Resins. The chelating agent-loaded resins were prepared by simply passing the solutions of 0.05 M sodium salt solutions of SSA, CTA, and IHQS, respectively, through the columns (3.0 × 50 cm) packed with about 50 g of purified Dowex 1-X8, chloride form. The loaded resin beds were washed with deionized water to remove the excess reagent and then were dried at 60–70 °C for a day.

Total Capacity of the Loaded Resin. The aqueous solution containing 100 ppm of metal ion, adjusted previously to the optimum pH value, was passed through the column packed with 1 g of the chelating agent-loaded resin. The flow rate was adjusted to 1.0 ± 0.1 mL per minute. The collected effluents were analyzed by atomic absorption spectrophotometry to obtain the chromatogram of frontal analysis from which the total capacity of the loaded resin was calculated. The value of the total capacity was expressed in mmol of metal ion per gram of dry resin.

Procedure for the Absorption of Metal Ions. In the batch method, aliquots (20–25 mL) of aqueous solution containing metal ion (ca. 100 μg) were shaken with weighed amounts of the chelating agent-loaded resin, ranging from 0.5 to 1.0 g, for about 1 h by a mechanical shaker. The amount of each metal ion absorbed by the resin was measured by atomic absorption spectrophotometry by comparing the concentration of equal aliquot portions of the solution before and after absorption.

The elution method was carried out using glass columns (1.0 × 40 cm) packed with a certain amount of the chelating agent-loaded resins.

All experiments were carried out at room temperature.

0003-2700/78/0350-0255$01.00/0 © 1978 American Chemical Society

Table I. Total Loaded Amount of Chelating Agent on Dowex 1-X8, Cl^- Form, 50- to 100- Mesh[a]

Chelating agent	Total loaded amount, mmol/g, resin	
	Elution method	Batch method
SSA	1.7 ± 0.1	1.9 ± 0.1
CTA	-	2.1 ± 0.1
IHQS	1.7 ± 0.1	1.7 ± 0.1

[a] Total capacity of Dowex 1-X8, Cl^- form: 3.7 mequiv/g.

RESULTS AND DISCUSSION

Nature of the Chelating Agent-Loaded Resins. The total loaded amount of SSA, CTA, and IHQS in the chelating agent-loaded resins was determined by both batch and elution methods (Table I). As shown in Table I, the amounts of SSA, CTA, and IHQS loaded were approximately the same, regardless of the differences in acidity and in nature of molecules. From the result, it is likely that the mechanism of the absorption of the chelating agent by the resin is due not only to the ion exchange between the chloride ion and the anionic sulfonate of the chelating agent. The other possible mechanism seems to be a certain molecular absorption between resin matrix and the molecule of the chelating agent. The molecular absorption mechanism, which is minor compared to that of ion exchange, was confirmed by evidence from the experiment itself as well as from literary sources.

It was observed that the chelating agents were held quantitatively by the resin even in the acidic media of 0.1 M $HClO_4$, HNO_3, H_2SO_4, and HCl. A number of studies reported were centered on the non-ion-exchange absorption of aromatic compounds such as carboxylic acids, phenols, alkylbenzene sulfonates, and aldehydes by ion exchangers (*18–23*).

The loaded resins were identified by the qualitative comparison of IR spectra of the resin itself, chelating agent, and the loaded resin with and without the metal ion. Furthermore, the coloration on the loaded resins after shaking or eluting with metal ion also aided in the qualitative identification of the loaded resins.

It was found that there was a limitation to this method in applying it to separation work in the laboratory; however it does not seem to pose a serious problem for practical applications. In the course of shaking the loaded resins with solution containing metal ions, a minute amount of SSA, CTA, and IHQS was removed from the loaded resins because of ion exchange between anionic sulfonate of the chelating agent absorbed and anion in the media.

In order to investigate how much the loaded chelating agent was removed from the loaded resin, the percentages of the removed chelating agents calculated from their total loaded amounts were measured as a function of concentration and nature of anion in the acid and salt media. As expected from the selectivity order of anions on Dowex 1 resin (*24*), it was observed that the effect of the nature of anion on the SSA- and IHQS-loaded resins in both acid and salt solutions decreased in the order $ClO_4^- > NO_3^- > Cl^- \approx SO_4^{2-} > CH_3COO^-$. In the case of CTA-loaded resin, the differences in percentage between anions was less significant because of its relatively strong absorption on the resin.

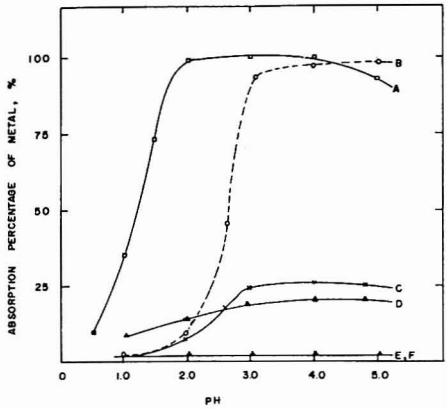


Figure 1. Effect of pH on the absorption of metal ions by SSA-loaded resin. (A) Fe(III), (B) Cu(II), (C) Ni(II), (D) Mn(II), (E) Pb(II), (F) Mg(II)

Concerning the effect of the anion concentration of the solution, it can be concluded that at the same concentration of 0.1 M of anions less than 1% CTA was removed with perchlorate and nitrate media, less than 0.5% CTA with sulfate and chloride, and approximately 0.1% CTA with the acetate medium. With concentration ranging from 10^{-3} to 10^{-2} M of anions, 1 to 10% SSA or IHQS was removed with perchlorate, nitrate, and sulfate medium, 1 to 5% SSA or IHQS with chloride, and 0.1 to 2% SSA or IHQS with acetate medium.

Absorption of Metal Ions by the Loaded Resins. In order to determine the optimum conditions, the optimum pH ranges were investigated by the batch method. For the SSA-loaded resin, the pH ranges were 2 to 4 for Fe(III), 3 to 5 for Cu(II), Ni(II), and Mn(II), respectively (Figure 1). These pH ranges are in accord with those for their chelations in the aqueous solutions. As shown in Figure 1, the difference in the values of the absorption percentage of metal between metal ions at their optimum pH ranges was likely due to the stabilities of their chelates. The absorption of metal ions by the SSA-loaded resin at the optimum conditions and the stability constants (*25–30*) are presented in Table II. On the other

Table II. Absorption of Metal Ions by the Chelating Agent-Loaded Resin by the Batch Method[a]

Metal ion	SSA, pH 3.5–3.8		CTA, pH 3.8–4.1		IHQS, pH 3.0–4.1	
	Absorbed, μg	Log K (ref.)	Absorbed, μg	Log K (ref.)	Absorbed, μg	Log K (ref.)
Fe(III)	100 ± 0.2	14.4 (*20, 21*)	22.7 ± 0.2	3.31 (*22, 23*)	16.1 ± 0.2	···
Cu(II)	97.7 ± 0.1	9.52 (*20*)	<0.1	13.92 (*22*)	100 ± 0.1	11.82 (*25*)
Cr(III)	···	···	<1	···	···	···
Cr(VI)	···	···	100 ± 1	8.21 (*24*)	···	···
Zn(II)	23.1 ± 0.1	6.1 (*21*)	<0.1	···	67.2 ± 0.1	7.74 (*25*)
Ni(II)	25.2 ± 0.5	6.42 (*20*)	<0.5	···	···	···
Pb(II)	0.8 ± 0.1	···	<0.1	···	100 ± 0.1	8.16 (*25*)
Mn(II)	19.1 ± 0.1	5.42 (*20*)	<0.1	···	16.0 ± 0.1	6.05 (*25*)
Mg(II)	<0.1	···	···	···	<0.1	4.12 (*25*)
Cd(II)	···	···	···	···	18.6 ± 0.1	6.99 (*25*)

[a] Resin: 1.0 g, total volume: 25mL, added amount of each metal ion: 100 μg, shaking time: 2 h.

Absorption of Metal Ions by the Loaded Resins. In order to determine the optimum conditions, the optimum pH ranges were investigated by the batch method. For the SSA-loaded resin, the pH ranges were 2 to 4 for Fe(III), 3 to 5 for Cu(II), Ni(II), and Mn(II), respectively (Figure 1). These pH ranges are in accord with those for their chelations in the aqueous solutions. As shown in Figure 1, the difference in the values of the absorption percentage of metal between metal ions at their optimum pH ranges was likely due to the stabilities of their chelates. The absorption of metal ions by the SSA-loaded resin at the optimum conditions and the stability constants (*25–30*) are presented in Table II. On the other

Table III. Total Absorption Capacities of the Chelating Agent-Loaded Resins[a]

Resin	Total absorption capacity, mmol/g, resin				
	Fe(III)	Cr(VI)	Cu(II)	Pb(II)	pH
SSA	1.28 ± 0.01	...	1.07 ± 0.01	...	3.0-3.5
CTA	0.65 ± 0.01	1.14 ± 0.01	-	...	3.0-3.5
IHQS	...	...	0.73 ± 0.01	0.70 ± 0.01	3.0-3.5

[a] Resin taken: 1.0 g, flow rate: 0.5 ± 0.1 mL/min.

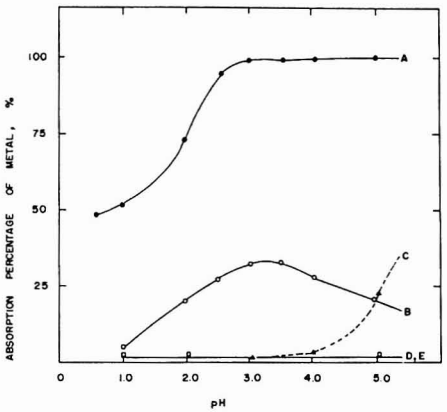


Figure 2. Effect of pH on the absorption of metal ions by CTA-loaded resin. (A) Cr(VI), (B) Fe(III), (C) Cu(II), (D) Mn(II), (E) Pb(II)

hand, the small absorption of Pb(II) and Mg(II) not forming chelates with SSA can be neglected because of the analysis error.

In the case of CTA-loaded resin, the pH ranges were 3 to 5 for Cr(VI) and 3.0 to 3.5 for Fe(III), respectively (Figure 2). In Table II, the absorption of Cu(II) by CTA-loaded resin was negligible at the pH range of 3.8–4.1 which is below the optimum condition for Cu(II).

It was observed that the optimum pH ranges for Pb(II), Cu(II), Zn(II), and Cd(II) in the case of IHQS-loaded resin were 3 to 5, while for Mn(II) it was 4 to 5.

The mechanism of the absorption is based on the chelating between the metal ion and the chelating groups of the sulfonated chelating agent in the loaded resin. As mentioned in the previous section concerning the nature of the loaded resins, the absorption of the chelating agent on the resin is based on both mainly ion exchange and partly molecular absorption. Therefore, the absorption of the chelating agent molecule by its chelating groups such as the hydroxyl group has to be taken into consideration.

However, in the process of the absorption of metal ion, the chelating groups must be free from the resin matrix to form metal chelates in the resin phase. Therefore, it might be predicted that not all the chelating groups present in the loaded resin were available for the chelation. This prediction is proved by the fact that the total absorption capacities of the loaded resins are smaller than those expected from the values of the total loaded amount of chelating agents (Table I).

The total absorption capacities of the loaded resins were determined at only the pH range of 3.0–3.5 (Table III). It was reported that in the solution with pH values less than 3, ferric and cupric ions reacted with SSA in 1:1 mole ratio to form reddish violet and blue chelate, respectively (*25, 31*). As shown in Table III, the total absorption capacities of SSA-loaded resin for Fe(III) and Cu(II) were much less than those calculated from the total loaded amount.

Table IV. Separation of the Synthetic Mixture of Metal Ions by the Elution Method

Resin	Sample No.	Metal ion	Amount added, μg	pH	Absorption, %	Resin bed, cm
SSA	I	Zn(II)	100		<0.1	
		Pb(II)	100		<0.1	
		Cu(II)	100	2.2	0.7	1.0 × 11.2
		Fe(III)	200		100[a]	
	II	Mg(II)	250		<0.1	
		Ni(II)	250	3.6	1.2	1.0 × 28.4
		Pb(II)	250		<0.1	
		Cu(II)	500		100[a]	
	III	Mg(II)	50 000		0.9	
		Pb(II)	50 000		<0.1	
		Mn(II)	50 000	3.6	1.8	1.0 × 28.4
		Fe(II)	50 000		<0.1	
		Cu(II)	50 000		16.9	
		Fe(III)	50 000		100[a]	
CTA	I	Pb(II)	500		<0.1	
		Mn(II)	500		<0.1	
		Cu(II)	500	4.3	<0.1	1.0 × 11.2
		Fe(III)	500		34.7	
		Cr(VI)	500		100[a]	
	II	Pb(II)	500		<0.1	
		Ni(II)	500		<0.1	
		Zn(II)	500	4.3	<0.1	1.0 × 11.2
		Cr(VI)	500		100[a]	
	III	Pb(II)	50 000		<0.1	
		Cu(II)	50 000		0.5	
		Fe(III)	50 000	4.3	23.7	1.0 × 17.6
		Cr(VI)	50 000		100[a]	
IHQS	I	Ca(II)	500		<0.1	
		Cd(II)	500		<0.1	
		Zn(II)	500	3.9	1.3	0.5 × 11.9
		Pb(II)	500		100[a]	
	II	Fe(II)	500		<0.1	
		Mn(II)	500	3.8	<0.1	0.5 × 11.7
		Cu(II)	500		100[a]	
	III	Ca(II)	50 000		<0.1	
		Cd(II)	50 000		2.6	
		Zn(II)	50 000	3.8	5.1	0.5 × 23.8
		Pb(II)	50 000		82.5	
		Cu(II)	50 000		98.4	

[a] 100% absorption means no detection of metal ion in the effluent by atomic absorption spectrophotometry.

In the case of CTA- and IHQS-loaded resins, it was the same because the mole ratios were 1:1 for all metal chelates (*27, 29, 30, 32*).

From the results, it can be concluded that the total absorption capacity of the loaded resin probably depended on some factors such as the stability of the metal chelates in the resin phase, the nature of the chelating agent-loaded resins, the availability of the chelating groups for the chelation, and the affinity of the chelating agent on the resin and so on.

For the application of this study to the separation of the mixture solutions, some examples were carried out by the

elution method. As shown in Table IV, the following separations are possible: Fe(III) from Zn(II), Pb(II), Mg(II), and Mn(II); and Cu(II) from Mg(II), Ni(II), and Pb(II) with SSA-loaded resin; Cr(VI) from Pb(II), Mn(II), Cu(II), Ni(II), and Zn(II) with CTA-loaded resin; and Cu(II) from Mn(II) and Fe(III); and Pb(II) from Zn(II) and Cd(II) with IHQS-loaded resin.

As a preliminary experiment for the application to industrial purposes, an attempt was made to remove Cr(VI) from the sample solutions collected from a tungsten mine effluent by using the CTA-loaded resin. It was possible to remove Cr(VI) ranging from 50 to 1 ppm from the effluents. The data were not presented because they were just for preliminary work.

LITERATURE CITED

(1) A. Dadone, F. Frache, and F. Baffi, *Chromatographia*, **7**, 258 (1974).
(2) A. M. Mulukozi, *Talanta*, **20**, 1341 (1973).
(3) A. M. Mulukozi, and D. M. S. Mosha, *Talanta*, **22**, 239 (1975).
(4) R. Smits, C. Vanroelen, and D. L. Massart, *Fresenius' Z. Anal. Chem.*, **273**, 1 (1975).
(5) R. A. A. Muzzarelli and R. Rocchetti, *Anal. Chim. Acta*, **69**, 35 (1974); **70**, 283 (1974).
(6) D. E. Leyden, T. A. Patterson, and J. J. Alberts, *Anal. Chem.*, **47**, 733 (1975).
(7) K. Kotsuli and S. Hayashi, *Bunseki Kagaku*, **23**, 802 (1974).
(8) J. S. Gill and S. N. Tandon, *J. Radioanal. Chem.*, **20**, 5 (1974).
(9) J. S. Gill and S. N. Tandon, *Talanta*, **19**, 1355 (1972).
(10) F. Vernon and H. Eccles, *Anal. Chim. Acta*, **72**, 331 (1974).
(11) C. W. Blount, D. E. Leyden, T. L. Thomas, and S. M. Guill, *Anal. Chem.*, **45**, 1045 (1973).
(12) A. Warshawsky, *Inst. Min. Metall.*, **83**, C101 (1974).
(13) R. Kroebel and A. Meyer, *Int. Sol. Ext. Conf. Lyon.*, 2025 (1974).
(14) D. E. Leyden and G. H. Luttrell, *Anal. Chem.*, **47**, 1612 (1975).
(15) T. Braun and A. B. Farag, *Anal. Chim. Acta*, **69**, 85 (1974); **71**, 133 (1974).
(16) T. Braun and A. B. Farag, *Anal. Chim. Acta*, **76**, 107 (1975).
(17) D. W. Lee and M. Halmann, *Anal. Chem.*, **48**, 2214 (1976).
(18) W. Funasaka, T. Kojima, G. Takeshima, and J. Kimoto, *Bunseki Kagaku*, **11**, 434 (1962).
(19) W. Rieman III, and H. F. Walton, "Ion Exchange in Analytical Chemistry", Pergamon Press, New York, N.Y., 1970, p 168.
(20) M. G. Chasanov, R. Kunin, and F. McGarvey, *Ind. Eng. Chem.*, **48**, 305 (1956).
(21) B. R. Kim, V. L. Snoeyink, and F. M. Saunders, *J. Water Pollut. Control Fed.*, **48**, 120 (1976).
(22) K. S. Lee and D. W. Lee, *Anal. Chem.*, **46**, 1903 (1974).
(23) K. S. Lee, D. W. Lee, and W. Lee, *Anal. Chem.*, **47**, 2270 (1975).
(24) S. Peterson, *Ann. N.Y. Acad. Sci.*, **57**, 144 (1953).
(25) C. V. Banks and R. S. Singh, *J. Inorg. Nucl. Chem.*, **15**, 125 (1960).
(26) A. Ringborn, "Complexation in Analytical Chemistry", Interscience, New York, N.Y., 1963.
(27) V. T. Athavale, N. Mahadevan, P. K. Mathur, and R. M. Sathe, *J. Inorg. Nucl. Chem.*, **29**, 1947 (1967).
(28) V. A. Nazarenko and F. A. Biryuk, *Zh. Anal. Khim.*, **24**, 44 (1969).
(29) S. K. Banerji and Said-ul-Zafar Qureshi, *Bull. Chem. Soc. Jpn.*, **38**, 720 (1965); *Chem. Abstr.*, **63**, 9421f (1965).
(30) A. Ekman, *Suom. Kemistil. B*, **35**, 111 (1962); *Chem. Abstr.*, **58**, 971c (1963).
(31) A. Ågren, *Acta Chem. Scand.*, **8**, 266 (1954).
(32) C. F. Richard, R. L. Gustafson, and A. E. Martell, *J. Am. Chem. Soc.*, **81**, 1033 (1959).

RECEIVED for review June 17, 1977. Accepted November 11, 1977.

Kinetics of Ion Exchange in Polydisperse Systems

Kurt Bunzl

Gesellschaft für Strahlen- und Umweltforschung mbH München, Institut für Strahlenschutz, 8042 Neuherberg, West Germany

The kinetics of ion-exchange processes in systems simultaneously involving ion-exchanger particles of different diameters was investigated in well stirred electrolyte solutions. Theoretical calculations, based on film diffusion controlled ion-exchange processes were performed for several important frequency distributions of the particle diameters in order to reveal the characteristics of such processes in comparison to monodisperse systems. It is shown that the smaller particles, always reacting more rapidly, will overshoot their eventual equilibrium value and, therefore, have to release after some time considerable amounts of these already sorbed counterions in favor of the slower reacting larger particles. As a result, even though in the later stages of the ion-exchange process considerable amounts of ions are still exchanged between the particles, the solution concentration will change after some time only very little and thus simulate an equilibrium state of the system, not yet attained by the ion-exchanger particles. Experimentally, the rates of ion exchange were measured in several polydisperse systems of a cation exchanger for the exchange Cs^+/H_3O^+. After determination of the kinetic properties of the individual fractions of the mixture in separate experiments, the rates of ion exchange of arbitrary polydisperse systems were calculated in quantitative agreement with the theory, without adjusting any parameter. If the polydisperse system consists of *I* different fractions, one has to solve for that purpose *I* differential equations simultaneously.

Even though much effort has been spent for many years on investigation of the kinetics of ion-exchange processes in monodisperse systems, very little is known about the rates in corresponding polydisperse mixtures, i.e., in systems where the size of the ion exchanger particles is not uniform. Yet, even commercially available ion-exchange resins, used on a large scale in the laboratory and in the industry for many purification and separation processes, are known, in general, to be not uniform in their diameters. This is even more true in the case of ion-exchange processes taking place in natural systems as, for example, in the soil, where the range of particle sizes of the substances involved (clay minerals, humic substances, sesquioxides) may cover several orders of magnitude. In all such cases, it will be interesting to know to what extent the rates of ion exchange in polydisperse mixtures differ from those observed in the corresponding monodisperse systems.

For this reason we investigated theoretically as well as experimentally the kinetics of such systems in well stirred dilute electrolyte solutions, where film diffusion is the rate-determining step. Since the system of differential equations, necessary to describe such a polydisperse system cannot be solved analytically, it is solved numerically by a computer for several important frequency distributions of the diameters of the ion-exchanger particles. These calculations yield not only the rates for the attainment of the equilibrium in the solution but also those for the different particle fractions of the ion exchanger. Experimentally this is, however, difficult to achieve. In a recent investigation (*1*) of the kinetics of competitive ion-exchange reactions involving only two different cation exchangers simultaneously in solution, we were able to measure independently the counterion concentration of all three phases (solution, ion exchanger A and B) as a function of time. In the present study, however, a rapid separation of the various fractions of the ion-exchanger beads

0003-2700/78/0350-0258$01.00/0 © 1978 American Chemical Society

after predetermined periods for subsequent analysis was not attempted and only the concentration of the ions in solution was measured as a function of time and compared with the calculated rates.

The polydisperse systems of the ion exchanger were prepared by mixing known amounts of five individually sieved, and thus approximately uniform, fractions of the material. In one case a commercially available polydisperse ion-exchange resin (100–200 mesh according to the manufacturer) was also investigated. The ion-exchange reaction considered, always involved the exchange of Cs^+/vs. H_3O^+ ions.

THEORY

The system considered shall consist of i fractions of a cation exchanger, differing only in their radii r_i (in cm) and their amounts Q_i (in mequiv), which are stirred simultaneously in V-mL solution, containing the counterions M and N (subscripts 1 and 2, respectively) in concentrations c_1 and c_2 (in moles electrolyte/L). Since all fractions of the ion exchanger will exchange counterions in an equivalent way, the total equivalent concentrations c (in mequiv/mL) will remain constant in the solution:

$$c = z_1 r_{1c} c_1 + z_2 r_{2c} c_2 \tag{1}$$

where z_1 and z_2 are the valences of the counterions M and N and r the stoichiometric coefficients for ionization of the two electrolytes $M_{r1c}D_{r1a}$ and $N_{r2c}D_{r2a}$ present in solution (D is the common co-ion).

The general differential equation for the rate of a film diffusion controlled ion-exchange process for particles of uniform diameter is given (*1*) as

$$\frac{d\bar{\gamma}_1}{dt} = R\cdot\frac{\alpha_2^1 r_{1c} c_1 z_1 (1-\bar{\gamma}_1) - z_2 c_2 r_{2c}\bar{\gamma}_1}{\alpha_2^1(1-\bar{\gamma}_1)(D_2/D_1) + \bar{\gamma}_1} \tag{2}$$

where $\bar{\gamma}_1 = z_1 C_1/C$ is the equivalent fraction of the counterions M in the ion exchanger. C_1 = the concentration of the counterions M (in moles of ions per liter) in the ion exchanger. C = volume ion-exchange capacity (in mequiv/mL) of the ion exchanger, t = time (s). $R = F\,D_2/\bar{V}\delta C$, where $F/\bar{V}$ is the surface to volume ratio of the ion exchanger particles. For spherical particles of radius r we thus can write $R = D_2/3rC\delta$. D_1, D_2 = diffusion coefficients, given as $D_1 = (D_{11}D_{22}r_{2c}z_2 - D_{12}D_{21}r_{2c}z_2)/(r_{1c}z_1D_{12} + r_{2c}z_2D_{22})$ and $D_2 = (D_{11}D_{22}r_{1c}z_1 - D_{21}D_{12}r_{1c}z_1)/(r_{1c}z_1D_{11} + r_{2c}z_2D_{21})$ where the D_{ij} is the set of four diffusion coefficients describing isothermal diffusion in the corresponding ternary solution H_2O–MD–ND at the same concentration as in the Nernst film. They can be determined by independent measurements, but as yet very few data are available. δ = thickness of the Nernst film.

The equivalent separation factor α_2^1 of the ion exchanger is given as

$$\alpha_2^1 = \frac{\bar{\gamma}_{1,\infty}\cdot\gamma_{2,\infty}}{\bar{\gamma}_{2,\infty}\cdot\gamma_{1,\infty}} \tag{3}$$

where γ_1 and γ_2 are the equivalent fractions of the counterions M and N in solution and the subscripts ∞ denote the equilibrium values ($t = \infty$).

Since Equation 2 has to hold for each fraction i of the polydisperse cation exchanger, we will thus have i differential equations. They can be considered as a system of differential equations which are all subject to the same boundary and initial conditions of the finite solution volume (batch operation) considered here.

This boundary condition is obtained from the material balance, which states that all counterions released by the i fractions of the ion exchanger have to appear in solution. If we have initially only ions M in the solution and only ions N in the ion exchanger:

$$\left.\begin{aligned}\bar{\gamma}_1 &= c_2 = 0\\ z_1 r_{1c} c_1 &= c\end{aligned}\right\} \text{ at } t = 0 \tag{4}$$

we can write

$$r_{2c} z_2 c_2 = C\sum_{i=1}^{i} w_i\bar{\gamma}_{1,i} = \frac{1}{V_i}\sum_{i=1}^{i} Q_i\bar{\gamma}_{1,i} \tag{5}$$

where $w_i = \bar{V}_i/V$, $\bar{V}_i$ = volume of the ith fraction of the cation exchanger in mL, and $Q_i = C\bar{V}_i$ = amount of exchanger of the fraction i in mequiv. The ion-exchange capacity C of the exchanger is independent of the particle radius and will be the same for each fraction i.

The quantities c_1 and c_2 in Equation 2 can now be eliminated with help of Equations 1 and 5 and we obtain, if we consider for simplicity monovalent ions only ($z_1 = z_2 = r_{1c} = r_{2c} = 1$):

$$\frac{d\bar{\gamma}_{1,i}}{dt} = R_i\cdot\frac{\alpha_2^1(1-\bar{\gamma}_{1,i})(c - \frac{1}{V_i}\sum_{i=1}^{i} Q_i\bar{\gamma}_{1,i}) - \bar{\gamma}_{1,i}\,\frac{1}{V_i}\sum_{i=1}^{i} Q_i\bar{\gamma}_{1,i}}{\alpha_2^1(1-\bar{\gamma}_{1,i})(D_2/D_1) + \bar{\gamma}_{1,i}} \tag{6}$$

where for spherical particles:

$$R_i = D_2/3r_iC\delta = \text{const.}/r_i \tag{7}$$

These i differential equations have now to be solved simultaneously in order to obtain the rates of ion exchange in each fraction i. After all $\bar{\gamma}_{1,i}$ are known as a function of time, the concentrations $c_2(t)$ and $c_1(t)$ in solution can be calculated with help of Equations 5 and 1.

At equilibrium, all equivalent fractions $\bar{\gamma}_{1,i}$ will approach the same value, since the separation factor is the same for all fractions i.

The system of differential Equations cannot be solved analytically. In order to show, however, in which characteristic way the concentrations of the ions in the different fractions of the ion exchanger and in solution will vary as a function of time, Equation 6 was solved simultaneously by a computer for several important particle size distributions of an ion exchanger, using the Runge–Kutta method (*2*).

MODEL CALCULATIONS

In all model calculations, a cation exchanger, consisting of five fractions with different particle radii r_i was considered. The values of these radii were $r_1 = 0.004$ cm; $r_2 = 0.007$ cm; $r_3 = 0.01$ cm; $r_4 = 0.013$ cm; $r_5 = 0.016$ cm.

The total amount of all fractions of the ion exchanger was always $Q_{tot} = C\bar{V}_{tot} = 0.5$ mequiv, loaded with counterions N (index 2) only, ($\bar{\gamma}_1 = 0$ at $t = 0$). This sample is added to V = 100-mL solution containing initially only counterions M (index 1) at a concentration $c_{1,t=0} = c = 0.01$ mequiv/mL. For the values of the other constants we used $\alpha_2^1 = 1.5$; $D_2/D_1 = 2$; $D_1 = 2.5 \times 10^{-5}$ cm^2 s^{-1}; $C = 5$ mequiv/mL; $\delta = 0.001$ cm. The values R_i can then be calculated (Equation 7) as $R_1 = 7.5$; $R_2 = 4.29$; $R_3 = 3.00$ $R_4 = 2.31$; $R_5 = 1.86$ cm^3 s^{-1} mequiv^{-1}. The amounts Q_1 to Q_5 of each fraction will depend on the special frequency distribution of the fractions considered.

Frequency distributions can be characterized either according to the weight m_i/M of each fraction (m_i = weight of each fraction; M = total weight of all fractions) or according to the number of particles of each fractions. n_i/N (n_i = number of particles of each fraction, N = total number of particles in all fractions). If the radius of the particles in each fraction is known, the n_i/N can be calculated from the m_i/M

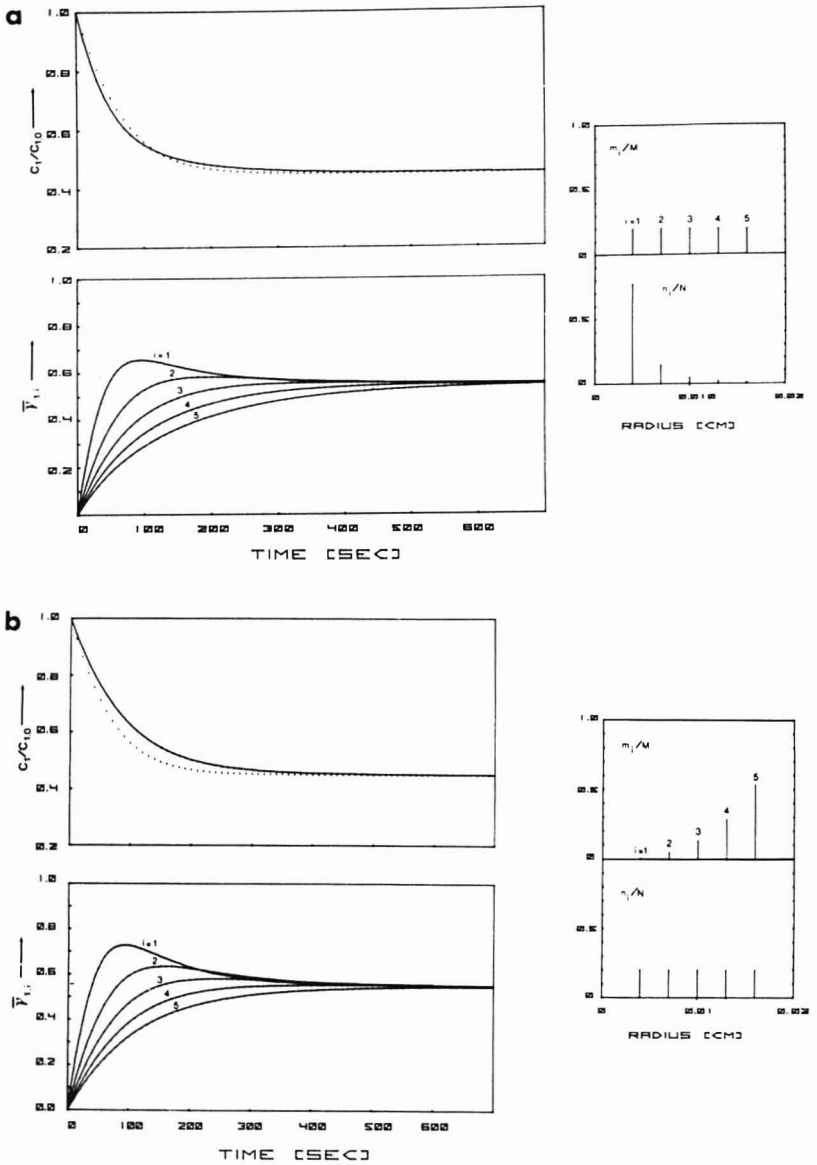
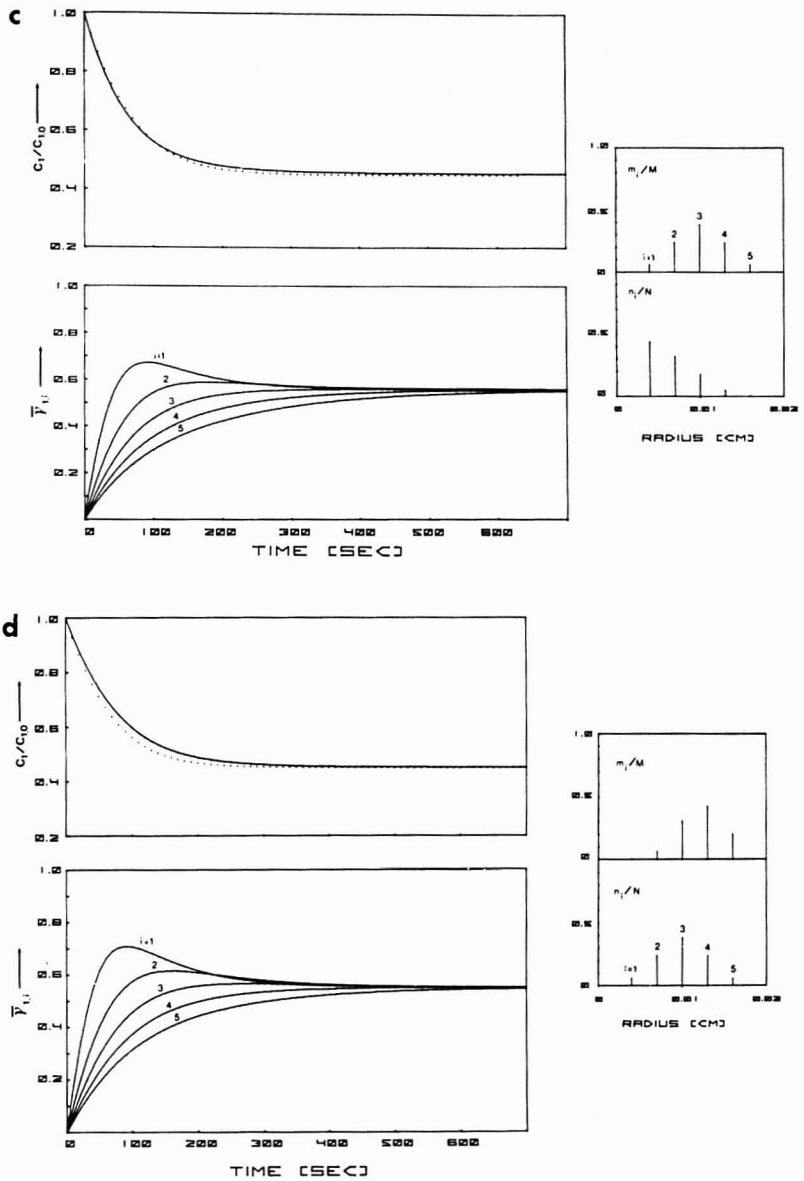


Figure 1. Equivalent fractions $\bar{\gamma}_{1,i}$ of counterions M in each of the five fractions (i = 1–5) of a polydisperse ion exchanger system (bottom) and concentration $c_1/c_{1,0}$ of ions M in the solution (top) as a function of time t, calculated according to Equations 6, 5, and 1. Initially ions M only in solution, but not in the ion exchanger. Dotted line: monodisperse system, r = 0.01 cm. (a) Rectangular distribution of the fractions according

and vice versa. It is a matter of convenience which basis is used. Since, however, the frequency distributions look quite different when given as n_i/M or n_i/N, we will characterize in the following all frequency distributions considered, both



to weight m_i/M. (b) Rectangular distribution of the fractions according to number of particles n_i/N. (c) Normal distribution of the fractions according to weight m_i/M. (d) Normal distribution of the fractions according to number of particles n_i/N

according to their weight and according to the number of particles in each fraction.

Rectangular Distribution of the Fractions According to Their Weight. First we will consider a particle size distribution, consisting of equal amounts of all five fractions. We thus have $Q_1/Q_{tot} = m_i/M = 0.2$; ($i$ = 1–5). Since we

already put $Q_{tot} = 0.5$ mequiv, this yields $Q_1 = Q_2 = Q_3 = Q_4 = Q_5 = 0.1$ mequiv.

This frequency distribution of the fractions can be also characterized according to the number of particles in each fraction. Using the above values for the radii of the particles in each fraction and those for Q_i/Q, one obtains $n_1/N = 0.772$; $n_2/N = 0.114$; $n_3/N = 0.0494$; $n_4/N = 0.0225$; $n_5/N = 0.01206$. These latter values are not necessary for the solution of the differential equations 6, but were calculated only for illustration of the frequency distribution of the above polydisperse system (see Figure 1a, right side).

Substituting the above values in Equation 6, we obtain a system of 5 differential equations, to be solved simultaneously. Using the Runge–Kutta method for the numerical solution of this system, one finds with help of a computer $\gamma_1(t)$ of the ion-exchange processes in each of the 5 fractions, and by substituing these values in Equations 5 and 1 the concentration of the ions in the solution as a function of the time. These results, together with the frequency distribution of the ion-exchanger particles are shown in Figure 1a. For comparison we also calculated (dotted line) the rate of ion exchange as observed in the solution phase, if one would use a monodisperse ion exchanger with a uniform radius of the particles of 0.01 cm, which is the radius of fraction 3 (central fraction).

Figure 1a illustrates clearly in which way the different fractions compete for the ions in solution. The fraction 1 with the smallest particles reacts comparatively fast because of its large surface and obviously absorbs initially more counterions M than the other fractions. Since, however, in equilibrium all fractions of the ion exchanger will approach the same equivalent fraction $\gamma_{1,\infty}$ (i = 1–5), the fractions 1 and 2 have to release some of their already sorbed counterions M in favor of the fractions 3, 4, and 5 which can react only relatively slow. As a result, the fractions 1 and 2 overshoot their eventual equilibrium value considerably.

A similar behavior was already observed both theoretically and experimentally in a mixture of two cation exchangers, which exhibited different surfaces and separation factors and thus also different reaction rates (*1*). The concentration of the ions M in solution (upper half of Figure 1a) decreases continually as a function of time. Compared to a monodisperse ion exchanger with the uniform radius $r = 0.01$ cm of the central fraction of the distribution (dotted line), the concentration of the ions M in solution in the polydisperse mixture decreases faster initially (because of the presence of smaller particles) but slower in the final stages of the reaction (because of the presence of the larger particles).

Rectangular Distribution of the Fractions according to the Number of Particles. Here we consider a frequency distribution, comprising an equal number n_i of particles in each fraction of the ion exchanger. We thus have $n_i/N = 0.2$; (i = 1–5). Using the above listed values of the radii of the particles in each of the five fractions, one can characterize this distribution also in terms of $m_i/M = Q_i/Q_{tot}$ and obtains $Q_1/Q_{tot} = 8.32 \times 10^{-3}$; $Q_2/Q_{tot} = 4.46 \times 10^{-2}$; $Q_3/Q_{tot} = 0.130$; $Q_4/Q_{tot} = 0.286$; $Q_5/Q_{tot} = 0.532$.

This distribution, together with the results of the numerical solution of Equation 6 using the above values of Q_i/Q_{tot} is shown in Figure 1b.

In this case we see again that the ion-exchanger particles with the smaller radii (fractions 1, 2, and 3) overshoot their eventual equilibrium values for the same reasons as in the preceding case. Fractions 4 and 5 on the other side, can approach their equilibrium only comparatively slowly. In the solution (upper half of Figure 1b) we can compare again the reaction of the polydisperse system (solid line) with the corresponding one of a monodisperse system of uniform particle radius $r = 0.01$ cm (dotted line). In contrast to the preceding distribution, we see that now the polydisperse system reacts slower than the monodisperse system throughout the whole exchange process. The explanation can be obtained from the frequency distribution of the particles shown in Figure 1b. Since here all fractions contain the same number of particles, the polydisperse system will consist on a weight basis m_i/M or Q_i/Q_{tot} mainly of large particles. Such a distribution will therefore always yield a comparatively slow reaction rate.

Normal Distribution of the Fractions according to Their Weight. The standard normal frequency distribution $h(r)$ of the radii of the particles is given as

$$h(r) = (2\pi)^{-1/2}\exp(-z^2/2) \qquad (8)$$

where $z = (r - \bar{r})/\sigma$; $\bar{r}$ = the mean radius and σ the standard deviation. In approximation we will substitute for the above continuous distribution a discrete function, consisting again of five fractions of particles. If we define $\bar{r} = r_3$; $r_4 = r_3 + \sigma$; $r_5 = r_3 + 2\sigma$; $r_2 = r_3 - \sigma$; $r_1 = r_3 - 2\sigma$, we obtain the same particle radii for the five fractions as used before by putting $\bar{r} = 0.01$ cm and $\sigma = 0.003$ cm. Using tabulated values for the area under the standard normal distribution curve (*3*) we find that the fractional amount $m_3/M = Q_3/Q_{tot}$ of particles between $(r_3 - \sigma/2)$ and $(r_3 + \sigma/2)$ will be 0.383, which we will use as the fractional amount of the particles with radius r_3. Similarly we obtain for the fractional amount of particles between $(r_4 - \sigma/2)$ and $(r_4 + \sigma/2)$ the value for $m_4/M = Q_4/Q_{tot} = 0.24$ and for $m_5/M = Q_5/Q_{tot} = 0.061$, which we will use as the fractional amounts of the particles with radii r_4 and r_5, respectively. Since the normal distribution function is symmetrical we also have $Q_1/Q_{tot} = Q_5/Q_{tot}$ and $Q_2/Q_{tot} = Q_4/Q_{tot}$. If we characterize this distribution also in terms of the fractional number n_i/N of particles with radii r_i, we obtain $n_1/N = 0.441$; $n_2/N = 0.324$; $n_3/N = 0.177$; $n_4/N = 0.0506$; $n_5/N = 0.00653$. A graphical illustration of the above distribution is shown in Figure 1c, right side.

Inserting in Equation 6 the above values Q_i/Q_{tot} and the values of the other constants, we obtain after solving numerically the resulting system of five differential equations the rates of ion exchange for the 5 fractions and in solution (see Figure 1c). Again we see that the ion-exchanger particles with the smaller radii (fractions 1 and 2) overshoot their eventual equilibrium values, while fractions 3, 4, and 5 approach their equilibrium only comparatively slowly. In solution (upper half of Figure 1c) we compare again the rate of ion exchange of the polydisperse system (solid line) with the corresponding one of a monodisperse system of uniform particle radius $r = \bar{r} = 0.01$ cm (dotted line). We see that, compared to the monodisperse system, the concentration of the ions M in the polydisperse system decreases faster initially but slower in the final stages of the reaction. A similar behavior was observed already for the polydisperse system exhibiting a rectangular distribution of the particles.

Normal Distribution of the Fractions according to the Number of Particles. If we consider a normal distribution of the particles according to the number of particles we can use the values for Q_i/Q_{tot} obtained in the preceding section for the n_i/N needed in this case and thus put $n_1/N = n_5/N = 0.061$; $n_2/N = n_4/N = 0.24$; $n_3/N = 0.383$. Using the above values for the radii of the particles of the five fractions, we can then characterize this distribution also according to the weight $m_i/M = Q_i/Q_{tot}$ of each fraction and obtain $Q_1/Q_{tot} = 3.13 \times 10^{-3}$; $Q_2/Q_{tot} = 0.0661$; $Q_3/Q_{tot} = 0.307$; $Q_4/Q_{tot} = 0.423$; $Q_5/Q_{tot} = 0.201$. This distribution is shown on the right side of Figure 1d.

Inserting in Equation 6 the above values Q_i/Q_{tot} and the values of the other constants, we obtain again after solving numerically the resulting system of differential equations the rates of ion exchange in each fraction and in solution as shown

in Figure 1d. Again we see that fractions 1 and 2 containing the smaller particles overshoot their eventual equilibrium value and have to release some of the already sorbed counterions. In solution (upper half of Figure 1d) we compare the rate of ion exchange of the polydisperse system (solid line) with the corresponding one of a monodisperse system of uniform particle radius $r = 0.01$ cm (dotted line). Compared to the monodisperse system we see that the above polydisperse system reacts slower throughout the whole exchange process.

EXPERIMENTAL

Apparatus. All kinetic experiments were performed in a glass-jacketed cylindrical beaker (10 × 7.5 cm diam.), thermostated at 25 ± 0.05 °C. The rate of ion exchange H_3O^+ vs. Cs^+ was measured in the solution continually by an immersed electrical conductivity electrode, connected to a conductivity meter and a recorder. The solution was stirred in the reaction vessel at 280 rpm.

Reagents. Analytical grade CsCl and HCl solutions (p.a. Merck) were used.

Material. The ion exchanger employed was AG-50 W X 8 (Bio-Rad Laboratories), a sulfonated polystyrene-type cation exchanger in the H^+ form. Five fractions of this material, available as spherical beads, were obtained by wet sieving, namely: (1) r = 0.025–0.05 mm; $\bar{r}_1 = 0.0375$ mm. (2) r = 0.05–0.01 mm; $\bar{r}_2$ = 0.075 mm. (3) r = 0.10–0.20 mm; $\bar{r}_3 = 0.15$ mm. (4) r = 0.20–0.40 mm; $\bar{r}_4 = 0.30$ mm. (5) r = 0.40–0.55 mm; $\bar{r}_5 = 0.475$ mm, where $\bar{r}_i$ denotes the mean radius of each fraction.

After sieving, all fractions were once again converted to the H^+ form by 1 N HCl solutions, washed with deionized water, and air dried according to standard procedures (*4*). The pure ion-exchange capacity of the above resin, as determined by the conventional titration method (*4*), using separately 0.2-g air dry samples of each fraction was in the average of all fractions 4.21 mequiv/g air dry resin with a relative standard deviation of 2.4%, which corresponds to 5.09 mequiv/g oven dry, when dried at 105 °C in a vacuum oven.

Procedure. In order to obtain an ion exchanger with a given frequency distribution of particle diameters, weighed amounts of the above air dried five fractions were mixed to a total of 1.00 g (corresponding to $Q_{tot} = 4.21$ mequiv ion exchanger). Since air dried resin ion-exchanger beads crack frequently when placed immediately into water, all mixtures were equilibrated after weighing with saturated water vapor for 24 h. In this way swelling of the beads proceeds very slowly and cracking of the samples was not observed when placed subsequently in the reaction vessel, filled with 300 mL deionized water. After stirring at 280 rpm for several hours, the final swelling and thermal equilibrium is attained and the initial conductivity of the solution is recorded.

The ion-exchange reaction is initiated by adding 2 mequiv Cs^+ (2 mL CsCl, 1 N) instantaneously by a piston pipet. Since the equivalent conductivity of the H_3O^+ ions released into the solution by the ion exchanger is considerably greater than the corresponding one of the Cs^+ ions disappearing, the conductivity of the solution will increase at the same rate as the ion-exchange reaction proceeds (*5*). With help of a suitable calibration curve, the amount of counterions exchanged by the sample at any time can thus be obtained from the continuously recorded values of the solution conductivity.

In this way the rates of ion exchange H_3O^+/Cs^+ were determined for several polydisperse mixtures of the ion exchanger as well as individually for each of the five fractions.

The error in the determination of concentration of the counterions in solution by the above conductivity method is about ±2% rel. With the exception of the first few seconds of the ion-exchange process, the error of the time measurement is always better than ±1% rel.

RESULTS AND DISCUSSION

With one exception, all polydisperse systems of the ion exchanger investigated were prepared by mixing several of the sieved and thus approximately monodisperse fractions. In order to understand, however, quantitatively the rates of ion exchange in polydisperse systems, we have to discuss first

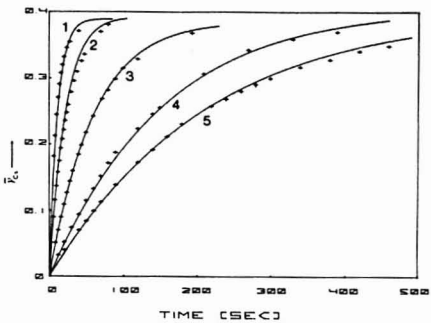


Figure 2. Equivalent fraction $\bar{\gamma}_{Cs}$ of the Cs^+ ions in each of the five fractions of the cation exchanger as a function of time, when placed in their H^+ form *individually* into the CsCl solution (monodisperse systems). Amount of each fraction Q = 4.21 mequiv. Solid line: calculated according to Equation 9; (+++) experimental values

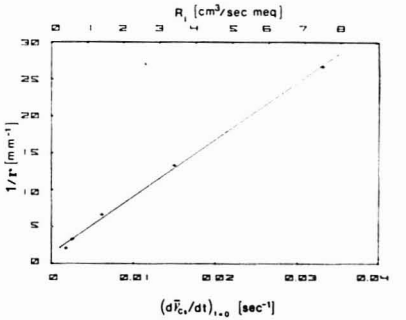


Figure 3. Initial slope $(d\bar{\gamma}_{Cs}/dt)_{t=0}$ of the rate curves of Figure 2 and rate coefficients R_i as a function of the inverse particle radius $1/r$ for each fraction (i = 1–5) of the ion exchanger

those observed for the individual fractions. Once we have evaluated for each fraction of the mixture the numerical value of R appearing in Equation 6, we should be able to describe the kinetic behavior of the polydisperse system. The values of the other constants in this equation, namely α_2^1, and D_2/D_1 have to be identical for each fraction and can be obtained separately, as described below.

Individual Fractions of the Ion Exchanger. The rates of ion exchange Cs^+/H^+, observed individually for each of the 5 fractions are shown in Figure 2. They are given as equivalent fractions $\bar{\gamma}_{Cs}$ of the Cs^+ ions in the resin as a function of time t. From the equilibrium values attained, one obtains the separation factor by using Equation 3 as $\alpha_H^{Cs} = 3.16 \pm 5\%$ rel. as an average value of all five fractions. The total equivalent solution concentration was in all experiments $c = 2/302 = 6.62 \times 10^{-3}$ mequiv/mL.

The theoretical rates of each of these ion-exchange processes can be obtained from Equation 2 by putting $z_1 = z_2 = r_{1c} = r_{2c} = 1$ and using the previous initial and boundary conditions $c_2 = 0$ and $c_1 = 1$ at $t = 0$; $c_2 = Q\bar{\gamma}_1/V$; $c = c_1 + c_2$ as

$$\frac{d\bar{\gamma}_1}{dt} = R\frac{\alpha_2^1(1-\bar{\gamma}_1)(c - Q\bar{\gamma}_1/V) - Q(\bar{\gamma}_1)^2/V}{\alpha_2^1(1-\bar{\gamma}_1)(D_2/D_1) + \bar{\gamma}_1} \qquad (9)$$

where R is of course different for each fraction but not D_2/D_1

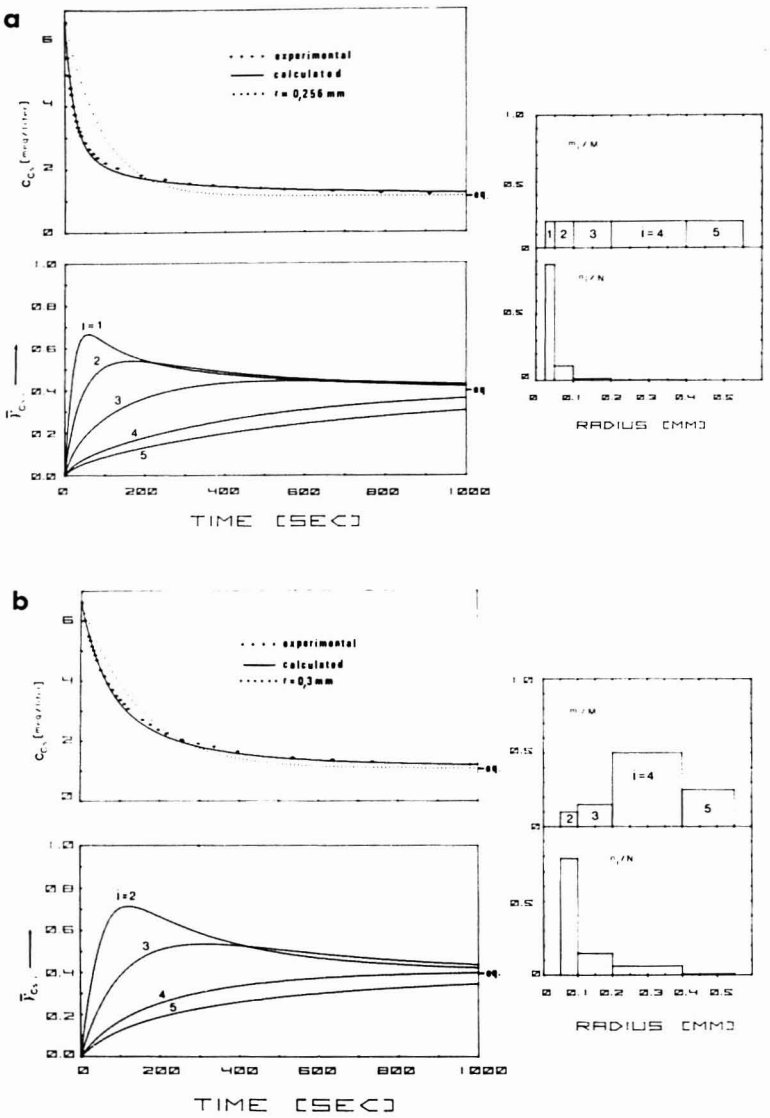
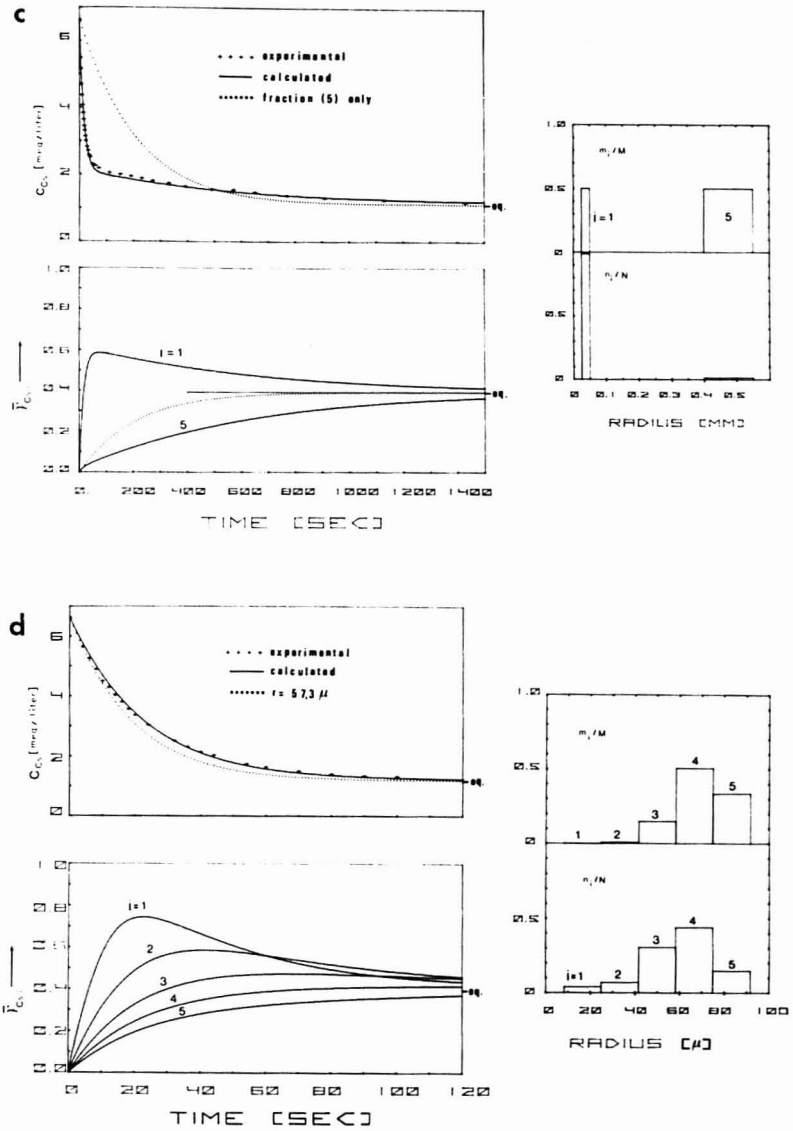


Figure 4. Experimental (+++) and calculated values (solid line) of the Cs^+ ion concentration c_{Cs} in solution (top) and of the equivalent fractions $\bar{\gamma}_{Cs}$ of the Cs^+ ions in each fraction of polydisperse ion-exchanger systems (bottom) as a function of time. Calculations according to Equations 6, 5, and 1. Initially Cs^+ ions only in the solution and H_3O^+ ions only in the ion exchanger. (a) Mixture of equal amounts of all five fractions of the ion exchanger according to weight $m_i/M = 0.2$ ($i = 1$–5). Dotted line: monodisperse system, $r = 0.256$ mm. (b) Mixture of four fractions

and $\alpha_{\frac{1}{2}}$. Equation 9 can be obtained also from Equation 6, when the latter is written for one single component ($i = 1$) only. The initial slope of the experimentally observed $\bar{\gamma}_1$ –

$$\left(\frac{d\bar{\gamma}_1}{dt}\right)_{t=0} = RcD_1/D_2 \qquad (10)$$



of the ion exchanger according to weight: $m_2/M = 0.1$; $m_3/M = 0.15$; $m_4/M = 0.5$; $m_5/M = 0.25$. Dotted line: monodisperse system, $r = 0.30$ mm. (c) Mixture of two very different fractions of the ion exchanger according to weight: $m_1/M = 0.5$. Dotted line: monodisperse system, $r = 0.475$ mm (fraction 5). (d) Commercial ion exchanger, sieved by the manufacturer to 100–200 mesh. Dotted line: monodisperse system according to the arithmetic mean particle radius of the distribution ($r = 57.3$ μm)

t plot (see Figure 3) can be derived from Eq. 9 as Eq. 10. Starting with an estimated numerical value for D_2/D_1 and using the experimentally observed value for $d\bar{\gamma}_{C_A}/dt$ at $t =$ 0, one can calculate with the help of Equation 10 a value of R. Substituting this value together with the other known constants ($Q = 4.21$ mequiv, $V = 302$ mL, $\alpha_H^C = 3.16$, $c = 6.62$

$\times 10^{-3}$ mequiv/mL) into Equation 9, one then calculates the rate of ion exchange and compares it with the corresponding experimental curve of Figure 2. This procedure is continued, using different values for D_2/D_1 until a good fit between the experimental and calculated rate curves is obtained. In the present case Equation 9 was solved numerically by a computer, using the same program as for the solution of Equation 6 by putting in the latter $i = 1$. An analytical solution of Equation 9 is, however, also available (*6*).

In this way one finds for fraction 1 of the ion exchanger, $R_1 = 7.5$ cm^3/s mequiv and $D_2/D_1 = 1.5$. For the other fractions, the same value of D_2/D_1 has to be used, since the same ions are involved in the diffusion process through the Nernst film. With the help of Equation 10 one finds then readily for the remaining fractions $R_2 = 3.4$; $R_3 = 1.4$; $R_4 = 0.58$; $R_5 = 0.415$ cm^3/s mequiv. Inserting these latter values in Equation 9 yields a good agreement between the experimentally observed values (+++ in Figure 2) and calculated ones (solid lines), even though for the other fractions D_2/D_1 could not be adjusted. The above value of D_2/D_1 is also supported by earlier experiments, where investigations of Cs^+/H^+ ion-exchange reactions (*1*) yielded the same value.

Equation 7 shows that R should be inversely proportional to the radius r of the beads of each fraction of the ion exchanger. Similarily, we see from Equation 10 that the initial slope of the rate curves should then also be proportional to $1/r$. That this is indeed observed experimentally also is shown in Figure 3, where the above quantities are plotted for each individual fraction of the resin. The regression line drawn in Figure 3 through the experimental points yields a correlation coefficient of 99.9%. This demonstrates that film diffusion is indeed the rate controlling step under our experimental conditions, since otherwise different rate laws would be observed (*4*).

Polydisperse Systems. After knowing the kinetic and equilibria properties of the individual fractions of the ion exchanger, we should now be able to describe quantitatively the kinetics of the exchange Cs^+/H^+ in an arbitrary mixture of them with the help of Equations 6, 5, and 1.

The first polydisperse system considered experimentally, consisted of 0.2 g air dry ion exchanger of each fraction, corresponding to $Q_i = 0.2$ (4.21) mequiv ($i = 1$–5) (rectangular distribution). Characterizing this frequency distribution of the beads in terms of the weight we have $m_i/M = Q_i/Q_{tot} = 0.2$; $i = 1$–5. For illustration we describe this system also according to the number of particles in each fraction. Using as an approximation for each fraction the corresponding average radius r given earlier, we obtain $n_1/N = 0.874$; $n_2/N = 0.109$; $n_3/N = 0.0137$; $n_4/N = 0.00171$; $n_5/N = 4.3 \times 10^{-4}$. A graphical representation of this frequency distribution can be found on the right side of Figure 4a. Since the initial and boundary conditions for the exchange Cs^+/H_3O^+ were the same as for the individual fractions described above, we have again: $c = 6.62 \times 10^{-3}$ mequiv/mL, $V = 302$ mL, $\alpha_R^{Cs} = 3.16$. Inserting these values together with the above values of D_2/D_1 and R_1 to R_5 in Equations 6, 5, and 1, we are now able to calculate the rate of ion exchange in the above polydisperse mixture. Comparison of the experimental and calculated values in the solution phase is shown in the upper half of Figure 4a, where the concentration of the Cs^+ ions in solution is given as a function of the time. As can be seen, a good agreement is obtained, even though no parameter could be adjusted. It is interesting to know to what extent the kinetics of this polydisperse system deviates from a monodisperse system, exhibiting the same radius of the beads as the average particle radius of the polydisperse mixture. For this reason we calculated with the help of Equation 9 the rates of ion exchange in a monodisperse system, using as uniform particle radius the average of the radii of the first and fifth fraction, i.e., $r = (0.0375 + 0.475)/2 = 0.256$ mm. The corresponding value for R, necessary for that calculation was obtained by interpolation from the curve shown in Figure 3. The result is shown in Figure 4a as a dotted line. As one can see, describing the polydisperse system by a monodisperse one, yields a rather poor approximation. Compared to the monodisperse system, the above polydisperse mixture reacts much faster initially but considerably slower towards the end of the ion-exchange process.

In the lower half of Figure 4a we plotted the calculated rates of the ion exchange processes, occuring simultaneously in each of the five fractions as a result of the competitive reactions among the beads. Similar to the results already obtained in the model calculations, we see that the small particles (fractions 1 and 2) absorb the Cs^+ ions initially so rapidly that they have to release them partially after some time in favor of the larger particles (fractions 4 and 5). An experimental proof of these overshooting effects was obtained earlier (*1*) for a more simple system.

Besides that, the rate curves for the five fractions in Figure 4a show another interesting phenomenon. Even though after about 1000 s the equilibrium in the solution is attained very closely, this is not so for the five fractions of the ion exchanger! At this point of time, all five fractions are still rather far away from their common equilibrium equivalent fraction $\bar{y}_{1,\infty} = 0.394$. The reason, why this very slow attainment of the equilibrium in the ion-exchanger phase does not show up in the solution phase can be, however, understood readily. In the final stages of the ion-exchange process the fractions with the smaller particles release Cs^+ ions to the solution, while the fractions with the larger particles absorb them. As a result, the Cs^+ concentration in the solution will change very little after this point and thus simulate an equilibrium, which is actually not yet attained.

In the next polydisperse system considered, we mixed 0.1 g air-dry ion exchanger of fraction 2, 0.15 g of fraction 3, 0.5 g of fraction 4, and 0.25 g of fraction 5. This yields $Q_1 = 0$; $Q_2 = 4.21$ (0.1) mequiv; $Q_3 = 4.21$ (0.15) mequiv; $Q_4 = 4.21$ (0.5) mequiv and $Q_5 = 4.21$ (0.25) mequiv. The frequency distribution according to the weight is thus $m_1/M = Q_1/Q_{tot} = 0$; $m_2/M = Q_2/Q_{tot} = 0.1$; $M_3/M = Q_3/Q_{tot} = 0.15$; $m_4/M = Q_4/Q_{tot} = 0.5$ and $m_5/M = Q_5/Q_{tot} = 0.25$. Using again for each fraction the corresponding average radii $\bar{r}_i$ we can calculate for illustration $n_1/N = 0$; $N_2/N = 0.784$; $n_3/N = 0.147$; $n_4/N = 0.0612$; $n_5/N = 0.00771$. The graphical representation of this frequency distribution of the particles is shown on the right side of Figure 4b.

Inserting the same numerical values for c, V, α_R^{Cs}, D_2/D_1, R_i as in the preceding example and the above values for Q_i in Equations 6, 5, and 1, the rates of ion exchange in the solution as well as in the ion-exchanger phase of each fraction can be calculated. The result is shown in Figure 4b. Again, a good agreement between experimental and calculated values is found. For comparison we calculated also in this case with help of Equation 9 the rate of ion exchange of a monodisperse system, exhibiting as uniform radius $r = 0.3$ mm, which is the average radius $\bar{r}$ of the "central" fraction 4 of the above distribution (dotted line in Figure 4b). Again we see that the kinetic behavior of this polydisperse system can be described only unsatisfactorily by a monodisperse approximation.

Inside the resin phase of each fraction we observe again the overshooting effects for the smaller particles and—comparted to the solution—the slow attainment of the equilibrium of each fraction for the same reasons as in the preceding example.

In the next example a mixture, consisting only of the very small particles of fraction 1 and of the large particles of fraction 5, is investigated, since one can observe in this case the slow reaction of the resin phase very clearly. Using 0.5 g air dry ion exchanger each of fraction 1 and 5, we have Q_1

$= Q_5 = 4.21$ (0.5) mequiv; $Q_1/Q_{tot} = Q_5/Q_{tot} = 0.5$. Using the average radii $\bar{r}$ of each fraction, one can calculate also in this case for illustration $n_1/N = 0.997$ and $n_5/N = 4.91 \times 10^{-4}$. This distribution is shown on the right side of Figure 4c. Inserting the same numerical values for C, V, α_H^{Cs}, D_2/D_1, R_1, and R_5 as before, together with the above values for Q_1 and Q_5, in Equations 6, 5, and 1, the rates of ion exchange can be calculated for this mixture (Figure 4c). Again a good agreement between experimental and calculated rates is observed. In the solution the Cs^+ ions disappear rapidly and—considering the solution only—the equilibrium is almost attained after about 200 s (upper half of Figure 4c). At this point of time, the ion-exchanger particles are, however, still very far away from their equilibrium values. But again, as observed before since the smaller particles (fraction 1) release after this time interval Cs^+ ions while the larger ones (fraction 5) absorb them, very little change of the Cs^+ concentration is observed in the solution. In fact, and this is surprising, the large particles (fraction 5) react slower in the above mixture than in a system containing fraction 5 only. This is also shown in Figure 4c, where the rate of ion exchange observed, if fraction 5 is the only ion-exchanger component in solution is drawn as a dotted line. As can be seen, in this case the equilibrium is attained quite closely after about 800 s, in contrast to the behavior of fraction 5 in the mixture, which is at this point still far away from equilibrium. The reason, why large ion-exchanger particles react slower in the presence of smaller particles can be understood readily. As is well known, the rate of a film diffusion controlled ion-exchange process depends on the momentary concentration c_1 of the counterions to be absorbed in solution (see Equation 2). Since, in a polydisperse mixture of an ion exchanger, the smaller particles react faster initially, c_1 diminishes *thus* rapidly in the solution. As a result, the larger particles of the mixture find only relatively few counterions to absorb and react now even slower than in the absence of the small particles. Thus, substituting in a system of uniform ion-exchanger particles part of them on a weight basis by smaller particles, results in a faster reaction in the solution phase but in a slower reaction in the ion-exchanger phase.

Finally, instead of the synthetic mixtures described so far, we also investigated a "natural" polydisperse mixture, namely the commercially available ion exchange resin DOWEX-50 W X 8, 100–200 mesh, which is essentially the same resin as the preceding one, except that it is less purified and exhibits a wider particle range. The frequency distribution of the particle diameters of this material according to the number n_i/N was determined under the microscope and distributed into five classes as shown in Figure 4d, right side. Using these values and the measured average radii of each fraction ($\bar{r}_1 = 16.7$; $\bar{r}_2 = 32.1$; $\bar{r}_3 = 50.0$; $\bar{r}_4 = 66.7$; $\bar{r}_5 = 83.3$ μm), one obtains $Q_1/Q_{tot} = 7.18 \times 10^{-4}$; $Q_2/Q_{tot} = 8.88 \times 10^{-3}$; $Q_3/Q_{tot} = 0.194$; $Q_4/Q_{tot} = 0.507$; $Q_5/Q_{tot} = 0.334$ (An alternative way to obtain the Q_i/Q_{tot} values would be a sieve analysis of the material and weighing of each fraction). The separation factor was found to have the same value i.e., $\alpha_H^{Cs} = 3.16$; the weight in quantity of the ion exchanger for the kinetic experiment was $Q_{tot} = 4.0$ mequiv. The values of R_i were found for each fraction with help of inter- and extrapolation of the $1/r$ vs. R curve shown in Figure 3. The values for c, V, and D_2/D_1 were the same as in the other cases. The experimental and calculated results of this system are shown in Figure 4d. Agreement between these values is again good. The arithmetic mean particle radius of this polydisperse resin was found from the counting statistics of $\bar{r} = 57.3$ μm. Describing the rate of ion exchange in the present polydisperse system by a monodisperse system using this mean radius, results in a rate curve, shown as a dotted line in Figure 4d. The poor agreement between this curve and the experimental results reveals that the particle range of this resin, sieved by the manufacturer to 100–200 mesh, is still too wide that it can be—from a kinetic point of view—considered monodisperse.

CONCLUSIONS

The rates of ion exchange in polydisperse systems exhibit in the concentration range, where film diffusion is the rate determining step, several characteristics, not observed in monodisperse systems.

Since the smaller particles always react faster than the larger ones, they will overshoot their eventual equilibrium value and have, therefore, to release after some time considerable amounts of these already sorbed counterions in favor of the larger particles.

Even though during the later stage of the reaction, counterions are still exchanged between the smaller and larger particles of the mixture, the concentration of the ions in the solution changes very little by these processes. As a result, monitoring only the solution concentration simulates an equilibrium of the polydisperse system, which is not yet attained by the ion-exchanger particles.

Attainment of equilibrium of the large ion-exchanger particles in a polydisperse system is slower than in a monodisperse system, containing the same total amount of ion exchanger in the form of large particles only.

LITERATURE CITED

(1) K. Bunzl, *J. Inorg. Nucl. Chem.*, **39**, 1049 (1977).
(2) L. Collatz, "The Numerical Treatment of Differential Equations", Springer Verlag, Berlin, 1960.
(3) L. Sachs, "Angewandte Statistik", Springer Verlag, Berlin, 1974.
(4) F. Helfferich, "Ion Exchange", McGraw-Hill Book Co., New York, N.Y., 1962.
(5) K. Bunzl, *J. Soil Sci.*, **27**, 32 (1976).
(6) K. Bunzl, A. Wolf, and B. Sansoni, *Z. Pflanzenernaehr. Bodenk.*, **4**, 476 (1976).

RECEIVED for review August 29, 1977. Accepted October 25, 1977.

Determination of Sulfur Compounds in High-Boiling Petroleum Distillates by Ligand-Exchange Thin-Layer Chromatography

Takashi Kaimai* and Atsushi Matsunaga

Nippon Mining Co., Ltd., Technical Research Center, 3 Niizo-Minami, Toda, Saitama 335, Japan

Determination of sulfur compounds in high-boiling petroleum distillates was carried out by ligand-exchange thin-layer chromatography (LETLC). Mercaptans, sulfides, and disulfides were separated from aromatic hydrocarbons by LETLC on a mercury-loaded silica gel. It was, however, difficult to separate dibenzothiophene from aromatic hydrocarbons. Alkyl mercaptan formed a strong complex with mercury and was not developed at all, even with polar solvent. Sulfur compounds were isolated by this procedure from petroleum aromatic concentrate and were identified by GLC/MS.

The problem of separating sulfur compounds from the hydrocarbons and other materials in petroleum has received much attention for many years. Many separation methods were proposed but no satisfactory method for the higher boiling fractions of crude oil has been reported.

Recently, procedures for class separation of organic sulfides, utilizing interaction of metals with sulfur compounds from hydrocarbons, have been developed. Nonaqueous ligand-exchange column chromatography has been used for separation of sulfides from other petroleum compounds (*1, 2*). The presence of cyclic and aryl sulfides was shown by mass spectral examination.

This paper describes a simple procedure for class separation of sulfur compounds and quantitative sulfur type analyses of heavier petroleum distillates. The separation was achieved by ligand-exchange thin-layer chromatography (LETLC) on mercuric acetate-impregnated silica gel plate. The determination of the ratio of sulfides to dibenzothiophenes was carried out with a densitometer.

EXPERIMENTAL

Apparatus. A sandwich chamber system (CF-TLC supplied by Toyo Roshi, Tokyo, Japan) was used for development of TLC. A densitometer (Dual-Wavelength TLC Scanner CS-910 obtained from Shimadzu Seisakusho, Kyoto, Japan) was used for quantitative type analysis (*3*).

Materials. Absorbents used were Silica gel H (Type 60), Aluminium oxide acidic (Type T), and Aluminium oxide basic (Type E) all obtained from Merck.

Procedure. Adsorbent layers of approximately 0.25-mm thickness were produced by coating 20 × 20 cm glass plates following the standard procedure. The coated plates were left to dry on the bench overnight and then sprayed with 1 wt % methanol solution of metal salts. These metal salts-loaded silica gel plates were left to dry on the bench and then used without any further activation. The spots on the chromatograms were revealed in either of two ways: (a) by inspection under UV light (254 nm) or (b) by spraying with palladous chloride solution.

Quantification of colored spots was carried out by a densitometer. Zigzag scanning and the reflectance mode were employed for measurements. Spots colored by spraying with palladous chloride were scanned at 380 nm, compensating background at 600 nm, for sulfur compounds analyses.

Diphenyl sulfide and dibenzothiophene were used as standard sulfur compounds for calibration.

Table I. R_s[a] Values of Standard Compounds by TLC (Solvent; *n*-Hexane)

Sample	Adsorbent: Silica gel	Alumina (acidic)	Alumina (basic)
n-Cetyl mercaptan	1.08	1.58	1.48
p-tert-Butyl thiophenol	1.08	1.38	1.00
n-Decyl sulfide	0.72	1.50	1.30
Benzyl phenyl sulfide	0.51	0.62	0.70
Di-*n*-octyl disulfide	1.04	1.62	1.35
Diphenyl disulfide	0.72	1.31	1.22
Dibenzo-thiophene	0.92	1.23	1.17
Liquid paraffin	1.92	-	-
Alkyl naphthalenes	1.84	-	-
Alkyl tetralins	1.84	-	-

[a] Reference compound, anthracene.

RESULTS AND DISCUSSION

Separation of Standard Sulfur Compounds. Separation of sulfur compounds from aromatic hydrocarbons was investigated with TLC on silica gel and alumina (acidic and basic) layers. Sulfur compounds and hydrocarbons used in these examinations are listed in Table I. *n*-Hexane was used as developing solvent. R_s values (reference compound: anthracene) of standard compounds are indicated in Table I. As shown, it was difficult to separate any sulfur compound from aromatic hydrocarbons and to make class separation of sulfur compounds with conventional adsorbents.

Table II shows R_s values of sulfur compounds in TLC on various metal salts-loaded silica gel layers with *n*-hexane as developer. Mercuric acetate and silver nitrate were effective for class separation of sulfur compounds. Any of the metal salts in Table II was effective for separation of *n*-cetyl mercaptan. *n*-Cetyl mercaptan was not developed because of its formation of strong complexes with metal salts, but not because of the formation of mercaptides. This was supported by the fact that *n*-cetyl mercaptan was developed by TLC on mercuric acetate-loaded basic alumina or florisil with *n*-hexane as developer. Zinc chloride, cadmium acetate, and copper acetate were effective for separation of *p-tert*-butyl thiophenol, but not so effective for sulfides and disulfides. This means that thiophenols form complexes with metal salts easily.

Table III shows R_s values of standard compounds in TLC on mercuric acetate-loaded silica gel with various developing solvents. Figure 1 shows the chromatogram developed with *n*-hexane. Alkyl mercaptan was not developed at all. Thiophenol and sulfides were developed a little. Disulfides

0003-2700/78/0350-0268$01.00/0 © 1978 American Chemical Society

Table II. R_s Values of Sulfur Compounds by TLC on Various Metal Salts-Loaded Silica Gel (Solvent, *n*-Hexane)

Sulfur compound	Metal salt				
	Mercuric acetate	Zinc chloride	Cadmium acetate	Copper acetate	Silver nitrate
n-Cetyl mercaptan	0	0	0	0	0
p-*tert*-Butyl thiophenol	0.13	0.32	0.19	0.10	0.18
n-Decyl sulfide	0.05	0.82	1.00	0.85	0
Benzyl phenyl sulfide	0.05	0.52	0.42	0.35	0.18
Di-*n*-octyl disulfide	0.86	1.64	1.30	1.30	0.53
Diphenyl disulfide	0.41	1.12	1.00	0.90	0.88
Dibenzothiophene	1.05	1.28	1.00	1.00	1.18

Table III. R_s Values of Standard Compounds by TLC on Mercuric Acetate-Loaded Silica Gel

Sample	Solvent		
	n-Hexane	Carbon tetrachloride	Benzene
n-Cetyl mercaptan	0	0	0
p-*tert*-Butyl thiophenol	0.13	0.24	0.40
n-Decyl sulfide	0.05	0.18	0.19
Benzyl phenyl sulfide	0.05	0.29	0.76
Di-*n*-octyl disulfide	0.86	0.78	1.00
Diphenyl disulfide	0.41	0.33	1.00
Dibenzothiophene	1.05	1.00	1.00
Liquid paraffin	2.45	1.24	1.00
Dialkyl benzenes	2.09	1.13	1.00
Alkyl naphthalenes	2.09	1.13	1.00
Alkyl tetralins	2.09	1.13	1.00

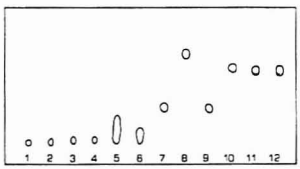


Figure 1. Chromatogram of standard compounds by TLC on mercuric acetate loaded silica gel. (1) *n*-Cetyl mercaptan, (2) *p*-*tert*-butyl thiophenol, (3) *n*-decyl sulfide, (4) benzyl phenyl sulfide, (5) di-*n*-octyl disulfide, (6) diphenyl disulfide, (7) dibenzothiophene, (8) liquid paraffin, (9) anthracene, (10) dialkyl benzenes, (11) alkyl naphthalenes, (12) alkyl tetralins

were developed with tailing. Dibenzothiophene was developed to the similar position of anthracene without tailing. Hydrocarbons were developed without tailing and gave larger R_f values. It is clear that the separation of sulfur compounds except dibenzothiophene from hydrocarbons is possible by the procedure mentioned above.

It was reported (*4*) that low molecular weight sulfides form complexes with mercuric ions and these complexes can be extracted from the organic to the aqueous layer. Such interaction may be responsible for the TLC separation procedure. Sulfur compounds may be developed while forming complexes. This analytical procedure could be expressed as ligand-exchange TLC.

Table IV. Sulfur Compounds Isolated from High-Boiling Distillates of Kuwait Crude Oil (Identified by GLC/MS)

Molecular ion (*m*/*e*)	Sulfur compound
250, 264, 278, 292, 306, 320	Alkyl thiophenols (Alkyl; $C_{10}H_{21}$-$C_{15}H_{31}$)
212, 226, 240, 254, 268, 282, 296, 310, 324	Alkyl hexahydrothiaindans (Alkyl; C_5H_{11}-$C_{13}H_{27}$)
214, 228, 242, 256, 270, 284	Alkyl tetrahydrothiapyrans (Alkyl; C_8H_{17}-$C_{13}H_{27}$)
210, 224, 238, 252, 266, 280, 294, 308, 322	Alkyl thiophenes (Alkyl; C_9H_{19}-$C_{17}H_{35}$)

Table V. Color Reaction with $PdCl_2$

Color	Sulfur compound
White	*n*-Decyl sulfide
Yellow	Benzyl phenyl sulfide, *n*-cetyl mercaptan
Orange	Diphenyl disulfide, dibenzothiophene, *p*-*tert*-butyl thiophenol
Brown	Di-*n*-octyl disulfide
Dark brown	Benzothiophene

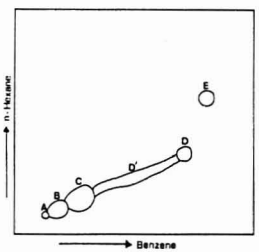


Figure 2. Chromatogram of standard sulfur compounds (two-dimensional development). (A) *n*-Cetyl mercaptan (white); (B) *p*-*tert*-butyl thiophenol, *n*-decyl sulfide (orange); (C) benzyl phenyl sulfide (brown); (*D*, *D'*) di-*n*-octyl disulfide, diphenyl disulfide (brown); (E) dibenzothiophene (orange)

Dibenzothiophene was different from other types of sulfur compounds and developed to the similar position of anthracene. For this reason, it is considered that dibenzothiophene cannot form a coordination compound with mercuric ion because of its steric hindrance. This is supported by the fact that alkyl thiophenes which have less steric hindrance than dibenzothiophene were separated from aromatic hydrocarbons in high-boiling petroleum distillates by preparative LETLC. (See Table IV.)

Sulfur compounds were classified as shown in Table V by color reaction with palladous chloride. Hydrocarbons do not react with palladous chloride.

Acidic alumina was found to be as effective a support for separation of sulfur compounds from hydrocarbons as silica

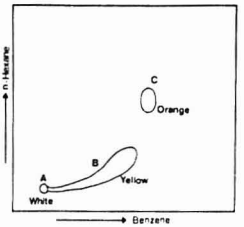


Figure 3. Chromatogram of sulfur compounds in transformer oil (two-dimensional development)

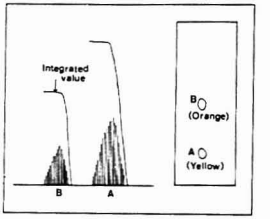


Figure 4. Densitometric scanning of the spots of diphenyl sulfide and dibenzothiophene (at 380 nm)

gel, but basic alumina, neutral alumina, molecular sieves, and Florisil were not effective. This means that the formation of complex can be accomplished under acidic state.

Two-dimensional development was carried out to attain a clear class separation of sulfur compounds on the mercuric acetate-loaded silica gel. Figure 2 shows a chromatogram of standard sulfur compounds by two-dimensional development. Dibenzothiophene was separated clearly from other sulfur compounds.

Separation of Sulfur Compounds in Lube-Stocks. Figure 3 shows a chromatogram of sulfur compounds in an aromatic concentrate of transformer oil by two-dimensional development. Two-dimensional development was effective for class separation of sulfur compounds in refined oil. An orange spot indicates the presence of dibenzothiophenes. A yellow part indicates the presence of sulfides and little presence of disulfides. This means that the main types of sulfur compounds in the transformer oil are dibenzothiophenes and sulfides.

Qualitative analysis was carried out on sulfur compounds in aromatic concentrate from high-boiling distillates (bp 280–440 °C) of Kuwait crude oil. Sulfur compounds except dibenzothiophenes were separated from aromatic hydrocarbons by LETLC on a preparative scale with *n*-hexane as developer. After separation, sulfur compounds except dibenzothiophenes on silica gel were scratched up (aromatic hydrocarbons and dibenzothiophenes are seen to be blue by inspection under UV light) and then dissolved in methanol. Table IV shows sulfur compounds identified by GLC/MS. Existence of thiophenols was confirmed by strong UV absorption at 316 nm.

Quantitative Analyses. Figure 4 shows the result of the densitometric scanning of the spots of diphenyl sulfide and dibenzothiophene after separation by LETLC and visualization. The extinction coefficient of colored complex varied with the difference of sulfur compound. For example, that of diphenyl sulfide was seven times as large as dibenzothiophene at 380 nm. The repeatability of this measurement was not so good, mainly because of the instability of the extinction coefficient of the complex. Therefore, it was necessary to standardize the interval from spraying to scanning. But even so, the variations of the results were in the range 2 to 4%.

The ratios of sulfides to dibenzothiophenes in several lubricant basestocks (150 neutral) were determined. Two type sulfur compounds were separated with two-dimensional development of LETLC. After visualization, densitometric scanning of the spots was carried out. The contents of sulfides in lubricant basestocks were 7 to 20 wt % of total sulfur compounds and dibenzothiophenes were 80 to 93 wt %. The ratios of sulfides to dibenzothiophenes depended on the crude source and refining process.

ACKNOWLEDGMENT

The authors thank Takeda Rika, Tokyo, for use of the densitometer. The authors are also grateful to K. Fujimori, and T. Akada for helpful discussions.

LITERATURE CITED

(1) L. R. Snyder, *Anal. Chem.*, **41**, 314 (1969).
(2) J. W. Vogh and J. E. Dooley, *Anal. Chem.*, **47**, 816 (1975).
(3) H. Yamamoto, T. Kurita, J. Suzuki, R. Hira, N. Nakano, H. Makabe, and K. Shibata, *J. Chromatogr.*, **116**, 29 (1976).
(4) T. Yotsuyanagi, T. Kamidate, and K. Aomura, *Jpn. Anal.*, **18**, 1487 (1969).

RECEIVED for review August 10, 1977. Accepted September 30, 1977.

Packed Microcapillary Columns in High Performance Liquid Chromatography

Takao Tsuda[1] and Milos Novotny*

Department of Chemistry, Indiana University, Bloomington, Indiana 47401

New high-pressure LC (packed microcapillary) columns are described which consist of small adsorbent particles drawn inside glass capillaries of 50–200 μm internal diameters. A typical ratio of the column inner diameter to particle size is 2, and a significant plate-height reduction is achieved with decreasing particle size. With typical flow rates of several μL/min through such columns, modified injection and detection techniques are necessary. The columns of different inner diameters and particle sizes were evaluated through the reduced plate height vs. velocity plots. The effect of column coiling diameter on chromatographic performance was also studied. Whereas sample capacity of packed microcapillary columns is low, typical column efficiencies are significantly higher than those obtained with the hitherto available LC columns.

The basic types of columns available in analytical gas chromatography (GC) are conventional packed columns, open tubular (capillary) columns, micropacked columns (with typical internal diameters around 1 mm), and packed capillary columns. These columns differ widely in terms of separation efficiency and sample capacity. Selection of a column type in liquid chromatography (LC) has been more restricted because of viscosities and solute diffusivities in the liquid phase which are orders of magnitude different from the values in the gas phase.

The most efficient columns presently used in LC are those packed with totally porous small particles (with particle size down to several micrometers). The other column types, as known in GC, have not been sufficiently explored. This is primarily due to the fact that the mass transfer is a diffusion-controlled process. Thus, capillary LC is unlikely to give desired efficiencies under the conditions of laminar flow.

Packed capillary columns studied extensively in GC by Halasz and Heine (*1*) and Landault and Guiochon (*2*) have rather unique characteristics. Their technology is different from other column types in that the adsorptive material is drawn inside the glass capillaries, in a way that is somewhat similar to the very common method for preparation of glass capillary helices (*3*). However, according to Halasz and Heine (*1*), the most important feature of such columns is the ratio of particle size to the internal column diameter. Whereas packed capillaries possess usual values of this ratio between 0.2 and 0.5, the conventional packed columns are typically well below 0.1. Thus, packed capillaries have certain geometrical characteristics of their own which are reflected in their analytical performance. Considering a rather loose packing of these columns used in GC, their efficiencies are quite high. Halasz and Heine (*1*) attribute this to the mobile-phase mixing effect that aids the radial diffusion and stress the importance of high column permeability.

When comparing the theoretical separating power of GC and LC with the actual situation, Giddings (*4*, *5*) and Golay (*6*) note that, unlike in GC where a reasonable approach has been made to its theoretical limit through the capillary column, there is a discrepancy in LC of many orders of magnitude.

Giddings (*4*) derived a simple relationship between the limiting number of theoretical plates, N_{lim}, and certain parameters involved in the chromatographic separation (time of analysis disregarded):

$$N_{lim} = \frac{d_p^2 \Delta p}{4\psi\gamma\eta D_M} \tag{1}$$

where ψ and γ are geometrical constants, d_p is the particle size, Δp is pressure gradient, η is viscosity, and D_M is solute diffusivity in the mobile phase. Thus, for the columns of the same geometrical characteristics used in GC and LC it applies that

$$\frac{N_{lim}(GC)}{N_{lim}(LC)} = \frac{\eta_L D_L}{\eta_G D_G} \approx \frac{1}{1000} \tag{2}$$

When substituting typical values into Equation 1, N_{lim} for LC can be as much as 10^8 theoretical plates.

It also appears from the above considerations that the pressure gradient Δp (and, subsequently, inlet pressure) is the most important variable in achieving higher column efficiencies. In modern LC using columns packed with micrometer-size particles, pressures up to several hundred atmospheres are typically employed. Although substantial reductions of the plate height are achieved while decreasing the particle size, there are some practical limits to this procedure. As pointed out by Halasz et al. (*7*), there are difficulties in uniform packing of very small particles, as well as the problem with the evolved heat of friction.

The present investigation explores a version of packed capillary columns for high-performance LC. However, since both particle diameters and internal radii of such columns are typically an order of magnitude lower than those used in GC, we will refer to them as "packed microcapillaries" throughout the text. Special technology has been developed to achieve uniform packing of these columns. As demonstrated by the presented results, capacities of packed microcapillaries are significantly lower than those of typical LC analytical columns. However, column efficiencies are significantly higher. Since the injector and detector connections (split sampling and the use of a make-up liquid flow) are crucial to the column performance, this chromatographic technique is strongly reminiscent of the use of capillary columns in GC.

In the present work, several column types with different particle size and the column internal diameter were investigated. Van Deemter plots obtained with the packed microcapillaries are presented and their shapes are discussed. Since the plate height, H, of such columns appears to be strongly affected by hydrodynamic factors, a possible role of column coiling was briefly investigated. Evaluations were made for columns of identical internal diameter and particle size, but different column coil radii.

EXPERIMENTAL AND RESULTS

Preparation of Packed Microcapillaries. A commercial glass drawing machine (Hupe and Busch, Groetzingen, West

[1] On leave from the Department of Applied Chemistry, Faculty of Engineering, Nagoya University, Nagoya, Japan.

0003-2700/78/0350-0271$01.00/0 © 1978 American Chemical Society



Figure 1. Microphotograph of a section of alumina-packed microcapillary. Column inner diameter, 75 μm; average particle size, 30 μm

Germany) was used for the preparation of columns. The drawing apparatus was placed in the vertical position while the packing material was introduced uniformly into the drawn microcapillary by means of gravity. The packing uniformity of the original glass column (typically, 5.5-mm o.d. and 0.25-mm i.d.) is very important; packing under the vibrator action aids this uniformity. The inner and outer column diameters can be varied through selection of the initial dimensions of glass tubing and drawing conditions. Because of its relatively low melting temperature, soft glass is a preferred material. Reproducible preparation of columns with internal diameters below 100 μm is relatively easy. A typical wall thickness of our columns is 250–300 μm.

The uniformity of packing inside the microcapillaries will strongly affect column efficiency. Thus, selection of a uniform particle size fraction is initially desirable. Whereas it is technically feasible preparing packed microcapillaries from a variety of materials that do not undergo undesirable irreversible changes during the drawing process, such columns require some variations of technology. The present fundamental investigations of packed microcapillaries were limited to the use of acidic and basic alumina packing materials. These were 30 μm and 10 μm activated alumina (LiChrosorb, AloxT, from E. Merck Reagents, Darmstadt, West Germany), 100 μm activated alumina (from M. Woelm, Eschwege, West Germany) as well as the corresponding particle size fractions obtained from the coarse column chromatography materials after grinding, mechanical sieving, and sedimentation sizing process.

Although various columns with different particle sizes and diameters were prepared and their analytical properties are described below, we presently consider columns with internal diameters between 50 to 80 μm, packed with particles around 30 μm, to be a good compromise between analytical performance and minimum difficulties of operating conditions (sample size, available inlet pressure, and sample introduction). The columns have a uniform appearance along their entire length. A microphotograph of a typical section of the alumina-packed microcapillary is shown in Figure 1. Technological importance of the ratio of capillary inner diameter to particle size must be stressed. Although the columns of larger diameters packed with small particles (e.g., 140-μm i.d. and 30-μm particle size) have uniform appearance, their structure collapses under the operating conditions, and clogging occurs.

Whereas the radius of most studied columns was 6 cm, the drawing apparatus had to be provided with home-made coiling tubes for the preparation of columns coiled into greater or smaller radii.

Analytical System. The high-pressure syringe pump and UV-detector of the Varian Model 4100 liquid chromatograph were used throughout the measurements. Since the problems of dead volume are considerably more severe with these column types than

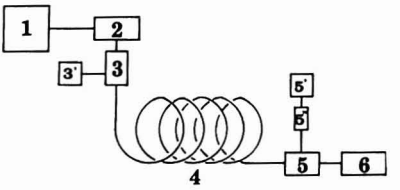


Figure 2. Microcapillary liquid chromatograph: 1, high-pressure syringe pump; 2, injection point; 3, splitter; 3′, metering valve to adjust split ratio; 4, packed microcapillary column; 5, make-up liquid mixing piece; 5′, liquid reservoir; 5″, flow restricting valve; 6, detector

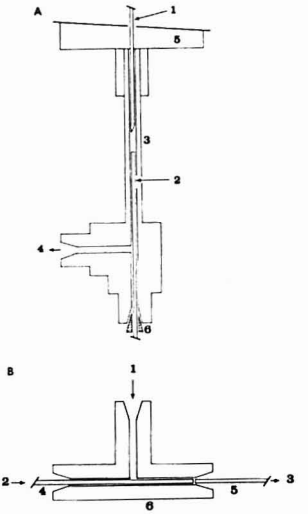


Figure 3. (A) Injector/splitter: 1, microsyringe needle; 2, column inlet; 3, 1.5-mm i.d. tube; 4, direction of discard flow; 5, injector flange; 6, polyimide ferrule. (B) Make-up liquid mixing piece: 1, entering make-up liquid; 2, column effluent; 3, liquid entering detector cell; 4, column outlet; 5, detector connecting capillary; 6, mixing tee

with the conventional LC columns, both injection and detection techniques were modified. In order to overcome these problems, we resorted to the commonly practiced techniques of capillary GC (sample splitting and the use of additional liquid flow at the column outlet). Figure 2 shows the schematic diagram of the system used, whereas Figure 3 details the parts of injector/splitter and the make-up solvent assembly.

Typical split ratios around 1:1000 resulted in the use of maximum detector sensitivity. However, the detector response is decreased by the use of an extra liquid flow to overcome the detector cell dead volume. Whereas such flow was around 20–50 μL/min, typical flow rates through 70-μm i.d. packed microcapillaries are less than 10 μL/min. As judged from reproducibility of retention times, flow appears constant among individual runs, once the inlet pressure is set to a desired value.

It should be emphasized that this work primarily addresses itself to fundamental column performance investigations. Thus, better sample introduction techniques and detectors with small internal volumes and greater sensitivities are needed for future work.

Column Efficiency Studies. Three different ratios of particle size and inner diameter were used in preparation of packed microcapillaries: 100/200, 30/70, and 10/50 μm. Van Deemter plots were measured for standard UV-absorbing solutes, introduced onto the columns in the amounts close to 10^{-8} g. As ex-

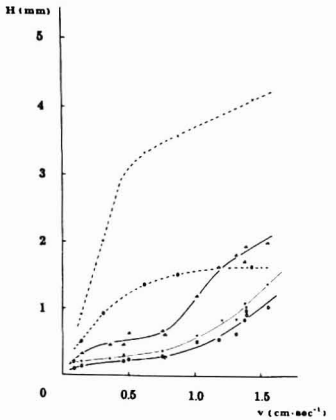


Figure 4. Plate height vs. velocity curves for standard solutes run on 100-μm (broken line) and 30-μm (solid line) particle size columns. O = benzene; x = methyl benzoate (retention relative to benzene, 1.34 for 100-μm column and 1.14 for 30-μm column); Δ = quinoline (retention relative to benzene, 1.71). To adjust approximately the same relative retention on both column, the mobile phase was hexane with 0.03% and 0.05% methanol, respectively, for a 30-μm and 100-μm column. Column lengths were 14 m and 40 m for 30-μm and 100-μm columns, respectively

pected, values of the height equivalent to a theoretical plate, H, were reduced with decreasing particle size, d_p. Figure 4 demonstrates differences in H vs. v (average linear velocity of the mobile phase) curves for a 100-μm compared to a 30-μm particle column. Whereas the minima of these H vs. v plots apparently lie at considerably lower velocity values than measurable, the plate heights at the lowest velocity values of Figure 4 roughly correspond to those theoretically predicted (*7*):

$$H_{min} = A + 2\sqrt{BC} \approx 3.6\, d_p$$

Shapes of H vs. v curves are important for both understanding the physical phenomena occurring in the columns as well as their analytical utility. Obviously, the measured curves fail to fit the usually proposed equations of liquid chromatography (*7*, *19*).

Whereas the initial nonlinearity of the measured curves is not unusual for some LC columns and can be explained by the coupling theory of Giddings (*8*), there appears no simple explanation for the further rise of H with flow rate. It should be stressed that this general curve shape (rise, a plateau, and a second steeper rise) is highly reproducible with sequentially prepared columns of the same particle size. As indicated below, the curve shape holds also for other d_p values, although particle size or packing geometry appears to determine the second onset of the curves. It is also unlikely that mechanical changes of the column bed due to high pressure and/or flow shear are implicated; repeatedly measured curves gave identical shapes.

Plots of reduced values (*8*) are generally considered as good indication of the column's chromatographic quality across a range of particle sizes. Figure 5 shows the reduced plots for three columns of different particle size. The plots were obtained using a nonretained (or only slightly retained) solute, benzene, in order to dissociate mass-transfer processes from those of hydrodynamic nature. The initial h values of the smallest-particle column (10 μm) are somewhat higher than those of other two columns. This is most likely a result of our present insufficient packing technology at this particle size and less homogeneous column bed. Figure 5 further demonstrates the effect of particle size on band broadening under the dynamic conditions. The shapes of curves obtained with retained solutes on the columns with different particles are nearly identical (Figure 6). With the current column technology, less than 10% column-to-column variation in H at a given velocity and retention time was observed.

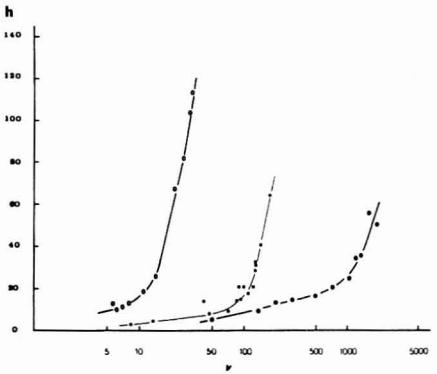


Figure 5. Reduced plate height vs. reduced velocity curves for benzene measured on O = 10-μm particle size column (length, 3.6 m), ■ = 30 μm (length, 14 m), and ● = 100 μm (length, 40 m). Mobile phase: same as Figure 4

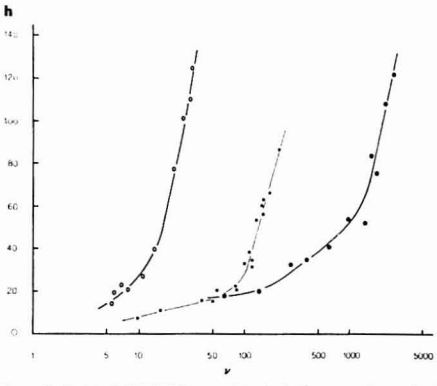


Figure 6. Reduced plate height vs. reduced velocity curves for retained solutes on same columns as indicated in Figure 5, under the same conditions. Solutes of similar relative retention were used: pyridine (10-μm column); quinoline (30-μm column); and methyl benzoate (100-μm column)

If hydrodynamic factors are involved in the zone broadening phenomena, it is of some interest to investigate whether the column coil radius can influence the plate height as well. This situation received some attention previously (*9–11*) with different column types. The results obtained with the columns of identical inner diameter and particle size, but different column coil radii, are shown in Figure 7.

Although analytical applications of packed microcapillaries will be a matter of future research, two important questions are of immediate interest: first, what are the typical column efficiencies to be expected, and second, what sample sizes can be tolerated.

A chromatogram of a standard mixture obtained on a "typical" packed microcapillary is shown in Figure 8. Whereas the total number of theoretical plates obtained on this run is not identical with the so-called effective plates (it is estimated that some 70% of the column space is occupied by the mobile phase), there is every indication of achieving column efficiencies approximately an order of magnitude higher than those currently available in practice of modern LC.

Sample capacity of a 10-μm particle column was investigated using benzene, methyl benzoate, and dimethyl phthalate introduced through the splitter in varying amounts (Figure 9).

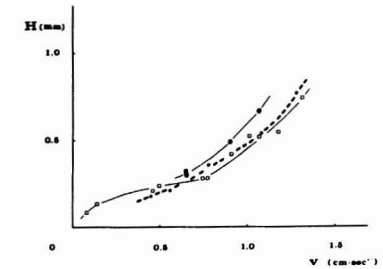


Figure 7. Effect of column coil diameter on plate height vs. velocity curves. Solute: benzene; all columns were 12 m × 75 μm i.d., packed with 30-μm alumina. Mobile phase: hexane with 0.05% methanol. Column coiling diameters: O, 30 cm; □, 12 cm; and ■, 5.7 cm

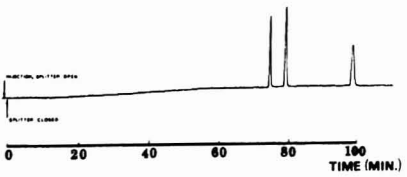


Figure 8. Chromatogram of the standard mixture on a 29 m × 75 μm i.d. (30-μm particle size) alumina-packed microcapillary column. Mobile phase: *n*-hexane with 0.05% methanol, flow linear velocity, 0.65 cm/s. Solutes: benzene, methyl benzoate, and quinoline (in the order of elution); number of theoretical plates for quinoline = 85 000; inlet pressure, 1500 psi; column permeability, 6.1×10^{-8}

Obviously, the plate height increases with sample size. Microcapillaries of somewhat wider diameters and greater lengths will be more tolerant to slightly larger samples. Nevertheless, a need for sensitive detection is clearly suggested for these columns.

DISCUSSION

The novel LC columns described in this paper may have utilization in three analytically important directions: (1) availability of greater resolving power; (2) the overall miniaturization of LC systems; and (3) increased compatibility of LC with mass spectrometry or other ancillary techniques that require low mobile-phase flow rates. The obtained results are discussed in view of these trends below.

Small-particle column technology has drastically improved the state of modern LC since several years ago. H values lower than 20 μm have been reported (*7*) for short columns packed with 4-μm particles. Whereas difficult-to-resolve pairs of solutes (e.g., various isomers) can frequently be separated through mobile-phase selectivity adjustments in LC, similar degree of resolution in GC may necessitate a "brute force" approach, i.e., a great number of theoretical plates. However, it is the overall efficiency of a given chromatographic column which is instrumental in separating complex mixtures. Alternatively, it is often of advantage to combine high plate numbers with selectivity. Just as with GC where the plate height values of capillary and best packed columns are roughly comparable, the column length that can be practically utilized for a given separation problem becomes crucially important.

Since the inlet pressure remains a single most important parameter in gaining higher efficiencies (*5*), longer columns are likely to be more emphasized in future LC separations. Present pressure limitations of the chromatographic equipment are less severe than is commonly believed. On the other hand, the approach of decreasing particle size with a simultaneous increase of column length in a usual way (slurry-packed columns) has its limitations. Namely, these include the evolved heat of friction, difficulties in packing extremely small particles, and joining shorter column sections together. The packed microcapillary columns described in this paper may provide an alternative solution. Their column technology is relatively easy.

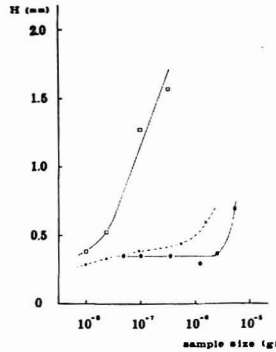


Figure 9. Plate height vs. sample size for a 10-μm particle size (3.6 m long) microcapillary. Mobile phase: hexane with 0.05% methanol, flow linear velocity, 0.4 cm/s. Solutes: O, benzene; ×, methyl benzoate; □, dimethyl phthalate; UV-detector sensitivity, 0.02–0.16 OD, full scale

The described columns are quite unique, both structurally and analytically. Whereas they are a microversion of packed capillaries used previously in GC, their analytical characteristics differ significantly from the irregularly packed columns investigated by Halasz and Walkling (*12*). These authors observed a turbulence-caused decrease of H. Their plate height values typically ranged from 2 to 10 mm.

Van Deemter plots constructed for various solutes and measured on the packed microcapillaries of varying internal diameter and particle size show quite unusual behavior. Whereas H values as low as 100 μm were achieved at very low flow rates and the curves remained flat over an analytically useful range of flow velocities, a sudden increase of H is observed at higher velocities. Interestingly enough, this increase demonstrates itself in the areas of velocities roughly comparable to those of decreasing H of the irregularly packed columns of Halasz and Walkling (*12*). Thus, some secondary flow effects are suggested. However, their interpretation may be a difficult matter.

Reduced plate heights are comparatively low for microcapillaries filled with different particles. Furthermore, such columns can be prepared with good reproducibility. The preparation of columns with 10-μm particles packed into 50-μm capillaries is somewhat exceptional, since they yield consistently less satisfactory results. The most likely reason for this is insufficient uniformity of 10-μm packing in the original (0.25-mm i.d.) glass tube. Indeed, particles of this size are known to be packed with difficulties in a dry state. In addition, the higher ratio of column diameter to particle size may also play some role.

Although the packing technology for small particles may still be improved in the future, we presently consider columns with 70-μm i.d., packed with 30-μm particles, to be a good compromise. Without excessive inlet pressures, good efficiencies are obtained. Adequate sample capacity is yet another consideration.

Since the packed microcapillaries of great lengths are coiled into helices, it has been of some interest finding whether there is some effect of column coiling on their performance. Long

ago, such a possibility was considered in chromatography by Giddings (*9*, *10*). A simple relation was derived (*10*) for the plate height contribution due to coiling:

$$H = \frac{7\upsilon r^4}{12R^2\gamma D_M} \quad (3)$$

where υ is flow velocity, r is column radius, R is coil radius, γ is the obstruction factor of the B term of the van Deemter equation, and D_M is the solute diffusion coefficient in the mobile phase. This contribution to the plate height primarily arises from the different velocities of the molecules encountered in different distances from the column wall. Whereas in gas chromatography, this contribution can be significant perhaps only in preparative-scale work, greater caution must be exercised in high-pressure liquid chromatography because of the considerably smaller values of D_M. The effect of column shape in LC was experimentally explored by Barth et al. (*11*). Significant H increases were observed with columns of conventional diameters, but no particular changes were observed for a 0.76-mm i.d. tube.

Even though the microcapillary radius is very small to amount to an appreciable increase of H through the coil effect (*9*, *10*) or the limitations by flow of the lateral mass transfer (*13*), some secondary flow phenomena could occur in the complex structure of packed microcapillaries. Because of the complexity of hydrodynamic conditions inside the column, Reynolds number would probably be a useless criterion. Whereas mass transfer is increased because of the secondary flow in open tubular columns (*14*), coiling may have only a minor effect on the performance of packed microcapillaries. Certainly, Figure 7 seems to indicate that. The differences in measurements with the columns of different coil radii are indeed very small and within the reproducibility range of column technology.

Miniaturization of equipment without sacrificing its resolving power is an important trend in analytical separation methods. As recently shown by Ishii (*15*), a miniature LC equipment is feasible that employs detector cells of very small volume. The packed microcapillaries described here naturally lend themselves to miniaturization, with typical flows of a few microliters per minute. Admittedly, the instrumental conditions used in this work are less than ideal and the necessary instrumentation has yet to be designed. In particular, smaller detection cells are needed.

In order to utilize more effectively the separating power of this technique, longer columns and correspondingly higher pressures are needed. The columns with diameters and lengths as described in this work seldom required inlet pressures over 200 atm. However, with the typical liquid flow volumes of these columns, there should be no major technological problems to utilize pressures around 1000 atm. Chromatography carried out under the extreme pressure conditions was demonstrated for both dense gases (*16*) and liquids (*17*).

Possibilities of combining LC with MS have now been under focus for several years. It appears that some technical problems of a successful coupling of these methods arise from excessive column liquid flows. Again, the described columns (or any other small-diameter columns) can potentially reduce these problems.

Whereas the present study is confined to one particular type of chromatography (the liquid–solid separation principle) and the alumina adsorbent, other column materials are worth exploring. Thus, in situ modifications of alumina with either salts (*18*) or liquids are clearly feasible, as is the preparation of bonded phases with this material (*19*). As described by Halasz and Heine (*1*), particles of graphitized carbon black can also be drawn inside the glass capillaries if special precautions are made. Obviously, a choice of sorption materials is limited to those of sufficient thermal stability. Finally, if the very useful siliceous materials are to be used, special techniques must be developed to regenerate the thermally lost surface hydrated structures. The surface silanol groups are needed for the preparation of chemically bonded stationary phases of different selectivities.

LITERATURE CITED

(1) I. Halasz and E. Heine, *Adv. Chromatogr.*, **4**, 207 (1967).
(2) C. Landault and G. Guiochon, in "Gas Chromatography 1964", A. Goldup, Ed., British Petroleum Institute, London, 1965, p 121.
(3) D. H. Desty, J. N. Haresnape, and B. H. F. Whyman, *Anal. Chem.*, **32**, 302 (1960).
(4) J. C. Giddings, *Anal. Chem.*, **36**, 1890 (1964).
(5) J. C. Giddings, Ref. 2, p 3.
(6) M. J. E. Golay, *Chromatographia*, **6**, 242 (1973).
(7) I. Halasz, R. Endele, and J. Asshauer, *J. Chromatogr.*, **112**, 37 (1975).
(8) J. C. Giddings, "Dynamics of Chromatography", Marcel Dekker, New York, N.Y., 1965.
(9) J. C. Giddings, *J. Chromatogr.*, **3**, 520 (1960).
(10) J. C. Giddings, *J. Chromatogr.*, **16**, 444 (1964).
(11) H. Barth, E. Dallmeier, and B. L. Karger, *Anal. Chem.*, **44**, 1726 (1972).
(12) I. Halasz and P. Walkling, *J. Chromatogr. Sci.*, **7**, 129 (1969).
(13) J. C. Giddings, "Dynamics of Chromatography", Marcel Dekker, New York, N.Y., 1965, p 52.
(14) R. Tijssen, *Chromatographia*, **3**, 525 (1970).
(15) D. Ishii, K. Mochizuki, and Y. Mochida, Abstracts of the 1977 Pittsburgh Conference on Analytical Chemistry and Applied Spectroscopy, Cleveland, Ohio, No. 385.
(16) L. McLaren, M. N. Myers, and J. C. Giddings, *Science*, **159**, 197 (1968).
(17) B. A. Bidlingmeyer, R. P. Hooker, C. H. Lochmüller, and L. B. Rogers, *Sep. Sci.*, **4**, 439 (1969).
(18) C. G. Scott and C. S. G. Phillips, Ref. 2, p 226.
(19) J. H. Knox and A. Pryde, *J. Chromatogr.*, **112**, 171 (1975).

RECEIVED for review July 20, 1977. Accepted November 7, 1977.

Determination of Penicillamine in Blood and Urine by High Performance Liquid Chromatography

Rolf Saetre and Dallas L. Rabenstein*

Department of Chemistry, University of Alberta, Edmonton, Alberta, Canada

New procedures are described for the determination of reduced penicillamine and total penicillamine (reduced plus oxidized penicillamine) in the nonprotein fractions of plasma, packed erythrocytes, whole blood, and urine. The procedures for reduced penicillamine are based on the separation by high performance liquid chromatography (HPLC) of reduced penicillamine from the other sulfhydryl-containing amino acids and peptides in the sample, followed by detection with a mercury-based electrochemical detector. The detector has a detection limit of ca. 5×10^{-7} M penicillamine, and at an electrode potential of +0.1 V vs. the SCE it is selective for sulfhydryl components in the biological fluids analyzed. Total penicillamine is determined by electrolytic reduction at a Hg pool electrode prior to the HPLC analysis. The procedures have been used to determine the reduced and total penicillamine in urine and blood from patients on penicillamine therapy for rheumatoid arthritis.

Penicillamine (β,β-dimethylcysteine; 3-mercaptovaline) is widely used for the treatment of Wilson's disease (*1*, *2*), lead poisoning (*3*), cystinuria (*4*), and rheumatoid arthritis (*5*). It also has been used to increase the rate of elimination of methylmercury in methylmercury poisoning (*6*), and its chemotherapeutic value against human malignancies is being studied (*7*). However, in spite of its wide use in medicine, the pharmacology of penicillamine is still not completely understood. The known metabolites of penicillamine in man are penicillamine disulfide (PSSP), the mixed penicillamine–cysteine disulfide (PSSC) and *S*-methylpenicillamine (*8*, *9*). In a recent study of the metabolism of penicillamine, metabolites could only account for some 50% of the penicillamine administered for the treatment of cystinuria (*9*).

Penicillamine is administered in doses up to several grams/day, possibly for lifetimes. Because highly toxic reactions can result, it is essential that there be sensitive and selective methods for monitoring the levels of penicillamine and its metabolites in the body fluids.

In this paper, we describe high performance liquid chromatography methods for the determination of reduced penicillamine (PSH) and the total penicillamine (reduced plus oxidized disulfide metabolites) in the nonprotein fraction of plasma, erythrocytes, whole blood, and urine. The procedures for reduced penicillamine involve separation from other sulfhydryl molecules on Zipax SCX cation-exchange resin followed by detection with a mercury-based electrochemical detector which has high selectivity and sensitivity for sulfhydryl-containing molecules (*10*). The total penicillamine is then determined by electroreduction of the disulfide metabolites in a second aliquot at a mercury pool electrode followed by HPLC analysis. Results are presented for blood and urine from rheumatoid arthritis patients on penicillamine therapy.

EXPERIMENTAL

Chemicals. Reduced penicillamine (ICN Pharmaceuticals), glutathione (Sigma), metaphosphoric acid (Mallinckrodt), disodium hydrogen phosphate (MCB), citric acid (Shawinigan), and EDTA (Aldrich) were used as received. Oxidized penicillamine (Aldrich) was used as received except in the glutathione disulfide exchange experiment, where it was recrystallized from a water–ethanol mixture to remove residual reduced penicillamine. The mixed cysteine–penicillamine disulfide was prepared by a literature procedure (*11*). Doubly distilled water was used throughout.

Apparatus. Separations were performed on a 0.2 × 30 cm column of Zipax SCX strong cation-exchange resin, with a 0.2 × 3 cm precolumn of Zipax SCX. Both columns were dry packed. When analyzing both blood and urine samples, the resin which first comes into contact with the sample turns brown after repeated use. The precolumn was used to avoid repacking the whole column. Sample aliquots of 10 μL were injected onto the column by syringe. A pH 3.0 phosphate/citrate buffer of 0.04 M ionic strength, deaerated with oxygen-scrubbed nitrogen, was used as eluent. An eluent flow rate of 0.6 mL/min was used. As discussed previously (*10*), the Teflon tubing which connects the eluent reservoir to the chromatographic column must be kept in an oxygen-free nitrogen atmosphere to avoid a large oxygen background current with the electrochemical detector. The tubing, connectors, valves, and columns were obtained from the Cheminert Division of Laboratory Data Control. A Milton Roy minipump having a maximum flow rate of 3 mL/min was used.

The mercury-based electrochemical detector described previously was used (*10*). The design in which the reference electrode is positioned approximately 0.5 cm from the Hg electrode was found to be satisfactory for the present application.

The penicillamine disulfides were reduced at a Hg pool electrode. The electrolysis cell (Figure 1) consists of a 1.5 × 5 cm tube with an inverted U-shaped side arm (1-mm i.d.) attached to the side approximately 1 cm from the bottom. A Hg pool of 0.7-cm depth was used. Electrical contact to the Hg was made via a Pt wire sealed into the bottom. The side arm is filled with saturated NaCl/2% Agar and dips into a beaker containing saturated NaCl and a Pt wire counter electrode. With a small magnetic stirring bar on top of the Hg pool, this cell is suitable for sample volumes down to a few hundred microliters. Samples were electrolyzed at a constant current of 6.43 mA, provided by a Leeds & Northrup constant current coulometer. This gave rise to a voltage drop of about 6 V across the cell. It was found convenient to reduce simultaneously several samples with multiple electrolysis cells connected in series. Oxygen-free nitrogen usually was passed over the solution during electrolysis.

The salt bridge has been attached to the side rather than having it dip into the solution from the top of the tube so that magnetic stirring can be used with sample volumes down to a few hundred microliters. Also, the cell resistance is smaller permitting the use of several cells in series without exceeding the output limit of the coulometer. Initially, the salt bridge was filled with saturated KCl/2% Agar. This, however, gave rise to decreased retention times for penicillamine and caused tailing of the peaks. During electrolysis at 6.43 mA for 10 min, the approximately 4×10^{-5} mol of H^+ which are reduced are replaced by cations from the salt bridge. When these are K^+ ions, they are more strongly retained on the Zipax SCX than are the Na^+ ions in the buffer. In high concentrations, they tend to saturate the column, thereby reducing the retention time for penicillamine. Saturated NaCl/2% Agar in the salt bridge eliminated this problem. When electrolyzing small samples, care must be taken to ensure that the samples are sufficiently acidic to avoid quantitative reduction of the protons. All samples were made 0.2 M in HCl prior to electrolysis.

Procedure for Penicillamine in Plasma. Five mL of blood is collected in a Vacutainer (Fisher Scientific) which contains a

0003-2700/78/0350-0276$01.00/0 © 1978 American Chemical Society

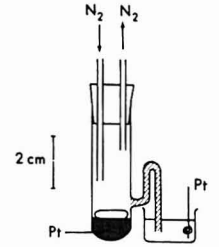


Figure 1. Electrolysis cell for the reduction of penicillamine disulfides. See text for details

K_3HEDTA solution. The Vacutainer is gently shaken to mix the contents, and then centrifuged immediately at 2500 rpm for 5 min. Then 0.8 mL of plasma is withdrawn and placed in a 10 × 75 mm test tube containing 0.2 mL of metaphosphoric acid solution (500 g/L). The tube is centrifuged at 2500 rpm for 10 min to remove protein precipitate. The supernatant liquid is withdrawn with a 1-mL tuberculin syringe, and forced through a 0.45-μM pore diameter filter, which is held in a filter holder (Millipore) fitted to the syringe. The filtrate is collected in a 10 × 75 mm test tube.

The reduced penicillamine in the filtrate is determined by analyzing 10-μL aliquots by HPLC. To determine the total penicillamine (reduced plus oxidized) in the filtrate, 0.4 mL of filtrate is placed in the electrolysis cell, acidified with 0.4 mL of 0.4 M HCl, and electrolyzed for 10 min. Then 10-μL aliquots of the electrolyzed solution are analyzed for reduced penicillamine by HPLC. The total oxidized penicillamine can be calculated by difference from these two results.

Procedure for Penicillamine in Packed Erythrocytes. Blood is collected and centrifuged in the Vacutainer as described above. After estimating the hematocrit, the plasma is withdrawn with a tuberculin syringe. The packed cells are then twice washed with their volume of normal saline solution and centrifuged at 2500 rpm for 5 min. The supernatant is withdrawn and 0.2 mL of packed cells is added to a 10 × 75 mm test tube containing 0.7 mL of EDTA solution (0.2 g Na_2H_2 EDTA/L). After 1 min, 0.1 mL of metaphosphoric acid solution (500 g/L) is added to the test tube and the contents are mixed well. After 10 min, the tube is centrifuged at 2500 rpm for 5 min. The supernatant is forced through a 0.45-μM pore diameter filter and the filtrate is collected in a 10 × 75 mm test tube.

The reduced penicillamine and the total of the reduced and the oxidized penicillamine in the filtrate are determined as described above for the plasma filtrate.

Procedure for Penicillamine in Whole Blood. Freshly drawn blood, 0.2 mL, is placed in a 10 × 75 mm test tube containing 0.7 mL of EDTA solution (0.2 g Na_2H_2 EDTA/L). The hemolyzed sample is treated and analyzed by the procedure described above for packed erythrocytes.

Procedure for Penicillamine in Urine. Urine, 2.25 mL, is acidified immediately after delivery with 0.25 mL of 2 M HCl to stabilize the reduced penicillamine. If precipitate forms, the sample is centrifuged at 2500 rpm for 5 min. For the majority of the samples encountered in this work, the penicillamine concentrations were so high that best results were obtained if the stabilized sample was diluted; 0.5 mL of the solution, or the supernatant if centrifugation is necessary, is transferred to a test tube and diluted 10-fold with 0.2 M HCl. Then 10-μL aliquots of this solution are analyzed for reduced penicillamine.

To determine the total penicillamine, 0.5 mL of the diluted solution is electrolyzed for 10–15 min. Next 10-μL aliquots of the electrolyzed solution are analyzed for reduced penicillamine. The longer electrolysis times are necessary if dilution is less than 10-fold.

RESULTS

Stability of Penicillamine Solutions. Since thiols are readily oxidized (*12*), the stability of reduced penicillamine solutions was studied to find stable conditions for standards and samples. Figure 2 shows the stability of 1.0×10^{-3} M PSH in distilled water (solution pH 6.2) stored at room temperature (curve A) and 4 °C (curve B), and of 1.0×10^{-3} M penicillamine in distilled water containing 1 g/L Na_2H_2EDTA at room temperature (curve C). A curve identical to C was obtained for a penicillamine/EDTA solution stored at 4 °C. EDTA apparently stabilizes the penicillamine solutions by complexing trace metals which catalyze thiol oxidation (*12*). Similar experiments with penicillamine in 0.2 M HCl solution, in normal urine to which 2 M HCl was added to give a final HCl concentration of 0.2 M, and in 50 g/L metaphosphoric acid solution indicated that penicillamine in these solutions is stable for at least a day at room temperature.

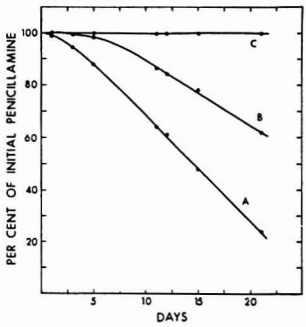


Figure 2. Time course for the stability of 1.0×10^{-3} M PSH (A) in distilled water (solution pH 6.2) stored at room temperature (25° C); (B) in distilled water stored at 4 °C, and (C) in distilled water containing 1 g/L Na_2H_2EDTA stored at room temperature

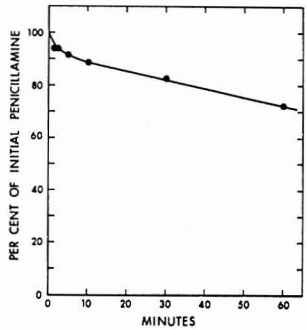


Figure 3. Time course for the stability of 1.1×10^{-4} M PSH in normal urine at room temperature

The stability of reduced penicillamine in urine was also studied to determine how soon after delivery the urine has to be acidified to avoid significant loss of penicillamine by oxidation. The results in Figure 3 indicate that urine samples should be acidified immediately after delivery. It was determined from similar experiments that the penicillamine concentration in plasma is not decreased significantly during the time required for centrifugation and analysis, possibly because the EDTA present initially in the Vacutainer complexes trace metals which catalyzed thiol oxidation.

Standard Curves were obtained by plotting peak height (nA) vs. the penicillamine concentration of standard solutions. The calibration curve for plasma was prepared from standard PSH solutions containing 50 g/L metaphosphoric acid. Calibration curves for reduced penicillamine in urine and for

Table I. Penicillamine Concentrations (mg/L) of Blood and Urine from Patients on Penicillamine Therapy for Rheumatoid Arthritis

	Urine		Plasma		Packed erythrocytes		Whole blood[a]		Hematocrit	Whole blood[b]	
Sample	(PSH)	$(PSH)_{Total}$[c]	(PSH)	$(PSH)_{Total}$[c]	(PSH)	$(PSH)_{Total}$[c]	(PSH)	$(PSH)_{Total}$[c]	%	(PSH)	$(PSH)_{Total}$[c]
1	25.4	374	1.08	4.2	0.59	0.81	1.1	3.3	33	0.92	3.1
2		254	2.60	8.1	0.70	0.75	1.7	4.2	45	1.74	4.8
3	47.0	223	1.91	5.2	0.91	1.00	1.6	3.5	40	1.50	3.5
4	29.4	86	2.80	6.9	0.81	0.98	1.8	3.7	45	1.90	4.2
5	2.5	89	0.90	2.7	-	-	0.70	1.8	-	-	-
6	203	1360	0.71	3.3	-	-	0.70	2.4	-	-	-
Av rel std dev[d]	2.3%	1.7%	3.9%	2.2%	16%	13%	11%	5.0%			

[a] Observed results. [b] Calculated from the observed results for plasma and packed erythrocytes and the hematocrit. [c] The total of the reduced penicillamine and the oxidized penicillamine in the nonprotein fractions. [d] Calculated from the results of 3–5 injections for each sample.

total penicillamine in plasma, erythrocytes, whole blood, and urine were prepared from standard PSH solutions in 0.2 M HCl. Calibration curves were linear from 5×10^{-7} M to 1×10^{-3} M penicillamine. At 5×10^{-7} M the signal-to-noise ratio was 5:1, where S/N = average signal amplitude/RMS noise with RMS noise = average peak-to-peak noise/2.5. To give some indication of the sensitivity of this method, 10 μL of 5×10^{-7} M penicillamine corresponds to 0.75 ng of penicillamine.

Disulfide Exchange Reactions. Thiols and disulfides undergo disulfide exchange reactions (*13*), the rates of which are pH dependent, decreasing rapidly as the pH decreases because the deprotonated form of the thiol is the reactive form (*14*). In the procedure for the determination of penicillamine in whole blood, the sample is first hemolyzed with a dilute EDTA solution at near neutral pH. Hemolysis releases the reduced and oxidized penicillamine as well as the other thiols and disulfides of the erythrocyte. After about 1 min, metaphosphoric acid is added which lowers the pH, thus essentially stopping any disulfide exchange, and precipitates the proteins. To determine if a significant amount of reduced penicillamine is formed or lost by disulfide exchange with oxidized or reduced glutathione, GSSG and GSH respectively, the forward rates for the disulfide exchange reactions represented by Equations 1 and 2 were measured.

$$PSSP + GSH \rightleftharpoons PSSG + PSH \quad (1)$$

$$GSSG + PSH \rightleftharpoons PSSG + GSH \quad (2)$$

The experiments were performed at 25 °C in phosphate/citrate buffer of pH 7.5 and ionic strength 0.04 M. All solutions were thoroughly deareated before mixing, and oxygen-scrubbed nitrogen was bubbled through the solutions during the reaction. In the study of Reaction 1, the PSH concentration was measured as a function of time by determining the PSH in aliquots. The reaction was stopped by making the aliquots 0.2 M in HCl. In the study of Reaction 2, the GSH concentration was measured as a function of time by HPLC (*10*).

The time course for formation of penicillamine by disulfide exchange in a solution initially containing 1.0×10^{-3} M PSSP and 1.0×10^{-3} GSH is shown in Figure 4. From the initial rate of the reaction, the forward rate constant (defined by Equation 3) for Reaction 1 was found to be 2.8×10^{-2} L/mol^{-1} s^{-1}.

$$\frac{d[PSH]}{dt} = k_f[PSSP][GSH] \quad (3)$$

The forward rate constant for Reaction 2 at similar conditions is 0.43 L/mol^{-1} s^{-1}. These rate constants coupled with the small concentrations of GSH and GSSG in the hemolyzed solutions indicate that essentially no PSH is lost or formed by disulfide exchange during the hemolysis step.

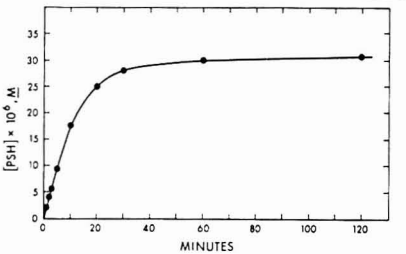


Figure 4. Time course for the formation of PSH by the disulfide exchange reaction, PSSP + GSH ⇌ PSSG + PSH. Solution conditions were phosphate/citrate buffer of pH 7.5 and ionic strength 0.04 M, 25 °C. The solution initially contained 1.0×10^{-3} M PSSP and 1.0×10^{-3} M GSH

Reduced Penicillamine. Figure 5 shows a typical chromatogram obtained for a urine sample from a rheumatoid arthritis patient on penicillamine therapy. The sharp, unretained peak at ca. 1 min after sample injection is due to a combination of double layer capacitance effects, which result from the sample medium being different from the mobile phase, and detector response to chloride, traces of cysteine, and, in the case of whole blood and erythrocyte samples, reduced glutathione in the sample. Both cysteine and reduced glutathione are essentially unretained with the chromatographic conditions used in this work.

The reduced penicillamine levels of the urine and blood from patients treated with 750 mg of D-penicillamine per day for rheumatoid arthritis are listed in Table I. The penicillamine was taken orally in doses of 250 mg. The average relative standard deviations for the determination of reduced penicillamine in the various sample media, calculated from the results of 3–5 injections for each sample, are also given in Table I. The relative standard deviations for the packed erythrocyte and whole blood results are generally larger than those for urine and plasma analyses because, after sample preparation, the penicillamine levels of the packed erythrocyte and whole blood samples encountered in this work approach the detection limit of the detector. Recoveries of 98 ± 3% and 99 ± 3% were obtained for reduced penicillamine added to plasma.

Total Penicillamine. The procedure for total penicillamine gives the sum of the reduced penicillamine and the oxidized penicillamine (PSSP and PSSC (*4*, *9*)) in the nonprotein fraction. The procedure is based on the quantitative reduction of the oxidized forms, followed by determination by HPLC of the total reduced penicillamine. Several methods of disulfide reduction were studied, in addition to the electrolysis method.



Figure 5. Representative chromatogram obtained for a urine sample from a patient on D-penicillamine therapy for rheumatoid arthritis. Peak height corresponds to 5.7×10^{-5} M PSH

A chemical reduction of PSSP with $NaBH_4$ at room temperature was attempted. This gave a yield of less than 5%, in agreement with reported results (*15*). Addition of Cu^{2+} as catalyst increased the yield to 66%. Other metal ions, e.g., Fe^{3+}, Zn^{2+}, and Hg^{2+}, as catalysts gave lower and irreproducible yields. Besides giving less than quantitative reduction, procedures with $NaBH_4$ were tedious and required complete deaeration of samples, which caused excessive foaming of urine samples. Reduction with sulfite was also attempted, but without success.

Electroreduction at a Hg pool cathode was found to be quantitative for both PSSP and PSSC, complete within 10–15 min at an electrolysis current of 6.43 mA, and does not require deaeration of the sample solution either before or during electrolysis. The recovery of PSSP (1.0×10^{-5} M) added to the urine of several rheumatoid arthritis patients on penicillamine therapy was 100 ± 3%, 98 ± 2%, and 97.5 ± 2%, and 98.2 ± 1.3% recovery was obtained for PSSP added to normal urine. Recoveries of 103 ± 3% and 97 ± 3% were obtained for PSSP added to the plasma of rheumatoid arthritis patients.

The total penicillamine levels of the urine and blood from patients treated with 750 mg of D-penicillamine per day for rheumatoid arthritis are given in Table I. The average relative standard deviations for the determinations, calculated as described above for reduced penicillamine, are also given in Table I.

To determine if the results listed in Table I for reduced and total penicillamine in plasma, packed erythrocytes, and whole blood are internally consistent, the reduced and total penicillamine concentrations of whole blood were predicted from the levels found for plasma and packed erythrocytes and the estimated hematocrit. The calculated and observed concentrations show good agreement.

Direct detection of oxidized penicillamine with the electrochemical detector at −1.2 V vs. the SCE was also attempted. The 0.2 × 30 cm Zipax SCX column was used with a phosphate/citrate buffer at pH 4.0 (ionic strength 0.1 M). Under these conditions, the detection limit was approximately 5×10^{-4} M PSSP, which is too high for direct detection to be applicable to the samples encountered in the present work.

DISCUSSION

The very low penicillamine detection limits of the procedures described in this paper result from the high sensitivity of the Hg pool electrode for the sulfhydryl group. Selectivity is achieved by coupling the electrode with a liquid chromatographic separation. Because the detector responds only to the sulfhydryl-containing amino acids and peptides in the sample when operated at a potential of +0.1 V vs. the SCE, it is necessary only that the chromatographic step separate penicillamine from the other sulfhydryl-containing molecules. This is easily and quickly done; with the mobile phase and chromatographic column used in this work, penicillamine is eluted with a retention time of ca. 3.3 min whereas cysteine and GSH are essentially unretained.

In contrast, the chromatographic step in autoanalyzer procedures with ninhydrin detection must resolve the penicillamine from all other ninhydrin-positive components of the sample. Because of the complexity of biological fluids, this can require long elution times. For example, in a recent study of penicillamine metabolism, elution times on the order of 8 h were necessary to elute penicillamine disulfide (*9*). It is of interest that with the autoanalyzer method no reduced penicillamine could be detected in fresh urine from patients on penicillamine therapy for the treatment of rheumatoid arthritis or cystinuria (*9*), which is considerably different from the findings of the present study (Table I). The failure to detect reduced penicillamine in the previous study could be due to its rapid oxidation since no mention is made of precautions to exclude oxygen from reagents or mobile phase, or to incomplete resolution of reduced penicillamine from other ninhydrin-positive components, perhaps glycine (*16*).

Reduced penicillamine in urine and plasma generally is determined colorimetrically as its Fe(III) complex (*17*), although this method has been reported to lack precision (*16*). Oxidized penicillamine generally is determined by autoanalyzer methods with ninhydrin detection. Other methods in the literature include a gas chromatographic determination of the esterified forms of reduced and oxidized penicillamine as their thiazolidine or Schiff base derivatives, respectively (*18*), and an autoanalyzer procedure for total penicillamine which is based on its quantitative conversion to penicillaminic acid by performic acid oxidation, with ninhydrin detection (*16*). An immunological assay also has been described (*19*). It would seem that the methods described in this paper offer advantages over the methods mentioned above in terms of simplicity, analysis time, and the ease with which this method can determine both the reduced and oxidized penicillamine.

For the patients encountered in this work, both the free and the oxidized penicillamine in the blood was distributed unevenly between the plasma and erythrocytes, with the reduced penicillamine concentration some 2–4 times higher and the total penicillamine some 5–10 times higher in the plasma. It also is of interest that the distribution between the reduced and oxidized forms is considerably different for plasma and red blood cells, as indicated by the ratio of total penicillamine to reduced penicillamine concentrations (Table II). Most significant, perhaps, is the finding that most of the penicillamine in the red blood cell is in the reduced form, since the reduced form is the active form in the treatment of methylmercury and lead poisoning by penicillamine, and in

Table II. Ratio of Total Penicillamine to Reduced Penicillamine[a]

Sample	Urine	Plasma	Packed erythrocytes	Whole blood
1	15	3.9	1.4	3.0
2	-	3.1	1.1	2.5
3	4.7	2.7	1.1	2.2
4	2.9	2.5	1.2	2.1
5	36	3.0	-	2.6
6	6.7	4.6	-	3.4

[a] Calculated from the results in Table I.

the postulated mechanism of action at the molecular level in the treatment of cystinuria (*20*).

ACKNOWLEDGMENT

The authors are indebted to F. F. Cantwell of the University of Alberta for his many helpful discussions, and gratefully acknowledge the cooperation of the Rheumatic Disease Unit of the Department of Medicine, University of Alberta, and their technician, A. Saetre, for providing numerous urine and blood samples from their patients on penicillamine therapy.

LITERATURE CITED

(1) J. M. Walshe, *Am. J. Med.*, **21**, 487 (1956).
(2) J. M. Walshe, *Br. J. Hosp. Med.*, **4**, 91 (1970).
(3) S. Selander, K. Cramer, and L. Hallberg, *Br. J. Ind. Med.*, **23**, 282 (1966).
(4) J. C. Crawhall, E. F. Scowen and R. W. E. Watts, *Br. Med. J.*, **1**, 1270 (1973).
(5) Multicenter Trial Group, *Lancet*, 257 (1973).
(6) F. Bakir, S. F. Damluji, L. Amin-Zaki, M. Murtadha, A. Khalidi, N. Al-Rawi, S. Tikriti, H. I. Chahir, T. W. Clarkson, J. C. Smith, and R. A. Doherty, *Science*, **181**, 230 (1973).
(7) G. Tisman, V. Herbert, L. Teng Go, and L. Brenner, *Proc. Soc. Exp. Biol. Med.*, **139**, 355 (1972).
(8) K. Gibbs and J. M. Walshe, *Q. J. Med.*, **40**, 275 (1971).
(9) D. Perrett, W. Sneddon and A. D. Stephens, *Biochem. Pharmacol.*, **25**, 259 (1976).
(10) D. L. Rabenstein and R. Saetre, *Anal. Chem.*, **49**, 1036 (1977).
(11) J. C. Crawhall, E. F. Scowen, and R. W. E. Watts, *Br. Med. J.*, **1**, 1411 (1964).
(12) P. C. Jocelyn, "Biochemistry of the SH Group", Academic Press, New York, N.Y., 1972, pp 94–110.
(13) Ref. 12, p 121.
(14) I. M. Kolthoff, W. Stricks, and R. C. Kapoor, *J. Am. Chem. Soc.*, **77**, 4733 (1955).
(15) K. Bir, J. C. Crawhall, and D. Mauldin, *Clin. Chim. Acta*, **30**, 183 (1970).
(16) K. Borner, *Z. Physiol. Chem.*, **341**, 264 (1965).
(17) P. R. Pal, *J. Biol. Chem.*, **234**, 618 (1959).
(18) E. Jellum, V. A. Bacon, W. Patton, W. Pereira, and B. Halpern, *Anal. Biochem.*, **31**, 339 (1969).
(19) E. S. K. Assem and M. R. Vickers, *Postgrad. Med. J., Suppl.*, **50**, 10 (1974).
(20) J. C. Crawhall, E. F. Scowen, and R. W. E. Watts, *Br. Med. J.*, **1**, 588 (1963).

RECEIVED for review September 12, 1977. Accepted November 4, 1977. This research has been supported by the University of Alberta and the National Research Council of Canada. Financial support to R.S. by a University of Alberta Scholarship is gratefully acknowledged.

Liquid Chromatographic Analysis of Analgesics on Amberlite XAD-7

Robert G. Baum and Frederick F. Cantwell*

Department of Chemistry, University of Alberta, Edmonton, Alberta, Canada, T6G 2G2

Amberlite XAD-7, a non-ionic polyacrylate resin, is used as a stationary phase for the separation of mixtures of analgesics. Binary and ternary solvent mixtures prepared from chloroform, ether, ethanol, and hexane are used as mobile phase. From plots of log adjusted retention volume of each compound vs. solvent composition, the optimum solvent mixture is chosen to achieve a given separation. Commercial products containing various combinations of ASA, salicylic acid, caffeine, phenacetin, salicylamide, and acetaminophen are analyzed. A mixture of all six compounds is base-line resolved on a 30 cm × 0.28 cm column. By choosing mobile phases in which separation factors are large, analgesic mixtures are also separated on short (10 cm) columns at low pressures. These systems represent a low-cost alternative to existing analytical methods.

Continued widespread use of multicomponent pain relief preparations has led to a long standing interest in improving assay methods for analgesics. Although methods based on direct spectrophotometry have been popular in the past (*1*, *2*) and occasionally appear in the current literature (*3*), chromatographic techniques constitute the bulk of recent methods.

Gas chromatography has been used for the determination of analgesics without the formation of derivatives, but compounds such as acetylsalicylic acid (ASA), salicylic acid, and acetaminophen which possess acidic hydrogens show considerable tailing on most columns (*4*, *5*). Consequently these compounds are usually derivatized prior to gas chromatographic analysis (*6*). Perhaps for this reason, gas chromatography is not widely used in the analysis of multicomponent analgesics. Column partition chromatography was used by Levine (*7*) for the separation of ASA, phenacetin, and caffeine with subsequent quantitation by ultraviolet spectrophotometry. This approach has been extended to more complex mixtures (*8–10*), and partition chromatography is the basis of some current official methods (*11*).

High efficiency liquid chromatography has been employed more frequently in recent years. Several investigators have used pellicular anion exchangers with aqueous buffers as eluents (*12–14*), and one group employed a pellicular cation exchanger (*15*). Walton et al. (*16*) investigated the use of macroporous and conventional gel-type ion-exchange resins for the separation of several analgesics using electrolyte-free alcohol–water mobile phases. Caffeine, phenacetin, ASA, and acetaminophen mixtures have been separated on an octadecylsilyl bonded phase using acetonitrile–water mobile phase containing ammonium carbonate (*17*), and these four compounds plus salicylamide were analyzed on a column of pellicular silica gel using organic solvent mobile phases (*18*).

The resin Amberlite XAD-7, a nonionic macroporous polymer of poly(methyl methacrylate) (*19*), has previously been studied as an adsorbent. Adsorption isotherms of fatty acids (*20*) and the adsorption of organic contaminants from drinking water (*21*) have been reported. It has been used as a stationary phase for chromatography of phenols and other acids with aqueous-organic mobile phases (*22*, *23*) and of a variety of compounds with both aqueous and nonaqueous mobile phases (*24*). A similar poly(methyl methacrylate) polymer, Hitachi Gel 3030, was used to separate aromatic hydrocarbons, dyes, and steroids (*25*).

In the present study Amberlite XAD-7 is used as the stationary phase for chromatographic separation and determination of ASA, salicylic acid, phenacetin, caffeine, salicylamide, and acetaminophen in analgesic tablets. The chromatographic systems described herein are more rapid and

0003-2700/78/0350-0280$01.00/0 © 1978 American Chemical Society

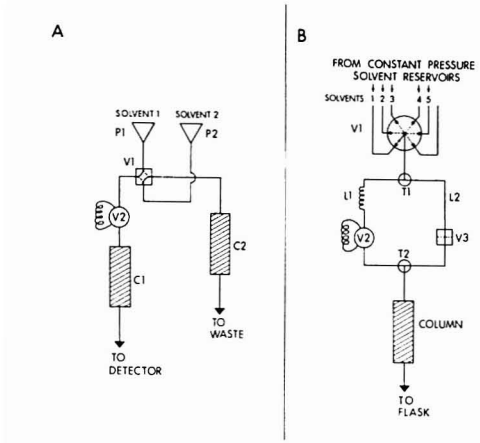


Figure 1. Diagrams of the liquid chromatographs (description in text)

efficient than traditional partition chromatography, while at the same time they are low-cost alternatives to higher pressure liquid chromatographic methods.

EXPERIMENTAL

Apparatus. A diagram of the liquid chromatograph that was used in most of the studies is shown in Figure 1A. Pump P1 (Model CMP-2VK), all valves, chromatographic columns, fittings and Teflon tubing were obtained from Laboratory Data Control, Riviera Beach, Fla. (Model numbers shown in parentheses). The water jacketed glass column C1 was either 50 cm × 0.28 cm i.d. or 30 cm × 0.28 cm i.d. (Type MB) and was dry packed with 0.82 or 0.47g of <325 mesh Amberlite XAD-7. Column void volumes V_m were 2.4 and 1.3 mL. The column was thermostated at 25 ± 1 °C. The detector was a Model 230 Absorbance Detector (Spectra-Physics, Santa Clara, Calif.) set at 280 nm. Peak areas were measured with a Model CSI-38 electronic integrator (Columbia Scientific Industries, Austin, Texas), and chromatograms were recorded on a Recordall Series 5000 recorder (Fisher Scientific Co.).

For the analysis of Excedrin Tablets using the chromatograph shown in Figure 1A, a 240-cm long section of 0.8 mm i.d. Teflon tubing was placed between V1 and V2 as a delay line. With valve V1 in the position shown (solid lines), P1 pumped Solvent 1 through the sample injection valve V2 and through the 30-cm analytical column C1. Simultaneously P2 (stainless steel syringe pump, Perkin-Elmer Corp., Norwalk, Conn.) pumped Solvent 2 to waste via valve V1 and the auxiliary column C2. When valve V1 was switched (dashed lines), Solvent 2 was pumped through the analytical column while Solvent 1 was diverted through C2 to waste. The auxiliary column C2 was also 30 cm × 0.28 cm i.d. packed with XAD-7 and was included in the system to eliminate repressurizing and the resultant flow rate change when V1 was switched. The sample was injected with Solvent 1 flowing through the analytical column C1 and Solvent 2 flowing through the auxiliary column C2. Immediately after caffeine eluted, valve V1 was switched and Solvent 2 was pumped through C1. The delay line between V1 and V2 allows ASA to elute before Solvent 2 reaches the detector. After elution of the fourth component, acetaminophen, V1 was switched back to the original position, and another injection made after a short equilibration period.

For the analysis of ASA, phenacetin, and caffeine (APC) mixtures on the 50-cm column, V1, P2, and C2 were removed, and P1 was connected directly to the sample injection valve V2. Likewise, when measuring adjusted retention volumes for Figures 2–4, C2, V1, and V2 were removed, pump P1 or pump P2 was connected to the 30 cm column via a septum injector (Model 183A8), and samples were injected with a Model 701-N, 10-μL syringe (Hamilton Co., Reno, Nev.).

A second chromatograph (Figure 1B) employed a 10 cm × 0.63 cm glass column, C, packed with 0.95 g of 200–325 mesh XAD-7. Column end fittings have been described previously (26). The constant pressure pump consisted of five steel vessels pressurized by a tank of compressed nitrogen (50 psig) and was based on the design of Fritz (22). The six-port valve V1 (R6031V6P) allowed the selection of any of the five mobile phases. T1 and T2 were tee-connectors (CJ3031), V3 was an on-off valve (CAV 2031) and V2 was a 0.50-mL rotary injector valve (R6031SV). In order to dissolve all of the tablet drug components, it was necessary to use a solvent (dioxane) which turned out to be a strong eluent for some of the drugs. Since the volume of sample solution injected was large, this deteriorated resolution between several of the compounds. In order to avoid this problem it is necessary to dilute the sample solution extensively with the mobile phase hexane after drawing it into the injection valve but before allowing it to enter the column. This in situ dilution was accomplished by the tee-loop arrangement shown in Figure 1B. The tubing L1 connecting T1 to V2 was 200 cm × 0.8 mm i.d., while the tubing L2 connecting T1 to V3 was only 20 cm × 0.8 mm i.d. Thus the ratio of flow rates through these two branches was approximately 1:10. After the sample had washed onto the column, V3 was closed, and mobile phase flowed through only the left branch of the loop. For studies involving this chromatograph no detector was employed, as the eluted sample components were collected in separate flasks and analyzed spectrophotometrically using a Cary 118 spectrophotometer (Varian Associates, Palo Alto, Calif.).

In the analysis of Excedrin Tablets, the dioxane tablet extract was injected and 15 mL of Solvent 1 (hexane) allowed to pump through the column. All four compounds are strongly retained at the top of the column. Thirty-four mL of Solvent 2 (35% ether) elutes ASA as well as any salicylic acid but leaves the other components strongly retained. Next, 37 mL of Solvent 3 (16% chloroform) elutes caffeine, leaving salicylamide and acetaminophen on the column. Thirty-four mL of Solvent 4 (50% chloroform) now elutes salicylamide, which has already been moved most of the way down the column ahead of acetaminophen by the previous solvents. Finally, 13 mL of Solvent 5 (50% ethanol) elutes acetaminophen. After elution of acetaminophen valve V1 was switched back to Solvent 1, valve V3 was opened again, and 23 mL of Solvent 1 was allowed to pump through the column before making the next injection. Total analysis time was 100 min. The eluted compounds were collected in separate 50-mL volumetric flasks and diluted to volume with the same solvent that was used to elute the given compound. Quantitative determinations were made spectrophotometrically using standard calibration plots. ASA was measured at 276 nm, caffeine at 275 nm, salicylamide at 308 nm, and acetaminophen at 286 nm. In the case of acetaminophen, measurements could not be made at the peak maximum because of interference which was caused by the presence of a small amount of benzene impurity in the hexane.

Reagents, Chemicals, and Solvents. Drug substances were USP or equivalent grade. Salicylic acid, ASA, salicylamide, and caffeine were assayed by USP or NF methods (27, 28) as 99.6%, 100.0%, 99.6%, and 99.4%, respectively. Acetaminophen and phenacetin were assayed spectrophotometrically using USP Reference Standards as 99.4% and 100.4%. Hexane and ethanol were anhydrous reagent grade and were distilled before use. Chloroform (J. T. Baker Chemical Co., Phillipsburg, N.J., approx. 0.75% ethanol), diethyl ether, and 1,4-dioxane were reagent grade and used as received.

Binary and ternary mobile phases were prepared by transferring measured volumes of a given solvent into a volumetric flask and diluting to volume with hexane.

Approximate solubilities, as w/v percent in chloroform and ether of salicylamide (0.7% and 4%) and acetaminophen (<0.1% and 0.3%), were measured by adding increments of solvent to a known weight of drug with vigorous stirring between each increment. Solubilities of other drugs in chloroform and ether were obtained from published values (29) as: salicylic acid (2% and 33%), ASA (6% and 8%), phenacetin (7% and 1%), and caffeine (18% and 0.2%).

Resin. Amberlite XAD-7 (Rohm and Haas Co., Philadelphia, Pa.) was ground in a triple porcelain roller mill (Erweka-Apparatebau-GMBH, Chemical and Pharmaceutical Industry Co.,

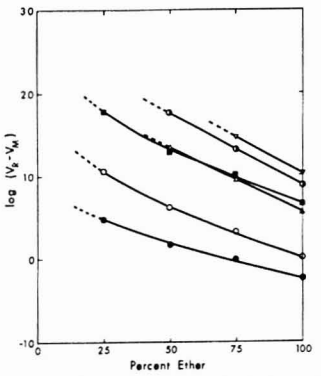


Figure 2. Plots of log ($V_R - V_M$) vs. percent ether in the mobile phase for salicylic acid (●), ASA (○), salicylamide (△), phenacetin (■), caffeine (◑) and acetaminophen (▽) on a 30 cm × 0.28 cm column of Amberlite XAD-7

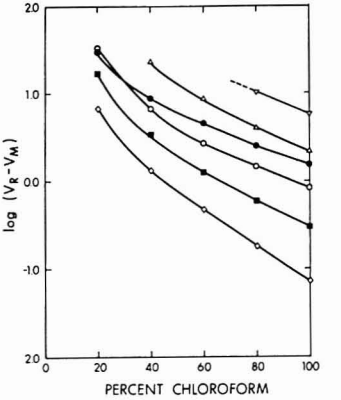


Figure 3. Plots of log ($V_R - V_M$) vs. percent chloroform in the phase for caffeine (◊), phenacetin (■), ASA (○), salicylic ac salicylamide (△) and acetaminophen (▽) on a 30 cm × 0.28 cm c of Amberlite XAD-7

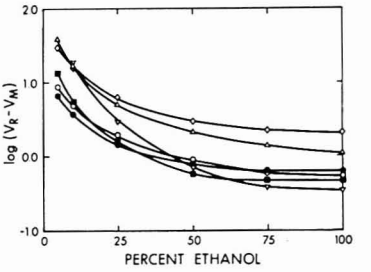


Figure 4. Plots of log ($V_R - V_M$) vs. percent ethanol in the mobile phase for acetaminophen (▽), phenacetin (■), ASA (○), salicylic acid (●), salicylamide (△) and caffeine (◊) on a 30 cm × 0.28 cm column of Amberlite XAD-7

Inc., New York, N.Y.), dried and classified on U.S. Standard Sieves, de-fined by decantation in methanol and dried in a 50 °C vacuum oven. The resin was dry-packed into columns and conditioned by washing with 10^{-3} M HCl in methanol followed by pure methanol and then chloroform. This conditioning was necessary to minimize tailing of ASA and salicylic acid.

Tablets, Blank, and Spiked Blanks. Commercial tablets were purchased at pharmacies in the United States. Average tablet weights were determined for each lot (*27*), and the tablets were ground to a fine powder. Sample solutions were prepared from one average tablet weight of the powdered tablet. Powdered APC tablets were weighed into 100-mL volumetric flasks, dissolved, and diluted to volume with chloroform. Powdered Excedrin tablets were weighed into 200-mL volumetric flasks, dissolved in 50.0 mL of dioxane and diluted to volume with chloroform. However, when Excedrin tablets were analyzed on the chromatograph in Figure 1B, the powdered samples were dissolved in 50.0 mL of dioxane. In all cases, undissolved inert ingredients were filtered out as the solution was drawn into the injection valve by placing a small plug of cotton in the valve inlet tube.

Lack of chromatographic interference by inert tablet ingredients was demonstrated by preparing a blank containing corn starch, talc, lactose, and stearic acid and analyzing it as for a tablet. Quantitative recovery of drug components was demonstrated by adding known amounts of the drugs to 75 mg of the blank mixture and analyzing it as a tablet.

RESULTS AND DISCUSSION

Chromatography of Analgesics. Salicylic acid, ASA, caffeine, phenacetin, salicylamide, and acetaminophen were chromatographed on a 30 cm × 0.28 cm i.d. column of XAD-7 using various ether/hexane, chloroform/hexane, and ethanol/hexane binary solvent mixtures as mobile phases. Their retention behavior is plotted in Figures 2–4 as log ($V_R - V_M$) vs. volume percent of the given solvent in hexane. Here V_R is the drug retention volume, V_M is the system void volume, which was measured as the retention volume of an unretained component, and $V_R - V_M$ is the adjusted (net) retention volume.

The retention behavior observed in Figures 2–4 is in marked contrast to what is usually observed for "polar adsorbents" such as silica gel and alumina. With these adsorbents it is usually possible to neglect the relatively small sample–mobile phase interaction energy in predicting retention volumes and to consider only the interaction energies between sample and adsorbent and between mobile phase and adsorbent (*30*). It is usually found that a given series of sample compounds exhibits the same elution sequence, regardless of the nature of the mobile phase. As a consequence "solvent strengths" follow approximately the same order regardless of the sample compound used to measure them, giving rise to the so-called "eluotropic series".

Although Amberlite XAD-7 is a more polar, or less hydrophobic, adsorbent than the styrene–divinylbenzene copolymers XAD-1, -2, and -4 (*24*), it is significantly less polar than silica gel and alumina. The consequence of this decreased adsorbent polarity is seen by comparing the elution sequences of the six compounds shown in Figures 2 and 3. With an ether-containing mobile phase, they elute in approximately the inverse order of their solubilities in ether (caffeine and acetaminophen order is reversed), while with a chloroform-containing mobile phase they elute in the inverse order of their solubilities in chloroform. Thus, for the compounds salicylic acid, ASA, phenacetin, and caffeine, the elution sequence, just as the solubility sequence, is *reversed* in the two solvent systems. Evidently, the sample–mobile phase interaction is not dwarfed by the sample–adsorbent and mobile phase–adsorbent interactions when the adsorbent is XAD-7.

The plots in Figures 2–4 may be used to select the mobile phase required to separate any two drug components. The details of this procedure have been discussed previously (*31*), and we will here only give as an example the selection of a

chloroform/hexane mobile phase to separate caffeine and phenacetin on a 50 cm × 0.28 cm i.d. column of XAD-7. First, it is necessary to multiply all of the values of $(V_R - V_M)$ by 50/30 since the curves in Figure 3 were obtained on a 30-cm column of the same diameter. This amounts to shifting all of the curves in Figure 3 upward by 0.22 log unit. Next, we will place three requirements on the separation: (A) Baseline resolution (R_s) between the less strongly retained component and any unretained components (including "solvent peaks" resulting from refractive index effects); (B) Baseline resolution between phenacetin and caffeine; (C) as short a retention volume for the more strongly retained component as is consistent with the first two requirements.

The 50-cm column exhibited plate heights of about 0.10–0.15 cm for most of the drugs with chloroform/hexane mobile phases, so that the number of theoretical plates $N \approx 400$. Peak width for an unretained component W_u is calculated as 0.4_8 mL by the relationship (*31*):

$$N = 16\left(\frac{V_M}{W_u}\right)^2 = 400 = 16\left(\frac{2.4}{W_u}\right) \quad (1)$$

Assuming that caffeine has a similar width when it is just baseline resolved from the unretained peak, then the minimum allowable net retention volume for caffeine is calculated as 0.7_2 mL from the expression:

$$R_s = 1.5 \approx \frac{V_R - V_M}{0.4_8} \quad (2)$$

From the (shifted) caffeine curve in Figure 3, it is seen that the mobile phase must contain not more than about 60% chloroform to meet requirement (A).

Requirements (B) and (C) are simultaneously fulfilled by finding the percent chloroform closest to, but not higher than, 60% which will give baseline resolution between caffeine and phenacetin. The value of R_s may be adequately approximated with Equation 3 in which k_p' and k_c' are capacity factors for phenacetin and caffeine and α is the ratio k_p'/k_c':

$$R_s \approx \frac{\sqrt{N}}{4}\left(\frac{\alpha - 1}{\alpha}\right)\left(\frac{k_p'}{k_p' + 1}\right) \quad (3)$$

The value of α is obtained by taking the antilog of the vertical distance between the curves for the two compounds at the appropriate percent chloroform. The value of α at 60% chloroform is 2.6_5 and k_p' is 0.8_8, yielding an R_s value of 1.5. Thus, in this example it is not necessary to consider lower percentages of chloroform since adequate resolution should be obtained with this solvent. Figure 5 shows the separation obtained between phenacetin, caffeine, and the unretained solvent peak on a 50-cm column using 60% chloroform.

Ethanol/hexane mobile phases do not provide large separation factors, α, for several of the compounds studied (Figure 4). On the other hand, ethanol is a strong eluent for most of the compounds and can be used in ternary solvent mixtures to reduce the retention volumes of otherwise strongly retained components. For example, although all six drugs in Figure 3 are well resolved on a 30-cm column of XAD-7 using 55% chloroform, the last two, salicylamide and acetaminophen, are retained too strongly, thus prolonging analysis time unnecessarily. Even with a gradient of increasing chloroform concentration, acetaminophen would be too strongly retained. However, if the solvent is changed from 55% chloroform to 55% chloroform/3.8% ethanol after the elution of salicylic acid, then all six components exhibit well defined peaks (Figure 6).

Analysis of Commercial Tablets. Mixtures containing ASA, phenacetin, and caffeine were analyzed on a 50-cm column using the liquid chromatograph diagramed in Figure 1A. The mobile phase was 60% chloroform in hexane. Quantitative determinations were based on peak areas, and linear calibration curves were obtained by injecting standard APC mixtures dissolved in chloroform. Relative average area deviations for the three compounds were between 0.1 and 0.8%.

To test the applicability of this chromatographic method to the analysis of APC tablets, a blank and spiked blank were prepared as described above. Chromatograms of the blank exhibited a flat baseline indicating no interference from any of the inert ingredients. Results of the analysis of the spiked

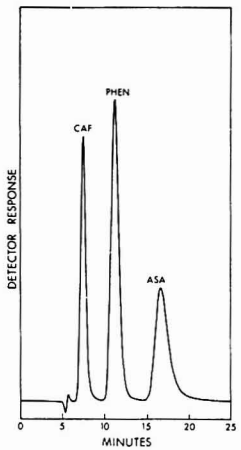


Figure 5. Chromatogram of Empirin tablet on a 50 cm × 0.28 cm column of Amberlite XAD-7 with 60% chloroform in hexane as mobile phase. Pressure 400 psig; flow rate 0.44 mL/min; Linear velocity 0.15 cm/s

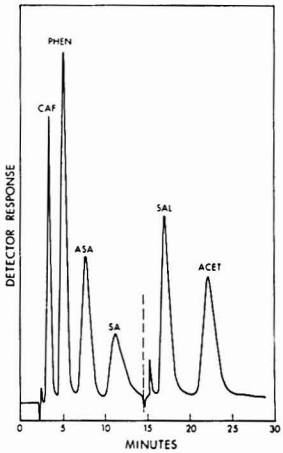


Figure 6. Chromatogram of caffeine (CAF), phenacetin (PHEN), ASA, salicylic acid (SA), salicylamide (SAL), and acetaminophen (ACET) on a 30 cm × 0.28 cm column of Amberlite XAD-7. Dashed line indicates mobile phase change from 55% chloroform to 55% chloroform/3.8% ethanol mobile phase. Pressure 400 psig: flow rate 0.6 mL/min. Linear velocity 0.23 cm/s

Table I. Results of Analysis

Product	Found mg/Tablet[a] (Label Claim mg/Tablet) Phenacetin	Caffeine	ASA	Salicylamide	Acetaminophen
Spiked blank[b]	161 (161)	31.6 (31.4)	223 (225)	-	-
Empirin (Lot 035-u)[c]	163 (162)	32.3 (32.4)	230 (227)	-	-
Empirin (Lot 357-p)[d]	160 (162)	32.2 (32.4)	230 (227)	-	-
Revco APC	154 (162)	30.6 (32.4)	231 (227)	-	-
Spiked blank[b]	-	64.0 (64.1)	195 (194)	129 (129)	96.0 (96.3)
Spiked blank (S.C.)[b,e]	-	63.2 (64.7)	194 (196)	131 (131)	97.8 (98.2)
Excedrin (Lot.6H10)	-	63.6 (64.8)	204 (194)	127 (130)	93.5 (97.2)
Excedrin (Lot.6H10) (S.C.)[e]	-	65.0 (64.8)	198 (194)	128 (130)	94.8 (97.2)
Excedrin (Lot.6F25)	-	67.1 (64.8)	189 (194)	134 (130)	100.4 (97.2)
Excedrin (Lot.6F25) (S.C.)[e]	-	65.2 (64.8)	195 (194)	131 (130)	96.8 (97.2)

[a] Assays of commercial products reported on basis of average tablet weight. [b] Amount in parentheses in this row is known amount added to blank. [c] Manufacturers analysis: phenacetin 164; caffeine 33.0; ASA 228. [d] Manufacturers analysis: phenacetin 160; caffeine 32.8; ASA 232. [e] S.C. indicates short column (10 cm × 0.63 cm i.d.) chromatograph.

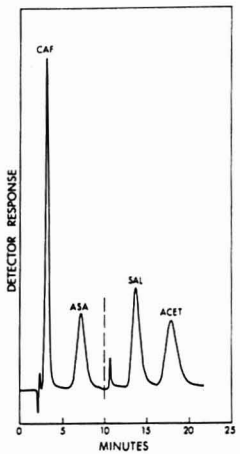


Figure 7. Chromatogram of Excedrin tablet on a 30 cm × 0.28 cm column of Amberlite XAD-7. Dashed line indicates change from 57% chloroform to 55% chloroform/3.8% ethanol. Pressure 400 psig; flow rate 0.6 mL/min; Linear velocity 0.23 cm/s

blank along with the assay values for three commercial formulations are presented in Table I. The assay values of the spiked blank are compared with the known quantities added, and those of commercial products are compared with the label claim and, where available, with the manufacturer's analysis. A typical chromatogram of an APC tablet is shown in Figure 5. Salicylic acid, the major degradation product of ASA, elutes after ASA and does not interfere in the analysis.

As another example, the chromatograph shown in Figure 1A, with a 30-cm column, was used for the analysis of samples containing a mixture of ASA, caffeine, salicylamide, and acetaminophen (Excedrin Tablets). A tablet blank chromatogram showed a flat baseline, and linear calibration curves based on peak areas were obtained for all components by injecting standard mixtures. Relative average area deviations for the four compounds were between 0.1 and 0.9%. Results of analysis of the spiked blank and two lots of commercial tablets are presented in Table I, and a typical tablet chromatogram is presented in Figure 7. Salicylic acid elutes between ASA and salicylamide and does not interfere in the analysis.

Determination of salicylic acid in ASA-containing tablets is best performed with an ether/hexane mobile phase and is the subject of a separate report (*32*).

Analyses Using Short Columns. As an alternative to high pressure liquid chromatographic systems, we were interested in developing simple systems involving short analytical columns operated at low pressures, with the eluted components collected in separate flasks for subsequent quantitation by spectrophotometry. The need for expensive pumps and detectors could thus be eliminated. Such a system using a 10 cm × 0.63 cm i.d. glass column is diagramed in Figure 1B. A tank pressure of 50 psig produced flow rates of 1.8 to 0.9 mL/min (linear velocity = 0.07 to 0.03 cm/s) depending on solvent viscosity. Plate heights were about 0.2 cm.

Using the data in Figures 2–4 it is possible to select mobile phases which produce large separation factors, α, for the various drug compounds. With these mobile phases it is then possible to sequentially elute the tablet components, each with a different mobile phase. As an example, Excedrin Tablets were analyzed for their four components by the procedure described in the Experimental section. For replicate injections, relative average deviations were between 0.4 and 2%. Results of analysis of a spiked blank and the two commercial Excedrin samples are listed in Table I. Assay values may be compared with those obtained above.

CONCLUSIONS

Amberlite XAD-7 is an inexpensive column packing which is suitable for use in both high and low pressure chromatographic systems. It shows long column life, is compatible with aqueous and nonaqueous solvents, and can be readily regenerated after solvent programming. On the one hand, it should be possible to increase column efficiency by packing stainless steel columns with smaller and more uniform particles while, on the other hand, larger particles would be used in gravity flow columns. Long analysis times encountered with the latter can be offset by running several columns in parallel and collecting the eluted compounds for subsequent quantitation.

The principles outlined in the discussion above and previously (*31*) along with the data in Figures 2–4 and a knowledge of the plate height of the column allow one to predict separation factors and select appropriate mobile phases and column lengths to achieve a given separation.

LITERATURE CITED

(1) T. V. Parke, A. M. Ribley, E. C. Kennedy, and W. W. Hilty, *Anal. Chem.*, **23**, 953 (1951).
(2) A. W. Clayton and R. E. Thiers, *J. Pharm. Sci.*, **55**, 404 (1966).
(3) F. Namigohar and J. Khorrami, *Ann. Pharm. Fr.*, **34**, 457 (1976).
(4) J. G. Nikelly, *Anal. Chem.*, **38**, 2248 (1964).
(5) L. L. Alber, M. W. Overton and D. E. Smith, *J. Assoc. Off. Anal. Chem.*, **54**, 620 (1971).
(6) S. L. Ali, *Chromatographia*, **6**, 478 (1973).
(7) J. Levine, *J. Am. Pharm. Assoc., Sci. Ed.*, **46**, 687 (1957).
(8) R. F. Heuermann and J. Levine, *J. Am. Pharm. Assoc., Sci. Ed.*, **47**, 276 (1958).

(9) K. T. Koshy, *J. Pharm. Sci.*, **53**, 1280 (1964).
(10) C. G. Cunningham and S. Barkan, *J. Assoc. Off. Anal. Chem.*, **57**, 728 (1974).
(11) "United States Pharmacopia", 19th Rev., Mack Publishing Co., Easton, Pa., 1975, pp 12, 39.
(12) R. A. Henry and J. A. Schmit, *Chromatographia*, **3**, 116 (1970).
(13) R. L. Stevenson and C. A. Burtis, *J. Chromatogr.*, **61**, 253 (1971).
(14) J. L. Mayell, C. F. Hiskey, and L. Lachman, *Anal. Chem.*, **46**, 449 (1974).
(15) J. A. Schmit in "Modern Practice of Liquid Chromatography", J. J. Kirkland, Ed., Wiley-Interscience, New York, N.Y., 1971, Chapter 11.
(16) P. Larson, E. Murgia, F. J. Hsu, and H. F. Walton, *Anal. Chem.*, **45**, 2306 (1973).
(17) D. Rosenbaum, *Anal. Chem.*, **46**, 2226 (1974).
(18) P. P. Ascione and G. P. Chrekian, *J. Pharm. Sci.*, **64**, 1029 (1975).
(19) "Preliminary Technical Notes, Amberlite XAD-7", Rohm and Haas Co., Philadelphia, Pa., 1972.
(20) J. Paleos, *J. Colloid Interfac. Sci.*, **31**, 7 (1969).
(21) A. K. Burnham, G. V. Calder, J. S. Fritz, G. A. Junk, H. V. Svec, and R. Willis, *Anal. Chem.*, **44**, 139 (1972).
(22) J. S. Fritz and R. B. Willis, *J. Chromatogr.*, **79**, 107 (1973).
(23) D. J. Pietrzyk and C-H. Chu, *Anal. Chem.*, **49**, 860 (1977).
(24) D. J. Pietrzyk and C-H. Chu, *Anal. Chem.*, **49**, 757 (1977).
(25) K. Fuzita, I. Shimokobe, Y. Arikawa, and S. Ganno, *Nippon Kagaku Kaishi*, **1975**, 999.
(26) F. F. Cantwell, *Anal. Chem.*, **48**, 2044 (1976).
(27) (a) "United States Pharmacopia", 19th Rev., Mack Publishing Co., Easton, Pa., 1975. (b) *Ibid*, 18th Rev., 1970, p 483.
(28) "National Formulary", 11th Rev., Mack Publishing Co., Easton, Pa., 1960.
(29) "The Merck Index", 8th Ed., Merck and Co., Rahway, N.J., 1968.
(30) L. R. Snyder, "Principles of Adsorption Chromatography", Marcel Dekker, New York, N.Y., 1968.
(31) H. Y. Mohammed and F. F. Cantwell, *Anal. Chem.*, in press.
(32) R. G. Baum and F. F. Cantwell, *J. Pharm. Sci.*, in press.

RECEIVED for review September 19, 1977. Accepted November 7, 1977. Presented in part at the 173rd National Meeting, American Chemical Society, New Orleans, La., March 1977. This work was supported by the National Research Council of Canada and the University of Alberta.

Quantitative Ion Probe Measurement Using Matrix Ion Species Ratios

J. D. Ganjei, D. P. Leta, and G. H. Morrison*

Department of Chemistry, Cornell University, Ithaca, New York 14853

A new method of empirical calibration has been developed using matrix ion species ratios to calibrate elemental sensitivity factors from external standards. A series of sensitivity factors is generated as a function of sample chamber oxygen pressure using an oxygen leak system. The method is applied to the analysis of three different metal matrices: steels, aluminum alloys, and copper alloys. The accuracy achieved with the method is on the order of 10% relative error.

The ion microprobe is currently one of the most sensitive techniques for surface microanalysis, achieving ppm detection limits within a volume of several monolayers. The in-depth profile and x-y lateral resolution capabilities are additionally valuable functions. One of the main limitations of the technique, however, is the difficulty of determining elemental concentrations. The relationship between elemental concentrations and measured secondary ion intensities is not a simple conversion factor because of the complexity of the secondary emission process from sputtered surfaces. As a result, ion probe measurements have usually been semiquantitative.

The empirical calibration approach, which is used in most other analytical techniques, has been hindered by relative secondary ion yield changes during ion microprobe analyses. Therefore, elemental sensitivity factors determined from external standards generally result in considerable error for secondary ion signals of unknown samples. Quantitative results are achieved only when sample and standard match in chemical composition and experimental conditions are kept constant.

A competing calibration approach is the development of physical models to simulate the ion-surface interaction. The most successful version to date has been the local thermal equilibrium (LTE) model as exemplified by Andersen and Hinthorne's computer program CARISMA (*1*). Although this model has been surprisingly successful in some cases, in general the accuracy of the results cannot be stated to better than a factor of 2 or 3 (*2-4*). In addition, the necessity for prior determination of several internal standard elements within the sampling area makes practical applications difficult.

A number of modifications of the empirical calibration approach have been proposed. McHugh (*2*) was the first to suggest matrix-sensitive correlation factors as a means of compensating for matrix effects. Some successful results have been reported using matrix ion species to correct secondary ion signals (*5, 6*). It should be noted that the use of MO^+/M^+ ratios to determine LTE parameters "temperature" and "electron concentration" have been previously suggested (*1*). The matrix ion species ratio (MISR) method essentially consists of using the ratio of such matrix ions as (M^+, MO^+, M_2^+) to calibrate elemental sensitivity factors. Through the admission of oxygen into the sample chamber during the external standard analysis, a series of elemental sensitivity factors and matrix ion species ratios are measured. Unknown samples' elemental concentrations are determined by using the matrix ion species ratio to select the appropriate sensitivity factor.

Data were obtained for the multielement analysis of three different metal matrices; steels, aluminum alloys, and copper alloys. The accuracy achieved with the MISR method is on the order of 10% relative error. These results are compared with single sensitivity factor corrected measurements obtained at residual instrument pressure and oxygen saturated conditions, respectively, and with data reported by other investigators using the LTE semitheoretical approach. In all cases the MISR method shows a substantial improvement in accuracy.

EXPERIMENTAL

Instrumentation. The study was accomplished using a CAMECA IMS-300 ion microprobe which has been previously described (*7*). The instrument was interfaced with a DEC PDP-11/20 computer, a Nuclide D/A converter, and a Preston high speed A/D converter. Peripheral devices included a 1.2 M word cartridge disk used for the RT-11 operating system, a

0003-2700/78/0350-0285$01.00/0 © 1978 American Chemical Society

Table I. Experimental Parameters

Instrument: CAMECA IMS-300 ion probe
Primary ions: O^-, O_2^+
Primary ion energy: 5.5 keV
Primary ion current density: 1×10^{-8} to 1×10^{-2} A/cm^2
Primary crater size: unrastered, $\sim 2 \times 10^{-3}$ cm^2
Mass resolution: 200
Secondary ion energy range: 0–15 V
Sampling area: 125- to 250-μm diameter circle
Detection system: Pulse count rate
Immersion lens aperture: 300-μm diameter

Versatec high speed printer and a GT-40 graphics display system.

Computer Software. Analyses were performed under computer control using Fortran and Assembler level programming. Data collection was accomplished by peak integration (twenty 100-ms points across each peak). A routine collection of data for 15 species of interest took approximately 1 min per total scan. Five scans were averaged for each analysis to minimize noise contributions.

Standards. The standards used in this study were the NBS low alloy steels SRM-661, 662, 663 and 664; the NBS iron and plain carbon steels 1042, 1044, and 1045; the Japanese M Steel series, M2 and M9 prepared by Sumitamo Metals and M16 and M25 prepared by Nippon Steel; the aluminum alloys AA2, AA3, AA4, and AA5 prepared by Johnson, Mathey and Co.; and the copper alloys series, CB0, CB1, CB2 also prepared by Johnson, Mathey and Co. Uncertified elemental concentrations in NBS-1042, 1044, and 1045 steels were verified in this laboratory utilizing neutron activation analysis and atomic absorption spectroscopy. During the analyses, one standard from each matrix was used as the external standard and the other standards were treated as "unknowns."

Sample Preparation. The samples were mounted in Sn-Bi eutectic and wet-sanded with SiC paper down to 600 grit. They were further polished with 1-μm and 0.3-μm alumina on a wet wheel polisher until no scratches were discernible under light microscope examination. Each sample was presputtered with a wide raster to approximately 0.1 μm in depth.

Procedure. The basic experimental parameters are presented in Table I. Several experimental conditions were varied for the three modes of analysis carried out on the samples. One analysis was performed at a residual instrument pressure of 3×10^{-8} Torr and a high beam density (1 – 5 mA/cm^2). The analysis at saturated O_2 conditions was executed with a low primary beam density (0.1 mA/cm^2) and an oxygen pressure of 1×10^{-5} Torr within the sample chamber. The MISR method was performed by bombarding the external standard at an intermediate beam density of 0.5 mA/cm^2 and incrementing the sample chamber oxygen pressure in several steps while monitoring the secondary ion signals. "Unknown" samples were then analyzed at high primary beam densities (1–5 mA/cm^2) with some oxygen present in the sample chamber (5×10^{-7} Torr). During the analyses, the primary beam was slightly defocused so that the sampled area was under continual bombardment. This allowed an equilibrium condition to exist between the rate of sputtering and oxygen adsorption. Normally, the CAMECA oxygen leak unit admits oxygen directly onto the sample surface and the actual sampling ambient pressure is somewhat greater than the total chamber pressure. However, during the MISR calibration the leak was modified so that the sample chamber pressure reflected the pressure at the surface. This provided uniform flooding of the chamber and reduced memory effects between pressure changes.

RESULTS AND DISCUSSION

In ion microprobe analysis, the elemental sensitivity factor is usually defined as

$$S_x = \frac{i_x}{C_x} \cdot \frac{C_{ref}}{i_{ref}} \qquad (1)$$

where i_x and i_{ref} are the signal intensities of element x and the reference element, respectively, and C_x and C_{ref} are the corresponding concentrations.

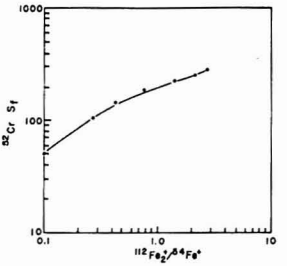


Figure 1. ^{52}Cr relative sensitivity factor plotted vs. matrix ion species ratio for low alloy steel NBS-662

In this unmodified empirical calibration procedure, a single sensitivity factor is determined for each element by measuring the signals from a standard sample. These sensitivity factors are then used to transpose secondary ion signals from other samples into elemental concentrations. In general, this procedure has been unsuccessful because a single sensitivity factor does not compensate for relative ion yield fluctuations. Good results are obtained only when experimental conditions are reproduced exactly and sample and standard matrices are a perfect match.

The MISR calibration procedure is predicated on the fact that conditions which induce changes in elemental ion yields also affect matrix ion species yields. The sampling environment is effectively indexed by a ratio of two matrix species. Thus, whenever elemental ion species are measured, a matrix ion species ratio is also determined. Following this approach, an elemental sensitivity factor is valid only when the sample's matrix ion species ratio matches the ratio of the standard.

This procedure would be impractical if only one sampling condition could be generated per external standard. In that case, the analyst would be required to obtain a large number of standards in order to cover a range of elemental sensitivity factors and matrix ion species ratios. We have solved this problem by using ambient oxygen to induce sampling environment changes. Thus, only one external standard is needed because the adsorbed oxygen produces a large range of secondary ion yields. The application of this calibration procedure is shown in Figure 1 where the Cr sensitivity factor in NBS-662 low alloy steel is plotted against a matrix ion species ratio ($^{112}Fe_2^+/^{54}Fe^+$). Both axes are presented as log scales because of the large variation in intensities. The curve was produced by increasing sample chamber oxygen pressure from residual pressure 3×10^{-8} Torr to 1×10^{-5} in several steps. At each increment, the elemental and matrix ion species signals were measured and then converted into sensitivity factors and matrix ion species ratios. The denominator of the matrix ratio was also used as the reference species for the elemental sensitivity factor. Other elemental ion signals were simultaneously measured and a similar curve was plotted for each constituent of interest within the standard sample. Secondary ion intensities of constituent elements and matrix species were later obtained from "unknown" samples. The matrix ratio was then used to select the appropriate sensitivity factor. As a result, changes in experimental conditions and matrix composition between samples were corrected. Since secondary ion yield fluctuations are a major source of error in ion microprobe analysis, the MISR correction is significant.

One important observation that should be clarified is that although oxygen pressure within the sample chamber is used to produce the MISR curves, pressure readings are not a valid substitute for the matrix ratios in the abscissa. This can be explained by two factors: (1) ion yields are dependent on

matrix chemical composition so that two samples may have different ion yields at the same ambient oxygen pressure, and (2) the actual amount of oxygen being adsorbed onto the surface may be different at equal chamber pressures because of divergent sputtering rates during the analyses.

In order for the MISR method to be properly applied, a number of requirements must be met during the analysis. One essential requirement is the availability of an appropriate external standard of the matrix containing the elements of interest at known concentrations. In addition, the spatial distribution of the elements within the standard must be determined so that sampling error of heterogeneous elements can be reduced to an acceptable level. Microsampling error is especially critical since most standard samples have been certified for much larger volumes by bulk analysis techniques.

A second requirement is two measurable matrix ion species whose ratio is sensitive to oxygen adsorption. Greater sensitivity is achieved by choosing matrix ion species which respond differently to sample chamber oxygen. For example, oxides show dramatic enhancement with increasing oxygen while polymer ions remain relatively stable or exhibit a small negative slope. If the ratio consists of ions from these two groups, small changes in ambient oxygen pressure will significantly affect the ratio value.

Suitable ions are usually easy to find because molecular species are prevalent in secondary ion spectra. In some cases the analyst may choose a matrix cluster ion such as M_2^+ instead of the matrix elemental ion for the reference signal. By so doing one can greatly increase sensitivity for trace elements since the instrument's dynamic range may prevent simultaneous measurement of weak signals and the intense matrix elemental ion.

Finally, some preliminary investigation of the sample matrix is necessary in order to optimize experimental conditions. The most critical parameter is primary beam density since this variable directly determines the sample's sputtering rate. The sputtering rate is important because it limits the amount of oxygen that is adsorbed onto the sample surface at different sample chamber pressures. Therefore, the MISR method requires adjustment of the primary beam density and sample chamber oxygen pressures until a series of different sampling environments are obtained in the external standard analysis. Once the external standard curve has been generated, experimental conditions are calibrated by the matrix ion species ratio so that a variety of conditions can be employed during unknown sample analyses.

The results from ion microprobe analysis of the various samples are presented in Tables II to V. In every instance the spatial distribution of the constituents was checked before analysis using the sampling procedure of Scilla and Morrison (7). Ion micrographs were recorded of each element and the elemental spatial distributions approximated by sampling constants determined with image analysis (8). The sampling constants were then used to estimate the minimum sampling area required for accurate (less than 10% relative error) analysis of bulk determined concentrations. In several samples, some elemental distributions were found to be too heterogeneous for microprobe analysis (over ten sampling areas of 250-μm diameter); in other samples the average signal from several sampling areas was required. These spatial heterogeneity problems are illustrated in Figure 2. The ion micrograph in Figure 2a shows Co in NBS-664 steel. The uniform intensity of the micrograph indicates a very homogeneous distribution. An intermediate distribution is shown in Figure 2b. The micrograph indicates that Nb is located in numerous small inclusions in NBS-662 steel. Since the inclusions are small and densely spaced, the heterogeneity of the Nb distribution can be overcome by averaging the signals from five sampling areas. Figure 2c illustrates a severe heterogeneity problem where the inclusions are large and sparsely distributed. As a result, ion microprobe analysis of Al in NBS-664 steel is impractical. Reduction of the sampling error to an acceptable level would require averaging the signal from approximately 100 sampling areas.

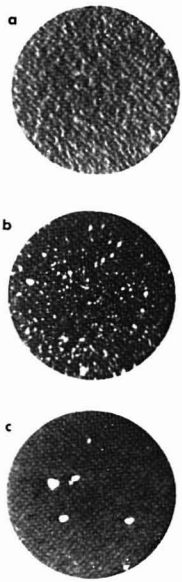


Figure 2. Ion micrographs. Field of view, 250-μm diameter. (a) Co in NBS-662; (b) Nb in NBS-662; (c) Al in NBS-664

In order to compare the MISR method with the unmodified empirical calibration procedure, three separate analyses were performed on each sample: unmodified empirical analysis at residual sample chamber pressure, at saturated oxygen conditions, and a third analysis using the MISR method. The relative error of each mode of analysis is presented under the labels residual, saturated, and MISR. In some cases, the error from the analysis at saturated oxygen conditions is not given because the low primary beam density required for saturation introduced low signal-to-noise ratios.

Table II presents the data from the analysis of the NBS-660 low alloy steel series. NBS-662 was used as the standard and $^{112}Fe_2^+/^{54}Fe^+$ was chosen as the matrix ratio. Ti, Zr, and Nb were determined by averaging the signals from five sampling areas. Al and Si in NBS-664 were found to be too heterogeneously distributed for ion probe sampling. Anomalous results were obtained from vanadium in NBS-663 and 664. This was attributed to vanadium being distributed in the carbide phase in these two steels while present in solid solution in the low V concentration steels. None of the empirically derived methods seem to be able to compensate for an element being present in two completely different chemical phases between standard and sample. Therefore, these two results are not included in the average percent error. Only Al, V, Cr, and Mn concentrations were determined at saturated oxygen conditions because of sensitivity problems as mentioned above.

Several other steel samples were analyzed using NBS-661 steel as the external standard and the results are shown in Table III. This was done in order to confirm the applicability of the MISR calibration to steels beyond the specially pre-

Table II. Analysis of NBS-660 Low Alloy Steels Series

Sample	Mode of analysis	C	Al	Si	Ti	V	Cr	Mn	Co	Zr	Nb	Av % rel error external standard
662	NBS concn[a]	0.16	0.09	0.39	0.084	0.04	0.30	1.04	0.30	0.19	0.29	
661	NBS concn[a]	0.38	0.02	0.223	0.02	0.011	0.69	0.66	0.03	0.009	0.022	
	Residual[b]	3%	31%	43%	18%	53%	14%	33%	8%	41%	50%	29%
	Saturated[b]		9%			5%	10%	5%				
	MISR[b]	16%	10%	19%	25%	10%	4%	14%	3%	6%	32%	14%
664	NBS concn[a]	0.87	0.008	0.067	0.24	0.10	0.06	0.25	0.15	0.068	0.15	
	Residual[b]	78%	-	-	8%	(53%)	72%	29%	0%	24%	41%	31%
	Saturated[b]		-	-		(226%)	53%	25%				
	MISR[b]	3%	-	-	25%	(70%)	2%	0%	13%	9%	7%	8%
663	NBS concn[a]	0.62	0.24	0.39	0.05	0.31	1.31	1.50	0.048	0.049	0.049	
	Residual[b]	19%	18%	18%	25%	(26%)	29%	20%	10%	35%	13%	21%
	Saturated[b]		18%			(90%)	20%	0%				
	MISR[b]	0%	25%	11%	16%	(75%)	0%	0%	6%	12%	4%	8%

[a] Weight %. [b] % relative error.

Table III. Analysis of 1040 Series and M Series Steels

Sample	Element	Relative error, % Residual	Saturated	MISR	Concn wt % (Cert.)
1042	Cr	13	40	5	0.006
	Mn	308	48	25	0.65
1044	Cr	15	5	10	0.02
	Mn	67	31	8	0.39
1045	Cr	20	38	0	0.01
	Mn	84	5	7	0.44
M2	Si	7	14	11	0.44
	Cr	5	21	5	2.10
	Mn	23	9	7	0.43
M9[a]	Si	10	48	10	0.63
	Cr	6	5	3	8.82
	Mn	52	21	13	0.44
M16[a]	Si	60	7	13	0.57
	Cr	29	2	15	16.33
	Mn	9	14	6	0.35
M25[a]	Cr	120	38	8	25.89
Average relative error =		52%	22%	9%	

[a] Sensitivity factors corrected for differences in Fe concentration between sample and standard.

pared NBS-660 series. The same ratio $^{112}Fe_2^+/^{54}Fe^+$ was used. Image analysis indicated that sampling error was insignificant for the elements of interest. The data obtained from the M series steels is especially interesting since the large increase in Cr concentrations did not produce errors in the MISR method values. In contrast, the residual pressure empirical results were substantially affected. The error in determining Cr in M25 was also significantly greater under saturated oxygen conditions.

A similar approach was used to determine Ti, Mn, Fe, and Cu in a set of aluminum alloy standards. These results are presented in Table IV. An intermediate standard AA4 was selected as the ion microprobe standard for the analysis. The matrix ion species ratio was chosen to be $^{70}Al_2O^+/^{54}Al_2^+$ because the ratio showed a large sensitivity to ambient oxygen pressure and the $^{27}Al^+$ signal was too intense to be simultaneously measured with the constituent signals. The relative errors of both the analyses under saturated oxygen conditions and the MISR method are extremely good. However, the Cu determination in AA2 was degraded by measurement noise during the saturated oxygen analysis.

Table V gives the data for the determination of Si, Mn, and Fe in a set of copper alloys. The secondary ion signals from the copper matrix were fairly insensitive to sample chamber oxygen compared to the Fe and Al samples. $^{142}Cu_2O^+/^{126}Cu_2^+$ was used as the matrix ratio since it showed a greater response

Table IV. Results from Al Alloys

Samples	Modes of analysis	Ti	Mn	Fe	Cu
AA4	J&M concn[a]	0.02	0.069	0.76	0.065
AA3	J&M concn[a]	0.011	0.0155	0.19	0.02
	Residual[b]	40%	580%	33%	160%
	Saturated[b]	13%	3%	7%	7%
	MISR[b]	14%	0%	4%	19%
AA5	J&M concn[a]	0.06	0.13	0.35	0.11
	Residual[b]	31%	15%	17%	13%
	Saturated[b]	20%	3%	30%	9%
	MISR[b]	50%	8%	2%	7%
AA2	J&M concn[a]	0.005	0.0053	0.10	0.006
	Residual[b]	82%	1430%	85%	270%
	Saturated[b]	40%	25%	15%	130%
	MISR[b]	26%	15%	12%	30%

[a] Weight %. [b] % relative error.

Table V. Copper Alloys

Sample	Modes of analysis	Si	Mn	Fe	Co
CB0	J&M concn[a]	0.05	0.0479	0.0537	0.0506
CB1	J&M concn[a]	0.0270	0.0189	0.0214	0.02101
	Residual[b]	36%	24%	0%	4%
	Saturated[b]	19%	21%	26%	15%
	MISR[b]	19%	12%	5%	6%
CB2	J&M concn[a]	0.0160	0.0094	0.0111	0.0104
	Residual[b]	280%	28%	21%	55%
	Saturated[b]	71%	15%	56%	40%
	MISR[b]	5%	23%	17%	41%

[a] Weight %. [b] % relative error.

relative to oxygen pressure. This sampling environment stability is reflected in the similar errors obtained by the three methods in the analyses of CB1 whose elemental concentrations are close to the external standard, CB0. The MISR method did achieve a substantial improvement over the single sensitivity factor determinations in the analyses of CB2. This improvement probably reflects the difference in matrix composition between CB2 and CB0. The saturated condition results were also degraded in the CB2 analysis by measurement noise.

In general, these data show that the poorest accuracy was obtained in the absence of admitted oxygen. A substantial improvement resulted from saturating the surface with oxygen but the most consistently accurate values were obtained with the MISR method. This is shown in Table VI where the average percent relative errors of the analyses are presented. Besides its accuracy we feel that the MISR method has several other advantages over analyses performed under saturated oxygen conditions. First, every secondary ion species exhibits

Table VI. Average % Relative Error of the 3 Modes of Analysis

Sample	Single S_x Approaches		
	Residual O_2	Satd O_2	MISR
660 series (Al, V, Cr, Mn)	33	16	7
M2 series (Si, Cr, Mn)	28	14	9
1040 Series (Cr, Mn)	85	28	9
Al alloy (Ti, Mn, Fe, Co)	230	25	15
Cu alloy (Si, Mn, Fe, Co)	56	33	14

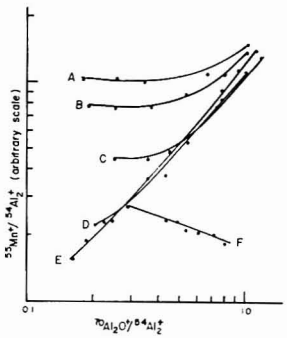


Figure 3. $^{55}Mn^+$ curves for aluminum standards: (A) AA1 Mn = 20 ppm; (B) AA2 Mn = 53 ppm; (C) AA3 Mn = 155 ppm; (D) AA4 Mn = 690 ppm; (E) AA5 Mn = 1300 ppm; (F) $^{55}Al_2H^+$ from pure aluminum

a different behavior with ambient oxygen (*9*). Usually no one optimum position exists where all the ions have a flat profile. Second, oxygen saturation is dependent on a slow sputtering rate so that oxygen can saturate the surface. As a result, low primary ion beam densities must be employed which greatly reduces instrumental sensitivity. Third, when a surface is saturated with oxygen, information about the chemical distribution of the elements can be disguised by the oxide layer. Oxide layer formation also prevents meaningful in-depth profiles due to oxide sputtering rate differences.

While investigating the MISR method, we have made the general observation that better accuracy and precision are achieved by introducing a small amount of ambient oxygen to the sample surface during the analysis of unknowns. Theoretically, the results from sample analyses should be the same regardless of experimental conditions since corrections are made on the basis of MISR values in the external standard sensitivity factor curve. In practice it was found that the intermediate ambient oxygen pressure (5 to 8 × 10^{-7} Torr) alleviated such surface conditions as uneven oxide formation and shifted the sensitivity factors toward the middle of the external standard curve. Therefore most "unknown" samples were analyzed with some oxygen present in the sample chamber. However, the low pressure and high primary beam density made the conditions far removed from saturation.

In one particular case, a total sensitivity factor profile of the samples enabled recognition of a mass interference. This is illustrated in Figure 3 where the profiles of $^{55}Mn^+$ in the five aluminum alloys are presented. The relative $^{55}Mn^+/^{54}Al_2^+$ ratios have been corrected for differences in Mn concentration in samples A, B, C, D, and E. At low $^{70}Al_2O^+/^{54}Al_2^+$ ratios which correspond roughly to low oxygen pressure, the profiles of AA2 and AA3 deviate markedly from the high Mn concentration samples. At higher ambient pressures, the curves come much closer to coinciding. Through the analysis of a pure aluminum sample, it was found that the profiles' deviations were due to $^{55}Al_2H^+$ whose profile is also shown by F in Figure 3. By analyzing the "unknown" samples at higher chamber oxygen pressures, the interference was reduced since the $^{55}Al_2H^+$ signal strength was minimized relative to $^{55}Mn^+$. The potential of total profiles for samples is pointed out by this example where the shape of the curves enabled recognition of an interference. However, the vast majority of analyses can be performed with just one measurement of the unknown sample's secondary ion signals.

Table VII. Comparison of Results Obtained for Analysis of NBS-661

Element	Concn %	% relative error			
		MISR	Newbury	CARISMA	Simon
Al	0.02	10	41	450	180
Si	0.223	19	105	(IS)	15
Ti	0.02	15	12	150	100
V	0.011	10	65	42	35
Cr	0.69	4	69	(IS)	10
Mn	0.66	14	17	(IS)	10
Co	0.03	3	9	-	30
Zr	0.009	6	31	20	-
Nb	0.022	32	20	2	35
Average % error		14	41	133	52

To further demonstrate the effectiveness of the MISR method of calibration, a comparison is made with published results for the NBS-661 standard obtained by both empirical and semitheoretical methods. This sample was chosen since the NBS-660 series has been a popular matrix for ion microprobe analysis and therefore provided the maximum number of literature values. The relative percent error using the respective methods is summarized in Table VII. The methods include a simple empirical approach by Newbury et al. (*3*), Andersen and Hinthorne's LTE model (*1*) using Si, Cr, and Mn as internal standards, and Simons and Evans (*4*) simplified modification of CARISMA utilizing Fe and Ni as internal standards. The MISR method shows a substantial improvement over the other approaches.

It should be pointed out that several other LTE model modifications exist. Especially noteworthy are those of Werner et al. (*9*) and Ishitani et al. (*10*). These researchers have analyzed similar steels without the use of internal standards. Ishitani et al. use the molecular ion species of Fe to fit the model's parameters, while Werner et al. need only the matrix ion. However, these methods still do not achieve the low relative error of MISR.

In conclusion, a general empirical calibration procedure has been developed to achieve quantitative ion microprobe analysis which employs matrix ion species to correct for sampling environment differences. The method involves: (1) selection of an external standard of similar matrix type containing the constituents of interest, (2) minimization of sampling error within the standard, (3) generation of a sensitivity factor series with sample chamber oxygen pressure, (4) use of a matrix ion species ratio to calibrate the sensitivity factors, and (5) analysis of unknown samples.

Further work is being performed in this laboratory to evaluate this method for other matrices such as semiconductors and insulators and in such applications as feature analysis and in-depth profiling.

LITERATURE CITED

(1) C. A. Andersen and J. R. Hinthorne, *Anal. Chem.*, **45**, 1421 (1973).
(2) J. A. McHugh, "Secondary Ion Mass Spectrometry" in "Methods of Surface Analysis", S. P. Wolsky and A. W. Czanderna, Ed., Elsevier, New York, N.Y., 1976.
(3) D. E. Newbury, K. F. J. Heinrich, and R. L. Myklebust, "Surface Analysis Techniques for Metallurgical Applications", ASTM STP-576, American

Society for Testing and Materials, Philadelphia, Pa., 1976, pp 101–113.
(4) D. S. Simons and C. A. Evans, Jr., *Anal. Chem.*, **48**, 1341 (1976).
(5) J. J. Larsson, A. Lodding, H. Odelius, and L. G. Petersson, "Calibration Methods for Ion Probe Application to Fluorine in Biological Hard Tissue", U.S.–Japan Joint Seminar on SIMS, Honolulu, Hawaii, 1975.
(6) H. Tamura, T. Ishitani, and I. Kanamota, "Correction for Ionization Yield", U.S.–Japan Joint Seminar on SIMS, Honolulu, Hawaii 1975.
(7) G. J. Scilla and G. H. Morrison, *Anal. Chem.*, **49**, 1529 (1977).
(8) J. D. Fassett, J. R. Roth, and G. H. Morrison, *Anal. Chem.*, **49**, 2322 (1977).
(9) A. E. Morgan and H. W. Werner, *Anal. Chem.*, **48**, 699 (1976).
(10) T. Ishitani, H. Tamura, and T. Kondo, *Anal. Chem.*, **47**, 1294 (1975).

RECEIVED for review August 15, 1977. Accepted October 27, 1977. Financial support was provided by the National Science Foundation under Grant No. CHE-7608531 and through the Cornell Materials Science Center.

Measurement of Electron Capture Rates for Chlorobenzene with Negative Ion Plasma Chromatography

Glenn E. Spangler*

MERADCOM, Attn: DRDME-O, Fort Belvoir, Virginia 22060

Phil A. Lawless

Research Triangle Institute, Research Triangle Park, North Carolina 27709

Theory and experimental procedures are developed to allow measurement of ion–molecule reaction rates with plasma chromatography. The procedures include the use of the exponential dilution flask. Diagnostically, the dissociative electron capture of chlorobenzene is shown to procede at a rate of $7.1 \pm 3.1 \times 10^{-11}$ cm^3 molecule^{-1} s^{-1} in agreement with similar results obtained with swarm beam techniques.

Plasma Chromatography is an analytical technique which has been developed in recent years to detect and identify trace constituents of organic vapors in gaseous mixtures under atmospheric pressure conditions. Review articles describing the technique have been provided by Karasek (*1*) and Metro and Keller (*2*). The vapors to be detected are ionized by ion–molecule reactions in the presence of a ^{63}Ni radioactive source and are sorted by a coupled ion mobility drift tube spectrometer (*3*). The readout is an arrival time spectrum of ion current peaks separated by mobility differences through the drift region. Among the parameters affecting the response of the instrument are the nature of the reactant ion and reaction paths available for the ion–molecule reactions (*4*), rate constants affecting the direction and speed of the ionization and recombination processes, efficiency for ion current extraction from the near radioactive source region, masking and/or false identification of ion mobility peaks due to the presence of interfering species (*5*), peak shape as it is affected by longitudinal diffusion and gate width settings, (*6*), and ion loss through transverse diffusion and/or charge detachment. Experimentally, changes in gate width, drift temperature, electrostatic drift field, reagent carrier gas composition, sample composition, and sample concentration can all significantly affect results. In particular, when nitrogen is used as drift and reagent carrier gases, electron capture processes are the reactions generally observed producing negative ions.

Karasek et al. (*7–9*) have studied the ionization of chlorobenzene and dichlorobenzene in plasma chromatography and have shown that these compounds dissociatively capture free electrons to form detached chloride anions. Resonance capture by these molecules is endothermic by about 0.86 and 0.36 eV, respectively. This is postulated to be due to the formation of an intermediate molecular anion before dissociation into an halide anion and a radical. Thermal electron capture is also possible (*10–12*). Although the relative attachment coefficients for organic compounds are generally referenced to that for chlorobenzene in the electron capture detector (*13–18*), the operating conditions utilized in plasma chromatography do not allow direct comparison with ECD data. Rather, E/P values of 0.28 V/cm-Torr, in nitrogen, typically chosen for optimum operation of the plasma chromatograph, allow the generation of electrons with an average energy of 0.3 eV (*19*). Endothermic reactions are consequently more probable than exothermic or thermal reactions in comparison with thermal electron data.

In the present work, dilution flask experiments that measure the efficiency of ionization of chlorobenzene in plasma chromatography are reported. A theoretical treatment is provided to describe the mechanisms of reaction involved in the reaction region of the instrument and to arrive at values for the dissociative capture rate constant.

EXPERIMENTAL

The experimental setup is illustrated in Figure 1. The data were collected on a Franklin GNO Beta/VII Plasma Chromatograph consisting of an ion–molecule reaction region and a coupled ion–mobility drift tube spectrometer. Mobilities of the product ions formed in the reaction region are measured in the drift region by either a one-grid or two-grid pulsing procedure. The one-grid pulsing procedure consists of measuring the ionic drift time spectrum from the pulsed shutter grid (grid 1) to the collector with fast electronics while the two-grid pulsing procedure utilizes a second grid as a variably delayed gate to sample a narrow band of the ion mobility spectrum. For the one-grid pulsing procedure, readout was accomplished with a Nicolet 1072 signal averager, Hewlett-Packard 7035 x-y recorder, and/or Tektronix 5103 oscilloscope. To collect dilution flask data, the two-grid pulsing procedure was used with an automatic baseline correcting circuit whose performance was checked by repetitive scanning and manual integration in the one-grid mode (*20*). Operating parameters used in the performance of these experiments are displayed in Table I.

The dilution flask was of cylindrical design and constructed of Pyrex glass. It was housed in a Thermolyne OV-10600 hot plate oven modified to sit above a Thermolyne Nucerite stirring hot plate. A magnetically driven rotor, with the magnet enclosed in glass, was included in the flask; speed could be adjusted by settings

0003-2700/78/0350-0290$01.00/0 © 1978 American Chemical Society

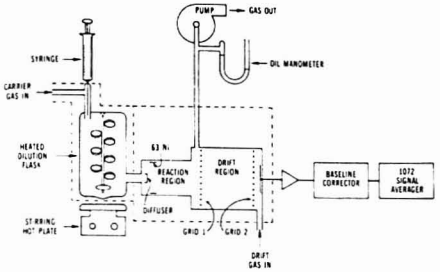


Figure 1. Experimental setup

Table I. Experimental Parameters

Plasma chromatograph	
Gate 1 width	0.2 ms
Gate 2 width	1.0 ms
Repetition rate	40/s
Carrier gas	Prepurified nitrogen
Drift gas	Prepurified nitrogen
Drift tube pressure	Atmospheric
Drift tube temperature	200 °C
Drift field	214 V/cm
Standing open grid current	
Electrons	5.25×10^{-10} A
Positive Ions	3.77×10^{-10} A
Reaction region geometry	
Cross-sectional area	1.56 cm²
Length	6.0 cm
Dilution flask	
Flask temperature	195 °C
Flask volume	469 cm³
Rotor speed	60 rpm
Carrier gas flow	48–101 cm³(NTP)/min (Data normalized to 50 cm³/min at 200 °C)

available on the stir plate. No significant difference was observed in the exponential decay of the sample concentration with the rotor stirring or not. Since the dilution flask was coupled directly to the plasma chromatograph, the carrier gas from the treatment system of the plasma chromatograph was delivered directly through the dilution flask to the inlet of the instrument. The flask was heated independently of the plasma chromatograph, and the carrier gas inlet line was heated by a wrapped heater tape. Syringe injection of sample into the flask established an initial concentration N_0 of sample within the flask.

The gas exit of the plasma chromatograph was connected to a variable speed suction pump in parallel with an oil manometer. This arrangement allowed pressure drops across the plasma chromatograph to be monitored and stabilized. The manometer pressure was adjusted to be less than atmospheric (0.5 cm of oil $< \Delta P <$ 1.0 cm of oil), but not enough less to draw laboratory air through the sample injection hole of the dilution flask. The latter condition was made evident by formation of negative molecular reactant ions (identities unspecified) from the free electrons normally generated in nitrogen. This slight underpressure minimized problems associated with backflushing of the injected sample.

Reagent grade chlorobenzene was used as the sample for these experiments. Gas or liquid syringes of various sizes were used to inject vapor or liquid samples, respectively, into the flask. Vapor samples were withdrawn from a closed 551-cm³ Erlenmeyer flask which had been flushed with nitrogen flowing at a rate of 450 cm³/min for 30 to 60 min, injected with 1 μL of pure chlorobenzene liquid, and then mixed for 20 min with a magnetic stir bar. Liquid samples were withdrawn from solutions of chlorobenzene with pesticide grade benzene (Fisher), prepared by volumetric dilution. Reproducibility was established by using clean glassware, preparing new batch samples periodically throughout the experiments, assuring syringe cleanliness by interposing benzene washes between injections, and establishing baselines with blank injections of pure benzene.

THEORETICAL

Ionization. The theory for the ionization of vapor species in plasma chromatography is derived from the theory developed for ion-mobility drift tube spectrometers (*21*). The transport equations describing the three-dimensional drift and diffusion of the reactant ion concentration n_R, neutral sample concentration N_P and the product ion concentration n_P in the presence of ion–molecule reactions are

$$\frac{dn_R}{dt} = D_R n_R - k_P n_R N_P \tag{1}$$

$$\frac{dN_P}{dt} = D_{LN}\frac{d^2N_P}{dz^2} - \frac{\dot{F}}{A_r}\frac{dN_P}{dz} - k_P n_R N_P \tag{2}$$

$$\frac{dn_P}{dt} = D_P n_P - \beta\alpha_P n_+ n_P + k_P n_R N_P \tag{3}$$

where k_P is the ionizing ion–molecule reaction rate, D_{LN} is the longitudinal molecular diffusion coefficient for the neutrals, A_r is the cross-sectional area of the cylindrical drift tube, $\dot{F}$ is the volumetric flow of carrier gas, and α_P is the ion–ion recombination coefficient describing loss of product ions during their exposure to positive ions in the near radioactive source region, which is a fraction β of the reaction region volume. D_R and D_P are operators given by

$$D_i \equiv \frac{D_{Ti}}{r}\left[\frac{d}{dr}\left(r\frac{d}{dr}\right)\right] + D_{Li}\frac{d^2}{dz^2} - v_i\frac{d}{dz} - \frac{dv}{dz}i \tag{4}$$

where D_{Ti} and D_{Li} are the transverse and longitudinal diffusion coefficients respectively for the various species and v_i is the ion drift velocity in the direction of the applied electrostatic drift field, E.

A term linear in the gradient of the drift velocity is included in Equation 4 to correct for space charge effects. Since the drift velocities are

$$v_i = \mu_i E \qquad i = R,P \tag{5}$$

where μ_i is the mobility, and since Poisson's equation stipulates

$$\frac{d^2V}{dz^2} = \frac{dE}{dz} = \frac{e(n_R + n_P)}{\epsilon_0} \tag{6}$$

where V is the electrostatic potential, e is the electronic charge, and ϵ_0 is the permittivity of free space, the space charge term becomes

$$\alpha_{space} = \frac{dv_i}{dz} \simeq \frac{e\mu_i(\overline{n_R + n_P})}{\epsilon_0} \tag{7}$$

where the ion concentrations are averaged over the observation time so that nonlinearity can be removed from the differential equations. Mathematical simplicity can be achieved in obtaining solutions by working near the limit of detection where $n_R \gg n_P$.

The steady state solution for the neutral concentration is

$$N_P = \frac{N_i\dot{F}}{\dot{F} - D_{LN}A_r m_N}\exp(m_N z) \tag{8}$$

where the spacial attenuation coefficient m_N is given by

$$m_N \simeq \frac{1}{2D_{LN}}\left\{\frac{\dot{F}}{A_r} - \sqrt{\frac{\dot{F}^2}{A_r^2} + 4D_{LN}k_P n_R}\right\}$$

$$\simeq -\frac{A_r k_P n_R}{\dot{F}} \qquad (9)$$

and N_i is the inlet concentration of sample introduced into the reaction region at $z = 0$. The coefficient of Equation 8 is independent of $\dot{F}$ and the expansion of Equation 9 is allowed when $\dot{F} > 1.5$ cm^3/min $> A_r(4D_{LN}k_P n_R)^{1/2}$. This condition is satisfied for the capture of free electrons in nitrogen (i.e., $k_P < 10^{-8}$ cm^3 molecule^{-1} s^{-1}, $n_R = 1.2 \times 10^4$ ion/cm^3, $v_R = 5 \times 10^5$ cm/s, $D_{LN} = 0.10$ cm^2/s). N_P is equivalent to N_i when $|m_N| \ll 1$ cm^{-1} which is generally satisfied in plasma chromatography under normal operating conditions.

Under the set of boundary conditions

$$\begin{aligned} n_P &= 0 && \text{at } r = a \\ n_P &= 0 && \text{at } r = 0,\ z = 0 \\ n_P &\text{ bounded} && \text{as } z \text{ becomes large} \end{aligned} \qquad (10)$$

the steady-state solution for the product ion concentration is

$$n_P = \sum_{s=1}^{\infty} \frac{k_P n_{R0} N_i}{\beta\alpha_P n_+ + \alpha_{space}}\left[1 - \exp\left(m_{Ps}z\right)\right] \times J_0\left(\frac{\eta_s r}{a}\right) \qquad (11)$$

where η_s ($s = 1, 2, 3$, etc.) are the zeroes of the zero-order Bessel function, J_0 (2.6, 5.5, 8.7, etc.), n_R is replaced by $\sum_s n_{R0}J_0(\eta_s r/a)$ and m_{Ps} is

$$m_{Ps} = \frac{1}{2D_{LP}}\left\{v_P \pm \sqrt{v_P^2 + 4D_{LP}\left(\alpha_{space} + \beta\alpha_P n_+ + D_{TP}\eta_s^2/a^2\right)}\right\}$$

$$\simeq -\frac{\alpha_{space} + \beta\alpha_P n_+ + D_{TP}\eta_s^2/a^2}{v_P} \qquad (12)$$

The approximation of Equation 12 holds only when s is small.

The average product ion current I_P measured at the collector of the plasma chromatograph is

$$I_P = A_r\gamma_1\gamma_2\gamma_3\overline{n_P}(z = l)\, ev_P \qquad (13)$$

where l is the length of the reaction region, γ_1 is the effective transmission coefficient for the grid structures of the instrument, γ_2 is the proportional amount of time the shutter grid is open (0.8% for the experimental data of Table I), and γ_3 is the effective transmission of the drift region corrected for longitudinal and transverse diffusion losses (100% for the experimental data for Table I).

A theoretical estimate of γ_1 was obtained by solving for the electrostatic flux transmission through a grid of parallel wires of radius R, separated by a center-to-center distance L. Assuming the ionic transmissivity, Ti, is equal to the fraction of electric flux transmitted through the grid, the result is

$$Ti = 1 - \frac{4R}{L} \qquad (14)$$

Using the values of R and L specified by the manufacturer for the shutter grids, Ti was calculated as 0.84 for grid 1 and grid 2. Only an optical transmissivity (0.80) was given by the manufacturer for the collector aperture grid, with no description of its configuration. By assuming that the aperture grid consisted of a crossed matrix of fine circular wires, an ionic transmissivity of 0.62 was calculated from Equation 14. Then γ_1, the product of the three grid transmissivities, is about 0.44.

It was recognized that electrons and ions exhibit different transmission properties through the grids, and so a measurement of the actual transmissivities was performed for both free electrons and negative reactant ions in dry air. This was done indirectly by measuring the current collected by the grid wires and comparing it with the current passed through the grid. A Keithley 153 Microvolt-Ammeter was used for the measurements, and its insulation rating limited the measurements to grid 2 only. It was necessary to assume that the transmissivities of grids 1 and 2 were equal, but since their construction is identical, this is not a bad assumption. The presence of leakage currents required difference measurements between currents with the grids open and currents with the grids closed.

For free electrons, the shutter grid transmissivities were 0.841, in excellent agreement with the theoretical calculation. The aperture grid transmissivity was 0.51, giving an overall γ_1 of 0.35. For the reactant ions, the shutter grid transmissivitives were 0.809 and the aperture grid transmissivity was 0.43 for an overall γ_1 of 0.29. The value for free electrons is used in calculating the electron concentration in the reaction region from the measured collector current and the value for ions is used in calculating the product ion concentration in the reaction region from the measured product ion current.

The average charge density $\bar{n}_p$ is obtained by averaging the Bessel function over the cross-sectional area of the reaction region as described by Carslaw and Jaeger (22). That is

$$\overline{J_0(\eta_s r/a)} = \frac{\int_0^a rJ_0(\eta_s r/a)\mathrm{d}r}{\int_0^a r\mathrm{d}r} = \frac{2}{\eta_s}J_1(\eta_s) \qquad (15)$$

where J_1 is the first-order Bessel function. Equations 11 and 13 imply that the product ion current is linearly dependent on sample concentration but is independent of carrier gas flow rate. Therefore, plasma chromatography belongs to the class of concentration-dependent detectors.

Calibration. The design, performance and use of exponential dilution flasks for detector calibration have been previously described (23-25). The technique consists of a vessel or flask of fixed volume through which a carrier gas flows at a known rate on its way to the detector. Measurements are made by injecting a known amount of calibrant gas or vapor into the flask and recording the dynamic change of the detector response as a function of time. When mixing is complete, the calibrant concentration in the flask satisfies

$$N_i = N_0 \exp(-\frac{\dot{F}}{V_f}t) \qquad (16)$$

where N_0 is the initial concentration of test vapor injected into the flask, $\dot{F}$ is the volumetric flow of carrier gas at the temperature of the flask, V_f is the geometric volume of the flask, and t is the time elapsed after introduction of vapor. If, however, incomplete mixing or adsorption occurs, the effective volume for the decay will deviate from the geometrical volume in a measurable way. Since the decay from the highest vapor concentration to the lowest detectable concentration allows departures in detector response to be observed, the exponential dilution method provides in one experiment a means whereby the limit of detection and linear dynamic range of a detection can be determined.

In calibrating the response of a plasma chromatograph, the dilution flask uses the same carrier gas as the plasma chromatograph. Without additional dilution, the concentration of calibrant delivered to the instrument N_i satisfies Equation 16. Due to mixing volumes within the instrument, the re-

Table II. Calculated Rate Constant Data

β	$\beta\alpha_p n_+ + \alpha_{space}$ (s^{-1})	E/P (V cm^{-1} $Torr^{-1}$)	k_p (cm^3 $molecule^{-1}$ s^{-1})	k_p (s^{-1} $Torr^{-1}$)	$\alpha(E/P)$ (cm^{-1} $Torr^{-1}$)
			Plasma chromatography (200 °C)		
0.04	0.50	0.282	5.1×10^{-11}	1.0×10^6	2.08
0.07	0.75	0.282	7.1×10^{-11}	1.4×10^6	2.89
0.10	1.00	0.282	8.8×10^{-11}	1.8×10^6	3.57
0.13	1.25	0.282	1.0×10^{-10}	2.1×10^6	4.16
0.15	1.50	0.282	1.2×10^{-10}	2.4×10^6	4.70
0.18	1.75	0.282	1.3×10^{-10}	2.6×10^6	5.15
0.21	2.00	0.282	1.4×10^{-10}	2.8×10^6	5.56
			Swarm beam method (room temperature)		
		0.275	7.0×10^{-11}	2.3×10^6 (1.4×10^6)[a]	5.5 (3.41)[a]

[a] Corrected to 200 °C.

sponse of the plasma chromatograph to calibrant injection is not immediate. Sedlak and Blurton discuss this problem and point out that the *area* under the dilution curve for a pure injected calibrant without background is independent of the value of the instrument response factor "λ" (*26*). For this reason, the response of the plasma chromatograph can be standardized by integration. This corresponds to substituting Equation 16 into Equation 11 and performing the integral

$$Q_P = A_r \int_0^\infty \overline{n_P(z = l)}\, v_P dt \qquad (17)$$

where Q_P is the total number of product ions generated in the reaction region per injection. The result is

$$Q_P = \sum_i \frac{2A_r k_p n_{R0} N_0 v_P V_f J_1(\eta_s)}{F\eta_s(\beta\alpha_p n_+ + \alpha_{space})} \left[1 - \exp(m_{P_s} l)\right] \qquad (18)$$

RESULTS AND DISCUSSION

Displayed in Figure 2 are data collected on Q_P as a function of the total quantity N_0V_f of injected calibrant. Q_P was experimentally determined to satisfy an inverse relationship with F, as expected from Equation 18, with a standard error of 4.7×10^9 ions in the 10^{10}–10^{11} ion range. This corresponds to a percentage error of about 5%. Figure 2 shows three regions of proportionality. The three regions will be labeled as background ($N_0V_f < 10^{15}$–10^{16}), intermediate linear (10^{15}–$10^{16} < N_0V_f < 10^{17}$), and saturation ($N_0V_f > 10^{17}$).

The level of the background region is dependent on size of injection and quantity of benzene present. A 10.7-μL injection of benzene gives a proportionally higher background than a 1.7-μL injection. Such a response is attributed to either a halogenated impurity in the pesticide grade benzene, displacement of chlorobenzene from the walls of the instrument due to scrubbing action by the injected benzene, or increased ionization efficiencies for chlorobenzene in the presence of electron thermalization by collision with benzene. Not enough data are available to conclusively determine the origin of the background. Because of these acknowledged difficulties, the theoretical considerations of this paper cannot be applied to the background ion current.

Saturation occurs as the calibrant concentration approaches the reactant ion concentration for increasing lengths of the dilution cycle. The broken curve fitting the data in Figure 2 satisfies an equation of the form $Q_P = A \ln(1 + BN_0)$, A and B are adjustable parameters, derivable from simple kinetic arguments for plasma chromatography under saturated conditions. The experiments are consequently no longer near the limit of detection and the assumptions underlying the theoretical treatment of the previous section become inappropriate. The region of theoretical interest is the intermediate linear region where there is a direct relationship between sample concentration and instrumental response.

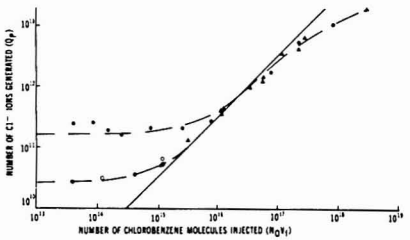


Figure 2. Efficiency of ionization for chlorobenzene in plasma chromatography. Sample preparation was achieved by gas phase dilution for the triangle data and was achieved by liquid phase dilution for the open circle (1.7-μL injections) and closed circle (10.7-μL injections) data. All data are normalized to 50 cm^3/min at flask temperature and atmospheric pressure

The constant of proportionality for the solid line in Figure 2 corresponds to an ionization efficiency (Q_p/N_0V_f) of $2.6 \pm 0.8 \times 10^{-5}$ ion/molecule. If this value is substituted into Equation 18, estimates can be made on the rate constant describing the dissociative capture process. For these calculations, mobility and diffusion coefficient data were taken from Spangler and Collins (*6*), the electron swarm drift velocity was taken as 5×10^5 cm/s from Huxley and Crompton (*27*), and the reactant concentration n_{R0} was taken as 1.2×10^4 electrons/cm^3. The reactant concentration n_{R0} was estimated from

$$n_{R0} = \frac{\text{Standing Open Grid (Electron) Current}}{2A_r e v_p \sum_s J_1(\eta_s)/\eta_s}$$

Recorded in Table II are values for the rate constant k_p and the attachment coefficient $\alpha(E/P)$, the rate constant divided by the electron swarm drift velocity, for various values of $(\beta\alpha_p n_+ + \alpha_{space})$. Also recorded in Table II are similar data taken by Christophorou, Crompton, Hurst, and Reinhardt using electron swarm beam techniques at room temperature (*10*).

The calculated values of β entered in Table II are determined from $(\beta\alpha_p n_+ + \alpha_{space})$ where the experimental parameters require that α_{space} be equal to 0.11 s^{-1}, n_+ be equal to $6.7 \pm 0.5 \times 10^6$ ions cm^{-3} and the low temperature Thomson Theory for recombination requires α_p be equal to $1.4 \pm 0.3 \times 10^{-6}$ cm^3 ion^{-1} (*28*). It is estimated that there is about a 40% experimental error in the determination of β. Roughly half of this is attributed to the scatter in the experimental data and half to the uncertainty in the positive ion concentration. Experimentally, β represents an effective reaction volume, approximately equal to the volume enclosed by the ^{63}Ni

radioactive source, in which recombination occurs. For a β of 0.07, k_p is $7.1 \pm 3.1 \times 10^{-11}$ cm^3 molecule^{-1} s^{-1} which lies close to the swarm beam data. For a β of 0.09, $\alpha(E/p)$ is 3.41 cm^{-1} Torr^{-1} in agreement with temperature corrected values reduced from swarm beam data. Christophorou et al. indicate that $\alpha(E/p)$ is independent of total pressure variations (*10*). Assuming that ion densities increase linearly over the radioactive source region, which occupies one sixth the length of the reaction region, these values for β bracket the expected value of 0.08 if the β of one sixth is reduced by a factor of two to correct maximum measured ion densities for average densities within the region. The 44% error in k_p may mask temperature related effects in the plasma chromatographic results (*28*).

A concluding remark is that the product of the ionization efficiency and the carrier gas flow rate is a constant for plasma chromatography. For chlorobenzene, this constant is 3.4×10^{-5} cm^3 (200 °C)/s for the reaction region before attenuation is imposed by the transmittance of the grid structures. For the operating parameters outlined in Table I, the constant is 7.7×10^{-8} cm^3 (200 °C)/s for the overall plasma chromatographic system.

LITERATURE CITED

(1) F. W. Karasek, *Anal. Chem.*, **46**, 710A (1974).
(2) R. A. Keller and M. M. Metro, *Sep. Purif. Methods* **3** (1), 207 (1974).
(3) E. W. McDaniel and E. A. Mason, "The Mobility and Diffusion of Ions in Gases", Wiley, New York, N.Y., 1973.
(4) G. E. Spangler and C. I. Collins, *Anal. Chem.*, **47**, 393 (1975).
(5) R. A. Keller and M. M. Metro, *J. Chromatogr. Sci.*, **12**, 673 (1974).
(6) G. E. Spangler and C. I. Collins, *Anal. Chem.*, **47**, 403 (1975).
(7) F. W. Karasek and O. S. Tatone, *Anal. Chem.*, **44**, 1758 (1972).
(8) F. W. Karasek, O. S. Tatone, and D. M. Kane, *Anal. Chem.*, **45**, 1210 (1973).
(9) F. W. Karasek and D. M. Kane, *J. Chromatogr.*, **93**, 129 (1974).
(10) L. G. Christophorou, R. N. Compton, G. S. Hurst, and P. W. Reinhardt, *J. Chem. Phys.*, **45**, 536 (1966).
(11) R. N. Compton, L. G. Christophorou, and R. H. Huebner, *Phys. Lett.*, **23** (11), 656 (1966).
(12) R. N. Compton, R. H. Huebner, P. W. Reinhardt, and L. G. Christophorou, *J. Chem. Phys.*, **48**, 901 (1968).
(13) J. E. Lovelock and N. L. Gregory, *3rd Int. Symp. Gas Chromatogr.*, Academic Press, New York, London, 1962, p 219.
(14) J. E. Lovelock, *Nature (London)*, **189**, 729 (1961).
(15) J. E. Lovelock, P. G. Simmonds, and W. J. A. VandenHeuvel, *Nature (London)*, **197**, 249 (1963).
(16) J. E. Lovelock, *Phys. Proc. Radiat. Biol., Proc. Int. Symp.*, 1963 (Pub. 1964), p 183.
(17) A. Zlatkis and J. E. Lovelock, *Clin. Chem. (Winston-Salem, N.C.)*, *11*, 259 (1965).
(18) G. Castello and G. D'Amato, *J. Chromatogr.*, **54**, 157 (1971).
(19) E. W. McDaniel, "Collision Phenomena in Ionized Gases", Wiley, New York, N.Y., 1964, p 536.
(20) P. A. Lawless and G. E. Spangler, *Rev. Sci. Instrum.*, **48**, 240 (1977).
(21) I. R. Gatland, *Case Stud. At. Phys.*, **4** (6), 371–437 (1974).
(22) H. S. Carslaw and J. C. Jaeger, "Conduction of Heat in Solids", Clarendon Press, Oxford, 1973, pp 196–201.
(23) J. E. Lovelock, "Gas Chromatography", R. P. W. Scott, Ed., Butterworths, Inc., Washington, D.C., 1960, p 26.
(24) A. Fontijn, A. J. Sabadell, and R. Ronco, *Anal. Chem.*, **42**, 575 (1970).
(25) J. J. Ritter and N. K. Adams, *Anal. Chem.*, **48**, 612 (1976).
(26) J. M. Sedlak and K. F. Blurton, *Anal. Chem.*, **48**, 2020 (1976).
(27) L. G. H. Huxley and R. W. Crompton, "The Diffusion and Drift of Electrons in Gases", Wiley, New York, N.Y., 1974, Chap. 14.
(28) E. W. McDaniel, "Collision Phenomena in Ionized Gases", Wiley, New York, N.Y., 1964, Chap. 12.

RECEIVED for review July 21, 1977. Accepted November 1, 1977. This research was conducted under the authority of the Department of Army Projects 1T161102AH51, 1T161101A91A, and 1W762712AH66, Fort Belvoir, Va.

Determination of Molybdenum by Neutron Activation and Srafion NMRR Ion Exchange Resin Separation

R. A. Nadkarni and G. H. Morrison*

Department of Chemistry, Cornell University, Ithaca, New York 14853

Srafion NMRR ion exchange resin has been used to separate molybdenum after neutron activation. The method is used to determine the trace amounts of molybdenum in steels, and geological, biological, and environmental standard reference materials.

Molybdenum is an essential trace element in biological systems, and in addition has important consequences in metallurgical and geological systems. Because of the low concentration levels involved, neutron activation methods of analysis appear to be most applicable. Direct determination of Mo in complex natural samples by instrumental neutron activation analysis (INAA) is difficult because of its low level in these materials. In addition, the low energy gamma peak of ^{99}Mo is masked by the radiation produced by the large amounts of ^{24}Na, ^{82}Br, ^{32}P, etc. upon neutron irradiation. Therefore, radiochemical separations are required for the accurate determination of trace amounts of Mo.

An ion exchange resin that has been shown to be very effective in radiochemical separations is Srafion NMRR. It has been used to quantitatively separate trace noble metals including Au and Ag (*1–9*), and Hg (*9–13*) and Cu (*14*) from geological, biological, and environmental materials. The resin binds ions with the d^8 electronic configuration forming square planar complexes; hence its selectivity for noble metals.

Recently Nadkarni and Morrison (*8*) and Muzzarelli and Rocchetti (*15*) studied the behavior of several common transition metals with Srafion NMRR resin, and only Mo was found to be quantitatively retained on the resin. The present study describes the use of this resin to separate Mo during neutron activation analysis of standard samples of steel, rock, coal, and plant and animal material. The results are in good agreement with the certified or literature values.

EXPERIMENTAL

Samples and Reagents. The following standard samples were analyzed for their Mo content: NBS Stainless Steel 121d, NBS Low Alloy Steel 661, USGS Basalt BCR-1, NBS Coal SRM-1632, NSB Orchard Leaves SRM-1571, NBS Bovine Liver SRM-1577, and Bowen's Kale. These materials were dried as specified by the suppliers.

Srafion NMRR ion exchange resin was obtained from Polycycle, Inc., Palo Alto, Calif. The resin was equilibrated with 0.5 N HCl for several hours before use. The resin was then packed in glass columns of 1.5-cm i.d. and 15-cm length. Irradiation standards

0003-2700/78/0350-0294$01.00/0 © 1978 American Chemical Society

Table I. Absorption of ^{99}Mo on Srafion NMRR Resin

Experiment	Absorption, %	Elution, %
pH 1.05	99.8	
pH 1.95	99.9	
pH 3.15	100	
pH 4.10	100	
pH 5.65	100	
pH 6.05	100	
0.5 N HCl		6.0
2 N HCl		11.2
8 N HCl		7.5
4 N NH_4OH		21.6
1 M KCNS		62.4
0.5 M EDTA		0.35

were prepared from diluted aliquots of molybdenum solution prepared with "Specpure" MoO_3. ^{99}Mo tracer was prepared by irradiating "Specpure" MoO_3.

Irradiation. Samples, 200–400 mg, in sets of four and a standard containing ~40 μg Mo were sealed in high purity quartz vials and were irradiated in the central thimble facility of the Cornell TRIGA Mark II reactor at a thermal neutron flux of 3 × 10^{12} n cm^{-2} s^{-1} for periods of 22 to 35 h.

Radiochemistry. The samples were allowed to cool for ~60 h before separating molybdenum. This considerably reduces the activity of other short-lived major nuclides such as ^{24}Na, ^{42}K, etc. The geological and coal samples were dissolved by alkali peroxide fusion; the biological samples were dissolved in an HNO_3 + $HClO_4$ mixture (1.5:1); and the steel samples were dissolved in aqua regia, all in the presence of 2 mg Mo^{6+} carrier. The pH of the solutions were adjusted to ~1 and then passed over Srafion NMRR columns at the rate of 1 mL/min. The resin was washed 10 times with 10-mL portions of distilled water. The washed resins were transferred to Pyrex Erlenmeyer counting flasks and made up to 25 mL with water. The standards were treated identically.

Counting. The samples and standards were counted using a coaxial 56 cm^3 Ge(Li) detector and a 4096 channel analyzer. The system had a 1.96-keV (FWHM) resolution, a peak-to-Compton ratio of 37:1 and the counting efficiency of 12.9%. The data were computed on a PDP-11/20 computer. No variations in the intensity of the 140-keV radiation resulting from different thicknesses of the flasks used were observed.

RESULTS AND DISCUSSION

Srafion NMRR was tested for its absorption behavior towards molybdenum by passing solutions containing 2 mg of Mo^{6+} carrier and a fixed quantity of ^{99}Mo tracer at varying pH over the resin column, and counting both the resin and the effluent phases. The results in Table I show that at least up to pH 6, Mo^{6+} is quantitatively absorbed. Absorption behavior above pH 6 was not checked, since well below pH 6, other metals will start precipitating as their hydroxides.

Several reagents were used to try to elute the absorbed Mo^{6+} from the resin. However, in no case was complete elution obtained. Maxium elution (62%) was achieved with 1 M KCNS (Table I). However, in view of quantitative absorption, it is unnecessary to elute Mo from the resin, and the whole resin phase is used for gamma spectroscopy.

In another experiment, 350 mg of unirradiated BCR-1 rock was mixed with ^{99}Mo tracer and run through the entire procedure. The absorption of ^{99}Mo on the resin was complete even in this case.

The only useful isotope of molybdenum for radiochemical work is ^{99}Mo (66 h half-life) with a 140-keV γ-ray peak. ^{99}Mo decays to its daughter ^{99m}Tc (6.05 h) and both have to be allowed to equilibrate before counting (40 h). The only interfering nuclear reactions in the molybdenum determination are ^{102}Ru(n,α)^{99}Mo, and ^{235}U(n,F)^{99}Mo. However, the amount of ruthenium in most materials is so low that the contribution from its reaction towards molybdenum activity is negligible. The ^{235}U(n,F)^{99}Mo reaction is important in most geological silicate samples where the ratio of Mo:U is unity or less. Under our irradiation conditions, 1 μg of U produced 0.82 μg of apparent ^{99}Mo. In biological and environmental analyses, where the Mo:U ratio is very large, e.g. Bovine liver, 4000; Kale, 228; Orchard Leaves, 10.3; the U contribution can be safely ignored.

Table II. Determination of Molybdenum in Standard Reference Materials

Material	Present, ppm[a]	Found, ppm[c]
NBS Stainless Steel 121d	0.165%[b]	0.167 ± 0.007%
NBS Low Alloy Steel 661	0.19%[b]	0.191 ± 0.003%
USGS Basalt BCR-1	1.5 (*16*); 1.15 (*17*)	1.39 ± 0.21
NBS Coal SRM-1632	0.2 (*18*); 3.08 (*19*); 3.4 (*20*); 5 (*21*)	3.14 ± 0.28
NBS Orchard Leaves SRM-1571	0.3 ± 0.1[b]	0.24 ± 0.02
NBS Bovine Liver SRM-1577	3.2[b]; 3.04 (*22*); 3.33 (*23*); 3.19 (*24*); 3.5 (*25*)	3.12 ± 0.26
Bowen's Kale	2.28 (*26*)	2.13 ± 0.12

[a] Reference numbers in parentheses. [b] NBS Certificates of Analysis. [c] Mean value ± standard deviation.

The proposed method was applied to several standard reference materials of metallurgical, geological, biological, and environmental nature. The results are given in Table II. In each case, four replicate analyses were carried out. The results are in excellent agreement with the certified and/or literature values where available. ^{59}Fe produced from steel samples also has a γ-ray peak at 143 keV, very near the 140 keV peak of ^{99}Mo; however, Srafion NMRR resin has been shown not to absorb any Fe^{3+} (*8*). Flanagan (*16*) gives 1.1 ppm as "magnitude" molybdenum value in the USGS standard basalt BCR-1; other workers have found 1.15 ppm by epithermal NAA (*17*). In silicate rocks where uranium content is high, the contribution from ^{235}U(n,F)^{99}Mo has to be corrected by irradiating a separate aliquot of uranium.

Among biological and environmental standard samples, NBS has not certified the molybdenum value for coal: SRM-1632; however, literature values range from 0.2 to 5 ppm, obtained by the techniques of photon activation analysis (*18*), epithermal NAA (*19*), and INAA (*20, 21*). The true value is probably around 3–4 ppm. Our value for NBS Orchard Leaves, SRM-1571, is in good agreement with the certified value by NBS. For Bovine Liver: SRM-1577, NBS has given 3.2 ppm as "information" value. Other workers also have found molybdenum close to this value by the techniques of radiochemical NAA (*22–24*) and proton induced x-ray emission (*25*). The value for molybdenum in Bowen's Kale is not certified, but Bowen (*26*) gives 2.28 ppm as a grand mean of molybdenum results by colorimetry and NAA.

In all cases our results are in good agreement with the recommended values. The accuracy of the results is better than 1% for steels, <5% for Bovine Liver and Coal, and 6–8% for Kale and BCR. Only in the case of Orchard Leaves, our value is lower by 20% than NBS certified value, though it is well within the error bars given by NBS. The precision of the results varies from 5–9% for most samples except BCR where it is 15%. Eight samples can be processed in four hours after irradiation. The final resins' γ-ray spectra do show small amounts of nuclides other than ^{99}Mo, such as ^{82}Br, ^{198}Au, ^{110m}Ag, etc.; however, in no way do they interfere with the determination of ^{99}Mo. Since the samples are allowed to "cool" prior to radiochemistry, large amounts of short to medium lived isotopes of major elements decay away to inconsequential amounts. The half-life of ^{99}Mo at the 140-keV peak was measured for several samples and was found to be

66 ± 2 h. The experimental detection limit was found to be 0.04 ppm with a 20-h irradiation and 1-h counting period. This can be improved by irradiating the samples for longer periods of time.

LITERATURE CITED

(1) T. E. Green and S. L. Law, *U.S. Bur. Mines, Rept. Invest.*, 7358 (1970).
(2) T. E. Green, S. L. Law, and W. J. Campbell, *Anal. Chem.*, **42**, 1749 (1970).
(3) H. A. Das, R. Janssen, and J. Zonderhuis, *Radiochem. Radioanal. Lett.*, **8**, 257 (1971).
(4) C. W. Blount, D. E. Leyden, T. L. Thomas, and S. M. Guill, *Anal. Chem.*, **45**, 1045 (1973).
(5) R. A. Nadkarni and G. H. Morrison, *Anal. Chem.*, **46**, 232 (1974).
(6) L. L. Sundberg, *Anal. Chem.*, **47**, 2037 (1975).
(7) R. A. Nadkarni and G. H. Morrison, *Anal. Chem.*, **47**, 2285 (1975).
(8) R. A. Nadkarni and G. H. Morrison, *J. Radioanal. Chem.*, **38**, 435 (1977).
(9) A. Warshawsky and S. Ehrlich-Rogozinski, *Microchem. J.*, **22**, 362 (1977).
(10) S. L. Law, *Science*, **174**, 285 (1971).
(11) S. L. Law, *Am. Lab.*, **5**, 91 (1973).
(12) P. J. Ke and R. J. Thibert, *Mikrochim. Acta*, 417 (1973).
(13) D. E. Leyden, *Adv. X-ray Anal.*, **17**, 293 (1974).
(14) E. S. Gladney, *Anal. Chim. Acta*, **91**, 353 (1977).
(15) R. A. A. Muzzarelli and R. Rocchetti, *Anal. Chim. Acta*, **70**, 465 (1974).
(16) F. J. Flanagan, *Geochim. Cosmochim. Acta*, **37**, 1189 (1973).
(17) E. Steinnes, *Anal. Chim. Acta*, **57**, 249 (1971).
(18) A. Chattopadhyay and R. E. Jervis, *Anal. Chem.*, **46**, 1630 (1974).
(19) J. J. Rowe and E. Steinnes, *J. Radioanal. Chem.*, **37**, 849 (1974).
(20) D. H. Klein, A. W. Andrer, J. A. Carter, J. F. Emery, C. Feldman, W. Fulkerson, W. S. Lyon, J. C. Ogle, Y. Talmi, R. I. Van Hook, and N. Bolton, *Environ. Sci. Technol.*, **9**, 973 (1975).
(21) R. R. Ruch, H. J. Gluskoter, and N. F. Shimp, *Environ. Geol. Notes*, 72 (1974).
(22) B. Maziere, J. Gros and D. Comar, *J. Radioanal. Chem.*, **24**, 279 (1975).
(23) E. Steinnes, *Anal. Chim. Acta*, **78**, 307 (1975).
(24) P. Lievens, R. Cornelis, and J. Hoste, *Anal. Chim. Acta*, **80** 97 (1975).
(25) R. D. Wills and R. L. Walter, *Nucl. Instrum. Methods*, **142**, 231 (1977).
(26) H. J. M. Bowen, *At. Energy Rev.*, **13**, 451 (1975).

RECEIVED for review October 14, 1977. Accepted November 16, 1977. This work was supported in part by the National Science Foundation through the Cornell Materials Science Center.

Determination of Silica in Bulk Iron Ore Samples by Neutron Activation Analysis

Mihai Borsaru* and Ralph J. Holmes

CSIRO Division of Mineral Physics, P.O. Box 124, Port Melbourne, Victoria 3207, Australia

A fast neutron activation technique has been developed for the determination of SiO_2 in 30-kg samples of iron ore of −6-mm particle size. Only a single irradiation with a Pu-Be neutron source is necessary, if particular care is taken to minimize the thermal neutron flux in the sample. By including the sample weight and the epithermal neutron flux in the regression equation, an accuracy of better than ±0.34% SiO_2 (95% confidence level) is achieved for silica concentrations ranging from 1 to 10% in the presence of low amounts of Al_2O_3 (up to 6%). Samples must be dried to <1% free moisture before analysis, if the best accuracy is required.

The need for developing bulk analysis techniques is twofold. First, measurements on large samples eliminate sample preparation errors and, second, it is a step towards on-stream analysis which is of benefit to the mining industry. Because of the great penetrating power of neutrons and high energy γ rays, nuclear techniques are suitable for this type of analysis.

In the present work, neutron activation analysis has been applied to the determination of silica in bulk iron ore samples. The fast neutron reaction $^{28}Si(n,p)^{28}Al$ employed here has been used extensively for the determination of silicon in various matrices (*1–4*). The simultaneous determination of silica and alumina in small samples, using a dual source technique has also been reported (*5–9*). However, in all cases, small samples were used, to minimize neutron flux perturbations due to the presence of the sample. One of the aims of the present work was to evaluate the magnitude of the neutron flux distortion by large bulk samples due to differences in bound water, free moisture, and density, as previously studied for the determination of Al_2O_3 in iron ores (*10*). The presence of large amounts of H_2O in bulk samples can be particularly serious in fast neutron activation as hydrogenous material rapidly thermalizes neutrons.

EXPERIMENTAL

Ore samples were irradiated with a 4-Ci Pu-Be neutron source ($\simeq 10^7$ neutrons/s) to induce the silicon reaction $^{28}Si(n,p)^{28}Al$. The radioactive isotope ^{28}Al produced by this fast neutron reaction decays by emitting a 1.78-MeV γ ray with a half-life of 2.3 min. The cross section for this reaction is very small for neutrons of energy less than 5 MeV and increases to 450 mb for neutrons of 7.5-MeV energy; hence the necessity to use a Pu-Be fast neutron source rather than a ^{252}Cf source which has lower average neutron energy.

The neutron source was located below the samples on a cadmium covered lead support, and was enclosed within a cadmium cylinder to remove any thermal neutrons emitted by the source, since these neutrons can produce the same radioactive isotope ^{28}Al through the thermal neutron reaction $^{27}Al(n,\gamma)^{28}Al$. Special care had to be taken also, to minimize the thermal neutron flux pervading the ore samples. Hence the ore was irradiated in a rectangular box (40 × 33 cm by 8 cm deep) constructed from brass rather than wood, since the latter would cause significant neutron thermalization. A steel plate of 9-cm thickness was located above the ore surface to reflect transmitted fast neutrons back into the ore. The lower face of the steel plate was covered with cadmium sheet to absorb any backscattered thermal neutrons.

Two Texlium spectrometric neutron detectors ($^3He/Kr$ filled) were placed underneath the box (next to the neutron source) to monitor the thermal and epithermal neutron fluxes in the vicinity of the ore samples. The epithermal neutron detector was located in a cadmium covered cylindrical polyethylene tube, thus increasing the detection efficiency by thermalization of epicadmium neutrons.

All samples ($\simeq$30 kg) were irradiated for 6 min, transferred laterally to the counting station (11-s delay), and counted for 5 min. The ^{28}Al radiation at 1.78 MeV was detected with a 126 × 126 NaI (Tl) detector. Variations in system gain were corrected

0003-2700/78/0350-0296$01.00/0 © 1978 American Chemical Society

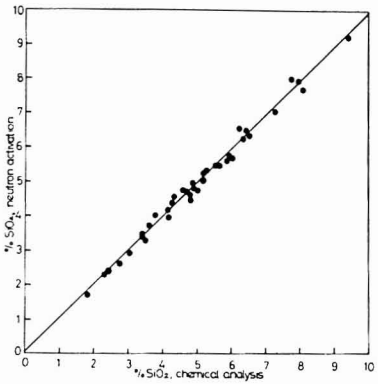


Figure 1. Comparison of neutron activation assays for SiO_2 with chemical analyses

with a Canberra Industries model 1520 analog stabilizer locked on the ^{60}Co γ-ray peak at 1.33 MeV originating from a small source located near the detector.

RESULTS AND DISCUSSION

Measurements. A total of 40 different iron ore samples of −6-mm particle size were available for the study. These were collected from various areas in several Australian mines, some several years apart in time. The investigation was limited to samples with up to 10% SiO_2, 6% Al_2O_3, and 6.6% chemically bound water, with free moisture levels <1%.

Neutron activation assays (y) for SiO_2 were obtained from a regression equation of the form:

$$y = A + B\gamma + Cw + Dn \quad (1)$$

where γ is the number of γ-ray counts (thousands) due to ^{28}Al, w is the weight of the ore sample (proportional to bulk density), n is a neutron parameter (discussed later), and A, B, C, and D are regression coefficients.

Without any correction for variations in neutron flux, the accuracy of the SiO_2 determination was ±0.40% SiO_2 at the 95% confidence level (2σ). This is improved to ±0.34% SiO_2 (95% confidence) when the epithermal neutron flux is included in the regression equation as follows:

$$SiO_2 = 6.70 + 1.65\gamma - 0.179w - 1.01n \quad (2)$$

where n is the epithermal neutron flux (10^6 counts/300 s). A comparison of neutron activation SiO_2 assays, given by the above equation, with chemical analyses (XRF) is presented in Figure 1.

The observed improvement in accuracy due to the introduction of the epithermal neutron flux into the regression equation indicates that this reflects the changes in fast neutron flux due to the presence of the bulk sample. The inclusion of the thermal neutron flux in the regression equation did not significantly improve the accuracy of the SiO_2 determination, although the thermal neutron measurement can be utilized to measure the total water content (free and combined) of the ore samples with an accuracy of ±0.7% H_2O at the 95% confidence level if required (Figure 2). The water determination is based on the well-known principle of fast neutron thermalization by hydrogenous material (*11*).

It should be mentioned that the value for the accuracy of SiO_2 determination, ±0.34% SiO_2, does not take any account of chemical analysis errors. The latter were estimated to be ±0.15% SiO_2 at the 95% confidence level from duplicate sampling and analysis data. When this correction is applied,

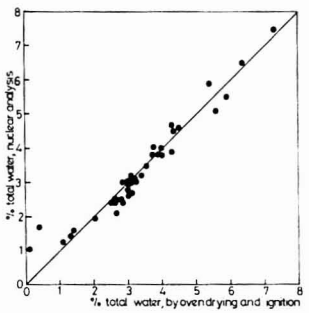


Figure 2. Comparison of neutron measurement of total water with oven drying and ignition method

the estimated accuracy of the nuclear determination of SiO_2 is improved to ±0.31% SiO_2 (95% confidence).

Interferences. There are several other nuclear reactions occurring in iron ore which are potential sources of interference with the SiO_2 measurement, namely $^{27}Al(n,\gamma)^{28}Al$, $^{56}Fe(n,p)^{56}Mn$, $^{55}Mn(n,\gamma)^{56}Mn$, and $^{31}P(n,\alpha)^{28}Al$. Of these the ^{27}Al interference is potentially the most serious.

The cross-section of the $^{27}Al(n,\gamma)^{28}Al$ reaction is 230 mb for thermal neutrons and is negligible for fast neutrons. However, despite the presence of some thermal neutrons in the samples, additions of up to 5% calcined alumina produced no detectable interference with the SiO_2 measurement. The Al_2O_3 level in Australian iron ores is typically <6%, so its interference can be discounted. This would not necessarily be the case with other ores, e.g. bauxites where the Al_2O_3 concentration is an order of magnitude greater. The determination of Al_2O_3 in iron ores using the thermal neutron reaction with ^{27}Al has already been developed (*10*), and can be combined with the present method to yield both SiO_2 and Al_2O_3.

Any interference from ^{56}Mn resulting from the fast neutron reaction $^{56}Fe(n,p)^{56}Mn$ and the thermal neutron reaction $^{55}Mn(n,\gamma)^{56}Mn$ is due to its 1.81-MeV γ ray, since it is not possible to resolve this radiation from the 1.78-MeV ^{28}Al radiation with NaI (Tl) detectors. However, the cross section of the $^{56}Fe(n,p)^{56}Mn$ reaction is approximately an order of magnitude lower than that of the $^{28}Si(n,p)^{28}Al$ reaction for equal neutron energies below about 9 MeV, and the half-life of ^{56}Mn is 2.58 h compared with 2.3 min for ^{28}Al. Consequently the interference from ^{56}Fe will be low. This was confirmed by measuring the residual activity in the ore after 25 min when essentially all the ^{28}Al has decayed. The number of counts recorded in 5 min was <2% of the average response due to SiO_2. It is worth noting, when considering the small ^{56}Fe interference, that it is the change in Fe concentration that is important rather than the actual concentration. The grade of the samples used in this study varied from 52% to 66% Fe, corresponding to a change of 14% Fe above a threshold of 52% Fe, the latter of which constitutes a constant background.

From the evidence discussed above, the interference from the thermal neutron reaction $^{55}Mn(n,\gamma)^{56}Mn$ is also small despite its high cross-section (13.3 b). This is due both to the low thermal neutron flux within the sample and the low concentration of Mn in most commercial Australian iron ores (<0.1% Mn).

Fast neutrons can also produce ^{28}Al via the reaction $^{31}P(n,\alpha)^{28}Al$ which has a cross section of 1.5 mb at 5 MeV. However, this interference is insignificant at the 0.05% P level typical of Australian iron ores, although more care would need to be exercised with high phosphorus ores.

CONCLUSIONS

The SiO_2 content of bulk samples (~30 kg) of iron ore fines containing up to 10% SiO_2 can be determined with an accuracy of better than ±0.34% SiO_2 at the 95% confidence level. Since the thermal neutron flux in the samples is minimized in the present method, only a single irradiation with a Pu-Be neutron source is necessary, provided the Al_2O_3 content of the ore is low (<6%). It is necessary, however, to include the sample weight and epithermal neutron flux in the regression equation, and to dry samples to <1% free moisture if the best accuracy is required.

The total measurement time of 11 min can be reduced if desired by using a stronger neutron source.

ACKNOWLEDGMENT

The authors thank P. L. Eisler, A. W. Wylie, and S. Youl of the Division of Mineral Physics for their assistance, and Hamersley Iron Pty Ltd for providing the assayed samples.

LITERATURE CITED

(1) D. De Soete, R. Gijbels, and J. Hoste, "Neutron Activation Analysis" (Vol. 34 of "Chemical Analysis", Monographs on Analytical Chemistry and its Applications), Wiley-Interscience, London, 1972.
(2) A. J. Lundan and O. P. Mattila, in "Nuclear Techniques in the Basic Metal Industries", IAEA, Helsinki, 1972, p 3.
(3) D. M. Bibby and J. P. F. Sellschop, *J. Radioanal. Chem.*, **22**, 103 (1974).
(4) D. M. Bibby, *Anal. Chim. Acta*, **79**, 125 (1975).
(5) F. Dugain and J. Tatar, *Ann. Inst. Geol. Publici Hung.*, **54**, 375 (1970).
(6) F. Dugain, Eurisotop Report No. 61, Eurisotop Office, Brussels, 1972.
(7) L. Alaerts, J. P. Op de Beeck, and J. Hoste, *Anal. Chim. Acta*, **70**, 253 (1974).
(8) L. Alaerts, J. P. Op de Beeck, and J. Hoste, *Anal. Chim. Acta*, **78**, 329 (1975).
(9) S. S. Gurna and A. S. Bhatnagar, *Indian J. Pure Appl. Phys.*, **11**, 805 (1973).
(10) M. Borsaru and R. J. Holmes, *Anal. Chem.*, **48**, 1699 (1976).
(11) "Neutron Moisture Gauges", Technical Report Series No. 112, IAEA, Vienna, 1970.

RECEIVED for review September 19, 1977. Accepted October 28, 1977.

Feedback Excitation Nuclear Magnetic Resonance Spectrometry and Its Application to Simultaneous Temperature Measurement

Drouet Warren Vidrine and Paul E. Peterson*

Chemistry Department, University of South Carolina, Columbia, South Carolina 29208

A new type of NMR based on feedback excitation of nuclei using the frequency difference between nuclear resonances is described. Circuits permitting its use in the lock circuit of the Varian XL-100 spectrometer for temperature determinations simultaneous to ordinary spectral acquisition are given. Thermometric mixtures containing compounds with temperature-sensitive ^{19}F chemical shifts have been calibrated between −50 and +60 °C to allow temperature determination ±1° to be made with this circuit. ^{19}F chemical shifts and shift sensitivities to temperature, relative to the ^{1}H resonance of TMS, have been measured for several fluorine compounds.

Temperature measurement in nuclear magnetic resonance has traditionally been accomplished either by thermocouple replacement (*1*) or by the measurement of a temperature-dependent frequency difference between two nuclear resonances (*1, 2*). If the two nuclei being used for thermometric measurement are of the same isotope as the nuclei being observed, they will appear superimposed on the observed spectrum unless measurement is accomplished by tube replacement. This superimposition often obscures the observed spectrum, especially in the narrow shift range of ^{1}H nuclei. Observing one isotope, then alternately another for temperature determinations, solves this problem. However, most NMR spectrometers are capable of observing only one isotope at a time, so temperature measurement simultaneous to spectral acquisition is ordinarily still impossible (*3*).

We describe here a modification of the Varian XL-100 lock circuit which permits accurate measurement of a frequency difference between the primary lock nucleus and another, secondary nucleus, without compromising the field stabilization function of the main lock circuit. The output of this supplementary circuit is an audio signal with a frequency exactly equal to the frequency difference between the resonance peak centers of the primary lock nucleus and a secondary lock nucleus. Using heteronuclear lock, this circuit permits a simultaneous measurement of temperature without interfering with the observed spectrum, and seems capable of higher precision than previous methods. In this paper we use a 2:1, v:v mixture of 1,2-dibromotetrafluoroethane and 1,2-difluorotetrachloroethane as the lock substance for the thermometric circuit.

To extend the usefulness of this method, we have calibrated over a wide temperature range the temperature sensitivities of several suitable mixtures of nuclei. In addition, our ^{19}F chemical shift measurements on the XL-100 have allowed us to report the temperature sensitivity of several ^{19}F chemical shifts relative to the ^{1}H resonance of TMS. The unique position of TMS as an NMR reference, the narrow shift scale of hydrogen, and the insensitivity to temperature of TMS relative to many other ^{1}H nuclei, make TMS a desirable reference.

Definitions and Properties of Chemical Shift Scales. In current practice, ^{1}H, ^{13}C, and ^{11}B (*4*) chemical shifts are measured using a "deshielding" scale which assigns positive shift values to deshielded (downfield) nuclei. The scale is defined by Equation 1,

$$\delta_{(1)} = [(\nu^{OBS} - \nu^{REF})/\nu^{REF}] \cdot 10^6 \quad (1)$$

where ν^{OBS} is the resonance frequency of the observed nucleus, and ν^{REF} is the resonance frequency of the reference, at constant field strength. All shift scales in this paper are defined in units of ppm (parts-per-million).

However, the shifts of ^{19}F nuclei (*5*) have been defined according to the old "physical" scale. In the older literature, the shift scales of many other nuclei, including ^{11}B and ^{13}C,

0003-2700/78/0350-0298$01.00/0 © 1978 American Chemical Society

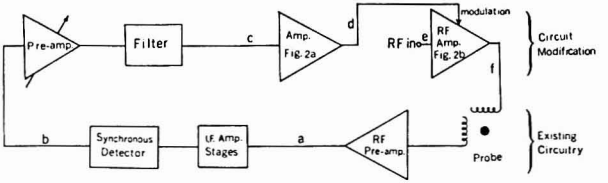


Figure 1. Block diagram of modification permitting feedback excitation of secondary lock nucleus. Frequencies present in Hertz (for $\Delta\nu_{nuclei}$ = 401 Hz and $\nu_{primary\ lock}$ = 94.184509 MHz): (a) 94 184 509, 94 184 910; (b) 401, 802, 1203, 1604, noise, dc bias; (c) 401; (d) 401 (6-V ac) 11-V dc bias; (e) 94 184 509; (f) 94 184 108, 94 184 509, 94 184 910

also were defined this way (*6*). This scale is defined by Equation 2,

$$\delta_{(2)} = [(H^{OBS} - H^{REF})/H^{REF}]\cdot 10^6 \quad (2)$$

where H^{REF} is the field strength required to bring the reference nucleus into resonance, and H^{OBS} is the field strength required to bring the observed nucleus into resonance, at a constant instrumental radiofrequency.

The field H at which any nucleus resonates at a constant frequency can be specified as a ratio H/H^{REF}. This ratio has a value identical to the ratio ν^{REF}/ν, for any particular field strength. Substituting this latter ratio into Equation 2, and rearranging, we obtain the corresponding Equation 3, for measurements made at constant field.

$$\delta_{(2)} = [(\nu^{REF} - \nu^{OBS})/\nu^{OBS}]\cdot 10^6 \quad (3)$$

The difference between the two scales, $\delta_{(1)}$ and $\delta_{(2)}$, is therefore not merely the fact that the one gives positive values to deshielded nuclei, and the other gives positive values to shielded nuclei. The "spread" of the scale is also affected. If the denominator of Equation 1 is the smaller of the two values in the numerator, the denominator of Equation 2 will be the larger of the two, and vice versa, provided the reference compound is not changed. Rearranging Equation 1, we obtain:

$$10^6\cdot\nu^{OBS}/\nu^{REF} = \delta_{(1)} + 10^6 \quad (4)$$

Likewise rearranging Equation 3:

$$10^6\cdot\nu^{REF}/\nu^{OBS} = \delta_{(2)} + 10^6 \quad (5)$$

Multiplying the two equations together, and rearranging, we obtain Equation 6, a statement of the true relationship between the two scales:

$$\delta_{(1)} + \delta_{(2)} = -\delta_{(1)}\cdot\delta_{(2)}\cdot 10^{-6} \quad (6)$$

This equation shows that in addition to the difference in signs, there is a difference in absolute value between the two scales when the same reference is used. Rearrangement of Equation 6 yields the general Equation 7 for conversion of "physical" scale shifts ($\delta_{(2)}$) to the more common shift scale ($\delta_{(1)}$), where the reference nucleus remains the same.

$$\delta_{(1)} = -10^6\cdot\delta_{(2)}(\delta_{(2)} + 10^6)^{-1} \quad (7)$$

To convert from one reference to another on the same $\delta_{(1)}$ scale requires the conversion shown in Equation 8 obtained from Equation 4:

$$\delta_{(new)} = [\nu^{REF}_{(old)}/\nu^{REF}_{(new)}][\nu_{(old)} + 10^6] - 10^6 \quad (8)$$

Because of the historical primacy of ^{1}H in NMR, these relationships have not often been appreciated. For ^{1}H, the two scales $\delta_{(1)}$ and $\delta_{(2)}$ typically differ by less than 0.0001 ppm in absolute value. However, the distinction should not be ignored in NMR of other nuclei, for the two scales can differ in absolute value by more than 0.3 ppm in the case of nuclei with large shift ranges, e.g., ^{13}C, ^{19}F, and ^{31}P. Attempts to convert data from one scale to the other by simply reversing the sign are theoretically wrong, and can cause errors.

In the current literature, several authors (*7*) are now reporting all NMR shifts on "deshielding" scales ($\delta_{(1)}$), and the International Union of Pure and Applied Chemistry now publicly recommends this (*8*). The ascendancy of Fourier-Transform NMR and the need for a consistent convention argue for the universal adoption of the frequency-based shift scale, $\delta_{(1)}$. Nevertheless, in this paper we use the accepted ^{19}F scale, based on $\delta_{(2)}$.

EXPERIMENTAL

Lock Circuit Modification. *Instrumentation.* The lock modulation circuit, described in the Construction section below, was assembled largely from modular equipment, described here. A Varian XL-100 NMR spectrometer was used in the normal, "frequency swept" mode, to provide ^{19}F lock and ^{1}H observe capability. This spectrometer used 41 kHz field modulation and single-sideband synchronous detection.

For audio noise and overtone rejection, a Krohn-Hite 3700 active filter was used in the "max flat" position. To filter an audiofrequency of approximately 420 Hz, for instance, the filter was set to give a constant gain of +20 dB between 300 and 600 Hz, while attenuating frequencies outside that band by 24 dB/octave, to a maximum attenuation of 80 dB below bandpass gain.

For observing the audiofrequencies, channel 2 of a Tektronix 454 oscilloscope was used. Channel 1 was used as a separate variable gain audio preamplifier (maximum gain 14 dB).

Frequency measurements were made by period-average counting on a Hewlett-Packard 5245L electronic counter with a time-base calibrated to an accuracy of ±50 ppb vs. National Bureau of Standards (1958) tables of microwave transition frequencies.

Thermocouple measurements were made using a copper/constantan junction calibrated to ±0.02 °C using a National Bureau of Standards-certified platinum resistance thermometer (*3*). Regulated voltages were each supplied by zener diodes acting through emitter-follower outputs.

Construction. The lock modulation circuit is shown diagrammatically in Figure 1. The input to the modification is the detected lock signal. This can be conveniently obtained by using the already available dc output of the existing lock synchronous detector. Simple diode detection of the 41-kHz intermediate frequency (I.F.) amplification stage of the lock signal amplifier also suffices. This detected signal is ac amplified (with the Tektronix preamp) and filtered using the Krohn-Hite active filter amplified to provide an ac output of up to 20 V peak-to-peak, biased to 11 V dc. This output is substituted for the normal 20-V power supply in the last stage (Figure 2b) of the existing radiofrequency (RF) transmitter of the spectrometer. Substitution is accomplished by plugging the modulation output (Figure 2a) into the modulation input jack (Figure 2b), our modification. When this output is not plugged in, the RF transmitter operates on its normal 20-V supply.

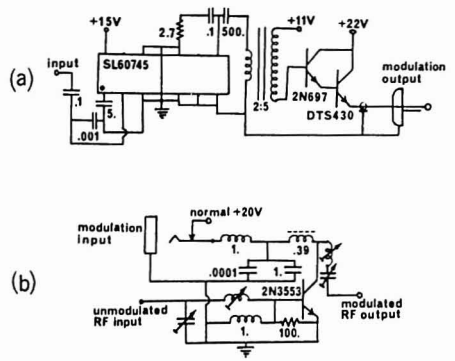


Figure 2. Schematic diagrams of lock circuit modification. (a) Diagram of the audio amplifier of our design with Darlington emitter-follower output supplying audio modulation power. (b) Last stage of existing RF transmitter amplifier, showing phono jack modification permitting RF modulation using modulated power supply. Resistance values, ±5%, in Ω. Capacitance values, are in μF. Capacitors of less than 1-μF capacitance ±10%; others are electrolytic capacitors with capacitance ±25%. Inductance values are in μH, ±20%. The module SL60745 is an ordinary 2.5-W integrated-circuit power amplifier (National Semiconductors, Inc.) thermally connected to 60 cm^2 of copper heat sink fins

Sample Tube Configurations. Operation of the lock modulation circuit has been demonstrated with both 5-mm and 12-mm tubes of ^{19}F thermometric mixture (2:1, v:v, $(CBrF_2)_2$:$(CFCl_2)_2$). Calibration of the thermometric mixture at 0.15 and 11.63 °C was accomplished in a 12-mm tube of thermometric mixture with a coaxially-mounted thermocouple, which was removed just before each measurement. This calibration was checked by mounting a 5-mm methanol tube in place of the thermocouple, and taking a ^1H spectrum of methanol while simultaneously determining the ^{19}F frequency difference with the lock modulation circuit. Temperatures calculated using the ^1H and ^{19}F thermometers agreed within 0.5 °C. Horizontal gradients were checked by placing ^{19}F lock thermometric mixture in the 5-mm coaxial inner tube and methanol in the outer tube. Vertical gradients were checked for by changing thermocouple position ±5 mm. No gradients were found at 0 °C.

Thermometric Mixtures. For thermometric measurements using the lock modulation method, mixtures were selected according to these criteria: (a) Stable compounds with a convenient liquid range, (b) possessing a spectrum of two singlets spaced a convenient width apart for the audio modulation circuit as built (Δν, 100–5000 Hz), and (c) having useable shift sensitivity to temperature relative to each other. Several chemical shift differences (in Δν at XL-100 field strength), and shift sensitivities to temperature are shown in Table I.

Calibration of ^{19}F Thermometric Mixtures between −50 and +60 °C. A Perkin-Elmer R-32 spectrometer operating at 90 MHz ^1H and 84.6 MHz ^{19}F was used to obtain chemical shift differences between nuclei (Δν) of thermometric mixtures at several temperatures. A melting-point capillary of acidified (0.03% 12 M HCl) methanol (*1*) mounted in a 5-mm tube of thermometric mixture was used. After 15-min equilibration, temperature drift was approximately 0.05 °C in 0.5 h. The spectrometer was locked on one ^{19}F nucleus, and Δδ measured by adjusting the observe frequency to the peak center of the other ^{19}F nucleus, then recording the value for $\nu_{lock} - \nu_{observe}$ indicated on the frequency meter, then converting to parts-per-million. The procedure was repeated for the ^1H resonances of methanol to determine temperature.

^{19}F Chemical Shifts Measured Relative to the ^1H Resonance of Neat TMS. *Apparatus.* A Varian XL-100 NMR spectrometer was set up for ^{19}F lock and ^1H observe capability. However, in the "field swept" mode, the functions of the lock and observe channels are reversed, providing ^1H lock and ^{19}F observe. Shifts of ^{19}F compounds were measured relative to the ^1H resonance of neat capillary tetramethylsilane (TMS) lock, after temperature equilibration of the probe for at least 20 min. The sample tube was a 5-mm tube containing a ^{19}F compound or mixture, with coaxial "melting point" capillary of neat TMS. Temperatures were measured by substitution of a Varian 5-mm methanol sample, and are accurate to ±2 °C.

Table I. Selected Chemical Shift Sensitivities to Temperature

	Nucleus	Frequency difference $\lvert\Delta\nu\rvert$ at 25 °C[a]	Sensitivity $d(\Delta\delta)/dT$[b]
$(CBrF_2)_2$:$(CCl_2F)_2$	^{19}F	409.2[c]	−0.795[c]
2:1 CCl_2=CF_2:CCl_3CF_3	^{19}F	606.4[d]	+0.727
$CFCl_3$:CBr_2F_2	^{19}F	637.3[c]	+0.131[c]
Methanol[e]	^1H	157.0	−0.913
1,2-Ethanediol[e]	^1H	165.3	−0.984

[a] At 23.51 kG (XL-100) field strength. Frequency units are used for convenience in interpretation of our lock circuit modification. [b] Between 0 and 25 °C at 23.51 kG. [c] This value was insensitive to the relative concentration over the range 1:4 to 4:1. [d] R-32 data converted to XL-100 field strength. [e] Contains 0.03% 12 M HCl to prevent splitting; data from Van Geet (*1*, *6*).

Defining a TMS-Based ^{19}F Scale. In our field-swept measurements on the Varian XL-100 NMR spectrometer with heteronuclear lock, the ^{19}F observe frequency was constant (94.18451 MHz), while the field strength was changed by varying the offset frequency on the ^1H lock until the peak maximum of a ^{19}F resonance was located (the ^1H lock frequency is 100.01515 MHz plus the ^1H offset frequency, which may be varied between 70 and 100 kHz). Let us consider an example in which trichlorofluoromethane (TCF) is initially in resonance at 25 °C and in which a change of offset of 100-Hz frequency brings a second fluorine compound, XF, into resonance.

The frequency change of 100 Hz is sensed by the TMS, and causes a field change of 23.487 mG, bringing XF into resonance. The fluorine instrument frequency remains unchanged. For fluorine, the 23.487-mG change in field is equivalent to 94.10 Hz. The chemical shift with a CCl_3F reference is calculated by Equation 2: $\delta_{(2)} = 10^6 \cdot (23.487 \times 10^{-3}/23487) = 1.000000$. Thus, it appears that the field referenced chemical shift for fluorine may be calculated directly from:

$$\delta_{(2)F} = 10^6 \cdot \Delta\nu_{offset}/\nu^{TMS} \quad (9)$$

Because the frequency ratio $\nu^{TCF}/\nu^{TMS} = 0.9409645$ at 25 °C, Equation 9 may also be written as:

$$\delta_{(2)F} = 10^6 \times 0.9409645\ \Delta\nu_{offset}/\nu^{TCF,25°} \quad (10)$$

This is the accurate field referenced shift with CCl_3F as the reference. Although the application of Equation 9 leads to a familiar chemical shift scale at 25 °C, the application at other temperatures has a more complex interpretation involving TMS as the ultimate reference, as will be described later. The frequency referenced shift $\delta_{(1)}$ follows by Equation 7. For our compound XF, it is equal to −0.9999990. Except for the change in sign, the difference between $\delta_{(1)}$ and $\delta_{(2)}$ is negligible, but it is not negligible for very large shifts.

It is also of interest to note the relationships between ^1H- and ^{19}F-based heteronuclear chemical shifts. During our measurements, the ^1H lock (TMS) frequency was 100.09359 MHz at an offset of 78439.9 Hz, the offset required to bring CCl_3F at 25 °C into resonance with the instrumental ^{19}F frequency of 94.18451 MHz (at this ^1H offset, the measured ratio between the ^{19}F frequency and the instrumental ^1H frequency is 0.940964473). Accordingly, the chemical shift of TMS relative to CCl_3F is by Equation 1

$$\delta^{TMS}_{(1)F} = 10^6 \cdot (\nu^{TMS} - \nu^{TCF})/\nu^{TCF} = 62739.379 \quad (11)$$

Alternatively, the shift of CCl_3F may be expressed relative to TMS on the ^1H scale

$$\delta^{TCF}_{(1)H} = 10^6 \cdot (\nu^{TCF} - \nu^{TMS})/\nu^{TMS} = -59035.527 \quad (12)$$

These are the frequency based shifts. The field based shifts, defined by Equation 2, follow by rearranging

$$\delta^{TCF}_{(1)} = [\frac{\nu^{TCF}}{\nu^{TMS}} - 1] \cdot 10^6 =$$

$$[\frac{H^{TMS}}{H^{TCF}} - 1] \cdot 10^6 = \delta^{TMS}_{(2)} \quad (13)$$

Similarly, $\delta^{TCF}_{(2)} = \delta^{TMS}_{(1)}$. Furthermore, $\delta^{TCF}_{(1)}$ and $\delta^{TCF}_{(2)}$ are related by Equation 7.

While the above relations express the chemical shift between TCF and TMS, any fluorine shift may be expressed on the ^1H scale. For example, for our compound XF, the frequency based shift is $\delta^{XF}_{TCF(1)} = -0.9999990 \approx -1.000$.

The shift relative to TMS may be calculated by Equation 8.

$$\delta^{XF}_{TMS(1)} = 10^6 \cdot (\nu - \nu^{TMS})/\nu^{TMS} \quad (14)$$

$$= (\nu^{TCF}/\nu^{TMS})(\delta^{XF}_{TCF(1)} + 10^6) - 10^6 \quad (15)$$

$$= 0.9409645\, \delta^{XF}_{TCF(1)} - 59035.527 \quad (16)$$

For our compound XF, $\delta^{XF}_{TMS(1)} = -59036.49$. This may be converted to a field referenced shift by Equation 7: $\delta^{XF}_{TMS(2)} = +62740.47$. Unlike Equation 8, Equation 7 is nonlinear.

Having considered the options available for reporting chemical shifts at 25 °C, we now turn to the application of Equation 9 at other temperatures. Operationally, it is equally simple to bring XF at another temperature into resonance by a change of offset. In this case the $\Delta\nu_{offset}$ reflects not only the change required to bring XF into resonance at 25 °C, but also the change in field (which affects ν_{XF}) resulting from the variability of the TMS ^1H frequency with temperature. In addition, the variability of the ^{19}F XF frequency with temperature is reflected. Although the latter is not separated from the variability of TMS with temperature, the range of fluorine–TMS temperature dependence indicates that the ^{19}F variability is sometimes large.

We may calculate an apparent chemical shift for XF at any temperature using Equation 9. Values of "δ" obtained in this way are tabulated in this paper. Although the reference nucleus for these values is ^1H of TMS, the zero point is the chemical shift of $CFCl_3$ at 25 °C. The "spread" is essentially that of the usual ^{19}F scale, allowing comparison of the magnitude of the apparent chemical shifts with the magnitude of the range of ^{19}F chemical shifts for various compounds. We again note that for ordinary ^{19}F shifts, the denominator would be a fluorine frequency taken at the same temperature, whereas it is not for these apparent δ values. Instead "ν^{TCF*}" of Equation 10 is actually $0.940964473 \cdot \nu^{TMS,T*}$. We may also note that because of this relationship the heteronuclear ^1H frequency-based scale values calculated by Equation 16 are valid TMS-referenced shifts at any sample temperature.

RESULTS

Circuit Operation. The circuit described in the Experimental section operates as outlined below. Circuit locations are shown in Figure 1. The resonance signals of the two lock nuclei (point *a*) are detected as an audio signal of which the fundamental frequency is equal to the frequency difference between the two resonances (point *b*). This audio signal is filtered to remove most of the harmonics and noise (point *c*), amplified (point *d*), and used to modulate the lock transmitter RF output (point *f*). The center frequency of the RF output continues to excite the primary lock nucleus, while one of the sidebands has the correct frequency to excite the secondary lock nucleus. Therefore, the whole circuit acts as a feedback oscillator, with the main frequency-selective element in the feedback loop being the frequency difference between the resonance peaks of the two nuclei.

Operation of the lock modulation circuit was investigated using a lock mixture of 2:1, v:v, $(CBrF_2)_2$:$(CCl_2F)_2$. The spectrometer was locked normally on the largest peak ($CBrF_2CBrF_2$). Then, the modulation circuit, with a preamplifier gain of −3 to +6 dB, was connected as shown in Figure 1. Modulation commenced spontaneously, growing to the maximum (clipping) level in 2–5 s, depending on the exact gain. The frequency of the audio sine wave output was determined to be 401.20 Hz by period-average counting for 10 000 cycles (~25 s), using the counter time base. The measured frequency varied less than 0.01 Hz over 10 min of successive counts.

The frequency was not affected by changing gain within the following limits: Decreasing the preamplifier gain >10 dB dropped the oscillator loop amplification to less than unity. Raising it (10–15 dB) to maximum caused considerable overmodulation and a decrease of the lock dc level, but no frequency change. Further increase in gain using an auxiliary amplifier (30 dB) caused extreme overmodulation and loss of lock. Frequency was also not changed by changing frequency filter settings, except when the filter bandpass did not encompass the audio frequency being measured (e.g., filter settings of 300–380 Hz for the 401-Hz signal), causing the audio circuit gain to be very frequency-dependent at the modulation frequency. Even then, $\Delta\nu$ only changed ~0.2 Hz.

Measurements Using the Feedback Circuit. The frequency difference between the two ^{19}F nuclei was measured by letting a 12-mm tube containing 2:1, v:v, $(CBrF_2)_2$:$(CCl_2F)_2$, with thermocouple immersed, equilibrate for 0.5 h, after first connecting the modulation circuit and adjusting the gain with the thermocouple. After equilibration, the thermocouple was removed, whereupon spinning commenced spontaneously, and the spectrometer was locked to one of the ^{19}F resonances. Modulation occurred spontaneously in a few seconds. The audiofrequency of the modulation circuit was measured to determine the $\Delta\nu$ between the two nuclear resonances. $\Delta\nu$ was found to be 429.341 Hz at 0.15 °C, and 420.058 Hz at 11.63 °C.

For a "temperature jump" experiment, the temperature was equilibrated at 0.8 °C (measured by ^{19}F $\Delta\nu$, using the linear approximation $\Delta\nu = 429.458 - (0.8083 \cdot t°C)$) and then the setting of the Varian temperature controller was increased 10°. The $\Delta\nu$ was measured by accumulating successive 10 000 cycle period-average counts for 14 min, and converting to temperature. The results (Figure 3) show the expected exponential approach to the new set temperature, with an initial lag of 0.30 min. Half-time of equilibration was 0.97 min, a figure in agreement with non-spinning thermocouple measurements. Interestingly, changes in probe tuning or magnet homogeneity caused small (0.1–0.4 °C) changes in the equilibration temperature of the sample, with a similar half-time but no initial lag, apparently due to changes in RF energy absorption. Increasing homogeneity always caused increases in temperature, supporting this hypothesis.

Calibration of Thermometric Mixtures. For use of fluorine nuclei as thermometric mixtures over a wider range, $\Delta\delta$ was determined at 6 temperatures between −50 and +60 °C, with a capillary of acidified methanol as an internal thermometer, using a Perkin-Elmer R-32 spectrometer.

Equations 17–21 are empirical least-squares curve fits of the data. The data pairs of Equations 17 and 18 (^{19}F $\Delta\delta$ and temperature) are reproducible to ±0.005 ppm, but the complex nature of the curves necessitates several parameters and leads to standard deviations greater than 0.005 ppm. Also, the best available calibration of the methanol thermometer (*1*) is only

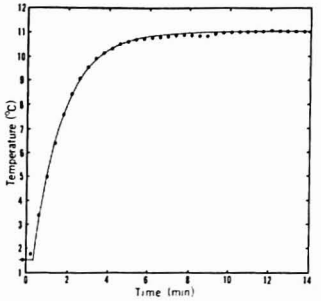


Figure 3. Temperature jump experiment. Dots represent experimental data. Line is calculated exponential approach to new set temperature, with initial lag of 0.3 min and half-time of 0.97 min

accurate to 0.8 °C, so temperatures calculated in Equations 17–19 should be considered to have standard (RMS) errors of approximately 0.8 °C. Equations 14 and 15 have standard errors of 0.002 ppm at high temperatures and 0.005 ppm at low temperatures.

For a 2:1, v:v, $(CBrF_2)_2$:$(CCl_2F)_2$ mixture, the following expression (Equation 17) fits the data with a standard deviation of 0.25 °C. Variations in relative amounts of the two compounds do not affect the calibration. This calibration curve also correlates with values obtained on the Varian XL-100 spectrometer using the lock modulation circuit, to ±0.5 °C.

$$1/T = -0.02177847 + 0.01546517 \cdot \Delta\delta_F - 0.003441595 \cdot \Delta\delta_F^2 + 0.000279336 \cdot \Delta\delta_F^3 \quad (17)$$

For a 2:1, v:v, $CF_2{=}CCl_2$:CF_3CCl_3 mixture, the following expression (Equation 18) fits the data with a standard deviation of 0.18 °C.

$$T = 3259.865 - 1738.553 \cdot \Delta\delta_F + 303.264 \cdot \Delta\delta_F^2 - 16.3522 \cdot \Delta\delta_F^3 \quad (18)$$

Temperatures are based on Van Geet's calibration of the methanol thermometer (*1*, *9*), here converted into a form directly useable on any spectrometer:

$$T = 403.0 - 29.46 \cdot \Delta\delta_H - 23.83 \cdot \Delta\delta_H^2 \quad (19)$$

This calibration curve also correlates with values obtained on the Varian XL-100 spectrometer using the lock modulation circuit, to ±0.5 °C.

Using the 100-MHz spectrometer in field-swept mode, the ^{19}F chemical shift (relative to ^1H TMS, as described in the Experimental section) was determined for $(CBrF_2)_2$ both neat and in solution. The ^{19}F shift of neat CCl_3F (TMS scale) was not investigated in detail, but varies approximately with $1/T$, and approximately fits the expression $1/T = 0.006534 \cdot \delta + 0.003354$. Newmark and Graves (*10*) have shown that ^{19}F shift sensitivity to temperature in 1,2-difluorotetrachloroethane is due at least in part to rotamer populations. A similar situation should obtain for 1,2-dibromotetrafluoroethane. They also noted the sensitivity of 1,1-dichlorodifluoroethene, although its cause was not investigated.

The ^{19}F resonance of $(CBrF_2)_2$ in 2:1, $(CBrF_2)_2$:$(CCl_2F)_2$ has a ^{19}F shift (scale, Equation 9) varying with temperature according to the following expression with a standard deviation of 0.0016 ppm in the temperature range −60 to +40 °C.

$$\delta_{(CBrF_2)_2 \text{ solution}} = 62.4622 + 575.74/T - 106897/T^2 \quad (20)$$

Table II. ^{19}F Chemical Shifts and Shift Sensitivities to Temperature, on TMS Scale

	Concentration (%, v/v)	^{19}F chemical shift in ppm at 25 °C $\delta_{F(TMS)}$	Temperature sensitivity $d\delta_{F(TMS)}/dT \cdot 10^3$ (ppb/°C)[a]
$CFCl_3$	Neat	0	+2.0
	80.0%[b]	−0.040	+1.5
	60.0%[b]	−0.080	+1.3
	50.0%[b]	−0.099	+1.3
	40.0%[b]	−0.116	+1.3
	20.0%[b]	−0.154	+1.5
CBr_2F_2	Neat	−6.962	−0.2
	80.0%[c]	−6.925	−0.2
	60.0%[c]	−6.881	−0.2
	50.0%[c]	−6.865	−0.2
	40.0%[c]	−6.847	−0.2
	20.0%[c]	−6.805	−0.3
$(CBrF_2)_2$	Neat	63.340	+3.5
	66.7%[d]	63.196	+3.0
	50.0%[e]	63.693	+0.2
	50.0%[f,g]	64.26	+0.9
CF_3CO_2-CH_2CH_3	Neat[g]	77.68	+3.7
	50.0%[g,h]	76.85	+4.7
	80.0%[d,g]	77.29	+3.8
	60.0%[d,g]	76.86	+4.3
	40.0%[d,g]	76.43	+4.7
	20.0%[d,g]	75.94	...[i]
$(CFCl_2)_2$	33.3%[h]	67.546	−5.8
	80.0%[f,g]	67.68	...[i]
	60.0%[f,g]	68.09	−6.2
	40.0%[f,g]	68.45	−7.0
	20.0%[f,g]	68.82	−7.6
$CF_3C_6H_5$	50.0%[h]	63.798	+6.1
CF_3COOH	90.9%[j]	78.142	−0.7
CF_3CH_2OH	90.9%[j]	79.035	−1.2

[a] From shifts measured at −30 °C and +25 °C. [b] In CBr_2F_2. [c] In $CFCl_3$. [d] In $(CFCl_2)_2$. [e] In $CF_3C_6H_5$. [f] In $CF_3CO_2CH_2CH_3$. [g] Shifts were reproducible within 0.005 ppm on any single day, but varied up to 0.1 ppm from week to week because of trace hydrolysis. [h] In $(CBrF_2)_2$. [i] Frozen at −30 °C. [j] Contains 9.1% D_2O.

Neat $(CBrF_2)_2$ has a ^{19}F shift (scale, Equation 9) varying with temperature according to the following expression with a standard deviation of 0.005 ppm in the temperature range −80 to +30 °C:

$$\delta_{(CBrF_2)_2 \text{neat}} = 63.0030 + 394.10/T - 87872/T^2 \quad (21)$$

A survey of other ^{19}F shift sensitivities to temperature was accomplished by measuring shifts at −30 and +25 °C, as shown in Table II. In common with ^1H and ^{13}C (*3*, *10*, *11*) shift sensitivities, salient features are: (a) Nonpolar molecules without rotational equilibria have small (~1 ppb/°C) sensitivities; (b) Polarizable compounds change sensitivity as well as chemical shift when solvent polarity changes; (c) Compounds with rotational equilibria have marked sensitivities; and (d) Both positive and negative sensitivities are found. For $(CBrF_2)_2$, ^{13}C shift sensitivities are about $^1/_3$ those found for ^{19}F. Increasing temperature deshields ^{13}C and shields ^{19}F in this compound. Splitting constants (accurate to 0.2 Hz) are not affected by temperature in the compounds $(CBrF_2)_2$ (J_{CF}, J_{CCF}) and CF_3CH_2OH (J_{FH}) (*11*).

DISCUSSION

A useful method of simultaneous temperature determination in NMR is described here. Without modification, the method should be applicable to ^1H and ^{19}F lock modes on the Varian XL-100 spectrometer, while observing any nucleus.

Calibrations of two ^{19}F thermometric mixtures are included. We have demonstrated the operability of the circuit as shown, but for extended or routine use of the circuit, helpful improvements might include: (a) Consolidation of preamplifier, filter, amplifier, and power supply onto a single chassis; (b) An automatic gain-control circuit in the audio preamplifier to render unnecessary the adjustment of circuit gain; (c) A phase-lock loop active filter to provide a narrow-bandpass, self-tuning filter, eliminating fine adjustments of bandpass frequency while improving filtering; and (d) A latch-and-hold circuit, probably as part of the phase-lock loop, permitting use with pulse lock. As an additional use of the circuit, frequency-to-voltage conversion of the audio signal might allow the circuit output to be used as sensor for a probe thermoregulator.

The circuit represents a new type of NMR, using continuously feedback signal for excitation. It differs from nuclear side-band oscillation in that the feedback is the frequency difference between two spectrum peaks. It resembles stochastic noise excitation NMR (*12*), which uses continuous noise for excitation and also produces a continuous time-domain spectrum. However, instead of noise, our system uses feed-back signal which is enriched in the resonance frequency to excite the secondary lock nucleus. The feedback loop character of the circuit and the presence of noise make the circuit self-activating and ensure an output which is the frequency difference between the two peak maxima, exact to better than $^1/_{10}$ of the peak widths. Possible areas for future investigation include: (1) Feedback NMR of more complex spectra, and (2) A circuit operating directly with the radio frequencies, contained wholly within the probe housing, with only the frequency differences as output.

The calibrations of $(CBrF_2)_2/(CFCl_2)_2$ and $CCl_2{=}CF_2/CCl_3CF_3$ solutions permit temperature determinations to an absolute accuracy of better than 1 °C. Also, the peak-center-seeking characteristic of the lock modulation circuit, plus the averaging inherent in a 10000 cycle (25 s) count, allows frequencies to be determined to <0.01 Hz, resulting in a temperature measurement precision of ~±0.01 °C. At subambient temperatures, the Varian temperature controller permits temperature stabilities around ±0.05°/min, after equilibration, limiting the practical usefulness of such precision. However, the circuit does permit accurate measurement of small temperature differences, and recent work (*13*) shows that improving the N_2 flow system on this type of temperature controller can permit sample temperatures stable within ±0.025 °C.

Reporting our data relative to neat TMS represents an approach to basing chemical shifts and shift sensitivities to temperature on some universal standard. Jameson and coworkers (*14*) in turn report values for the temperature sensitivity of TMS shifts vs. an absolute standard (^{129}Xe at 0 atm) to ±0.02 ppm, between −53 and +27 °C. This permits our ^{19}F sensitivities to be converted (with reduced accuracy) to absolute temperature sensitivities. Schneider, Freitag, and Schommer (*15*) have discussed this approach in connection with an earlier study from Jameson's laboratory (*16*).

ACKNOWLEDGMENT

The authors thank Harold C. Walsh for able assistance in the design and construction of the electronics circuits used.

LITERATURE CITED

(1) A. L. Van Geet, *Anal. Chem.*, **42**, 679 (1970).
(2) M. L. Kaplan, F. A. Bovey, and H. N. Cheng, *Anal. Chem.*, **47**, 1703 (1975).
(3) D. W. Vidrine and P. E. Peterson, *Anal. Chem.*, **48**, 1301 (1976).
(4) E. J. Stampf and J. D. Odom, *J. Organomet. Chem.*, **131**, 171 (1977).
(5) C. H. Dungan and J. R. Van Wazer, "Compilation of Reported ^{19}F NMR Chemical Shifts", Wiley-Interscience, New York, N.Y., 1970.
(6) J. W. Emsley, J. Feeney, and L. H. Sutcliffe, "High Resolution NMR Spectroscopy", Vol. 2, Pergamon Press, London, 1966.
(7) G. R. Langford, M. Akhtar, P. D. Ellis, A. G. MacDiarmid, and J. D. Odom, *Inorg. Chem.*, **14**, 2937 (1975).
(8) *Pure Appl. Chem.*, **45**, 219 (1976).
(9) A. L. Van Geet, *Anal. Chem.*, **40**, 2227 (1968).
(10) R. A. Newmark and R. E. Graves, *J. Chem. Phys.*, **72**, 4299 (1968).
(11) D. W. Vidrine and P. E. Peterson, manuscript in preparation.
(12) R. R. Ernst and W. A. Anderson, *J. Magn. Res.*, **3**, 28 (1970).
(13) J. J. Windle, *J. Magn. Res.*, **22**, 487 (1976).
(14) C. J. Jameson, A. K. Jameson, and S. M. Cohen, *J. Magn. Res.*, **19**, 385 (1975).
(15) H. J. Schneider, W. Freitag, and M. Schommer, *J. Magn. Res.*, **18**, 393 (1975).
(16) A. K. Jameson and C. J. Jameson, *J. Am. Chem. Soc.*, **95**, 8559 (1973).

RECEIVED for review March 2, 1977. Accepted October 5, 1977.

Electron Spin Resonance Spectrometric Study of Free Radicals in Coals

Leon Petrakis* and D. W. Grandy

Gulf Research & Development Company, P.O. Drawer 2038, Pittsburgh, Pennsylvania 15230

The presence, concentration, and nature of free radicals in several coals, coal fractions, and pyrolyzed coals have been ascertained by electron spin resonance (ESR) spectrometry. Careful measurements of *g* values, lineshapes, linewidths, and integrated intensities of the observed signals have been made. The nature and concentration of free radicals present in a given coal are determined by rank, thermal history, and particle size. Significant changes in radical concentration and, in some cases, in the chemical nature are observed as pyrolysis temperature is increased. Interpretation of the data is based on earlier work on pure macerals and on literature *g* values of pure compounds. The implications of free radicals in coal liquefaction processes are examined.

Free radicals are generally assumed to play a significant role in the behavior of coals during liquefaction processes. Coals have an appreciable concentration of stable free radicals in their native form, presumably formed in the "coalification" process. In addition, when most coals are heated, bonds are broken and free radicals are formed with the concomitant release of volatile material, mainly water and light hydrocarbons. Upon further heating, coals pass through a temperature of maximum fluidity and ultimately solidify or repolymerize. Thus, free radicals can also be associated with problems in coal liquefaction, such as reactor coking and poor conversion yields. Despite the ubiquity and their apparent great significance, free radicals in coal are not really well understood and well characterized. This is surprising for the further reason that free radicals offer an excellent way of understanding the structure of coals, or at least that part of their structure that has unpaired electrons. This study of free

0003-2700/78/0350-0303$01.00/0 © 1978 American Chemical Society

Table I. Chemical Analysis (MAF)

Wt %	Wyodak Gillette, Wyoming	Illinois #6	Lower Dekoven, Illinois[a]	Pocahontas #3 West Virginia
C	72.2	82.0	80.6	86.4
H	5.5	5.4	5.8	3.9
O	21.0	9.5	4.8	6.8
S (org)	0.3	1.0	7.7	0.9[b]
N	1.0	1.7	1.8	1.2
Ash (M.F.) wt %	9.2	6.5	21.9	3.3
Rank (ASTM)	Subbituminous C	HVB	HVA	LV

[a] Data provided by P. Given, The Pennsylvania State University. [b] Total sulfur.

radicals in coals was initiated to gain some insight as to the number and types of free radicals in coals under various conditions. Electron spin resonance (ESR) spectrometry has been used in the study of coal by many workers (*1–4*) since the discovery of free radicals in coal by Uebersfeld (*1*) and Ingram (*2*). The technique is attractive, since radical concentration and chemical information can be obtained with relative ease in a minimal period of time. Four coals of various bituminous and subbituminous ranks were studied since these are the types of most interest for liquefaction purposes.

The ESR spectral parameters of interest are the *g* value of the radicals, radical concentration, peak-to-peak linewidth of the first derivative signal and in some cases, the spectral lineshape. The *g* value is a parameter which is particularly sensitive to the chemical environment of the unpaired electron in a radical. Radical concentration is a measure of the number of unpaired electrons (spins) in a given amount of sample. The spectral linewidth, in the case of mixtures such as those in coal, is probably determined by the proximity of the unpaired electron to nuclei with magnetic moments, such as protons or nitrogen (hyperfine interactions). Spectral lineshapes in these samples are largely affected by unresolved hyperfine structure and anisotropic effects. Because of the complex mixture of compounds present in coal, the *g* value, linewidth, and lineshape are composite properties of all radicals present in a sample. The position and characteristics of the signal envelope are greatly influenced by the relative concentrations of the different radicals.

Throughout the course of this work, we have attempted to gain some understanding of the chemical structure of the radicals in these coals and selected fractions before and after thermal treatment. The *g* value of a coal sample is possibly the most useful single parameter available in terms of structural information. Although they are often neglected in the literature, there are a sufficient number of *g* values catalogued so that structural information on the radicals in coal can be obtained by comparison with the *g* values of compounds or compound types that might reasonably be expected to be found in coal. It must be remembered, however, that the *g* value found for a coal sample reflects the nature of *all* of the radicals present and is not the isotropic *g* value of a pure compound. Although comparisons between *g* values of a mixture of radicals in the solid state with the isotropic *g* values of pure compounds in the literature must be made cautiously and with a number of solid state effects in mind (vide infra), they may still be very useful in characterizing the paramagnetic species present in coal and gaining structural information. We will show that ESR, along with other spectrometric techniques and some analytical data, can be used to learn much about the structure of free radicals in natural and thermally altered coals.

EXPERIMENTAL

The four coals selected were examined by ESR at room temperature after a variety of treatments. All of the coals were dried overnight in air at 110 °C before further use. A portion of each sample lot was sieved with those particles <44 μm and those >298 μm being set aside. The total unsieved coal and these two sieve fractions were used for most of this work. Other sieve fractions were occasionally used. An upper limit on particle size of 2 mm was imposed by sample tube diameter. All evacuation–heat treatments were conducted by first evacuating the sample to ~10^{-4} Torr for 2 h at the treatment temperature and then sealing. In some cases where samples were rerun at a later date, some effects due to sample age were noted. These effects were restricted to linewidth and lineshape. Duplicate samples were prepared at a later date for many of the samples to check reproducibility. Analytical data for the coals studied are shown in Table I.

All spectra were recorded at room temperature with Varian V-4500 single- and dual-cavity spectrometers. Concentration measurements were done with the dual-cavity instrument by the usual sample–standard interchange method. A solution of DPPH in benzene was used as the primary standard for concentration and *g* value measurements. To minimize the effect of differences in lineshape between samples, peak areas used in concentration calculations were obtained by photocopying spectra, and cutting and weighing the signals. Reproducibility between duplicate samples was usually within 20% and is much better than this on the same sample. The possibility of "skin" effects in pyrolyzed samples affecting the concentration measurements was considered. Coals carbonized to 600 °C have resistivities on the order of 10^3 Ω-cm (*5*). This allows an estimation of skin depth at *x* band frequencies of about 10 mm (*6*) and, consequently, such skin effects are probably not important. Linewidths and *g* values were calculated from spectra obtained with a single-cavity spectrometer equipped with a Ventron NMR gauss meter and a Hewlett-Packard frequency counter. A minimum of three spectra was taken for each sample in these determinations. Microwave frequency and magnetic field values were taken at a minimum of three points per scan. Noise and other factors limit *g*-value determinations to slightly better than 1 part in 10^5 or about ±1 in the last place shown. Linewidth determinations were of variable quality, depending on the signal-to-noise ratio and lineshape. Errors in linewidths are 10% or less in most cases. Spectral lineshapes were examined for many of the samples. In some cases, multiple superimposed signals were observed.

RESULTS

Room Temperature Experiments. *g Values.* The results obtained in the ESR experiments on the total coals, Table II, are essentially in agreement with the results obtained by earlier workers (*4*). The *g* values show a substantial difference between the Wyodak subbituminous coal and the three higher ranking coals. Since the *g* value of a radical is quite sensitive to the chemical environment of the unpaired electron, some information as to the types of radicals in coal can be obtained. In the case of the higher ranking coals, the *g* values are typical of those found for π-type aromatic hydrocarbon radicals (see Table III). If present in these radicals, heteroatoms are not likely to participate in the molecular orbital of the unpaired electron to any significant degree. The subbituminous coal, on the other hand, has a much higher *g* value which indicates that atoms other than carbon and hydrogen (probably oxygen) are important in the electronic structure of the radical. Oxygen is believed to be the atom responsible for changes in *g* values with rank for several reasons (see Figure 1). Among

Table II. ESR Parameters of Coals and Coal Fractions

Sample	g value	Linewidth in air	ΔH (Gauss) in vacuum	Radical concentration per gram × 10^{-18}	
				In air	In vacuum
Wyodak subbit. C, total coal	2.0037	7.2	7.4	4.9	5.8
<44 μm	2.0037	6.7	7.0	3.8	3.8
>298 μm	2.0033	7.3	7.4	3.3	3.6
Illinois #6 HVB total coal	2.0029	1.3	1.3 & 6.0	9.8	6.8
<44 μm	2.0030	4.3	1.0	9.9	6.9
>298 μm	2.0029	6.4	1.3 & 5.7	6.3	
Lower Dekoven, Illinois, HVA total coal	2.0028	0.9	0.9	5.3	4.1
<44 μm	2.0029	2.9	0.9	8.0	5.6
>298 μm	2.0029	4.1	1.2 & 4.9	4.4	3.9
Pocahontas #3 LV total coal	2.0029	2.6	0.97 & 6.01	18.9	15.8
<44 μm	2.0030	5.9	1.0	28.8	
>298 μm	2.0029	5.6	1.0	26.8	

Table III. Values of Some Possible Compound-Types in Coal

Radical type	g value	References
(1) Aromatic hydrocarbons, π radicals		
1-5 rings	2.0025 (cation) 2.0026-2.0028 (anion)	(*7, 8*)
7 rings (coronene)	2.0025 (cation) 2.00291 (anion)	(*7, 8*)
(2) Aliphatic hydrocarbons, π radicals	2.0025 to 2.0026 (neutral)	(*9*)
(3) Oxygen-containing free radicals		
σ type π type	2.0008-2.0014 (neutral)	(*10, 11*)
Quinones 1-3 rings Ethers	2.00469-2.00380	(*7, 12*)
1-ring, mono-, di-, trimethoxybenzenes	2.00350-2.00398 (cation)	(*13*)
(4) *N*-containing radicals	2.0031	(*14*)
(5) *S*-containing radicals	2.0080-2.0081	(*14*)
(6) Graphite	2.0025-2.015	(*15*)

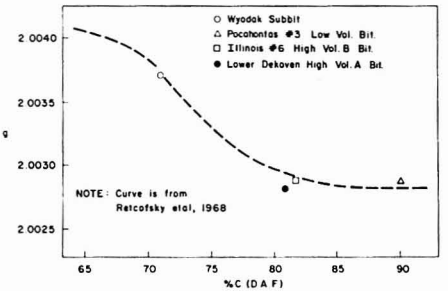


Figure 1. Plot of *g* values vs. coal rank

the heteroatoms found in the hydrocarbon framework of coal, oxygen content varies in a regular fashion with rank, whereas nitrogen and sulfur content are more or less constant (*4*). Sulfur-containing radicals have *g* values considerably higher than those found in coals and nitrogen-containing radicals, which have *g* values similar to those containing oxygen, usually have much broader linewidths, if exchange effects are negligible. Correlations between *g* values of coals and oxygen content, which varies from 20% to 4% by weight going from low- to high-ranking coals, have been made and it has been suggested that the radicals may be of the quinone type (*4*). Generalizations regarding trends in *g* values with size and substitution of semiquinones would suggest that such molecules having 4 to 9 rings would have the proper range of *g* values (*7*). Methoxy benzene radicals and related compounds are known to have *g* values typical of those found in the lower rank coals, around 2.0035 to 2.0037 (*13*). In view of the current opinions regarding the structure of coal, either or both may be possibilities, depending on the rank of the coal in question. Among the other hypotheses proposed for the structure of coal (*16*), are the aromatic model and the aliphatic or polyadamantane model (*17*). In the polyadamantane model, coal is viewed as a collection of complex three-dimensional aliphatic cages with small aromatic molecules attached. The older and more widespread aromatic model shows coal as composed of clusters of polycyclic aromatic molecules tied together by short aliphatic chains or by single bonds. The number of rings per cluster is thought to increase with rank until a structure resembling graphite is approached. This view is supported by x-ray studies and the reflectance anisotropy exhibited by anthracites (*18*). It is possible that the severe pressures of sedimentation may cause the molecular structure of coal to change from the three-dimensional polyadamatane type of structure to the two-dimensional, oriented aromatic structure by thermally induced rearrangements as the coalification process proceeds. Radicals possessing the proper range of *g* values could be of the methoxy benzene type in the polyadamantane structure or the large, multi-ring quinone type in the aromatic model.

Linewidth. The spectral linewidth ($\Delta H_{p\text{-}p}$) of all samples was measured as run in air or vacuum. With the exception of the subbituminous coal, many evacuated samples yielded spectra which consist of a sharp line ($\Delta H_{p\text{-}p}$ ~1 gauss) superimposed on a broader signal. In some cases, it was possible to measure separate values of $\Delta H_{p\text{-}p}$; in others, the components were clearly there but were not resolvable. Except for a few of the samples which exhibited some effects of age when rerun, the majority of the samples have much broader linewidths in air or, as for those samples with two resolvable components, the narrow component often disappears. This is the expected result of dipolar broadening by paramagnetic molecular oxygen. As noted by Retcofsky (*4*), spectra of some lithotypes found in coal show large differences when the samples are

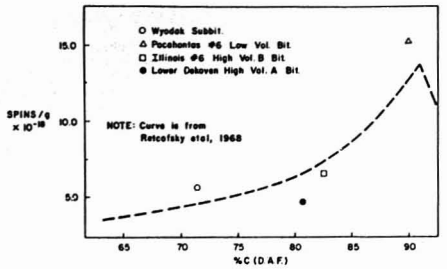


Figure 2. Free radical concentration vs. rank

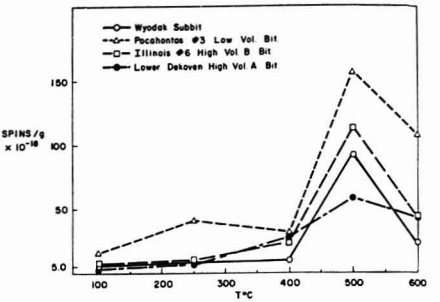


Figure 3. Free radical concentration vs. temperature, coals as received

evacuated relative to those run in air. Fusain, or mineral charcoal, exhibits considerable spectral broadening (approximate factor of 3) when exposed to air, whereas vitrain, the main lithotype in most coals shows no such "oxygen effect". A very small amount of fusain (~1%) in coal can account for the sharp component seen in spectra of some evacuated samples. In nearly every instance in the coals studied, the finer sieve fraction of each coal had the narrower linewidth. Because of the greater friability of fusain, its concentration is known to be highest in the smaller sieve fractions (*19*). The greater linewidths found for the subbituminous samples, compared to the higher rank coals, are likely to be caused by structural differences in the radicals involved since hydrogen content is essentially the same for all of the coals for which analytical data are available, i.e., ~5.4 to 5.8% H. This would imply that atoms with attached hydrogens participate more in the molecular orbital of the unpaired electron in subbituminous radicals than in the higher ranking coals, if exchange effects are unimportant.

Spin Concentration. Concentration measurements were performed to find the number of unpaired electrons (spins) per gram of sample. The radical concentrations found for the four coals in air follow the expected increase with rank (see Figure 2). One high-volatile bituminous coal, Lower Dekoven, Illinois, had a slightly lower spin concentration than expected; however, this may be due to the extremely high ash content of this coal, about 22% vs. 6.5% found in the Illinois #6 high-volatile bituminous coal. With regards to particle size, the finer sieve fraction has a higher spin concentration than the coarse fraction. Again, the difference may be attributed to the concentration of fusain in the fine fraction since fusain is known to have a spin concentration about five times greater than associated vitrains (*4*).

All of the coals, except the Wyodak subbituminous, show a decrease in radical concentration when evacuated. This result is unexpected and its cause is unknown. It is interesting to note, however, that it is the subbituminous coal again which exhibits a different behavior upon evacuation, as was the case with the linewidths. Another abnormality is the difference in concentration of the total coal compared to the sieve fractions. It was expected that the total coal would have a concentration somewhere between that of the sieve fractions. Such is not the case with two of the four coals. One possibility is that the remaining portion (>44 μm, <298 μm) has a spin concentration which would cause the sum of the parts to be equal to the whole.

Lineshapes. The lineshapes of the spectra were estimated whenever possible. The two lineshape functions considered were the Lorentzian function, which is of the form $ka(a^2 + x^2)^{-1}$, and the Gaussian function, which is $\exp(-a^2x^2)$. The Lorentzian function has the property of approaching the baseline very slowly, whereas the Gaussian function is narrower and drops off very quickly. Evacuated samples yielded spectra which range from some nearly equal linear combination of the two functions, as is the case with the subbituminous coal, to the very broadly sloping, multicomponent spectra of the higher rank coals. Multicomponent spectra were more common in total coal and coarse samples. All of the spectra tended to drop off more rapidly in the wings than in the main portion of the signal, i.e., the lineshape function changed on going from the point of maximum amplitude to the baseline. Such a lineshape is not uncommon (*20, 21*), and could possibly be due to unresolved hyperfine or anisotropic effects, or both. Of those samples run in air, only the subbituminous coal had appreciable Gaussian character. The higher rank coals often had very broad lineshapes which, in some cases, sloped linearly from the baseline to the peak in the derivative curve. Signal asymmetry, which caused some problems in *g*-value determinations, was far more prevalent in air-exposed samples than those which were run while evacuated.

The ESR parameters of these coals have values which are, for the most part, in the range expected for their rank. It is very likely that the radicals in the lowest rank coal studied are of a different type than those of the higher rank coals, the subbituminous coal radicals probably containing more heteroatoms in the vicinity of the unpaired electron. Differences in ESR parameters observed between different sieve fractions, such as linewidth and concentration, are probably due to differences in lithotype concentration.

Heat Treated Coals. *Spin Concentration.* The four coals and available sieve fractions were evacuated and heated to temperatures up to 600 °C. Radical concentration, *g* value, and linewidth were monitored for each sample. The radical concentration of the total coals is seen to change dramatically over the temperature range studied (see Figure 3). Up to 400 °C, only moderate changes in radical concentration occur. Radical concentration increases sharply between 400 and 500 °C and drops substantially on going to 600 °C. This behavior is qualitatively in agreement with the work of Smidt and VanKrevelen (*22*), among others; however, their work was done with "hand-picked vitrains of high purity" whereas this work was done on coals as received and their sieve fractions. The change in free radical concentration as a function of temperature may be due to the rupture of bonds starting around 400 °C and continuing to a point where the coal becomes fluid enough for the radical sites formed on bond-breaking to combine and the coal then resolidifies or polymerizes into a char. A possible explanation of the preference of temperatures in the range of 400 to 450 °C for coal liquefaction (*23*) and the observed softening point range of 375 to 475 °C for high-volatile and higher rank coals (*24*) may be such a rupture of bonds with the attendant formation of free radicals. Free radical combination, as indicated by the decrease in con-

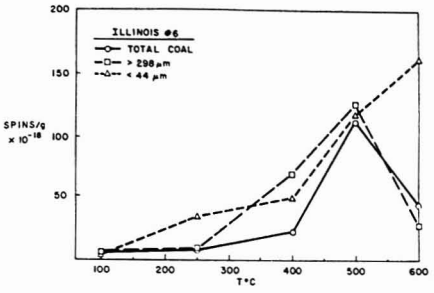


Figure 4. Free radical concentration vs. temperature, Illinois #6

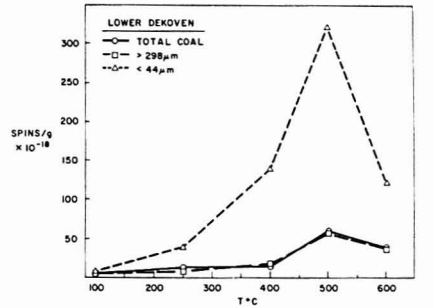


Figure 5. Free radical concentration vs. temperature, Lower Dekoven

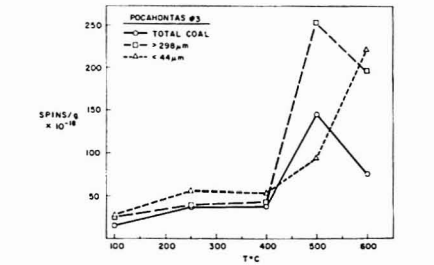


Figure 6. Free radical concentration vs. temperature, Pocahontas #3

centration above 500 °C, could account for the resolidification of these same coals between 440 and 540 °C. It is expected from the studies of vitrains of various carbon contents (22) that some rank dependence in the temperature of maximum radical concentration will be found.

The temperature dependence of radical concentration is found to be somewhat different for some sieve fractions relative to the total coal (see Figures 4, 5, and 6). In most cases the temperature dependence of the radical concentration of the fine (<44 μm) sieve fraction departs substantially from that of the coarse fraction (>298 μm) and that of the total coal. The degree of difference between the total coal and the sieve fractions is largely determined by the size distribution of the coal as received. For example, the Wyodak subbituminous coal exhibited almost no differences between the total coal and the fine sieve fraction, not surprising in view of the lack of enough coarse particles for study. The most plausible reason for differences among the fractions is an unequal

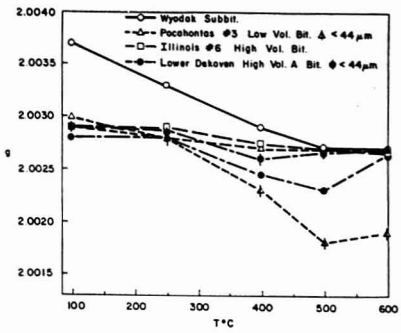


Figure 7. *g* values vs. temperature

distribution of the types of macerals. From ESR studies of pure macerals, it is know that each behaves differently with temperature, particularly above 400 °C (25). However, among any given maceral, no dependence of radical concentration on particle size is found (26). Since it is known that exinite and vitrinite are the most susceptible macerals to liquefaction (27) and that these same macerals show the largest increase in free radical concentration upon heating (25), it is likely that materials which undergo the largest increases in radical concentration upon heating will be the most desirable for liquefaction. If such is the case, free radical formation may be very desirable in liquefaction materials, provided repolymerization does not take place (28). Because of the long commercial applicability of methods for petrographic separation (SOVACO method) (29), the use of particular lithotypes in coal liquefaction may be feasible.

g Values. Figure 7 shows the change in *g* values of the radicals in the total coals as a function of temperature. Two of the coals, the Pocahontas #3 coking coal and the Illinois #6 high-volatile bituminous coal, show a minor decrease in *g* values from 2.0029 to 2.0027. Such a change in *g* values shows a relatively minor change in radical structure, the radicals tending to become pure hydrocarbon in nature. This may be due to either molecular rearrangements or some loss in oxygen as volatile material, or both. The Wyodak subbituminous coal shows a very large decrease in *g* value, from 2.0037 to 2.0027, which occurs below 500 °C. It is known from vacuum distillation studies of a subbituminous Wyoming coal that water, carbon dioxide, and carbon monoxide are the predominant products up to 450 °C (30). Mass spectrometric analysis of the gas evolved while heating this Wyodak coal for 2 h at 500 °C shows that about 85% of the gas evolved is carbon monoxide and carbon dioxide on a weight basis. The water content of the gas was negligible; however, our sample was predried for two days at 105 °C. The carbon oxides account for about 40% of the oxygen present in the original coal on a moisture-free basis. Since radical concentration does not change below 400 °C in this coal, the removal of oxygen from the molecular framework as gaseous products below 400 °C must be taking place in the pre-existing radical centers or in a part of the molecule with appreciable spin density. Removal of oxygen from other parts of the molecule could not account for the decrease in *g* value. One of the bituminous coals, Lower Dekoven, Illinois, shows some interesting changes in *g* value when heated. Between 250 and 500 °C, the *g* value decreases to an abnormally low value of 2.0023. There are several possible explanations for this behavior, among these is the appearance of σ-type radicals. Many σ radicals have *g* values around 2.0024 and some are known to have *g* values as low as 2.0008 (10). Sigma-type radicals are those formed by bond

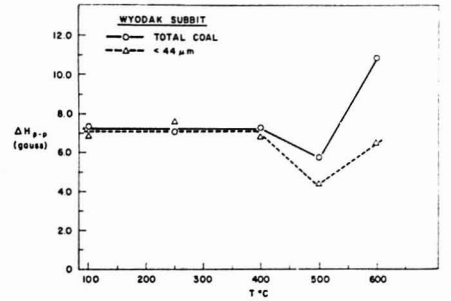
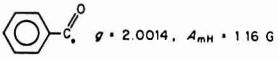


Figure 8. Spectral linewidth vs. temperature, Wyodak subbituminous

breakage, often hydrogen abstraction. These radicals often have large hyperfine coupling constants which, in the case of coal, would be unresolved and would cause the linewidths to be quite broad. However, in the case where hydrogen atoms are not close, three bonds or more from the radical center, the hyperfine coupling is small and, hence, the linewidth in coal would be quite narrow. An example is the radical formed by irradiation of benzaldehyde shown below (*11*).



From the increase in the g value of the radicals in the Lower Dekoven coal on heating to 600 °C and the decline in radical concentration, it is likely that these radicals are involved in recombination reactions.

The g values of the sieve fractions are very similar to those of the total coals, with two exceptions (see Figure 7). The fine fraction of the Lower Dekoven coal behaves in a manner similar to the other high-volatile bituminous coal (Illinois #6) and its sieve fractions rather than the total coal. The fine sieve fraction of the Pocahontas #3 coking coal shows a trend in g values with increased temperature very different from the total coal. The g value is 2.00275 at 100 °C, drops to 2.0018 at 500 °C, and increases only slightly to 2.0019 at 600 °C. The reason for this g-value temperature dependence is very likely to be due to the formation of σ radicals. The relatively small change in g value on going from 500 to 600 °C is not surprising since this sieve fraction shows little tendency to repolymerize; indeed, the radical concentration at 600 °C is double that at 500 °C. The possibility of the formation of a graphite-like substance was considered but rejected since the g values of graphite are 2.0025 to 2.015, depending on sample history (*15*), and those of highly carbonaceous materials such as *meta*-anthracite are around 2.0028 (*4*).

Linewidth. The spectral linewidth of the total coals and sieve fractions is found to vary considerably with temperature. Interpretation of the data is complicated by the presence of several components in the spectra of some samples. The subbituminous coal and the <44-μm sieve fraction behave in a similar fashion with spectra at all temperatures having only one apparent component. The temperature dependence of the linewidth, shown in Figure 8, is very similar to that found by Smidt and VanKrevelen (*22*) for coals of slightly higher carbon content and is basically characteristic of vitrinite and exinitic material (*25*). The linewidth for these materials changes very little up to 400 °C where a decrease begins, followed, in turn, by an increase at higher temperatures. The point of minimum linewidth appears to be rank dependent (*22*). The three other coals, high-volatile bituminous and coking coals, often gave spectra in which two components of different width were clearly resolvable or, from the nearly linear shape from the baseline to the inflection points, suggest many components which could not be resolved. At lower temperatures (≤250 °C) the narrow component is likely to be due to some fusanitic material (*4*). At higher temperatures, this component is often not resolvable, probably because of the rapid increase in signal strength of the vitrinitic and exinitic components up to 500 °C (*25*). The decrease in linewidth between 500 and 600 °C found for most samples is characteristic of coals of bituminous rank, which then show an increase in linewidth at still higher temperatures. The decrease in linewidth is probably due to electron delocalization which, in excess, leads to increased electron–electron interaction and increased broadening.

ACKNOWLEDGMENT

The authors gratefully acknowledge P. Given of The Pennsylvania State University for helpful discussions and for making available to us analytical data on the Lower Dekoven coal sample. The authors also acknowledge A. V. Fareri's diligence and assistance with the experimental aspects of this work.

LITERATURE CITED

(1) J. Uebersfeld, A. Étienne, and J. Combrisson, *Nature (London)*, **174**, 614 (1954).
(2) D. J. E. Ingram, J. G. Tapley, R. Jackson, R. L. Bond, and A. R. Murnaghan, *Nature (London)*, **174**, 797 (1954).
(3) B. C. Gerstein, C. Chow, R. G. Pembleton, and R. C. Wilson, *J. Phys. Chem.*, **81**, 565, 1977.
(4) H. L. Retcofsky, J. M. Stark, and R. A. Friedel, *Anal. Chem.*, **40**, 1699 (1968).
(5) P. L. Waters, "Proceedings of the Fifth Conference on Carbon", Vol. 2, Pergamon Press, The Macmillan Co., New York, N.Y., 1963, p 142.
(6) L. S. Singer, "Proceedings of the Fifth Conference on Carbon", Vol. 2, Pergamon Press, The Macmillan Co., New York, N.Y., 1963, p 43.
(7) M. S. Blois, Jr., H. W. Brown, and J. E. Maling, "Free Radicals in Biological Systems", Academic Press, New York, N.Y., 1961, p 130.
(8) B. G. Segal, M. Kaplan, and G. K. Fraenkel, *J. Chem. Phys.*, **43**, 4191 (1965).
(9) R. W. Fessenden and R. H. Schuler, *J. Chem. Phys.*, **39**, 2147 (1963).
(10) P. Smith, R. A. Kaba, L. M. Dominguez, and S. M. Denning, *J. Phys. Chem.*, **81**, 162 (1977).
(11) P. J. Krusic and T. A. Rettig, *J. Am. Chem. Soc.*, **92**, 722 (1970).
(12) M. Adams, M. S. Blois, and R. H. Sands, *J. Chem. Phys.*, **28**, 774 (1958).
(13) P. O'Neill, S. Steenken, and D. Schulte-Frohlinde, *J. Phys. Chem.*, **79**, 2173 (1975).
(14) "Atlas of Electron Spin Resonance Spectra", Bielski and Gebicki, Ed., Academic Press, New York, N.Y., 1967, pp 38, 606, 611.
(15) Gerald C. Michael, Ph.D. Thesis, The Pennsylvania State University, 1969.
(16) F. R. Mayo, J. Huntington, and N. Kivshen, "Oxidation of Coal, Coal Fractions and Coal Models", SRI Coal Chemistry Workshop, August 26–27, 1976.
(17) T. Aczel, M. L. Gorbaty, P. S. Maa, and R. H. Schlosberg, Exxon Research and Engineering Company, "Studies on the Organic Structural Types in Coals", SRI Coal Chemistry Workshop, August 26–27, 1976.
(18) "Coal and Coal Bearing Strata", Duncan Murchison and T. Stanley Westoll, Ed., Oliver and Boyd, Edinburgh and London, pp 250–252.
(19) "International Handbook of Coal Petrography", International Committee for Coal Petrology, 2nd ed., Centre National de la Recherche Scientifique, Paris, 1963.
(20) Charles P. Poole, Jr., "Electron Spin Resonance", Wiley Interscience, New York, N.Y., 1967, p 807.
(21) L. Petrakis, *J. Chem. Educ.*, **44**, 432 (1967).
(22) J. Smidt and D. W. VanKrevelen, *Fuel*, **38**, 355 (1959); "Coal", Elsevier, Amsterdam, 1961, pp 393–399.
(23) Juan J. Correa and Jack M. Hochman, U.S. Patent No. 3,726,784, Exxon Research and Engineering Company, April 10, 1973.
(24) "Chemistry of Coal Utilization", National Research Council Committee, H. H. Lowry, Ed., Vol. 1, John Wiley and Sons, New York, N.Y., 1945, p 302.
(25) D. E. G. Austen, D. J. E. Ingram, P. H. Given, C. R. Binder, and L. W. Hill, "Coal Science", *Adv. Chem. Ser.*, **55**, 344 (1966).
(26) C. R. Binder, Ph.D. Thesis, The Pennsylvania State University, 1965, p 38.
(27) P. H. Given, D. C. Cronauer, W. Spackman, H. L. Lovell, A. Davis, and B. Biswas, *Fuel*, **54**, 40 (1975).
(28) Richard C. Neavel, *Fuel*, **56**, 237 (1976).
(29) "Coal Preparation", J. W. Leonard and D. R. Mitchell, Ed., AIMMPE, New York, N.Y., 1968, pp 1–15.
(30) H. H. Lowry, Ed., Ref. 24, p 763.

RECEIVED for review June 6, 1977. Accepted November 3, 1977.

Interference of Salt Matrices in the Determination of Copper by Atomic Absorption Spectrometry with Electrothermal Atomization

D. J. Churella[1] and T. R. Copeland*

Department of Chemistry, Northeastern University, Boston, Massachusetts 02115

This work examines the concentration dependent interferences of several alkali and alkaline earth halides in the atomic absorption spectrometric determination of copper using a carbon cup electrothermal atomizer. The unusual interference of $NaClO_4$ is also investigated. The addition of Na_2O_2 is shown to eliminate or substantially reduce the interferences caused by these salts both in pure solutions and in seawater. Occlusion of the analyte is proposed as the primary mechanism of these interferences.

When electrothermal (nonflame) atomization techniques were first being developed by L'vov, Massman, Amos, and others (*1–5*), it was a common opinion that, in contrast to flame methods, determinations could be made relatively free from interferences caused by the matrix. With the advent of commercial instrumentation and a mushrooming interest in the method, it was discovered that the signal obtained for a metal was very much a function of the matrix involved and many interferences were noted.

There is little general agreement among the authors of interference studies (*6–11*) as to the exact mechanism of interferences. West et al. (*7*) show that suppressions are due to gas-phase interactions between atomic species and condensing interferents, Aggett and Sprott (*8*) and Segar and Gonzalez (*9*) cite metal and compound volatility as the major consideration in interferences, and Cruz and Van Loon (*10*) and Smeyers-Verbeke et al. (*11*) support the occlusion hypothesis of interference. They all agree, however, that interferences are probably due to complex combinations of several factors.

In order to understand the mechanisms of interference, it is important to know something of the mechanism of atomization of the analyte. Campbell and Ottaway (*12*) proposed a mechanism based on the reduction of the metal atoms in the gaseous state. Appearance temperatures for several metals were shown to be in agreement with the lowest temperatures at which the carbon reduction reaction becomes thermodynamically feasible. Kinetic studies by Fuller (*13, 14*) showed that the most probable reaction mechanism involves a slow first-order reduction of metal oxide by carbon followed by rapid volatilization of the metal formed.

Comparison of these and other studies must be done with consideration for the equipment employed and the chemical composition of the matrix. Commercially available equipment differs greatly in the total mass of the atomizer and the power supplied to it. Consequently the rate of change of the drying, ashing, and atomizing temperatures varies widely. The rate of temperature elevation, final temperature of each cycle, and length of time the sample remains at the temperature maxima, all would be expected to affect the size and composition of the crystals formed from remnants of the matrix. Measurement of parameters such as appearance temperatures from standard solutions (*12*) is largely independent of the time required to reach that temperature and reasonable agreement with thermodynamic calculations could be expected. However, calculations based on thermodynamics for atomizers (such as employed in this study) where temperature changes over 500 °C/s are common, are essentially meaningless.

Kinetic interpretations of matrix interferences must also be made with care. The kinetic studies of atomization processes carried out by Fuller (*13, 14*) indicate a slow first-order reduction of the metal oxide by the carbon atomizer followed by rapid vaporization of the metal formed. This rate would be significantly affected by the size of the matrix/carbon interface (crystal size) as well as the actual crystal composition. Thus, although thermodynamic and kinetic studies of atomization are valuable in predicting important parameters in the atomization process, they do not necessarily afford information predicting the causes and extent of matrix interferences.

Electrothermal atomization has several advantages over flame atomization including extremely small sample volume, improvements of up to 2–3 orders of magnitude in sensitivity, and the elimination of lengthy pretreatment for the destruction of organic matter (*8*). It is thus of particular use in biological analysis where one is often working with very small samples of tissue which contain trace amounts of the metal of interest.

Biological samples, by nature, contain rather large amounts of salts (e.g., 1000–3500 μg/mL NaCl and 1400–6300 μg/mL KH_2PO_4 in addition to others (*15*)) and these salts can have a distinct effect on the accuracy of an analysis. Also, in wet digestion of samples, it is common practice to add acids such as HNO_3 and $HClO_4$ to the sample. If these acids are not completely destroyed in the digestion process, they will be present during the analysis and could have an effect on the response of the analyte. It was the purpose of this study to determine what effect these salts would have on the analysis for copper and to perhaps shed some light on the poorly understood origin, nature, and extent of these interactions.

EXPERIMENTAL

Apparatus. All experiments were performed on a Varian-Techtron AA-6 Atomic Absorption Spectrophotometer equipped with a CRA-63 electrothermal atomizer, a BC-6 background corrector, and a Varian Aerograph model A-25 recorder. Jarrell-Ash and Varian single element hollow cathode lamps were used as light sources. Graphite cups were used in the atomizer and N_2 was employed as the sheath gas. The CRA-63 atomizer offers both step and ramp atomizer modes. The voltage step mode afforded larger more reproducible signals and was used exclusively in this study. The 324.75-nm copper resonance line was employed for all analyses using a spectral bandpass of 0.5 nm and a slit height of 10 mm.

Experiments were performed to determine whether significant differences in the degree of signal suppression would be found measuring peak heights rather than areas. For all solutions studied, peak heights and mechanically or electronically integrated areas showed identical % suppression within experimental error. Consequently, absorbances were determined by measuring peak heights. Peak heights were measured from the recorder traces rather than using the AA-6 peak mode as the former was found

[1] Present address, Polaroid Corp., Cambridge, Mass. 02139.

0003-2700/78/0350-0309$01.00/0 © 1978 American Chemical Society

to be more reproducible. Thus the measurement time constant was primarily that of the recorder, measured to be 0.3 s full scale. The peak height mode of the AA-6 also exhibited % suppressions identical to the other measurement modes within their (larger) experimental error.

Samples were dispensed into the cup using a 5-μL micropipet with disposable plastic tips.

Atomizer temperatures were measured using a model 95 Pyro Micro-optical pyrometer. The area of the cup where temperatures were measured was inside the cup just below the optical path representing a temperature intermediate between the floor of the cup and the temperature in the optical path.

Electron micrographs of the matrix residues in the atomizer cups were obtained using an AMR 1000 scanning electron microscope and Polaroid type 52 film.

Reagents. All chemicals used were reagent grade. Water was distilled and doubly deionized and had a minimum resistivity of 2.0 MΩ.

All volumetric glassware was cleaned in hot, concentrated nitric acid before first use and was soaked overnight in ~1 M nitric acid between uses. Glassware was marked and used exclusively for one metal.

Stock solutions, 1000 μg/mL, of metals were prepared by dissolving 1.000 g of pure metal in a minimum amount of concentrated HNO_3 and diluting to 1 L. Solutions were stored in polyethylene bottles. Solutions of matrix compound, 20 000 μg/mL, were prepared as needed. Working solutions were freshly prepared before use by adding appropriate volumes of stock metal and salt by buret to 100-mL flasks and diluting to volume. Unless otherwise noted, all solutions contain 1.0 μg/mL copper.

General Procedure. Nonspecific absorption of salt matrices was checked by running a sample of 20 000 μg/mL salt solution in total absorbance mode. If peak heights greater than 5 mm (2% of full scale) were obtained, the whole series was run in the background corrected mode.

In a given series, the pure metal solution was run first, then the metal plus salt solutions were run in order of increasing salt concentration. Since results are reported relative to the response of the pure metal solution, this solution was run periodically throughout the series and at the end of the series. If the response of the pure solution changed during the series because of cup deterioration, the other solutions were compared to the most recent run of the pure solution. At least three replicate samples of each solution were run for each set of conditions.

In the two-number system of notation used in this work to specify dry, ash, and atomize setting, the first number indicates the relative voltage and the second number is the time in seconds for the particular cycle as read from the CRA-63 power supply. The drying time was generally kept at 25 s and the drying voltage adjusted so that the sample just finished drying at the end of the cycle. Ash settings of 5/10 and 7.25/30 were used.

The low ash setting of 5/10 resulted in a final temperature of 350 to 400 °C. The high ash temperature reached 975 to 1050 °C depending on the condition of the cup and support rods. Unless otherwise noted, the atomize setting was 8/3 which resulted in a final temperature of 2500 °C. The cups were fired at least three times between sample injections to ensure that any residual matrix had been removed.

RESULTS AND DISCUSSION

Effect of Mineral Acids. Solutions were analyzed which were 1.0 μg/mL in Cu and either 1.0 M or 0.001 M in various mineral acids. Solutions with these same concentrations of Cu and acids in addition to being 3000 μg/mL NaCl were also run to determine the effect of these acids on the interference of NaCl. The results are shown in Table I.

The data are presented as Δ% which is the amount the copper absorbance has changed in the presence of the interferent relative to the copper absorbance in a distilled water solution. It is calculated according to the equation:

$$\Delta\% = \frac{P_m - P_s}{P_s} \times 100 \quad (1)$$

where P_m is the peak height of the analyte in the presence of the matrix and P_s is the peak height of the standard solution. This method normalizes the data, overcoming slight day-to-day variations in the absolute absorbance of the standard solution, and makes possible the direct comparison of the effect of various matrices. Except for 1 M $HClO_4$ and H_3PO_4, the acids alone caused generally small changes in the Cu signal. High ash conditions resulted in a slightly greater loss in Cu signal than low ash. However, $HClO_4$ and H_3PO_4 caused marked reductions in the signal at low ash (-55% and -30.7%, respectively), with considerable improvement in high ash (-16.8% and -14.2%, respectively). The 0.001 M concentrations of these acids were consistent with the other acids in causing only small reductions in the signal.

Table I. Effect of Various Acids on NaCl Interference

Acid	Cu + acid, Δ%		Cu + acid + NaCl vs. Cu, Δ%		Cu + acid + NaCl vs. Cu + NaCl, Δ%	
	Low ash	High ash	Low ash	High ash	Low ash	High ash
NaCl only			-64	-26		
1 M HCl	-4	-3	-73	-40	-26	-19
0.001 M HCl	-1	-3	-65	-28	-4	-3
1 M HNO_3	-1	-4	-26	-26	+104	0
0.001 M HNO_3	-3	-6	-42	-18	+60	+11
1 M H_2SO_4	-2	-5	-30	-29	+92	-4
0.001 M H_2SO_4	-4	-2	-33	-26	+84	0
1 M $HClO_4$	-55	-17	-96	-89	-88	-84
0.001 M $HClO_4$	-4	-8	-66	-41	-8	-20
1 M H_3PO_4	-31	-14	-21	-15	+119	+15
0.001 M H_3PO_4	-7	-9	-56	-50	+22	-33
1 M CH_3COOH	-6	-13	-65	-46	-4	-27
0.001 M CH_3COOH	-8	-13	-67	-38	-8	-17

These same acids in the presence of NaCl presented an entirely different picture. When compared to the peak height of the pure Cu solution (center two columns of Table I), these matrices caused a much more severe depression of the signal than with the acids alone in all cases except for 1 M H_3PO_4 at low ash.

When compared to the response of a solution containing only Cu + NaCl (right two columns), HNO_3, H_2SO_4, and H_3PO_4 caused an enhancement of the Cu signal. In other words, they suppressed the interference of NaCl. The most effective suppression of the NaCl interference was achieved with a 1 M concentration of these acids at low ash conditions. High ash conditions resulted in an enhancement of the signal in only two cases, 1 M H_3PO_4 and 0.001 M HNO_3. These results are in agreement with Matousek (*16*) who found that H_3PO_4 significantly reduced the interference of NaCl on Cu and Pb solutions.

Effect of Various Salts. Matrix solutions containing either 0.5 μg/mL or 1.0 μg/mL Cu and varying amounts of inorganic salts were also investigated. The interference trends for LiCl and NaCl (Figures 1 and 2) are the same, their curves being almost superimposable. There is no interference until about 300 μg/mL salt, then a gradual increase in interference until at 10 000 μg/mL, about 80% of the Cu signal is lost. Using the high ash cycle decreases the interference and causes the Δ% curve to drop off more gradually. The curves for KCl and KI are the same as for NaCl and are not included.

$AlCl_3$ (Figure 3) follows the same general trend as the above salts except that the curves drop off at considerably lower concentrations and tend to level off above 3000 μg/mL salt.

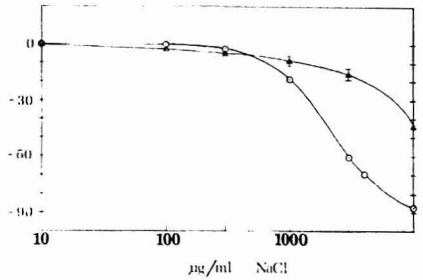


Figure 1. Effect of NaCl on Cu absorbances. 1 μg/mL Cu, (Δ) high ash conditions, (O) low ash conditions

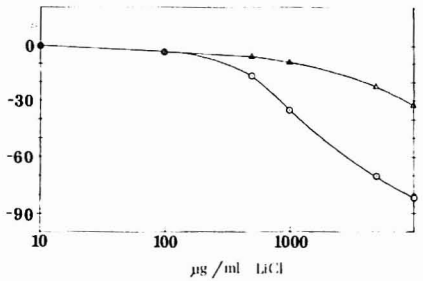


Figure 2. Effect of LiCl on Cu absorbances. 1 μg/mL Cu, (Δ) high ash conditions, (O) low ash conditions

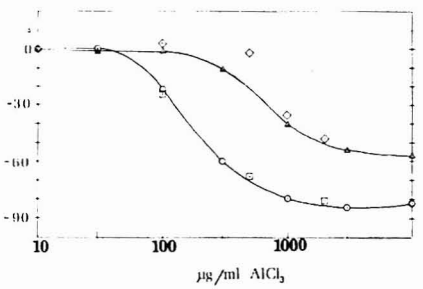


Figure 3. Effect of $AlCl_3$ on Cu absorbances. (Δ) high ash, 1 μg/mL Cu; (◊) high ash, 0.5 μg/mL Cu; (O) low ash, 1 μg/mL Cu; (□) low ash, 0.5 μg/mL Cu

The high ash curve for $MgCl_2$ (Figure 4) is the same as the curves for $AlCl_3$ and has a "normal" shape. The low ash curve, however, is quite different in that it passes through a minimum of −56Δ% at about 250 μg/mL and then rises to −34Δ% at 10000 μg/mL. $CaCl_2$ shows some indication of a similar effect, the data were however highly scattered.

For several salts, the effect of a matrix was determined on a lower concentration of Cu to determine if the ratio of Cu to interferent or the absolute amount of interferent was the dominant factor. The copper concentrations were varied from 0.1 to 1.0 μg/mL. In all cases studied, the same absolute amount of interferent caused the same degree of interference. This is illustrated for 0.5 μg/mL Cu in $AlCl_3$ and $MgCl_2$ (Figures 3 and 4). This would indicate that the interference is due to a physical effect rather than a stoichiometrically dependent chemical effect.

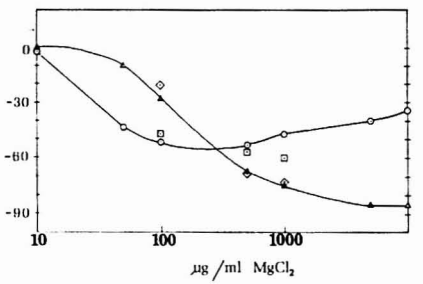


Figure 4. Effect of $MgCl_2$ on Cu absorbances. (Δ) high ash, 1 μg/mL Cu; (◊) high ash, 0.5 μg/mL Cu; (O) low ash, 1 μg/mL Cu; (□) low ash, 0.5 μg/mL Cu

The results presented thus far are consistently explicable by an interference mechanism dominated by the occlusion of the analyte in matrix crystals. The analyte atoms are trapped in microcrystals or agglomerates of matrix material which is not destroyed in the ash cycle and some fraction of which is large enough to be thrown from the atomizer in the atomize cycle without decomposing to free the analyte.

For the alkali chlorides studied, these microcrystals are most likely chloride or perhaps mixed chloride–oxide species. The similarity of boiling points (and hence vapor pressures and evaporation rates) of LiCl, NaCl, and KCl (1380 °C, 1465 °C, and 1407 °C, respectively) would explain the great similarity of their interference curves. $MgCl_2$, $CaCl_2$, and $AlCl_3$ interferences are also consistent with an occlusion mechanism. $AlCl_3$ upon addition to water evolves HCl and thus the most likely "crystal" to form upon drying is a mixed hydroxide chloride which would become predominantly an oxide matrix during either a high or low ash cycle and thus parallel the behavior of the alkali halides discussed above. The high ash decomposition of magnesium and calcium should also follow this behavior. However, the low ash temperature (350–400 °C) is close to the decomposition temperatures of $Mg(OH)_2$ (350 °C) and $Ca(OH)_2$ (580 °C). Thus, several hydrates of the chlorides as well as hydroxides, and hydrated oxychlorides would be favored for the low ash decomposition of these species. Several of these compounds decompose upon heating to release HCl. Thus, as the matrix content of these salts increases, a gelatinous film of matrix would most likely form which would enhance the formation of small crystals of matrix in intimate contact with the graphite cup. This ashing behavior would explain the apparently anomalous behavior of $MgCl_2$ at low ash and the anomalous and irreproducible behavior of $CaCl_2$ at low ash. Since $CaCl_2$ forms mono-, di-, and hexahydrates in addition to $Ca(OH)_2$ which decomposes just above the low ash temperature, high variability would be expected.

Occlusion is also supported by the nonstoichiometric nature of the salt interferences. Occlusion is a physical process and is not dependent on the stoichiometric ratio of analyte to interferent as are chemical processes.

The effects exhibited for the NaCl interference in the presence of acids are also consistent with occlusion. The HNO_3 could assist in the removal of the salt by forming volatile $NaNO_3$ and HCl resulting in the observed enhancement. H_2SO_4 and H_3PO_4 are both rather viscous acids and would lower the ionic mobility during the drying process and dry more slowly, resulting in smaller crystals. These smaller crystals have a larger surface area to volume ratio, would have a greater contact area with the carbon cup, would evaporate faster, and would be less likely to occlude the analyte, resulting in less interference. These acids would also

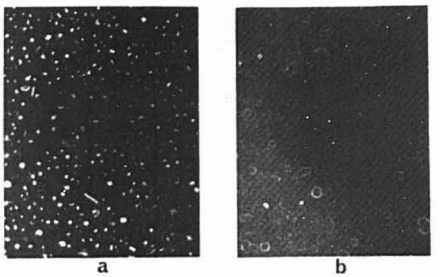


Figure 5. SEM photographs of the sample cup. Low ash conditions, (a) NaCl + 1 M H_2SO_4, (b) NaCl + 1 M H_3PO_4 (See text)

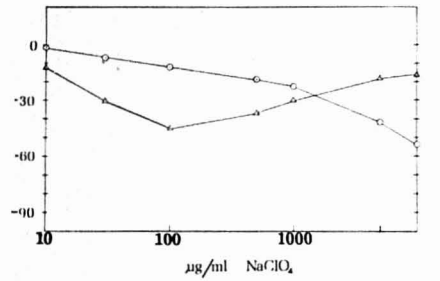


Figure 6. Effect of $NaClO_4$ on Cu absorbances. 1 μg/mL Cu, (Δ) high ash conditions, (O) low ash conditions.

tend to retain water of hydration in the crystals which upon ashing or atomization would be rapidly vaporized, fracturing the salt crystals and releasing trapped analyte atoms. This effect would be diminished by the more thorough drying of the high ash cycle, as is observed for these solutions.

Further evidence of the variation in crystal size formed is seen in Figure 5. These photographs are electron micrographs of the bottom of the graphite cups after low ash cycle. The cups contained 3000 μg/mL NaCl, 1 μg/mL Cu and 1 M H_3PO_4, or H_2SO_4. Both are at ~80× magnification under which each photograph represents ~75% of the surface of the bottom of the cup. Each previously unused cup was fired 4 times to decontaminate, then fired 3 times with the normal dry, ash, atomize settings with the appropriate solution added. A fourth injection of solution was made and the dry and ash cycles were performed. The cup was then removed from the atomizer and the SEM photos were taken. For a comparison of the crystal size obtained for pure 3000 μg/mL NaCl, 1 μg/mL Cu solutions, refer to Figure 9. It is obvious that the acids significantly affect the crystals formed. H_2SO_4 leaves much smaller crystals than pure NaCl, and H_3PO_4 leaves a dust of matrix distributed over the surface of the cup with higher concentrations in the grain boundaries of the graphite.

Such dramatically different crystal sizes led to the investigation of salts which would either evolve gases or produce a gel stage during the dry or ash cycles to determine which process was most likely to produce microcrystalline deposits.

$NaClO_4$ interfered with the Cu absorbance unlike any other salt tested in this work. Figure 6 is a point-by-point average of five separate sets of $NaClO_4$ data run at various times throughout the work. The individual curves were always the same general shape and were displaced vertically over a maximum range of 10Δ%. The low ash curve drops off linearly to 1000 μg/mL, then more steeply to a minimum of −66Δ% at 20000 μg/mL. Under high ash conditions the $NaClO_4$ begins to cause a suppression of the Cu absorbance almost immediately. The interference curve drops off rather steeply to a minimum of −45Δ% at 100 μg/mL, then increases to a maximum of −16Δ% at 10000 μg/mL, then drops off very steeply to −50Δ% at 20000 μg/mL.

Figure 7 shows the cups after low and high ash for 3000 μg/mL $NaClO_4$. Under low ash conditions, slightly more deposit is left than for the NaCl/acid matrices discussed above. Under high ash conditions the deposits appear finely dispersed and most of the matrix has been destroyed as is evident by the lack of crystals in the X600 magnification (Figure 7c). Only a few extremely small crystals remain near the center of the cup (the round raised mass at the upper left of the photograph). Evidently the matrix is being destroyed by decomposition of the $NaClO_4$ with fracturing of the crystals and some varying loss of solid material during the high ash. This is consistent with the known decomposition of $NaClO_4$ at ~650 °C.

$$NaClO_4 \rightarrow NaCl + 2O_2$$

Studies of Cu response vs. ash temperature in the presence of $NaClO_4$ indicated that ash settings between 6 and 7 were necessary to cause the high ash suppression of the Cu signal. This corresponds to a temperature of about 700 °C which is

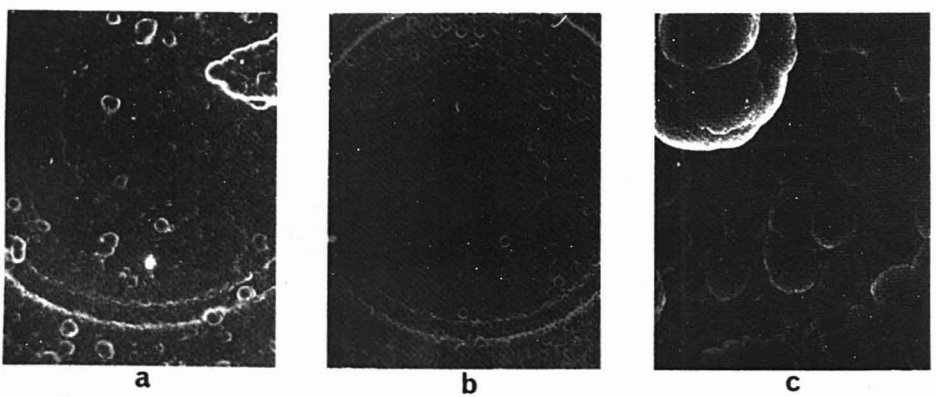


Figure 7. SEM photographs of cups containing $NaClO_4$. (a) 80X, low ash, (b) 80X high ash, (c) 600X high ash (cup center in upper left corner)

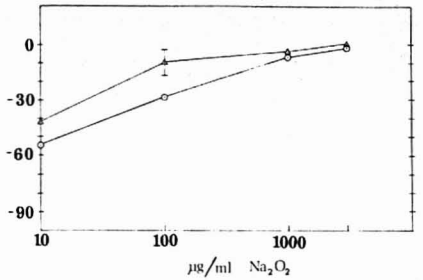


Figure 8. Suppression of the NaCl interference using Na_2O_2. All solutions contain 1 μg/mL Cu, 3000 μg/mL NaCl, and varying Na_2O_2

Table II. Effect of Na_2O_2 on Interference of Various Salts

Solution	Low Ash Peak height	Low Ash Δ%	High Ash Peak height	High Ash Δ%
Cu only	216.4	-	214.7	-
+ Na_2O_2	189.6	−12.4	200.3	−6.7
Cu + NaCl	90.5	−58.2	149	−30.6
+ Na_2O_2	211.7	−2.2	215.9	+0.6
Cu + $NaClO_3$	144.6	−24.6	162.5	−9.7
+ Na_2O_2	187.0	−2.6	171.2	−4.9
Cu + $NaClO_4$	144.2	−39.4	205.6	−13.6
+ Na_2O_2	211.6	−11.1	214.1	−10.0
Cu + $AlCl_3$	24.0	−90.2	18.8	−91.6
+ Na_2O_2(DI)[a]	189.6	−23.0	190.5	−15.0

[a] DI = Double Injection (see text).

very close to the decomposition temperature of $NaClO_4$ at ~650 °C. Since the interference effect was different from that of NaCl, the presence of oxygen in the cup during the high ash cycle was implicated as a major factor in the observed interferences. To test this hypothesis, sodium peroxide, Na_2O_2, was added to the cup as another source of oxygen. The result was the nearly complete elimination of the interferences normally caused by the salts.

Figure 8 illustrates the effect of increasing amounts of Na_2O_2 on the Cu signal in the presence of 3000 μg/mL NaCl. Rather dramatic increases in the signal are observed until at 3000 μg/mL Na_2O_2, both high and low ash signals are within 2% of the response for the pure Cu solution.

The effect of adding 3000 μg/mL Na_2O_2 to several other salts is shown in Table II. The concentrations of Cu and of salt in all these solutions are 1.0 μg/mL and 3000 μg/mL, respectively. These solutions were run at different times and their Δ%'s are calculated relative to the pure Cu response at that time, not necessarily the one listed in the table. Na_2O_2 suppresses the interference of the salt and improves the signal in all cases. There is very little difference between the response under high ash and low ash conditions.

Figure 9 illustrates the differences in crystal size obtained. The deposits of pure NaCl under low ash conditions are quite large and are diminished only somewhat by the high ash cycle. The addition of sodium peroxide results in a rather uniform covering of small crystals with a few larger deposits. The high ash with Na_2O_2 added results in an extremely fine, uniform powder from which no occlusion occurs.

The oxidizing ability of Na_2O_2 could also play a minor role in its elimination of interferences. In the presence of Na_2O_2, a heated solution of $CuCl_2$ dries as the black oxide whereas without Na_2O_2, it dries as the green chloride. If CuO is formed by the Na_2O_2 during the dry cycle, occlusion would be less

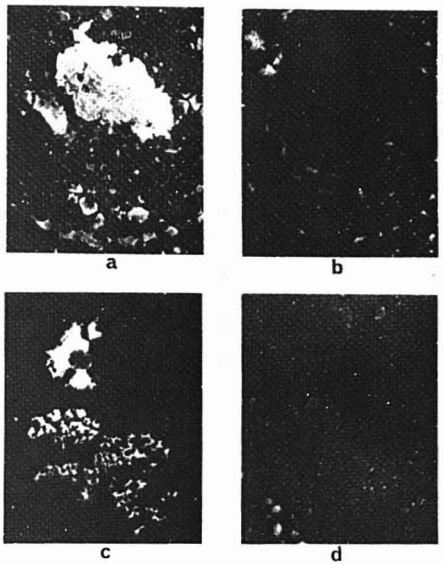


Figure 9. SEM photographs of sample cups. (a) 3000 μg/mL NaCl, low ash; (b) 3000 μg/mL NaCl + 3000 μg/mL Na_2O_2, low ash; (c) 3000 μg/mL NaCl, high ash; (d) 3000 μg/mL NaCl + 3000 μg/mL Na_2O_2, high ash

likely because the larger, insoluble CuO molecule would not fit into a forming halide salt crystal as easily or be as available as a Cu^{2+} ion. Na_2O_2 would form oxides of other species in the cup such as the volatile and easily atomized Na_2O which would boil off at high ash temperatures and help to eliminate the matrix. Having all the Cu in the form of CuO would make it more available for carbon reduction as shown by Campbell and Ottaway and others (*12*, *13*).

Addition of Sodium Peroxide to Seawater. Seawater is an excellent test of the capacity of Na_2O_2 to remove salt interferences. Synthetic and natural seawater was obtained from the New England Aquarium and samples were spiked with 0.2 μg/mL Cu and with 0.2 μg/mL Cu + 3000 μg/mL Na_2O_2. The addition of both the Cu and the Na_2O_2 resulted in a 14% dilution of the seawater.

The results shown in Table III indicate once again that the Cu signal is improved in all cases by the addition of Na_2O_2. Recovery of the Cu signal is not quite as complete with the seawater as it was with the salt solutions but the total concentration of salt (36900 μg/mL for synthetic seawater) is also much greater. Considering this concentration of salts, the recovery is remarkable.

Na_2O_2 was also added to the spiked seawater by a double injection technique (signified by DI in Table III) whereby the seawater sample is injected into the cup in the normal manner, then a 5-μL volume of 3000 μg/mL Na_2O_2 solution is also injected, and the dry–ash–atomize sequence is initiated. This results in the same amount of material in the cup as with the premixed method and simplifies solution preparation. However, it requires very careful adjustment of the dry voltage and time settings so that the solution dries completely without boiling out of the cup. With both the synthetic and natural seawater, this double injection technique resulted in a greater improvement in the signal than the premixed method, perhaps because the Na_2O_2 has had less time to decompose.

Table III. Effect of Na_2O_2 on Response of Cu in Seawater

Solution composition	pH	Low ash			High ash		
		Peak ht	Δ%	RSD	Peak ht	Δ%	RSD
Pure 0.2 μg/mL Cu	3	81	-	1.9	79	-	2.5
0.2 μg/mL Cu + 3000 μg/mL Na_2O_2	12.5	66.5	−17	0.5	64.5	−18	1.1
Synthetic seawater	6.5	0	-	-	0	-	-
Syn. + 0.2 μg/mL Cu	4.5	48.3	−40	8.6	34.0	−45	10.8
Syn. + Cu + 3000 μg/mL Na_2O_2	10	59	−27	6.7	76	−4	15.6
Syn. + Cu + Na_2O_2(DI)[a]	-	72.4	−10	4.0	73.3	−7	11.3
Natural seawater	6.5	0	-	-	0	-	-
Nat. + 0.2 μg/mL Cu	4.5	9.6	−89	3.5	11.8	−85	6.0
Nat. + Cu + 3000 μg/mL Na_2O_2	10	59.3	−31	10.8	61.8	−21	7.6
Nat. + Cu + Na_2O_2(DI)[a]	-	63.3	−26	18.2	70.3	−10	1.9
Nat. + Cu + 3000 μg/mL NaOH(DI)[a]	-	50.3	−41	1.8	56.0	−28	16.8
Nat. + Cu + 30% H_2O_2(DI)[a]	-	27.3	−68	7.1	30.3	−61	4.1

[a] DI = Double Injection (see text).

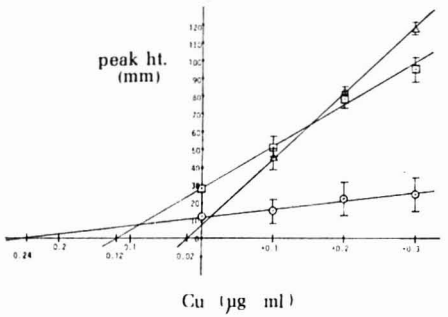


Figure 10. Standard addition analysis of seawater for Cu. (Δ) blank; (O) high ash, no Na_2O_2; (□) high ash, 3000 μg/mL Na_2O_2

When Na_2O_2 is added to water, some of the Na_2O_2 reacts to form NaOH and O_2, causing the solutions to become very basic and effervesce. There is also a slow evolution of oxygen from the solutions upon standing. Because of this, the effect of NaOH alone was determined with natural seawater. The addition of 3000 μg/mL by double injection resulted in an improvement of the Cu signal but not to the extent of the Na_2O_2 improvement (Table III). The spiked seawater was also run with 30% H_2O_2 by double injection and this resulted in an improvement of 20 Δ%—the smallest improvement of all.

One of the most common methods for compensating for matrix effects is the method of standard additions. To determine what effect the presence of Na_2O_2 would have on standard additions plots, natural seawater spiked with 0.1 μg/mL Cu was analyzed with and without the addition of 3000 μg/mL Na_2O_2. The standard addition plots, Figure 10, show rather dramatically the advantages to be gained by the addition of Na_2O_2. The graph for seawater with Na_2O_2 gives a value for the Cu concentration of 0.12 μg/mL which, when corrected for the standards blank, becomes 0.10 μg/mL—exactly the amount added. Without Na_2O_2, however, the value obtained is 0.24 μg/mL—twice the actual value. This graph also has larger standard deviations for the individual points and is less sensitive because of the very small slope of the line. The addition of Na_2O_2 to the seawater clearly enhances the precision and accuracy of the analysis.

It is evident that the physical size and chemical composition of a sample/matrix deposit can dramatically affect the signal achieved. Occlusion of the analyte in the matrix is the predominant mechanism of interference. Occlusion is reduced by compounds forming smaller crystals by forming viscous gels upon drying (NaOH, H_3PO_4, Na_2O_2, HNO_3), by forming unstable crystals which fracture via gas evolution ($MgCl_2$, Na_2O_2, $NaClO_4$), by forming volatile matrix compounds (Na_2O_2, HNO_3, $NaClO_4$), or by a combination of these. Adding one compound to a matrix to cause one of the above effects is in some instances advantageous. For example, L'vov (*17*) has added $LiNO_3$ to some NaCl matrices and found a decrease in interference.

However, such additions must be made with caution as evidenced by the results of large excesses of $NaClO_4$ in this study. It appears that addition of a substance which provides a uniform dispersion of extremely small crystals is the most desirable matrix interference suppresser. The only obvious alternative is to use an atomizer which has an extremely long pathlength so that crystals containing occluded analyte are totally decomposed before exiting the atomizer. Studies employing long pathlength atomizers and extending the present study to include more volatile elements and other potential interference suppressers are currently under way.

LITERATURE CITED

(1) B. V. L'vov, *Spectrochim. Acta, Part B*, **24**, 53 (1969).
(2) H. Massman, *Spectrochim. Acta, Part B*, **23**, 215 (1968).
(3) M. D. Amos, *Am. Lab.*, **2** (8), 33 (1970).
(4) D. C. Manning and F. Fernandez, *At. Absorpt. Newsl.*, **10**, 94 (1971).
(5) J. P. Matousek, *Am. Lab.*, **3** (6), 45 (1971).
(6) G. Baudin, M. Chaput, and L. Feve, *Spectrochim. Acta, Part B*, **26**, 425 (1971).
(7) D. Alger, R. G. Anderson, I. S. Maines, and T. S. West, *Anal. Chim. Acta*, **57**, 271 (1971).
(8) J. Aggett and A. J. Sprott, *Anal. Chim. Acta*, **72**, 49 (1974).
(9) D. A. Segar and J. G. Gonzalez, *Anal. Chim. Acta*, **58**, 7 (1972).
(10) R. B. Cruz and J. C. Van Loon, *Anal. Chim. Acta*, **72**, 231 (1974).
(11) J. Smeyers-Verbeke, Y. Michotte, P. Van den Winkel, and D. L. Massart, *Anal. Chem.*, **48** 125 (1976).
(12) W. C. Campbell and J. M. Ottaway, *Talanta*, **21**, 837 (1974).
(13) C. W. Fuller, *Analyst (London)*, **99**, 739 (1974).
(14) C. W. Fuller, *Analyst (London)*, **100**, 229 (1975).
(15) B. J. Stevens, *Clin. Chem. (Winston-Salem, N.C.)*, **18**, 1379 (1972).
(16) J. P. Matousek, Paper 306, 3rd Annual Meeting of the Federation of Analytical Chemistry and Spectroscopy Societies, Philadelphia, Pa., Nov. 1976.
(17) B. V. L'vov, Paper 214, 3rd Annual Meeting of the Federation of Analytical Chemistry and Spectroscopy Societies, Philadelphia, Pa., Nov. 1976.

RECEIVED for review September 12, 1977. Accepted November 1, 1977.

Determination of Industrial Dyes in Water by Laser Excited Resonance Raman Spectrometry

Laurent Van Haverbeke,[1] Patricia F. Lynch, and Chris W. Brown*

Department of Chemistry, University of Rhode Island, Kingston, Rhode Island 02881

Industrial fabric dyes were detected in distilled water at concentrations below 100 ppb and identified at concentrations below 200 ppb using resonance Raman spectrometry. The method was tested on doped samples of river and seawater. In both cases dyes could be detected and identified at the 200-ppb level. Detection and identification limits were higher in the natural samples because of an increase in the spectral background; however, the results show that the method is practical for "real world" samples.

In recent years, laser Raman spectrometry has been shown to be a promising method in water pollution studies. In the early 1970's, Bradley and Frenzel (*1*) reported the detection of benzene in water at concentrations around 50 ppm, and Baldwin and Brown (*2*) found minimal detectable concentrations of 25 to 75 ppm for various inorganic anions. Later, Ahmadjian and Brown (*3*) demonstrated the use of Raman spectrometry in remote detection measurements. More recently, Cunningham, Goldberg, and Weiner (*4*) were able to reduce the detection limits to 5 to 40 ppm for various solutes.

Up to now, the practical use of Raman spectrometry in pollution studies was restricted because, for most compounds, the minimum detectable concentration was too high. An important limitation is the Raman spectrum of the solvent, water, which shows up as a background above which the spectrum of the compound of interest is observed (*5*).

It is possible to increase the strength of the Raman signal of the solute without increasing the one of water by taking advantage of the resonance Raman effect. When the excitation frequency approaches the frequency of an electronic absorption band, the resultant Raman signal may be enhanced several orders of magnitude. Since water does not have an absorption band in or close to the visible region, enhancement of the water Raman signal is not observed.

Because of their strong absorption in the visible region, dyes lend themselves readily to monitoring by resonance Raman spectrometry. In a recent study on FD&C dyes, Brown and Lynch (*6*) have shown that dyes can be detected and identified in commercial solutions such as juice mixes and sodas at concentrations as low as 5 ppm without significant interference from other substances present.

In the present contribution we have determined the detection and the identification limits for a number of red industrial fabric dyes. A comparison with visible spectral detection is also presented. Furthermore, we have tested the method on two natural water samples doped with a dye.

EXPERIMENTAL

The Raman spectra of the dye solutions were recorded on a Spex Industries Model 1401 monochromator, equipped with a CRL Ar^+ ion laser and a photon counting detection system. We used both the 488-nm and 514.5-nm lines of the Ar^+ laser as exciting sources with 1-W output at the sample. All samples were contained in a cylindrical cell (~10-mm diameter), mounted in the Spex standard illumination chamber. Instrumental conditions for obtaining maximum signal-to-noise (S/N) ratios were thoroughly investigated. For natural water samples, the maximum S/N ratio was obtained with a spectral slit-width of ~5 cm^{-1}. A time constant (integration time) of 10 s was used for measuring the spectra; the S/N ratio was improved by using longer integration times, but the time required to measure a spectrum was too long for a practical method. Spectra were scanned at 5 or 10 cm^{-1}/min using a 10-s time constant.

Visible absorption spectra were recorded on a Cary Model 15 UV-visible spectrophotometer using a standard 5-cm quartz cell.

The fabric dyes used in this study were Superlitefast Rubine, Procion Red, Lyrazol Fast Red, and Direct Red 83. These commercial dyes were supplied by Kenyon Piece and Dye Works and by the Bradford Dyeing Association, and were used without further purification. They were dissolved in distilled water at concentrations around 200 ppm, diluted ten times to around 20 ppm, and then diluted consecutively to 50% to obtain lower concentrations.

Table I. Resonance Raman Spectra of the Dyes in the Region 1100–1500 cm^{-1} [a]

Superlitefast Rubine	Procion Red	Lyrazol Fast Red	Direct Red 83
1277 (7)	1123 (2)	1196 (3)	1248 (3)
1290 (9)	1180 (3)	1223 (3)	1317 (8)
1334 (7)	1230 (4)	1257 (3)	1359 (10)
1346 (8)	1251 (4)	1322 (4)	1421 (7)
1387 (8)	1286 (10)	1357 (10)	1446 (6)
1422 (10)	1344 (4)	1412 (4)	1482 (5)
1451 (3)	1368 (2)	1439 (6)	
1496 (2)	1430 (6)		
	1498 (2)		

[a] The first figure gives the position of the band (in cm^{-1}). The value in parentheses is the relative height (maximum = 10).

RESULTS AND DISCUSSION

The visible absorption spectra of Superlitefast Rubine, Procion Red, Lyrazol Fast Red, and Direct Red 83 are shown in Figure 1. All four dyes show at least one absorption band in the vicinity of both the 514.5- and 488-nm lines of the Ar^+ laser. Therefore, we used both lines as resonance Raman excitation frequencies. One of the dyes, however, (Procion Red) shows an intense fluorescence between 1000 and 2000 cm^{-1} when the 514.5-nm line was used as exciting frequency. Since under these conditions a minimum concentration cannot be determined, we restricted our measurements on Procion Red to the 488-nm excitation.

The most useful region of the Raman spectra of these dyes is the region between 1000 and 1500 cm^{-1}. Below 1000 cm^{-1}, no intense bands are observed. On the other hand, intense bands in the region 1500 to 1800 cm^{-1} will be masked by the water band at 1640 cm^{-1} upon dilution. Except for Procion Red, no major differences were observed between the spectra obtained with 488- and 514.5-nm excitation frequency. The

[1] Present address, Labortorium Anorganische Scheikunde, Rijksuniversitair Centrum Antwerpen, Groenenborgerlaan, 171, B2020 Antwerp, Belgium.

0003-2700/78/0350-0315$01.00/0 © 1978 American Chemical Society

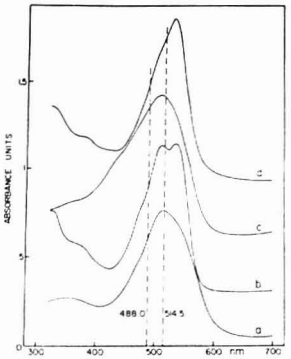


Figure 1. Visible absorption spectra of fabric dyes. (a) Superlitefast Rubine (11.35 ppm), (b) Procion Red (6.32 ppm), (c) Lyrazol Fast Red (7.38 ppm), (d) Direct Red 83 (12.15 ppm)

Table II. Minimal Detection and Identification levels[a]

Dye name	Raman		Visible spectrophotometry
	Detection	Identification	
Superlitefast Rubine	35	75	66
Procion Red	30	140	30
Lyrazol Fast Red	45	160	40
Direct Red 83	55	175	50

[a] All values in parts per billion (ppb).

strongest bands in the 1000–1500 cm^{-1} region for each of the dyes at 488 nm excitation are listed in Table I. The table demonstrates very clearly that this region of the spectra is very characteristic and can be used as a fingerprint-like recognition pattern.

More and more of the smaller bands are lost in the noise of the spectrum as the dye solutions are diluted. We considered the 1000–1500 cm^{-1} region of the spectrum suitable for identification purposes at a certain concentration when at least three bands are visible, i.e., they have a signal-to-noise ratio >3. The lowest concentrations for which this occurs are given in Table II. The spectra shown in Figure 2 are obtained from solutions close to these identification levels. In the same way, we consider a dye detectable at a certain concentration when at least one band is visible with a signal-to-noise ratio of at least three. The detection levels for the four dyes are also given in Table II.

From Table II we can see that there is a large variation in both the detection levels and the identification levels, but there is no relationship between them. The reason for this can be found in the pattern of the spectrum. If a large number of bands have the same intensity, both the level of detection and identification are similar. If, however, the spectrum is composed of one or two intense bands and a large number of smaller bands, there will be a significant separation between the two levels.

Table II also contains the minimally detectable concentrations when using visible absorption spectrometry. A 5-cm pathlength cell was used and a minimally detectable absorption of 0.004 was assumed (7). As can be seen, the detection levels for resonance Raman spectrometry are of the same order as the ones obtained by visible spectrometry. The former has, however, the advantage of better identification capabilities.

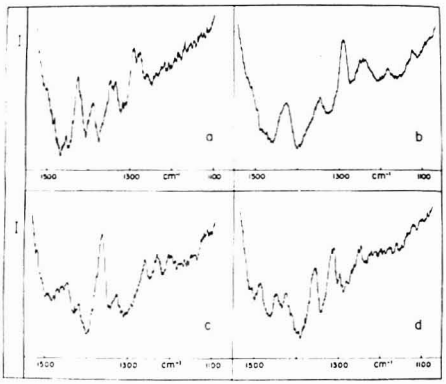


Figure 2. Resonance Raman spectra of fabric dyes close to the identification level. (a) Superlitefast Rubine (88 ppb), (b) Procion Red (192 ppb), (c) Lyrazol Fast Red (210 ppb), (d) Direct Red 83 (190 ppb)

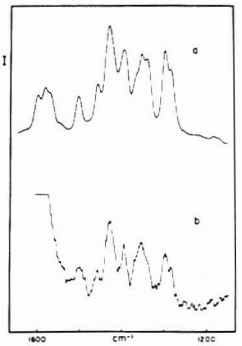


Figure 3. Resonance Raman spectra of (a) Superlitefast Rubine in distilled water at 24.3 ppm; (b) Superlitefast Rubine in river water at 288 ppb

To investigate the practical use of the resonance Raman technique in pollution determinations, we simulated a real situation. A 250-mL water sample, collected from the nearby Pettaquamscutt River, was polluted with 3 mL of a 24.3 ppm solution of Superlitefast Rubine in distilled water, resulting in a dye concentration of 288 ppb in river water. From this sample, resonance Raman spectra were measured with both the 488- and 514.5-nm laser lines. The spectrum obtained using the 488-nm laser line showed a huge fluorescence, which made identification of the dye bands practically impossible. However, the 514.5-nm excited spectrum showed very little fluorescence. The region between 1200 and 1600 cm^{-1} is shown in Figure 3b. For comparison, the spectrum of the same dye in distilled water at a concentration of 24.3 ppm is displayed in Figure 3a. The spectral background level of the river water spectrum was ~3000 counts/s (with an integration time of 10 s and a spectral slit-width of 5 cm^{-1}), and the ratio of the Raman intensities to the background was ~1:5.

Seawater from Narragansett Bay was doped with the same dye and its spectrum measured. The water was collected from the Bay during August, doped with the dye, and the spectrum measured on the same day. The spectral background was ~7500 counts/s (with an integration time of 10 s and a spectral slit-width of 5 cm^{-1}), and the ratio of the Raman

intensities to the background was ~1:15. Furthermore, suspended particles occasionally caused "spikes" in the spectrum as they moved through the laser beam. However, a spectrum with a signal-to-noise ratio of ~10 was obtained at a concentration of 444 ppb. Using the criterion of having three bands with a signal-to-noise ratio of >3, we can identify the dye in the seawater and the river water at the 200-ppb level.

The results of this study show that Raman spectrometry is a viable method for detection and identification of chemicals in water when those chemicals exhibit resonance Raman scattering. The increased scattering caused by the resonance effect makes it possible to obtain reasonable spectra even when the spectral background is relatively high as in natural water samples.

LITERATURE CITED

(1) F. B. Bradley and C. A. Frenzel, *Water Res.*, **4**, 125 (1970).
(2) S. F. Baldwin and C. W. Brown, *Water Res.*, **6**, 1601 (1972).
(3) M. Ahmadjian and C. W. Brown, *Environ. Sci. Technol.*, **7**, 452 (1973).
(4) K. M. Cunningham, M. C. Goldberg, and E. R. Weiner, *Anal. Chem.*, **49**, 70 (1977).
(5) G. Braunlich, G. Gamer, and M. S. Petty, *Water Res.*, **7**, 1643 (1973).
(6) C. W. Brown and P. F. Lynch, *J. Food Sci.*, **41**, 1231 (1976).
(7) L. de Galan, "Analytical Spectrometry", Adam Hilger Ltd., London, 1971.

RECEIVED for review April 27, 1977. Accepted October 13, 1977. This research was partially supported by the National Sea Grant Program, National Oceanic and Atmospheric Administration. One of us (L.V.H.) gratefully acknowledges financial support from the State University Center of Antwerp and a N.A.T.O. Research Fellowship.

Analytical Chemistry of Amygdalin

Thomas Cairns,* Jerry E. Froberg, Steve Gonzales, William S. Langham, and John J. Stamp

U.S. Food and Drug Administration, Los Angeles, California 90015

John K. Howie and Donald T. Sawyer

Department of Chemistry, University of California, Riverside, California 92521

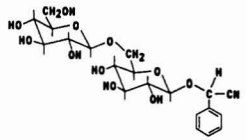
High performance liquid chromatography, carbon-13 nuclear magnetic resonance, chemical ionization mass spectrometry, and gas chromatography with flame ionization detection have been employed for the identification and quantitative determination of the epimers of amygdalin. The results indicate that a combination of techniques is required to understand total sample profiles and the pharmaceutical composition of current drug samples. Notably, injectable preparations of amygdalin are epimeric and below declared concentration, while tablet dosage forms contain epimerically pure (*R*)-amygdalin.

History. Amygdalin (I), a naturally occurring cyanogenetic glycoside (*1*) found in the kernels or seeds of members of the *Rosaceae* (almond, apple, apricot, cherry, peach, pear, plum, quince), was first isolated in 1830 (*2*). Subsequently it was discussed that amygdalin could be hydrolyzed by a nitrogenous enzyme associated with the glycoside in the almond. The hydrolysis product, "oil of bitter almonds", was in fact a mixture of benzaldehyde, hydrocyanic acid, gentiobiose, and glucose (*3*).

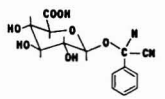
The structural elucidation of amygdalin (I) and various synthetic approaches were first published in 1923/1924 by a number of workers (*2*, *4*, *5*). About ten years later, the biochemistry of amygdalin as well as the physical, chemical, and physiological characterization of the compound and its hydrolysis products, notably HCN, was discussed by Viehoever and Mack (*3*).

Stereochemistry. Amygdalin (I), a gentiobioside of mandelonitrile, contains several chiral (asymmetric) centers which potentially can give rise to a large number of epimeric species. The chiral centers of the gentiobiose moiety, however, are well defined (derived from β-D-glucose) and are stable. The aglycone entity or nonsugar derived chiral center of mandelonitrile is susceptible to epimerization, particularly under basic conditions, because of the weakly acidic character of the benzylic proton. Because these epimers (derivatives of (*R*)- and (*S*)-mandelonitrile) will have different physiochemical properties and possible different pharmacological and toxicological properties, analytical procedures for amygdalin should be capable of their identification and quantitative determination. The naturally occurring amygdalin that is extracted from the kernels and seeds of members of the *Rosaceae* has the *R* configuration.

Laetrile vs. Amygdalin. To avoid any risk of the further proliferation of confusion in nomenclature, amygdalin is not structurally synonymous with Laetrile. Amygdalin (I)



(I)
Amygdalin
$C_{20}H_{27}NO_{11}$
D-mandelonitrile-beta-D-glucoside-6-beta-D-glucoside



(II)
Laetrile
$C_{14}H_{15}NO_7$
l-mandelonitrile-beta-glucuronic acid

is a naturally occurring cyanogenetic glycoside that is present in the kernels of almonds and related fruits. Laetrile (II), according to the patents issued (*6*, *7*) results (a) from hydrolysis of amygdalin and subsequent oxidation of the L-mandelonitrile-β-glucoside product with platinum black, or

0003-2700/78/0350-0317$01.00/0 © 1978 American Chemical Society

Table I. Analysis of Amygdalin-Containing Samples[a]

No.	Sample type	Wt, g	Declared	^{13}C-NMR[b] Found, %			HPLC, Found, %			GC/FID, Found, %		
				R	S	R/S	R	S	R/S	R	S	R/S
1	Tablet	0.86		15	0		14	0		27	0	
2a	Tablet	0.64		72	0		68	0		100	0	
2b		0.65		70	0					72	0	
3	Tablet	0.41		32	0					24	0	
4a	Injectable preparation		3 g/10 mL	26	38	0.70	25	35	0.72	41	54	0.75
4b			3 g/10 mL	28	38	0.73	24	35	0.70	32	43	0.74
5a	Injectable preparation		3 g/10 mL	12	16	0.75	11	19	0.58	9	21	0.43
5b			3 g/10 mL	19	28	0.70	18	27	0.67	26	33	0.78
5c			3 g/10 mL	8	10	0.76	7	11	0.62	14	18	0.77

[a] Analysis made on different lots of same product. [b] Based solely on purity of organic matter assay.

(b) by condensation of mandelonitrile with glucose followed by oxidation, or (c) by condensation of mandelonitrile with glucuronic acid. All attempts to prepare Laetrile (II) by the patented procedures have been unsuccessful (*8*). Recently, however, the synthesis of Laetrile in a one-step procedure by use of a solid phase immobilized glucuronyltransferase has been accomplished (*9*). The failure of the patented synthetic procedures as well as the great expense required to achieve the enzymatic synthesis of Laetrile established that this trade-marked compound exists only in extremely limited quantities. The proponents of Laetrile and the popular press have confused the situation by their use of this name to describe amygdalin (I). Presently, the drug that is offered as an anticancer agent is amygdalin (I).

In this paper, we report analytical protocols for the specific identification and quantitation of amygdalin and its epimers by use of HPLC, ^{13}C-FTNMR, GC/FID, and GCMS.

EXPERIMENTAL

Reagents. (a) *Acetonitrile.* Nanograde. (b) *Ethanol.* 95% and absolute. (c) *Trifluoroacetic Acid Sodium Salt.* Eastman Organic Chemicals, Rochester, N.Y. (d) *Trifluoroacetic Anhydride.* Available from Eastman Organic Chemicals, Rochester, N.Y. (e) *Reaction Mixture.* Trifluoroacetic anhydride was mixed with an equal volume of acetonitrile that contained 10% trifluoroacetic acid, sodium salt. (f) *Petroleum Ether.* Pesticide grade. (g) *Amygdalin.* Aldrich Chemical Co. The material was recrystallized by dissolving 2 g in 100 mL 95% ethanol that was heated to boiling. The resulting solution was filtered twice through a fritted glass filter funnel, prior to its evaporation to 20 mL, and allowed to recrystallize. The resulting trihydrate crystals were then dissolved in 100 mL of boiling absolute ethanol and concentrated to less than 10 mL. After recrystallization, the crystals were dried in a 60 °C vacuum oven for 18 h (mp 215 °C) and stored in a desiccator.

Addition of 1 drop of aqueous ammonia (5 mL concentrated ammonia diluted to 25 mL) to an amygdalin sample solution (0.4 g/5 mL) resulted in an epimeric mixture.

Apparatus. (a) *Gas Chromatograph.* Equipped with a flame ionization detector with (1) a 6 ft × 3.5 mm i.d. glass column packed with 2% OV-101 on CWHP; operating conditions: purified nitrogen flow 60 mL/min; temperatures, column 220 °C, detector 250 °C, injection 220 °C; (2) a 6 ft × 2 mm i.d. glass column packed with 2% F-50 versilube on CWHP; operating conditions: purified nitrogen flow 30 mL/min; temperatures, column 180 °C, detector 300 °C, injector 250 °C.

(b) *Gas Chromatograph–Mass Spectrometer.* Finnigan Model 3300 with Data System 6000 or equivalent. Operating conditions: 5 ft × 2 mm i.d. glass column packed with 3% OV-101 on Chromosorb 750, 100–120 mesh, methane as carrier and reagent gas at 30 mL/min; temperatures, column 220 °C, source 150 °C, injector 250 °C; MS accelerating voltage, 150 V; MS inlet pressure, 1 Torr.

(c) *^{13}C-Nuclear Magnetic Resonance Spectrometer.* ^{13}C-NMR spectra were recorded on a Bruker WH-90 pulsed Fourier Transform multinuclear NMR spectrometer or equivalent equipped with quadrature phase detection. The spectrometer was internally locked on the deuterium resonance of the solvent, 1:4 (v/v) D_2O:H_2O. The ^{13}C fixed frequency transmitter (22.638 MHz), probe head, and preamp were used. Two 8K free induction decays (FIDS) were collected at a sweep width of 5000 Hz, yielding an acquisition time of 1.638 s and digital resolution of 0.61 Hz. Satisfactory signal to noise ratio was obtained after 2200 4.5-μs pulses (90° pulse, 13.4 μs); total data collection time, 1 h. Exponential multiplication was performed on the FIDS prior to transformation by use of a line broadening constant of 0.5 Hz.

(d) *Liquid Chromatograph.* A Spectro-Physics Model 3500 or equivalent equipped with 250 × 3 mm i.d. 10-μm spherisorb ODS column and UV detector at 254 nm was used at ambient temperature. Operating conditions: (a) for the quantitative determination of the *R* form and to screen samples for epimers, solvent 4% CH_3CN/H_2O, flow rate 1.6 mL/min; (b) for the quantitative determination of *R* and *S* forms, solvent 0.2% CH_3CN/H_2O, flow rate 1.2 mL/min.

Sample Preparation. (a) *Injectable Preparations.* A quantity of sample equivalent to 10–30 mg amygdalin was diluted with distilled water for HPLC determination or derivatized for GC determination (*10*).

(b) *Tablets and Powders.* A sample equivalent to 10–30 mg of Amygdalin was weighed and diluted with distilled water prior to filtration through 0.45-μm Millipore filter for HPLC determination. For GC analysis, the diluted sample was extracted according to the procedure in the following paragraph.

(c) *Fatty Products.* Samples were ground to pass through a 30-mesh sieve, then weighed and extracted twice with 100 mL of petroleum ether. Sufficient sample was used to yield 10–30 mg of amygdalin. The solid portion was filtered with a glass fritted funnel and then extracted twice with 60-mL portions of boiling 95% ethanol, boiling gently for 2–3 min each time. The resulting solution was filtered through a glass fritted funnel and then evaporated to near dryness with the aid of vacuum and a heat source. With the aid of two portions of absolute ethanol, the product was recrystallized. The concentrations were adjusted to allow amounts injected within the linear range between 400 to 2000 ng for both HPLC and GC.

RESULTS

A representative sampling of amygdalin tablets and injectables that currently are manufactured in Mexico has been examined by a combination of techniques—HPLC, GC/FID, GCMS, and ^{13}C-NMR (Table I).

Gas Chromatography. Because amygdalin has gentiobiose as the parent glycoside, the present investigation has utilized the technique of trifluoroacetic acid derivatization (TFA) for GC analysis as previously suggested for mono- and disaccharides in cocoa products (*10*). Methodology has been developed for the extraction and clean-up of amygdalin from food products, tablets, and injectables. The increased volatility of TFA–amygdalin relative to the corresponding TMS derivative is noteworthy. On a nonpolar column such as OV-101

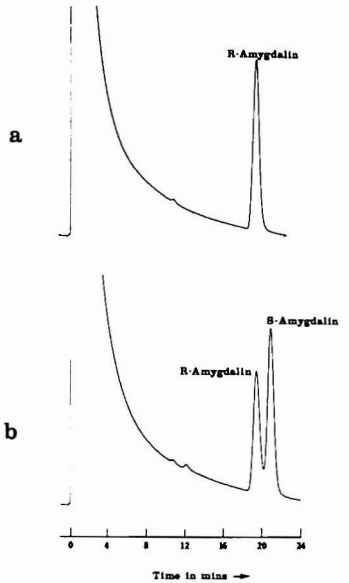


Figure 1. GC separation of TFA derivatives of (*R*)- and (*S*)-amygdalin: (a) tablet, (b) injectable preparation. GC conditions: 6 ft × 2 mm i.d. 2% versilube F-50 column, 30 mL/min N_2, 180 °C isothermal

TFA–amygdalin chromatographs in about 3.75 min at 220 °C as compared to 5 min at 280 °C for the TMS–amygdalin (*11*). However, separation of the epimers of amygdalin could not be achieved on OV-101 by use of TFA derivatives. Nahrstedt (*11*) has reported a partial separation of (*R*)- and (*S*)-amygdalin (as their TMS derivatives) on both OV-1 and OV-17. In an attempt to resolve the epimers as their TFA derivatives, conditions have been optimized for the OV-210 stationary phase. A partial separation has been achieved, but the experimental conditions caused both column bleed and decomposition of the TFA derivatives. Subsequently, a 2% F-50 (G.E. versilube, 10% trichlorophenyl:methyl silicone) column has proved to be effective for the separation of the amygdalin epimers as their TFA derivatives (Figure 1). The McReynold's constant (*12*) for versilube F-50 is about the same as OV-101 (229 and 240 respectively) while that of OV-210 is 1520. Hence, the effectiveness of F-50 for the epimeric separation is surprising in view of the failure of OV-101 to resolve the peaks. The success of F-50 must be due to a specific interaction of the TFA groups with the trichlorophenyl entity of the stationary phase.

Gas Chromatography–Mass Spectrometry. In an attempt to establish the identity of the TFA derivative of amygdalin, GC-MS has been employed. Figure 2 illustrates the separation of the mono- and disaccharides (apparently present in original samples) from amygdalin in various products. The elution time of TFA–amygdalin relative to the other sugars indicates that amygdalin can be derivatized intact and chromatographed as such. The observance of the parent ion for derivatized amygdalin (1129 amu) with chemical ionization has not been possible because the mass spectrometer system has a limit of 1000 amu. However, the presence of abundant ions at *m/e* 319, 547, 769, and 883 indicates that the derivatized amygdalin is an intact species. The gas chromatographic and GC-MS studies provide convincing

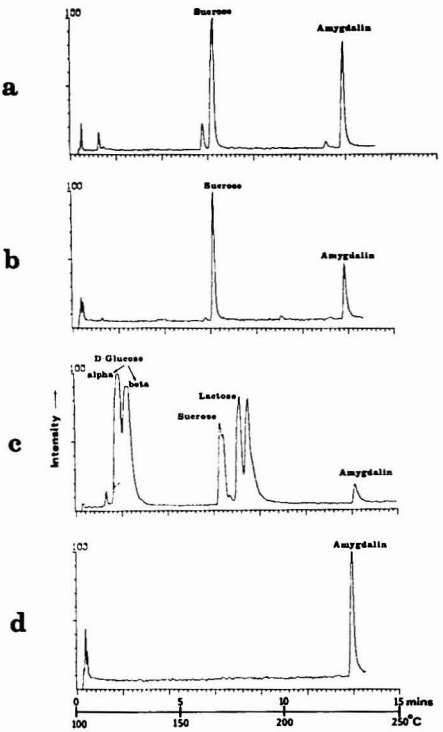


Figure 2. GCMS Total Ion Chromatograms of TFA-derivatized extracts of (a) apricot kernels, (b) a commercial standard, (c) a health food supplement, and (d) an injectable solution from Mexico. GC conditions: 5 ft × 2 mm i.d. 3% OV-101 column, 30 mL/min methane, and temperature programmed. MS conditions: acceleration voltage, 150 V; inlet pressure, 1 Torr

evidence that the TFA derivative of amygdalin is totally derivatized and is chromatographically separated intact. Furthermore, the mass spectra of the TFA derivatives of the two epimers are identical. The four major ion peaks are characteristic of derivatized amygdalin and can be used for a quantitative assay procedure by the multiple ion detection technique (Figure 3).

^{13}C-Nuclear Magnetic Resonance. The ^{1}H-NMR spectra of a large number of cyanogenetic glycosides, including amygdalin, have been previously reported (*13*). Proton NMR provides evidence of the presence of epimers by two distinctly different methine chemical shift values (6.00 ppm for (*R*)-amygdalin and 6.09 ppm for (*S*)-amygdalin) for the benzylic proton attached to the chiral aglycone carbon atom. The second resonance results when (*R*)-amygdalin is epimerized by base-catalysis (*14*). To reinforce this conclusion and to obtain absolute and unambiguous proof of the presence of both (*R*)- and (*S*)-amygdalin in base extracted materials, ^{13}C-NMR experiments have been conducted on the nine representative samples already analyzed by GC/FID and GCMS (Table I). Figure 4 illustrates the salient features discovered in a comparison study between (*R*)-amygdalin and an epimeric mixture. Natural abundance broad-band proton-decoupled ^{13}C-NMR spectra of amygdalin (0.4 g/5 mL), of epimerized amygdalin (0.4 g/5 mL), and of a Mexican pharmaceutical

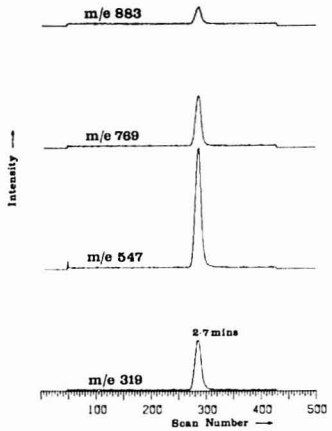


Figure 3. GC-MS Multiple Ion Detection chromatograms of (R)-amygdalin. GC conditions: 5 ft × 2 mm i.d. 3% OV-101 column, 30 mL/min methane, 220 °C isothermal. MS conditions: acceleration voltage, 150 V; inlet pressure, 1 Torr

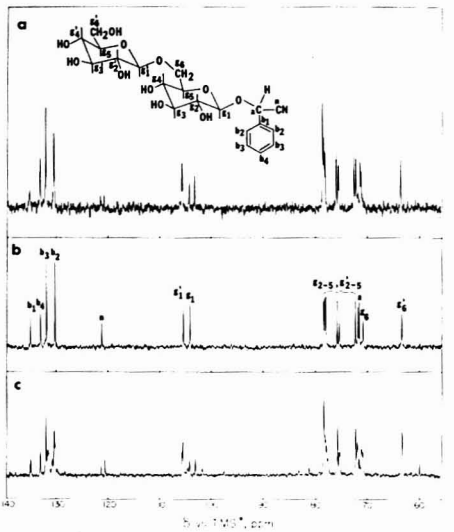


Figure 4. ^{13}C-NMR spectra of (a) Aldrich amygdalin standard, base epimerized with ammonia, (b) Aldrich amygdalin standard, and (c) Mexican injectable sample of amygdalin

sample of an aqueous solution of "amygdalin" (0.8 g/5 mL) are illustrated in Figure 4. Off-resonance continuous-wave decoupling experiments cause the carbon resonances that are labeled b_1 and n to remain singlets; carbon resonances g_6 and g_6' to become triplets; and all the other carbon resonances to split into doublets. When the epimerization experiment is repeated with pure D_2O as the solvent, the acidic hydrogen atom at the carbon labeled a is exchanged for a deuterium atom. This causes the ^{13}C resonance of this carbon to have a substantial decrease in intensity (less Nuclear Overhauser Effect). The ^{13}C spectrum of the Mexican "amygdalin" sample clearly shows that the material is not pure. Epimerization has occurred at some stage of the processing. Based on the relative intensities of the nitrile resonances (*R* epimer to the sum of *R* and *S* epimers), only 37% of the amygdalin present in the sample is the *R* epimer. Some of the additional aromatic resonances present in the Mexican sample may be due to a paraben added to the material as an antioxidant. Others, however, are apparently due to further base-catalyzed decomposition of the starting material. When Reagent Grade amygdalin is epimerized with an excess of ammonia (five times that used for the spectrum illustrated in Figure 4), several new aromatic resonances are observed within 3 h. A spectrum that is recorded after such an exposure to ammonia exhibits aromatic resonances virtually identical to those of the Mexican sample. The exact nature of this decomposition product is not known, but the decomposition reaction may involve a base-catalyzed hydrolysis of the nitrile group. On the basis of the total ^{13}C spectrum of the Mexican sample, the maximum purity (in terms of carbon content) is 87% (*R*)- and (*S*)-amygdalin. Hence, the net assay for the sample is only 32% (*R*)-amygdalin.

Assignment of the Resonances. The off resonance decoupling experiments indicate that the carbon resonances labeled b_1 and n come from carbon atoms to which no protons are bound. The chemical shifts establish that the b_1 resonance is due to carbon-1 of the phenyl ring and that the n resonance results from the nitrile carbon. Resonances g_6 and g_6' are due to the methylene carbons of the glucose rings. The assignment of the downfield resonances to the g ring is based on the magnitude of the differences in chemical shifts between the *R* and *S* epimer when some of the *S* epimer is generated in the presence of base. This is based on the rationalization that the closer a given carbon atom is to the asymmetric carbon labeled a, the greater the magnitude of the chemical shift difference between the *R* and *S* epimers. The assignments of the other carbon resonances of the sugar rings and the aromatic ring have been made on the same basis. The assignment of the carbon resonance labeled a is based on the differences in intensity of these resonances in the H_2O and D_2O epimerization experiments. Substitution of a deuterium atom for the hydrogen atom in carbon a causes a decrease in the intensity of the resonance in the broad-band proton-decoupled spectrum because of the lack of the proton-induced Nuclear Overhauser Effect.

Optical Purity. The carbon-13 spectrum of the recrystallized Reagent Grade amygdalin confirms that the compound is free of organic impurities. All of the 18 different types of carbon atoms display distinct resonances. This spectrum, viewed in conjunction with the epimerized spectrum, demonstrates that the material is isomerically pure as well. The large chemical shift differences for many of the resonances between the *R* and *S* epimers is remarkable and clearly demonstrates the ability of ^{13}C-NMR to distinguish isomers in compounds with more than one asymmetric center (*15*). The inequality of ^{13}C environments between the epimers is even experienced by carbon atoms of the glucose ring far from the asymmetric carbon a.

High Performance Liquid Chromatography. Because of the demonstrated differences in physical properties exhibited by the epimers of amygdalin, the possibility of their separation by HPLC is attractive because sample preparation would be limited to dissolution in water for tablet preparations and dilution for injectable preparations. By use of a reverse phase column technique with 4% CH_3CN/H_2O solvent mixture at a flow rate of 1.6 mL/min, partial separation of the epimers is observed (Figure 5). These conditions provide a convenient screening technique for suspected amygdalin samples and can be used to determine the total amygdalin content (*R* + *S* epimers). To determine (*R*)- and (*S*)-am-

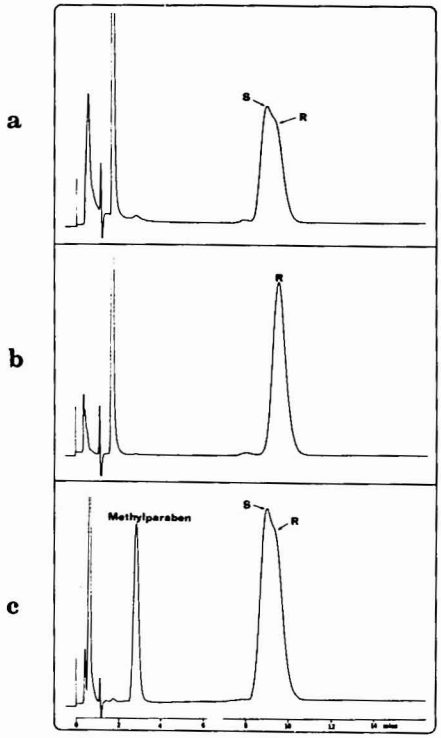


Figure 5. HPLC chromatograms of (a) Aldrich amygdalin standard, base epimerized with ammonia, showing R and S epimers. (b) Aldrich (R)-amygdalin standard, and (c) Mexican injectable sample of amygdalin showing R and S epimers. LC conditions: 25 cm × 3 mm i.d. ODS column 4% CH_3CN/H_2O mobile phase; flow rate, 1.6 mL/min

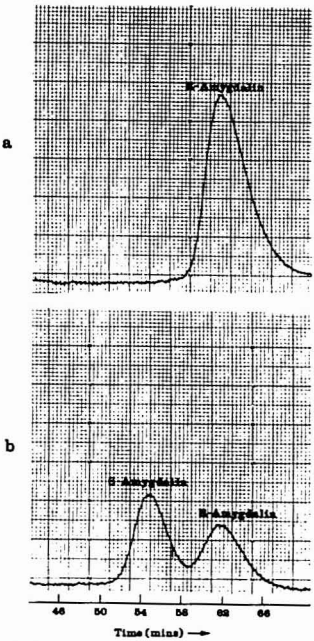


Figure 6. HPLC chromatograms illustrating the separation achieved for (R)- and (S)-amygdalin: (a) tablet, (b) injectable. LC conditions: 25 cm × 3 mm i.d. ODS column; 0.2% CH_3CN/H_2O mobile phase; flow rate, 1.2 mL/min

ygdalin as separate entities, the solvent system has to be adjusted (0.2% CH_3CN/H_2O) and the flow rate reduced (1.2 mL/min). For such conditions, the epimeric pair is completely resolved in about 60 min and both forms can be determined quantitatively by use of (R)-amygdalin as a standard (Figure 6). This use of one standard to determine both epimeric forms has been made on the basis that both epimers are equally responsive to the UV detector that has been employed. Indeed, the ratio of R/S found agrees well with that observed by the other two quantitative techniques (Table I).

DISCUSSION AND CONCLUSIONS

Because of the presence of epimeric forms of amygdalin, any deliberately designed analytical procedure for quantitation must relate to a stereochemical assay. The epimeric equilibrium that is indicated by the samples in Table I appears to have a mean ratio value of 42% (R)-amygdalin to 58% (S)-amygdalin. The best data for these ratios are provided by HPLC because the ^{13}C-NMR results can suffer from counting errors. In particular, the low ratio reported for sample No. 5 is the result of an insufficient number of scans for accurate spectral summation and quantitation. However, the analytical results support the conclusion that an epimeric equilibration occurs in alkaline solutions. Interestingly, all of the solid dosage forms in Table I contain only (R)-amygdalin while the injectable preparations contain epimeric mixtures close to the apparent equilibrium constant. Depending on the information required (qualitative vs. quantitative) a number of salient features should be emphasized.

Qualitative Assay. Each of the techniques that have been employed has some advantages in relation to the sample composition. The ^{13}C-NMR techniques, beyond establishing the presence and assay of the epimers of amygdalin, can detect other organic impurities, additives, and decomposition products. The organic assay results listed in Table I indicate that in the tablets and injectable preparations other organic materials are sometimes present. The HPLC technique can provide a rapid screening of samples for epimeric purity without a great deal of sample preparation. Other UV detectable molecules may also be detected such as methylparaben (Figure 5). With regard to analysis by GC/FID and GCMS, the derivatization procedure can provide quick identification of amygdalin and detection of other extractable saccharides present (Figure 2).

Quantitative Assay. The prime choice of methodology for the quantitative determination of the epimers of amygdalin is HPLC, based on the ease of sample preparation and speed of analysis. The screening procedure developed can quickly answer (in about 10 min) the question of epimeric purity and provide quantitation of (R)-amygdalin (assuming only the R form is present) or total amygdalin ($R + S$) present (if epimeric). Separation and quantitation of the epimers as individual entities can be achieved by a change in the solvent system and flow rate. The carbon-13 method provides an elegant technique to determine the presence of epimers and to obtain a semiquantitative assay of organic purity. It also can sense the presence of any carbon-containing impurities

and provide the means to their identification. Both HPLC and ^{13}C-NMR have proved to be valuable quantitative techniques in dealing with aqueous solutions of amygdalin. These techniques avoid the derivatization procedures that are required for the GC/FID and GC-MS methods and provide a distinct advantage for the analysis of injectable preparations of amygdalin. Although thermal epimerization has not been observed when derivatization procedures are used, analysis of aqueous solutions by HPLC and ^{13}C-NMR avoid the risk of induced epimerization. The major utility of the GC/FID and GC-MS techniques for the quantitative determination of amygdalin and its epimers is for those situations where HPLC is not available to the analyst. The correlation between the various techniques firmly establishes each as an independent analytical method for the qualitative and quantitative determination of amygdalin.

ACKNOWLEDGMENT

The authors are grateful to Milton A. Luke and Gregory M. Doose for their helpful suggestions and laboratory assistance. The authors also express their thanks to Roselyn Erneta of the U.S. Customs for the amygdalin samples.

LITERATURE CITED

(1) E. E. Conn, *J. Agric. Food Chem.*, **17**, 519 (1969).
(2) "The Merck Index", 9th ed., (1976), p 81.
(3) A. Viehoever and H. Mack, *Am. J. Pharm.*, **107**, 397 (1935).
(4) W. N. Haworth and Wylam, *J. Chem. Soc.*, **123**, 3120 (1923).
(5) C. S. Hudson, *J. Am. Chem. Soc.*, **46**, 483 (1924).
(6) E. T. Krebs and E. T. Krebs, Jr., U.S. Patent Office, No. 2,985,664 (1961).
(7) E. T. Krebs and E. T. Krebs, Jr., Br. patent, 788,855 (1958).
(8) W. Benson, FDA Bureau of Drugs, 200 C Street, S.W., Washington, D.C. 20204, private communication.
(9) C. Fenselau, Department of Pharmacology and Experimental Therapeutics, The Johns Hopkins University, Baltimore, Md. 21205, private communications.
(10) M. A. Luke, *J. Assoc. Off. Anal. Chem.*, **54**, 937 (1971).
(11) A. Nahrstedt, *J. Chromatogr.*, **50**, 518 (1970).
(12) W. O. McReynolds, *J. Chromatogr. Sci.*, **8**, 685 (1970).
(13) D. S. Seigler, *Phytochemistry*, **14**, 9 (1975).
(14) J. W. Turczan, FDA New York District Laboratory, 850 Third Avenue, Brooklyn, N.Y. 11232, private communications.
(15) J. I. Kroschwitz, M. Winokur, H. J. Reich, and J. D. Roberts., *J. Am. Chem. Soc.*, **91**, 5927 (1969).

RECEIVED for review July 27, 1977. Accepted November 11, 1977.

Ionic Interference in the Determination of Arsenic in Water by the Silver Diethyldithiocarbamate Method

Shingara S. Sandhu*

Claflin College, Orangeburg, South Carolina 29115

Peter Nelson

South Carolina State College, Orangeburg, South Carolina 29117

The extent of ionic interference in the use of the standard silver diethyldithiocarbamate (SDDC) method for arsenic determination in water and waste water is quantitatively evaluated. The absorbance peak at 410 nm is assigned to the formation of a hydrogen–SDDC rather than a chromium–SDDC complex. The SDDC method provides reliable data for arsenic, even in fairly polluted water and its recovery up to 0.5 μg (0.01 mg L^{-1}) from such waters is quantitative. Antimony and mercury interfere with arsenic color development by yielding complexes, with maximum absorbance at 510 and 425 nm, respectively. Recovery of arsenic, released on digesting standard solutions of natural water as well as cacodylic acid, (sodium salt) is also quantitative.

Arsenic is widely distributed in the human environment and any sample of water, if analyzed by a suitably sensitive method, will be found to contain at least a small quantity of arsenic (*1*). The U.S. Public Health Service recommends that arsenic concentration in drinking water should not exceed 0.01 mg L^{-1} and that water with an arsenic concentration greater than 0.05 mg L^{-1} should be rejected for human consumption (*2*). The arsenic concentration of potable water is generally less than 0.005 mg L^{-1} although a concentration as high as 0.1 mg L^{-1} has been reported (*3*). Arsenic is a suspected carcinogen (*3*); consequently, there is growing interest in arsenic contamination of the environment.

Several methods (*4–13*) are available for the determination of arsenic but silver diethyldithiocarbamate (SDDC) (*10*) is the only recommended method for the separation and quantitative determination of arsenic in water samples. This method consists of reducing inorganic arsenic in a water sample by acid zinc reaction to arsine (AsH_3) which is scrubbed through lead acetate impregnated glass wool and is absorbed in silver diethyldithiocarbamate dissolved in pyridine. The color developed due to the arsine (AsH_3) silver diethyldithiocarbamate reaction is photometrically measured at 535 nm. Conflicting reports (*12*, *14*) have been published on the role of chromium as an interfering ion in the standard method. Though chromium supresses arsine generation (*10*), a color enhancement ascribed to chromium interference in the determination of arsenic by the SDDC method was observed. The authors (*14*) speculated that the chromium–SDDC complex was responsible for the absorbance peak at 410 nm. Certain other metals—cobalt, copper, mercury, molybdenum, nickel, platinum, and silver—have also been reported to interfere in the generation of arsine (*10*) but their limits of interference have not been thoroughly investigated. It has been indicated that the presence of antimony in a water sample interferes in the development and photometric measurement of the SDDC–arsenic complex color (*10*), but a recent report indicates that antimony concentrations up to 0.2 mg L^{-1} do not show any significant interference. This

0003-2700/78/0350-0322$01.00/0 © 1978 American Chemical Society

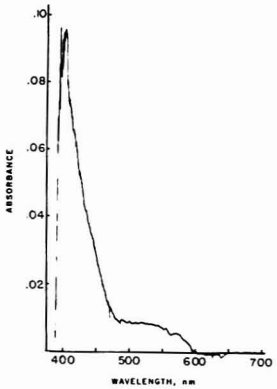


Figure 1. Absorbance spectrum of a reagent blank recorded vs. a SDDC solution as reference

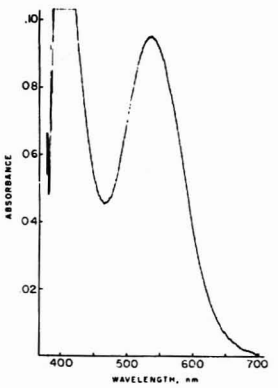


Figure 2. Absorbance spectrum of 2 μg of arsenic alone and in combination with 1 mg L^{-1} each of Cr(VI), Co(II), Cu(II), Mo(VI), and Ni(II) recorded vs. a SDDC solution as reference

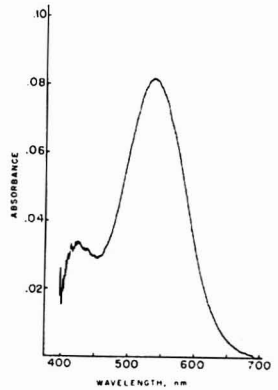


Figure 3. Absorbance spectrum of 2 μg of arsenic alone and in combination with 1 mg L^{-1} each of Cr(VI), Co(II), Cu(II), Mo(VI), and Ni(II) recorded vs. a reagent blank as reference

article presents data to resolve the confusion that surrounds the use of the SDDC method for the determination of arsenic in water and waste water.

EXPERIMENTAL

Apparatus. The generator and absorber assembly have been previously described (*10*) and were purchased from Fisher Scientific (Catalogue No. 1-405). A Beckman Model 24/25, double-beam scanning spectrophotometer with 1-cm cells, equipped with a digital read out system and a strip chart recorder, was used for spectrum study and absorbance measurements.

Materials. The stock solutions for arsenic (III), arsenic(V), chromium, cobalt, copper, mercury, molybdenum, nickel, phosphate, and antimony containing 1 g L^{-1} of ionic concentration were prepared from arsenic trioxide (As_2O_3), sodium arsenate ($Na_2HAsO_4{\cdot}7H_2O$), potassium chromate (K_2CrO_4), cobalt chloride ($CoCl_2{\cdot}6H_2O$), copper nitrate ($Cu(NO_3)_2{\cdot}3H_2O$), mercury(II) chloride ($HgCl_2$), ammonium molybdate ($(NH_4)_6Mo_7O_{24}{\cdot}4H_2O$), nickel nitrate ($Ni(NO_3)_2$), potassium dihydrogen phosphate (KH_2PO_4) and antimony trichloride ($SbCl_3$) respectively. Intermediate solutions were prepared by diluting the stock solutions 1:10, and working solutions containing requisite concentrations of various ions were obtained by diluting the intermediate solutions. Analytical grade reagents were used.

Procedure. The procedure adopted for the present study is similar to the one given for the standard method (*10*) except that a 50-mL water sample is used which requires the use of 7.5 mL of concentrated hydrochloric acid, 2.0 mL of potassium iodide and 0.5 mL of stannous chloride in hydrochloric acid. The reaction is allowed to proceed for 15 min at room temperature, following the addition of 3.0 g of zinc, after which the generator is transferred to a water bath at about 50 °C for another 15 min. The solutions, from the absorber tubes, are poured directly into a 1-cm cell and scanned for a complete absorbance spectrum (700–350 nm), using a SDDC solution and a reagent blank (SDDC solution treated in the absorber tube similar to the experimental procedure but without arsenic) as references. Though the concentration of arsenic(III) as well as arsenic(V) in the prepared standards and river water is maintained at 2.0 μg or less per 50 mL of sample (0.04 mg L^{-1} or less), the amount of interfering ions is varied up to 350 μg per 50 mL (7.0 mg L^{-1}). An absorbance calibration curve using 0.0, 1.0, 2.0, 4.0, and 5.0 μg of arsenic was prepared.

RESULTS AND DISCUSSION

Complete absorbance spectra for a reagent blank, arsenic(III), and arsenic(III) in combination with chromium(VI), cobalt(II), copper(II), molybdenum(VI), and nickel(II), each at 1 mg L^{-1} level (total interfering ionic concentration 5.0 mg L^{-1}), vs. an SDDC solution, as reference, are given in Figures 1 and 2, respectively. Each spectrum shows an absorbance peak around 410 nm which disappears, or is considerably reduced, (Figure 3) when the same absorbance is recorded vs. a reagent blank.

An absorbance peak at 410 nm similar to Figures 1 or 2 is seen in all observations, no matter which one of the numerous interfering ions is used in the generator, either alone, or in combination with arsenic, if the absorbance of the SDDC complex developed in the absorber tube is read vs. a SDDC solution rather than vs. a reagent blank. Although no mechanism for the transport of chromium from the arsine generator to the absorber, which contains SDDC solution, was suggested, the absorbance peak at 410 nm was speculated to be due to the formation of a chromium diethyldithiocarbamate complex (*14*). The information presented here (Figures 1–3) does not substantiate the previous report (*14*), but rather demonstrates that none of the interfering ions is responsible for the absorbance peak at 410 nm. The absorbance peak at 410 nm is observed even when the generator has nothing in it except the deionized water, hydrochloric acid, and zinc. The addition of stannous chloride alone or in combination with

Table I. Recovery of Various Forms of Arsenic from Demineralized and River Waters, Concentration mg L^{-1}

	Demineralized water			River water		
Theoretical	Determined[a]	Recovery, %	Std dev	Determined[b]	Recovery, %	Std dev
			As(III)			
0.01	0.0102	102	5.7	...	...	...
0.02	0.0196	98	4.3	0.0214	107	5.6
0.04	0.0410	102	3.4	0.043	108	4.5
			As(V)			
0.01	0.0100	100	5.8	...	...	...
0.02	0.0208	104	4.9	...	...	...
0.04	0.0395	99	4.0	...	...	...
			As(III) + As(V) (50:50)			
0.01	0.0095	95	5.6	...	...	...
0.02	0.0201	100	3.1	...	...	...
0.04	0.0405	101	3.5	0.044	109	5.8

[a] Mean of 35 determinations. [b] Mean of 20 determinations.

potassium iodide does not change the nature of this absorbance peak in any way.

Accordingly, it is suggested that the absorbance at 410 nm is due to the reaction of hydrogen (generated by the acid zinc interaction) with SDDC reagent. It is further observed that the presence of arsenic in the generator, alone or in combination with the other ions, remarkably increases the peak height at 410 nm over reagent blank or interfering ions alone (Figures 1 and 2). It is speculated that during the reaction of arsine (AsH_3) with SDDC, a certain amount of additional atomic hydrogen becomes available for simultaneous combination with SDDC, resulting in the formation of the additional hydrogen SDDC complex responsible for increased absorbance at 410 nm.

$$\text{SDDC} + AsH_3 \rightarrow \text{SDDC-Arsenic complex} + \text{SDDC-Hydrogen complex}$$

The peak at 410 nm is not precisely reproducible (±30%), and is seen to be preferentially destroyed over the arsenic–SDDC complex peak of 535 nm. The arsenic–SDDC complex is developed as described in the procedure and the absorbance spectrum is recorded. The solution is poured back into the absorber tube and concentrated hydrochloric acid is added, a drop at a time, to the solution in the absorber tube and the absorbance spectrum is taken again. This is repeated until the peak at 410 nm disappears. Molarity of hydrochloric acid, calculated from the volume of acid added, when plotted vs. the change in absorbance at 410 nm, shows a negative linear relation, whereas the absorbance at 535 nm, except for a minor dilution effect, remains the same. The instability of the complex, responsible for absorbance at 410 nm, is an additional indication that a hydrogen–SDDC complex rather than a metal–SDDC complex is probably responsible for an absorbance peak at 410 nm.

The single ion absorbance spectra for Cr(VI), Co(II), Cu(II), Mo(VI), and Ni(II) are not different from the reagent blank spectrum and do not show any noticeable peak within 700 to 350 nm, if the readings are taken vs. a reagent blank. Therefore, it appears that these ions should not show any positive interference, as suggested previously (*14*), in the evaluation of arsenic by the standard method. However, if the absorbance spectrum of the complex formed in the absorber tube is recorded, using a SDDC solution instead of a reagent blank as reference, a large absorbance peak at about 410 nm is noticed, which causes the elevation of the baseline (Figures 1 and 2), leading to an inaccurately high arsenic estimate (about 10%) for a given water sample.

The water samples containing 0.30 mg L^{-1} of antimony and 2.0 mg L^{-1} of mercury show absorbance peaks at 510 nm (average absorbance 0.007) and 425 nm (average absorbance 0.005) respectively, thus these ions are expected to interfere positively in the determination of arsenic by the standard method. Possible positive interference by antimony has been suggested in the past (*10*) but similar interferences by mercury have not been reported. Ionic mercury reacts with stannous chloride in hydrochloric acid to produce metal mercury (*15*).

$$2Hg^{2+} + SnCl_2 + 2Cl^- \rightarrow Hg_2^{2+} + SnCl_4$$

$$Hg_2^{2+} + SnCl_2 + 2Cl^- \rightarrow 2Hg^0 + SnCl_4$$

There is a distinct possibility that mercury vapors are carried over from the generator to the absorber tube containing SDDC reagent, resulting in the formation of a mercury–SDDC complex, responsible for an absorbance peak at 425 nm.

The amount of arsenic recovered from demineralized water is quantitative up to an arsenic concentration of 0.5 μg or 0.01 mg L^{-1} (Table I). Arsenic recovery from demineralized water in the presence of various interfering single ions is presented in Table II. This information suggests that the recovery of arsenic is not affected in the presence of chromium(VI), cobalt(II), copper(II), molybdenum(VI), nickel(II), nitrate, and phosphate, up to an individual ion concentration of 5.0 mg L^{-1}. But when the single metal ion concentration is increased beyond 5.0 mg L^{-1}, a decrease in arsenic recovery from standard solutions is observed and at the 7.0 mg L^{-1} level, the arsenic recovery decreases by about 10%. Nitrate and phosphate concentrations up to 100 mg L^{-1} do not show any observable effect on the arsenic recovery.

It has been reported (*12*) that antimony concentrations up to 0.2 mg L^{-1} did not produce any observable interference in determining arsenic by the SDDC method. In the present study, antimony concentration of 0.2 mg L^{-1} does not show any significant change in the recovery of arsenic from standard solutions, however, when the antimony concentration is raised to 0.3 mg L^{-1}, the apparent rate of recovery for arsenic increased by about 10%. The location of the arsenic absorbance peak shifts toward 510 nm in the presence of antimony. This shift seems proportional to the amount of antimony present in a solution containing 0.04 mg L^{-1} of arsenic. The mercury concentrations at 1.5 mg L^{-1} and above show a significant positive interference in the recovery of arsenic.

Interference by several ions in combination was studied by preparing standard solutions, containing 0.04 mg L^{-1} of arsenic and varying the concentrations of each ion, chromium(VI), cobalt(II), copper(II), molybdenum(VI), nickel(II), phosphate,

Table II. Recovery of Arsenic from Demineralized and River Water in the Presence of Interfering Ions, Concentration mg L^{-1}

Ions[a] added individually	Demineralized Water			River Water	
	Theoretical	Recovery, %[b]	Std dev	Recovery, %[c]	Std dev
5	0.02	99.6	5.9	107	6.6
5	0.04	98.9	5.7	108	6.5
7	0.04	89.5	4.3	97	8.3
Sb					
0.2	0.04	99.6	4.7		
0.3	0.04	109.3	4.9		
Hg					
1.5	0.04	107.5	4.5		
5.0	0.04	134.2	4.4		
Collectively[c]					
5.6, 0.8 each	0.04	96.2	4.7	103.3	7.2
7.0, 1.0 each	0.04	89.4	4.0	97.1	9.3
Cr(VI) + Co(II)					
3.5 each	0.04	88.2	3.5		
Mo(VI)[d] + Cu(II)					
3.5 each	0.04	90.2	4.2		

[a] Ions used: Co(II), Cr(VI), Cu(II), Mo(VI), NO_3^-, Ni(II) and PO_4^{-3}. [b] Mean of 12 determinations for each system. [c] Mean of 6 determinations for each system. [d] Results for other combinations, not reported here.

and nitrate, up to 1.0 mg L^{-1}. The results on the recovery of arsenic in the presence of a combination of ions are also given in Table II. There is no significant interference by these ions up to a combined concentration of 5.6 mg L^{-1} (0.8 mg L^{-1} each ion) but when the combined concentration is increased above this level, there is an observable decrease in the recovery of arsenic from demineralized water. A combined concentration of 7.0 mg L^{-1} (1.0 mg L^{-1} each ion) decreases the arsenic recovery from standard solutions by about 10%.

A combined concentration of two ions, chromium(VI) and cobalt(II), each at 3.5 mg L^{-1}, decreases the arsenic recovery by about 10%. A molybdenum(VI) and copper(II) combination, as well as the combination of any other two metal ions in this category at a total concentration of 7.0 mg L^{-1}, shows similar results (Table II). It appears that under the present set of experimental conditions, the ionic specificity of the elements that interfere in arsine generation, is not as important as their total concentration in inhibiting the recovery of arsenic from the standard solutions.

The studies were also carried out using natural water from the Edisto River, Orangeburg, S.C., which was spiked with arsenic as well as with interfering ions. Because only inorganic arsenic is reduced to arsine (*10*), a digestion step, as suggested in the literature, using nitric and sulfuric acids (*12*) was tried for the release of organically bound arsenic. Data on the recovery of arsenic using this digestion method are acceptable for standard solutions but the recovery of arsenic, added to the river water, is inconsistent and reproducibility is very poor. Consequently, the potassium permanganate method (*16*) with minor modification is adopted for the digestion of water samples. One-tenth milliliter of 5.0% potassium permanganate, followed by 5.0 mL of concentrated sulfuric and 0.3 mL of nitric acids, is added to 50 mL of water sample, containing at least 1 μg of arsenic. The water sample is placed in a water bath at 35 °C for an hour and the excess of potassium permanganate is destroyed by adding 1.5% hydroxylamine hydrochloride. Hydroxylamine hydrochloride is added a drop at a time to avoid its excess in the generator. The reliability of the potassium permanganate method was further investigated using known concentrations (2 μg and 1 μg of arsenic per 50 mL) of dimethylarsenic acid (cacodylic acid, sodium salt). This method not only gives an acceptable recovery and reproducibility for arsenic in natural water as well as in organoarsenicals (88.8% arsenic recovery for cacodylic acid), but is less laborious than the acid digestion method previously used (*12*). The recovery of arsenic from the river water is greater than the amount added (Tables I and II). The difference approximately equals the amount of arsenic found in the Edisto River.

LITERATURE CITED

(1) H. K. D. Lee, "Metallic Contamination and Human Health", Academic Press, New York, N.Y., 1972.
(2) United States Department of Health, Education and Welfare, Public Health Service, "Drinking Water Standards", Public Health Service Publication No. 956, U.S. Government Printing Office Washington, D.C., 1962.
(3) Subcommittee on Air and Water Pollution of the Committee on Public Works, United States Senate, "Water Pollution" Part 4. United States Senate, Ninety-first Congress, Second Session, U.S. Government Printing Office, Washington, D.C., 1970.
(4) J. C. Caldwell, R. Lishka, and E. McFarren, *J. Am. Water Works Assoc.*, **65**, 73 (1973).
(5) A. L. Chaney and J. M. Harold, *Ind. Eng. Chem., Anal. Ed.*, **12**, 691 (1940).
(6) I. M. Kolthof, and A. Elias, *Ind. Eng. Chem., Anal. Ed.*, **12**, 177 (1940).
(7) D. Liederman, F. E. Brown, and O. I. Milmer, *Anal. Chem.*, **30**, 1543 (1958).
(8) G. W. Powers, *Anal. Chem.*, **31**, 1590 (1959).
(9) D. C. Ballinger, R. J. Lishka, and M. E. Gales, *J. Am. Water Works Assoc.*, **54**, 1424 (1962).
(10) American Public Health Association, American Water Works Association and Water Pollution Control Federation, "Standard Methods for the Examination of Water and Waste Water", 13th ed., American Public Health Association, Washington, D.C., 1971.
(11) K. C. Tam, *Environ. Sci. Technol.*, **8**, 73 (1974).
(12) J. F. Kopp, *Anal. Chem.*, **45**, 1786 (1973).
(13) S. S. Sandhu, *Analyst (London)*, **101**, 856 (1976).
(14) G. C. Whitnack and H. H. Martens, *Science*, **171**, 383 (1971).
(15) A. B. Garret, H. H. Sisler, J. Bonk, and R. C. Stoufer, "Semimicro Qualitative Analysis", 3rd ed., Blaisdell Publishing Company, Waltham, Mass., 1957.
(16) Perkin-Elmer Corporation, "Analytical Method for Atomic Absorption Spectrophotometer, Mercury Analysis System;" 303-3119, Norwalk, Conn., 1972.

RECEIVED for review July 7, 1977. Accepted November 21, 1977. This work is supported by EPA Grant R8041640-10.

Determination of Sulfides and Application to Shale Oil Analysis

Raphael P. D'Alonzo,[1] Alan P. Carpenter, Jr., Sidney Siggia,* and Peter C. Uden

Department of Chemistry, GRC Tower I, University of Massachusetts, Amherst, Massachusetts 01003

Organic sulfides are oxidized to the corresponding sulfoxide using aqueous sodium metaperiodate. Simultaneously the periodate is reduced to iodate which can be quantitatively precipitated by the addition of silver ion in nitric acid. The precipitate is filtered and dissolved in ammonium hydroxide, and the resulting solution analyzed for its silver content by atomic absorption spectrometry. Sodium metaperiodate is shown to be a good reagent which oxidizes the sulfide completely to the sulfoxide without any further oxidation to sulfone. The sensitivity of the method is greater than or equal to most existing methods. Selectivity is good; however, compounds such as thiols and diols which are also oxidized will interfere. Also, compounds in the sample which reduce silver ion will cause high results. The precision of the method is ±2.0–4.0% over a range of 1.0–5.0 μmol/mL of sulfide. The method has been applied to the determination of nonpolar organic sulfides in Green River shale oil.

The goal of this work was to first develop a general method for the determination of organic sulfides with high selectivity and, second, to modify the procedure for sulfide quantitation in shale oil. Past procedures for sulfide analysis have depended heavily upon both chemical and instrumental methods with a strong emphasis on oxidative approaches.

The determination of thioethers employing oxidation with bromine has been accomplished using a variety of oxidizing reagents such as: bromine water (*1*), bromate–bromide mixture (*2*), and electrically generated bromine (*3*). The end point can be determined amperometrically, potentiometrically, iodometrically, or by the color of bromine. These reagents react with the sulfide to produce the corresponding sulfoxide.

$$\text{R-S-R}' + \text{Br}_2 + \text{H}_2\text{O} \rightarrow \text{R-SO-R}' + 2\text{HBr} \quad (1)$$

However, it has been shown (*4*) that bromine oxidations often lead to high results, since some sulfoxide may further oxidize to the corresponding sulfone.

$$\text{R-SO-R}' + \text{Br}_2 + \text{H}_2\text{O} \rightarrow \text{R-SO}_2\text{-R}' + 2\text{HBr} \quad (2)$$

Since oxidation to the sulfone is seldom complete, stoichiometry is indefinite.

A microchemical method based on bromine oxidation was described by Belcher and co-workers (*5*). Direct titration on small samples (about 50 μg) was accomplished employing 0.02 N $KBrO_3$. However, some problems with overoxidation were also reported.

Oxidation of thioethers with hypochlorite has been reported by Leutch (*6*). This method employs a 0.1 N sodium hypochlorite solution but more dilute hypochlorite solutions were found to rapidly deteriorate. Thus, difficulties were encountered when adapting the method to the micro scale.

Lewin (*7*) presented a macro method for the assay of organic sulfides using perbenzoic acid as the oxidizing reagent.

$$\text{R-S-R}' + 2\text{C}_7\text{H}_6\text{O}_3 \rightarrow \text{R-SO}_2\text{-R}' + 2\text{C}_7\text{H}_6\text{O}_2 \quad (3)$$

Perbenzoic acid is a strong oxidizing agent, oxidizing the sulfide to the sulfone; thus, any intermediate sulfoxide present will interfere. In this procedure, a measured amount of perbenzoic acid is used, and the excess peroxide is determined iodometrically after oxidation is complete. Once again, this method was not found to be suitable as a micro method, because of the instability of dilute perbenzoic acid solutions.

Puchalsky (*8*) describes a method for the analysis of organic sulfides by titration of their hydrogen peroxide-formed sulfoxides. Sulfides are treated with hydrogen peroxide in acetic acid at room temperature to produce the corresponding sulfoxide.

$$\text{R-S-R}' + \text{H}_2\text{O}_2 \xrightarrow{\text{HOAc}} \text{R-SO-R}' + \text{H}_2\text{O} \quad (4)$$

Subsequent potentiometric titration of the formed sulfoxide derivative in acetic anhydride is accomplished using $HClO_4$. Interference due to overoxidation is prevented, since oxidation to the sulfone is sufficiently slow.

The analysis of organic sulfides by column chromatography has been investigated by many authors. For an excellent review of these procedures, see ref. 9.

Many instrumental methods for the assay of thioethers have been described. Some of the more interesting techniques involve UV spectrophotometry, gas chromatography, nuclear magnetic resonance, and isotope exchange.

Iodine interacts with dialkyl sulfides to produce a complex with a strong absorbance maximum at 310 nm (*10*). A spectrometric method, based on the interaction with iodine, for the determination of sulfides in hydrocarbons, has been developed by Hastings (*11*). Hastings has also pointed out the importance of the free iodine–iodine complex equilibrium (*12*), and the necessity of a large excess of iodine in the reagent to force the reaction to the right. This complexation has been used analytically, employing both isooctane (*11*) and carbon tetrachloride (*13*) as the reaction medium.

$$\text{R-S-R}' + \text{I}_2 \rightleftarrows (\text{R-S-R}' \cdot \text{I})^+\text{I}^- \quad (5)$$

The method to be described utilizes atomic absorption spectrometry for the analysis of some selected aliphatic and aromatic thioethers, as well as potassium penicillin G. An aqueous sodium metaperiodate reagent oxidizes the organic sulfide to the corresponding sulfoxide. The reduced periodate is quantitatively precipitated in the form of silver iodate, which is removed from the reaction mixture by filtration using a fine glass frit filter. After washing to remove excess silver, the filtered silver iodate is dissolved in ammonia, and the resulting solution analyzed for its silver content by means of atomic absorption spectrometry. Sodium metaperiodate is found to be a good reagent to oxidize the sulfide completely to the sulfoxide without any further oxidation to produce sulfone. The reagent, unlike periodic acid, is stable to light. The reaction conditions are mild with quantitative oxidation accomplished at low temperatures (0–25 °C). The general procedure calls for a reaction time of 15 h. The sensitivity of the method is greater than or equal to most existing methods and selectivity is quite good, since many other functional groups such as benzyl, phenyl, and carboxyl do not interfere. The adjacent hydroxyl group is known to interfere, but these groups and sulfides are rarely found in the presence

[1] Present address, Procter and Gamble Company, Winton Hill Technical Center, Cincinnati, Ohio 45224.

0003-2700/78/0350-0326$01.00/0 © 1978 American Chemical Society

of each other. The precision of the method is ±2.0–4.0% over a range of 1.0–5.0 μmol/mL of sulfide.

The refining of petroleum and shale oils by catalytic cracking procedures is adversely affected by the presence of heteroatom compounds. In particular, the problems due to the presence of sulfur compounds in petroleum oils and the need to study their structure has been discussed (*14*). This difficulty is also common to the refining of crude shale oils because of the presence of sulfur compounds. For example, one of the potentially most useful sources of oil, the Green River oil shale deposit, yields oil with sulfur levels between 0.61 to 0.87% (*15*). Green River shale oil sulfur compounds have been determined as being predominately thiophenes and sulfides, with traces of disulfides and mercaptans also present (*16–19*). The absence of more highly oxidized forms of sulfur is due to the pyrolysis conditions present in the production of the shale oil.

The study of sulfide sulfur compounds in petroleum and shale oil distillates has been performed in the past with an emphasis on reactive extraction techniques. Complexation with metal salts (*17, 18, 20*), extraction with strong acids such as HI (*18, 20*) and H_2SO_4 (*21*), and the formation of sulfonium salts using methyl iodide or sodium-*p*-toluenesulfonate (*18, 20*), have all been used as methods to separate sulfides from the oils studied. The sulfides are then regenerated from the salts and recovered by extraction or distillation. The amount of sulfur (from elemental analysis) in each distillate fraction gives an estimation of the amounts of sulfur compounds present (*18*). The limitations of these methods are: the less than quantitative yield obtained in derivatization and regeneration of the sulfides (*18, 20*), the contamination of the extracts of the oil with unsaturates (*18, 20*), and the lack of a suitable method for measuring the total sulfur present (*20*).

In this study, a crude shale oil obtained from The Oil Shale Corporation (TOSCO) was fractionated using a silica gel adsorption column, as has been done in past work (*18, 22–24*). This was done in order to separate the nonpolar sulfur compounds from the bulk of the polar constituents, such as the nitrogen components, which are found in shale oil. This step removed any polar materials which might cause reduction of the silver ion in the precipitation step. The isolation of the aromatic and nonpolar sulfur compounds was followed by reaction with $NaIO_4$. This initial preparative separation in combination with $NaIO_4$ oxidation is quite specific for the determination of neutral organic sulfides in Green River shale oil. A check of the percent recovery of sulfides from the silica column separation procedure was undertaken using standards of butyl sulfide and phenyl sulfide. The quantitative elution of these standards from the adsorption column with a benzene eluent indicates the validity of this procedure.

EXPERIMENTAL

Reagents. *Periodate Reagent.* Sodium metaperiodate (certified ACS) was obtained from Fisher Scientific Company. A 15 μmol/mL solution of this reagent is prepared by dissolving approximately 0.78 g in 250 mL of distilled deionized water. This reagent is reported to be stable (*25*), but was stored in the dark if it was to be used over an extended period of time.

Acid–Silver Reagent. Silver used for precipitation of the iodate formed was prepared by mixing equal volumes of a 3:1 concentrated nitric acid (Baker Analyzed Reagent) solution with 2 M silver nitrate solution. Silver nitrate, 2M, (Fisher) was prepared by dissolving 84.94 g $AgNO_3$ in 250 mL of distilled deionized water. This reagent was stored in the dark for no more than two weeks before use.

Silver Stock Solution for AAS. A stock solution of $AgNO_3$ (Fisher) was prepared according to guidelines given in ref. 26. Standard solutions for calibration were prepared by diluting appropriate aliquots of stock solution in 100-mL volumetric flasks. All silver solutions were protected from light and fresh standards were prepared from the stock weekly.

Standard Sulfide Solutions. Phenyl sulfide (gold label–99+%) was obtained from Aldrich. Butyl sulfide, isobutyl sulfide, hexyl sulfide, benzyl sulfide, L-(−)-methionine, DL-methionine, and *N*-acetyl-DL-methionine were all received from Eastman Kodak Co. A sample of penicillin G potassium salt was obtained from Wyeth Laboratories. This sample was refrigerated to prevent degradation of its β-lactam ring. All sulfides purchased were the purest grades available. Microanalysis for sulfur was carried out on all sulfides as a purity check, percent purities greater than 98% being obtained. Standard sulfide solutions were prepared by weighing out 10–50 mg of the compound, dissolving in either distilled water or 2:1 acetone (Fisher spectro grade)–water solution, and diluting to volume in a 100-mL volumetric flask with the solvent. These solutions were used immediately after preparation.

Apparatus. A Perkin-Elmer 403 Atomic Absorption Spectrophotometer was used to measure all absorbances at 328.1 nm with a single element silver hollow cathode lamp at an operating current of 20 mA. All determinations were made using an air–acetylene flame in accordance with the guidelines given in reference 26. All absorbances measured were an average of 100 readings.

A filtering apparatus consisting of six fine frit (4–5:5 μm) Pyrex glass funnels was used for simultaneous filtering of 1–6 samples. Eppendorf pipets (Brinkmann Instruments) were used to pipet all reagent and sample solutions. A Mettler microbalance was used for weighing all sulfide samples.

Procedure. *General Method.* A 1-mL sample of sufide solution is pipeted into a 50 × 150 mm test tube. The amount of sulfide taken should range between 100 to 500 μg, this corresponding to a concentration of 1–5 μmol/mL for a sulfide of molecular weight 100. One milliliter of reagent sodium metaperiodate solution is added to the sample, and the top of the test tube sealed with parafilm. This provides a 3–15 times molar excess of periodate to sulfide. The test tube is placed on a mechanical shaker and allowed to shake overnight (15 h). After shaking, 1 mL of acid–silver reagent is pipetted into the reaction mixture to precipitate the iodate formed. The test tube is again shaken for an additional 10 min to flocculate the $AgIO_3$ precipitate. The test tube is then placed in a freezer, maintained at −15 °C, for 30–60 min to promote further coagulation and suppress solubility of the $AgIO_3$. The test tube is removed from the freezer and its contents are immediately transferred, with a 3-mL rinse of 1:1 acetone–water (0 °C), to the filtering apparatus. The precipitate is rinsed three times with acetone–water washing portions from the test tube. Each washing portion is allowed to pass completely through the filter before the next portion is added; otherwise, high blank values will result due to incomplete washing of the excess $AgNO_3$. After filtering and washing of the precipitate is completed, clean filter flasks are transferred to the filtering apparatus after rinsing of the filter stems before transfer to prevent any possibility of contamination. Concentrated ammonium hydroxide (5 mL) is added to the test tube and transferred to the filter funnel to dissolve the $AgIO_3$ precipitate. Suction is applied and the filter rinsed with three 15-mL portions of distilled deionized water from the test tube. The suction flask is then removed from the filtering apparatus and its contents are transferred to a clean 100-mL volumetric flask, which is made up to volume with distilled deionized water rinsings from the filter flask. The silver content of the resulting solution is then determined by atomic absorption spectrometry. For further procedural details, see reference 27.

Silica Column Separation of Shale Oil Sulfur Concentrate. A 2–3 g sample of crude shale oil (from TOSCO; Golden, Colo.) is placed on a 2 cm × 25 cm column of silica gel (60–200 mesh, Fisher Scientific) previously activated at approximately 130 °C for 24 h. Hexane (100 mL) is passed through the column to remove the paraffin portion of the oil. Spectrograde benzene, 150 mL, (Fisher Scientific) is then passed through the column and collected, the eluate containing the aromatic and sulfur compounds of the oil (*18*). Other more polar constituents of shale oil, such as oxygen- and nitrogen-containing compounds remain adsorbed on the column during the separation.

Reaction of Sulfides in Shale Oil with $NaIO_4$. The benzene eluent from the silica column preparative separation is divided into three 50-mL volumes and the benzene evaporated to 2–5 mL on a hot plate held at 50 °C. Blanks are prepared using 50 mL of benzene solvent. At this point, the sulfur concentrates and

Table I. Determination of Organic Sulfides by Atomic Absorption Spectrometry

Compound	Concentration, μmol/mL	Micromoles Taken	Micromoles Found	Recovery, %[a]
Butyl sulfide	5.015	5.015	5.145	102.6 ± 3.2 (6)
Isobutyl sulfide	4.476	4.476	4.610	103.0 ± 4.8 (6)
Hexyl sulfide	1.547	1.547	1.524	98.5 ± 4.4 (6)
Phenyl sulfide	3.688	3.688	3.577	97.0 ± 3.2 (6)
Benzyl sulfide	3.207	3.207	3.095	96.5 ± 2.2 (6)
L-(−)-Methionine	2.746	2.746	2.716	98.9 ± 2.2 (6)
DL-Methionine	2.611	2.611	2.663	102.0 ± 2.4 (6)
Potassium penicillin G	1.151	1.151	1.105	96.0 ± 6.0 (5)

[a] Figures in parentheses indicate number of determinations.

Table II. Determination of Total Sulfide in a Mixture

Mixture	Concentration, μmol/mL	Micromoles Taken	Micromoles Found	Recovery, %[a]
Butyl sulfide, 2.5075 μmol, + isobutyl sulfide, 2.2380 μmol	4.7455	4.7455	4.8879	103 ± 1.1 (6)
Hexyl sulfide, 1.739 μmol, + benzyl sulfide, 2.342 μmol	4.081	4.081	4.069	99.7 ± 3.4 (6)

[a] Figures in parentheses indicate number of determinations.

blanks are placed in 125-mL Erlenmeyer flasks and 10 mL of $NaIO_4$ (70 μmol/mL) added with 20 mL of acetone. The flasks are stoppered and shaken on a mechanical shaker for 12–16 h. The H_2O/acetone/benzene layer is then separated from the dark surface oil layer using a separatory funnel and the formed iodate then precipitated by 2 mL of acid–silver reagent. The flasks are then placed in a refrigerator at −10 °C for 30 min. After cooling, the samples are filtered through fine fritted glass funnels and the $AgIO_3$ precipitate is washed three times with 1:1 acetone:H_2O (at 0 °C). The $AgIO_3$ is then dissolved in 10 mL of concentrated ammonia and diluted to a final volume of 100 mL with distilled, deionized water. Blanks are treated in an identical manner. The resulting solutions are analyzed for their silver content by atomic absorption spectrometry.

Standard Addition Method. To each of the 50-mL portions of the benzene eluent from the silica column separation is added 10 mL of 0.22 mg/mL phenyl sulfide in benzene. Each sample is then evaporated down to 2–5 mL volume and treated as described earlier.

Calculations for the level of sulfides present in shale oil by this method assume that the 2.2 mg of phenyl sulfide added is completely reacted. The total equivalents of sulfide found minus the equivalents of sulfide added equals the equivalents of sulfide in the oil sample.

RESULTS AND DISCUSSION

Calibration Curve. Appropriate dilutions of silver nitrate stock solution were used for the construction of a calibration curve. Absorbances were measured at 328.1 nm and were found to be linear over a range of 2–10 ppm Ag. This corresponds to a sulfide concentration range of 1.9–9.2 μmol/mL.

Reaction Conditions and Concentrations. The concentration of reagent periodate and sulfide sample is not critical in this procedure, since quantitative oxidation of the sulfide to the sulfoxide can be accomplished over a large range of concentrations without the production of higher oxidized species, such as sulfones. It is, however, necessary that periodate be in excess, and it should be remembered that more dilute concentrations require longer reaction times. In this procedure, the final concentration of sulfide, after the addition of reagent to sample, was 0.5–2.5 μmol/mL while the final concentration of periodate was approximately 7.5 μmol/mL. These concentrations were found to give satisfactory results for some selected thioethers as reported in Table I. The reaction time required at these concentrations was found to be approximately 15 h. Longer reaction times do not result in higher recoveries, because of the ability of the reagent to stop oxidation at the sulfoxide stage.

Effect of Other Functionalities. Compounds listed in Table I show that the substitution of other functional groups on the molecule have no effect on the theoretical recovery of silver iodate. The aromatic ring in both phenyl and benzyl sulfide shows stability to the periodate reagent. Methionine, both pure and mixed isomers, gave excellent results, showing no interference from its carboxyl or amino group. These results demonstrate the selectivity of the periodate reagent toward the sulfide group. However, all attempts made to quantitate *N*-acetyl-DL-methionine failed. The high recoveries of silver from this compound cannot be explained with certainty. It may be possible that the oxidized acid product is precipitated upon the addition of silver ion, unlike methionine, whose amino group promotes solubility under acid conditions. In addition to precipitation of the acid, inclusion of silver ion seemed to be indicated from the poor precision of the 12 determinations.

Interference. The ability of periodate to react with adjacent hydroxy functions has been known for some time and has been used as the basis for the quantitation of these groups. A comprehensive review of these methods is given by Kolthoff and Belcher (*28*). Older methods measured excess periodate by adding an excess of sodium arsenite followed by back titration with standard iodine solution.

$$HIO_4 + Na_3AsO_3 \rightarrow Na_3AsO_4 + HIO_3$$

This method has been used to estimate adjacent hydroxy functions in both glycols and carbohydrates. Pesez has quantitated 1,2-dihydroxyacids by fluorimetry using sodium metaperiodate to form the oxidized product which is then coupled with resorcinol (*29, 30*). However, interference from diols presents little problem since they are rarely found in the presence of organic sulfides. Other functional groups which have been reported (*31–34*) to reduce periodate are α-hydroxy aldehydes, α-hydroxy ketones, 1,2-diketones, α-hydroxy acids, and α-amino alcohols.

Iodate Precipitation. The ability to precipitate iodate in the presence of periodate with silver under acid conditions has made it possible to determine iodate directly. This separation was the basis of a method developed by Oles (*35*) for the determination of adjacent hydroxyl groups. Prior to this, no accurate method existed to determine the quantity of iodate in the presence of periodate. Thus, older methods

Table III. Quantitation of Sulfide in Shale Oil

Method	Equiv Sulfide S/g oil	% Sulfide S in oil	% total S in oil	% of total S as Sulfide S
Direct	$2.77 \times 10^{-5} \pm 9.8\%$	0.089	0.85	10.4
Standard addition	$2.58 \times 10^{-5} \pm 8.5\%$	0.083	0.85	9.7

measured excess periodate as discussed in the previous section. The solubility of silver iodate, and factors which affect its solubility, can be found in ref. 35. The important feature here is the decrease of silver iodate solubility due to the high concentration of silver ion, the low temperature of the wash solution (0 °C), and the high acidity of the reaction solution.

Blank Value. A study on the source of the blank for this system is reported in detail in ref. 35. It was found that a wash solution consisting of equal volumes of water and acetone containing HNO_3 (0.2% v/v) resulted in a small reproducible blank value of 0.35–0.44 ppm Ag^+ in a 50.0-mL volume. This paper is in agreement with the present work, in which an average blank value of 0.2 ppm Ag^+ was found in a 100.0-mL volume.

Determination of Total Sulfide. The determination of total sulfide in mixtures has been accomplished. The results of this study for two mixtures of sulfides are reported in Table II.

Recovery Study. A column identical to that used in the separation of sulfur concentrate from the oil was used in this study. Butyl sulfide and phenyl sulfide in hexane were introduced onto the column and eluted with benzene. The collected benzene eluent was studied for its content of both standard sulfides by gas chromatography using a $^1/_8$-inch × 6 ft, 8% OV-7 on ABS (mesh size 70/80) column equipped with a flame ionization detector. The recovery of each sulfide from the column using this procedure was 95 ± 2%.

Determination of Total Sulfide in Shale Oil. The results from direct and standard addition measurements of sulfides in shale oil are reported in Table III. From the percent sulfur in the shale oil, as determined by microanalysis, the total sulfur in the form of sulfides may be calculated.

The good agreement between the two methods indicates that the benzene eluent matrix does not significantly affect the quantitative reaction of sulfides with $NaIO_4$ under these conditions. In order to determine if interfering reactions were occurring in the oxidation of the sulfides, the reaction of a standard disulfide and thiol with $NaIO_4$ was studied, since disulfides and thiols will also be present in the sulfur concentrate from the oil sample. The reaction of butyl disulfide did not proceed to any measureable extent while hexane thiol reacted to an extent of approximately 30% under the conditions used for sulfide reaction. This interference is negligible when applied to shale oil since thiols are present only at about 1% of the total sulfur in the oil (*36*). In cases where thiol interference is important, it may be desirable to perform a separate analysis for thiols by a selective method such as silver reaction to form mercaptides. This has been accomplished using amperometric (*37*) and atomic absorption techniques (*38*).

Quantitative estimation of sulfur compounds in the naphtha cut (IBP to 200 °C) of N-T-U shale oil has put sulfides at approximately 15–20% of the total sulfur in this fraction (*18*, *20*). This is difficult to correlate with the levels of sulfides found in the crude shale oil because the naphtha comprises only about 18% of the total crude (*15*). No other data from past work are available concerning the levels of sulfides in shale oil and shale oil distillates. In the present study, the sulfides have been found to be about 10% of the total sulfur in crude TOSCO II shale oil. Because of the limitations of the adsorption method in separating the sulfur compounds, this analysis is applicable only to the "neutral" sulfides in the oil. Any sulfide groups in compounds containing nitrogen and oxygen are not analyzed by this method because of their strong adsorption on silica.

LITERATURE CITED

(1) J. R. Sampey, K. H. Stagle, and E. E. Reid, *J. Am. Chem. Soc.*, **54**, 340 (1932).
(2) S. Siggia and R. L. Edsberg, *Anal. Chem.*, **20**, 938 (1948).
(3) J. W. Sease, C. Nieman, and E. H. Swift, *Anal. Chem.*, **19**, 197 (1947).
(4) B. Gauthier and J. Maillard, *C. R. Hebd. Seances Acad. Sci.*, **236**, 1178 (1953).
(5) R. Belcher, Y. A. Gawargious, and A. M. G. MacDonald, *Mikrochim. Acta*, **6**, 1114 (1966).
(6) S. L. Leutch, *J. Franklin Inst.*, **239**, 334 (1945).
(7) L. N. Lewin, *J. Prakt. Chem.*, **2**, 118, 282 (1927).
(8) C. B. Puchalsky, *Anal. Chem.*, **41**, 843 (1969).
(9) J. Churacek, *J. Chromatogr. Libr.*, 1975, 3 (Lig. Column Chromatogr.), 927–937.
(10) S. Siggia, "Instrumental Methods of Organic Functional Group Analysis", Wiley-Interscience, New York, N.Y., 1972.
(11) S. H. Hastings, *Anal. Chem.*, **25**, 420 (1953).
(12) S. H. Hastings and B. H. Johnson, *Anal. Chem.*, **27**, 564 (1955).
(13) H. V. Drushel and J. F. Miller, *Anal. Chem.*, **27**, 495 (1955).
(14) G. P. Hinds, *Proc. Am. Pet. Inst.*, **42**, 18 (1962).
(15) M. T. Atwood, *Chem. Tech.*, **3**, 617 (1973).
(16) W. E. Cady and H. S. Seelig, *Ind. Eng. Chem.*, **44**, 2636 (1952).
(17) G. U. Dinneen, R. A. Van Meter, J. R. Smith, C. W. Bailey, G. L. Cook, C. S. Allbright, and J. S. Ball, *U.S. Bur. Mines, Bull.*, **593** (1961).
(18) G. U. Dinneen, R. A. Van Meter, J. R. Smith, C. S. Allbright, and W. R. Anthoney, *Anal. Chem.*, **27**, 185 (1955).
(19) G. U. Dinneen, *Proc. API 1962 Summer Sym.*, **42**, 41 (1962).
(20) H. T. Rall, C. J. Thompson, H. J. Coleman, and R. L. Hopkins, *U.S. Bur. Mines, Bull.*, **659**, 60 (1972).
(21) S. F. Birch, T. V. Cullum, R. A. Dean, and R. L. Denyer, *Ind. Eng. Chem.*, **47**, 240 (1955).
(22) D. Haresnape, F. A. Fidler, and R. A. Lowry, *Ind. Eng. Chem.*, **44**, 2691 (1949).
(23) R. A. Dean, *Proc. Am. Pet. Inst.*, **42**, 54 (1962).
(24) R. A. Dean and E. V. Whitehead, *7th World Pet. Congr. Proc.*, **9**, 165 (1967).
(25) N. J. Leonard and C. R. Johnson, *J. Org. Chem.*, **27**, 282 (1962).
(26) C. P. Parker, "Water Analysis by Atomic Absorption Spectroscopy", Varian Techtron Pty. Ltd., Palo Alto, Calif., 1972.
(27) R. P. D'Alonzo, Ph.D. Dissertation, University of Massachusetts, Amherst, Mass., 1977.
(28) I. M. Kolthoff and R. Belcher, "Volumetric Analysis", Vol. 3, Interscience, New York, N.Y., 1957, p 475.
(29) M. Pesez, *Bull. Soc. Chim. Fr.*, (5) 3,676,2072 (1936).
(30) M. Pesez, and J. Bartos, *Talanta*, **14**, 1097 (1967).
(31) N. D. Cheronis and T. S. Ma, "Organic Functional Group Analysis by Micro and Semimicro Methods", John Wiley & Sons, New York, N.Y., 1964, p 507.
(32) R. J. B. Reddaway, *Analyst (London)*, **82**, 506 (1957).
(33) R. L. Shriner, R. C. Fuson, and D. Y. Curtin, "The Systematic Identification of Organic Compounds", 5th ed., John Wiley & Sons, New York, N.Y., p 146.
(34) R. Adams, "Organic Reactions", Vol. II, John Wiley & Sons, New York, N.Y., 1944.
(35) P. J. Oles and S. Siggia, *Anal. Chem.*, **46**, 2197 (1974).
(36) A. P. Carpenter, Jr., Ph.D. Dissertation, University of Massachusetts, Amherst, Mass., 1977.
(37) I. M. Kolthoff and W. E. Harris, *Ind. Eng. Chem., Anal. Ed.*, **18**, 161 (1946).
(38) J. Marhevka, Ph.D. Dissertation, University of Massachusetts, Amherst, Mass., 1976.

RECEIVED for review September 2, 1977. Accepted November 9, 1977. This work was supported by grants CHE76-07378 and CHE74-15244 from the National Science Foundation.

Micro-Size Potentiometric Probes for Gas and Substrate Sensing

C. P. Pui, G. A. Rechnitz,*[1] and R. F. Miller

Departments of Chemistry and Physiology, State University of New York, Buffalo, New York 14214

The design, construction and evaluation of micro gas sensing probes for ammonia and carbon dioxide is described in detail. It is shown that the resulting sensors have promise for biological measurements in terms of tip size (less than 10 μm), sensitivity, and dynamic response. The micro ammonia sensing probe is further utilized to prepare a micro urea sensor by immobilizing urease enzymes at the electrode tip.

Potentiometric gas sensing probes have been used as the basis of many enzyme sensor systems in addition to their utility for direct gas measurement. A classical gas sensing membrane probe employs a double membrane system in which a thin layer of an appropriate filling solution separates an external gas permeable hydrophobic membrane from an internal sensing electrode of the ion-selective membrane type. The solution layer and internal sensing electrodes are so chosen that the gaseous species to be measured shifts a chemical equilibrium in the filling solution to produce an ion activity change that can be sensed by the internal membrane. Recently, a new type of gas sensor known as the air-gap sensor has been reported (*1*). The sensor is based on the same principle as other gas sensors except that the gas permeable membrane is replaced by an air gap which separates the electrolyte layer (adsorbed as a very thin film on the surface of an ion-selective electrode) from the sample, the entire system being contained in a gas-tight measuring chamber. The advantages of each type of gas sensor have been well established. (*1–6*).

Currently, potentiometric gas sensors for measuring a wide range of gases are commercially available. The application of these sensors has been extended to include assays of biological samples. However, one limitation of these commercially available sensors results from their relatively large size which makes in vivo measurements in biological systems difficult, if not impossible. It would clearly be advantageous for many biological applications to reduce the sensing tip size so that its insertion into living tissue is practical. We report here a gas sensing probe design made of glass micropipets, with a tip diameter of less than 10 μm; it seems likely that this tip diameter might be further reduced with the possibility of achieving small enough tips for intracellular applications. Such sensors can be fabricated to serve as micro gas sensing devices or, with the addition of an enzyme immobilized at the tip, can form the basis of a highly selective micro biological substrate sensor. Micro-size ammonia and carbon dioxide sensors are reported here and a micro urea sensing enzyme probe based on the ammonia system is described.

EXPERIMENTAL

Materials. Analytical grade reagents were used to prepare buffers, constant ionic strength solutions, and standard ammonium chloride, sodium bicarbonate, and urea solutions. Distilled and deionized water was used throughout for these preparations. Enzyme urease (Type VI: Highly purified powder from Jack Beans) and Bovine serum albumin (BSA, Fraction V powder) were obtained from Sigma Chemical Company and glutaraldehyde (25% solution in water) from J. T. Baker Chemical Co. Dimethyl dichlorosilane, obtained from Ventron Corp., was made up as a 4% solution in analytical reagent grade carbon tetrachloride.

Sealing of micropipets and electrodes was carried out using halocarbon wax Series 6-00 (Halocarbon Products Corp., Hackensack, N.J.), glass cover cement (Kroenig) (Chrome-Gessellschaft Schmid & Co.), high vacuum wax Apiezon W100 (Apiezon Products Limited, London) and 5 minute epoxy (Devon Corp., Mass.). Corning Code 0150 pH sensitive glass tubings (1 mm o.d., 0.5 mm i.d.) were obtained from Corning Glass Works while all other glass tubing was obtained from Glass Company of America, Inc.

Micro Sensor Fabrication. The gas sensing probes reported in this work function via pH changes within an appropriate internal solution. For the fabrication of various micropipets, we found it convenient to use two different vertical pipet pullers, one from David Kopf Instruments (Mode 700C) and the other from Narishige Scientific Instruments Laboratory. A noninverting binocular microscope (Ernst Leitz Wetzlar) was used to monitor much of the sensor fabrication.

Micro pH Electrodes. Methods for making various types of micro glass pH electrodes have been well established (*7–9*). For the purpose of this work, spear-type glass micro pH electrodes were prepared as follows. A 7-cm length of pH tubing was pulled into two very finely tapered micropipets using the DKI vertical puller. A long heating coil, a strong solenoidal pull, and high heat were necessary to achieve the desired pipet profile. The tips of the micropipets were then sealed using a De Fonbrune microforge. An incomplete seal was generally indicated by the taking up of water when the electrodes were soaked in distilled water. The sealed pH electrodes were then filled by boiling in deionized distilled water under vacuum for about 20 min. The water in the electrodes was replaced by 0.01 M HCl using a fine steel tubing attached to a hypodermic syringe. The dc resistances of the electrodes were then measured using a Keithley electrometer (Model 601B). An electrode with a sealed tip generally had a dc resistance close to 10^9 Ω.

Insulating pipets were pulled from ordinary Pyrex glass tubing (1.6-mm o.d., 1.2-mm i.d.) under moderate heat and a moderate pull, using the Narishige vertical puller equipped with a long heating coil. Under microscopic observation, the tip of the insulating pipet was broken off mechanically until a tip diameter of a few micrometers was obtained. The pipet tip was filled with insulating wax or cement by simply dipping the tip into heat-melted halocarbon wax or glass cover cement and by applying a slight vacuum at the open end of the pipet. The insulating pipet was cut to a length of about 1 cm shorter than the pH electrode to be insulated.

The insulating pipet was then mounted on a Plexiglas holder, with plasticine, on the microscope platform and the pipet tip was gently heated with a heating coil. The micro pH electrode, held by a micromanipulator (PRIOR, England), was carefully inserted into the insulating pipet such that only about 50 μm of the sensitive tip protruded out of the insulating pipet. Any excess wax or cement adhering to the tip was removed using a fine electrically heated wire. At the wide end, the space between the pipet and the electrode was filled with glass cover cement so that the air trapped would help to prevent the entry of aqueous solution through the lower seal.

The pH response of the insulated pH electrode was measured against a calomel electrode (Corning Catalogue No. 476017) in standard buffers. Electrodes with the slopes of at least 50 mV per unit pH were used. The dc resistance of the pH electrodes after insulation was generally increased by a hundred-fold.

[1] Present address, Department of Chemistry, University of Delaware, Newark, Del. 19711.

0003-2700/78/0350-0330$01.00/0 © 1978 American Chemical Society

Because of the high resistances associated with these electrodes, all resistance and potential measurements were carried out in a Faraday cage. The potential measurements were made using a high input impedance (10^{14} Ω) Orion digital 801 meter and were recorded using a Heath/Schlumberger Model EC1 200-02 recorder.

Micro Air-Gap Gas Sensor. Glass tubings of 5 mm o.d., 3.4 mm i.d. were thoroughly cleaned, rinsed with millipore-filtered distilled water, and dried in an oven. By means of the D.K.I. vertical puller equipped with a short heating coil, the tubing was first extended 1 to 2 cm under high heat. It was then realigned and subsequently pulled by gravity using minimum heat. The pipet had a very short tapered profile with a tip diameter usually of a few micrometers. The total length of the pipet was cut to about 2.5 cm. The tip of this micropipet was then made hydrophobic by repeatedly dipping into millipore-filtered dimethyl dichlorosilane (4% solution in carbon tetrachloride) and heating with a heating coil. Slight vacuum was also applied at the wide end of the pipet during this operation. This pipet is designated as the outer pipet.

A second pipet, designated as the inner pipet, was pulled from a glass tubing of size 3-mm o.d., 2.4-mm i.d. with the Narishige vertical puller. A medium length heating coil, low heat, and a low pull were used. The profile of this pipet should be such that the shank of the pipet is sufficiently large to accommodate an insulated micro pH electrode and itself fit into the outer pipet. The tip of the pipet was then broken off to a diameter of about 10 μm. A small drop of high vacuum wax was then melted onto the shank of the pipet close to the tip.

The outer pipet was mounted on a Plexiglas holder on the microscope platform and firmly secured with a Plexiglas clamp. The inner pipet, held by a micromanipulator, was carefully inserted into the outer pipet. Gentle heating was applied to slightly melt the vacuum wax on the inner pipet so that the tip could be inserted to a distance approximately 150 to 200 μm from the tip of the outer pipet. Continuing gentle heating brought the wax seal very close to the tip of the inner pipet, thus forming an air space within the tip of the outer pipet. The space between the outer and the inner pipets at the wide end was sealed with quick setting epoxy.

The inner pipet was then filled with an appropriate internal solution (0.1 M NaCl and 0.005 NH_4Cl or $NaHCO_3$, saturated with silver chloride). Some agitation might be necessary to bring the internal solution right to the tip of the inner pipet, and this could be achieved readily by means of a finely etched tungsten wire (ac current in sodium nitrite) or a very fine micropipet. An insulated micro pH electrode was then very carefully inserted so that the pH tip almost protruded out of the internal solution. A fine silver wire (0.127 m) electrolytically coated with silver chloride was finally inserted to contact the internal solution. The pH and the reference electrodes were firmly sealed to the inner pipet at the wide end using glass cover cement. The complete assembly of a micro air-gap sensor is shown in Figure 1.

Measuring Techniques for Ammonia and Carbon Dioxide. To test the micro air-gap ammonia or carbon dioxide sensors, the standard addition technique was used. Gaseous ammonia was generated by adding a standard solution of 1 M ammonium chloride to a 100-mL sample of 0.1 M Na_2PO_4NaOH buffer (pH 11.0) in a thermostated cell (T = 25 °C). In the case of carbon dioxide, 1 M sodium bicarbonate solution was added to a 100-mL sample of 0.5 M sodium chloride solution, acidified to pH 1.9 with concentrated sulfuric acid. Potential readings were taken after a steady state was reached as indicated on the digital meter and strip chart recorder.

Preliminary Investigation of a Micro Biosensor for Urea. Five milligrams of urease enzyme was dissolved in 25 μL of 15% BSA solution (prepared in Tris buffer, 0.2 M, pH 8.5), and this enzyme solution was stored under refrigeration until use. The inner pipet, after assembly with the outer pipet as described above, was filled with a solution containing 5×10^{-3} M ammonium chloride and 10^{-1} M sodium chloride saturated with silver chloride. The tip of the outer pipet was then broken off very slightly to a tip diameter of about 10 μm in order to make the very tip hydrophilic. A drop of enzyme solution held at the tip of a graduated micropipet (Gilmont) was brought in contact with the tip of the outer pipet and a small column of enzyme solution collected within the tip was allowed to dry by evaporation. The process was repeated until a thin layer of enzyme residue formed at the tip. A drop of 25% glutaraldehyde was then brought in contact with the enzyme layer in the tip for several minutes and polymerization formed a sturdy layer of enzyme at the pipet tip. The top was then washed thoroughly with distilled water or Tris buffer to remove excess glutaraldehyde or unbound enzyme. The micro pH electrode and the silver–silver chloride wire were then inserted to complete the sensing unit.

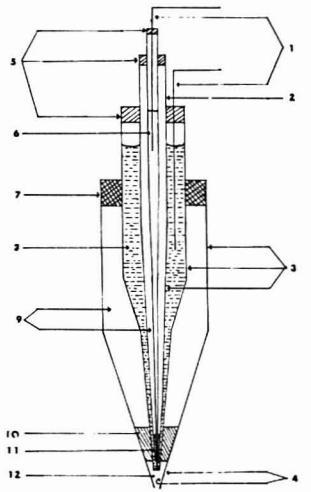


Figure 1. Construction of a micro air-gap gas sensing probe. (1) Ag/AgCl wires, (2) insulated micro pH electrode, (3) ordinary Pyrex glass, (4) hydrophobic surface, (5) glass cover cement, (6) 0.01 M HCl, (7) epoxy resin, (8) 0.005 M NH_4Cl or $NaHCO_3$ + 0.01 M NaCl, (9) air space, (10) high vacuum Apiezon wax, (11) glass cover cement or halocarbon wax, (12) air gap

The potential response of the micro urea probe was tested by the standard addition technique. Urea solution, 1 M, in Tris buffer, 0.2 M, pH 8.5, was added to a 100-mL sample of Tris buffer, 0.2 M, pH 8.5, contained in a thermostated cell (T = 25 °C) and steady-state potentials were recorded. Tris buffer, 0.2 M, pH 8.5, was prepared by dissolving a weighed amount of tris(hydroxymethyl)aminomethane in distilled deionized water. The pH was adjusted with hydrochloric acid.

RESULTS AND DISCUSSION

Sensor Design. The construction of a micro air-gap gas sensor is shown in Figure 1 and a photograph of an actual gas sensing tip is shown in Figure 2. The internal ion sensing electrode (the pH electrode) fits snuggly in the inner pipet containing the appropriate filling electrolyte. The electrolyte is held in place within the pipet by capillarity, and it contains a fixed activity level of the ion (chloride ion) to which the reference electrode (silver–silver chloride) responds. The hydrophobic tip of the outer pipet essentially acts as a gas permeable membrane. Thus, when the micro probe is immersed into a sample solution, the air trapped in the gap and the hydrophobicity of the sensing tip prevents the entry of the aqueous solution but allows the gas to pass freely through the tip into the air gap. The process will continue until the partial pressure of the gas in the internal electrolyte at the tip of the inner pipet equals that of the sample solution. Since the amount of electrolyte surrounding the micro ion-sensitive electrode tip is small, as is the size of the air gap, this equilibrium is quickly established. The equilibrium concentration of the gas in the thin layer of electrolyte determines its ionic activity (the pH) which is measured by the micro



Figure 2. A micro air-gap sensing tip under 400 times magnification (internal electrolyte was not incorporated in the inner pipet for clarity)

ion-sensitive electrode (micro pH electrode). The ionic activity of the thin layer of electrolyte is proportional to the logarithm of the partial pressure of gas in the sample.

In general, the probe potential is related to the determinand concentration by the equation

$$E = \text{Constant} \pm \frac{2.3\,RT}{F} \log_{10} [X]$$

where X is the determinand, R is the gas constant, T is the temperature, F is the Faraday constant and E is the potential; the sign of the last term is positive for an acidic gas and negative for a basic gas. The theoretical significance of this equation has been published previously (*1*, *10*).

Although the micro air-gap gas sensor is in an early stage of development, there are several unique features associated with the basic design which should be emphasized. Apart from the relatively simple construction, the sensor shares the advantage of a conventional air-gap probe in that the lack of a membrane phase facilitates the free diffusion of gaseous molecules into the internal electrolyte. However, the electrolyte layer on the pH-sensitive tip does not need to be removed after every measurement in order to maintain accuracy as required in the conventional air-gap sensors. The inner pipet serves to retain the bulk of the internal electrolyte, which stabilizes the composition of the thin layer of the sensitive tip by slow but continuous exchange. The micro air-gap gas sensor can be used in direct contact with the sample and requires no special reaction vessel. As is evident from Figure 2, it should be possible to further miniaturize the micro air-gap gas sensor without too much difficulty.

Micro Air-Gap Gas Sensing Probes. The potential response of a micro air-gap ammonia sensor is shown in Figure 3. The internal electrolyte employed was a solution of 0.005 M ammonium chloride and 0.1 M sodium chloride, and the measurement of ammonia gas was carried out by total conversion of ammonium chloride over the concentration range of 10^{-5} to 5×10^{-2} M. Also included in the figure is the calibration curve obtained under the same experimental conditions using a commercial barrel type Orion ammonia probe (Model 95-10). As can be seen, a linear calibration curve with a slope of −60 mV per decade concentration change of ammonia is obtained over the total range studied, comparable to that obtained for the commercial barrel type ammonia sensor. The micro ammonia sensor had the following dimensions: outer tip diameter, 8 μm; inner tip diameter, 15 μm; insulating tip diameter, 8 μm; pH sensitive tip length, 50 μm; distance between inner and outer tips, 165 μm.

For the micro ammonia sensors studied, in addition to the general factors (temperature, osmotic pressure, electrolyte composition, etc.) which affect the response of all gas sensing probes (*1*, *5*, *6*, *11*), the sensitivity was found to be largely determined by the sensitivity of the internal micro pH electrode and by the geometry of the electrolyte surrounding the pH sensitive tip. The sensitivity decreased significantly

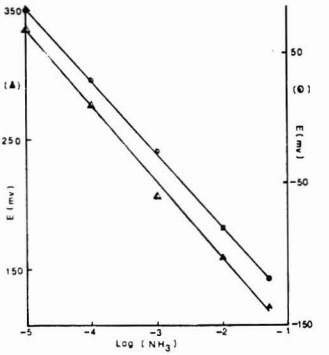


Figure 3. Potential response of a micro air-gap ammonia sensor. (Δ) micro air-gap sensor, (O) Orion ammonia sensor (Model 95-10)

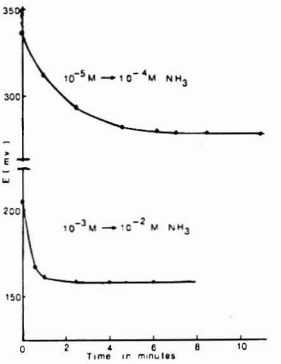


Figure 4. Dynamic response curves of a micro air-gap ammonia sensor

with increasing thickness of the electrolyte layer at the pH sensitive tip. Hence, for a good micro ammonia sensor, the tip of the micro pH electrode should almost protrude out of the electrolyte. The wax-sealed micro pH electrodes were satisfactory for the present work and have the advantage of being relatively easy to prepare; however, with prolonged use (several hours), the wax-seal insulation slowly broke down because of the intrusion of electrolyte, leading to decreasing sensitivity of the micro pH electrode which in turn affected the ammonia response. This problem can be circumvented by using glass-to-glass-seal insulated micro pH electrodes (*7–9*).

The dynamic response at two different concentration levels obtained for the micro ammonia sensor is shown in Figure 4. The response time is short (2–3 min) particularly at high ammonia concentrations. The response appeared to be predominantly a function of the geometry of the sensing probe itself, since a good micro pH electrode is effectively instantaneous in its response. Thus, with an outer tip size of a few micrometers, the response time is largely determined by the tip size and the shape of the inner pipet, the pH sensitive tip length, and the size of the air gap.

The potential reproducibility of the micro ammonia probe is, of course, dependent on the reproducibility of the internal micro pH electrode. For the micro ammonia sensor described above, the potentials between successive measurements were reproducible to about 1 mV above the ammonia concentration of 10^{-4} M, until the micro pH electrode showed sign of de-

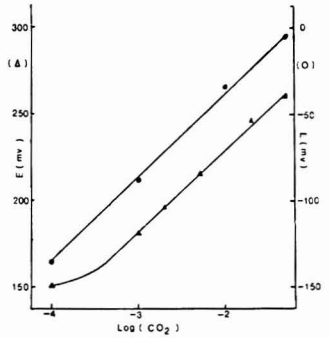


Figure 5. Potential response of a micro air-gap carbon dioxide sensor. (Δ) micro air-gap sensor, (O) Corning carbon dioxide sensor (Catalogue No. 476107)

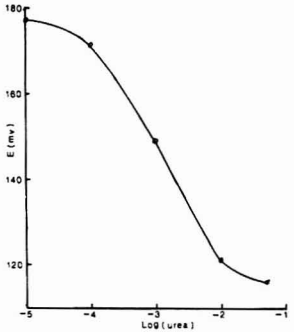


Figure 6. Potential response of a micro urea sensor

terioration. Equilibration between two successive measurements was slow, and this was almost certainly due to the slow diffusion of the confined layer of electrolyte surrounding the relatively long pH sensitive tip with the bulk electrolyte. Re-equilibration times were tested in alkaline buffer (pH 11.0), air, and dilute sulfuric acid, and were found to be quickest (~1 h) in acid solution. This would also appear to be consistent with the continuous rapid decrease in ammonia partial pressure in the air gap and internal electrolyte as a result of the continuous decrease of partial pressure of ammonia in acid solutions due to the formation of ammonium ions.

The use of the micro air-gap sensor is not limited to ammonia; fabrication of other gas sensors also seems feasible. Figure 5 shows the response of a micro air-gap carbon dioxide probe, made by employing a solution of 5×10^{-3} M sodium bicarbonate and 0.1 M sodium chloride as an internal electrolyte. The measurement of carbon dioxide was tested in determining sodium bicarbonate by means of the total conversion method. As can be seen, the calibration curve has a slope of 50 mV per decade concentration change of carbon dioxide which is comparable to that obtained for the commercial barrel carbon dioxide sensing probe (Corning Catalogue No. 476107) over the concentration range studied. This micro air-gap carbon dioxide sensor appeared to have some advantages over the recently reported micro carbon dioxide membrane probes (*12, 13*) whose potential responses for carbon dioxide were sub-Nernstian and whose micro hydrophobic membranes were difficult to fabricate.

The lower detection limit of the micro air-gap gas sensors has not been fully examined but is expected to be largely a function of the sensitivity of the internal micro pH electrode, the geometry of the electrolyte surrounding the pH sensitive tip and the composition of the internal electrolyte. The overall results obtained from this work indicate that it may be feasible to develop additional micro gas sensors by judiciously selecting the inner ion sensing electrodes, for instance, a H_2S sensor with a micro sulfide electrode, a HF sensor with a micro fluoride electrode, a HCN sensor with a micro silver electrode, and a Cl_2 sensor with a micro chloride electrode.

Micro Biosensor for Urea. The simplicity in design of the micro air-gap sensors also makes them attractive as building blocks for fabricating micro biosensors. This is particularly true because the sensing tip does not require a hydrophobic gas permeable membrane which could make immobilization of enzyme(s) difficult and could itself act as a partial barrier for gas diffusion. The tip may also be bevelled for tissue penetration and thus, if an enzyme can be immobilized within the sensing tip, the sensor may eventually prove to be useful for extra- and intracellular recording of biological substrates.

We have carried out a preliminary study of the feasibility of fabricating such a biosensor using the well established urease–urea system (*14, 15*) and the results obtained are highly promising as shown in Figure 6. The micro urea probe was fabricated simply by chemically binding a thin layer of urease enzyme within the sensing tip (10-μm tip size) of a micro air-gap ammonia sensor. Hence, when the probe was immersed into a urea substrate sample, the gaseous ammonia produced by the urease-catalyzed reaction at the tip diffused through the air gap and altered the hydrogen ion activity of the internal electrolyte monitored by the internal micro pH electrode. Such a micro sensor is highly selective, if not specific, because the enzyme provides the specificity of the chemical reaction and the micro air-gap sensor provides the high selectivity and sensitivity for measuring the gaseous product produced from the reaction.

The response of the micro urea probe was quick, requiring only several minutes to reach a steady-state potential. Although the sensitivity of the probe is low, which may be due to the low sensitivity of the micro pH electrode used (50 mV per unit pH) and insufficient quantities of enzyme, further optimization of the probe is likely to improve urea response.

ACKNOWLEDGMENT

We thank M. E. Meyerhoff for his continued interest in this work and R. Dacheux for some technical assistance.

LITERATURE CITED

(1) J. Ruzicka and E. H. Hansen, *Anal. Chim. Acta*, **69**, 129 (1974).
(2) E. H. Hansen, H. B. Filho, and J. Ruzicka, *Anal. Chim. Acta*, **71**, 225 (1974).
(3) J. Ruzicka, E. H. Hansen, P. Bisgarrd, and E. Reymann, *Anal. Chim. Acta*, **72**, 215 (1974).
(4) E. H. Hansen and J. Ruzicka, *Anal. Chim. Acta*, **72**, 353 (1974).
(5) P. L. Bailey and M. Riley, *Analyst (London)*, **100**, 145 (1975).
(6) J. W. Ross, J. H. Riseman, and J. A. Krueger, *Pure Appl. Chem.*, **36**, 473 (1973).
(7) G. Eisenman, "Glass Electrodes for Hydrogen and Other Cations", Marcel Dekker, New York, N.Y., 1967.
(8) M. Lavallee, O. F. Schanne, and N. C. Hebert, "Glass Microelectrodes", John Wiley & Sons, New York, N.Y., 1969.
(9) L. C. Clark, Jr., D. W. Lubber, I. A. Silver, and W. Simon, "Ion and Enzyme Electrodes in Biology and Medicine", University Park Press, Baltimore, Md., 1976.
(10) D. Midgley and K. Torrance, *Analyst (London)*, **97**, 626 (1972).
(11) P. L. Bailey and M. Riley, *Analyst (London)*, **102**, 213 (1977).
(12) C. R. Caflisch and N. W. Carter, *Anal. Biochem.*, **60**, 252 (1974).
(13) M. Sohtell and B. Karlmark, *Pflugers Arch.*, **363**, 1979 (1976).
(14) D. S. Papastathopoulous and G. A. Rechnitz, *Anal. Chim. Acta*, **79**, 17 (1975).
(15) M. Mascini and G. G. Guilbault, *Anal. Chem.*, **49**, 795 (1977).

RECEIVED for review September 16, 1977. Accepted November 29, 1977. Financial support by a grant from the National Institutes of Health is gratefully acknowledged.

Identification of Fuel Oils by Low Temperature Luminescence Spectrometry

Scott H. Fortier and DeLyle Eastwood*

U.S. Coast Guard Research and Development Center, Avery Point, Groton, Connecticut 06340

A low temperature luminescence method for identification of fuel oils was developed after optimization of experimental parameters such as solvent, sample concentration, excitation wavelength, etc. Fluorescence instrumentation, both corrected and uncorrected, were compared. Typical emission peaks for representative fuel oils excited at 254 nm are tabulated for classification information. Low temperature luminescence spectra showed more structure than room temperature fluorescence spectra, thereby enhancing oil identification capabilities.

Low temperature luminescence of petroleum oils for identification purposes is still a relatively little explored area. Studies by previous investigators (*1–3*) have shown that room temperature fluorescence is a rapid and accepted analytical technique for oil identification. Earlier low temperature measurements by Parker (*2*) and Hornig et al. (*4, 5*) showed that the increased spectral structure found at liquid nitrogen temperatures is useful in distinguishing among closely similar oils. Also, at 77 K, one may see phosphorescence as well as fluorescence.

In the present study, petroleum fuel oils were analyzed by low temperature luminescence and the resulting procedure was optimized with respect to experimental parameters. Preliminary application of this procedure has shown it to be a useful tool for identifying the source of an oil spill by direct comparison of spectra of spill samples with those from suspected sources. Typical wavelengths for emission peaks for representative fuel oils of each class on excitation at 254 nm are tabulated for classification purposes.

EXPERIMENTAL

Apparatus. A Baird-Atomic Fluorispec SF-100 fluorescence spectrophotometer was used to generate the majority of the spectra for this study. This instrument has double monochromators on both the excitation and emission sides, with the excitation and emission gratings blazed at 300 nm and 500 nm, respectively. A Hamamatsu R136 photomultiplier operated at 800 V was used as the detector and a Houston Instrument Model 2000 X-Y recorder was employed for graphic display.

Spectra were also generated on a Perkin-Elmer MPF-4 fluorescence spectrophotometer. This instrument is equipped with a single monochromator blazed at 300 nm on each side, a Hamamatsu 446-UR photomultiplier as detector, and a corrected spectra accessory. A Perkin-Elmer Model 56 strip chart recorder was used with this instrument.

Spectra generated on both the Baird-Atomic and the Perkin-Elmer instruments are uncorrected unless stated otherwise.

Suprasil quartz sample tubes and Dewars were obtained from Baird-Atomic because they were of superior quality in having a low fluorescence background. A special holder was designed to adapt the Dewars to the Perkin-Elmer instrument.

A Baird-Atomic phosphoroscope was used with the Fluorispec to produce a few typical phosphorescence spectra.

Selection of Oils for Study. Fuel oils were chosen as representative of each class on the basis of room temperature fluorescence and infrared spectra of over 150 fuel oils which had been previously analyzed at the Coast Guard Research and Development Center.

These specially selected representative oils included 19 fuel oils which were broken down as follows: four No. 1, four No. 2, five No. 4, three No. 5, and three No. 6 fuel oils. One No. 2 fuel oil was chosen for an exhaustive study on two different spectrofluorometers, varying parameters such as slit width, wavelengths, sample concentration, and solvent. After optimum experimental conditions were established, all other oils were analyzed using these parameters.

Selection of Solvents for Study. Solvents evaluated included: cyclohexane, methylcyclohexane, and hexane (all spectroquality from Matheson, Coleman and Bell (MCB); heptane (spectroquality from Mallinckrodt); octane (practical grade from MCB); and tetrahydrofuran and 2-methylpentane (chromatoquality from MCB). When methylcyclohexane, cyclohexane, and heptane were used as solvents, spectra with good structure were obtained, whereas spectra of oil solutions in tetrahydrofuran showed the least structure because of the high polarity of this compound. Methylcyclohexane was chosen as the most suitable solvent because it forms a clear glass at liquid nitrogen temperatures and was found to give more reproducible spectra than either heptane or cyclohexane, which form snows.

Selection of Concentration. Concentration effects with respect to changes in spectral shape for emission spectra were studied over a range from 100 to 1 ppm, and 10 ppm was selected as the standard concentration. This concentration represents a reasonable compromise in that sharp spectral structure can be achieved and reabsorption effects minimized while obtaining a good signal to noise ratio with no appreciable interference from solvent impurities.

Procedure. Oil solutions were prepared at 10 ± 0.3 ppm (w/w) in spectroquality methylcyclohexane in low-actinic glass volumetric flasks. An aliquot of the solution in a sample tube was lowered slowly (~30 s) into the Dewar containing liquid nitrogen. This avoids strain to the organic glass and ensures good spectral reproducibility.

Instrumental Conditions. Slit widths used, unless otherwise stated, were 6 nm for the stationary monochromator and 4 nm for the scanning monochromator. Wavelengths used for excitation were 254, 290, and 340 nm, although Hornig et al. (*5*) as well as the present investigators checked other wavelengths. A Corning 0-52 (Corning glass No. 7380) filter, with cut-off below 360 nm, was inserted at 480 nm (readjusting gain to compensate for filter absorption) during those spectral scans when the excitation was 254 or 290 nm in order to eliminate second-order light interference.

All oil solutions were used in equilibrium with the atmosphere, although other experimenters (*6*) have indicated that degassing can increase spectral intensity and structure for oil solutions at low temperature. Degassing would increase the complexity of the method and therefore would affect reproducibility for matching purposes because of required additional sample handling.

RESULTS AND DISCUSSION

The value of low temperature luminescence as an analytical tool is illustrated in Figure 1 which shows a comparison between the room temperature and low temperature emission spectra of a No. 2 fuel oil excited at 254 nm. The room temperature spectrum exhibits a single broad peak (~355 nm) while the low temperature emission spectrum for the same oil shows much sharper spectral structure and the emission extends to longer wavelengths because of phosphorescence.

0003-2700/78/0350-0334$01.00/0 © 1978 American Chemical Society

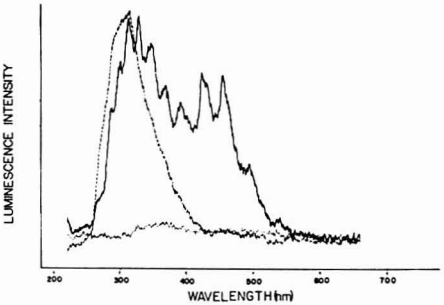


Figure 1. Comparison of room (---) and low (——) temperature spectra of a No. 2 fuel oil excited at 254 nm. Low temperature solvent blank (...) is included

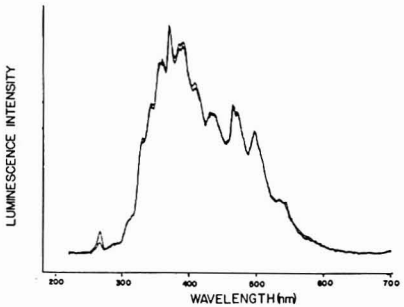


Figure 2. Spectral reproducibility for a No. 2 fuel oil excited at 254 nm. Peaks at 254 nm represent 1st order scatter

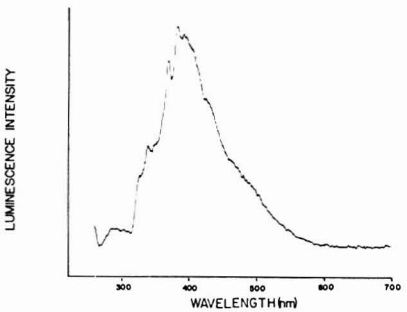


Figure 3. Spectrum of a representative No. 1 fuel oil excited at 254 nm

The solvent blank shown is that obtained at low temperature since impurities are more likely to be detected at these temperatures where fluorescence, and especially phosphorescence, quantum yields are higher.

Reproducibility. A typical example of reproducibility is shown in Figure 2 for a No. 2 fuel oil. A fresh sample was used for each of the spectral scans. A consistently uniform clear glass can be obtained and maximum reproducibility achieved using the slow (30-s) cooling rate.

Typical Spectra. Figures 3–6 illustrate low temperature luminescence spectra of other classes of fuel oils excited at

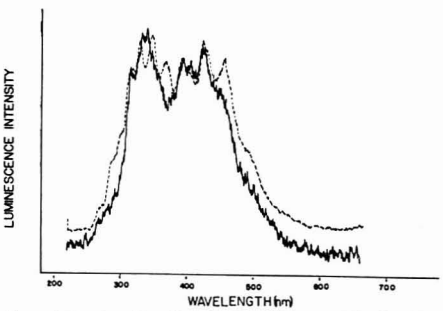


Figure 4. Spectra of two [(——) and (---)] representative No. 4 fuel oils excited at 254 nm

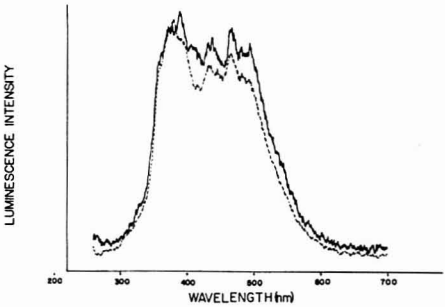


Figure 5. Spectra of two [(——) and (---)] representative No. 5 fuel oils excited at 254 nm

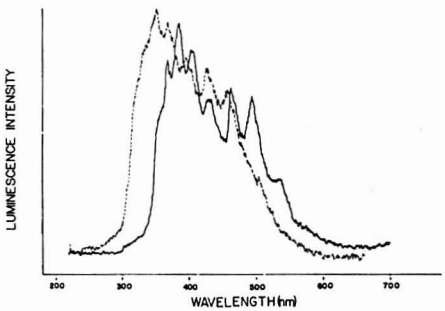


Figure 6. Spectra of a light (---) and a heavy (——) representative No. 6 fuel oil excited at 254 nm

254 nm. Figure 3 depicts a spectrum of a No. 1 fuel oil and Figures 4, 5, and 6 show spectral comparisons of two No. 4, two No. 5, and two No. 6 fuel oils, respectively. For each class, the spectra shown are typical of the class and represent the limits of spectral variability within the class. For No. 1 fuel oils, relatively little variability occurs and therefore only one example was included. Progressing from the lighter to the heavier fuel oils, the changes in the spectra are readily apparent. The spectrum of a No. 6 fuel oil, for example, is considerably different from a No. 2 fuel oil excited at the same wavelength and, in general, is shifted to longer wavelengths. Even for a No. 6 fuel oil, sometimes difficult to identify by

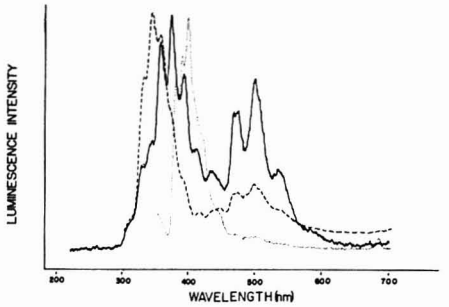


Figure 7. Spectra of a No. 2 fuel oil excited at 254 nm (——), 290 nm (- - -) and 340 nm (...)

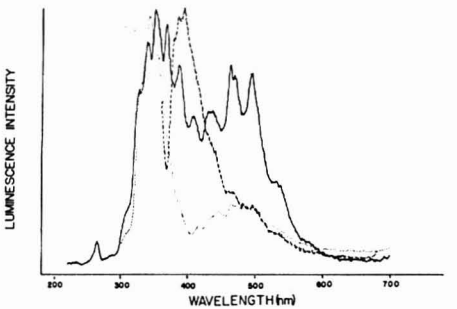


Figure 8. Comparison of spectra of a representative No. 2 fuel oil excited at 254 nm (——), 290 nm (...), and 340 nm (- - -)

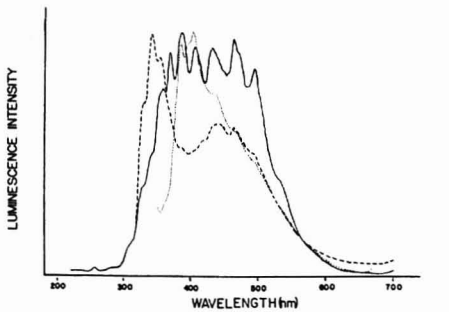


Figure 9. Spectra of a representative No. 4 fuel oil excited at 254 nm (——), 290 nm (- - -), and 340 nm (...)

room temperature fluorescence, there is considerable structure to characterize the oil.

Varying Excitation Wavelength. Examples of the effect of varying excitation wavelength on spectra of different fuel oil types are shown in Figures 7–10; Figures 7 and 8 for two different No. 2 fuel oils, Figure 9 for a No. 4 fuel oil, and Figure 10 for a No. 6 fuel oil. Useful information can be obtained at all three wavelengths (254, 290, and 340 nm) and, by utilizing selected wavelengths for excitation, advantages may be gained in terms of avoiding interference from impurities or in displaying only certain peaks for greater contrast. Excitation at 254 nm excited a larger proportion of aromatic

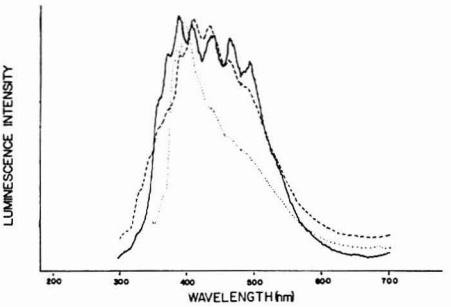


Figure 10. Spectra of a representative No. 6 fuel oil excited at 254 nm (——), 290 nm (- - -), and 340 nm (...)

Table I. Characteristic Luminescence Peaks for Fuel Oil Types at 254 nm Excitation[a,b]

Fuel oil	No. studied	Wavelengths
No. 1	5	326, 339, 369, 384, 407
No. 2	6	328, 341, 353, 369, 388, 410, 432, 465, 496
No. 4	6	356, 372,[c] 384,[c] 435, 465
No. 5	5	380, 390, 418, 433, 468, 482, 494
No. 6	5	434, 465, 497[c]

[a] Wavelength reproducibility is ±1 nm. [b] Wavelengths of all peaks are ±2 nm except where noted otherwise. The wavelength variability represents the maximum variability within a class. [c] Wavelengths of these peaks are ±3 nm.

hydrocarbons and produced more structured emission.

Wavelengths Corresponding to Characteristic Luminescence Peaks for Fuel Oil Types. Data on the spectra of 27 fuel oils of various types are summarized in Table I, which lists the wavelengths at which principal peaks occur on excitation at 254 nm. Although the primary purpose of this paper is to present a technique useful for identification, Table I lists data which are useful for classifying fuel oils. Table I was constructed using spectral data from the following fuel oils: five No. 1; six No. 2, six No. 4, five No. 5 and five No. 6. For each class of oils, Table I indicates the wavelengths corresponding to major peaks common to all oils within a class as well as the maximum variation for each peak position. Therefore, additional peaks which were found only for some oils within a class are not included.

The wavelengths are grouped in a pattern suggesting common classes of compounds in the oils. Minor shifts (e.g. between No. 1 and No. 2 fuel oils 339 to 341 nm or 384 to 388 nm) could possibly be ascribed to different luminescent backgrounds or to different members of the same class of compounds.

Additional information useful for identification is supplied by the peak ratios, additional structure not common to all oils within a class and differences in peak shapes or luminescence envelopes. Ranges of peak ratios could also have been tabulated, but for uncorrected spectral data would have been of value only to those using the same instrumentation.

Data generated on 17 fuel oils excited at 290 nm (not tabulated) showed that several, but not all, of the same peaks appear. For example, for a No. 2 fuel oil excited at 290 nm, peaks were observed only at 320, 342, and 353 nm (Figures 7 and 8 and Table I). In addition, excitation at 290 nm produced peaks which would not be characteristic of that fuel oil type on excitation at 254 nm. A No. 4 fuel oil, when excited at 290 nm exhibited peaks at 331 and 343 nm which were not

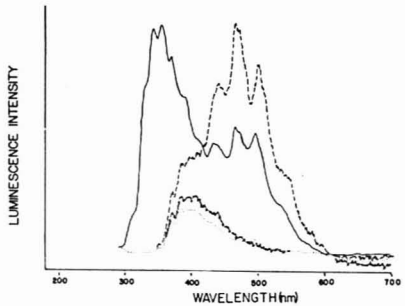


Figure 11. Comparison of the low temperature luminescence spectrum (——) with the phosphorescence spectrum (---) of a No. 2 fuel oil excited at 254 nm. The luminescence (...) as well as the phosphorescence (-X-) blanks are included. Excitation slit width, 21 nm; emission, 6 nm

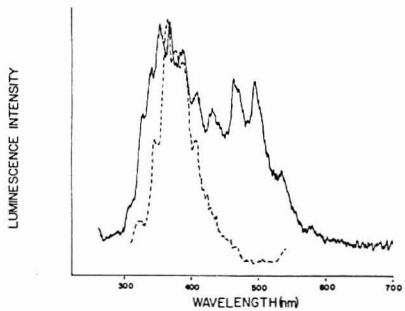


Figure 12. Comparison between uncorrected low temperature luminescence spectra of a No. 2 fuel oil excited at 254 nm run on the Baird-Atomic Fluorispec (——) and the Perkin-Elmer MPF-4 (---). Excitation slit width for MPF-4, 16 nm; emission slit width, 4 nm

characteristic of this oil type at 254 nm excitation (Figure 9 and Table I).

The wavelengths for prominent peaks can be correlated with aromatic ring systems as comparisons with spectra obtained from model ring systems show. For example, the peak at 326 ± 2 nm for a No. 1 fuel seems to be attributable to naphthalene-type compounds (*7, 8*), and the peak at 384 ± 3 nm may be ascribed to pyrene-type compounds (*7*).

Phosphorescence. Although most measurements were made as luminescence (fluorescence and phosphorescence), some measurements were needed to determine the phosphorescence separately. These phosphorescence measurements were made using a delay time of approximately 1 ms. Varying the delay time over the available range 0.5–30 ms (*9*) did not change the shape of the spectra appreciably, which is reasonable since many aromatic compounds have lifetimes of at least 0.1 s. Figure 11 shows the low temperature luminescence spectrum of a No. 2 fuel oil as well as the phosphorescence spectrum of the same oil. Recording the phosphorescence spectrum required the use of wider slits for instrumental reasons.

Instrumental Comparison. Figure 12 compares uncorrected emission spectra generated on instrumentation from different manufacturers. The uncorrected low temperature emission spectrum of a No. 2 fuel oil generated on the double monochromator Baird-Atomic Fluorispec is contrasted with the corresponding uncorrected spectrum obtained on the single monochromator Perkin-Elmer MPF-4. The detected signal appeared weaker on the MPF-4 and therefore a wider excitation slit width (16 nm) was used.

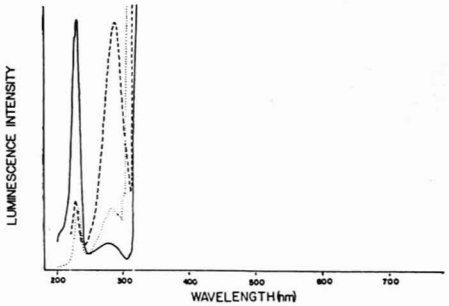


Figure 13. Comparison of uncorrected and corrected excitation spectra for a No. 2 fuel oil on the two instruments detecting at 323 nm. Baird-Atomic uncorrected spectrum (---) and Perkin-Elmer MPF-4 uncorrected (...) and corrected (——) spectra. Excitation slit width for MPF-4, 2 nm; emission slit width, 21 nm

The spectra differ partly because the excitation slits are different and partly because use of a filter (Spectro-Film Incorporated with cut-off at 265 nm) was necessary to eliminate first-order scatter. Also, the Perkin-Elmer grating is blazed at 300 nm while the gratings in the Baird-Atomic double monochromator are both blazed at 500 nm, which makes the peaks near 500 nm relatively much stronger as measured on the Baird instrument. Considerably more structure was obtained on the Fluorispec, partly because of the difference in the excitation slits. For low temperature measurements, the double monochromators in the Baird proved of value in reducing scatter; more scatter was noticed with the Perkin-Elmer MPF-4 with single monochromators.

Excitation Spectra. In addition to luminescence emission spectra, luminescence excitation spectra were also obtained detecting at major emission peaks. In some cases, closely similar oils could be more easily distinguished by examining excitation spectra.

To compare corrected and uncorrected spectra, and to compare instruments further, excitation spectra were generated on the Baird-Atomic Fluorispec and the Perkin-Elmer MPF-4. This is illustrated in Figure 13 for a No. 2 fuel oil. The apparent rapid drop-off in intensity at shorter wavelengths, observed for uncorrected spectra run on both instruments, is an instrumental artifact, especially noticeable for a double monochromator instrument such as the Fluorispec. The relative intensity of the short wavelength peak (~230 nm) increases considerably in the corrected spectrum obtained with the MPF-4.

Spectral Correction—Corrected vs. Uncorrected Instruments. For all spectrofluorometers, neither the source/excitation monochromator combination nor the emission monochromator/photomultiplier combination is flat in spectral response. Therefore, for uncorrected instruments, relative luminescence intensity is not independent of wavelength and the correct peak ratios are not obtained. As long as all data are taken on the same instrument and under the same experimental conditions, uncorrected spectra may be compared to identify oils. For corrected spectrofluorometers, at least in principle, it should be possible to compare spectral data and peak ratios taken on different instruments.

Useful information may be overlooked by using uncorrected spectra, principally on the short wavelength end of excitation spectra and on the long wavelength side of emission spectra.

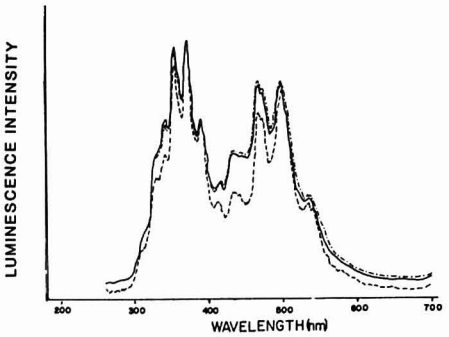


Figure 14. Example of the low temperature luminescence method as used for identification purposes in a real world spill case. Three No. 2 fuel oils are compared: the spill sample (——); the suspect sample which was a definite match (-.-); and the suspect sample which was a definite mismatch (- - -)

By correction, the intensities in these spectral regions are amplified to produce the correct relative intensity of all of the fluorescence peaks, which allows more accurate comparison of peak ratios. Also, in comparing data taken on different instruments, results may be incompatible unless suitably corrected spectra are used. Spectrally corrected spectrofluorometers are now commercially available. Even with corrected instruments, however, unless adequately dilute solutions (~0.05 Å at excitation wavelength) are used, geometric effects may prevent the comparison of spectra run on different instruments.

Identification Procedure. Presently, identification is made by using visual overlays to compare spectra. Two samples may be considered to have originated from a common source if their emission spectra match to within ±4% of full scale over the spectral range from 300 to 600 nm. In-house weathering studies, which will be reported later, showed that light oils weathered more than two days or heavy oils weathered more than one week fall outside of these tolerances.

Figure 14 shows an example of oil identification by this low temperature luminescence method taken from a real-world spill case. Using the criteria stated above, the weathered spill sample of No. 2 fuel oil was compared to two possible source samples: one of which proved to be a definite match (both by physical evidence and by experimental results from other analytical methods such as infrared spectroscopy and gas and thin-layer chromatography) and the other a non-match.

CONCLUSION

Fuel oil identification capabilities have been enhanced by the use of low temperature luminescence. A considerable increase in spectral structure is obtained by low temperature luminescence for fuel oils at 77 K as compared to conventional room temperature fluorescence. At room temperature, fuel oils of a given type may yield similar broad and featureless signatures with only minor spectral differences which could be confused by inexperienced operators. These subtle spectral differences are enhanced and sharpened in low temperature luminescence spectra. The sharp structure observed with low temperature luminescence is invaluable when comparing spectra of spilled fuel oil and suspect source samples to identify the correct origin of an oil spill. The rigid matrix formed at liquid nitrogen temperature is responsible for the spectral sharpening (*2, 10, 11*) because of a lack of collisional broadening and reduction of other broadening and quenching mechanisms.

Optimum conditions determined for the low temperature luminescence method were excitation at 254 nm, methylcyclohexane as solvent, and 10 ppm as a standard concentration. If all measurements are performed on the same instrument under identical experimental conditions, both corrected and uncorrected instrumentation can be used.

The low temperature luminescence method described in this paper is presently being used as an auxiliary technique for oil identification. It is part of a multimethod approach for oil spill investigations which includes room temperature fluorescence and infrared spectroscopy as well as gas and thin-layer chromatography and is most successfully employed for oil identification dealing with closely similar fuel oils. The low temperature luminescence method extends the power of room temperature fluorescence where uncertainty occurs in fuel oil identifications. It is also evident, from the data presented, that spectral patterns exist which can be correlated with fuel oil type and may therefore be utilized to classify these oils.

ACKNOWLEDGMENT

The authors thank Arthur W. Hornig for stimulating technical discussions.

LITERATURE CITED

(1) "Oil Spill Identification System", Chemistry Branch–U.S. Coast Guard Research and Development Center, Report No. CG-D-41-75, October 1974. (Available to the public through the National Technical Information Service, Springfield, Va. 22151. No. ADA003803.)
(2) C. A. Parker, "Photoluminescence of Solutions", Elsevier Publishing Company, New York, N.Y., 1968.
(3) A. D. Thruston and R. W. Knight, *Environ. Sci. Technol.*, **5**, 64 (1971).
(4) A. W. Hornig and D. Eastwood, "Development of a Low Temperature Molecular Emission Method For Oils", Program No. 16020GBW prepared for EPA Water Quality Office by Baird-Atomic, Inc., 15 October 1971.
(5) A. W. Hornig, D. Eastwood, and J. Guilfoyle, "Development of a Low Temperature Molecular Emission Method For Oils", Program No. 16020GBW prepared for EPA Water Quality Office by Baird-Atomic, Inc., 18 August 1971.
(6) A. W. Hornig, D. Eastwood, J. Guilfoyle, and F. Kawahara, "Molecular Luminescence Studies of Petroleum Oils at 77 °K", presented at the Pacific Conference on Chemistry and Spectroscopy, San Francisco, Calif. 16–20 October 1972.
(7) J. F. McKay and D. R. Latham, "Fluorescence Spectroscopy in the Characterization of High-Boiling Petroleum Distillates", presented at the 163rd National Meeting of the American Chemical Society, Boston, Mass., April 1972.
(8) I. B. Berlman, "Handbook of Fluorescence Spectra of Aromatic Molecules", Academic Press, New York, N.Y., 1971.
(9) J. J. Hanks, "Oil Fingerprinting by Phosphorescence—A Feasibility Study", Academy Scholar's Report–U.S. Coast Guard Academy, 13 May 1975.
(10) J. B. Birks, "Photophysics of Aromatic Molecules", Wiley-Interscience, New York, N.Y. 1970.
(11) S. P. McGlynn, T. Azumi, and M. Kinoshita, "Molecular Spectroscopy of the Triplet State", Prentice-Hall, Inc., Englewood Cliffs, N.J., 1969.

RECEIVED for review May 16, 1977. Accepted November 21, 1977.

Dual-Flame Photometric Detector for Sulfur and Phosphorus Compounds in Gas Chromatograph Effluents

Paul L. Patterson,* Robert L. Howe, and Ahmad Abu-Shumays[1]

Varian Instrument Division, 2700 Mitchell Drive, Walnut Creek, California 94598

A new dual-flame photometric detector is described for use in the specific detection of phosphorus- and sulfur-bearing compounds in the effluent of a gas chromatograph. A first hydrogen-rich flame is used to decompose samples from the gas chromatograph, and a second flame is used to produce light emission from S_2 and HPO molecules. Because sample decomposition occurs in the first flame, the light emission in the second flame exhibits a more uniform response with respect to sample concentration and composition in comparison to previous single-flame detectors. For those sulfur compounds tested, a pure square-law dependence of emission intensity vs. sample amount is obtained in agreement with theoretical expectations for S_2 emissions. A phosphorus detectivity of 5×10^{-13} g P/s and a sulfur detectivity of 5×10^{-11} g S/s are achieved. Selectivity with respect to hydrocarbon emissions is 5×10^5 g C/g P in the phosphorus mode, and ranges from 10^3 g C/g S to 10^6 g C/g S in the sulfur mode. The burner is further capable of handling large volume solvent injections without extinguishing the flames.

The flame photometric detector (FPD) has seen widespread use in gas chromatography as a specific detector for sulfur- or phosphorus-bearing compounds. This detector operates on the principle that phosphorus and sulfur compounds emit characteristic green and blue colorations, respectively, in hydrogen-rich, hydrogen–air flames (*1*). In the case of phosphorus, the green emission is due to the HPO molecule, and the intensity of this emission is known (*2*) to vary linearly with phosphorus atom flow into the flame. In the case of sulfur, the blue emission is due to the S_2 molecule, and the S_2 emission intensity is theoretically expected (*3*) and is usually found (*2*) to vary as the approximate square of sulfur atom flow into the flame.

The most widely used version of the FPD has been that design first described by Brody and Chaney (*2*) in 1966. Brody and Chaney employed a diffusion flame in which a mixture of the gas chromatograph (GC) effluent and air was conveyed to the center orifice of a flame tip, and an excess of H_2 was introduced from the outer periphery of the flame tip. With this burner and flow configuration, interfering light emissions from hydrocarbons occurred mainly at the base of the flame in close proximity to the burner orifices, whereas sulfur and phosphorus emissions occurred in the diffuse upper portions of the flame. Brody and Chaney enhanced the selectivity of their detector by using an opaque shield about the flame base so as to prevent hydrocarbon emissions from reaching a photomultiplier tube viewing the flame from the side.

Most of the known limitations (*4*) of the Brody–Chaney burner can be related to the fact that a single flame is used to both decompose samples and produce the desired phosphorus or sulfur emissions. Samples in the GC effluent can include compounds of complex molecular structure, and such compounds can change the flame environment and adversely affect the production of light. One well-known limitation of the Brody–Chaney burner is its susceptibility to solvent flameout (*2, 5*). Solvent peaks corresponding to GC injections of more than a few μL volume, momentarily starve the flame of oxygen and cause it to be extinguished. Burgett and Green (*5*) have reported that an interchange of the H_2 and air supplies to the burner can overcome this flameout problem. Such a gas stream interchange probably also negates the advantage of an opaque shield at the flame base, because incoming hydrocarbons do not encounter oxygen-containing flame regions until further downstream of flame tip orifices. It is in the oxygen-enriched regions of the diffusion flame that hydrocarbon emissions are most prevalent.

Another limitation of a single flame FPD is that the sulfur response is not always a pure square-law dependence on sulfur content. In fact, there have been reports (*6–11*) claiming the S response varies anywhere from a linear to a pure square-law response depending on such factors as the exact design of the burner, the flame gas flow rates, the concentration of sample, or the type of compound analyzed. A related problem is the known variation in sensitivity depending on the molecular structure of the sample being analyzed. Finally, it is also known that the sulfur or phosphorus light emissions in single flame detectors are severely quenched if there exists simultaneously a hydrocarbon background in the flame (*12–16*).

Most of the above limitations can be overcome if the region of sample decomposition chemistry is removed from the region of optical emission. This is accomplished in the present work through the use of a dual-flame burner. One flame is used to achieve the decomposition of incoming samples, and a second longitudinally separated flame is used to produce the desired optical emission.

There have been two previous reports of dual-flame burners used for sulfur or phoshorus detection. van der Smissen (*17*) employed an optically transparent Smithells-type (*18*) chimney to achieve two longitudinally separated H_2–air flames. One flame burned in a H_2-rich environment at a flame tip located inside the lower end of the chimney, and a second flame burned at the chimney exit where the excess H_2 combined with surrounding ambient air. Unlike the present work, van der Smissen viewed mainly the optical emission that occurred in the glow region between the two flames. A disadvantage of this burner was that S and P emissions occurred at different spatial locations within this glow region, so that the optical viewing axis had to be relocated if a change from S to P modes of detection was desired. Also, the requirement for an optically transparent chimney meant that the burner was constructed of high temperature glass which typically has a very low thermal conductivity and contains significant alkali impurities. Consequently, both flames in the van der Smissen burner generally exhibited background colorations due to alkali impurities outgassed from hot glass walls, even with a cooling water jacket surrounding the chimney.

Rupprecht and Phillips (*12*) also described the use of a dual-flame burner for the analysis of sulfur in hydrocarbon streams. In this case, an initial oxygen-rich flame was used

[1] Present address, Varian Instrument Division, 611 Hansen Way, Palo Alto, Calif. 94303.

0003-2700/78/0350-0339$01.00/0 © 1978 American Chemical Society

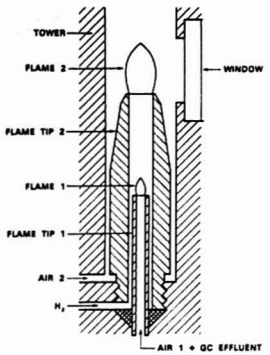


Figure 1. Schematic diagram of the dual-flame burner

to oxidize incoming hydrocarbons and sulfur compounds. S_2 emission was then generated and detected in a second H_2-rich flame located downstream of the oxidizer flame. A major disadvantage of this burner was the requirement of an elaborate ignition sequence in order to achieve successful ignition of both the oxidizer and detector flames. Like the van der Smissen burner, this burner was also constructed of glass, and alkali emissions were a source of interfering light in the flames. In addition, the region between the two flames constituted a sizeable dilution volume such that the S_2 emission in the H_2-rich flame exhibited very poor sensitivity.

The dual-flame burner employed in the present work differs from previous burners by being mostly an all metallic structure. Consequently, interfering emissions from alkali impurities are largely eliminated. In addition, the volume between the two flames is kept small so that excellent S and P sensitivity is still maintained when emissions in the second flame are viewed. In the present burner, a simple on–off control of an air source allows an easy conversion to a single flame mode, so that advantages and disadvantages of single- vs. dual-flame operation can be readily evaluated. A companion paper (*19*) describes such a comparison of single- vs. dual-flame operation, especially with respect to hydrocarbon quenching in the flame. The present paper is concerned mainly with burner design and performance characteristics in the dual-flame mode.

EXPERIMENTAL

Instrumentation and Chemical Reagents. The detector described in this paper is the flame photometric detector manufactured by Varian (Palo Alto, Calif.). All chromatographic data were obtained using a Varian Model 3700 gas chromatograph. Chromatographic columns and operating conditions are indicated where used. Solvents used to prepare test and calibration samples were nanograde 2,2,4-trimethylpentane obtained from Mallinckrodt (St. Louis, Mo.) and 99% pure grade *n*-hexane obtained from Phillips (Bartlesville, Okla.). Thiophosphate pesticides were obtained from Polyscience (Niles, Ill.) as 1% solutions by weight in benzene. These thiophosphate samples were further adjusted to desired concentrations by dilutions in 2,2,4-trimethylpentane. All other sample mixtures were prepared by dilutions in either 2,2,4-trimethylpentane or *n*-hexane using pure chemicals obtained from Chem Service (West Chester, Pa.).

Burner Design. A schematic illustration of the dual-flame burner is shown in Figure 1. A first flame is achieved by combining a source of air and hydrogen at a first flame tip such that the amount of H_2 is in excess of that required for complete combustion of the air. The excess H_2 is then combined with a second air source at another flame tip located downstream of the first flame. The two flames are ignited by igniting first the top flame, and then a mild flashback process ignites the lower flame. Similarly, when solvent peaks come through the detector, the lower flame may be momentarily extinguished, but the top flame stays lit because of an abundant supply of air located at the outer periphery of the top flame. Flashback then causes the lower flame to automatically reignite after the solvent passes. The purpose of the first flame is to decompose complex chemical compounds coming from the GC and convert them into combustion products consisting of relatively simple molecules. In the case of sulfur and phosphorus compounds, a region of light emission characteristic of S_2 and HPO molecules occurs in the volume between the first and second flames, and this emission indicates that sample decomposition is successfully achieved in the first flame. The purpose of the second flame is to regenerate light emission from S_2 and HPO molecules by burning again the combustion products from flame 1. Although both flames produce light, only that light produced in flame 2 is viewed photometrically. This is because the optical emission environment in flame 2 is much less disturbed by incoming samples from the GC than is the light produced at the first flame.

The flame tips and tower illustrated in Figure 1 were constructed of type 316 stainless steel, whereas the optical viewing window was Pyrex glass. Compared to high temperature glasses, stainless steel has a higher thermal conductivity and a negligible alkali impurity content (*20*). As a result, heat generated by the flames could be adequately dissipated by conduction such that neither flame 1 nor flame 2 exhibited any background flame colorations caused by materials outgassed from hot burner components. Flame tips 1 and 2 could probably also be constructed of high purity alumina ceramic, since that material has a thermal conductivity comparable to that of stainless steel. Some typical dimension of the burner components shown in Figure 1 were as follows: flame tip 1, i.d. = 1.5 mm, o.d. = 3.2 mm; flame tip 2, i.d. = 3.6 mm, o.d. = 4.6 mm at the top to 11 mm at the bottom; tower i.d. = 13 mm; and separation between ends of flame tip 1 and flame tip 2 = 17 mm.

All gas flows to both flames were completely controlled. On the Varian 3700 gas chromatograph, the control valves for H_2 and air supplies provide the dual capacity of flow regulation and flow shutoff. Once a gas flow was adjusted to its desired rate, that control valve could be turned off and on again without disturbing the flow rate setting. For optimum sulfur and phosphorus sensitivity and selectivity, the best flow rates were determined to be as follows: GC carrier gas, He = 30 mL/min; H_2 = 140 mL/min; air 1 = 80 mL/min; and air 2 = 170 mL/min. The sum of the two air supplies was sufficient to consume approximately 70% of the H_2 supplied to the burner. Hence, flame 2 as well as flame 1 was normally operated in a H_2-rich environment.

In a H_2–air flame, the presence of large concentrations of H, O, and OH flame radicals play an important role in both the sample decomposition chemistry and in the chemical reactions that result in light emission (*1*, *3*). An important consideration in a diffusion flame is the fact that the H_2 and air do not mix instantaneously. Consequently, such a flame contains spatial regions that are locally rich in H radicals, and other spatial regions that are locally rich in O and OH radicals. Sample decomposition chemistry, the type of combustion products formed, and the spatial distribution of light produced can all have a strong dependence on whether the sample is introduced to the diffusion flame via the H_2 gas stream or via the air gas stream. In the present burner, samples eluting from the GC enter flame 1 mixed with air. Consequently, these samples initially are exposed to a flame region with an abundance of O and OH radicals, and shortly thereafter they encounter a flame region with a large excess of H atoms. The region between flame tip 1 and flame tip 2 can be described qualitatively as containing a mix of combustion products, unburnt H_2, inert gases, and probably some residual H atoms. The presence of highly reactive H atoms in this interflame volume probably helps minimize sample losses due to absorptive interactions with the metal walls. The environment of flame 2 can be described as consisting of a central core region rich in H atoms, surrounded by an outer periphery region with an abundance of O and OH radicals. Since the desired S_2 and HPO emissions are well-known to occur in H-rich flame regions, the flame tip geometry and gas flow rates were chosen to maximize the spatial extent of the inner core of flame 2, while minimizing the spatial extent of the outer periphery. In flame 2, both the

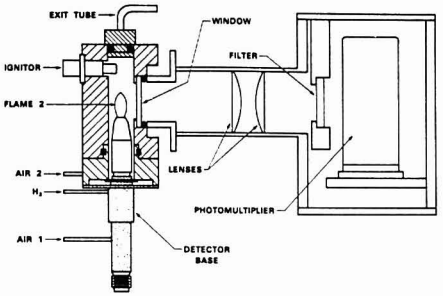


Figure 2. Schematic diagram of the FPD burner and photometric viewing components

S_2 and HPO emissions occur in a well-defined inner conical region extending to approximately 7 mm above the top of flame tip 2. Interfering hydrocarbon emissions occur primarily in a halo-type region located at the outer periphery and in near proximity of the top of flame tip 2.

In addition to dual-flame operation, the burner illustrated in Figure 1 can also be operated in a single-flame mode. This single-flame operation is achieved by simply turning off the air 1 supply. Also, if so desired, an oxygen-rich emission environment can be achieved at flame 2 by decreasing the H_2 flow and increasing the air 2 flow so that there is an excess of O_2.

Photometric Viewing. Figure 2 shows a schematic illustration of the burner and the photometric viewing components contained in the Varian FPD. The flame tips are surrounded by a cylindrical tower that is pneumatically sealed such that all gas flows to the burner can be measured at the top exit port of the tower. Light produced in flame 2 of the burner is viewed through the window in the side of the tower. A pair of optical lenses focuses an image of the flame through an optical filter and onto the photocathode of a photomultiplier tube. The lens arrangement shown in Figure 2 collects radiation from the flame at $f/2.5$ and provides a magnification near unity. The photomultiplier used in this detector is a side-viewing Hamamatsu R906 or an RCA 4552.

The FPD in this work used an unconventional choice of filter for sulfur detection, and that bears some further explanation. To aid in this discussion, there are shown in Figure 3 the spectral distributions of light emitted from the S_2 molecule, from the HPO molecule, and from the CH and C_2 radicals of a typical hydrocarbon. At the bottom of Figure 3, there is also shown the spectral response of the photomultiplier used, as well as the transmissions of the sulfur and phosphorus filters. Based upon high resolution spectral tracings of the S_2 molecular emission bands, most prior FPD's have used a 394-nm interference filter for S detection. Typically such interference filters have spectral bandwidths of approximately 8–10 nm. The second spectral tracing in Figure 3 shows that at a resolution of 8 nm, the discrete emission bands of the S_2 molecule merge and largely disappear. Hence, from the standpoint of maximizing the S signal, it really does not matter much whether the filter is centered precisely at 394 nm or at 380 or 400 nm. Also, the flame noise characteristics of the present detector were such that the signal-to-noise ratio remained the same whether the S emission was viewed at 360 nm or at 394 nm. Hence, the ultimate choice of S filter was based largely on the requirement for minimizing interferences from hydrocarbon and phosphorus emissions, and the spectral tracings of these interferences indicated that the S emission should best be viewed at wavelengths of 380 nm or less. The actual S filter used was a broad-bandpass, colored glass filter with peak transmission at 365 nm. For phosphorus detection, the filter used was a narrow-bandpass interference filter peaked at 530 nm.

RESULTS AND DISCUSSION

Effects of Gas Flow Rates. For a dual-flame burner with the dimensions described earlier, the sustained operation of both flames requires the H_2 and air-flow rates to be main-

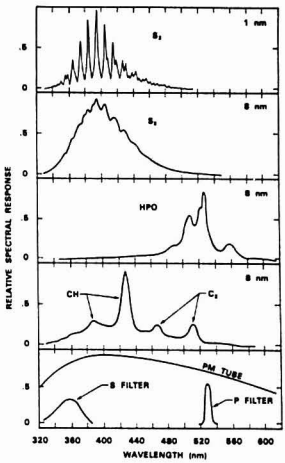


Figure 3. Relative spectral distributions of light emitted from S_2 and HPO molecules, and CH and C_2 radicals of a typical hydrocarbon, S_2 emission is shown at both high (1 nm) and low (8 nm) spectral resolution. Spectral response of photomultiplier tube and transmissions of S and P filters are indicated in bottom plot

tained within the following ranges: H_2, between 70 and 150 mL/min; air 1, between 70 and 120 mL/min; air 2, greater than 160 mL/min. In addition, the burner can accommodate GC carrier gas flows ranging up to 100 mL/min. Either He or N_2 can be used as the GC carrier gas. However, He is the preferred gas because it results in a slightly lower flame background and higher sample response than does N_2.

As expected, the FPD performance is strongly dependent on the relative magnitudes of H_2 and air flows supplied to the burner. The set of flow rates described earlier in this paper were chosen to provide the best combination of sensitivity, selectivity, and signal-to-noise ratios while maintaining a positive combustion environment for both flames. A very convenient feature of the present burner is that the optimum sulfur and phosphorus responses are achieved with exactly the same set of gas flows. Consequently, a change from S mode to P mode of detection requires only a change in optical filter.

Illustrated in Figures 4–6 are the relative variations of sulfur (I_S), phosphorus (I_P), hydrocarbon (I_C), and flame background (I_B) emission intensities as a function of variations in the H_2, air 1, and air 2 flow rates. In generating the data in these figures, hexanethiol was used as the S compound, tributylphosphate was used as the P compound, and *n*-pentadecane was used as the hydrocarbon. Other sulfur, phosphorus, and hydrocarbon compounds studied exhibit similar dependencies on flow. All emission intensities have been normalized to unity response at the normal operating flow rates. It is clear from these plots that both sensitivity and selectivity of the FPD are strongly dependent on the H_2 and air flows.

In the present burner, the flame environment that emits the observed light contains sizeable spatial gradients in chemical species and flame temperature along the line of viewing. However, in the core of flame 2, the sulfur and phosphorus species can be expected to be very well mixed with the unburnt H_2 and other combustion products emanating from flame 1. As a result, it is possible to correlate the H_2 dependencies of I_S and I_P with flame reaction mechanisms that have been previously proposed (*1*, *3*).

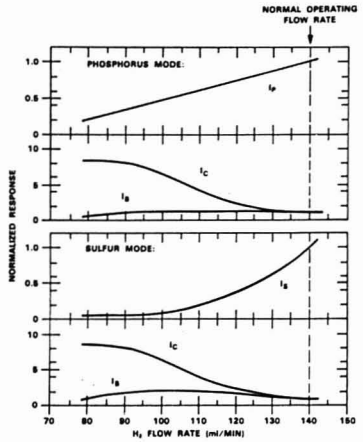


Figure 4. Variations in emission intensities of sulfur I_S, phosphorus I_P, hydrocarbon I_C, and flame background I_B as a function of variations in H_2 flow. Other flows: He, 30 mL/min; air 1, 80 mL/min; air 2, 170 mL/min. All data normalized to unity at normal operating flow rate of 140 mL/min

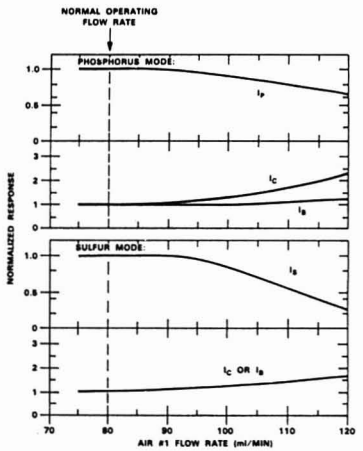


Figure 5. Variations in emission intensities as a function of variations in air 1 flow. Other flows: He, 30 mL/min; H_2, 140 mL/min; air 2, 170 mL/min. All data normalized to unity at normal operating flow rate of 80 mL/min

In the case of sulfur, it is generally believed that incoming sulfur-bearing compounds are decomposed irreversibly to yield H_2S as a primary combustion product. In the present burner, this decomposition occurs largely in flame 1. The H_2S then further reacts with H atoms in the hydrogen-rich flame to yield S_2 molecules. Sugden et al. (*3*) have derived the following expression for the S_2 concentration:

$$[S_2] \propto [S]_0^2[H]^2/[H_2]^3 \quad (1)$$

where $[S]_0$ represents the concentration of total added (monatomic) sulfur, [H] is the concentration of hydrogen atoms, and $[H_2]$ is the concentration of hydrogen molecules. Then according to Gilbert (*1*), the S_2 emission can be generated by the chemiluminescent reaction, $S_2 + H + H \rightarrow S_2^* + H_2$. Hence,

$$I_S \propto S_2^* \propto [S_2][H]^2 \quad (2)$$

Combinding relations 1 and 2 gives

$$I_S \propto [H]^4[S]_0^2/[H_2]^3 \quad (3)$$

Assuming small variations in H_2 do not appreciably change flame temperature, and further assuming that equilibrium prevails in the core of flame 2, then the known (*21*) flame reaction, $3H_2 + O_2 = 2H + 2H_2O$, yields the relation $[H] \propto [H_2]^{3/2}$. Substituting into relation 3 gives the prediction that $I_S \propto [H_2]^3$.

In the case of phosphorus, incoming phosphorus-bearing compounds are believed to be decomposed to yield PO as a primary combustion product. Again, in the present burner this decomposition occurs in flame 1. Then according to Gilbert (*1*), either of the following two reactions could generate the HPO^* emission:

$$PO + H + M \rightarrow HPO^* + M \quad (4)$$

where M is an inert third body; or

$$PO + OH + H_2 \rightarrow HPO^* + H_2O \quad (5)$$

Again assuming equilibrium prevails in the core of flame 2, the flame reaction, $H_2 + O_2 = OH + OH$ then yields the relation $[OH] \propto [H_2]^{1/2}$. Hence, both reactions 4 and 5 predict that $I_P \propto [H_2]^{3/2}$.

In Figure 7 there are plotted a graph of $I_S^{1/3}$ vs. H_2 and a graph of $I_P^{2/3}$ vs. H_2. Within the accuracy of the data, both graphs exhibit a straight line dependence at H_2 flows above 105 mL/min. Although these power law fits of the data are not necessarily unique, the graphs in Figure 7 do indicate that the observed variations in S_2 and HPO emissions are qualitatively consistent with predictions based upon the probable reaction mechanisms occurring in the flames.

Sample Response. Figure 8 shows the FPD response in both the phosphorus and sulfur modes. Plotted on logarithmic scales are the sample peak height response in nA vs. the heteroatom flow rate in ng P/s or ng S/s. Data are shown for three different substances. One substance contains only

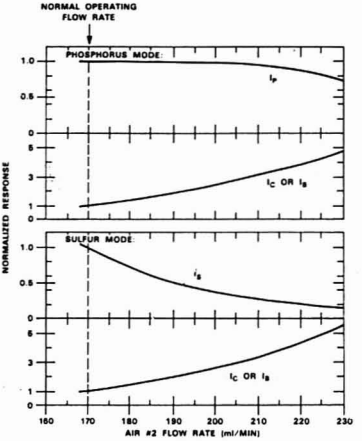


Figure 6. Variations in emission intensities as a function of variations in air 2 flow. Other flows: He, 30 mL/min; H_2, 140 mL/min; air 1, 80 mL/min. All data normalized to unity at normal operating flow rate of 170 mL/min

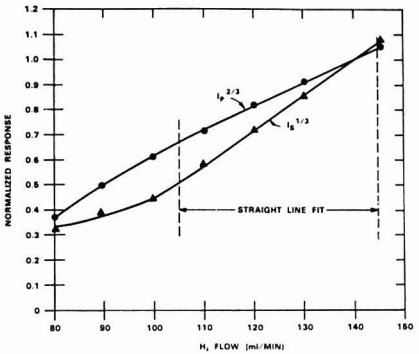


Figure 7. Graphs of $I_P^{2/3}$ and $I_S^{1/3}$ vs. H_2 flow. Data normalized to unity at 140 mL/min

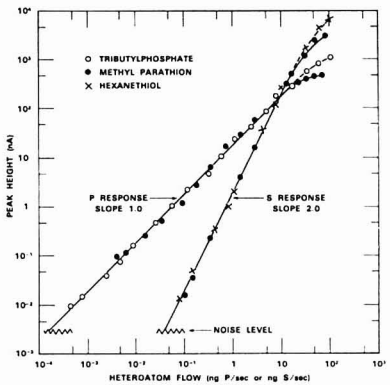


Figure 8. Plot of peak height response for P and S modes of detection. GC conditions: column, 200 cm × 6 mm o.d. × 2 mm i.d., Pyrex, 5% OV-101 on 100/120 Chrom W; carrier flow rate, 25 mL/min He; detector temperature, 230 °C; injector temperature, 230 °C; column temperature, 220 °C for tributylphosphate, 230 °C for methyl parathion, and 110 °C for hexanethiol

phosphorus, one contains both phosphorus and sulfur, and one contains only sulfur. In the phosphorus mode, the data for tributylphosphate and methyl parathion exhibit exactly the same sensitivity except at the very highest sample amounts. The P response has a slope of 1.0 on this logarithmic plot, meaning the P response is linear over approximately a range of 10^5 in sample amount. In the sulfur mode, the data for hexanethiol and methyl parathion again exhibit exactly the same sensitivity except at the very highest sample amounts. The S response has a slope of 2.0 on this logarithmic plot, meaning the S response of both sulfur samples follows a pure square-law dependence on sulfur amount. The sulfur response extends over a range of 10^3 in sample amount. Sulfur compounds that have been analyzed and found to have a pure square-law dependence include the following: carbon disulfide, thiophene, hexanethiol, dodecanethiol, hydrogen sulfide, sulfur dioxide, sulfur hexafluoride, methyl mercaptan, disyston, methyl parathion, malathion, methyl trithion, and ethion.

At low sample concentrations, the noise level indicated in Figure 8 is due to flame noise, and that is typically an order of magnitude greater than photomultiplier tube dark current noise. At high sample concentrations, the upper limits of sample response correspond to the onset of self-absorption effects in the emitting flame. At these high sample amounts, the concentration of ground state S_2 and HPO molecules becomes sufficient to cause some reabsorption of light emitted from excited S_2^* and HPO* molecules.

The data shown in Figure 8 correspond to sample compounds having different chromatographic retention times. In comparing peak height responses of these different compounds, it is noteworthy to point out that the relevant parameter is heteroatom flow rate in ng P/s or ng S/s. In the case of phosphorus compounds, the P flow rate was determined by dividing the P weight in the GC sample peak by the peak width at half height. In the case of sulfur, the peak amplitude varies according to a square-law dependence, so the peak width at one-fourth the maximum peak height was used in the calculation of S atom flow rate.

For phosphorus, the FPD sensitivity can be defined as follows:

$$S_P = \text{Peak Height/P Atom Flow Rate}$$

For the data shown in Figure 8, S_P = 20 nA/(ng P/s). Similarly, in the case of sulfur, the FPD sensitivity can be defined as follows:

$$S_S = \text{Peak Height/(S Atom Flow Rate)}^2$$

For the data of Figure 8, S_S = 2.0 nA/(ng S/s)^2. Both S_P and S_S can be varied by changing the gain of the photomultiplier tube through a change in its power supply voltage. However, the flame noise also changes accordingly, such that the ratio of sensitivity to noise stays approximately constant. A better indicator of FPD response is, therefore, the detectivity which is defined as follows:

$$D_P = 2 \times \text{noise}/S_P$$

and

$$D_S = \sqrt{2 \times \text{noise}/S_S}$$

where noise is measured in nA, S_P in nA/(ng P/s), D_P in (ng P/s), S_S in nA/(ng S/s)^2, and D_S in (ng S/s).

For the data in Figure 8,

$$D_P = 5 \times 10^{-4} \text{ ng P/s}$$

and

$$D_S = 5 \times 10^{-2} \text{ ng S/s}$$

The selectivity of the FPD is illustrated by the chromatograms shown in Figure 9. The sample analyzed contained 4000 ng of a C_{15} hydrocarbon, 20 ng of a sulfur-containing compound (dodecanethiol), 20 ng of a phosphorus-containing compound (tributylphosphate), and 20 ng of a compound containing both phosphorus and sulfur (methyl parathion). In the S mode, the chromatogram reveals the two S compounds along with a small peak for the C_{15}, but there is no trace of the P compound. In the P mode, the chromatogram reveals the two P compounds with no trace of the S compound or the C_{15}.

FPD selectivity ratios can be determined by ratioing the phosphorus (S_P), sulfur (S_S), and hydrocarbon (S_C) sensitivities with respect to each other. In the phosphorus mode, the S_P/S_C selectivity is greater than 5×10^5 g C/g P or greater than 10^6 atoms C/atoms P. This means that it takes more than one million C atoms to produce the same light signal as one P atom. The S_P/S_S selectivity is variable depending on the amount of interfering sulfur. This is because the S interference depends quadratically on S amount while the P signal varies only linearly with P amount. Hence, at very low levels of sulfur, the S_P/S_S selectivity is 5×10^4 g S/g P while at high

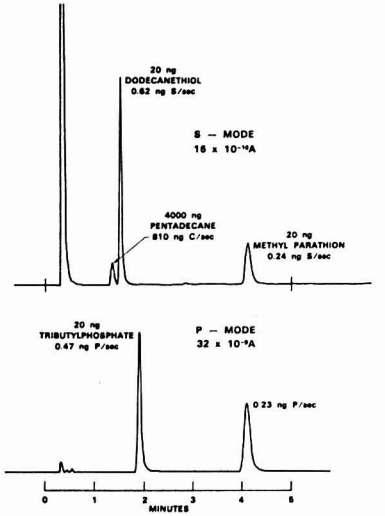


Figure 9. Chromatograms showing analysis of a test sample containing pentadecane, dodecanethiol, tributylphosphate, and methyl parathion. Same sample analyzed in both the S and P modes of detection. GC conditions: column and carrier flow, same as Figure 8; detector temperature, 220 °C; injector temperature, 220 °C; column temperature, 210 °C

sulfur levels, the S_P/S_S selectivity drops to about 50 g S/g P.

In the sulfur mode, the S_S/S_C selectivity varies from 10^3 g C/g S at low sulfur content to better than 10^6 g C/g S at high sulfur content. Again the variable selectivity is due to the fact that the S signal varies as the square of sulfur content while the C interference varies only linearly with C content. The S_S/S_P selectivity varies from 10 g P/g S at low sulfur content to greater than 10^4 g P/g S at high sulfur content.

Figure 10 provides an example of the capability of the present burner for handling large sample volume injections into the GC. The chromatogram shown represents the analysis of a 60-μL injection of *n*-hexane containing a 500-ppb trace of *n*-hexanethiol. The flames satisfactorily survive this large hexane solvent peak without being permanently extinguished. In addition, excellent sensitivity to hexanethiol is obtained even though this peak is not completely resolved from the tail of the hexane solvent peak.

In Figure 10, the hexane solvent response consists of an initial off-scale peak followed by a smaller secondary peak. Such double-peaked solvent responses often occur in those instances where the flow rate of solvent into the burner is sufficient to momentarily extinguish the first flame. The secondary peak in the solvent response coincides with the reignition of the lower flame. During the time that the lower flame is out, the FPD response is of questionable quantitative value since the burner is no longer functioning in a dual-flame mode. However, it should be recognized that it is the rate of flow of solvent molecules into the burner that determines whether the first flame is extinguished rather than the total amount of solvent. For any given volume of solvent injected into the GC, the rate of flow of solvent into the burner will depend on GC operating parameters such as injector temperature, column temperature, and carrier gas flow rate through the column. Consequently, it is always possible to find a set of GC operating conditions which allows both flames

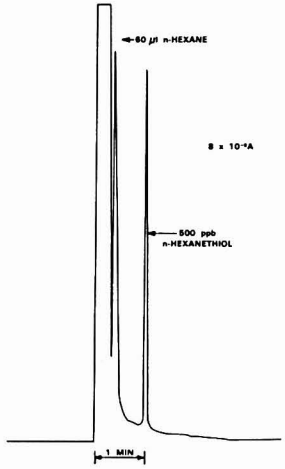


Figure 10. Chromatogram illustrating analysis of a 60-μL injection of *n*-hexane containing a 500-ppb trace of *n*-hexanethiol. GC conditions: column and carrier flow, same as Figure 8; detector temperature, 150 °C; injector temperature, 130 °C; column temperature, 120 °C

in the burner to continously function irrespective of the amount of solvent injected. In most cases, momentary flameout of the lower flame is a phenomenon that occurs only for solvent peaks at very early retention times in the chromatogram.

ACKNOWLEDGMENT

The authors thank Vincent Hornung for the design and construction of the electronics module used to operate the FPD.

LITERATURE CITED

(1) P. T. Gilbert, "Nonmetals", in "Analytical Flame Spectroscopy", R. Mavrodineanu, Ed., Macmillan and Co., Ltd., London, 1970, Chap. 5.
(2) S. S. Brody and J. E. Chaney, *J. Gas Chromatogr.*, **4**, 42 (1966).
(3) T. M. Sugden, E. M. Bulewicz, and A. Demerdache, in "Chemical Reactions in the Lower and Upper Atmosphere", Proceedings of an International Symposium, San Francisco, Calif., 1961, Interscience Publishers, New York, N.Y., 1961, pp 89–108.
(4) S. O. Farwell and R. A. Rasmussen, *J. Chromatogr. Sci.*, **14**, 224 (1976).
(5) C. A. Burgett and L. E. Green, *J. Chromatogr. Sci.*, **12**, 356 (1974).
(6) A. I. Mizany, *J. Chromatogr. Sci.*, **8**, 151 (1970).
(7) R. K. Stevens, J. D. Mulik, A. E. O'Keefe, and K. S. Krost, *Anal. Chem.*, **43**, 827 (1971).
(8) T. Suglyama, Y. Suzuki, and T. Takeuchi, *J. Chromatogr. Sci.*, **11**, 639 (1973).
(9) T. Suglyama, Y. Suzuki, and T. Takeuchi, *J. Chromatogr.*, **77**, 309 (1973).
(10) J. G. Eckhardt, M. B. Denton, and J. L. Moyers, *J. Chromatogr. Sci.*, **13**, 133 (1975).
(11) C. H. Burnett, D. F. Adams, and S. O. Farwell, *J. Chromatogr. Sci.*, **15**, 230 (1977).
(12) W. E. Rupprecht and T. R. Phillips, *Anal. Chim. Acta*, **47**, 439 (1969).
(13) S. G. Perry and F. W. G. Carter, "The Chromatography of Sulphur Compounds", in "Gas Chromatography 1970", R. Stock, Ed., Proceedings of the 8th International Symposium on Gas Chromatography, Dublin, 1970, Institute of Petroleum, London, 1971, p 381.
(14) T. Suglyama, Y. Suzuki, and T. Takeuchi, *J. Chromatogr.*, **80**, 61 (1973).
(15) C. D. Pearson and W. J. Hines, *Anal. Chem.*, **49**, 123 (1977).
(16) D. A. Clay, C. H. Rogers, and R. H. Jungers, *Anal. Chem.*, **49**, 126 (1977).
(17) C. E. van der Smissen, U.S. Patent 3,213,747, Oct. 26, 1965.
(18) A. Smithells and H. Ingle, *Trans. Chem. Soc.*, **61**, 204 (1892).
(19) P. L. Patterson, *Anal. Chem.*, **50**, following paper in this issue.
(20) F. Rosebury, "Handbook of Electron Tube and Vacuum Techniques", Addison-Wesley, Reading, Mass., 1965.
(21) K. Schofield and H. P. Broida, "Flame Kinetic Studies," in "Methods of Experimental Physics", L. Marton, Ed., Vol. 7, Part B, Academic Press, New York, N.Y., 1968.

RECEIVED for review August 22, 1977. Accepted November 4, 1977.

Comparison of Quenching Effects in Single- and Dual-Flame Photometric Detectors

Paul L. Patterson

Varian Instrument Division, 2700 Mitchell Drive, Walnut Creek, California 94598

A recently developed dual-flame photometric detector can be easily converted to a single-flame mode. Using this burner, single- vs. dual-flame operation was compared with respect to problems of quenching of light emissions. In the case where both sample decomposition and light emission occur in a single flame, light emissions from sulfur and phosphorus compounds are severely quenched by the presence of a hydrocarbon background in the flame. In addition, single-flame operation exhibits quenched sample responses dependent on the molecular structure of the sample. By separating the region of sample decomposition from the region of optical emission in a dual-flame mode of operation, these quenching effects are minimized. A good application of the dual-flame operation is shown to be the analysis of sulfur compounds in gasoline.

In gas chromatography, the flame photometric detector (FPD) is commonly used for the specific detection of sulfur- or phosphorus-bearing compounds. This detector senses light emissions from S_2 and HPO molecules that are formed by the combustion of samples in hydrogen-rich, hydrogen–air flames. In the past, the most popular version of the FPD (*1*) has utilized a single flame for the dual purpose of decomposing incoming samples as well as generating the desired optical emissions. Two well-known problems in these single-flame detectors have been sample responses which are strongly compound dependent (*2*), and sample responses which are severely quenched by the presence of a hydrocarbon background in the flame (*3–7*). In order to overcome the hydrocarbon quenching problem, it has been necessary to ensure that the detected sulfur or phosphorus compounds are well-resolved from major organic compounds which also elute from the gas chromatograph (GC) column. For complex samples, this requirement has often dictated the use of very high-resolution GC columns such as capillary columns (*8*).

In a preceding paper by Patterson, Howe, and Abu-Shumays (*9*), the design and performance of a new dual-flame FPD is described. One of the features of the burner employed in this dual-flame FPD is that a simple on-off control of an air source allows an easy conversion to a single-flame mode of operation. Consequently, the same burner can be operated in either a single- or a dual-flame mode so that the two methods of operation can be readily compared. The purpose of the present paper is to describe such a comparison of single- and dual-flame operation, especially with respect to the problem of quenching of emissions in the flames. It will be shown that one of the most significant advantages of dual-flame operation is the minimization of quenching effects on the sulfur and phosphorus emissions.

EXPERIMENTAL

The work described in this paper employed the flame photometric detector manufactured by Varian (Palo Alto, Calif.) and a Varian Model 3700 gas chromatograph. Chromatographic columns and operating conditions are indicated where used. Solvents used to prepare test samples were nanograde 2,2,4-trimethylpentane obtained from Mallinckrodt (St. Louis, Mo.) and chromatoquality grade butyl alcohol obtained from Matheson, Coleman, and Bell (Norwood, Ohio). Thiophosphate pesticides were obtained from Polyscience (Niles, Ill.) as 1% solutions by weight in benzene. These thiophosphate samples were further adjusted to desired concentrations by dilutions in 2,2,4-trimethylpentane. All other sample mixtures were prepared by dilutions in either 2,2,4-trimethylpentane or butyl alcohol using pure chemicals obtained from Chem Service (West Chester, Pa.). Gasoline samples were obtained from service stations representing two major oil companies and two independents.

In the Varian dual-flame FPD, hydrogen and air flow rates normally supplied to the burner are as follows: H_2, 140 mL/min; air 1, 80 mL/min; and air 2, 170 mL/min. The combination of H_2 and air 1 forms a first flame which is used to achieve sample decomposition. The unburnt H_2 and combustion products from the first flame are then combined with air 2 to form a second flame for the purpose of generating the desired optical emissions. For operation in a single-flame mode, the air 1 source is turned off, and the single-flame formed from the combination of H_2 and air 2 then is used for both sample decomposition and generation of the optical emission. From signal-to-noise considerations, the H_2 and air 2 flow rates listed above are reasonable optimal choices for single-flame as well as dual-flame operation.

For sulfur detection, the Varian FPD employs a broad-bandpass filter with peak optical transmission at 365 nm. For phosphorus detection, the filter is a narrow-bandpass filter peaked at 530 nm. In the dual-flame mode of operation, the sulfur response varies according to a square-law dependence on sulfur amount, while the phosphorus response is a linear dependence on phosphorus amount.

RESULTS AND DISCUSSION

In Figure 1 there is shown a simple analysis of a 10-ppm concentration of carbon disulfide (CS_2) in butyl alcohol. In this analysis, the CS_2 comes off the GC column first, followed by the butyl alcohol solvent peak. In the chromatograms shown in Figure 1, the sample was injected twice with the second injection timed so that the second CS_2 peak came off the column at the same time as the butyl alcohol peak from the first injection. Figure 1 shows that the dual-flame burner produces a peak for the second CS_2 sample which is approximately 80% of the peak height of the first CS_2, even though the second peak is present in the detector at the same time as a large concentration of butyl alcohol. When the FPD burner is operated in a single-flame mode, Figure 1 shows that the first CS_2 peak is larger than that obtained with dual flames, but there is absolutely no response for the second CS_2 peak. In other words, in the single-flame mode the butyl alcohol solvent so alters the flame environment that light emission is drastically quenched, including light emission from the butyl alcohol as well as the CS_2. The observed difference in sensitivities in the case of the first CS_2 peak may be associated with different concentrations of H atoms in the emission flames. Sulfur emission depends strongly on H-atom concentration (*9*), and the additional air 1 supply in the dual-flame mode could result in a lowering of the H-atom concentration.

The chromatograms shown in Figure 1 provide a clear illustration of the hydrocarbon quenching effect in the single-flame FPD. The chromatograms shown in Figure 2 provide a more subtle example of this hydrocarbon quenching. In

0003-2700/78/0350-0345$01.00/0 © 1978 American Chemical Society

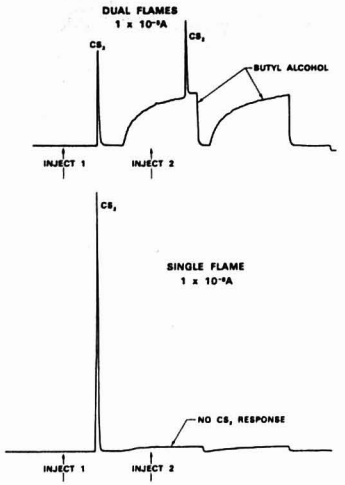


Figure 1. Dual- and single-flame analyses of 10 ppm CS_2 in butyl alcohol with the second injection timed to cause CS_2 to pass through FPD at the same time as butyl alcohol. GC conditions: column, 200 cm × 6 mm o.d. × 2 mm i.d., Pyrex, 5% OV-101 on 100/120 Chrom W; carrier flow, 25 mL/min He; column temperature, 60 °C; injector temperature, 130 °C; detector temperature, 230 °C

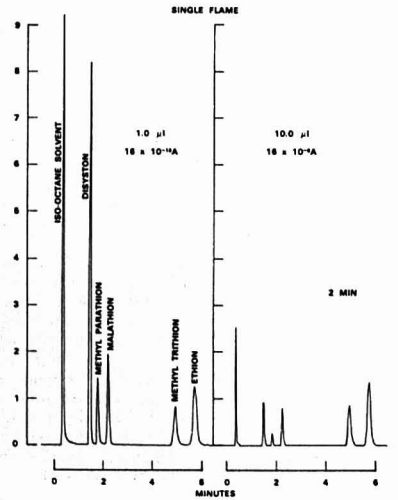


Figure 2. Single-flame chromatograms of sample containing 5 ppm each of five thiophosphate pesticides. GC conditions: column, same as Figure 1; carrier flow, 30 mL/min He; column, injector, and detector temperatures all 200 °C

Figure 2, there is illustrated an analysis of a sample containing approximately 5 ppm each of five different thiophosphate pesticides. The analysis was performed using the single-flame mode and using the S filter. The two chromatograms shown correspond to injections of 1.0 and 10.0 µL of the sample with the current range for the 10.0-µL injection being 100 times greater than that of the 1.0-µL injection. If these sulfur

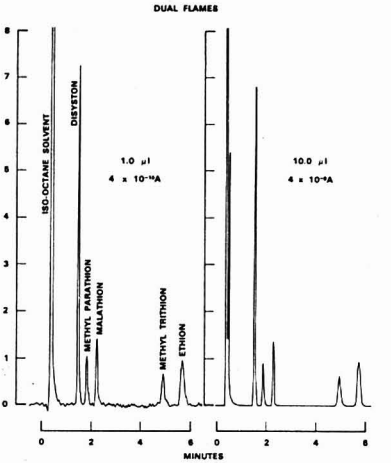


Figure 3. Dual-flame chromatograms of same sample and GC conditions as Figure 2

emissions obeyed a pure square-law dependence on sulfur content, then the heights of the sample peaks should be the same in the two chromatograms. That clearly is not the case. In the 10-µL chromatogram, the three peaks at early retention times are greatly diminished in amplitude. This effect is caused by the underlying tail of the isooctane solvent peak which is much greater in the case of the 10.0-µL injection than in the case of the 1.0-µL injection. Although this solvent tail does not show up on the chromatogram because it does not give off any detectable light, that solvent tail is nevertheless present in the FPD flame, and it quenches the light emission from the sample peaks at early retention times. These two chromatograms also provide a good illustration of the confusion that can develop concerning the sulfur response of single-flame detectors. For example, from the data shown in Figure 2, it could be erroneously concluded that the disyston response is approximately linear with sample amount, the methyl trithion and ethion responses exhibit a pure square-law dependence on sample amount, and the methyl parathion and malathion responses are somewhere between a linear and a pure square-law dependence on sample amount. However, if the injected sample volume is held fixed at 1.0 µL, and sulfur response is checked instead by varying sample concentrations, then it is found that all five sulfur compounds exhibit a square-law response. Consequently, variations in both sample volume and sample concentration revealed in this case that solvent quenching is occurring in the data shown in Figure 2.

Figure 3 shows the use of the dual-flame burner for the same sample analysis described in Figure 2. With dual flames, both the 1.0-µL and 10.0-µL chromatograms exhibit the same relative peak height distribution. Also, all five sample peaks exhibit a square-law sulfur response within the accuracy of the GC analysis. Hence, the dual-flame burner eliminates the distortion of the chromatogram caused by the quenching of sample response by an underlying solvent tail. Figure 3 also illustrates the advantage of injecting larger sample volumes. By increasing sample volume by a factor of 10, the signal-to-noise ratio has been increased by a factor of 100. Also, the selectivity of sulfur response can be expected to improve with larger sample volumes because sulfur peaks increase as the square of sample amount while interfering hydrocarbon peaks

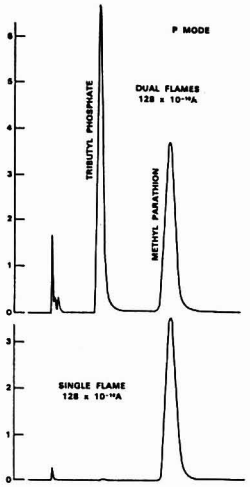


Figure 4. Dual- and single-flame analyses of 20 ng each of tributylphosphate and methyl parathion in isooctane solvent. 1.0 μL sample volume. GC conditions: column, 50 cm × 3 mm, 5% OV-101 on 100/120 Chrom G; carrier flow, 30 mL/min He; column temperature, 180 °C; injector and detector temperatures, 220 °C

increase only linearly with sample amount.

Figure 4 illustrates the analyses of 20 ng each of tributylphosphate and methyl parathion using the P filter and both the dual- and single-flame modes of operation. With dual flames, the FPD responds to tributylphosphate and methyl parathion with exactly the same sensitivity of 20 nA/(ng P/s). However, in the single-flame mode, the response to tributylphosphate is negligible. In this case, it seems unlikely that the absence of response to tributylphosphate is due entirely to quenching by the solvent tail. Rather, it appears that this single-flame chromatogram is exhibiting a quenching effect associated with the different molecular structures of tributylphosphate and methyl parathion. Similar observations of compound-dependent sample responses have been reported in previous work with single-flame detectors (2).

Another area where quenching of sample response has been a problem in the past is in the analysis of samples so complex that the GC column does not completely separate the sulfur and phosphorus compounds from overlapping hydrocarbon compounds. An example of this situation is the analysis of gasoline using a packed column. Figure 5 shows two chromatograms representing the analysis of a gasoline sample on a packed column using column oven programming from 35 to 200 °C. The top chromatogram in Figure 5 was obtained with the dual-flame FPD operated with an oxygen-rich emission flame and a special optical filter peaked at the most intense hydrocarbon emission. This chromatogram of hydrocarbon emissions shows that there are a great many unresolved hydrocarbon peaks being eluted from the GC column. The bottom chromatogram in Figure 5 shows the same analysis performed using the dual-flame FPD with a normal hydrogen-rich emission flame and using the sulfur filter. Despite the simultaneous presence of many overlapping hydrocarbon compounds, the S-mode chromatogram reveals a relatively small number of large, well-resolved peaks. The identity of these S-mode peaks was not established. However, if the sample volume was increased by a factor of two, most of the peak heights increased by a factor of four. Hence, most

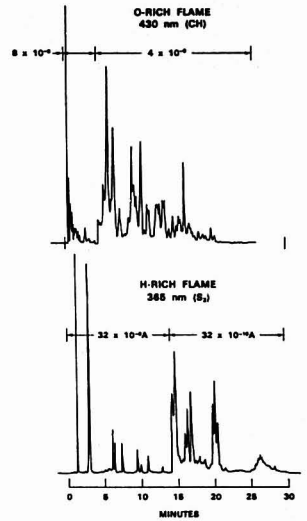


Figure 5. Analysis of 2 μL gasoline sample using dual-flame FPD in hydrocarbon-responsive mode in top chromatogram and sulfur mode in bottom chromatogram. GC conditions: column and carrier flow, same as Figure 1; injector and detector temperatures, 200 °C; column temperature program, hold at 35 °C for 3 min, program at 4 °C/min from 35 to 120 °C and 84 °C/min from 120 to 200 °C, hold at 200 °C for 3 min

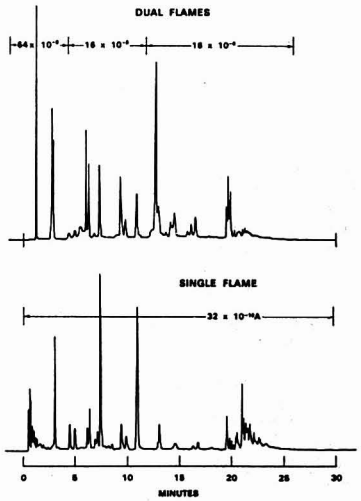


Figure 6. Analysis of same gasoline sample as Figure 5 using dual-flame and single-flame FPD operation. Column temperature program, hold at 35 °C for 3 min, program at 4 °C/min from 35 to 100 °C and 84 °C/min from 100 to 200 °C, hold at 200 °C for 2 min. Other GC conditions same as Figure 5

of the prominent peaks in the bottom chromatogram exhibited the square-law response dependence expected for S-containing compounds.

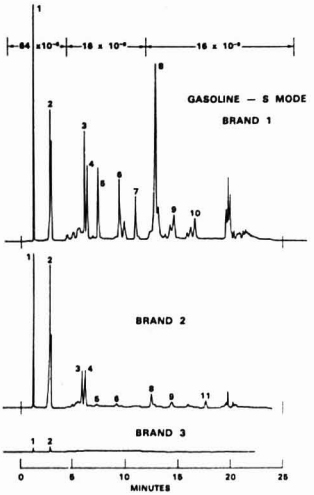


Figure 7. Dual-flame, sulfur-mode analyses of 2-μL samples of three different gasoline brands. GC conditions same as Figure 6

Figure 6 shows the same gasoline sample analyzed with both the dual-flame method and a single-flame method. Changes in the attenuation factors and a slight change in the column oven program account for a difference in appearance of the dual-flame chromatogram in Figure 6 from that shown in Figure 5. There are three significant differences between the single-flame chromatogram and the dual-flame chromatogram. First, the peaks exhibited in the dual-flame chromatogram are a factor of 10 to 100 times larger than the peaks in the single-flame chromatogram. Second, at early retention times the single-flame chromatogram exhibits some of the same unresolved hydrocarbon peaks seen in the oxygen-rich chromatogram of Figure 5. Finally, the single-flame chromatogram is completely missing a few of the very largest peaks present in the dual-flame chromatogram. Hence, it is clear that the dual-flame method is much superior to the single-flame method in the analysis of complex mixtures such as the gasoline samples described here.

Figures 7 and 8 illustrate the potential application of the dual-flame FPD to the analysis of sulfur compounds in different brands and grades of gasoline. In Figure 7, there are shown chromatograms of three different brands of gasoline. All three chromatograms were obtained under exactly the same attenuations. Hence, it can be seen that there are significant differences in peak amplitudes as well as peak distributions between the three gas samples. Figure 8 shows the analysis of a fourth brand of gasoline, and illustrates the difference between the regular and premium grades of that brand. Again, there are significant differences in the distribution of peaks present in the two chromatograms.

CONCLUSIONS

Unlike the single-flame FPD, the dual-flame method of operation allows excellent sample response to be obtained even for analyses where there exists a hydrocarbon background eluting from the GC column at the same time as the sulfur

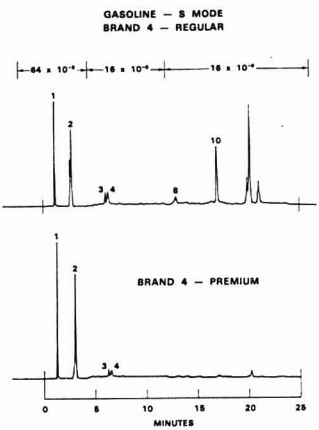


Figure 8. Dual-flame, sulfur-mode analyses of 2-μL samples of different grades of same gasoline brand. GC conditions same as Figure 6

or phosphorus compounds. This characteristic of the dual-flame FPD means that low resolution GC columns can often suffice to analyze complex mixtures. It also suggests that less elaborate sample preparations may be employed before selectively analyzing samples for S or P compounds. However, some reduction of sample response can still occur at very high levels of hydrocarbon background. Consequently, for accurate quantitative results, the dual-flame FPD should be calibrated with standards prepared in a sample matrix that resembles as much as possible the matrix of the unknown samples.

For some sulfur compounds which are well resolved from hydrocarbon interferences, the single-flame method of operation can give greater sample response than dual-flame operation. However, single-flame operation is more likely to provide sample responses that are strongly dependent on the molecular structure of the sample compound. Also, single-flame detectors are known (*10*) to often exhibit sulfur responses that deviate from the expected pure square-law dependence, with the amount of deviation again being compound-dependent.

Dual-flame FPD operation may not be as sensitive as single-flame operation in some cases. However, dual-flame operation will generally provide more uniform response to samples, irrespective of sample composition or concentration.

LITERATURE CITED

(1) S. S. Brody and J. E. Chaney, *J. Gas Chromatogr.*, **4**, 42 (1966).
(2) S. O. Farwell and R. A. Rasmussen, *J. Chromatogr. Sci.*, **14**, 224 (1976).
(3) W. E. Rupprecht and T. R. Phillips, *Anal. Chim. Acta*, **47**, 439 (1969).
(4) S. G. Perry and F. W. G. Carter, "The Chromatography of Sulfur Compounds", in R. Stock, Ed., "Gas Chromatography 1970", Proceedings of the 8th International Symposium on Gas Chromatography, Dublin, 1970, Institute of Petroleum, London, 1971, p 381.
(5) T. Sugiyama, Y. Suzuki, and T. Takeuchi, *J. Chromatogr.*, **80**, 61 (1973).
(6) C. D. Pearson and W. J. Hines, *Anal. Chem.*, **49**, 123 (1977).
(7) D. A. Clay, C. H. Rogers, and R. H. Jungers, *Anal. Chem.*, **49**, 126 (1977).
(8) L. Blomberg, *J. Chromatogr.*, **125**, 389 (1976).
(9) P. L. Patterson, R. L. Howe, and A. Abu-Shumays, *Anal. Chem.*, **50**, preceding paper in this issue.
(10) C. H. Burnett, D. F. Adams, and S. O. Farwell, *J. Chromatogr. Sci.*, **15**, 230 (1977).

RECEIVED for review August 22, 1977. Accepted November 4, 1977.

Simultaneous Determination of Vancomycin, Anisomycin, and Trimethoprim Lactate by High Pressure Liquid Chromatography

R. L. Kirchmeier* and R. P. Upton

Pfizer Inc., Quality Control, Special Testing and Analytical Development Laboratories, Groton, Connecticut 06340

A reverse phase, high pressure liquid chromatographic method for the rapid, accurate, precise, and simultaneous determination of vancomycin, anisomycin, and trimethoprim lactate has been developed, and applied to the determination of these compounds in antibiotic mixtures. No chemical methods for the determination of anisomycin have previously been reported. The methods reported in the literature for the determination of vancomycin, and/or trimethoprim lactate are imprecise, nonspecific, or time consuming, and do not allow the simultaneous quantitation of anisomycin, vancomycin, and trimethoprim. Precision of the high pressure liquid chromatographic assay was found to be ±1.8%, ±1.1%, and ±2.2% for vancomycin, anisomycin, and trimethoprim lactate, respectively (two standard deviations relative to the average).

With the recent development of an antibiotic mixture for use as an inhibitor for the selective culture of *Neisseria gonorrhoeae* (*1*), containing vancomycin, anisomycin, and trimethoprim lactate, the development of a rapid, accurate, and precise chemical method of analysis for these materials in the presence of each other was desired. No previous reports of a method for the chemical determination of anisomycin content appear in the literature. Vancomycin has in the past been analyzed and/or quantitated by column chromatography (*2*), or TLC (*3–5*). Chemical methods reported for the determination of trimethoprim involve the use of spectrofluorimetry (*6*), paper chromatography (*7*), TLC (*8*, *9*), and GLC (*10*). Although the GLC method reported above for trimethoprim (*10*) is precise and accurate, the simultaneous determination of vancomycin and anisomycin is not possible because of their low volatilities. Simultaneous analysis of vancomycin, anisomycin, and trimethoprim by TLC or paper chromatography would not be feasible for lack of precision and specificity. A fluorimetric TLC procedure for trimethoprim (*9*) requires 24 h of development time for the fluorimetric determination of low levels of trimethoprim. Since all of the methods described above suffer from one or more limitations, i.e., they are either nonspecific, involve long sample preparation and/or analysis tmes, or are not amenable to the simultaneous determination of vancomycin, anisomycin, and trimethoprim lactate, the development and application of a reverse phase high pressure liquid chromatographic procedure was undertaken.

EXPERIMENTAL

Apparatus and Operating Conditions. A Waters Associates Model 6000A high pressure metering pump at a flow rate of 1.0 mL/min in conjunction with a Schoeffel Model SF770 multiwavelength UV detector set at 225 nm (0.2 Absorbance Units Full Scale (AUFS)) were used for the analysis of all samples. A Valco Model CV-6-UHPa-C-20 loop injection valve (7000 psi pressure rating) fitted with a 25-μL sample loop was employed for sample injections. Spectra were recorded with a Varian Model A-25 recorder (10 mV) set at a chart speed of 10 in./h.

Column. A 30 cm × 4 mm i.d. Waters Associates μ Bondapak C_{18} column (a monomolecular layer of octadecyltrichlorosilane chemically bonded to totally porous μ-Porasil particles having an average diameter of 10 μm) was used at ambient temperature.

Reagents and Standards. Acetonitrile distilled in glass was purchased from Burdick and Jackson. Reference standards for vancomycin (1070 μg/mg base), anisomycin (100%), and trimethoprim lactate (98–100%) were received from Elanco, Pfizer Inc., and Burroughs Wellcome, respectively, and used without further purification.

Mobile Phase. Mobile phase is prepared by mixing 125 mL of acetonitrile and 875 mL of pH 6, 0.05 M potassium dihydrogen phosphate buffer solution in a 1-L vacuum flask. Degassing is accomplished via house vacuum (640 Torr, approximately) with magnetic stirring for 10 min prior to use in the liquid chromatograph.

Calibration Curves. Calibration curves for vancomycin, anisomycin, and trimethoprim lactate were determined on separate standard solutions (in mobile phase) containing from 0.01 to 0.07, 0.05 to 0.4, and 0.03 to 0.07 mg/mL of vancomycin, anisomycin, and trimethroprim lactate, respectively. For each solution, 25 μL was injected into the chromatographic system, and the resulting peak height was plotted vs. concentration.

Sample Preparation. No sample pretreatment was required for the samples assayed in this study. Approximately 40 mg of the antibiotic mixture to be assayed (containing up to 5 mg each of vancomycin and trimethoprim and up to 30 mg of anisomycin) was accurately weighed out into a 100-mL volumetric flask, and diluted to volume with mobile phase.

RESULTS AND DISCUSSION

Reverse phase high pressure liquid chromatography was a logical choice for the simultaneous determination of vancomycin, anisomycin, and trimethoprim lactate. Figure 1 indicates the structures for anisomycin and trimethoprim base. Although the complete structure of vancomycin is not know, several reports of the determination of the partial structure and approximate molecular weight (1388) of vancomycin appear in the literature (*11–13*). Separation of vancomycin from anisomycin and trimethoprim was accomplished on a Sephadex G 10 column with a 0.02 M, pH 7.0 phosphate buffer mobile phase; however, trimethoprim and anisomycin were not resolved (*14*). In addition, approximately 4 h were required for the complete elution of vancomycin, anisomycin, and trimethoprim lactate from the column.

The separation of vancomycin into three biologically active components via liquid chromatography on a Sephadex C-50 column has been previously reported (*2*). The average distribution (% by peak area measured at 280 nm) of the biologically active vancomycin components was found to be 51.5 and 73.3% (most biologically active), 20.1 and 16.8% (medium biological activity), and 15.4 and 10.1% (least biologically active) for the two vancomycin hydrochloride preparations. Under the high pressure liquid chromatographic conditions employed in this study, the chromatography of two separate preparations of vancomycin hydrochloride (Elanco Lot OAY56A and Elanco Lot 8FW78F) resulted in the elution of one major, and several minor components (by peak height measurement at 225 nm, see Figure 2). Standard curves obtained by measuring the peak height of the major component, and plotting this peak height vs. concentration, agreed to within 1.2% for the two vancomycin preparations. The vancomycin eluate was monitored at several wavelengths, including 280 nm; however, no significant change in the

0003-2700/78/0350-0349$01.00/0 © 1978 American Chemical Society

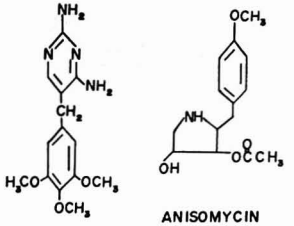


Figure 1. Structure of anisomycin and trimethoprim base

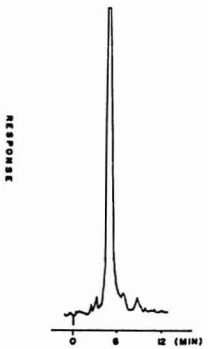


Figure 2. Chromatographic trace of vancomycin eluate at 225 nm

proportion of the major component was noted in either vancomycin preparation (by measurement of observed peak heights at the various wavelengths). In addition, a sample of vancomycin HPLC eluate was collected, lyophilized, and its bioactivity was determined vs. an unchromatographed vancomycin sample at the same concentration in the same phosphate matrix by a previously reported biochemical procedure (*15*). Both samples were assayed against vancomycin hydrochloride Elanco Lot 8FW78F. No significant difference in bioactivity was found between the chromatographed and control sample of vancomycin. Thus 0.75 and 0.72 μg/mg of vancomycin hydrochloride were found in the chromatographed and control samples, respectively.

The effect of mobile phase composition on the retention volumes of vancomycin, anisomycin, and trimethoprim lactate is given in Table I. Optimum conditions for a particular column result in the elution of all three components within approximately 20 min. Peak heights observed for vancomycin, anisomycin, and trimethoprim lactate as a function of detector wavelength are given in Table II.

The chromatographic trace of a standard mixture containing vancomycin, anisomycin, and trimethoprim lactate obtained at 225 nm is shown in Figure 3.

Calibration curves for vancomycin, anisomycin, and trimethoprim lactate were prepared on a single day. Correlation coefficients were 0.998, 0.9999, and 0.9985 for vancomycin, anisomycin, and trimethoprim lactate, respectively. The mean value of y and the y-intercept were found to be 346 and −13, 553 and +11, and 3.45 and +0.35 for vancomycin, anisomycin, and trimethoprim lactate, respectively. Repeated injections of standard solutions of vancomycin (seven injections on two separate days), anisomycin (six injections on two separate

Table I. Retention Volume vs. % Acetonitrile in Mobile Phase

Mobile phase: % acetonitrile in 0.05 M, pH 6 phosphate buffer	Retention volume, mL		
	Vancomycin	Anisomycin	Trimethoprim lactate
20	3.0	6.0	6.8
17.5	···	10.0	12.5
15	3.5	13.3	17.0
14	4.6	16.5	21.5
12.5	6.1	···	···
10	19.5	34.5	46.5

Table II. Observed Peak Height vs. Detector Wavelength

Detector wavelength, nm	Observed peak height		
	0.04 mg/mL of vancomycin, cm	0.2 mg/mL of anisomycin, cm	0.05 mg/mL of trimethoprim lactate, cm
218, 0.1 AUFS	17.0	46.4	29.8
225	14.6	32.4	27.4
230	12.6	13.4	24.4
235	10.1	3.1	19.7
254	1.2	3.5	5.6
280	2.1	4.6	5.2

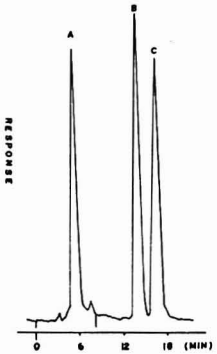


Figure 3. Chromatographic trace of a standard mixture containing 0.05 mg/mL each of vancomycin (A), and trimethoprim lactate (C), and 0.3 mg/mL of anisomycin (B)

days), and trimethoprim lactate (six injections on two separate days), gave rise to one standard deviation relative to the average peak heights of 0.6%, 0.3%, and 0.4%, respectively. Thus, single point standards were used for the determination of vancomycin, anisomycin, and trimethoprim lactate by this HPLC method.

Table III summarizes the analytical data obtained by this method on a series of 17 samples containing vancomycin, anisomycin, and trimethoprim lactate. Values are reported in terms of percent of component as determined by high pressure liquid chromatography relative to the label claim for each component. The values thus reported by HPLC tend to be 6% high for vancomycin, 2.2% low for anisomycin, and 2.0% low for trimethoprim lactate. The precision of the HPLC method as determined on four separate weighings of a single sample on two separate days was found to be ±1.8%, ±1.1%, and ±2.2% (two standard deviations relative to the average) for vancomycin, anisomycin, and trimethoprim lactate, respectively. Sample stability studies were undertaken, and indicated no trend in assay values obtained by

Table III. Analysis of Inhibitory Antibiotic Mixture by HPLC

Sample No.	Vancomycin content by HPLC (% relative to label claim)	Anisomycin content by HPLC (% relative to label claim)	Trimethoprim lactate by HPLC (% relative to label claim)
1	102	99	100
2	106	96	99
3	102	98	99
4	102	100	101
5	98	96	96
6	99	100	101
7	107	99	101
8	109	102	102
9	104	98	98
10	104	94	93
11	108	98	97
12	106	96	95
13	113	99	99
14	107	94	94
15	106	97	95
16	109	95	95
17	114	101	99

HPLC with respect to temperature or pH for samples stored under various conditions for periods of several months.

Samples of vancomycin, anisomycin, and trimethoprim lactate were also subjected to both acidic and basic hydrolysis (standard solutions of each material were treated with 0.1 N NaOH and 0.1 N HCl for periods of up to 2 h). High pressure liquid chromatography of these partially decomposed materials revealed no interfering eluates. Aglucovancomycin, prepared via the acid hydrolysis of vancomycin (*16*), was found to elute at the solvent front under the HPLC conditions used in this study. No other specific interferences were tested.

In conclusion, the application of this reverse phase, high pressure liquid chromatographic approach for the simultaneous determination of vancomycin, anisomycin, and trimethoprim lactate results in a rapid, accurate, precise method of analysis. The procedure should be applicable to determination of these materials in biological matrices subsequent to extraction of the components of interest, and application to the study of vancomycin and decomposition products obtained by various chemical means may aid in the further elucidation of the vancomycin structure.

ACKNOWLEDGMENT

The authors are indebted to F. Hochstein for supplying the standard materials used, and to R. Holmwood and J. Beyer for valuable aid in the development and application of this method. Appreciation is also given for the bioassay of vancomycin samples by J. Stankewich.

LITERATURE CITED

(1) J. Martin and J. Lewis, *J. Assoc. Public Health Directors*, in press.
(2) G. K. Best, N. H. Best, and N. N. Durham, *Antimicrob. Agents Chemother.*, 115 (1968).
(3) B. B. Korchagin, L. I. Serova, Z. I. Vtorova, I. I. Vagina, E. Z. Olpinska, and S. P. Dementieva, *Epidemiol., Mikrobiol. Infekts Bolez.*, *8*, 50 (1971).
(4) I. J. McGilveray and R. D. Strickland, *J. Pharm. Sci.*, **53**, 77 (1967).
(5) V. Betina, *J. Chromatogr.*, **15**, 379 (1964).
(6) D. E. Ernest, B. A. Koechlin, and R. E. Weinfeld, *Chemotherapy*, **14**, 22 (1969).
(7) L. Reio, *J. Chromatogr.*, **60**, 183 (1972).
(8) M. Bidlo and D. Bobak, *Lucr. Conf. Nat. Chim. Anal., 3rd*, **4**, 199 (1971).
(9) C. W. Sigel and M. E. Grace, *J. Chromatogr.*, **80**, 111 (1973).
(10) F. L. Fricke, *J. Assoc. Off. Anal. Chem.*, **55**, 1162 (1972).
(11) K. A. Smith, D. H. Williams, and G. A. Smith, *J. Chem. Soc., Perkin Trans. 1*, **20**, 2369 (1974).
(12) N. K. Kochetkov and O. S. Chizov, *Biochim. Biophys. Acta*, **83**, 134 (1964).
(13) H. Bjorndal, C. G. Hellerquist, B. Lindberg, and S. Svensson, *Angew. Chem., Int. Ed. Engl.*, **9**, 910 (1970).
(14) F. A. Hochstein, Pfizer Inc., Groton, Conn. unpublished work, 1976.
(15) "Code of Federal Regulations", **21**, April 1, 1976 rev., U.S. Government Printing Office, Washington, D.C., p 216.
(16) F. J. Marshall, *J. Med. Chem.*, **8**, 18 (1965).

RECEIVED for review September 6, 1977. Accepted November 28, 1977.

Thin-Mercury-Film Voltammetry of Inorganic Lead(II) Complexes in Seawater

Lloyd M. Petrie* and Rodger W. Baier[1]

Graduate School of Oceanography, University of Rhode Island, Kingston, Rhode Island 02881

Cyclic voltammetry of 10^{-5} M Pb(II) model solutions proved useful in revealing that electron transfer of Pb(II) at thin mercury film electrodes was reversible for glassy carbon electrodes at scan rates ≤10 mV/s and less reversible for wax-impregnated graphite electrodes. Electron transfer was reversible for PbCl, quasi-reversible for $PbSO_4$ and $PbCO_3$, and least reversible for PbOH. Anodic stripping voltammetry (ASV) and use of ^{210}Pb radiotracer in 10^{-8} M Pb(II) model solutions revealed similar trends. ASV of organic-free seawater at pH 8.5 gave peak currents less than theoretical for Pb(II), even taking into account cell material adsorption. This was largely due to the electrochemical inactivity of PbOH. At pH 3, the peak currents were proportional to the seawater Pb(II) concentration.

[1]Present address, Department of Chemistry, Duke University Marine Laboratory, Beaufort, N.C. 28516.

Because of its extensive use, its persistence in the marine environment (400 years), and its toxicity, the biogeochemical impact of lead on the marine environment needs to be more fully characterized (*1–5*). To more effectively predict the transport and biological effects of lead and other trace metals in the marine environment, it is necessary to determine not only their concentrations but their chemical speciation (*6, 7*).

Because of precise and sensitive levels of detection and the capability for discrimination of discrete metal complexes, voltammetric techniques such as anodic stripping voltammetry (ASV) have been widely used to characterize metal speciation in seawater (*8–10*). Generally, two types of working electrodes have been used: (1) the hanging mercury drop electrode (HMDE) and (2) the thin mercury film electrode (TMFE), which consists of a liquid mercury film on an inert substrate, usually wax-coated graphite or glassy carbon. Both electrodes have distinct advantages and disadvantages with the HMDE claiming superior precision and the TMFE superior sensitivity

0003-2700/78/0350-0351$01.00/0 © 1978 American Chemical Society

and selectivity (*11*, *12*).

Efforts to fully utilize the capability of voltammetry in Pb(II) speciation studies have been frustrated by several difficulties: (1) contamination (*13*), (2) rapid adsorption of Pb(II) species onto electrochemical cell materials (*14*), and (3) incomplete data about the electroactivity of individual Pb(II) complexes (*15*). While much concern has been directed toward these first two difficulties, the last one is also critical to proper interpretation of voltammetric data. Voltammetric classification of Pb(II) present in seawater into various operational fractions (e.g., soluble inorganic species, soluble organic chelates, particulate phases) requires knowledge of which Pb(II) species are electroactive. Even for the principal inorganic species in seawater, information is incomplete. Pb(aquo) and PbCl apparently undergo reversible electron transfer at both HMDEs and TMFEs (*15–17*). Reversible electron transfer has not been demonstrated for PbOH, $PbSO_4$, or $PbCO_3$.

The objective of this work was to interpret Pb(II) voltammetric responses of organic-free seawater by taking into account the electroactivity of principal species and adsorption onto cell materials. TMFEs were evaluated because few detailed studies of this electrode type have been reported (*16–20*). Cyclic voltammetry of 10^{-5} M Pb(II) model solutions was used to evaluate the electron-transfer properties of individual inorganic Pb(II) species. Although widely used to study electron transfer at HMDEs and bare substrate electrodes, cyclic voltammetry has not been performed with TMFEs. ASV was next performed on 10^{-8} M Pb(II) model solutions. A pH-dependent seawater speciation model was constructed from formation constants determined from cyclic voltammetry. Then the ASV response of UV-irradiated seawater vs. pH was interpreted based on predicted distribution and electroactivity of inorganic Pb(II) species.

The most complete mathematical treatment of reversible electron transfer at a thin, planar, mercury film is the deVries and van Dalen model (*21–23*). For the limiting case of very thin mercury films (semiinfinite diffusion of Pb(II) into and out of the Hg layer) the following relationships apply:

$$H = \frac{l^2 nFv}{RTD_R} \leqslant 1.6 \times 10^{-3}$$

$$i_{pc} = 2.4953 \times 10^{11}\, n^{3/2} A C_O^{\circ} D_O^{1/2} v^{1/2}\ (\mu A)$$

$$n(E_{pc} - E_{1/2}) = -38.45 + 29.58 \log H\ (\text{mV})$$

$$i_{pa} = 1.1157 \times 10^{12}\, n^2 A C_R^{\circ} l v\ (\mu A)$$

$$n(E_{pa} - E_{1/2}) = -1.43 + 29.58 \log H\ (\text{mV})$$

$$nb_{1/2} = 75.53\ (\text{mV})$$

where

H	dimensionless flux ratio parameter
i_{pc}	cathodic (reduction) peak current, μA
E_{pc}	cathodic (reduction) peak potential
$E_{1/2}$	polarographic 1/2-wave potential
i_{pa}	anodic (oxidation) peak current, μA
E_{pa}	anodic (oxidation) peak potential
$b_{1/2}$	width of anodic peak at 1/2 peak height, mV
l	Hg film thickness, cm.
n	number electrons transferred
F	Faraday constant = 96 500 C/equiv
v	potential scan rate, V/s
R	8.314 J/K mole
T	temperature = 296 K
D_R	diffusivity of reduced species in Hg film, cm^2/s
A	electroactive area, cm^2
C_R°	initial concentration of reduced species in Hg film, mol/cm^3
C_O°	initial concentration of oxidized species in solution, mol/cm^3
D_O	diffusivity of oxidized species in solution, cm^2/s

EXPERIMENTAL

Apparatus. A Princeton Applied Research PAR 174 Polarographic Analyzer and Hewlett-Packard 7035B X–Y recorder were used. A Perkin-Elmer 56 recorder was used for chronoamperometry. Wax-impregnated graphite electrodes were obtained from Princeton Applied Research. Glassy carbon electrodes were made by gluing a 6 mm diameter × 3 mm GC-A chip (Tokai Industries, Ltd.) inside a Pyrex tube. Mercury was placed in the bottom inside of the electrode and a 24-gauge Pt wire inserted for electrical contact. The reference electrode was a Sargent-Welch miniature Ag/AgCl (saturated KCl) electrode and the counter electrode was a 1-mm diameter WIGE. The cell and bubbler were both Pyrex. An ordinary rubber stopper was used to hold the electrodes and bubbler in place. N_2 or CO_2 from pressurized cylinders was fed through a Manostat flowmeter and into the bubbler through acid-washed Tygon tubing. A Heath EU-302A pH meter was used.

For electropurification of solutions, a 250-mL Pyrex Erlenmeyer flask fitted with a glass stopcock was used. The working electrode was a glass-embedded 24-gauge Pt wire placed in a Hg pool. Both the reference and counter electrodes were 24-gauge Pt wires. A Heath Model EUA-19-2/4 Polarographer module was used. The Hg layer and overlying solution were stirred by a Teflon-coated stirring bar.

Liquid scintillation counting was performed with either a Beckman LS-133 or Picker Liquimat. Seawater was photooxidized by a UV Photo-Oxidation Unit (La Jolla Scientific Co.). Computation and regression analyses were performed on a Digital Equipment Corporation PDP 11 and Tektronix 4012 display unit. Planimetry was done with a Keuffel and Esser Rolling Disc Planimeter, Model 62-0110.

Reagents. All reagents, except as noted, were ACS reagent grade from Fisher Scientific. Merck Suprapur 1.0 N HNO_3 was used for ASV experiments. The seawater was collected at 1000 m by a plastic balloon at position 32°25′ N and 75°59′ W, transferred to 20-L polyethylene bottles and stored in darkness at 5 °C. The water for solution make-ups and washing was well water distilled in stainless steel, sent through two mixed ion-exchange beds in series, and sent through an activated charcoal filter. For liquid scintillation, Aquasol cocktail (New England Nuclear) and 20-mL glass vials (Kimble) were used.

Procedures. Fifteen-milliliter samples were used. All experiments were performed at a temperature of 23 ± 0.5 °C and ionic strength (I) of 0.7 ± 0.01. For solutions containing high concentrations of ligands, a mixture of ligand salt and KNO_3 was used to maintain I = 0.7. The solution pH was adjusted by introducing small volumes of purified HNO_3 or KOH. All potentials are reported vs. Ag/AgCl (saturated KCl). Before each experiment, all electrodes and glassware were washed with 1 N HNO_3 and rinsed with deionized water.

Before each experiment, the working electrode was polished and cleaned. After 5 minutes deaeration, stock $Hg(NO_3)_2$ was added to give an initial Hg concentration of 3.95×10^{-5} M. Then –0.4 V was imposed on the working electrode for 1–2 min before being changed to 0.0 V. Plating continued until 0.024 C of charge had been passed.

The standard solution for cyclic voltammetry was 10^{-5} M Pb(II) in 0.7 M KNO_3 at pH 5.00 ± 0.05 to which ligands were then added. Potential scans began at –0.2 V except for those shifted considerably cathodically by complexation of Pb(II) (i.e., PbOH and $PbCO_3$). For these the cyclic scan was initiated between –0.2 and –0.3 V. However, manual switching of the potential was always 200 mV past the cathodic peak in accordance with Nicholson and Shain for HMDEs (*24*). The solution was bubbled for 15 s and left for 30 s to become quiescent before initiating a new cyclic scan.

The test solution for chronoamperometry was 10^{-5} M Pb(II) in 0.7 KNO_3 at pH 5.00 ± 0.05. The supporting electrolyte was tested individually to substract out background current. After 15-s agitation, the solution was allowed to stand for 30 s before –0.6 V was imposed on the working electrode and the current vs. time recorded. Runs were repeated in triplicate for both WIGE

Table I. Measured vs. Theoretical Peak Currents and Peak Potentials Using a Wax-Impregnated Graphite Electrode[a]

Scan rate, mV/s	i_p (cathodic), μA		E_p (cathodic)[b]		i_p (anodic), μA		E_p (anodic)[b]		$b_{1/2}$, mV[c]
	Measured	Theor.[d]	Measured	Theor.[d]	Measured	Theor.[e]	Measured	Theor.[d]	
2	0.32 ± 0.00	0.35	−0.466 ± 0.001	−0.473	2.11 ± 0.05	1.80 ± 0.05	−0.441 ± 0.001	−0.455	38 ± 0
5	0.47 ± 0.00	0.56	−0.460 ± 0.001	−0.467	2.77 ± 0.01	2.35 ± 0.03	−0.433 ± 0.001	−0.449	39 ± 0
10	0.64 ± 0.01	0.79	−0.458 ± 0.001	−0.463	3.67 ± 0.03	2.94 ± 0.02	−0.428 ± 0.001	−0.445	39 ± 0
20	0.88 ± 0.01	1.12	−0.457 ± 0.001	−0.459	4.69 ± 0.02	3.66 ± 0.04	−0.420 ± 0.001	−0.440	41 ± 0
50	1.22 ± 0.03	1.77	−0.463 ± 0.001	−0.453	6.57 ± 0.18	4.12 ± 0.29	−0.409 ± 0.001	−0.434	47 ± 0
100	1.35 ± 0.04	2.50	−0.477 ± 0.001	−0.448	6.56 ± 0.07	6.24 ± 0.24	−0.400 ± 0.001	−0.430	64 ± 0

[a] Av ± std dev for 3 runs of 10^{-5} M Pb(II) in 0.7 M KNO_3 at pH 5.00 ± 0.05 and T = 23 ± 0.5 °C. [b] Peak potentials vs. A AgCl (saturated KCl). [c] $b_{1/2}$ = width of anodic peak at $^1/_2$ the peak height = 38 mV theoretically at all scan rates. [d] Deviations estimated to be less than 1%. [e] Standard deviations estimated from variances in determination of Pb(0) concn in Hg film.

Table II. Measured vs. Theoretical Peak Currents and Peak Potentials Using a Glassy Carbon Electrode[a]

Scan rate mV/s	i_p (cathodic), μA		E_p (cathodic)[b]		i_p (anodic), μA		E_p (anodic)[b]		$b_{1/2}$, mV[c]
	Measured	Theor.[d]	Measured	Theor.[d]	Measured	Theor.[e]	Measured	Theor.[d]	
2	0.27 ± 0.00	0.24	−0.466 ± 0.000	−0.469	1.57 ± 0.00	1.37 ± 0.02	−0.446 ± 0.000	−0.450	38 ± 0
5	0.42 ± 0.00	0.39	−0.461 ± 0.000	−0.463	2.15 ± 0.00	1.88 ± 0.01	−0.440 ± 0.001	−0.444	38 ± 0
10	0.58 ± 0.00	0.55	−0.457 ± 0.000	−0.458	2.93 ± 0.01	2.34 ± 0.00	−0.435 ± 0.000	−0.440	38 ± 0
20	0.80 ± 0.00	0.77	−0.453 ± 0.000	−0.454	3.94 ± 0.01	3.00 ± 0.00	−0.431 ± 0.000	−0.435	39 ± 0
50	1.21 ± 0.00	1.22	−0.446 ± 0.000	−0.448	6.01 ± 0.00	4.10 ± 0.02	−0.425 ± 0.000	−0.429	40 ± 0
100	1.66 ± 0.02	1.72	−0.442 ± 0.000	−0.443	8.08 ± 0.02	5.33 ± 0.08	−0.421 ± 0.000	−0.425	42 ± 0

[a] Av ± std dev for 3 runs of 10^{-5} M Pb(II) in 0.7 M KNO_3 at pH 5.00 ± 0.05 and T = 23 ± 0.5 °C. [b] Peak potentials vs. Ag/AgCl (saturated KCl). [c] $b_{1/2}$ = width of anodic peak at $^1/_2$ the peak height = 38 mV theoretically at all scan rates. [d] Deviations estimated to be less than 1%. [e] Standard deviations estimated from variances in determination of Pb(0) concentration in Hg film.

and glassy carbon working electrodes.

All stock solutions except Suprapur HNO_3 and seawater used in ASV experiments were electropurified at −1.2 V for 48–72 h. ASV of stock solutions revealed that purification reduced the Pb(II) concentrations approximately two orders of magnitude to the following representative values:

Solution	Pb(II) concentration, M
0.7 M KNO_3	$0.9 \pm 0.4 \times 10^{-9}$ (3 samples)
0.7 M KCl	$1.7 \pm 0.9 \times 10^{-9}$ (4 samples)
0.23 M Na_2SO_4	$1.3 \pm 0.7 \times 10^{-9}$ (3 samples)
1.0 M $NaHCO_3$	7.1×10^{-9} (1 sample)
0.7 M KOH	8.4×10^{-9} (1 sample)

Purified solutions were poured directly into polyethylene bottles that were pre-washed with 0.5 N Suprapur HNO_3 and rinsed with deionized water.

ASV was performed with a deposition potential of −0.8 V for 2.75–11.5 min with N_2 agitation and a 15- to 30-s quiescent period, respectively. The scan rate was 5 mV/s. After the background concentration was determined, 0.1 mL Pb(II) standard or ^{210}Pb(II) standard was added to raise the sample Pb(II) concentration by 5.0×10^{-9} M or 2.9×10^{-9} M, respectively. Duplicate runs were performed at each condition.

The initial activity of radioactive samples was $1.25 \pm 0.5 \times 10^6$ dpm/mL. Liquid scintillation counting was performed on 0.1-mL samples added to 10 mL Aquasol, stored in darkness for 6 h, and counted on either scintillation counter with a 0–0.055 MeV energy window to less than 1% error (*14*). Solution blank activities were less than 2% of the sample activities.

Organic-free seawater was prepared by irradiating 1000 m slope water for 6 h with high intensity ultraviolet light in 500-mL quartz tubes.

RESULTS AND DISCUSSION

$Pb(H_2O)_n$ Electroactivity vs. deVries–Van Dalen Model. Cyclic voltammetry was used to compare TMFE electron-transfer of $Pb(H_2O)_n$ at a wax-impregnated graphite electrode (WIGE) and a glassy carbon electrode (GCE) to the deVries–Van Dalen reversible model.

Diffusivities were obtained by interpolating published data (*25, 26*): $D_R = 1.25 \times 10^{-5}$ and $D_O = 8.10 \times 10^{-6}$ cm²/s. The electroactive areas of the two electrodes were determined by chronoamperometry utilizing the Cottrell equation:

$$i_t = \frac{nFAD_O^{1/2}C_O^\circ}{\pi^{1/2}t^{1/2}}$$

Where C_O° = solution concentration of oxidized species, mol/cm³; and t = time elapsed, s. When i_t vs. $t^{-1/2}$ data were plotted for WIGE and GCE, the data produced the expected linear relationships. The slope = $(nFD_O^{1/2}C_O^\circ/\pi^{1/2}) \times A$ relationships were evaluated for the electroactive areas, A, of both electrodes:

$$A \text{ (WIGE)} = 0.395 \text{ cm}^2$$

$$A \text{ (GCE)} = 0.272 \text{ cm}^2$$

Although the mercury film is really a series of closely packed Hg droplets (*16, 27*), the solution diffusion layer, δ, is orders of magnitude thicker than calculated Hg film thicknesses, l:

$$\delta \text{ (0.7 M KNO}_3\text{)} = 0.01 \rightarrow 0.1 \text{ cm}$$

$$l \text{ (WIGE)} = 6.2 \times 10^{-6} \text{ cm}$$

$$l \text{ (GCE)} = 6.8 \times 10^{-6} \text{ cm}$$

A reasonable approximation would be to neglect local transport effects of Hg droplets, consider Pb(II) transport from the scale of δ, and assume a very thin continuous Hg film. When this was done, the calculated flux ratio, H, for both electrodes was much less than 1.6×10^{-3}. Therefore, the deVries–Van Dalen limiting case applied.

The half-wave potential for Pb(II) → Pb(O) was interpolated from published data (*28*): $E_{1/2}$ (0.7 M KNO_3) = −0.357 vs. Ag/AgCl (satd KCl).

Tables I and II show the comparison between measured experimental values averaged from three runs and calculated theoretical values for peak potentials and peak currents. Figure 1 shows a typical TMFE cyclic voltammogram.

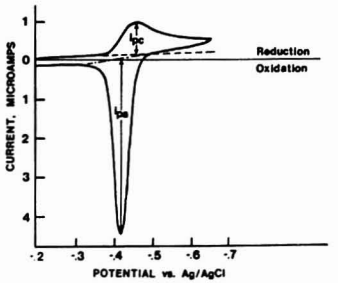


Figure 1. Typical cyclic voltammogram of Pb(II) with a thin mercury film electrode. Reproduced from experimental data

Table III. Reversibility Criteria Comparison

Scan rate, mV/s	ΔE, mV[a]		$b_{1/2}$, mV[b]	
	WIGE[c]	GC[d]	WIGE[c]	GC[d]
2	25 ± 2	21 ± 0	38 ± 0	38 ± 0
5	27 ± 2	21 ± 1	39 ± 0	38 ± 0
10	30 ± 2	22 ± 0	39 ± 0	38 ± 0
20	37 ± 2	22 ± 0	41 ± 0	39 ± 0
50	54 ± 2	21 ± 0	47 ± 0	40 ± 0
100	77 ± 2	21 ± 0	64 ± 0	42 ± 0

[a] $\Delta E = E_{p(cath)} - E_{p(anod)} = 19$ mV theoretically at all scan rates. [b] $b_{1/2}$ = anodic $^1/_2$ peak width = 38 mV theoretically at all scan rates. [c] Wax-impregnated graphite electrode data from Table I. [d] Glassy carbon electrode data from Table II.

Comparison to theoretical was relatively good for both electrode types at slow scan rates (Tables I and II); however, the GCE gave better results.

To more clearly determine compliance with the deVries–Van Dalen reversible model, two parameters serve as good reversibility criteria. First, there is the difference between the anodic peak potential (E_{pa}) and the cathodic peak potential (E_{pc}):

$$E_{pc} = \frac{1}{n}(-38.45 + 29.58 \log H) + E_{1/2}(\text{mV})$$

and

$$E_{pa} = \frac{1}{n}(-1.43 + 29.58 \log H) + E_{1/2}(\text{mV})$$

Therefore,

$$E_{pa} - E_{pc} = \Delta E = \frac{37.02}{n} = \frac{37}{2} = 19 \text{ mV}$$

ΔE is independent of the approximations in determining l, H, or C_R^* scan rate. Second, there is $b_{1/2} = 75.53/2 = 38$ mV. $b_{1/2}$ is independent of H and scan rate. Table III reveals the trends of both electrodes toward increased irreversibility with increased scan rate.

Therefore, the GCE conformed well to the deVries–Van Dalen reversible model at potential scan rates ≤10 mV/s, superior to the WIGE. As a result, subsequent work was performed with the GCE at $v = 5$ mV/s.

Electroactivity of Pb(II) Inorganic Complexes. Increasing concentrations of Cl^-, OH^-, SO_4^{2-}, or CO_3^{2-} were added to the standard solution, 10^{-5} M Pb(II) in 0.7 M KNO_3, and cyclic voltammetry was performed.

Table IV. PbCl Electroactivity[a]

(Cl^-), M	ΔE, mV	$b_{1/2}$, mV	$\frac{i_{pc}(PbCl)}{i_{pc}(Pb^{2+})}$	$\frac{i_{pa}(PbCl)}{i_{pa}(Pb^{2+})}$
0.02	21 ± 0	38 ± 0	1.00 ± 0.00	1.02 ± 0.03
0.05	21 ± 0	38 ± 0	0.99 ± 0.01	1.03 ± 0.01
0.1	21 ± 0	38 ± 0	0.99 ± 0.02	0.99 ± 0.02
0.2	21 ± 0	38 ± 0	1.00 ± 0.03	1.03 ± 0.01
0.3	21 ± 0	38 ± 0	1.00 ± 0.01	1.05 ± 0.03
0.4	21 ± 0	38 ± 0	1.00 ± 0.01	1.03 ± 0.01
0.5	21 ± 0	38 ± 0	1.02 ± 0.01	1.07 ± 0.04
0.6	21 ± 0	38 ± 0	1.04 ± 0.00	1.07 ± 0.00
0.7	21 ± 0	38 ± 0	1.04 ± 0.02	1.09 ± 0.04

[a] Av ± std dev for 3 runs of 10^{-5} M Pb(II) in 0.7 KNO_3–KCl at pH 5.00 ± 0.05 and $T = 23 \pm 0.5$ °C.

Table V. PbOH Electroactivity[a]

pOH	ΔE, mV	$b_{1/2}$, mV	$\frac{i_{pc}(PbOH)}{i_{pc}(Pb^{2+})}$	$\frac{i_{pa}(PbOH)}{i_{pa}(Pb^{2+})}$
<9.00	21 ± 0	38 ± 0	1.00 ± 0.00	1.00 ± 0.00
8.51 ± 0.00	22 ± 1	38 ± 0	1.05 ± 1	1.04 ± 0.04
7.98 ± 0.06	29 ± 2	39 ± 1	1.09 ± 0.06	0.96 ± 0.01
7.49 ± 0.04	65 ± 13	39 ± 1	1.15 ± 0.09	0.96 ± 0.01
6.95 ± 0.06	63 ± 17	44 ± 5	1.26 ± 0.11	0.98 ± 0.11
6.58 ± 0.07	72 ± 10	43 ± 3	1.42 ± 0.13	0.97 ± 0.08
5.92 ± 0.01	84 ± 2	49 ± 1	1.53 ± 0.06	0.87 ± 0.12
5.47 ± 0.02	76 ± 4	61 ± 1	1.52 ± 0.07	0.63 ± 0.01
5.00 ± 0.04	69 ± 6	71 ± 3	1.69 ± 0.06	0.57 ± 0.02
4.55 ± 0.05	55 ± 9	62 ± 5	1.72 ± 0.06	0.59 ± 0.03
4.02 ± 0.03	51 ± 3	66 ± 6	1.69 ± 0.23	0.59 ± 0.09
3.50 ± 0.04	48 ± 3	58 ± 4	1.44 ± 0.19	0.56 ± 0.02
3.02 ± 0.03	46 ± 3	56 ± 4	1.39 ± 0.18	0.64 ± 0.06

[a] Av ± std dev for 6 runs of 10^{-5} M Pb(II) in 0.7 M KNO_3 at $T = 23 \pm 0.5$ °C.

Table VI. $PbSO_4$ Electroactivity[a]

(SO_4^{2-}), M	ΔE, mV	$b_{1/2}$, mV	$\frac{i_{pc}(PbSO_4)}{i_{pc}(Pb^{+2})}$	$\frac{i_{pa}(PbSO_4)}{i_{pa}(Pb^{+2})}$
0.013	21 ± 0	38 ± 0	1.00 ± 0.00	1.00 ± 0.00
0.026	21 ± 1	38 ± 1	0.97 ± 0.01	0.97 ± 0.01
0.05	23 ± 1	38 ± 0	0.89 ± 0.05	0.92 ± 0.05
0.10	25 ± 1	38 ± 0	0.82 ± 0.07	0.85 ± 0.03
0.15	24 ± 1	38 ± 0	0.77 ± 0.05	0.80 ± 0.04
0.18	25 ± 1	38 ± 0	0.72 ± 0.03	0.75 ± 0.04
0.20	24 ± 0	38 ± 0	0.77 ± 0.03	0.79 ± 0.04
0.233	24 ± 1	38 ± 0	0.76 ± 0.05	0.78 ± 0.12

[a] Av ± std dev for 6 runs of 10^{-5} M Pb(II) in 0.7 M KNO_3 at pH 5.00 ± 0.05 and $T = 23 \pm 0.5$ °C.

Table VII. $PbCO_3$ Electroactivity[a]

(CO_3^{2-}), 10^{-5} M	ΔE, mV	$b_{1/2}$, mV	$\frac{i_{pc}(PbCO_3)}{i_{pc}(Pb^{2+})}$	$\frac{i_{pa}(PbCO_3)}{i_{pa}(Pb^{2+})}$
0.61	22 ± 0	38 ± 0	1.01 ± 0.02	1.00 ± 0.06
2.39	22 ± 1	39 ± 1	0.90 ± 0.05	0.89 ± 0.04
5.01	23 ± 1	40 ± 1	0.69 ± 0.01	0.71 ± 0.01
7.42	26 ± 2	40 ± 0	0.57 ± 0.01	0.69 ± 0.04
10.64	26 ± 2	41 ± 2	0.51 ± 0.01	0.67 ± 0.12
13.91	27 ± 2	41 ± 2	0.47 ± 0.01	0.55 ± 0.02
20.37	31 ± 2	42 ± 2	0.49 ± 0.03	0.56 ± 0.04
28.83	30 ± 1	41 ± 1	0.50 ± 0.02	0.56 ± 0.04

[a] Av ± std dev for 3 runs of 10^{-5} M Pb(II) in 0.7 M KNO_3 at pH 4.0 → 7.20 ± 0.10 and $T = 23 \pm 0.5$ °C.

Tables IV–VII show the cyclic voltammetric electroactivity for PbCl, PbOH, $PbSO_4$, and $PbCO_3$. Changes in the cathodic and anodic peak currents with the onset of complexation were

Table VIII. ASV of Dilute Pb(II) Model Solutions[a]

Condition	Predominant species	$i_{pa}(PbL)$ / $i_{pa}(Pb^{2+})$	^{210}Pb activity (PbL) / ^{210}Pb activity (Pb^{2+})
0.7 KCl pH 5.0 ± 0.05	PbCl 86%	1.02 ± 0.04	0.90[b]
0.233 Na_2SO_4 pH 5.0 ± 0.05	$PbSO_4$	0.75 ± 0.02	1.00[b]
0.7 KNO_3			
pH 5.0 ± 0	Pb^{+2} 91%	0.99 ± 0.02	0.94 ± 0.02
pH 5.5 ± 0.1	Pb^{+2} 76%	0.95 ± 0.07	0.88 ± 0.03
pH 6.2 ± 0.1	PbOH 61%	0.40 ± 0.08	0.81 ± 0.05
pH 6.5 ± 0.1	PbOH 76%	0.22 ± 0.04[c]	0.79 ± 0.06[c]
pH 6.9 ± 0.1	PbOH 89%	0.15 ± 0.03	0.71 ± 0.12
8.5 > pH > 7.5	PbOH 90%	no measurable response	0.84 ± 0.05
4.6×10^{-3} M CO_3^{2-} pH 7.20	$PbCO_3$ 96%	0.45 ± 0.06	1.00 ± 0.03[c]

[a] Av ± std dev for 3-4 runs at each condition except as noted. Supporting purified electrolyte was 0.7 M KNO_3. $T = 23 \pm 0.5$ °C. $(Pb^{2+})_{total} = 3\text{–}6 \times 10^{-9}$ M depending upon solution blank. [b] Only one data point. [c] Only two data points.

represented as ratios of measured peak currents at a given ligand concentration to measured peak currents with no ligand present:

$$\frac{i_{pc}\,(PbCl)}{i_{pc}\,(Pb^{2+})} \text{ and } \frac{i_{pa}\,(PbCl)}{i_{pa}\,(Pb^{2+})}$$

PbCl electron-transfer was reversible. The slight increase in peak currents with increased Cl^- concentration may be due to adsorption of electroactive Pb species (*29*, *30*). OH^- complexation resulted in large deviations from reversible electron-transfer. Both ΔE and $b_{1/2}$ went through maxima at intermediate pOH values. i_{pc} increased with OH^- concentration while the i_{pa} decreased. This suggested electrode adsorption of Pb(II)–hydroxy species. SO_4^{2-} and CO_3^{2-} complexation resulted in slightly irreversible behavior. The decline in peak currents with increased CO_3^{2-} concentration was largely due to $PbCO_3$ precipitation, as determined with ^{210}Pb radiotracer.

ASV of Pb(II) Model Solutions. The electroactivity of inorganic Pb(II) complexes at dilute concentrations was determined by ASV of 10^{-8} M Pb(II) model solutions spiked with ^{210}Pb (Table VIII). For PbCl and $PbSO_4$ solutions electrochemical responses for the 10^{-9} M Pb(II) media compared favorably with the 10^{-5} M Pb(II) media. The disparity between voltammetrically measured and actual solution $PbCO_3$ concentration was greater for ASV than for cyclic voltammetry. The ASV peak current of Pb–hydroxy complexes was much lower than for the actual Pb(II) concentration. The nonreversible electron-transfer behavior of PbOH and $PbCO_3$ during cyclic voltammetry manifested itself in ASV peak currents that were much lower than theoretical, even considering Pb(II) adsorptive losses.

Voltammetric Formation Constants. In polarography, increased complexation of a metal, which undergoes *reversible* electron transfer, results in cathodic shifts of $E_{1/2}$:

$$\Delta E_{1/2} = E_{1/2}(Pb^{2+}) - E_{1/2}(PbL_m) = \frac{0.0591}{n} \log \frac{\beta \gamma_{Pb} D_{PbL}^{1/2}}{\gamma_{PbL} D_O^{1/2}} + \frac{0.0591\, m}{n} \log C_L \gamma_L$$

where

β	overall formation constant of Pb(II) complex
γ_{PbL}	activity coefficient of Pb(II) complex
D_{pbL}	diffusivity of Pb(II) complex, cm^2/s
m	coordination number of ligand
γ_L	activity coefficient of ligand
C_L	concentration of ligand, M
D_O	diffusivity of Pb(II) ions, cm^2/s

Table IX. Voltammetric Formation Constants[a]

Species	Peak shift	log β	n^b	r^{2c}	Literature[d]
PbCl	Cathodic	0.96	1.04	0.94	0.88–1.50
	Anodic	0.95	1.07	0.95	
PbOH	Cathodic	8.00	0.97	0.89	6.2–7.9
	Anodic	7.98	1.27	0.90	
$PbSO_4$	Cathodic	1.02	0.60	0.95	1.0–2.7
	Anodic	0.85	0.50	0.94	
$PbCO_3$	Cathodic	7.05	1.25	0.97	4.6–7.5
	Anodic	6.21	1.08	0.97	

[a] Determined by computer linear regression. [b] n = coordination number. [c] r^2 = correlation coefficient. [d] From references (*31–33*).

However, E_{pc} and E_{pa} are related to the $E_{1/2}$:

$$E_{pc} = \frac{1}{n}(-38.45 + 29.58 \log H) + E_{1/2}$$

$$E_{pa} = \frac{1}{n}(-1.45 + 29.58 \log H) + E_{1/2}$$

When a complexing ligand is added to Pb(II)-containing media, $E_{1/2}$ will be shifted cathodically. H, however, contains no terms that change with complexation of Pb(II). Consequently, E_{pc} and E_{pa} will shift cathodically by the amount $E_{1/2}$ is shifted. Representing

$$E_{pc}\,(Pb^{2+}) - E_{pc}\,(PbL) = \Delta E_{pc}$$

and

$$E_{pa}\,(Pb^{2+}) - E_{pa}\,(PbL) = \Delta E_{pa}$$

then for Pb(II) complexation,

$$\Delta E_{pc} = \Delta E_{pa} = \Delta E_{1/2} = 0.0296 \log \frac{\beta \gamma_{Pb}^{2+} D_{PbL}^{1/2}}{\gamma_{PbL} D_{Pb}^{1/2}} + 0.0296\, m \log (C_L \gamma_L)$$

Although electron transfer was not reversible for all inorganic complexes tested, conditional formation constants were calculated from cathodic shifts in the cyclic voltammograms (Table IX) With the exception of the SO_4^{2-} case, coordination numbers were close to integral values. The log β values compared favorably with literature values. Correlation coefficients were generally high.

Pb(II) Inorganic Speciation Model for Seawater. To predict the voltammetric response of seawater, the distribution

Table X. ASV of Organic-free Seawater[a]

pH	Predominant species[b]	i_{pa}(pH) / i_{pa}(pH3)	^{210}Pb activity (pH) / ^{210}Pb activity (pH3)	E_{pa}
8.5 ± 0.1	PbOH (88%), $PbCO_3$ (10%)	0.01 ± 0.00	0.24 ± 0.01	−0.479 ± 0.003
7.5 ± 0.1	PbOH (82%), PbCl (14%)	0.36 ± 0.01	0.55 ± 0.03	−0.462 ± 0.001
7.0 ± 0.1	PbOH (60%), PbCl (32%)	0.46 ± 0.01	0.64 ± 0.02	−0.456 ± 0.001
6.5 ± 0.1	PbCl (54%), PbOH (32%)	0.52 ± 0.02	0.69 ± 0.04	−0.453 ± 0.002
6.0 ± 0.1	PbCl (69%), PbOH (13%), Pb^{2+} (13%)	0.62 ± 0.04	0.73 ± 0.06	−0.452 ± 0.001
5.5 ± 0.1	PbCl (76%), Pb^{2+} (15%)	0.74 ± 0.03	0.81 ± 0.02	−0.452 ± 0.001
5.0 ± 0.1	PbCl (79%), Pb^{2+} (15%)	0.81 ± 0.01	0.87 ± 0.06	−0.452 ± 0.001
4.5 ± 0.1	PbCl (79%), Pb^{2+} (15%)	0.92 ± 0.01	0.93 ± 0.03	−0.452 ± 0.001
4.0 ± 0.1	PbCl (79%), Pb^{2+} (15%)	0.92 ± 0.01	1.00 ± 0.02	−0.452 ± 0.001
3.0 ± 0.1	PbCl (79%), Pb^{2+} (15%)	1.00	1.00	−0.452 ± 0.001

[a] Av ± std dev for 2-3 sets of data from 5 runs. T = 23 ± 0.5 °C. Deposition potential = −0.800 V vs. Ag/AgCl (saturated KCl). [b] From inorganic speciation model in the paper (Figure 2).

of inorganic Pb(II) species needed to be known. However, a comparison of the several published speciation models revealed great disparities (*7*, *34–36*). For the model of Baier (1971), the predominant species in seawater at pH 8.2 was PbCl(30%), $PbHCO_3$(25%), Pb^{2+}(20%), $PbCO_3$(15%); Zirino and Yamamoto (1972), $PbCO_3$(80%), PbCl(10%); Bilinski and Stumm (1973), PbOH(42%), $PbCO_3$(32%), PbCl(12%); and Dryssen and Wedborg (1974), $PbCl_2$(42%), PbCl(19%), PbOH(10%). This is not surprising since, except for Bilinski and Stumm, researchers were forced to use data from several sources, approximate missing data, and make assumptions regarding activity coefficients. To reduce assumptions and to have a model that more accurately reflected TMFE voltammetric responses of seawater, an ion-association model was constructed from these experimental data (*34*, *35*):

(a) $(Pb)_{total} = (Pb^{2+}) + (PbCl) + (PbCl_2) \ldots + (PbOH) \ldots + (PbCO_3)$

(b) Since $(Pb(L_j)_n) = \beta_j(Pb^{2+})(L_j)^n$,
$(Pb)_{total} = (Pb^{2+}) + \sum_j \beta_j(Pb^{2+})(L_j)^n$

(c) Fraction $Pb(L_j)_n$ of total $= \dfrac{(Pb)(L_j)_n}{(Pb)_{total}} = \dfrac{\beta_j(Pb^{2+})(L_j)^n}{(Pb^{2+}) + \sum_j (\beta_j(Pb^{2+})(L_j)^n} = \dfrac{\beta_j(L_j)^n}{1 + \sum_j (\beta_j(L_j)^n)}$

Variations in HCO_3^- and CO_3^{2-} as a function of pH were calculated from Allen (*37*). Figure 2 shows the inorganic speciation of Pb(II) in seawater. Note the predominance of PbOH in the usual pH range of seawater (i.e., 7.8–8.6).

ASV of Organic-Free Seawater. Since PbOH is the dominant species in organic-free seawater and demonstrates a lower than theoretical current response, it was predicted that the ASV current responses would be much lower than theoretical. Table X shows that at high pH the ASV peak response was lower than theoretical, even taking into account cell material adsorptive losses. This was principally due to the electrochemical inactivity of PbOH. Once the seawater was acidified, the comparison between ASV current responses and solution Pb(II) concentrations was good. It might be noted that E_{pa} for 10^{-8} M Pb(II) in 0.7 M KNO_3 was −0.430 ± 0.001. For seawater at low pH, ΔE_{pa} = −0.452 − (−0.430) = −22 mV, which is a peak shift expected for PbCl. The ΔE_{pa} for pH 8.5 seawater to $Pb(H_2O)_n$ was −49 mV, a shift expected for PbOH formation.

CONCLUSIONS

(1) Cyclic voltammetry was useful for demonstrating that electron-transfer of Pb(II) at a TMFE with glassy carbon was simple and reversible at scan rates ≤10 mV/s, according to the deVries–Van Dalen model. Performance for the GCE was superior to that for a WIGE.

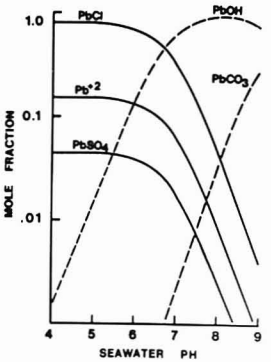


Figure 2. Inorganic Pb(II) speciation model for seawater as a function of pH

(2) Electron transfer of PbCl was reversible with $PbSO_4$ and $PbCO_3$ being quasi-reversible. Electron transfer of PbOH deviated from the reversible model in a complicated manner, suggesting electrode adsorption.

(3) Reasonable log β values were obtained for PbCl, PbOH, and $PbCO_3$ by cyclic peak shift analysis. The measured value for $PbSO_4$ was probably low.

(4) An inorganic speciation model for Pb(II) in organic-free seawater based on cyclic voltammetric formation constants revealed that about 90% of the Pb(II) would exist as PbOH.

(5) Measurement by ASV of 10^{-8} M Pb(II) solutions revealed peak current responses for $PbCO_3$ and PbOH solution lower than expected for the actual solution Pb(II) concentration, even correcting for adsorption.

(6) As expected, measurement by ASV of organic-free seawater at high pH resulted in a lower than theoretical current response, due to electrochemical inactivity of PbOH. The voltammetric response of pH 3 seawater was according to theory since $Pb(H_2O)_n$ and PbCl are reversibly electroactive.

ACKNOWLEDGMENT

We thank William Gutknecht, Chemistry Department, Duke University, for his helpful comments during the course of this work and during preparation of this manuscript.

LITERATURE CITED

(1) "Marine Environmental Quality", National Academy of Sciences, Washington, D.C., 1971, pp 14–15.
(2) S. S. Shulka and H. V. Leland, *J. Water Pollut. Control Fed.*, **45**, 1319 (1973).

(3) P. B. Brewer in "Chemical Oceanography", J. P. Riley and G. Skirrow, Ed., 2nd ed. Academic Press, New York, N.Y., Vol. 1, 1975, pp 417–420.
(4) H. V. Rice, D. A. Leighty, and G. C. McLeod, *Crit. Rev. Microbiol.*, **3**, 27 (1973).
(5) "Baseline Studies of Pollutants in the Marine Environment and Research Recommendations: The IDOE Baseline Conference, May 24–26, 1972", E. D. Goldberg, Ed., New York, 1972, pp 2-4.
(6) D. R. Kester in "The Nature of Seawater", E. D. Goldberg, Ed., Dahlem Konferenzen, Berlin, Germany, 1975, pp 17–42.
(7) W. Stumm and P. A. Brauner in "Chemical Oceanography", J. P. Riley and G. Skirrow, Ed., 2nd ed., Academic Press, New York, N.Y., Vol. 1, 1975, pp 174–239.
(8) A. Zirino, S. H. Lieberman and M. L. Healy in "Marine Electrochemistry", J. B. Berkowitz et al., Ed., The Electrochemical Society, Princeton, N.J., 1973, pp 319–332.
(9) H. W. Nurnberg and P. Valenta in "The Nature of Seawater", E. D. Goldberg, Ed., Dahlem Konferenzen, Berlin, Germany, 1975, pp 87–136.
(10) M. Whitfield in "Chemical Oceanography", J. P. Riley and G. Skirrow, Ed., 2nd, ed., Academic Press, New York, N.Y., Vol. 4, 1975, pp 1–154.
(11) T. R. Copeland and R. K. Skogerboe, *Anal. Chem.*, **14**, 1257A (1974).
(12) G. E. Batley and T. M. Florence, *J. Electroanal. Chem.*, **55**, 23 (1974).
(13) Meeting Report, *Mar. Chem.*, **2**, 69 (1974).
(14) L. Petrie and R. Baier, *Anal. Chim. Acta*, **82**, 255 (1976).
(15) T. F. Sharpe in "Encyclopedia of Electrochemistry of the Elements", A. J. Bard, Ed., Vol. 1, Marcel Dekker, New York, N.Y., pp 249–56.
(16) W. R. Matson, Ph.D. Dissertation, Massachusetts Institute of Technology, Cambridge, Mass., 1968.
(17) T. Copeland, Ph.D. Dissertation, Colorado State University, Fort Collins, Colo., 1973.
(18) W. Lund and M. Salberg, *Anal. Chim. Acta*, **76**, 131 (1975).
(19) W. Lund and D. Onshus, *Anal. Chim. Acta*, **86**, 199 (1976).
(20) Z. Stojek and Z. Kublik, *J. Electroanal. Chem.*, **77**, 205 (1977).
(21) W. T. deVries and E. Van Dalen, *J. Electroanal. Chem.*, **8**, 366 (1964).
(22) W. T. deVries, *J. Electroanal. Chem.*, **9**, 448 (1965).
(23) W. T. deVries and E. Van Dalen, *J. Electroanal. Chem.*, **14**, 315 (1967).
(24) R. S. Nicholson and I. Shain, *Anal. Chem.*, **36**, 706 (1964).
(25) A. Baranski, S. Fitak, and Z. Galus, *J. Electroanal. Chem.*, **60**, 175 (1975).
(26) V. M. Stackelberg, M. Pilgram, and V. Toome, *Z. Elektrochem.*, **57**, 342 (1953).
(27) D. N. Hume and J. N. Carter, *Chem. Anal. (Warsaw)*, **17**, 747 (1972).
(28) I. M. Kolthoff and J. J. Lingane, "Polarography", Interscience, New York, N.Y., 1946, pp 149–52.
(29) R. H. Wopschall and I. Shain, *Anal. Chem.*, **39**, 1514 (1967).
(30) D. J. Barclay and F. C. Anson, *J. Electroanal. Chem.*, **28**, 71 (1970).
(31) "Stability Constants of Metal-Ion Complexes", *Chem. Soc., Spec. Publ.*, **17**, L. G. Sillen and A. E. Martell, Ed., The Chemical Society, London, England, 1967.
(32) "Stability Constants of Metal-Ion Complexes", *Chem. Soc., Spec. Publ.*, **25**, L. G. Sillen and A. E. Martell, Ed., The Chemical Society, London, England, 1967.
(33) H. Bilinski, R. Huston, and W. Stumm, *Anal. Chim. Acta*, **84**, 157 (1976).
(34) R. Baier, Ph.D. Dissertation, University of Washington, Seattle, Wash., 1971.
(35) A. Zirino and S. Yamamoto, *Limnol. Oceanogr.*, **17**, 661 (1972).
(36) D. Dryssen and M. Wedborg in "The Sea", E. D. Goldberg, Ed., Wiley Interscience, New York, N.Y., 1974, pp 181–195.
(37) H. Allen, Ph.D. Dissertation, University of Michigan, Ann Arbor, Mich. 1974.

RECEIVED for review May 16, 1977. Accepted November 11, 1977. This research was supported by the Oceanographic Section, National Science Foundation, NSF Grant DES74-12831.

Solvent Extraction Method for Determination of Plutonium in Soft Tissue

Narayani P. Singh,* Shawki Amin Ibrahim, Norman Cohen, and McDonald E. Wrenn

Institute of Environmental Medicine, New York University Medical Center, 550 First Avenue, New York, New York 10016

A simple, quick, and accurate method has been developed for the determination of plutonium isotopes in soft tissues. First ^{242}Pu tracer is added and then the tissues are digested using concentrated nitric acid followed by a mixture of nitric and sulfuric acids. Plutonium is then coprecipitated with iron carrier after the addition of ammonium hydroxide. The precipitate is dissolved in HNO_3 (1:1) after complete removal of sulfate ions and the acidity adjusted to 3 M. Plutonium is maintained in the +4 valence state and extracted twice with 25% trilaurylamine in xylene (pre-equilibrated with 3 M nitric acid). The organic phase is washed twice with equal volumes in 10 M HCl to remove traces of thorium and then with HNO_3 to remove iron and uranium. Plutonium is then scrubbed from the trilaurylamine phase two times with 2 M H_2SO_4, evaporated almost to dryness, electrodeposited onto a platinum planchet, and counted by alpha spectrometry with a surface barrier silicon diode. The final recovery ranged from 49–85% with a mean of 61%.

All people living in the northern hemisphere since 1945 have been exposed to plutonium isotopes from nuclear weapons detonation tests. Accordingly, such human tissues are slightly contaminated with plutonium. Because of the need to have background information on the plutonium content of human tissue (*1*, *2*), it has become imperative to develop reliable, accurate, and rapid analytical techniques for the determination of plutonium in these samples. Although a number of techniques have been described for the determination of plutonium in food, soil, and rock (*3–10*), little consideration has been given to plutonium measurement in human soft tissues.

Some investigators have employed liquid scintillation counting techniques for determining plutonium in biological materials using thenyltrifluoroacetone (TTA) (*11*), dibutylphosphoric acid (DBP) (*12*), and bis(2-ethylhexyl)phosphoric acid (D_2-EHPA) (*13*) as solvent extraction agents. Recently the Energy Research and Development Administration's Health and Safety Laboratory (HASL) (*14*) has published a technique for determining plutonium in tissues using ion-exchange separation followed by electrodeposition and alpha spectrometry. Since ion exchange is a time-consuming technique, a much more rapid solvent extraction procedure using trilaurylamine (TLA) as an extracting agent has been developed at our laboratory. Since knowledge of the isotopic composition of plutonium in human tissues is important in predicting sources of exposure, alpha spectrometry is the final stage of the determination. In addition, alpha spectrometry is a reliable technique for determining the degree of potential interference from other alpha-emitting nuclides, the most probable being the natural isotopes of uranium, radium, and thorium, and eliminating the interference therefrom.

EXPERIMENTAL

Reagents and Apparatus. All reagents used are of analytical grade. Trilaurylamine (TLA), Pfaltz and Bauer, Inc.; 25% TLA solution is prepared in xylene and shaken with one-third volume of 3 M HNO_3 for 10 min. The organic phase is centrifuged and separated before use. A working solution of TLA cannot be stored for extended periods since it begins to deteriorate after 24 h. Once equilibrated with HNO_3, it must be used the same day. The 2 M H_2SO_4, 3 M HNO_3, and 10 M HCl are prepared by appropriate dilution of concentrated acids with deionized, distilled water.

0003-2700/78/0350-0357$01.00/0 © 1978 American Chemical Society

Other reagents and equipment employed include: ^{242}Pu tracer, methyl red indicator, platinum planchets, nickel disks, electrolytic cell (*14*), electrolytic analyzer (motor driven platinum electrode and a power supply).

Sample Preparation. Transfer 500–1000 g of tissue to a 4-L beaker and add 1–2 dpm of ^{242}Pu tracer. Add just enough concentrated nitric acid to immerse the tissues and cover the beaker with a watch glass. Heat gently over a magnetic stirrer hot plate until frothing ceases. Raise the temperature slowly to approximately 100 °C and continue heating until the volume is reduced to approximately 100 mL. Heat at higher temperature and add a few drops of concentrated HNO_3 occasionally until a clear solution is obtained. At this stage add 200 mL of 1:1 HNO_3:H_2SO_4 mixture and heat vigorously until all the nitric acid is driven off. Add a few drops of HNO_3 occasionally with constant heating until a clear colorless solution is obtained ensuring almost complete decomposition of organic material. Remove most of the sulfuric acid by evaporation before proceeding further. In cases of tissues containing refractory plutonium oxide, the tissues, particularly the lung, must be treated with hydrofluoric acid or by fusion to ensure the complete dissolution of refractory oxides; however, this is not required for tissues from the general population exposed to fallout plutonium which is readily soluble in nitric and hydrochloric acid.

Procedure. Add 300 mL of 1:3 HCl to the clear solution thus obtained and boil for several minutes. Cool and add 1 mL of iron carrier (100 mg $FeCl_3$/mL) and swirl the beaker for proper mixing. Add ammonium hydroxide very gently until precipitation is complete (the pH of the solution should be 8 or greater). The precipitate is gently heated with constant stirring for fast settling and then allowed to stand overnight for complete precipitation. Remove the supernatent after centrifugation of the precipitate in a 50-mL centrifuge tube. Dissolve the precipitate in 4–5 mL of concentrated HNO_3 and reprecipitate $Fe(OH)_3$ with ammonium hydroxide. Plutonium is coprecipitated with iron hydroxide along with several other metals. Repeat the process several times to ensure the complete removal of sulfate ions. The precipitate thus obtained is free of sulfate ions and is dissolved in a minimum volume of 1:1 HNO_3; the acidity of this solution is determined by titrating a 100-μL aliquot against a standard sodium hydroxide solution. The acidity is adjusted to 3 M by adding a calculated volume of nitric acid of appropriate concentration.

Solvent Extraction. Heat the solution thus obtained gently and add 25 mg $NaNO_2$ (solid $NaNO_2$ is preferred since it does not increase the volume). Cool the solution to room temperature and add an equal volume of 25% TLA (pre-equilibrated with 3 M HNO_3 for 10 min). Shake gently for 10 min and centrifuge for 20 min at 2000 rpm. Vigorous shaking should be avoided to prevent emulsion formation. Remove the aqueous phase into another 40-mL tube without disturbing the organic phase. This organic phase is the first extract. Repeat the extraction with an equal volume of 25% TLA and remove the aqueous phase. Add the second organic phase to the first extract. Add an equal volume of 10 M HCl to the total organic phase and shake for 10 min. Centrifuge for 10 min and remove the aqueous phase. Repeat the process once again to ensure the complete removal of thorium. Finally, wash the TLA phase with an equal volume of 1:1 HNO_3 to remove iron and uranium and scrub the plutonium with an equal volume of 2 M H_2SO_4 (contact time is 10 min). Remove the aqueous phase into a beaker and repeat the scrubbing with 2 M H_2SO_4 once again. Remove this aqueous phase to the same beaker which contains the aqueous phase from the first scrubbing. Evaporate the solution to dryness and electrodeposit plutonium on a platinum planchet. Sometimes, while separating the aqueous phase, some organics from TLA become entrained with H_2SO_4 which might interfere in electroplating. To avoid this possibility, add several drops of HNO_3 when black floating organics are present. The HNO_3 should completely decompose the organics in the presence of H_2SO_4.

Electrodeposition *Apparatus.* The plating cell consists of an elongated 22-mm cap which holds a 1-oz polyethylene bottle with the bottom removed. The cap, which has space for an 18-mm diameter platinum plating disk and a nickel backing disk, may be firmly screwed into the polyethylene bottle forming a leak-tight plating cell (*14*). A threaded brass bushing is molded into the cap, thus making the electrical contact with the platinum disk cathode by clip leads. The cell is supported on a brass pedestal which is heavy enough to remain stationary in an ice water bath. The anode is a 1.59-mm diameter platinum disk riveted at one end. It is connected through a constant speed stirrer to the positive outlet of the power supply (*14*).

A power supply furnishes a constant current ranging between 0–10 A and a constant voltage ranging between 0–30 V.

Procedure. Add 1 mL of 2 M H_2SO_4 to the beaker in which the solution, obtained after scrubbing with 2 M H_2SO_4, was evaporated to dryness and heat gently at low temperature on a hot plate before transferring to the plating cell. Wash two times with 1 mL of 2 M H_2SO_4 and transfer the solution to the cell to ensure the complete transfer of plutonium to the plating cell. Add one drop of methyl red indicator and titrate with 1:1 NH_4OH dropwise to a yellow color. An excess of ammonia might decrease the electroplating efficiency. Bring the solution back to a red color by adding 2 M H_2SO_4 dropwise with 3–4 drops extra to obtain the desired pH of the plating solution. The volume should not exceed more than 3–4 mL. Electroplate at an initial current of 1.2 A for 1 h. Quench the electrolyte with 3–4 drops of ammonium hydroxide at the end of 1 h. Dismantle the cell and rinse the platinum disk with distilled water, alcohol and flame it to red heat over a burner to convert plutonium to oxide; determine the plutonium recovery and isotope composition after counting the disk with a surface barrier silicon diode (Ortec, Inc.) and multichannel analyzer which permits identification of ^{238}Pu and $^{239,240}Pu$ and also permits energy discrimination against naturally-occurring alpha emitters which are not completely eliminated by the radiochemical procedure.

Standardization. The counting efficiency of the counter and energy calibration was determined with an electrodeposited standard source containing ^{242}Pu, ^{239}Pu, and ^{238}Pu which have their major alpha energies at 4.90, 5.16, and 5.50 MeV, respectively.

RESULTS AND DISCUSSION

Since the ion-exchange technique for determining plutonium in soft tissues is time-consuming, this faster and highly efficient technique was developed using solvent extraction. The choice of TLA was made because of its high discrimination factor against uranium which favors a high extraction coefficient for plutonium (*15*) (K_d Pu(IV) is 311 and K_d U(VI) $\sim$ 0.5).

At early stages of the development, when the extraction was carried out on tissue samples which had been wet ashed with nitric acid only, the recovery was poor. This may be the result of interference in solvent extraction by undecomposed organic material. It is essential, therefore, to decompose organic matter completely by wet ashing with a mixture of HNO_3 and H_2SO_4. Unfortunately the iron hydroxide coprecipitation of plutonium may then contain insoluble $(NH_4)_2SO_4$ trapped into the precipitate, which because of the strong complexing tendency of sulfate ions will lower the extracting efficiency of TLA resulting in a poor yield for Pu (Table I). It is essential, therefore, to remove sulfate ion completely by dissolving and reprecipitating the $Fe(OH)_3$.

The complete removal of organic matter in the wet-ashing step and sulfate ions in reprecipitating and washing the iron hydroxide resulted in an enhanced recovery of plutonium from a single extraction by TLA and a single backwashing with 2 M H_2SO_4 to approximately 45% from the original value of 22%. Introducing two extractions of plutonium from aqueous solution of tissues with two back-extractions with 2 M H_2SO_4 enhanced the recovery further to about 65%. When the volume of the plating solution exceeded 5 mL, the recovery decreased. When the volume of solution was maintained at 3–4 mL, the final recovery was approximately 72%. A similar effect was found by Mitchell, who observed decreased efficiency in the electrodeposition of ^{239}Pu with increasing volume (*16*).

Finally, it was noted that when the TLA phase was washed once with equal volumes of 1:1 dilute HNO_3 after washing with 10 M HCl and before the scrubbing of plutonium with 2 M

Table I. Recovery of Plutonium from Beef Liver for Different Experimental Conditions

Extracting conditions	Plutonium, dpm Added	Plutonium, dpm Recovered	Recovery, %	General experimental conditions
I. Extraction at 3 M HNO_3 with 25% TLA and scrubbed with 2 M H_2SO_4	3.84 1.06	0.83 0.21	22 20	The organic materials from tissues were not completely decomposed
II. Extraction at 3 M HNO_3 with 25% TLA and scrubbed with 2 M H_2SO_4	36.40 1.99	8.32 0.36	23 18	The iron hydroxide precipitated was not free of SO_4 ions before extraction
III. One extraction at 3 M HNO_3 with 25% TLA and scrubbed with 2 M H_2SO_4	49.40 1.20	20.40 0.54	41 45	Free of organics and sulfate ions before extraction
IV. Two extractions with 25% TLA and two scrubbings with 2 M H_2SO_4	5.04 1.7	3.29 1.20	65 68	Free of organics and sulfate, but the volume of plating solution not controlled
V. Two extractions with 25% TLA and two scrubbings with 2 M H_2SO_4	2.53	1.84	73	Volume of plating solution controlled to 3-3.5 mL
VI. Two extractions with 25% TLA, one washing with 1:1 HNO_3 and two scrubbings with 2 M H_2SO_4	1.22	1.03	84	Final condition of electroplating (vol. 3-3.5 mL)

Table II. Recovery of Plutonium from Beef Liver Using Method VI of Table I

Sample	Amount of ^{242}Pu added, dpm	Amount found, dpm	Recovery, %[a]
1	2.534	1.264 ± 0.086	50.0 ± 3.4
2	0.173	0.081 ± 0.013	49.1 ± 7.5
3	0.940	0.488 ± 0.058	62.5 ± 6.2
4	1.224	1.031 ± 0.062	84.2 ± 5.1
5	1.166	0.720 ± 0.051	61.0 ± 4.4
6	1.104	0.702 ± 0.069	63.3 ± 6.3
7	1.522	0.690 ± 0.065	45.3 ± 4.3
8	0.806	0.509 ± 0.047	63.1 ± 5.8
9	1.573	0.963 ± 0.064	61.2 ± 4.1
10	1.062	0.623 ± 0.049	58.7 ± 4.6
11	0.775	0.656 ± 0.064	84.8 ± 8.2
12	1.896	0.964 ± 0.071	50.8 ± 3.8

[a] Average recovery = 61.2 ± 12.5. Median recovery = 61.2.

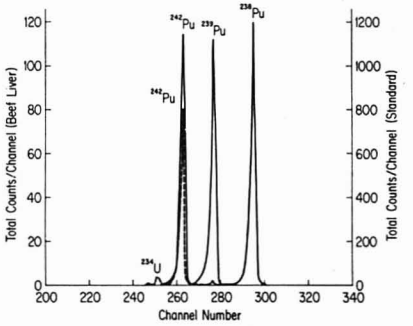


Figure 1. Alpha spectrum from a beef liver sample and plutonium standard. Counting time = 1200 min. Dotted lines indicate the alpha spectrum obtained with a beef liver sample with added ^{242}Pu tracer. Solid lines are for a ^{238}Pu, ^{239}Pu, and ^{242}Pu standard

H_2SO_4, the plate appeared clean and the plating recovery improved once again to 85%. It is essential, therefore, to remove iron by washing with 1:1 HNO_3 before scrubbing plutonium.

Since the alpha energies for ^{228}Th and ^{238}Pu (5.43 and 5.50 MeV respectively) are almost identical, it is essential to remove thorium completely before electroplating. Using this method, the discrimination against thorium exceeded 3×10^4, as determined from the addition of known amounts of ^{228}Th (about 120 dpm).

Employing these final conditions of extraction, backwashing and electroplating, 12 beef liver tissues (100–150 g) to which known amounts of ^{242}Pu has been added were analyzed for plutonium; the results are summarized in Table II. Recoveries between 49 and 85%, with a mean of 61%, were obtained. The recovery experiments were carried out with added ^{242}Pu activity from 0.173 dpm/sample to 2.534 dpm. This covers the most probable range of concentrations of environmental plutonium plus added tracer, since the mass of the added tracer will exceed the mass of $^{239,240}Pu$ or ^{238}Pu found in most soft tissue. The equivalent amount of ^{239}Pu to 2.5 dpm of ^{242}Pu is 16 times greater, or 40 dpm (18 pCi). (See Figure 1 for representative alpha spectrum.)

Table III gives the natural level of ^{239}Pu in beef liver, which could be measured only when large masses of tissue (~500 g) were analyzed and the samples counted for 2000 min or longer. The counting efficiency was 28%. The plutonium

Table III. Plutonium Content of Beef Liver

Sample No.[a]	Amount of tissue, g	Yield, %	$^{239,240}Pu$, pCi/kg
1	450	58 ± 5	0.0088 ± 0.0050
2	450	55 ± 5	0.0059 ± 0.0041
3	340	46 ± 5	0.0076 ± 0.0046
4	441	44 ± 4	0.0069 ± 0.0026

[a] Samples 1 and 2 are taken from aliquots of the same pool of beef liver. Samples 3 and 4 are both taken from another pooled sample. The difference in $^{239,240}Pu$ concentrate in the two pools is well within the counting error.

concentration is almost 100 times lower than in human liver (*17*). This difference may occur because cattle coming to slaughter have been exposed to plutonium in the environment for a much shorter time. It has been suggested, based on a comprehensive review of the literature, that plutonium content in mammals should increase with age, starting from virtually zero at birth (*18*).

In short, concentrations of ^{239}Pu in air were at a maximum in the middle 1960's, whereas the concentration of ^{239}Pu in the mid 1970's was an order of magnitude lower (*1*). However, it is reasonable that beef liver from steers or cows slaughtered in the mid 1970's which were only several years old would tend

to have much lower Pu in liver, if inhalation from primary fallout was the only source.

LITERATURE CITED

(1) B. G. Bennett, **WASH-1359**, U.S. Department of Energy, Dec. 1976.
(2) W. J. Bair, C. R. Richmond, and B. W. Wachholz, **WASH-1320**, U.S. Department of Energy, Sept. 1974.
(3) P. J. Mango, P. E. Kauffman, and B. Schleien, *Health Phys.*, **13**, 1325 (1967).
(4) H. Levine and A. Lamanna, *Health Phys.*, **11**, 117 (1965).
(5) M. C. deBortoli, *Anal. Chem.*, **39**, 375 (1967).
(6) K. C. Pillai, R. C. Smith, and T. R. Folsom, *Nature (London)*, **203**, 568 (1964).
(7) N. Y. Chu, *Anal. Chem.*, **43**, 449 (1971).
(8) E. L. Geiger, *Health Phys.*, **1**, 405 (1959).
(9) C. W. Sill, K. W. Puphal, and F. D. Hindman, *Anal. Chem.*, **46**, 1725 (1974).
(10) J. C. Veselsky, *Int. J. Appl. Radiat. Isot.*, **27**, 499 (1976).
(11) L. C. Schwendiman, J. W. Healy and D. L. Reid, Hanford Works Report, H.W. 22680, Richland, Washington, Nov. 1951.
(12) D. L. Horrocks and M. H. Studier, *Anal. Chem.*, **30**, 1947 (1958).
(13) R. F. Keough and G. J. Powers, *Anal. Chem.*, **42**, 419 (1970).
(14) Health and Safety Laboratory, U.S. Department of Energy, HASL Procedures Manual, 1976.
(15) N. SriNivasan, M. V. Ramaniah, C. L. Rao, P. K. Khopkar, G. M. Nair, and N. P. Singh, *B.A.R.C.* 374 (1968).
(16) R. F. Mitchell, *Anal. Chem.*, **32**, 327 (1960).
(17) M. E. Wrenn, N. Cohen, I. M. Fisenne, and J. W. Neton, New York University Medical Center, Institute of Environmental Medicine, Annual Report COO-2968-1 (1977).
(18) M. E. Wrenn, *Braz. Acad. Sci.*, 131 (1977).

RECEIVED for review October 11, 1977. Accepted November 29, 1977. This research was supported by Grant No. E (11-1) 2968 from the U.S. Energy Research and Development Administration and is part of a center program supported by Grant No. ES 00260 from the National Institute of Environmental Health Sciences and Grant No. CA 13343 from the National Cancer Institute.

Improvement of Detection Limits in Laser-Excited Atomic Fluorescence Flame Spectrometry

S. J. Weeks,[1] H. Haraguchi,[2] and J. D. Winefordner*

Department of Chemistry, University of Florida, Gainesville, Florida 32611

Laser-excited atomic fluorescence flame spectrometry with a pulsed nitrogen laser pumped tunable dye laser has been investigated with respect to analytical figures of merit, especially in terms of improvement of detection limits. The detection limits for 19 elements in an air–acetylene flame and for 5 elements in a nitrous oxide–acetylene flame are evaluated in the cases of both resonance and nonresonance atomic fluorescence lines. The detection limits obtained have been improved about 10 to 200 times. Detection limits for many elements excited by the frequency doubled dye laser output are reported for the first time. Now, most elements examined can be detected at the ng mL^{-1} (ppb) level or less with analytical curve linearities of over five orders of magnitude. Improvement of the detection limits was achieved mainly by expanding the diameter of the laser beam to illuminate a larger analyte volume in the flame and by using a low dispersive spectrometric system. The optical arrangement employed reduced the scatter signal and improved the signal-to-noise ratio (SNR). Although a low dispersive spectrometric system (spectral bandwidth of $\Delta\lambda_M$) was employed, the spectral resolution of the system was determined by the spectral bandwidth of the laser, $\Delta\lambda_L$ ($\Delta\lambda_L << \Delta\lambda_M$). Conditions for optimizing analytical results are discussed. The results indicate that laser-excited atomic fluorescence spectrometry is potentially superior to atomic absorption spectrometry, atomic emission flame spectrometry, atomic emission induction coupled plasma spectrometry, and conventional source atomic fluorescence spectrometry, in terms of analytical figures of merit.

In recent years, tunable organic dye lasers have been increasingly used as excitation sources for atomic fluorescence spectrometry with flame atomizers (*1–14*) and with furnace atomizers (*15–22*). In these studies, pulsed (ruby, Nd^{3+}:YAG, and nitrogen laser or flashlamp pumped laser) or continuous wave (CW) dye lasers have been employed as excitation sources for atoms. Good detection limits for sodium and barium have been reported with CW dye excitation (*11*, *13*). However, the available wavelength range of CW dye lasers is presently limited to the longer visible wavelength region, primarily above 520 nm, making a CW dye laser of limited analytical use. With frequency doubled flashlamp pumped dye lasers, magnesium at 285.2 nm and lead at 283.3 nm have been studied by laser-excited atomic fluorescence spectrometry, and very good limits of detection have been reported (*9*, *15*). However, flashlamp pumped and CW dye lasers require large volumes of expensive dye solution. Pulsed nitrogen (N_2) laser pumped tunable dye lasers offer the greatest advantages to date, primarily because of the high peak spectral irradiances and the wide wavelength range (≈220 to ≈950 nm) which can be quickly and easily obtained. So far, laser-excited atomic fluorescence flame spectrometry with a N_2 laser pumped dye laser has produced detection limits comparable to those obtained by flame emission spectrometry and atomic absorption flame spectrometry (*3–5*, *10*). Detection limits in laser-excited atomic fluorescence spectrometry have been comparable with those obtained in atomic fluorescence flame spectrometry using conventional narrow line light sources, such as hollow cathode lamps, and electrodeless discharge lamps, and xenon arc continuum sources (*23*, *24*). Unfortunately, previous results obtained with laser excitation have not been as good as expected based upon the high irradiance (*25*). Therefore, the experimental arrangement and conditions in laser-excited atomic fluorescence flame spectrometry needed to be more fully investigated; a pulsed source with high spectral irradiance combined with gated detection should be a nearly optimal analytical system for improvement of detection limits and signal-to-noise ratios (SNR) in atomic fluorescence, as has been predicted (*24*, *26–28*).

A pulsed laser excitation-gated detection system was therefore used in the present studies. Such a system has the following characteristic features: (i) high spectral irradiance;

[1] Present address, Analytical Chemistry Division, Institute of Material Research, National Bureau of Standards, Washington, D.C. 20234.
[2] On leave, Department of Chemistry and Physics, National Institute for Environmental Studies, Yatabe, Ibaraki, Japan.

0003-2700/78/0350-0360$01.00/0 © 1978 American Chemical Society

(ii) pulsed output; (iii) narrow spectral bandwidth of the excitation source; (iv) wide range of wavelength tunability; (v) high beam collimation; and (vi) minimization of flame emission background (noise). From Omenetto et al. (28), the advantages of gated detection are a result of high peak power (i) and a low duty cycle (ii). The highest average power consistent with the lowest duty cycle (also called duty factor) are desirable operating conditions. For resonance fluorescence, the Rayleigh scatter shot noise will limit the SNR under ideal conditions. For nonresonance fluorescence, the lowest detectable signal will be limited by dark current noise, and/or amplifier noise, and/or flame background emission noise, and/or molecular fluorescence background noise. However, because not all elements have strong nonresonance fluorescence lines, a system should be designed to optimize, as best possible, both resonance fluorescence and nonresonance fluorescence signals in order that the system be generally analytically useful.

The narrow spectral bandwidth of the laser (item iii) and gated detection minimize the emission background noise (item vi), allowing the use of a large optical throughput measurement system. The small beam diameter of the laser output is considered to be essential in those laser spectroscopic studies where saturation of energy levels is required or where spatial diagnostic measurements in flames or plasmas are needed (see Ref. 27 for discussion of application and benefits of saturation). A small beam diameter, however, is not necessarily required in (analytical) atomic fluorescence flame spectrometry. In fact, using spectral irradiances greater than the saturation spectral irradiance, will at most only double the atomic fluorescence signal, while the scatter signal will continue to increase linearly with source power, i.e., laser power is being wasted and SNR decreased (24, 26). However, assuming the atomic vapor is excited to near saturation conditions with the expanded beam as well as with the beam not expanded, the fluorescence signals will increase in direct proportion to the ratio of the illuminated volumes. However, operating at near saturation conditions maintains many of the benefits achieved with saturation (e.g., large signal levels and large linear dynamic range).

When the system is source-carried shot noise limited, the full advantages of pulsed excitation-gated detection are not realized; this case will be encountered in many resonance fluorescence measurements, as pointed out by some workers (1, 3). Therefore, efforts to reduce the scatter have been made in the present studies. By laser beam expansion and proper use of light traps, apertures, and light baffles, the source scatter signal and noise were greatly reduced. This system has provided improved analytical figures of merit.

EXPERIMENTAL

Chemicals. All the chemicals used were reagent grade. Stock solutions of each element (1000 $\mu g\ mL^{-1}$) were prepared in accordance with the directions by Smith and Parsons (29). Deionized water was used as a blank solution in all the experiments.

Instrumentation. A schematic diagram of the present laser-excited atomic fluorescence flame spectrometric system is shown in Figure 1. The experimental components used in the system are described in Table I. Organic dyes used are listed in Table II, where the concentrations of the dyes, solvents, and their peak output wavelengths and wavelength ranges are also given.

The nitrogen laser was operated under the following conditions: applied high voltage 26–28 kV; pressure of nitrogen in laser channel 50 Torr; and repetition rate 20 Hz. The N_2 laser had a 10-ns pulse width and ca. 400-kW peak output power at 337.1 nm. The dye laser, which was pumped by the N_2 laser, had 6 dye cells mounted in a carousel which rotated the desired dye cell into the optical path of the laser cavity. Each cell contained ca. 2 mL of dye solution, which was magnetically stirred during operation. The output of the dye laser had ca. 3–8 ns pulse width and ca.

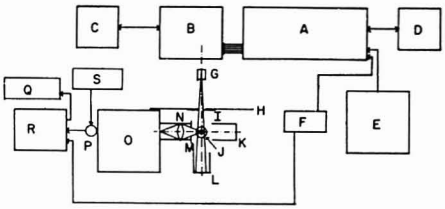


Figure 1. Schematic diagram of laser-excited atomic fluorescence flame spectrometry system. (A) N_2 laser, (B) dye laser, (C) dye laser control unit, (D) vacuum pump, (E) N_2 laser power supply, (F) trigger source, (G) beam expander, (H) panel, (I) diaphragm, (J) burner/nebulizer, (K) light trap, (L) light trap, (M) diaphragm, (N) light baffle and lens, (O) monochromator, (P) photomultiplier detector, (Q) recorder, (R) boxcar integrator, (S) photomultiplier power supply

Table I. Experimental Components of Laser-Excited Atomic Fluorescence Flame Spectrometric System

Component	Model No.	Company address
Nitrogen laser/ power supply	UV-400 TG 100	Molectron Corp., Sunnyvale, Calif. 94086
Trigger source		
Dye laser	DL 200	
Dye laser control unit	DL-040A and DL-050	
Vacuum pump	Type 1030	Alcatel Vacuum Products, Hanover, Mass. 02339
Beam expander	...	Laboratory constructed
Nebulizer and premix burner assembly	303-0110 290-0107	Perkin-Elmer, Norwalk, Conn. 06852
Nebulizer and premix burner assembly	20851-01 42240	Instrumentation Laboratory Inc., Wilmington, Mass. 01887
Capillary burner head	...	Laboratory constructed
Monochromator	EU-700	Heath Co., Benton Harbor, Mich. (now McPherson Inst., Acton, Mass. 01720)
Photomultiplier	R212UH or R818	Hamamatsu TV Co., Middlesex, N.J. 08846
Power supply	412B	John Fluke Manuf. Co., Seattle, Wash. 98133
Boxcar integrator	160 or 162/164	Princeton Applied Research, Princeton, NJ 08540
Recorder	Servo/Riter II	Texas Instrument Co., Houston, Texas 77006

1–80 kW peak power depending upon the dye and wavelength. The mode structure for this Hänsch-type dye laser has recently been reported (30). The beam diameter of the dye laser output was ca. 0.3 nm. A beam expander (12.5-mm focal length lens) was placed in the optical path of the dye laser beam. The beam expander was mounted on a support with fine x, y, z adjustments. A pinhole (spatial filter) was used to minimize the fluorescence background of the dye laser output and to produce a spatially more uniform irradiance. The beam diameter at the flame position was about 5 mm. A panel fitted with an adjustable diaphragm was placed between the beam expander and burner in order to minimize the scattered light level.

A standard capillary burner head 10 mm in diameter (about 50 capillaries of 1-mm i.d. for the air/C_2H_2 flame and of 0.84-mm i.d. for the N_2O/C_2H_2 flame arranged into an area 10 mm in diameter) was used with an inert gas sheath which provided flame

Table II. List of Laser Dyes Used[a]

Dye	Concentration (mol/L)	Solvent	Wavelength peak, nm	Wavelength range, nm (10% points)
PBD	5×10^{-3}	toluene/ethanol 50/50	366, 378	360-386
BBQ	2.5×10^{-3}	toluene/ethanol 50/50	386	373-399
PBBO	5×10^{-4}	toluene/ethanol 70/30	400	391-411
DPS	saturated $< 1.2 \times 10^{-3}$	*p*-dioxane	406	396-416
Bis-MSB	1.2×10^{-3}	*p*-dioxane	421	411-430
7D4MC	10^{-2}	ethanol	457	440-478
C102	10^{-2}	ethanol	470	453-495
7D4TMC	10^{-2}	*p*-dioxane	483	460-517
C500	10^{-2}	ethanol	500	473-547
C495	10^{-2}	ethanol	536	515-583
R6G	5×10^{-3}	ethanol	579	568-605
RB	5×10^{-3}	ethanol	609	594-643
R6G + CVP	2.5×10^{-3} 3.3×10^{-3}	ethanol	660	641-687

[a] From "Molectron Dye List" by Molectron Corp., Sunnyvale, Calif. 94086.

"separation" (*31*). Phosphine and acetone traps were used in the acetylene gas line (*32–34*). The flow rates of gases were passed through rotameters and were calibrated with a linear mass flowmeter (Model ALK 50k, Hastings-Teledyne, Hampton, Va.).

The fluorescence was imaged on the monochromator entrance slit through a lens (76-mm focal length, 50-mm diameter). The diaphragm was set to maximize the fluorescence signal with respect to the scatter signal and SNR. The monochromator was a 0.35-m focal length Czerny-Turner grating spectrometer (2.0 nm/mm reciprocal linear dispersion, 1180 lines/mm grating blazed at 250 nm).

The detection system consisted of a photomultiplier tube, a boxcar integrator, and a chart recorder. The photomultiplier base circuit was modified for pulsed, high current application (*3*). The photomultiplier was operated at a high applied voltage for best transient response (1000 V for the R212 UH and 1200 V for the R818). The boxcar integrator (see Table I) was operated with 50-Ω input, an aperture time ca. 15 ns, and an observed time constant between 0.5 and 5 s.

Procedure. The gas flow rates were ca. 2.3 L min^{-1} of acetylene and 12.3 L min^{-1} air for the air–acetylene flame, and ca. 6 L min^{-1} of acetylene and 10.6 L min^{-1} of nitrous oxide for the nitrous oxide–acetylene flame. Most measurements were performed under slightly fuel-rich flame conditions. The atomic fluorescence signals were maximized with respect to the flow rate of acetylene in both of the flames. A more fuel-rich flame was used in some cases (e.g., Al, Bi, Cr). A fuel-lean flame yielded slightly better results for Ni, Ag, Cu. The flame height at which the atomic fluorescence measurements were taken was ca. 20–30 mm above the burner head. The position of the exciting beam in the flame was not extremely critical due to the large beam diameter. Argon gas with ca. 10–15 L min^{-1} flow rate was used for flame separation. No significant difference in signal or SNR was observed between the "separated" and "unseparated" flames.

An 800- or 1000-μm slit width of the monochromator was used in most resonance fluorescence cases, unless scatter and background noises were found to be small, in which case 2000-μm slit widths were used. In most nonresonance fluorescence cases, 2000-μm slit widths were used.

After optimization of the experimental arrangement and conditions, analytical curves were measured for each element at their atomic fluorescence lines in suitable flames. The root mean square noise levels were evaluated by measuring $^1/_5$ of the observed peak-to-peak noise on the baseline (*35*) while aspirating deionized water (blank). The detection limits were then evaluated by extrapolating the analytical calibration curves to a signal-to-noise ratio of 3 (*36*).

RESULTS AND DISCUSSION

Optimization of the System. *Reduction of Scatter Signal.* The pulsed excitation–gated detection system is ideally suited to the measurement of nonresonance fluorescence lines assuming fluorescence background noises are negligible. However, because many elements, such as Ba, Ca, Cd, Li, Mg, and Sr (mostly alkali and alkaline earth elements), have only one strong resonance fluorescence line, source-carried shot noise can deteriorate their detection limits. In order to overcome this situation for resonance fluorescence lines, an effort was made to reduce the scatter noise and optimize the optical system. Strontium was chosen as a diagnostic element (Sr only has available a resonance atomic fluorescence line). Replacing the beam expander with a focusing lens does not improve the SNR because of lower signal levels and the larger scatter signal levels are observed. The low signal level was probably due to the excitation and observation of a smaller flame volume. It should be stressed here that the addition of only the beam expander without a spatial filter enhanced the atomic fluorescence signal, but also increased proportionally the scatter signal. The large scatter signal, which varied with wavelength, was clearly a result of radiation scattered by the laboratory surroundings and not due to scatter from the analyte flame volume. The proper use of apertures and light traps markedly reduced the scatter signal level. The best SNR was obtained using the beam expander and properly apertured and baffled optical paths, the SNR was improved by more than a factor of 10, and the fluorescence signal-to-scatter signal ratio by a factor of 75, compared to those obtained by the use of only a focusing lens. The scatter signals for most analyses were found to be very small and due mainly to scatter from the environment.

Slit Width vs. SNR. The spectral narrowness of the laser source allowed much larger slit widths (compared to conventional fluorescence spectrometry) to be used with only a solid angle consideration for collection of scattered light at resonance wavelengths (i.e., additional radiation from a spectral continuum or inert gas lines (*37*) did not exist and the fluorescence background of the laser beam was orders of magnitude smaller and could be minimized or spatially filtered if necessary). In other words, the laser was a tunable source with only one narrow spectral line. In laser-excited atomic fluorescence spectrometry, spectral resolution depends upon the *spectral bandwidth of the laser output*, $\Delta\lambda_L$, *not upon the spectral bandwidth of the monochromator*, $\Delta\lambda_M$. An example of signal selectivity is shown in Figure 2A in terms of the fluorescence excitation of sodium D lines (doublet separated by 0.6 nm). The spectral bandwidth of each line was ca. 0.03 nm despite the use of an 800-μm monochromator slit width ($\Delta\lambda_M \sim 1.6$ nm) i.e., spectral resolution is determined by the laser, $\Delta\lambda_L \sim 0.03$ nm (a spectral profile of

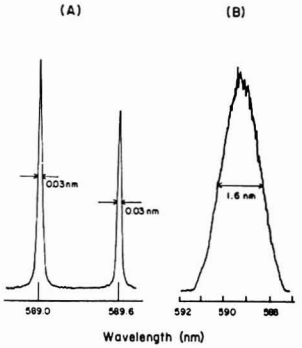


Figure 2. Fluorescence excitation and fluorescence emission profiles of sodium D lines (at 589.0 and 589.6 nm) in the air-acetylene flame. (A) Profile observed by scanning the laser. (B) Profile observed by scanning monochromator. Slit width was 800 μm in both cases

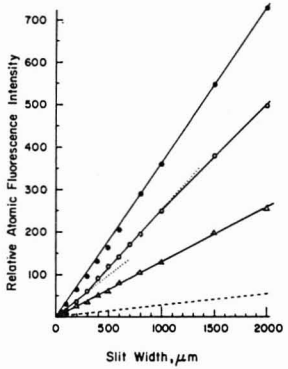


Figure 3. Dependence of atomic fluorescence signal of Na and Tl on slit width observed in the air-acetylene flame. (-O-) Resonance fluorescence of sodium. Excited at 589.0 nm, observed at 589.0 nm. (—: scatter level). (-●-) Resonance fluorescence of thallium. Excited at 377.6 nm, observed at 377.6 nm. (-Δ-) Nonresonance fluorescence of thallium. Excited at 377.6 nm, observed at 535.0 nm

sodium atomic fluorescence observed by wavelength scanning the monochromator spectrometer is shown in Figure 2B, where an 800-μm slit width was used). Because the emission signal of sodium was essentially negligible due to the low duty factor (3×10^{-7} here) of the pulsed source-gated detection system, wide monochromator slit widths can be used. In Figure 3 a plot of fluorescence signal vs. slit width is shown for sodium (resonance atomic fluorescence; excited at 589.0 nm and observed at 589.0 nm) and thallium (both of resonance and nonresonance atomic fluorescence; excited at 377.6 nm and observed at 377.6 nm and 535.0 nm, respectively). In the case of sodium, the curve has three different slopes in the ranges of 0–300 μm, 300–1000 μm, and >1000 μm. At slit widths less than 300 μm, fluorescence from only the excited 589.0-nm Na is observed. With the slit width wider than 400 μm, fluorescence from both of the sodium D lines was observed by the spectrometer (*simultaneous multiple line observation*). This gave larger signals (i.e., a larger slope in Figure 3) observed by the spectrometer in the slit width range 300–1000 μm. The simultaneous multiple line observation suggests another advantage of laser-excited atomic fluorescence

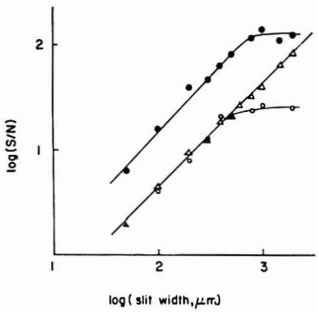


Figure 4. SNR vs. slit width of Na and Tl in the air-acetylene flame. (-O-) Resonance fluorescence of sodium. Excited at 589.0 nm, observed at 589.0 *nm*. (-●-) Resonance fluorescence of thallium. Excited at 377.6 nm, observed at 377.6 nm. (-Δ-) Nonresonance fluorescence of thallium. Excited at 377.6 nm, observed at 535.0 nm

spectrometry, when multiplet lines of an element are within the spectrometer spectral band pass used (e.g., Mn), in that greater signal levels are easily obtainable. In Figure 3, the slope of the curve for sodium becomes smaller for slit widths exceeding 1000-μm slit width because saturation of the photomultiplier (anodic current) causes nonlinearity; saturation was evaluated by using the neutral density filters to reduce the signal to the photomultiplier detector. For analyses at high concentrations, the monochromator slit width could also be reduced to minimize saturation of the photomultiplier.

In Figure 4, the curves of SNR vs. monochromator slit width are shown in the cases of sodium and thallium (same experimental conditions as those in Figure 3). For both the Na and Tl resonance cases, the SNRs reached plateaus at slit widths between 800 and 1000 μm. Source-carried noise limited the maximum SNR at slit widths >1000 μm. Scatter signal levels are shown in Figure 3 for Na. Considerations which determine the optimum monochromator slit width in atomic fluorescence are: type of transition; source irradiance; optical configuration (i.e., efficiency of signal collection); saturation of photomultiplier anode current; flame background fluorescence; and spectral bandwidth of source radiation and spectrometer. In the present experimental arrangement, an 800- or 1000-μm slit width provided a generally useful setting, because the source-carried noise limit is apparently approached here as was determined experimentally for Na and Tl by the SNR vs. slit width plot (Figure 4).

However, in the nonresonance case, no leveling off of the slope in SNR vs. slit width curve was observed. This indicated that the signal was not source-carried noise limited and that a detection system with a larger optical conductance could be employed.

Analytical Figures of Merit. *Limits (Powers) of Detection.* The detection limits and analytical curves were obtained for 23 elements, including 37 transitions, and 7 different fluorescence processes. Ten elements were reported using the frequency doubled dye laser output, most of which represent the first time these transitions have been observed by laser-excited atomic fluorescence. The work also demonstrated the wide tuning range of the N_2 laser pumped dye laser as a single "line" source for atomic spectrometry as elements from Cd at 228 nm to Li at 671 nm were observed.

The limits of detection have been improved by a factor of ca. 10–200 times over those previously obtained with a N_2 laser pumped tunable dye laser system for all elements examined, except cobalt. The linearity of the analytical curves have also been extended to about five orders of magnitude for almost

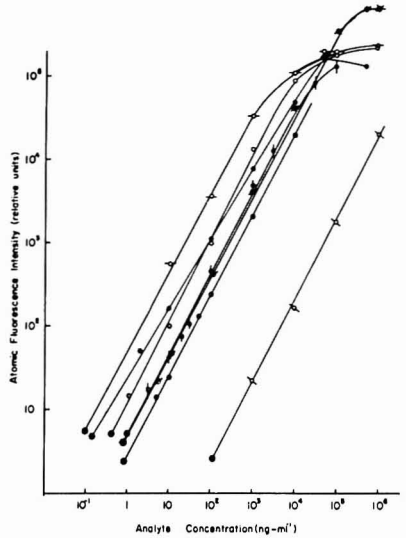


Figure 5. Analytical calibration curves for elements having only strong resonance transitions above 355 nm in air–acetylene flame, $\lambda_{ex} = \lambda_{fl}$, nm, given in parentheses. ( ) Resonance fluorescence of Ba (554), (–O–) resonance fluorescence of Ca (422), ( ) resonance fluorescence of Cr (359), (⊙) resonance fluorescence of Li (670), (ϕ) resonance fluorescence of Mn (403), (•) resonance fluorescence of Na (589), (O) resonance fluorescence of Sr (460). (● indicates the limit of detection.)

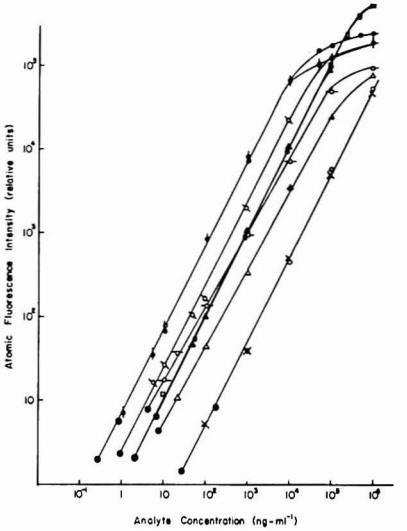


Figure 6. Analytical calibration curves for elements having both strong resonance and nonresonance transitions excited above 355 nm in an air–acetylene flame, λ_{ex}, nm and λ_{fl}, nm given in parentheses respectively. (▲) Resonance fluorescence of Ga (403, 403), ( ) nonresonance fluorescence of Ga (403, 417), (•) resonance fluorescence of In (410, 410), ( ) nonresonance fluorescence of In (410, 450), (□) nonresonance fluorescence of Ni (361, 352), (O) resonance fluorescence of Pb (405, 405), (×) nonresonance fluorescence of Pb (405, 283), (–O–) resonance fluorescence of Tl (377, 377), (△) nonresonance fluorescence of Tl (377, 535). (● indicates the limit of detection)

all elements examined. These results are presented in Table III together with all pertinent data and conditions necessary for discussing detection limits except for the system time constant which was 1 s for most cases. In all cases, at least five time constant intervals were allowed before signals were measured. The noise level was evaluated by taking $^1/_5$ the peak-to-peak noise over at least a 50-s time period when only the blank was being aspirated (*35*). This approach was equivalent to calculating the standard deviation of 16 separate measurements for evaluating the noise, N. The limit of detection (LOD) was calculated on the basis of a signal-to-noise (SNR) equal to three (as recommended by IUPAC (*36*)). However, it is generally accepted that a SNR ≥ 10 should be used for practical determinations.

In Tables III and IV, our results are compared with previous laser-excited fluorescence studies in flames and furnaces, and with the best values for the limits of detection obtained by conventional source flame and furnace atomic fluorescence (AF), flame atomic emission (AE), flame and furnace atomic absorption (AA), and by atomic emission induction coupled plasma (ICP). It should be noted that all limits of detection except those determined in the present work were based on a SNR = 2 value. Table IV clearly shows that laser-excited atomic fluorescence flame spectrometry compares quite favorably to all the methods listed where pneumatic nebulizers are used. The use of an ultrasonic nebulizer should also provide ca. 10-fold improvement in detection limits (*38*) for laser excited AF. The limits of detection for nonresonance fluorescence are typically an order of magnitude better than for the corresponding resonance fluorescence cases.

Analytical Calibration Curves and Linear Dynamic Ranges. The analytical calibration curves plotted in Figures 5–8 are divided according to whether the element: (i) has transitions which are excited by the fundamental (>355 nm) or frequency doubled (<355 nm) dye laser output; (ii) has only strong resonance transitions or has both strong resonance and nonresonance transitions; and (iii) is best excited in an air–acetylene or nitrous oxide–acetylene flame.

The *linear dynamic range* is determined by the lower and upper concentration limits. The *upper limit* of concentration is determined from the analytical calibration curve by that signal level which deviates from linearity by 5%. The *lower limit* of concentration is the limit of detection. The upper and lower limits of concentration, as well as the linear dynamic ranges are reported in Table III. The linear dynamic ranges for almost all elements examined by laser-excited atomic fluorescence flame spectrometry were about 5 to 7 orders of magnitude. The linear dynamic ranges were equivalent to those obtained by the ICP (4–7 orders of magnitude), about one or two orders of magnitude better than by conventional source atomic fluorescence spectrometry and atomic emission spectrometry, and about 2 to 4 orders of magnitude greater than flame atomic absorption and furnace atomic absorption. The high degree of linearity obtained by pulsed laser-excited atomic fluorescence spectrometry was due to the low noise and the high spectral irradiance of the laser resulting in lower limits of detection; at high concentrations, there was minimal self-absorption and also there was a minimal prefilter effect due to the atomic vapor being excited to near-saturation conditions (*6*, *12*, *28*). The slopes of the analytical calibration curves (sensitivity) shown in Figures 5–8 are all close to unity (within 5%) except for Na, Tl, and Mo resonance fluorescence, which are attributed to a combination of postfilter and self-absorption effects, source irradiances insufficient to

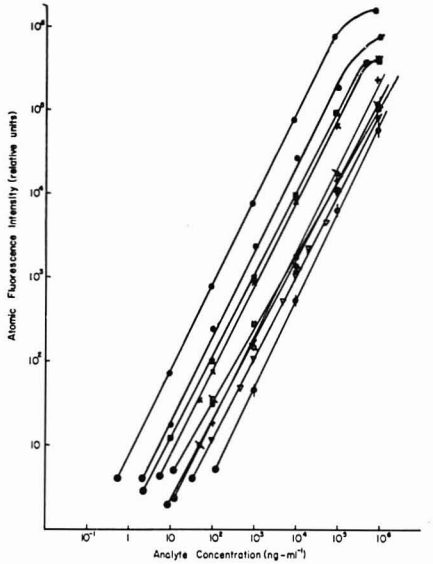


Figure 7. Analytical calibration curves for elements having transitions excited above 355 nm in a nitrous oxide–acetylene flame, λ_{ex}, nm and λ_{fl}, nm given in parenthese, respectively. (■) Resonance fluorescence of Al (396, 396), (O) nonresonance fluorescence of Al (394, 396), (◠◡) resonance fluorescence of Ba (553, 553), (+) resonance fluorescence of Mo (380, 380), (□) resonance fluorescence of Mo (390, 390), (•) resonance fluorescence of Tl (365, 365), (×) resonance fluorescence of Tl (400, 400), (▽) nonresonance fluorescence of V (370, 411), (◇) resonance fluorescence of V (411, 411). (● indicates the limit of detection)

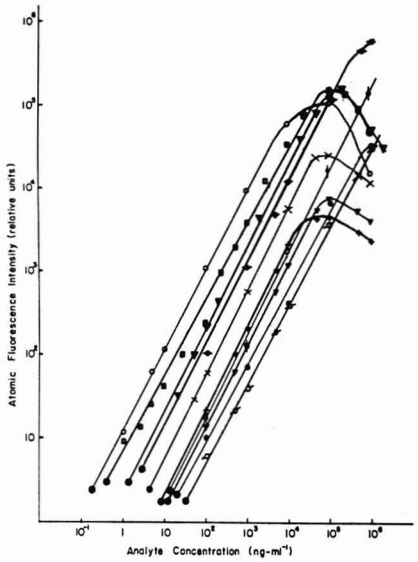


Figure 8. Analytical calibration curves for elements having transitions excited below 355 nm in an air–acetylene flame, λ_{ex} nm and λ_{fl} nm given in parentheses, respectively. (×) Resonance fluorescence of Ag (328, 328), (-●-) resonance fluorescence of Bi (306, 306), (+) resonance fluorescence of Cd (228, 228), (▼) resonance fluorescence of Cu (325, 325), (◠◡) nonresonance fluorescence of Fe (296, 373), (O) resonance fluorescence of Mg (285, 285), (□) resonance fluorescence of Mn (280, 280), (▽) resonance fluorescence of Ni (232, 232), (•) resonance fluorescence of Pb (283, 283), (◇) nonresonance fluorescence of Pb (283, 405). (● indicates the limit of detection)

produce "saturation" conditions, and ionization of the analyte. All of the analytical calibration curves for resonance lines obtained with doubling of the dye laser output bend over at high analyte concentrations, typical of the analytical growth curves for low spectral irradiance narrow line source excitation (*39*). The spectral bandwidth of the dye laser varies with wavelength and is likely to be ≲0.01 nm in the UV but somewhat larger in the visible, e.g., ~0.03 nm.

For precise and accurate data over a long time period, which is necessary in any practical analytical work, the atomic fluorescence signal (under beam expansion of the dye laser output) must in most cases be measured relative to the intensity of the laser output (*assuming the measurements are being performed on the linear region of the fluorescence intensity vs. source intensity curve*). This was due to the fact that the dye laser output decreases with time to varying degrees dependent upon the individual dye degradation. Ratioing was simple to accomplish by reflecting a small amount of the laser output off a quartz plate onto a photodiode and using a dual channel boxcar integrator to ratio the signal.

Spectral Interferences. Due to the narrow spectral bandwidth of the laser output *and* its pulsed operation, N_2 laser pumped dye laser-excited atomic fluorescence with gated detection essentially has no, or can be adjusted to have no spectral interferences. The typical spectral bandwidth of the dye laser output is 0.01 nm and using frequency narrowing techniques is typically 0.001 nm. This is shown in Table V and Figure 9 for the case of Mn and Ga at 403.3 nm. Ga has lines at 403.30 and 417.21 nm. Mn lines are at 403.08, 403.31,

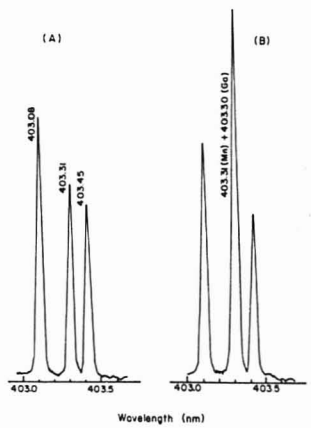


Figure 9. Fluorescence excitation spectrum for: (A) a 1 ppm Mn solution; and (B) 1 ppm Mn + 5 ppm Ga solution

and 403.45 nm. The spectral separation of the two lines for Ga and Mn near 403.3 nm is only 0.01 nm. The specificity factor (the ratio of interferent to analyte concentration which contributes 100% interference using low dispersion) for the analysis of Mn at 403 nm in the presence of Ga is 5 (*40*). Part

Table III. Detection Limits by Laser-Excited Atomic Fluorescence Flame Spectrometry

			This work[c]			Previous works[c]			
Element	Ex/Fl, nm[a]	Type of AF[b]	LOD, ng mL^{-1}	UL, mg mL^{-1}	log (LDR), units	LOD, ng mL^{-1}	UL, mg mL^{-1}	log LDR, units	Ref
Ag	328.1	RF$^{\dagger e}$	4	0.06	4.2	...	...	...	...
Al	396.1	E-RF$^{\Delta}$	2	0.6	5.4	300	0.1	4	3
	394.4/396.1	S-DLF$^{\Delta}$	0.6	0.3	5.7	5	0.2	4.6	3
Ba	553.7	RF†	100	10	5	8	>1	>5	11
	553.7	RF$^{\Delta}$	8	>1	>5	40	...	...	13
Bi	306.8	RF†	3	0.5	5.2	...	...	...	...
Ca	422.7	RF†	0.08	0.006	4.9	5	0.05	4	3
Cd	228.8	RF†	8	0.03	3.5	...	...	...	...
Co[d]	357.5/347.4	AS-DLF†	1000	>2	>3.3	200	0.2	3	3
	230.9	RF†	1000	>2	>3.3	...	...	...	...
Cr	359.3	RF†	1	0.3	5.5	20	0.02	3	3
Cu	324.7	RF†	1	0.1	5	...	...	...	...
Fe	296.7/373.5	S-DLF†	30	>1	>4.5	...	...	...	...
Ga	403.3	RF†	7	0.3	4.6	100	0.5	3.7	3
	403.3/417.2	S-DLF†	0.9	0.2	5.4	20	0.02	3	3
In	410.4	RF†	0.8	0.4	5.7	10	0.5	3.7	3
	410.4/451.1	S-DLF†	0.2	0.3	6.2	2	0.5	4.4	3
Li	670.8	RF†	0.5	>0.001	>4.3	...	...	...	...
Mg	285.2	RF†	0.2	0.02	5	0.3	...	...	9
Mn	403.1	RF†	1	0.08	4.9	10	0.02	3.3	3
	279.5	RF†	0.4	0.1	5.4	...	...	...	...
Mo	379.8	RF$^{\Delta}$	12	>1	>4.9	1000	0.1	2	3
	390.3	RF$^{\Delta}$	12	>1	>4.9	300	0.1	2.5	3
Na	589.0	RF†	<0.1	0.05	>5.7	0.1	...	...	13
	589.6/589.0	TA-SLF†	1	0.06	4.8	...	...	...	...
Ni	232.0	RF†	12	0.1	3.9	...	...	...	...
	361.0/352.4	E-AS-DLF†	2	1	5.7	50	0.2	3.6	3
Pb	405.8	E-RF†	180	>1	>3.7	6	...	...	10
	405.8/283.3	AS-DLF†	30	>1	>4.5	...	...	...	...
	283.3	RF†	20	1	4.7	...	...	...	...
	283.3/405.8	S-DLF†	13	>1	>4.9	30	...	...	9
Sr	460.7	RF†	0.3	0.03	5	10	0.02	3.3	3
Ti	399.9	RF$^{\Delta}$	5	1	5.3	100	0.2	3.3	3
	365.4	RF$^{\Delta}$	2	0.4	5.2	...	...	...	...
Tl	377.6	RF†	4	0.3	4.9	1000	0.05	1.7	3
	377.6/535.0	S-DLF†	7	0.6	4.9	200	0.1	3.7	3
V	411.2	E-RF$^{\Delta}$	50	>1	>4.3	...	...	...	...
	370.4/411.2	E-S-SLF$^{\Delta}$	30	>1	>4.5	500	...	...	5

[a] Ex/Fl = excitation wavelength/fluorescence wavelength (if different than excitation wavelength). The energy levels involved in the transition and their *gf* and *gA* values can be found in Reference 42. [b] RF = resonance fluorescence; E-RF = excited resonance fluorescence; S-DLF = Stokes direct line fluorescence; AS-DLF = anti-Stokes direct line fluorescence; TA-SLF = thermally assisted stepwise line fluorescence; E-AS-DLF = excited anti-Stokes direct line fluorescence; and E-S-SLF = excited Stokes stepwise line fluorescence. (See Reference 43 for detailed discussion). [c] LOD = Limit of Detection, UL = Upper Limit of linearity, and LDR = linear dynamic range = UL/LOD. [d] Experimental difficulty was encountered in obtaining good laser output at the Co lines attempted. [e] † A/A or air/acetylene flame. $^{\Delta}$ represents N/A or nitrous oxide/acetylene flame.

(i) of Table V shows that by exciting the 403.08-nm transition of Mn and observing the "resonance" fluorescence with a low dispersive spectrometric system (1.6-nm bandpass), no interference of Ga on the analysis of Mn is observed even when Ga is present at a concentration 1000-fold greater than that of Mn. This simply demonstrates that because of the narrow spectral bandwidth of the laser, no Ga is being excited and that because of the low duty factor, Ga flame emission is negligible. Part (ii) of Table V shows that Mn does interfere with the analysis of Ga approximately in the ratio expected; however, this interference is simply eliminated by using nonresonance fluorescence which detects the Ga fluorescence signal at 417.01 nm, as seen in part (iii) of Table V.

Spectral interferences in conventional source AF, AA, and in AE due to concomitants and flame background in various flames and furnaces and inert fill gas lines in lamps, are well-known (*33, 34, 37, 40*). Spectral interferences occur in ICP spectrometry unless sufficiently high resolution detection is employed, because of the high temperatures occurring in the plasma. Nonspectral interferences occurring with the ICP have been found to be relatively small but complex, and the setting of the principal experimental parameters of the ICP are critical as they affect the magnitude of these interferences (*41*). A CW dye laser-excitation AF system will also be subject to flame background noise.

The only significant potential interferences foreseen in pulsed laser-excited atomic flame fluorescence spectrometry with gated detection would arise from molecular fluorescence of species formed in the flame by concomitants and flame gases, and excited by the laser (*33*). The ground state resonance transition of V at 385.54 nm was not observed because of the difficulty of finding this transition among the strong CN molecular fluorescence in this region. These potential interferences are currently being investigated.

Concluding Statements. Pulsed source laser-excited atomic fluorescence with gated detection is potentially superior to all other elemental methods compared here in terms of the analytical figures of merit obtainable. The ease of operation of the system is solely dependent on the state-of-the-art of tunable dye lasers. The high cost of the excitation-measurement system and the requirement of single element detection (slew scanning of the dye laser is possible) will have

Table IV. Comparison of Detection Limits in Flame and Furnace Spectrometry and Inductively Coupled Plasma (ICP)

	Detection limit, ng mL^{-1}					
					ICP	
Element	AF,[a] laser, this work	AF,[b] conventional source	AE[b]	AA[b]	Pneumatic nebulization[c]	Ultrasonic nebulization[d]
Ag	4	0.1β[e] (0.4)	2	1 (0.01)	4†	...[f]
Al	0.6β	100	3	30* (0.1)	2	0.5**
Ba	8	...	1	20 (0.6)	0.1†β	0.01
Bi	3β	5β (10)	20 000	50 (0.4)	50†	...
Ca	0.08β	20 (0.1)	0.1β	1* (0.04)	0.07†β	0.0001
Cd	8	0.001β (0.01)	800	1 (0.008)	1.0	0.07*
Co[g]	1000	5β (1)	30	2β (0.2)	2β	0.1*
Cr	1β	5	2β	2β (0.2)	0.9β	0.08*
Cu	1	0.5 (1)	0.1β	1* (0.06)	0.2β	0.04*
Fe	30	8 (10)	5	4 (1)	0.2β	0.09
Ga	0.9β	10 (50)	10*	50 (0.1)	14†	0.6
In	0.2β	100	0.4β	30 (0.04)	30†	...
Li	0.5	...	0.02β	1 (0.3)	...	...
Mg	0.2β	0.1β (1)	5*	0.1β (0.004)	0.7†	0.003
Mn	0.4β	1 (5)	1	0.8 (0.02)	0.1β	0.01*
Mo	12β	500	100	30 (0.3)	4β	0.2
Na	<0.1β	...	0.1β*	0.8	0.2†β	0.02
Ni	2β	3β (5)	20	5β (0.9)	4β	0.2
Pb	13β	10β (3)	100	10β (0.2)	10β	1*
Sr	0.3	30	0.2	5 (0.1)	0.02†β	0.003
Ti	2β	4000	30	90* (4)	3†β	0.03
Tl	4β	8β (20)	20	20 (1)	200†	...
V	30	70	7	20 (0.3)	1β	0.06

[a] Limits of detection represent concentrations required to produce a line signal three times as great as the standard deviation of the background noise. All other values listed in the table represent concentrations required to produce a line signal twice as great as the standard deviation of the background noise, except where noted. [b] Values taken from J. D. Winefordner, J. J. Fitzgerald, and N. Omenetto, *Appl. Spectrosc.*, **29**, 369 (1975) except for those designated *, which were taken from V. A. Fassel and R. N. Kniseley, *Anal. Chem.*, **46**, 1110A (1974). Values in parentheses are for furnace AF and AA. [c] All values taken from K. W. Olson, W. J. Haas, Jr., and V. A. Fassel, *Anal. Chem.*, **49**, 632 (1977) except those with †, which are from V. A. Fassel and R. N. Kniseley, *Anal. Chem.*, **46**, 1110A (1974). [d] All values taken from P. W. J. M. Boumans and F. J. deBoer, *Spectrochim. Acta, Part B*, **30**, 309 (1975) except those designated *, which were taken from K. W. Olson, W. J. Haas, Jr., and V. A. Fassel, *Anal. Chem.*, **49**, 632 (1977) and those designated **, which were taken from M. H. Abdallah, R. Diemiaszonek, J. Jarosz, J. M. Mermet, J. Robin, and C. Trassy, *Anal. Chim. Acta*, **84**, 271 (1976). Limit of detection designated ** represent concentrations required to produce a line signal six times as great as the standard deviation of the background noise. [e] β designates best value with pneumatic nebulization. All values within a factor of 3 are considered to be equal. [f] ... indicates no value reported. [g] Experimental difficulties were encountered in obtaining good laser output at the Co lines.

Table V. Investigation of Spectral Interferences between Manganese and Gallium

Composition	Relative atomic fluorescence intensity
(i) Excited at 403.08 nm/Observed at 403.08 nm [Observe manganese atomic fluorescence]	
Mn 1 ppm	69
Mn 1 ppm + Ga 5 ppm	70
Mn 1 ppm + Ga 100 ppm	68
Mn 0.5 ppm + Ga 100 ppm	34
Mn 0.1 ppm + Ga 100 ppm	7
(ii) Excited at 403.30 nm/Observed at 403.30 nm [Observe gallium atomic fluorescence]	
Ga 5 ppm	67
Ga 5 ppm + Mn 1 ppm	108
(iii) Excited at 403.30 nm/Observed at 417.01 nm [Observe gallium atomic fluorescence]	
Ga 5 ppm	151
Ga 5 ppm + Mn 1 ppm	151

to be weighted against the need for trace analysis by the analyst. It will also be necessary to investigate other nebulization (e.g., ultrasonic) and atomization sources (e.g., furnaces, ICP, etc.). For nonresonance fluorescence, a nondispersive system, using, for example, only interference filters and neutral density filters before the photomultiplier, should yield the optimal system (i.e., lowest limit of detection and largest linear dynamic range). Experiments are currently in progress to optimize the optical configuration for the nonresonance case and compare with the resonance cases. It should also be noted that because fluorescence is emitted in 4π steradians, a system could be designed using two detectors and two optical arrangements to optimize both resonance and nonresonance signals with little added expense or inconvenience. A pulsed source laser-excited atomic fluorescence system which optimizes both resonance and nonresonance fluorescence signals via SNR determinations and considers spectral irradiance in terms of approaching saturation will provide the best method for trace analysis to date. The authors believe that in most cases the detection limits and linear dynamic range could be improved by up to 4 orders of magnitude depending on the type of spectral lines being measured by: (i) optimization of the optical system (≥1 order); (ii) optimization of laser beam diameter (i.e., spectral irradiance) (<1 order); (iii) consistently good quality of laser beam shape over entire spectrum (<1 order); (iv) higher output powers (especially in the frequency doubled wavelength region) (≥1 order); (v) use of ultrasonic (or much improved pneumatic) nebulization (≥1 order); (vi) improvement in flame stability and homogeneity by improved flow system and mixing chamber design (<1 order); (vii) a more suitable burner configuration (<1 order); (viii) optimization of the electronic detection system (e.g., fast transient response photomultiplier tube and base, pulse stretching, and preamplification) (≥1 order); and (ix) reduction in radio frequency interference noise (≤1 order).

ACKNOWLEDGMENT

The authors thank Hamamatsu for the use of R818 and R212UH PM tubes and Arthur P. Grant and staff for assistance from the machine shop.

LITERATURE CITED

(1) L. M. Fraser and J. D. Winefordner, *Anal. Chem.*, **43**, 1693 (1971).
(2) M. B. Denton and H. V. Malmstadt, *Appl. Phys. Lett.*, **18**, 485 (1971).
(3) L. M. Fraser and J. D. Winefordner, *Anal. Chem.*, **44**, 1444 (1972).
(4) N. Omenetto, N. N. Hatch, L. M. Fraser, and J. D. Winefordner, *Anal. Chem.*, **45**, 195 (1973).
(5) N. Omenetto, N. N. Hatch, L. M. Fraser, and J. D. Winefordner, *Spectrochim. Acta, Part B*, **28**, 65 (1973).
(6) N. Omenetto, L. P. Hart, P. Benetti, and J. D. Winefordner, *Spectrochim. Acta, Part B*, **28**, 301 (1973).
(7) N. Omenetto, P. Benetti, L. P. Hart, J. D. Winefordner, and C. Th. J. Alkemade, *Spectrochim. Acta, Part B*, **28**, 289 (1973).
(8) J. Kuhl, S. Neumann, and M. Kriese, *Z. Naturforsch. A*, **28**, 273 (1973).
(9) J. Kuhl and H. Spitschan, *Opt. Commun.*, **7**, 256 (1973).
(10) D. R. de Olivares, Ph.D. Thesis, Indiana University, 1976.
(11) R. B. Green, J. C. Travis, and R. A. Keller, *Anal. Chem.*, **48**, 1954 (1976).
(12) J. A. Gelbwachs, C. F. Klein, and J. E. Wessel, *Appl. Phys. Lett.*, **30**, 489 (1977).
(13) B. W. Smith, M. B. Blackburn, and J. D. Winefordner, *Can. J. Spectrosc.*, **22**, 57 (1977).
(14) J. W. Daily and C. Chan, University of California, Berkeley, Calif., unpublished work.
(15) J. Kuhl and G. Marowsky, *Opt. Commun.*, **4**, 125 (1971).
(16) S. Neumann and M. Kriese, *Spectrochim. Acta, Part B*, **29**, 127 (1974).
(17) W. M. Fairbanks Jr., T. W. Hänsch, and A. L. Schawlow, *J. Opt. Soc. Am.*, **65**, 199 (1975).
(18) H. L. Brod and E. S. Yeung, *Anal. Chem.*, **48**, 344 (1976).
(19) B. L. Sharp and A. Goldwasser, *Spectrochim. Acta, Part B*, **31**, 431 (1976).
(20) S. Mayo, R. A. Keller, J. C. Travis, and R. B. Green, *J. Appl. Phys.*, **47**, 4012 (1976).
(21) M. A. Bolshov, A. V. Zybin, L. A. Zybina, V. G. Koloshnikov, and I. A. Majorov, *Spectrochim. Acta, Part B*, **31**, 493 (1976).
(22) J. P. Hohimer and P. J. Hargis, Jr., *Appl. Phys. Lett.*, **30**, 344 (1977).
(23) J. D. Winefordner, J. J. Fitzgerald, and N. Omenetto, *Appl. Spectrosc.*, **29**, 369 (1975).
(24) N. Omenetto, *Anal. Chem.*, **48**, 75A (1976).
(25) N. Omenetto, G. D. Boutilier, S. J. Weeks, B. W. Smith, and J. D. Winefordner, *Anal. Chem.*, **49**, 1076 (1977).
(26) N. Omenetto, L. M. Fraser, and J. D. Winefordner, *Appl. Spectrosc. Rev.*, **7**, 147 (1973).
(27) G. D. Boutilier, J. D. Bradshaw, S. J. Weeks, and J. D. Winefordner, *Appl. Spectrosc.*, **31**, 307 (1977).
(28) N. Omenetto and J. D. Winefordner, Chapter on "Atomic Fluorescence Spectroscopy with Lasers", in "Analytical Laser Spectroscopy", John Wiley, New York, N.Y., in press.
(29) B. W. Smith and M. L. Parsons, *J. Chem. Educ.*, **50**, 679 (1973).
(30) A. A. Pease and W. M. Pearson, *Appl. Opt.*, **16**, 57 (1977).
(31) H. Haraguchi and J. D. Winefordner, *Appl. Spectrosc.*, **31**, 195 (1977).
(32) H. Haraguchi, W. K. Fowler, D. J. Johnson, and J. D. Winefordner, *Spectrochim. Acta, Part A*, **32**, 1539 (1976).
(33) W. K. Fowler and J. D. Winefordner, *Anal. Chem.*, **49**, 944 (1977).
(34) R. Mavrodineanu and H. Boiteux, "Flame Spectroscopy", John Wiley, New York, N.Y., 1965, p 62.
(35) N. W. Bower and J. D. Ingle, Jr., *Anal. Chem.*, **48**, 686 (1976).
(36) IUPAC, Nomenclature, Symbols, Units, and Their Usage in Spectrochemical Analysis, Part II, Section 4.1, Revision 1975.
(37) L. de Galan and G. F. Samaey, *Spectrochim. Acta, Part B*, **24**, 679 (1969).
(38) K. W. Olson, W. J. Haas, Jr., and V. A. Fassel, *Anal. Chem.*, **49**, 632 (1977).
(39) J. D. Winefordner, S. G. Schulman, and T. C. O'Haver, "Luminescence Spectrometry in Analytical Chemistry", John Wiley, New York, N.Y., 1973.
(40) B. E. Buell, "Flame Emission and Atomic Absorption Spectrometry", J. A. Dean and T. C. Rains, Ed., Marcel Dekker, New York, N.Y., 1969, p 270.
(41) P. W. J. M. Boumans and F. J. DeBoer, *Spectrochim. Acta, Part B*, **31**, 355 (1976).
(42) C. H. Corliss and W. R. Bozman, "Experimental Transition Probabilities for Spectral Lines of Seventy Elements", *Natl. Bur. Stand. (U.S.) Monogr.*, **53** (1962).
(43) N. Omenetto and J. D. Winefordner, *Appl. Spectrosc.*, **26**, 555 (1972).

RECEIVED for review August 22, 1977. Accepted November 9, 1977. This research has been supported by AFOSR-AF-F44620-76-C-0005. One of the authors (H.H.) would also like to thank the Agency of Science and Technology, Japan, for a travel fellowship.

Trimethylsilyl Ether Formation to Quantitate Hydroxyls by Nuclear Magnetic Resonance Spectrometry

F. K. Schweighardt,* H. L. Retcofsky, S. Friedman, and M. Hough

U.S. Department of Energy, Pittsburgh Energy Research Center, 4800 Forbes Avenue, Pittsburgh, Pennsylvania 15213

An NMR method is described for the characterization and quantitation of hydroxyl groups in complex organic mixtures by formation of their trimethylsilyl (TMS) derivatives. A series of model compounds was used to demonstrate the ninefold enhancement in proton NMR sensitivity, which subsequently gave a calculated hydroxyl content with an average error of 5% for both reproducibility of the measurement and agreement to the known hydroxyl content. This study also showed the unique chemical shift attributed to each class of hydroxyl-containing compounds. The method was then applied to the characterization of hydroxyl groups found in coal liquefaction oils and asphaltenes.

Although a number of methods exist for the determination of hydroxyl groups in simple mixtures (*1*) and petroleum oils (*2*), a more reliable and independent method is still needed to correlate the total hydroxyl content and the nature of the hydroxyl moiety. Following the introduction of the method of forming trimethylsilyl (TMS) ether derivatives by Martin (*3*) some 25 years ago, others have made further use of the technique for isolation purposes (*4*), mass spectrometry (*5*), gas chromatography (*6*), NMR quantitation of fatty acids (*7*), infrared and NMR quantitation of hydroxyl in coal (*8*, *9*), and gravimetric estimation of hydroxyl groups in coal asphaltenes (*10*). We now propose the use of proton NMR of the TMS derivatives to aid in quantifying the number and kind of hydroxyl groups present in complex mixtures, such as coal-derived oils.

It has long been known that hexamethyldisilazane (HMDS) reacts quantitatively with hydroxyl groups according to Equation 1,

$$2\mathrm{ROH} + (\mathrm{CH_3})_3\mathrm{SiNHSi}(\mathrm{CH_3})_3 \xrightarrow[\text{(HMDS)}]{} 2\mathrm{ROSi}(\mathrm{CH_3})_3 + \mathrm{NH_3} \quad (1)$$

The resulting trimethylsilyl ethers are thermally stable and appear to resist oxidation. It is important to point out that the starting compounds are easily recovered from the ether by hydrolysis.

Langer et al. (*11*) reported that it is possible to distill off phenolic portions of coal hydrogenation products as TMS ethers at atmospheric pressure without undue decomposition. They reported that TMS ether derivatization of alcohols

0003-2700/78/0350-0368$01.00/0 © 1978 American Chemical Society

generally increases their boiling points by some 15 °C, while the boiling points of TMS ethers of phenols are decreased some 25–40 °C. Amines and mercaptans, for which hydrogen bonding of the parent compound plays only a small role, show an increase in boiling point of the TMS derivative by some 60 °C. This is contrary to the general belief that TMS derivative formation always decreases the boiling point. In fact, TMS derivative boiling points parallel those of comparable acetates. It is because of the success of TMS derivative formation on both hydrogen-bonded and hindered hydroxyls that we have extended its use to direct quantitation of hydroxyls by NMR.

EXPERIMENTAL

NMR Spectra. The time-sharing NMR spectrometer (*12*) at the National Institutes of Health Biomedical Facility, Mellon Institute, Pittsburgh, Pa., was used to obtain the 250-MHz ^1H NMR spectra. The spectrometer was operated in the correlation (*13*) mode, and each spectrum is the result of 100–250 time-average scans. Samples were run as CS_2 solutions (25 mg/mL) at 26 °C. After an NMR spectrum was taken for integral intensity measurements, tetramethylsilane was added to act as an internal standard for chemical shift measurement. In each case, the sample was permitted to come to thermal equilibrium prior to recording the spectrum.

Infrared Spectra. Immediately after a TMS derivative was formed from either a model compound or a coal-derived product, it was freed of solvent and its IR spectrum taken in CS_2. The spectrum was run on a dilute solution in 3-mm liquid cells with a Perkin-Elmer Model 180 infrared spectrophotometer. Completion of TMS derivative formation was confirmed by the absence of the absorption band at 3590 cm^{-1}, assigned as the free OH stretch. Comparison of the intensity of the band at 3480 cm^{-1}, assigned to an N–H structure of pyrrole or carbazole, was made before and after TMS derivative formation in the case of coal-derived oils. In no case did we observe a significant decrease in intensity of this N–H band. Our experimental parameters were devised to provide mild reaction conditions for TMS derivatization of hydroxyls. Formation of an N–H derivative is possible (*11*) under more demanding conditions of heat, acid catalysis, and duration of reflux. Hence, we conclude that the observed TMS derivatives were substantially derived from hydroxyl moieties. It should be pointed out that our earlier work (*14*) on IR of TMS derivatives of coal-derived asphaltenes showed a small band at 3560 cm^{-1} that did not disappear by formation of a TMS ether. The exact nature of this band is still in question, but it appears to be a highly hindered hydroxyl.

Sample Preparation. Fifty milligrams of the compound or mixture was weighed into a 25-mL sidearm filtering flask. The sidearm was fitted with a Bunsen valve to release solvent pressure and the top sealed with a neoprene stopper. To the sample were added 10 mL of pesticide grade benzene, 0.5 mL of hexamethyldisilazane, 0.5 mL of *N*-trimethylsilyldimethylamine and 50 μL of pyridine-d_5. This mixture of reagents was found to react with a broad range of hydroxyl-containing compounds and mixtures. We found that pyridine-d_5 was required for the more hindered hydroxyl to react and therefore used it throughout to standardize our procedures. The sample flask was placed on a hot plate, brought to slow reflux, and over the course of 30–60 min the flask was gently swirled. It was found that for even the most hindered hydroxyl samples complete reaction required no more than 60 min. After refluxing, dry nitrogen gas was used to purge the flask. The solution was transferred to a 50-mL round bottom boiling flask with a 5-mL benzene wash. This entire solution was freeze-dried for 15 min to sublime the benzene, then 2 mL of CS_2 was added. One half of the sample was examined by IR for the disappearance of the OH absorption band. If the band was absent, the remaining sample was put in a 5-mm NMR tube, flushed with nitrogen, and sealed with a double locking pressure cap.

RESULTS AND DISCUSSION

Evaluation of the sensitivity and quantitation of the technique were performed on cholesterol ($C_{27}H_{46}O$), pyrenol-1 ($C_{16}H_{10}O$), cyclohexanol ($C_6H_{12}O$), and 3,5-dimethylphenol ($C_8H_{10}O$). These model systems were chosen to give a general comparison of spectrometer operation over the entire proton NMR spectrum. Our results are given in Table I and indicate that a reasonable degree of accuracy can be obtained for dilute solutions. Accuracy did drop off if a signal-to-noise ratio of less than 25:1 for the TMS ether resonance was obtained. With the NMR spectrometer system employed and its associated computer hardware, a 2.5 mg/mL sample of cholesterol in CS_2 gave a hydroxyl proton percent of 2.3 ± 0.10. In general, compounds of the type studied, with one or two hydroxyl groups, gave a 5% error of the known hydroxyl content. The greatest source of error, which could be controlled, was the presence of water in solvents, leading to the formation of hexamethyldisiloxane. The NMR signals from hexamethyldisiloxane are centered about internal tetramethylsilane and are readily determined during a blank run.

Table I. Hydroxyl Percentages as Calculated from Their TMS Derivative

Sample	Formula	At. % H as OH	TMS ether calculated at. % H as OH ±5%
Cholesterol	$C_{27}H_{46}O$	2.17	2.3
Pyrenol-1	$C_{16}H_{10}O$	10.00	10.6
Cyclohexanol	$C_6H_{12}O$	8.33	7.9
3,5-Dimethylphenol	$C_8H_{10}O$	10.00	10.3

It was evident from our work that if careful control was maintained of solvent and reagent purity, the precision (reproducibility) of the technique would be an acceptable 5%. Our work with the model compounds required us to add pyridine to facilitate the general acid/base reaction of TMS ether formation. Preliminary studies showed that with coal-derived samples, *no* pyridine or *N*-trimethylsilyldimethylamine was required to achieve complete reaction; only HMDS in benzene was necessary. We chose to use pyridine-d_5 (100 at. %) in 50-μL amounts so that the resulting proton spectrum was not disturbed if the pyridine could not be entirely removed by freeze drying.

The chemical shift of each TMS derivative formed was found to vary, in general, with the nature of the hydroxyl group, alcohols and benzylic hydroxyls being the most shielded and polynuclear aromatic carboxylic acids and oximes least. Figure 1 gives the chemical shift at 250 MHz of 22 model compounds. Note that the chemical shifts of the TMS derivative of the alcoholic–benzylic hydroxyl groups fall between 0 and 45 Hz, phenolic hydroxyls between 40 and 70 Hz, and carboxylic acids and oximes from 65 to more than 110 Hz downfield from internal tetramethylsilane.

There is one case, *o*-phenylphenol, that lies at −2 Hz and at first appears to be out of place. However, this can be explained as being the result of a conformation which allows the methyl protons attached to silicon to be directly over an aromatic ring. Shapiro and Proulx (*15*) indicated that preference for such conformations is, in turn, the result of rotational preferences exhibited by the "flat" aromatic ring. Such chemical shifts should therefore be expected when the system in question contains a free phenyl ring adjacent to a hydroxyl. A model of the trimethylsilyl ether of this system has two of the three methyl groups sitting directly above the phenyl rings. We find that the unusually high chemical shift of the *o*-phenylphenol TMS ether can be explained if the rings are twisted 50–60° out of plane (*16*, *17*).

Superimposed on Figure 1 is a proton spectrum of the acid components of a coal-derived asphaltene as their TMS ethers in CS_2 solution. Note that the spectrum has two major areas—one centered at the alcoholic–benzylic hydroxyl and another covering the phenolic and carboxylic acid TMS

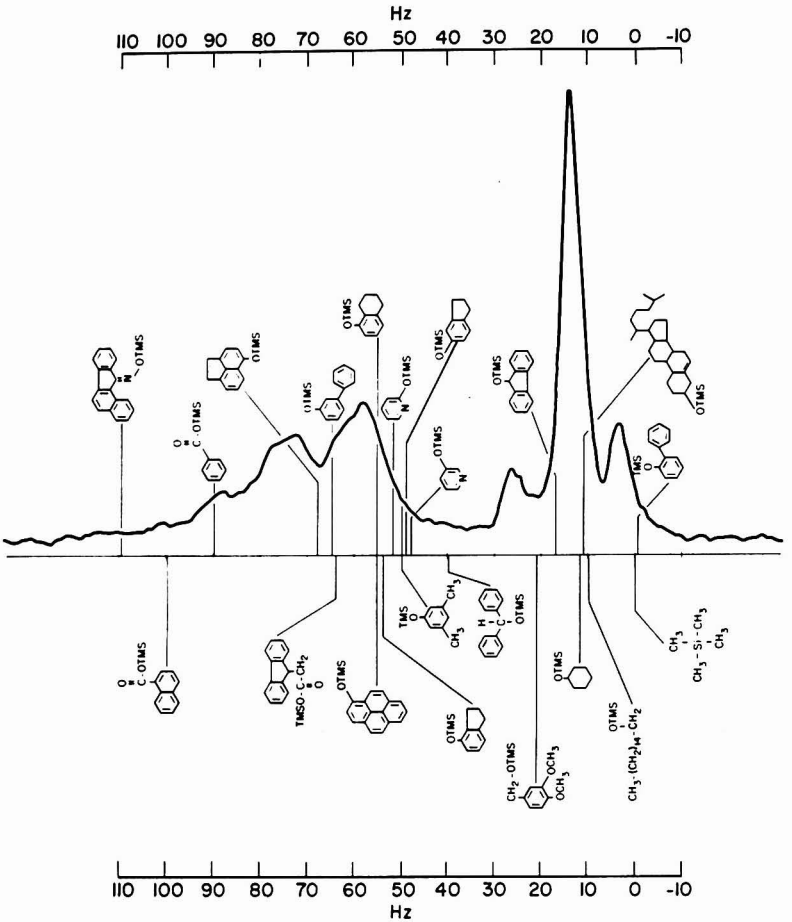


Figure 1. Chemical shift of TMS derivatives of model compounds at 250 MHz. Overlaid spectrum is that of a coal-derived acid/neutral fraction from an asphaltene

Table II. Percentage of Hydroxyl in Coal-Derived Fractions Calculated from Their TMS Derivatives

	Fraction of coal liquid				
Composition (MAF)	1 Pentane, soluble oils	2 Asphaltenes	2a Asphaltenes, acid/neutral	2b Asphaltenes, base	3 Preasphaltenes, THF soluble
At. %[a]					
C	44.8	52.5	50.2	52.9	56.1
H	53.6	44.1	46.6	43.6	39.0
O	0.9	2.0	2.1	1.6	3.2
N	0.4	1.2	0.6	1.5	1.2
S	0.1	0.2	0.3	0.3	0.1
TMS calculated					
% H as OH	1.2	2.0	2.0	1.5	3.0
% O as OH[b]	67%	43%	44%	49%	35%

[a] Error ±5%, as determined by replicate measurement. [b] Error ±10%, estimated sum of all errors.

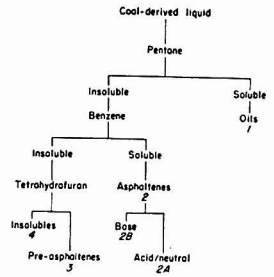


Figure 2. Separation scheme for coal-derived liquids

derivatives. We have observed a similar distribution of hydroxyl TMS ethers from fractions derived from Figure 2. The degree of spectral complexity increases as one explores fractions 1–3. Table II summarizes the pertinent physical and chemical properties of each of the fractions. The remaining oxygen contained within the coal-derived samples may be assigned to ether linkages (e.g., furan) because the infrared data do not show a carbonyl band.

If we examine Figure 1 in more detail, we can distinguish two major, but overlapping, areas of TMS ethers of the acid components of a coal-derived asphaltene. The chemical shifts of the model compounds allow us to assign portions of the spectrum as being alcoholic or hindered phenolic, 0–50 Hz, or simple phenols, 45–100 Hz. This is the first reported observation of a distinct distribution of hydroxyls in coal-derived oils and asphaltenes. The NMR data of the TMS ether derivatives suggest the presence of phenols, hindered phenols, and benzylic hydroxyls.

ACKNOWLEDGMENT

The authors acknowledge the cooperation of Sayeed Akhtar and Nestor Mazzocco in providing the coal liquefaction products and associated process data.

LITERATURE CITED

(1) "Handbook of Analytical Chemistry", L. Meites Ed., McGraw-Hill Book Company, New York, N.Y., 1963, Section 6, pp 1–101.
(2) N. Linnet, "A Discussion of the ASTM Method for Determination of Acid and Base Number in Oils", Radiometer, Denmark, ST43.
(3) R. W. Martin, *J. Am. Chem. Soc.*, **74**, 3024 (1952).
(4) M. M. Sprung and L. S. Nelson, *J. Org. Chem.*, **20**, 1950 (1955).
(5) A. G. Sharkey, Jr., R. A. Friedel, and S. H. Langer, *Anal. Chem.*, **29**, 770 (1957).
(6) S. H. Langer, P. Pantages, and I. Wender, *Chem. Ind., London*, **1958**, 1664.
(7) A. Hase and T. Hase, *Analyst (London)*, **97**, 998 (1972).
(8) S. Friedman, C. Zahn, M. L. Kaufman, and I. Wender, *U.S. Bur. Mines, Bull.*, **No. 609**, (1963).
(9) J. D. Brooks and J. R. Steven, *Fuel*, **46**, 13 (1967).
(10) S. Friedman, M. L. Kaufman, W. A. Steiner, and I. Wender, *Fuel*, **40** (33), 26 (1961).
(11) S. H. Langer, S. Connell, and I. Wender, *J. Org. Chem.*, **23**, 50 (1958).
(12) J. Dakok, R. F. Sprecher, A. A. Bothner-by, and T. Link, Paper presented at the 11th Experimental NMR Conference, Pittsburgh, Pa., 1970.
(13) J. Dadok and R. F. Sprecher, *J. Magn. Reson.*, **13**, 243 (1974).
(14) F. R. Brown, S. Friedman, L. E. Makovsky, and F. K. Schweighardt, *Appl. Spectrosc.*, **31**, 241 (1977).
(15) B. L. Shapiro and T. W. Proulx, *Org. Magn. Reson.*, **8**, 40 (1976).
(16) H. Suzuki, *Bull. Chem. Soc. Jpn.*, **32**, 1350 (1959).
(17) J. B. Clews and K. Lonsdale, *Proc. R. Soc. London Ser. A*, **161**, 493 (1957).

RECEIVED for review August 22, 1977. Accepted November 29, 1977. Use of brand names facilitates understanding and does not necessarily imply endorsement by the U.S. Department of Energy.

CORRESPONDENCE

Chemical Ionization Mass Spectrometry as a Tool for the Elimination of Surface Related Phenomena in the Spectra of Unstable Compounds

Sir: The occurrence of surface related reactions in mass spectrometer ion sources has long been recognized. The products of gas–surface reactions, involving surface ionization on the filament and pyrolysis on hot surfaces, often contribute minor peaks to electron impact (EI) mass spectra, and complications can be severe in the analysis of reactive or thermally unstable compounds. The resulting mass spectra may lead one to assume the presence of impurities not actually in the sample, or even cause errors in the identification of unknown compounds and mixtures. The purpose of this correspondence is to present an example of such surface related phenomena and to point out how these problems may be avoided utilizing chemical ionization (CI) mass spectrometry.

The compound used to illustrate this problem is the brominated derivative of polymeric sulfur nitride, $(SN)_x$ (*1*). $(SN)_x$ has been previously found to produce a noncyclic $(SN)_4$ species upon sublimation (*2*). The brominated derivative, of empirical formula $SNBr_{0.4}$ (*1*), was expected to yield $(SN)_4$ plus an unknown brominated species upon sublimation; hence, identification of the bromine containing species was of particular interest. In work reported elsewhere (*3*), we have discussed the chemistry and characterized the vapor phase species sublimed from brominated $(SN)_x$.

The electron impact mass spectrum of $SNBr_{0.4}$ obtained at 125 °C is given in Figure 1a. This spectrum was obtained on a Hewlett-Packard 5980A mass spectrometer, equipped with a dual EI-CI source, using a 70-eV electron energy during the slow sublimation of brominated $(SN)_x$ from a solids probe over a 40-min period. Comparison to previously published

0003-2700/78/0350-0371$01.00/0 © 1978 American Chemical Society

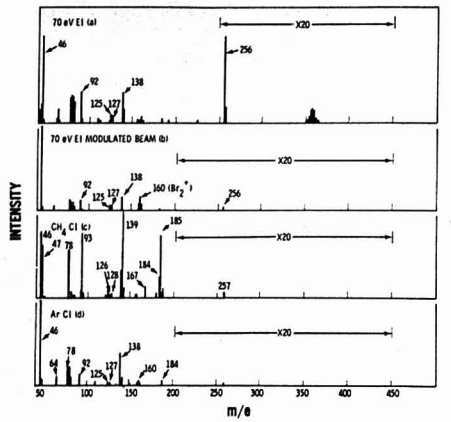


Figure 1. Comparison of mass spectra of $SNBr_{0.4}$. (a) 70-eV EI spectrum, (b) 70-eV EI spectrum obtained using a modulated beam mass spectrometer sampling an effusive beam from a Teflon Knudsen cell, (c) CH_4 CI spectrum, and (d) Ar CI spectrum. The high mass peaks in the conventional 70-eV EI spectrum have their origin in surface related phenomena in the mass spectrometer ion source. All spectra were obtained at 120 to 130 °C. All ions in the CI and modulated beam spectra may be attributed to either S_xN_y, SNBr, HBr, Br_2, or S_8

spectra of $(SN)_x$ (2) suggests the presence of $(SN)_4$ (MW = 184), Br_2, and several additional bromine containing compounds (3). (A small amount of water present during the synthesis also results in a small HBr impurity (3).) The spectrum of brominated $(SN)_x$ shows distinct multiplets centered at approximately m/e 358, 438, and 519, with the series of peaks around m/e 358, the most intense. These multiplets may be ascribed to one or more compounds containing 3, 4, and 5 bromine atoms, respectively. Although it was not possible to identify the other elemental constituents of these species, they do contain elements other than sulfur, nitrogen, hydrogen, and bromine.

The relative importance of these high mass clusters may be reduced somewhat by shutting off the source heaters and allowing the source to cool, or simply running the solids inlet probe at a lower temperature. (Modulated molecular beam experiments, discussed below, clearly show this behavior is not due to changes in the vapor composition resulting from temperature changes (3).) However, these approaches were plagued by increased background, rapidly decaying and changing source conditions due to the build up of surface contaminants, and a greatly reduced signal intensity due to the decreased rate of sublimation and to condensation on the cooler parts of the source.

To determine the relative importance of surface related reactions, the conventional EI spectrum (Figure 1a) were compared to EI spectra obtained using a modulated molecular beam sampled from a Teflon Knudsen cell at temperatures of 70 to 150 °C. The molecular beam, effusing through a 1-mm orifice in the Knudsen cell into a differentially pumped region (maintained at $\leq 10^{-6}$ Torr), is directed at a molecular beam skimmer, which allows a well-collimated beam to enter the separately pumped analyzer section (3). The molecular beam is modulated using a rotating toothed wheel and subsequently passes through the axial molecular beam ionizer of an Extranuclear mass spectrometer (Extranuclear Laboratories, Inc., Pittsburgh, Pa. 15238) where ionization occurs using 70-eV electrons. The absence of surface related phenomena in the molecular beam technique allows one to study unstable or reactive species in the effusive beam; the molecules studied do not collide with surfaces after leaving the Knudsen cell (2, 3). Similarly, all background components and molecules scattered off surfaces will have concentrations independent of the modulation frequency and will not contribute to the mass spectra. A typical spectrum is shown in Figure 1b. Detailed studies have clearly demonstrated the vapors of brominated $(SN)_x$ to be a mixture of S_4N_4, SNBr, Br_2, and small amounts of HBr and S_8 (3). Spectra obtained by free vaporization and Knudsen effusion are also quite similar; i.e., the same molecular species are sublimed from both the solids inlet probe and the Knudsen cell.

A comparison of the modulated beam EI spectrum to the conventional 70-eV EI spectrum (Figures 1a and 1b) shows the presence of surface related phenomena. The higher mass multiplets are entirely absent from the modulated beam spectrum and the contribution at m/e 256 from molecular sulfur (a known decomposition product of $(SN)_x$ (2)) is greatly reduced. Similar high mass clusters have been observed for this compound in other laboratories under EI conditions (see Acknowledgment), but were not observed in the modulated beam experiment under any mass spectrometer conditions for similar heating rates and temperatures from 50 to 150 °C.

Although modulated beam mass spectrometry offers a method for the elimination of surface related contributions to mass spectra, such instruments are costly, rarely found in an analytical laboratory, require a considerably longer time in both sample preparation and actual data acquisition, and consume one to two orders of magnitude more sample. An alternative technique available to many laboratories, involves the use of chemical ionization (CI) mass spectrometry to eliminate, or greatly reduce, contributions due to surface related phenomena.

In an attempt to identify the high mass species indicated by conventional electron impact (Figure 1a), we failed to observe any ions indicative of these heavier species using either argon, methane, isobutane, or ammonia as CI reagents. At least one of these CI reagents should yield quasi-molecular ions if these species are not due to surface reactions. Repetitions of these experiments using a number of samples, instrumental conditions, heating rates, CI reagent gas pressures, and temperatures up to 200 °C failed to show these high mass ions, or probable fragment ions. All the ions in the Ar, CH_4, isobutane, and NH_3 CI spectra may be attributed to the S_xN_y, SNBr, HBr, Br_2, and S_8 species identified in modulated beam experiments (3). (It should be noted that several peaks in the CI spectra may be attributed to addition of the CI reagent ion, e.g., $S_3N_3{\cdot}C_2H_5^+$ at m/e 167.)

Thus, the CI spectra clearly show the absence of the unidentified high mass species also absent in the modulated beam experiment. The elimination of these ions in the spectra clearly shows that CI offers a mechanism for the elimination or reduction of surface related processes in mass spectrometer ion sources. The reduced contributions of surface reactions in the CI mode are most likely due to the relative isolation of the ion source chamber from the hot filament and the relatively high pressure gas flow across the sample into the source, which decreases the probability of diffusion to a hot surface prior to ionization.

A comparison of the four spectra in Figure 1 shows that argon (in the absence of a large water impurity) offers a distinct advantage for the analysis of mixtures over more commonly used methane, isobutane, and ammonia as a CI reagent. The latter involve relatively low energy proton transfer processes; hence, molecular species such as Br_2 and S_8 are not ionized by isobutane and NH_3 CI. Charge transfer from argon ions (Ar^+ and Ar_2^+, are the major reagent ions in this work) is a much higher energy process and is capable of

ionizing most molecules. Additionally, the fragmentation patterns produced by Ar CI often resemble conventional electron impact spectra (*4*). Except for a few changes in the fragmentation pattern, the Ar CI and 70-eV EI modulated beam spectra shown in Figure 1 are quite similar. Although this similarity is obviously somewhat fortuitous, in view of the differences in ionization energy (and mechanism) and the quite different instruments, it does facilitate interpretation of the spectra.

These results emphasize an advantage of chemical ionization mass spectrometry not previously reported: the elimination or reduction of contributions due to surface related phenomena. The CI approach has several major advantages over modulated molecular beam mass spectrometry, including both speed and cost. The use of argon as a CI reagent offers the advantage (for mixtures) of being highly nonspecific and producing spectra similar to electron impact spectra, without contributions due to surface related phenomena. Thus, chemical ionization offers a way to avoid the errors and complications which may unknowingly contribute to conventional EI spectra.

ACKNOWLEDGMENT

We thank G. B. Street (IBM Research Laboratory, San Jose, Calif.) and J. J. DeCorpo (Naval Research Laboratory, Washington, D.C.) for discussing their mass spectral results prior to publication, G. B. Street for providing samples of brominated $(SN)_x$, and D. M. Schoengold for assistance in several of the CI experiments.

LITERATURE CITED

(1) G. B. Street, W. D. Gill, R. H. Geiss, R. L. Greene, and J. J. Mayerle, *J. Chem. Soc., Chem. Commun.*, 407 (1977).
(2) R. D. Smith, J. R. Wyatt, J. J. DeCorpo, F. E. Saalfeld, M. J. Moran, and A. G. MacDiarmid, *J. Am. Chem. Soc.*, **99**, 1726 (1977).
(3) R. D. Smith and G. B. Street, *Inorg. Chem.*, in press.
(4) D. F. Hunt and J. F. Ryan, *Anal. Chem.*, **44**, 1306 (1972).

Richard D. Smith*
Philip W. Ryan

Chemical Methods and Kinetics Section
Physical Sciences Department
Battelle, Pacific Northwest Laboratories
Richland, Washington 99352

RECEIVED for review July 25, 1977. Accepted November 14, 1977. This paper is based on work performed under United States Energy Research and Development Administration Contract No. EY-76-C-06-1830.

Simplified Solids Mass Spectrometer Combining a Glow Discharge Source with a Quadrupole Mass Filter

Sir: The analysis of trace elements in bulk solids by mass spectrometry—an area which has become loosely known as solids mass spectrometry by its practitioners—has utilized chiefly the pulsed rf spark source (*1*, *2*) for ionization. This source provides high sensitivity, broad applicability, and relatively little interference, but a spark source mass spectrometer is a complex and expensive instrument and yields data of often less than satisfactory precision. Alternative or complementary ion sources have been described (*2*) but none has been broadly accepted. More recently, the glow discharge has been investigated as an atomization-ionization source (*3–6*) which offers several advantages, notably simplicity and stability, for solids mass spectrometry. We have combined this source with a versatile quadrupole mass filter for trace element analysis of conducting solids or solution residues. This report describes a simple solids mass spectrometer currently used in our laboratory as an alternative instrument to our spark source mass spectrometer.

EXPERIMENTAL

A cross section of the solids mass spectrometer is shown in Figure 1. The stainless steel housing was constructed from 6-inch o.d. tubing, subdivided to form chamber 1, into which the ion source (3) protrudes, and the higher-vacuum chamber 2 which houses the energy analyzer (4), quadrupole filter (5), and the electron multiplier detector (6). The glow discharge source is formed from two separate housings: a standard glass joint, vacuum sealed by a Viton O-ring to the stainless steel flange, and an inner stainless steel body similarly sealed to the flange and attached by machine screws. The hollow cathode (7) is secured by a set screw to the stainless steel body and is adjustable along the ion beam axis. The discharge is localized to the cathode interior by use of a ceramic insulator which surrounds the cathode; a glass sleeve isolates the stainless steel housing from the discharge. The anode (8) is adjusted to give a 1.90-cm interelectrode separation. Three ports on the glass housing provide access for the gas inlet (9), thermocouple vacuum gauge (10), and an auxiliary pumping port (11). The 0.5-mm cathode nozzle orifice directs an expanding jet of argon and sputtered species across a 5-mm separation onto the skimmer cone (12) which has a 1.0-mm orifice to select a central fraction of the beam for transmission to the energy analyzer. A Bessel Box type energy analyzer allows a selected ion-energy window to pass a fraction of the ions to the quadrupole for mass analysis. The neutral species in the beam are removed by a central metal stop in the energy analyzer.

Typical pressures are 0.5–3 Torr in the glow discharge source, 10^{-4} Torr in chamber 1 and 10^{-6} Torr in chamber 2. Argon is used as the discharge gas at a sample flow rate of 1.5 mL min^{-1}. The discharge is operated at currents up to 40 mA and voltages ranging from 400 to 600 V.

The Bessel Box energy analyzer (Model 616-1), quadrupole mass filter (Model 324-9), and associated quadrupole control equipment are made by Extranuclear Laboratories, Inc. The vacuum chamber and ion source were constructed at the University of Virginia. Two 1200 L sec^{-1} Varian (Model VHS-4) diffusion pumps provide the required pumping.

RESULTS

Because the prime interest in our laboratory is trace element analysis, we wished to have high throughput of the sputtered and subsequently ionized species for good detection limits. This would be better accomplished without the ion energy analyzer, but spectra taken under such conditions showed the broadening effects of high energy (>50 eV) ions. The energy analyzer was necessary to obtain adequate resolution and peak shape. Sampling directly from the cathode, where field effects of the cathode dark space (*7*) may influence ion energy, a significant energy spread is not surprising. Previous work (*8*) indicated a lower energy spread when sampling through the anode out of the negative glow, but this mode also resulted in poorer sensitivity. Extraction directly from the rear of the hollow cathode, as in Figure 1, samples a region of high ion density for maximum sensitivity. Typical mass spectra of copper and molybdenum isotopes in NBS steels are shown in Figure 2.

0003-2700/78/0350-0373$01.00/0 © 1978 American Chemical Society

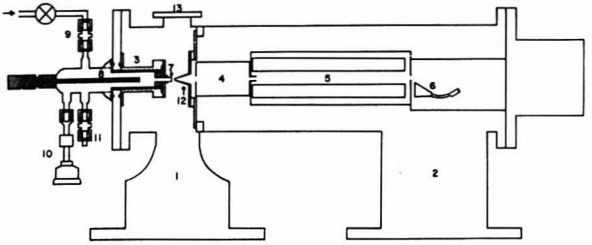


Figure 1. Cross section of solids mass spectrometer: (1) intermediate chamber, (2) analyzer chamber, (3) ion source, (4) Bessel Box energy analyzer, (5) quadrupole filter, (6) detector, (7) hollow cathode, (8) anode, (9) gas inlet, (10) thermocouple gauge, (11) auxiliary pumping port, (12) skimmer cone, (13) view port

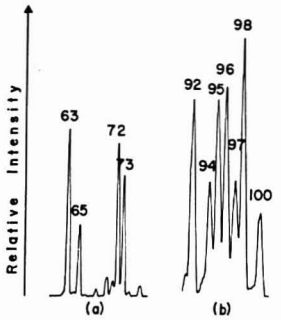
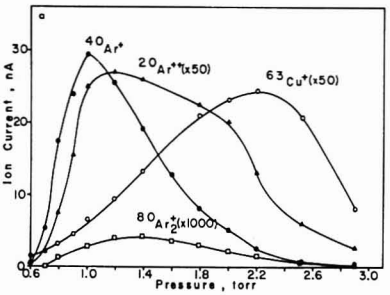


Figure 2. Isotopic display of copper and molybdenum in steels. (a) Copper at 0.015% in NBS 801, m/e 72, 73 = FeO, FeOH, (b) molybdenum at 0.22% in NBS 811a



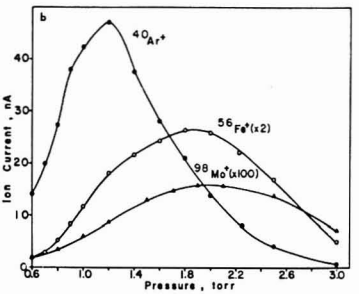


Figure 3. Effect of pressure on selected discharge species: (a) copper hollow cathode, (b) stainless steel hollow cathode

Ions of the sputtered cathode species normally make up a small percentage of the total ion population (*9*). The bulk of the ion beam, consisting of Ar^+, ArH^+, Ar^{2+}, and Ar_2^+, can cause spectral interference both at their nominal mass to charge ratio and also in combination with sputtered species (e.g., $CuAr^+$). A study of the effect of gas pressure on the hollow cathode discharge showed it is possible to discriminate against the discharge gas species as shown in Figure 3. The optimum pressure for the sputtered species produces a significant reduction of the discharge-gas ion current. The copper isotopes (Figure 3a) can then comprise 15–20% of the total ion beam, while iron (Figure 3b) can be as large as 35–40% of the total beam. Further discrimination is possible by adjustment of the ion-energy window to favor the ions arising from the sputtered atoms. Judicious selection of both pressure and ion energy conditions can produce at the entrance to the quadrupole filter an ion beam which may be up to 50–60% cathode species.

Preliminary precision and sensitivity studies are encouraging. Using NBS steel cathodes, the peak heights of minor to trace constituents show a reproducibility in the 2–6% RSD range for 10–15 consecutive scans. Table I shows results obtained for copper isotopes in a steel cathode. There is a small but consistent discrepancy in the absolute values of the isotopic ratios when using a quadrupole mass filter (*10*). However, our precision data represent an improvement over the 20–30% range shown in spark source mass spectrometry. Elemental detection limits determined to date have been mainly in the low ppm to sub-ppm values. Only metal cathodes have been evaluated.

Compared to the spark-source mass spectrometer, the glow discharge solids mass spectrometer has the advantages of greater simplicity, significantly reduced cost, and greater precision. Its comparative disadvantages include certain spectral interferences from the discharge gases and—at this point—somewhat reduced elemental sensitivity. Studies are under way to evaluate a modified ion sampling and optics system for sensitivity enhancement.

Table I. Reproducibility of Copper Peaks in Consecutive Mass Spectra Taken from NBS 801 Steel. Copper Present at 0.015%

	Trial 1[a]		Trial 2[b]	
m/e	63	65	63	65
RSD%	1.69	2.24	3.26	3.25

[a] 10 scans. [b] 15 scans.

LITERATURE CITED

(1) A. J. Ahearn, Ed., "Mass Spectrometric Analysis of Solids", Elsevier, Amsterdam, 1966.
(2) A. J. Ahearn, Ed., "Trace Analysis by Mass Spectrometry", Academic Press, New York, N.Y., 1972.
(3) J. W. Coburn and E. Kay, *Appl. Phys. Lett.*, **19**, 350 (1971).
(4) H. Oechsner and W. Gerhard, *Phys. Lett.*, **40A**, 211 (1972).
(5) W. W. Harrison and C. W. Magee, *Anal. Chem.*, **46**, 461 (1974).
(6) B. N. Colby and C. A. Evans, Jr., *Anal. Chem.*, **46**, 1236 (1974).
(7) G. F. Weston, "Cold Cathode Glow Discharge Tubes", Iliffe, London, 1968.
(8) E. H. Daughtrey, Jr., and W. W. Harrison, *Anal. Chem.*, **47**, 1024 (1975).
(9) J. W. Coburn and E. Kay, *Appl. Phys. Lett.*, **18**, 435 (1971).
(10) G. K. Wehner, *Appl. Phys. Lett.*, **30**, 185 (1977).

C. G. Bruhn[1]
B. L. Bentz
W. W. Harrison*

Department of Chemistry
University of Virginia
Charlottesville, Virginia 22901

[1] On leave from Departamento de Análisis Instrumental, Escuela de Química y Farmácia, Universidad de Concepción, Concepción, Chile.

RECEIVED for review October 7, 1977. Accepted November 10, 1977. This work supported by NIH GM-1456910.

Data Treatment in Cyclic Voltammetry

Sir: The peak current ratio ($i_{p,f}/i_{p,b}$) of forward and backward potential scans is an important parameter in cyclic voltammetry (CV) (*1*, *2*). It is known (*1*) that $i_{p,b}$ must be measured against the extrapolated value of the primary process. The basic equations for CV are complicated, the current function being presented numerically or graphically (*1*, *2*). The absence of an analytical solution makes it difficult to extrapolate the primary process to the second peak and to determine $i_{p,b}$. Nicholson and Shain (*1*) have described two experimental procedures for obtaining such a baseline: (a) to extend the forward scan beyond the selected switching potential (if another reaction does not interfere) or (b) by stopping the sweep at some potential past the peak and recording the constant potential i–t curve. Procedure (a) is often impossible, and for procedure (b) special equipment is needed. Polcyn and Shain (*3*) presented a semiempirical method for calculations of the descending part of the peak. It was given as a part of the multistep charge transfer analysis and remained, apparently, unnoticed. Thus, in most cases data treatment is restricted to peak potential interpretation.

This work presents a simple method for the extrapolation of the forward current to the back peak potential (or time). The same approach is used as in (*3*) but the results obtained differ and the method is also extended to the case of the following chemical reactions. The method is based on the facts that (a) potentials far beyond the forward peak correspond to the limiting current region of classical polarography (i.e., depolarizer surface concentration approaches zero); and (b) the potential axis is simultaneously the time axis. Therefore beginning from definite potential (or time), any further potential shift does not change the electrolysis conditions for the reaction under study and the faradaic current–potential curve is actually a potentiostatic current–time curve. This "convergence point" may be calculated from classical polarographic equations: for the condition $i_t > 0.99^*I$ and 25 °C these potentials are: $E' > E_{1/2}^{r} + 0.119/n$ (V) and $E' > E_{1/2}^{irr} + 0.119/\alpha n$ (V), where i_t is the instantaneous current, I is the classical polarographic diffusion current, E' is the "conversion" potential, $E_{1/2}^{r}$ and $E_{1/2}^{irr}$ are the polarographic half-wave potentials for reversible and irreversible electrode reactions (absolute values of the potentials are used), α is the symmetry factor. Beyond this conversion potential, the only change of the current is its decrease due to decreasing depolarizer flux toward the electrode.

Cottrell's potentiostatic equation (*4*) describes the current–time relationship for single pulse at a planar electrode:

$$i_t = nFSC\sqrt{\frac{D}{(t-t_o)}} = \frac{\text{const}}{(t-t_o)^{1/2}} \qquad (1)$$

where S is the electrode area, C is the bulk concentration of the depolarizer, t is the time and t_o is the point at which the pulse starts (usually $t_o = 0$). In the present case, t_o is neither the moment at which electrolysis commences nor the time of E'. At the moment when $E = E'$, there is a finite diffusion layer and the depolarizer concentration in the vicinity of the electrode is less than its bulk value. Therefore, a virtual time, t_o, may be calculated; when used in the Cottrell equation, it will give the experimentally observed CV-currents, starting at $E = E'$. The potential axis becomes, in effect, the time axis only beyond E'. Since experimental curves are recorded in current–potential coordinates, Equation 1 may be rewritten:

$$i_t = \frac{A}{(E-B)^{1/2}} \qquad (1a)$$

where A and B are the constants, B corresponds to t_o in the time domain. From the practical point of view, it is convenient to operate with normalized current ($i_t = i_t/i_p$, i_p is the peak current) and to measure potentials relative to the peak potential, E_p.

For the reversible charge transfer, such curves were constructed for the theoretical curve due to Nicholson and Shain (Table I in Ref. 1), and for the experimental CV-curves of $[Fe(CN)_6]^{4-}$-oxidation (see Figure 1). As expected, all the normalized curves are superposed. The constants for Equation 1a were calculated for this generalized curve:

$$\bar{i}^2 = \frac{0.0256}{(E-0.0445)} = \left[\frac{F}{RT}(E-0.0445)\right]^{-1} \qquad (2)$$

Calculations were done for a one-electron transfer; otherwise nF/RT must be employed. It must be noted that the field of application of Equation 2 and its constants differ from those in (*3*). A similar equation is valid for irreversible peaks:

$$\bar{i}^2 = \left[\frac{\alpha nF}{RT}(E-0.01)\right]^{-1} \qquad (3)$$

It is remarkable that the coefficients in Equations 2 and 3 are found to be equal to nF/RT and $\alpha nF/RT$. In this connection

0003-2700/78/0350-0375$01.00/0 © 1978 American Chemical Society

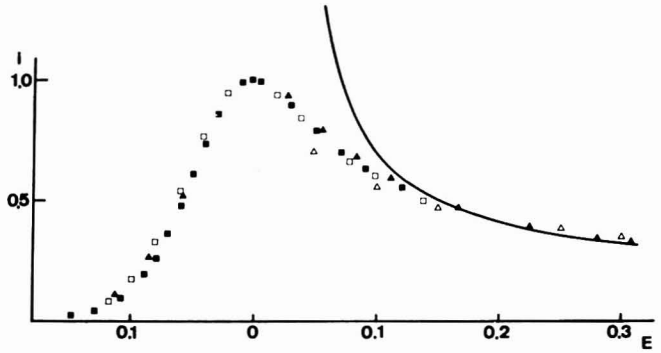


Figure 1. Stationary polarograms and calculated base line. i is the normalized current (see text), E is the potential in volts relative to the peak. The solid curve was calculated by Equation 2. (■) represents the simple reversible case. (□) reversible charge transfer followed by a chemical step, both from Nicholson and Shain's calculations (Ref. 1, Tables I and IX). (▲) represents oxidation of $[Fe(CN)_6]^{4-}$ with potential sweep of 0.011 V/s. $[Fe(CN)_6]^{4-}$, concentration is 0.001 M, supporting electrolyte, 1 M Na_2SO_4; the working electrode was a vertical disk with area 1.4 cm^2. (△) calculated according to (*3*)

let it be noted that Reinmuth (*5*) has found a linear relationship for the rising portion of the peak between $\ln |(i_p - i)^{1/2}/i|$ and E with slopes equal to RT/nF for reversible and $RT/\alpha nF$ for irreversible charge transfer. Equation 3 is less exact than Equation 2, because of the absence of available theoretical calculations in the region extended to the field of the classical polarographic limiting current (*1*), Equation 30 from Ref. 3 gives, according to the authors, a better approximation for irreversible charge transfer. As constants, 12 mV for $(E - E_p)\alpha n$ and 0.992 for γ could be recommended. Use of these equations supposes a knowledge of α. The latter can be determined from the difference peak–half peak potentials, from their dependence on the rate of potential scan (*1*), or with the help of the above mentioned Reinmuth procedure. All the constants in Equation 1a may be obtained from a few experimental points at proper potentials which correspond to the polarographic diffusion current. In the last case, the knowledge of α is unnecessary; this procedure has been used during on-line data treatment by computer (*6*).

The presented method could be used also in cases when the charge transfer is followed by the chemical reaction (see Figure 1).

As stated above, this approach is valid after a conversion point. One can see from Figure 1 that the calculated base line is in agreement with the experimental points beginning at about $\sim 160/n$ mV after the peak. For irreversible peaks, this field must be even more shifted from the peak potential.

Nicholson has proposed (*7*) the calculation procedure for the case of the reversible electron transfer followed by chemical reaction. This procedure allows the calculation of the anodic peak height from experimental data without knowledge of the baseline. The method given here and by Polcyn and Shain (*3*) allows not only determination of the peak heights but separation between the previous and following stationary polarograms. The method can find application in data treatment for two consecutive or overlapped peaks on the forward scan (also with an intermediate chemical reaction) and/or for the case when the reaction under study is close to supporting electrolyte discharge.

LITERATURE CITED

(1) R. S. Nicholson and I. Shain, *Anal. Chem.*, **36**, 706 (1964).
(2) H. Matsuda, *Z. Elektrochem.*, **61**, 689 (1959). H. Matsuda and Y. Ayabe, *Z. Elektrochem.*, **59**, 494 (1955).
(3) D. S. Polcyn and I. Shain, *Anal. Chem.*, **38**, 370 (1966).
(4) See for example: D. O. Raleigh, *Electroanal. Chem.*, **6**, 112 (1973).
(5) W. H. Reinmuth, *Anal. Chem.*, **33**, 1793 (1961).
(6) P. E. Whitson, H. W. Van den Born, and H. Evans, *Anal. Chem.*, **45**, 1298 (1973).
(7) R. S. Nicholson, *Anal. Chem.*, **38**, 1406 (1966).

Gregory Ginzburg

Department of Chemistry
Ben Gurion University of the Negev
Beer Sheva, Israel

RECEIVED for review August 5, 1977. Accepted November 1, 1977.

Comment on Determination of Fluoride by Neutron Activation Analysis

Sir: In the recent article by Knight et al. (*1*), the discussion of interfering nuclear reactions with the $^{19}F(n,\gamma)^{20}F$ determination of F is inadequately developed. Such interferences severely limit the usefulness of this neutron activation technique to simple matrices. The $^{23}Na(n,\alpha)^{20}F$ reaction, with a threshold of 4.0 MeV, produces a prohibitively strong interference in materials where $Na/F > 10^4$. It has been noted (*2*) that 1 mg of Na yields an apparent F content of 42 ± 6 ppm under reactor conditions present at the Instituut Nucleaire Wetenschappen in Gent, Belgium, a fairly typical reactor with a flux of 10^{12} $n/cm^2/s$. Knight et al. (*1*) discuss the interference of ^{38}Cl in the determination of F, as Figure 2D (*1*) clearly illustrates. Unless unusually high levels of F are present, detection will be impossible.

0003-2700/78/0350-0376$01.00/0 © 1978 American Chemical Society

The reactor used for irradiation must have its neutron flux spectrum carefully characterized. This information is not offered by the authors (*1*). The cadmium ratio is an important consideration for assessing the Na interference.

An alternative reaction, also of short half-life, can be considered. The $^{19}F(n,p)^{19}O$ reaction, with a threshold energy of 4.22 MeV and $t_{1/2}$ = 26.9 s, seems to have fewer interferences. However $^{18}O(n,\gamma)^{19}O$ must be considered. Oxygen-18 has a low natural abundance (0.20%) and a low neutron capture cross section (0.0002 barn), but many matrices have up to 50% oxygen content.

The authors' procedure appears to be fine for Teflon and other such special materials, but the implication of pursuing analysis of more complex matrices is not supported by the data presented.

LITERATURE CITED

(1) H. G. Knight, A. K. Furr, and T. F. Parkinson, *Anal. Chem.*, **49**, 1507 (1977).
(2) R. Dams, J. Billiet, and J. Hoste, *Int. J. Environ. Anal. Chem.*, **4**, 141 (1977).

Ernest S. Gladney*
David B. Curtis

Los Alamos Scientific Laboratory
P.O. Box 1663 MS 490
Los Alamos, New Mexico 87545

RECEIVED for review October 11, 1977. Accepted October 25, 1977. This work performed under the auspices of the U.S. Energy Research and Development Administration.

AIDS FOR ANALYTICAL CHEMISTS

Automated Analysis for Trace Organic Components in 32% Hydrochloric and 28% Hydrobromic Acid Process Streams

Kenneth W. Grubaugh* and Gerald E. Stobby

Analytical Laboratories, 258 Building, Dow Chemical U.S.A., Midland, Michigan 48640

The chemical process industries are blessed with many process streams which, because of their hostile nature, do not adapt well to standard direct methods of analysis and yet accurate, reliable analytical data are needed on a continuous basis to provide good process and environmental control. Prime examples, and the subject of this paper, are the analysis of the inorganic acids hydrochloric and hydrobromic that are formed during the halogenation of organic molecules. Whether the acid thus formed is to be used in a downstream process or is to be salvaged for its halogen content, the organic components must be kept low to prevent undue contamination in subsequent operations. Utilizing a stripping column and head space analysis techniques, the authors have developed the "MOPS" or Multiple Organic in Process Streams analyzer to achieve these goals. Traditionally, this analysis has been achieved by extracting a sample with a suitable solvent and then analyzing the enriched solvent. This has been a time consuming and labor intensive analysis. Attempts to automate this type of procedure have not always been successful.

Commerically available analyzers, such as the Perkin-Elmer Head Space Analyzer and the Tekmar Liquid Sample Concentrator, which utilize a head space analysis concept, were reviewed prior to the MOPS development. While each gave good sensitivity and they were excellent for their intended use, none were judged acceptable for meeting our objectives for a completely automated on-line analytical system. These analyzers require large amounts of operator time for sample preparation and instrument loading and are not designed for on-stream analysis. As a result considerable lag time exists between the results obtained and the current composition of the process stream which does not permit rapid response to process variations. A third instrument, the Arcas "COW" or Chlorinated Organics in Water Analyzer, most nearly met our needs.

This instrument, which was developed by personnel of Dow Chemical U.S.A.'s Louisiana Division, features the simultaneous mixing of a water sample stream with a stripping gas in a short length of $^1/_4$-inch stainless steel tubing. Partitioning occurs during the residence time in the tube and the enriched stripping gas is subsequently separated and analyzed utilizing gas chromatography. Because of incomplete mixing and short residence time, this instrument may not provide the sensitivity needed to monitor certain compounds. It is, however, a truly automated, continuous analyzer and provided the genesis for the MOPS analyzer.

EXPERIMENTAL

The MOPS apparatus (Figure 1) employs a corrosion proof stripping column in which a purge gas is used to partition the organics dissolved in the sample stream into the gas phase. The enriched purge gas is then analyzed by utilizing standard analytical techniques. The advantage associated with this approach is the fact that volatile components can be separated in sufficient quantities for analysis from hostile sample matrices which would otherwise prohibit direct analysis.

The 1-inch diameter Pyrex piping, fittings, and clamps used in pilot work provided a convenient source of parts for construction of a separator. Custom glass parts were fabricated by the Michigan Division's Glass Fabrication Department. The initial work was performed utilizing a 6-inch long column packed with $^1/_4$-inch Beryl saddles. This provided the needed surface area and liquid residence time to give a substantial increase in sensitivity over the COW analyzer. However, because of the porous nature of the saddles, and the resultant cleaning problem between samples, it was decided to try a 6-inch length of inverted Vigreux column. This achieved the same sensitivity and is used routinely for most applications. The Vigreux column was inverted to ensure maximum wetting of the interior surfaces. Circular Teflon screens are placed above and below the top port ring to prevent upward splashing of the sample stream and to diffuse the sample stream

0003-2700/78/0350-0377$01.00/0 © 1978 American Chemical Society

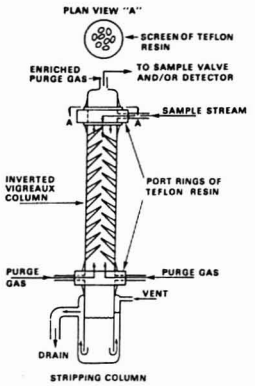


Figure 1. Stripping column

as it drops into the Vigreux column. In practice the sample stream is introduced at the top of the separator and allowed to percolate down through the column. The purge gas is introduced at the base of the Vigreux column from opposite sides and flows upward countercurrent to the liquid flow. A 6-inch length of glass pipe is attached to the bottom of the Vigreux column and port ring and placed in a reservoir which permits sufficient head to assure that the purge gas is continually flushed out of the top of the column. A volume ratio of ten parts of sample stream to one part of purge gas is maintained to provide optimum contact between liquid and gas. The experiments required a minimum sample stream flow rate of 50 mL/min and a purge gas flow rate of 5 mL/min. Lower flow rates resulted in a loss of sensitivity. The enriched purge gas is passed through a double sample valve fitted with 2-mL sample loops. The sampling valve consists of two 4-way slider valves fitted with two pneumatic actuators. This configuration permits the sampling of one loop while the second is being purged. Frequency of analysis is then limited only by the time necessary to produce a chromatogram. At a preselected schedule, which is controlled by a timer, the 2 mL of enriched purge gas is flushed into a gas chromatograph for separation and detection of the gaseous components. The chromatographic column is connected directly to the sample valve and by-passes the injection port. The separator and sample valve are located in a controlled oven to permit the use of temperature as a variable to achieve optimum results. In this configuration a gas chromatograph is used as a detector but the enriched purge gas could be analyzed using other analytical techniques such as infrared or mass spectrometry.

PROCEDURE AND RESULTS

Identification of Contaminants. Approximately 3 L of the acid stream under study were placed in a 1-gal. narrow mouth glass jug. The mouth of the jug was fitted with a two-hole stopper and a $^1/_4$-inch × 10-inch fritted glass tube which extended well into the sample. The second hole was fitted with either an activated carbon or silica gel slug of the type used in air sampling. A purge gas was then passed through the sample via the fritted glass tube; the volatile organics were stripped from the sample and absorbed in the slug. The stripping operation was allowed to continue overnight. The organic compounds collected in the slug were then stripped from the absorbent using carbon disulfide and identified utilizing infrared spectrometry. The hydrochloric acid stream was found to contain benzene, monochlorobenzene, and dichlorobenzene. The hydrobromic acid sample was found to contain methylene chloride and methylene chlorobromide.

Preparation of Standards and Sample Analysis. The acid samples that resulted from the stripping action described

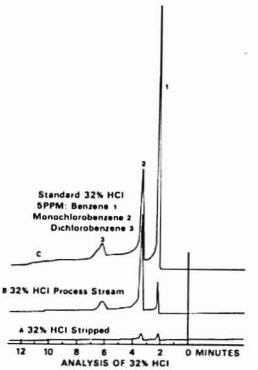


Figure 2. Analysis of 32% HCl

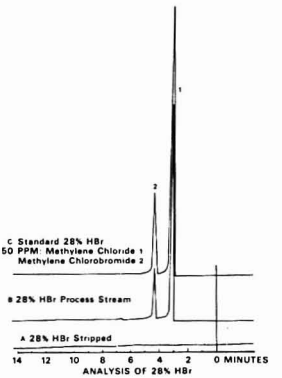


Figure 3. Analysis of 28% HBr

in the previous paragraph were circulated through the MOPS analyzer and found to be essentially free of organic contaminants as evidenced by the straight base line produced by the gas chromatograph. Known amounts of organic contaminants were then dissolved in the appropriate acid. The 32% hydrochloric acid was prediluted on a one to one volume basis before analysis.

Hydrochloric Acid, 32%. Benzene, monochlorobenzene, and dichlorobenzene, 5 ppm each, were dissolved in the diluted, stripped hydrochloric acid which was then circulated through the MOPS analyzer. Figure 2 depicts the chromatographs obtained with the stripped hydrochloric acid (A), a sample stream analysis (B), and the stripped hydrochloric acid sample spiked with known amounts of the contaminants (C). Comparison of the sample and standard chromatographs indicated that the process stream contained: 1 ppm benzene, 5 ppm monochlorobenzene, and 2 ppm dichlorobenzene.

Hydrobromic Acid, 28%. Methylene chloride and methylene chlorobromide, 50 ppm each, were dissolved in the stripped hydrobromic acid which was then circulated through the MOPS analyzer. Figure 3 depicts the chromatographs obtained with the stripped hydrobromic acid (A), a sample stream analysis (B), and the stripped hydrobromic acid spiked with known amounts of the contaminants (C). Comparison of the sample and standard chromatographs indicated that the process stream contained 40 ppm methylene chloride and 36 ppm methylene chlorobromide.

Chromatographic Conditions. Using a Varian Aerograph Model 1400, conditions were: attenuation, 64×10^{-11}; column temperature, HCl, 165 °C and HBr, 90 °C; detector, flame ionization; detector temperature, 200° isothermal; flow rate, 60 mL/min; carrier gas, nitrogen; and column, 14-ft 20% OV 275 80/100 Chromasorb W/AW.

PRECISION

A sufficient amount of the process stream was collected to permit ten determinations to be made. The reproducibility of peak height response was observed to be ±5% and the linearity of response over the expected concentration range also fell within this limit.

RECEIVED for review July 27, 1977. Accepted November 9, 1977.

Gas Chromatography of High Molecular Weight Hydrocarbons with an Inorganic Salt Eutectic Column

Lloyd R. Snowdon*

Institute of Sedimentary and Petroleum Geology, 3303-33rd Street N.W., Calgary, Alberta, Canada, T2L 2A7

Eric Peake

Environmental Sciences Centre (Kananaskis), University of Calgary, Calgary, Alberta, Canada, T2N 1N4

Gas chromatographic analyses of isoprenoid and normal alkanes and of steranes and triterpanes often play a key role in environmental studies of oil spills (*1–3*) and in petroleum geochemistry (*4–6*). The C_{19} saturated isoprenoid hydrocarbon, pristane, and the C_{20} saturated isoprenoid, phytane, are usually determined by gas chromatography in the presence of saturated normal alkanes. The ratio of these isoprenoids to selected normal alkanes is used as an indicator of biochemical alteration of crude oils (*7*).

Conventional packed gas chromatographic columns coated with such liquid phases as OV-101, SE-30, and Apiezon L often produce only partial resolution of these isoprenoid hydrocarbons from the adjacent C_{17} and C_{18} normal alkanes. Capillary columns and open tubular columns operated under ideal conditions (*2*) are capable of the desired resolutions but examples in the literature show that this frequently is not achieved. There is a need for a column which will completely resolve isoprenoid and normal alkanes, which is easy to operate and which will produce rapid analysis for the routine examination of large numbers of samples. The conventional packed columns described in this paper meet these requirements.

EXPERIMENTAL

Column packing consisting of 30% by weight of eutectic salt (*8, 9*) on 60/80 mesh Chromosorb W (Johns-Manville) was prepared by dissolving the salt, 54.55 wt % KNO_3, 27.3 wt % $LiNO_3$ 18.2 wt % $NaNO_3$ (Analabs) in water and adding this to the solid support which was pre-wet with methanol. The resulting slurry was reduced to near dryness by rotary evaporation and then dried in an open container overnight at 400 °C. A 3.35 m by 3.2 mm outside diameter stainless steel column and a 3.66 m by 2 mm inside diameter glass column were packed and stabilized by heating at 350–400 °C for several hours with a carrier gas flow of about 10 mL/min of helium. The choice of the steel and glass columns was made on the basis of availibility, gas chromatograph geometry, and standard operating procedure used in the authors' laboratories.

Crude oil samples and saturated hydrocarbons extracted from sedimentary rocks were routinely analyzed in the stainless steel column in one laboratory using a Hewlett-Packard model 5710A gas chromatograph equipped with a flame ionization detector.

A helium carrier flow of about 30 mL/min and heating rate of 8 °C/min resulted in the optimum high-speed separation of the saturated hydrocarbons. A slower heating rate (4 °C/min) resulted in peak spreading and a faster rate (16 °C/min) apparently reduced the column/sample interaction. Lower carrier gas flow rates also reduced the resolution, while higher flow rates required very high pressures on the front of column.

Hydrocarbons were extracted from crushed Green River oil shale with benzene, transferred to isooctane, and the normal alkanes removed with a 5 Å molecular sieve, leaving a mixture of isoprenoids, steranes, triterpanes, and lesser amounts of other branched and cyclic compounds. This was chromatographed in the other laboratory in the 3.66 m by 2 mm glass column in a Varian 2100 gas chromatograph equipped with flame ionization detectors. The helium carrier gas flow rate was initially 85 mL/min, dropping to 60 mL/min at the maximum oven temperature of 400 °C. A program rate of 10 °C/min was found to give adequate separation with minimum analysis time. A standard mixture containing 22 polycyclic aromatic hydrocarbons was also chromatographed in the 3.66-m glass column but a program rate of 4°/min was required to achieve optimum resolution.

RESULTS AND DISCUSSION

The sodium, lithium, potassium nitrate eutectic salt mixture proved to be an effective gas chromatographic coating phase for the rapid separation of saturated isoprenoids and *n*-alkanes in the nC_4 to nC_{40} carbon range. Mixtures of saturated isoprenoid and normal alkanes, such as those found in crude oils and in sedimentary rocks, were readily resolved with complete separation of pristane and phytane away from the adjacent *n*-alkanes (Figures 1a and 1b). Separation of these components by the salt mixture is often equal or superior to that obtained with capillary columns coated with Apiezon L (*10*), OV-101 (*11, 12*), or SE-52 (*2*), primarily because the pristane and phytane isoprenoid peaks fall approximately halfway between the nC_{17} and nC_{18} and the nC_{18} and nC_{19} normal alkanes, respectively. Other liquid phases gave retention times for pristane and phytane similar to those of nC_{17} and nC_{18}, respectively. Chromatograms of the same sample run on both salt eutectic and a commercially prepared OV-101 SCOT column gave essentially identical quantitative results of the heavy *n*-alkanes indicating that losses due to adsorption

0003-2700/78/0350-0379$01.00/0 © 1978 American Chemical Society

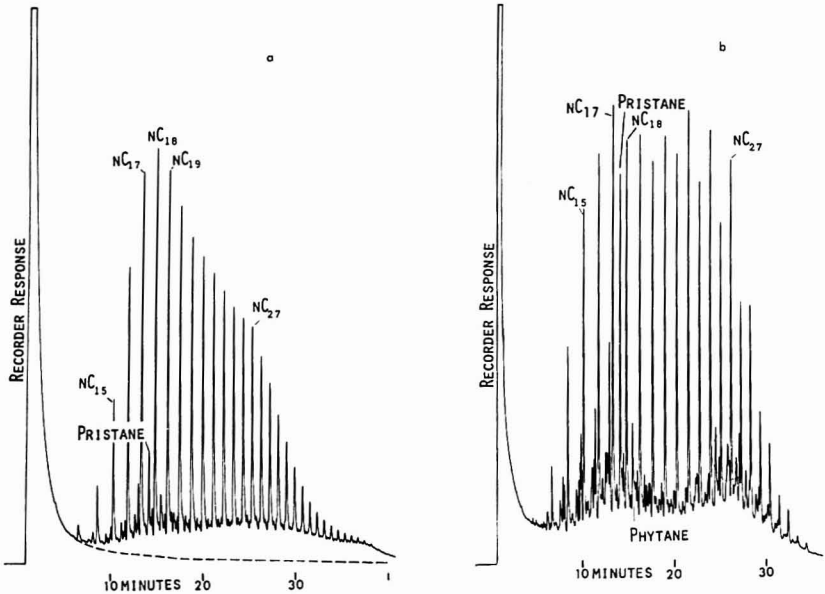


Figure 1. Gas chromatograms of (a) a whole crude oil from the Altamont Bluebell Field, Unita Basin, and (b) saturated hydrocarbons from a Canadian Arctic Islands sedimentary rock

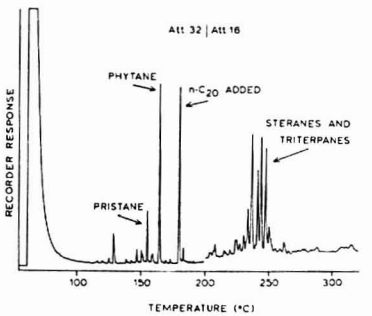


Figure 2. Gas chromatogram of branched and cyclic saturated hydrocarbons from the Green River oil shale

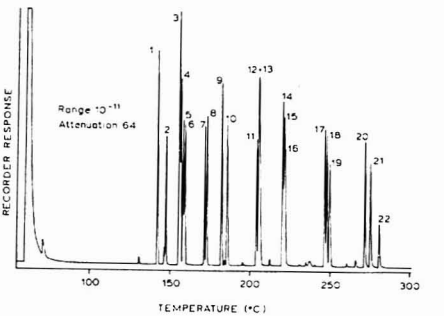


Figure 3. Gas chromatogram of a standard mixture of polycyclic aromatic hydrocarbons (1) fluorene, (2) 9-methylfluorene, (3) phenanthrene, (4) anthracene, (5) 2-methylfluorene, (6) 1-methylfluorene, (7) 1-methylanthracene, (8) 2-methylanthracene, (9) pyrene, (10) fluoranthene, (11) 3,4-benzofluorene, (12 and 13) 1,2-benzofluorene and 2,3-benzofluorene, (14) triphenylene, (15) chrysene, (16) benz[*a*]anthracene, (17) benzo[*e*]pyrene, (18) benzo[*a*]pyrene, (19) benzo[*b*]fluoranthene, (20) benzo[*ghi*]perylene, (21) *o*-phenylenepyrene, (22) 1,2,3,4-dibenzanthracene

are insignificant. Rapid program rates, up to 10 °C/min, together with column stability to 400 °C allowed analyses of crude oils for major saturated hydrocarbons to be conducted in about 30 min.

Samples for the analysis of minor cyclic and branched saturated components are usually prepared by removal of the normal saturated alkanes with molecular sieve (*13*). As shown in Figure 2, the branched-cyclic saturated hydrocarbon fraction of the Green River oil shale was readily resolved into isoprenoids and a group of compounds previously identified as C_{27} to C_{30} steranes and triterpanes (*14*). Resolution of the sterane–triterpane components was comparable to that previously achieved with a 15.2-m SE-30 SCOT column (*15*). Tricyclic diterpanes, found in some extracts of sedimentary rocks, gave peaks in the vicinity of nC_{18} whereas the retention times of the triterpanes and steranes fell in the range of the nC_{28} alkane.

The versatility of the eutectic salt mixture as a stationary phase was demonstrated by its ability to resolve a mixture of polycyclic aromatic hydrocarbons as shown in Figure 3. Of particular interest is the resolution of benzo[*a*]pyrene, a well known carcinogen, and its isomer, benzo[*e*]pyrene, which frequently occur in atmospheric particulate samples.

Loss of resolution resulted if moisture was adsorbed on the column either by exposure of the hydroscopic salt to the atmosphere or by the use of impure carrier gas; however,

resolution was readily regained by conditioning the column overnight at 400 °C with helium carrier gas flow.

LITERATURE CITED

(1) M. Gruenfeld, Proceedings of Joint Conference on Prevention and Control of Oil Spills, Washington, D.C., March 13–15, 1973, pp 179–193.
(2) E. B. Overton, J. Bracken, and J. L. Laseter, *J. Chromatogr. Sci.*, **15**, 169 (1977).
(3) J. G. Pym, J. E. Ray, G. W. Smith, and E. V. Whitehead, *Anal. Chem.*, **47**, 1617 (1975).
(4) J. G. Bendoraitis, B. L. Brown, and L. S. Hepner, *Anal. Chem.*, **34**, 49 (1962).
(5) I. R. Hills, G. W. Smith, and E. V. Whitehead, *J. Inst. Pet.*, **56**, 27 (1970).
(6) J. D. Brooks, K. Gould, and J. W. Smith, *Nature (London)*, **222**, 257 (1969).
(7) N. J. Bailey, A. M. Jobson, and M. A. Rogers, *Chem. Geol.*, **11**, 203 (1973).
(8) W. W. Hanneman, C. F. Spencer, and J. F. Johnson, *Anal. Chem.*, **32**, 1386 (1960).
(9) J. M. Hunt, in vonder Borch et al., "Initial Reports of the Deep Sea Drilling Project", Vol. 22, U.S. Government Printing Office, Washington, D. C., 1974, pp 673–675.
(10) J. Han and M. Calvin, *Geochim. Cosmochim. Acta*, **33**, 733 (1969).
(11) B. W. Jackson, R. W. Judges, and J. L. Powell, *Environ. Sci. Technol.*, **9**, 656 (1975).
(12) W. E. Reed, *Geochim. Cosmochim. Acta*, **41**, 237 (1977).
(13) M. T. Murphy in "Organic Geochemistry", G. Eglinton and M. T. Murphy, Ed., Springer-Verlag, Berlin, 1969.
(14) E. J. Gallegos, *Anal. Chem.*, **43**, 1151 (1971).
(15) D. E. Anders and W. E. Robinson, *Geochim. Cosmochim. Acta*, **35**, 661 (1971).

RECEIVED for review July 29, 1977. Accepted October 24, 1977.

Drying Small Amounts of Solvent for Use in Nuclear Magnetic Resonance Spectrometry

Joseph B. Alper

Department of Biochemistry, College of Agricultural and Life Sciences, University of Wisconsin—Madison, Madison, Wisconsin 53706

A major problem in the area of high field proton magnetic resonance (PMR) spectroscopy is the contamination of solvents with water (*1*). This problem is especially acute when using very small amounts of sample; the water signal can obscure sample peaks as well as cause computer-associated dynamic range problems when using time averaging techniques. We have developed a simple, fast, and efficient method of drying such solvents as dimethylsulfoxide (DMSO), acetone, and chloroform using a surplus gas chromatograph (GC), a broken 10-mL volumetric pipet, a 6-inch syringe needle, a Pyrex, Leur-lock syringe, Swagelok fittings and 4Å molecular sieves.

EXPERIMENTAL

The column was constructed as follows and the end result is shown diagrammatically in Figure 1. The ends of a 10-mL volumetric pipet were cut and bent in such a manner as to allow a good fit in the GC oven: the end to be connected to the GC inlet was fitted with Swagelok fittings and the outlet end was joined to the syringe barrel. The barrel of the pipet was then packed with 4-Å molecular sieves obtained from Altex Corp. A small hole ($^1/_8$-inch) was made in the back of the GC oven to accommodate the syringe needle, which is attached to the Leur-lock fitting of the syringe. The use of a syringe needle as the exit port allowed the dry solvent to be collected directly into a dry sample containing a NMR tube fitted with a septum cap. A small gauge needle is inserted through the cap during collection to allow for pressure relief. The column was then heated at 240 °C for 12 h, with a slight stream of dry nitrogen flowing during this time, to activate the molecular sieves. This procedure is also carried out after a day's use; we have found that after 9 months of daily use and overnight baking, the molecular sieves should be replaced.

Samples are prepared in our laboratory by dissolving between 0.2–4.0 mg of a peptide in a small amount of water, lyophilizing in the NMR tube to give a dry, white solid. The NMR tube is then fitted with a suitable septum cap (Aldrich) and dry solvent was collected after fitting the NMR to the exit needle of the GC column. The GC oven is set at 100 °C for Me_2SO-d_6 and 50 °C for both $CCDl_3$ and acetone-d_6; an injector temperature of 150 °C for Me_2SO-d_6 and 100 °C for $CDCl_3$ and acetone-d_6 is used. Dry nitrogen was used as the carrier gas and the flow was such that 15 min after injection all solvent had been eluted from the column. Up to 4.0 mL of solvent has been dried at one time.

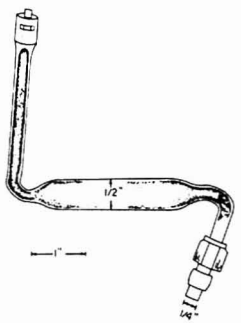


Figure 1. Diagram of the apparatus used to dry small amounts of solvents as described in this paper

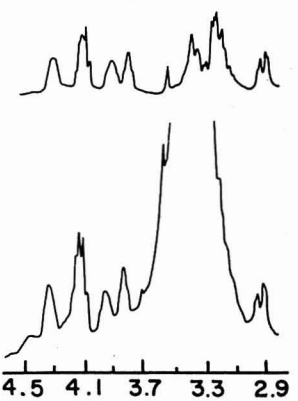


Figure 2. C_α proton region of the NMR spectra of tocinamide in Me_2SO-d_6. The bottom spectrum was taken using Me_2SO-d_6 taken from a sealed ampule. The top spectrum was taken using Me_2SO-d_6 dried using the method outlined in this paper

0003-2700/78/0350-0381$01.00/0 © 1978 American Chemical Society

RESULTS AND DISCUSSION

Figure 2 is the C_α region of the NMR spectra of tocinamide (*1*), a hexapeptide, in Me_2SO-d_6 which had been taken directly from a sealed ampule using a dry pipet; this was done in a dry glove bag. The water peak is very noticeable and caused problems by obscuring resonances from the glycine and cysteine residues. Figure 2 is the same region of an identical sample only prepared using Me_2SO-d_6 taken directly off the above described GC column. The water peak is missing and all resonances are fully visible. Similar results have been obtained with chloroform and acetone. In all cases, residual water contamination is less than 50 μM as estimated by comparison of peak heights due to a known concentration of proton to the residual water peak, which is visible only upon extreme magnification.

This procedure is much superior to storing solvents over molecular sieves and transferring them directly to the NMR tube. We have found that water contamination is still very noticeable, although less than with no drying at all. Thus, our transfer procedure is where this method stands out, and it should solve a major nuisance to NMR spectroscopists.

ACKNOWLEDGMENT

Les Licholls kindly supplied the NMR spectra of tocinamide.

LITERATURE CITED

(1) L. J. F. Nicholls, C. R. Jones, and W. A. Gibbons, *Biochemistry*, **16**, 2248 (1977).

RECEIVED for review September 12, 1977. Accepted November 16, 1977. This research was supported by the College of Agricultural and Life Sciences of the University of Wisconsin by grants from the NIH (AM 18604) and the NSF (BMS-74, 23819). The Biochemistry 270 MHz Facility was made possible by grants from the Graduate School and The National Science Foundation (No. BMS 74-23826).

Vacuum Envelope for High Pressure Mass Spectrometry Applications

Eric Grimsrud

Department of Chemistry, Montana State University, Bozeman, Montana 59717

Some of the most important developments in the area of mass spectrometry for chemical analysis in recent years have involved the use of ion sources in which the pressure is high relative to that of the conventional electron impact mass spectrometry technique. The now well-established and widely-used Chemical Ionization (*1*) method of generating mass spectra utilizes an ion source pressure of about 7 Torr. More recently, ultrahigh detection capabilities have been demonstrated by the method of Atmospheric Pressure Ionization (*2*) mass spectrometry which requires an ion source pressure of 7 atm. Because of the high gas flow rates inherent in these methods, perhaps the most significant modification required in the high pressure mass spectrometers results from the need of much greater pumping capacity on the vacuum envelope. The most simple and least costly way to do this modification is to install a single and relatively large pump on the vacuum envelope (*2*). Depending on the magnitude of gas flow, however, this approach may result in an inadequate vacuum, especially when baffles, traps, and isolation valves are added with the pump. The differentially pumped method (*3*), using two vacuum pumps in semi-isolated regions of the vacuum envelope, is generally recommended for high pressure mass spectrometers because lower pressures can be maintained in the critical volumes enclosing the mass analyzer and detector, while tolerating fairly high gas flow rates from the ion source into the first stage of the vacuum envelope. Of course, greater expense and complexity must be accepted with the differentially pumped system because of the additional pump and its associated baffles, traps, isolation valves, foreline pump, and fail-safe devices. We would like to report here an envelope design for high-pressure mass spectrometry methods which has some of the advantages of both of the above methods, that is, simplicity and low cost along with significant pressure differentiation between critical and noncritical volumes of the mass spectrometer envelope. Our application is for Atmospheric Pressure Ionization, but the principle could be applied equally well to a Chemical Ionization mass spectrometer or other applications of mass spectrometry in which high gas flow rates are inherent, such as an Electron Impact Ionization mass spectrometer which is sampling the entire effluent from a gas chromatograph (*4*).

EXPERIMENTAL

Our mass spectrometer shown in Figure 1 is similar to the single-pump design of Horning et al. (*2*) for Atmospheric Pressure Ionization. Between the 6-in. diffusion pump (Edwards model E06) and the mass spectrometer envelope are a baffle and a 6-in. butterfly isolation valve. The baffle is homemade from straight stainless strips of 1.5 in. in width, soldered into the vacuum envelope each at a 45° angle. The ion source encloses a 1-cm^3 volume, the walls of which are formed by a ^{63}Ni-impregnated platinum foil. Most of the carrier gas entering the ion source is vented to the room air after passing through the cell. About 3.8 cm^3 atm min^{-1}, however, passes into the vacuum envelope via a 20-μm aperture. This aperture is in the center of a nickel disk (Perforated Products, Inc.) of 25-μm thickness which forms the back wall of the ionization volume. The nickel disk is sealed between the ion source and the flange of the vacuum envelope with a gold O-ring. For these measurements, the ion source was maintained at room temperature.

Within the vacuum envelope, a quadruple mass spectrometer (Extranuclear Laboratories, Inc.), including the quadruple rods and electron multiplier detector are mounted to the rear flange. The rods and detector are each housed in stainless steel cans which, except for the ion entrance aperture (3-mm diameter), was entirely closed when first received from the manufacturer. An effective curtain was fabricated to separate the volumes indicated as A and B in Figure 1 in the following manner. A stainless disk ($^1/_{16}$-in.thick) was welded to the interior walls of the vacuum envelope and to the top of one of the baffle fins in the position shown. This disk has a hole of 5 in. in diameter centering on the quadruple axis. A piece of stainless plate, fitting from the bottom edge of the above-mentioned baffle fin to the axis of the butterfly baffle was welded to the fin and envelope walls. Another disk (5.5 in. in diameter) and an attached collar were made to fit over the quadrupole housing as shown. The fit is such that the collar is snug, but easily movable. With the addition of this part to the quadruple housing, the separation of volumes A and B is caused by placement of the rear flange and all of the components attached to it onto the mass spectrometer. As shown in Figure 1, with the butterfly valve open, the separation of volumes A and B extends to the throat of the diffusion pump. To ensure that the pressure near the quadrupole rods and the detector is that of region B, several holes were drilled into the jackets of the detector and the

0003-2700/78/0350-0382$01.00/0 © 1978 American Chemical Society

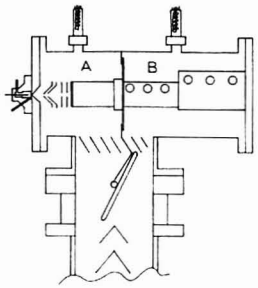


Figure 1. Atmospheric pressure ionization mass spectrometer with a curtain separating critical from noncritical regions of the vacuum envelope

quadruple rods behind the quadruple housing collar.

The pressure in regions A and B was monitored by two ionization gauges (Leybold-Heraeus, Inc., Ionvic 2). The manufacturer's pressure calibration was used. Accuracy was verified by interchanging three tubes and three controllers of the same type and obtaining identical pressure readings.

RESULTS AND DISCUSSION

The measurements of pressure in regions A and B of the vacuum envelope under different test conditions are shown in Table I. By removing the disk and collar of the quadruple housing, the first condition tests the situation where no curtain separating regions A and B exists. As is expected, no difference in pressures in regions A and B is seen, both having a pressure of 1.0×10^{-4} Torr. It will be shown later that this is about the magnitude of pressure expected given the source sampling aperature, the diffusion pump, baffle, and isolation valve of our system. It is important to note that operation of quadruple rods and an electron multiplier at this pressure is not recommended by the manufacturer because of the likelihood of vacuum discharges causing damage to the rods and the premature death of the detector (5).

Replacing the quadruple housing collar results in an effective separation of regions A and B down to the diffusion pump throat, except for the small ion entrance aperture of the quadruple housing. The result is that the pressure in region A increases to 1.6×10^{-4} Torr, but the pressure in region B decreases to 2.3×10^{-5} Torr. Since the quadruple rods and detector will also experience the pressure of region B, this simple alteration of the vacuum envelope has decreased the pressure in critical regions by a factor of 4. The successful operation of our quadruple rods and detectors for long periods of time may be a reasonable expectation at this pressure of nitrogen (5).

For the sake of this study, the result of one further alteration of the vacuum system, blocking the ion entrance aperture of the quadruple housing, is shown in Table I. Here the regions A and B are entirely separated down to the diffusion pump throat. In region A, a pressure of 1.6×10^{-4} Torr is observed and in region B, a pressure of 2.3×10^{-5} Torr. Since these are the same values observed with the ion entrance aperture open, it is clear that the presence of a small hole the size of the ion entrance aperture (3 mm) has little effect on the differential pressures established in regions A and B.

The results of Table I can be shown to be in harmony with known laws describing the behavior of flowing gases (6). The flow rate of nitrogen through the mass spectrometer is limited by the 20-μm aperture of the ion source. The conductance, C, of this aperature can be calculated from the equation for viscous flow of air at 20 °C, $C = 20\ A$ L s^{-1}, where the area, A, is expressed in cm^2. The flow rate, $Q = C \times \Delta P$, where ΔP is the pressure differences across the aperture (about 643 Torr in Bozeman) is then calculated to be 4.0×10^{-2} L Torr s^{-1} or 3.8 cm^3 atm min^{-1}. The pumping speed of our pump is reported to be 1400 L s^{-1} by the manufacturer. For the valve and a baffle very similar to ours, the manufacturer of our valve and pump report a throughput efficiency of 50% for each device. Thus, the net pumping speed, S, of our stack will be about 1400 L s^{-1} × 0.50 × 0.50 = 350 L s^{-1}. Thus, with no curtain separating regions A and B of our envelope, a pressure of $P = Q/S = 4.0 \times 10^{-2}/350 = 1.15 \times 10^{-4}$ Torr should be attained. This value is in good agreement with the result of the first test condition shown in Table I where a value of 1.0×10^{-4} was observed. Perhaps the greatest uncertainty in our calculations results from the uncertainty in the size of the ion source aperture (±10%).

Table I. Pressure Observed in Two Regions of the Mass Spectrometer under Various Physical Conditions of the Vacuum Envelope

Condition of vacuum envelope	Pressure, Torr Region A	Region B
Quadruple housing collar NOT used	1.0×10^{-4}	1.0×10^{-4}
Envelope curtain in place	1.6×10^{-4}	2.3×10^{-5}
Curtain in place and quadruple ion aperture closed	1.6×10^{-4}	2.3×10^{-5}

With the envelope curtain intact, the cross-sectional area of the pumping stack exposed to region A is reduced by about one-third the total area. Thus the pumping speed to region A should now be about 0.66 × 350 = 230 L s^{-1} and a pressure in region A of $P = Q/S = 4.0 \times 10^{-2}/230 = 1.7 \times 10^{-4}$ Torr is predicted. A value of 1.6×10^{-4} Torr was measured. To compute the pressure predicted in region B under this condition, gas flow from two directions, from the ion entrance lens of the quadruple housing and from the throat of the diffusion pump, must be considered. The conductance of the 3-mm ion entrance aperture can be calculated from the molecular flow equation for air at 20 °C through an orifice, $C = 12\ A$ L s^{-1} where the area is in units of cm^2. The flow is then $Q = C \times \Delta P = 8.5 \times 10^{-1}$ L s^{-1} × 1.6×10^{-4} Torr = 1.35×10^{-4} Torr L s^{-1}. The pumping speed to region B will be 350 × 0.33 = 115 L s^{-1}, and a pressure of $P = Q/S = 1.17 \times 10^{-6}$ Torr is predicted for region B from flow through the ion entrance aperture alone. This value is an order of magnitude less than the value of 2.3×10^{-5} Torr observed in region B under this condition. It must be concluded, therefore, that flow through the ion entrance aperture plays a minor role in determining the pressure of region B. The other effect, flow to and from the diffusion pump throat can be easily perdicted. The pressure anywhere in a vacuum system having a single pump can never be lower than the pressure at the throat of the pump since this region experiences maximum pumping speed. Assuming that region B is completely sealed from region A down to the throat of the diffusion pump, no *net* flow between B and the pump can occur, and the equilibrium pressure established in region B must be the same as the pressure at the throat of the pump. Thus, to calculate the limit of achievable pressure in region B predicted from the equilibrium flow from the pump alone, we need only to calculate the pressure predicted at the diffusion pump throat. This is $P = Q/S = 4.0 \times 10^{-2}/1400 = 2.9 \times 10^{-5}$ Torr. This value is much larger than the effect on region B predicted for flow through the ion entrance aperture and is, therefore, most important and a determining factor of the pressure in region B. The measured value of 2.3×10^{-5} Torr in region B is in good agreement with this prediction. The last condition tested, that of blocking the ion entrance aperture completely, conclusively illustrates that the pressure of region B is being

limited to that at the pump throat, since no effect of this change is reflected in the measured pressures.

The advantages of this system for our application are obvious, and further interesting consequences might be predicted. For example, if additional baffling or trapping is desired in a vacuum system and if these are installed in a manner which maintains a curtain continuously down to the pump throat, it would still be possible to achieve the ultimate pressure of the diffusion pump throat or very close to it throughout the critical volume. In other words, the pressure achievable in a selected region of a vacuum system is limited only by the gas flow rate entering the entire envelope and the size of the pump evacuating it, and can be made independent of the baffles, traps, and isolation valves also used. Another potentially useful prediction is that a lower pressure in the critical volume might be obtained by using a larger diffusion pump even if the diameter of the pump exceeds that of the port and vacuum system to which it is attached. In a singly pumped system, one would gain little by this alteration because the net conductance of the pumping stack is limited by its smallest dimension.

The major limitation of the vacuum design described here compared to a conventional differentially pumped system is, as has been shown, the ultimate vacuum achievable with it is inherently limited for a given gas flow rate and vacuum pump. As is possible with the truly differentially pumped system, the pressure of the critical volume cannot be continuously lowered by decreasing the size of the aperture connecting the two envelope volumes. Furthermore, for a given system, much lower pressures in the critical volumes can be obtained with a conventional differentially pumped system. In our application, for example, the pressure in region B could be reduced to about 1×10^{-6} Torr by the proper addition of a second diffusion pump stack of modest size. Nevertheless, for many applications, the envelope design described here can offer satisfactory results at a minimum of expense and instrumental complexity, and certainly provides a significant improvement in performance over the conventional singly-pumped vacuum envelope.

LITERATURE CITED

(1) B. Munson, *Anal. Chem.*, **43** (13), 28A (1971).
(2) E. C. Horning, M. G. Horning, D. I. Carroll, I. Dzidic, and R. N. Stillwell, *Anal. Chem.*, **45**, 936 (1973).
(3) M. McKeown and M. W.Siegel, *Am. Lab.*, Nov. 1975.
(4) E. P. Grimsrud and R. A. Rasmussen, *Atmos. Environ.*, **9**, 1010 (1975).
(5) Extranuclear Laboratories, Inc., Instruction Manuals for Preamp counting head, model 032-3, and for particle multipliers, model 051, Oct. 1975.
(6) S. Dushman, "Scientific Foundations of Vacuum Technique", 2nd ed., J. M. Lafferty, Ed., John Wiley and Sons, New York, N.Y., 1962, Chapter 2.

RECEIVED for review October 4, 1977. Accepted November 14, 1977. Acknowledgment is made to the Donors of the Petroleum Research Fund, administered by the American Chemical Society; to Research Corporation; and to the National Science Foundation for support of this research.

CORRECTION

Chemically-Bonded Aminosilane Stationary Phase for the High-Performance Liquid Chromatographic Separation of Polynuclear Aromatic Compounds

In Table I of this article by S. A. Wise, S. N. Chesler, H. S. Hertz, L. R. Hilpert, and W. E. May, *Anal. Chem.*, 49, 2306 (1977), the logarithm of the retention index for pyrene on μBondapak NH_2 should be 3.26 rather than 3.68.

Author Index

Abu-Shumays, A. 339
Alper, J. B. 381
Anson, F. C. 223
Arvia, A. J. 229

Baier, R. W. 351
Baum, R. G. 280
Beck, R. A. 200
Bentz, B. L. 373
Bond, A. M. 216
Borsaru, M. 296
Brown, C. W. 315
Bruhn, C. G. 373
Bunzl, K. 258

Cairns, T. 317
Calandra, A. J. 229
Cantwell, F. F. 280
Carpenter, A. P., Jr. 326
Castellano, C. E. 229
Churella, D. J. 309
Cohen, N. 357
Copeland, T. R. 309
Curtis, D. B. 376

D'Alonzo, R. P. 326
Davis, E. R. 202

Eastwood, D. 334
Eng, F. 197

Fortier, S. H. 334
Friedman, S. 368
Froberg, J. E. 317

Ganjei, J. D. 285
Garner, W. L. 251
Giger, W. 243
Ginzburg, G. 375
Gladney, E. S. 376
Gonzales, S. 317
Grandy, D. W. 303
Grimsrud, E. 382
Grubaugh, K. W. 377
Gupta, R. N. 197

Hadjiioannou, T. P. 205
Haraguchi, H. 360
Harrison, W. W. 373
Hieftje, G. M. 209
Higuchi, T. 232
Holland, M. K. 236
Holmes, R. J. 296
Hough, M. 368
Howe, R. L. 339
Howie, J. K. 317
Hunter, T. W. 209

Ibrahim, S. A. 357

Janzen, E. G. 202
Johnson, D. C. 240

Kaimai, T. 268
Kirchmeier, R. L. 349
Knechtel, J. R. 202
Kolling, O. W. 212
Korus, R. A. 249
Koval, C. A. 223

Langham, W. S. 317
Larochelle, J. H. 240
Lawless, P. A. 290
Lee, D. W. 255
Lee, K. S. 255
Lee, W. 255
Leta, D. P. 285
Lewis, D. 197
Lynch, P. F. 315

Martins, M. E. 229
Matsunaga, A. 268
Melcher, R. G. 251
Miller, R. F. 330
Mitchell, J. W. 194
Morrison, G. H. 285, 294

Nadkarni, R. A. 294
Nelson, P. 322
Nikolelis, D. P. 205
Novotny, M. 271

O'Halloran, R. J. 216

Patterson, P. L. 329, 345
Peake, E. 379
Peterson, P. E. 298
Petrakis, L. 303
Petrie, L. M. 351
Pietri, C. E. 236
Pui, C. P. 330

Rabenstein, D. L. 276
Rechnitz, G. A. 330
Retcofsky, H. L. 368
Rosser, R. W. 249
Ruzic, I. 216
Ryan, P. W. 371

Saetre, R. 276
Sandhu, S. S. 322
Sawyer, D. T. 317
Schaffner, C. 243
Schweighardt, F. K. 368
Severs, L. W. 251
Siggia, S. 326
Singh, N. P. 357
Smith, D. E. 216
Smith, R. D. 371
Snowdon, L. R. 379
Spangler, G. E. 290
Srianujata, S. 232
Stamp, J. J. 317
Sternson, L. A. 232
Stobby, G. E. 377

Tsuda, T. 271

Uden, P. C. 326
Upton, R. P. 349

Vaccaro, J. R. 251
Van Haverbeke, L. 315
Vidrine, D. W. 298

Weeks, S. J. 360
Weiss, J. R. 236
White, W. R. 232
Winefordner, J. D. 360
Wrenn, M. E. 357

Future Articles

Effect of Solute Ionization on Chromatographic Retention on Porous Polystyrene Copolymers
D. J. Pietrzyk, E. P. Kroeff, and T. D. Rotsch

Kinetic Determination of Borate at the Parts per Million Level
J. C. Gijsbers and J. G. Kloosterboer

Curie-Point Pyrolysis and Field Ionization Mass Spectrometry of Polysaccharides
H.-R. Schulten and W. Gortz

Elimination of Beta-ray Interference with Magnetic Fields in Measurement of X-rays Following Neutron Activation
M. Mantel, Z. B. Alfassi, and S. Amiel

Evaluation of Benzene as a Charge Exchange Reagent
S. C. S. Rao and C. Fenselau

Preservation of Some Trace Metals in Samples of Natural Waters
K. S. Subramanian, C. L. Chakrabarti, J. E. Sueiras, and I. S. Maines

Analysis of Carotenoid and Porphyrin Pigments of Geochemical Interest by High-Performance Liquid Chromatography
S. K. Hajibrahim, P. J. C. Tibbets, C. D. Watts, J. R. Maxwell, and G. Eglinton

Stationary Cold-Vapor Atomic Absorption Spectrometric Method for Mercury Determination
S-L. Tong

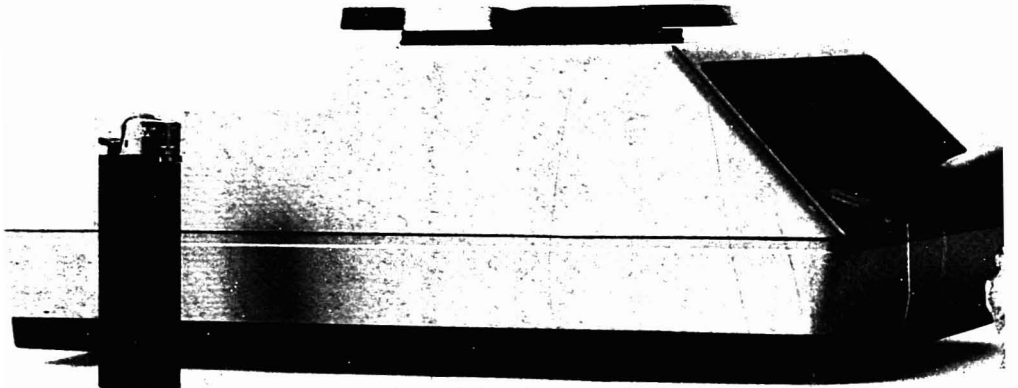
Two-Phase Buffer Systems I. Theoretical Considerations
T. J. Janjic and E. B. Milosavljevic

Liquid Chromatographic Analysis of Pharmaceutical Syrups Using Pre-Columns and Salt Adsorption on Amberlite XAD-2
H. Y. Mohammed and F. F. Cantwell

Experimental and Theoretical Consderations of Flow Cell Design in Analytical Chemiluminescence
S. Stieg and T. A. Nieman

SARTORIUS DOES IT AGAIN!

Introducing new microprocessor-equipped electronic balances with new capabilities, new add-on data keyboards, and new low (from $1,295) prices.



Last year, Sartorius introduced a major advance in fully electronic weighing with the revolutionary Series 3700 Balances.

This year, Sartorius does it again with its new MP models. These extremely versatile electronic top-loading balances utilize Texas Instruments microprocessors to vastly expand data handling and processing capabilities.

With optional plug-in keyboards that can be added anytime, MP models can be used to convert weight data, select programs, recall information and even calculate results.

Some typical applications for these balances include: instantaneous conversion from metric to non-metric calibration (weighings in pounds, ounces, carats, grains, pennyweights, etc.), parts counting, mean weight determination, percentage weighing, and variable integration time for more precise animal weighings.

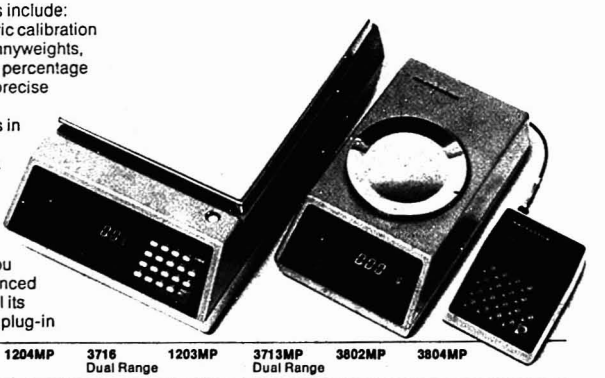
MP models also provide complete weighings in 1-2 seconds, instant electronic taring, automatic overload protection, a built-in vibration filter, data storage memory, and are available with BCD and analog outputs.

Can you afford to buy a new balance without these capabilities?

When you choose a Sartorious MP model, you have selected a balance that will be quite as advanced tomorrow as it is today. Even if you do not need all its capabilities now, the purchase of the appropriate plug-in keyboard makes the needed capability instantly available any time in the future. Only Sartorius offers this flexibility.

For all their advanced technology, Sartorius MP models, priced as low as $1,295 are significantly less expensive than many other electronic balances without such features. For literature, write: Sartorius Balances Division, Brinkmann Instruments, Inc., Cantiague Road, Westbury, N.Y. 11590.

sartorius



MODEL (Partial Listing)	1205MP	1202MP	1212MP Dual Range	1204MP	3716 Dual Range	1203MP	3713MP Dual Range	3802MP	3804MP
Weighing Range	0-160g	0-300g	0-30g 0-300g	0-1200g	0-120g 0-1200g	0-3000g	0-300g 0-3000g	0-6000g	0-16000g
Readability	0.001g	0.01g	0.001g 0.01g	0.01g	0.01g 0.1g	0.1g	0.01g 0.1g	0.1g	0.1g
Price	$2295.	$1295.	$1650.	$2195.	$1845.	$1595.	$2495.	$3340.	on request

CIRCLE 28 ON READER SERVICE CARD